NASA SP-376

ACTIVE MICROWAVE WORKSHOP REPORT

NATIONAL AERONAUTICS AND SPACE ADMINISTRATION

NASA SP-376

ACTIVE MICROWAVE WORKSHOP REPORT

The report of a working group meeting at
Lyndon B. Johnson Space Center, July 22-26, 1974,
on the utilization of
active microwave systems in applications programs

Edited by

Richard E. Matthews
NASA Lyndon B. Johnson Space Center

Scientific and Technical Information Office 1975
NATIONAL AERONAUTICS AND SPACE ADMINISTRATION
Washington, D.C.

For Sale by the Superintendent of Documents,
U.S. Government Printing Office, Washington, D.C. 20402
Price $5.60 Stock No. 033-000-00624-1
Library of Congress Catalog Card No. 75-600062

Foreword

ON JANUARY 15, 1974, the National Aeronautics and Space Administration issued an announcement entitled "Opportunities for Participation in a Working Group for Utilization of Active Microwave Systems in Future Applications Programs." The purpose of the announcement was to initiate the formation of an ad hoc Active Microwave Working Group whose objective would be "to review and define the anticipated advantages of active microwave systems in future aerospace Applications Programs."

The Working Group, which was implemented by the Lyndon B. Johnson Space Center (JSC) on behalf of NASA, met in Houston, Tex., from July 22 to 26, 1974. The membership of the Working Group was selected from those persons responding to the NASA announcement. Approximately one-third of those responding were selected; the limitation on numbers was imposed primarily by facility and funding constraints. The excellent response assured that all Working Group areas of interest were more than adequately covered. In a great many cases, the Steering Committee was forced to choose one person from among several who were equally qualified in a particular interest area.

The interest areas of the Working Group dictated its division into three discipline panels (Earth/Land, Ocean, and Atmosphere) and a Technology Support Group. The Working Group was chaired by Richard A. Moke assisted by Richard E. Matthews, both of JSC. The chairmen of the subgroups were as follows.

Earth/Land Panel: J. W. Rouse, Jr., and M. W. Molloy
Ocean Panel: F. O. Vonbun
Atmosphere Panel: W. R. Bandeen
Technology Support Group: W. E. Brown, Jr.

A Steering Committee coordinated the efforts of the various panels. JSC was assisted in implementation of the Working Group by the Remote Sensing Center and the Industrial Economics Research Division of Texas A&M University.

Many people contributed significantly to the activities of the Working Group and to list their contributions individually is not possible. However, special thanks are due to the Working Group members and to members of the Steering Committee for their support and contributions.

A word of caution is in order regarding this report. It will be noted that individual author identity is missing. To assure better continuity and coverage, each chapter was written as a unified entity rather than as a series of individually authored papers. However, when the various sections of a chapter were blended together, the differences in use of symbols and notation by the various contributors presented a problem. Although

attempts were made to eliminate confusing or ambiguous symbol usage, the goal of establishing symbol uniqueness was not achieved. Consequently, care must be exercised when comparing equations from different sections of the report.

The contents of this report represent the collective knowledge, views, and opinions of the Working Group members. The recommendations and conclusions contained in the report are those of the Working Group members and do not necessarily represent the policy and program direction of NASA.

LYNDON B. JOHNSON SPACE CENTER

MARCH 27, 1975

Contents

CHAPTER 5—ACTIVE MICROWAVE SENSOR TECHNOLOGY

TABLES

CHAPTER 1

Summary of the Active Microwave Workshop

INTRODUCTION

NASA Applications Objectives

NASA is responsible for planning, directing, and conducting aeronautical and space activities. To help meet this responsibility, the NASA applications program has the following objectives:

1. To develop and test procedures, instruments, spacecraft, and interpretive techniques in the various disciplines in applications.
2. To accomplish long-range studies of potential benefits to be gained from, and the problems involved in, the utilization of space capabilities.
3. To conduct a comprehensive and meaningful space applications program to help maintain U.S. scientific, technological, and economic leadership.

These objectives can be met by the use of aircraft and spacecraft systems for obtaining information about the Earth, the oceans, and the atmosphere. Remote sensor systems for providing improved data in a variety of discipline areas are the core of the missions to be performed with these aircraft and satellites.

In the past, the major emphasis on remote sensor systems in the applications program has been on visible-region sensors for both aircraft and satellites. Camera, vidicon, and multispectral scanner systems have been used extensively in the space program aboard Earth resources aircraft and on spacecraft such as Apollo, Nimbus, Earth Resources Technology Satellite (ERTS), Skylab, and others. Similar systems are planned for future spacecraft, such as the Earth Observatory Satellite (EOS) series. As a result of these and associated activities, such as the development of large multispectral data-processing centers, there exists a significant amount of empirical data and data analysis results supporting the application potential of visible-region sensors.

In comparison, active microwave sensors have had limited application, and the amount of usable empirical data is inadequate. Thus, the application potential cannot be documented with similar confidence. The active microwave sensing field has the advantage of a far more extensive background in theoretical and analytical modeling studies, and many of the applications presented in this report are based on these fundamental studies of the physical phenomena measurable in the microwave region.

The Active Microwave Workshop (AMW) is the first concerted effort made to bring together the several elements of the active microwave remote-sensing field in such a way as to demonstrate the applications of this technology. The results presented in this report convincingly show the desirability and feasibility of using active microwave sensors on future Earth observations missions.

Objectives of the AMW

The basic objective of the AMW was to review and define the anticipated advantages of active microwave systems in future aerospace and applications programs. Specific objectives included the following:

1. Definition of user/applications requirements in each of three areas of interest—namely, Earth/land, oceans, and atmosphere.

2. Description and specification of active microwave systems and signature data that can be obtained or are needed to meet user/applications requirements in each area of interest.

3. Identification of active microwave sensor technology capabilities and anticipated technological developments that might impact overall area objectives.

4. Formulation of guidelines and recommendations for applying active microwave systems technology to NASA programmatic goals and future mission planning.

The approach taken by the three discipline panels—Earth/land, oceans, and atmosphere—to meet the AMW objectives was

1. To identify needed Earth observations applications in which active microwave sensor techniques are potentially useful.

2. To divide these applications into those known to be feasible and those believed to be feasible.

3. To outline the experiments and systems needed to implement presently feasible methods and to bring others to the feasible stage.

Structure of the AMW

The active microwave working group, composed of approximately 70 scientists and engineers, was directed by a 12-man steering committee. The selection of the working group members was based on the applicants' experience in the Earth observations areas of interest and/or in active microwave systems. The membership of the working group is shown in appendix 1A. The multidisciplinary objectives of the AMW required the formation of three discipline panels (Earth/land, oceans, and atmosphere) and a technology support group.

A 2-day meeting of the participants was held April 24 and 25, 1974, in Houston, Tex., to acquaint the participants with the objectives and scope of the AMW program, to structure the AMW report, and to assign tasks to the participants for specific contributions to this report.

The AMW was held from July 22 to 26, 1974, in Houston, Tex. The participants submitted contributions to the AMW report in advance of the AMW meetings to facilitate compilation of a working draft for the 5-day session in July. These advance contributions were abstracted, evaluated, reproduced, and distributed to the participants 3 weeks in advance of the AMW meetings.

During the weeklong AMW working sessions, the advance contributions were rewritten, edited, reviewed, and summarized by the panels and the support group to form a draft of the full AMW report. The draft formed the basis for the final report.

PANEL RECOMMENDATIONS

Earth/Land Panel

The panel recommends the following activities to bring active microwave remote sensing to its full potential:

1. Program development: Initiate a coordinated interdisciplinary program for development of active microwave sensing of the Earth.

2. Measurements: Establish multifrequency, multipolarization, ground-based/aircraft experiments and develop modeling programs to study the characteristics of microwave energy interaction mechanisms associated with measurements of soil moisture, surficial materials, vegetation penetration, crop moisture effect, vegetation species, snow moisture content, frozen ground, and others.

3. Interpretation: Train a wide range of users in interpretation of radar images to take advantage of unique and full-time operational capability. Develop image interpretation methodology for use with active microwave images.

4. Operational tests: Conduct semioperational demonstrations for those imaging radar applications that are identified as feasible, that are potentially useful, and that capitalize on the unique characteristics of radar.

5. Satellite experiment: Conduct a satellite imaging radar experiment using a single- or dual-wavelength imaging radar system to

establish the effect of orbital operation on the system and the radar data.

6. Data analysis: Place high priority on the data analysis and interpretation techniques and their funding in all present and future active microwave programs.

Oceans Panel

Programmatic recommendations.—The programmatic recommendations are as follows:

1. Immediately develop a focused and coordinated program for the specific use of aerospace microwave systems for oceanographic applications.

2. Increase the emphasis on research and development in (1) the proper interpretation of microwave signals returned from the sea or ice surface, and (2) the mathematical modeling of ocean-surface phenomena as applicable to microwave observations.

3. Initiate a vigorous program in the development of end-to-end data processing for ocean phenomena as detectable by active microwave systems.

4. Initiate an active microwave test program using aircraft dedicated to the study of oceanographic phenomena.

5. Explore the complementary role of passive sensors used in conjunction with active microwave systems.

6. Explore coastal zone requirements that can be satisfied by using airborne remote active microwave systems together with other sensors.

Technical recommendations.—Particular priority should be given to the design and development of—

1. A high-resolution imaging radar (10-m resolution, 200-km swath width).

2. A high-precision radar altimeter (2- to 5-cm accuracy).

3. A high-precision scatterometer (0.2-dB accuracy, 30-km spatial resolution).

4. Digital techniques for ocean data handling for active microwave systems.

Further emphasis should be placed on acquiring—

1. A microwave remote-sensing device for measuring surface wind velocity (as high as 50 m/sec, $\pm 10°$ direction, ± 10 percent speed, 25-km resolution).

2. A real aperture aircraft radar potentially including Doppler capacity (10-m resolution).

3. A wave directional spectrometer (ocean wavelength of 30 to 50 m; angle resolution of $\pm 10°$, ± 10 percent).

4. A multifrequency, multipolarization radar.

Atmosphere Panel

The atmosphere panel recommendations are as follows:

1. A single cohesive research program should be established in NASA to develop active microwave techniques to be applied to requirements in the meteorological discipline as well as the oceanographic and Earth resources disciplines. The concepts discussed in this report, virtually for the first time, indicate that the applications may be feasible from space.

2. The scientific commonality of certain requirements between two or more disciplines should be recognized and emphasized. For example, both the oceanographic and atmospheric disciplines measure ice cover over polar regions.

3. The technological commonality of active microwave systems required by the meteorological, oceanographic, and Earth resources disciplines should be studied to achieve maximum cost effectiveness. It appears possible that one active microwave system (e.g., an imaging pulse radar), if suitably designed, may satisfy some of the requirements of more than one discipline. This possibility should be thoroughly investigated.

4. A major allocation of resources should be designated for the reduction, validation, analysis, and interpretation of data to be acquired in the flight program. Too often in the past, the analysis of data received little support in flight programs. The panel believes that the comprehensive and timely analysis of the data is of such importance

that, if necessary, it would be preferable to eliminate an entire flight experiment to provide for adequate data analysis rather than devote essentially all the available resources to flight systems and prevent the adequate exploitation of the data. In addition to the primary analysis, such exploitation should provide for the acquisition of "truth" data (e.g., from ships, instrumented aircraft, etc.) to be used in validating the satellite observations.

5. A downward-looking, scanning pulse radar technique should be developed for satellite use in a low-altitude orbit. The instrument resulting from this development would provide global measurements of rain intensities, heights of echo top, and the melting level in rain clouds. In addition, it may be possible to combine this instrument with the scatterometer proposed by the oceans panel for measuring ocean surface winds. These techniques are important in short- and long-term weather forecasting.

6. In-depth feasibility studies of the active microwave systems proposed in this report should now be undertaken. Initial evaluations have shown these systems to have promise. Calculations of required resolutions and sensitivities should be matched with expected technological capabilities. Furthermore, the panel thinks that fundamental research on active remote-sensing techniques should be broadened to include frequencies other than microwave. For example, the possible use of a carbon dioxide Doppler laser system operating at a wavelength of approximately 10 μm for measuring cloud boundary motion or clear air motion by means of scattering from aerosols, either from a geostationary or a low-altitude satellite, is discussed in the section entitled "Satellite-Borne Radar With Doppler Capability" in chapter 4. However, insufficient data exist now for the assessment of the utility of the method; hence, further theoretical and experimental work is needed to permit such an assessment.

Technology Support Group

The technology support group recognizes an urgent need for establishing a program to develop a spaceborne onboard digital data-handling system for processing imaging radar data. Fundamental areas to be considered include the requirements for multiple-look processing and the tradeoff criteria between data compaction and image interpretability.

The technology support group also recommends a program be established to develop lightweight, space-deployable antennas to satisfy swath width and resolution requirements to meet the measurement objectives set forth by the discipline panels. If such an ongoing program in the communication area exists, a medium should be established to allow radar technology to interact with the program.

In reviewing the overall technological goals in using active microwave sensors in Earth resources applications, it is recommended that NASA establish a unified radar sensor development and applications program. A pertinent aspect of this program should be to provide ways and means for various investigations to have a common source of information. A central repository for reports would be highly desirable. A centrally located area where investigators could work individually or in a group on various pertinent problems would allow NASA to focus on key application areas and thereby provide long-term cost savings.

A concerted experimental program should be established with the data acquisition and analysis objectives focused on answering the important questions related to near-future missions. Sensor calibration and application studies on a local-area basis are prerequisites to establishing system requirements for orbital spacecraft missions. Such a program will require the use of one or two dedicated aircraft. At least one high-altitude aircraft is needed.

Data acquisition and instrument development activities should be emphasized in future NASA programs, whereas study tasks resulting in no data acquisition and/or no hardware development should be deemphasized. The study programs have reached a

state of maturity that must now be supported by system technology development.

PANEL SUMMARIES

Earth/Land Panel Summary

The Earth/land panel performed its tasks against the backdrop of the extensive ERTS applications studies, which have dominated the attention of the remote-sensing field for more than 2 yr. Consequently, the application areas addressed are familiar, and the value of acquiring remotely sensed data in support of these applications has been well established (app. 1B). The panel determined that active microwave sensors can significantly improve the acquisition of information needed to effectively exploit these application areas. The Earth/land panel report (ch. 2) is the most extensive document available on active microwave remote sensing of terrain features and will prove to be an invaluable reference for all future Earth observations programs.

Scope of study.—The Earth/land panel was composed of four subpanels, each of which considered a different class of discipline needs: mineral resources and geologic applications, water resources, vegetation and soils, and land use and urban environment.

The active microwave sensor applications identified by each subpanel are as follows:

1. Mineral resources and geologic applications:
   - *a.* Landform identification and terrain analysis
   - *b.* Mineral deposit location
   - *c.* Petroleum exploration
   - *d.* Ground water exploration
   - *e.* Crustal motion
   - *f.* Civil works
     - (1) Major construction site monitoring
     - (2) Construction material location
2. Water resources applications:
   - *a.* Lake ice monitoring
   - *b.* Flood forecasting and monitoring
   - *c.* Lake level determination and eutrophication
   - *d.* Coastal wetlands mapping
   - *e.* Water pollution monitoring
   - *f.* Frozen water hydrologic observations
     - (1) Snowfields
     - (2) Glaciers
     - (3) Permafrost
3. Agriculture, forestry, range, and soil applications
   - *a.* Crop identification
   - *b.* Crop cover and condition
   - *c.* Range inventory and biomass assessment
   - *d.* Soil types and properties mapping
   - *e.* Soil moisture determination
     - (1) Watershed management
     - (2) Crop yield prediction
4. Land use, urban, regulatory, and cartographic applications
   - *a.* Disaster monitoring
     - (1) Floodwater and coastal inundation
     - (2) Fire
     - (3) Wind damage
     - (4) Snowfall damage
     - (5) Earthquake damage
     - (6) Landslides
   - *b.* Land use monitoring
     - (1) Existing land use
     - (2) Transportation networks
     - (3) Location of engineering materials
   - *c.* Regulatory monitoring—oil spills
   - *d.* Cartography

Status.—Perhaps the most significant results of the AMW effort were, first, the recognition of the current lack of adequate experimental results to verify the feasibility of active microwave sensors for select applications and, second, the subsequent identification of immediate research needs. In many cases, there exist theoretical studies of basic electromagnetic interaction mechanisms that suggest the potential application, but many of these models are inadequately supported by experimental results.

In summarizing the status of active microwave sensor applications, the following applications were found to have proven feasibility:

1. Lake ice monitoring

2. Flood mapping
3. Oil-spill detection
4. Landform identification and terrain analysis
5. Grain crop identification
6. Broad-class land-use mapping

Those applications for which the basic phenomena of interest are believed to be measurable by active microwave sensing techniques are as follows:

1. Soil moisture determination
2. Soil-type mapping
3. Petroleum exploration
4. Rangeland inventories
5. Crop condition and biomass estimates
6. Mineral deposit mapping
7. Coastal wetlands mapping
8. Snowfield mapping

Each of these areas requires additional experimental investigation to confirm the feasibility of microwave remote-sensing methods. These areas represent the principal applications for which immediate research is needed. For example, petroleum exploration and mineral deposit mapping are two geological applications in which the unique capability of active microwave sensors to penetrate surface vegetation could be extremely valuable. Operation at 50-cm wavelengths is feasible from satellite altitudes, and aircraft systems operating at 100-cm wavelengths are practical. These long-wavelength signals penetrate most natural vegetation and should suit the geologist's needs. However, the experimental data to confirm this potential are inadequate.

Comparison with visible-region sensors.— Because the visible-region sensors have such a commanding lead over microwave sensors in documented applicability to Earth observations, the panel accepted the need to show the relative merits of microwave sensors in the applications areas addressed. The examples in table 1–I illustrate how such a comparison confirms the desirability of microwave systems in future Earth observations efforts.

Unique applications. — Imaging radar, among the fine-resolution sensors, is uniquely suited to monitoring soil moisture. As previously stated, this is partly because of its ability to penetrate the soil, whereas the color seen by visible-region sensors changes as soon as the very top millimeter becomes wetter or drier. Active microwave sensors can detect soil moisture because the dielectric properties of the soil are affected by the amount of moisture present due to the large differences between the permittivity of dry soil and that of water. Such measurements have numerous applications to flood forecasting, agricultural production estimates, and watershed management.

The moisture content of snow strongly influences the scattered microwave signal because the amount of compaction and the amount of liquid-free water in the snow have a major influence on its permittivity and therefore on the volume scatter from within the snow. Although this application has not yet been turned into a proven quantitative measure, the phenomenon has been observed qualitatively and can be fully justified on physical grounds.

Frozen ground can often be readily distinguished from unfrozen ground by active microwave sensors because of the change in dielectric properties as the moisture in the soil changes from liquid to solid form. This application has important consequences in forecasting flood runoff.

The strong microwave effects associated with edges in lake and river ice make the structure of the ice much more visible on radar images than on visible images; consequently, active microwave sensors have special application to monitoring ice structure in the Great Lakes and major rivers.

The ability to control the angle of incident radiation with active microwave sensors has led to unique applications in geology and geomorphology. When illumination and observation are at relatively shallow grazing angles, the shadowing that can be observed in areas of small relief permits discrimination of structural features much better than the comparable features that can be observed

TABLE 1–I.—*A Comparison of Active Microwave Sensors and Visible-Region Sensors*

Application	Unique capabilities of active microwave sensors	Unique capabilities of visible-region sensors	Capabilities shared by both sensors
Crop identification and assessment.	Plant moisture condition may be recordable. Soil moisture condition may be recordable. Temporal behavior can be recorded on timely basis.	Spectral reflectance data.	Plant structure. Canopy cover. Areal extent. Computer-compatible data.
Soil moisture determination.	Vegetation and surface can be penetrated. Moisture changes on diurnal cycle may be recordable. Temporal behavior can be recorded on timely basis.	No quantitative capability.	Vegetation response to soil moisture change. Computer-compatible data.
Soil type and property mapping.	Vegetation and surface can be penetrated. Dielectric characteristics may be recordable. Soil moisture retention characteristics may be recordable. Temporal behavior on indicator vegetation can be recorded on timely basis.	Soil color.	Vegetation identification for soil-type mapping. Computer-compatible data.
Range inventory and biomass assessment.	Plant moisture condition may be recordable. Soil moisture condition may be recordable. Temporal behavior can be recorded on timely basis.	Spectral reflectance data.	Plant structure. Canopy cover. Areal extent and distribution. Computer-compatible data.
Disaster monitoring.....	Floodwater boundaries in vegetated areas can be detected. Earthquake-caused surface structure changes can be enhanced. Storm and fire damage can be assessed through clouds and smoke, day or night. Disaster events can be recorded on timely basis.	High-resolution color information.	Two-dimensional broad-area images. Land-use patterns and cultural features. Computer-compatible data.
Mineral deposits location.	Vegetation can be penetrated. Location is dependent on surface texture. Illumination angle can be controlled for feature enhancement. Polarization-dependent	Surface material color (where exposed).	Two-dimensional broad-area data. Vegetation indicator. Computer-compatible data.

TABLE 1–I—*Continued*

Application	Unique capabilities of active microwave sensors	Unique capabilities of visible-region sensors	Capabilities shared by both sensors
Mineral deposits location —Con.	surface information can be provided. Maps in regions of extensive cloud cover can be provided.		
Lake ice monitoring.....	Sensor is sensitive to ice type/thickness. Ridges, open water, and shoreline under snow cover can be delineated. Temporal behavior can be recorded on timely basis through clouds.	None.	Two-dimensional broad-area images. Computer-compatible data.
Flood forecasting and monitoring.	State of soil (i.e., frozen) may be recordable. Floodwaters under vegetation may be recordable. Soil water retention characteristics may be recordable. Soil moisture may be recordable. Temporal behavior can be recorded on timely basis through clouds.	More sensitive to flood-induced vegetation stress.	Two-dimensional images. Areal extent of floods. Computer-compatible data.
Coastal wetlands mapping.	Soil moisture may be recordable. Plant moisture may be recordable. Vegetation can be penetrated. Polarization-dependent soil conditions can be recorded. Temporal behavior can be recorded on timely basis.	Spectral reflectance data.	Plant structure. Canopy cover. Areal extent. Computer-compatible data.
Frozen water hydrologic observations.	Soil below surface can be penetrated. Snow cover can be penetrated. Sensor is sensitive to snow moisture content. Sensor is sensitive to subsurface dielectric properties. Temporal behavior can be recorded on timely basis through clouds.	Albedo of snow cover recordable.	Image format data. Computer-compatible data.

with passive sensors at any wavelength. This effect has been widely used in the commercial application of radar imagery by mineral companies and the application by governmental agencies that map geological phenomena.

Ocean Panel Summary

Oceans have an effect on everyone in some manner, whether by the food they produce or their effect on the weather and climate. However, because of their vastness, conventional studies of oceans have been, and can only be, economically attempted on a local scale. Trying to instrument the oceans on a global basis would be prohibitive in cost. The advent of remote sensing from aircraft, and especially from satellites, permits complete synoptic, sequential coverage. Using such techniques, the cost per data point will be several orders of magnitude less than when using conventional techniques. Remote-sensing techniques provide the means of achieving an unparalleled increase in the knowledge and thus the use of all the oceans of the world.

Practical applications and considerable economic benefits may be derived from remote sensing of the oceans by active microwave systems. These applications include improved warning systems for protection of life and property, more accurate weather forecasting, better monitoring of environmental quality, more efficient management of marine resources, improved commercial fishing, greater safety of shipping and navigation, better information for ship and coastal structure design, and enhanced knowledge of deviations from the geoid.

The benefits will be many faceted; they fall, in general, into the eight categories mentioned. Safety of life and property in the coastal areas has heavily depended in the past (and will heavily depend in the future) on the behavior of the ocean waters nearby. Tides, storm surges, pileups, and currents all have a large impact. Because these phenomena are all detectable by using active microwave techniques, such systems can give the proper information for forecasts and warnings. Data on wave direction, wave spectra, and wave diffraction, in particular, are economically detectable only if such systems are used.

The benefits of better weather forecasting are closely related to the previously mentioned coastal phenomena. In addition, the anticipated international agreement on increasing the "economic coastal region" to 360 km will require monitoring an area approximately 20 times larger than has been historically required. Furthermore, with the increased number of people living in the coastal States (where approximately 80 percent of the U.S. population resides), the cultural stress placed on U.S. coastal waters is ever increasing.

Spaceborne active microwave systems with a 10- to 50-m spatial resolution and a swath width of approximately 200 km could, for instance, be immediately applied to monitoring the aerial extent of this economic coastal region for detection of oil spills, management of marine resources, enhancement of commercial fishing, observation of ship activities in support of international agreements, warning of storm surges, indication of shoaling, and monitoring of ice conditions on the Great Lakes, North Slope, and polar regions.

The importance of observing and subsequently forecasting the ocean environment is illustrated by three examples. First, the determination of the wave climate near shore areas will offer invaluable support to ongoing coastal activities—for example, ongoing construction and planning for future projects. Second, a better understanding of the influence of the heat exchange phenomena is essential to long-term weather modeling. Third, monitoring the open water areas in the northern regions is very important for the shipping industry. The oceans panel determined that airborne, and particularly spaceborne, active microwave systems are essential for synoptic remote sensing of both local and large-scale phenomena.

Local phenomena are those oceanic and coastal phenomena with dimensions up to

100 km. These phenomena include surface waves and wind, internal waves, land/sea interaction, and the properties of inland and estuarine waters. Man's activities at sea are very much influenced by gravity waves. These are, in general, classified as waves with lengths of 2 cm to 500 m and heights to 30 m; they change shorelines, damage structures and cargo, and slow the progress of ships. A better understanding of such waves, their structure, diffraction, energy-exchange mechanism, and prediction will benefit marine activities.

Wave forecasting, an important factor in coastal management, can greatly benefit by the measurement or determination of surface wind fields. For centuries, seafarers have known that ocean waves increase in size with increasing windspeed. To determine the proper relationship between wind and waves is important not only for the coastal areas but also for the open ocean. The degree of vessel rolling, and hence the potential for cargo damage, is a function of wave height, wave direction with respect to the heading of the ship, and wave period with respect to the speed of the ship.

Land/sea interactions are most pronounced on the continental shelf and in the vicinity of islands. It is estimated that approximately 90 percent of man's ocean activities are in water depths less than 30 m, in which wave-effect forecasting is important but, unfortunately, is in a rather embryonic stage because of problems connected with shoaling, refraction, bottom friction, and breaking. Studies of these phenomena are far more than academic, considering man's heavy activities in the continental shelf areas.

Large-scale phenomena include the topography of the ocean surface—a complicated compound of geoidal variations and quasi-static spatial variations caused by tidal and meterological forces. Geostrophic currents and the polar ice coverage are also large-scale phenomena. The physical surface of the oceans is ever changing and is influenced by tides, air pressure, winds, salinity, temperature, density or pressure gradients, and geologic changes associated with the melting of glaciers. The determination of the deviation of this surface from the geoid (5 to 20 cm) is of importance for the computation of large-scale geostrophic currents. Because these currents transport large amounts of heat energy on a global scale, their improved measurement is important for improved methodology for forecasting weather and climate. The same is true for monitoring oceanic tides for possible applications of tidal-power harnessing and for better estimation of the Earth tides—that is, ocean loading of coastal areas as it relates to Earth dynamics (earthquake studies). Storm surges and wind setups are further dynamic manifestations of the same effect; both contribute to the danger of flooding of low coastal areas.

Global wave statistics, another large-scale consideration, are needed to establish a reference condition for planning ship routes and for designing ships and offshore structures. The same is true for the polar ice regions. Knowledge of the heat exchanged between the atmosphere and open water areas in these regions is essential for long-range weather forecasting and ship routing.

The oceans panel conclusions are as follows:

1. Certain all-weather, synoptic, high-resolution observations can best be provided by spaceborne active microwave systems. These observations include wave height, wave spectra, wave diffraction, distribution of sea and lake ice and open water areas within them, subsurface structure of glacier ice, the ocean geoid, and the static and dynamic topography of sea surfaces.

2. To date, the only Earth-oriented spaceborne active microwave systems in orbit were on Skylab. The information obtained from the S193 altimeter experiment has considerably exceeded all expectations and has provided unique oceanographic data. Surface variations with an accuracy of 1 to 2 m on a local scale and 5 to 20 m on a global scale have been detected. Preliminary indications from the S193 radiometer/scatter-

ometer (RADSCAT) system suggest that windspeeds as high as 20 m/sec are measurable from spacecraft.

3. Because many important ocean events are time dependent and short lived, it has been difficult to acquire the proper data because of the lack of dedicated oceanic research aircraft. The problem is further compounded by the lack of integrated planning and timely assignments of aircraft to ongoing in situ observations.

4. Quantitative relationships between radar signatures and oceanographic geophysical parameters have not been firmly established in many cases, primarily because of insufficient observations.

5. Development programs for active microwave sensors for ocean observation appear to be dispersed and have only limited coordination.

Atmosphere Panel Summary

The atmosphere panel considered the possible applications of active microwave systems in terms of more than three decades of operating experience with ground-based weather radar systems and in terms of a well-established meteorological satellite program extending back more than 14 yr, during which more than 30 experimental and operational satellites have been launched into both near-Earth and geostationary orbits. The satellites have carried a large variety of instruments that passively sensed radiation in the ultraviolet, visible, infrared, and microwave regions of the spectrum. An iterative exchange between discipline scientists and radar technologists led to the development of a list of applications using the following criteria:

1. The application must be of value to the discipline and in support of one or more of the following six NASA meteorology program objectives.

a. Operational support: Support the development of the operational meteorological satellite system.

b. Weather prediction: Develop space technology for determining the vertical structure of the atmosphere globally, which, when supplemented by simulation techniques, models, and conventional observations, will provide required data with emphasis on large-scale long-term weather forecasts.

c. Atmospheric pollution: Develop a space-sensing capability to identify and quantitatively monitor the distribution of natural and manmade pollution in the lower and upper atmosphere on global and regional scales.

d. Climate and weather modification: Apply space-acquired data from remote sensors, data collection systems, and/or in-flight experiments requiring unique orbital conditions (such as a gravity-free environment) to the development of models and the establishment of mechanisms for the rational examination of deliberate and inadvertent means for modifying weather and climate.

e. Weather danger and disaster warning: Develop and establish a system for continuous observation of atmospheric features to permit early identification and quantitative measurement of atmospheric conditions conducive to the formation of severe atmospheric phenomena (e.g., thunderstorms, tornadoes, hurricanes, etc.) to serve as a basis for timely warning to the public.

f. Processes and interactions: Investigate fundamental atmospheric processes and interactions on various temporal and spatial scales within the atmosphere, in response to solar inputs, and at the air/surface interface through the observation of the structure, composition, and energetics of the atmosphere for the purpose of effectively applying space capabilities in pursuance of the previously mentioned objectives.

2. The application must be reasonably achievable by active microwave means or by a combined active/passive system.

3. The application must be unique to active microwave systems or must be accomplished more effectively by active microwave techniques than by other means (e.g., passive radiometry in the visible, infrared, or microwave region).

The resulting applications are as follows:

1. Mapping maximum echo heights in rain clouds to provide an indication of storm intensity and rainfall production.

2. Measuring the height of the 273-K level in rain clouds as input to numerical weather prediction models and for assessing the intensity of tropical storms.

3. Mapping rain intensities over the globe as an input for future numerical models for long-range forecasting.

4. Quantitatively measuring liquid water content, drop-size spectra, and rainfall rates on a global scale: Condensed water is a critical component in the heat and water budgets of dynamic processes in the atmosphere; it is also important in short-range forecasting of local weather and in flood prediction.

5. Mapping horizontal motion within cloud systems: The measurement of horizontal winds is useful in weather forecasting. At present, radiosonde wind measurements are made manually and are essentially point measurements. A satellite Doppler radar wind measurement would map wind motion in a continuous manner throughout the storm. Wind field convergence properties of large systems may also be obtained efficiently.

6. Measuring surface pressure globally along the subsatellite track: These measurements would provide a major breakthrough for meteorological surface analysis and weather forecasting. If successful, such measurements would obviate the need for the myriad surface pressure measurements made daily over the globe. Even more importantly, these measurements would increase the accuracy of forecasts by extending the ground-based observations to oceans and other inadequately covered regions. A primary use would be to serve as a reference level for the temperature profiles now obtained routinely from atmospheric sounders on operational satellites, thus markedly increasing the accuracy of the profiles for updating forecast models.

7. Measuring surface winds over the oceans: These measurements would provide a new set of initial-state parameters for improving synoptic-scale weather forecasting; they would provide valuable information for weather danger warnings—for example, hurricane winds and storm surges. These measurements would assist in improving the understanding of the tropical atmosphere.

8. Mapping polar sea ice cover to measure the atmospheric heat balance in polar regions: This mapping would serve also as an input to numerical models of the general circulation for weather prediction purposes.

9. Applying bistatic measurements to communications needs such as attenuation and fading statistics for radio links: If coupled with depolarization measurements, bistatic measurements can provide information on raindrop and ice crystal sizes, shapes, and number density. Forward scatter geometries are also especially suited for detection of clear air turbulence. Because data from geostationary communications satellites contain meteorological information (generally considered to be "noise" in the communications system) and are available at little or no cost to the meteorologist, they should be used for atmospheric research.

10. Continuously monitoring maximum echo heights of storms from a geostationary satellite: If this monitoring could be done, it would be of extreme importance for monitoring the development and motion of severe storms and would lead to improved short-term forecasts and improved disaster warnings.

These 10 applications together with the 8 types of active microwave systems required to obtain the necessary measurements are summarized in table 1–II. A preliminary compilation of systems design criteria is shown in table 1–III.

Technology Support Group Summary

Many of the scientific objectives of the discipline panels, when translated into sensor requirements, indicate the need for imaging radar systems. Furthermore, the imaging radar performance specifications that can be inferred from the various application re-

TABLE 1–II.—*Application Requirements and Corresponding Active Microwave Systems*

Application requirements	Applicable active microwave systems [a]
Global coverage from low-altitude satellites	
1. Map maximum echo heights in rain clouds.	A. Downward-looking scanning pulse radar (design study).
2. Map height of melting layer in rain clouds.	A. Downward-looking scanning pulse radar (design study).
3. Map precipitation intensity.	A. Downward-looking scanning pulse radar (design study).
4. Map liquid water content and drop-size spectra (plus all above).	B. Multiwavelength radar (design study).
5. Map horizontal motion within cloud systems (e.g., tropical storms).	C. Doppler radar (feasibility study).
6. Determine surface pressure.	D. Active microwave transmissivity measurement in 5-mm oxygen (O_2) band (feasibility study).
7. Map surface winds over ocean areas.	E. Radiometer/scatterometer (RADSCAT) (ocean panel).
8. Map polar sea ice cover.	F. Synthetic aperture radar (SAR) (ocean panel).
Regional coverage at high temporal resolution from geostationary satellites	
9. Investigate fundamental atmospheric parameters (e.g., absorption, scattering, polarization, turbulence, etc.).	G. Data from existing and planned communications satellite systems (e.g., Applications Technology Satellite 6 (ATS–6)).
10. Continuously monitor maximum echo heights (development and intensity) of storms.	H. Short-wavelength radar with large antenna (feasibility study).

[a] Letters reference these systems to those in table 1–III.

quirements can, for the most part, be met by the current radar technology. Certain areas, such as data-handling capacity and deployment of large antennas in space, require further development to establish the technology to meet necessary performance requirements. Such development will likely be accomplished within 5 yr.

A significant portion of the sensor requirements necessary to meet the Earth/land and the oceans panels objectives could be satisfied by a single spaceborne imaging radar system. The multifrequency (Ka-, X-, and L-bands), multipolarization imaging radar configuration being considered for Space Shuttle flights should satisfy a high percentage of the user needs outlined by these panels. The nature of radar systems dictates that initial mission efforts include engineering and calibration objectives. Unlike the performance of some sensors (e.g., cameras), which can be measured either on the ground or in aircraft, the performance of active microwave sensors can be accurately assessed only under actual in-flight conditions. The first real test of the system comes when the radar is in orbit.

The need for other types of active microwave systems (i.e., scatterometers, altimeters, and sounders) is limited to a few special applications. Scatterometers are useful primarily in measuring surface windspeed over the ocean, and altimeters are required for measuring the shape of the geoid.

Advancement in radar technology is hampered in many areas by a lack of knowledge of the interaction of surface properties and the echo characteristics. Oceanographic and some agricultural application studies are maturing, but the success of these programs depends on an adequate data base. Additional

TABLE 1–III.—*Systems Design Criteria*

Applicable systems	Coverage	Circular orbit		Number of spectral bands	Wavelength cm	Frequency, GHz	Polarization	IFOV,* deg	Type of scan	Scan angle from nadir, deg	Swath width, km	Average power, W	Diameter of antenna, m	Vertical resolution, km	Frequency of coverage, hr
		Height, km	Inclination, deg												
A. Pulse radar	Global	~400	Not critical	1	0.8 or longer	Up to 37	No	0.3 beam	Transverse	±45	750	10	2.6 or more	1 to 2	12
B. Multiwavelength radar	Global	~400	Not critical	2, 3, or 4	0.5, 1, 3, or 10	3, 10, 30, or 60	Circular (both components	0.3 beam	Transverse	±45	750	—	2.6 or more	1 to 2	12
C. Doppler radar	Global	500	58 or Sun-synchronous	1	5 to 6	6 to 5	No	0.3 multi-beam	Conical (360°)	60	2200	100 (per beam)	11	3 (3 to 5 layers)	12 12
D. Active microwave transmissivity instrument for surface pressure	Global	Not critical	Not critical	4	~.6	~50	No	10 to 20	Nadir-looking	NA[b]	NA	10	0.3	NA	12
E. RADSCAT	Global	800	108	1	2.2	13.9	No	25 to 50	Transverse	45	2 swaths×500=1000	50	0.4	NA	12
F. SAR	Selected polar regions	800	85 to 95	1	3.0	10	No	3 to 30	NA	NA	100	200	8 by 5	NA	12
G. Communications satellite for meteorological use	Earth disk	36 000 (geostationary)	0	1 or 2	≤3	≤10	Orthogonal, linear, or circular	[c]	[c]	[c]	NA	2	≤10	NA	Continuous
H. Short-wavelength radar for geostationary satellites	Earth disk	*36 000* (geostationary)	*0*	1	≤.3	≥94	—	*15*	Transverse	±*10* (Earth disk)	*Earth disk* (to great circle angle ~50°)	*100 to 200*	≥*10*	*NA*	*0.25*

* Instantaneous field of view.
[b] Not applicable.
[c] Depends on number and location of ground stations.

research results in this critical area would help to determine the need for advanced technology and to define the performance requirements for future active microwave systems.

General status of sensor technology.—The technology for transmitting and receiving microwave energy in a manner that provides high-resolution range and azimuth spatial information is well developed. The power and weight demands of such systems no longer prohibit their use on spacecraft. For example, an L-band synthetic aperture imaging radar (providing a 100-km swath of approximately 30-m spatial resolution imagery from a 186-km altitude) requires less than 350 W of average power and would weigh less than 159 kg. Such a system would require an 8-m-long antenna.

Few active microwave systems and no imaging radar systems have been operated on spacecraft; therefore, there exists very limited experience in spacecraft antenna design. This problem is significant because the large engineering development cost for these antennas must be borne by the first few such systems used. In addition, the necessary design criteria are yet to be established. For rigid antenna structures, such as the antenna being considered for a Space Shuttle imaging radar, the aircraft antenna technology should be adequate to support the development. However, for the larger structures necessary for wide-swath-width imaging or narrow-beamwidth operation, considerably more development will be required.

The problem of handling the volume of data acquired by active microwave sensors is no more or no less severe than with any remote-sensor system. The required processing equipment to handle radar image data having a scale and resolution comparable to those of ERTS is approximately the same as that now used on ERTS–1. However, as with visible-region sensor data, the data-handling problem is a major obstacle to satellite remote sensing with fine-resolution active microwave sensors. Improved digital data-handling techniques are needed in the near future if the full potential of orbiting sensor systems is to be realized.

Projection of present technology.—The present trend in solid-state electronics indicates that future active microwave systems will continue to decrease in power, size, and weight requirements. Antenna design is also improving, but at a less dynamic rate. The most promising area of rapid technological development, relative to active microwave remote sensing, is in the field of data-handling techniques and hardware. The continual advancement in the state of the art of digital data handling and storage should soon remove the most serious obstacle to effective satellite remote sensing with high-resolution synoptic sensors.

It is expected that, within 10 yr, a multispectral imaging microwave system will be competitive in power, size, weight, and cost to the present ERTS multispectral scanner (MSS) system. Furthermore, it is expected that the data-handling capabilities will have an improved 10- to 30-m spatial resolution, without overloading the data-handling system.

CONCLUSIONS

This report provides an overview of the utility, feasibility, and advantages of active microwave sensors for a broad range of applications. In many instances, the material provides an in-depth examination of the applicability and/or the technology of microwave remote sensing, and considerable documentation is presented in support of these techniques.

Active microwave sensors can contribute significantly to Earth observations because of their capability to perform one or more of the following functions:

1. As unique sensors providing information on the phenomena under study that is unobtainable by any known practical means.
2. As complementary sensors providing an extension of the spectral description of the phenomena under study.
3. As supplementary sensors providing an

extension of the observation coverage of the phenomena under study.

The unique capability of microwave sensors to provide data night or day during nearly all weather conditions is only significant if the data have a quality and information content level adequate to supply the needs of the application. An assessment of the relative strengths and weaknesses of active microwave sensor data indicates that satisfactory data are obtainable for several significant applications.

Briefly summarized, the strengths and weaknesses of active microwave sensors are as follows:

1. Strengths:
   - *a.* Records otherwise unobservable phenomena
     - (1) Penetrates vegetation and near-surface material
     - (2) Dependent on surface composition and roughness
     - (3) Sensitive to vegetation, soil, and snow moisture
     - (4) Has controlled viewing angle for feature enhancement
     - (5) Provides broad spectral range information
   - *b.* Has coincident capability with visible sensors for many applications
     - (1) Provides two-dimensional image data
     - (2) Has broad areal coverage with moderate-to-high spatial resolution
     - (3) Records land-use patterns and changes
     - (4) Has computer-compatible information
     - (5) Sensitive to vegetation type and condition
   - *c.* Provides day/night, near-all-weather operation
2. Weaknesses:
   - *a.* Cannot record color-dependent phenomena
   - *b.* Data not spatially coincident with other sensors
   - *c.* Geostationary imaging operation not practical

The complementary and supplementary capabilities of active microwave sensors are significant, and it is probably in these capacities that active microwave systems will be introduced into satellite remote-sensing programs. However, a major effort of the active microwave working group was devoted to identifying the unique capabilities of active microwave sensors to establish clearly the advantages offered by these sensing techniques. The following list delineates the applications, by discipline area, for which active microwave sensors provide the most practical, the most advantageous, or the exclusive means of obtaining the needed information.

1. Earth/land:
   - *a.* Determine soil moisture for crop yield prediction
   - *b.* Map snowfields and glaciers
   - *c.* Monitor lake ice
   - *d.* Assess disasters for assistance and recovery
   - *e.* Perform landform identification and terrain analysis
   - *f.* Perform flood forecasting and watershed management
2. Oceans:
   - *a.* Determine sea state and surface winds
   - *b.* Map sea ice and iceberg locations
   - *c.* Monitor coastal processes
   - *d.* Monitor wave buildup in storm areas
   - *e.* Measure undulations of the geoid
3. Atmosphere:
   - *a.* Map freeze level height in rain clouds
   - *b.* Map rain intensity
   - *c.* Measure liquid water content
   - *d.* Map horizontal motion within cloud systems
   - *e.* Measure surface winds over the oceans
   - *f.* Map polar sea ice cover
   - *g.* Monitor maximum echo heights of storms

Each panel assessed the potential of active microwave systems from the distinctive perspectives associated with the disciplines involved. The applications identified and the techniques selected to address these applications evolved from the individual backgrounds of the Earth scientists, oceanographers, and meteorologists who guided the development of the material presented in this report. The common viewpoint shared by each panel was the awareness that active microwave sensors have unique capabilities that are not being adequately used.

The principal conclusions of the report are as follows:

1. Studies of microwave energy interaction with Earth surfaces, oceans, and the atmosphere (many supported by experimental evidence) clearly indicate the potential of active microwave sensors for numerous applications in these areas; these are applications for which the needed information can be obtained by no other more practical means than by active microwave sensors.

2. Active microwave sensors have unique capabilities for acquisition of descriptive data on many physical phenomena that may be otherwise obscured because of lighting or cloud conditions or that are unobservable by any other sensing method. These data are comparable in information content to visible-region sensor data.

3. Many applications for which the unique, supplementary, or complementary capabilities of active microwave sensors are invaluable have been identified in this report. Many of these applications can be addressed immediately by using available technology and analysis capabilities. For other applications, the research needed to establish firmly the operational feasibility of these sensors is indicated; many of the needed research results are close at hand. The difficulty in acquiring the necessary information is caused partly by the lack of ground-based and aircraft microwave sensors available to support experimental research. These systems and the funds to analyze the resultant data must be made available if the potential of microwave remote sensing is to be realized.

4. The active microwave sensor technology now available is completely adequate to support a majority of the applications identified in this report. The rapid development of solid-state electronics is continuing to enhance the hardware capabilities for sensor systems and data processing. The power, weight, and size parameters, long thought to be deterrents to spaceborne microwave systems, are compatible with modern spacecraft specifications. However, the current lack of experience with actual satellite imaging radar configurations, particularly the antenna assemblies, can only be overcome by conducting orbital tests on such systems. These tests are a necessary first step in the development of future satellite microwave remote-sensing systems for operational Earth observations.

5. The concentration of attention and resources on the ERTS and Skylab Programs, especially with regard to aircraft facilities and research funds, has had the effect of slowing the development of microwave remote sensing after 1970. As a result, an adequate base of information to firmly establish the feasibility of these techniques does not exist for many of the most important applications.

6. The coordinated multidisciplinary "team" concept, which stimulated remote-sensing activities during the 1960's and provided guidance for the rapid development of the field, should be reestablished to encourage the orderly introduction of microwave sensors in future Earth observations missions.

APPENDIX 1A

ORGANIZATION AND ADDRESSES OF THE AMW GROUP

The AMW group consisted of a steering committee, an Earth/land panel, an atmosphere panel, an oceans panel, and a technology support group.

STEERING COMMITTEE

William R. Bandeen, Atmosphere Panel Chairman
Code 910
NASA Goddard Space Flight Center
Greenbelt, Md. 20771

Walter E. Brown, Jr., Technology Support Group Chairman
Building 183, Room 701
NASA Jet Propulsion Laboratory
4800 Oak Grove Drive
Pasadena, Calif. 91103

W. Linwood Jones, Code MS 490
NASA Langley Research Center
Hampton, Va. 23665

Jules Lehmann, Code ERF
NASA Headquarters
Washington, D.C. 20546

Richard E. Matthews, Code HC
NASA Lyndon B. Johnson Space Center
Houston, Tex. 77058

Richard A. Moke, Steering Committee Chairman
Code HC
NASA Lyndon B. Johnson Space Center
Houston, Tex. 77058

Martin W. Molloy, Earth/Land Panel Cochairman
Code ERR
NASA Headquarters
Washington, D.C. 20546

William Nordberg, Code 650
NASA Goddard Space Flight Center
Building 21, Room 215
Greenbelt, Md. 20771

Andrew E. Potter, Code TF3
Chief of Applied Physics Branch
Office of Earth Resources
NASA Lyndon B. Johnson Space Center
Houston, Tex. 77058

J. W. Rouse, Jr., Earth/Land Panel Cochairman
Remote Sensing Center
Texas A&M University
College Station, Tex. 77843

Joe Siry, Code ES
NASA Headquarters
Washington, D.C. 20546

F. O. Vonbun, Oceans Panel Chairman
Code 900
NASA Goddard Space Flight Center
Greenbelt, Md. 20771

EARTH/LAND PANEL

Steven A. Arcone
U.S. Army Cold Regions Research and Engineering Laboratory
Hanover, N.H. 03755

Bruce J. Blanchard
U.S. Department of Agriculture
Box 400
Chickasha, Okla. 73018

M. Leonard Bryan
Environmental Research Institute of Michigan
P.O. Box 618
Ann Arbor, Mich. 48107

A. W. England
U.S. Geological Survey
Federal Center
Building 25
Denver, Colo. 80225

John E. Heighway, Code 301
NASA Lewis Research Center
Cleveland, Ohio 44135

Pieter Hoekstra
U.S. Army Cold Regions Research and Engineering Laboratory
Hanover, N.H. 03755

Richard A. Hoppin
Department of Geology
University of Iowa
Iowa City, Iowa 52242

Edward T. Kanemasu
Evapotranspiration Laboratory
Kansas State University
Manhattan, Kans. 66406

Leons Kovisars
Exploration Research Division
Research and Development Department
Continental Oil Co.
Ponca City, Okla. 74601

Anthony J. Lewis
Department of Geography and Anthropology
Louisiana State University
Baton Rouge, La. 70808

A. O. Lind
Department of Geography
University of Vermont
Burlington, Vt. 05401

A. A. Loomis
Jet Propulsion Laboratory
4800 Oak Grove Drive
Pasadena, Calif. 91103

Jerry R. Lundien
U.S. Army Corps of Engineers
Waterways Experiment Station
P.O. Box 631
Vicksburg, Miss. 39180

Harold C. MacDonald
Geology Department
University of Arkansas
Fayetteville, Ark. 72701

Roger M. McCoy
Department of Geography
University of Utah
Salt Lake City, Utah 84112

Paul M. Merifield
Department of Geology
University of California
Los Angeles, Calif. 90024

R. K. Moore
Remote Sensing Laboratory
Nichols Space Technology Building
2291 Irving Hill Drive, Campus West
University of Kansas
Lawrence, Kans. 66045

Stanley A. Morain
Remote Sensing Laboratory
Nichols Space Technology Building
2291 Irving Hill Drive, Campus West
University of Kansas
Lawrence, Kans. 66045

J. Plevin
European Space Research Organization
Space Applications Division
114 Avenue Charles de Gaulle
92200 Neuilly-sur-Seine
France

Gerald G. Schaber
U.S. Geological Survey
601 East Cedar Avenue
Flagstaff, Ariz. 86001

David S. Simonett
Earth Satellite Corporation
1747 Pennsylvania Avenue NW.
Washington, D.C. 20006

James V. Taranik
Chief of Remote Sensing
Iowa Geological Survey
16 West Jefferson Street
Iowa City, Iowa 52240

Thomas W. Thompson, Code 183–701
Space Sciences Division
NASA Jet Propulsion Laboratory
4800 Oak Grove Drive
Pasadena, Calif. 91103

Gene A. Thorley
Department of the Interior
Earth Resources Orbiting Satellite Data Center
Sioux Falls, S. Dak. 57701

Stanley H. Ward
Department of Geology and Geophysics
University of Utah
Salt Lake City, Utah 84112

G. L. Wilfert
Battelle Observatory
Battelle Northwest Laboratories
Richland, Wash. 99352

ATMOSPHERE PANEL

David Atlas
Director, National Hail Research Experiment
National Center for Atmospheric Research
P.O. Box 3000
Boulder, Colo. 80303

Lt. Col. Gordon A. Beals
HQ AWS/DNT
Scott Air Force Base, Ill. 62225

Charles W. Bostian
Electrical Engineering Department
Virginia Polytechnic Institute and State University
Blacksburg, Va. 24061

Thomas A. Croft
Center for Radar Astronomy
Stanford University
Stanford, Calif. 94305

Richard J. Doviak
National Severe Storms Laboratory
National Oceanic and Atmospheric Administration
1313 Halley Circle
Norman, Okla. 73069

Isadore Katz
Applied Physics Laboratory
Johns Hopkins University
8612 Georgia Avenue
Silver Spring, Md. 20910

Roger M. Lhermitte
Division of Atmospheric Science
School of Marine and Atmospheric Science
University of Miami
Miami, Fla. 33100

Hans J. Liebe
U.S. Department of Commerce
Office of Telecommunications
Institute for Telecommunication Sciences
Boulder, Colo. 80302

Gordon E. Peckham
Physics Department
Heriot-Watt University
Edinburgh, Scotland
United Kingdom

Allan C. Schell
Research Electronic Scientist
Air Force Cambridge Research Laboratories/LZ
L. G. Hanscom Field
Bedford, Mass. 01730

Paul L. Smith, Jr.
Institute of Atmospheric Sciences
South Dakota School of Mines and Technology
Rapid City, S. Dak. 57701

Robert A. Stokes
Battelle Observatory
Battelle Northwest Laboratories
Richland, Wash. 99352

Richard R. Weiss
Department of Atmospheric Sciences
Cloud Physics Group
University of Washington
Seattle, Wash. 98195

Raymond Wexler, Code 910
NASA Goddard Space Flight Center
Greenbelt, Md. 20771

Carl A. Wiley
Rockwell International
P.O. Box 4182
Anaheim, Calif. 92803

OCEANS PANEL

John R. Apel
Ocean Remote Sensing Laboratory
Atlantic Oceanographic and Meteorological Laboratories
National Oceanic and Atmospheric Administration
15 Rickenbacker Causeway
Miami, Fla. 33149

Donald E. Barrick
Wave Propagation Laboratory
National Oceanic and Atmospheric Administration
Environmental Research Laboratories
Boulder, Colo. 80302

William J. Campbell
U.S. Geological Survey
113 Thompson Hall
University of Puget Sound
Tacoma, Wash. 98416

David E. Cartwright
Institution of Oceanographic Sciences
Bidston Observatory
Birkenhead, Cheshire L43 7RA
United Kingdom

Thomas W. Godbey
General Electric Company MD 323
French Road
Utica, N.Y. 13503

Kumar Krishen
Lockheed Electronics Co., CO9
16811 El Camino Real
Houston, Tex. 77058

Lee S. Miller
Applied Science Associates, Inc.
P.O. Box 949
Apex, N.C. 27502

Jean-Marie Monget
Centre d'Informatique Géologique
École des Mines
25 Rue St. Honoré
77 Fontainebleau
France

Lionel Moskowitz, Code 5328
Naval Research Laboratory
Washington, D.C. 20375

Willard J. Pierson
University Institute of Oceanography
The City College of City University of New York
c/o Bronx Community College
181st Street and University Avenue
Bronx, N.Y. 10453

Claes G. H. Rooth
School of Marine and Atmospheric Sciences
University of Miami
10 Rickenbacker Causeway
Miami, Fla. 33147

Omar H. Shemdin
Coastal and Oceanographic Engineering Laboratory
Weil Hall 336
University of Florida
Gainesville, Fla. 32601

John W. Sherman III
National Oceanic and Atmospheric Administration
National Environmental Satellite Service
Spacecraft Oceanography Group
Suite 405
3737 Branch Avenue
Hillcrest Heights, Md. 22031

F. Y. Sorrell
North Carolina State University
P.O. Box 5130
Raleigh, N.C. 27607

Robert H. Stewart
Scripps Institution of Oceanography
P.O. Box 1529
La Jolla, Calif. 92037

C. T. Swift, Code MS 1490
NASA Langley Research Center
Hampton, Va. 23665

E. J. Walsh, Code E106
NASA Wallops Flight Center
Wallops Island, Va. 23337

Ben Yaplee, Code 7110
Naval Research Laboratory
Washington, D.C. 20375

TECHNOLOGY SUPPORT GROUP

Louis H. Bauer
Goodyear Aerospace Corp.
Arizona Division
Litchfield Park, Ariz. 85340

Chi-Hau Chen
Department of Electrical Engineering
Southeastern Massachusetts University
North Dartmouth, Mass. 02747

D. E. N. Davies
Professor of Electrical Engineering
University College
London WC1E 7JE, England
United Kingdom

Richard G. Fenner, Code ED63
NASA Lyndon B. Johnson Space Center
Houston, Tex. 77058

H. L. Groginsky
Raytheon Corp.
Wayland, Mass. 01777

Preben E. Gudmandsen
348, Technical University of Denmark
Laboratory of Electromagnetic Theory
DK–2800 Lyngby
Denmark

Donald Howell
Motorola Government Electronics Division
8201 East McDowell Street
Scottsdale, Ariz. 85252

Rolando, Jordan, Code 183–701
NASA Jet Propulsion Laboratory
4800 Oak Grove Drive
Pasadena, Calif. 91103

Richard W. Larson
Environmental Research Institute of Michigan
P.O. Box 618
Ann Arbor, Mich. 48107

Leonard J. Porcello
Environmental Research Institute of Michigan
P.O. Box 618
Ann Arbor, Mich. 48107

M. I. Skolnick
Naval Research Laboratory
Washington, D.C. 20375

F. C. Williams
Hughes Aircraft
Aerospace Group
Radar Avionics Organization
Culver City, Calif. 90230

APPENDIX 1B

EARTH RESOURCES SURVEY PROGRAM USING ACTIVE MICROWAVE SENSING: RECOMMENDATIONS FOR THE FUTURE

This appendix outlines the following areas of the Earth resources program:

1. The general accomplishments of the Earth resources survey program and future mission plans.
2. The importance of active microwave sensing, especially in terms of unique features and operational potential; the state of the art, including European activity; and the need for research and development, stressing the need to conduct measurements aimed at increased understanding of interactions between microwave energy and natural/man-made materials.
3. The potential applications and benefits of active microwave sensing, both near term (within 5 yr) and longer term (within 10 yr).
4. The outline of a program plan, identifying operational goals, experimental program, and overall schedule.

REVIEW OF EARTH OBSERVATION PROGRAM

Applications Research

The NASA Applications Aircraft Research Program has led to the emergence of remote sensing as an important scientific discipline and tool for many uses. The ERTS and Skylab Earth resources experiment package (EREP) sensors evolved from this program, and commercial radar mapping services began partly because of the interest created by results of the program.

This program was started in 1964 by the Manned Space Science Division. The original program was conceived as an adjunct to the development of sensors for mapping the lunar surface from orbit. The sensors were to be developed for use during the Apollo Program and tested in Earth orbit by observing designated terrain features alongside those features being observed as lunar analog test sites.

Initially, the program developed around a series of "instrumentation teams," each of which combined individuals and agencies having instrument expertise with those having expertise in uses of the data and in automatic data processing and analysis. This effort appears to have been the first major attempt in the United States to bring together groups of civilian users and instrumentation specialists. The major teams were as follows: photography, chaired by John Cronin of the Air Force Cambridge Research Laboratories; infrared, chaired by R. J. P. Lyon of Stanford University; radar, chaired by R. K. Moore of the University of Kansas; and passive microwave, chaired by Frank Barath of the Jet Propulsion Laboratory (JPL). Aircraft support was provided by the cooperation of military agencies and by the NASA Lyndon B. Johnson Space Center (JSC).

Radar was included among the sensors considered for the lunar landing program because of the potential for obtaining information about subsurface features due to the postulated low absorption of microwave energy by the lunar-surface materials; this assumption was later verified by the lunar sounder experiment conducted during the Apollo 17 mission. The Earth-oriented users in the early stages were especially interested in active microwave sensors and the ability of radio waves to penetrate farther than waves in the visible and infrared regions, regardless of whether this penetration was through clouds, vegetation, or upper soil layers. Many scientists recognized that timely remote-sensing measurements would be required for many applications and that most of the Earth is covered by clouds often enough so that only microwave sensors could provide the information at the time it was needed. Other scientists were interested in information about surfaces covered by vegetation that might be penetrated by microwave sensors but not by the shorter wavelength sensors. Still other scientists hoped to obtain geological information by penetrating the topsoil to reveal underlying structure. The ability of active microwave sensors to detect phenomena in which shape and context were the prime discriminants was recognized, but little knowledge was available to indicate whether these sensors could also provide unique information about materials that had to be distinguished by tone or spectral/polarization signatures. A major contribution of this program has been the demonstration that many of these desirable features could be identified from radar image tone and texture; therefore, the advantages of cloud and vegetation penetration were realized in practice. Other unique applications of active microwave data for distinguishing geologic structure and so forth have been discovered serendipitously. However, some of the hopes for deep soil penetration have been impossible to fulfill.

Activities of the Radar Team

The radar team was formed in May 1964 and was active for approximately 2 yr. The University of Kansas undertook leadership of the team, which included members from many institutions (notably, the U.S. Geological Survey (USGS), the Naval Oceanographic Office, the University of Michigan, the University of California, and several Department of Defense (DOD) agencies).

The first extensive radar flight program under these auspices was conducted during the period 1965 to 1966 with the Westinghouse APQ–97 real aperture multipolarization radar under contract to NASA. More than 500 000 km^2 were imaged in different parts of the United States. Application of these images was made to numerous research efforts, which included geology, natural vegetation, agriculture, land use, hydrology, and coastal studies. Data from these flights are still being studied, and important results are still forthcoming. The use of these data by many groups led to the decision to use the APQ–97 radar to provide the first commercial imaging radar service in 1969. This service and subsequent commercial imaging radar services by Aero Services/Goodyear and by Grumman/Motorola have provided millions of square kilometers of worldwide images for both governments and private mineral firms.

Initially, efforts were made to obtain various military radar systems for NASA aircraft. Finally, in 1967 an experimental unfocused synthetic aperture system, the Philco-Ford DPD–2, was acquired and placed in operation on the NP–3A. This system was flown over numerous sites in the United States and also provided images through cooperative ventures with Mexico and Brazil. Although the Brazilian images were not of especially high quality, they demonstrated the potential to the extent that Brazilians, introduced to remote sensing by the NASA program, arranged for commercial imaging of the entire Amazon Basin. This offshoot of the NASA Applications Aircraft Re-

search Program is the largest single active microwave remote-sensing effort to date.

The University of Michigan Willow Run Laboratory (now the Environmental Research Institute of Michigan (ERIM)) high-resolution, X-band, synthetic aperture radar system developed for DOD was flown for the Earth Resources Aircraft Program (ERAP), and useful information was obtained for agriculture and geology. The system was modified to add an L-band capability under this program, and the two-frequency system has been especially valuable in demonstrating potential for multispectral radar. This system has also been used in studies of ice in the Great Lakes. A real aperture X-band radar was also flown for this purpose under NASA Lewis Research Center support during the 1973–74 ice season. Excellent practical results were obtained relative to extension of the ice navigation season.

Near the beginning of the program, the Naval Research Laboratory (NRL) four-frequency radar was used for scatterometry; however, it soon became apparent that this system could be modified to produce synthetic aperture images. The images from this system were the first to clearly demonstrate uses of multispectral radar.

Another two-frequency radar, developed at JPL, was an outgrowth of systems developed at L-band frequency for Venus studies and at lower frequencies for lunar sounding. This system, which has been used especially for oceanographic and geologic imaging, has the unique characteristic of providing altimetry directly on the image.

The radar scatterometers flown during this program have been instrumental in the development of oceanic wind measurement techniques tested on Skylab and planned for SEASAT. The 13.3-GHz NASA scatterometer was used in six flights over the North Atlantic at yearly intervals to test the wind measurement capability. The results obtained in these flights have been verified by the Skylab S193 microwave device.

The emphasis of ERAP necessarily shifted from the active microwave sensors as preparations for ERTS became more important. One of the earlier major programs that took much aircraft time was the corn blight watch in 1971 and 1972. With the Skylab launch, these facilities were even more in demand for spacecraft underflights, and ERAP provided a very large quantity of useful collateral data to many ERTS and EREP investigators. However, during this period, the ERIM two-frequency side-looking airborne radar (SLAR) was improved. An X-band frequency was added to the JPL SLAR, and the advanced application flight experiments (AAFE) RADSCAT was constructed. Much research in the microwave area during this period concentrated on oceanic wind and wave measurements, partly in support of the Skylab S193 experiment. The AAFE RADSCAT was flown over the ocean numerous times and also provided some underflight data over the land.

The first opportunity to fly an active microwave system to look at the Earth from space was on Skylab in the S193 experiment of EREP. The altimeter experiments and the oceanic RADSCAT results are discussed in chapter 3. An example of the Skylab altimetry data is shown in figure 2–3 of chapter 2.

One of the major purposes of the scatterometer terrain measurements was to ascertain the likely range of scattering coefficients. Histograms illustrating this have been prepared and are now being analyzed. An example is shown in figure 1B–1. The design information provided in this experiment should aid greatly in answering the question concerning the power required for a spaceborne imaging radar.

The ERAP has led to major advancements in the ability to monitor the Earth. Part of this advancement has been due to the direct measurements acquired within the program, and part has been due to the development of a community of users and interpreters of remotely sensed data, which was large enough to become self-supporting and self-expanding.

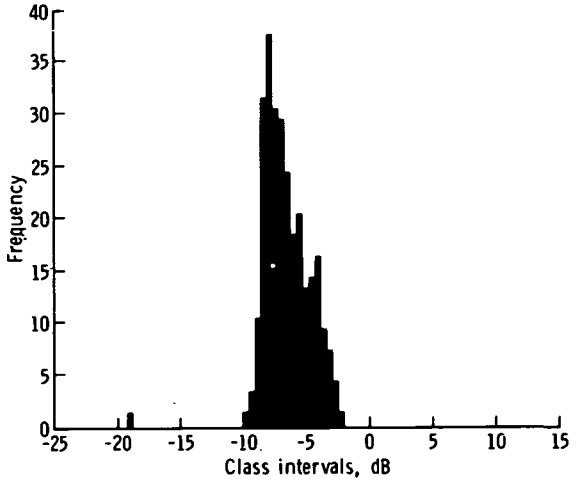

FIGURE 1B–1.—Histogram of a distribution of differential backscattering coefficient.

Future Elements

The success of ERTS–1 has clearly demonstrated, both in the United States and throughout the world, the practical value of orbital remote-sensing methods and their relevance to many of the critical problems of today. As a result of the success of ERTS–1, a second satellite, ERTS–B, has been approved for launch in 1975. In addition, the possibility of launching an ERTS–C, which would include a five-channel MSS, is being discussed.

A range of satellite systems (fig. 1B–2) is being studied that has a direct interest to applications in the Earth/land area. Perhaps the most important system is the EOS series. The first of these satellites, EOS–A, is currently scheduled for launch into a near-polar orbit in the late 1970's. A major systems objective for EOS is to provide a low-cost design based on a modular "building block" concept. This approach enables simple reconfigurations of the basic satellite to be made for different combinations of sensor types and also introduces the possibility of in-orbit repair or retrieval by using the Space Shuttle. The main sensors presently planned for the EOS–A mission are the thematic mapper and the high-resolution pointable imager. Later satellites in the EOS series are expected to include synthetic aperture radar systems for applications related to geological surveys, land-use monitoring, and water/ice monitoring.

The requirements for continuous or near-continuous observations of dynamic phenomena and the need to make measurements through gaps in cloud cover or at specific times of day have led to the study of high-resolution imagery obtained from synchronous altitudes. The Synchronous Earth Observatory Satellite (SEOS) is currently scheduled for launch in the early 1980's to monitor the continental and coastal regions of the United States in the following application areas: Earth resources, mesoscale weather phenomena, and timely warnings and alerts (e.g., floods and storms). The prime sensor for SEOS will be the multispectral large Earth survey telescope (LEST), which is capable of imaging in the visible and infrared (IR) bands. The predicted subsatellite ground resolutions for image data are 100 m in the visible bands and 800 m in the thermal IR bands. In addition to the LEST instrument, other candidate sensors for SEOS include atmospheric sounders, imaging microwave radiometers, microwave sounders, and a framing camera.

In addition to major facilities such as the proposed EOS and SEOS systems, low-cost applications Explorer spacecraft have been studied. These spacecraft could be launched by a Scout vehicle into a wide range of orbits from equatorial to polar inclinations. The system flexibility is such that a variety of instrument requirements could be accommodated without significant subsystem modifications. The first mission to be examined in detail is a heat capacity mapping mission to be flown in the late 1970's. The main sensor will be a cooled two-channel imaging radiometer providing data in the 0.8- to 1.1-μm and the 10.5- to 12.5-μm bands. Measurements will be made of thermal emission and surface albedo to develop models that use remotely sensed data to determine surface composition

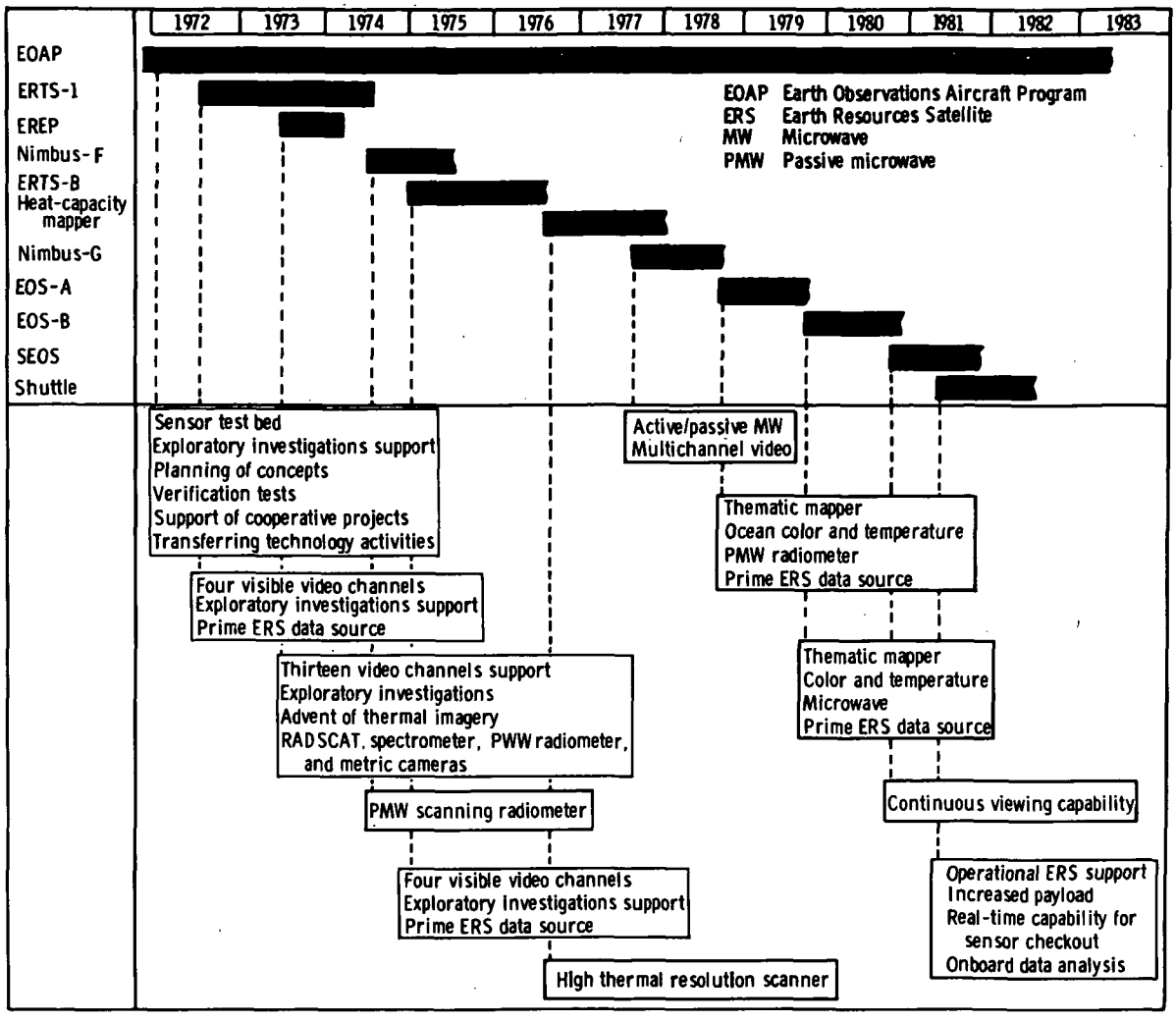

FIGURE 1B–2.—Diagram showing a range of satellite systems being studied and having applications in the Earth/land area.

from thermal measurements. Expected applications include surface geology, soil moisture, and investigations into transient thermal effects.

The introduction of the Space Transportation System (Space Shuttle, Spacelab, and Space Tug) at the end of this decade is expected to have a major effect on future experimental and operational Earth observation satellites. Automatic spacecraft such as EOS can be placed into orbit by the Space Shuttle and, if necessary, recovered for in situ repair or returned to Earth for refurbishment and eventual relaunch. Many missions for the post-1980's are being planned for Spacelab in the areas of science, applications, and technology. Spacelab is a modular system comprising a manned pressurized module and an unpressurized instrument-carrying pallet that fits into the cargo bay of the Space Shuttle and is carried into orbit for sortie missions of 7 days, which can be extended up to 30 days. The modular concept enables various module and pallet lengths to be used between the extremes of flying a long module with no pallet to pallet-only missions. Preliminary studies on the role of Spacelab for Earth resources surveys

have highlighted its value as a flexible orbital laboratory that could be used to link the present experimental aircraft programs to the future automatic operational satellite programs. Secondary Spacelab roles have also been identified, such as in-orbit testing and qualifications of sensors before their integration into automatic satellites and certain operational applications in which synoptic high-resolution data are required at infrequent intervals.

ACTIVE MICROWAVE SENSING

Importance to Earth/Land Area

The reasons for using active microwave sensors in place of or in addition to sensors in the visible IR range of the spectrum are as follows:

1. To provide timely information despite clouds or darkness (operational potential).
2. To penetrate vegetation and thin soil.
3. To complement (or replace) photography.
4. To provide special applications.

Probably the most important use is the capability to observe the terrain when clouds or darkness obscure the ground. This capability was the primary reason for developing the early airborne bombing radars, which were the predecessors of all airborne imaging radars.

A unique reason for using active microwave sensors is the ability of radio waves to penetrate vegetation and soil. The shorter wavelength signals in the microwave region cannot penetrate extremely dense vegetation all the way to the ground, and no microwave wavelength usable from space penetrates more than a few decimeters or meters into the soil. However, this amount of penetration makes visible many phenomena not observable at the shorter wavelengths.

The use of color in photography and its MSS extension into the thermal-IR region is well established for aiding interpretation of aerial imagery; the addition of almost two decades of spectrum in the microwave region enables extending the concept of color much further. This means that multispectral (or even single wavelength) active microwave sensors can add to the information available with multispectral scanning in the visible-IR region, thus making identification of ground objects easier. When clouds are present, microwave "color" may replace visible-IR color as a discriminant for differences in ground properties.

Active microwave sensors also have certain unique applications dependent particularly on the physics of microwave sensing—that is, applications in which visible-IR sensing will not work even if cloud and vegetation penetration is of no significance. Surface scatter from the ocean for wind sensing, volume scatter from snow and soil for moisture sensing, and detection of frozen ground are examples of this fact.

Details of the need for active microwave sensing are presented for introductory purposes. No examples are presented for the complementary role of active microwave sensing in adding to the available spectrum.

Cloud penetration.—Cloud penetration is particularly important when operational information must be gathered on a timely basis —that is, when there is no time to wait for the clouds to clear. Immediate monitoring of the extent of flooding is often important for warning those downstream and for dispatching help to the inundated areas. Monitoring flood damage as soon as possible after it occurs can aid in effective allocation of resources for repair and for aiding victims. Monitoring the full extent of a flood can also be important in forecasting its effect (positive and negative) on agriculture in the flooded area. Examples of the operational need for cloud penetration are as follows:

1. To monitor floods and flood damage.
2. To map lake ice.
3. To measure soil moisture.
4. To monitor harvest progress.

Great Lakes ice distribution must be observed on a timely basis if ship-route forecasting is to be effective. This monitoring is already being done in the U.S.S.R. Further-

more, because of the changing nature of the icepack, this monitoring must be repeated frequently.

Soil moisture measurements are important for many hydrologic and agricultural applications. Because the moisture conditions change rapidly, timely observations are important.

The progress of harvesting a particular crop is important not only to agricultural agencies but also to transportation agencies. Facilities for transporting the crop to its destination must be dispatched efficiently, and (at least in the U.S. Great Plains) harvest machinery and itinerant labor must be in the right place at the right time to take full advantage of the crop calendar. Because of the synoptic view provided by remote sensing, automatically processed sensor output can be more effective for this purpose than land communication networks that depend on gathering information from thousands of individual points. However, such a remote-sensing system cannot work if it must await good weather for photography.

Vegetation penetration.—Numerous applications of remote sensing require knowledge of conditions beneath the top of a plant canopy or a thin soil layer. Boundaries between different soil types and surface lithologies may be observed directly if the vegetation canopy can be penetrated, and a suitable choice of microwave sensor wavelength and incidence angle enables the penetration of most vegetation except dense forests. Some boundaries are also identifiable from the vegetation differences, which may be observed on either visible-IR or radar images, particularly if the observation is made at exactly the right time in the phenologic cycle. Examples of the operational need for vegetation penetration are as follows:

1. To map surface soil and rock boundaries.
2. To monitor floods in forested areas.
3. To measure soil moisture.
4. To inventory forests.
5. To map surficial materials.
6. To improve geologic mapping.

Floods often occur in forested areas where the extent of floodwaters is very difficult to measure with photography because of the leaf canopy. One leaf between the camera and surface can prevent observation; however, radar can normally penetrate significant amounts of canopy, depending on incident angle and wavelength.

The moisture content at the surface of bare soil can be inferred from visible-IR sensor data. However, if the soil is covered with dense vegetation, monitoring changes in moisture content is impossible without using the penetrating capability of microwave signals. Furthermore, even with bare soil, the capability of the microwave signal to obtain responses from some distances (centimeters to meters) within the soil means that moist subsurface layers can be observed even if the top centimeter has dried. The effect of a recent small rainfall or heavy dew in barely wetting the surface can be discounted when microwave sensors observe the integrated effect of the surface and near-subsurface. The wavelength of the microwave sensors is particularly important for this application because longer wavelengths can penetrate more vegetation and soil.

Forest inventory by photographic remote sensing involves very fine resolution so that individual tree-crown sizes can be measured and counted. The penetration capability of longer wavelength radar should enable estimating the volume of timber (rather than only of leaves) without using the fine resolution required for photography. Although this has not been proved, it will probably be an important use of active microwave sensors, at least in monospecific stands of timber.

Unique applications.—Moisture content of snow strongly influences the scattered microwave signal, whereas it has little effect on the visible response of the snow. The amount of compaction and liquid-free water in the snow has a major influence on its permittivity and therefore on the volume scatter from within the snow. Although this application has not yet become a proven quantitative measure, the phenomenon has been observed qualita-

tively and can be fully justified on a physical basis.

Frozen ground can often be readily distinguished from unfrozen ground by active microwave sensors because of the change in dielectric properties as the moisture in the soil changes from liquid to solid. This application has important consequences in forecasting flood runoff.

The strong microwave effects associated with edges in lake and river ice make the structure of the ice much more visible on radar images than on visible images; consequently, active microwave sensors have special application to monitoring ice structure in the Great Lakes and major rivers.

Among the fine-resolution sensors, imaging radar is uniquely suited to monitoring soil moisture because of its ability to penetrate the soil, whereas the color seen by other sensors changes as soon as the very top millimeter becomes wetter or drier. Active microwave sensors can detect soil moisture because the dielectric properties of the soil are affected by the amount of moisture present due to the large difference between the permittivity of dry soil and that of water. Such measurements have numerous applications to flood forecasting, agricultural production estimates, and watershed management.

The ability to control the angle of incident radiation with active microwave sensors led to unique applications in geology and geomorphology. The shadowing that can be observed in areas of small relief, when illumination and observation are at relatively shallow grazing angles, enables discrimination of structural features that cannot be observed with passive microwave sensors. This effect has been widely used in the commercial application of radar imagery by mineral companies and in the application by governmental agencies responsible for mapping geological phenomena. Some of the unique applications of active microwave systems are as follows:

1. Monitoring moisture content of snow.
2. Monitoring frozen ground.
3. Mapping lake and river ice.
4. Mapping structures in areas of low relief.
5. Monitoring soil moisture.

Summary of the importance of different factors to Earth/land applications.—Table 1B–I summarizes the unique features of active microwave sensing and their relative value to Earth/land applications. Clearly, some element from each of the application classes has proved feasible and important, and, in every instance, some part of the application requires the all-weather capability of active microwave sensors. The need for nighttime sensing is not so critical in many instances, and, in other instances, the need has yet to be demonstrated. In every situation, however, the ability to sense at night aids in more rapid acquisition of data because the number of useful passes over a given area is more than doubled relative to sunlight-dependent sensors.

Status of Active Microwave Sensing of Earth/Land

Microwave sensing of the land for civilian purposes was conducted to a limited degree before 1962 with plan position indicator (PPI) radar systems in aircraft and some specialized ground-based systems. However, the first significant studies of this topic began in 1963. Imaging radars used for such research have all been developed originally for military purposes. The L-band modification of the ERIM synthetic aperture radar and the recently completed S-band real aperture radar at the University of Kansas were the first systems constructed with civil use in mind. This means that parameters of the radars used were those considered appropriate for military reconnaissance, and the selection of frequencies, polarizations, and other parameters specifically for Earth/land sensing has been very limited.

Airborne sensing in which the goal is the development of civil applications of imaging radar has also been conducted using scatterometers. These instruments were developed primarily for collecting design and applica-

TABLE 1B–I.—*Unique Features of Active Microwave Sensing and Their Relative Value* [a] *to Earth/Land Applications*

Application	All weather	Day/ night	Penetra- tion	Dielectric constant	Surface roughness	Structural sensi- tivity [b]	Incident angle effects	Polariza- tion effects	Wave- length effects	Azimuth angle effects	Ground texture	Shadow- ing slopes
Land (solid earth), geology, minerals, civil works, and so forth	1	3	1	1	1	1	1	1	2	1	2	1
Soils and soil moisture	1	1	1	1	2	2	1	2	2	3	2	1
Vegetation (natural and cultivated)	1	1	1	1	2	1	1	1	1	2	1	4
Land use (urban and rural)	1	4	1	2	1	1	2	1	2	2	1	2
Water (inland water surfaces)	1	1	3	3	1	3	2	1	2	3	3	3
Snow and ice	1	1	1	1	2	1	2	2	2	2	2	2

[a] No. 1 is a proven or strong indication of value (research may still be needed for optimization and for unproven subareas); No. 2 is a potentially important value (needs research and development); No. 3 is no major value; and No. 4 is an unknown value.

[b] Sensitivity to shape of objects above or within a surface (e.g., vegetation, buildings, and volume scatter in ice). To be distinguished from roughness of soil, water, or ice and from the air-surface interface.

tion data for NASA; they have also been limited in their characteristics and terrain uses.

Ground-based (or truck-mounted) systems have been used by various experimenters for fundamental studies, and measurements have been made over a wider range of frequencies than with the airborne systems. The first significant study of this kind was conducted by Ohio State University. Since 1970, truck-mounted scatterometers covering an octave or more in bandwidth have been used at the University of Kansas, but no other broadband systems of this kind are known. By the summer of 1973, measurements over the 1- to 18-GHz range had been made with this system, but the objects sensed were restricted primarily to soils and crops.

This background clearly shows that the determination of the optimum frequency and polarization combination for most applications of active microwave sensors has not been accomplished. Nevertheless, many useful applications have been identified and proved. For example, imaging radars are widely used today in mineral exploration.

State of the art in mineral resources and geologic applications.—In many respects, this class of active microwave sensor applications is further developed than any other, because most of the interpretation techniques used in photogeology are readily extended to radar geology. This fact is partially due to the extensive demonstration project conducted in Panama by the U.S. Army Corps of Engineers and partially due to the use of imagery collected for NASA from 1964 to 1966.

The ability to map geologic structure and to map or infer lithology has been demonstrated in numerous environments. This activity is conducted extensively by both Government agencies and mineral/petroleum exploration companies in many countries. Perhaps the largest project is radar of the Amazon (RADAM) in Brazil, but the U.S.S.R. has used this kind of mapping since approximately 1968.

In the Panama project and elsewhere, identification of landforms was demonstrated and terrain analysis was conducted. This identification and analysis has been extended to some of the other countries imaged by the commercial systems.

The ability to identify possible construction material on radar images has been demonstrated. The U.S. Army Corps of Engineers conducted Project Sand, which demonstrated this capability first in Vietnam and later in Mississippi. Much research needs to be done in this area, but the application has definitely been successful.

State of the art in water resources applications.—Monitoring of ice and ice movements on the Great Lakes was demonstrated during the 1973–74 season with a low-resolution X-band system flown by Lewis Research Center. The effect of finer resolution has been demonstrated by the ERIM X-band system, and the utility of a combined X- and L-band system with modest resolution was demonstrated in 1973–74 by the same group.

Monitoring soil moisture is important in forecasting floods and in agricultural applications. Important fundamental work in this area, with application to bearing strength of soil, has been conducted for many years at the U.S. Army Corps of Engineers Waterways Experiment Station. The relationship between soil moisture and dielectric properties of soil has been well established in that program, particularly in the L-band region. Airborne scatterometer measurements by NASA show that recently irrigated agricultural fields can be clearly distinguished from drier fields, with and without vegetation cover, at angles of incidence within 40° of the vertical. Studies with a microwave spectrometer have demonstrated that a direct relationship exists between appropriate soil-moisture indicators for the surface layer and the observed radar signal. However, these studies also have shown some of the complications resulting because of different responses for soils prepared in different ways by plowing.

Studies of the coastal wetlands have been conducted by several investigators. The utility of imaging radar at the Ka-band was

demonstrated in these studies, and cross-polarized returns proved especially helpful in making distinctions. Multifrequency measurements in the coastal wetlands have proved the value of the combination of X- and L-band frequencies.

Oil pollution has been studied at the NRL, and elsewhere, in saltwater environment; the results were so successful that the U.S. Coast Guard is in the process of obtaining a microwave system for semioperational use in harbors and along the coast. No work has been done to determine whether this technique applies to inland waters, but the physical principle indicates that it should work in those cases in which the water is disturbed by wind or turbulent currents.

The ability to determine the moisture content of snow would be of great economic benefit. No quantitative measurements have yet been made to support the ability of radar to make such measurements, but qualitative work by Waite and MacDonald (ref. 1B–1) indicates that old, probably wet, snow shows up clearly on Ka-band images, with the nature of the return indicating a volume-scatter phenomenon.

Minor work on glaciers was conducted in the United States in the late 1960's, and the indication was that dry snow covering the glacier and its environs could be penetrated by the radar signal. Thus, the desired location of the glacial boundary could be determined even in the winter. Interesting work conducted by the U.S.S.R. on glacier studies with active microwave sensors is reported in chapter 2.

State of the art in agriculture, forestry, range, and soils applications.—Some crop identification was conducted at Ohio State University with a truck-mounted scatterometer, but the area observed was limited. Studies using imaging radars and scatterometers have been conducted since 1965. In addition, microwave spectrometer measurements of crops have been made extensively during the last 3 yr. The ability of cross-polarized returns to help distinguish crops was demonstrated for the months of August and September by using Ka-band imagery. July crop identification using this single-frequency system was not as satisfactory. However, the single-frequency Ku-band DPD–2 flown by JSC demonstrated that wheat could be identified clearly and that a yield model giving 95 percent accuracy could be applied to a countywide area in Kansas.

The use of multiple frequencies for crop identification has been tested with a microwave spectrometer. Although data analysis is not complete, initial indications are that a proper choice of frequencies can enable accurate identification of several commercial crops. The optimum frequencies have not yet been ascertained, but one frequency should be relatively high, probably well above the X-band. Best results were obtained using a 14-GHz frequency in combination with either a 7- or 4-GHz frequency. No attempt has been made to show the value of a third frequency or to try other high frequencies, but cursory examination of the available data indicates that any possible ambiguities in the two-frequency data (and some do exist at certain incident angles) could be easily resolved by using three frequencies.

Another two-frequency experiment was conducted using the ERIM X- and L-band system at Garden City, Kans. Analysis of these data by photointerpretation techniques showed that moderately good separation was achieved but that the L-band did not add as much to the separation ability as the 4-GHz frequency used with the spectrometer in eastern Kansas. This difference was probably because the L-band penetrates to the soil for some of the crops, whereas the higher frequencies do not do so for well-developed crops at suitable incident angles.

No quantitative work of consequence has been conducted to determine crop condition with active microwave sensors. During the 1972 summer, a small patch of corn blight was observed with the University of Kansas spectrometer, and a distinctive signature was observed that enabled clear separation of this diseased patch from healthy corn. This single example is not statistically significant; it is

reported only as a suggestion of what research may show. Furthermore, examination of radar images consistently shows patterns within fields that can only be caused by differences in the vigor of the plants, but no such images have been available soon enough after a flight in past experiments to enable ground checking.

Similarly, only qualitative indications of the ability to discriminate range conditions have been observed. On several occasions, interpreters have observed that rangeland on opposite sides of a fence in the sandhills near Garden City, Kans., showed significant differences in tone on X- and Ka-band radar, which could have been caused only by differences in range conditions (almost certainly due to differences in grazing pressure).

The ability to forecast runoff from watersheds is a significant factor in managing agricultural water resources, both for retaining water for future use and for preventing floods. McCoy (ref. 1B–2) demonstrated conclusively in a study of more than 30 basins in different environments that the appropriate stream-length and slope parameters could be derived from radar imagery by human interpretation; he also showed there may be promise in automated analysis of such basins.

The mapping of natural vegetation has been demonstrated successfully but not often used. Morain and Simonett (ref. 1B–3) showed that certain vegetation classes could be mapped quite well with the combination of like- and cross-polarized Ka-band imagery in a relatively arid mountainous region in Oregon. The same technique was used to map the gross vegetation types in Yellowstone National Park and was also successful in Utah. Extensive vegetation maps have been prepared in conjunction with various parts of the South and Central America radar mapping projects. An attempt to use Ka-band imagery for forest mapping in the Sierra Mountains of California was less successful.

State of the art of active microwave applications to land-use problems.—Various land-use maps have been prepared on a regional basis by different investigators using radar imagery. One of the first successful regional land-use maps was made by Nunnally (ref. 1B–4). In addition, several land-use maps of urban areas have been prepared with radar imagery. Although these maps have been moderately successful, the radar imagery used did not have sufficient resolution to enable detailed mapping; thus, the maps are of rather general categories and nowhere near as detailed as one can compile from aerial photography.

The potential use of moving target indicators to determine traffic flow in cities has been demonstrated in principle, but apparently no research has been conducted to apply this technique to the traffic-monitoring problem.

Identifying parked cars in industrial parking lots, in parking lots associated with recreational or residential complexes, or even identifying cars on major thoroughfares, without ascertaining whether they are moving, could lead to improved knowledge of human and industrial activity. Cars provide relatively strong returns on like-polarized imagery but weak returns on cross-polarized imagery. A pair of images of JSC showed strong returns from the buildings on both polarizations, but only the like-polarized image had strong returns from parking lots full of cars. Thus, the potential exists for use of this phenomenon.

Flood monitoring with radar is clearly feasible under some conditions. Images produced during the 1973 flooding of the Mississippi River appear to delineate the boundaries of flooded areas. These images were made in rural areas, and their application has not been tested in cities and suburbs where trees and buildings are present.

In addition to the previously discussed activities of the United States, a growing interest in active microwave sensing methods exists in many foreign remote-sensing programs. For example, the European Space Research Organization (ESRO) has recently completed a feasibility study on a synthetic aperture radar satellite system (ref. 1B–5).

One of the principal objectives of this study was to demonstrate that active microwave sensors are potentially capable of satisfying the operational requirements of the user community. Additional objectives were to identify critical technological areas and to indicate the research and development steps required to achieve the operational system. The main results of the study indicated the need for a 10-GHz focused synthetic aperture imaging radar capable of providing spatial resolutions of 50 m for a swath width of 80 km. Based on the results of the ESRO study, more detailed investigations are presently underway on radar systems for use on Spacelab missions as a preparatory step before the definition of the eventual operational system. The European scientists clearly recognize that a considerable amount of progress is possible by using ground-based instrumentation and airborne measurements. Accordingly, efforts are now underway to increase the number of fundamental measurements like those currently being conducted by DeLoor and Jurrieens (ref. 1B–6) in the Netherlands.

Need for Research, Development, and Training

Research, development, and training of interpreters are essential parts of a program to apply active microwave sensors to those operational functions for which their unique abilities provide an advantage over visible-IR sensors. Because many of the applications depend on the use of relatively conventional interpretation techniques, one of the most pressing needs is to train interpreters already familiar with aerial photography to work with radar images. Many applications appear sound from a physics viewpoint, but they have not been tried; consequently, applications research is needed to demonstrate that these potential uses of active microwave sensors can be made operational. Much additional research is needed to determine the optimum parameters for active microwave systems and to determine radar signatures so that multifrequency, multipolarization systems can use their "color" capability to discriminate among the various terrain phenomena of interest.

Need to develop expertise in conventional interpretation of radar images.—Many applications exist for which context, shape, timing, and texture are the most important interpretation tools. These same parameters are used in analysis of aerial photography and scanner images, and a large number of interpreters are familiar with their use. Professional photointerpreters normally use these techniques, but geologists, urban and regional planners, foresters, soil conservationists, and other researchers also use them regularly. Hence, a most important need is to insure that such users of photography are able to use radar images.

One of the most important needs is to overcome the natural hesitancy of these users to work with an unfamiliar medium. Breaking this resistance is most important because many applications can be handled better with radar images using exactly the same methods as photography.

Another problem that can be overcome with such a training program is the natural tendency of interpreters to want more resolution than they really need. This tendency has inhibited many researchers from using ERTS images; however, users of ERTS have demonstrated that even its relatively poor resolution can be applied to many problems for which "need matrices" have, in the past, specified much finer resolution. For many uses, fine resolution actually inhibits proper interpretation; yet interpreters often judge the quality of an image by looking at it to see what kinds of objects can be resolved. Thus, the problem really is one of overcoming prejudice.

Geometric effects on radar images are different from those on photographs and scanner images. For some applications, an understanding of these differences is important, particularly in mountainous terrain. This understanding can be gained quickly, and the interpreter who understands these

differences can then proceed to use his normal technique.

Needs for active microwave sensor application and signature research.—The application discussed in chapter 2 require different kinds of research and development. Applications depending primarily on conventional photointerpretation methods require research into the ability of these methods to satisfy the application needs with radar images and requires development of operational techniques for using active microwave sensors. Some such applications are nearly frequency independent in the sense that the radar images currently available (almost all in the few-centimeter-wavelength regime) seem capable of being used without regard to the exact frequency chosen. Other applications depend on geometric, texture, context, and timing factors, but use of a relatively low frequency for the radar is indicated. For such applications, similar research on use of conventional methods is required, but a low-frequency synthetic aperture radar is required to produce images. These needs are outlined in table 1B–II, in which the applications presented in chapter 2 are compared with the type of research and development needed.

Although many applications appear somewhat wavelength dependent, an optimum frequency probably exists for distinguishing the boundaries and textures that are important for each application. One reason no optimum frequency can be specified at this time is that multifrequency imagery is exceedingly scarce, and experiments conducted in such a way that the relative value of different frequencies can be compared are totally nonexistent for most of the listed applications. Choice of polarization has been the subject of more research than choice of wavelength, and a significant amount of imagery with multiple polarizations has been produced in the United States. Nevertheless, definitive research to establish the best single polarization is also almost totally lacking, because most multipolarization research has been aimed at determining the value of polarization combinations. Consequently, research is needed for determining the best wavelength-polarization combination for most applications as indicated in table 1B–II.

Many applications require the use of multiple frequencies and polarizations to produce "signatures" that permit fine distinctions to be made between classes of objects. These needs are particularly important in vegetation imaging, just as they are in the visible-IR part of the spectrum. Other such needs exist because varying depths of penetration with the different frequencies can be used jointly to learn more about a surface than could be learned with a signal that penetrates only to a single depth (under given conditions). Spectral signature studies have been conducted only for a very small number of materials under very specialized conditions; thus, this research area needs great expansion. The applications for which this kind of research is needed are listed in table 1B–II.

When signatures and temporal variations in response are important, fundamental understanding of the scattering process can contribute significantly to improved system design and to recognition of those areas in which microwaves may have great promise or in which applications may be more limited than indicated by present speculation. However, some applications, such as those depending on identification of land-water boundaries, are well understood from the standpoint of the physics of scattering, and such research is not likely to contribute to them. Some of the areas in which fundamental research shows most promise are itemized in table 1B–II.

PROGRAM PLANS

Active Microwave Sensing Experimental Program

Previous research and demonstrations have shown that active microwave systems are ready for many practical applications appropriate for both aircraft and spacecraft platforms. Systems that would be quite

TABLE 1B–II.—*Applications and Needed Research*

Application	Need for research on conventional techniques			Need to establish best single frequency/ polarization	Need for signature research	Need for fundamental research
	Any frequency	High frequency	Low frequency			
Mineral resources and geologic applications						
Landform identification and terrain analysis	X		X	X		
Mineral deposit location	X		X	X	X	
Petroleum exploration	X		X	X		
Ground water exploration	X		X	X		
Crustal motion						X
Major construction sites	X		X	X	X	
Construction materials	X		X	X	X	
Water resources applications						
Lake ice monitoring				X	X	X
Flood forecasting (soil moisture)	X		X	X	X	X
Flood mapping	X		X	X		
Lake-level determination	X			X		
Lake eutrophication	X			X	X	X
Coastal wetlands mapping	X		X	X	X	
Water pollution monitoring	X			X	X	X
Snowfields		X		X	X	X
Glaciers	X			X		
Permafrost			X			X
Agricultural, forestry, range, and soils applications						
Crop identification				X	X	X
Crop cover and condition	X			X	X	X
Range inventory		X		X	X	
Soils mapping	X		X	X	X	
Soil moisture:						
Watershed management	X		X	X	X	
Crop yield				X	X	X
Forestry	X		X	X	X	X
Land use mapping						
Basic image analysis	X			X	X	
Traffic	X			X	X	X
Parked cars	X			X		
Disaster assessment						
Flooding (urban/suburban)	X		X	X		
Previously flooded areas	X			X	X	
Wind damage	X	X		X	X	
Fire damage	X			X		
Earthquake damage	X			X		
Volcano activity	X		X	X	X	

useful could be implemented without further research. Nevertheless, many of the most promising applications, in which active microwave sensors are strongly needed, require considerable research to show whether or not the promise of the present can be fulfilled. For applications in which active microwave systems are clearly ready to contribute, there is still little evidence whether such a choice would be optimum or whether (for many applications) the wavelength chosen makes much difference. Hence, a coherent research program is needed that places priorities both on developing the most important and promising applications and on investigating those that cannot be described as promising because of lack of knowledge.

Because many applications use conventional image interpretation techniques, a major effort should be made to provide these images to potential users and user-oriented researchers as soon as possible. In some instances, little ground truth is needed and existing images may be used; in other instances, new flights to provide imagery must be accompanied by extensive ground truth provided by investigators. Many applications require repeated coverage at frequent intervals or require very timely single coverage. An efficient mechanism is needed to make such coverage possible.

Many other applications depend on determining an optimum frequency that is critical enough to require experimental radars with several frequencies. When signature analysis is likely to be significant or when a considerable search must be made for the right wavelength, ground-based scatterometer/spectrometers will often be the most economical research instruments.

Fundamental studies, both theoretical and and experimental, can lead to understanding the phenomena associated with some applications well enough so that the costs of field and aircraft experiments can be significantly reduced. Such studies should be supported in which this kind of potential payoff can be identified and qualified researchers are available.

Sensors.—Sensors to be used in such research are available in several forms. The recommended active microwave research sensors are as follows:

1. Aircraft imaging systems:
   - *a.* One multifrequency (four or five), multipolarization, fine-resolution synthetic aperture radar on NASA aircraft
   - *b.* One single-frequency (probably X-band), multipolarization, fine-resolution synthetic aperture radar on NASA aircraft
   - *c.* One or two existing multifrequency synthetic aperture radars on appropriate aircraft
   - *d.* Two to six simple real aperture SLAR's on investigator aircraft
2. Airborne scatterometers:
   - *a.* One AAFE RADSCAT
   - *b.* One or two simple fan-beam systems (possible frequencies in the Ku-, X-, C-, and L-band) on small aircraft
3. Ground scatterometers and spectrometers:
   - *a.* Four broadband spectrometers (multioctave) under control of actual researchers
   - *b.* Four simple panchromatic but relatively narrowband scatterometers under control of actual researchers

The major national facilities suggested for NASA aircraft are complicated systems intended to answer the questions requiring fine resolution, requiring a full complement of polarizations, or requiring images at several frequencies. Such facilities must be scheduled relatively tightly because of the demand from many users both for these systems and for nonradar sensors on the aircraft. Because of the cost of such sensors, they are not appropriate for individual investigator groups. Existing systems, such as those at ERIM and JPL, might be used together with these central systems.

Although major systems are recommended for NASA aircraft, several (two to six) simple, inexpensive systems are recom-

mended for use on aircraft under the control of investigators. Therefore, these systems need not be subject to the scheduling constraints, nor to the costs of flying on a large high-performance aircraft. These systems should be particularly valuable for experiments requiring frequent repetition of flights to observe time-dependent phenomena or requiring fewer flights in which timing is dependent on some unpredictable event. The kind of system used might be the APS–94 (used by Lewis Research Center and by USGS for ice studies) of the University of Kansas system, which could be duplicated for under $50 000 per unit. These systems have modest resolution and are not multifrequency, nor are they dual polarization, although this might be added relatively easily.

Much research can be accomplished by using available imagery. The 500 000 km^2 of Ka-band imagery obtained in 1965–66 are still useful for much research. Goodyear Aerospace has a computer-accessed library of U.S. Air Force images that cover many parts of the United States. Other image sources may also exist that could be used for some studies not requiring ground truth obtained at flight time.

The airborne scatterometer is a specialized instrument that can provide quantitative data from a wider range of areas than a ground-based system, but it does not provide an image. Its principal advantages are that it is inexpensive to add an additional frequency and that it provides multiangle data. Such systems can be flown on small aircraft that are inexpensive to operate.

One way to answer questions about optimum frequencies, polarizations, and their combinations in which images are not required is with swept-frequency scatterometer/spectrometers. At present, the 1- to 18-GHz system operated by the University of Kansas is the only system like this, but the development of three additional systems by qualified investigator groups is recommended. Such systems are much less costly to operate than multifrequency, multipolarization airborne systems, but they can only be used in relatively restricted areas at any particular time. Several of these systems need to be operating simultaneously in different areas if all the unanswered questions are to be addressed in a reasonable time period.

The number of groups capable of supporting such a sophisticated system and at the same time providing it with meaningful applications research is limited; hence, the development of approximately four additional simpler single-frequency systems is recommended so that these systems can be used by groups primarily oriented toward applications and without extensive engineering support. Such systems should be panchromatic (broadband) to guarantee that fading will not make data collection too difficult.

With this complement of sensors (distributed between operation by a national facility, such as the JSC, and by experimenters themselves), a program can be developed that should lead to the best use of limited resources in achieving the goals outlined in this report.

User-engineer-physicist coordination.— Every effort should be made to "team up" the user and application scientists with engineers or physicists interested in the relationship between the microwave signal and the terrain sensed. Experience from past programs has shown that many errors have been made by user scientists attempting to understand the electromagnetic fundamentals without adequate training. However, much of the research into applications of radar by engineers not teamed with users has produced meaningless data because the appropriate collateral data were not collected.

This "teaming up" of users and electromagnetic specialists can be achieved either by having both at the same institution or by assuring an institutional arrangement that encourages cooperation between persons located at different organizations. In the programs conducted to date, models exist for both of these arrangements.

Further coordination is necessary between these groups at a national and probably at

an international level. A steering group should be established to advise NASA on the conduct and progress of the program. Such a group should meet at least semiannually. Its members should come from NASA and ESRO personnel, from appropriate user/agency personnel, and from researchers representing both the users and the electromagnetic interaction community. At least one representative should be selected from the radar hardware development community, and at least one should be selected from the data-processing community.

Meetings of this group should include occasional formal presentation of research or applications, but a major part of each meeting should be devoted to informal, but structured, discussion of the work in progress at various major and minor research groups in areas of interest. The meeting should also include reviews of the direction of the program and recommendations of priorities for future work.

If a set of instruments such as that described can be combined with an inspired research program conducted by multidisciplinary groups of the type outlined here, numerous active microwave space applications should emerge that will be of great economic and social benefit both to the United States and the world.

Balance Between Allocations for Data Acquisition and Data Analysis

Optimum allocation of resources requires a balance be maintained between the cost of acquiring remote-sensing data and the cost of data analysis. Acquisition involves tangible costs such as the price of an instrument, the cost of a carrier vehicle and its operation, and the cost of communication and computer time in data processing. However, data analysis requires large amounts of scientific and paraprofessional manpower over a long period. Because the acquisition costs are so readily quantified and because of a desire for relatively quick "proof" that these investments are worthwhile, allocations of funds often are for too small an amount and for too short a time. Consequently, vast amounts have been spent on collecting data that were never used because the funds were not allocated for their analysis.

Nearly all scientists agree that the cost of worthwhile data analysis is as high or higher than the usual cost of instruments and acquisition of data. A cursory review of the history of remote sensing and similar programs shows that this point is often overlooked in funding allocations. Furthermore, the length of time required to reach the analysis stage can result in fund withdrawal because of mission changes. This situation has resulted in the reacquisition of data at a later time, which could have been avoided had the earlier programs been carried to the proper conclusion. The future NASA active microwave program should give appropriate consideration to both the analysis and the acquisition phases.

REFERENCES

1B–1. WAITE, WILLIAM P., AND MACDONALD, HAROLD C.: Snowfield Mapping with K-band Radar. Remote Sensing of Environment, vol. 1, no. 2, Mar. 1970, pp. 143–150.

1B–2. MCCOY, ROGER MICHAEL: An Evaluation of Radar Imagery as a Tool for Drainage Basin Analysis. Ph.D. Dissertation, Univ. of Kansas, 1967.

1B–3. MORAIN, S. A., AND SIMONETT, D. S.: Vegetation Analysis With Radar Imagery. Proceedings of the Fourth Symposium on Remote Sensing of Environment, Univ. of Michigan, 1966, pp. 605–622.

1B–4. NUNNALLY, NELSON R.: Integrated Landscape Analysis With Radar Imagery. Remote Sensing of Environment, vol. 1, no. 1, Mar. 1969, pp. 1–6.

1B-5. EUROPEAN SPACE RESEARCH ORGANIZATION: Side-Looking Radar Systems and Their Potential Application to Earth-Resources Surveys. ESTEC Contract No. 1537/71, 1973.

1B–6. DELOOR, G. P., AND JURRIEENS, A. A.: The Radar Backscatter of Vegetation. AGARD Propagation Limitations in Remote Sensing, Oct. 1971.

CHAPTER 2

Active Microwave Remote Sensing of Earth/Land

Active Microwave Working Group

Earth/Land Panel:

J. W. ROUSE, JR., *Cochairman*
MARTIN W. MOLLOY, *Cochairman*

Steven A. Arcone
Bruce J. Blanchard
M. Leonard Bryan
A. W. England
John E. Heighway
Pieter Hoekstra
Richard A. Hoppin
Edward T. Kanemasu
Leons Kovisars
Anthony J. Lewis
A. O. Lind
A. A. Loomis
Jerry R. Lundien
Harold C. MacDonald
Roger M. McCoy
Paul M. Merifield
R. K. Moore
Stanley A. Morain
J. Plevin
Gerald G. Schaber
David S. Simonett
James V. Taranik
Thomas W. Thompson
Gene A. Thorley
Stanley H. Ward
G. L. Wilfert

INTRODUCTION

The objectives of the Earth/land panel were (1) to identify needed Earth resources survey and solid Earth applications in which active microwave techniques are potentially useful, (2) to divide these applications into those known to be feasible and those believed to be feasible, and (3) to outline the experiments and systems needed to implement presently feasible methods and to bring other methods to the feasible stage. A summary of the Earth/land panel tasks and recommendations is presented in chapter 1.

The Earth/land panel undertook its work in the following sequence: (1) to identify broad areas of Earth resources and solid Earth applications; for example, agriculture, (2) to define key applications within these broad areas; for example, crop condition, (3) to specify information of value to users responsible for resource management decisions; for example, plant moisture content for crop yield forecasts, (4) to identify physical phenomena that must be measured to gain this information of value; for example, permittivity, (5) to specify preliminary functional requirements concerning data acquisition, processing, analysis and distribution (including required ground truth); for example, wavelength, repetition rate, time of year, and timeliness of data delivery to ultimate user, and tradeoffs among functional requirements, (e.g., spatial resolution compared to swath width), (6) to indicate

needed research, covering the complete range from theory and laboratory experimentation to field, aircraft, and spacecraft tests; for example, experiment plan flow diagram, and (7) to identify any issues raised by the foregoing analysis; for example, changes needed in the way responsible institutions currently use remote-sensing data to derive information for resource management.

The Earth/land panel report is divided by broad applications areas into (1) mineral resources and geologic applications (including earthquakes and crustal motions); (2) water resources; (3) agriculture, forestry, range, and soils (including soil moisture); and (4) land use, urban, environmental, and mapping applications. Appendix 1B of chapter 1 presents a review of the Earth observation program, the importance of active microwave sensing, and the program plans.

PART A

MINERAL RESOURCES AND GEOLOGIC APPLICATION

GENERAL OBJECTIVES

The objectives of part A are to describe the geoscience applications of active microwave systems. The unique contribution of imaging radars for mineral resource, petroleum and ground-water exploration, and geomorphic analysis in the cloud-shrouded tropics has been demonstrated. In the area of civil works, applications are found in the selection and evaluation of sites for major construction, such as nuclear powerplants, dams, pipelines, schools, and hospitals. In solid Earth studies (including geophysics), the possibility of utilizing active microwave sensors to detect small crustal movements before earthquakes appears to have some potential.

Active microwave systems should provide unique terrain data to facilitate geoscience interpretations. An obvious need for signal penetration exists where vegetation or a thin soil cover masks shallow outcrop patterns; thus, multifrequency microwave systems may provide this capability. In addition, the feasibility of obtaining multipolarization terrain parameters and an insight into dielectric properties may provide data for terrain analysis not otherwise available when using existing airborne systems.

The objectives of the various remote-sensing systems are quite similar. Ideally, remote sensing should provide quick, economic, and accurate data about the surface of the Earth. This requirement is particularly true for instances in which repetitive observations are required or in which traditional ground observations would be costly and impractical.

DEMONSTRATED REMOTE-SENSING OBSERVATIONS COMPARED TO OBJECTIVES

Earth Resources Technology Satellite 1

The major geologic objectives of Earth Resources Technology Satellite (ERTS) investigations are to delineate large structures, recognize new mineral and oil deposits (or at least promising areas for ground exploration), prepare maps of poorly known areas, and monitor geologic hazards. Most published analyses have been done by more-or-less conventional photogeologic interpretation, supplemented by additive color enhancement. Enhancement techniques, such as spectral band ratioing involving digital tape, have been done by only a few specialized facilities. These techniques will undoubtedly become more important in future lithologic identification.

The most important feature seen on the imagery is the linear, or the larger and more complex lineament. Therefore, much interpretation has been concerned with linear

analysis. Linears have been found to correlate with known faults and with ground-measured fracture trends. The remaining features are mainly topographic or tonally expressed lithologic contacts or are indeterminate. In northern California, linear systems (patterns) have been recognized and dated relatively on the basis of truncations. Mine-hazard maps based on ERTS linear traces have been made and verified in Indiana.

Many previously mapped high-angle faults have been identified. Several of these faults have been extended beyond known limits and connections have been established between formerly separated faults. A major right-slip fault zone along the California-Nevada State line has been discovered. In Alaska, a comparison of seismicity with linears has shown that some of the linears have not been mapped as faults. On the other hand, in the Southwest United States, faults with evidence of recent movements but not related to present seismicity may be keys for potential seismic hazard. Low-angle faults are difficult or impossible to discern.

Some new folds have been discovered, but other apparent folds on ERTS imagery have been found not to exist when field checked. Several circular features have been noted, not all related to any known geologic feature. Alinements of volcanic or plutonic activity may lie along unmapped fault zones. Some loci of igneous activity may be related to intersections of linears.

Mapping of lithologies has been only partially successful with ERTS data. Distinctive iron formations and some other Precambrian lithologies have been outlined in Wyoming. Remote-sensing units usually do not correspond to stratigraphic units, but nevertheless are helpful in delineating structure in some areas. In many cases, units are mainly separable on physiographic criteria. Correlation of ERTS geomorphological units with geostructural units has been made in Bolivia. In the same area, some success has been achieved in determining regional boundaries and relative ages of volcanics. Volcanic formations (and, similarly, other lithologies) are not always distinguishable unless they exhibit a characteristic morphology.

No direct evidence of ore deposits has been found. Known mineralized areas have been plotted on ERTS images to determine if there are correlations with linears, intersections, color-tonal anomalies, large structural bends, and discontinuities. The ERTS analysis suggests general areas that must be subjected to detailed field and geophysical studies.

The ERTS resolution of spatial detail is poor in areas of flat-lying rocks and low relief. However, some enhancement of topography and linears is observed on winter scenes with low Sun angle and where snow cover is not too deep.

Regular and continuing repetition of coverage is not necessary for geologic problems other than for monitoring volcanic activity and possibly some hazards. However, multiple coverage (winter, later spring, and fall) is desirable because of seasonal changes in vegetation and soil moisture and variations in atmospheric haze and cloud cover.

There is general agreement that the synoptic coverage and the orthophotographic characteristic of the ERTS images are the most valuable features of the system. Synoptic coverage provides a regional view under nearly uniform illumination and thus avoids the need for mosaics made from conventional aerial photographs. Because of the lack of scale distortion, the orthophotographic characteristic allows the image to be directly compared or overlaid with base maps of scales as large as 1:250 000.

High-quality color composites have been the most useful form of data, but all images have their advantages. Multispectral scanner (MSS) band 5 (red) emphasizes vegetational and other tonal contrasts, whereas MSS band 7 (infrared (IR)) emphasizes topography. The southeast look direction has subdued the northwest trends. Stereographic viewing is helpful, but complete coverage will not be available because of orbital design constraints.

Skylab

Few results are available from Skylab at present. Most geological studies are using the S190–A multispectral camera (black and white, color IR, and color) and the S190–B Earth terrain camera (high-resolution black and white, color IR, or color). Objectives of these studies are much the same as those of ERTS–1.

The black-and-white film (red band) and color film from S190–A and S190–B provide excellent detail, considerably better than ERTS. Stereographic coverage along many of the flight lines is complete. Individual frames provide a good regional view, although not of as large an area as ERTS. Skylab does not provide complete coverage of a given project area. The lack of repetitive coverage means that any portion of a project area may have too much cloud cover.

In northern Wyoming, southern Montana, and western South Dakota, Skylab imagery, where cloud free, allows for much more detailed structural and lithologic mapping than ERTS. Many more folds can be recognized and certain linears (faults) can be traced with more confidence. In the Coachella Valley of southern California, major faults can be traced under alluvium because they act as ground-water barriers, which support lines of vegetation at the surface. In Nevada, exposures of limestone were located in areas thought to be covered by volcanics. Therefore, aeromagnetic anomalies in these areas are related to features at depth (plutons which might be sources of metals), not to volcanics.

Apollo Lunar Sounder Experiment

The Apollo lunar sounder experiment (ALSE) flown on the Apollo 17 mission is providing a first good test of advanced orbital planetary radar concepts. It is an active microwave system designed to compromise between sounding and imaging. The ALSE is not optimum for Earth applications; however, it offers the following features, which can be readily incorporated into resources-oriented radar:

1. Multispectral (3 bands at 5.0 to 5.5 MHz, 15 to 16.5 MHz, and 150 to 164 MHz).
2. Coherent synthetic aperture.
3. Large dynamic range.
4. Amplitude calibration.
5. Coherent optical data processing.
6. Image dissection to produce digital data.
7. Digital data processing.
8. Holographic data display.
9. Stereographic data display.

Data products from the ALSE experiment are the surface radar imagery, the surface topographic profile, and the subsurface sounding. The surface radar imagery has several important uses, among which is the study of volcanic and tectonic features of radar backscatter and radar albedo. The data can also be used in conjunction with other lunar data to study various evolutionary processes that have shaped the lunar surface.

The continuous radar profile of the Moon can be used in conjunction with the laser altimeter data and stereophotography to study both the features of the Moon and local and regional lunar topography. For example, local topographic information from the surface profile can be used to study the mare basin structure in relationship to the mascon structure. Some interesting examples of crater rebound phenomena are also apparent in the local topographic profile.

The ALSE subsurface sounding will provide information on the subsurface stratigraphy and hence may be used to study volcanic flows, ejecta blankets, and regolith thickness. Relative changes in the surface profile and subsurface stratigraphy can provide information on the processes of tectonic activity such as intrusion and faulting.

Present Aircraft Systems With Imaging Microwave Systems

Two side-looking radar imaging systems are available for contract survey work at present. The Aerospace Division of Westinghouse was first to offer services using an APQ–97 installed in a DC–6B aircraft with complete onboard processing facilities. This

conventional real aperture system has moderate resolution and operates at 0.86 cm (Ka-band). Imagery can be acquired of a swath 20 km wide from either side of the aircraft at a nominal altitude of 6 km. The imagery scale is approximately 1:200 000. Early in 1971, the Goodyear Electronic Mapping System 1000 was installed in a Caravelle jet operated by Aero Service Corp. This radar system, a modification of the APS–102, is an X-band synthetic aperture system. The data film is processed in an optical correlator to produce ground-range imagery of good resolution. Two adjacent swaths are imaged simultaneously in both look directions, totaling 37 km. Missions have been flown with a 26-percent overlap, which provides approximately a 50-percent stereographic coverage. Nominal flight altitude is 12 km. Imagery is produced at a 1:400 000 scale but usually is delivered at a 1:250 000 scale.

Several organizations have side-looking radar systems for research projects related to civil remote-sensing activities; they include the NASA Lyndon B. Johnson Space Center (JSC), the University of Michigan, the U.S. Geological Survey, the U.S. Coast Guard, and the Jet Propulsion Laboratory (JPL).

MAJOR MINERAL RESOURCES AND GEOLOGICAL APPLICATIONS OF ACTIVE MICROWAVE SENSING

This section reviews the following areas in which radar imagery can provide useful information:

1. Mineral exploration.
2. Petroleum exploration.
3. Ground-water exploration.
4. Civil works.
5. Geologic mapping.
6. Landform identification and terrain analysis.

A state-of-the-art summary for each area is given in table 2–I. A concluding subsection briefly outlines the research needs for earthquake mechanisms and crustal motion.

Mineral Exploration

Radar imagery provides a useful information base on which to plan specific ground exploration programs. In the past, apart from problems of access and movement, a major hindrance has been the absence of a regional geologic map to which mineral occurrences could be related with an imaging radar. Areas having indicators of potential mineralization may now be more confidently defined. An example of a radar image is given in figure 2–1.

The common surface indicators signaling mineralization to the radar interpreter include fracture zones, veins, and rock-type association. The sites of igneous plugs, or volcanic centers in general, are highly prospective for metal mineralization (e.g., sulfide veins), especially if they are associated with fractures having obvious tensional orientations. The margins of discrete igneous intrusive bodies such as stocks are similarly prospective, especially where fault swarms, radial faults, or other tensional fractures coincide. A detailed geologic study using radar imagery of eastern Panama has highlighted potential mineralized areas based on most of the previously stated criteria (ref. 2–2). Wing also documented the utility of radar imagery for inferring the location of placer deposits. Based on the work of MacDonald and Waite (ref. 2–3), it seems feasible to identify and map sand and gravel deposits, which are critical to the construction industry.

Several other radar exploration programs concerning minerals have been completed in the tropics. For example, in November 1971, a side-looking airborne radar (SLAR) survey of the entire country of Nicaragua was undertaken for the Nicaraguan Government. The 1:250 000-scale imagery obtained was compiled into a 1:100 000- and 1:500 000-scale mosaic series by a commercial firm. The interpretations were directed at topography, geomorphology, land use, vegetation, and geology overlays for the 1:100 000-scale radar mosaics. It was concluded from this Nicaraguan study that the potential exists

TABLE 2–I.—*State-of-the-Art Summary of*

Discipline	Special functional requirements	Application	Parameters to be measured or identified
Mineral exploration [a]...	Steerable antenna; multiple look directions; multiple polarizations; multiple frequencies; measurement of dielectric properties.	Worldwide location of economic mineral deposits (metals, nonmetals, coal, clay, including bentonite, aggregate/sand, and gravel).	Surface texture and roughness; porosity and dielectric properties of rocks; plant types/stress possibly indicating geochemical anomalies; drainage patterns and topography indicating underlying rock type and structural control (possible indicators of mineralization/alteration "halos").
Petroleum exploration [a].	Pointable antenna; multiple look directions; multiple polarizations; multiple frequencies; measurement of dielectric properties.	Petroleum exploration (oil, gas, and surficial petroleum deposits such as tar, asphalt, oil, and shale); delineation of structure, rock type, and surficial material; composition for location of favorable oil and gas structures or surficial petroleum deposits.	Structure and rock type; morphology of the land surface beneath the vegetation canopy; vegetation types and boundaries; texture and composition of surficial materials; soil and moisture linears. (These parameters lead to direct mapping of rock type and structure and permit the location of favorable drill sites.)
Ground-water exploration	Simultaneous short- and long-wavelength data.	Location and determination of ground-water resources.	Same as for mineral exploration; determination of stream drainage parameters and ground-water seepage.
Civil works.....	Multiple frequencies advantageous for determining terrain texture parameters; requirement for subsurface penetration to determine soil thickness and soil properties.	Selection, evaluation, and monitoring of major construction sites/routes; location of construction materials.	Physical properties of soils (porosity, permeability, grain size, and shear strength); subsurface structure (primarily planes of weakness); rock type.
Geologic mapping [b].....	Long wavelength; low depression angle; synoptic	Mapping for minerals, petroleum, and	Surface texture and roughness; dielectric properties

Radar Imagery for Exploration

Information objectives	Feasibility	Research needed
Delineation of surface occurrences of economic materials (direct evidence); distribution and structure of bedrock at surface from which interpretations of structure, rock type, and possible occurrences at depth can be made.	Present active microwave systems give excellent topographic information—for example, an intrusive discovery in Venezuela shows differences exist in laboratory dielectric measurement of rocks and surficial materials.	Penetration of vegetation and soils to yield direct information on bedrock and structure; if feasible, spectral signatures of different rocks and metallic mineral alteration; image enhancement by multifrequency polarization; image ratioing; pattern recognition emphasizing texture; spectral classification; edge enhancement of structures; coordinated aircraft and ground data; coordinated data on temporal aspect of geologic information, especially snow cover and extreme moisture conditions; data on value of long-wavelength active microwave sensors (imager and profiler/sounder) in vegetated area for determining surface morphology.
"Hazy" anomalies, if real; structural traps (fault dome, etc.); stratigraphic (pinch-out and porosity) traps.	Feasibility has been established for petroleum exploration with single-frequency radar imagery —for example, location of drill sites in Colombia using commercial imagery. Offshore oil seep detection with microwave systems is underway.	Same as for mineral exploration.
Mapping aquifer and recharge areas; location of ground-water effluents; position of water table, if feasible; water quality, if feasible; surface seepage and areas of surface water/ground water; sources of ground-water contamination relative to changing land usage.	Inference can be made on most of the parameters except soil moisture detection, ground-water effluents, and water quality.	Same as for minerals and civil work; also soil moisture detection and ground-water effluents and water.
Slope stability; ease of excavation of Earth; bearing capacity; suitability of Earth materials; geologic hazards (subsidence, avalanches, landslides, and active faults); grain size and column depth of sand, gravel, and fill materials.	Feasibility has been established for grain size of soils; faults, joints, and bedding planes; and inferences concerning subsurface structure and rock type.	Low-frequency systems capable of penetrating surface to determine physical properties of Earth materials and saturated/unsaturated condition.
Distribution and structure of rocks at the surface.	Present active microwave systems provide textural and topo-	Delineation of major lithologic boundaries in areas of uniform, heavy

TABLE 2–I.—*State-of-the-Art Summary of*

Discipline	Special functional requirements	Application	Parameters to be measured or identified
	coverage; and subsatellite point profiling.	ground water; civil works; geologic hazards.	of rocks; drainage patterns, topography, and lineaments as an indicator of rock type and structure.
Landform identification and terrain analysis	Addition of a radar interferometer and perhaps a scatterometer for terrain slope data; accurate recording of depression angles across the range and, if required by a specific need, the presentation of such data directly on the image; extension of depression angle in the far range to 5° or less, if feasible; processing techniques to enable the enhancement of subtle tonal changes usually lost in radar signals in both excessively dark or light tones.	Landform identification and terrain analysis for oil and mineral exploration, civil engineering, land use mapping, land capability, soil mapping, flood prediction, and so forth.	Terrain slope; slope length; elevation; relative relief; drainage anomalies; landform distribution; surface configuration; other parameters directly interpretable by standard geophotographic techniques.

[a] Dynatrend (ref. 2–1) estimates that, at 1972 values, U.S. oil companies could save $62.5 million on the cost of reconnaissance surveys. For other minerals, industry might save as much as $12 million.

[b] The Dynatrend survey (ref. 2–1) estimates that the cumulative savings in military geology mapping, topographic mapping, and in U.S. Geological Survey regional and small-scale geologic mapping could approach $1.4 million annually.

for application to forestry, livestock, and general agriculture and that selected areas urgently deserve systematic search for mineralization.

During the fall of 1972, President Rafael Caldera of Venezuela announced a new mineral find "of great importance," including iron and possibly uranium, as a result of radar mapping in south Venezuela. The SLAR used was the Goodyear 102 system, and the imagery was contracted by a company created to promote development of southern Venezuela. Two contractor geologists were credited with the actual discovery. The imagery does not show mineral deposits but indicates to geologists where ground surveys should be made. Caldera said that the find, named "Cerro Impacto," contains a complex combination of minerals of great commercial and strategic value including a high content of iron, manganese, thorium, niobium, and radioactive materials.

Petroleum Exploration

Imaging microwave sensing for oil involves interpretation of surface geology. The interpreter relies strongly on trends that are apparent at the surface and meaningful to the particular investigation. A few of the phenomena noted and placed on the base map are the type, thickness, and attitude of formations and the fault traces and disposition. The interpreter also uses associative clues indicating structure and lithology as well as stream patterns and vegetation. Interpreta-

Radar Imagery for Exploration—Concluded

Information objectives	Feasibility	Research needed
	graphic data from which geologic maps showing rock formations and structure can be prepared.	forest cover; enhanced drainage and topographic detail areas of very low relief and flat-lying nonresistant rocks; detection of growth faults.
Radar shadow (both length and frequency); standard photointerpretation keys such as tone, texture, stereograph, site, and situation.	Research feasibility of collecting valid morphometric data has been established in mountainous terrain; operational feasibility has also been demonstrated under select situations in which standard photographic coverage and field mapping are prohibitive.	The utility of morphometric data from radar imagery in lowland areas cannot be evaluated until radar imaging systems with depression angles less than 5° are developed. Further refinements of slope-measuring techniques are needed. A complete documentation of the importance of radar image interpretation in other environments outside the tropics and the introduction of automatic interpretation are also necessary. Morphometric information from interferometer data should also be investigated (i.e., automatic slope-measurement capability). Automatic data processing techniques must be established.

tion of radar imagery is similar in these respects to that used in photogeology.

Depending on the terrain configuration, radar imagery is often superior to vertical aerial photographs for display and detection of surface features such as faults, fold patterns, and lineaments (refs. 2–4 to 2–6). Although vertical aerial photographs may more clearly reveal the smaller details of structural elements and patterns, radar imagery can often show, as well or better, the true nature and extent of structural patterns. Figure 2–2 is a striking example of the detail available on radar imagery.

Many radar mapping programs have been conducted by petroleum companies; however, because of the proprietary nature of this information, published reports are not available. Areas of extensive recent radar mapping include Brazil, Venezuela, Colombia, Panama, Nicaragua, Indonesia, New Guinea, and Australia. The only published report concerned specifically with radar mapping and petroleum exploration was completed in eastern Panama and northwestern Colombia by Wing and MacDonald (ref. 2–7). These authors concluded that "with the exception of those data provided by field investigation, the geologic information interpretable from the radar imagery of eastern Panama far exceeds those data previously available through conventional airborne reconnaissance methods." Certainly, radar remote sensing offers the only practical technique for reconnaissance mapping in the wet tropics; however, even where conventional

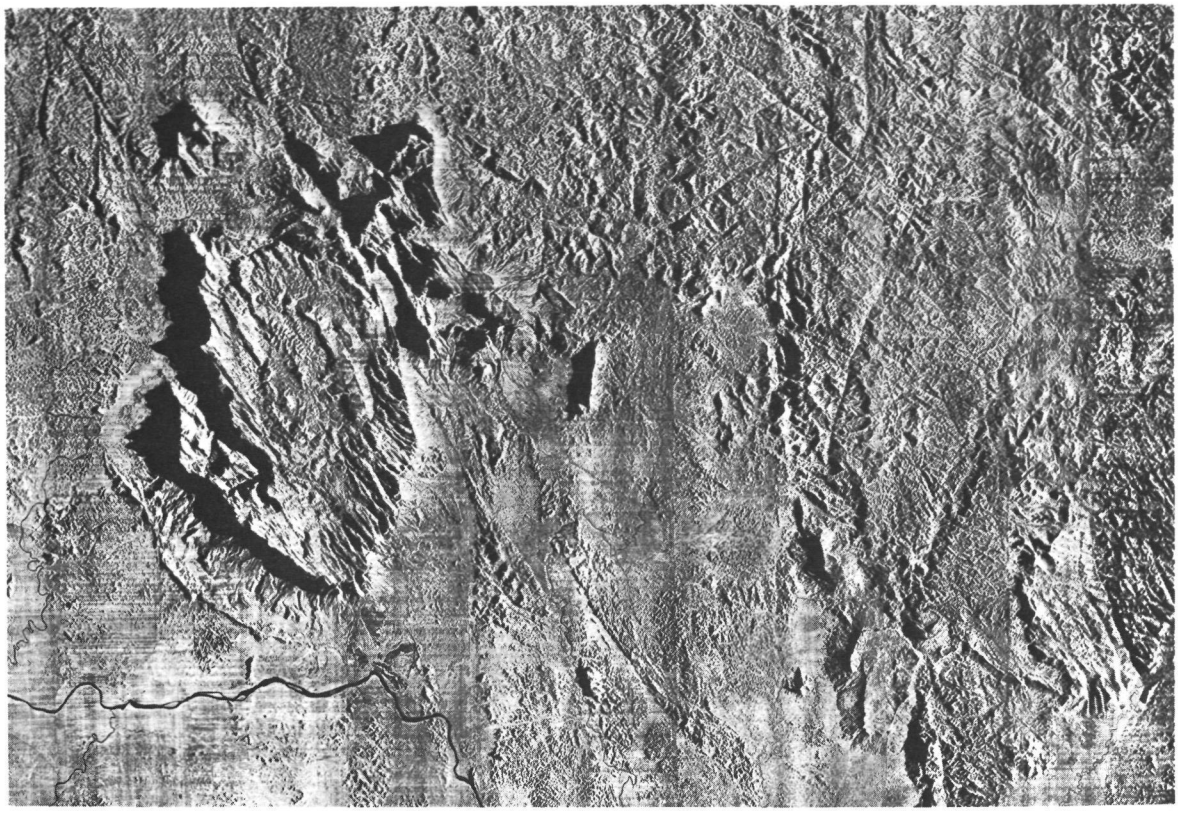

FIGURE 2–1.—Mosaic of an area in Venezuela using a synthetic aperture AN/APQ–102 radar system (31-mm wavelength).

aerial photographic coverage can be obtained, radar imagery can be a valuable supplement because of its unique data content.

Ground-Water Exploration

The overall objective of ground-water exploration is to define the geologic and hydrologic conditions relating to occurrence, quantity, and quality of ground water. The surface phenomena of interest include topography and drainage (structure and lithology), vegetation differences, soil moisture, springs, and possibly permafrost indicators (ref. 2–8). Surface hydrologic features relate mostly to those terrain parameters previously outlined. Soil moisture information would be especially helpful for locating springs or areas of seepage associated with perched water tables or faulted aquifers. Because springs and seepage areas have variations in discharges depending on the time of year, the temporal aspect of microwave coverage must be considered.

Vegetation can sometimes be a good surface indicator of ground water, especially in arid and semiarid regions. Fracture trend analysis has special application to ground-water exploration in certain terrain configurations. In the Apollo 9 photographs, the apparent coincidence of gross linears with areas of known anomalies of stream flow and of large capacity wells and springs, suggests a method for ground-water exploration (ref. 2–9).

In carbonate terrains, techniques of radar mapping in conjunction with techniques of fracture analysis for locating high-yield water wells could be substantially more effective than the usual random approach. In addition to satisfying the requirement for a

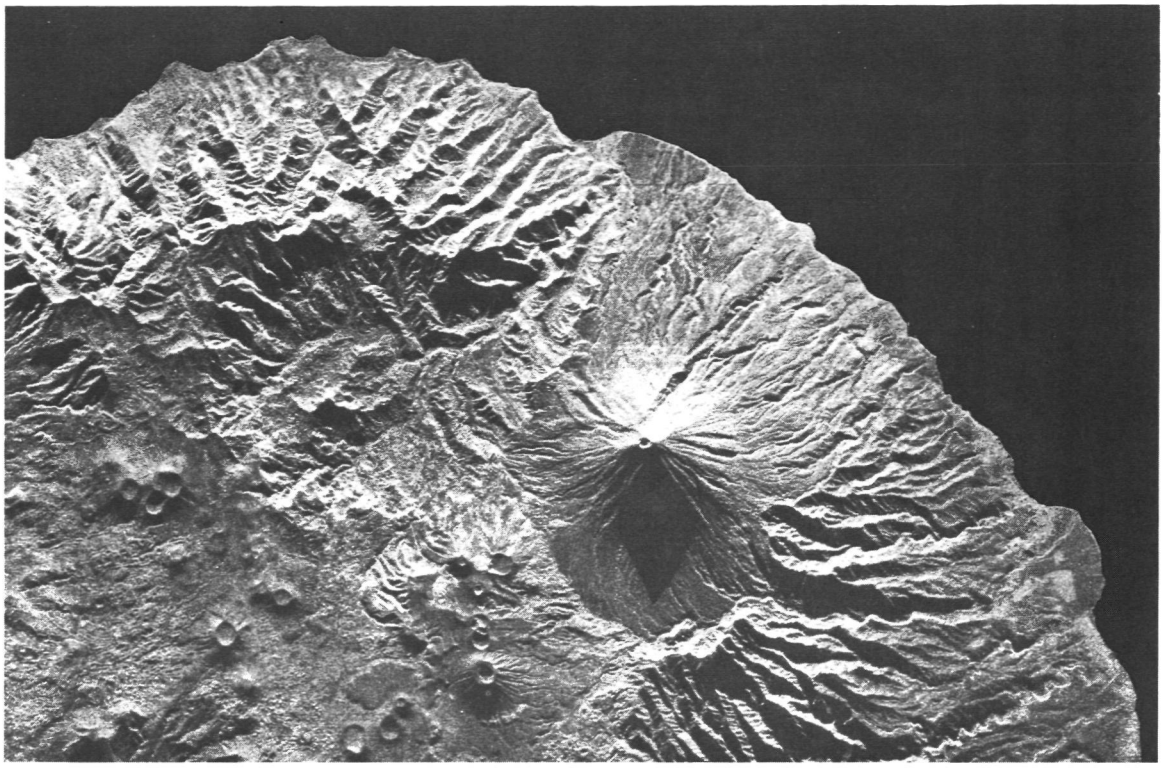

FIGURE 2–2.—Radar image of volcanic terrain on the Island of Bali, Indonesia, using the AN/APQ–102 radar system (31-mm wavelength).

rapid and synoptic terrain data-gathering technique, broad-spectrum microwave measurements of soil reflectivity provide evidence that variations in soil moisture may also be available with imaging radars. Microwave measurements are sensitive to the moisture content of the soil surface, and the potential for aiding in the detection of fracture trends is particularly appealing for ground-water exploration (ref. 2–10).

The regional applicability of using SLAR data for ground-water studies was provided by Feder and Barks (ref. 2–11). Using SLAR imagery, these investigators identified a losing drainage basin in the Missouri Ozarks by examining distinctive tonal and textural contrasts. More recently, a study by MacDonald and Waite (ref. 2–3) has shown that certain hydrologically significant characteristics of desert valleys and playas can be defined using imaging radars. For example, alluvial fans are avenues for the recharge of many valley aquifers, and localities near the toes of fan deposits generally contain important areas of water-well development. Water wells yielding moderate quantities can sometimes be drilled near the fringes of playas where coarser alluvial deposits interfinger with playa sediments. These zones of contrasting surface roughness are easily defined by shorter wavelength imaging systems.

Civil Works

In civil works, the primary goal is to improve the process for selecting and evaluating sites for major engineering projects, such as powerplants, dams, aqueducts, pipelines, and tunnels. Postconstruction monitoring is considered a necessary part of the site evaluation process.

The site selection and evaluation process involves (1) the determination of land capa-

bility for the proposed foundations and excavations; (2) the identification and assessment of risk from such geologic hazards as earthquakes, landslides, and subsidence; and (3) the nature and location of natural construction materials.

Regional analysis for site selection is often conducted by using image interpretation to rapidly identify and characterize landforms and materials. Conventional photointerpretation of imagery relies heavily on recognition of drainage patterns and associated landforms. These patterns and landforms indicate active land-forming processes, composition of unconsolidated materials, and bedrock characteristics. This type of analysis uses identification of tonal differences associated with differential Sun illumination reflectance differences of materials.

The radar shadow effect enables the effective determination of drainage patterns (ref. 2–12), which are indicative of the character of Earth materials (including grain size, weathering, and erosion characteristics) and planes of weakness. Long-wavelength active microwave sensors are especially applicable in forested areas where the signal must penetrate cover to detect patterns.

The ability of radar to effectively delineate fractures in Earth materials is well documented (refs. 2–2 and 2–13 to 2–16). In engineering geology, investigations of this capability pertain to earthquake risk assessment (ref. 2–17) and to identification of surface fracturing, which is incipient to subsidence and landsliding. In addition, information on terrain slopes and individual geomorphic features has been demonstrated by Lewis (ref. 2–18). Other possible applications include the use of low-frequency radar to determine the depth to the water table or the overburden depth; however, these applications have not been demonstrated.

Radar reflectance differences permit the identification of surficial Earth materials (refs. 2–3, 2–19, and 2–20). In civil works projects, this property applies to soil mapping, the location of construction materials (sand, gravel, fill), and identification of recently deposited stream alluvium as a means of assessing flood hazards. The usefulness of active microwave sensors for engineering soils interpretation has been summarized by Barr (ref. 2–20).

1. It is possible to interpret regional engineering soil types from SLAR imagery by means of an inference technique based on recognition and evaluation of repetitive characteristic patterns. The SLAR imagery shows pattern elements, average areal tones, and image texture, which, in various combinations, form SLAR image patterns indicative of specific terrain surface conditions.

2. The extent to which inferences can be made concerning local land-surface conditions such as surface roughness or vegetative cover is governed by the dynamic range of tone values expressed on the imagery.

3. The systematic SLAR image interpretation technique provides a logical basis for interpretation of engineering soil types and insures results consistent in derivation. The confidence with which an interpretation can be made is greatly increased if adequate field data are available. The technique attains a maximum usefulness if used to extend knowledge from areas with known conditions.

4. The relatively small scale at which SLAR imagery is obtained and the resolution of typical imagery are considered advantageous for regional engineering soils interpretation. A synoptic view of terrain, unconfused by minor tonal contrasts, is afforded by SLAR imagery.

The use of radar imagery in conjunction with photographic systems for civil works site selection and evaluation is desirable because it can provide more information on materials and landforms than conventional aerial cameras. More information is provided for these reasons:

1. Microwave signals are strongly dependent on composition of the illuminated area, moisture content of materials, and surface roughness of materials.

2. Vegetation associated with materials

can be eliminated or enhanced by selection of appropriate microwave wavelengths.

3. Terrain can be differentially illuminated by side-looking radars, thus enhancing landform and drainage patterns.

4. Active microwave sensing is time and weather independent.

Geologic Mapping

The geologic map is the basic foundation from which interpretations and recommendations can be made that concern the discovery of mineral and oil accumulations, delineation of geologic hazards, planning of civil works, reclamation, and many other applications.

The geologic map is a compilation of rock-type distributions (mostly represented by "formation," the mapping unit of the geologist) and of geologic structure. Rock types are generally separated on the basis of composition (lithologies) and orientation at the surface (many are tabular and it is important to determine their degree of inclination from the horizontal). From this map of the attitudes and distributions of various rock bodies, particularly as they indicate folding and faulting, the geologist makes interpretations of the geology beneath the surface. These interpretations at depth lead to recommendations for drilling and geophysical surveys to gain more detailed subsurface information that can lead to discovery and later exploitation of buried mineral and oil deposits.

Geological maps are compiled from mapping on the ground, from photogeologic analyses of aerial and satellite photography, and from radar imagery. When possible, the geologist uses all these techniques. Though mapping on the ground ultimately provides the greatest amount of detail and is the most accurate, it is also the most time consuming and not the most efficient method for reconnaissance. Satellite imagery has its greatest value at the reconnaissance level.

The ERTS and Skylab results indicate that much of the geologic information obtained is through geomorphic analysis, primarily of topography and drainage patterns. Though this satellite imagery provides an excellent map basis because of lack of distortion, adequate mapping can be restricted because of low resolution, poor weather, single look direction, heavy vegetation, low relief, and so forth. Radar has demonstrated its capability for providing detailed physiographic information that is free of most of these adversities and that has a choice of look direction and angle.

Utilization of satellite altimetry over land regions permits profiling the subsatellite point. This was attempted with the S193 altimeter aboard Skylab. Figure 2–3 shows a pass over the Midwest States. The altimeter profile is compared with topographic maps over the same groundtrack, and the correlation is extremely good.

Future uses of this concept will enable topographic mapping of remote regions. In addition, with accurate tracking of satellites, the topographic features can be positioned with accuracies equal to or better than conventional means.

The task of the interpreter using microwave remote sensing for geological analysis is to identify features (such as faults, folds, and lateral changes in rock units) exhibited or reflected by the Earth surface and faithfully reproduced in the imagery. Like photogeology, microwave terrain data interpretation is an attempt to understand geologic conditions, the existence of which can be inferred from radar image analysis of stream patterns, soil textures and patterns, lineations, shapes of hills and valleys, and the presence or absence of specific vegetation types. Some geologic features are so clearly expressed in their landform configuration that they can be identified directly; the nature of other geologic features can be determined only by ground examination. The extent to which geology can be mapped from microwave remote-sensing terrain data varies considerably, depending on the geologic and geomorphic characteristics of a region, the climate and density of vegetation, and the amount of surficial debris. Regardless of the sensor used, the principal kinds of geo-

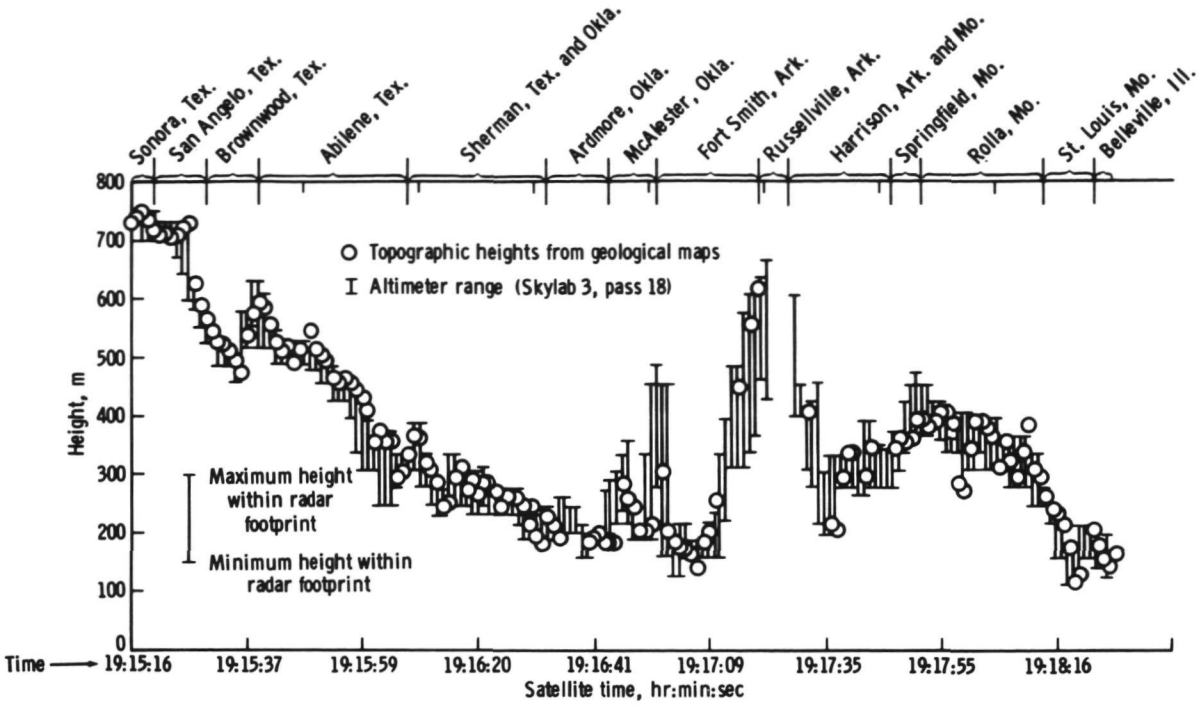

FIGURE 2–3.—Topographic heights from Skylab altimeter (Skylab 3, pass 18) compared with topographic heights from geological maps.

logic mapping information may be broadly grouped into two categories: lithologic and structural.

A few of the more important surface parameters of prime concern for making lithologic inference are—

1. Topography and microrelief.
2. Material type and texture.
3. Vegetation cover, type, and extent.
4. Moisture content, permeability, and porosity.
5. Unit thickness and stratification.

Published regional and localized lithologic studies using imaging radars have been conducted in California (ref. 2–21), Arizona (ref. 2–22), and Panama (refs. 2–3, 2–23, and 2–24). The practicality of using an imaging radar for regional lithologic mapping has also been demonstrated in many unpublished mapping programs in countries such as Nicaragua, Brazil, Colombia, New Guinea, and Venezuela.

Identification of rock types with airborne or spaceborne sensors has long been a goal that consistently remains elusive. The accuracy of a geologic map is generally dependent on selecting rock units that have sufficient areal extent to be significant and that are distinctive enough on the radar format to be easily mapped. In those regions where broad expanses of rock are exposed and/or are closely reflected in the terrain configuration, generalized rock types and regional facies changes in major sedimentary units might be mapped from evidence presented on a radar data format. However, in those areas having the combination of low relief and heavy vegetation or mantle cover, or in areas having poorly exposed rock units, diagnostic or suggestive lithic criteria may be completely absent. Previous lithologic data interpreted from radar imagery have been derived from surrogates rather than through direct identification.

Geologic structures frequently exert a strong influence on surface topography. As with photointerpretation, structural analysis

with radar is an attempt (1) to mark attitudes, distribution, continuity, and discontinuity of key horizons, and (2) to deduce the structural relationship from this information. Resistant relief-forming strata usually provide good key beds; however, any horizon that can be traced over a sufficiently large area will generally provide a satisfactory marker bed. Structural discontinuities, such as fractures, joints, and faults, are generally more easily eroded than surrounding rock, which results in linear segments (usually depressions) in the landscape. Consequently, the analyses of drainage, lineament, soil texture, and vegetation patterns help corroborate any structural interpretation. Recording of slopes and slope changes on various landforms is important in deducing a coherent structural picture.

Where topographic relief is great, the oblique angle of illumination of an imaging SLAR system can cause extensive shadowing, which may be a detriment to structural interpretation. However, there is no doubt that, in low-relief areas, the highlight and shadow effect tends to enhance subtle terrain features such as fault and joint patterns.

The most significant radar study of structural features was provided by Wing (ref. 2–25). This comprehensive investigation shows the usefulness of SLAR imagery when other terrain data were limited or not available.

An airborne radar image strip may be several hundred kilometers land and tens of kilometers in swath width. This strip gives the interpreter a synoptic view of the terrain and aids him in making regional geologic generalizations, which are a necessary preliminary for selecting areas for more detailed study.

All geologic data, from whatever source, are plotted on planimetrically accurate base maps. When good topographic base maps are available, radar imagery can usually be correlated with the topographic map. Hence, any geologic data and interpretations can be transferred to the base map by inspection. However, in areas in which base maps are poor or nonexistent, a rectified radar image is needed to provide the necessary planimetric base maps. In conducting mineral exploration, for example, it was found that there were no reliable maps of interior New Guinea and that aerial photography could not be obtained because of perpetual cloud cover. The SLAR imagery was obtained, which provided a drainage base map that finally enabled the pursuit of ground reconnaissance.

Three research areas are suggested to aid in the preparation of improved geologic maps using active microwave sensors.

1. The delineation of major lithologic boundaries is needed in areas of uniform, heavy forest cover. For example, in the Black Hills region, it is impossible to separate the Precambrian rocks from the Paleozoic rocks with any confidence when using any of the available photographic imagery. Analysis of ERTS imagery has shown that perhaps there are textural differences in the topography on the two major rock types, but the low spatial resolution is a hindrance to a satisfactory study. The higher resolution of Skylab may help, and analysis is currently being conducted. Unfortunately, Skylab coverage of the Black Hills is incomplete. Radar imagery might provide a better textural distinction between the Precambrian crystalline rocks and the younger sedimentary rocks and between the granitic and schist terrains within the Precambrian core. The economically valuable pegmatites, iron formations, and gold deposits are found in the Precambrian rocks. The ability to outline such areas of potentially valuable crystalline rocks in other regions would greatly assist mineral exploration. The ability of radar imagery to provide lithologic information in much greater detail than that obtainable from ERTS imagery has been shown in the heavily forested Amazon region.

2. Enhanced drainage and topographic detail is needed in areas of very low relief and flat-lying nonresistant rocks. Examples are the Powder River Basin and the Big Horn Basin. Satellite imagery is unsatisfactory

for revealing structures buried beneath the Eocene and younger rocks. Attempts have been unsuccessful in locating deeper domes and anticlines by using aerial photography to find drainage anomalies at the surface. Radar imagery using a low look angle and multiple look directions could provide much greater detail. A more important aspect, particularly in the Powder River Basin, is that many of the known buried oil traps are stratigraphic, which, in turn, may be related to major buried faults. These faults are not always expressed at the surface (or at least have not been identified), but their presence may possibly be detected by subtle features at the surface. Economic accumulations of oil are associated on the side of the fault where porosity has developed in dolomitized limestones. Many of these deep faults have been active several times in the geologic past and have affected the thickness and distribution of sedimentary facies, which are factors influencing the occurrence of oil. Therefore, any means of detecting these deep faults at the present surface has great economic value.

3. Detection of growth faults is needed. These faults are well-known features in the Gulf Coast and similar geologic environments, but active ones are not always easily recognizable on the ground or are not readily apparent in photographs. Growth faults are important in the localization of oil traps and have important implications in urban areas where they are breaking through roads, pipelines, and other types of construction. Again, radar imagery might reveal these features better than any other means.

Landform Identification and Terrain Analysis

Landform identification and terrain analysis (geomorphology) is a discipline that has applications in geologic exploration, civil engineering, soil mapping, land-use planning, and water resources management.

Most geomorphologists are interested in describing or identifying landform features or regions and understanding the processes responsible for shaping the landscape. This study can be qualitative or quantitative. Radar imagery is extremely helpful in either approach. Qualitatively, radar imagery can be used for regionalization of landform units as well as for identifying individual landform features. Quantitative landform data, relative relief and slope, can also be determined by using inherent radar distortions, radar foreshortening, shadowing, and, to a lesser degree, layover and parallax.

Regional geomorphology.—The texture, pattern, and shapes of the radar shadows resemble a typical Raisz diagram of the region and allow accurate and easy delineation of discrete landform units. Landform units mapped on radar have been found to agree well with units derived from topographic maps (refs. 2–18 and 2–26). In fact, along a proposed sea-level canal route in Panama, the agreement between map-derived and radar-derived units was remarkable. When only three landform units (plains, hills, and mountains) were compared, more than a 90-percent agreement was found in all cases (fig. 2–4). Exploration geologists have used the same surface expression, so evident on radar imagery, for the location of possible mining sites. Bauxite deposits have been discovered in Brazil by correlating terrace units having known bauxite deposits with previously unmapped terraces delineated on radar images. Other lithologic units have considerable surface expression characteristics and can therefore be mapped as geomorphic units.

Individual features.—Many geomorphic features are detectable on radar imagery. Some features are of interest to exploration geologists; for example, ring dikes, plugs, faults, fractures, calderas, shell bars, estuarine meanders, and drainage patterns. Evidence of glaciation (ref. 2–27), stream piracy (ref. 2–28), coastal erosion and deposition (ref. 2–18), and karst topography (ref. 2–24) have also been reported.

Quantitative geomorphology.—The accurate description of landforms is the first step in any geomorphic study. The three most

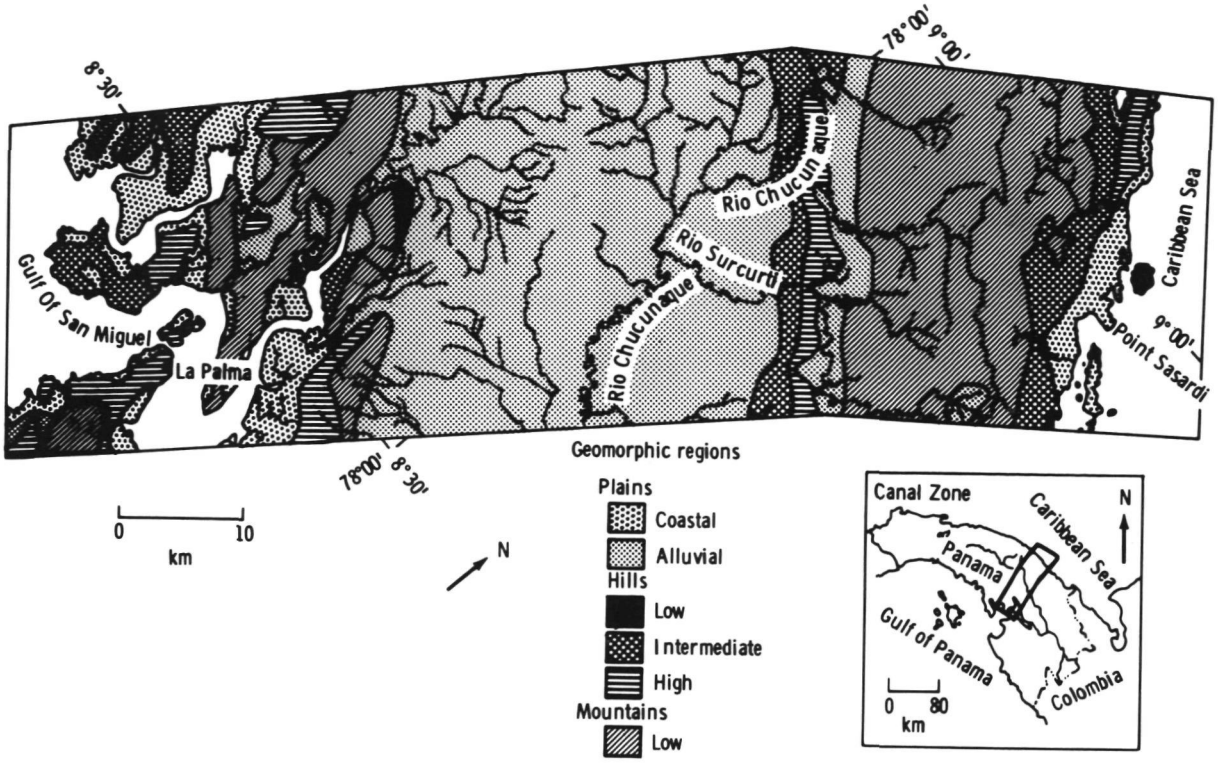

FIGURE 2–4.—Radar-derived geomorphic regions in area of possible route for sea-level canal in Panama.

important vertical dimensions used in landform analysis are elevation, relative relief, and slope. Of the three dimensions, slope is most widely used. By using inherent distortions of radar imagery (such as radar foreshortening, parallax, layover, and radar shadowing), relative relief and slope data can be collected (fig. 2–5).

Although active microwave sensing can, in some cases, be used to determine individual slope values, its real value concerns the determination of slope-angle distribution on a regional scale. Radar foreshortening (ref. 2–29), radar shadows (ref. 2–30), and radar power return (ref. 2–18) have all been evaluated as a source of slope data by comparing the radar-derived data with map-derived data. The studies referenced met with varying success, although radar layover and parallax are, in part, slope dependent and therefore are a potential source of

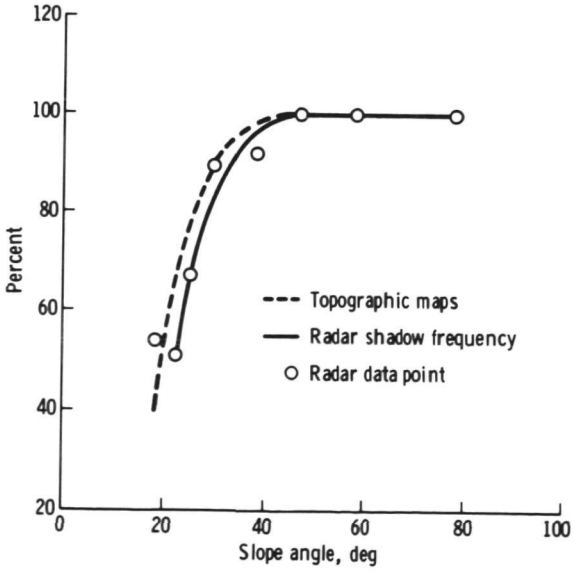

FIGURE 2–5.—Cumulative frequency curves of map-derived and radar-derived terrain slope α data (Annamoriah, West Virginia).

morphometric data. The difficulty of accurately measurable layover and parallax on radar imagery is a severe limitation.

The most practical source of morphometric data is radar shadowing. Although radar-derived slope data can be obtained for all types of terrain, shadowing is prominent. Radar foreshortening is most practical in moderate- and low-slope regions. However, foreshortening is limited by the extremely fine accuracy required by the foreshortening equation (ref. 2–18).

The use of radar power return as measured from radar image tone was tested as a source of slope data and met with little success. Although there is a linear correlation between radar tone and power return (ref. 2–31), the assumption that vegetation remains constant is impractical. However, using radar scatterometry and/or interferometry data would eliminate the problem and presumably make the measuring of terrain slope from interferometry power return a viable application.

The determination of relative relief is a logical extension of any slope-measuring method that requires the slope length as a known parameter; namely, radar foreshortening and radar layover. However, radar shadows can be used to measure relative relief by measuring shadow length instead of frequency. Of all the methods evaluated, shadow length was the most accurate, having a correlation coefficient value of 0.86, when compared with map-derived regional values.

Geomorphic summary.—The qualitative regionalization of landform regions and subsequent measuring of regional and individual morphometric parameters is of special value to the environmental geologist/physical geographer because it provides insight into landscape dissection, terrain surface roughness, and terrain mobility. The exploration geologist should be able to relate landform morphometric data to stratigraphic and lithologic units and to regional anomalies.

Earthquake Mechanisms and Crustal Motion

General objectives.—Measurement of solid Earth strain patterns may lead to a further understanding of earthquake mechanisms. It is of special interest to measure strains on a repetitive basis because the repetitions and accuracies are capable of discerning horizontal and vertical displacements of the surface that precede earthquake activity. Such premonitory strains are well known when on a large enough scale and near a natural or manmade gaging system—for example, the shoreline tilts recorded in Japan. Smaller scale motions (or those motions occurring in areas with no benchmarks for comparison) may occur often but remain undetected.

In particular, the phenomenon called dilatancy, a volumetric dilation of rocks ready to fail and generate an earthquake, has been described from observations in the Kuril Island chain by the U.S.S.R. Such a dilation should be accompanied by a vertical rise of the land surface above the volume affected. The extent of the rise is variously estimated to be between approximately 1 mm and 1 m, and undoubtedly varies from case to case, if, in fact, it occurs in a significant percentage of cases.

Vertical motions over large areas would tend to remain undetected if the strain is distributed broadly and neither local cracking nor tilting is involved. If an inland area were to rise a meter or more and the strain were distributed fairly uniformly over regions with dimensions of approximately 1000 km, the only effects would be similar to Earth tides and would rarely be detected. Although several programs are now in operation or are being planned to monitor horizontal strains, very few projects have been undertaken to monitor tilts or vertical changes, and no projects have been initiated to monitor the vertical positions of dozens of points in an area of earthquake interest. A system that could measure the relative elevations of numerous points on the Earth surface to an accuracy of a few centimeters would complement the existing horizontal ranging sys-

tems and could provide data necessary for a test of the hypothesis of dilatancy. One possible system would involve the principle of multilateration to numerous targets from aircraft or perhaps spacecraft.

Users of such data would be consulting engineering geologists and municipal, State, and Federal agencies. The end users are municipal, county, and State planning boards, the engineering and architectural professions, insurance underwriters, disaster-fighting operations, and others.

Functional requirements and discussion.— To secure measurements of dilatant uplift and the effects of strain, a system is required that enables relatively inexpensive portable devices to be moved from benchmark to benchmark over wide expanses of mountain and desert. These devices could facilitate establishing positions with true accuracies of 1 to 4 cm in three-dimensional space. Operators could know immediately when they have obtained useful results, without waiting for elaborate and costly computer reduction.

In analytical efforts to date, various methods of determining relative movement of non-line-of-sight points on the Earth surface were investigated: radar, distance-measuring equipment (DME), multilateration, and interferometry. Tradeoff analyses of each method support a final system choice of a unique multilateration scheme using active two-way microwave distance measurement. The system could use an aircraft platform that collects distance-measurement information of earthbound markers. Radar and electronic hardware either presently existing or currently under commercial development almost certainly will enable a suitable system to be built that is capable of 1- to 4-cm accuracy in three dimensions to relate benchmarks in local networks of precision survey points to a larger scale regional grid in which the grid points are established by another technique, such as satellite tracking. Such a system is described in appendix 2A.

GENERAL FUNCTIONAL REQUIREMENTS

Frequencies

The use of simultaneous multiple wavelengths appears to have great potential in the microwave remote-sensing field; however, examples of terrain applications are few because only a limited amount of multifrequency radar imagery has been available to the geoscientist. The obvious need for information on signal penetration exists where vegetation or a thin soil cover masks shallow outcrop patterns. In semiarid and arid terrain environments, the applicability of longer wavelength radars has been noted. For example, two multifrequency studies were conducted at the Pisgah Crater area in California (refs. 2–32 and 2–33). Both authors have recognized the surficial-cover-penetration potential of relatively long-wavelength imaging systems and note the necessity of obtaining simultaneous multiband coverage.

Many investigators have proposed using multiple frequencies to take advantage of the varying amounts of penetration or the change in roughness relative to wavelength. Most investigators have proposed as broad a coverage as is practical and consistent with orbital operation. On the high-frequency end, 35 GHz seems a reasonable choice in view of the difficulties encountered with atmospheric absorption and scattering at higher frequencies. This choice is consistent with equipment availability because considerable microwave work has been performed at this frequency.

A variety of low frequencies has been proposed ranging from 400 MHz to approximately 2 GHz. In general, proposals have been made to extend to the lowest practical frequency for orbital synthetic aperture operation. Limitations will depend on the phase resolution required and will probably be a tradeoff between the effect of Faraday rotation and the length of the synthetic aperture required for the desired ground resolution. The range of 30 cm is probably a reasonable choice. The utility of low-frequency data cannot be assessed at this time

because few data analyses in this frequency range have been performed. Data required by the Environmental Research Institute of Michigan (ERIM) L-band system should, if widely disseminated, remedy this situation. The major reason for requesting low-frequency data has been the desire to increase penetration, particularly through vegetation, and to decrease the effects of roughness.

The upper and lower frequencies are principally chosen from considerations of operational constraints. Virtually every investigator has recommended at least one intermediate frequency, and this choice seems to consistently fall in the X-band region because of a combination of data and equipment availability. This choice is questionable. If use is to be made not only of the differing information at each frequency but also of the variation in scattering due to frequency change, the data must be compared with some type of predictive model. The bulk of the models that may be used for this purpose predict a variation in return at different frequencies proportional to some function of the wavelength ratio. If this criterion is used and limiting frequencies of 1 and 35 GHz are assumed, the choice for a single intermediate frequency would be approximately 6 GHz, which is very dependent on the low-frequency limit. For example, using limits of 0.5 and 35 GHz would give a middle frequency centered on 4 GHz. The literature available in the area of soil moisture prediction with microwaves indicates a need for using the lowest practical frequency. This consensus tends to favor 4 GHz as a more reasonable choice of intermediate frequency.

Even a simplified argument such as that presented here shows the need for additional investigations in the frequency dependence of the scattered return before selection of frequency parameters. If possible, this investigation should be conducted not by funding one or two investigations of frequency dependence, but by making available to a wide variety of investigators imagery taken at frequencies other than the traditional X- and Ka-bands. This procedure would serve to possibly uncover new applications and to insure that the data are evaluated for several different applications in widely different disciplines.

Resolution

Because of the coherent nature of the illumination with active microwave sensors, no determination of resolution can intelligently be made without simultaneously considering scintillation and scale. For example, a 10-m resolution in a radar imaging system is not equivalent to a 10-m resolution in a photographic imaging system. If the radar sensor is assumed to be a fully focused synthetic aperture system, a single 10-m resolution cell from a homogeneous population represents only a single sample from a randomly varying distribution, which, in the case of Rayleigh fading, has a 5- to 95-percent range of approximately 18 dB. Thus, obtaining a reasonable estimate of signal intensity (or gray tone) requires the averaging of numerous independent samples. This averaging, in turn, decreases the effective resolution of the system for the sensing of area-extensive targets. However, for a photographic system with a listed 10-m resolution using panchromatic illumination, the signal intensity of a single cell is the sum of the contributions from many independent samples spaced in frequency. The gray tone of a homogeneous region is thus even, and the effective resolution is essentially the same as the listed system resolution.

The image scale is a consideration because it is the most frequently used means of performing the required averaging for fading in the radar image. In a small-scale format in which the image resolution cell is not resolvable by the eye, the eye will perform the necessary averaging. However, on magnification, the image will start to break up and exhibit graininess as the visual resolution approaches that of the image. Assuming a 10-m, fully focused, synthetic aperture system and taking 16 cells as the necessary number of independent samples, the effective resolution is actually 40 m. Thus, scale may

be adjusted only to match this figure with the visual resolution of the interpreter. Any magnification beyond this point is useless in the interpretation of area-extensive targets.

An example of the confusion caused by this effect may be cited from the two major systems currently flying commercial radar imagery. Both have system resolution listed as 10 m; however, one is a synthetic aperture system, and the other a real aperture system. The real aperture operation provides some averaging; thus, the effective resolution is somewhat better. This result may best be seen by magnifying imagery from both systems to larger scales where the breakup occurs at a slightly larger scale, or increased magnification, for the real aperture system.

In summary, the specification of resolution should be in terms of the effective resolution with consideration given to the statistics of the fading return. It would also be helpful to the individual investigator to transform this need into a specification of largest usable scale. The "user" evaluation of variable-resolution radar systems has not received adequate research support.

Dellwig has provided some information by attempting to define the geologic utility of variable-resolution radar (refs. 2–34 and 2–35). The amount of topographic detail recorded on relatively high-resolution radars provides increased detectability of specific terrain features; however, specific geologic utility has not been demonstrated. Certainly an increase in the number of lithic or structural units inferred from a radar format would improve the geologist's interpretation; however, Dellwig and McCauley (ref. 2–35) concluded that, in regional or large-scale studies, coarser resolution appears to be more desirable.

General

Spectral resolution can have two widely different interpretations. First, it can refer to the specification of multiple discrete frequencies to adequately describe the variations over the spectral region of interest. Second, as exemplified in the panchromatic visual imaging system, additional independent samples may be obtained in the frequency domain and averaged before image formation. In this case, the spectral resolution (or system bandwidth) could be significantly greater than that associated with the equivalent pulse length for the 10-m-range resolution.

The first specification is, of course, intimately related to the specification of the operating frequencies. In fact, the specification of three discrete frequencies implies sufficient knowledge of the target spectral response and frequency correlation function to determine that three independent frequency samples are all that are contained in the spectral region of interest. The discussion in the section entitled "Frequencies" should demonstrate that this knowledge is not available and that the selection of the number and value of discrete frequencies is little more than an educated guess.

To intelligently select the number and value of operating frequencies requires definition of the spectral response for the range of targets of interest. This task would best be accomplished by performing continuous frequency measurements over the frequency range of approximately 0.5 to 40 GHz and over all classes of targets. Alternatively, this task requirement could be better defined with wide dissemination to several different disciplines of multiple-frequency imagery acquired over target areas of interest. As noted earlier, the only widely disseminated imagery at this time is at the X- and Ka-bands. Little of this imagery is available over the same areas, and it is not acquired at the same time.

Obviously, the acquisition of calibration curves of continuous spectral response over all possible targets is impossible; however, it appears essential that this type acquisition be performed for at least a limited number of target classifications. These data may then be extrapolated to additional targets when simultaneous multiple-frequency im-

agery is available to investigators from a variety of disciplines.

Analysis of the ERIM simultaneous X- and L-band data will undoubtedly help clarify this problem. However, care should be taken not to be unduly influenced by a limited analysis of these discrete frequency data for a single restrictive objective such as moisture detection. If the results obtained from this system are to be one of the principal criteria for the determination of operating frequencies, these data should be made available to a much wider community of potential investigators.

Temporal

Seasonal variations provide contrasts in the geological information available on ERTS imagery. In addition, snow-enhanced ERTS imagery has proven to be of value for geologic mapping. Although snow enhancement provides a mechanism to increase the geologic utility of visible- or near-IR imagery acquired by terrestrially oriented satellite systems, this effect may not be true for microwave systems. Waite and MacDonald (ref. 2–36) have noted that subtle landform features may be completely obliterated on radar imagery if specific kinds of snow cover are present. However, seasonal variations do enhance the information in radar images (e.g., the imagery of woodland swamps with defoliated tree cover as compared to trees with full foliage) has been noted (ref. 2–3). In general, the temporal aspect of gathering microwave terrain data has not been well documented.

Dynamic Range

As discussed previously, the tradeoff with resolution involves the variance of the return (or the effective resolution of area-extensive targets). Any tradeoff of spatial resolution to compress the dynamic range of the already-averaged signal intensity would be a serious mistake.

Unquestionably, the dynamic range of the return far exceeds that of the image film; thus, compression of the dynamic range is a necessity in most instances. The dynamic range of the return signal, even without considering fading effects, is from 50 to 60 dB, whereas the image film can accommodate only approximately 20 dB. Obviously, if the full dynamic range of the signal is compressed to that of the film, it will only be at the expense of intensity (amplitude) resolution.

Current imaging systems do not attempt to display the full dynamic range of the signal return; data loss occurs at both the high and low extremes. The center range is controlled by some form of slow-response automatic gain control (AGC), which centers the mean signal intensity of the scene in the center of the film range. In most instances, this technique works acceptably; however, there are important exceptions. The return from old snow (or firn) has been shown to saturate the film of the APQ–97 system in virtually all cases. However, the returns from relatively smooth surfaces, such as playas, sand bars, and so forth, have been shown to be below the film sensitivity threshold. To include these extremes in the image dynamic range would seriously affect the intensity resolution and thus many other applications using midrange variations in intensity. For instance, applications such as soil-moisture detection or crop identification require the distinction of subtle tonal changes caused by signal variations of approximately 1 to 2 dB. Decreasing the intensity resolution of the image would completely obliterate many of the boundary distinctions that can be made with the currently available imagery.

The best solution to this problem appears to be either control of the dynamic range compression or, preferably, control of the portion of the signal dynamic range presented on the image film; that is, in essence, control of the AGC so that midrange signals could be permitted to saturate when it is desirable to view extremely low amplitude variations with good intensity resolution. The same technique in reverse could obvi-

ously be used to view high-amplitude variations in the return from firn while permitting the midrange variations to go below the film threshold.

Because orbital active microwave imaging systems will almost certainly use a synthetic aperture, implementation of this type control may be done with multiple processing of the image film. However, this does imply that preprocessing of the received signal will not sacrifice the dynamic range of the signal. Thus, any techniques for onboard preprocessing before downlink transmission to conserve information bandwidth should be weighed against the possible degradation of the inherently large dynamic range present in the Doppler return compared to that used in the formation of a single image.

Polarization

The potential value of simultaneously recorded like- and cross-polarized radar return was demonstrated by Dellwig and Moore (ref. 2–21), who made a preliminary evaluation of anomalously depolarized return signals in the Pisgah Crater area. About the same time, Morain (ref. 2–37) noted that the relatively uniformly textured and even-toned return from the vegetation on the like-polarized return was separable into areas of variable tones on the cross-polarized return. The degree of depolarization was directly related to vegetation type, the area boundaries paralleling those defined by the U.S. Forest Service map.

A better defined capability of dual-polarized radar is in the revelation of a qualitative estimate of soil moisture content by MacDonald and Waite (ref. 2–38). These two authors, utilizing like- and cross-polarized returns, discriminated between wet and dry areas in the near range in portions of the Gulf Coast with sufficient accuracy to warrant further investigation of this capability. Realizing the high degree of correlation between the electrical properties of soil and soil-moisture content, indications are that areas of permafrost in the Arctic regions could be easily delineated in a similar manner. Definition of soil-moisture content having been achieved with Ka-band imagery suggests an even greater potential for determination of soil moisture content for the as-yet-untested long-wavelength microwave systems.

Depression Angle

For geologic practicality, it is assumed that the most significant and immediate contribution of active microwave imaging sensors will be in those geographic regions containing relatively inaccessible, poorly mapped, mountainous terrain where photography cannot be obtained. However, data presented in a recent study by MacDonald and Waite (ref. 2–38) reveal that, for certain terrain configurations, the amount of retrievable geologic information will be of marginal utility unless the geometry of both the imaging system and the terrain is carefully considered.

In low-relief areas, the oblique illumination and resultant shadowing by imaging radar can generally provide enhancement of topographically expressed geological features; however, in mountainous terrain, radar shadowing can deter geologic interpretation. Especially in rugged terrain, two inherent disadvantages of a radar imagery format that can hinder geologic interpretation are extensive shadowing and layover. Radar depression angle and terrain slope define the range over which shadow and layover will occur, but the extent of either parameter is defined by relative relief. From most operational side-looking radar systems, the interpretive data loss increases as terrain slopes exceed 35° and local relief surpasses 1000 m. Tradeoffs between loss of geologic data caused by radar shadow and layover as compared to swath coverage should be evaluated. Similarly, the advantage of slight radar shadowing in low-relief areas should be considered.

The selection of the depression angle ranges in high-relief areas should be biased slightly toward the higher values, which will increase the occurrence of layover but de-

crease the occurrence of shadowing. The justification for this approach is that in such high-relief areas the near-range slope is severely foreshortened, whereas the far-range slope is presented near its true length. The slight intentional bias toward layover is introduced to sacrifice the least usable portion of the imagery.

The tradeoff decisions for selection of optimum depression angles is considerably easier for the categories with lower slope and relief. The probability of obtaining both layover and shadowing near the same angular range is less, and the decisions involve more the extent of shadowing desirable. In the lowest relief areas, shadowing is deliberately introduced to provide topographic enhancement.

It is apparent from the preceding discussion that an aircraft imaging system designed to maximize geologic data gathering should be capable of high-altitude operation and coverage of a range of depression angles from 10° to 55°, with a minimum elevation beamwidth of 20° to 25°. The adjustment of depression angle may be made by using an antenna with a broad elevation beamwidth that spans the entire range with the area imaged varied by adjustment of time delay and sweep rate. A higher gain antenna with a minimum elevation beamwidth of 20° to 25° could also be used with a mechanical drive system capable of varying the antenna pointing angle by approximately 25°. A spacecraft imaging radar system, although having the advantage of increased coverage for a small range of depression angles, should also be capable of a similar range of adjustments.

Look Direction

Because of the large areal coverage, SLAR imaging systems enable the eye to integrate subtle topographic differences over long distances. This synoptic presentation in conjunction with an oblique angle of incident illumination provides enhancement of topographic features that are not evident on conventional aerial photography, even when viewed stereoscopically. Thus, the geologist is able to see the terrain portrayed in a configuration that is normally not available to him. Many examples have been cited in the literature in which radar has actually defined structural features such as lineaments and faults, which had not been previously detected by using normal geological reconnaissance methods (refs. 2–14, 2–22, 2–34, and 2–39 to 2–42). Multiple-imagery passes were not available for most areas previously studied; therefore, the capability for repeatedly recognizing these anomalous geologic features on multiple-imaging passes and the influence of a preferred look direction (direction orthogonal to the groundtrack of the aircraft) could not be investigated. However, the availability of multiple flight coverage from eastern Panama and northwestern Colombia provided sufficient data for a semiquantitative look-direction analysis in which the detection of certain geologic features under a variety of terrain conditions could be examined.

Depending on the relative topographic relief, effective incident angle, and look direction, geologic features can be advantageously enhanced or can be completely suppressed. Maximum data retrieval from radar geological reconnaissance in poorly mapped areas necessitates imaging the specific region from two orthogonal look directions (ref. 2–43).

The effect of look direction on the detectability of linears in radar image data using a spatial frequency analysis technique, which uses a coherent-optics system, has been presented in a quantitative fashion by Eppes and Rouse (ref. 2–44). The authors concluded that the detectability factor of off-normal features can be improved by spatial filtering in the Fourier plane of a single look-direction image. A much less complicated and certainly more practical technique (image presentation or format still retained) for detecting linears can be achieved by using the widely accepted and inexpensive Ronchi grating (ref. 2–45). The Ronchi grating has been used as an effective method for determining geologic structure from radar im-

agery in coal-mining areas of Virginia (ref. 2–46). Radar imagery viewed through a Ronchi grating reveals lineaments enhanced by diffraction image overlap only when the grating lines are perpendicular to the lineament direction. The frequency and spacing of linear features determine the degree of enhancement. Because the linear trend is always added to the spurious images produced by objects with no actual alinement, the lineament direction is always more conspicuous. In those terrain environments in which manmade linear features (such as fence lines, field boundaries, etc.) occur with natural linears, the task of the geoscientist becomes complex if the imagery itself is not viewed.

The conclusion that might be apparent to a nongeoscientist from the previous discussion is that spatial filtering might negate the necessity of obtaining multiple-look-direction imagery over the terrain to be examined for geological studies. Unfortunately, geologic interpretation from any remote sensor image entails considerably more than just the mapping of linears or lineaments. For example, dip slopes are an integral component of any structural analysis and were one of the geologic parameters examined in the original look-direction study by MacDonald et al. (ref. 2–43). These authors concluded that the influence of radar foreshortening, as dictated by look direction, is inherently related to the nondetectability of dip slopes. The state-of-the-art data processing (including the two techniques previously described) does not provide detection improvement for dip slopes; however, orthogonal look directions would provide a realistic alternative for optimum data retrieval.

Radar Stereoscopy

Radar relief displacement is an inherent characteristic of SLAR systems. This displacement is toward the nadir if the object is above the datum (topographic high), and it is away from the nadir if the object is below the datum (topographic low). Therefore, the relief displacement is in the opposite direction from the displacement direction in optical systems.

Because the appearance of high-resolution radar imagery is similar to a photograph, a visual stereographic image can be formed with appropriate radar stereographic coverage. However, adverse shadowing conditions are more predominant in radar imagery because of the oblique angle of illumination. In addition, radar foreshortening and layover make radar stereoscopy exceedingly difficult to obtain where terrain relief is relatively great. When one object is imaged twice at two different look directions at the same altitude (i.e., opposite-side configuration) or at two different altitudes (i.e., same-side configuration), then radar stereoscopy can be obtained. Especially in rugged terrain with the opposite-side configuration, shadowing may be sufficient to negate the utility of stereoscopy. However, in those areas where terrain slopes are minimal, radar stereoscopy will aid geologic interpretation.

SUMMARY

Major application areas for active microwave remote sensing include (1) exploration of petroleum, mineral, and ground water resources; (2) mapping surface and structural features; (3) terrain analysis, both morphometric and genetic; (4) application in civil works; and (5) application in the areas of earthquake prediction and crustal movements.

Although the success of radar surveys has not been widely publicized, they have been used as a prime reconnaissance data base for mineral exploration and land-use evaluation in areas where photography cannot be obtained. Radar imagery is providing a "first look" at some 6 million km^2 throughout the world.

Microwave remote sensing, especially from aircraft or satellites, has several important attributes that establish its desirability for mineral resources and geologic applications:

1. Expediency: Conventional field measurement can be time consuming, inconvenient, and costly.

2. Efficiency: Large areas can be covered in a short time.

3. Vantage: Some measurements are practicable only from air.

4. Coverage of areas is possible when not directly accessible because of local conditions.

5. Unique and corroborative data contribution is available only in the microwave portion of the electromagnetic spectrum.

Several unique characteristics of microwave sensors make them valuable for geologically oriented investigations. The proven application of an all-weather day/night sensor is an obvious advantage in many poorly mapped regions (especially tropical) of the world, and the low angles of oblique illumination have been demonstrated to emphasize subtle terrain features, which normally would have been overlooked when using standard photographic techniques. Where vegetation cover masks the ground surface, the radar signal may be influenced by the combination of the vegetation and the terrain surface beneath the vegetation; consequently, the extent to which terrain parameters can be mapped from microwave terrain data varies considerably depending on (1) the geologic and geomorphic characteristics of a region, (2) the climate, (3) the density of vegetation, and (4) the amount of surficial debris. However, the feasibility of using multifrequency microwave data over heavily vegetated areas may increase the accuracy of measuring many terrain parameters. Where vegetation is sparse or absent, an imaging radar becomes extremely sensitive to the actual surface roughness; thus, surface particle size and texture dominate the microwave return signal. The feasibility of obtaining multifrequency-multipolarization terrain data and an insight into dielectric properties will provide terrain information that is not available with existing airborne systems.

A few of the more important terrain parameters of prime concern to the interpreter, which may be inferred with operational microwave systems, include—

1. Geologic structure and lithology, especially faults, folds, fractures, rock stratification, and thickness.

2. Vegetation cover, type, and extent.

3. Surficial materials (nonvegetated) such as texture and microrelief.

4. Landform parameters such as size, shape, slope, relative relief, and elevation.

Systems data generally available to users during the past 10 yr are from high-frequency systems (K- and X-bands), with which no significant penetration should be expected. Limited studies show that with the long-wavelength radars (P- and C-bands), some penetration will be obtained even though the effect is somewhat clouded by the smoothing of surfaces (resulting in low return) that appear rough to short-wavelength radars. However, an important future potential is indicated. Certainly, the aspect of some vegetative penetration might provide insight into the true surface morphology of areas masked by a tree canopy.

At present, resolution is limited in nonclassified systems at approximately 10 m. Whether or not improvement in resolution would be desirable depends on the nature of the survey; for example, a reconnaissance or "first-look" survey (for which radar is best suited) requires no better resolution than that provided by existing commercial systems.

Priority areas of future research include understanding system-terrain interaction. For example, it has been found that the depolarizing of incident energy varies somewhat over the classes of terrains that backscatter microwave energy; thus, if energy of a given polarization is transmitted, the relative amounts of energy returned with like polarization and cross-polarization are different from different terrain classes. There are also differences in the variation of backscattering with wavelength and incident angle. Understanding the many parameters that influence the radar return signal is expected to provide a measure of detailed terrain analysis (ref. 2–47). The potential applications for multipolarization-multifrequency microwave systems, as outlined in

this section, provide exciting possibilities for retrieving terrain information. For future microwave systems, any terrain parameter that can be measured as additional data or with improved accuracy will probably be valuable. Even if not useful itself, it may provide surrogate data about another vital parameter.

SPECIFIC RESEARCH AREAS

The cover and subsurface penetration in a multifrequency radar system would aid in the following areas:

1. Determining true surface morphology.
2. Determining soil thickness.
3. Determining depth to bedrock.
4. Detecting offshore oil seep.

The following research observations are noteworthy:

1. Contrasts in coastal wetlands vegetation on dual-polarized radar imagery appear to provide an additional data source.
2. Dielectric properties of terrain surficial materials would aid considerably in determining rock or soil composition, the physical properties of Earth materials, and variation due to saturated and unsaturated conditions.
3. Interferometry may provide a means of determining regional or local slope parameters, including the aspect of automatic slope mapping.
4. Quantitative data extraction relative to depression angle dependency for specific slope or terrain configurations has not been thoroughly investigated.
5. The specific needs for calibrated microwave data are not known; however, slope determination from power return seems feasible.
6. Data processing, including spectral ratioing and image enhancements, is needed. Spectral signatures of different rocks, metallic minerals, and alteration zones, together with pattern recognition emphasizing texture and tone are necessary. Need for temporal data has not been fully documented, especially in foliated as compared to nonfoliated terrains. Snow cover is of special concern.

PART B

WATER RESOURCES

This section concerns the various applications and projected applications of active microwave instruments for studying water resources. Most applications involve use of an imaging system operating primarily at wavelengths of less than 30 cm (i.e., K-, X-, and L-bands). Discussion is also included concerning longer wavelength nonimaging systems for use in sounding polar glaciers and icecaps (e.g., Greenland and the Antarctic).

The section is divided into six topics: (1) stream runoff, drainage basin analysis, and floods; (2) lake detection and fluctuating levels; (3) coastal processes and wetlands; (4) seasonally and permanently frozen (permafrost) ground; (5) solid water resources (snow, ice, and glaciers); and (6) water pollution.

SURFACE WATER

Runoff Prediction, Models, and Stream Networks

Runoff potential and modeling.—The general objective is the prediction of runoff potential of ungaged medium-size watersheds that lack prior records. In this context, medium size is defined as a 2- to 500-km^2 drainage area.

Storm runoff is related to the amount of storage available in or on the surface (inter-

ception, surface storage, and infiltration). Measurement of one or all of the characteristics can improve current manual techniques for estimation of coefficients for storm runoff equations. In the commonly used Soil Conservation Service (SCS) runoff reference (eq. (2–1)), the coefficient *CN* is based on the soil-cover complex over a watershed surface.

$$Q = \frac{(P - 0.2S)^2}{P + 0.8S} \qquad (2\text{–}1)$$

where Q is inches of runoff; P is rainfall (storm); S is water storage factor equal to $(1000/CN) - 10$; and CN is function of soil type, cover, roughness, and soil moisture.

Active microwave systems of appropriate wavelengths are sensitive to soil particle size, vegetation, roughness, and scene moisture; thus, a good possibility exists that the integrated influence of these characteristics can be quantitatively measured by microwave systems. Present technology favors active rather than passive microwave systems for imaging with longer wavelengths. The application is an area of primary research concern because it has not been tested with an active microwave system.

Application: The application for active microwave sensing would be to obtain data on the watershed runoff of medium-sized watersheds.

Acquisition: The data would be acquired by use of the following techniques:

1. Multifrequency wavelengths (X- and L-bands or longer).
2. Minimum of 20 data points per km^2 using seven-bit digital data.
3. Vertical and horizontal polarization.
4. Steepest possible depression angle and onboard tape recording.
5. Processing with data reduced to digital interface (registered) computer-compatible tape (CCT).
6. Gridded film output for location of data in irregularly shaped areas.
7. Display and distribution (as minimum user requirements) of CCT and film output or average value of each polarization of each wavelength used for requested surface area.

Justification: This system would provide all-weather capability and improve evaluations of hydrologic classification of soil by imaging in longer wavelengths than now available in passive images. The system could be used for space platforms and could improve ERTS saving by $2.5 million a year.

Anticipated results using active microwave sensing: Improved prediction of storm runoff used in the design of flood-control structures is anticipated (accuracy: 5 yr, 80 percent; 10 yr, 95 percent). The resulting information would be of use to the U.S. Department of Agriculture SCS, the U.S. Department of the Interior, and underdeveloped countries.

The ERTS studies by Blanchard (ref. 2–48) indicate that the SCS parameter *CN* can be related to the difference between MSS bands 4 and 5 in the southern Great Plains, especially during dry, dormant conditions. The ERTS scenes for such conditions are not always available when they are most needed for these measurements; however, benefits from this application have been estimated at $2.5 to $5.0 million if applied nationwide. This ratioing technique has not yet been tested using Skylab data. The Passive Microwave Imaging System (PMIS) measurements at X-band over eight small watersheds indicate the feasibility of microwave measurements of the coefficient *CN*. Figure 2–6 illustrates the apparent relationship of horizontally polarized PMIS temperature to the SCS runoff coefficient *CN* from these watersheds in central Oklahoma.

Cost/benefit.—The 1973 Dynatrend report (ref. 2–1) lists annual benefits in excess of $200 million at 1972 values. A modest saving is recognized for improvements in monitoring impounded water forecasts of irrigation water availability.

Recommendations.—The first requirement is to define and measure *CN* for the SCS equation. The second requirement is to attempt measurements of individual parameters for use in existing complex runoff equations (soil moisture, soil porosity or infiltration capacity, interception storage, etc.).

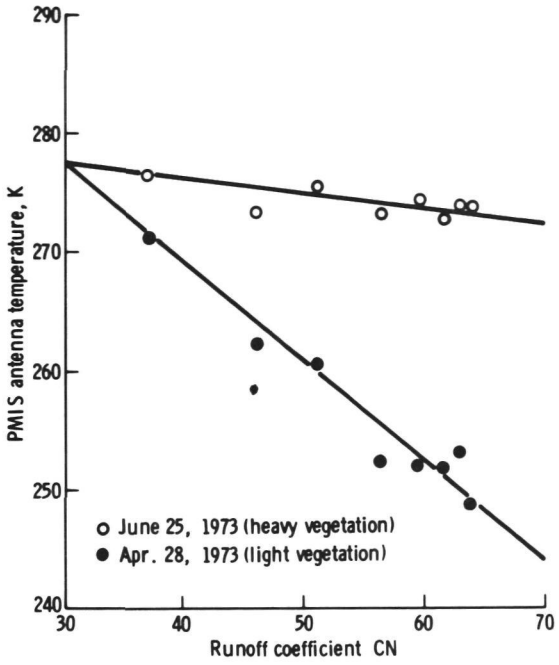

FIGURE 2–6.—Apparent relationship of the horizontally polarized PMIS temperature to the SCS runoff coefficient *CN* from watersheds in central Oklahoma.

During the first phase, aircraft platforms should be used over intensely instrumented watersheds to develop the relationship between microwave response and runoff coefficient. A second set of watersheds should then be used to test these prediction coefficients. Such a program could have results in 2 to 5 yr.

The second phase should be concurrent with the first and should involve use of a truck-mounted system over controlled plots. The experimental design might closely follow the design already initiated at the University of Kansas. After establishing basic relationships for each hydrologic variable, the knowledge must be repackaged for aircraft application.

Estimates of streamflow based on network analysis.—The objective of this application is to measure a different parameter of storm runoff; namely, Strahler numbers. This analysis is independent of the drainage-basin size and could therefore be more universally applicable than the previously discussed SCS runoff equation.

In the evaluations of ERTS–1 imagery, several investigators have shown the capability of satellite imagery for defining basin shapes, sizes, and drainage patterns. The extent and direction of streamflow were defined by imagery, and high-quality correlative streamflow data have been acquired by the data collection system (DCS) and used by State and Federal agencies. Historical streamflow data, which were routinely collected at gaging stations, have been extrapolated to ungaged sites by relating stream discharge to geometric and surface characteristics of the drainage basin. Some of the basin variables most easily extracted from ERTS–1 imagery are amount of open water, area of vegetative cover, area of snow cover, network geometry, drainage area, and major basin modifications by man; that is, urban development or cultivation.

The application of airborne radar to the identification and measurement of drainage-basin variables has been investigated by McCoy (ref. 2–49) and Lewis (ref. 2–18) (fig. 2–7). Investigation has shown that each different radar system yields different amounts of detail; however, the consistency of information content in any given radar system allows extrapolation of data to the level of detail that would be available on a 1:24 000 topographic map. This potential exists for each of the stream network variables in drainage basins, but it is strongest for basin area, total network length, total number of stream segments, and basin perimeter. High levels of correlation were found to exist between data derived from topographic maps and radar imagery. Figure 2–8 illustrates this general conformity. Because radar imagery can be the base for a reasonably accurate map of drainage-basin networks, it has proved to be very useful in compiling and updating drainage maps of inaccessible, cloudy environments such as the Amazon Basin.

Drainage area and stream network length are readily measured from radar images, and

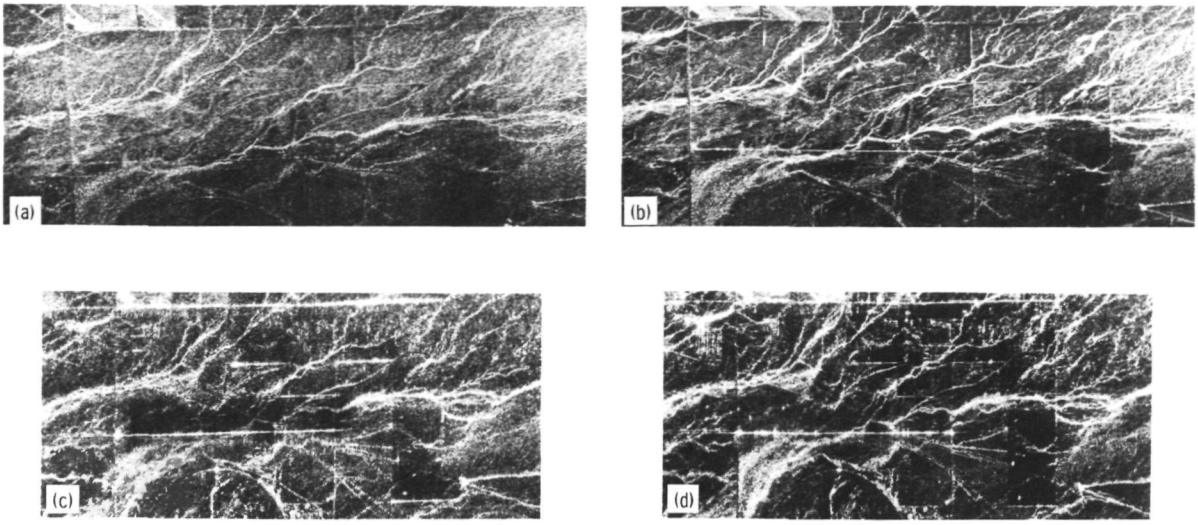

FIGURE 2–7.—Simultaneously obtained dual-frequency radar imagery of creek drainage patterns east of Gilbert, Ariz. (April 5, 1974); resolution is 10 by 10 m. (*a*) An X-band parallel polarization. (*b*) An X-band cross polarization. (*c*) An L-band parallel polarization. (*d*) An L-band cross polarization.

each is a significant variable related to streamflow. Assuming that terrain texture (expressed as network length) and drainage area are valid expressions of the surface characteristics affecting runoff, radar imagery can provide useful hydrologic information. To illustrate the potential of radar imagery in streamflow estimates, length measurements from radar imagery were compared to their rendition on existing maps and later correlated with streamflow. Figure 2–9 shows the relationship of network lengths obtained by edge enhancement of radar imagery and by manual measurement on topographic maps. Figures 2–10 and 2–11 show relationships of streamflow to terrain variables taken from topographic maps but that are available from radar images.

Functional requirements.—The functional requirements of the system are as follows:

1. Frequency: K- and X-band imaging has been successfully used; no information is available for other frequencies.

2. Resolution: A 15- to 100-m resolution has been tested satisfactorily. Better resolution appears not to be required.

3. Coverage: Large areas of coverage (as much as 100 km^2) within a zone of shallow depression angles (20° to 50°) would be most useful for low-distortion mapping of large basins.

4. Repetition: Regular repetition is important only when a DCS is being used. For basin geometric measurements, repetition is not necessary.

Justification: Drainage mapping and measurement of drainage geometry obtained from active microwave sensor data give results comparable to topographic maps (1:24 000). The added advantage of large areal coverage in a single frame is important.

Anticipated results: Water management agencies at the State and national levels would be able to establish streamflow or unit area runoff models for ungaged drainage basins that would be of great benefit in surveys of potential water yield. Water-supply estimates would become available for regions where no data are now available.

Recommendation.—Two key research areas

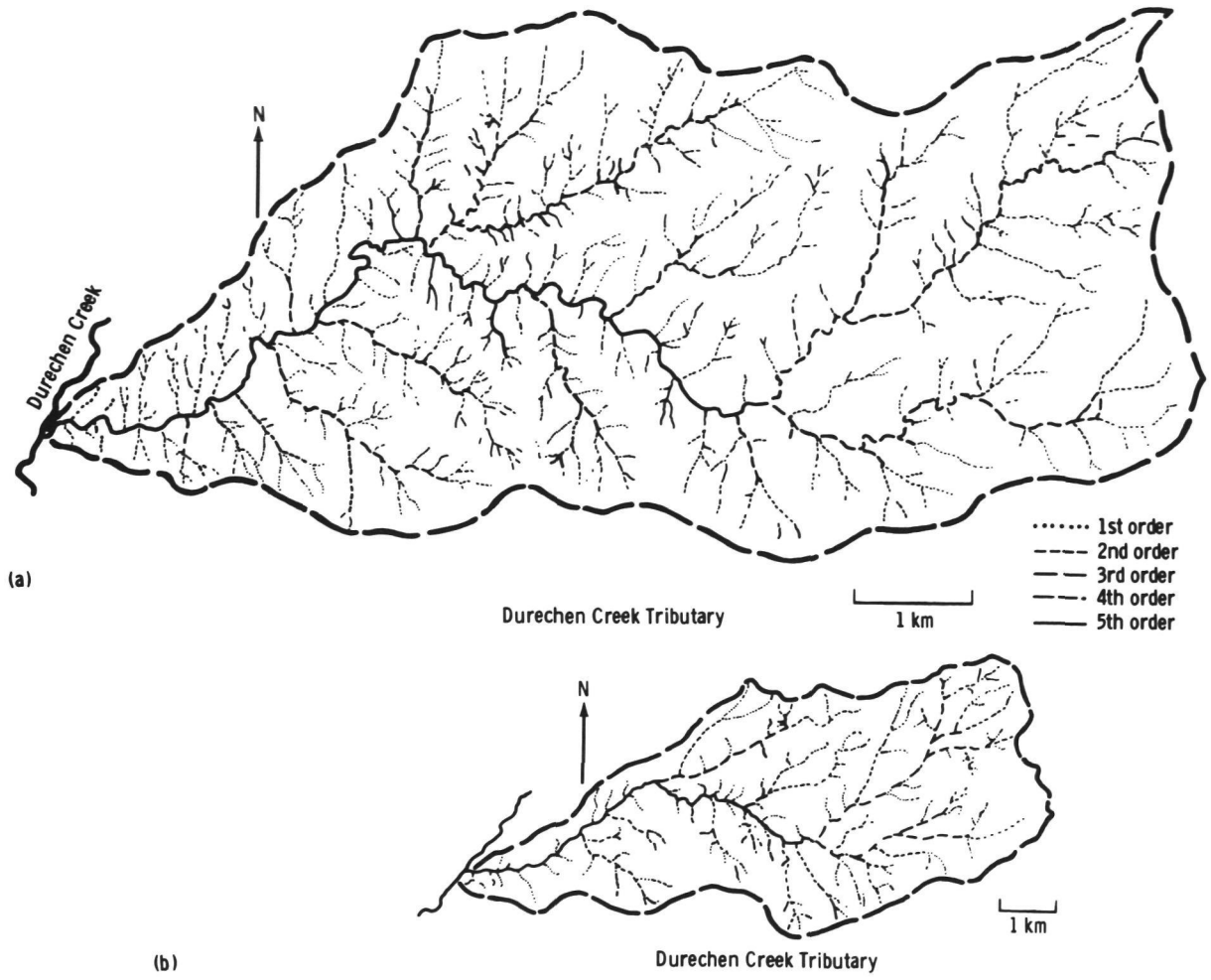

FIGURE 2–8.—Correlation between drainage basin data derived from topographic map and from radar imagery of the Durechen Creek tributary. (*a*) Topographic map; scale of 1:24 000. (*b*) K-band radar.

should be pursued: (1) Models relating hydrologic variables to terrain variables obtained from radar imagery should be developed and tested, and (2) techniques for automatic measurement of terrain variables from radar imagery should be developed further.

Flood Mapping

General objectives.—The general objectives are to study the extent, duration, and seasonality of flooding in both rural and urban settings. Data concerning the extent and duration are needed in real time, whereas seasonality requires long-term repetitive coverage for several years. Ground-cover analysis is viewed by many as an approach to determine infrequent or singular flooding (e.g., 100-yr floods). A program of flood mapping would provide additional remote-sensing data for delineating flood plains and thus be a primary benefit to land use planning authorities.

Demonstrated remote-sensing performance compared to objectives.—Evaluation of available satellite and aicraft imagery of floods has indicated that feasible methods exist for mapping the extent of inundation several

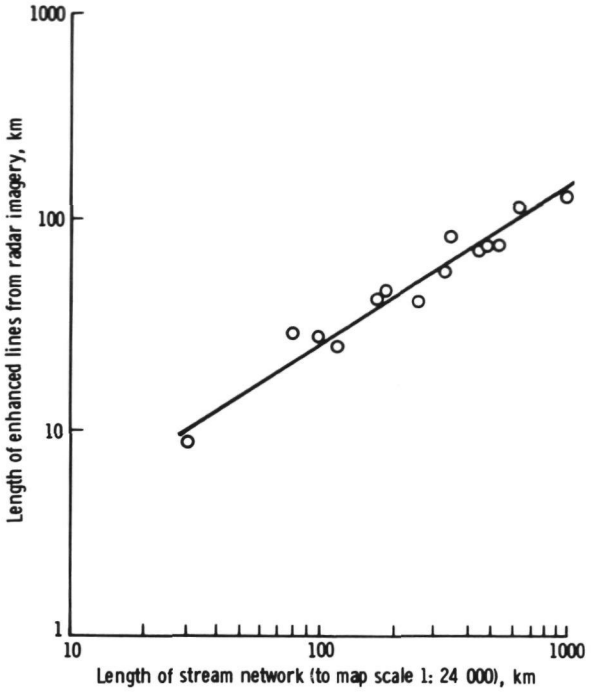

FIGURE 2–9.—Stream length measurements based on radar imagery compared with manual measurements on topographic map.

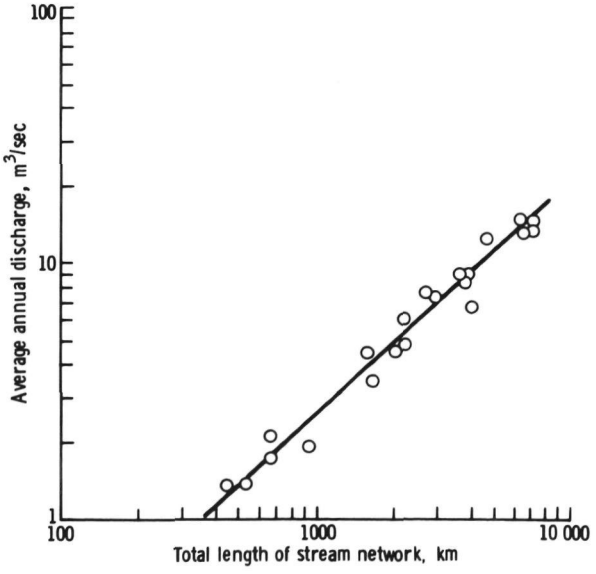

FIGURE 2–10.—Average annual discharge of stream as a function of the total length of stream network.

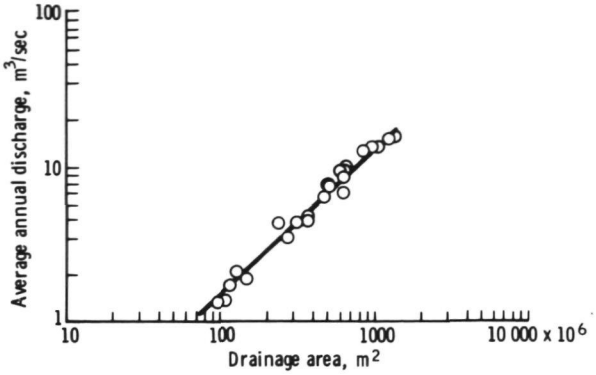

FIGURE 2–11.—Average annual discharge of stream as a function of the stream drainage area.

days after floodwaters have receded. The main phenomena mapped are the latent effects of high soil moisture on soil reflectivity and plant reflectivity. Characteristics of IR radiation (including the absorption of near-visible IR wavelengths by water, the reduced IR reflectance of wet soil and stressed plants, and the different reflective properties of snow and ice at IR wavelengths) have shown that IR photographic techniques are satisfactory for flood mapping (ref. 2–50). In addition, it has been demonstrated that Kodak IR Aero film 2424 with an 89B Wratten filter produces imagery that permits detection of floodwater levels following the recession of those waters. For example, such a study dealt with the floods in southeastern Michigan following a northeasterly storm on Lake Erie in the spring of 1973 (ref. 2–51). The items detected were the flotsam line remaining at the high-water mark.

Major flooding originates in a drainage basin, generating a pulse of water that eventually reaches a major tributary moving downstream. Flood crest at a given point may occur during nondaylight hours or at times when photographic sensing is not possible. Real-time knowledge of the extent of local inundation is vital for improving civil defense procedure. In a less real-time context, data could be used for flood-plain management.

Active microwave sensors could significantly enhance real-time data acquisition. In

addition, active microwave sensors should provide excellent flood inundation mapping because of the high moisture dependence of the electrical properties (e.g., dielectric constant) of the soils. Figure 2–12 shows APQ–97 imagery of the 1973 Missouri River flood. Some wavelength radar systems capable of reasonable penetration into the soil (2 to 5 cm) have been used to map changes in near-surface soil moisture for bare soils. Operation of wavelengths in the 20- to 30-cm range appear to enable soil moisture monitoring even under vegetative canopies (ref. 2–52).

Functional requirements for active microwave measurements.—The functional requirements are as follows:

1. Frequency: L-band (30 cm).
2. Resolution: 30 m.
3. Coverage: 20-km swath width.
4. Polarization: Dual polarization (like and cross).
5. Stereographic: Highly desired.

Processing.—The data will be processed as follows:

1. Onboard processing required for aircraft and Space Shuttle.
2. Display and distribution to consist of real-time capability, permanent record on print developed onboard aircraft, and digital tapes to be recorded for later processing and enhancement.
3. Real-time ground truth required and documentation with conventional aerial photographic techniques where possible.
4. Satellite data to be telemetered and processed in real time at data collection centers; data to be rapidly transmitted to users by telecom links.

Unique justification for active microwave sensing.—Nighttime and all-weather observations are required.

FIGURE 2–12.—Radar imagery of the May 1973 Missouri River flood. Water appears as black, which indicates areas of no signal return, because its surface is smooth to a wavelength of approximately 3 cm.

Anticipated active microwave results in 5 to 10 yr.—After 5 yr, 95 percent accuracy is anticipated in the use of active microwave sensing for flood-disaster monitoring and 100 percent accuracy is expected after 10-yr use. After 5 yr, 70 percent accuracy is anticipated for flood-plain mapping; after 10 yr, 95 percent accuracy is expected.

Users.—Two primary uses will be made of the data by the agencies shown in the following list.

1. Extent and duration of flooding: U.S. Geological Survey, State geological surveys, U.S. Army Corps of Engineers, U.S. Office of Emergency Preparedness, and State civil defense offices.

2. Seasonality of flooding: U.S. Department of the Interior, U.S. Environmental Protection Agency, State offices of planning and programing, and State land-use planning agencies.

Value.—Conventional flood-mapping investigations cost thousands of dollars and require months and even years to complete. Remotely sensed data of floods offer timeliness and synoptic coverage at low costs. (When active microwave sensors are used, timeliness is improved as a result of all-weather observations.) By improving runoff predictions, an annual saving of approximately $150 million in flood damage has been estimated (ref. 2–1).

Recommendations.—Active microwave research investigations of flooding and flood plains should be conducted to define the optimum sensor configuration for aircraft and satellite systems.

Mapping of Lakes

General mapping.—The general objectives of this water resource activity are to (1) map surface water bodies, (2) measure their surface areas, (3) calculate their changing levels for predicting floods or estimating hydroelectric potential, and (4) interpret and map the resource base of wetland environments.

Demonstrated performance.—The near-IR bands (6 and 7) of the ERTS MSS produce large tonal contrasts between land and water, which clearly define the land/water interface. Lakes less than 0.5 hm^2 and streams only 65 m across have been identified on ERTS imagery. Turbidity and plume patterns are also discernible on the visible and near-visible bands.

Reports on the utility of ERTS imagery for wetland studies have indicated that mapping the land/water interface, upper wetland boundary, plant community boundaries, spoil banks, and dredge and fill operations are all feasible on 1:250 000 ERTS imagery (refs. 2–53 and 2–54). At larger scales (1:125 000), information on transition zones, plant communities (such as *Spartina patens* and *Juncus roemerianas*), and drainage on mosquito ditches can be identified (ref. 2–54).

The application of side-looking radar to the detection of water bodies has received little attention. The one study that discusses this topic in depth is by Roswell (ref. 2–55). Roswell determined that the detection of lakes on radar imagery is based on (1) the large contrast between radar return from the land and water, (2) the frequency occurrence of bright return from the far range of the water body, and (3) the drainage elements around the water body.

Environmental parameters (relief, slope, and drainage) were found to influence microwave detectability. The relationship is such that lake detectability decreases with increasing relief and slope and decreasing drainage (i.e., poorly drained environs). As expected, the highest percentage of lake detection is in well-drained lowlands. In these areas, 60 percent of the lakes between 1 and 3 hm^2 and 93 percent of the lakes larger than 15 hm^2 were detected on imagery having a 15-m resolution. Simpson (ref. 2–56) reported a 100-percent detection of all lakes larger than 4 hm^2 on imagery from the same system. Radar imaging systems might therefore be valuable for updating maps ranging in scale from 1:250 000 to 1:24 000.

Roswell states that, although detectability

increases with lake size, the extent of radar shadowing and layover is more important than the resolution of the radar system. Roswell's data indicate that lake detection is consistently lower in the near range than in the middle or far range. No single look direction proved better for lake detection, but, in high-relief and slope areas, multiple looks increase detection.

Functional requirements.—Based on Roswell's data, it appears that an X-band system would be adequate for lake detection, although the optimum frequency is unknown. Resolution of approximately 5 to 10 m would also be adequate. With respect to depression angles, detectability is poorest in the near range. Therefore, angles of 15° to 45° are suggested. Repetition, including multiple looks, is important for both increasing detection and monitoring lake-level changes.

Processing may also be important. By processing the data to favor the variation of return from the lake rather than land surface, radar imagery may provide more than a medium for lake detection. Added information, such as windspeed and direction based on water-surface roughness or the detection of oil slicks, might possibly be obtained.

Unique applications.—Three applications unique to active microwave sensing are (1) monitoring lake-level changes, (2) monitoring spring thaw of ice-covered lakes, and (3) studying wind patterns over water.

Anticipated results.—The surface-water hydrology of many parts of the world is relatively unknown. Radar imagery could provide accurate information at very low cost. Mapping ephemeral lakes in arid and semiarid regions would also improve regional climatic data to permit the introduction of new land-use practices.

Recommendations.—Future work should document the conditions under which lakes can be detected on radar images. The practicality of active microwave systems for supplying flood prediction and regional climatic data by lake monitoring should be emphasized.

Specific applications: lake levels, lake flooding, and eutrophication.—Active microwave sensors can contribute data on at least two limnological characteristics: seasonal change in lake levels and eutrophication. Areas flooded by high lake levels could be identified with radar and could provide guidance regarding potential shoreline uses to Federal, State, and local planners and resource managers. Seasonal lake-level data would also be useful for assessing water supply. Eutrophication is an important clue to the ecological balance around a lake and to man's impact on the local environment. Eutrophication affects wildlife and drastically alters the local recreational resource and water supply.

Remote sensing of lake levels.—Lake-level changes can be approached by studying temporal changes in shoreline positions. Conventional aerial photography has been used to document lake-level changes and shoreline positions in Lake Rudolf. Lind (ref. 2–57) has applied ERTS data to assess seasonal changes in lake levels in Lake Champlain. Satellite observations have also been conducted on saline lakes in the United States.

For large lakes, synoptic and systematic coverage of the type that can be obtained from aircraft or satellites is desirable and can yield useful information on the effects of lake-level change. Active microwave sensors offer special advantages because they can be applied on demand when, for example, maximum or minimum stages have been reached. For many of the tropical regions, where cloud cover usually obscures the high-lake stage of the annual cycle, active microwave sensor data offer the only reliable means for assessing those lake levels.

The application of active microwave sensors should include not only large freshwater bodies (e.g., Great Lakes), but also farm ponds, beaver ponds, prairie potholes, and sinkholes. Microwave remote sensing can also apply to the brackish and saline water bodies along desert margins. Such information may facilitate the use of lake waters for irrigation purposes and for water supply (through possible desalinization). Fresh,

brackish, and saline lakes are scattered throughout the developing countries of the world, and data on water quality and fluctuation patterns could provide the basis for use of the waters and shores in a manner consistent with the individual environmental settings.

Resolutions of 3 to 10 m could conceivably provide the necessary data for lake-level studies. Other functional requirements that apply are those associated with existing conventional SLAR systems.

Seasonal coverage is a critical temporal requirement due to the fluctuation pattern of lakes. For mid- and high-latitude lakes, a minimum of two annual synoptic coverages would be needed to encompass the extreme periods of fluctuation. For tropical lakes, a somewhat greater frequency seems desirable because there are often interseasonal fluctuations. Thus, four annual synoptic coverages spaced to include the extremes and the transition periods leading to maximum and minimum levels would provide minimum data. On a worldwide scale, weekly observations would be needed to cover the time range of fluctuations for the diverse lake-level regimes.

Processing.—Processing the image data can be accomplished through standard photointerpretation procedures or through semiautomated or automated optical processing. An overlay procedure used in the mapping of lake levels for Lake Champlain is just as applicable for radar image data.

Display and distribution.—A map format involving the transfer of shoreline position to suitable base maps would provide users with a readily usable product; however, basic processed radar images could also provide data for resource management decisions. The scale of presentation is somewhat dependent on the resolution of the data involved. A scale of 1:62 500 is satisfactory for larger areas. Larger scales (e.g., 1:10 000) could be possible with finer resolution data.

Supplementary data.—When available, lake gage data should be related to the remotely acquired data to establish a relationship between specific gage values and shoreline changes. Thus, it would be possible to establish certain critical gage levels relating to specific shoreline positions. However, because most of the lakes of the world are ungaged, the remote-sensing data would need to be sufficient. For areas where reliable topographic maps exist, some relatively crude relationships might be established. Though useful, gage data are not critical to successful remote sensing.

Justification.—Because they can be applied at the appropriate times regardless of cloudiness and time of day, active microwave sensors would provide an especially valuable source of data on lake-level changes and effects. Reliability on a temporal scale is critical to assessing lake levels; thus, because many lakes are in the cloudiest portions of the globe, radar could make an important national and worldwide contribution. Although especially important limnologically, this contribution has considerable practical resource significance.

Anticipated active microwave results.—If properly researched and developed, the application of radar could pave the way toward—

1. Providing basic data for mapping seasonal lake-level changes on a systematic basis regardless of cloud-cover problems, which severely limit visible sensors.
2. Establishing lake fluctuation models based on water budgets (relationship to key climatic factors).
3. Providing maps and/or processed images of seasonal or multiseasonal fluctuations in lake level.

Because the technology for the study of lake levels is already available, implementation of a program of such surveys using active microwave sensors could be easily established within a 5-yr period. Improvements in resolution to provide the best possible data for this task will probably result in a 90-percent mapping accuracy. This level of accuracy may already be attainable, but no detailed studies exist to confirm it.

Cost/benefit considerations.—No cost/benefit studies seem to exist that address this application area even at a local level. Increases in data-gathering efficiencies attributable to radar and the multiple use of radar data for other applications would seem to provide at least a moderate-level benefit. This benefit, combined with the fact that lake-level data for most lakes of the world are nonexistent and could be supplied through radar applications, seems to tip the balance toward a favorable cost/benefit ratio.

Recommendations.—The mapping of lake levels with active microwave sensors can be implemented without much further research. Research relative to mapping accuracies seems to be needed; however, the overall application should not be hindered by this need.

Although aircraft could be used for highly detailed studies, the base data for large-scale investigations involving lakes in different climatic regions could be obtained from satellite vantage points and Space Shuttle vehicles. Because data processing can be done with known techniques, the results could be made available within a short time and without major expense for data processing. In summary, radar surveys of seasonal lake-level changes should provide immediate and useful results.

Eutrophication and plant growth in lakes.—The application of active microwave sensors for lake eutrophication is limited to detection of various floating and surface-protruding plantlife forms that often accompany the advanced stages of eutrophication. Color and color IR aerial photography have generally been used for investigations of lake plant growth; for example, Scherz (ref. 2–58) and Kiefer and Scherz (ref. 2–59). Only one investigator (ref. 2–60) has indicated the potential that radar may have for these studies. Many plant forms come to the water surface and therefore would be susceptible to radar detections. Algal mats, extensive water-lily and water-hyacinth infestations, and various water weeds are examples. These plant growths may attain such large proportions that they affect the qualities of lakes. In parts of the tropics and subtropics, for example, water-hyacinth infestations have ruined entire lakes. Some assessment of the degree of plant growth in lakes is of considerable importance. Microwave remote sensing provides a means for systematically monitoring detrimental plant growth in lakes, which is illustrated in figure 2–13.

Observations with like- and cross-polarized radar show that a clear distinction can be made between vegetation-covered water bodies (ricefields in Texas) and adjoining land or vegetation-free lakes. On like-polarized imagery alone, the vegetated water surface might be mistaken for land; on cross-polarized imagery the presence of vegetation might be missed.

Functional requirements.—Research is needed to establish accuracy levels for both detection and mapping. The following functional requirements are estimates:

1. Spatial resolution: 3 to 10 m.
2. Gray scale resolution: 5 to 10 dB.
3. Wavelength: 1 to 30 cm.
4. Polarization: horizontal transmit/horizontal receive (HH) and horizontal transmit/vertical receive (HV).
5. Wavelength bands: 2 to 3.
6. Swath width: 20 km.
7. Ground truth: to establish accuracies in detection and mapping.
8. Collateral sensors: visible and IR, which may not be required.
9. Underflight sensors: visible.
10. Timing: seasonal (three to four times a year minimum).
11. Format to user: maps and processed images.

Justification.—Water resources and management agencies are especially concerned with the problem of plant growth in lakes. Active microwave sensor data would provide the agencies with information on the extent of infestation. Although this phenomenon can be assessed with conventional visible sensors, radar offers a supplemental coverage in those regions where cloudiness would prevent the timely use of conventional sensors and in

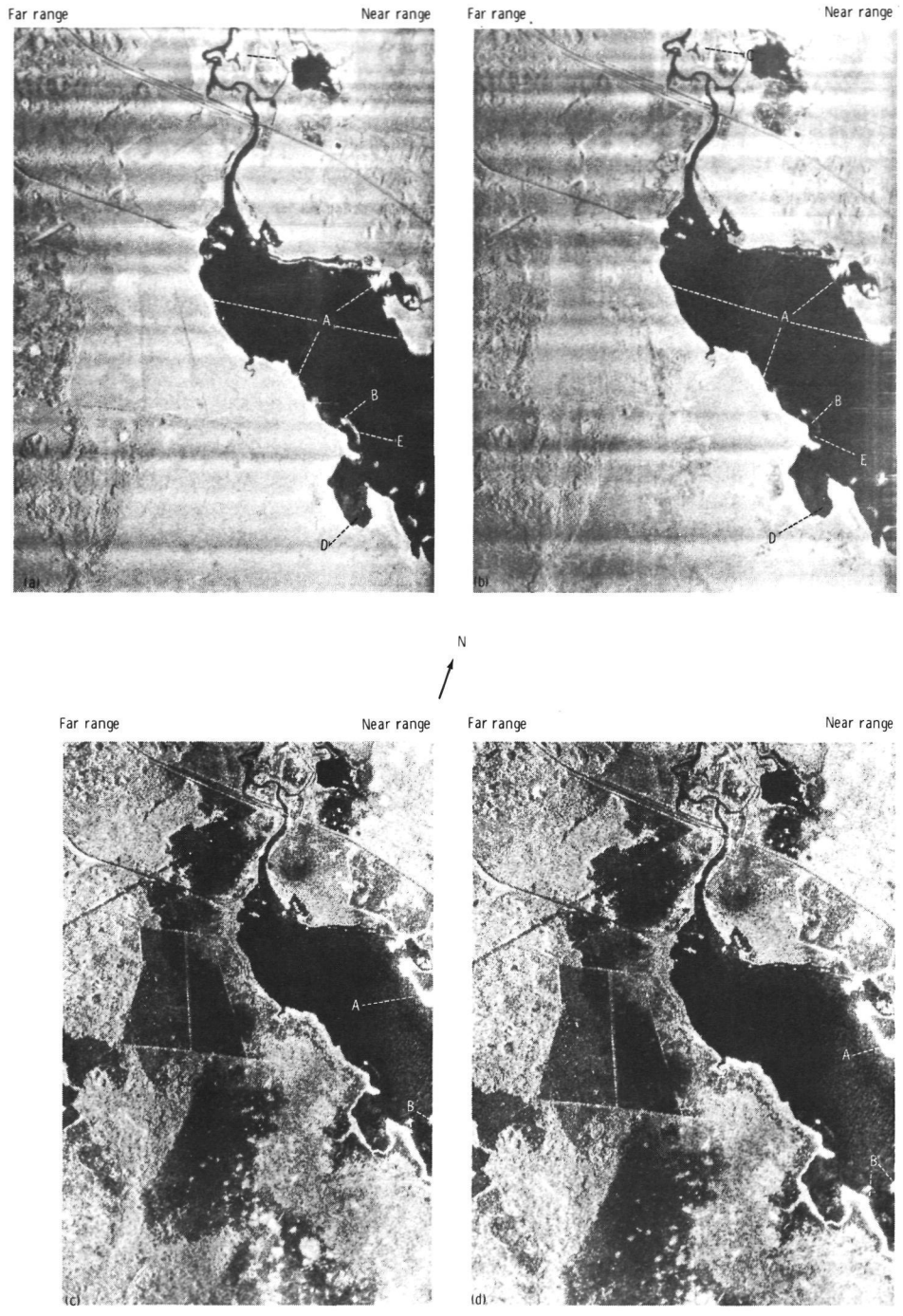

FIGURE 2–13.—Simultaneously obtained dual-wavelength radar imagery of Lake Poinsett region, St. Johns River, Brevard County, Florida; resolution of 10 by 10 m. (A—stationary water hyacinths, B—floating (migrating) water hyacinths, C—region of river channels choked with water hyacinths, D—water lilies, E—reeds growing and anchored in river.) (*a*) An X-band parallel polarization. (*b*) An X-band cross polarization. (*c*) An L-band parallel polarization. (*d*) An L-band cross polarization.

other regions where persistent cloudiness is found.

Recommendations.—Because radar has not been previously used for this application, a research effort is required to establish accuracy levels for detection and mapping and to establish radar system parameters. Such research could be completed within 5 yr. After the necessary experimentation, the operational use of radar could be implemented, which could occur within 5 to 10 yr.

Coastal Wetlands

General statement of problem.—The coastal zone is a unique environment in which three spheres interact: lithosphere (land), hydrosphere (ocean), and atmosphere (air). The coastal zone is therefore a highly variable, dynamic, and complex region. The high utility of the coastal zone is affirmed by high land values and population densities. Pressures are being exerted on the land, water, and air by those who wish to use the region for recreational, industrial, and commercial development. Not enough is known of the coastal zone to properly evaluate these uses.

Coastal geomorphologists interested in the frequently cloud-obscured coastal zone are increasingly using active microwave systems. Imaging radar provides a continuous image strip exhibiting a high-contrast coastline. Because coastal change is often greatest during the height of a storm (ref. 2–61), the near-all-weather ability of microwave systems should provide data that would aid in better understanding the process of coastal erosion.

Demonstrated remote-sensing observations.—Coastal maps have been updated by using radar (ref. 2–62). In addition, a variety of coastal zone features has been mapped in Panama and Colombia (refs. 2–18, and 2–62 to 2–64). An example is shown in figure 2–14. Most of these features were mapped for the first time and, as a consequence, pro-

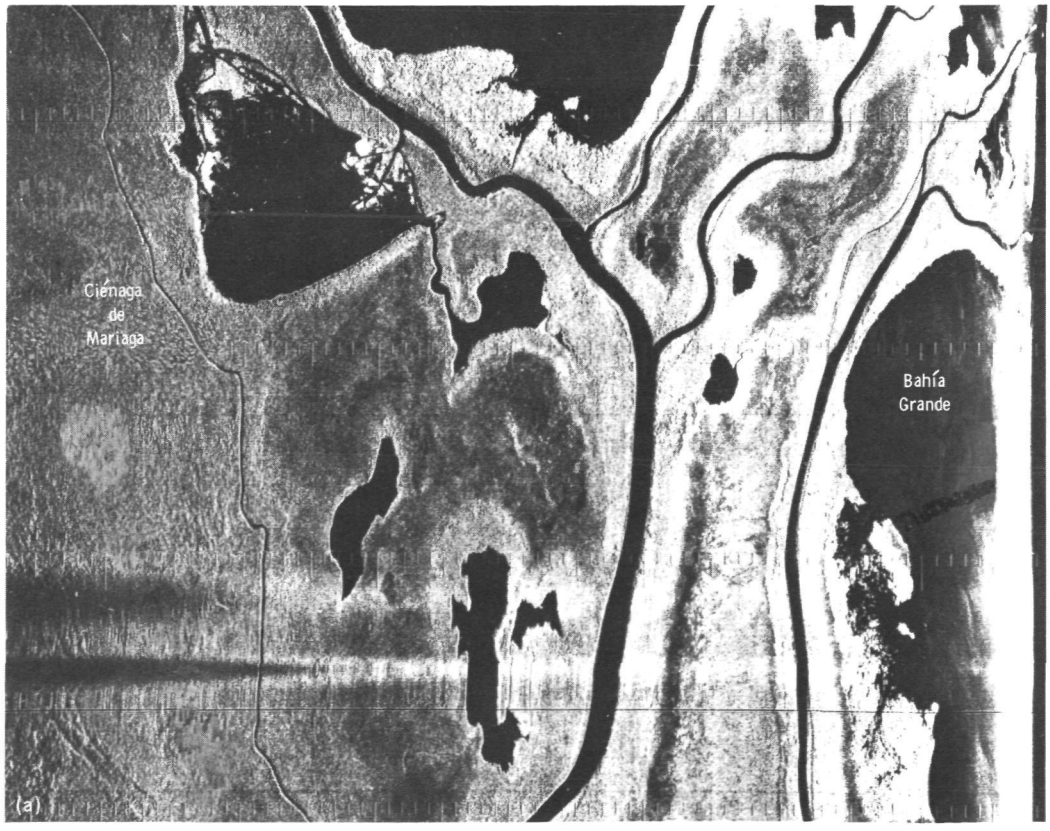

FIGURE 2–14.—Coastal map and radar image of an area of Panama. (*a*) Radar image.

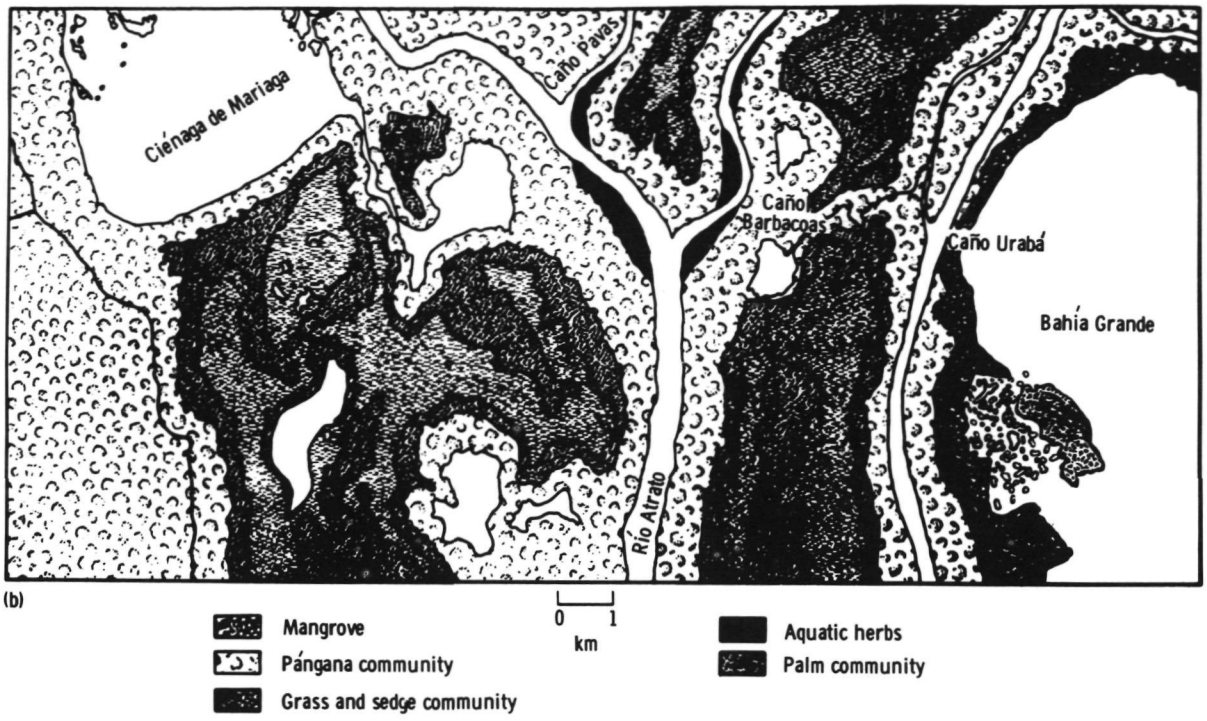

(*b*) Radar-derived map showing various coastal zone features.

vided information on the tidal influence, wave energy, and climate not previously known (ref. 2–18).

The detection of tidal zone features, such as mud flats and shell reefs, and the surf zone has subsequently been found to be strongly affected by position in the range (fig. 2–15). Like the detection of lakes, these features are better detected in the near range (ref. 2–65).

Cultural features unique to coastal/wetland environments are also evident on radar imagery. These features include marsh buggy tracks, access canals and pipelines, offshore oil platforms, ships and accompanying wakes, jetties, groins, piers, and buoys. The effect of groins can be monitored by noting the deposition on the upcurrent side of the groin.

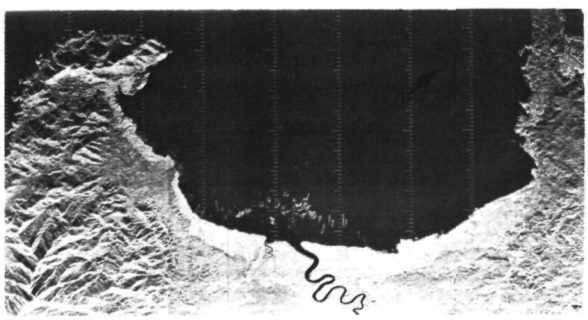

FIGURE 2–15.—Example of radar imagery showing coastal features.

For strictly freshwater coasts, a study conducted under the ERTS program is pursuing the comparison of several near-simultaneous imagery sets for identification of the extent of coastal flooding. This study used aerial IR photography, ERTS–1 MSS imagery, and dual-frequency, dual-polarization SLAR imagery. The analysis has not been completed, but the correlation between the preliminary interpretation of the imagery from the three sensors is quite high. Figures 2–16 to 2–18 are maps derived from these data.

Functional requirements.—Most data requirements could be satisfied by an aircraft-mounted sensor. Periodically gathered satellite data would serve best for change

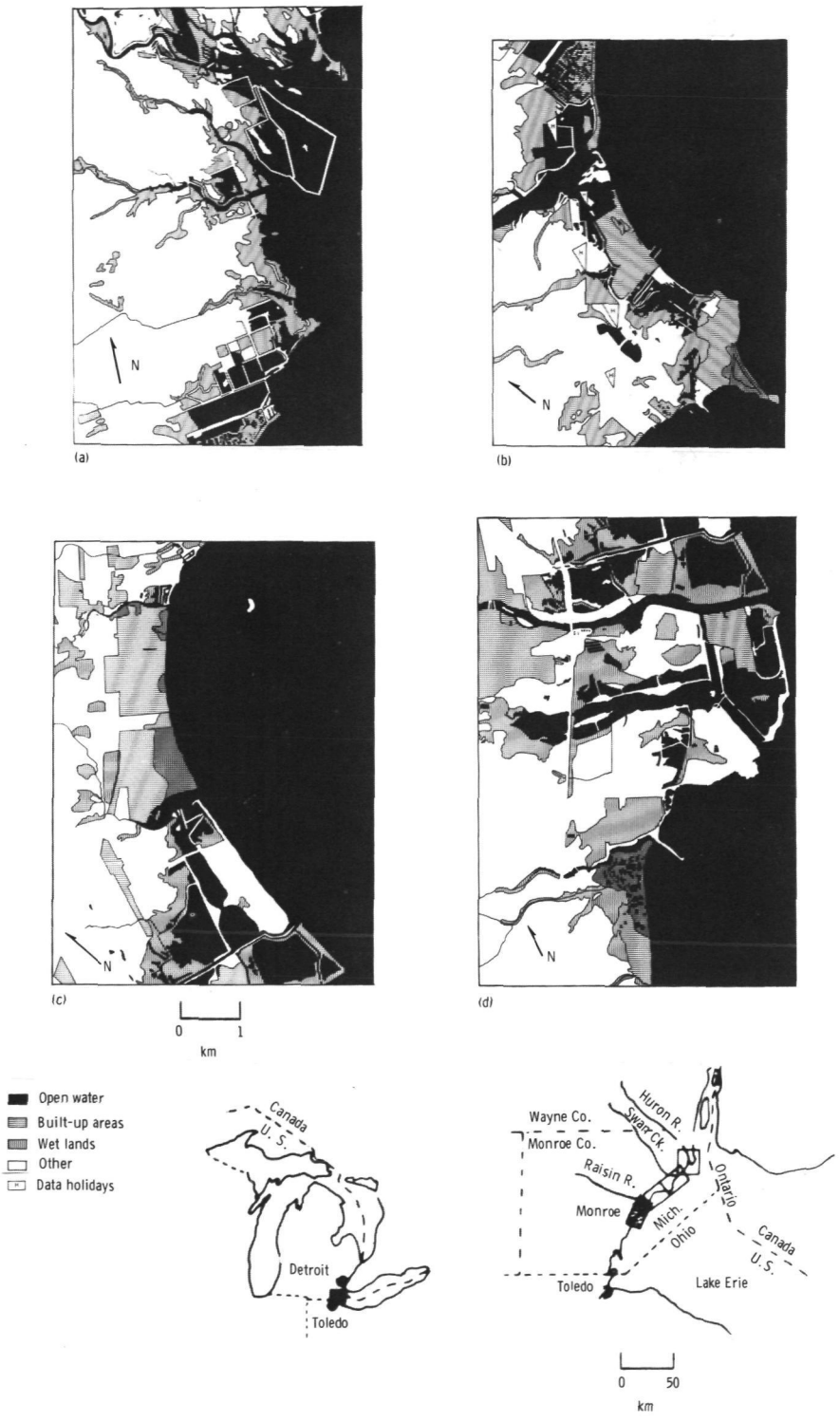

FIGURE 2–16.—Interpretation of aerial IR imagery of coastal flooding in the Great Lakes region. (*a*) View 1. (*b*) View 2. (*c*) View 3. (*d*) View 4.

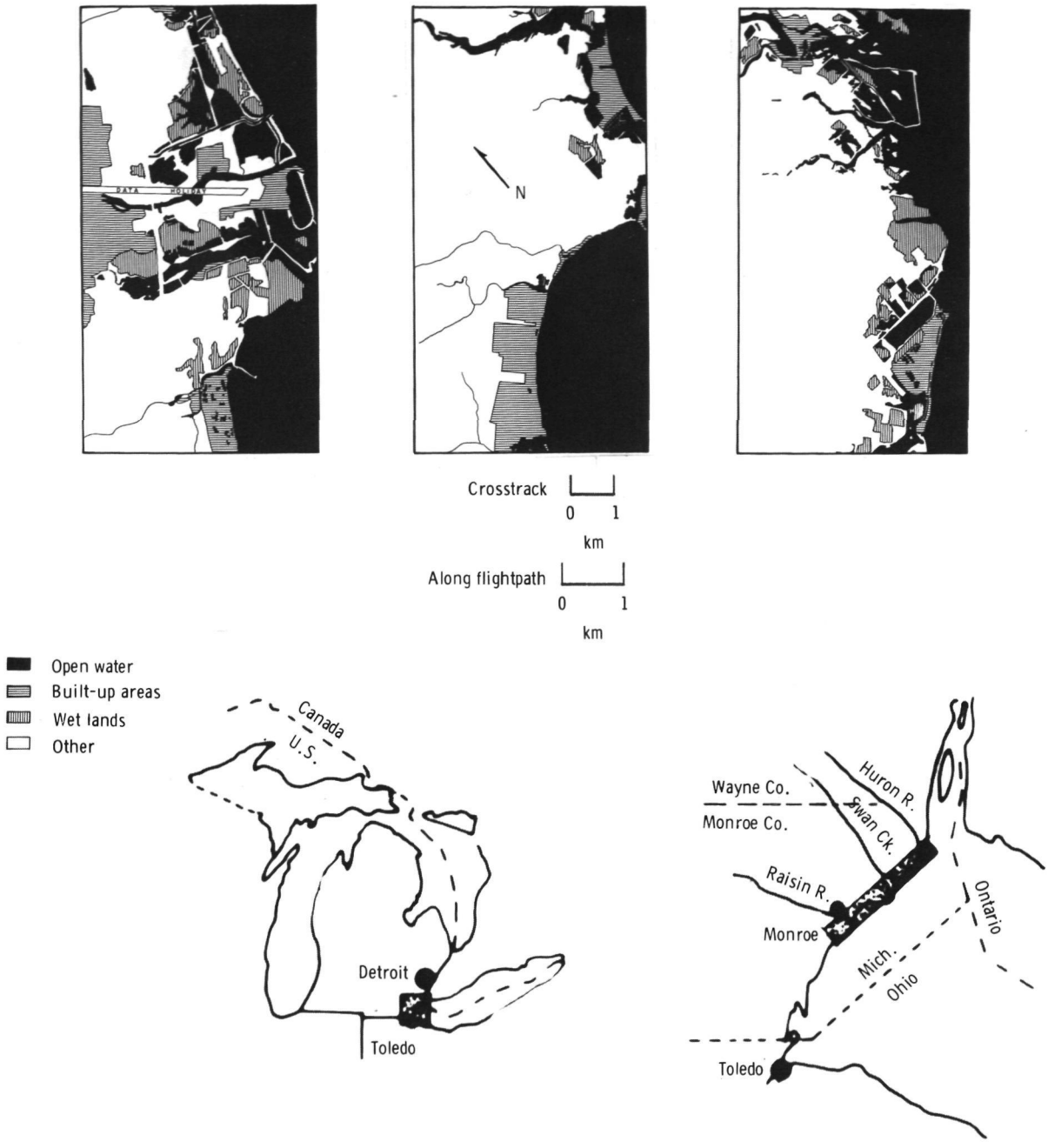

FIGURE 2–17.—Interpretation of SLAR imagery of the Great Lakes area.

detection, whereas data on random or ephemerous phenomena would require more flexible aircraft systems.

Resolution requirements and other system specifications would vary, depending on the scale of the study and the features or processes involved. For example, the 15-m resolution of most of the imagery previously used is generally suitable for coastal mapping of scales of 1:125 000. Occasionally, detailed

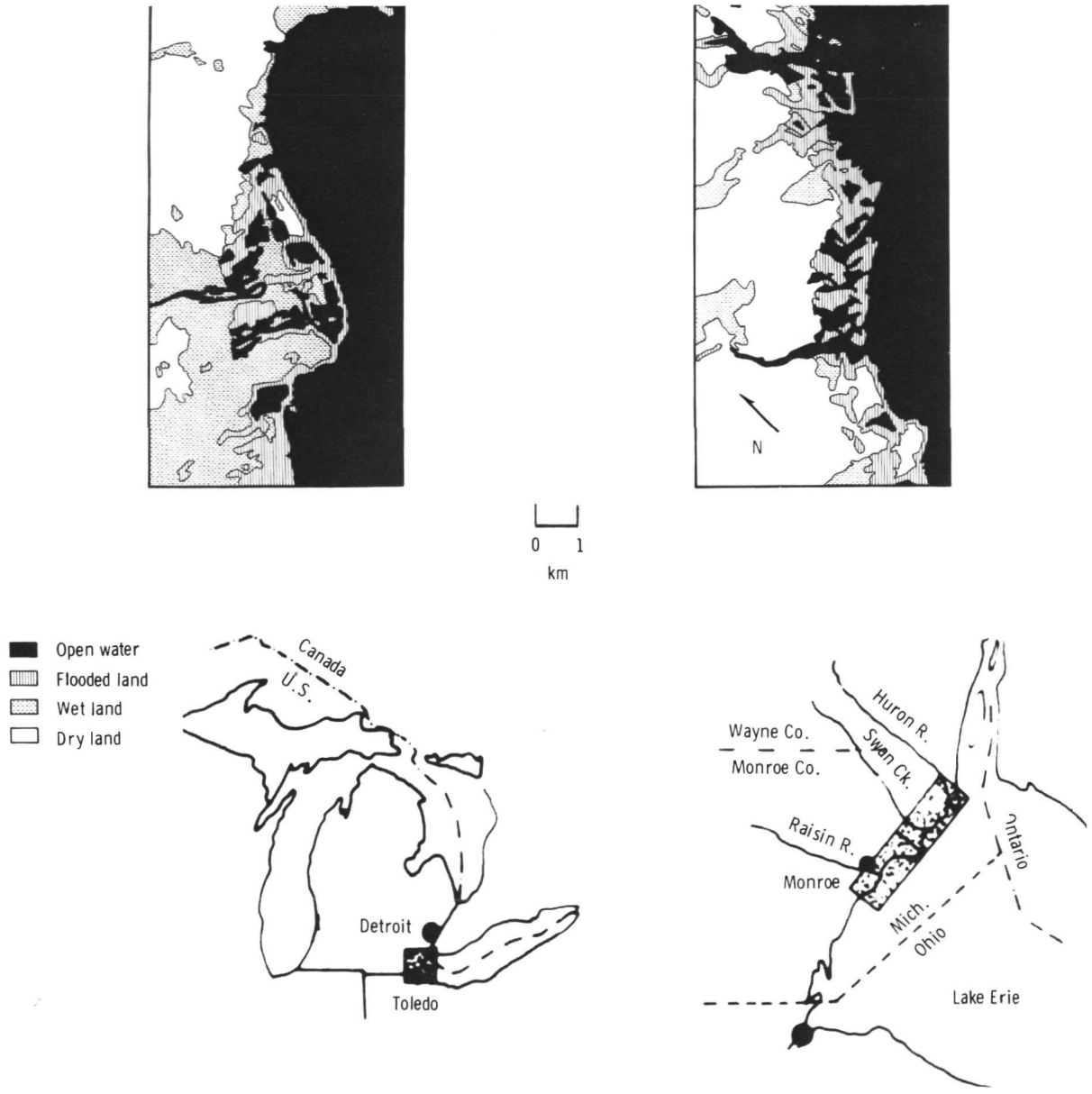

FIGURE 2–18.—Interpretation of ERTS–1 MSS imagery of the Great Lakes area.

mapping at 1:62 500 can be accomplished. An increase in resolution to 3 m would disclose new uses for active microwave systems not mentioned previously.

The optimum depression angles vary with both the type of region (coastal mountain as compared to coastal plain) and the features to be identified. In flat coastal plains, shallow depression angles between 3° and 17° would provide maximum topographic information. The use of low depression angles results in the enhancement of topography and suppression of vegetation or surface material information. Radar shadowing is increased and would be undesirable in other than flat terrain with subtle topographic relief or slope angle.

The use of high depression angles (be-

tween 45° and 76°) is valuable in mapping mangroves (ref. 2–62), lakes (ref. 2–55), tidal flats, shell reefs, and surf zones (ref. 2–65). These features are much easier to define in the near range of present operating systems.

Alteration of the gain setting to record the subtle tonal changes in the low-return areas of open sand, some marsh vegetation, and water would provide information not available with the radar imagery taken with AGC setting for the normally high-return land targets. The use of magnetic tape to record the signal and special processing techniques would be one approach to solving the problem and providing the user with a sliding, expanding, or contracting dynamic range.

In low coastal plain environments, look direction is not especially important. However, the best look direction appears to be with the aircraft flightpath parallel to the shoreline and with the imaging system over the water looking toward land. This look direction is especially important for high-cliffed or mountainous coasts; otherwise, the shoreline would be obscured by radar shadow.

STUDY OF HYDROLOGY OF SOLID WATER

This section briefly explores the literature concerning remote sensing of ice and snow surfaces. Four areas of interest are considered: (1) permafrost, seasonally frozen ground; (2) glacial ice (both cold and temperate), including the concept of sounding polar icecaps with a nonimaging radar; (3) snow, with special reference to the study of the free water content and water equivalent and the use of these data for hydrologic applications; and (4) freshwater lake ice, including a description of a presently operational system oriented to problems of navigation through the ice in the upper Great Lakes of the United States and Canada.

The problems of remote sensing of the Earth surface materials are highly complex and have been the subject of numerous articles. With snow and ice, there are constraints not associated with many other materials. The most obvious constraint is temperature, because the maximum attainable temperature is 273 K. A second constraint is that, at this maximum temperature, water can exist in two states: liquid and/or solid. To a degree, this dual state can also occur at slightly lower temperatures if the liquid phase is transitory or newly introduced from without. Also, snow generally has a fairly high albedo in the visible portion of the electromagnetic spectrum, which makes it readily seen against darker, natural backgrounds.

Aerial photography and satellite photography are excellent sensors for identification of snow-covered areas (refs. 2–66 to 2–69). In addition to conventional photography, radar has been useful in identifying snowfields (ref. 2–36) and could be used for delineating aerial distribution of these features. Active microwave sensors have an output that is computer compatible, have essentially all-weather capabilities, and could provide near-real-time information.

Permafrost

Introduction.—Permafrost is defined as a temperature condition of the ground, and permafrost is said to exist when the temperature is permanently below 273 K. Often, but not always, this condition coincides with the presence of frozen ground; that is, ground in which ice is present.

Permafrost poses severe problems in geotechnology, construction of pipelines, roads, airfields, dams, and oil and mineral exploration and recovery. These problems are often associated with volume percentages of ice in excess of the pore volume of the soil and rock matrix; thus, melting of the ground can result in collapse and soil failure. The large-scale activities planned in Alaska—transportation corridors, the Alaskan oil and gas pipeline, and the military pipeline from the Naval Petroleum Reserve—might benefit from more reliable remote sensor data. The need for or location of heat pipes along the Alaskan pipeline is an example of the possible integration of two technologies.

Basic objectives of remote sensors for

permafrost.—The information sought from sensors for geotechnical endeavors are—

1. Delineating permafrost bodies in the discontinuous zone.
2. Locating permafrost "windows" in the continuous zone.
3. Determining ice content of permafrost.
4. Determining the thickness of permafrost.
5. Determining the depth of thaw of the active layer.
6. Monitoring degradation of permafrost caused by natural (e.g., forest fires) and manmade activities.

Sensor capabilities.—To adequately discuss sensor capabilities, some basic facts about permafrost must be outlined.

1. Permafrost occurs in almost every known soil and rock type; thus, the variations in geological and dielectric properties of permafrost are as large as those observed in unfrozen ground. Only by comparing similar material types in the frozen and thawed state are certain differences discerned. For example, permafrost with resistivities less than 50 ohm-m were observed in marine sediments at Barrow, Alaska, whereas permafrost at Galbraith Lake had a resistivity of 10^6 ohm-m (greater than frozen limestone).
2. The top 0.5 to 1 m of permafrost thaws in the summer and is frozen in the winter. This "active layer" often consists of a saturated, organic material. The large seasonal variation in surface properties greatly influences sensor capabilities.
3. The depth of permafrost varies from 1 km in the most northern regions of the U.S.S.R. to less than 1 m at the southern boundary of permafrost (e.g., Copper River Basin in Alaska).

Geotechnical endeavors often require that the information listed previously (in the section regarding basic objectives) be obtained to a depth of 15 m. For example, the thaw bulb under the buried section of the proposed Alaskan pipeline will reach a depth of approximately 10 to 15 m after 2 yr of operation.

Table 2–II lists the geophysical, electrical, and electromagnetic sensors used in the past and planned for the future to probe permafrost to depths of 15 m or more. The application of these methods relies on the fact that frozen and unfrozen ground differ in electrical resistivity (fig. 2–19) and that the ice content of the ground is related to resistivity (fig. 2–20).

The dielectric properties of frozen ground at ultrahigh frequency (uhf) and microwave frequencies are mainly determined by the amount of liquid water in frozen soil. The dielectric loss of a frozen soil as a function of temperature is shown in figure 2–21. Based on these data and on the fact that in the summer the top 0.5 m of permafrost is thawed and water saturated, active microwave sensors will lack the penetration required to satisfy the geotechnical objectives previously listed.

However, this limitation does not mean that active microwave sensors have no use

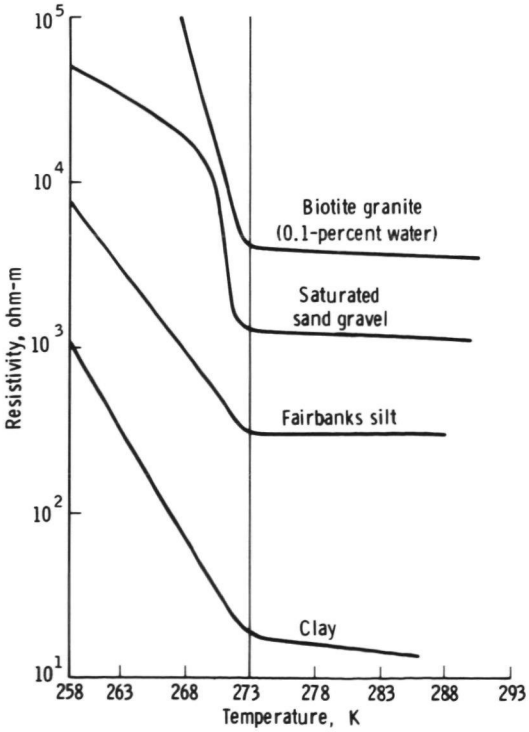

FIGURE 2–19.—Resistivity of soil types and a rock type as a function of temperature.

C, 2

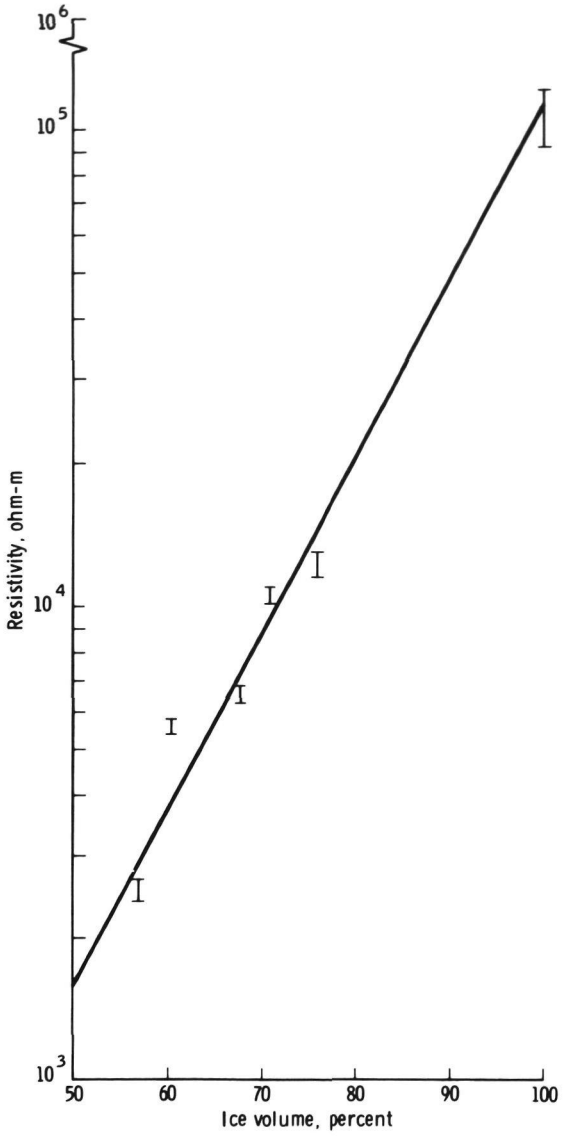

FIGURE 2–20.—The resistivity of frozen Fairbanks silt as a function of ice content by volume.

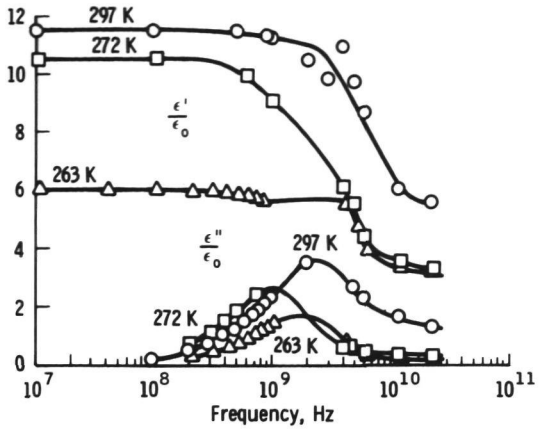

FIGURE 2–21.—The dielectric constant ϵ'/ϵ_0 and the dielectric loss ϵ''/ϵ_0 for a clay soil at several temperatures as a function of frequency.

in permafrost regions. The starting point of any exploration program is a good base map of the area on, for example, a 1:2500 scale. Because of the all-weather and day/night operation, SLAR may significantly reduce the cost of photocoverage.

Finally, the previous statements apply to geotechnical exploration. Permafrost differs from other regions of the world only in the presence of permanently frozen ground. All objectives pertaining to geology, surface water, and oil and mineral exploration apply equally to polar regions, perhaps even more so, because of the general inaccessibility of Arctic regions.

Demonstrated remote sensor observations.—Next to surficial geological mapping from aerial photographs, the most promising sensors for reducing the cost and improving the quality of subsurface exploration in the Arctic are those used in airborne resistivity mapping techniques. Several airborne surveys have been conducted in Canada and Alaska, and more are planned.

The ERTS imagery of Alaska has provided some high-quality photographs of all areas of Alaska. These images are used for—

1. General landform mapping.
2. Determining areas covered by lakes and some estimates on the depth of the lakes.
3. Maps of snow cover extent.

The U.S. Geological Survey Mohawk aircraft with SLAR imaging equipment were flown over the coastal plains near Barrow, Alaska. The images distinguished between lakes frozen to the bottom and lakes with a certain amount of water under the ice. Conventional photographic coverage has been used to monitor the environmental effect of recent construction.

Functional requirements.—Functional re-

TABLE 2–II.—*Summary of Geophysical, Electrical, and Electromagnetic Sensors Used and Planned for Permafrost Mapping*

Sensor type	Frequency	Comments	Present users
Galvanic resistivity measurements.	dc	Deep penetration possible; area coverage expensive.	Sensor is frequently used in U.S.S.R., Canada, and United States for onsite exploration.
Ground and airborne radiowave methods.	15 kHz to 1 MHz	Penetration as much as 91 m; cost approximately $30 per line mile.	First surveys were flown by Geological Survey of Canada, U.S. Geological Survey, and Cold Regions Research and Engineering Laboratory (CRREL) in 1973; system is going into routine operation.
Ground and airborne dipole-dipole methods.	100 Hz to 10 kHz	Ground method in use; airborne methods under development.	Several geophysical companies offer equipment and service for ground measurements; airborne equipment is available for mining technology only.
Magnetotelluric measurements.	0.001 Hz to 10 kHz	Under development and testing.	Sensor is used by the U.S. Geological Survey, Geological Survey of Canada, and CRREL.

quirements are identical to those listed under geology, cartography, oil and mineral exploration, and surface waters.

Permafrost summary.—The greatest need for remote sensing of permafrost areas of Alaska, Canada, and the U.S.S.R. is in geotechnology, route selection, and site selection. Sensors need to be developed that reduce the amount of exploratory drilling and provide better extrapolation between drill holes. Improved subsurface information will reduce environmental damage to permafrost terrain.

Because of the depth required in geotechnology, the most successful sensors should operate in the frequency range from 100 Hz to 1 MHz. High-altitude aircraft and satellite sensors may have a supporting role in geotechnical exploration.

Except for the study of geotechnology, the sensor requirements for permafrost regions do not differ from the sensor requirements for other areas of the world. Hence, the objectives pertaining to geology, land use, and surface waters apply equally to permafrost terrain.

Glacial Sounding

A unique application of active microwave systems exists in the cold glaciers of the world (glaciers in which the temperature is permanently below 273 K). Two major examples are the Greenland and Antarctic ice sheets. Because of the low signal attenuation in snow and ice, microwave radiation penetrates to great depths. A pulse that is transmitted from an antenna mounted under an aircraft is partially reflected from the air-ice interface and partially transmitted into the ice where it is subsequently reflected from the ice-bedrock surface and from other layers in the ice.

Attempts have been made to use similar systems on temperate glaciers, sea ice, and lake ice. In general, signal attenuation, limited thickness, and inhomogeneities have caused problems. Some of these problems may be alleviated in future systems.

Snow Cover

For many drainage basins in the temperate zones of the world, melt waters represent a major part of the annual yield of the basin. To properly use this water resource and to control flood drainage from high-stream discharges during the melt period, hydrologists must have timely information to perform their long- and short-term forecasts. Long-term forecasts are important for irrigation,

navigation, hydroelectric power, and water supply. These forecasts are usually made on an annual basis. The initial prediction is made at the beginning of winter, based on moisture conditions existing in the drainage basin at that time, and the basin response (annual runoff) is projected to various levels of snow accumulation (normal, above normal, and below normal) during winter months. The initial forecasts are revised as additional data on the areal extent of snow cover, depth of cover, and water equivalent become available. This forecasting process continues through the snowmelt period when additional data become important in determining the volume of melt-water runoff.

Therefore, the basic objective of the long-term forecast is to provide as accurate a prediction of annual runoff from snowmelt as possible and with sufficient leadtime to provide maximum use of the runoff. Attaining this objective requires accurate monitoring of snow cover. Specific uses and user agencies would include

1. Irrigation: Irrigation districts, U.S. Department of Agriculture, U.S. Bureau of Reclamation, and State regulatory agencies.
2. Hydroelectric power: U.S. Army Corps of Engineers, U.S. Bureau of Reclamation, Bonneville Power Administration, public power utilities, and private power companies.
3. Water supply: U.S. Bureau of Reclamation, State regulating agencies, water supply districts, and municipalities.
4. Navigation: U.S. Army Corps of Engineers.

Short-term forecasts are primarily involved in flood prediction and assessment of flood-hazard potential. Severe snowmelt floods have occurred in the upper Missouri River and Mississippi River basins in 1965 and 1969. Although flood damage was extensive in both instances, good forecasts of the flood potential and advanced planning by Federal, State, and local authorities served to mitigate the amount of damage. Improved techniques for forecasting could result in even less damage. For flood-forecasting purposes, accurate definition of the areal distribution of the snow cover, snow depth, and water equivalent of the snow are important, as well as the rate of production of snowmelt runoff. The principal Federal agencies involved in flood forecasting are the National Weather Service (NWS) and the U.S. Army Corps of Engineers. Numerous agencies are involved at the State and local level.

Demonstrated remote sensing observations.—Barnes (ref. 2–70) reports results indicating that ERTS imagery from MSS bands 4 and 5 have substantial practical application for snow mapping. The author states that snow cover can be mapped in more detail than is depicted on aerial survey snow charts. Barnes also indicates that ERTS MSS band 7 may be used to distinguish between wet snow and dry snow. Meier (ref. 2–71) reports that, for cloud-free and nonforested terrain, ERTS imagery enables rapid measurement of snow cover for specific drainage basins, but he reports that cloud cover causes problems in identification. Weisnet (ref. 2–72) performed a comparison of ERTS NOAA–2 data for snow-cover mapping and obtained good results.

Haefner et al. (ref. 2–73) have used imagery from ERTS for mapping snow cover in the Swiss Alps. The authors believe the imagery has potential, although many problems remain to be solved.

Active microwave results.—Knowledge of radar return from snow is limited. It is known that old snow gives strong isotropic returns at 35 GHz, at least in summer. It is also known that snow returns at 35 GHz (in the spring at Quebec) are strong enough to obscure the underlying terrain features. Dielectric properties of snow are known. Dry-cold snow has a permittivity close to unity and has low loss. Compacted cold snow has a higher permittivity but has low loss. Snow containing water in unfrozen form has much higher permittivity and loss. Research by Waite and MacDonald (ref. 2–36) indicates a feasibility for mapping the extent of old snow cover by using K-band imagery, regardless of most weather conditions. Their

work also indicates a significant difference in signal return between old and new snow.

Functional requirements.—Active microwave sensor requirements for snow mapping are dictated by the need to measure moisture content of snow, depth and extent of snow, and moisture content or freeze/thaw status of soil. A dual-wavelength microwave system is desired to give short-wavelength response from snow cover and long-wavelength penetration data. A spatial resolution of 15 m is desired, but a resolution of 100 m would be useful. Systematic, reliable coverage on a weekly basis is needed.

If a proper model of the dielectric and geometric properties of natural snow in its various states were available, a theory could be developed to show optimum frequencies and polarizations for the different measurements. Enough is known about the physics of snow and backscatter to permit starting such research immediately.

Although theory can guide system development and data interpretation when properly validated, experiments are needed both to validate the theory and to obtain information for conditions not included by the theory. Furthermore, airborne experiments will be required to develop techniques for use in operational systems.

Ground-based measurements should include the following: (1) controlled and artificially simple snow conditions, (2) natural snow conditions at a site that can be monitored continuously throughout a winter season in which snow remains on the ground for several months, and (3) natural snow conditions in a variety of locations. Because of numerous sites, only occasional measurements can be made of each site. Measurements should be made with a swept or stepped frequency system covering a range of approximately 4 to 40 GHz. Because frequencies above 20 GHz may not soon be usable in space, the measurement might stop at 18 to 20 GHz, but comparison with existing 35-GHz images would certainly be desirable. Multiple polarizations are necessary initially, although early data should be scanned to determine the utility of multipolarized data.

Aircraft measurements will require radar systems at appropriate frequencies; thus, an early attempt should be made to verify the applicability of the X-band. Although synthetic aperture radar will be needed in space, a real aperture system can be used on an aircraft, which will simplify the task of scheduling and locating suitable radars. This system should make flights over test sites having a variety of conditions. For most purposes, operational considerations can determine whether multiple flights over a few sites or a few flights over widely differing sites should be made. However, repeated flights over at least one site should be made to enable testing of change detection.

Repeated aircraft missions are required in the research phase. As the system becomes operational, aircraft mission needs will change, but they may not diminish. Spacecraft can provide regular surveys that will suffice for mapping large-scale phenomena. For short-range forecasting, aircraft missions flown between spacecraft missions will be desirable in areas where meteorological conditions favor rapid melting. The magnitude of this need can be determined only after more information is known on the radar response of snow cover of different kinds.

Spacecraft missions will need to cover critical areas in the mountains biweekly from first snow until near the end of spring melt. Whether weekly coverage by spacecraft is desirable during the melt or whether this need can be satisfied by aircraft should be the subject of a tradeoff study.

Freshwater Ice

Several questions are asked concerning the relationship of remote sensing to lake ice: (1) What do sensors really measure? (2) What can be inferred from these measurements? and (3) What information about lake ice is really needed?

Interpretation of remotely sensed data on lake ice is available (e.g., refs. 2–36, 2–74, and 2–75), but generally these data have

been qualitative rather than quantitative. Larrowe interpreted images by comparing airborne photographs taken simultaneously with the radar imagery (X-band, HH polarization). In all the studies, the lack of ground truth seriously limited any real study of the radar imagery concerning ice structure and thickness, crystal orientation, pressure and thrust features, cracking, and similar features.

In the study of seasonal lake ice, the day-to-day changes in the structure and distribution of snow on the surface of the ice sheet will possibly affect the structure of that ice sheet. Newly fallen snow and the drifting of this snow around and in the lee of obstacles on the ice sheet is, if sufficiently thick, capable of producing a significant insulative cover on the ice and thus retarding ice growth (ref. 2–76). In addition, when snowfall is small, ice growth is greater assuming that other climatological and limnological parameters are constant. The possibility also exists that, on a sheet of thin lake ice, the snowfall may be sufficiently great to exceed the bearing strength of the ice, causing it to crack. Cracks may also be caused by thermal expansion and contraction (ref. 2–77). Water, infiltrating through such a crack, may mix with and saturate the overlying snow, forming a slush layer that, when frozen, forms a highly granular ice layer (referred to as "snow ice" or "white ice"). This type of ice is uniquely identifiable on SLAR imagery (ref. 2–78).

Another commonly identifiable feature is called an ice foot. An ice foot is described as being "composed of any combination of frozen spray or lake water, snow accumulations, brash, stranded ice floes, and sand that is either thrown on the ice by wave action or is blown out from the exposed beaches" (ref. 2–79). Although an ice foot is a localized feature, because it occurs only on shorelines of relatively large lakes, it is an important indicator of geomorphic activity along the shoreline. Ice foots often persist into the spring after much of the lake ice has been melted or blown into the lake; thus they act as breakwaters, protecting the shoreline from erosion and deposition. If not removed from the shoreline, ice foots can present a hazard to navigation in a manner similar to icebergs in the North Atlantic. Several recent papers have described these ice foots (refs. 2–78, and 2–80 to 2–82), which are clearly visible on SLAR imagery (fig. 2–22).

Some attributes of lake ice that may be measurable by microwave remote sensing are—

1. Ice thickness, temperature profiles, rates of growth, and structures.
2. Snow accumulation, moisture content and density, and metamorphic stage.
3. Spatial and temporal distribution and thickness of both ice and snow cover, together with the spatial and temporal distributions of open water.

Lake-ice monitoring is an area in which the prototype for an operational system is most advanced. During the winter of 1973 to 1974, the initial steps for an ice information system were taken by a joint agency effort involving the U.S. Coast Guard, NWS, NASA, and the U.S. Army. The system used X-band SLAR imagery from two U.S. Army aircraft and one aircraft operated by NASA Lewis Research Center. Images were interpreted by the research team at Lewis Research Center, following the return of the SLAR-equipped plane to its base; and the image, together with an interpretive chart, was relayed for approval to the Ice Information Center at Cleveland, Ohio. After inclusion of data obtained from visual flights and inclusion of thickness data acquired by NWS, the approved ice chart, together with the radar image, was transmitted to those ships and shore installations having telefacsimile equipment. Approximately 200 such ice-chart radar image products were produced and distributed during the ice season (fig. 2–23).

Midway through the ice season, data from a short-pulse-radar ice thickness profiler, being developed by Lewis Research Center, were incorporated into the ice information system. This special radar was mounted on a C–47 aircraft operated by Lewis Research

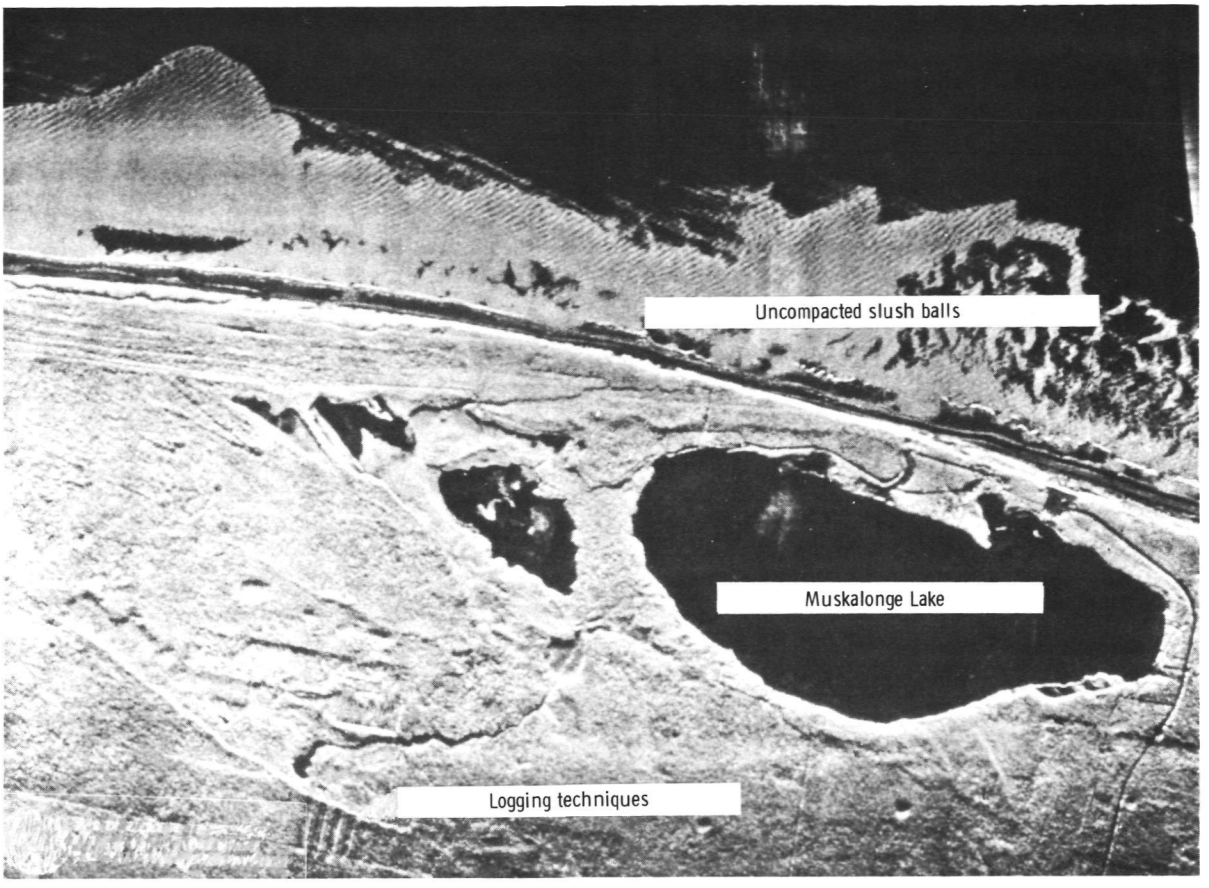

FIGURE 2–22.—X-band radar imagery of northern Michigan shoreline. Bright ridge along the shoreline is an ice foot; note the disconnected ice foots along shore between the slush balls and Muskalonge Lake.

Center and was capable of measuring ice thickness with an accuracy of approximately 5 cm from altitudes up to 1500 m.

Although further studies will be required, preliminary results from this study indicate that the dynamic range of reflected power from the entire range of natural ice/water targets spans only 20 dB. If this fact is true, it is especially important because considerable simplifications in data recording, telemetry, and processing systems could be affected. However, some data from the real aperture system operated by Lewis Research Center seem to indicate a larger dynamic range.

The functional requirements for lake-ice monitoring may be summarized as follows:

1. Frequency: X-band, cross-polarized seems to be adequate.

2. Resolution: 40-m spatial resolution and 2-dB intensity resolution are adequate. Intensity should be recorded over a 20-dB range.

3. Coverage: A swath width of 100 km is adequate, if properly centered.

4. Repetition: Daily coverage would be desirable; however, several passes each day, as would be possible for an equatorial satellite system, are preferred.

5. Recording medium: Digital tape recording onboard is preferred.

6. Timeliness: Update is desired daily; old data are of no use in navigation. However, ice forecasters can use data, together

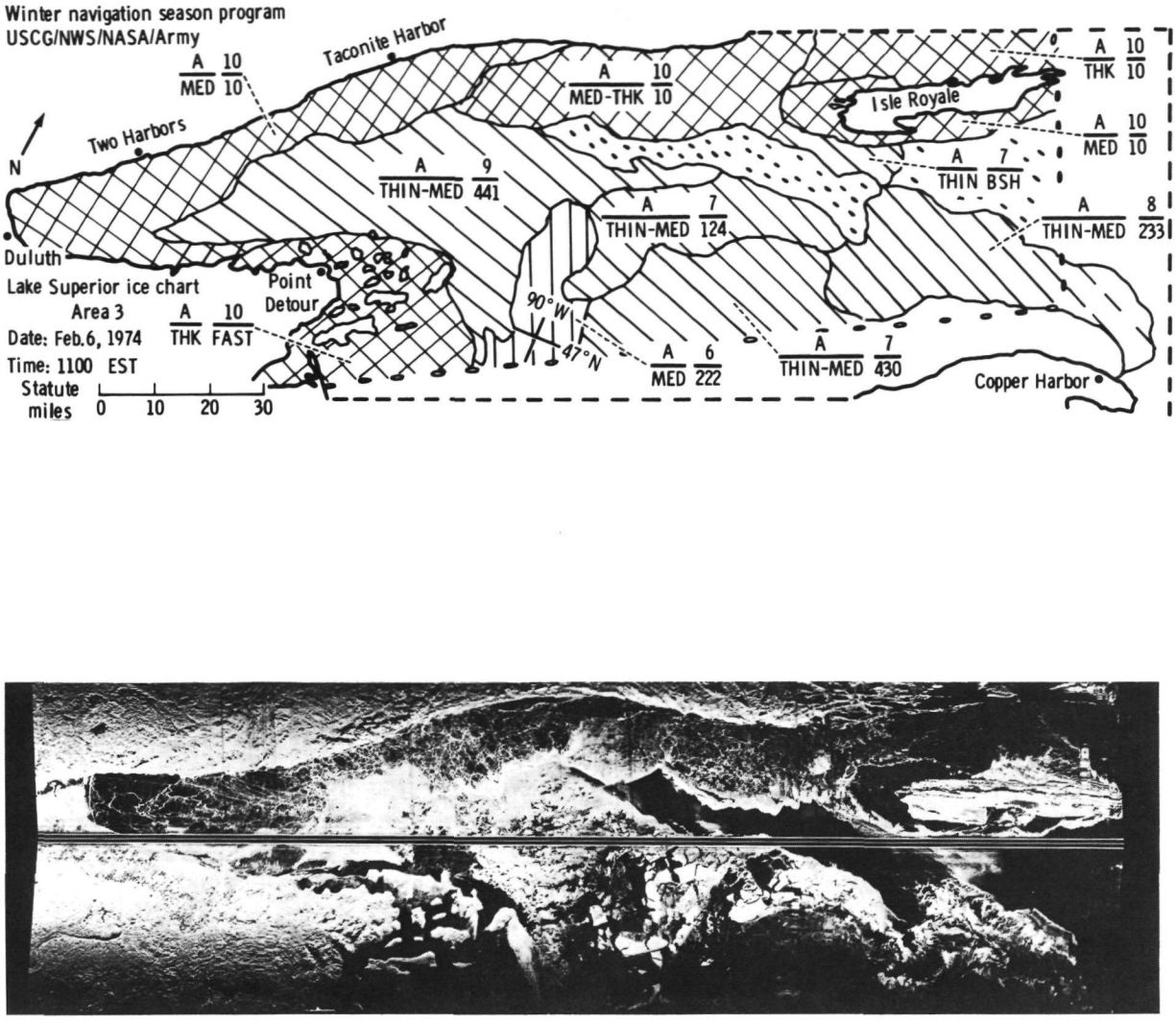

FIGURE 2–23.—Example of an ice chart and the related X-band radar image for the Lake Superior area.

with meteorological data, to predict freezeup and thaw.

7. Scale and projection: Generally, a scale of 1:1 000 000 is used, but for some areas the scale is 1:500 000. The type of projection is irrelevant.

Summary for Hydrology of Solid Water

This section is divided into three topics: (1) permafrost, (2) snow cover, and (3) lake ice. Glaciology, per se, is not directly addressed. However, valid inferences can be drawn from information presented here.

The major objectives of permafrost sensing are location and depth measurement. For many problems involving signal penetration, active microwave systems will be of minimal use. However, the primary contribution of active microwave systems will be the collection of data for base maps to be used in

geophysical exploration. Functional requirements are essentially the same as those pertaining to geology, mineralogy, and civil works (table 2–I).

Snow-cover sensing demands a high priority because of the need for better data in runoff prediction, water management, and flood prediction. Much research is needed to determine the feasibility of acquiring data for both water content of snow and the determination of the snow-water equivalent.

With respect to lake ice, a relatively low-resolution (50 m) system would be adequate for operational navigational problems in the upper Great Lakes. A prototype operational system using existing radars has already been initiated. Ice thickness is still a major problem because there are, at present, no known surrogates to aid interpretation. Several short pulse radars that could provide this much-needed data are operational, but their utility in space is marginal.

For lake-ice hydrology, the major needs are more intense ground truth and development of interpretation techniques. Existing radars will probably fulfill the vast majority of the data needs.

WATER POLLUTION

General Objectives

Many governmental agencies are interested in water pollution data. Although the Environmental Protection Agency is the major Federal agency empowered to investigate pollution problems, the U.S. Army Corps of Engineers, the U.S. Geological Survey, and the U.S. Coast Guard also have jurisdictional responsibilities. Amendments to the Federal Water Pollution Control Act, passed October 18, 1972, began a two-phase program to eliminate the discharge of pollutants into navigable waterways. In response, the U.S. Coast Guard began a program of pollution monitoring using remote-sensing techniques, including microwave remote sensing.

Because local, Federal, and international environmental/water resource agencies have the chief responsibilities of identifying, monitoring, and inventorying water pollution, they become data users and must either establish their data collection systems or depend on systems provided by other agencies. Remote sensors have both complementary and supplementary capabilities to provide data not otherwise available. A general objective in remote sensing is to provide rapid assessment of pollution accidents and to provide both supplementary and complementary data relating to pollution monitoring from continuous and semicontinuous sources. For active microwave sensing, the following objectives can be outlined.

1. Determine the nature and extent of inadvertent or intentional oilspills and monitor their dispersion either as they occur or shortly afterward. Possibly assess oil-slick thicknesses.
2. Determine the nature and extent of debris spills and monitor their dispersion.
3. As a complementary sensor, monitor pollution outfalls for surface effects and extent (i.e., scums, flotsam, foam, and water turbulence).
4. As a supplementary sensor, monitor pollution sources during nighttime and during weather conditions that prohibit the use of other remote sensors.
5. As a complementary and supplementary sensor, assess the effects of pollution (i.e., development of excessive algal growth and degradation of shore vegetation).

Demonstrated Remote-Sensing Observations

Aircraft platforms.—Aerial photographic systems have been extensively used in water pollution. Color and color IR imagery have been evaluated by several investigators as summarized in table 2–III by Welch (ref. 2–83). Qualitative studies have predominated, but there have been attempts to measure spectral properties of pollutants and their backgrounds. Examples of such studies include Neumaier and Silvestro (ref. 2–84), Villemonte et al. (ref. 2–85), Lillesand et al. (ref. 2–86), and Piech (ref. 2–87). To date, there has been limited success in quantifying heavy concentrations of industrial wastes.

TABLE 2–III.—*Photographic Specifications for Water Pollution Studies*

Problem	Best film-filter combination [a]	Best black-and-white film-filter combination [a]	Smallest scale used successfully	Notes
Water movement	Color, 1A	Pan, 25A Pan, 58 Pan, 90	1:60 000	Some water impurities caused confusion.
Detection of pollutants.....	Color, 1A	Pan, 25A Pan, 90	1:60 000	Color is significantly better than black and white.
Oil pollution	Pan, 47B Ortho, 18A	Pan, 47B Ortho, 18A	1:8000	Overcast day appeared to be best.
Inventory of kelp	Color IR, 12	IR, 89B	1:24 000	Sun glare caused problems.
Selecting underwater park sites.	Color IR, 12	None used	1:10 000	Stereoscopic vertical and oblique views were very useful.

[a] Numbers designate Wratten filters. A partial list of suitable film includes the following:
Color: Kodak Aero Negative (MS), Ektachrome Aero, Ektachrome X, and Kodachrome II, Anscochrome.
Color IR: Kodak Ektachrome IR Aero.
Pan (Panchromatic): Kodak Plus-X Aerographic, Double-X Aerographic, and Tri-X Aerocon.
Ortho: Kodak Royal Ortho, commercial.
IR: Kodak IR Aerographic.

A few attempts have been made to interpret other forms of pollution such as algae and aquatic plant concentrations. For example, plant growth on lakes can be outlined with color IR photography (ref. 2–59). Oil slicks have also received attention. Sensors ranging from ultraviolet (ref. 2–88) to thermal IR (ref. 2–89) to radar (ref. 2–90) have been studied. Many other studies have been undertaken for surveillance of thermal discharges using IR scanning (refs. 2–91 and 2–92).

Satellite platforms.—Sensing from orbital altitudes has taken various forms, ranging from assessment of large water bodies to study of individual point sources. The synoptic view provides a basis for documenting such aspects of water quality as general turbidity and eutrophication. Industrial pollution has been detected and mapped in a qualitative way (ref. 2–57). A variety of seasonal data relevant to the dispersal and distribution of pollutants is provided by satellite coverage (e.g., current, turbidity patterns, and flooding), whereas the applications to specific, local water-quality problems seem to concern mainly aircraft remote sensing. This situation could change with the development of new techniques.

Of all water pollution problems listed, radar has contributed most to the detection and mapping of oil slicks. Estes and Senger (ref. 2–93) and Guinard (refs. 2–90, 2–94, and 2–95) have reported on this application. Guinard concluded that a strong functional relationship exists between radar wavelength, sea state, and oil-film thickness. Evidence suggests the use of low frequencies, combined with low sea states, for detecting thin oil films. Thicknesses as small as 0.5 μm have been detected. Also 30- to 100-m resolution cells were sufficient with radar incident angles in the range from 2° to 20°.

The application of radar to other aspects of water pollution has been limited by the basic characteristics of radar signal interactions with water. Radar does provide information on surface features that either float on the water or change its surface geometry. Oil slicks and kelp beds are examples. Oil slicks smooth the water surface and thus reduce the radar cross section of the water

compared to its surroundings. Kelp beds have an opposite effect.

With the prospect of using high-resolution radar, some of the surface effects resulting from local pollution, such as surface scums and foam, should be detectable. No significant research has developed in recent years regarding the application of radar for pollution monitoring of these types of surface phenomena, probably because relatively high resolutions are required, and these data have not been generally available.

Functional Requirements for Active Microwave Measurements

Table 2–IV provides an estimation of certain important functional requirements, based on what little has been done and on some theoretical considerations of radar capabilities.

Data processing.—Image data are required for most analyses. Imagery may be derived directly, as with current operational radar, or may be obtained from CCT. The CCT may be processed in much the same way that conventional scanner data are manipulated to produce a spatial pattern.

Image rectification is an important consideration because correlations with output from other sensors are sometimes required, and these correlations will have to be transferred to a data base. In the case of water pollution data, a map base is needed; and, in many cases, absolute locations must be determined. As noted by Moore (ref. 2–96), all images should be converted to the radar equivalent of orthophotographs when correlation is needed with other remote-sensing images for data analysis. However, because of the state of the art with respect to radar, it is clear that further research is required.

Supplementary data.—Substantial ground-truth data are required to properly evaluate water pollution. Mensuration of the complex nature of certain types of effluents is not yet feasible by remote sensing, and possibly may never be feasible. However, the distinct vantage point provided by aerial and space remote-sensing platforms does provide at least qualitative data that may prove valuable. The significant factor is that a rapid assessment of the spatial dimensions of a problem is usually possible. Assessing the specific attributes of any water pollution problem, whether oil spills or industrial effluents, requires more than can be provided by aerial or space remote-sensing platforms and systems. Thus, surface sampling stations are usually needed. In addition, radar missions would need the support of other proven conventional remote-sensing systems to provide maximum information for most water pollution problems.

Accuracy of calibration.—Because most remote-sensing information is rendered in spatial formats, some type of mapping accuracy must usually be considered. The degree of accuracy required becomes a function of the purpose of the available data. Further research on data accuracy problems within the water-pollution/remote-sensing framework is needed.

Cost/Benefit Considerations

As indicated, remote sensing of water pollution has its principal value in presenting a synoptic view of the areal extent of the problem. It has been estimated that with ERTS, mapping can be reduced to costs as low as $0.03 per square kilometer. Assessment of the distributional patterns of water pollutants often requires numerous simultaneous observations, which are costly in both equipment and manpower. Although it would seem that the cost/benefit ratio could have favorable results, actual evaluations have not yet been performed. The U.S. Coast Guard experience with X-band radar could provide an important test case.

Recommendations

It must be recognized that radar may have limited application in the surveillance of

TABLE 2–IV.—*Estimated Radar Functional Requirements for Monitoring Water Pollution*

Objective	Frequency radar band [a]	Spatial resolution, m	Gray resolution	Temporal aspects	Polarization	Look direction	Angle, deg	Complementary remote sensors required	Platform
Oil slick detection and monitoring.	X	10 to 30	Conventional	Spill report and monthly in hazard areas.	Vertical	Side.	>20	No, but desirable	Aircraft
Debris spill detection and monitoring.	P, X, L, C	0.5	Fine under some conditions	Spill report and monthly in problem areas.	Vertical and horizontal.	Side and down.	Unknown	Yes	Aircraft
Surface effects of effluent discharge detection and monitoring.	P, X, L, C	0.5	Fine under some conditions	Intervals specified by control agencies.	Vertical and horizontal.	Side and down.	Unknown	Yes	Aircraft
Monitoring pollution effects, algal mats, and so forth.	P, X, L, C	1 to 10	Fine under some conditions	Seasonal or semiannually.	Vertical and horizontal.	Side and down.	Unknown	Yes	Aircraft and possibly spacecraft

[a] Synthetic aperture.

water pollution problems; thus, actual demonstration of the utility of radar must yet be produced. The best developed radar application appears to be in detecting, monitoring, and possibly assessing the thickness of oil slicks. However, application of radar for this purpose in the inland freshwaters needs to be demonstrated.

Other aspects of water pollution that result in surface roughness alterations, although theoretically detectable, have not been addressed.

Summary

Two major areas of water pollution are considered: oilspills and plant growth. Oilspills are the strongest area of study and application, not necessarily in terms of present operational status, but because of economic and environmental impact and importance. Present radar systems provide usable data, although more work is necessary for determining the optimum sensors for this work. One of the most important needs is in the area of interpretation and analysis.

PART C

AGRICULTURE, FORESTRY, RANGE, AND SOILS

INTRODUCTION AND GENERAL OBJECTIVES

In remote sensing of vegetation and soils, the important factor is the region of the electromagnetic spectrum to be sensed. Green vegetation absorbs strongly in the blue and red wavelengths primarily because of its chlorophyll content. Figure 2–24 shows a typical spectral reflectance pattern of a closed crop canopy and the corresponding spectral bands of the ERTS–1 MSS. The strong reflectance in the near IR is the result of matrices of cells and intercellular spaces, differing refractive indices, and large critical angles formed by cell walls in plant leaves.

The wavelengths used in microwave sensing are considerably longer than those used by ERTS. Therefore, the microwave return from vegetation is primarily influenced by the roughness (crop morphology) and dielectric properties rather than the cellular and molecular structure of plants. Thus, the determination of crop species, crop cover and/or leaf area, and crop vigor by microwave sensing depends on the effects of those factors on the crop structure and/or dielectric properties.

Crop vigor can be affected by many factors; for example, overgrazing, nutrition, drought, flooding, disease, and insects. One of the primary factors affecting agronomic production is plant-water deficit. Slight changes in plant-water content can cause significant decreases in growth and production. Some plant species change leaf orientation and hence basic geometry during periods of water deficit. Such changes in structure may be more readily detected by microwave than by visible or near-IR sensors. Dielectric properties of crops depend primarily on water content. Therefore, if small changes in dielectric properties of the crop can be detected, microwave sensors may prove valuable in detecting water deficits and the beginning of disease and insect damage. Extreme drought, disease, and insect damage would certainly be detectable because of leaf loss and consequent large changes in both crop morphology and dielectric properties.

The most important advantage of microwave sensing in agriculture is the all-weather capability. Timeliness in gathering data at specific growth stages in the ontogeny of the plants cannot be overstated.

Several promising applications for sensing of soil properties are made possible by some of the unique penetration capabilities of mi-

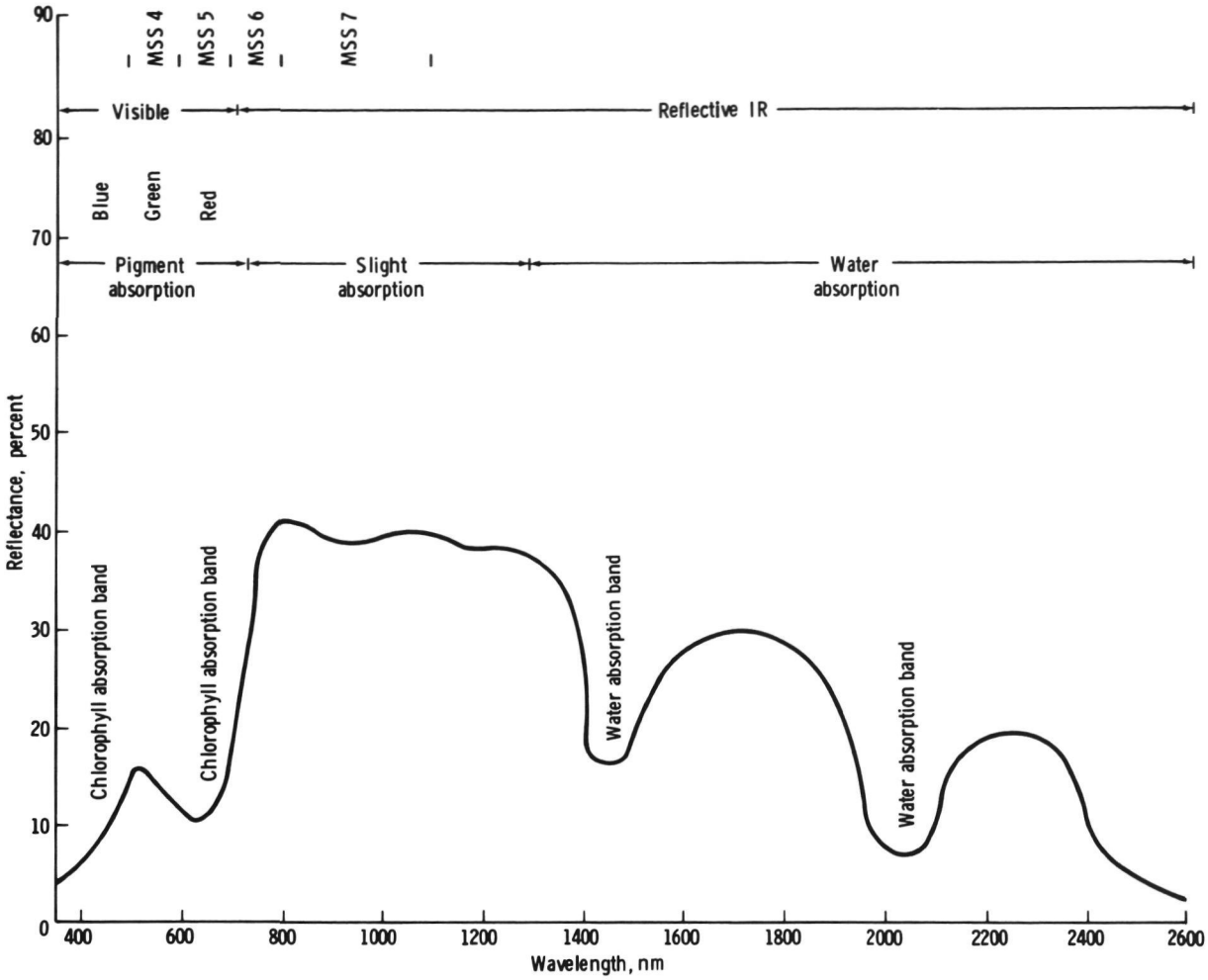

FIGURE 2–24.—Spectral hemispherical reflectance of a typical green crop canopy. The spectral response of ERTS–1 MSS bands and the primary absorption bands of chlorophyll and water are shown.

crowave systems. Measurement of soil water content would allow the development of a soil-moisture index that, in turn, could be used as input to prediction models for watershed runoff, crop yield, and soil strength or trafficability. Microwave measurements also offer possible new techniques in soil-type mapping for agricultural and military use. Other applications of regional value appear to be possible because of the ability of microwave sensors to readily distinguish differences in state (i.e., ice and water).

The primary need for measurement of soil moisture over large areas comes from the desire to develop more precise mathematical models for water-resources and crop-yield predictions. The spatial distribution of soil moisture indicates that such a measurement is feasible with active microwave systems.

Complex continuous watershed models have been developed in the past decade to mathematically represent the movement of water in the Earth-surface portion of the hydrologic cycle. These models are presently the only means of calculating "low flow" or continuous streamflows. Low-flow values for streams and the temporal distribution of flow volumes are extremely important for the

study of water supplies and the environmental input of changes in a watershed drainage area. Presently, soil moisture input to the models cannot be measured and is generated by submodels based on parameters developed by fitting the overall model to existing watershed data. The use of complex models is thereby restricted to use on watersheds with existing historical records.

Development of a soil-moisture index for use as input to crop-yield models is also very important. Crop-yield models are vital to improving timely estimates of world food production. However, no adequate system for measurement of moisture available to the plant root zone has been developed. Laboratory experiments on penetration and soil-moisture measurement with microwave systems indicate that reasonable estimates of moisture availability for plant growth are feasible.

Other applications in the areas of soil and soil moisture will require more refined spatial measurement; however, with improved technology in the following decade, most of the applications should become useful.

The general objectives of agricultural remote sensing are—

1. To provide information that is not readily available for decisionmaking in the agricultural extension, marketing, and processing industries.

2. To provide a better method for obtaining data for the Statistical Reporting Service, Agricultural Stabilization and Conservation Service, SCS, and Economic Research Service.

3. To monitor changes in agricultural land use for general research and development.

The specific objectives of microwave remote sensing are—

1. To identify major crops as one of a family of sensors to insure a timely and continuous remote-sensing capability.

2. To perform inventories of major crops, particularly those that either develop during the cloudy season (e.g., tropical rice) or may be identifiable on the basis of internal spatial structures rather than by visible/near-IR response (e.g., rubber).

3. To determine crop condition, disease severity, insect damage, leaf area index, and ontogeny to the extent that these factors affect either the plant-water status, gross crop morphology, or yield.

4. To determine the extent and timing of certain crop management practices such as irrigation, fertilization, and rotation.

CROPS, FOREST, AND RANGE

Demonstrated Remote-Sensing Observations for Crop, Forest, and Range Resources

The ERTS–1 observations.—The feasibility of crop identification from ERTS–1 has been demonstrated for selected crops and test areas: corn, alfalfa, and soybeans in South Dakota; wheat in Kansas; and various field and vegetable crops in California (ref. 2–97). An accuracy of 90 percent can be accomplished for field sizes larger than 10 hm^2. Usually, correct identification can be accomplished by knowing each crop calendar in each crop region.

Identification and mapping of major large-field crops (a prerequisite to yield and production estimates by remote sensing) is considered feasible. Once the crop has been identified, field mensuration is feasible with an accuracy of 70 to 90 percent using ERTS data. Timely and accurate estimates of winter wheat acreage, yield, and production in southwest Kansas were shown to be possible by Morain and Williams (ref. 2–98).

Feasibility for determining water deficit and disease severity from the ERTS data has not yet been determined. One of the primary difficulties has been the collection of data on a timely basis. Diseases spread rapidly, and the possibility that clouds might obscure the ground on a given ERTS pass can completely preclude their timely detection (ref. 2–99). The MSS has been used for determining leaf area and percent cover. The ratio of MSS band 4 to 5 has been found to relate to the amount of leaf area for wheat in Kansas,

whereas the ratio of MSS band 5 to 7 is best for estimating the leaf area for cotton and sorghum in Texas. This difference in ratioing techniques is apparently due to the low leaf area of wheat compared to the higher leaf areas of cotton and sorghum.

Forest discrimination into coniferous and deciduous types has been developed to a 90- to 95-percent accuracy level. Using multistage sampling techniques, the timber volume of a national forest district has been estimated to a confidence level and standard deviation acceptable to the U.S. Forest Service at a very favorable cost/benefit time/benefit ratio (ref. 2–100).

Range species/plant community vegetation mapping has been accomplished at various levels of success (70- to 90-percent accuracy). Several investigators have obtained encouraging initial results in range biomass estimation and range readiness predictions. If results continue to indicate good agreement between biomass and ratioed radiance levels, such data can be used not only as planning information for regional purposes but also as range-carrying-capacity decisionmaking information for the area manager at the field level on a near-real-time basis. A principal problem area in implementing this application is the requirement for data turnaround no more than 10 days after satellite acquisition.

A serious limitation documented by the NASA review of the ERTS–1 investigations is the frequent occurrence of cloud cover at critical periods in the growing cycle of crops (ref. 2–101). Persistent cloud cover is especially troublesome over Europe and tropical forest areas.

Active microwave observations.—Several published examples illustrate the capability of radar to differentiate both cultural and natural vegetation classes (refs. 2–102 to 2–104). Annotated examples of the imagery used in these studies are shown in figures 2–25 to 2–27. For agriculture, specifically, the feasibility for identifying crops has been shown for a combination of Ka-, Ku-, and X-band imagery. The values in table 2–V summarize the current capability as derived from film density data extracted from images.

The percent crop segregation in table 2–V was calculated as a percent of all fields comprising the fractional codes, not as a fraction of all fields of a given crop type. For example, grain sorghum on commercial imagery for September 1965 comprised 69 percent of all crops contained in the data space bounded by an upper and lower hyperplane, but approximately 95 percent of all grain sorghum fields plotted on the scattergram occurred within that data space. In other words, although most of the sorghum fields occur

TABLE 2–V.—*Percent Crop Segregation on Scattergrams as a Function of Radar Frequency and Date in the Growing Season*

Crop	Radar, band, and date			
	Westinghouse AN/APQ–97, Ka-band, July 1966	NASA DPD–2, Ku-band, Sept. 4, 1969	Westinghouse AN/APQ–97, Ka-band, Sept. 15, 1965	Michigan, X-band, Oct. 1969
Wheat	Not present	—	—	—
Grain sorghum	—	—	69	77
Corn	82 (cropped)	28	92	—
Alfalfa	—	50	—	—
Sugarbeets	92	—	97	64
Bare ground	91[a]	90	83	91

[a] Including wheat stubble.

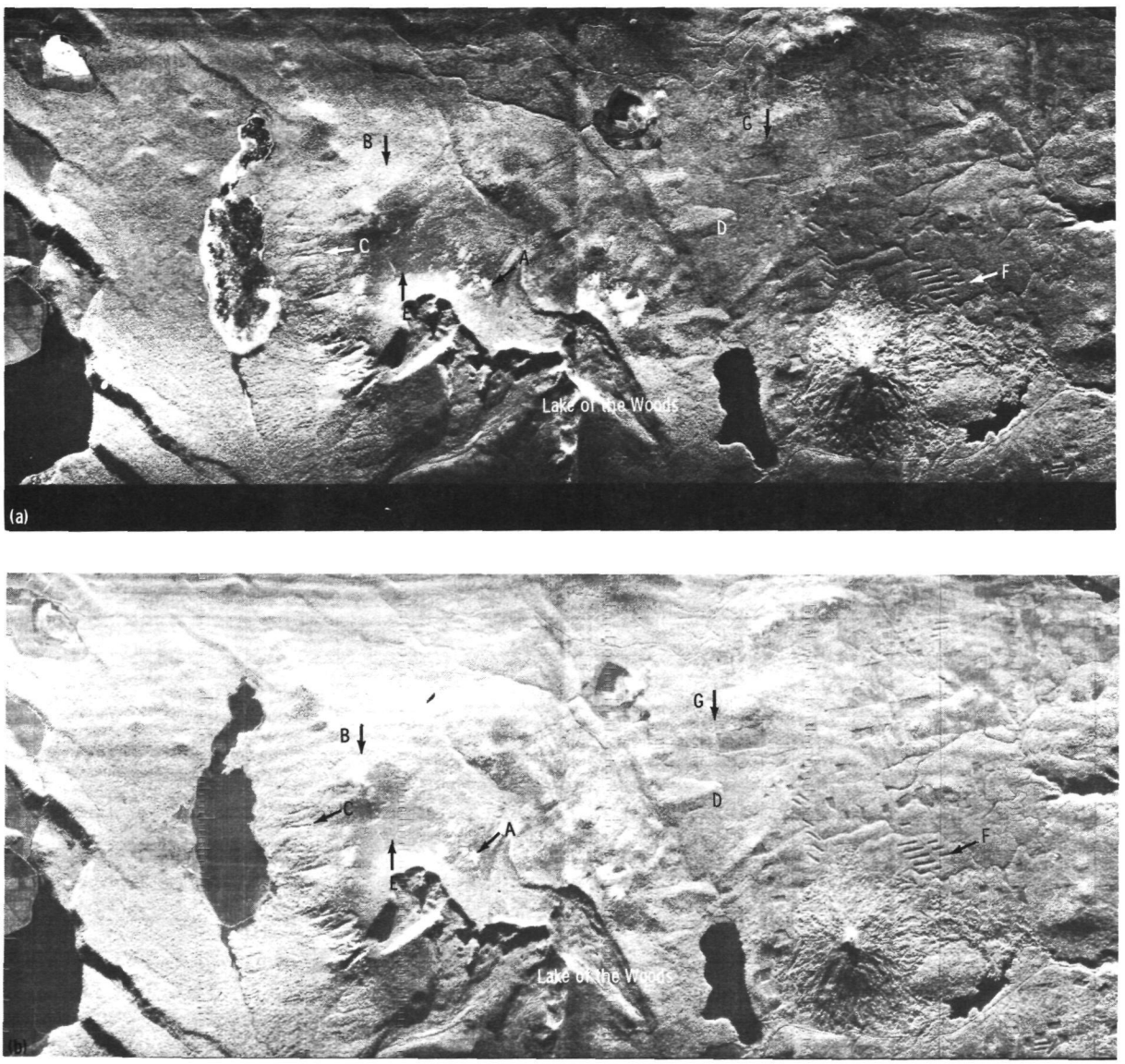

FIGURE 2–25.—Dual-polarization Ka-band images of a forested area east of Klamath Falls in southern Oregon. Forest tones and textures on different polarizations are findings of dominant species. Irregular breaks in the forest canopy are burn scars that can be categorized by age according to successional stages (compare the clarity of boundaries at *A*, *B*, and *C*). Most of the area is dominated by ponderosa pine (*D*) with sizable areas of white fir (*E*). Clear-cut logging operations are evident (*F*), which can be categorized by age according to regrowth. Both the logged-over and burned areas are dominated in early successional stages by chaparral, a favored habitat for deer; later stages are characterized by the encroachment of trees and, at this time, begin to acquire a textured appearance on radar (*G*). For further examples see reference 2–104. (*a*) An HH polarization. (*b*) An HV polarization.

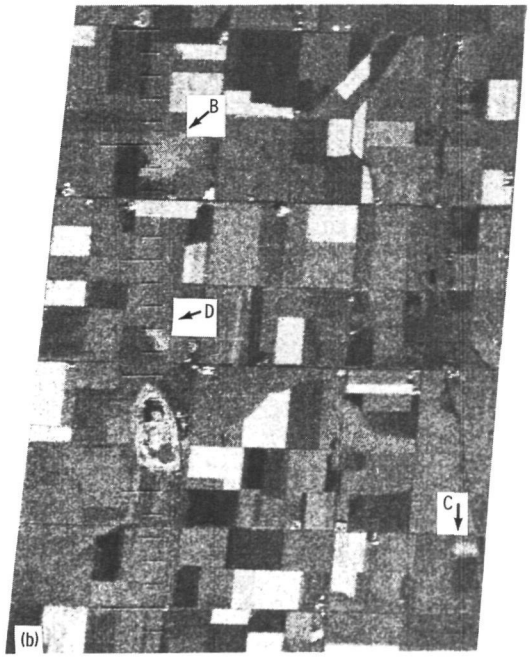

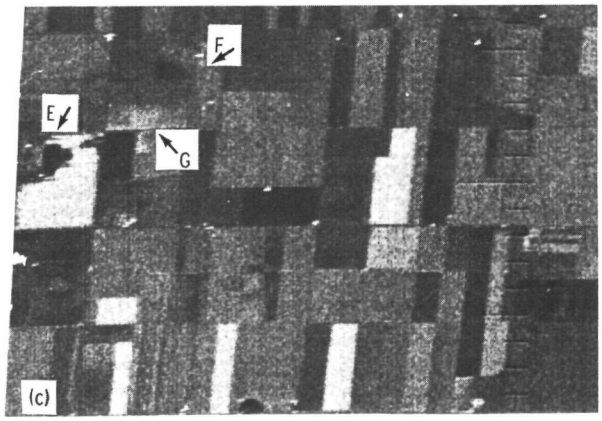

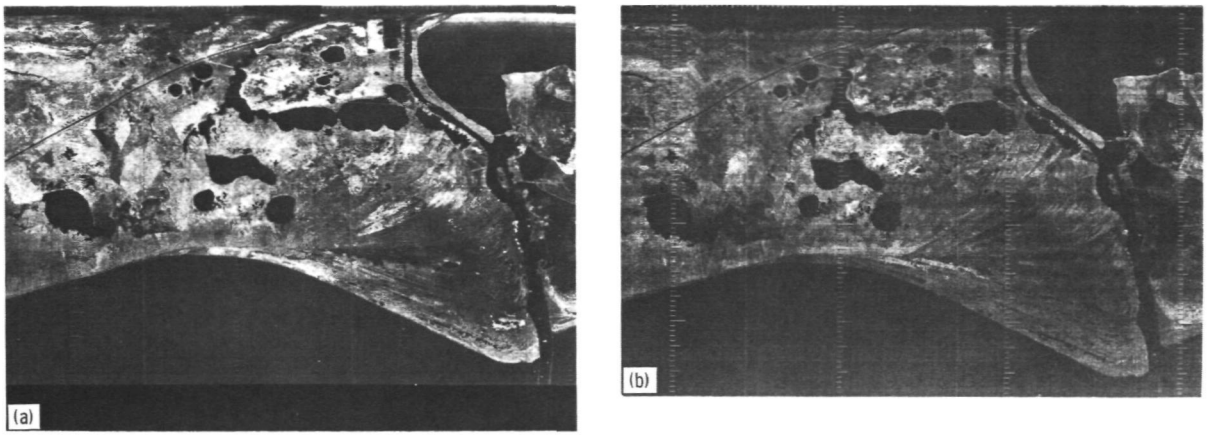

FIGURE 2–27.—Dual-polarization imagery of a grassland and marshland area along the gulf coast of Texas. Of striking interest is the difference in the pattern of bright areas on the two views. On the HH image, the brightness caused by moisture is added to the brightness contributed by surface scattering. The HV imagery is less sensitive to moisture and surface scattering but more sensitive to volume scattering; the area of high signal return is therefore much reduced on the HV imagery. Because of evidence such as this, it is believed that radar may have a unique role in grassland (rangeland) moisture monitoring, rice surveys, aquatic-plant density surveys in recreational areas, and plant phenological studies. For more information on the role of radar in phenology see reference 2–105. (*a*) An HH polarization. (*b*) An HV polarization.

within a fairly well defined data space, they cannot be unambiguously discriminated from many other crops.

From these efforts has come the basic justification for current ground-based microwave research in agriculture experiments by DeLoor and Jurrieens (ref. 2–106), Ulaby (ref. 2–107), and others. These experiments are extending the knowledge of signal interactions with crops and soils under differing cover, moisture, and plant morphology conditions. Generally, increase in plant cover is associated with increasing scene moisture; hence, the microwave response also increases. As crops decline in leaf area, dry out, or are harvested, signal strength drops. These cy-

FIGURE 2–26.—Examples of Ka-band HH images of agricultural patterns near Garden City, Kansas. (*a*) A general scene showing field pattern and ability to discriminate crop types. In this September scene, the lighter gray fields are corn, the medium gray fields are dominantly mature corn and sorghum with some newly planted (sparse cover) wheat. The darkest fields are bare or newly planted wheat. The fact that plow patterns are detectable (*A*) suggests that look direction and soil roughness are important considerations in SLAR interpretation. Crop moisture throughout the scene is generally low because the crops are maturing and drying out. New wheat has higher moisture but covers little of the ground. Therefore, the overall appearance of the image shows reduced gray scale contrast. (*b*) An area showing increased gray scale contrast resulting from higher moisture differential between crop types. The brightest fields are sugar beets with large turgid leaves. Moisture patterns within fields can be observed as irregularly shaped areas (*B*, *C*, and *D*), which suggest that information about crop condition may be obtained from radar. (*c*) An image similar to that in figure 2–26(*b*) but indicating an additional potential for radar to distinguish areas of flooding and faulty irrigation practices (*E*). Gradual tone transitions at points *F* and *G* also relate to crop or field condition.

clical trends can be useful for crop identification; also, when viewed under anomalous circumstances, they might aid as stress indicators.

However, to monitor and interpret seasonal trends, it is abundantly clear that sequential data must be obtained at several frequencies, polarizations, and viewing angles. Among the most fundamental issues to be resolved are tradeoffs in signal response from initially bare soils to partly covered fields to fully covered fields and their continuously varying moisture regions. Related tradeoffs, also to be quantified, include depth of signal penetration under variable moisture conditions.

For a large-area inventory of a single crop for which identification can be achieved on the basis of its unique phenology (e.g., winter wheat) or environmental conditions (e.g., flooded rice), active microwave sensing may not require the level of research effort alluded to previously. For example, a survey of winter wheat acreage was performed for Finney County, Kans., using Ku-band imagery. The results (table 2–VI) indicate the feasibility of accurately tabulating acreage for this particular crop. Once the acreage is determined, the application of an appropriate yield model enables the calculation of total production for a given area.

In conducting an inventory of natural vegetation, Morain and Simonett (ref. 2–108) investigated methods for the interpretation of vegetation from radar imagery by using an image discrimination, enhancement, combination, and sampling system developed at the University of Kansas. The study concerned various color combinations possible with HH- and HV-polarization K-band imagery on which various forms of level slicing and data-space sampling were performed. In this study, probability density functions confirmed that data-space sampling on a single image, or in two-space on two images, together with color combinations, is a valid discriminatory tool in studying natural plant communities.

Viksne, Liston, and Sapp (ref. 2–109) reported on the use of SLAR for forestry purposes in tropical zones. A great advantage of radar was that operations could be started and finished on schedule regardless of the weather. The authors briefly described the mapping of vegetation over an area of 17 000 km^2 in Panama. Coverage with overlap was obtained in approximately 4 hr with a YEA–3A aircraft having a groundspeed of 180 m/sec. The APQ–97 SLAR, which operates at K-band, was chosen for this area because near-perennial cloud cover limits the application of aerial photography. Because K-band signals do not penetrate vegetative cover at low depression angles, the technique enabled the evaluation of various vegetation types based on their radar return characteristics. Only very broad regions can be delineated in Colombia from radar imagery (scale approximately 1:220 000) of the area between Tumaco, Barbacoas, and Guapi. These regions are based on physiographic differences obtained from the interpretation of the radar imagery bands:

1. Region 1: Coastal zone influenced by the sea.
2. Region 2: Alluvial plains and low terraces subject to inundation.
3. Region 3: Terraces intersected by low hills.
4. Region 4: High hills and high plains.

TABLE 2–VI.—*Quadruplicated Automatic Data Processing Acreage Estimate for Wheat in Finney County* [a]

[Ku-band NASA imagery for June 1971]

Trial number	Estimated acreage	Comparison to SRS,[b] percent difference
1	181 081	5.7 low
2	177 559	8 low
3	171 776	11 low
4	204 687	6 high

[a] Unpublished research conducted at Kansas University Center for Research.

[b] The acreage reported by the Statistical Reporting Service (SRS) was 192 000 acres.

Only subsequent interpretation of small-scale aerial photographs (in Colombia approximately 1:40 000), visual aerial reconnaissance, and knowledge of the vegetation enabled further subdivision of these regions into two to five vegetation types on smaller areas.

Nicaragua information on 1:250 000-scale radar imagery flown in 1971 by Hunting is given by Francis.[1] A commercial radar, operating in the Ka-band, reveals similar units to those previously described but also shows *Pinus caribeae* stands to be darker than the other units. It was possible to distinguish three density classes in the pine stands. For areas larger than 15 000 km^2, radar was cheaper than black-and-white photography. A disadvantage is that a relatively large aircraft is required.

Perhaps the most ambitious use of radar in tropical forest land inventory has been in Brazil. Project Radar of the Amazon has acquired radar imagery of more than 5 million km^2 of the Amazon Basin. Radar mosaics at a scale of 1:200 000 are being produced from commercial synthetic aperture SLAR images. Brazilian scientists interpret the imagery and conduct ground-truth operations to produce maps of the geology, geomorphology, hydrology, vegetation cover, soil types, and land-use potential of this vast area. These maps will be used to select priority areas for more detailed remote sensing and ground survey.

An additional paper of interest, which emphasizes the potential aspects of radar for vegetation studies, is by Daus and Lauer (ref. 2–110). The principal conclusions of Daus and Lauer are summarized as follows:

1. Two primary characteristics of the SLAR imagery were found useful in analyzing wild-land vegetation resources: image tone and texture.

2. In this wild-land area, vegetation was the major factor affecting the texture, whereas slope and aspect were the main factors affecting tone.

3. A skilled interpreter can delineate differences in major vegetation cover types, especially in areas of nearly flat terrain.

4. In areas that were nearly flat and level, timber stands were consistently distinguished from everything else because of their relatively coarse texture.

5. Slight differences in topographic relief or change in slant range often caused two nearly identical timber stands to appear quite different on the SLAR imagery.

[1] Personal communication, 1972.

Functional Requirement for Active Microwave Sensing in Agricultural, Forestry, and Range Applications

With the possible exception of crop inventory and identification, fundamental ground and aircraft research must still be performed to determine the microwave response of important crops at various stages of growth and moisture status. Only then can these crop parameters be incorporated into useful models for predicting yield, biomass, and erodibility or incorporated as input into many managerial decisions. Research for all agricultural applications requires repetitive and/or multifrequency data collection over a range of viewing angles.

In general, the functional requirement for an operational active microwave program in agriculture depends on timely and repetitive coverage. It is impossible to be more specific concerning the number of required "looks" because this number varies as a function of crop species and geographic location. Inventories require relatively few looks (perhaps six per growing season) with a tolerable envelope of as much as 2 weeks. However, crop cover and vigor measurement leading to yield predictions or managerial decisions require near-real-time data with a tolerable envelope of not more than 3 days.

Available evidence shows the need for either a sweep frequency or multifrequency system operating in the 1- to 12-cm-wavelength region (and perhaps longer) over a variety of viewing angles from 30° to 70° off vertical. A spatial resolution of 15 m is desirable (particularly for small-field agricultural systems), but 30 m would suffice

for many useful applications. Gray scale resolution will need to be from 1 to 2 dB. Polarization and swath width are less easily predicted on the basis of current evidence. Probably, HH and cross-polarizations would be most generally useful, and swath width could vary without serious effect as a function of other design parameters.

Anticipated Microwave Results

It is anticipated that crop identification (and subsequent use in crop inventory) using a microwave system will be as accurate as those reported using the ERTS MSS (i.e., 90 to 95 percent for large fields of wheat, sorghum, corn, soybean, and alfalfa). There are many geographical locations where cloud cover has precluded any attempts to use MSS data. This would not be the case if a microwave system were the primary sensor.

Predictions of crop production rely heavily on soil-moisture conditions and crop vigor (e.g., disease and insect damage). Therefore, there is potential for a major contribution in this area for microwave sensors. Another area in which microwave sensing can make a unique contribution is in the assessment of areas of potential erosion in which crop cover and surface moisture are important parameters. Other areas of potential contribution are rangeland surveys and crop water deficits.

It has been postulated that long-wavelength microwave sensors capable of penetrating the vegetative cover of forests will provide returns from tree trunks and stems, thus allowing accurate estimates to be made of their volume. This theory must be tested; however, classification of major vegetation types in areas of moderate relief will be possible, perhaps for the first time in areas with persistent inclement weather.

Anticipated users.—Crop identification represents the first step in agricultural remote sensing. Thus, success in this task is potentially useful to the entire agricultural community. Government agencies such as the Statistical Reporting Service, Foreign Agricultural Service, and Economic Research Service are perhaps the primary users together with particular commodity groups such as the National Association of Wheat Growers. State and local tax-assessing boards have a vested interest in accurate crop identification for tax purposes. Other groups are interested in projecting water use and allocation.

Assessment of crop condition is immediately useful at local levels of agriculture and all the supporting agricultural businesses (fig. 2–28); consequently, farm and farm-support communities probably comprise most of the users. When crop condition impinges on yield and productivity, the users previously cited should also be included. For crop cover assessment, the Wind Erosion Laboratory of the U.S. Department of Agriculture Agricultural Research Service, the Soil Conservation Service, and similar organizations might be included.

Use and management of national rangeland by the individual owners and operators involve management decisions on a day-to-day basis. These decisions involve determination of optimum grazing density, regional animal movement, grain-feed demand, spraying to prevent encroachment, and decisions resulting from the effects of regional drought. Estimates of quality and quantity of rangeland on a regional basis affect decisions involving relocation of animals, natural grazing as compared to feedlot operations, and marketing practices. In the six Great Plains States extending from Texas to North Dakota, there are approximately 400 000 independent ranchers and farmers concerned with rangeland conditions. These six States produce 40 percent of the Nation's beef. The beef industry in this region exceeds $10 billion annually, but it is inadequately provided with regional rangeland condition information. The *Weekly Weather and Crop Bulletin* provides a gross rangeland condition map derived from county agents; however, these data are inadequate to support effective management practices on a regional basis.

The current lack of synoptic, regional

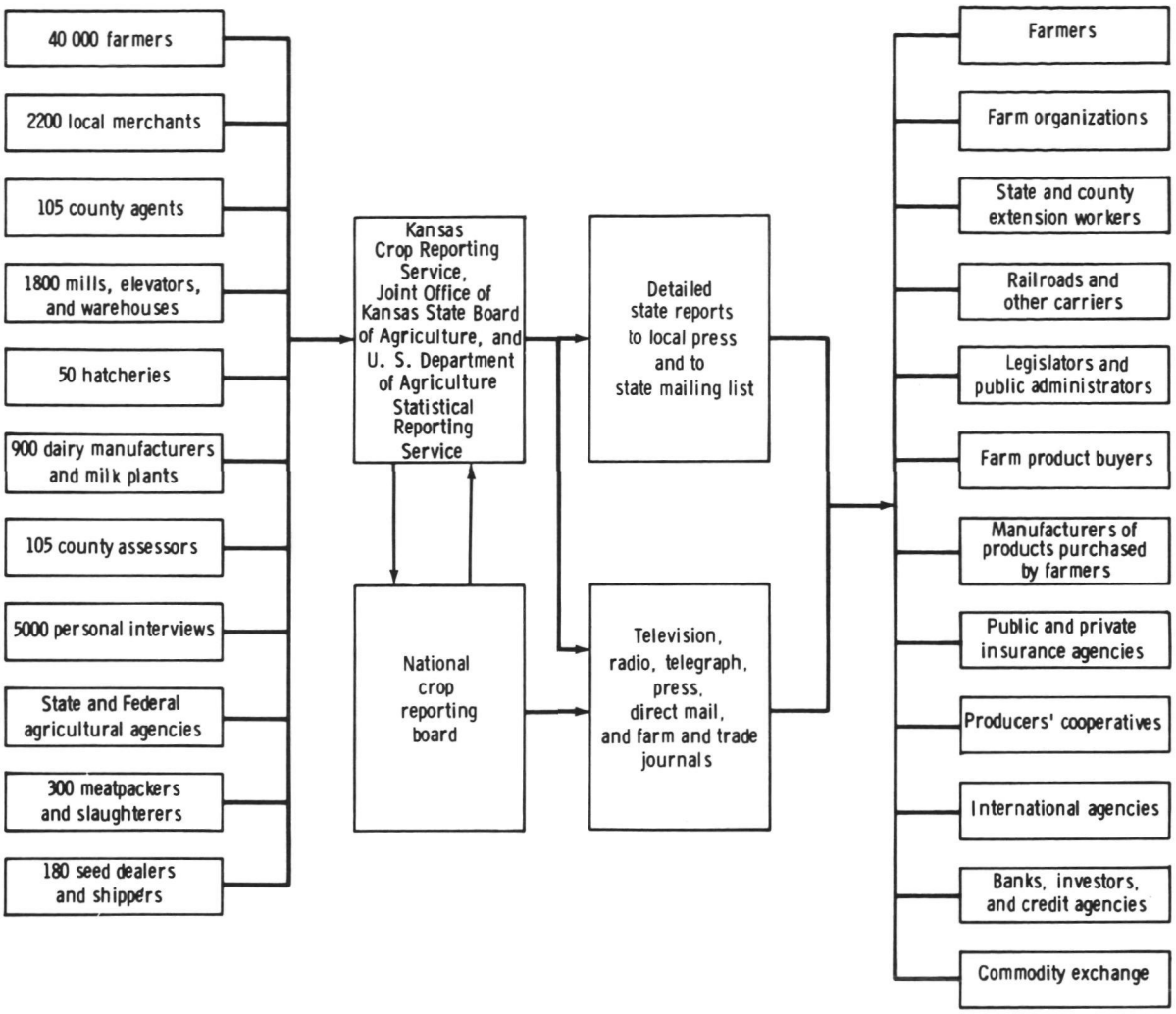

FIGURE 2–28.—Sources and uses of Kansas crop and livestock reporting information.

rangeland condition information has hampered effective use of this natural resource. The availability of regional ERTS data is expected to improve the coordination of rangeland management practices over large segments of the country. Assuming the acceptance of this new information source by managers, the need for more reliable rangeland condition information will become evident. Forest-land managers in the United States normally require more detailed information than can be provided by spaceborne radar systems. However, large areas of the globe are characterized by sparse population and/or persistent inclement weather, including parts of northern Europe, Asia, and North America; the equatorial rain forests of Africa, Asia, and South America; and parts of the tropics and subtropics. The land managers in these areas need the type data provided by SLAR to make forest classification maps and to document land-use change.

Value to the users.—The Dynatrend report (ref. 2–1) estimates that the annual benefit to U.S. users from accurate location and identification of major crops might approach $2 million (1972 dollar value). The bulk of this benefit is expected to result from improvements in remote sensing, especially if

identification accuracies can be improved for irregularly shaped fields smaller than 50 hm^2.

Furthermore, the report indicates that half the annual benefit derived from more timely and accurate crop inventories could be contributed by remote sensing; that is, an expected total of $5.6 billion (1972 dollar value). According to estimates, the annual value of improved inventories for wheat approached $100 million; an additional $100 million accrues for other major wheat-growing countries (Argentina, Australia, Canada, France, West Germany, and Italy). Improved rice inventories are expected to benefit U.S. decisionmakers in excess of $45 million and to benefit the rest of the rice-growing world considerably more.

Based on incomplete evidence concerning crop condition, the Dynatrend assessment suggests that remote sensing may contribute approximately 20 percent of the annual benefits from this activity (approximately $113 million at 1972 values). It is too early to assess the value of monitoring crop diseases from space or by microwave systems, because current sensors show limited capacity to satisfy these tasks on a timely basis.

Finally, the Dynatrend report lists several beneficial applications relating to management practices. Knowledge of diurnal and season transpiration rates, evaporation mapping, detection of faulty irrigation practices, soil-moisture mapping, improved range management, and other factors is crudely estimated to have annual world benefits of $500 million (1972 value). This number is projected into the tens of billions during the next several years. Because of electromagnetic limitations and resolution, present sensors are incapable of contributing to much of this annual benefit. Given the necessary research and development support for active microwave sensing, there is good reason to believe that some, and perhaps a large part, of this benefit could be achieved through decisions based on microwave sensing.

In forest resources, improvement in location of marketable resources and their identification by type should have an annual national benefit of $1.5 to $3 million and a worldwide benefit of perhaps $50 million. Accurate estimates of timber yield could benefit forest industries by $30 million annually ($1.6 billion worldwide). Finally, if forest-fire detection and damage assessment become operational applications, the Dynatrend report states that benefits in the range of an additional $1.5 to $3 million would accrue. To the extent that active microwave sensing can contribute, it can be assumed that developmental costs for sensing this flow resource would be worthwhile.

Cost/Benefit

There are complex economic considerations concerning the benefit portion of any cost/benefit analysis. Typical estimated benefits have already been presented. However, considerations of cost can be quite accurately determined and vary only according to the completeness of the line items included. For active microwave sensing in the next 5 to 10 yr, most costs are anticipated to be in sensor design and testing and in development of interpretation skills, including model building and data-processing techniques.

Principal Application Areas

The major advantage of including active microwave sensors among the systems for agricultural use is that it provides a continuous temporal capability. The unique contribution of microwave sensing is the potential for detecting crop-water phenomena that are major factors in limiting yield and production and that are important input in current yield-prediction models.

Large area crop inventory.—To accurately determine the acreage of a specific crop for inventory, the identity and area of the cropped field must be determined. This determination is equally true for range surveys. To identify the field and determine its area, knowledge of the crop calendar and the crop signature is required. Therefore, measurements of microwave return must be made at specific times corresponding to various

growth stages. Because the signal strength will depend primarily on structure and the dielectric properties of the viewed surface, there is an urgent need for information on the influence of crop morphology on microwave scattering and for separation of the scattering contribution of the underlying soil surface from that of plants.

Crop production estimates and erosion assessments.—The success of estimating crop production and rangeland biomass depends on the ability to identify the crop species. Although the range surveys are lower priority than crop inventories, they are an important application, especially in the Great Plains States. The current lack of synoptic regional range-condition information has hampered effective use of this natural resource.

Crop production estimates require inputs such as soil moisture and crop vigor. Surveillance of crop vigor will require data acquisition on a timely basis. Subtle changes in plant-water content must be detectable to be useful in assessing crop vigor. Soil-water potential in the root zone must be determined. Crop-cover and surface-moisture content will also be required for erosion assessment.

Depending on the success of measuring crop condition, active microwave data could provide solutions to many problems affecting managerial decisions, among which are—

1. Erodibility.
2. Irrigation scheduling.
3. Overgrazing.
4. Encroachment of undesirable range species.
5. Infestation by insects.
6. Epidemiology of disease.
7. Assessment of flooding or other storm damage.

Forest-land classification.—Classification of forest lands is the first step in the inventory and monitoring of this important resource. In many areas of the world, information of the type and extent of forest resources is lacking due to adverse ground conditions and persistent inclement weather, which hampers acquisition of aerial photography. The SLAR can provide the basic data necessary for production of reconnaissance maps and monitoring of shifting cultivation.

Principal Research Areas

Signal/terrain interactions.—Three simultaneous programs need to be established, each with a critical path and decision points to insure that research in the next decade is productive: (1) the development of theories and models, (2) the testing of these models using ground-based microwave systems, and (3) the integration of ground-based measurements with aircraft and eventually spacecraft sensors and with data from other sensor systems. Among theories and models, the most urgent needs are for data on crop morphology (leaf sizes, stalk lengths, leaf area index, fruit size, shape, arrangement, etc.) and the influence of crop morphology on scattering. Laboratory and field studies should be continued and expanded to determine the quantitative or, at least, the relative contribution of geometry and moisture content to signal backscatter over a range of frequencies and polarizations. In this regard, microwave sensing is at the developmental stage experienced in visible and IR multispectral scanning during the early to middle 1960's.

In addition to studies on signal/plant interactions, research should be supported on the spatial relationships of crops in fields (i.e., the areal dimensions of crops are as important as the shape of the individual plants that comprise the field). Subresolution phenomena (such as row spacings) and other spatial attributes (such as row direction) need to be studied to determine their contribution to crop identification. Signal returns from different canopy covers, soil-moisture contents, surface plow treatments, surface-moisture films, and so forth, need to be compared as functions of viewing angle, frequency, and polarization. The purpose of all the studies recommended here should be to develop broadband microwave systems as

prime sensors for crop condition and vigor assessment.

Major research areas in forestry include the development of procedures to compensate for changes in signal strength resulting from topography and the testing of multispectral radar (including long wavelengths) to aid volume inventory and classification of multistoried forest communities.

While the basic signal/plant and signal/crop relationships on the ground are being studied, efforts should be directed at simultaneously imaging the phenomena from aircraft. The purpose is to keep the interpretive and data-processing arts abreast of developments in signal/terrain understanding. In the past, there has been a tendency to interpret radar imagery as though it were panchromatic photography. A specific program should be initiated to stimulate the proper interpretation of imagery based on microwave principles.

Supporting research.—Effective use of active microwave sensors will require a thorough understanding of the sensor environment. Research should be initiated at different but appropriate levels of intensity to (1) document system transfer functions; (2) evaluate atmospheric effects (e.g., the comparative reflectance from dry terrain compared to terrain that was recently wet, scatter affected by nighttime moisture films compared to scatter under dry but windy conditions, etc.); (3) establish sampling strategies for plant and crop morphometry and for plant and soil moisture (areally and vertically); (4) determine depth of signal penetration in different angular, frequency, and moisture domains; and (5) develop calibrated spectral data for integrating active microwave and MSS data in processing schemes.

Recommendations

The following are recommendations for the development of remote sensing of crops, forests, and ranges:

1. Continue and expand the program for ground-based microwave studies.
2. Relate threshold detectable moisture conditions to critical soil and plant water limits.
3. Design models for relating detectable moisture phenomena and ground cover to crop vigor and yield.
4. Support efforts to establish levels of acceptable accuracies required by the user community, which should be done for specific applications at several levels in the user hierarchy.
5. Continue and expand the program in active microwave sensor data processing to insure its compatibility with other sensor data and to promote its interpretability at the user levels.
6. Continue and expand programs of testing multispectral active microwave systems over cultural and natural vegetation communities.

SOIL MAPPING WITH ACTIVE MICROWAVE SENSORS

Introduction

Although aerial photographs have been used extensively in national soil surveys, little use has been made of radar imagery in soil surveys. This situation is the result of several factors, but a major restriction on the use of radar imagery is the present inability to interpret the radar image. The success of aerial photography for soil surveys has been built on an ability to relate soil patterns, usually not actually visible on the imagery, with the distribution of other landscape features visible on the imagery. Radar studies have lacked the dual understanding of image pattern and soil distribution that has been essential in the use of aerial photography. This limitation is largely the result of a tendency to regard the radar image simply as a photograph and to ignore its special characteristics.

Previous research on radar reflectance from soils has used one of two approaches. The first approach is laboratory research such as that conducted by Lundien (refs. 2–111 and 2–112), who measured radar re-

flectance from artificially structured soils at several texture and moisture conditions. A second approach, used by Sheridan (ref. 2–113), Simonett (ref. 2–114), and Barr and Miles (ref. 2–115), applied airphotographic interpretation procedures to radar imagery to demonstrate that natural soil distributions in the field correspond, in some areas and under certain conditions, to patterns observed on radar imagery. However, their interpretations largely ignore the differences between radar and photography and present strictly empirical interpretations, without an explanation of the soil properties recorded on the imagery. The objective of this section is to outline an approach combining both these techniques to produce image interpretations based on analysis of microwave behavior and reflectance properties of Earth materials. The result will be a preliminary outline of (1) the kinds of soil properties that can be expected to appear on radar images, and (2) the necessary conditions for such imaging.

Functional Requirements for Active Microwave Sensing

Review of theory.—The SLAR operates by transmitting a known signal and receiving that portion reflected back toward the receiver from objects on the ground. The power returned to the receiver from any reflecting element is a function of the transmitted power, the gain of the antenna, the wavelength of the transmitted energy, the scattering cross section for the element, some function of the incident angle and beamwidth, and the distance to the target. Each sensor parameter can be controlled so that the only variable is the scattering cross section of the specific ground object.

Black-and-white line-scan imagery is produced by converting the backscattered energy into a spot of light, which is regulated in intensity according to the strength of the received signal. A strong reflection will produce relatively bright tones, whereas a weak signal will result in relatively dark tones. These tones are described as relative because they presently cannot be converted into absolute values of scattering cross section. Nevertheless, relative values can be useful if factors determining reflection strength can be applied to image interpretations and if these factors can be related to landscape patterns. These factors can be divided into ground variables and system variables. The most important ground variables for soil mapping are (1) dielectric properties, determined mostly by moisture content, and (2) surface roughness, determined mostly by the textural composition of the soil, microrelief, and vegetative cover. In addition, image interpretation must also consider the microwave variables of frequency, incident angle, and resolution. Interaction between ground and system variables produces the tone observed on the image. Because these interactions operate in a predictable fashion, they can be used as clues in image interpretation.

Effects of microwave variables on soil mapping.—Dielectric properties of soil are directly related to water content (ref. 2–112). The nature of the relationship has been empirically derived by Lundien (ref. 2–111) for Richfield silt loam at four radar frequencies (fig. 2–29). For all frequencies

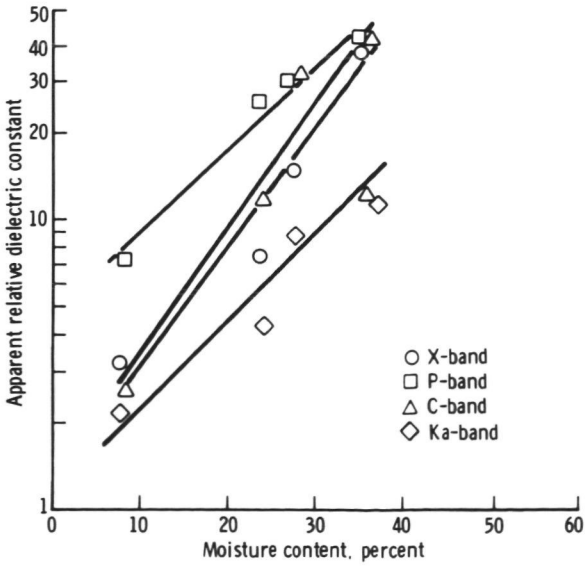

FIGURE 2–29.—Apparent relative dielectric constant of Richfield silt loam as a function of moisture content.

measured, the dielectric constant increased with increasing moisture. In a similar manner, for any two soils having nearly the same characteristics of particle size, shape, and arrangement (together with pore size, shape, and arrangement), the soil with the higher water content should have the higher dielectric constant and appear in relatively light tones on imagery. The relationship is such that one would expect a small increase in soil moisture near wilting capacity to result in a significant increase in radar reflectivity and, hence, image tone. However, the addition of moisture to an already moist soil should not significantly alter its already high reflection.

These general observations have led interpreters to regard radar as a potentially useful sensor for mapping regional soil moistures and for monitoring the relative moisture status of fallow fields. The usefulness of tonal changes, however, will depend on the position of these changes on the wetting and drying curves. Therefore, the case for radar as a monitor of available moisture depends upon future research demonstrating that radar is sensitive to changes between field capacity and wilting point. For the present, only gross differences in image tone between saturated and nonsaturated soils have been reported (ref. 2–38).

Relationships between wavelength and soil texture are shown in figure 2–30. In this diagram, the radar wavelength for "rough" (2λ) and "smooth" ($\lambda/10$) surfaces for midpoints in the bandwidths of V-, K-, X-, and L-bands are matched with U.S. Department of Agriculture soil texture classes. Several assumptions are inherent: (1) that the re-

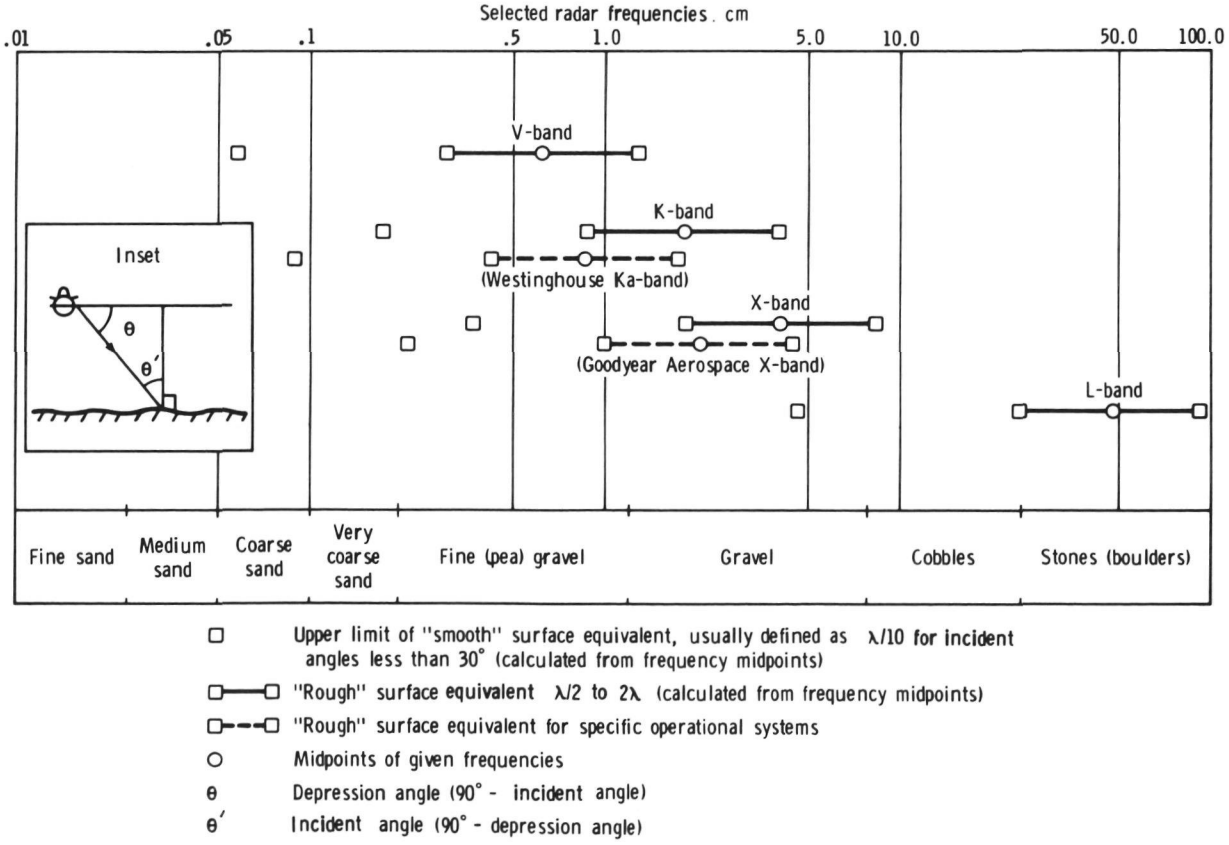

FIGURE 2–30.—Theoretical relationships between soil texture and wavelength for "smooth" and "rough" surfaces.

flecting terrain is sufficiently flat that reflection differences related to slope are negligible, (2) that the surface elements are uniform in size and distribution, and are sufficiently free of vegetation so that complications from composite reflection do not arise, (3) that signal returns are from surface rather than subsurface phenomena, and (4) that increases in return as a result of moisture are negligible. Based on the knowledge that rough surfaces have stronger reflection than smooth surfaces, the diagram suggests that at V-band, for example, returns should be highest for surfaces covered by small (pea-sized) to medium gravel and least for all textures finer than medium sand. At progressively lower frequencies (e.g., K-, X-, and L-bands), all other factors being equal, radar reflection from bare ground should be dominated by progressively coarser textured materials. Thus for L-band at incident angles less than 30°, boulder surfaces should give relatively brighter returns than their finer textured surroundings. Simultaneously produced imagery from both X- and L-bands should show gravel surfaces to be light gray or white at X-band and dark gray or black at L-band.

These relationships are expectations based on theory. In practice, identification of surface materials is much less precise because of the variable importance of moisture content and vegetal cover. Nevertheless, Sheridan (ref. 2–113) has verified from field examinations near Bishop, Calif., that on Ka-band imagery, gravelly soils image in comparatively light-gray tones, whereas silty and clayey soils appear in darker tones. His observations were made over an incident-angle range from 30° to 65°. Morain and Campbell (ref. 2–104) believe that arid lands offer the best opportunity for surface material identification because there is little surface moisture or dense vegetation to complicate the situation.

Kellogg and Orvedal (ref. 2–116) state that, at a scale of 1:50 000, the minimum mappable soil area is approximately 10 hm^2. At 1:1 000 000, the minimum area is approximately 4000 hm^2. At a scale of 1:50 000, a radar imaging system having 10-m resolution would have 1000 independent cells from which to generate an average gray level for every 10-hm^2 area. This number is more than that necessary for statistical significance. The resolution of images contained in figures 2–31 (*a*) and 2–31 (*b*) ranges from 12 to 15 m. For cartographic purposes, such resolution is satisfactory for generalized soil mapping.

However, for actual image interpretation, the adequacy of resolution depends on vegetation density and incident angle. Three idealized surfaces are as follows: (1) exposed soil of uniform moisture and texture having microrelief less than $\lambda/2$; (2) a similar, densely vegetated surface; and (3) a similar but partially vegetated surface. For exposed smooth surfaces, the major factors affecting reflection are soil texture, structure, cloddiness (microrelief), and moisture. These factors contribute so much to tone that, for practical purposes, average returns would be the same, whether the resolution cell was 3 or 15 m. Similarly, in densely vegetated scenes, soil studies by direct interpretation are precluded, whether radar or photography is used. Uncertainties surrounding the depth of signal penetration and the effects of moisture in vegetation make soil interpretations highly suspect. In densely vegetated areas, finer resolution alone will not improve the utility of radar for generalized soil mapping.

However, in the case of partially vegetated surfaces, resolution is an important consideration for image interpretation because, in each resolution cell, the process of signal averaging sums the reflectivities of different objects. Thus, signal returns from elements of varying sizes, shapes, and arrangements are averaged in different proportions depending on system resolution. The proportion of soil surface to vegetation is maximum at vertical incidence and declines as the incident angle increases to grazing. For radar systems having a wide angular range, there should be more soil information contained in the near-range portion of the image.

These considerations indicate that resolu-

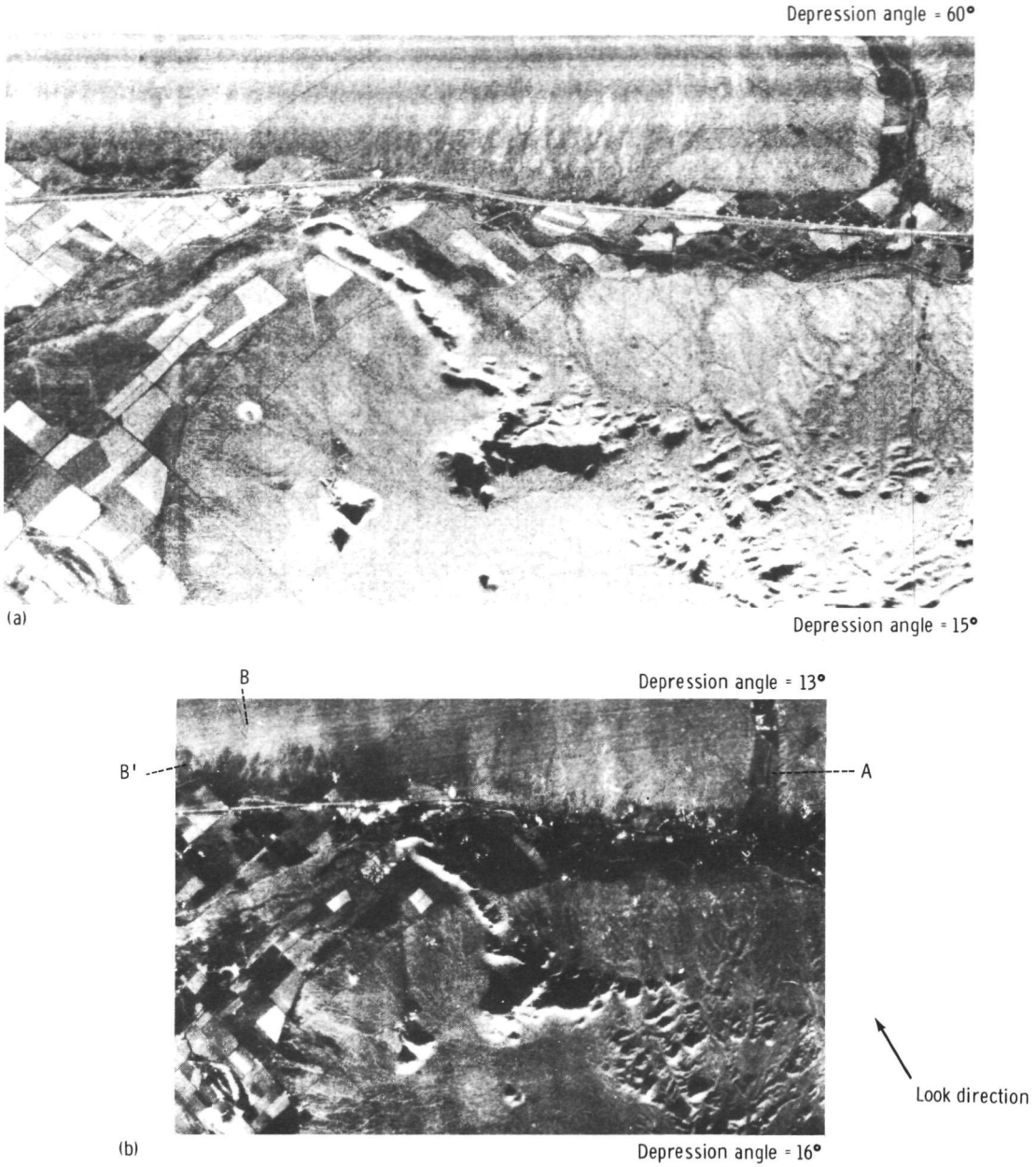

FIGURE 2–31.—Radar images in the vicinity of Tucson Mountains, Arizona. (*a*) Ka-band (0.86 cm) real aperture image; 15-m resolution; scale, 1:136 000 (October 1965). (*b*) X-band (3 cm) synthetic aperture image; 12-m resolution; scale, 1:195 000 (April 1971).

tion requirements for radar soil studies depend on radar incident angle and vegetation patterns. For practical reasons, it seems unlikely that resolution better than a few meters would greatly improve the production of soil maps from radar.

For a fixed resolution cell size, the scattering cross section has angular dependencies that are a function of the roughness, volume scattering, and resonances determined by object geometry. "Smooth" surfaces, those with reflecting facets (surface height devia-

tions from a mean plane) less than $\lambda/10$, are characterized by specularlike reflection. At incident angles between 10° and 30°, these objects reflect signals away from the receiver and appear very dark gray or black on the image. "Rougher" surfaces (usually defined as those with reflecting facets between $\lambda/2$ and 2λ) function more nearly as isotropic reflectors. In extreme cases, these surfaces tend to have more or less equal reflecting potential, regardless of incident angle. In a natural scene with two or more materials contributing to the radar return, the situation is more complex.

To investigate the application of this principle in a real landscape (near Tucson, Ariz.), Morain and Campbell (ref. 2–104) estimated the amounts of soil and vegetation visible at several incident angles. Quadrats similar in size to a resolution cell in figure 2–31 were laid out, and, within each, the size and location of each shrub were recorded. The only two terrain elements present were soil and creosote bush (*Larrea divaricata*). In the laboratory, these data were used to reconstruct models of the quadrats, which were then photographed at several angles. The resulting negatives were scanned by an area integrator, and the percentages of shrub and soil were calculated. The results from a typical quadrat clearly indicated that, for these rather simple landscapes, soil is the dominant visual element, even at incident angles as high as 75°. Since soil studies are equally concerned with mapping and determinations of soil-moisture status, active microwave systems should be designed for steep depression angles (from 60° to perhaps 75° off horizontal).

Anticipated Microwave Results

Soil surveys for generalized maps are less intensive and narrower in objectives than detailed surveys. Their purpose is usually to determine the range of variability likely to be found in a region to provide an outline for initial development and to select areas requiring more detailed mapping. Observations are made at wider intervals than in detailed surveys, and the mapping units are usually soil associations or broad soil patterns (ref. 2–117).

The main contribution of SLAR imagery (or any imagery) for generalized mapping is to provide knowledge of geographic distributions and estimates of relative areas of soil units. Most of the actual pedologic information cannot come from the imagery but must come from collateral information, field surveys, and the knowledge of the soil scientists. The imagery can only provide information about soil distributions. To interpret this information, the soil scientist must have a general knowledge of local climate, vegetation, and topography; identical requirements apply for producing a map by conventional methods. In addition, a knowledge of radar theory enables the interpreter to separate soil patterns from other patterns on radar images.

Morain and Campbell (ref. 2–104) illustrate this principle by applying radar theory to analysis of two SLAR images. An image of an area near Tucson, Ariz., shows a pattern related to variable vegetation densities, which are, in turn, closely related to soil and topographic patterns.

A site from Arizona was selected because an area with relatively low and uniform ground moisture was needed so that the effects of roughness could be studied independently of moisture. Furthermore, arid-zone vegetation is relatively sparse and soil-vegetation relationships are strongly expressed. The authors were fortunate in locating a region northwest of Tucson imaged by two different SLAR systems having slightly different system variables (fig. 2–31). Attention was focused on the nonagricultural lands because they were subject to relatively few changes during the interval between data collection and field observations. There were no available soil surveys for this particular environment, but the work of Gile and Hawley (ref. 2–118) with a similar environment near Las Cruces, N. Mex., assisted the interpretation. The authors identified Entisols and two orders of Arid-

isols on the alluvial fans. The approach was to examine a range of soil-vegetation types and to compare ground conditions with patterns on the radar images. These comparisons produced generalizations regarding the interpretation of soils from SLAR imagery.

A summary of observations for one particular landscape is given in figure 2–32, which shows a portion of the 3-cm (X-band) image together with landscape photographs and respective closeup photographs of the terrain types. Three terrain types are defined: (1) the riparian vegetation (*d*) and (*e*), which appears in light-gray tones; (2) transitional (*c*), the gentle shrub-mantled slopes (3°) that appear in medium-gray tones; and (3) interfluves (*b*) characterized by angular gravel pavement. These last two appear as dark filaments on the image. Two other land-surface entities are included in figure 2–32. The first is an abandoned airstrip (*a*), which does not appear in the SLAR image; the second is a streambed that does not appear on the SLAR image because, in that particular area, no drainage line was wide enough to be visible through the ri-

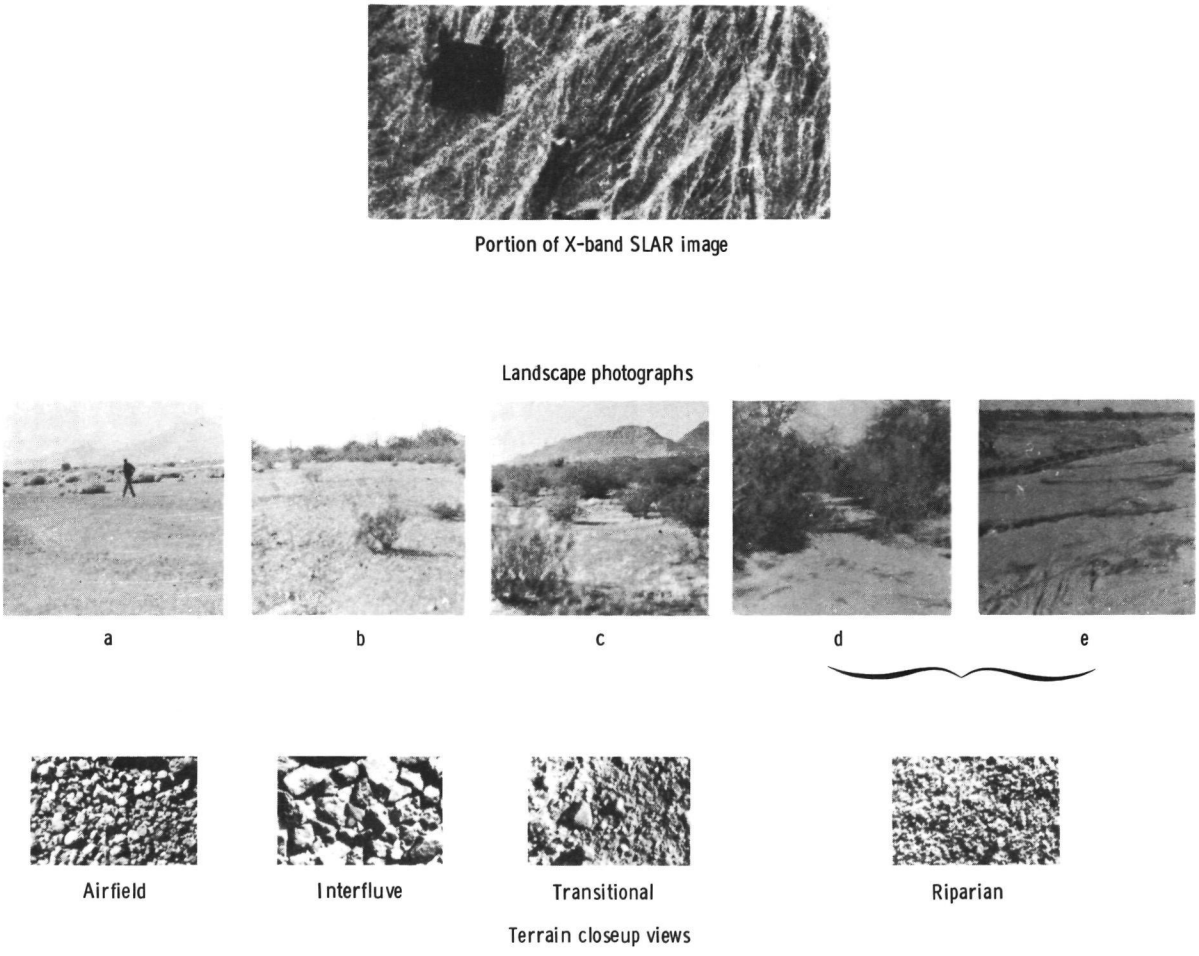

FIGURE 2–32.—Summary of observations for a designated landscape. Top: X-band SLAR image; center: landscape photographs (*a*) to (*e*) of the same area; bottom: closeup views of respective terrain types.

parian vegetation. When the look direction is oblique (as in this case) or orthogonal to the drainage, streambeds will not image unless they are sufficiently wide that vegetation along the banks does not obscure the bed from radar observation. Such a streambed appears as a thin black line on figure 2–31 (*b*) (arrow *A*).

"Rough" surfaces are defined as having reflecting facets in the range from $\lambda/2$ to 2λ (where $\lambda=3$ cm) or, in this case, in the gravel range from 1.5 to 6 cm. Such gravel surfaces should image in dark gray tones at K- and X-bands. In the insets of figure 2–32, it appears that both the airstrip and streambed have narrow particle-size ranges centering on 0.5 and 0.2 cm, respectively (the detailed insets have a 1-cm scale). The interfluve and transition categories appear to have wider particle-size ranges including infrequent cobbles up to several centimeters. Most surface materials appear to have particle sizes of approximately 1.0 and 0.05 cm. Photographs of the surfaces of all five terrain types indicate that no surface has a particle size exceeding 1.5 cm. Theoretically, when exposed and dry, these surfaces should all appear in similar dark tones. The fact that they do not appear this way on the image is explained by variations in vegetation density.

As the proportion of soil to vegetation increases, the strength of signal return decreases. For example, the areas marked *B* and *B′* on figure 2–31 (*b*) are almost identical creosote bush landscapes. No apparent surface textural differences were observed between them. The only significant difference is that, in area *B′*, the shrubs are shorter and farther apart. From this evidence, it is concluded that *B′* appears darker than *B* on the image because there is less radar reflection from vegetation.

This knowledge, combined with topographic information, provides a basis for matching image patterns with the soil categories that Gile and Hawley found in similar environments in New Mexico. The major pattern found on the alluvial fan is shown in the SLAR image in figure 2–33 (*a*). The distribution of brighter tones corresponding to riparian vegetation is shown in figure 2–33 (*b*). These tones correspond to areas of

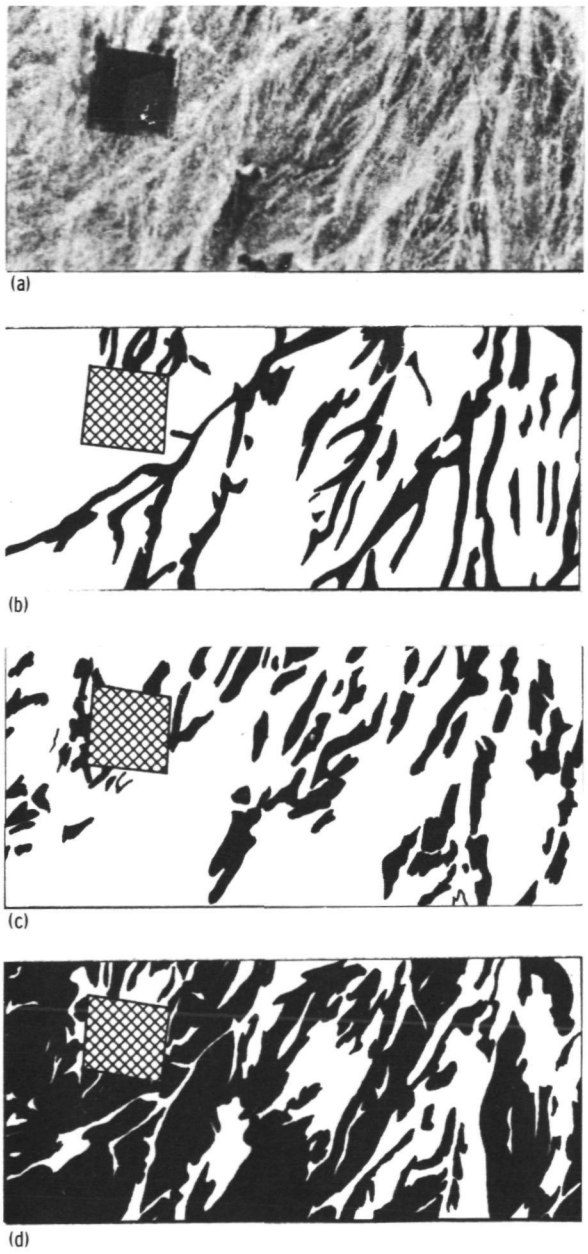

FIGURE 2–33.—Soil categories identified on the SLAR image of alluvial fan. (*a*) Major pattern of SLAR image. (*b*) Distribution of brighter tones corresponding to riparian vegetation. (*c*) Distribution of darkest tones, which are the interfluves and are characterized by desert pavements of stones and cobbles. (*d*) Soil categories positioned between those in figures 2–33 (*b*) and 2–33 (*c*).

riverwash and are probably bordered by small areas of Torrifluvents. In figure 2–33 (*c*), the darkest tones are shown, which are the interfluves characterized by desert pavements of stones and cobbles. The interfluves represent the oldest and most stable surfaces, and the soils are probably Haplargids. Figure 2–33 (*d*) shows the types positioned between those in figures 2–33 (*b*) and 2–33 (*c*), which are likely to be Camborthids.

In dry environments, the attributes most influencing radar returns are size, shape, and arrangement of the reflecting material rather than moisture content. Microphyll species have leaves comparable in size to gravelly and cobbly veneers. The tendency for desert plants to minimize evaporative loss through pubescence, thorniness, and schlerophylly suggests that little plant moisture would be visible to radar signals. It is suspected that the effect of shrubs on radar reflectance from desert terrain is confined to surface roughness and that this influence adds to reflectance from soil surfaces.

Microrelief contributes more to radar reflectivity than soil texture. However, because image tone is determined basically by roughness at the wavelength scale, it would seem that only those forms of microrelief having a commensurate scale should be important; for example, ripple marks in sand. Some plow patterns on bare soil are reported to increase radar reflection from cultivated fields (ref. 2–119), but no examples from natural landscapes have been reported. Field investigations at Tucson confirmed, in all cases, that exposed soil surfaces imaged in very dark gray or black tones at X- and Ka-bands. This type imaging occurred despite the variable microrelief, which in some cases exceeded 2λ by a factor of 3.

MacDonald and Waite (ref. 2–38) demonstrated that imaging radars are, under certain conditions, sensitive to gross soil-moisture variations. Morain and Campbell (ref. 2–104) have also observed moisture patterns of an area west of Hutchinson, Minn. (fig. 2–34). The numerous white and light-gray spots observable on the image are one of

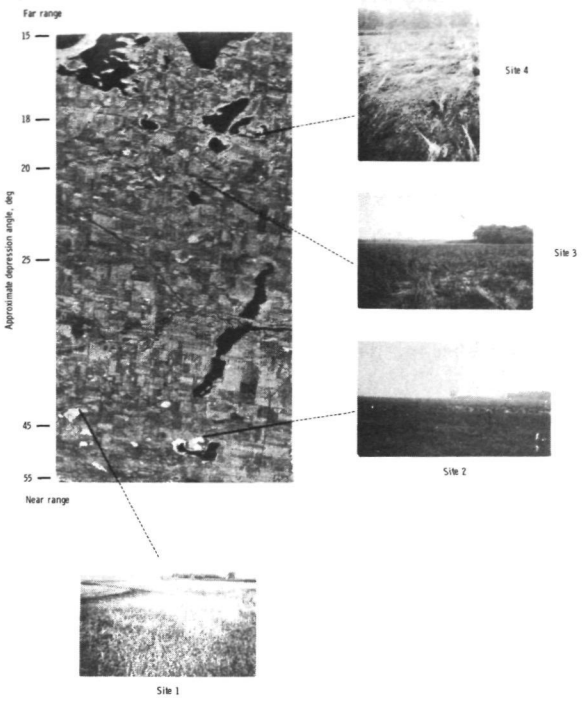

FIGURE 2–34.—Radar image and related landscape photographs showing moisture patterns of an area west of Hutchinson, Minn. Sites 1 and 2, imaged at a depression angle of approximately 45°, have bright tones of similar intensity. Sites 3 and 4, positioned at 20° and 18° depression angles, respectively, appear brighter than surrounding agricultural and wooded areas, although not as bright as sites 1 and 2.

the expressions of that moisture. Topographic maps, soil maps, and field observations reveal that these spots correspond in size, shape, and position to poorly drained depressions usually mapped as peat or muck soil.

The importance of incident angle on the magnitude of the received signal from a moist surface is illustrated in figure 2–34. At more nearly vertical angles, signal strength declines and gray tones are observed on the image. All sites have approximately the same vegetation and moisture characteristics. Sites 1 and 2, imaged at approximately the same depression angle (approximately 45°), have bright tones of similar intensity. Sites 3 and 4, positioned at 20° to 18° de-

pression, respectively, appear brighter than surrounding agricultural and wooded areas, although not as bright as sites 1 and 2. Moore (ref. 2–120) states that at shallow depression angles the height of vegetation may have a significant effect on reflection, particularly if the plants have a high moisture content. Therefore, it is possible that the bright spots at steep depression angles result from the cumulative effects of plant and soil moisture. At shallow angles, the topographic depressions are still somewhat brighter than their surroundings because they are relatively wetter, but the contrast is reduced by stronger returns from vegetation.

High moisture content and rough texture (relative to wavelength) tend to increase reflection. Thus, it is easy to envision situations in which an interpreter could not distinguish between reflection from a fine-textured moist soil and that from a coarse-textured dry soil. Theoretically, both types should appear as bright tones on an image and should not be easily distinguishable with a single radar frequency. In practice, however, an interpreter should resolve such confusion with multiple coverage using different radar characteristics, much the same as different film and filter combinations are used in photography.

Cost/Benefit

Much work should be done to document the economic factors associated with improved soil type and association mapping. The Dynatrend report (ref. 2–1) notes several studies of benefits in this area of remote-sensing applications, but these are considered questionable.

For cataloging soil environmental characteristics, the world might benefit to the extent of $30 million annually. Use of satellite data for locating and surveying potentially cultivable soils might save developing countries an additional $75 million. These values may be an order-of-magnitude low or high (probably not the latter), but in either case they suggest that there is valid economic reason to improve soil-mapping capabilities.

Conclusions

Radar sensors will not completely replace photography as a mapping aid for either detailed or generalized soil surveys. Nevertheless, the unique contributions of active microwave sensing for resource inventories in arid and semiarid environments or the perennially cloudy tropic and arctic zones should be pursued. These contributions are especially important when the penetration capabilities of longer wavelength systems are considered. Only a small portion of the electromagnetic spectrum has presently been used (mostly the visible portion) in remote sensor studies of the soil. Unique and valuable information on texture and texture-related phenomena, moisture, and possibly even subsurface texture contrasts could probably be partially provided by radar imagery.

Observations from aerial photographs have shown that local experience and knowledge are important factors in soil interpretation. These same factors will probably be important for interpretations from SLAR. Knowledge of the sensor principles and operation is of greater importance in SLAR studies because of the unfamiliarity of most people with this sensor. As a result, soil interpretations from SLAR are unlikely to progress without individuals having combined knowledge of local soils, soil science, and SLAR theory. Because such imagery is available only for certain areas and because the combination of interpretation skills is possessed by only a few interpreters, advances in radar mapping have been slow.

Additional research is needed to ascertain the relationships of radar reflection to system frequency, polarization, dielectric constant, and incident angle. Investigations confirm that near-vertical incident angles are best for detecting differences in soil moisture and, possibly, for discriminating soil types on the basis of their surface texture. In reviewing the theory and observations, the relative reflection strengths caused by moisture and texture are believed to intersect in both the frequency and angular domains; thus, interpreters cannot readily distinguish between

a moist fine-textured soil and a dry coarse-textured soil if all other parameters are equal. These tradeoffs should be reconcilable by comparing the reflection characteristics of soils over a broad range of microwave frequencies, angles, and moisture conditions. In the same way that various film-filter combinations aid in the interpretation of objects that otherwise look the same on panchromatic photography, it should be possible to distinguish between soil-moisture and texture differences by judicious selection of radar parameters.

SOIL MOISTURE MEASUREMENT

Introduction

Civilization and the existence of water in soil are inseparable; thus, when prolonged droughts occur, civilizations vanish. As presently demonstrated in Africa, even the lack of water in soils for periods of weeks can seriously alter the precarious balance between food supply and demand. The ability to monitor and predict moisture in soils on a global scale has been a longstanding objective that has thus far eluded man. Active microwave sensors offer a promising approach based on scientific reasoning and preliminary results. Additional research and development is required to arrive at a functional capability.

Two promising applications for sensing of soil properties are made possible by some of the unique penetration capabilities of microwave systems. Measurement of soil water content would allow the development of a soil moisture index that could be used as input to watershed runoff and crop-yield models. Soil moisture monitoring for irrigation requirements has local value and may be accomplished after more precise techniques are developed.

The primary need for soil-moisture measurements over large areas stems from a desire to improve prediction models for water resources and crop yield. The spatial distribution of soil moisture indicates that such measurements are feasible with active microwave systems.

Complex, continuous watershed models have been developed in past decades to mathematically represent the movement of water in the Earth-surface portion of the hydrologic cycle. Presently, these models are the only means of calculating "low flow" or continuous streamflows. Low-flow values for streams and the temporal distribution of flow volumes are extremely important for the study of water supplies and the environmental input of changes in a watershed drainage area. Presently, soil-moisture input to the models cannot be measured, and the input is generated by submodels based on parameters developed by fitting the overall model to existing watershed data. The use of complex models is thereby restricted to use on watersheds with existing historical records.

Development of a soil-moisture index for use as input to crop-yield models is also very important. Crop-yield models are vital to improvement in timely estimates of world food production. Identification and mapping of some major crops are considered feasible. However, no adequate system has been developed for measuring the moisture available for the plant root zone. Laboratory experiments on penetration and soil-moisture measurements with microwave systems (refs. 2–121 and 2–122) indicate that reasonable estimates of moisture availability for plant growth are feasible.

Demonstrated Remote-Sensing Observations

ERTS–1 and aircraft photography.—Preliminary results from ERTS suggest that relative soil-moisture variations can be detected in desert playas and areas of alkaline soils (refs. 2–123 and 2–124). Quantitative measurements cannot be made based on spectral appearance in the visible region. The MSS's and cameras on aircraft platforms show similar feasibility for moisture detection. In general, soils that are moist have somewhat darker tones in comparison to their dry state. However, no known mathe-

matical relationship exists between soil color and moisture content.

Skylab S193 and aircraft radar observations.—Several research programs have centered on laboratory studies regarding the measurement of electrical properties of the soil-water mix (refs. 2–112, 2–125, and 2–126). These studies have shown that the water content has a major effect on the electrical properties of soil media. Differences in soil type do not have an important effect on the relative dielectric constant.

Other research programs have demonstrated the use of radar measurements from elevated platforms to detect changes in soil properties (refs. 2–107, 2–111, 2–112, and 2–121). These efforts have indicated that near-vertical measurements are more desirable than low-depression-angle measurements because the predominance of the surface-roughness comparison of the total radar backscatter is reduced, and the significance of the reflection from vegetation is reduced. Field studies by Morain and Campbell (ref. 2–104) confirm these observations. When measurements are made on smooth surfaces at these near-vertical angles, the reflectance can be correlated with soil moisture. In addition, when skin depths are significantly large, subsurface composition can be inferred.

The S193 scatterometer on Skylab made numerous measurements over test sites from which soil-moisture data are available or for which soil moisture can be inferred from nearby rainfall measurements. Because these data are being analyzed at this time, no conclusive results can be reported. However, the general indications are that soil moisture may correlate with measurements made with the truck-mounted radar and airborne scatterometers. In cursory examination of Skylab data, vegetation appeared to have a disturbing influence on the K-band measurements.

Wavelengths from 0.8 to 21 cm and incident angles from vertical to 50° have been used in passive microwave measurements on soils (ref. 2–122). Because these microwave devices measure the natural emission from the target, they are sensitive to the target temperature and emissivity. The natural emission from a soil target is very dependent on surface roughness and on bulk electrical properties. Thus, a change in the water content in a soil would show up in an apparent change in temperature. The depth at which the bulk of the energy originates is determined by the wavelength and the water-content profiles.

A truck-mounted passive microwave system has been used recently to determine antenna temperature changes as a result of changes in soil moisture, roughness, and vegetation. Preliminary measurements indicate that an L-band (1.41 GHz) radiometer wil be necessary to overcome some of the influence of roughness and vegetation on soil-moisture measurement (ref. 2–127). However, limitations on antenna size may prevent design of radiometers in a scanning mode at L-band. Another study using an L-band radiometer (S194) on Skylab has shown good correlation between antenna temperatures and a 30-day decayed antecedent precipitation index. An index of this nature would be adequate for prediction of moisture for wheat production if repeated coverage could be provided over the Great Plains at 2-week intervals. At best, the passive systems are hampered by antenna size requirements that do not restrict the active microwave systems.

Functional Requirements

The response of microwave energy in soil media is determined by the electrical properties of soil and their spatial distribution. The use of microwave sensors is advancing because of known relationships between electrical properties of soils and water content. The electrical conductivity of soils at low frequency is almost exclusively ionic and occurs as a result of the motion of free or exchangeable ions in the soil solution. Because exchangeable ions often dominate over free ions in solutions, clays have a higher conductivity than coarser grained soils. Typically, the conductivity of soils varies

from 10^{-1} mho/m for clay soils to 10^{-3} mho/m for sands and gravel. Because of these high conductivities, conduction currents dominate over displacement currents for frequencies above approximately 10^6 Hz.

Water content influences the conductivity of soils, but other factors such as soil and clay type are as important as water content in determining the conductivity of soils. At frequencies above 10^7 Hz, the influence of conductivity of soils on the propagation constant begins to diminish and the relaxation of water in soils becomes important. Figure 2–35 shows the relative dielectric constant of typical soils as a function of volumetric water content at a frequency of 1.074 GHz (parallel and perpendicular polarization). The 12 soils included sands, silts, and clays. Increasing the frequency to 10^{10} Hz causes the relative dielectric constant to decrease significantly from its low-frequency value (ref. 2–125), as will subjecting the soil to low temperatures.

A transverse electromagnetic wave normally incident on a smooth surface, which has a finite conductivity, will be partly reflected at the surface, and the remainder will penetrate into the soil. The electric and magnetic fields in the ground will decay exponentially with depth. The skin depth in soil media can have values as much as several meters in the 10^8- to 10^9-Hz frequency range. In the 10^9- to 10^{10}-Hz range, the skin depth can shrink to only a few centimeters. Thus, by selecting a number of frequencies for operation, it may be possible to define soil media as a function of depth.

Images produced from SLAR systems can be divided into areas of relatively consistent tonal and texture patterns. A relatively few samples from these areas of consistent patterns will serve to identify the physical properties of these areas. Thus, information from a few bench-mark stations can be extrapolated to large surface areas. These bench-mark stations can be entirely composed of ground-truth measurements or a limited amount of ground truth supplemented by direct measurements with airborne or truck-mounted radars.

The functional requirements for active microwave systems to measure soil moisture vary considerably with the required ultimate operational system. Three areas of application for soil moisture data are (1) modeling of watersheds, (2) crop-yield predictions, and (3) scheduling of irrigation. Table 2–VII outlines some of the characteristics required in active microwave systems desired

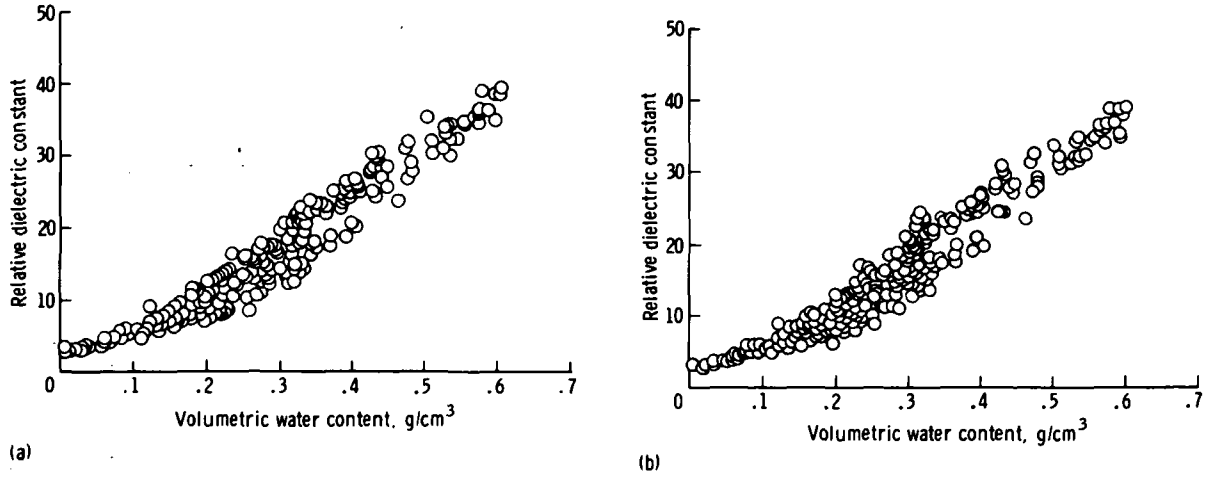

FIGURE 2–35.—Effect of water content on the relative dielectric constant of soils (sands, silts, and clays) at a frequency of 1.074 GHz. (*a*) Parallel polarization. (*b*) Perpendicular polarization.

for these applications in the soil-moisture area.

Anticipated Microwave Results

The applications and unique capabilities of active microwave systems are summarized in table 2–VII. Other applications in the area of soil moisture will require more refined spatial and spectral measurement. However, with improved technology in the following decade, most applications should become feasible.

Several researchers have reported results from airborne microwave measurements (refs. 2–38 and 2–128). Most results can only be reported in rather broad categories of soil-moisture content (e.g., dry or wet). The fact that soil-moisture conditions can be observed in these measurements indicates that such data may be adequate for large-area prediction models. Conventional measurement of soil-moisture distribution over large areas is not presently feasible. Part of the problem concerns the available ground truth at the time the flights were made. Although most laboratory experiments are conducted with highly controlled targets of rather small dimensions, field programs must sample large areas of highly variable properties. Ground truth has been adequate in very few field measurements.

Cost/Benefit

Accurate measurement of soil moisture affects so many vital areas of modern civilization that cost/benefit statements are difficult to formulate or document. The importance of soil moisture for agriculture, runoff prediction, flood-hazard prediction, locust infestation prediction, erodibility, and numerous other uses cannot be overstated. As a fundamental attribute of the terrestrial environment, soil-moisture data become a basic input to all models. By the most conservative estimates, the benefits exceed any costs involved in the data collection.

TABLE 2–VII.—*Soil Properties Capabilities Chart*

Environmental parameter	Application	Unique key capability of active microwave systems	Competing sensors or systems
Water content of soil..	Input to crop-yield models and monitoring crop vigor.	Penetration of soil, penetration of clouds, and vegetative cover.	Visual and IR.
	Input to complex watershed models.	Penetration of soils and all-weather capability.	
	Soil strength and trafficability.	.....	Geophysical techniques.
State of water in soil surface (frozen or liquid).	Detection of danger from sheet runoff. Infiltration restriction. Restriction of soil moisture evaporation.	.....	IR
Soil type	Soil type mapping Input to trafficability models.	Penetration of soil, all-weather capability and penetration of vegetative cover, vegetation mapping and soil reflectivity.	Geophysical techniques.

Conclusions

Research is recommended along two parallel lines: (1) attempts to empirically correlate scattering coefficients and images from present systems with field measurements of soil moisture, and (2) research to build a store of knowledge from which system behavior can be predicted. For some applications, the empirical approach is the only feasible approach (e.g., runoff prediction of watersheds) because the areal extent of the entity to be sensed does not allow control. For irrigation scheduling, the second approach is the most economical way to proceed, because the relationship between the quantity to be measured and its microwave signature varies from one setting to another (e.g., the relationship between microwave signature and water content in Arizona may be unique to that location). To predict the extent to which a certain observed correlation persists in other settings of soil type, vegetation, water, and temperature regime, the interactions between microwave radiation and the Earth need to be fully understood.

Figure 2–36 is a flowchart for required research. Level I research should be a low-level continuous effort conducted simultaneously with research at level II. At level II, the empirical approach and the controlled ex-

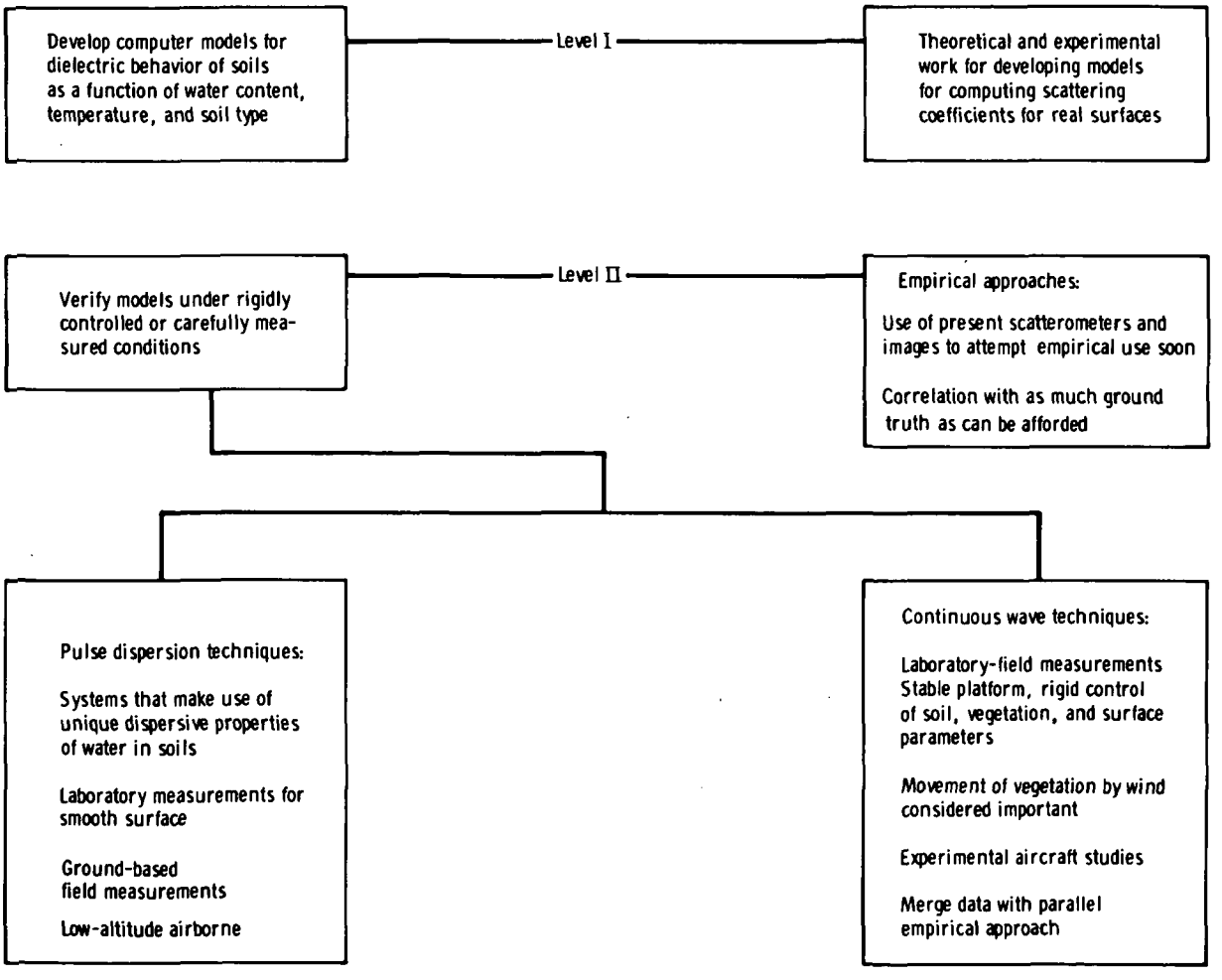

FIGURE 2–36.—Flowchart showing required research for simultaneously measuring moisture content and soil type with microwave sensing.

periments are also recommended to be conducted simultaneously.

SUMMARY

The objectives for active microwave sensing in agriculture, forestry, range, and soils extend those indicated for other sensors. The most unique contribution is expected to be in measurements of soil moisture as input to models of crop and rangeland production, watershed runoff, and trafficability. Theory and preliminary results show the feasibility of measuring moisture status, although research is needed to quantify many complex tradeoffs in signal return as a function of moisture content, vegetational cover, signal penetration, soil structure, root densities, and so forth. Further work will be needed to develop quantitative image interpretation techniques. The functional requirements for such a system will include a multifrequency design with a 1-dB intensity resolution and 50-m spatial resolution. Most important is the need for timely coverage.

For vegetational resources, crop identification for inventory and for yield and production estimates is most feasible. Active microwave sensors are unique in providing continuous temporal monitoring; thus, they are regarded as prime sensors for agricultural survey. The most significant contribution for both agricultural and rangeland surveys is in the potential ability of active microwave sensors to detect crop-water phenomena and total leaf area. Both these parameters are important as input to yield-prediction and crop-vigor models. For tropical agricultural systems, active microwave sensors may have a singular role in monitoring the rate and direction of riceland flooding during the cloudy monsoon season. These flood data can be translated into valuable information on basic rice type and production.

Apart from moisture- and water-related phenomena, active microwave systems are viewed as prime sensors for recording structural and spatial data related to crops and forests. These data are important attributes in determining leaf area indices and, ultimately, crop or timber yield. Tropical tree crops (e.g., rubber, oil, and palm) are expected to be more discernible from their forest surroundings because of the regular spacing and orientation of trees comprising individual plantations. Canopy penetration is essential for obtaining returns from tree trunks to discern the regularity, and only microwave sensors have this ability.

Functional requirements for an operational active microwave system in agriculture include multifrequency (wavelengths of 1 to 12 cm for crops and 1 to 50 cm for forests) and multipolarization (HH, VV, and cross) capabilities. Spatial resolutions of 15 to 30 m and spectral resolutions of 1 to 2 dB are desired over a viewing-angle range from 30° to 70° off vertical. As with all biological sensing, timeliness of data collection is absolutely essential.

The most important application for rangeland sensing is to measure available biomass as input to decisions on animal grazing capacity and improvement of range conditions. Plant cover, moisture status, and soil moisture are key parameters in assessing biomass. Essentially, the same system considerations that pertain to agricultural crops apply to rangelands.

Applications for active microwave sensors in forestry focus on typing community structures with the objective of producing physiognomic maps and, ultimately, to estimate timber volumes in economically important areas. Forest-clearing sites (as in clear-cut logging operations in the Pacific Northwest or tropical slash and burn agriculture) are readily visible on radar images in regions of low relief. Equally interpretable are successive stages of forest regrowth after a clearing or fire. Difficulties occur in mountainous terrain. Functional requirements include a multifrequency, multipolarization system and stereographic coverage having almost complete (90 percent) overlap to satisfactorily image mountainous environments.

Research programs are suggested for advancing knowledge of signal/plant and signal/crop interactions and for learning to

interpret images and digital data obtained from aircraft and spacecraft sensors. Even very conservative estimates of dollar benefits suggest that these efforts could have enormous economic benefit for agricultural businesses and society.

PART D

LAND USE, URBAN, ENVIRONMENTAL, AND CARTOGRAPHIC APPLICATIONS

LAND USE, DISASTER, AND ENVIRONMENTAL MONITORING

Effective State, regional, and national land-use planning requires the compilation of a wide range of areal data. These include data on static components of the environment (including soils, slope, geology, and hydrologic systems) and on dynamic cultural land use and related components (including transportation routes, urban and rural land use, and public infrastructure). In the interplay of these natural and cultural features, with natural features relatively static and cultural features to a greater or lesser degree dynamic, planning is accomplished. Monitoring the changes in land use is of value not only in itself but also for determining the interaction with other land uses and with the background environment. This section focuses on radar applications and land-use analysis in the monitoring of land-use change, especially the more dynamic components, and the interaction between land use and dynamic features of the environment (floods, hurricanes, etc.). Because public awareness of land planning is relatively new, a more detailed discussion of land planning in relationship to remote sensing is included in this section.

Although the relationships between land use and environmental quality are not well defined and are not conducive to orderly simple analysis (ref. 2–129), general public awareness has increased and has helped focus attention on land-use planning and management as one means of achieving a reasonable balance between economic well-being and environmental quality.

Growth in economic productivity has caused a greater demand for leisure and recreational services, which are highly dependent on environmental quality. Environmental quality is becoming more highly valued in relationship to potential increases in economic standards of living. Growth in productivity depends on increasingly powerful technologies and therefore has greatly increased the geographic and temporal extent of each person's effect on the environment. The results of these trends have been recognized, and new laws have been passed; new institutions have been created for protecting the environment. As new policies have been developed and implemented for controlling specific types of environmental effects, there has been increasing recognition that land-use patterns have a strong influence on the relationship between future economic production and environmental quality. These overall land-use patterns influence such key factors as (1) the location of environmental disruptions that arise from the extraction of resources; (2) the magnitude of wastes generated, especially from transportation activities; and (3) the costs of treatment to lessen the impact of residuals discharged into the environment.

More fundamentally, the experience of the last 5 yr has furthered the recognition that land-use patterns determine who shares which environments and with whom. As this sharing and the resulting external effects include more people over larger areas and for longer times, the potential economic, environmental, and social benefits from more centralized, comprehensive land-use planning

increase. These benefits have provided the incentive for a restructuring of the Federal, State, and local land-use planning processes and techniques. The beginnings of this restructuring are evident in recent legislation, and its effects will have a strong influence on spacecraft remote-sensing systems during the next several decades. A parallel reaction by the private sector is already underway.

Recently, there has been increasing concern in the Congress about what many Americans perceive to be a national land-use crisis. Evidence of congressional concern is demonstrated by the following facts:

1. More than 120 land-use-related bills were introduced in the 91st Congress.
2. More than 200 such measures were considered in the 92d Congress.
3. By March 10, 1973, more than 50 land-use-related bills had been introduced into the 93d Congress.

Presently, Congress has temporarily tabled a Land Use Policy and Planning Assistance Act to encourage the establishment of the decisionmaking framework and to assist in the development of data collection techniques. This act may be reintroduced and passed within the next 2 yr. The desire of many officials to pass such an act indicates the belief that land-use planning is beneficial. If passed, the act will establish broad requirements for data collection, part of which may be accomplished with satellite data (including active microwave sensor data). Related trends are evident in State legislation. Three recent reports (refs. 2–130 to 2–132) summarize the changes in the land-use planning and control activities of various States and local jurisdictions.

The Rubino-Wagner report (ref. 2–130) identified five States that have already developed land-use plans—Hawaii, Alabama, Delaware, New York, and Rhode Island—and seven other States that have recently initiated innovative State legislation in the field of land use.

The Bosselman-Callies report (ref. 2–131) provides detailed descriptions of the experiences of recent land-use control legislation in Hawaii, Vermont, San Francisco, Minneapolis, St. Paul, Massachusetts, Maine, Wisconsin, and New England.

The Haskell report (ref. 2–132) views the changes in land-use planning practices from a somewhat different perspective than either of the other reports. Although the primary focus of the report is on organizational and institutional design over the entire range of environmental problems, it also includes some techniques used for various specific areas of environmental management, including land management and regulation.

These reports indicate an increasing trend toward innovation in State land-use planning activities, which will create an increasing need for data on which to base land-use planning decisions. The Haskell report states: "A first tool used by some states to strengthen their land planning effort is the generation of an adequate data base, and the development of analytical capabilities needed to make effective use of such data."

Several developments in analytical capabilities appear to enhance the potential benefits from use of satellite data in land-use planning. The first development is the use of computerized information storage and retrieval systems for handling land-related data. Several States have developed or begun such systems, including Minnesota, New York, Maryland, and Arizona. Efficient and low-cost means for handling large arrays of data through parallel processing technology can be expected to enable the satellite systems to produce large data arrays much more efficiently than at present. These methods of data handling will apply not only to future ERTS-type systems but also to digital radar image systems.

A second related development is the work on models capable of partially simulating the complex interrelationships of socioeconomic activities, land-use patterns, and the resulting effects on natural resources and environmental conditions. Such models can help land-use planners analyze land-related data to assess more accurately the tradeoffs

between economic production and environmental quality and thus increase the benefits from satellite systems.

General Objectives of User Agencies and Industries

Land-use planning, monitoring, and regulation.—Traditionally, most U.S. land-use data have been for counties and various metropolitan planning agencies. Counties have rarely been of sufficient size or commanded sufficient capital to include regular land-use inventory as part of their planning function. However, counties have been the principal arena for interplay between the public and private sector when zoning and development are in conflict. Small undercapitalized planning departments have been no match for private interests, and zoning decisions frequently remain only as long as the more powerful private interests are not included. Although the balance between public and private interests—as represented by metropolitan planning agencies, councils, and private developers—has perhaps been more even than at the county level, there are numerous examples of the protagonists of "the highest and best use" in a strictly economic sense, which ignore environmental and neighborhood quality considerations.

These facts have stimulated the intense Federal and State interests in land-use inventory, monitoring, and planning. The Federal initiatives in this area focus on stimulating State-level activity. Thus, the natural interests of the State (reflecting citizen concern for a more forceful public voice) and the Federal pressures for State action have converged in making the State and, in some areas and for some problems, regional groups of States the prime focus of the current trends in land-use planning.

Constitutionally, the State governments have the authority to determine powers of local government units. Although the trends in land-use planning do not indicate State reassertion of authority for land-use control, they do show a complex reworking of intergovernmental relationships in which the State governments play a more active role in providing framework, data, information systems, overall guidelines and coordination, and many of the public facilities and services that influence land-use decisions.

Although these trends and pressures are still evolving, it is highly probable that, by the time spacecraft active microwave systems are used in land-use planning, a wider and stronger role for the State will have developed. Similarly, State-sized areas and regional groups of States concerned with common environmental problems (for example, Rocky Mountain States and Northern Plains States concerned with strip mining and oil-shale development) will have developed and strengthened.

The counties are too small in many instances to benefit from space-derived data because their problems are too detailed and require information that cannot be obtained from remote sensing, but the State is, in many ways, a prime candidate (in area, scale of problems, and information needs) for the capabilities of high- and moderate-resolution spacecraft remote sensing. The general objectives of user agencies and industry must therefore be considered in relationship to the trends to strengthen State land-use planning, which is aided both by Federal legislation and funds and by public pressure.

The principal interests of the States are converging in the development of statewide geobase information systems as part of the planning base and in the possible integration of economic modeling and forecasting through use, on a small-area basis, of the geobase data on natural and human resources. The ability to overlay and spatially examine finely disaggregated economic and census data (at the census tract level), land use, and static and dynamic environmental background data is now seen as a major area for State agency planning and development. The State Department of Planning in Maryland is already working in this area.

In a parallel manner, the interests of major corporations are converging in large-area analysis. Corporations with large or scat-

tered real estate holdings, with land owned in sensitive areas, with requirements for utility-site and route selection and planning, and with concerns for general community development are beginning to anticipate the need in their planning departments for pre-environmental effect analyses in which geobase data on land-use change are essential. Examples are visible in planning departments of major electrical utilities in which public and private funds are used jointly to prepare land use and other data for entry into geobase information systems. The many regulatory and monitoring requirements in existing and planned Federal and State legislation will hasten the process and offer opportunities for remote sensing of (1) land use, (2) changes in land use, (3) environmental stress, and (4) illegal or undesirable actions in the private sector.

Desirable monitoring, planning, and minimization.—In addition to the previously mentioned environmental and land-use monitoring concerns, both Federal and State agencies together with private corporations and relief agencies have shown increasing interest in planning for natural disasters. This interest is expressed by concern with insurance programs, disaster relief, damage area and value assessment during and following the event, population resettlement, and related matters.

Several State and Federal agencies realize that detailed land-use information, together with data on the extent of the disaster in relationship to various land uses, is one of the most effective ways to obtain perspective on the scope and intensity of a disaster and on the conditions that will partly dictate the response.

Detailed land-use data by area will aid in the assessment of the number of lives endangered and the property value at risk. For example, in flood-plain land use, the critical method for assessment during a flood is the interaction between the extent, depth, and persistence of floodwaters and the effects by class of land use of such extents, depths, and persistences. Studies are now beginning but will be of increasing importance as State-developed information systems begin storage of land use, census, and relevant socioeconomic data by city block and census tract.

Certainly, one of the widely anticipated advantages of a statewide geobase information system is its ability to rapidly provide data in disaster situations, and refinements such as anticipatory planning for river flood and coastal area damage through storage of high-density data are expected to become commonplace.

Objectives Relative to Active Microwave Capabilities

Both of the concerns mentioned (land-use planning and disaster monitoring) are directly relevant to active microwave remote sensing. For disaster monitoring, the use of active microwave sensors is obligatory because they are the only sensors that can obtain data on demand. Therefore, active microwave sensors must be the prime sensors for a disaster-monitoring system designed to obtain data on the extent and progress of riverine floods, hurricanes, great fires, tidal waves, volcanic eruptions, earthquakes, landslides, and blizzards. Data on these events must be obtained at night, through clouds, rain, smoke, dust, fog, and smog. Only imaging radar meets these requirements.

Active microwave sensors are of at least equal rank with visible-region sensors in a general program of land-use monitoring, updating, and regulatory management. The purposes of active microwave remote-sensing systems may be summarized as follows. (Refer also to tables 2–VIII and 2–IX.)

1. The systems will provide data in areas partly obscured by clouds and, by cross-calibration with visible-region sensors, may be used for partial extrapolation at a single time.

2. By assuring systematic, orderly acquisition of data, active microwave remote sensors will enable the establishment of monitoring systems in which continuity of data acquisition is a primary factor. Such situations will occur when regulatory matters are

TABLE 2–VIII.—*Functional Requirements of Active Microwave Systems*

Requirements	Area of application	
	Input for complex watershed and crop-yield models	Irrigation scheduling
Desired incident angle, deg from vertical	0 to 40	0 to 40
Wavelength:		
Minimum, cm	1	1
Maximum, cm	100	100
Desired number of channels:		
Aircraft	4	3 to 4
Spacecraft	2	
Laboratory		5 to 10
Minimum number of channels	2	2
Polarization:		
Research mode	All combinations	All combinations
Operational mode	1 or 2	1 or 2
Swath width:		
Aircraft, km	10 to 40	10 to 20
Spacecraft, km	200 to 350	NA[a]
Spatial resolution:		
Desired, m	30	10
Maximum, m	100	30
Gray scale resolution:		
Desired, dB	20	20
Allowable, dB	10	10
Calibration accuracy:		
Type	Relative	Relative
Accuracy, dB	2	1
Ground truth:		
Operational system	Monitor key large fields with two fields (extreme wet and dry) having recording rain-gage records.	Same as application in preceding column.
Research system	Gravimeteric sampling of fields with full range of soil moisture (two sets); one set to develop prediction scheme, other set to verify penetration.	Laboratory controlled (gravimetric samples).
Need for real-time data (operational)	Daily values required for watershed models in real time; 1- to 18-day interval may satisfy crop-yield models.	Real-time values essential for operational systems, not needed for research.
Data format	CCT and images.	CCT and images.
Special techniques needed	Computer programing for rapid extraction and computation of soil-moisture output (most vital requirement for this application).	New computing developments for operational systems.
Probable ultimate platform	Spacecraft.	Aircraft.

[a] Not applicable.

TABLE 2–IX.—*Relative Probabilities of Conditions Restricting Photography in World Environments*

Environment type	Relative probability of adverse imaging condition for visible and/or IR
Wet Tropics	High probability of persistent clouds, haze, and rain.
Midlatitude west coast	Seasonally high probability of fog, clouds, and rain.
Arid Tropics	Seasonally medium probability of dust.
Arctic	High probability of long-term darkness, clouds, and snow.
Midlatitude continental areas	Medium probability of clouds.

involved and when progressive change is a key element in land-use analysis. This purpose may be described as the provision of key time data in which active microwave remote sensing is essential for the effective functioning of the monitoring system. Certainty of data acquisition will frequently be the deciding factor in a decision to initiate a satellite remote-sensing monitoring system. Just as a manufacturing plant at the mercy of irregular supplies of key materials incurs high costs and may be forced to operate below peak efficiency, an information system subject to sporadic arrivals of data, long time gaps, partial data at a single time, and similar problems would be forced to operate at low efficiency or, possibly, go out of business.

3. In areas of persistent cloud cover (such as parts of western Europe, wet Tropics, and Northwest United States), in areas of rain and fog, or in high latitude during winter, the active microwave systems will be the only sensors on which a rational program can be built. For such areas, the active microwave sensor is obligatory.

4. In land-use (including agricultural areas) data acquisition programs that use multistage sample designs, it is commonplace to find that these designs are not strong in the face of missing data. A purpose of active microwave sensors may be to provide key complementary information.

If imaging radar systems are provided to meet the short-term data-gathering requirements previously outlined for disaster monitoring (2 hr to 10 days) and for midterm land-use monitoring, updating, and regulatory management (11 to 100 days), the opportunity will also occur to use active microwave sensors for other, less time-dependent, but system-essential roles. These additional roles mainly involve once-a-year surveillance at a key time of the year. The long-term monitoring programs (100 days or more), though required infrequently, may nevertheless have critical time-dependent features that restrict the period of data acquisition. The usefulness of active microwave sensing will be proved by its applicability to short-term and midterm land-use monitoring. Once the decision is made to use them, many secondary opportunities in land use will occur, principally the long-term-monitoring type providing backup to visible-region sensors.

Demonstrated Remote-Sensing Observations

To compare performance to objectives for several sensors, two approaches will be used: (1) the ability of a given sensor to obtain the data needed by sensor type and resolution, independent of considerations of weather and timeliness, and (2) the ability of the sensors to obtain data rapidly (2 hr to 10 days) and under less severe time constraints (greater than 100 days). These time periods respectively relate to disasters, land use, regulatory monitoring programs, and annual (or longer) updating programs.

The ERTS–1.—The ERTS–1 has demonstrated a high-level capability to update land-use maps at levels I and II of the Anderson et al. classification system (ref. 2–133) shown in table 2–X. The usefulness of data at this level varies from State to State, depending on its size and land-use characteristics. With few exceptions, all categories were identified in one or more studies as shown in table 2–XI. The land-use classification (ref. 2–133) in level II is still highly generalized, and many States find

TABLE 2–X.—*Land-Use Classification System for Use With Remote Sensor Data* [a]

Level I	Level II
Urban and built-up land.	Residential.
	Commercial and services.
	Industrial
	Extractive.
	Transportation, communications, and utilities.
	Institutional.
	Strip and clustered settlement.
	Mixed.
	Open and other.
Agricultural land	Cropland and pasture.
	Orchards, groves, bush fruits, vineyards, and horticultural areas.
	Feeding operations.
	Other.
Rangeland	Grass.
	Savannas (palmetto prairies).
	Chaparral.
	Desert shrub.
Forest land	Deciduous.
	Evergreen (coniferous and other).
	Mixed.
Water	Streams and waterways.
	Lakes.
	Reservoirs.
	Bays and estuaries.
	Other.
Nonforested wetland.	Vegetated.
	Bare.
Barren land	Salt flats.
	Beaches.
	Sand other than beaches.
	Bare exposed rock.
	Other.
Tundra	Tundra.
Permanent snow and icefields.	Permanent snow and icefields.

[a] Classification system defined in ref. 2–133.

either that data at this level are unacceptable for State planning purposes or that the data require extensive support data.

The question of the accuracy of land-use determination using the ERTS–1 is still under review because few investigations have reported quantitative results. In some situations, accuracies at level I are 90 percent or better. Generally, accuracies drop to as low as 60 percent at level II. Accuracies are not assessable at level III.

In several studies, level III categories were distinguished, but the number varies from State to State, depending on the particular natural land use and cultural patterns of the area. No consistent nationwide or statewide level III identification system could be based on ERTS–1 data. Nevertheless, the situation is much better than was anticipated for ERTS–1 imagery because the data were expected to be useful only for level I. The ERTS–1 has performed better than anticipated, which is encouraging for future spacecraft sensing.

Additional land cover/use categories [2] (level III categories) identified in ERTS–1 studies (in addition to level II categories contained in ref. 2–133) are as follows: mobile homes, parking lots, unimproved open space (bare), improved open space (irrigated), unimproved open space (with trees), low-density residential, high-density residential, developed open space (urban), rural open land, rights-of-way in forest, rural settlements, wooded rangeland, soybeans, corn, exposed soil, winter ryegrass, and stubble. Other categories were high-density single family, low-density single family, mixed multiple and single family, agricultural (plowed), agricultural (nonplowed), extractive (mines), extractive (tailing pipes), extractive (basins), extractive (gravel pits), sanitary landfill, water (natural basin), water (excavated basin), wetlands (northern bogs), wetlands (southern perennial), wetlands (southern seasonal), low-income residential, middle-income residential, coastal strand, coastal salt marsh, coastal sage, woodland savanna, and riparian vegetarian.

Regarding the two principal areas of concern—disaster monitoring and land-use change and regulatory monitoring—ERTS–1 has performed the following:

1. A limited, but not satisfactory, role in disaster monitoring, being severely limited

[2] Unpublished data from M. T. Heinz et al.

TABLE 2–XI.—*A Sample of Experiments Delineating Land-Use Categories From ERTS–1 Data* [a]

Experiment	Total number of land cover/user categories delineated	Level of categories involved	Technique used
Wray/census cities	11	I, II, III	Automated/manual.
Simpson/New England ...	11	I, II, III	Manual.
Henry/Alabama	6	I	Manual.
Erb/Houston	32	I, II	Automated/manual.
Sweet/Ohio	19	I, II	Manual.
Ingles/Mississippi	13	I, II	Automated.
Sizer/Minnesota	34	I, II, III	Manual.
Thomas/Maryland	6	I	Manual.
Raji/Los Angeles County..	12	I, II, III	Automated.
Houston/Wyoming	19	I, II, III	Automated/manual.
Sattinger/Michigan	9	I, II	Automated.
Colwell/California	17	I, II, III	Manual.

[a] Unpublished data from M. T. Heinz et al.

(by weather, timing, and resolution) to occasional usefulness in long-term persistent floods in less cloudy areas

2. A limited, but not fully satisfactory, role in land-use monitoring and regulatory processes, being limited by cloud cover, timing, resolution, and ambiguities in identification

The Skylab Program.—A recently completed study (ref. 2–134) concerns Skylab instrument performance in land-use mapping. The instruments studied were the S192 multispectral scanner, the S190A camera, and the S190B Earth terrain camera. Comparisons were made with land-use data in the Washington-Baltimore area and the Eastern Shore of Maryland to level IV and, in some cases, to level V. Modifications of existing classifications and a new classification developed for the study were used.

The Earth terrain camera was extraordinarily valuable; it was capable of enlargement to 1:24 000 scale (enlargements to 1:10 000 are possible), and updating of land-use classes with virtually no (or very low) ambiguity was possible. In addition, the results of mapping with S190B data compared very favorably with land-use mapping using high-altitude color IR aircraft photography (RB–57). When mapping was prepared with aircraft data, updating by using Earth-terrain-camera data for longer detection proved readily feasible, particularly for classes involving land clearing for urban development, for which the resolution was good enough that peripheral information enabling separation of plowed land from land cleared for development could be obtained. These results suggest the following applications:

1. For disaster monitoring (2 hr to 10 days), a future shuttle spacecraft could obtain excellent data in noncloudy areas, especially if resolutions better than the 2 m of S190B were obtained. Such data would be calibrated against radar imagery for use when radar is the only data available. Under all inclement or night conditions, the camera and scanners of Skylab (except thermal IR at night) would be of no use.

2. For land-use monitoring (11 to 100 days), high-resolution photography on a shuttle-type vehicle would be invaluable for updating land-use data in arid and semiarid areas where the probability of obtaining data is high. In all other environments, to insure orderly provision of data, radar imaging would at least equal the photography, and, in the more humid environments, it would be the obligatory sensor.

Active microwave results.—The principal studies with imaging radar concerning the

identification of land-use classes comparable to those found in levels I and II (ref. 2–133) are those described in references 2–28, 2–102, 2–119, 2–133, and 2–135 to 2–151.

In addition, extensive but unpublished studies have been used in the assessment of current and projected capabilities of radar images in land-use mapping. The studies were performed in Brazil during Project Radar of the Amazon and in New Guinea by D. S. Simonett, who used X- and Ka-bands, respectively; in Michigan by M. L. Bryan, who used X- and L-band multiple-polarization data; and in Kansas by R. K. Moore, who used a three-frequency multiple-polarization system for crop identification studies.

Summarizing the results of this literature review and analysis of the unpublished data, the following conclusions were reached:

1. A single-frequency radar with single polarization in X- or Ka-bands and with 15-m resolution could distinguish all level I and II categories (table 2–X) virtually without ambiguity.

2. Improvement of the radar system by adding polarizations and, especially, additional frequencies in the range of 1 to 50 cm will make many categories at level III and several categories at level IV distinguishable.

3. Improvement of spatial resolution to approximately 8 m would make the multipolarization, polychromatic radar system highly competitive with color photography in shape and content evaluation and identification and would make many identification classes superior because of the wider multispectral capability.

4. Because of the wavelengths of radar (1 to 50 cm in the areas under consideration) and the spatial frequencies and geometries of natural and artificial land-use features, multifrequency, multipolarization radar is expected to have a high land-use-information content, probably as high as any multifrequency system in the visible region. The strongest indications of this assumption are in the unpublished data of M. L. Bryan and R. K. Moore.

In summary, the evidence strongly supports the view that multispectral sensing in the radar region will probably be at least as successful as that in the visible and near-IR regions with, of course, different strong and weak areas.

All the studies previously listed are empirical, and most are quantitative or semiquantitative. Thus, although issues of theory and modeling have been bypassed, the general area of measurement and quantification of identification accuracies with manual, digital, and statistical analyses has been addressed. The research completed is sufficient to provide a good quantitative base for judgment.

Functional Requirements for Active Microwave Investigations of Land Use

The main variables within functional requirements are the timing of data gathering and the return of data to the user. These variables tend to govern the data storage, transmission, and processing techniques used. If an active microwave system is designed to provide optimal data for the broadest spectrum of actual users, then the functional requirements for short-term applications will dictate the optimal microwave system for land-use analysis. The functional requirements for midterm and long-term applications comprise the greatest applications area for active microwave systems.

Short-term events (floods, earthquakes, etc.) often require data collection under cloudy, foggy, or smoky conditions. Short-term events require data within a 12- to 48-hr period. Rapid data transmission to the user is mandatory. To be of practical value, data should be made available from within a few hours (near real time) to 1 day. Data acquisition should be possible at any time of the day or night and during any time of the year. A satellite system should have the option to take data on command and perhaps to acquire very-high-resolution data of 50- by 50-km areas. Shuttle systems should have the option of modifying mission plans to allow for data acquisition within a 2-hr period.

An active microwave system used in this

application should be broadband and use the 3- to 30-cm wavelength region of the spectrum. The system should be multispectral; however, multispectral (multifrequency) radars will have to be tested in spacecraft and aircraft to determine optimal bandpass. A multiple-polarization capability is important, and HH, vertical transmit/vertical receive (VV), and cross-polarizations should be available. Instantaneous coverage on a synoptic level (100 by 100 km) will be desirable for monitoring; however, high-resolution coverage of small areas may be desirable on a command basis.

Worldwide repetitive coverage on a demand basis will encompass the largest user community. The desired resolution of 15 m is allowable if a narrow strip of very-high-resolution data can be embedded in lower resolution data. A 50-dB dynamic range in 2-dB steps would be desirable for gray-scale resolution. Design of the active microwave system should approach a −30-dB scattering coefficient. Ground truth, together with very-high-resolution color photography to calibrate active microwave interpretive procedures, should be acquired in selected areas. Data storage, transmission, analysis, and dissemination should be a key development area. Multispectral analysis techniques, both optical and manual, and computer processing must be used. Multistage data analysis and cross-comparative data analysis will be an important functional requirement.

Data reduction and analysis.—As discussed later, the spacecraft and aircraft radar data are expected to be in three principal formats that will govern the data reduction and analysis processes: black-and-white image format, color-combined images, and CCT's.

The CCT data would enable multispectral pattern analysis and digital image enhancement and should be considered in precisely the same way as multispectral scanner data for processing and analysis options. These options will include the use of time-congruenced digital images for areas of very low relief.

Color-combined and black-and-white images will be interpreted manually to provide major land-use boundaries, which may then be registered to the CCT's by using interactive terminals (graph tablet, light pen, etc.). Within these manually determined boundaries, detailed multispectral classification will be conducted by using computer classification. Within the next 10 yr, parallel processing will cause a sharp reduction in the cost per pixel classification and will result in interactive identification and mapping programs.

Display and distribution timeliness.—Data needed for disaster monitoring are required within 12 to 48 hr, preferably 12 hr. Data for land use and regulatory monitoring should be obtained within 1 week of acquisition. Data for longer term monitoring should be obtained within 2 weeks to 1 month, preferably 2 weeks.

Formats.—The data obtained from aircraft and spacecraft imaging systems will be in the form of CCT's and images prepared from the digital tapes, which include enhanced preprocessed images.

Scales and projections.—All images derived from the CCT's should be outputted on universal transverse Mercator (UTM) projection, with indexing to UTM coordinates and latitude/longitude coordinates. Scales may be variable, but a recommended group of scales would be 1:24 000, 1:50 000, and 1:100 000.

Ground truth.—Ground truth should be obtained (mainly in the form of field observations of land-use categories) during the experimental phases of the aircraft testing needed to define the limits of data interpretability. During spacecraft research and development and later operational missions, training sets should be established and updated regularly as small samples for extrapolation. Studies are needed on the proportions and types of ground truth essential for regulatory monitoring and disaster situations.

Accuracy of calibration.—Two forms of calibration are required: absolute calibration

to 2 dB and relative calibration to 1 dB. Ground calibration with corner reflectors may be needed in some instances.

Unique Justification of Microwave Sensing

The unique justifications of microwave sensing are as follows:

1. Disaster monitoring (2 hr to 10 days): Radar is the only sensor capable of monitoring the progress of a disaster under inclement conditions.

2. Land-use monitoring (11 days to 100 days): Radar is the only sensor that can guarantee data acquisition and thus is essential to the effective initiation and functioning of a truly responsive monitoring system.

3. Long-term land-use update (100 days or more): Radar does not have a unique role in this area; it is secondary or supportive.

Anticipated Active Microwave Results and Accuracies Within 5 to 10 Yr

The results and accuracies shown in tables 2–XII and 2–XIII might be anticipated between 1978 and 1984, if a prompt commitment is made to construct a flexible aircraft research radar system capable of testing resolution, wavelength, polarization, bandwidth, swath width, depression-angle effects, and azimuth-angle effects on the radar return with completion before June 1977, and if a systematic testing program is initiated.

Value of disaster monitoring.—The annual loss of life resulting from disasters is large, and the annual monetary cost of such disasters is roughly estimated to be $300 million in the United States and $10 billion on a worldwide basis. The degree to which these losses could be reduced through the introduction of a quick monitoring system, which could be used to direct relief operations, recovery, land management practices, etc., is largely unknown and will require a systematic and thorough analysis. Savings of 1 percent in the United States and 2 percent on a worldwide basis for areas of poor communications would total $3 million and $200 million, respectively.

TABLE 2–XII.—*All-Weather Monitoring of Disaster Areas, Intensities, Persistencies, and Effects*

Disaster characteristics	Percent accuracy	
	5 yr	10 yr
Flood area	95	98
Flood area and time by class of land use	90	95
Fire damage (large area)	80	85
Wind damage	60	70
Earthquake damage	30	50
Blizzard effects	60	70

TABLE 2–XIII.—*All-Weather Monitoring of Land-Use Change, Regulatory Monitoring, and Updating of Land-Use Classes*

Category	Percent accuracy	
	5 yr	10 yr
Level I	95	98
Level II	92	96
Level III	60	80
Level IV (accuracy based on good identification, 90 percent of a small number of classes)	10	15

The cost of testing a disaster-monitoring system using a standby shuttle vehicle and a multifrequency radar system is estimated at less than $25 million per year, which does not include development costs of the system or systems.

Value of land-use monitoring.—To decisionmakers, the value of an integrated geobased land use information system using radar for systematically updating to level III is estimated to be $6 million annually. Throughout the world, such a system might be worth 10 times that amount. If borne exclusively by a single land-use monitoring program, the cost of operating the multifrequency system would probably exceed $20 million annually. The problem of double counting for both cost and benefits will arise when the same data serve multiple purposes.

Cost/Benefit Considerations

The complexity of cost/benefit analysis is evidenced in the studies now being conducted

for the U.S. Department of the Interior. These studies indicate the types of analyses required and the difficulty of pinpointing the benefits for the United States and other parts of the world.

Conclusions and Recommendations

The principal conclusions of the panel regarding presently demonstrated feasibility is that published and unpublished studies strongly support the view that radar imagery at one or two frequencies and several polarizations can be used satisfactorily for mapping and updating land use to level II in the Anderson et al. (ref. 2–133) land-use classification system.

The present capability leads to the consideration of a full-scale multifrequency, multipolarization, digitally recorded, synthetic aperture, 8-m resolution system as a candidate for spacecraft use in disaster and land-use monitoring. The development of a polychromatic system is important because land-use data at level III (not considered in the Anderson et al. paper (ref. 2–133)), and possibly at level IV, are much more useful for State-level geobase information system functioning and for disaster monitoring, when penetration of tree cover is important and a diversity of wavelengths up to 50 cm (short of the limiting region of Faraday effects) is required.

Research is needed in the scanning of detailed land-use classes to level III and the scanning of disaster areas in a systematic testing program with a flexible polychromatic radar system. The detection of land-use change for regulatory monitoring and the interaction between disaster and detailed land-use classes constitute the basis of the experiments needed in which the following radar parameters should be systematically and repeatedly examined against these classes.

1. Wavelength: 1 to 50 cm; 4 to 5 bands.
2. Polarization: Linear, HH, VV, HV.
3. Bandwidth: One band of greater than usual bandwidth (e.g., ½ octave).
4. Resolution: Experiment with one band of very-high-resolution, narrow-swath-width imagery embedded in moderate resolution.
5. Swath width: 20 to 100 km.
6. Depression angles: 50° to 80°.
7. Azimuth angles: Multiple flight directions.
8. Stereoscopy: 60 percent sidelap.

Recommendations on data gathering for which imaging radar is the obligatory sensor.—A class of management and policy decisions exists in both public and private sectors that requires timely rapid-response data under inclement conditions of night, cloud, rain, fog, smog, dust, and smoke. Many of these decisions relate to national and especially international emergencies caused by great storms, earthquakes, fires, volcanic eruptions, blizzards, floods, tidal waves, landslides, oilspills, and related events. Only active microwave sensors can meet these needs. Timely data on the interaction between these events and land uses in time and space will be critical in defining the areas affected, the types of property damage anticipated, emergency operations, the progress of flood recession, and so forth, especially for developing countries.

The development of an emergency preparedness system including the following components is necessary.

1. Single- or dual-frequency radar spacecraft imaging system.
2. Digital onboard processing of wide bandwidth transmission to a central facility in the United States.
3. Rapid-analysis teams at the central facility.
4. Provision of alternative information to emergency headquarters and field teams by means of—
   a. Provision of hardcopy images.
   b. Multicolor-enhanced interpreted images.
   c. Commercial satellite television transmission of enhanced interpreted images.

Recommendation 1: A significant effort should be initiated by NASA to define the

most effective radar system to image the diverse group of areas and emergency conditions. This effort should explore multiple resolutions, wavelengths, bandwidths, polarizations, incident angles, azimuth angles, and swath widths by theoretical analyses and aircraft data gathering.

Recommendation 2: For the purpose of defining a radar system for emergency conditions and for many other less-time-dependent uses of radar imagers, NASA should develop a flexible aircraft multiplex radar system (or systems) in which the interrelationships between system parameters and target response may be systematically examined.

The aircraft system (or systems) should have the capability to explore basic questions on target and background radar response with variations in resolution, wavelength, bandwidth, polarization, depression angle, azimuth angle, and swath width.

Recommendation 3: With the aircraft system (or systems) of recommendation 2 available, NASA should examine to at least level III in the Anderson et al. (ref. 2–133) land-use classification system the target/background interactions before, during, and following major hurricanes and similar disasters in the United States. These data will set bounds on interpretability, decisions, management options, etc., and will define the spacecraft radar designs.

Recommendation 4: Following successful research analysis and development through the previous recommendations, NASA, the European Space Research Organization, and the United Nations should take the steps necessary to establish emergency interpretation and data dissemination facilities and to explore the methods and techniques of hard-copy and television transmissions.

Recommendations on data gathering for which radar is required for effective functioning of a land-use monitoring and change detection system.—Many States are concerned with monitoring land-use changes (1) for compliance with regulations at both the State and Federal level, (2) for the normal updating needed in a geobase information system, (3) for using changing land-use data to level III as a basis for economic and forecasting models, (4) for maintenance of planning options, and (5) for anticipation and planning of new public and private sector cooperative planning of utility sites and routes, development works, population shifts, and related matters. In many cases, the original decision to establish a remote-sensing satellite-based monitoring system will be conditioned on the ability of the system to reliably and orderly supply data and information as needed to facilitate key land-use management decisions. The value of active microwave sensors in insuring that the system will function independently of weather conditions should not be deemphasized. Radar imagery will probably meet many, if not all, monitoring needs. Visible-region sensing will be adequate in some subhumid and arid areas but will benefit significantly from radar support in cloudy areas.

URBAN AND TRANSPORTATION APPLICATIONS

A series of Government-sponsored ongoing research programs concerned with the collection and use of data from urban areas is underway. Many of these programs are concerned primarily with using a set of remote sensors, including multiband photography, multispectral scanners, and SLAR mounted either in aircraft or spacecraft. Most data that have been properly collected, analyzed, and used in application programs for decisionmaking have been confined to the visible and IR portions of the electromagnetic spectrum. The microwave portion of the spectrum has been sparingly used as a viable data source for urban information.

Some uses of active microwave imaging systems, specifically SLAR, for urban data collection are discussed in this section. The usefulness of SLAR data is compared with data collected by other sensors, and the applications of these SLAR data for urban studies are identified. Therefore, this dis-

cussion is a continuation and extension of previous work by NASA (ref. 2–152) in identifying Earth resources from space, with specific emphasis on urbanized areas and active microwave sensors. The objectives of such programs are as follows:

1. To determine the capabilities of various remote sensors to record physical data, both natural and cultural, about the atmosphere, oceans, and terrain of the Earth.
2. To identify potential applications of these data in scientific and resource management fields.
3. To design information systems based on both the needs of users and the capabilities of forthcoming remote-sensing satellites.

Work on these objectives has not progressed as a unit. Usually, after completing a functional data collection system, the data collected by the system are subjected only to modest analysis. In urban studies, this type analysis is especially relevant because the problems are only partially within the immediate domain of technology. Social problems, which are not really amenable to the technologist's approach or to the scientific method (ref. 2–153), are an integral part of the problem that must be solved before stating the usefulness of active microwave sensor data.

Definition of Subject and Problem

Urban studies measure three parameters: population density, functional use, and morphology. Population density is often measured and expressed by housing density and population size and density. The rural/urban fringe is delineated by using population density. Another means for delineating the fringe is by counting street intersections per square kilometer. Normally, the sources of these data are Federal, State, and local census-gathering projects, aerial photographs, and topographic maps. However, some measurements, especially street intersections per square kilometer, could be interpreted from radar imagery.

Functional boundaries within a city are also defined primarily by census-type data and high-resolution aerial photographs. These data would be more difficult to derive from existing SLAR systems, although several studies indicate that this can be accomplished at relatively low levels of accuracy.

Defining morphological regions is difficult because the definitions vary from region to region. Generally, the information wanted is the shape and texture of features such as the central business district, the alinement of street patterns, or the pattern of commercial development. As will be documented later in this chapter, active microwave sensors can provide part of these data.

Transportation, a key to urbanism, must also be considered because, without the ability to move people and goods quickly and cheaply, urban centers would not exist. The fact that streets occupy from 10 to 20 percent of the surface in urban areas is proof of their importance.

Determination of transportation network and site usage has importance for land planning and management at all levels of government. Conventional photographic techniques are limited by (1) the requirement for repetitive coverage at large scales (1:6000) and high resolutions, (2) weather conditions, (3) daytime observation, and (4) vegetative cover. Active microwave sensors may provide accurate data, especially if they can result in the identification of moving (transient) subjects.

Land-Use Classification

In urban areas, where most of the surface is covered by artificial construction, the determination of actual land use is difficult under any circumstances. Asphalt and other petroleum derivatives are used for racetracks, roads, parking lots, driveways, and roofs. The actual use of the asphalt is determined by the original intent, age, and changing spatial context. The use may also be multipurpose, with each use being valid and possibly time dependent (e.g., a parking lot during business hours may become a recreational area at night and on weekends).

Using photographic remote sensing, which detects only the surfaces (e.g., the tops of trees, roofs, or bottoms of gravel pits), the functional uses of these surfaces or of the surfaces they obscure from view are difficult to determine.

Existing systems for classification of urban land use are separated into levels of generalization based on the amount of detail described. The level of generalization is usually dependent on the scale and target detection capabilities of the imagery. Also, the level of generalization of urban land-use data may be determined by the requirements of the user. Map users at the national scale would normally require only the highest level of generalization, whereas users at the local scale would need detailed information available at a second or third level in a land-use classification system. Table 2–XIV shows the relationship of user needs to levels of generalization in urban land-use classifications (refs. 2–133 and 2–154).

Urban land-use classification systems are similar at the first level of generalization but vary to suit conditions as more detail is added. Urban land-use maps based on radar imagery at aircraft altitudes show that imagery of urban areas can be classified adequately to produce maps that include most level II categories shown in table 2-XV. In a few instances, a refinement to a level III category has been possible (i.e., relative residential densities and relative ages of residential areas).

TABLE 2–XIV.—*Land-Use/Scale Relationships* [a]

User scale	Level of generalization	Source of information
National	I [b]	Satellite imagery and high-altitude photography.
State	I and II	Same as for "National."
Local (city or county).	III and IV [c]	Medium- and low-altitude photography.

[a] Refs. 2–133 and 2–154.
[b] Most generalized.
[c] Most detailed.

TABLE 2–XV.—*Land-Use Classification System for Use With Remote Sensor Data* [a]

Level I	Level II
01. Urban and built-up land.	01. Residential. 02. Commercial and services. 03. Industrial. 04. Extractive. 05. Transportation, communications, and utilities. 06. Institutional. 07. Strip and clustered settlement. 08. Mixed. 09. Open and other.

[a] Ref. 2–133.

Demonstrated Remote-Sensing Observations

Present methods of collecting data about urban areas and the analysis of these data are time consuming, costly, and rather inefficient. Normally, these methods involve extensive fieldwork, interviews, and similar operations (e.g., census data and origin-destination studies). To provide management and decisionmakers with current information, emphasis has been placed on the development of new systems and analysis techniques, which include exploring the potential of remotely sensed data, including SLAR. Most previous research in remote-sensing data-collection analysis and management has used photographic systems (black and white, color, color-IR, and multilens cameras). Thermal imagery and radar have received relatively minor attention (ref. 2–155).

Photography and ERTS.—Urban land-use data from aerial photographs are feasible on both a block and parcel basis; however, mapping parcels usually requires supplemental data (ref. 2–156). Block mapping can be accomplished on photographs at scales as small as 1:100 000. By using ERTS imagery, eight major land-use categories have been mapped in Rhode Island at a level

to meet standards set in State land-use maps published in 1960 (ref. 2–155).

Aerial photographs are standard tools in transportation studies. Highway departments use photogrammetric and interpretive techniques for route selection, road design, and recording the various stages of construction. Mapping traffic-flow patterns, planning future parking facilities, and determining necessary road maintenance are other demonstrated applications of aerial photographs.

Current high-resolution large-scale photographs can provide accurate data on transient events by repetitive aircraft overflights. Though more cost effective than ground surveys, this approach is still expensive in terms of time and money, because (1) repetitive coverage over small areas at low altitudes is required and (2) large volumes of data must be analyzed by conventional photointerpretive methods. Current quasi-operational satellites (ERTS) do not have the resolution or repetitive frequency required for detection and identification of transient subjects.

Other urban-oriented applications of aerial photographs are as follows:

1. Planning collection routes (e.g., garbage, sewage, and buses) and zoning changes.
2. Establishing the rights-of-way for powerlines and pipelines.
3. Monitoring atmospheric pollution.
4. Determining dwelling units and estimating population.
5. Determining housing quality.

Active microwave.—Radar imagery has been used much less frequently than aerial photography. However, published reports indicate that radar imagery is a potential source of urban data. Radar has been used to map land-use patterns within urban areas (refs. 2–28, 2–148, and 2–149). An example of this application is shown in imagery of San Diego, Calif. (fig. 2–37). Industrial, commercial, and residential zones and vacant lots were delimited in all cases. Finer divisions were possible in a smaller and less complex urban area; parks, cemeteries, golf courses, and relative ages of residential regions were delineated.

The relationship between population and the radar-derived area of urban regions has been studied and tentatively established (ref. 2–151). Settlement detection was evaluated for 100 percent of the cities with a population larger than 7000, for 80 percent of the towns with populations between 800 and 7000, and for 50 percent of the villages with populations between 150 and 800 (ref. 2–146). Differentiating rural from urban areas was found to be consistently possible.

Other studies (refs. 2–148 and 2–137) have evaluated polarization schemes for detecting cultural features. Polarization is important in the delineation schemes for detecting cultural features. Polarization is important in the delineation of railroads and powerlines (fig. 2–38), the separation of parks from urban areas, the distinction between residential areas differing in age or building materials, and the detection of bridges. Bryan (ref. 2–147) recently conducted similar studies using a two-frequency, two-polarization imaging radar system. His studies concentrated on two areas in the Detroit metropolitan area: one was near the central city with heavy industries and large railroad yards, and the other was a suburb composed primarily of residential areas. The residential areas and the heavy industrial areas (fig. 2–39) on this 10-m-resolution imagery were clearly and accurately delimited. Generally, the accuracies of identification of the residential areas were approximately 75 percent correct, whereas industrial areas were discriminated with accuracies of approximately 63 percent. These accuracies may appear to be low; however, they were made solely on the basis of the existing SLAR imagery.

Anticipated Microwave Results

Because most urban changes do not occur within a 2-day timespan when cloud cover or daylight could be critical and because most urban areas are concentrated in the well-developed countries, radar imagery is in com-

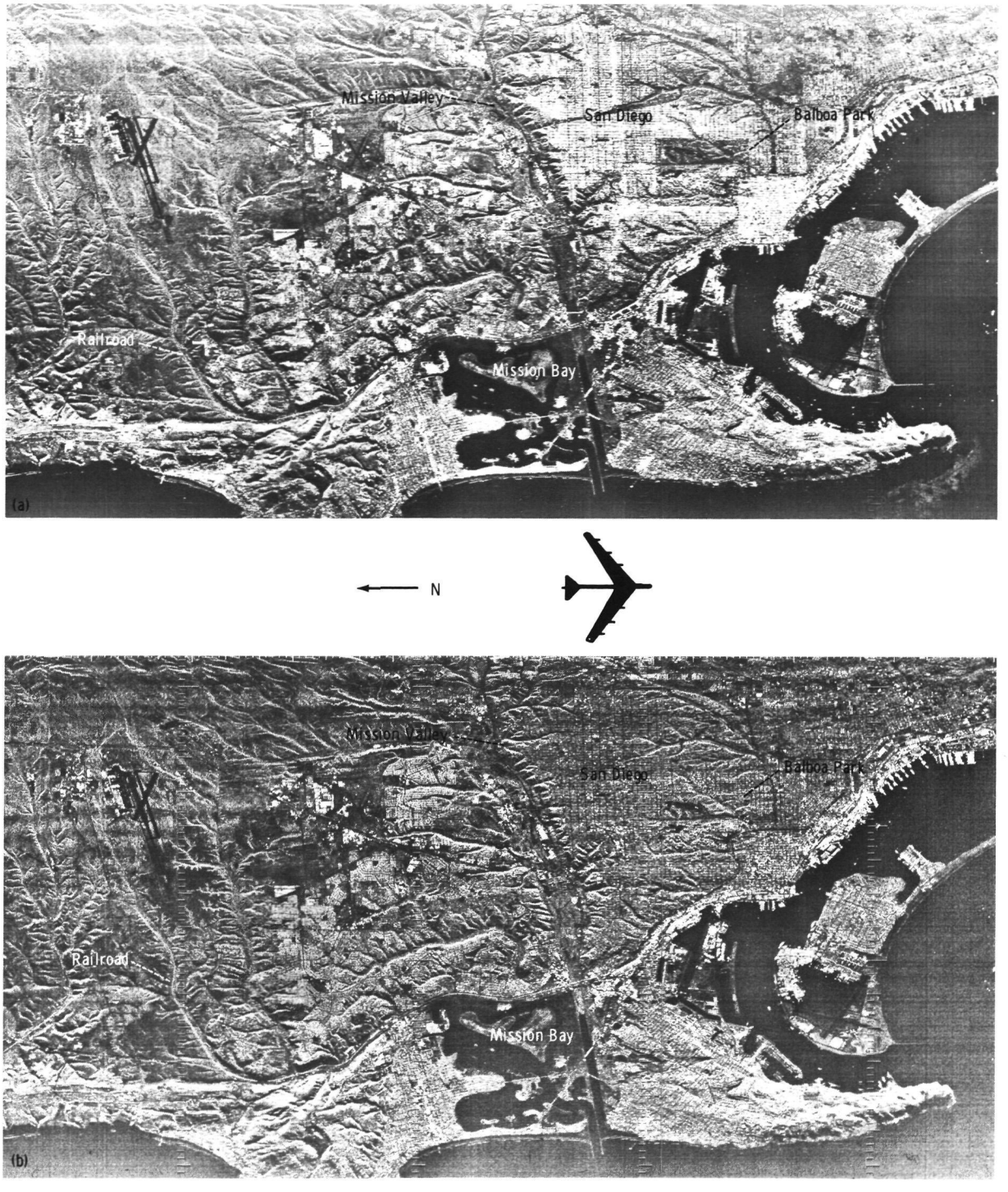

FIGURE 2–37.—Imagery of San Diego, Calif., showing separation of residential, park, and business areas by using two radar polarizations. (*a*) An HH polarization. (*b*) An HV polarization.

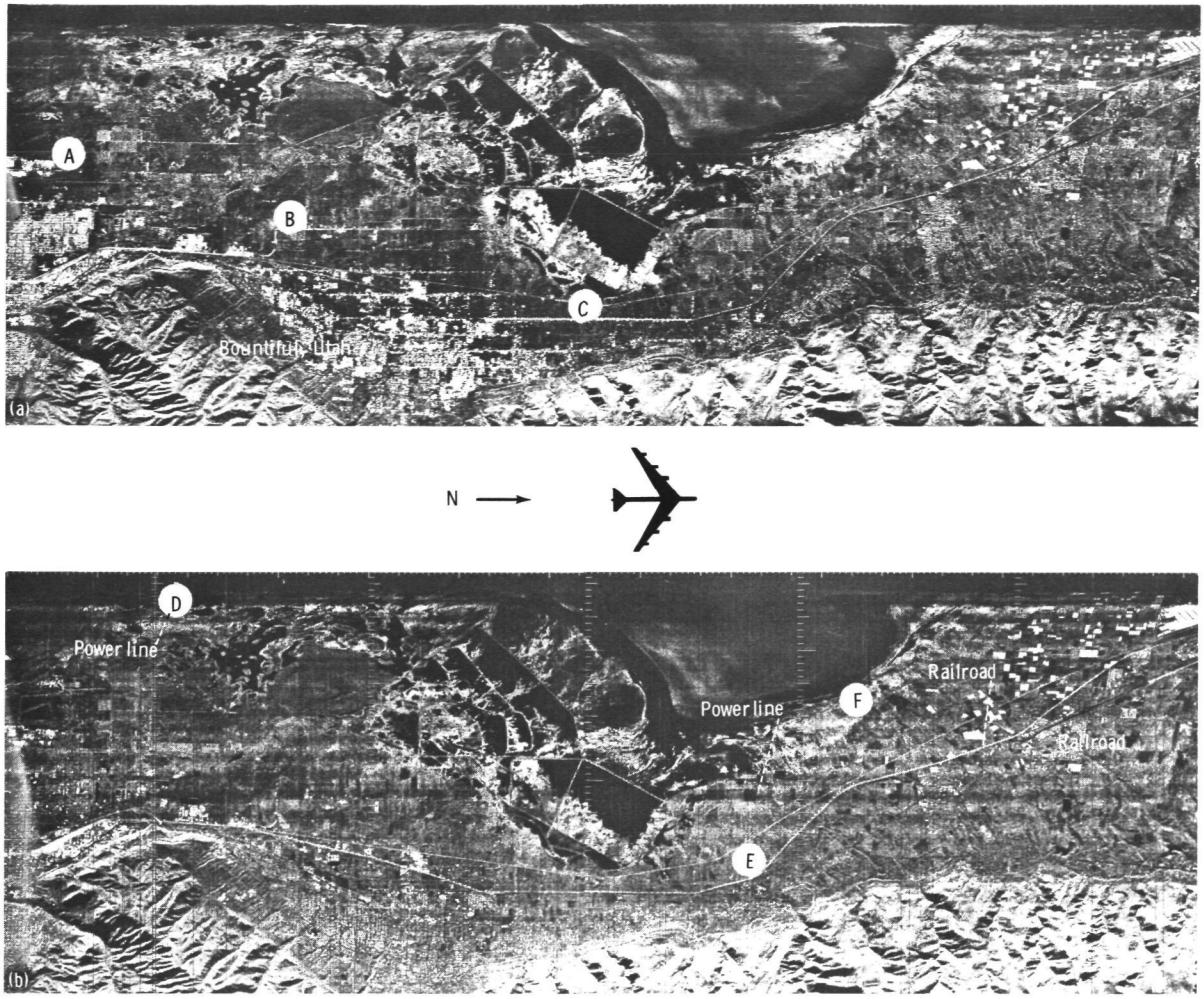

FIGURE 2–38.—Imagery showing delineation of railroads and powerlines near Bountiful, Utah, using two radar polarizations. (*a*) An HH polarization. (*b*) An HV polarization.

petition with aerial photography as a source of data. Existing active microwave systems may provide the technology necessary for frequency-of-use analysis based on identification of transient subjects. Microwave systems with resolutions of 10 m (with different polarizations and with moving-subject analysis) may possibly be used to identify the transient subjects previously outlined. Moving-target analysis using active microwave sensors has been proved feasible. Radar may also provide data on (1) short-term phenomena, such as urban flooding related to high-intensity rainfall; (2) nighttime-related activities; and (3) urban or commercial activities in the tropics and underdeveloped countries. The near-all-weather capability of active microwave sensors makes possible the collection of such short-term information without the loss of critically timed data.

Active microwave sensors aboard a spacecraft could produce imagery capable of mapping to a level of generalization suitable to users at a national and regional scale; that is, level I. Furthermore, radar imagery from a satellite should enable mapping of certain in-

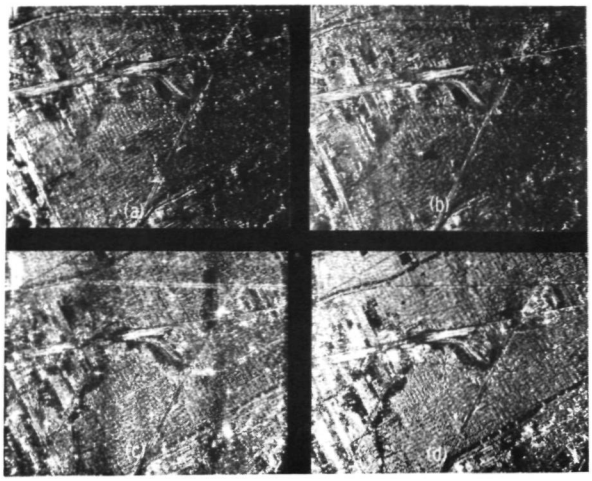

FIGURE 2–39.—Four-channel simultaneous SLAR imagery of a portion of Detroit, Mich. (*a*) An X-band, HH polarization. (*b*) An X-band, HV polarization. (*c*) An L-band, HH polarization. (*d*) An L-band, HV polarization.

formation at level II in the classification system.

Other time- and place-dependent data can also be obtained from radar imagery.

1. Monitoring traffic on waterways.
2. Search-and-rescue operations in coastal and fluvial environments.
3. Nighttime surveillance of movement across borders and possible contraband.
4. Monitoring use of recreation facilities during periods of inclement weather.
5. Documenting urban flooding related to local weather conditions.
6. Supplying local, State, and Federal agencies with timely information on traffic-flow patterns, concentrations of activity in urban and rural areas, recreational site usage, and so forth, so that management plans can be developed to maximize land use and to minimize the negative effect of people on the environment.

Functional Requirements

The following requirements are recommended for use of active microwave sensor data for study of urban scenes:

1. Resolution: A 5-m resolution is recommended; 10-m resolution is acceptable (fig. 2–40).
2. Swath width: A width of approximately 15 to 20 km is required.
3. Repetition: One pass over each scene every 14 days is required.
4. Wavelength: Two wavelengths, collected simultaneously, are recommended: shorter wavelength in the Ka- or X-band (1 to 3 cm), longer wavelength in the L-band (20 to 30 cm).
5. Polarizations: The HH and HV polarizations are strongly recommended and should be available for each wavelength.
6. Depression angles: Depression angles should range from 20° to 60°. The actual image swath should be centered within this range.
7. Timeliness: For nonemergency studies, data should be delivered to the users within 2 weeks of data collection. For emergency studies (e.g., floods, hurricanes, and disaster assessments), data should be delivered within 2 hr of collection.
8. Processing: Onboard processing is desirable for aircraft and Space Shuttle. Digital tapes are required for later processing to enhance data. Low-altitude aircraft underflights are required for documentation of ground conditions and for calibrations. Unmanned satellite data are to be telemetered and processed at data collection centers.
9. Format to user: Formats will be raw imagery at time intervals, a map format showing frequency of use, and printouts showing inventory of transient subjects in specified areas.
10. Unique justification for active microwave: Active microwave sensing can identify moving subjects and make nighttime and all-weather observations possible.
11. Identification of users: No independent evaluation of the potential users of SLAR imagery from urban areas has been conducted. However, a brief review of the literature indicates some potential users.

In a series of discussions (ref. 2–157) concerning urban planning and data needs for the Denver, Colo., metropolitan area plan-

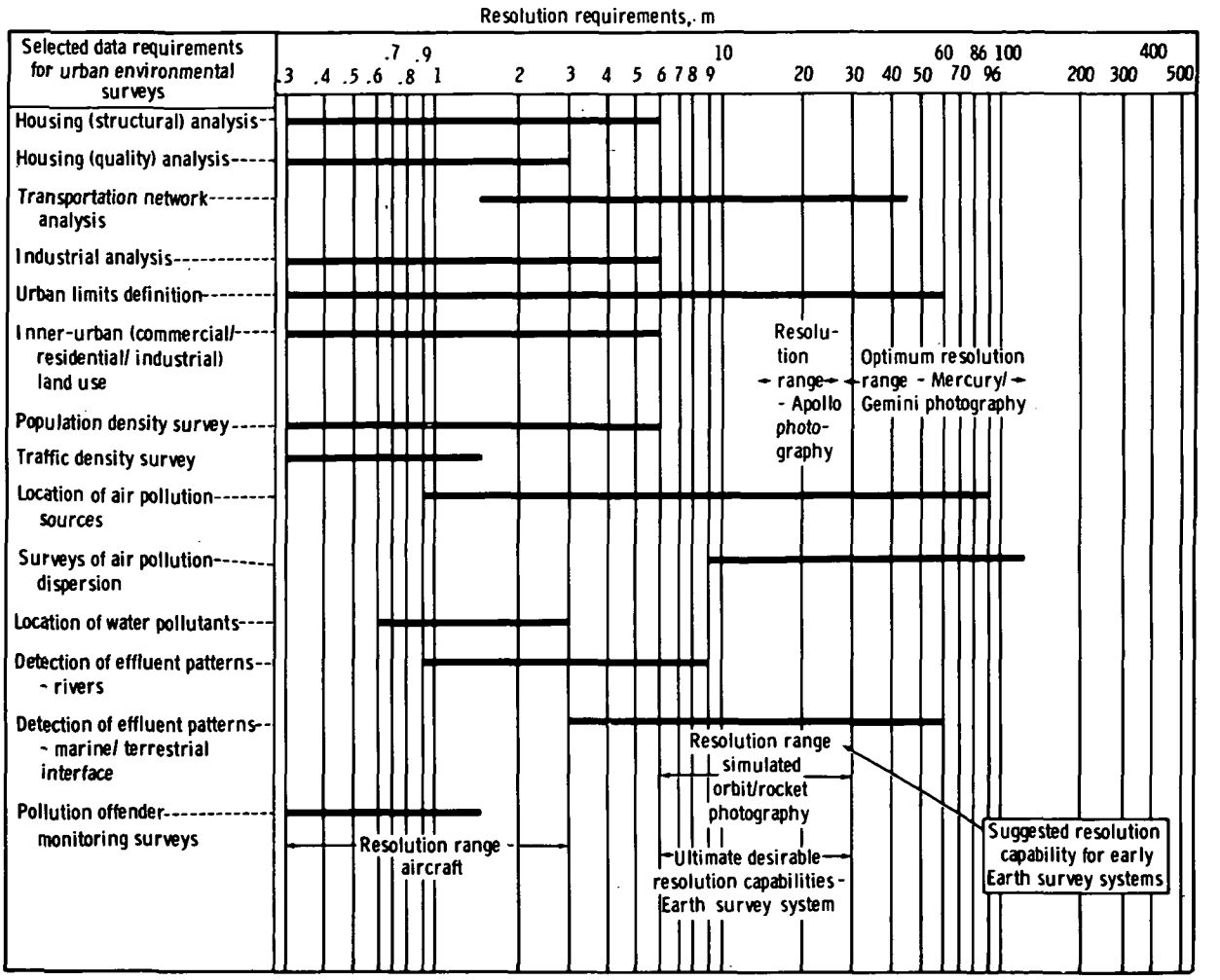

FIGURE 2–40.—Optimum level of detail (resolution) requirements for selected data categories related to urban environmental surveys.

ning community, the following potential users were identified:

1. State Planning Office
2. State Land Use Commission
3. Denver Council of Governments
4. State Highway Commission
5. City of Denver Planning Office
6. City Engineer's Office
7. Urban Drainage and Flood Control Commission
8. Traffic Engineer's Office
9. Zoning Board
10. Assessor's Office
11. City Water Board
12. Urban Renewal Authority
13. Model Cities Program
14. Community Renewal Program
15. Office of Economic Opportunity
16. Colorado Water Conservation Board
17. Regional Transportation District

The following applications for remote sensing were identified as having the highest potential (ref. 2–158):

1. Natural resources and economic development.
2. Recreation and culture.
3. Agriculture.
4. Transportation.
5. State planning agencies.

6. Regional planning agencies.
7. Local city and county planning agencies.

In the present context, the last four items are of special interest. To state definitively the complete listing of possible users would be an extensive task and would, in essence, identify all individuals, groups, agencies, and offices that are involved in various aspects of the structure, morphology, and extent of the urbanized area.

One metropolitan area should be selected as an example, and, within the selected area, all potential user agencies for SLAR should be identified. It is assumed that other States would have, within the same general categories, the same or similar organizational hierarchies, which would fit the general format of the original test case.

Recommendations

As previously noted, visual interpretation of SLAR data will probably provide the greatest immediate benefits. Later benefits will be derived from both visual and machine analysis because photographic interpretation techniques are indispensable for identifying those areas that cause confusion during visual interpretation.

Because only a few studies of the microwave response of urban landscapes have been accomplished, a well-documented and sustained program should be developed to explore sensor capabilities. The following sequence is suggested:

1. Identify study areas that include a complete spectrum of urban conditions.
2. Collect relevant SLAR imagery using a system comparable to that selected for satellite development.
3. Interpret the data by concentrating on the following items:

a. Develop optimum land-use classifications with consideration of those classifications that are presently being used by the local planning and land-use agencies.

b. Document the interpretation accuracies for combinations of wavelengths, polarizations, and resolutions.

Active microwave instrumentation should be developed with a multifrequency, multipolarization, and multiresolution capability; thus, aircraft and Space Shuttle missions can be flown to define the optimal resolutions, frequencies, and polarizations required to detect and identify transient phenomena. Data-processing techniques should be developed to further aid identification of transient subjects by moving-subject analysis.

SUMMARY AND RECOMMENDATIONS

A reliable and timely update of changes in a data base is a major need in land-use planning. These changes may be considered in a very short term period, such as disasters, and in mid- and long-term periods, such as developmental change. For each of these needs, active microwave sensors can be important.

For disaster sensing, radar is the only sensor that can obtain data with certainty on demand, regardless of obscuration. Radar can rapidly provide complete coverage and monitoring of the extent and progress of floods, hurricanes with destructive winds, coastal inundations, great fires, tidal waves, volcanic eruptions, earthquakes, landslides, and blizzards. To be timely, data on these events must be independent of night, clouds, rain, smoke, or fog; and only radar can provide that independence.

In the developmental change of land use, the urgency of timely coverage is reduced, and the status of radar becomes coequal or, in some cases, subordinate to sensors of the visible wavelengths. In these applications, active microwave sensors will provide missing data in areas partially obscured by clouds and will assure an orderly and systematic continuity of data. The assurance of complete data is a key consideration when monitoring regulation of progressive land-use change is practiced. In cloudy environments (even in the United States), imaging radar would provide strong support to aerial photography in the management of land use. In very cloudy

areas, active microwave sensors would perforce become the obligatory sensor for a monitoring program. In many such situations, the decision to establish the ground information system will be made possible only by the assurance of data acquisition, which is given by the active microwave sensor components of the monitoring system.

The obligatory role of active microwave sensors in the monitoring of disasters requires that data be acquired at high resolution (8 to 10 m) over a wide swath (50 to 100 km) using a wavelength that is certain to penetrate clouds (3 to 10 cm). Furthermore, the data must be provided to the user within a few hours (12 to 48 hr) in a hard-image format.

The supportive use of radar for land-use data collection requires identification of surface cover by active microwave multispectral, multipolarization, multistage analyses. Therefore, instruments with 1-, 3-, and 10-cm wavelengths should be used together with combinations of polarizations. The data should be available to the user in intervals of a few weeks in both hardcopy and digital tape. Lower resolution (10 to 20 m) would be acceptable, but a high-resolution strip embedded within approximately 5 percent of the coverage would be highly advantageous.

A basic need for the development of an active microwave land-use change information system is a determination of optimum radar system parameters. For this purpose, a flexible variable-parameter aircraft radar system (or systems) should be developed, and a research program should be initiated to determine the radar and target interactions with respect to variations in resolution, wavelength, bandwidth, polarization, depression angle, azimuth angle, and swath width. The research will help determine the limits of interpretability and the spacecraft radar designs. Ultimately, the research program should initiate development of national and international emergency data dissemination facilities. Experiments are needed to define the abilities of radar imagery for detection, identification, and mapping of land uses to level III of the Anderson et al. land-use classification system (ref. 2–133).

A land-use monitoring system will require the same aircraft testing of land-use category mapping and inventory to level III, systematically viewed against variable radar-instrument parameters of wavelength, polarization, bandwidth, resolution, depression angle, azimuth angle, and swath width, which were previously listed for disaster monitoring.

Each category to level III should be systematically reviewed by repeated flights in representative areas of the United States to define radar performance in multispectral digital pattern recognition, manual updating, and interactive identification.

REFERENCES

2–1. DYNATREND, INC.: Final Report: Evaluation of Benefits and System Features of an Earth Resource, Satellite Operational System. Dynatrend, Inc. (Burlington, Mass.), Aug. 1973.

2–2. WING, R. S.: Structural Analysis From Radar Imagery of Eastern Panama Isthmus. Mod. Geol., vol. 2, 1971, pp. 1–21 and 75–127.

2–3. MACDONALD, H. C., AND WAITE, W. P.: Imaging Radars Provide Terrain Texture and Roughness Parameters in Semi-Arid Environments. Mod. Geol., vol. 4, no. 2, 1973, pp. 145–158.

2–4. WING, R. S., AND DELLWIG, L. F.: Radar Expression of Virginia Dale Pre-Cambrian Ring-Like Complex, Wyoming/Colorado. Geol. Soc. Amer. Bull., vol. 81, 1970, pp. 293–298.

2–5. WING, R. S.; OVERBEY, W. K., JR.; AND DELLWIG, L. F.: Radar Lineament Analysis, Burning Springs Area, West Virginia; An Aid in the Definition of Appalachian Plateau Thrusts. Geol. Soc. Amer. Bull., vol. 81, 1970, pp. 344–347.

2–6. GILLERMAN, ELLIOT: Roselle Lineament of Southeast Missouri. Geol. Soc. Amer. Bull., vol. 81, no. 3, Mar. 1970, pp. 975–982.

2–7. WING, R. S., AND MACDONALD, H. C.: Radar Geology; Petroleum Exploration Technique, Eastern Panama and Northwestern Colombia. Amer. Assoc. Pet. Geol. Bull., vol. 57, no. 5, 1973, pp. 825–840.

2–8. LYON, R. J. P., AND LEE, KEENAN: Remote

Sensing in Exploration for Mineral Deposits. Econ. Geol., vol. 65, no. 7, 1970, pp. 785–800.

2–9. POWELL, W. J.; COPELAND, C. W.; AND DRAHOVZAL, J. A.: Delineation of Linear Features and Application to Reservoir Engineering Using Apollo 9 Multispectral Photography. Alabama Geol. Survey Open File Report, Information Series 41, Univ. of Alabama, 1970.

2–10. WAITE, W. P., AND MACDONALD, HAROLD C.: Fracture Analysis With Imaging Radars. EOS Trans. Amer. Geophys. Union, vol. 53, no. 9, Sept. 1972, p. 981.

2–11. FEDER, G. L., AND BARKS, J. H.: A Losing Drainage Basin in the Missouri Ozarks Identified on Side-Looking Radar Imagery. U.S. Geol. Survey Prof. Paper 800–C, 1972, pp. C249–C252.

2–12. CANNON, P. J.: The Application of Radar and Infrared Imagery to Quantitative Geomorphic Investigations. Proceedings of the Second Annual Remote Sensing of Earth Resources Conference, vol. 2, Univ. of Tennessee Space Institute (Tullahoma, Tenn.), Mar. 1973, pp. 503–519.

2–13. DELLWIG, L. F.: Pluses and Minuses of Radar in Geological Exploration. Earth Resources Aircraft Program Status Review, vol. 1, NASA MSC (Houston, Tex.), Sept. 1968, pp. 14–1 to 14–25.

2–14. HACKMAN, R. J.: Geologic Evaluation of Radar Imagery in Southern Utah. NASA CR–80782, 1966.

2–15. ROBERTS, RALPH J.: Geological Evaluation of K-Band Radar Imagery, North-Central Nevada. U.S. Geol. Survey Technical Letter NASA–49 (Washington, D.C.), Aug. 1966.

2–16. SNAVELY, P. D., JR., AND WAGNER, H. C.: Geologic Evaluation of Radar Imagery, Oregon Coast. NASA CR–75449, 1966.

2–17. KEDAR, E. Y., AND SHIN-YI, HSU: Side-Looking Radar Imagery Applied in Seismic-Risk Mapping. Proceedings of the Eighth International Symposium on Remote Sensing of Environment, vol. II, Univ. of Michigan, Oct. 1972, pp. 1195–1198.

2–18. LEWIS, A. J.: Geomorphic Evaluation of Radar Imagery of Southeastern Panama and Northwestern Colombia. CRES TR–133–18, Center for Research in Engineering Science, Univ. of Kansas, 1971.

2–19. HOLMES, ROBERT F.: Engineering Materials and Side-Looking Radar. Photogramm. Eng., vol. 33, no. 7, July 1967, pp. 767–770.

2–20. BARR, DAVID J.: Use of Side-Looking Airborne Radar Imagery for Engineering Soils Studies. Ph.D. Dissertation, Purdue University, 1968.

2–21. DELLWIG, L. F., AND MOORE, R. K.: The Geologic Value of Simultaneously Produced Like- and Cross-Polarized Radar Imagery. J. Geophys. Res., vol. 71, no. 4, July 1966, pp. 3597–3601.

2–22. MACDONALD, H. C.; BRENNAN, B. A.; AND DELLWIG, L. F.: Geologic Evaluation by Radar of NASA Sedimentary Test Site. IEEE Trans. Geosci. Electronics, vol. GE–5, no. 3, Dec. 1967, pp. 72–78.

2–23. VIKSNE, ANDRIS; LISTON, THOMAS C.; AND SAPP, CECIL D.: SLR Reconnaissance of Panama. Geophysics, vol. 34, no. 1, Feb. 1969, pp. 54–64.

2–24. MACDONALD, H. C.: Geologic Evaluation of Radar Imagery From Darien Province, Panama. Mod. Geol., vol. 1, no. 1, Nov. 1969, pp. 1–63.

2–25. WING, R. S.: Cholame Area—San Andreas Fault Zone, California: A study in SLAR. Mod. Geol., vol. 1, 1970, pp. 173–186.

2–26. SCHWARZ, D. E., AND MOWER, R. D.: The Potential for Deriving Landform Regions From Radar Imagery: A Puerto Rican Example. The Utility of Radar and Other Remote Sensors in Thematic Land Use Mapping From Spacecraft: Annual Report, D. S. Simonett, ed., U.S. Geol. Survey, Interagency Rep. NASA–140, May 1968, pp. 22–27.

2–27. MCCAULEY, J. R.: An Evaluation of Radar Imagery in Areas of Alpine Glaciation (abs.), Geol. Soc. Amer. Abstr., vol. 4, no. 4, 1972, p. 285.

2–28. PETERSON, R. M.: Observation on the Geomorphology and Land Use of Part of the Wasatch Range, Utah. U.S. Geol. Survey Interagency Rep. NASA–140, May 1968, pp. 75–113.

2–29. DALKE, GEORGE W., AND MCCOY, ROGER M.: Regional Slopes With Non-Stereo Radar. Photogramm. Eng., vol. 35, no. 5, May 1969, pp. 446–452.

2–30. LEWIS, A. J., AND WAITE, W. P.: Cumulative Frequency Curves of the Darien Province, Panama. AGARD Propagation Limitations in Remote Sensing, Oct. 1971, pp. 10.1–10.10.

2–31. COSGRIFF, R. L.; PEAKE, W. H.; AND TAYLOR, R. C.: Terrain Scattering Properties for Sensor System Design. Engineering Experiment Station Bull. no. 181, Ohio State Univ. Press (Columbus, Ohio), 1960.

2–32. DELLWIG, L. F.: A Geoscience Evaluation of Multifrequency Radar Imagery of Pisgah Crater Area, California. NASA CR–101829, 1968.

2–33. MOORE, R. K.: Radar Imaging Applications: Past, Present, and Future. Proceedings of the Seventh International Aerospace Instrumentation Symposium (England), Mar. 1972.

2–34. DELLWIG, L. F.; KIRK, J. N.; AND WALTERS, R. L.: The Potential of Low Resolution Radar Imagery in Regional Geologic Studies. J. Geophys. Res., vol. 71, no. 20, 1966, pp. 4995–4998.

2–35. DELLWIG, L. F., AND MCCAULEY, J. R.: Evaluation of High Resolution X-Band Radar in the Ouachita Mountains. CRES TR–177–21, Center for Research in Engineering Science, Univ. of Kansas, Aug. 1971.

2–36. WAITE, W. P., AND MACDONALD, H. C.: Snowfield Mapping With K-Band Radar. Remote Sensing Environ., vol. 1, no. 2, Mar. 1970, pp. 143–150.

2–37. MORAIN, S. A.: Field Studies on Vegetation at Horsefly Mountain, Oregon, and Its Relation to Radar Imagery. CRES Rep. 61–22, Center for Research in Engineering Science, Univ. of Kansas, Jan. 1967.

2–38. MACDONALD, J. C., AND WAITE, W. P.: Soil Moisture Detection With Imaging Radars. Water Resour. Res., vol. 7, no. 1, Feb. 1971, pp. 100–110.

2–39. DELLWIG, L. F.; MACDONALD, H. C.; AND KIRK, J. N.: The Potential of Radar in Geological Exploration. Proceedings of the Fifth Symposium on Remote Sensing of Environment, Univ. of Michigan, Apr. 1968, pp. 747–763.

2–40. KIRK, J. N., AND WALTERS, R. L.: Preliminary Report on Radar Lineaments in the Boston Mountains of Arkansas. Compass Sigma Gamma Epsilon, vol. 45, no. 2, Jan. 1968, pp. 122–127.

2–41. LEVINE, D.; COLBERT, C.; GRAHAM, L. C.; CRANE, P.; AND SCHEPS, B. B.: Combinations of Photogrammetric and Radargrammetric Techniques. Manual of Photogrammetry. Third ed. Amer. Soc. of Photogramm., Banta Publ. Co. (Mensha, Wis.), 1966, pp. 1003–1048.

2–42. CAMERON, H. L.: Radar as a Surveying Instrument in Hydrology and Geology. Proceedings of the Third Symposium on Remote Sensing of Environment, Univ. of Michigan, Oct. 1964, pp. 441–452.

2–43. MACDONALD, H. C.; KIRK, J. N.; DELLWIG, L. F.; AND LEWIS, A. J.: The Influence of Radar Look Direction on the Detection of Selected Geological Features. Proceedings of the Sixth Symposium on Remote Sensing of Environment, Univ. of Michigan, Oct. 1969, pp. 637–650.

2–44. EPPES, THOMAS A., AND ROUSE, JOHN W., JR.: Viewing-Angle Effects in Radar Images. Photogramm. Eng., vol. 40, no. 2, Feb. 1974, pp. 169–173.

2–45. POHN, H. A.: Remote Sensor Application Studies Progress Report, July 1, 1968, to June 30, 1969: Analysis of Images and Photographs by a Ronchi Grating. PB 197–101, U.S. Dept. of Commerce, 1970.

2–46. ELDER, C. H.; JERAN, P. W.; AND KECK, D. A.: Geologic Structure Analysis Using Radar Imagery of the Coal Mining Area of Buchanan County, Virginia. BM–RI–7869, Bureau of Mines Rep. of Invest. (Pittsburgh, Pa.), Jan. 1974.

2–47. Earth Resources Radar for a Remote Sensing System. Rep. GAP–4947, Rev. A, Goodyear Aerospace Corp. (Litchfield Park, Ariz.), Oct. 1970.

2–48. BLANCHARD, B. J.: Measuring Watershed Runoff Capability With ERTS Data. NASA GSFC Third ERTS–1 Symposium (Washington, D.C.), vol. 1, sec. B, Dec. 1974, pp. 1089–1098.

2–49. MCCOY, R. M.: An Evaluation of Radar Imagery as a Tool for Drainage Basin Analysis. CRES TR–61–31, Center for Research in Engineering Science, Univ. of Kansas, Aug. 1967.

2–50. HOYER, B. E.; HALLBERG, G. R.; AND TARANIK, J. V.: Summary of Multispectral Flood Mapping. Iowa Geological Survey Public Information Circular No. 7, 1974.

2–51. SATTINGER, I. J.; SELLMAN, A. N.; ISTVAN, L. B.; AND COOK, J. J.: Remote Sensing in Michigan for Land Resource Management. NASA CR–135639, July 1973.

2–52. ROUSE, J. W.: Geoscience Specifications for Orbital Imaging Radar. Tech. Rep. RSC–52, Texas A. & M. Univ. Remote Sensing Center, Mar. 1974.

2–53. CARTER, VIRGINIA; MCGINNESS, JOHN; AND ANDERSON, RICHARD R.: Mapping Northern Atlantic Coastal Marshlands, Maryland-Virginia, Using ERTS Imagery. Remote Sensing of Earth Resources, vol. II, Univ. of Tennessee Space Institute, 1973, pp. 1011–1020.

2–54. ANDERSON, RICHARD R.; CARTER, VIRGINIA; AND MCGINNESS, JOHN: Mapping Southern Atlantic Coastal Marshlands, South Carolina-Georgia, Using ERTS Imagery. Remote Sensing of Earth Resources, vol. II, Univ. of Tennessee Space Institute, 1973, pp. 1021–1028.

2–55. ROSWELL, C.: Detectability of Water Bodies by Side-Looking Radar. CRES TR–177–

16, Center for Research in Engineering Science, Univ. of Kansas, 1969.

2–56. SIMPSON, R. B.: Geographic Evaluation of Radar Imagery of New England. NASA CR–121426, 1969.

2–57. LIND, A. O.; HENSON, E. B.; AND PELTON, J.: Environmental Study of ERTS–1 Imagery: Lake Champlain and Vermont. Symposium on Significant Results Obtained From the Earth Resources Technology Satellite-1, vol. 1, sec. A, NASA SP–327, 1973, pp. 643–650.

2–58. SCHERZ, J. P.: Monitoring Water Pollution by Means of Remote Sensing Techniques. NASA CR–126640, 1971.

2–59. KIEFER, RALPH W., AND SCHERZ, JAMES P.: Aerial Photography for Water Resources Studies. ASCE Natl. Water Resources Eng. Meeting (Phoenix, Ariz.), Jan. 1971.

2–60. DRAKE, B., ET AL.: The Application of Airborne Imaging Radars (L- and X-Band) to Earth Resources Problems. ERIM Rept. 104000–1–F, Environmental Research Institute of Michigan (Ann Arbor), May 1974.

2–61. EL-ASHRY, M. R., AND WANLESS, H. R.: Shoreline Features and Their Changes. Photogramm. Eng., vol. 33, no. 2, 1967, pp. 184–189.

2–62. MACDONALD, H. C.; LEWIS, A. J.; AND WING, R. S.: Mapping and Landform Analysis of Coastal Regions With Radar. Geol. Soc. Amer. Bull., vol. 82, Feb. 1971, pp. 345–358.

2–63. MACDONALD, H. C., AND LEWIS, A. J.: Radar Detection of Estuarine Meanders in Eastern Panama and Northwestern Colombia. Mod. Geol., vol. 1, 1970, pp. 187–196.

2–64. LEWIS, A. J., AND MACDONALD, H. C.: Mapping of Mangrove and Perpendicular-Oriented Shell Reefs in Southeastern Panama With Side-Looking Radar. Photogrammetria, vol. 28, Dec. 1972, pp. 187–199.

2–65. HANSON, B. C., AND DELLWIG, L. F.: Radar Signal Return From Near-Shore Surface and Shallow Subsurface Features, Darien Province, Panama. Proc. Amer. Soc. Photogramm., Oct. 1973, pp. 1017–1031.

2–66. COOPER, C. F.: Snow Cover Measurements. Photogramm. Eng., vol. 31, no. 4, July 1965, pp. 611–619.

2–67. FRITZ, SIGMUND: Snow Surveys From Satellite Pictures. Rocket and Satellite Meteorology, John Wiley & Sons, 1963.

2–68. ROBINOVE, CHARLES J.: Space Technology in Hydrologic Applications. The Progress of Hydrology, vol. 1, Univ. of Illinois, 1967, pp. 88–107.

2–69. SABATINI, R. R.; RABCHEVSKY, G. A.; AND SISSALA, J. E.: Nimbus Earth Resources Observations. NASA CR–122348, 1971.

2–70. BARNES, JAMES C.: Evaluate the Application of ERTS–A Data for Detecting and Mapping Snow Cover. NASA CR–133884, 1973.

2–71. MEIER, M. F.: Evaluate ERTS Imagery for Mapping and Detection of Changes of Snow Cover on Land and on Glaciers. NASA CR–135878, 1973.

2–72. WEISNET, D. R., AND MCGINNIS, D. F.: Evaluation of ERTS Data for Certain Hydrologic Uses. NASA CR–136000, 1973.

2–73. HAEFNER, H.; GFELLER, R.; AND SEIDEL, K.: Mapping of Snow Cover in the Swiss Alps from ERTS–1 Imagery. Paper presented at 16th Plenary Meeting, COSPAR (Konstanz, West Germany), June 1973.

2–74. LARROWE, B. T.: Fine Resolution Radar Investigation of Great Lakes Ice Cover. Univ. of Michigan, Rep. 1900–1–F (U), Jan. 1971.

2–75. LARROWE, B. T.; INNES, R. B.; RENDLEMAN, R. A.; AND PORCELLO, L. J.: Lake Ice Surveillance Via Airborne Radar: Some Experimental Results. Proceedings of the Seventh International Symposium on Remote Sensing of Environment, vol. I, Univ. of Michigan, May 1971, pp. 511–512.

2–76. BILELLO, M. A.: Water Temperatures in a Shallow Lake During Ice Formation, Growth, and Decay. CRREL Rep. 213, U.S. Army Terrestrial Sciences Center (Hanover, N.H.), Dec. 1967.

2–77. WILSON, J. T.; ZUMBERGE, J. H.; AND MARSHALL, E. W.: A Study of Ice on an Inland Lake. Rep. 5, part I, U.S. Army Corps of Engineers, Snow Ice and Permafrost Research Establishment (Wilmette, Ill.), Apr. 1954.

2–78. BRYAN, M. L., AND MARCUS, M. G.: Physical Characteristics of Near-Shore Ice Ridges. Arctic, vol. 25, no. 3, Sept. 1972, pp. 182–192.

2–79. MARSHALL, F. W.: Air Photo Interpretation of Great Lakes Ice Features. Univ. of Michigan, Great Lakes Research Division (Ann Arbor), 1966.

2–80. MARSH, W. M.; MARSH, B. D.; AND DOZIER, J.: Formation, Structure and Geomorphic Influence of Lake Superior Icefoots. Amer. J. Sci., vol. 273, no. 1, 1973, pp. 48–64.

2–81. EVENSON, EDWARD B.: The Ice-Foot Complex; Its Morphology, Classification, Mode of Formation, and Importance as a Sediment Transporting Agent. Mich. Acad., vol. 6, no. 1, Summer 1973, pp. 43–57.

2–82. FAHNESTOCK, R. K.; CROWLEY, D. J.; WILSON, M.; AND SCHNEIDER, H.: Ice Vol-

canoes of the Lake Erie Shore Near Dunkirk, New York, U.S.A. J. Glaciol., vol. 12, no. 64, 1973, pp. 93–99.

2–83. WELCH, R. I.: The Use of Color Aerial Photography in Water Resource Management. New Horizons in Color Aerial Photography Proc., ASP–SPSE, June 1969, pp. 315–321.

2–84. NEUMAIER, GERHARD, AND SILVESTRO, FRANK: Measurement of Pollution Using Multiband and Color Photography. Seminar on New Horizons in Color Aerial Photography, Proc., ASP–SPSE, 1969, pp. 47–58.

2–85. VILLEMONTE, J. R.; HOOPES, J. A.; WU, D. S.; AND LILLESAND, T. M.: Remote Sensing in the Mixing Zone. NASA CR–137304, 1973.

2–86. LILLESAND, T. M.; SCARPACE, F. L.; AND CLAPP, J. L.: Photographic Quantification of Water Quality in Mixing Zones. Amer. Soc. Photogramm., Proc. Annual Meeting, Mar. 1974, pp. 333–357.

2–87. PIECH, K. R.: Industrial Effluent Diffusion in Rivers: A New Approach to Theory and Measurement. Paper presented at the 15th Annual Meeting of the Institute of Environmental Sciences (Anaheim, Calif.), Apr. 1969.

2–88. WELCH, R. I.: Case Studies in Water Pollution Detection by Remote Sensing—Multiple Spectral Approach. Earth Satellite Corp. (Washington, D.C.), 1970.

2–89. CHANDLER, PHILIP B.: Remote Detection of Oil Pollution Within the 8–14 Micron Infrared Region. Amer. Soc. Photogramm., papers from the 36th Annual Meeting, 1970, pp. 405–421.

2–90. GUINARD, N. W.: The Remote Sensing of Oil Slicks. Proceedings of the Seventh International Symposium on Remote Sensing of Environment, vol. II, Univ. of Michigan, 1971, pp. 1005–1026.

2–91. WHIPPLE, JANICE M.: Surveillance of Water Quality. Photogramm. Eng., vol. 39, 1973, pp. 137–145.

2–92. New Techniques for Signal Processing of Thermal Data. Daedalus Enterprises, Inc. (Ann Arbor, Mich.), 1970.

2–93. ESTES, JOHN E., AND SENGER, LESLIE W.: The Multispectral Concept as Applied to Marine Oil Spills. Remote Sensing Environ., vol. 2, no. 3, Oct. 1972, pp. 141–163.

2–94. GUINARD, N. W.: Radar Monitoring of Oil Pollution: NASA MSC Third Annual Earth Resources Program Review. Hydrology and Oceanography, vol. 3, 1970.

2–95. GUINARD, N. W., AND PURVES, C. G.: The Remote Sensing of Oil Slicks by Radar. U.S. Coast Guard Office of Research and Development (Washington, D.C.), 1970.

2–96. MOORE, R. K.: A Radar Research and Development Program for ESRO. Consultant Report Submitted to the European Space Research Organization, Aug. 1973. (Available from Univ. of Kansas, Lawrence, Kans.)

2–97. Symposium on Significant Results Obtained From the Earth Resources Technology Satellite-1. NASA SP–327, 1973.

2–98. MORAIN, S. A., AND WILLIAMS, D. L.: Extraction of Agricultural Statistics From ERTS–1 Data of Kansas. NASA CR–137047, 1974.

2–99. KANEMASU, E. T., ET AL.: ERTS–1 Data Collection System Used to Predict Wheat Disease Severities. Remote Sensing Environ., vol. 3, no. 2, 1974, pp. 93–97.

2–100. NICHOLS, J. D.; GIALDINI, M.; AND JAAKKOLA, S.: A Timber Inventory Based Upon Manual and Automated Analysis of ERTS–1 and Supporting Aircraft Data Using Multistage Probability Sampling, vol. 1, sec. A, NASA GSFC Third ERTS–1 Symposium (Washington, D.C.), 1974, pp. 145–157.

2–101. SMITH, O. G., AND GRANGER, H., eds.: Report on Significant Results and Projected Applications Obtained From ERTS–1 Principal Investigator Interviews. NASA JSC (Houston, Tex.), May 1974.

2–102. HARALICK, R. M.; CASPALL, F. C.; AND Simonett, D. S.: Using Radar Imagery for Crop Discrimination: A Statistical and Conditional Probability Study. Remote Sensing Environ., vol. 1, no. 2, 1970, pp. 131–142.

2–103. MORAIN, S. A., AND SIMONETT, D. S.: Vegetation Analysis With Radar Imagery. Proceedings of the Fourth Symposium on Remote Sensing of Environment, Univ. of Michigan, 1966, pp. 605–622.

2–104. MORAIN, S. A., AND CAMPBELL, J.: Radar Theory Applied to Generalized Soil Mapping. Soil Sci. Soc. Amer. Proc., Sept./Oct. 1974.

2–105. MORAIN, S. A.: Phenology and Remote Sensing. Phenology and Seasonality Modelling. Springer-Verlag, 1974.

2–106. DELOOR, G. P., AND JURRIEENS, A. A.: The Radar Backscatter of Vegetation. AGARD, Propagation Limitations in Remote Sensing, June 1971, pp. 12–1—12–7.

2–107. ULABY, F. T.: Radar Response to Vegetation. CRES TR–177–42, Center for Research in Engineering Sciences, Univ. of Kansas, Sept. 1973.

2–108. MORAIN, S. A., AND SIMONETT, D. S.: K-Band Radar in Vegetation Mapping. Photo-

gramm. Eng., vol. 33, no. 7, July 1967, pp. 730–740.

2–109. VIKSNE, ANDRIS; LISTON, THOMAS C.; AND SAPP, CECIL D.: SLR Reconnaissance of Panama. Photogramm. Eng., vol. 36, no. 3, Mar. 1970, pp. 253–259.

2–110. DAUS, S. J., AND LAUER, D. T.: Testing the Usefulness of Side Looking Airborne Radar Imagery for Evaluating Forest Vegetation Resources. Final Report, Forestry Remote Sensing Laboratory, Univ. of California, May 31, 1971.

2–111. LUNDIEN, J. R.: Radar Responses to Laboratory Prepared Soil Samples: Terrain Analysis by Electromagnetic Means. Tech. Rep. 3–693, Rep. 2, U.S. Army Engineers Waterways Experiment Station (Vicksburg, Miss.), 1966.

2–112. LUNDIEN, J. R.: Laboratory Measurement of Electromagnetic Propagation Constants in the 1.0–1.5 GHz Microwave Spectral Region. Terrain Analysis by Electromagnetic Means, Tech. Rep. 3–693, Rep. 3, U.S. Army Engineers Waterways Experiment Station (Vicksburg, Miss.), 1967.

2–113. SHERIDAN, M. F.: Preliminary Studies of Soil Patterns Observed in Radar Images, Bishop Area, California. NASA CR–80643, 1966.

2–114. SIMONETT, D. S.: Potential of Radar Remote Sensors as Tools in Reconnaissance, Geomorphic, Vegetation, and Soil Mapping. NASA CR–101456, 1969.

2–115. BARR, DAVID J., AND MILES, ROBERT D.: SLAR Imagery and Site Selection. Photogramm. Eng., vol. 36, no. 11, 1970, pp. 1155–1170.

2–116. KELLOGG, C. E., AND ORVEDAL, A. D.: Potentially Arable Soils of the World and Critical Measures for Their Use. Advan. Agron., vol. 29, 1969, pp. 109–170.

2–117. MOON, J. W.; LIGON, W. S.; AND HENDERSON, J. R.: Soil Classification and Soil Maps: Original Field Surveys. Soil Sci., vol. 67, Feb. 1949, pp. 169–175.

2–118. GILE, L. H., AND HAWLEY, J. W.: The Prediction of Soil Occurrence in Certain Desert Regions of the Southwestern United States. Soil Sci. Soc. of Amer. Proc., vol. 36, no. 1, 1972, pp. 119–124.

2–119. MORAIN, S. A., AND COINER, J. C.: An Evaluation of Fine Resolution Radar Imagery to Making Agricultural Determinations. CRES TR–177–7, Center for Research in Engineering Science, Univ. of Kansas, Aug. 1970.

2–120. MOORE, RICHARD K.: Ground Echo. Radar Handbook, Chap. 25, Merrill I. Skolnik, ed., McGraw-Hill Book Co., 1970.

2–121. ULABY, F. T.; CIHLAR, J.; AND MOORE, R. K.: Active Microwave Measurement of Soil Water Content. CRES TR–177–46, Center for Research in Engineering Science, Univ. of Kansas, Nov. 1973.

2–122. NEWTON, R. W.; LEE, S. L.; ROUSE, J. W., JR.; AND PARIS, J. F.: On the Feasibility of Remote Monitoring of Soil Moisture With Microwave Sensors. Proceedings of the Ninth International Symposium on Remote Sensing of Environment, vol. I, Univ. of Michigan, Apr. 1974, pp. 725–738.

2–123. YOST, E. F.: In Situ Spectroradiometric Qualification of ERTS Data. NASA CR–130864, 1972.

2–124. SEEVERS, PAUL M., AND DREW, JAMES V.: Evaluation of ERTS–1 Imaging in Mapping and Managing Soil and Range Resources in the Sand Hills and Region of Nebraska. Symposium on Significant Results Obtained From the Earth Resources Technology Satellite, vol. 1, sec. A, NASA SP–327, 1973, pp. 87–89.

2–125. HOEKSTRA, P., AND DELANEY, A.: Dielectric Properties of Soils at UHF and Microwave Frequencies. J. Geophys. Res., vol. 79, no. 11, Apr. 1969, pp. 1699–1708.

2–126. WIEBE, M. L.: Laboratory Measurements of the Complex Dielectric Constant of Soils. NASA CR–123294, 1971.

2–127. LEE, S. L.: Dual Frequency Microwave Radiometer Measurements of Soil Moisture for Bare and Vegetated Rough Surfaces. Tech. Rep. RSC–56, Texas A. & M. Univ. Remote Sensing Center, Aug. 1974.

2–128. DICKEY, F. M.; MOORE, R. K.; KING, C.; AND HOLTZMAN, J. C.: Moisture Dependency of Radar Backscatter From Irrigated and Non-Irrigated Fields at 400 MHz and 13.3 GHz. CRES Tech. Memo. 177–33, Center for Research in Engineering Science, Univ. of Kansas, Sept. 1972.

2–129. SIMONETT, D. S.; BROONER, W. G.; CONTE, D.; GOEHRING, D. R.; AND HAYNES, J. L.: Land Use Change and Environmental Quality in Urban Areas: Some Comparative Studies. Earth Satellite Corp. (Washington, D.C.), Apr. 1973.

2–130. RUBINO, R. G., AND WAGNER, W. R.: The State Role in Land Resource Management. Council on State Governments (Lexington, Ky.), 1972.

2–131. BOSSELMAN, FRED, AND CALLIES, DAVID: The Quiet Revolution in Land Use Control. Council on Environmental Quality (Washington, D.C.), Dec. 1971.

2–132. HASKELL, ELIZABETH H., ET AL.: Managing the Environment; Nine States Look for New Answers. Woodrow Wilson International Center for Scholars (Washington, D.C.), Apr. 1971.

2–133. ANDERSON, J. R.; HARDY, E. E.; AND ROACH, J. T.: A Land-Use Classification System for Use With Remote Sensor Data. U.S. Geol. Survey Circ. 671, 1972.

2–134. SIMONETT, D. S., AND RHODE, W. G.: Land Use Studies With Skylab Data—Baltimore, Maryland, and Washington, D.C. NASA CR–139542, 1974.

2–135. BEATTY, F. D., ET AL.: Geoscience Potentials of Side-Looking Radar. Raytheon Autometric Corp. (Alexandria, Va.), 1965.

2–136. HARDY, N. E.; CONER, J. C.; AND LOCKMAN, W. O.: Vegetation Mapping With Side-Looking Airborne Radar: Yellowstone National Park. NASA CR–125451, 1971.

2–137. LEWIS, A. J.; MACDONALD, H. C.; AND SIMONETT, D. S.: Detection of Linear Cultural Features With Multipolarized Radar Imagery. Proceedings of the Sixth International Symposium on Remote Sensing of Environment, vol. II, Univ. of Michigan, Oct. 1969, pp. 879–893.

2–138. MORAIN, S. A.; HOLTZMANN, J.; AND HENDERSON, F. M.: Radar Sensing in Agriculture, A Socio-Economic Viewpoint. IEEE EASCON Conv. Rec., vol. 70, 1970, pp. 280–287.

2–139. MORAIN, S. A.; WOOD, C.; AND CONTE, D.: NASA Earth Observations Survey Program 90-Day Mission Analysis Report, NASA MSC Mission 102, Site 76. CRES Tech. Memo. 169–4, Center for Research in Engineering Science, Univ. of Kansas, 1970.

2–140. NUNNALLY, N. R.: Integrated Landscape Analysis With Radar Imagery. Remote Sensing Environ., vol. 1, no. 1, 1969, pp. 1–6.

2–141. PETERSON, R. M.; COCHRANE, G. R.; MORAIN, S. A.; AND SIMONETT, D. S.: A Multi-Sensor Study of Plant Community Density and Boundaries at Horsefly Mountain, Oregon. Remote Sensing in Ecology, Univ. of Georgia Press, 1969, pp. 63–93.

2–142. PIERSON, W. J.; SCHEPS, B. B.; AND SIMONETT, D. S.: Some Applications of Radar Return Data to the Study of Terrestrial and Oceanic Phenomena. Proceedings of the Third Goddard Memorial Symposium on Scientific Exploration for Manned Orbital Flight, Amer. Astron. Soc., Mar. 1965, pp. 87–137.

2–143. SCHWARZ, D. E., AND CASPAL, F. C.: The Use of Radar in the Discrimination and Identification of Agricultural Land Use. Proceedings of the Fifth Symposium on Remote Sensing of Environment, Univ. of Michigan, 1968, pp. 233–248.

2–144. SIMONETT, D. S.: Remote Sensing With Imaging Radar; A Review. Geoforum, no. 2, 1971, pp. 61–74.

2–145. SIMONETT, D. S.; EAGLEMAN, J. E.; ERHARD, A. B.; RHOADES, D. C.; AND SCHWARZ, D. E.: The Potential of Radar as a Remote Sensor in Agriculture: A Study With K-Band Imagery in Western Kansas. CRES Rep. 61–211, Center for Research in Engineering Science, Univ. of Kansas, 1967.

2–146. SIMPSON, R. B.: APQ–97 Imagery of New England: A Geographic Evaluation. Proceedings of the Sixth International Symposium on Remote Sensing of Environment, Univ. of Michigan, 1969, pp. 909–925.

2–147. BRYAN, M. L.: Extraction of Urban Land Cover Data From Multiplexed Synthetic Aperture Radar Imagery. Proceedings of the Ninth International Symposium on Remote Sensing of Environment, vol. I, Univ. of Michigan, Apr. 1974, pp. 271–288.

2–148. LEWIS, A. J.: Evaluation of Multiple Polarized Radar Imagery for the Detection of Selected Cultural Features. U.S. Geol. Survey Interagency Rep. NASA–130 (Washington, D.C.), Dec. 1968.

2–149. MOORE, E. G.: Side-Looking Radar in Urban Research: A Case Study. U.S. Geol. Survey Interagency Rep. NASA–138 (Washington, D.C.), 1969.

2–150. NUNNALLY, N. R., AND WITMER, R. E.: Remote Sensing for Land-Use Studies. Photogramm. Eng., vol. 36, no. 5, 1971, pp. 449–454.

2–151. SABOL, JOSEPH: The Relationship Between Population and Radar-Derived Area of Urban Places. The Utility of Radar and Other Remote Sensors in Thematic Land Use Mapping from Spacecraft, Annual Report, U.S. Geol. Survey Center Interagency Rep. NASA–140, May 1968. (Also CRES TR–117–1.)

2–152. WESTERLUND, F. V.: Urban and Regional Planning Utilization of Remote Sensing Data: A Bibliography and Review of Pertinent Literature. USDI–U.S. Geol. Survey Interagency Rep. USGS–242 (Washington, D.C.), Apr. 1972.

2–153. DUBOS, RENÉ JULES: Reason Awake: Science for Man. Columbia Univ. Press (New York), 1970.

2–154. HORTON, F. D.: Remote Sensing: Techniques and Urban Data Acquisition. Introductory Reader in Remote Sensing, J. E. Estey and L. W. Senger, eds. (Santa Barbara, Calif.), 1972.

2–155. LINDGREN, D. T.: Urban Applications of Remote Sensing. Remote Sensing: Techniques for Environmental Analysis, chap. 9, J. C. Estes and L. W. Senger, eds., Hamilton Pub. Co. (Santa Barbara, Calif.), 1974.

2–156. HOWARD, W. A., AND KRACH, J. B.: An Assessment of the Usefulness of Small-Scale Photographic Imagery for Acquiring Land Use Information Necessary for the Urban Planning Function. U.S. Geol. Survey Interagency Rep. USGS–207, 1971.

2–157. GRIFFITHS, T. M.; HOWARD, W. A.; AND KRACHT, J. B.: Developing Remote Sensing Display Modes to Satisfy Urban Planning Data Input Needs. U.S. Geol. Survey Interagency Rep. USGS–207, 1971.

2–158. GOODELL, H. G., AND REED, W.: Environmental Application of Remote Sensing Methods to Coastal Zone Land Use and Marine Resource Management. The Potential of Remote Sensing as a Data Base for State Agencies—The Virginia Model. NASA CR–119721, 1971.

APPENDIX 2A

EARTHQUAKE MECHANISMS AND CRUSTAL MOTION

To be competitive, a new system for crustal motion measurements must have at least one advantage over conventional geodesy; it must be more accurate, be more economical, or be capable of reaching inaccessible areas. Therefore, it is necessary first to ascertain the state of the art of conventional geodesy. The National Geodetic Survey claims a very high degree of accuracy and economy; therefore, correspondingly high standards must be set as criteria that a system must attain to be worth building.

Horizontal control and vertical control are performed by independent techniques in conventional geodesy, and the accuracies and costs are therefore estimated separately. First-order horizontal control is presently attained by building networks of triangles, each side of which is measured by a laser ranging device. Each triangle is solved by a side-side-side formula of plain trigonometry. This technique replaces the use of theodolites and an angle-side-angle formula working from a single invar-taped baseline, and this technique is far less sensitive to errors produced by horizontal refraction. Nevertheless, the principal source of error is still the varying index of refraction of the atmosphere. The atmosphere increases the time of propagation of a light pulse over what it would be in vacuo; therefore, the range measurement is increased by approximately one part in 3375 in the red wavelength characteristic of a Model 8 Geodimeter (6328×10^{-10} m). That quantity, in turn, varies by approximately 1 part in 300 for every Kelvin of temperature change along the line of sight and by approximately 1 part in 10^5 N/m^2 change of atmospheric pressure. Because it is not possible to calibrate the atmosphere more accurately than 1 K for a line of sight along the ground, the net accuracy of laser ranging is not more accurate than approximately 1 ppm—that is, 1 cm per 10 km (ref. 2A–1). The cost of first-order horizontal work is approximately $3000 per triangulation station occupied, regardless of the spacing between stations.[1]

Vertical control is obtained by a technique called differential leveling, which consists of sighting on a graduated rod (called a stave) by spirit level, reading the elevation, and stepping through the countryside at approximately 50-m intervals. Measurements are taken in both directions along the traverse—that is, all lines are fore- and back-leveled. Estimates of accuracy vary. In 1948, the International Geodetic Association redefined high-precision leveling as having a standard deviation (in meters) of $\sigma = (2.9 \times 10^{-3}) L^{3/2}$, where L is traverse length in kilometers (ref. 2A–1). This presumably includes both random and systematic errors, which were treated separately in an older definition. However, there is some evidence that sys-

[1] Private communication, H. Schmid and J. Bossler, National Oceanographic and Atmospheric Administration, National Geodetic Survey, Rockville, Md., Dec. 1973.

tematic effects may be larger than the definition implies. The National Oceanographic and Atmospheric Administration, National Geodetic Survey, examined rates of vertical crustal movement in the eastern part of the United States by comparing the 1929 combined level net of the United States and Canada with the releveling performed at a mean date of 1965. The discrepancy between these results and the tide gage data along the Atlantic coast totaled 4 mm/yr from Maine to New Jersey, or approximately 144 mm in 36 yr over 500 km, which is one-half larger than the definition would allow between two independent first-order levelings. The Survey Division of the Los Angeles County Engineers has stated that there is a discrepancy of approximately 1 mm/km (almost four times what the definition would allow) revealed by the failure to attain closure on the line between Long Beach and San Diego.

A serious limitation in conventional leveling is that it attains high accuracy only when traversing flat country. But flat country in the American Southwest typically connotes intermontane regions filled with loosely consolidated alluvium, which may be expected to display large vertical movements, depending on the amount of underground water, and which masks the important crustal movements beneath. The greatest advantage that a new system may offer, especially in its early development when the cost may be high and the accuracy low, is the location of stations on bedrock in hilly or mountainous country. Good strategy requires that developing such capability be given high priority in the system design.

The basic mathematical technique used for the proposed system was developed by Rinner (ref. 2A–2) and depends on what he called a transfer network. In this case, grids of radar-reflecting geodetic control points are flown so no fewer than six can be viewed from the airplane system at one time. Rinner's equations are used to solve simultaneously by multilateration for the relative positions of the six grids. The equations are then used to propagate the solution along a chain, adding new stations and dropping others as they pass through the zone of visibility of the radar.

Unfortunately, Rinner restricted his examination to numerical analysis of multilateration by using a high satellite; thus, it is necessary to analyze a case using the low-flying airplane. Nevertheless, a few generalizations from his work apply to this discussion.

1. The smallest total error in the three-dimensional positions of the geodetic control points on the ground is obtained when the height of the vehicle is approximately equal to the separation between ground points. Thus, for an aircraft flying at an altitude of 10 km, the control points should be placed at 10-km intervals.

2. It is not possible to solve for positions from a single overpass of the aircraft. It is necessary to make two overflights at different altitudes so the equations of position will not be singular. The errors in calculated position decrease linearly with the separation in altitude of the two passes.

3. The errors are approximately inversely proportional to the square root of the number of points that can be ranged at one time.

4. The horizontal errors increase with the square root of the number of links in the chain, but Rinner's numbers indicate that the vertical sigmas increase linearly with the chain length. This point must be carefully checked because it implies that the rate of propagation of vertical error in a system would be unacceptably large. It will be necessary to calculate the effect of Earth tides on the ground points.

Several requirements are imposed on the aircraft flight plans and on the distribution of the ground markers by the mathematics of multilateration. These requirements are summarized in the following theorem: A simultaneous ranging system can obtain no unique solution for marker coordinates if all the markers lie on a plane curve of the second order, or if all markers and aircraft ranging positions lie on a surface of the second order. Two implications of this theorem are as follows:

1. The aircraft must vary its altitude by a large factor—for example, by a factor of 2—during data acquisition, which can be done most simply by having the aircraft overfly the markers twice, once at high altitude and once at a much lower altitude. This dual overflight sets a strong upper limit to the spacing between ground markers. Even if a U–2 is used, which can fly one of the passes at an altitude of 30 km, the second flight must be performed at 15 km, and because little weight is added to the solution by points at elevation angles below 12°, there must be a complete set of markers in a square of approximately 75 km on a side. This fact implies that the ground markers (receivers) must be spaced fairly evenly at an average density of one every 30 km, even if the aircraft is a U–2. If a commercial plane is used, then the markers must be spaced at one every 15 km, because a minimum of six markers must be simultaneously visible from the aircraft to obtain a solution for relative coordinates.

2. The aircraft must vary its groundpath and altitude between the two passages. It seems probable that the aircraft must fly preassigned routes determined by computer simulation, which will not be straight lines, but the turning radii need not be smaller than 30 km.

One of the most troublesome problems in the system design is the detection of reasonable-size targets observed by the signal returning from the background landscape, and the most important factor in detection is the frequency of the system. The signal-to-noise ratio is set by the "clutter," the reflection from the countryside surrounding the target, and it cannot be improved by increasing the transmitted power because signal and "clutter" rise proportionately. The signal-to-noise ratio can be improved in only two ways: by increasing the size and efficiency of the target and by improving the resolution of the radar so that the smallest distinguishable area of the landscape is reduced to a minimum.

If the new system attains the accuracy of 3, 4, 6, and 10 cm, then the system will exceed conventional leveling in accuracy for spacing greater than 40, 60, 100, and 200 km, respectively.

REFERENCES

2A–1. BOMFORD, GUY: Geodesy. Third ed. Oxford Press, 1971.

2A–2. RINNER, K.: Systematic Investigations of Geodetic Networks in Space. Annual Technical Report, U.S. Army, European Research Office, Technische Hockschuk (Graz, Austria), 1967.

CHAPTER 3

Active Microwave Remote Sensing of Oceans

Active Microwave Working Group

Oceans Panel:

F. O. VONBUN, *Cochairman*
J. W. SHERMAN III, *Cochairman*

John R. Apel
Donald E. Barrick
William J. Campbell
David E. Cartwright
Thomas W. Godbey
Kumar Krishen
Lee S. Miller
Jean-Marie Monget
Lionel Moskowitz
Willard J. Pierson
Claes G. H. Rooth
Omar H. Shemdin
F. Y. Sorrell
Robert Stewart
C. T. Swift
E. J. Walsh
Ben Yaplee

A rationale is developed in this chapter for the use of active microwave sensing in future aerospace applications programs for the remote sensing of the world's oceans, lakes, and polar regions. This chapter is divided into five major parts: (1) Applications, (2) Technical Background, (3) Local Phenomena, (4) Large-Scale Phenomena, and (5) Technical Approaches. Summaries pertaining to applications, local phenomena, and large-scale phenomena are given in chapter 1. A discussion of orbital errors is presented in appendix 3A.

The technical background section is a detailed account of the general physical interaction of an electromagnetic wave with the ocean surface. Large ocean waves (gravity waves) behave like an ensemble of specular reflectors so that the strength of the scatterer is proportional to the slope of the gravity waves. However, ocean waves comparable to the wavelengths of the microwave systems used show resonant (Bragg) scattering effects for angles of incidence larger than 20°. This type of scattering is controlled by the capillary waves, which in turn depend on the local short-term surface wind field and the ocean water surface tension. The latter changes when an oil film covers the water surface, resulting in a modification of the character of the capillary waves (smoother because of the greater surface tension of oil), and the presence of oil is thus detectable with active microwave systems.

The section concerning technical approaches is a discussion of specific instruments and their needed characteristics. Radar altimeters, scatterometers, and imaging radars are the major instruments needed to accomplish the many applications outlined.

For the detection and determination of sea-surface topographic features, which relate to many important phenomena, the altimeter (corrected for orbital perturbations) is the only instrument able to economically supply the needed information on a global scale. This ability was demonstrated by the recent, very successful Skylab altimeter experiment in which height variations of the sea surface were detected with a precision of 1 to 2 m on a local scale (as large as 200 km). In the future, the broadening effect on the radar-return pulse will also provide accurate information about significant wave height as well as the surface height probability density function.

The scatterometer viewing the oceans at 0° to 10° incident angles provides sea-state information through the detection of the slope statistics of the ocean waves. For higher incident angles, local wind fields can be determined. The Skylab experience demonstrated that wind velocities as high as 20 m/sec are detectable by such methods.

Imaging radars may be the most versatile instruments for ocean-surface observations. These instruments can provide information on global wave climatology, coastal wave refraction, and buildup of waves in large storm areas. In addition, radar images of sea ice, polar ice, open water areas, and Great Lakes ice conditions will provide important practical application for weather forecasting, coastal structure design, fishing, and shipping.

In conclusion, airborne and, particularly, spaceborne active microwave systems are essential for almost all previously mentioned applications.

No actual attempt was made to reduce the applications and requirements outlined herein to specific operational flight hardware and missions. Further, active tracking systems such as radar, lasers, range and range-rate systems, and satellite-to-satellite tracking systems are not discussed; these systems are very important for some of the oceanographic measurements to be made but are adequately covered in the literature. Also, documentation already exists (and is cited in the section entitled "Current User Needs") that outlines in some detail the requirements for oceanographic data using aerospace technology. These requirement reports are being coordinated by the Interagency Coordination Committee, Earth Resources Survey Program, and some coordination was accomplished at the recent National Academy of Engineering Study, July 1 to 13, 1974, at Snowmass, Colo. System performance parameters, such as measurement accuracies and intervals, spatial and time resolution, coverage, etc., are addressed in those documents and have been used with modification in this report. Therefore, a restatement of those requirements is not included in this document. However, it is recommended that some of the requirements be updated in view of the evolving knowledge and technology discussed in this document.

PART A

APPLICATIONS

CURRENT USER NEEDS

User needs for a large portion of the ocean community have been compiled and integrated in documents by the National Oceanic and Atmospheric Administration (NOAA) (ref. 3–1) and the U.S. Coast Guard (USCG) (ref. 3–2). Other information concerning the use of oceanographic observations has been documented by the National Academy of Sciences and the National Academy of Engineering. Also, a SEASAT User Working Group within the NASA Earth and Ocean

Physics Application Program (EOPAP) has defined the ocean communities' physical oceanographic data needs.

Briefly, the total need may be defined as an increasing requirement for improved marine environmental monitoring. This, in turn, may be subcategorized as monitoring of physical parameters; forecasting of weather, winds, waves, and circulation; hazards warning; ice surveillance; and the detection and monitoring of ocean and near-shore pollution events.

The environmental monitoring requirements may be broadly grouped into three regions: estuarine and coastal (including the Great Lakes), open ocean areas with major current systems, and open oceans. The polar regions could be regarded as a fourth general area, but the requirements are very similar to those of the coastal region. The U.S. territorial waters and proposed coastal economic zones are of immediate importance for monitoring man's activities in the oceans.

BENEFITS

The benefits that may ultimately be derived from an aerospace remote-sensing system are as multifaceted as the impact of the oceans on the affairs of people. These benefits generally fall into the categories of protection of life and property along the coasts and at sea; improvement of commercial fisheries and the management of marine resources, particularly in the coastal environment; safety and navigation of U.S. shipping and maritime interests; enhancement of the quality of the environment; improved ship and oceanic structures design; and improved long-range weather forecasts for the ocean and continental environment.

The general problem of defining coastal circulation in detail is an important feature that affects most coastal-related activities. This need is common to all coastal studies; for example, in fisheries, the prevailing current system moves larval forms from the spawning grounds to other regions where they either grow or perish; water quality is subject to change at any point as a function of the tidal system and prevailing currents; and, for protection of life and property, the focusing of wave energy in the coastal region is gradually altered by both the methodical action of daily currents and the dramatic effects of storms as they change the bathymetry and shape of the coastline.

Substantial benefits would be derived from active microwave sensing. It must be noted that the development of remote sensors addresses only a part of the entire system necessary to fully achieve the benefits. Thus, not only is it necessary to develop the technology, but the involvement and acceptance of the new technology by the user is also required.

Improved Environmental Forecasting

Because of the large area of ocean compared to land and the coupled complex interactions between ocean and atmosphere, much of the world's weather is created over the water and ice that comprise the surface of the Earth's oceans. The combination of surface measurements and meteorological and oceanographic satellite data would significantly help to achieve the goal of meaningful 1- to 2-week forecasts. An accurate 5-day forecast would immediately improve U.S. shipping operations. These 5-day forecasts should reduce the present international shipping cargo damage losses of approximately $500 million per year globally by estimates of 5 to 10 percent, and permit reductions in transoceanic transit time of as much as 10 percent.[1]

Hazard Warnings

It is difficult to consistently predict the landfall of a major weather disturbance (e.g., tropical cyclones and the resultant storm surge) to within 200 km and 24 hr in advance. With the increase in the number of people living along the coasts, where approximately 80 percent of the U.S. population now reside, and in the number of offshore facilities contemplated for this region, the potential for loss of life and property has been

[1] From 12 to 24 hr in the Atlantic Ocean and 12 to 60 hr in the Pacific Ocean.

increased proportionately. In the world's low-lying areas, particularly in the U.S. Gulf of Mexico region where more than 30 million people dwell, early warning of severe hurricanes is absolutely essential to initiate evacuation of the population. Observations of sea/air interactions, sea-surface temperature, wind, waves, and an increased understanding of the storm surge process will constitute a large step forward in providing the required early warnings.

Not only are forecasts needed but compilation of such data as wave spectra, focusing of wave energy, and storm-induced alongshore currents is also critically needed to improve ship and oceanic structures design. The 2000 to 3000 doubtful shoals presently located on the world's hydrographic charts are potentially confirmable by high spatial resolution instrumentation operating in both the visible and microwave portions of the electromagnetic spectrum. Such shoals, which may or may not even exist, require avoidance by as much as 50 km for the conservative ship navigator.

Fisheries Improvement

From 1959 to 1969, the deficit in the U.S. balance of payments attributed to fisheries accounted for 19 percent of the total deficit. Since the late 1950's, this deficit has been on the order of hundreds of millions of dollars and currently is about $1.5 billion per annum, with about 70 percent of its products imported. An increase in fisheries productivity and protection in U.S. coastal waters is needed to reduce the dependency on other nations. Active microwave sensors will benefit the U.S. fishing industry from two standpoints. First, improved forecasting of marine environmental conditions will enhance decisions concerning those regions of the oceans where efficient operations can occur without loss of nets, vessels, or life. Second, the anticipated increase in the "economic coastal region" to 370 km will require monitoring of all vessel operations in a region nearly 20 times larger than historically required. Radar imaging systems could provide initial detection of localized activity that could be monitored by aircraft or geostationary satellite systems.

One specific fisheries application is the use of spaceborne sensors to make surface salinity and temperature isomaps. These maps can be used as an index of possible density distribution of those game and commercial fish species having definite salinity and/or temperature habitat preferences, with obvious potential for increased yield. Such maps would be of particular use in pinpointing local low-temperature anomalies indicative of coastal upwelling and its attendant high biological productivity.

Ice Surveillance

The Arctic region has a significant impact on global meteorological and climatological conditions. It has been estimated that, at any time in the Arctic region, approximately 10 percent of the ocean surface is open water. The heat flow through the water/air interface is two to three orders of magnitude greater than the heat flow through the water/ice/air interface. The dynamics and forecasting of ice strain in terms of ice type, leads, and polynyas are thus important not only to shipping but also to long-term weather forecasts, which are significantly affected by major points of energy input. The Polar Experiment, as a part of the Global Atmosphere Research Program (GARP), should be a major program during the next decade. This experiment will be supported by microwave sensors. The first benefits will be scientific and are threefold: the synoptic view of ice conditions; the availability of surface truth for instrument calibration and validation; and an area for international cooperation.

In addition to the aforementioned effects of ice and water on weather predictions, marine transportation in various parts of the continental United States and Alaska is subject to hazardous ice conditions. Increasing emphasis is being placed on the Great Lakes, the central river system, and New England. Nearly all iron ore transported in the Great

Lakes region is carried by ship. Significant amounts of wheat, oil products, coal, and finished goods also move across these regions by ship.

Ordinarily, domestic icebreaking is provided for vessels that are not designed to move through ice-covered waters. Therefore, an ability to determine ice coverage, clear water passages, pressure ridges, and ice thickness is material to the successful extension of the navigation season. An interim USCG report on the extension of the St. Lawrence River and Great Lakes navigation season beyond the December 15 closing date estimated the economic gains listed in table 3–I.

These gross estimates are based on a number of factors, some of which are improved ice surveillance, data analysis and prediction, all-season aids to navigation, and increased icebreaking activity. No attempt has been made to assess the economic benefit of each of these contributing programs. Therefore, estimating that portion of the potential benefit to be derived by improved ice surveillance and forecasting is not possible at this time.

Arctic and Antarctic icebreaking have historically been conducted in support of scientific investigations and, to a limited degree, military operations. Discovery of oil deposits on Alaska's North Slope and the political and economic ramifications of a dependency on Middle East oil supplies have spurred further activity in the far north. Scientific and geological surveys, commercial oil drilling, ocean transport, and support of icebreaking requirements in the high latitudes will place increasing emphasis on all-weather monitoring and prediction of ice extent, ice-free passages and polynyas, ice thickness and pressure ridges, and on the discrimination of new ice from multiyear ice. The benefits of more complete data gathering and ice forecasting should be more efficient icebreaking operations, reduced damage to vessels and structures, increased safety of personnel, and more economic or other advantageous vessel transport of petroleum and other resources.

TABLE 3–I.—*Economic Gains Resulting From Extension of Navigation Season of the St. Lawrence River and Great Lakes*

Navigation season extended to—	Economic gains, millions of dollars	
	By 1975	By 1985
Jan. 31	40	85
Feb. 28	58	123
Year round	68	145

Ocean Pollution

Oil pollution constitutes a major threat to U.S. water resources, marine life, waterfront property values, and the recreational industry. Oil pollution incidents are generally agreed to be a direct result of the number of transfer operations between vessels and shore facilities, the volume of oil transferred, the number and length of vessel passages within U.S. waters, and the number of offshore oil wells.

The size of the area to be monitored is significant; it includes thousands of kilometers of rivers, lakes, harbors, and coastlines. Remote-sensing techniques that enhance the ability to observe oil discharge will materially assist in the enforcement of applicable laws and tend to ameliorate the environmental damages by more rapid response and cleanup.

The USCG has observed marked decreases of as much as 25 percent in the number of oilspills when continued surveillance of critical areas was used. Although much of this decrease could be attributed to increased attention to handling and transfer methods, the fact that better and more complete surveillance is being conducted would tend to dissuade the intentional polluter.

Cost estimates of USCG daily observation of certain harbors and waterways with existing vessels and aircraft are $2 to $4 million annually. Extension to a dedicated surveillance of major U.S. continental lakes and coastlines for pollution may exceed $18 million. High-resolution radar, imaging micro-

wave radiometers, and multispectral low-light-level television are presently being installed on aircraft for low-altitude flight. Sensor systems that could detect a surface oil sheen of 1000 m^2 or greater from high-altitude aircraft with corresponding increased swath width could decrease yearly costs from $11 to $18 million.

Monitoring of Endangered Marine Life

The Marine Mammal Act of 1972 (Public Law 92–522) focused on the need to assess the stock of specific species of marine life to insure their continued existence and on the ultimate goal or restoring and maintaining a viable commerce with certain of these species. The prime current need is to conduct a census of many of these mammals, including, for example, sea otters, and gray and bowhead whales, walrus, and seals. Three specific forms of space technology appear appropriate for development.

1. Tracking of animals by surface, aircraft, or spacecraft techniques, potentially using radar transponders, to determine the habits of the creature; in particular, the time in and out of the water.

2. Overflights by aircraft to determine the herd sizes and numbers of animals in the herds.

3. Where appropriate, satellite tracking of icefields to assess and forecast the location of ice where these animals are most likely to be found, thus reducing aircraft search time.

Benefits are difficult to establish beyond the preservation and conservation of these marine animals.

PART B

TECHNICAL BACKGROUND

SUMMARY

This section describes the physics of electromagnetic scattering from the sea and is presented as a guideline to relate an observable (such as the radar cross section) to the hydrodynamics or physical properties of the sea.

At microwave frequencies, the ocean produces two types of scattering processes. The larger ocean waves essentially behave as an ensemble of specular reflectors such that the strength of the scatter is proportional to the tilts (or slopes) of the gravity waves. Because the length of the ocean wave is much greater than the height, quasi-specular scattering occurs only at angles close to the nadir direction (usually within 25°). Therefore, near nadir, the active microwave system is closely linked with the physics that controls the gravity wave slope. For angles beyond 20°, resonant (Bragg) scattering occurs from those waves that are comparable to the wavelength of the incident electromagnetic wave. At microwave frequencies, this type of scattering is controlled by the capillary wave structure. Because the capillaries have a short time constant for growth and decay, the scattering strength is linked to the local wind fields and the surface tension of the ocean surface.

As specific examples of the interdisciplinary science of electromagnetics and geophysical oceanography, the physics is discussed in connection with data provided by three instruments; namely, the scatterometer, the altimeter, and the imaging radar. These instruments are selected because of the availability of generally consistent data resulting from numerous experiments conducted from stationary platforms, aircraft, and satellites. The data provided by each instrument are discussed in context with

specular point and Bragg scattering theories.

Although the scope of the Active Microwave Working Group is active systems, the physics of the microwave radiometer is discussed as a complementary instrument. Finally, the degrading effect of extraneous sources of noise is discussed as a limiting mechanism of the accuracy of the ocean surface measurement.

PHYSICAL MECHANISMS OF THE RADAR ECHO

Radar echo from the sea was first observed during World War II on shore- and ship-based surveillance systems. Because this echo represented an unwanted signal that often masked the desired target signals, it was referred to as "clutter." Early systems used straightforward techniques to suppress the echoes from these nearly stationary sea scatterers to enhance the returns from faster moving targets. However, little attention was devoted to the actual nature of the sea echo and the scatter mechanisms until the late 1950's.

The first definitive studies on this subject were experimental. Crombie (ref. 3–3) deduced from measured sea echo Doppler spectra that the dominant scatter mechanism at high frequency (hf) (approximately 30 m wavelength) is resonant (or Bragg) scatter, which originates from ocean wavetrains for which the spatial period is one-half the radar wavelength (for backscatter near grazing), and which is traveling toward and away from the radar. Measurements of microwave sea return (approximately 3-cm wavelength), although not immediately identifying the applicable scatter mechanism, showed definite regions and trends in the echo that were functions of frequency, sea state (windspeed), polarization, and incident angle. Reviews of these early investigations can be found in references 3–4 to 3–6.

Theoretical efforts (refs. 3–7 and 3–8) on the subject of rough surface scattering have also contributed significantly to the interpretation of the physical mechanisms responsible for sea scatter. In particular, the two-scale scattering model (refs. 3–7 and 3–9) has offered satisfactory explanations for most of the observed characteristics of the sea return.

For returns near normal incidence (incident angles less than approximately 20°), theoretical results indicate that the large gravity waves (which are at least several radar wavelengths across) are the dominant contributors to sea return. These gravity waves act as quasi-specular reflectors to which physical optics theory is applicable. The problem may be approached either by computing the surface autocorrelation function (ref. 3–10) needed in the physical optics formulation for a randomly rough surface using the sea spectrum obtained by oceanographers, or by modeling the sea surface by a collection of plane facets (ref. 3–11) and using the measured sea slope distribution for the facets. Such theories have given correct predictions for both the angular and the wind dependence in this region. They also indicate that wind dependence is related directly to the changes in the slope of the density function of the sea surface (ref. 3–12).

For returns away from the normal (incident angles larger than 20°), the dominant contributor to sea return in the microwave region is the capillary wave to which the standard small perturbation theory is applicable (ref. 3–13). The first-order perturbation result shows that the Bragg resonance alone cannot explain the difference in wind dependence between the horizontally and vertically polarized returns (ref. 3–14). The two-scale scattering theory indicates that the interaction between the gravity and the capillary waves must be considered. Such an interaction leads to a stronger wind dependence for the horizontally polarized return, which is exactly what has been observed experimentally (ref. 3–14). The two-scale scattering theory also shows that wind dependence in this angular region is due primarily to the growth of the sea spectrum with the wind, a fact reported by many oceanographers (ref. 3–15).

Before attempting to design a radar experiment for remotely sensing sea state from space, a thorough understanding of the mechanisms responsible for the scattering process should be achieved. Having the mechanisms and the quantitative models that they produce, one can then sensibly analyze a proposed experiment concerning its feasibility, sensitivity, and cost.

The physical mechanisms presently known and accepted as responsible for scatter from the sea are summarized in table 3–II. Bragg scatter is illustrated in the experimental record at 10 MHz shown in figure 3–1. The two dominant "spikes" in the Doppler spectrum occur at shifts of $\pm[g/(\pi\lambda)]^{1/2}$, where g is the acceleration of gravity and λ is the radar wavelength. This is confirmed by derivations from the first-order theory, which is summarized as

$$\sigma_{VV}(\eta) = 2^5\pi k_0^4 \left[\sin\theta_i \sin\theta_s + \cos(\phi_i - \phi_s)\right]^2 \left[S_{\pm}(\kappa_{rx}, \kappa_{ry})\,\delta(\eta \pm \omega_g)\right] \quad (3\text{–}1)$$

where

$\sigma_{VV}(\eta)$ = normalized Doppler spectrum backscattering cross section for vertical-transmit, vertical-receive polarization states

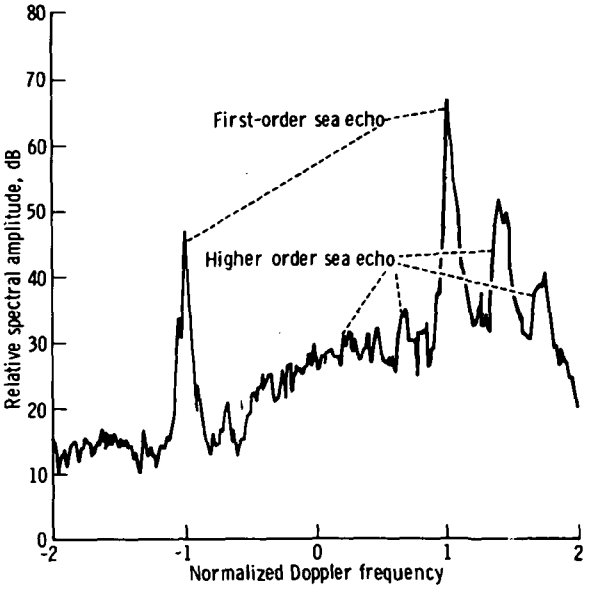

FIGURE 3–1.—Illustration of Bragg scatter at 10 MHz.

η = radian Doppler shift from carrier $= \omega - \omega_0$

ω = temporal wave number of ocean wave

ω_0 = radian wave number of radio carrier frequency

κ_r = sum of incident and scattered radar wave numbers $= \mathbf{k}_i + \mathbf{k}_s$

$\mathbf{k}_i = k_0(\sin\theta_i \cos\phi_i\,\mathbf{x} + \sin\theta_i \sin\phi_i\,\mathbf{y} - \cos\theta_i\,\mathbf{z})$

$\mathbf{k}_s = k_0(\sin\theta_s \cos\phi_s\,\mathbf{x} + \sin\theta_s \sin\phi_s\,\mathbf{y} + \cos\theta_s\,\mathbf{z})$

k_0 = radar wave number $= 2\pi/\lambda$

ω_g = Doppler shift of advancing and receding resonant gravity waves $= g^{1/2}(\kappa_{rx}^2 + \kappa_{ry}^2)^{1/4}$

$S_{\pm}(\kappa_{rx}, \kappa_{ry})$ = directional wave-height spectrum of ocean waves, where the $\pm$ subscript refers to spectra representing waves advancing and receding along κ_r (x, y)

(θ, ϕ) = polar angles associated with transmitted and received wave directions

s,i = subscripts indicating scattered and incident, respectively

$\mathbf{x},\mathbf{y},\mathbf{z}$ = unit vectors along the x-, y-, and z-axis, respectively

λ = radar wavelength

δ = Dirac impulse function

In equation (3–1), the Doppler spectrum is shown to consist of two impulse functions (or spikes) in the frequency domain centered at shifts $\pm[(2k_0g)/(2\pi)]^{1/2} = [g/(\pi\lambda)]^{1/2}$ for backscatter near grazing ($\phi_s = \phi_i$, $\theta_s = \theta_i =$

TABLE 3–II.—*Physical Mechanisms of Radar Scatter From the Sea*

Scatter	Physical mechanisms
mf/hf (1000 m > λ > 10 m)[a]	Bragg (diffraction grating) effect.
Microwave (1 m > λ > 1 mm)	Quasi-specular reflections (diffraction) (within 15° of specular direction).
	Bragg (diffraction grating) effect and interaction between large- and small-scale waves (beyond 15° of specular direction).

[a] Medium frequency/high frequency; λ = wavelength.

$\pi/2$). Furthermore, the magnitude of the echo as contained in these spikes is proportional to the wave-height directional spectrum evaluated at twice the radar wave number ($2k_0$). Bragg scatter in other directions follows analogously. The ocean wave train that scatters in a given direction (θ_s, ϕ_s) has a spatial period $L=2\pi/|\kappa_r|$ and orientation given by $\phi_r=\tan^{-1}(\kappa_{ry}/\kappa_{rx})$ with respect to the x-axis.

At microwave frequencies, the average radar backscattering cross section as a function of angle of incidence typically has the shape shown in figure 3–2. The scattered echo signal in the region with 15° to 25° from the vertical is referred to as the quasi-specular component and can be explained by reflections from plane facets. In the high-frequency limit, the average backscatter cross section per unit surface area for this component is given as

$$\sigma^\circ = \pi \sec^4\theta\, P(\zeta_{xsp}, \zeta_{ysp})\, |R(0)|^2 \quad (3\text{–}2)$$

where

σ° = average backscatter cross section per unit area for polarized component

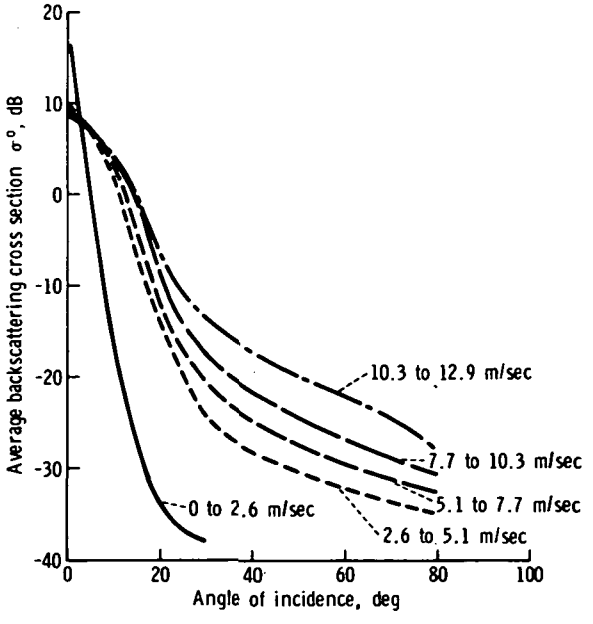

FIGURE 3–2.—Typical average backscattering cross section as a function of incident angle (1.25 cm).

$P(\zeta_x, \zeta_y)$ = probability density function of surface slopes ζ in x and y directions

$\zeta^2_{xsp}+\zeta_{ysp}$ = required specular (mirror) reflection condition at surface facet $=\tan^2\theta$

$R(0)$ = Fresnel reflection coefficient of sea at normal incidence

θ = angle of incidence (angle between local normal at the surface of scattering and the incident wave direction)

For the sea, the probability density function for the surface slopes is nearly Gaussian. The nature of the continuous sea surface (except under extreme conditions of breaking waves) is such that the slope rarely exceeds 15° to 25°; hence, specular point return would become very weak for incident angles beyond approximately 25°. Because the slope itself is a function of sea state and windspeed, this limit will vary somewhat: between approximately 8° and 15° for the sea states between about sea state 1 (2.5-m/sec wind) and sea state 6 (16-m/sec wind).

One further effect is worth noting in this quasi-specular region: both theory and experiment show that the return is not polarization sensitive. As long as the "polarized" component of backscatter is being received (e.g., vertical received for vertical incident, horizontal received for horizontal incident, left-circular received for right-circular incident, etc.), the magnitude as a function of incident angle is the same; no depolarization is predicted in the near-vertical angular region. This is not true as one moves away from the quasi-specular region, where the vertically polarized backscatter return is usually much larger than the horizontally polarized return in the Bragg scatter region.

Beyond incident angles of approximately 15° to 25°, microwave sea backscatter can be explained to a large extent by the Bragg diffraction grating mechanism. Although the theory appears strictly justifiable only when the overall height of the surface is small in terms of the radar wavelength (which is never true for the sea in the microwave re-

gion), an argument can be made that the sea is really a two-scale composite surface, in which a small-scale slightly rough component is riding on top of much larger waves. According to this composite theory (refs. 3–7, 3–9, 3–16, and 3–17), it is mainly the small-scale component that the radar is observing at these large angles. Although the mathematical justification of the theory can be questioned, extensive experimental work by Guinard and Daley (ref. 3–18), Moore et al. (ref. 3–14), Bradley (ref. 3–19), and Wright (ref. 3–7) indicates that this explanation and theory are reasonably accurate. The magnitude of the radar return as a function of incident angle, the polarization dependence, the frequency dependence, and the Doppler characteristics are all predictable from this two-scale surface model.

Experiments to determine the radar response of the sea have been carried out by numerous investigators. The empirical observation that radar cross section increased with increasing sea state was evident from the start. Some of the conclusions reached by the many investigators have been confusing, however, because of the variety of incident angles used and because of difficulties in obtaining adequate measurements of the sea and wind to compare with the radar observations.

The recent programs (since about 1966) conducted by the Naval Research Laboratory (NRL) and NASA Lyndon B. Johnson Space Center (JSC) have led to a fuller understanding of both the wind response of the capillary waves and the corresponding increase in microwave backscatter.

Claassen et al. (ref. 3–20) reported information on the increase in capillary wave spectral components with windspeed as shown in figure 3–3 (ref. 3–21), where $D(U_*)^{1/2}$ is a wind-dependent coefficient of the capillary part of the wave spectrum. Because the previously described theories indicate that the radar signal should increase as the capillary wave components of the sea increase, the result reported by these authors is most encouraging.

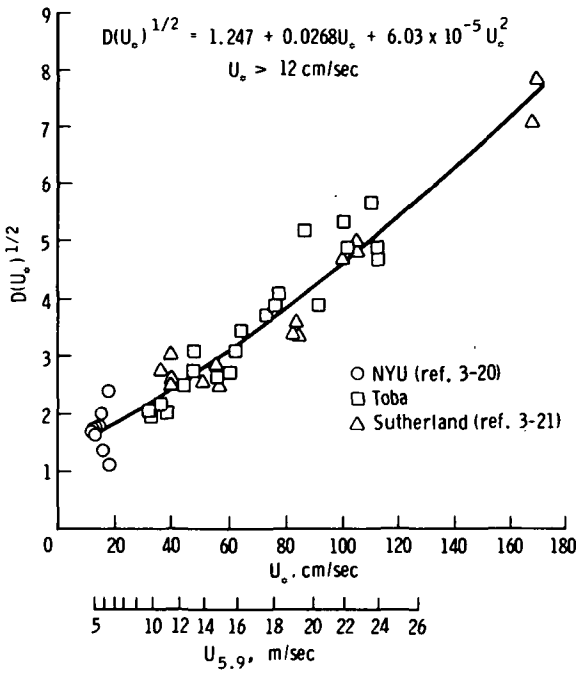

FIGURE 3–3.—The wind dependence of $D(U_*)^{1/2}$ for capillary waves, where U_* is the friction velocity at the ocean surface, and $U_{5.9}$ is the wind velocity at an elevation of 5.9 m above the ocean surface (refs. 3–20 and 3–21).

The JSC and NRL measurements are summarized in reference 3–14. In both cases, measurements made in different years were separated from each other by biases, but individually they exhibited approximately the same wind response. Figures 3–4 and 3–5 show examples of the two data sets plotted on logarithmic scales (the linear decibel scale is a logarithmic amplitude scale). The slope of the trend lines on these curves is the exponent of the wind response for the angle, frequency, polarization, and direction. These responses were found to vary between linear and square law; that is, the exponents were between 1 and 2. Figure 3–6 shows the upwind vertical polarization case.

The variation of response with angle between wind direction and look direction for the radar was somewhat uncertain until the Advanced Application Flight Experiments (AAFE) radiometer/scatterometer (RADSCAT) instrument was flown. This instru-

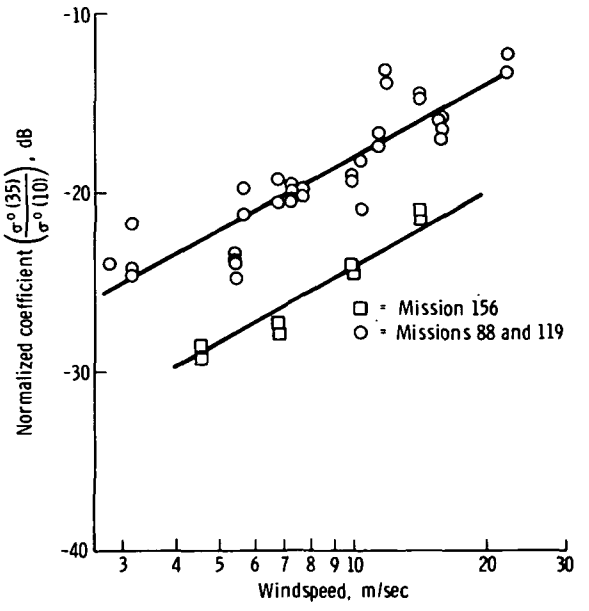

FIGURE 3–4.—Wind response of JSC scatterometric data for crosswind observations (vertical transmit/vertical receive polarization).

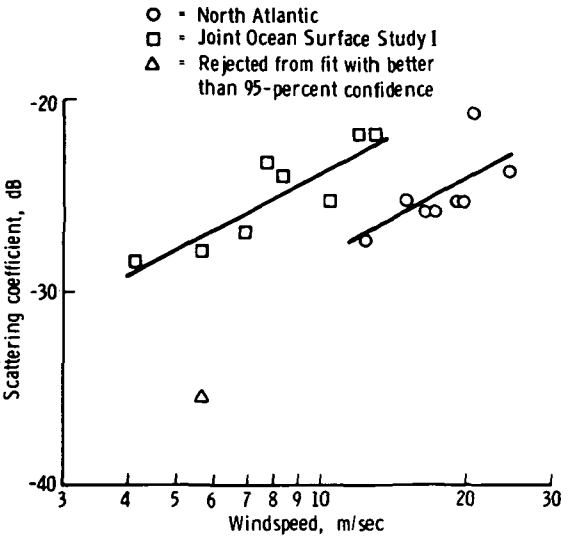

FIGURE 3–5.—Wind response of NRL X-band data for upwind observations at an incident angle of 60° (vertical transmit/vertical receive polarization).

ment gave a much clearer identification of the angular variation that must be considered in using backscatter data for wind determination than had previously been available.

Skylab S193 results, although presently incomplete, tend to confirm the previous experiments and to reduce the variance associated with the aircraft experiments. Figure 3–7 shows some of the early results for horizontal polarization (after aspect angle correction).

THE PHYSICS OF THERMAL EMISSION IN THE MICROWAVE BAND

Thermodynamics of Radiometric Emission

The basic physics of thermal emission, regardless of the electromagnetic wavelength, is based on the Planck radiation law. In the microwave region, the Rayleigh-Jeans limit is applicable, and the received power is given by

$$\frac{P_r}{k\Delta f} = T_A = \frac{\int f(\Omega)\, T_B(\Omega)\, d\Omega}{\int f(\Omega)\, d\Omega} \qquad (3\text{–}3)$$

where

P_r = received power
k = Boltzmann constant
Δf = receiver bandwidth
T_A = antenna temperature
$f(\Omega)$ = normalized pattern function of the receiving antenna
$T_B(\Omega)$ = brightness temperature
Ω = solid angle

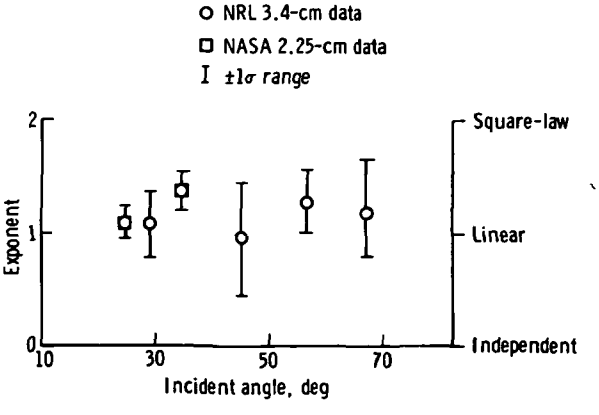

FIGURE 3–6.—Wind response of scatterometer (upwind, vertical transmit/vertical receive polarization).

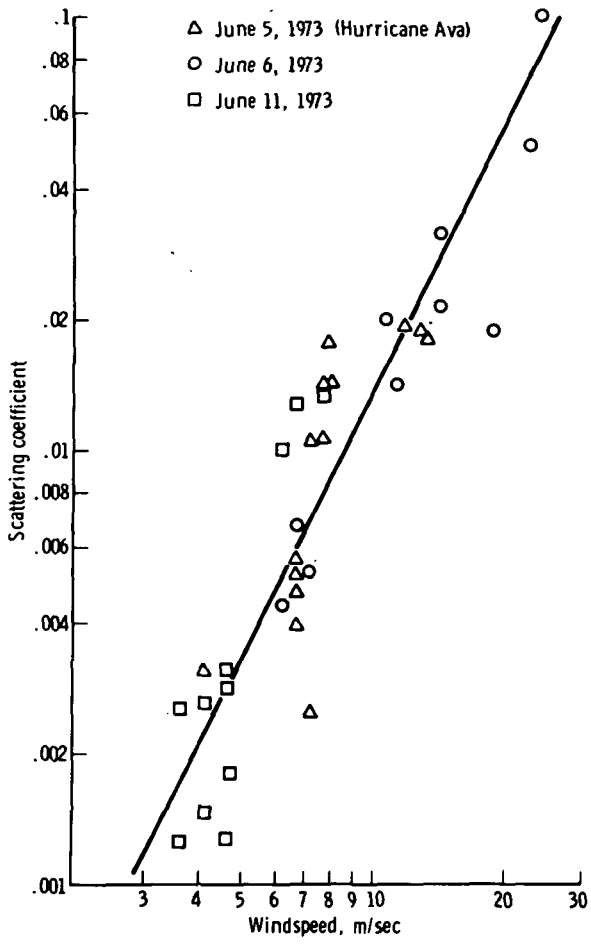

FIGURE 3–7.—The S193 scatterometer response to wind at sea, 30 days into the first Skylab mission (horizontal polarization; 50° angle with vertical).

If atmospheric contributions are ignored, the quantity $T_B(\Omega)$ is the product of the surface emissivity and the molecular temperature of the source.

Emission From a Specular Surface

If the surface is flat, the emissivity E is

$$E = 1 - |R|^2 \qquad (3\text{–}4)$$

where $|R|^2$ is the reflection coefficient, defined by the usual Fresnel expressions. In general, $|R|^2$ is a function of polarization, viewing angle, operating frequency, and dielectric constant. The emissivity of seawater (at the vertical viewing angle) increases from approximate values of 0.3 at 1 GHz to 0.5 at 35 GHz, so that the brightness temperature ranges between 100 and 150 K within the microwave region. As the wavelength decreases to the millimeter range, the emissivity gradually increases to unity.

In addition to radiation being emitted by the surface, sky noise is reflected from the surface into the instrument. This noise is generated by molecular species (principally oxygen and water vapor) and condensed water (clouds and rain) and requires a correction to the radiative transfer order to properly interpret the surface characteristics. The correction is made by using the standard radioactive transfer equations. The atmospheric radiation depends strongly on electromagnetic frequency, relative humidity, and rainfall rate. As a numerical example, the sky temperature increases from approximately 5 K at 1 GHz to approximately 100 K at 22 GHz.

If the surface is indeed flat, or specular, the radiometric emission is a function of only two parameters; namely, the salinity and the temperature of the water. If the water is covered by a layer such as ice, oil, or foam, the reflection coefficient will vary according to the thickness of the layer. If the losses of the layer are not too appreciable, the reflection coefficient will alternately exhibit maximums and minimums at quarter wavelength (layer thickness) intervals. An example of this behavior is shown in figure 3–8, which typifies the way the reflection coefficient

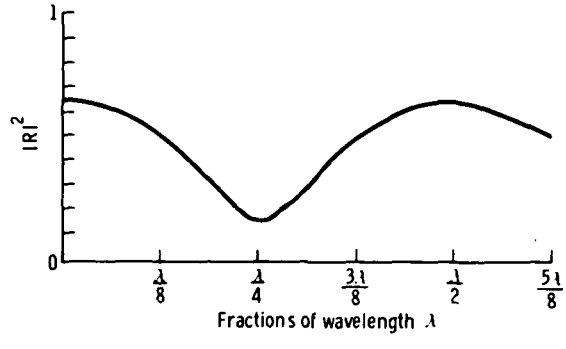

FIGURE 3–8.—Variation in reflection coefficient as a function of thickness in fractions of wavelengths within an ice layer (normal incident angle).

varies as a perfectly smooth ice layer thickens over freshwater. This curve clearly indicates that (1) it is possible to measure the *thickness of smooth layers over the surface* of the water and (2) as the dielectric constant of the layered medium approaches a matched condition, with $|R|^2 \rightarrow 0$ at odd quarter-wavelength intervals, the change in thickness can radically alter the radar cross section.

Relationship Between Microwave Emission, Sea State, and Winds

The determination of sea-state and surface wind fields over the oceans by remote passive microwave sensing has generated much interest during the last decade. Measurements of this type on a temporal, global, and all-weather basis would be of great value to the meteorologist and oceanographer and would be of general maritime use.

The microwave brightness temperature dependence on sea state (windspeed W) arises from two effects. The first effect is a result of the increasing roughness of the compact water surface, and the second effect is a result of the increasing coverage of whitecaps and sea foam with increasing windspeed. Although both are properly termed roughness *effects, the first will be referred to as the* surface roughness and the second as the sea-foam effect. Surface roughness has been investigated theoretically using a geometric optics model (ref. 3–22) based on the sea-surface slope distribution of Cox and Munk (ref. 3–23) and using a physical optics model (refs. 3–16 and 3–24) that depends on the correlation function heights.

Multiple-scatter and shadowing effects, which become important at large angles of incidence, have been investigated using a one-dimensional geometric optics model (ref. 3–25). These investigators have shown that the emission from a rough surface is intimately related to the radar scattering coefficient and is explicitly given by

$$E = 1 - \frac{1}{4\pi \cos\theta} \iint \sigma^\circ(\Omega)\, d\Omega \qquad (3\text{–}5)$$

where θ is the incident angle. The quantity σ° also replaces the reflection coefficient to account for the scattered sky component. If σ° is computed from the geometric optics expression, results typical of those shown in figure 3–9 are obtained. These curves show

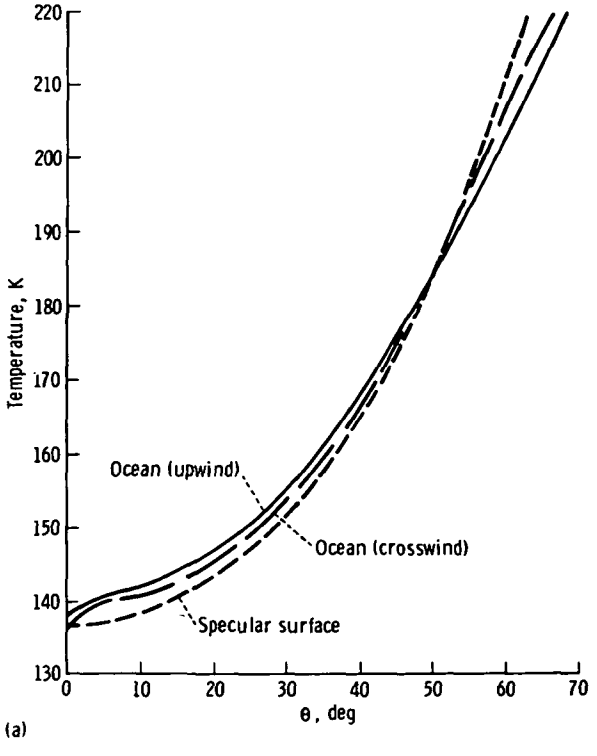

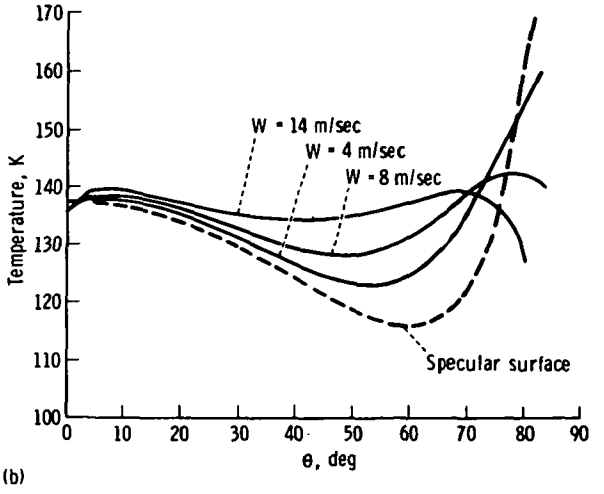

FIGURE 3–9.—Brightness temperature as a function of incident angle with wind-roughened ocean surface as a parameter (frequency of 19.4 GHz, water temperature of 290 K). (*a*) Vertical polarization (windspeed of 14 m/sec). (*b*) Horizontal polarization.

that, for the vertical polarization, there is a crossover point; that is, roughness causes an increase in brightness temperature for angles near nadir and a decrease in brightness temperature as the incident angle approaches grazing. Hence, the radiometric temperature is invariant with roughness at the crossover point. For the horizontal polarization, roughness generally causes an increase in brightness temperature over all incident angles. The rather complicated behavior of the family of curves beyond an incident angle of 60° is due to scattered atmospheric radiation, which can be a predominant factor near grazing.

The very high microwave brightness temperature of sea foam compared to that of the average sea surface, which results in the sea-foam effect, was first suggested by Williams (ref. 3–26) and has been supported theoretically on the basis of a physical model for foam (ref. 3–27). Measurements of the microwave brightness temperature of sea surface indicate a dependence on surface roughness and sea foam that is correlated with windspeed (refs. 3–28 to 3–31).

Surface roughness effects will dominate at the lower windspeeds. However, because of the increasing prevalence of sea foam with increasing sea state and the high microwave brightness temperature of foam, the microwave emission characteristics of the sea will be determined by sea foam at very high speeds. The transition windspeed between the two effects is not known but is probably between 15 and 20 m/sec. An estimate of the combined effect of surface roughness and sea foam with windspeed, as viewed from a satellite, is shown in figure 3–10 (ref. 3–32). The effect of surface roughness is seen to predominate at windspeeds to approximately 20 m/sec, with foam being the major factor at higher windspeeds. The combined effects result in a strong windspeed dependence that allows remote sensing of surface wind fields over the entire range of windspeeds from calm to 30 m/sec and higher.

To cover the entire range of windspeeds, observations will be necessary at larger incident angles because the roughness effect is less at the smaller angles. Because the surface roughness effect decreases with decreasing frequency and the foam effect is also likely to decrease, the sensitivity to surface windspeed is greater at higher frequencies. The relative effects of surface roughness and foam may best be studied by simultaneous measurements of both vertical and horizontal polarization at 55° incident angle. The vertical component is sensitive only to foam, whereas the horizontal component is affected by both foam and roughness.

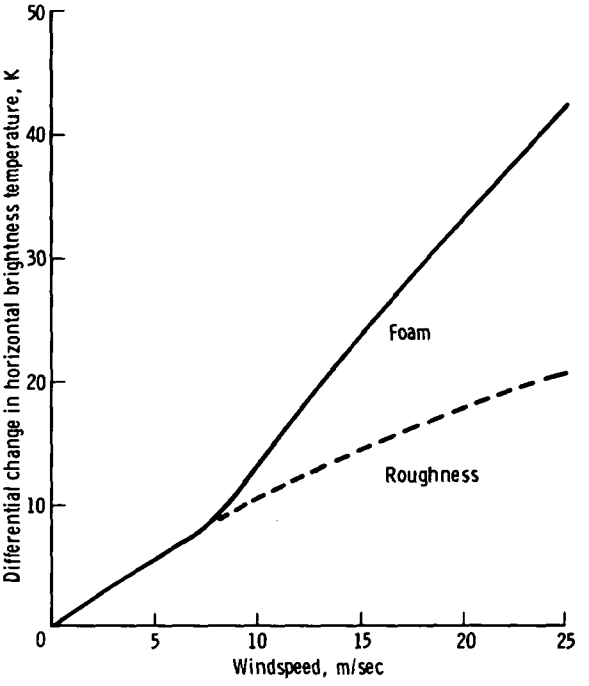

FIGURE 3–10.—Total windspeed dependence at 55° incident angle. The estimated total differential change in horizontal brightness temperature at 19.34 GHz and 55° incident angle is shown as a function of windspeed by the upper solid line. The relative contributions due to surface roughness and sea foam are indicated.

In summary, the microwave brightness temperature of the ocean is significantly dependent on the surface wind fields. This dependence offers the potential to remotely sense surface winds over the entire range of windspeeds from calm to 30 m/sec and higher from a satellite on an all-weather and global

basis. The dependence results primarily from surface roughness effects for windspeeds as high as approximately 15 to 20 m/sec and is largely due to the effects of ocean foam for higher windspeeds. Sensitivity to windspeed increases with frequency and is most pronounced for horizontal polarization at larger incident angles.

ATMOSPHERIC ATTENUATION AND SKY NOISE

When radar measurements of a desired observable are conducted through a long path length of intervening medium, several undesirable results may occur. First, the medium can remove electromagnetic energy from the beam by attenuation and scattering, which will reduce the amount of power received by the radar and therefore restrict the dynamic range of the instrument, or even eradicate the measurement entirely. Another undesirable aspect is that the index of refraction of the medium will affect the group velocity of the electromagnetic wave, thereby resulting in unwanted dispersion and time delay for altimetry. Finally, the noise temperature of the intervening medium increases with absorption, resulting in a reduction of the signal-to-noise ratio.

The pertinent medium is, of course, the atmosphere. The atmosphere removes power from the beam either through resonant absorption by molecular species or by condensed water vapor. Pulse dispersion occurs because the index of refraction is frequency dependent. Absorption and dispersion are most severe when the radar system is tuned to operate near the resonant lines of the atmosphere at 22 GHz (water vapor) and 60 GHz (oxygen).

Details of the undesirable effects can be inferred from the papers concerning the sensing of atmospheric properties. As a general statement, any physical phenomenon that enhances the atmospheric measurement results in a degradation of the oceanographic measurement. This is particularly true if the experiments are conducted from space.

The strongest source of sky noise is the Sun. The radiometric temperature of the quiet Sun ranges from 10^4 K at X-band to 10^5 K at L-band. The "slowly varying component," which is due to sunspot activity, raises these numbers by one to two orders of magnitude, and bursts will raise the temperatures to 10^9 to 10^{10} K. If a radar or radiometer is pointing at an area of the ocean where a strong specular component of the Sun is being reflected from the water, noise may saturate the receiver.

PHYSICAL PROPERTIES OF WATER

The physical properties of water that affect the electromagnetic interaction are the salinity and temperature of the water. These two quantities are important because the complex dielectric constant, and hence the reflectivity, is a function of both salinity and temperature.

Experiments currently indicate that the complex dielectric constant can be cast in the Debye form

$$\epsilon = \epsilon' + i\epsilon'' = \epsilon_\infty + \frac{\epsilon_s - \epsilon_\infty}{1 - i\omega\tau} + i\frac{\rho}{\omega\epsilon_0} \qquad (3\text{–}6)$$

where

ϵ' = dielectric constant
ϵ'' = loss factor
ϵ_∞ = the relative dielectric constant as $\omega \to \infty$
ϵ_s = the relative dielectric constant as $\omega \to 0$
$\omega = 2\pi f$
τ = relaxation time (sec)
ϵ_0 = permittivity of free space (8.854×10^{-12} F/m)
ρ = dielectric conductivity
$i = (-1)^{1/2}$

The quantities ϵ_s, τ, and ρ are all functions of temperature and salinity. Stogryn (ref. 3–33) has examined the experimental data and developed analytical expressions for these quantities in terms of regression series. When the dielectric constant is specified, the reflection coefficient $|R(0)|^2$ can be derived from the Fresnel formulas, which, for normal incidence, is given by

$$|R(\theta = 0)|^2 = \left|\frac{1 - \sqrt{\epsilon}}{1 + \sqrt{\epsilon}}\right|^2 \qquad (3\text{–}7)$$

It is of interest to note that the geometric optics expression for the radar scattering coefficient of rough surfaces is proportional to $|R(\theta=0)|^2$.

Figure 3–11 shows a plot of reflection coefficient as a function of frequency values that $|R(0)|^2$ may assume because of extreme variations in the water temperature and salinity content (0 to 35‰). At frequencies above 5 GHz, the change in $|R(0)|^2$ is primarily due to the influence of water temperature. As the frequency decreases below 5 GHz, salinity becomes a more important parameter. The gross knowledge of the reflection coefficient is important for the system design. First, the scattered signal is 2 to 3 dB less than what it would be if the ocean were a perfect reflector; second, if $|R(0)|^2$ is less than unity, thermal radiation is emitted that decreases the signal-to-noise ratio of the measurement. The detailed knowledge of the variation of reflection coefficient with salinity and temperature appears to be of minor importance. Because the data in figure 3–11 only span 1.88 dB, the measurement of σ° must be done to within a few hundredths of a decibel for active systems to provide accurate temperature ($\Delta T = 10°$) and salinity ($\Delta S = 1‰$) measurements

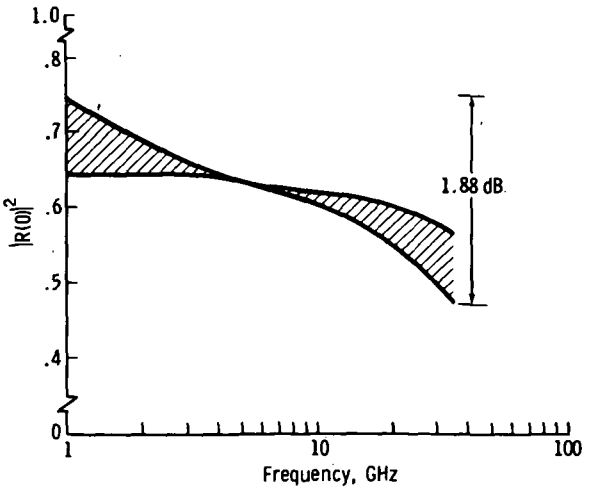

FIGURE 3–11.—Plot of reflection coefficient as a function of frequency over the microwave band of 1 to 35 GHz.

of water. Such measurements can apparently best be done with microwave radiometers. When water turns to ice, the static dielectric constant remains unchanged; however, the relaxation time τ increases by several orders of magnitude. Assuming that the ice is frozen freshwater (i.e., $\rho=0$), then a large $\omega\tau$ in the Debye equation gives a value ϵ of approximately ϵ_∞ plus a small imaginary part (or $\epsilon \approx 4.9$), in which case $|R(0)|^2$ is approximately 0.14. This very low loss, which results from the significant increase in $\omega\tau$, serves to increase the skin depth and enables the radar to illuminate features covered by snow and ice.

APPLICATIONS OF PHYSICS TO RADAR SENSING TECHNIQUES

The purpose of this section is to examine several concepts for instruments that could possibly measure some of the important properties of sea state. In this section, the various instruments will not be compared concerning their sensitivity, performance, and cost; that will be done in a subsequent section of this document. Rather, the physical mechanism of radar scatter in the operation of the instrument will be examined and it will be shown how the theoretical concepts and equations of the section entitled "Physical Mechanisms of the Radar Echo" can be applied to quantitatively explain the performance of the sensors. The principal instruments to be examined in this respect are as follows.

1. Scatterometer: Mean slopes near vertical are sensitive to sea state. Bragg scatter from capillary waves at angles sufficiently removed from nadir is sensitive to the instantaneous windspeed.

2. Altimeter: Distribution of specular points at vertical is proportional to the height distribution of the largest waves.

3. Imaging radars/wave spectrometers: Local tilts of specular points (and hence local echo intensity) vary with the slope of longer waves.

In addition to these well-known sensors, several other concepts that could also have spacecraft application will be described.

Scatterometry

The scatterometer is the simplest form of microwave radar. It senses the (averaged) absolute power return from the sea surface. The instrument parameters that can usually be varied for a particular scatterometer system are the incident angle and the polarization states. Because the instrument is usually well calibrated, it is possible to measure $\sigma°$, the average radar backscatter cross section of the sea surface per unit surface area, as a function of incident angle and polarization state. The scatterometer has already been flight tested aboard numerous aircraft and has been flown on Skylab; specific results are discussed in subsequent sections of this report.

The normal incident angle range of the instrument is from the vertical out to 60°. Near the vertical ($\theta<20°$), the specular-point theory discussed in the section entitled "Physical Mechanisms of the Radar Echo" is applicable. The radar scatter model is given in equation (3–2). Because the slopes for the sea are usually Gaussian distributed, equation (3–2) can be rewritten

$$\sigma° = \frac{\sec^4\theta}{2\zeta_x\zeta_y}\exp\left(-\frac{\tan^2\theta}{2\zeta_x}\right)|R(0)|^2 \qquad (3\text{–}8)$$

where ζ_x and ζ_y are the root-mean-square (rms) sea slopes in the x and y directions, with the x-direction here being taken to lie along the surface in the plane of incidence. Again, $R(0)$ is the Fresnel reflection coefficient of a smooth sea at normal incidence. Thus, by measuring $\sigma°$ as a function of θ, one can potentially measure the surface slopes of the sea. Because these slopes are related to sea state and/or windspeed, it should be possible to determine these meteorological parameters with the scatterometer.

An example of one possible straightforward relationship between surface slope and windspeed is shown in figure 3–12 (ref. 3–34), which gives both measured data and a theoretical prediction for the variation of the sea surface slope with windspeed. If the further simplifying assumption is made (though it may not be necessarily valid) that the sea-slope distribution is isotropic, then the expression for $\sigma°$ can be simplified still further. In this case, $\zeta_x^2=\zeta_y^2=\zeta^2/2$, where ζ^2 equals $\zeta_x^2+\zeta_y^2$ and is the total mean-square slope of the surface. Then, at the vertical,

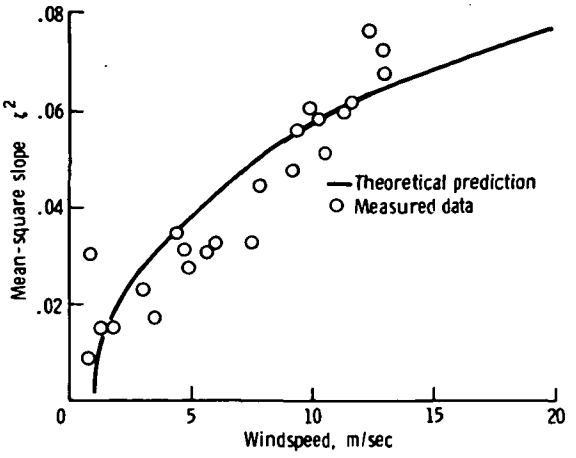

FIGURE 3–12.—Example of possible relationship between sea surface slope and windspeed.

$$\sigma° = \frac{|R(0)|^2}{\zeta^2} \qquad (3\text{–}9)$$

The slope-dependent specular-point theory can provide a reasonable basis for the design and interpretation of scatterometer data out to incident angles of approximately 20°.

An important question that has an impact on scatterometer accuracy is the variance around the apparent mean of the measured sea-echo points, which is evident in experimental data. No simple theoretical model completely explains the reason for this variance. It is quite obvious that this variance in sea echo, combined with instrumental and propagation loss variances, will ultimately limit the accuracy of the scatterometer for measuring the surface winds.

The bulk of scatterometer data, which has been obtained by NRL, NASA JSC, and NASA Langley Research Center (LaRC), has concentrated on the response at viewing

angles greater than 25°. The rationale behind the desire to operate in this mode is twofold: first, the scattering data are proportional to the local wind sector (which is of interest for meteorological forecasting), and second, the wide-angle scan will give wide-area global coverage from satellite platforms. As previously mentioned, Bragg scattering dominates in this mode of the scatterometer. Specific descriptions of the theoretical model and a discussion of flight results are presented in detail in a subsequent section. Scatterometers have also been used in the detection of oil spills (ref. 3–35).

Altimetry

An orbiting microwave altimeter transmits a pulse with an effective spatial length that is short compared to typical wave heights (e.g., usually less than 0.5 m). As the pulse interacts with waves beneath the satellite, it is scattered back toward the satellite by specular points on the larger gravity waves. The short pulse is "stretched" temporarily by the ocean waves, and the degree of this stretching is a direct measure of the mean heights of the waves at the suborbital point. The radar altimeter has been tested on various aircraft and on Skylab. The pulse length on Skylab, however, was insufficiently short to allow a good test of the sensor for measuring wave height. The primary satellite tests of the instrument are to be conducted with the Geodynamic Experimental Oceanic Satellite (GEOS–C), which is to be launched in 1975.

The radar cross section can be expressed as a function of the height of the radar pulse interaction region, as shown in equations (3–10) and (3–11). From the specular-point theory discussed in the section entitled "Physical Mechanisms of the Radar Echo," backscattered strength from N specular points is

$$\sqrt{\sigma_B} = \sum_{i=1}^{N} \sqrt{\pi g_i}\, e^{i2k_0 Z_i \cos\theta} \qquad (3\text{–}10)$$

where

g_i = Gaussian curvature at the ith specular point
Z_i = height of the ith specular point above mean surface
k_0 = radar wave number
θ = angle of incidence from vertical

When equation (3–10) is squared, written as a distribution over height, and averaged, it becomes

$$\eta^\circ(Z) = \pi \int_0^\infty n(Z,g)\, g\, dg \qquad (3\text{–}11)$$

where $\eta^\circ(Z)$ is the average backscatter cross section per unit area per unit height increment at height Z, and $n(Z, g)$ is the average number of specular points per unit area for heights between Z and $Z+dZ$ and for Gaussian curvature between g and $g+dg$.

The physical illustration of a radar pulse of spatial width $\Delta Z \cos\theta = (c\tau)/2$ advancing over the ocean is shown in figure 3–13. If this model is used, and it is assumed that a symmetric Gaussian distribution of sea-wave heights exists, the expression in equation (3–12) is obtained for the average radar cross section of the sea as a function of time. Radar altimeter power return ($H \ll a$) is

$$G^2\sigma(t) = \sqrt{\pi^3}\,\frac{H x_w}{s^2} \exp\left[\left(\frac{t_p}{t_s}\right)^2 - \frac{2t}{t_s}\right] \left[1 - \phi\left(\frac{t_p}{t_s} - \frac{t}{t_p}\right)\right] \qquad (3\text{–}12)$$

where

G = antenna gain as a function of time
$\sigma(t)$ = average radar cross section as a function of time
H = height of the radar altimeter
a = "radio" radius of the Earth ($\approx$4/3 times actual Earth radius)
s^2 = total slope
$x_w = (c\tau)/[4(\ln 2)^{1/2}]$
$t_p = [2(x_w^2 \quad 2h^2)^{1/2}]/c$
$t_s = (2H^2\Psi_c^2)/c$
$1/\Psi_c^2 = [\,(8 \ln 2)/\Psi_B^2] + (1/s^2)$, where Ψ_c and Ψ_B are shown in figure 3–14
h^2 = mean-square sea wave height
$\phi(x)$ = error function of argument x

Two constants t_p and t_s appear in this model. In normal satellite operation, t_s will be much larger than t_p; this is defined as the "pulse

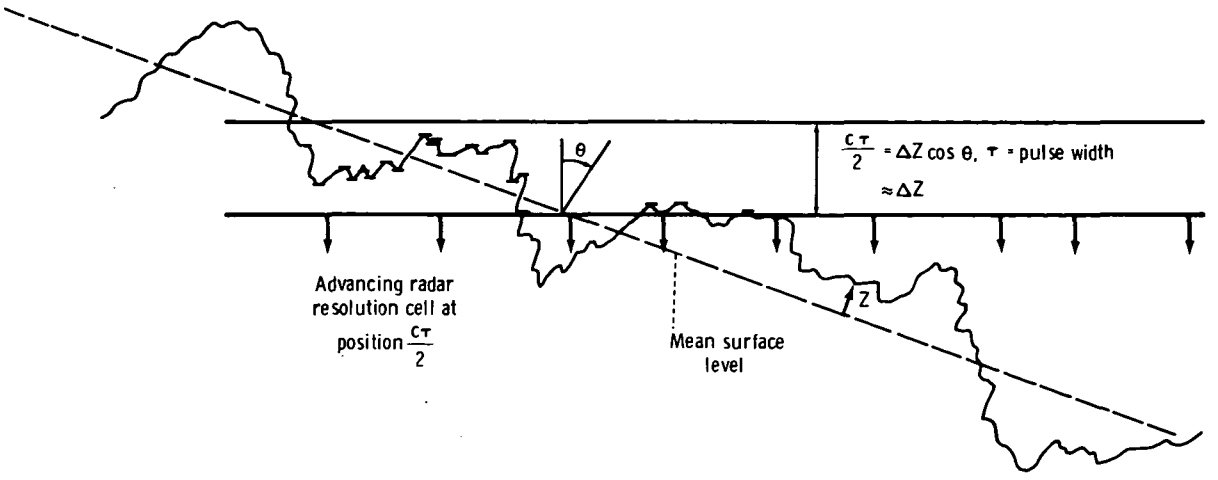

FIGURE 3–13.—Physical illustration of specular point scatter (specular points are highlighted).

limited" mode of altimeter operation. In this case, the return signal (as expressed by the average radar cross section as a function of time in eq. (3–12)) is as shown in figure 3–15. The slope of the leading edge of the signal is a function of the significant sea-wave heights $H_{1/3}$ at the suborbital point. This portion of the signal is the one that must be used to extract "sea state."

The constants t_p and t_s have simple geometric interpretations that help to explain the nature of the received signal. As shown in figure 3–16, t_p represents the amount that the incident signal (propagating vertically downward) gets stretched by ocean waves of height h. The constant t_s is a measure of the time that the radar echo is being received from the sea, as shown in figure 3–14. In the pulse-limited mode ($t_s \gg t_p$), this return will be received from a spherically advancing resolution cell as long as (1) there are specular points with slopes large enough to backscatter, and (2) the antenna beamwidth is great enough to permit illumination of the sea. For pulse-limited operation, the length of the trailing edge of the pulse shown in figure 3–15 is essentially t_s.

Because the information on significant sea-wave height for pulse-limited altimeter operation is contained in the slope of the leading edge, one way of retrieving the height distribution information is to differentiate (as a function of time) the averaged leading edge. This derivative is then essentially a pulse that is directly proportional to the ocean-wave height probability density function. This effect is shown in figure 3–17, in which a more realistic height distribution than the symmetric Gaussian function is now used. Oceanographers have known that, for greater wave heights, the height probability

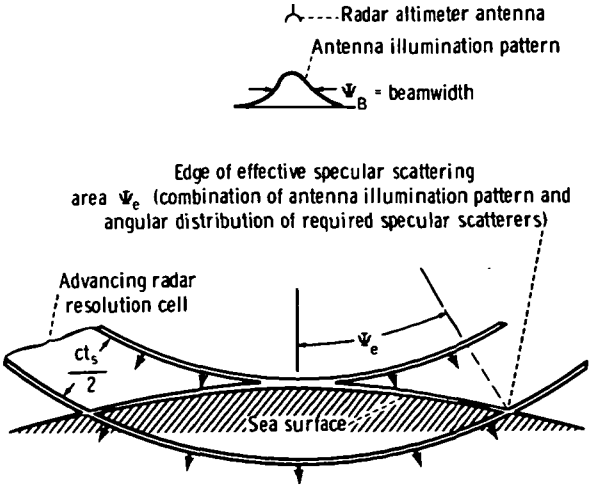

FIGURE 3–14.—Interpretation of altimeter model constant t_s.

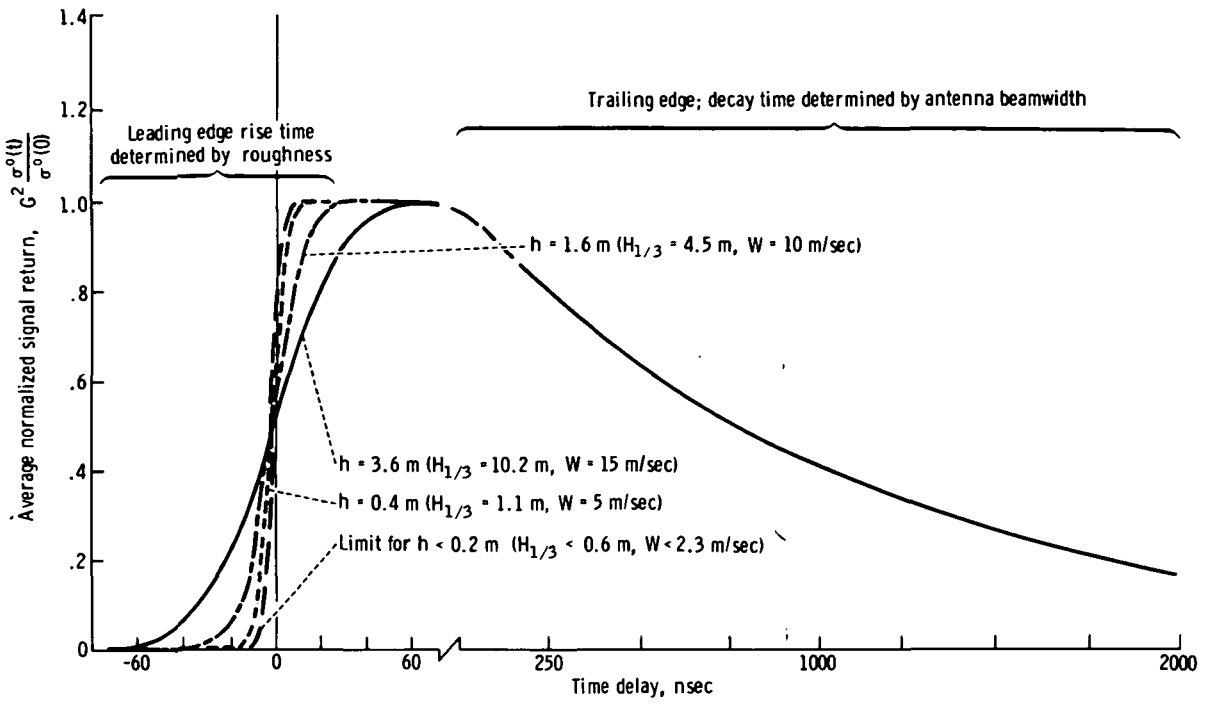

FIGURE 3–15.—Average radar cross section as a function of time (where $H_{1/3}$ is significant wave height and W is windspeed).

density function is skewed toward heights above the mean plane. This skewness can be described by a parameter δ, which can be as high as 0.4. Hence, the upper graphs in figure 3–17 show wave probability density functions (with and without skewness) for various wave heights. The lower graphs show the time derivative of the averaged leading edge of the received signal for a 10-nsec transmitted pulse (in the absence of noise). This signal, for greater wave heights, is stretched in direct proportion to the width of the height probability density function. However, note that when the height density function is skewed (dashed curve), the radar return is also skewed, but in the opposite direction. This has been observed experimentally, where the radar "centroid" of the measured altimetry return appears to move toward the troughs and away from the wave crests. The theoretical model explains this shift and can be used as a correction to quantitatively determine the error factor introduced by wave skewness for the purpose of determining the mean sea position.

The specular-point model, and its extension to radar altimetry, therefore adequately explains the interaction mechanism with the sea and can permit both the design of the sensor and the interpretation/extraction of sea-wave height information from the received signal.

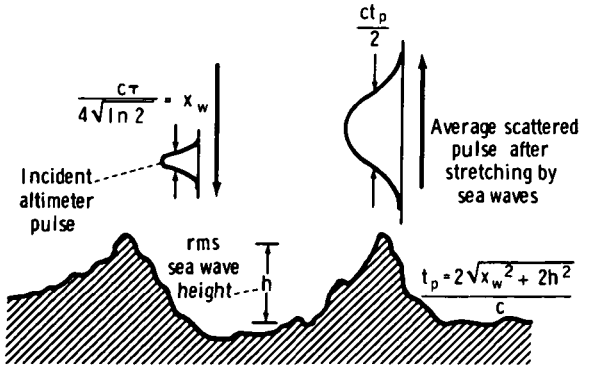

FIGURE 3–16.—Interpretation of altimeter model constant t_p.

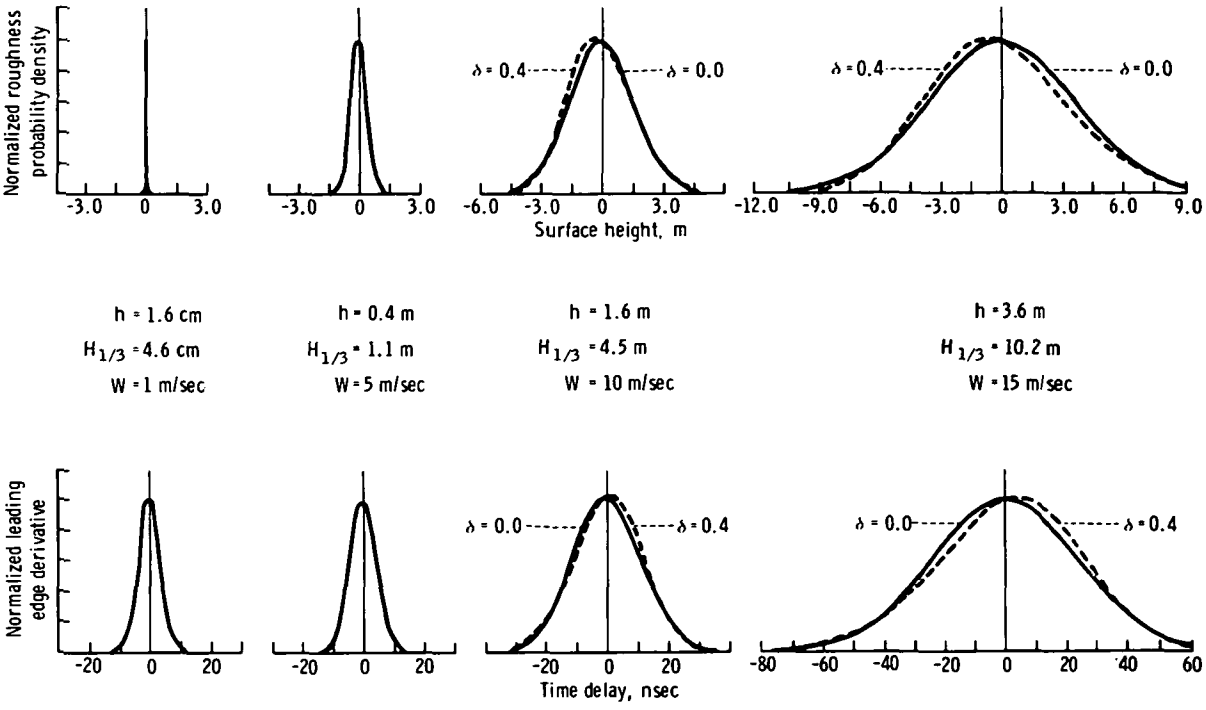

FIGURE 3–17.—Wave probability density functions.

Imaging Radars

Recently, airborne imaging radars have recorded very striking radar "pictures" of longer ocean-wave patterns that very clearly show the periods and directions of the various "swell type" wave components present on the sea. These high-resolution radar images are formed by synthetic aperture techniques, in which fine detail parallel to the flightpath is obtained by "synthesizing" a long antenna from the small aircraft antenna by combining the received signals at different points along the aircraft flightpath.

The purpose of this section is to explain that factor in the scatter process that permits the imaging radar to see the long gravity waves. For this purpose, it is adequate to consider only a high-resolution radar with a resolution cell size that is small in terms of the ocean wavelengths under observation, and to ignore the mechanical details of how the signal is processed aboard the aircraft to actually achieve this image. Because the imaging radar appears to have such great long-term potential for oceanic sensing from spacecraft, this understanding of the scatter process appears to be essential to the proper interpretation of the images in terms of sea state (or the wave-height directional spectrum).

The fact that the imaging radar "sees" gravity waves tens of meters in length (when the radar wavelength itself is only centimeters) indicates that the long wave is "modulating" the intensity of the echo over different parts of the wave. The most distinctive wave patterns in these radar images appear within approximately 25° from the vertical. The specular-point theory explains scatter in this region (see the section entitled "Physical Mechanisms of the Radar Echo"). Because the specular points producing scatter at centimetric radar wavelengths are themselves ocean-wave features with dimensions that are centimetric in scale, these small-wave features obviously must be affected by the presence of the long wave on which they are riding.

There are mechanisms by which modulation of the small specular-point scatterers can be produced by a long underlying gravity wave, thus enhancing the radar visibility of the long gravity wave. If one assumes (to first order) that the total slope of the surface is the sum of the slopes of all the surface components present, then the long gravity wave causes all the surface components present and also causes all the small-wave specular points to be tilted according to its own slope. Thus, for the radar look direction shown, more specular points will be on the forward face of the wave than on the back side. The diagram in figure 3–18 illustrates this modulation pattern as a "radar reflectivity plot," in which the heavier shading corresponds to the greater reflectivity on the forward wave face. Hence, a periodic pattern of radar reflectivity is produced that corresponds to the long underlying gravity wave. The equations under the plot use the previous specular-point model (eq. (3–2)) to show how the slope probability density function of the small wavelets is modified to account for the presence of the long wave slope ζ_x^ℓ. The second equation expands the small-scale slope density function in a Taylor series, showing that (to first order) the radar cross section is indeed proportional to the slope of the long underlying gravity wave. This explains why the longer wave is visible and also provides a quantitative estimate of the intensity of this modulation.

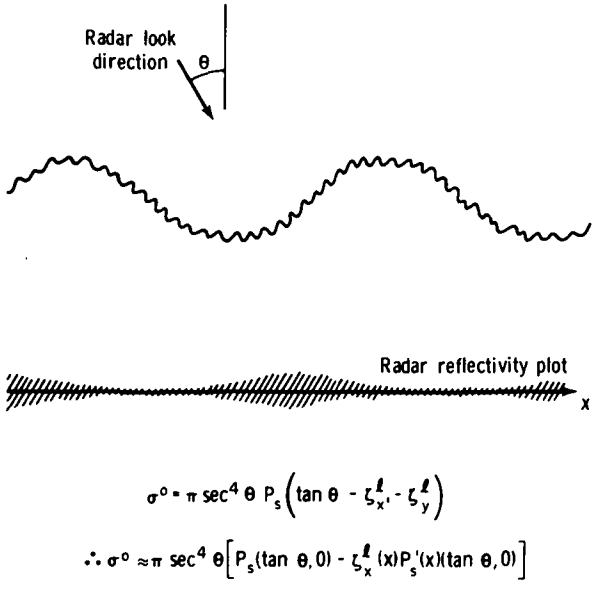

FIGURE 3–18.—Specular-point tilt superposition (where P_s is the probability density function in the specular direction).

A second mechanism (fig. 3–19) can also produce a radar reflectivity pattern that carries the modulation of a long underlying gravity wave. As a result of hydrodynamic nonlinear interactions involving straining and surface tension, short capillary waves tend to be concentrated more on the leading edge of the long gravity wave. The leading edge is defined as the side of the long wave the normal of which points in the same direction as its phase velocity. Capillary waves are excited by very gusty, strong winds and hence may be absent entirely when there is little wind. When they are present, however, they will arrange themselves in a spatial pattern with the periodicity of the underlying gravity wave and thereby produce a radar cross section that (to first order) varies directly with the slope of the underlying gravity wave. The proportionality constants, which depend on wind, are presently unknown. They could be estimated either theoretically or experimentally.

One final effect may (in some cases) account for the "wave" patterns seen by an imaging radar. This effect is the orbital velocity of the short radar-reflecting capillary waves due to the presence and motion of the long underlying gravity wave. These scat-

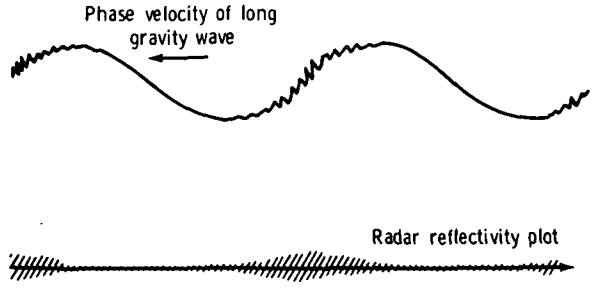

FIGURE 3–19.—Capillary bunching on leading edge.

C.13

tering specular points on the larger gravity wave execute a circular motion as the longer wave passes beneath them. For a given position of the long wave, the direction of this circular motion is in the directions shown by the arrows in figure 3–20. The speed v_0 of this motion is constant and equals $2a[(2\pi g)/L]^{1/2}$, depending on the amplitude a and length L of the long wave. Therefore, at some points on the long wave, the specular points have no component of motion along the radar direction (where the vector is perpendicular to the radar line of sight). At other points (in particular, within two regions over one period of the longer wave), the orbital velocity component lies along the radar look direction, and the specular points are moving relative to the radar and hence changing their phase with time, as observed at the radar receiver. Because the return from the sea in an imaging radar is observed and integrated for some finite period of time T, the distance traveled by these "maximum radial velocity" specular regions during this time is v_0T. If this distance is greater than one-quarter of the radar wavelength, destructive phase interference will occur in these regions and the "image" will appear weaker (or effectively "blurred"). For example, for a long wave with an amplitude of 1 m and a length of 15 m, destructive interference will occur for processing times greater than 6 msec when viewed at S-band frequencies (10 cm).

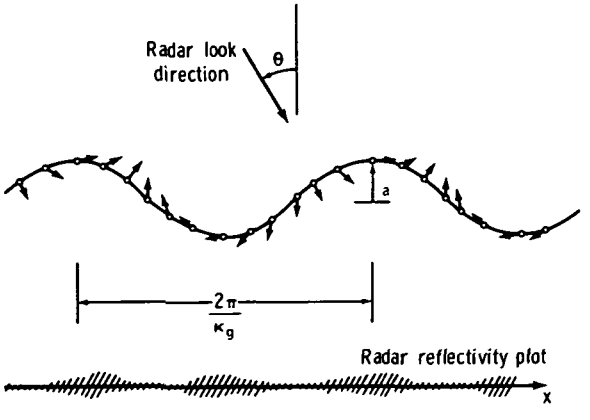

FIGURE 3–20.—Capillary motion caused by orbital velocity.

The radar reflectivity plot corresponding to this temporal smearing effect is shown in figure 3–20. The important fact is that this effect, unlike the previous two, produces a reflectivity plot that appears as a second spatial harmonic of the fundamental gravity wave. Thus, the radar image would give the misleading impression that the ocean wave seen by the radar was one-half its actual length.

Which of the three mechanisms is dominant is not clear. Because only the first has been analyzed quantitatively, the others, at this time, can only be qualitatively described and said to have some part in the production of the radar image. Further analysis is required on the latter two to ascertain their quantitative role in the process. As can be seen from the reflectivity plots and from the equations, the three effects do not always reinforce each other constructively for all angles. Because, in addition, the specularly reflecting capillary waves are present on top of the long swell-type gravity waves only in gusty wind conditions, there may be several situations that involve combinations of effects in which the long gravity waves are not visible at all on radar images. This may explain the "sometimes" nature of swell patterns in radar images when compared to optical photographs.

MICROWAVE RADIOMETRY APPLICATIONS

The rationale of including a discussion on microwave radiometer measurements of the ocean surface is that some oceanographic parameters can best be made with radiometers (rather than radars). As noted in a previous section, using a radar to accurately measure ocean-surface temperature and salinity is unrealistic. Microwave radiometers, however, offer a very attractive possibility. A plot of brightness temperature as a function of salinity content of the water is shown in figure 3–21 for 1.0 and 5.4 GHz. Brightness temperature as a function of

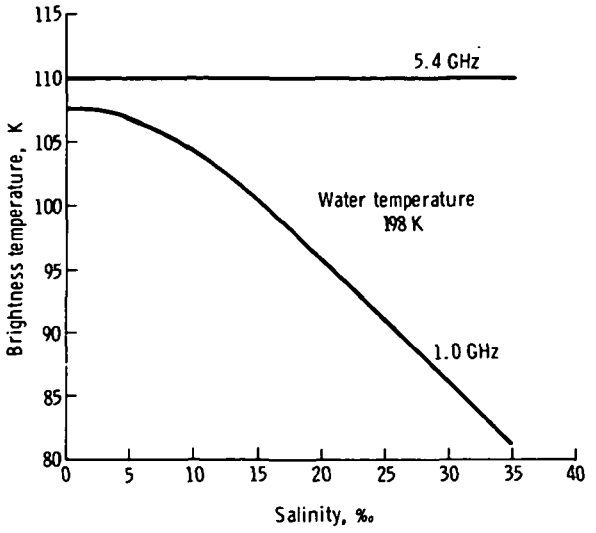

FIGURE 3–21.—Brightness temperature as a function of salinity content.

water temperature is plotted for the same two frequencies in figure 3–22.

The relative independence of brightness temperature with salinity at C-band coupled with the strong salinity dependence at L-band suggests that an airborne two-frequency radiometer system can be used to measure water temperature and salinity. An S-band radiometer developed for the NASA AAFE has demonstrated the capability of measuring brightness temperature to an accuracy of 0.3 K. A companion instrument operating at L-band (which is being constructed at LaRC) would open the possibility of simultaneously measuring water temperature and salinity to respective accuracies of at least 1 K and 1‰. The 1‰ accuracy figure for the salinity measurement is valid only if the salinity is greater than 5‰.

The most attractive use of the microwave radiometer is as an instrument to complement the scatterometer for wind measurements. Radiometers may be required to provide atmospheric corrections for active measurements.

CONCLUSIONS AND RECOMMENDATIONS

There is firm experimental evidence to conclude that the electromagnetic backscattering process at microwave frequencies is due to (1) specular-point reflections when the viewing angle is within 20° of nadir, and (2) resonant (Bragg) scattering when the viewing angle is beyond 20° from nadir. The first phenomenon is intimately linked to the tilt of gravity waves, and the second is due to the spectral characteristics of the capillary or short gravity wave spectrum.

The response of the radar altimeter can be interpreted in terms of the specular-point theory; that is, the impulse response is stretched in time in a manner that is proportional to the vertical distribution of specular points.

The scatterometer measures sea slope near vertical incidence as a result of the change in the rms tilt of specular points. At angles sufficiently removed from the vertical, the scatterometer responds to the wind fields because of the instantaneous change in the Bragg spectrum of short waves.

More analytical work is required to define the scattering process associated with promising experimental techniques, including the imaging radar. Microwave radiometers

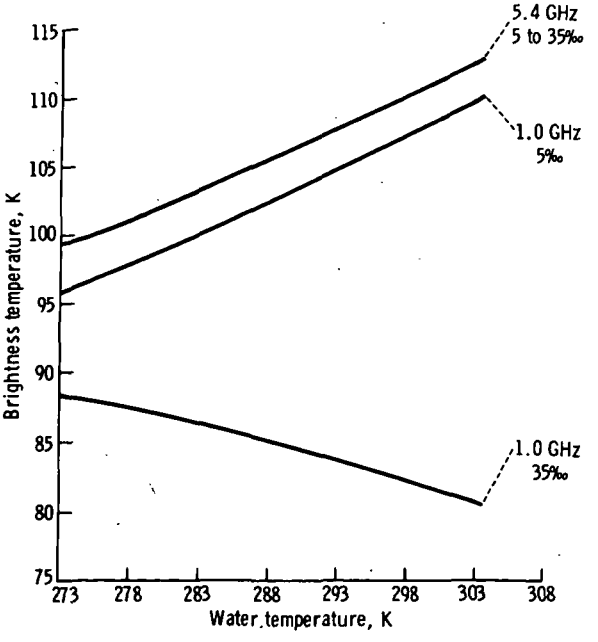

FIGURE 3–22.—Brightness temperature as a function of water temperature.

should be incorporated as complementary instruments, specifically in regard to ocean temperature measurements, salinity measurements, and inference of high windspeeds due to the presence of surface foam.

Parallel analytical and experimental efforts are recommended to establish the accuracy with which windspeed can be measured from the percent foam coverage.

PART C

LOCAL PHENOMENA

This section is devoted to the oceanic and coastal phenomena with dimensions ranging to 100 km. The two major categories discussed are waves (their generation and dynamics) and ocean-land related problems.

The dynamics of surface waves in both capillary and gravity ranges indicates that microwave technology provides a superior means of measuring simultaneously the spatial and temporal properties of ocean waves. The need for basic studies of physical phenomena in support of active microwave sensing is indicated. Active microwave scattering from surface waves is discussed in terms of wave dynamics. Ocean waves receive most of their energy from wind. The state of the art in wind measurements by conventional methods shows a gross inadequacy of present surface-sampling techniques for global weather and wave forecasting; microwave technology offers the potential to alleviate many of the problems. Global aspects of wind climatology are included in the discussion of large-scale phenomena in the section entitled "Global Wave Statistics." The subject of internal waves is relatively new and is less well understood in comparison with surface waves. Internal waves, even though they exist well below the microwave skin depth, are frequently detectable through surface manifestations such as convergence zone slicks, which have been visible in Earth Resources Technology Satellite (ERTS) imagery. Internal waves may also possibly be detected from surface temperature anomalies in the divergence zones. Thus, by monitoring surface properties with microwave sensors, a mathematical model for the prediction of internal waves might be developed.

The second category deals with the interaction between the ocean and its land boundaries in the coastal zone. The monitoring of shoreline changes is very important for coastal engineering and oil-drilling structures, beach erosion, coastal navigation, and recreation. The wave climate, the single most important parameter affecting coastal processes, could be monitored in great detail over large areas by satellite-borne active microwave sensors.

All these phenomena influence the ocean-surface structure in various ways, which are detectable by active microwave instruments. The signatures of signals obtained by such instruments and their relationships to oceanic and coastal processes provide an invaluable aid to understanding these processes.

WAVES

Human activities on the sea are very much influenced by waves, which damage structures and cargoes, change shorelines, and slow the progress of ships. A better understanding of waves and better wave predictions will benefit marine activities and yield concomitant economic benefits.

In the past, wave measurements have been difficult, and understanding of the generation, propagation, mutual interaction, and decay of waves on the ocean is based on several good oceanographic experiments. In

the following paragraphs, the present understanding of wave spectra is outlined, and the ways in which microwave systems may facilitate wave measurement and how this might provide scientific and economic benefits are discussed.

Ocean waves may be defined as undulations of the surface with time scales in the range from 0.025 to 25 sec, corresponding to wavelengths in the range from 0.02 to 1000 m, respectively. These are subclassified as (1) gravity waves, with time scales in the range from 0.1 to 25 sec, length scales from 2 cm to 500 m, and heights to 30 m, or (2) capillary waves, with time scales in the range from 10^{-1} to 10^{-2} sec, length scales from 0.5 to 2.0 cm, and heights of less than 1.0 cm. Ocean waves are random, and a time record of the ocean-surface displacement in a storm region may contain wave periods in the entire range indicated earlier. Far from a storm center, waves become more organized as the longer waves propagate more rapidly out of the region. Long waves occurring away from storm centers are referred to as swells. Long waves approaching a coastline are influenced by the drag of the bottom and become shallow-water waves. Wave energy is eventually dissipated through breaking in an active near-shore area called the surf zone. Wave energy is also dissipated offshore through viscous effects and by breaking, which is evidenced by the presence of whitecaps. The processes of wave generation by wind; the transfer of energy between the various wave spectral components by wave-to-wave interaction; and the dissipation of energy by viscosity, breaking, and bottom effects are extremely complex and constitute a research area under intensive investigation by theoreticians and experimentalists.

The statistical properties of gravity waves vary slowly in time and space and can be described locally by a three-dimensional Fourier transform $F(k, \phi, \omega)$; that is, the sea surface can be considered as a superposition of waves of all wavelengths $L=(2\pi)/k$ and periods $T=(2\pi)/\omega$ traveling in all possible directions ϕ. Usually, the larger waves ($L>1$ m) are assumed to obey the dispersion relation applicable to infinitesimal amplitude gravity waves ($\omega^2=gk$). This reduces the dimension of the spectrum by one, and the resulting function is the directional spectrum $\psi(k, \phi)=\psi_1(\omega, \phi)$. The sea surface is now described as a superposition of plane waves with various wavelengths and directions. These wave components are generated by the wind, interact with other wave components, propagate away from their generating area, and eventually decay. Clearly, study of these processes requires a simple, routine method of measuring these individual components of the wave spectra. Such a method does not now exist.

Integration of the function $\psi(k, \phi)$ over all angles yields the one-dimensional spectrum $\psi(\omega)$. This is the more easily measured spectrum of sea-surface elevation measured at a point. Integration of $\psi(\omega)$ gives the variance of wave height at this point $<Z^2>$. This statistic is frequently reported in terms of the significant wave height $H_{1/3}$, which historically has been defined as the average of the highest one-third of waves present in a sea. More recently, it has been taken to be

$$H_{1/3}=4<Z^2>^{1/2} \qquad (3\text{–}13)$$

where $<>$ indicates ensemble average.

The statistics of the ocean surface, especially the statistics of wave-number distribution, are poorly known. In fact, $F(k, \phi, \omega)$ has never been measured. In discussing what is known about the various spectra, it is convenient to consider the simplest first.

From the wave-height variance, the rms wave height, $<Z^2>^{1/2}$, and significant wave height are easily estimated. Most data come from "eyeball" estimates of significant wave height reported by transient ships and, less commonly, from accelerometers on weather ships and buoys. Large amounts of data are available: atlases give wave climate over the world's oceans, wave height is routinely included in weather reports from ships, and wave height is routinely predicted by such groups as the Fleet Numerical Weather Central and the National Weather Service.

The one-dimensional spectrum is commonly measured with wave staffs or accelerometers mounted on buoys and ships. The general shape of the function and its relation to windspeed, duration, and fetch are reasonably well known for wavelengths greater than 1 m. Little is known of $\psi(\omega)$ in the region between 1 m and 1 cm because few measurements have been made. The equivalent function $\psi(k, \phi)$ is almost unknown for these wavelengths because the dispersion relation $\omega^2 = gk$ cannot be applied accurately to short waves. This has important consequences. Microwave signals are Bragg scattered by ocean wavelengths in this band, and lack of knowledge of the generating mechanisms of these waves hinders, to some extent, the application of active microwave systems that use sea scatter for inferring such factors as oceanic winds. Conversely, the Bragg scatter can be used to investigate this wavelength region of ψ.

The directional spectrum $\psi(k, \phi)$ is not well known. Measurements have been taken a few times in a few selected places, but the dependence on windspeed, duration, and fetch could be better described.

Capillary waves have been traditionally investigated by theoreticians and experimentalists with academic interests. More recently, and with the onset of microwave instruments as remote sensors, capillary waves have attracted more attention from a more practical point of view. The roughness of the sea is interpreted by the density and structure of capillary waves, which respond to windspeed. The detection of sea-surface roughness by active microwave instruments offers the potential of remote determination of windspeed.

Laboratory studies by Wright and Keller (ref. 3–36) indicate that Bragg scattering dominates radar return signals for angles greater than 20° from the vertical. The primary return is from capillary waves. The dynamics of capillary waves, therefore, assume central importance in understanding radar return at higher angles of incidence.

Capillary waves are sensitive to wind forcing, local currents, orbital velocities of long gravity waves, and changes in surface tension due to slicks induced by oil spills or biological activity. Laboratory experiments by Shemdin et al. (ref. 3–37) (fig. 3–23) indicate that a linear relationship exists between capillary wave slope energy ϕ_s and windspeed W for each frequency. A saturation level is achieved at a certain windspeed beyond which the slope energy remains constant. Higher frequencies achieve saturation at higher windspeeds. The same study (fig. 3–24) also indicates the influence of long waves on capillary waves at various windspeeds. These results provide an understanding of the scatter evidenced in relating windspeed to radar backscatter. Indeed, windspeed is only one of the variables that affect capillary waves, which in turn determine the magnitude of the backscatter.

Imaging radar has the capability of detecting long gravity waves and directions primarily because capillary waves vary in intensity along the profile of long waves. The variation is induced directly or indirectly by the orbital velocities of the long waves. The interaction between capillary waves and long gravity waves is nonlinear, and a com-

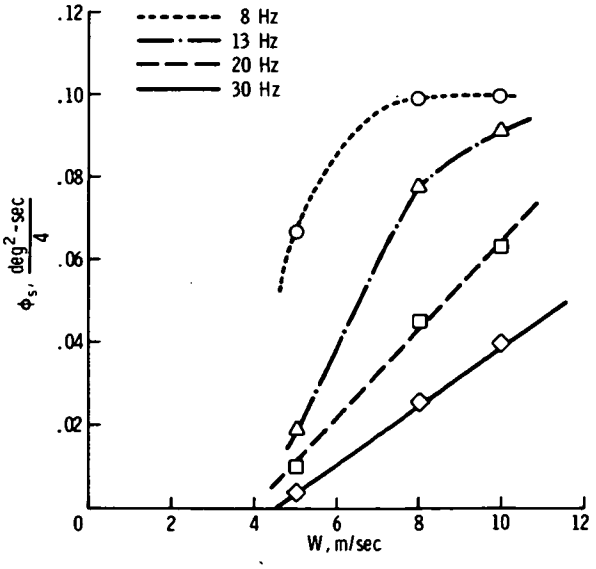

FIGURE 3–23.—Wind dependence of slope spectral values at different frequencies.

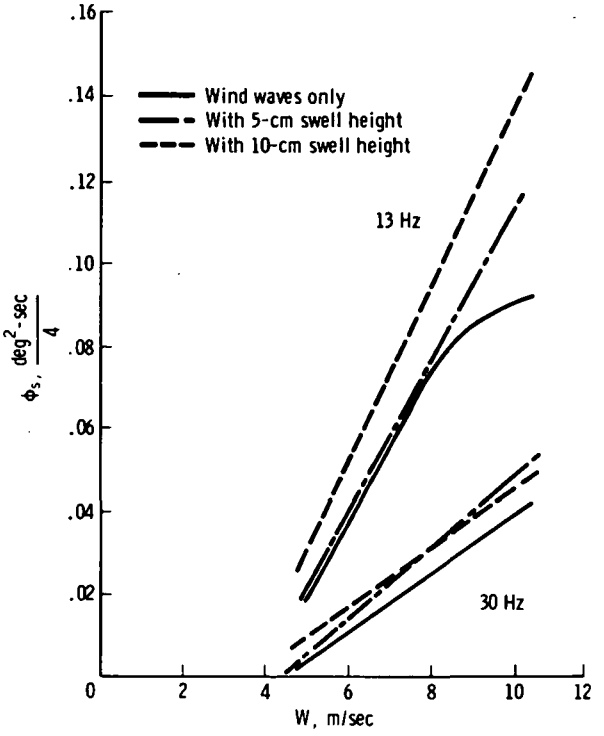

FIGURE 3–24.—Dependence of slope spectral values at 13 and 30 Hz on mechanically generated waves.

plete understanding of the process is under investigation. Presently, it is not evident how one may obtain heights of the long gravity waves from variations of the radar imager return from various phase positions along the profiles of the long waves. The remote determination of the directional wave spectra is of central importance to users involved in structural design and protection in coastal and offshore areas.

Microwave technology now provides a means of simultaneously measuring the spatial and temporal properties of ocean waves. This is far superior to the traditional methods of measuring the time history of water-surface elevation at a fixed position or the spatial distribution of waves from a photograph. The dynamics of wind-generated capillary waves as revealed by a Doppler radar mounted on a wave tank are far more complex than the traditional understanding based on hydrodynamics. The surface drift, for example, can increase wave dispersion by as much as 100 percent. The modulation of capillary waves by long gravity waves can be more easily investigated by active microwave instruments in a wide range of windspeeds.

For larger ocean waves, active microwave measurements are expected to produce routine estimates of significant wave height $H_{1/3}$ and of the directional wave spectrum $\psi(k, \phi)$. The dispersion of a high-resolution altimeter pulse gives $H_{1/3}$ directly. High-resolution real and synthetic aperture radars have shown images of waves. Suitable optical or digital processing is expected to yield the directional spectrum (or slope spectrum) of large ocean waves.

Satellite measurements of the directional spectrum of ocean waves are expected to have a number of important benefits to pure research, ocean engineering, and marine activities. First, development of the satellite instruments will lead to simple, reliable techniques for measurement of the spectrum. Given the development of such a technique, substantial benefits will accrue from the increased knowledge of ocean waves.

Wave forecasting models can benefit greatly by direct measurement of wind and waves with appropriate microwave sensors. Daily global coverage of areas of approximately 1000 km^2 will verify and update numerical models for forecasting wind and waves. Representative spot measurements over areas of approximately 5 km^2 will be more useful. Windspeed resolution of approximately ± 2 m/sec over a range up to 50 m/sec will be needed to cover storm areas. Measurement of wavelengths from perhaps 25 to 500 m and a resolution of 5 to 25 m will also be needed.

For pure research, measurements of the spectrum as a function of windspeed and fetch can be used to test theories of wave generation. To date, only a few measurements of wave growth have been published. Measurements near the edge of strong currents can test theories of wave trapping and refraction by current shears; the effect could be substantial but has never been measured.

Measurements made in conjunction with simultaneous oceanic internal wave fields can test theories for the generation of internal waves by surface waves; internal waves have often been measured. Internal waves affect the propagation of sound in the sea, but no generally accepted theory for their generation exists.

Routine measurements of wave size and direction will lead to reliable catalogs of wave climatology of benefit to marine engineering activities. A few examples can be listed as follows:

1. Offshore structures are designed to withstand the largest expected waves from a particular direction. Improved wave climatology will lead to more reliable, less costly, and safer designs.

2. The siting and design of breakwaters and harbors depends on the expected direction of arrival of large waves, and these data can be supplied by satellite.

3. Ships are often slowed and their cargoes damaged by large waves. If the oceanic wave field were known, ship routing predictions could be optimized for most economic operation. The wave field will be measured by satellite and its future development will be predicted from the improved models of wave generation that are themselves produced from satellite data.

4. The wave spectra are also important in more accurate forecasting of mixed layer dynamics, and hence the entire range of fluxes of heat, momentum, and energy between the ocean and the atmosphere.

As indicated, the dynamics of capillary waves have a central function in radar return from the ocean surface at angles greater than 10° from the vertical. Field measurements of capillary waves are extremely limited at the present time and must be developed. Recent laboratory measurements of capillary waves by Shemdin et al. (ref. 3–37) verify the existence of strong interactions between capillary waves and long gravity waves. Wright and Keller (ref. 3–38) more recently placed an X-band Doppler radar over the same laboratory facility and found that the return from the water surface is strongly modulated by the long gravity waves. Sufficient evidence already exists that suggests that radar return is governed not only by wind but also by all physical and dynamical factors that control the generation and decay of capillary waves.

The imaging radar detection of long gravity waves is another manifestation of the aforementioned observations. Although the wavelength and direction can presently be obtained from the imaging radar, wave height is not yet obtainable. Research into the dynamics of capillary wave modulation by long waves and the effect on surface backscatter may be useful in relating heights of long gravity waves to the modulation of the capillary wave backscatter over the wave profile. Photographic methods exist (ref. 3–39) by which directional wave-number spectra of long waves can be obtained. The aim must be to develop the methodology by which the imaging radar information can be treated as an all-weather "photograph" from which directional wave-number spectra can be extracted.

The full utilization of active microwave instruments for remote sensing will require a comprehensive program of basic studies of physical phenomena, evaluation of instruments, and comparisons with sea truth. The basic studies must include the response of instruments to wind and capillary waves in the presence of long gravity waves, currents, and surface agents. Field and laboratory programs will both help toward this end. Of paramount importance will be the availability of an adequately instrumented field station to monitor wind, capillary and gravity waves, currents, temperature, and surface tension. Airborne microwave instrument measurements can then be compared directly to the sea truth to delineate the various factors influencing the return.

The existing capability to predict ocean waves is primitive compared to what might be done subsequent to further development of satellite microwave instruments as remote sensors. The potential can only be realized

in conjunction with numerical models, because the satellite coverage will not be frequent enough to monitor continuously the rapid changes normally encountered in storms. The periodic coverage will be best utilized to improve numerical models, which then become useful on an operational basis with continuous updating of new information.

WINDSPEED

From a historical standpoint, airborne remote sensing for oceanography began in January 1785 with the first balloon flight over the English Channel, from Dover, England, to the forest of Guines, France. However, the only remote-sensor system available at that time, and for a long time to come, was the human eye. The only observable phenomena probably seen on the sea surface by the observers were surface waves and whitecaps. At that time, the balloon flight itself was more important that any observations made. It is interesting to note that, once again, lighter-than-air craft are being considered as a platform for remote-sensing experiments.

In the early 19th century, technology had not yet advanced to the point at which instrumentation existed for the purpose of measuring windspeed and wave height. Probably the oldest and best known of the relationships between windspeed and wave height is the Beaufort wind scale (table 3–III) designed by Admiral Sir Francis Beaufort in 1805. The scale was based on the effects of various windspeeds on the amount of canvas that a full-rigged frigate of the period could carry. Table 3-III, a condensed modern version of the original Beaufort scale, describes the sea surface appearance as a function of windspeed.

With the development of the cup anemometer in the second half of the 19th century, (supposedly) accurate information on windspeed could be obtained. Although other, more accurate wind-measuring systems have been developed through the years, data from any windspeed sensor located on the sea surface should be considered with caution.

Ever since man has been able to estimate or measure windspeed and wave height, he has attempted to form some empirical rela-

TABLE 3–III.—*Condensed Version of Beaufort Wind Scale*

Beaufort number	Definition	Windspeed, m/sec	Description of effects on sea surface
0	Calm	Under 0.5	Sea mirror smooth.
1	Light air	0.5 to 1.5	Ripples present without foam crests.
2	Light breeze	2.1 to 3.1	Small wavelets; crests glassy but do not break.
3	Gentle breeze	3.6 to 5.1	Large wavelets; crests begin to break; occasional whitecap.
4	Moderate breeze	5.7 to 8.2	Small waves becoming longer; frequent whitecaps.
5	Fresh breeze	8.7 to 10.8	Moderate waves; many whitecaps.
6	Strong breeze	11.3 to 13.9	Large waves form; white foam crests more extensive; streaks develop.
7	Moderate gale	14.4 to 16.9	Sea builds up: streaks very noticeable in wind direction.
8	Fresh gale	17.5 to 20.6	Moderately high waves; well-defined streaks.
9	Strong gale	21.1 to 24.2	High waves; dense streaks.
10	Whole gale	24.7 to 28.3	Very high waves; sea surface appears white.
11	Storm	28.8 to 32.4	Exceptionally high waves; sea covered with large patches of foam.
12	Hurricane	32.9 or more	Air filled with spray and foam; sea completely white; driving spray.

tionship between the two. Probably the most famous of the studies was that of Sverdrup and Munk (ref. 3–40). For the first time, an attempt was made to relate windspeed to the significant wave height (the average of the one-third highest waves in a long sequence of waves at a given location) and predict the significant wave height at other locations from wind-velocity information. The significant wave-forecasting technique lends itself readily for computer application and, indeed, continues in operation on a daily basis by both the National Weather Service and the Navy's Fleet Numerical Weather Central. Unfortunately, the significant wave method is not able to fully describe what is occurring at the sea/air interface. For this purpose, the directional wave spectrum and momentum transfer rates are needed.

In the late 1940's, the English pioneered in experimenting with wave spectral processing, which led eventually to techniques for obtaining shipborne ocean-wave records with the Tucker meter. The wave spectral concept received added impetus from the superposition theory, which describes the sea surface as an infinite number of sinusoidal waves with different heights, periods, and phases all traveling in different directions. This theory is the basis for numerical prediction of ocean-wave spectra. Within 11 yr, many spectral forms were developed that purported to describe the limiting wave spectrum for a specific windspeed (i.e., a fully developed sea).

The fundamental requirement for producing accurate ocean-wave spectral forecasts is accurate wind velocity data over a dense data network. This data network is scarce at the present. In addition, the quality of available wind-velocity data is questionable. Numerous factors can adversely affect wind-velocity observations at sea as well as any unknown possible malfunction in the anemometer system itself. Some of these factors are the following:

1. Instrument sheltering: Mast-mounted anemometers could be sheltered by the mast and produce erroneous observations.

2. Anemometer height: Most anemometers aboard ships are not located at a standard height above the sea surface. Because windspeed does vary with elevation above the surface, windspeeds should be adjusted to a standard level.

3. Atmospheric stability: Atmospheric stability is important in determining how windspeed varies as a function of elevation above the sea surface. Stability is a function of sea-air temperature difference. Under neutral stability conditions, when the air and sea-surface temperatures are equal, windspeed varies logarithmically with elevation. This neutrally stratified air may range in thickness from a fraction of a meter to perhaps 1500 m in the extreme.

4. Ship motion: Ship motion will tend to truncate high- and low-windspeed estimates by changing the effective anemometer height; hence, the rougher the sea, the greater the effect. The wind-velocity vector must also now be corrected for the forward translation of the ship.

Windspeeds at sea are sometimes estimated by nonanemometer means such as the following:

1. Wind estimates from visual wave-height estimates: Observers would estimate the wave height and then correlate their observations with a windspeed/wave-height scale such as the Beaufort scale.

2. Whitecap density: The windspeed could be estimated from the percentage of whitecaps and foam present on the sea surface. Whitecap production begins with a 6- to 7-m/sec windspeed. At approximately 12 m/sec, the wind hurls the whitecaps downwind in the form of streaks.

3. Navigational estimates: Wind velocity could be estimated by vector addition from the position, heading, and drift of a ship.

Windspeed may also be inferred from the following other data:

1. Synoptic weather maps: Geostrophic and gradient winds may be estimated from surface weather maps where there are no ship observations.

2. Ocean-wave records: Windspeed may

be inferred from the variance of a wave spectrum obtained by spectrally analyzing an ocean-wave record.

From the previous discussion, one can see that the deficiency in oceanic wind data is due not only to technology but also to the paucity of ships at sea at any specific time. At no time are there more than six weather ships systematically obtaining ocean wave records on the world's oceans. Furthermore, there are no longer any weather ships flying the U.S. flag. The primary means for obtaining wave data at sea is by visual techniques. For the purposes of wave forecasting and describing what is occurring at the sea/air interface, visual wave observations are inadequate. A visual wave-height observation does not supply enough information. In addition, accurate visual wave-height observations are difficult to make in rough seas and at night.

The wave records obtained systematically at the six foreign weather ship locations have proved to be invaluable. Unfortunately, processing of these wave records for spectral content is delayed for as long as 30 days or more because each ship remains on station for several weeks and no processing facilities are aboard. Furthermore, not all the wave records are processed: those that are processed are not widely distributed and are mainly used for research. The processed wave records from the Tucker-type shipborne wave recorders yield only a one-dimensional spectrum. The most desirable method for ocean-wave prediction is the directional wave spectrum (i.e., the distribution of spectral wave energy with wavelength and direction). Although techniques exist for obtaining directional wave information, there remains no operational program (except in research experiments) for obtaining these data.

The orbiting of an active microwave sensor aboard a satellite has the potential for revolutionizing the methods by which global ocean wind and wave information are obtained and for improving the quality of presently obtained information. For both meteorologists and oceanographers, this could represent a great increase in the amount of global ocean wind and wave information to become available on a regular basis for both short- and long-range weather and wave prediction. The knowledge of Southern Hemisphere sea-surface conditions would improve tremendously, because little information is presently available from the Southern Hemisphere oceans by conventional means. Large-scale air/sea interactions between the Northern and Southern Hemispheres could be monitored and studied. Predictions of upper-air meteorological parameters would improve as a result of more reliable lower boundary (surface) input parameters. The total impact of an active microwave system orbiting the Earth cannot now be determined; however, the process of monitoring and forecasting the marine environment could be revolutionized by having such a system in orbit.

To provide the most meaningful information about global-scale ocean winds and waves, certain minimum specifications are required for parametric values (table 3–IV).

TABLE 3–IV.—*Sensor Specifications for Remote Sensing of Surface Winds and Waves*

(*a*) Deep Water (global)	
Surface winds:	
Velocity, m/sec	2 to 50 (±2 or 10 percent)
Direction, deg	0 to 360 (±20)
Field of view, km	20 by 20
Sample intervals, km	250
Waves:	
Length, m	50 to 500 (±25)
Direction, deg	0 to 360 (±10)
Height, m	0.5 to 30 (±0.5 or 10 percent)
Field of view, km	20 by 20
Sample intervals, km	250
(*b*) Shallow water (local)	
Surface winds:	
Velocity, m/sec	2 to 50 (±2 or 10 percent)
Direction, deg	0 to 360 (±5)
Field of view, km	3 by 3
Sample intervals, km	50
Waves:	
Length, m	50 to 500 (±25)
Direction, deg	0 to 360 (±5)
Height, m	0.5 to 30 (±0.5 or 10 percent)
Field of view, km	3 by 3
Sample intervals, km	50

Active microwave technology has not yet been proved capable of providing information over the entire windspeed range recommended. As a result, a complementary multifrequency passive microwave system should be part of the total sensor package aboard a given orbiting satellite. This system would allow more complete coverage of the required windspeed range, although greater complexity is necessitated by the inclusion of a passive system. The incident angle, polarization (preferably both horizontal and vertical), frequency, and atmospheric attenuation become important factors to be considered. Before operational deployment of such a combined system, a breadboard version should be tested aboard the Space Shuttle or as a scientific experiment aboard another satellite.

Information on global sea-surface conditions has many applications. Accurate sea-surface conditions are important to commercial fishing, both near shore and in the open ocean; naval operations; optimum-time ship routing; search-and-rescue operations; deep-sea and near-shore drilling operations; long-range weather prediction; hurricane detection, tracking, and prediction; near-shore recreational activities; and further scientific research. Within these major categories are numerous smaller categories. Essentially, a satellite system providing global wind and wave information on an operational basis will be immediately cost effective. Such a global ocean system has long been awaited by meteorologists and oceanographers.

INTERNAL WAVES

The existence of modes of internal oscillation in a stratified fluid has been known since the early part of the century, when such waves were postulated to explain the phenomena of "dead water" in Norwegian fiords. An internal wave is simply a trapped gravity wave propagating in a medium having vertical density variations, with the normal gravitational restoring force reduced by the buoyancy presented by the density changes. The dominant mode is a low-frequency, low-speed oscillation that exhibits very little surface amplitude but appreciable horizontal surface velocities.

Internal waves can be generated by a variety of mechanisms. Wind stress that excites a spectrum of surface gravity waves is one source; the surface waves scatter and form an interference pattern that is felt at depth, thereby generating an internal wave that propagates freely. Another mechanism is the scattering of tides by bottom roughness or depth discontinuities presented by the edges of continental shelves and island areas. A third mechanism is shear-flow instability caused by current systems such as the Gulf Stream.

The usual method for observing internal waves involves towing thermistor strings through the water to sense the associated temperature variations. Recently, Apel et al. (ref. 3–41) have shown that periodic surface slicks seen in ERTS–1 images serve to "tag" the underlying internal wave and thereby render them visible on a synoptic scale for the first time. Such slicks are probably due to the concentrations of oils arising from the convergence of wave-associated surface currents mentioned earlier. The oil damps the small capillary wave structure that is largely responsible for variations in the optical reflectivity of the surface. The periodic nature of the internal waves then leads to periodic surface slicks, which are a familiar sight at sea, especially on the Continental Shelf. In shallow water (200-m depth), these slicks usually appear in packets of a few kilometers in extent and consist of individual striations spaced at 500 to 1000 m. The slicks are generally oriented parallel to the local bottom topography.

Because changes in X-band radar reflectivity of the ocean surface result from essentially the same sources as do changes in optical reflectivity (i.e., capillary wave variations), one would expect internal wave-slick patterns to be visible to an imaging radar under conditions similar to those occurring for visible radiation.

Whether such waves have ever been observed on radar images is not known; nor is

it readily apparent what frequencies, polarizations, or incident angles are needed. However, an estimate is obtainable from the variation in radar cross section with windspeed and incident angle. From unpublished curves of radar cross section available elsewhere in this study, one deduces that, for windspeeds below perhaps 5 m/sec, X-band frequencies at incident angles from 15° to 35° might be suitable. Resolutions of 10 m on the ocean surface should be more than adequate.

Further vague indications also exist that deepwater internal waves may leave very subtle signatures that might conceivably be visible with imaging radar. Observations of this sort would represent a significant advance in the understanding of an important oceanic phenomenon.

LAND/SEA INTERACTION

Land/sea interactions are most pronounced on the Continental Shelf and in the vicinity of islands. An estimated 90 percent of man's ocean activity occurs in water depths shallower than 30 m. In this region, the wave climate represents the single most important environmental factor affecting offshore planning and design. Tides and currents are equally important for navigation, fishing, and recreation. The Continental Shelf has a width scale of approximately 100 km and a mean maximum depth of less than 200 m. Around islands, ocean/land interaction can occur over a region 500 km along a given dimension.

Significant modification of the wave climate occurs in shallow water through shoaling, refraction, bottom friction, and breaking. In the presence of sharp discontinuities, wave diffraction is dominant in spreading the wave energy. Available procedures for wave forecasting are predominantly for deep water. The state of the art for extending deepwater forecasts to shallow water is in the embryonic stage. Isolated procedures exist for evaluating refraction and diffraction of simple waves. Attenuation of waves by bottom friction has been assessed with the aid of quadratic friction coefficients, which have been shown not to be completely satisfactory. Combined refraction and diffraction schemes have also been tried for single wave components. Directional spectra methods are being developed by the oil industry, but the results have not been published.

The use of remote-sensing methods can aid in providing significant information on the transformation of wave direction across a continental shelf. The return from a radar image can provide an all-weather photograph of waves over the entire region from deepwater to shore. Existing refraction and diffraction schemes can be verified. A low-altitude altimeter with a 3- by 3-km spot size can provide wave-height information along a path transecting the shore.

The catastrophic changes imposed on the shoreline by major storms in the coastal regions are obvious because the changes occur rapidly. Such monitoring of shoreline changes is particularly suited to observation by radar systems, which can assess shoreline damage and changes even before the storm has subsided enough to permit visual observation.

In addition to this use for storm damage assessment, aerospace radar systems are applicable to shoreline form analysis. During the last decade, there has been increasing scientific interest in alongshore variations in coastal processes and their relationship to rhythmic and crescentic beach morphology, shoreline erosion, and overwash processes. Efforts are underway to formulate the physical processes responsible for the alongshore variation; however, research is needed to characterize the beach features, their distribution in both time and space, and their relationship to erosion trends and overwash processes. Alongshore variations in coastal processes and shoreline form were not under investigation until the 1950's. Consequently, only recently have the effects of these dynamic features on the beach dune system been recognized. Aerial photographs of the coastline have assisted in this recognition. Radar imaging systems can extend the observation.

The study of shoreline form is far more than an academic exercise. Briefly, significant alongshore features of sandy coasts are cusp-like forms of that shoreline called shoreline sand waves, which migrate along the coast. The wavelength of the features range from approximately 100 m to 10 km. The larger sand waves are fundamental to the stability of the shoreline; therefore, the success or failure of the several types of costal engineering structures and facilities depends on an understanding and surveillance of these shoreline phenomena. The shoreline sand waves are part of a hierarchical pattern, the elements of which are often superimposed. These elements include (1) small cusps, or cusplets, only 1 m across; (2) beach cusps, which are up to tens of meters in length; (3) the shoreline sand waves, or giant beach cusps already mentioned; (4) secondary cusps spaced from 25 to 50 km; and (5) cusps spaced from approximately 100 to 200 km. Dolan has shown (ref. 3–42) that sand waves are important in focusing the destructive power of storm surges and storm erosion damage.

In addition, these sand waves migrate approximately 200 m/yr along the mid-Atlantic coast. Accelerated erosion (associated with the passage of a shoreline sand wave embayment) can severely damage a barrier dune (if one is present), cause the loss of valuable shore property, or destroy structures located too close to the shore. Passage of the sand wave point, or horn, leads to propagation of the beach. The point of focus of storm surge energy is gradually changed. Thus, the forecasting of storm effects must be modified in accordance with shoreline changes.

A significant advantage of radar imagery over visual photography is the acquisition of both shoreline shape and wave-energy spectrum information. Thus, the interactive system can be studied. The application of active microwave techniques to the coastal region is more extensive than the specific task of storm damage interaction and assessment.

Optimum use of remote-sensing instruments will require coverage over a 100-km-wide area with a 3- by 3-km spot size over 10-km intervals. Wavelength measurements are needed in the range from 25 to 500 m, with height measurements to 20 m. Wind measurements to 50 m/sec, with a resolution of ± 2.0 m/sec, are desirable to monitor storm propagation across the Shelf. In the vicinity of islands, somewhat larger coverage, spot size, and sampling interval would be useful.

Further improvement in remote-sensing capability can be achieved by the comparison of remotely sensed data with high-altitude photographs in good weather. The presence of directional wave gages will aid in interpreting results. Direct measurements can be used to test existing numerical schemes for wave transformation in shallow water and to develop new ones.

The derived benefits from improved shallow water wave climate data will be primarily in beach erosion prevention and minimization of hazards along the shoreline. The design and placement of offshore structures such as nuclear power plants, deepwater oil ports, and oil drilling rigs will also benefit.

INLAND AND ESTUARIAL WATERS

The objectives of a study done by D. E. Bowker of LaRC were to define the needs in the coastal zone related to the four LaRC-established national priority areas of pollution, fisheries, hazards, and geography/cartography. The approach to this study was to fund four independent contractors—The Virginia Institute of Marine Science (VIMS), Old Dominion University (ODU), TRW Systems Group (TRW), and Ocean Data Systems, Inc. (ODSI)—to study the problem. The results are summarized in appendix 3B.

PART D

LARGE-SCALE PHENOMENA

This section deals with oceanic phenomena with horizontal scales from approximately 100 km up to the widths of the oceans themselves. Their very size makes these phenomena difficult to monitor by surface-based methods, so that satellite-mounted active microwave techniques are especially valuable and may be the only way of gathering the information needed for scientific progress.

An important class of large-scale features consists of those concerned either directly or indirectly with the vertical topography of the ocean surface, estimated from the center of the Earth. This class includes the shape of the geoid, which is determined by the internal mass structure of Earth; the quasi-stationary anomalies due to spatial variations in sea density and steady current systems; and the time-dependent variations due to tidal and meteorological forces and to varying currents. These features are discussed in subsequent sections. All these features make use of the techniques of radar altimetry, although currents can also be studied by satellite tracking of floats.

Certain large-scale phenomena could, in principle, be usefully observed by satellite altimeters; however, it is unlikely that the necessary precision (approximately 1 cm) could be obtained in the near future. Steric variations in sea level, due to time-dependent changes in water density, notably at annual and semiannual periods, are known from shore-based tide gages to have amplitudes of less than 10 cm in most parts of the ocean. Tsunamis sometime reach meters of amplitude at a coastline, but in the open ocean where they would be most useful to measure, they merely consist of long waves of a few centimeters' amplitude and some tens of kilometers' wavelength. Prospects for detecting tsunamis by altimetry are discussed by Greenwood et al. (ref. 3–43).

MARINE GEODESY

Background

The primary function of geodesy is to determine the shape of the Earth by carefully measuring the geometric distance between points on its surface. For years, this approach seemed to be satisfactory because the surveyed areas were limited to portions of continental crusts and the measurements were not required to consider the micromovements of the solid Earth crust, which was considered as a perfectly rigid body. Problems related to the choice of a common reference datum for all those local determinations were approached through the use of a theoretical surface called the geoid, which is an equipotential of the Earth gravity field.

The geoid on land is not a physical surface; it is determined through a numerical process that involves the computation of an integral of gravity anomalies called the Stokes formula. The geoid on the oceans was long considered to be in coincidence with the physical surface of the sea (refs. 3–44 and 3–45).

During the last 10 yr, the problems of geometric geodesy have been extended to the open oceans mainly through the needs of accurate navigation and positioning. Marine geodesy has appeared as a separate scientific endeavor because most of the hypotheses of practical "land" geodesy were found to poorly match the physical properties of the ocean environment. At the same time, the accuracies of the available instruments for distance measurements were drastically improved so that movements of the crust of very small amplitude had to be considered.

Presently, serious difficulty is encountered in coping with the shape of the Earth per se, and marine geodesy must be concerned with four important surfaces (ref. 3–46): the physical surface of the Earth crust, the phys-

ical surface of seawater, the geoid, and the mean sea level.

The physical surfaces are experimentally accessible but the others are concepts with definitions that unfortunately tend to vary slightly from one author to another. Following is a brief overview of the problems encountered when dealing with those surfaces.

The physical surface of the Earth crust.—The Earth crust is the solid surface of Earth, including that portion underlying the seas and the oceans. Long regarded as perfectly rigid, the Earth crust is, in fact, the outer shell of a "pulsating" elastic medium in everlasting slow movement. Those displacements are essentially as follows:

1. The solid Earth tides (20 to 40 cm, vertical).
2. The continental drift (a few centimeters a year, horizontal).
3. Movements caused by earthquakes and fault displacements (a few centimeters to a few meters in any direction).
4. Tilt of coastal areas caused by the rising and falling of ocean tidal motions (a few centimeters in any direction).
5. Movements caused by the modification of loading conditions on the crust (erosion-sediments piling).

Some of those effects would have to be considered very carefully when using a radar altimeter with a 10-cm resolution capability.

The physical surface of the sea water.—The water surface changes position for many reasons, some of which are ocean tides; air pressure; winds; temperature, density, or pressure gradients; movements caused by sudden variations in the physical surface of the ocean floor (earthquakes, fault displacements); and geologic changes associated with the melting of glaciers (ref. 3–47).

This fast-moving surface is obviously difficult to match with the present concept of the geoid over the open seas; a fresh look at the problem is badly needed. Other important interactions that may occur between the two surfaces are the cross-coupling of ocean tides and solid Earth tides and the movements of the sea surface due to movements of the ocean floor. Both these interactions tend to be very difficult to decipher in the coastal zone areas.

The geoid.—The only satisfactory definition of the geoid from the mathematical viewpoint is that of an equipotential of the Earth gravity field with a certain absolute potential. However, an empirical approach has been imposed by practical considerations so that local geoids have been defined by each national geodetic agency as equipotential surfaces passing through a defined point (datum point), usually chosen in the countries having oceanic borders near the mean sea level. Unfortunately, those local geoids do not coincide over the total surface of the Earth because the datum points have not been chosen on the same equipotential.

One of the greatest contributions of satellite altimetry (using coast-to-coast tracking across the Atlantic Ocean) will be to provide experimental data ultimately useful in the choice of a common datum for North America and Europe. This datum should be chosen as a reference for the North Atlantic marine geoid.

Three ways of mapping the shape of the geoid are available today.

1. Measurement at sea of gravity and integration through the Stokes formula.
2. Measurement at sea of the vertical deflection of gravity and integration through the Veining-Meinez formula.
3. Measurement of the altitude of a satellite over the physical surface of the sea leading to the shape of the geoid with the use of appropriate correction and filtering of the data.

Gravity at sea cannot be measured, in the foreseeable future, to an accuracy better than 0.01 m/sec^2, thus leading to uncertainties in the geoidal heights computed from the sea of at least a few meters. Deflections of the vertical could be measured to an accuracy of 0.5 sec of arc with the GEON system (ref. 3–48) and to a few seconds of arc using an inertial navigation system (ref. 3–49).

The wealth of geoidal information available from radar altimetry has been ade-

quately demonstrated by data from the Skylab S193 altimeter experiment (ref. 3–50). Figures 3–25 and 3–26 are two examples. Figure 3–25 shows the profile of the Puerto Rican trench area, which represents a mass deficiency, and figure 3–26 shows the effect of a sea mount, which corresponds to a mass concentration. Because the geophysical value of such information is well known, this discussion will be directed toward geoidal feature resolution available from altimetry.

To discuss the large-scale resolution capabilities of radar altimetry, it is first necessary to examine geoid spectrum and altimeter-related characteristics. Figure 3–27 shows a geoidal power spectral density of the Puerto Rican trench area, computed by using Skylab S193 data from McGoogan et al. (ref. 3–50) and Miller and Brown (ref. 3–51). This area was selected because it should contain short-wavelength components of substantial magnitude; therefore, the analysis should yield an approximate upper boundary on geoidal data processing requirements for GEOS–C. Figure 3–28 shows the spatial filter transfer function of the altimeter, which was computed based on the specific tracking system used in the GEOS–C altimeter. The minimum-mean-square linear filter for processing altimeter data may be derived based on the power spectrum and spatial filter models discussed and on known altimeter random error characteristics. Optimum impulse response functions are shown in figure 3–29. Referring again to figure 3–27, the half-power bandwidth of the optimum filter is seen to be 40 km for the GEOS–C design.

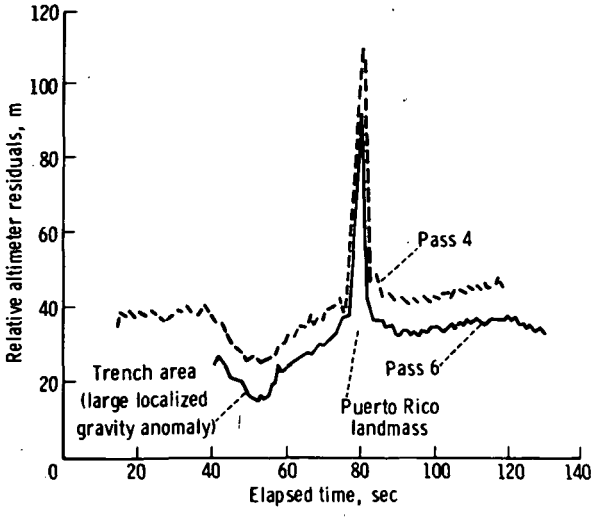

FIGURE 3–25.—Geoidal profile of the Puerto Rican trench area from Skylab passes 4 and 6 (ref. 3–48).

These findings indicate that future altimeter systems will be able to provide substantial improvement in resolution of features to wavelengths as short as 5 km.

The mean sea level.—The geodesist, looking for a reference surface from which land heights could be measured, adopted the average height of the ocean surface in coastal areas as defining segments of its reference surface, the hypothesis being that the geoid and the mean sea level coincide all along the coastal lines.

The basic idea was that proper averaging in time of tide gage logs taken in ports along the coast would provide reliable estimates of the true position of the geoid. Coastal geodesists have developed complex schemes for filtering out all tidal influences. Unfortunately, other systematic effects are still present in their computations. It is well known that a 10-m discrepancy exists between the two ends of the eastern coast of the United States. High correlations of the residuals with atmospheric pressure variations (ref. 3–52) have been noted by oceanographers all along the Mediterranean coast.

The mean-sea-level computations could be corrected with radar altimeter measurements, but this is a very difficult task indeed. Radar altimeters take instantaneous profiles of the physical surface of the sea, whereas mean sea level is computed from time logs taken at fixed points. The only method of comparison would be by the averaging of many profiles measured by the altimeter. Such a time-consuming task would only be fulfilled many years from now after many successful launches of radar altimeters aboard satellites.

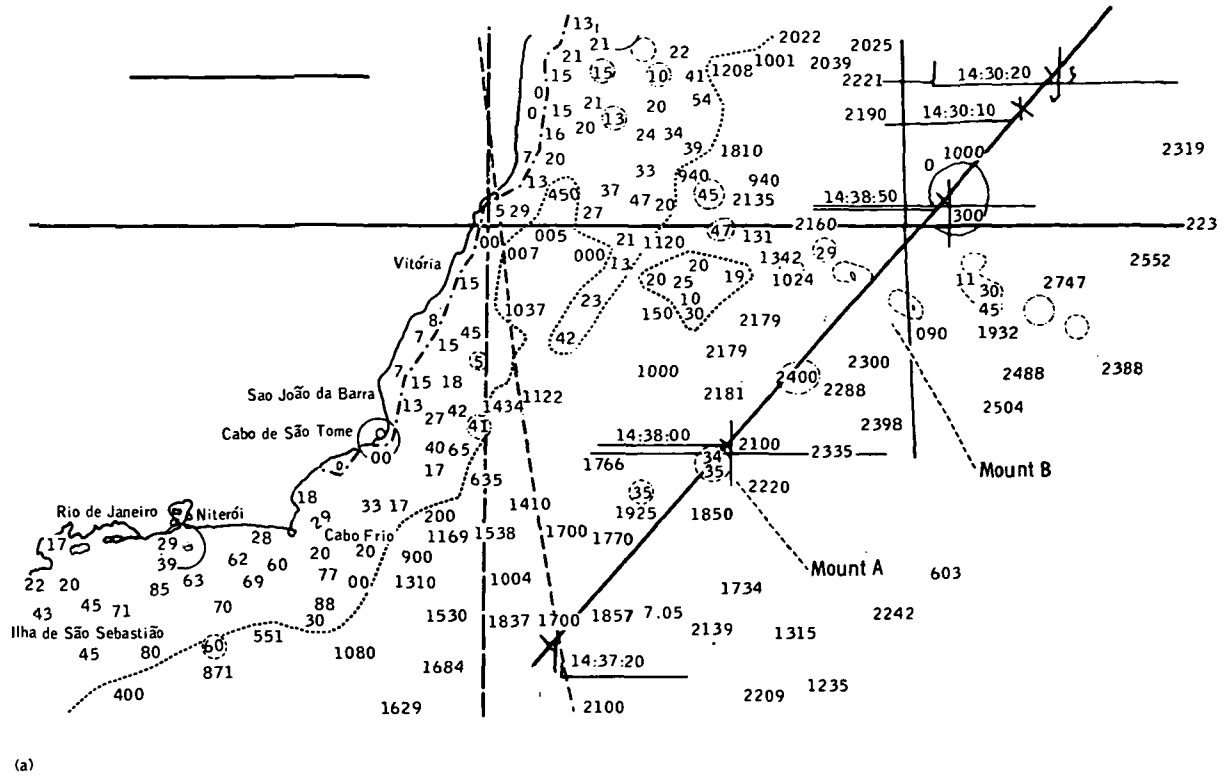

FIGURE 3–26.—Effects of subsurface features on altimeter data; Skylab 3, pass 11. (*a*) Geographic area and ocean bottom topography (numbers indicate water depth). (*b*) Altimeter relative profile.

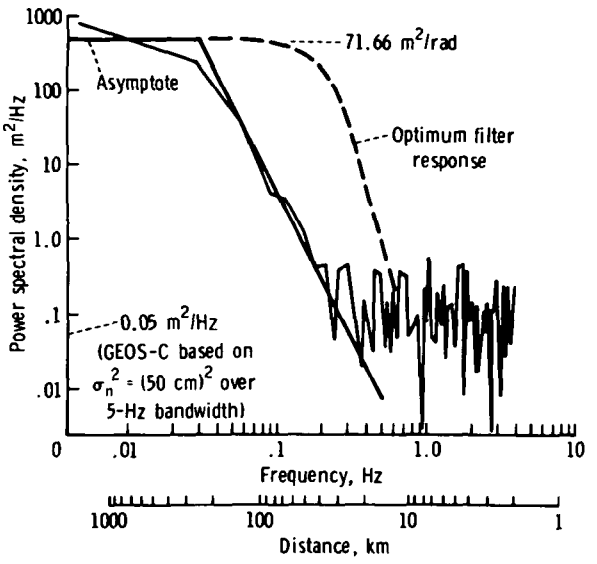

FIGURE 3–27.—Geoid undulation spectrum of Puerto Rican trench and Wiener filter transfer function.

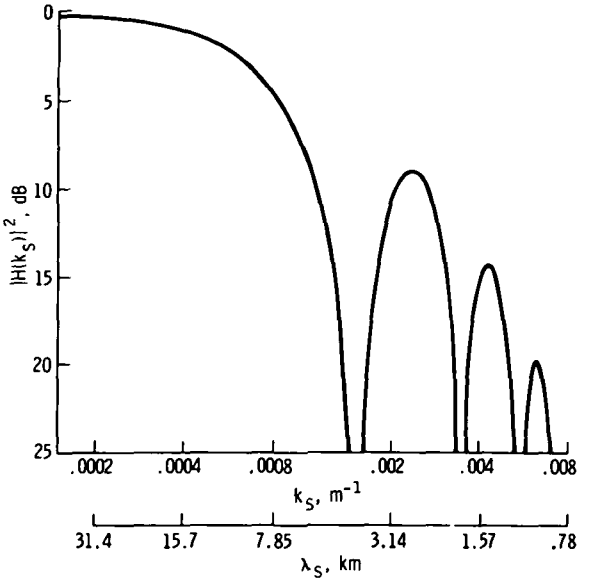

FIGURE 3–28.—Spatial filter transfer function, where altimeter altitude is 440 km and antenna beamwidth is 1.5° (rectangular gate). (From ref. 3–50.)

Figure 3–30 presents ideas on how an integrated system for marine geodesy could be built around the short-arc coast-to-coast tracking of a radar altimeter. Signals T_1, T_2, and T_3 are time references transmitted by the satellite to synchronize all the ocean and Earth tides logs.

Applications

The need for high-accuracy geoidal information to support studies such as crust deformation and solid-Earth models is well known (ref. 3–53). Marine geodesy is concerned with two main applications: the positions of objects on the Earth solid surface in a marine environment, and the average position of an object on the water surface.

Requirements of users for each category are summarized in tables 3–V and 3–VI (ref. 3–54) and are expressed in terms of needed precisions in geocentric (ϕ, λ) position and height (h) above the geoid. Many of the specifications can only be fulfilled if a marine geoid has been determined with a relative precision of better than 1 m ($\approx$50 cm) and an absolute precision of a few meters ($\approx$5 m).

A secondary requirement for high-accuracy ($<$10 cm) geoidal information is that of supporting ocean topography activities. If oceanographic applications of remote-sensing activities are to achieve their full potential, it will be necessary to define the geoidal, or permanent, contours to a resolution comparable to the magnitude of oceanographic effetcs.

OCEANIC TIDES

Historically, tidal research has concentrated on the immediately practical problems of computing tide tables for the major ship-

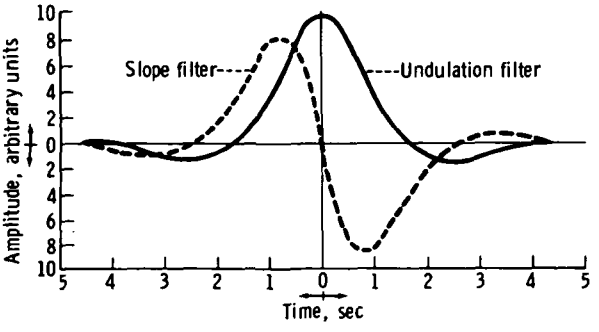

FIGURE 3–29.—Derived weighting function for geoidal data processing.

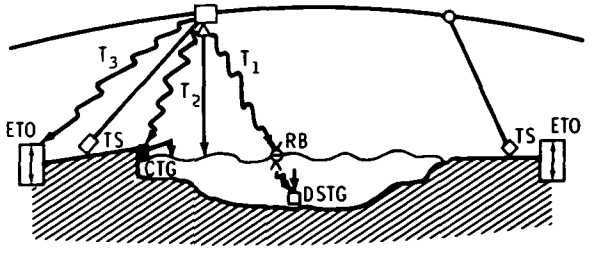

TS = Tracking station (laser)
ETO = Earth tides observatory
CTG = Coastal tide gage
DSTG = Deep sea tide gage
RB = Time relay buoy
T_1, T_2, T_3 = Time references

FIGURE 3–30.—Concepts of an integral coast-to-coast radar altimeter system for marine geodesy.

ping ports. Unfortunately, this can be done quite accurately by a purely empirical process that teaches one almost nothing about tidal dynamics. Since the work of the 18th- and 19th-century French mathematician, Laplace, it has been clear that the proper understanding of tidal dynamics demands a knowledge of the tides in the open ocean, where they are generated by the Newtonian gravity field of the Moon and the Sun. Such knowledge would not only be a fundamental contribution to oceanography but would also, in principle, enable the computation of the propagation of tidal energy into the shallow seas and estuaries and, hence, give predictions of both tidal elevations and streams in any location that may be required for future practical purposes.

No one has yet succeeded in attaining this knowledge. Computing the disturbing gravitational field that drives the system is fairly easy, and Laplace's field equations have been written in countless learned scientific papers, but their solution for the complex geometry and topography of the actual ocean presents great difficulties. The difficulties arise partly from the large number of possible normal modes of oscillation, partly from the fact that all the ocean basins interact (so that partial solutions for a single ocean are impossible without independent tidal measurements around its entire boundary), and partly from the necessity to model the dissipation that is concentrated in the intricate network of shallow seas. Analytical solutions in geometrically defined basins are only of qualitative value. Numerical solutions for actual ocean topography tax even the largest modern computers and ultimately only show the extreme sensitivity to fine topographical detail and to the yielding of the Earth crust, factors previously considered negligible.

The lack of definitive global maps for the oceanic tides is a major lacuna in modern geophysical knowledge. Apart from the intrinsic interest in defining the response of the ocean to the known gravitational forces and the driving mechanism for the co-oscillating tides in all the shallow seas, reliable tidal maps are fundamental to the solution of a

TABLE 3–V.—*Positions of Motionless Objects on the Solid Surface of the Earth*

Activity	Precision, m		Absolute (A) or Relative (R)
	ϕ, λ	h	
Coastal landmarks	1	0.5	R
Island positioning	20	20	A
Deap sea mining	10	3	A
Drilling platforms	20	—	R
Shallow water topography	20	—	R
Geologic mapping	50	—	R

TABLE 3–VI.—*Average Position of an Object on the Surface of the Water*

Activity	Precision, m		Absolute (A) or Relative (R)
	ϕ, λ	h	
Oceanographic buoys	70	—	A
Oceanographic ship on station	35	—	A
Drifting buoys	50	—	R
	200	—	A
Oceanographic vessel en route	100	—	R
Submarine cable operation	100	—	R
Hydrographic vessel on station	5	—	R
	70	—	A

number of other geophysical problems. Researchers on tides of the Earth and of the atmosphere, on geomagnetisms, and on the momentum balance of the Earth rotation are increasingly finding their work hinging on the oceanic tides. They turn to the oceanographers, who are unable to supply the required data.

State of the Art

Approximately six maps of the M_2 tide (lunar semidiurnal constituent) exist that have been computed for most of the world's oceans in recent years by various methods and assumptions. Assumptions vary, but the most fundamental divisions occur (1) between those who force the solutions to agree with assumed continental boundary tidal conditions and those who eschew the use of all empirical data, and (2) between those who attempt to allow for crustal yielding and those who assume a rigid Earth. (For a modern review, see Hendershott (ref. 3–55).) Two of the most authoritative and advanced results are compared in figure 3–31. They are in fair agreement on certain features, such as the tidal configuration in the North Atlantic, but their results for the South Atlantic are quite different. Such disagreement, here and in other oceans, is typical of all cotidal maps to date. Ironically, it is extremely difficult even to obtain the measurements necessary to find out which interpretation, if any, is correct. Maps of the diurnal tides are rarer, but those that are published show a similar lack of agreement.

Much of the controversy about global tidal computations centers on ocean/land interaction, which is rather complicated, but there are also limitations due to the lack of proper information to be fed into the computer model from the boundaries bordering shallow seas. A typically crucial area for the Atlantic Ocean appears to be the Patagonian Shelf, but reliable data from here and many other places are sparse. Computer models would also benefit from measurements across transoceanic sections, which would provide boundary conditions for separate evaluation of smaller zones. Isolated spot measurements at certain places where the tidal amplitude is known to be large would also be valuable.

Seabed pressure sensors for measuring tides in the open sea have been increasing in numbers over the last decade, but they are expensive devices with a high risk of loss and require expert supervision and many ship deployments. The sensors are supported only by a few nations that have well-developed oceanographic technologies; thus, the chances of obtaining data in the foreseeable future, from most of the Southern Hemisphere at least, are remote. To date, the only tidal data that have been taken from the open sea (apart from islands) have been from within a few hundred kilometers of North America, Northwestern Europe, and South Australia. Monitoring the tides in all the world's oceans by direct measurement, or even obtaining the minimal data that might enable computation, is not possible at this time.

Radar altimetry from spacecraft will transform the measurement situation. The difference between satellite range and altimeter height above the sea surface, suitably corrected for various biases and errors, will vary from a variety of causes discussed elsewhere in this report (ref. 3–45). The variables may be divided into (1) permanent or quasi-permanent features of ocean topography, (2) features that vary in time at any given Earth location, and (3) tracking and other errors. Variables of type (1), including the geoid and steady dynamic features, although approximately 1 to 100 m, can in principle be extracted either from independent knowledge or, in due course, by averaging from repeated satellite passes. Variables of type (2) include the tides, up to approximately ± 2 m in amplitude, and also include random variations caused by the weather, on the order of 0.1 to 0.3 m. (Transients such as surges and tsunamis may be ignored in this context because their amplitudes are appreciable only in shelf seas.) A large proportion of the weather influence is a direct reflection of atmospheric pressure at 1 m of sea level per N/m^2. This can be removed by means of

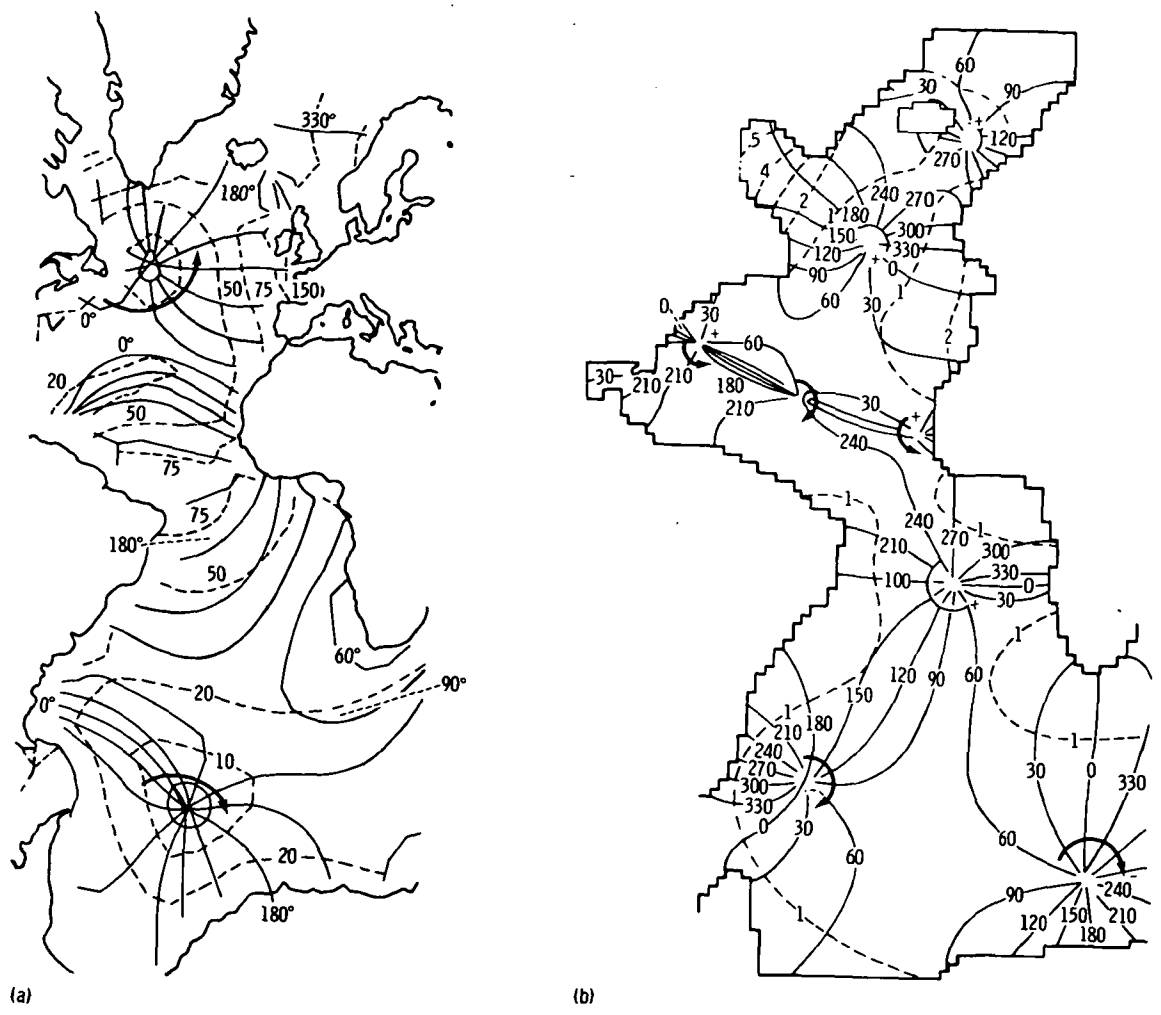

FIGURE 3–31.—Cotidal maps of the Atlantic Ocean using different methods and boundary conditions. (*a*) Cotidal maps computed by Pekeris and Accad, 1969 (ref. 3–56). (*b*) Cotidal maps computed by Hendershott, 1972 (ref. 3–55).

synoptic meteorological data computed on land. The residual signal will therefore be considerably tide dependent, provided variables of type (3) are well below 1 m. This dependence is further enhanced by using the strong coherence that exists between any oceanic tidal variable and the perfectly calculable tide-generating potential of the Moon and Sun (ref. 3–57).

Requirements

As in all applications of satellite altimetry, the only basic requirement demanded is accuracy of the interpretable signal. Because modern trends in altimeter design enable its accuracy to be reduced to a few centimeters, the major requirement is in the accuracy of orbital tracking over as wide a global coverage as possible. Stating minimal requirements outside the context of discussion of approaches to various problems is difficult, but the situation may be summarized as "given any reasonable accuracy, one can expect to learn so much tidal information and no more." With 1- to 2-m accuracy, there is some hope of gaining useful information about the oceanic regions with largest tides, such as

parts of the North Atlantic. With 0.5-m accuracy, one should certainly obtain good information from such regions and could hopefully consider wider oceanic fields. Complete tidal definition over the world's oceans would require 5- to 10-cm accuracy. In any case, continuous signals for many months or years are assumed.

An altimeter "footprint" of approximately 100 km should be adequate for most tidal work in the deep ocean. To resolve the smaller horizontal scale of tides in most shelf seas, resolution better than 20 km would be needed.

Technical Approach

At some stage in the interpretation of the altimeter tidal signal, one will have to allow for the fact that the signal differs fundamentally from the usual land-based concept of the ocean tide. If z' is the anomaly in sea level sensed by a tide gage, that sensed by the altimeter is $z=z'+z''$, where z'' is the tidal elevation of the Earth crust, approximately 0.2 m. (See ref. 3–55 for a full dynamical discussion.)

A large part of z'' consists of a direct yielding of the body of the Earth to the gravitational forces, which is easily calculable, but there is a smaller residue of approximately 0.1 m that can only be calculated in terms of global integrals of the ocean tide itself (i.e., the "loading tide"). Clearly, for some purposes, one can interpret z in terms of z' merely by approximating to z'' by the simple body tide, with small loss of accuracy. For higher precision, a fair approximation to the loading tide could be computed from one of the existing rough cotidal maps. The entire situation procedure is, in any case, one of successive approximations.

Two possible approaches to data analysis are possible. One method relies on obtaining many traverses of a given track zone; that is, for example, 500 km wide. After correcting for the geoid (which preferably should not vary too steeply in the chosen area), for atmospheric pressure, and for any other known anomalies, the successive altimeter readings in any 500-km-square section are treated as a signal that is partly coherent with both the diurnal and semidiurnal parts of the tide-generating potential, calculated at the appropriate times, together with a random noise due to tracking errors. One would attempt to extract perhaps as many as eight arbitrary constants to describe the coherent signals in terms of "admittances" to the potential, with one further arbitrary constant to absorb a residual error in the geoid.

Applying numerical filters aimed at isolating the M_2 tide is similar in principle (ref. 3–58). With orbital height errors of approximately 0.5 m and tidal amplitudes of approximately 1 m, one could obtain solutions of reasonable accuracy from about 50 passes. Larger numbers of passes give greater accuracy or permit more refined definition of admittances. Several possible variants could be considered. The admittances could be treated as arbitrary functions of distance along an entire oceanic track, or as localized functions of two dimensions, constrained to satisfy the tidal dynamical equations. In some places, the diurnal tide could be ignored. The ultimate result would be empirical tidal measurements in a network of grid areas covering a chosen zone.

The other approach would be to compare every traverse of an ocean, on whatever track, with the corresponding simultaneous solution of a given computer model of oceanic tides, again after removing the major part of the geoid and other variations assumed known. The residual variance about space-located averages would be compounded because of tracking errors and errors in the computer model. The computations would be repeated for the same data with variation of frictional and other uncertain parameters in the model until the residual variance was minimized. One could then say that the model output was "correct" for the ocean area considered, and a refinement of the geoid would also result.

In any approach to tidal analysis of altimeter signals, the accuracy of the solution will obviously be a function of the tracking

error variance divided by the number of track repetitions. Any means of reducing this quotient is beneficial and will extend the scope of any investigation; for example, to regions of smaller tidal range. With current practices, vertical errors can apparently be as little as 0.2 m in the vicinity of tracking stations, worsening to 1 to 2 m in areas remote from these stations. Increasing the number of tracking stations would have obvious advantages. However, oceanic zones exist where the tide is already known to an accuracy of 0.5 m or better, either from pelagic measurements or by approximate calculations where the tidal range is known to be very small. These zones could be used as "surface truth" to identify the tracking errors where they might otherwise be large. A program can also be envisioned of pelagic tidal measurements in oceanic zones selected for this purpose. (The surface measurements do not necessarily have to be taken simultaneously with the altimetry.) However, 0.5-m accuracy is hardly sufficient to resolve tidal signals in the controversial South Atlantic (fig. 3–31), where, according to island data, the amplitudes are approximately 0.3 m (ref. 3–59). Such areas would have to be computed from altimeter measurements along boundary zones where the tidal range is larger.

Applications

Finally, assuming that all errors can be reduced to useful levels and all the analysis has been done, what applications would knowledge of ocean tides have, both to science and to the practical world of mankind? The scientific uses have been outlined by Munk and Zetler (ref. 3–60), and their conclusions are restated here.

1. The knowledge of oceanic tides on a global basis is necessary to properly interpret nearly all geophysical measurements at tidal frequencies, including measurement of gravity, magnetic field, etc.

2. Measurements of oceanic tides will lead to improved tidal models and ultimately to improved calculations of tidal dissipation in the ocean, which, when subtracted from dissipation obtained from changes in the length of day, will yield the dissipation in the solid Earth. These measurements will provide important information concerning the plastic properties of the solid Earth.

3. Oceanic tidal currents, when coupled with electric and magnetic field measurements on the ocean bottom, can probe the conductivity (and thus temperature) within the upper mantle as a function of frequency (depth). Horizontal gradients of temperature should exist near volcanic belts, in areas of downthrusting plates, and at postulated upper mantle "hotspots."

4. Finally, the response of the Earth to the shifting weight of the oceans, as measured by Earth strain or tilt meters, gives information about the local elastic structure of the Earth. This, too, is expected to vary near margins of lithospheric plates.

Knowledge of oceanic tides at the boundaries of shallow land-bounded seas enables better computation of the tides and tidal streams in such seas for purposes of navigation of ships, tidal power-generating schemes, and flood warning (see the following section). The inland Earth tide, which requires the oceanic tide for proper computation, is of value to geodetic leveling, surveying procedures, and the accuracy of astronomical siting.

STORM SURGES AND WIND SETUP

Storm surges may be defined as transient anomalies in sea-surface elevation (and currents) caused by storms, with time scales in the region of 10^4 to 10^5 sec, horizontal scales of approximately 10^2 to 10^3 km, and vertical excursions as high as approximately 6 m. The associated currents may be regarded as determinable from the gradients of elevation and will not be considered here as independent variables. Storm surges are largely confined to shelf seas, partly because the dynamic effect of wind stress is inversely proportional to water depth, and also because critical wave speeds in shallow water are

comparable with speeds of propagation of weather systems, causing more efficient coupling with the atmosphere than with the deep ocean. Storm surges have been intensely studied in certain sea areas where they present a frequent danger of flooding to adjacent lowland, such as in the southern part of the North Sea, the Adriatic Sea near Venice, and the shelf seas bordering the Eastern and Southern United States. Flood danger also depends on the coincident state of the tide, and, to some extent, study of storm surges and local tides are inseparable.

An important ingredient of some storm surges is a quasi-static pileup of water toward the coastline, caused by the onshore wind stress and the radiation stress in the associated waves. This effect is usually called "wind setup." In some areas, where wind strength and direction persist for many days and coastal topography prevents the formation of steady currents, wind setup may form a steady deformation of sea level of some decimeters. However, although such a setup may not be thought of as a storm surge, its dynamics are not essentially different.

When tidal predictions were sufficiently well developed for sea level to be approximately partitioned into "astronomical tide" and "surge residual," researchers observed that the latter was to some extent a direct function of local weather and tried to express it as a simple linear regression of wind components and local atmospheric pressure. Results varied from passable to poor, and obviously neglected the spatial as well as the time history of the weather patterns and the transmission of energy from other parts of the shelf in the form of a free wave (sometimes called an "external surge"). More complex response operators, which take into account the spatial and temporal wind and pressure fields, have been developed with some success, but scientific practice has tended to veer away from such empirical approaches, whereby "prediction constants" are estimated from data by a least-squares calculation. The modern tendency is to predict storm surges by numerical solution of the wave equations over a network of small areas covering the shelf sea concerned; at each area, the three components of atmospheric stress are specified at regular increments of time.

State of the Art

Three examples of disastrous surges are shown in figures 3–32 and 3–33. Figure 3–32 shows elevations in the North Sea computed over a numerical grid from the dynamical equations. The surge of February 17, 1962, reached more than 3 m above tide level and caused severe flooding in the Cuxhaven-Hamburg area of Germany. Figure 3–33 shows the surge height, exceeding 7 m, along the U.S. gulf coast during the passage of Hurricane Camille.

The principal features and causes of storm surges are fairly well understood and, within certain limits, can be roughly reproduced by integrating the wave equations with driving stresses from the wind and pressure fields. But the demand continues for further research and information to help understand the finer scale features, such as their interaction with the tide and with coastal topography, and the response to unusual weather conditions. Because wind stress is the most important factor, success in predicting or understanding storm surges depends on the accuracy with which the winds over the sea can be specified. A serious hindrance to research is the lack of observational data of surface elevations offshore. With few exceptions, nearly all the observations of surges come from coastal tide gages, but these observations can give a distorted and/or limited picture of their main structure in the open sea because waves and currents cause steep gradients near the shoreline. Like the ocean tide problem, the logistics of offshore recording are difficult. Stormy shallow seas present a particularly hostile environment for recording equipment and data transmission systems.

Active microwave technology could help research on storm surges in two ways. Wind determination over the sea by the "scatter-

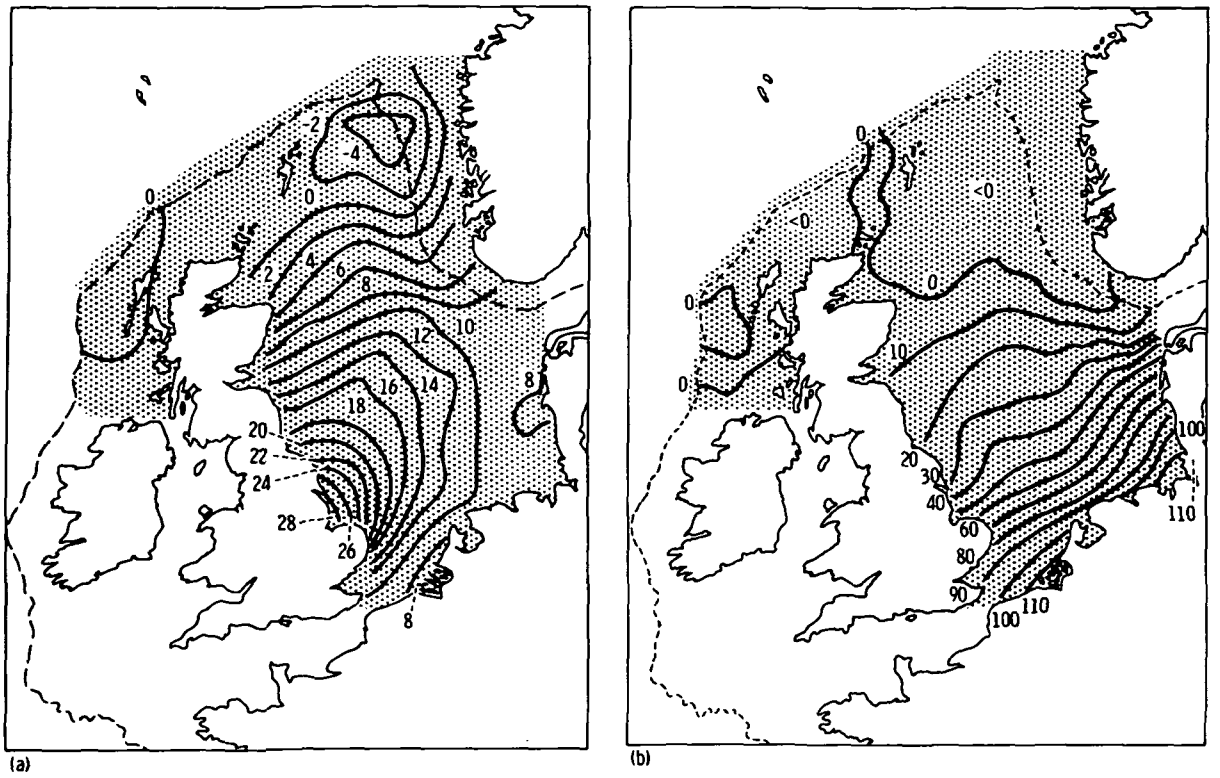

FIGURE 3-32.—North Sea storm surge. (*a*) September 14, 1962. (*b*) September 17, 1962.

ometer" technique would give a more accurate picture of the driving forces than is usually obtainable from computations based on the pressure field, and altimeter tracks over surge-ridden seas would give valuable information on the open-sea structure of the surge itself.

The scatterometer data would be more frequently available, because the wide swath of the instrument would include a given sea area on a large number of tracks. By the nature of altimeter tracks, the chance of sensing a large storm surge, which may occur only once or twice in a year, would be correspondingly less. However, as in the case of tsunamis, a single fortuitous track could provide useful data for checking a computer model that would be virtually unobtainable by conventional methods. Any track across the sea in calm weather would naturally provide useful information about the tides.

Requirements

Requirements of the scatterometer would be at least twice-daily coverage of a given sea area with dimensions of approximately 1000 km, with interpretation to windspeed over a grid spacing of approximately 100 km. To improve on surface-based estimates, windspeed would require precision to approximately 2 to 3 m/sec. Because, in storm conditions, the wind field may change considerably in a few hours, the winds measured by the satellite would not in themselves be sufficient to follow the full time history of a storm surge, but the data for intermediate times could be supplied from a computed weather model, which would itself be improved by the scatterometer data.

The altimeter "footprint" would need to be smaller than that required for oceanic tidal research. A diameter of approximately 20 km would be satisfactory. Vertical precision

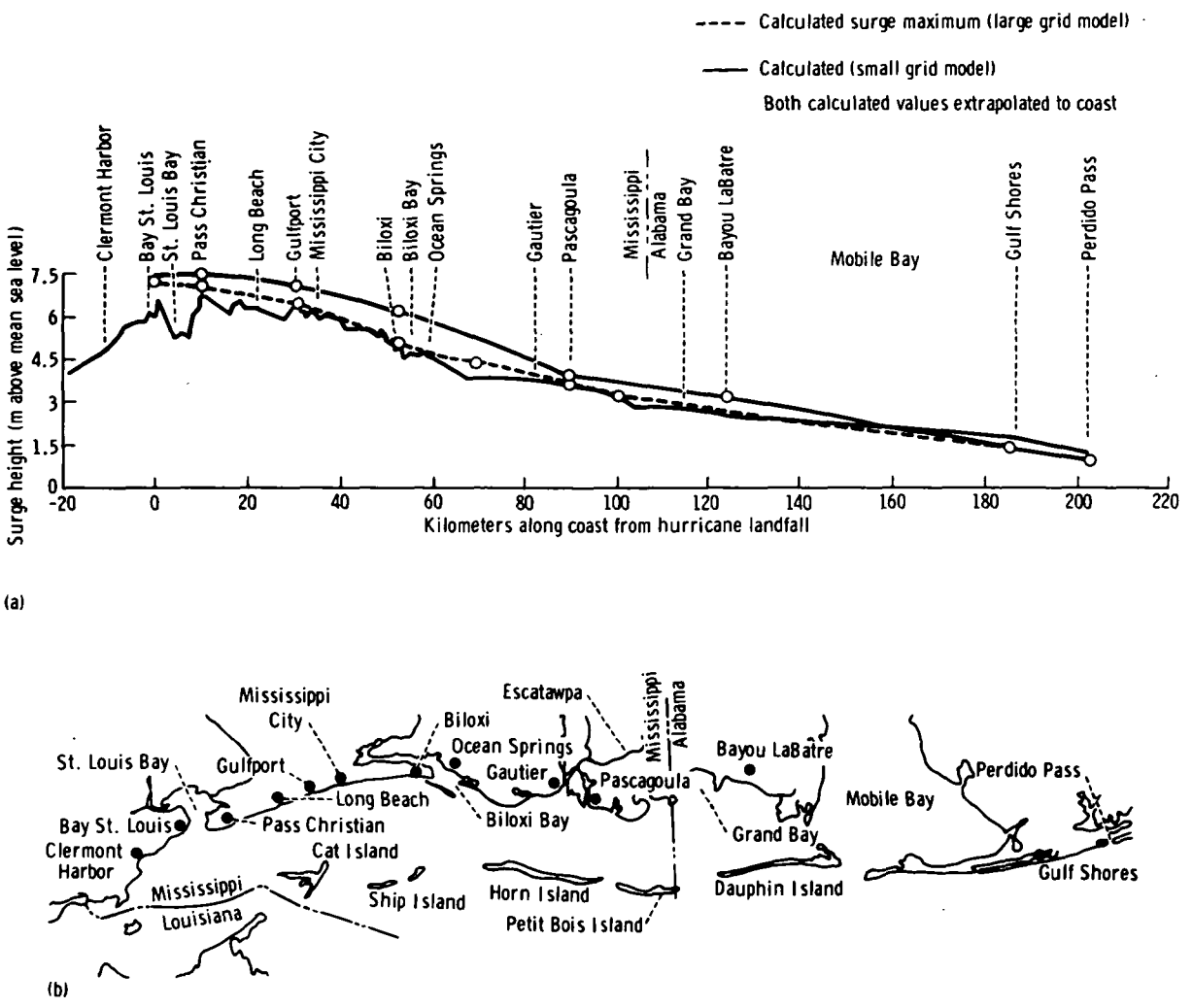

FIGURE 3–33.—Comparison of observed and calculated surge height maximums along the Gulf Coast during Hurricane Camille. (*a*) Surge height compared to distance along coast. (*b*) Geographical map.

of 0.5 m in the altimeter signal would be useful for measuring a large surge, but because the chances of encountering a large surge are slight, one would like in any case to record the more frequent small surges with an accuracy of 0.2 m. At the same time, orbital tracking errors and other systematic errors that do not vary by more than a few centimeters in 100 km can be neglected, because the seas of interest are always well provided with coastal tide gages and only the gradients of the sea surface are really required from the altimeter.

Applications

One application of these data would be to improve computer models designed to forecast storm surges. These models in turn are used as a basis for warning the public of danger from floods and for alerting sea defense operators. Another use of these models, of growing importance, is in warning large ships of unusual shoaling caused by "negative surges"; that is, depressions in sea level associated with the more familiar positive surges.

CURRENTS

Until recently, the methods of study in oceanography were limited to the standard shipbound tools. By comparing the area that can be covered by a ship in a reasonable amount of time to the total ocean, trying to understand the entire ocean by using the standard methods is equivalent to trying to understand the nature of a very large forest by painstakingly examining each tree. Many of these methods and their shortcomings are discussed in detail by Fomin (ref. 3–61) and Neumann (ref. 3–62). This does not imply that the traditional methods are useless; in understanding some particular aspects of the ocean, they are actually indispensable. However, as far as the global ocean model or large-scale phenomena are concerned, the traditional methods are not effective enough to produce a synoptic view. This shortcoming can be compensated to a large extent by the newly developed remote-sensing techniques.

Remote-sensing techniques are the only observation methods that are capable of fast scanning over a vast area. Because of this unique capability, these techniques will become the most important tools in large-scale physical oceanographic research. However, because of the way data are collected, all the information thus obtained is confined to the surface. But the environment of the ocean is a complicated one; all the physical processes in the ocean are controlled by both surface and subsurface parameters. These parameters act and interact to produce the phenomena actually observed. Remote-sensing techniques are only effective in measuring those phenomena controlled by surface parameters. Fortunately, such phenomena include most of the crucial problems in physical oceanography. Furthermore, some subsurface phenomena such as internal waves can also be inferred indirectly from microwave measurements of the surface.

The most severe deficiency of the traditional methods is the time factor. All ocean phenomena change with time as well as space. The traditional methods, because they are shipbound, are highly time constrained. They cannot produce any synoptic data of global scale. As a result, the so-called global data are actually patched-up works from different times and different cruises. For example, the meandering of the Gulf Stream is a well-known feature of the motion. If, as shown in figure 3–34, the stream path from A to B is P_1 at time t_1 and a ship surveys the area in time interval t_2-t_1, the path changes continuously to P_2 in the same time interval. The result of the survey will produce a path P that is not a path of the event at any time.

Another view of this deficiency of time factor is the spatial restriction. To cover a reasonable area in a given time interval, the ship will have to move with a minimal amount of delay, thus occupying fewer stations. Therefore, the gaps will be wide. This discrete set of data will create problems when interpolation is used in processing the data.

The combined effect of the space and time deficiencies is to eliminate the possibility of getting field data to improve the accuracy of global condition prediction, which depends not only on a local system but also on the interrelation between different systems. The Gulf Stream, for example (fig. 3–35), is dominantly controlled by the wind field of the northern Atlantic as a whole, rather than by local winds. However, events in the south-

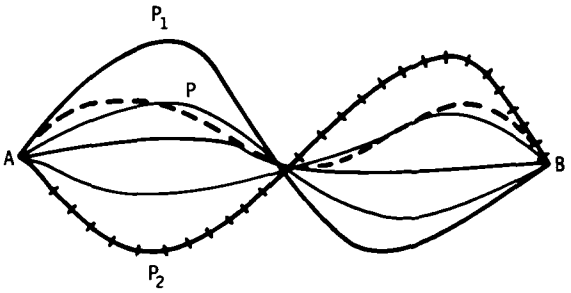

FIGURE 3–34.—Sketch illustrating problem with traditional methods of data gathering. Time for a ship to travel from A to B is t_2-t_1.

ern Atlantic will eventually feed to the Gulf Stream through current systems (nos. 15, 2, 20, etc., in fig. 3–35).

Although severely limited, the traditional method can produce data on the water column under the surface. Such information is important in studies on interval waves and baroclinic current, etc.

Advantages of Remote Sensing

Because remote-sensing techniques are capable of rapidly scanning large areas, they can be used to obtain continuous data on a global scale. Such data are essential to the predictive models on weather and sea state. From remote sensing, useful data can be obtained concerning the mean sea level, the sea state, and the surface temperature field. (Also see fig. 3–36.)

The first method of measuring ocean currents by remote sensing was by satellite tracking of drifting buoys. This was the French meteorological EOLE satellite system (Cooperative Application Satellite CAS–A) that was launched from the NASA Wallops Island Station on August 16, 1971. The EOLE data collection and positioning system has been operational since early September 1971. The satellite tracks and collects data from drifting buoys during each pass by interrogating the buoy transponders. The stored range and range-rate observations are later transmitted to ground telemetry stations and processed at the Centre National d'Etudes Spatiales (CNES) computing center in Brétigny, France. In the future, the observations will be processed at the NASA Goddard Space Flight Center.

Although originally designed for balloon tracking, the EOLE system has proved to be an ideal tool for applications such as drafting objects positioning (icebergs and

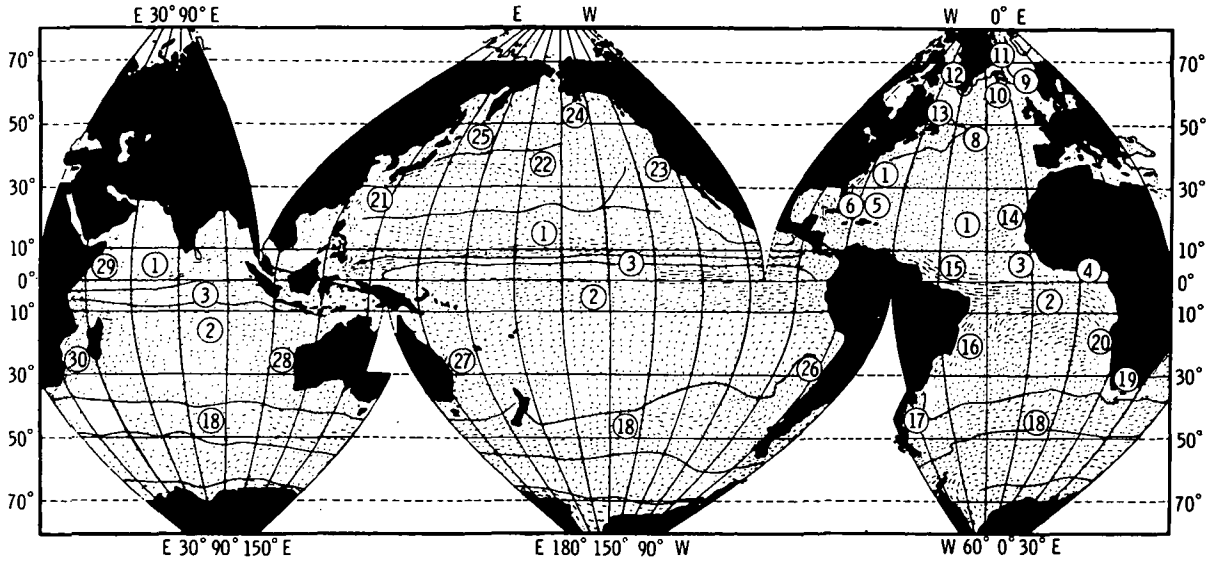

Note: 1 = North Equatorial Current, 2 = South Equatorial Current, 3 = Equatorial Countercurrent, 4 = Guinea Current, 5 = Antilles Current, 6 = Florida Current, 7 = Gulf Stream, 8 = North Atlantic Current, 9 = Norwegian Current, 10 = Irminger Current, 11 = East Greenland Current, 12 = West Greenland Current, 13 = Labrador Current, 14 = Canary Current, 15 = Guiana Current, 16 = Brazil Current, 17 = Falkland Current, 18 = Antarctic Circumpolar Current, 19 = Agulhas Current, 20 = Benguela Current, 21 = Kuroshio, 22 = North Pacific Current, 23 = California Current, 24 = Aleutian Current, 25 = Oya Shio, 26 = Peru Current, 27 = East Australian Current, 28 = West Australian Current, 29 = Somali Current, 30 = Mozambique Current, 31 = (Indian) Monsoon Current (Northern Hemisphere summer).

FIGURE 3–35.—World chart of ocean currents during Northern Hemisphere winter (ref. 3–62).

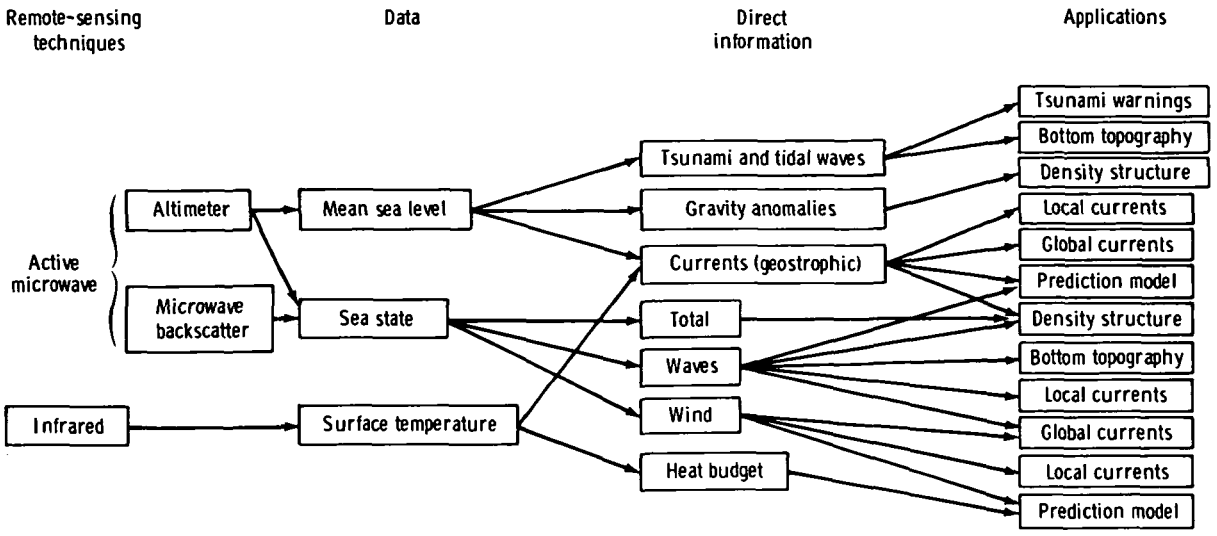

FIGURE 3–36.—Uses of remote-sensing techniques.

buoys). Routine operation can provide positions with accuracies of approximately 2 to 3 km.

The Virginia Institute of Marine Sciences started drifting buoy experiments using the EOLE positioning system in September 1972. The main objective is a study of currents along the coast of Virginia, outside the mouth of the Chesapeake Bay. The buoys are round disks carrying the radio and EOLE antennas, under which is attached a cubic case containing the electronics. A 5- to 20-m cable links it to a submarine crosslike sail.

Although the drifting buoy system uses satellites for data acquisition, it has many of the disadvantages of the traditional methods discussed previously. In this sense, this system does not offer many of the real advantages achieved by remote sensing.

The most promising method for measurement of ocean-surface currents has been developed from increasingly accurate radar or active microwave altimeters. The basis for current measurement using satellite-borne altimeters is that most important ocean currents are driven by changes in the ocean-surface elevation.

By measuring the surface slope alone, the surface-current velocity can be determined. This calculation is not new, but the practical implications of this approach have only recently been realized through the possibility of accurate measurements of ocean-surface slope by satellite-borne radar altimeters. The accuracy to which the slope is measured directly determines the accuracy of the surface current.

Measurement of surface current seems simple; however, difficulties arise because data obtained from satellite altimeters still contain substantial amounts of noise. To analyze the data and to calibrate the instrument, the satellite measurements must be related to models of the ocean-surface relief. To do this, one must rely on in situ hydrographical data available in the literature. The most useful data are measurements that lead to surface relief by means of dynamic height.

Requirements

The expected change in surface elevation due to geostrophic currents for areas of well-defined current integrity is approximately 0.5 to 1.0 m change in elevation over distances of 25 km or larger. Current features in these regions, such as eddies or weaker subcurrent systems, cause a height variation of approxi-

mately 25 cm. To detect the transient topographic signatures of these magnitudes, the permanent topographic features must first be determined to somewhat higher resolution. On the basis of defining permanent features to within 10 cm with 80 percent confidence (over a 25-km spatial extent), using nominal satellite groundtrack velocities, the required resolution translates to 12 cm rms for altitude samples that are statistically independent for a 1-per-second data rate. In some special situations, the height change may occur over distances less than 25 km, in which case a resolution (footprint) of approximately 1 to 3 km is recommended.

Technical Approach

The present technical approach is to measure the surface elevation and use this measurement to compute surface currents. Computed currents can be compared with currents from in situ measurements of dynamic height or measured elevations compared with measured values of dynamic height. At places where the density profile is known, the subsurface currents may also be computed. The accuracy of the surface current computed by this method depends on the accuracy of the measured height and the geostrophic assumption. In most situations, the geostrophic assumption is good and the accuracy of the surface elevation is the only parameter affecting accuracy.

If subsurface currents are desired, then the density profile is also required. The density profile cannot be measured remotely; therefore, any computation of subsurface currents will require local measurements.

The present approach is based on data obtained solely from an altimeter. The increased development of remote sensing will permit the measurement of many parts of the wave spectrum. Presently, the high-frequency or high-wave number part of the spectrum can be measured by active microwave backscatter as shown by Krishen (ref. 3–63); Daley (ref. 3–64), and Valenzuela et al. (ref. 3–65). In addition, part of the low wave number spectrum can be obtained for an altimeter by the measurement of significant wave height $H_{1/3}$ or by imaging radar. Huang et al. (ref. 3–66) have shown that there is a relation between nondirectional wave spectrum, surface wind, and current. Moreover, they have determined the change in wave spectrum with surface current using windspeed as a parameter. This was done by using the Pierson-Moskowitz-Kitaigorodskii (ref. 3–67) spectrum for the zero current condition. Figure 3–37 shows the wave number spectrum as a function of surface current u for a windspeed W of 10 m/sec. If the surface wind and the spectrum can be obtained, this would provide an alternate method of current measurement.

It may not be possible, at least in the near future, to remotely sense the entire wave spectrum. Because of this, Huang et al. (ref. 3–66) have computed the relation between rms surface roughness and current. Surface roughness also depends on surface wind, and figure 3–38 shows the rms slope as a function of windspeed with current speed u as a parameter. In principle, surface roughness could be used for current measurements. Figure 3–39 contains the same information as figure 3–38, but with windspeed as the parameter.

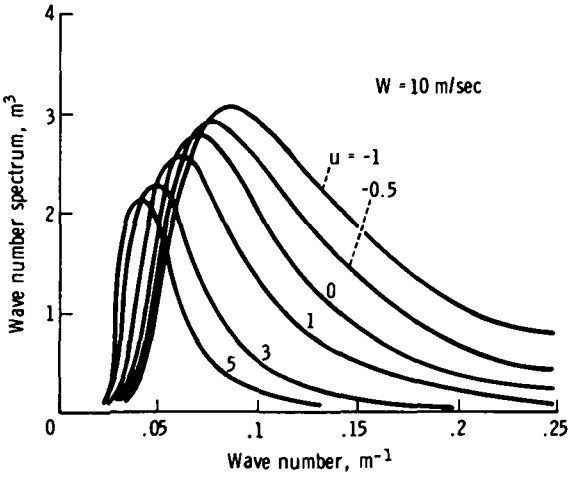

FIGURE 3–37.—Changes of wave number spectra for a 10-m/sec windspeed under different current conditions.

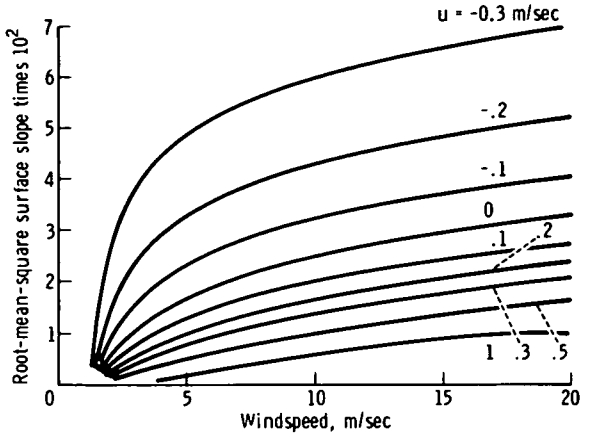

FIGURE 3–38.—Variation of rms surface slope with windspeed, using current speed as a parameter.

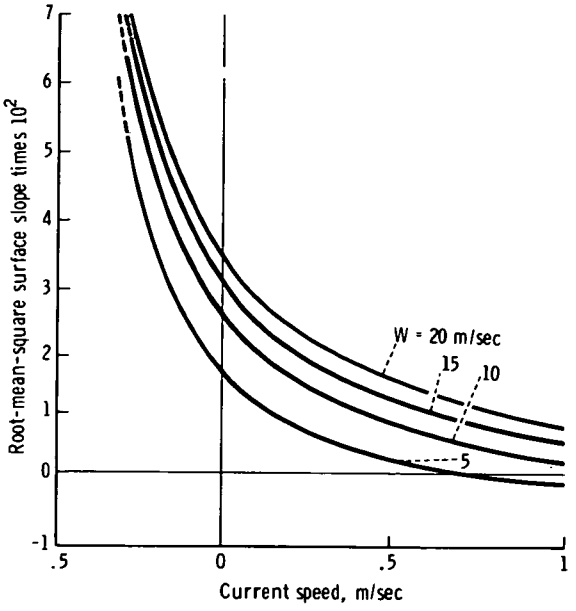

FIGURE 3–39.—Variation of rms surface slope with current speed, using windspeed as a parameter.

The surface roughness or the energy in the high wave number waves increases quite rapidly with wind (see figs. 3–38 and 3–39). Thus, an increase in the energy in the high wave number region can be caused by either adverse currents or the wind. At high windspeeds, the effect caused by the wind will probably overshadow any change in wave spectra caused by currents. Therefore, it is postulated that only in low winds can surface roughness be used to measure current. At this time, however, additional efforts must be made to separate the two effects. This alternate method of current measurement, at least at low windspeeds, can be used as a check (also obtained by remote sensing) on the currents obtained from the satellite altimeter.

The ultimate goal must be remote sensing of the complete directional wave-height spectrum. This is slightly different from the present approach of measuring the high-frequency spectrum by means of backscatter and of inferring wind by a relation between wind and the wave-height spectrum at specific (high) wave numbers. If, by using various remote-sensing systems and possibly models of the spectra, the total wave-height spectrum can be obtained, then the high-frequency portion could be used to infer wind; and the rest of the spectrum, including the high-frequency portion, would be used to measure currents and other parameters of interest (e.g., wave energy, significant wave heights, etc.).

Applications

Virtually all ocean waves are influenced by ocean currents and, thus, information is required on these currents. Any activity using ships will be able to use surface current information to reduce time en route, to lower costs or fuel consumption, and to avoid bad weather. Some examples are shipping and naval operations, fishing operations, and search-and-rescue operations. Access to measured or predicted ocean-surface currents will be of immediate benefit to all these users.

Long-range weather forecasting and/or weather models also require a global picture of the surface currents. The proposed current information will benefit both. As the ocean becomes more crowded, pollution and the ability to predict pollution becomes increasingly important. Surface currents are also needed for predictions of pollution from any known source. Moreover, slicks detected

by a measurement of the high wave number spectrum can reveal pollution or salt intrusion.

GLOBAL WAVE STATISTICS

Any dynamic phenomena on the ocean surface, such as ship motion and forces on anchored or stationary platforms, are governed by the actual and/or expected sea state. Because the ocean surface is random, the only way to define it is by statistical description. The usual method used to describe wave motion is by the wave-number or wave-frequency spectrum and the expected variation of this spectrum under different conditions. Therefore, models to predict the expected wave spectra for given geographical and meteorological conditions have received much attention.

The primary mechanism by which waves are generated is the surface wind. Moreover, in the open ocean (i.e., without boundaries) with no currents, the wind uniquely determines the wave spectrum. However, the relationship between wind conditions and the sea state is still not completely resolved. When boundaries or currents are present, the prediction of wave statistics becomes increasingly difficult.

Because of the inability to uniquely predict the wave spectrum, the approach must be to measure the wave spectrum, or wave statistics, so that mathematical models may be refined by observations and thus yield the desired data. The measurements must be made on a global scale because some of the factors (e.g., storms, geostrophic currents, etc.) that affect the spectrum extend for hundreds of kilometers. Because of these large-scale processes that influence the sea state, measurements at a single point or at several points at different times are difficult to interpret. Therefore, remote sensing offers a great many advantages in developing global wave statistics. Such statistics have two immediate and widely useful purposes:

1. To establish reference conditions to be used for design and planning, and for evaluating global wave models.

2. To monitor any changes from the reference condition, such as those caused by storms, currents, topography, pollution, etc. The change in wave spectra can be used to evaluate the size and nature of these phenomena.

A less-immediate goal is the generation of improved methods of predicting and modeling ocean-wave spectra.

State of the Art

The first work on a model to predict ocean-wave characteristics was undertaken by Cornish (ref. 3–68). Little work followed this until Sverdrup and Munk (ref. 3–40), motivated by the necessity of wave information for naval operations, developed a model to predict wave characteristics. Their analysis was concerned with a relation between wave heights and periods and did not deal with the concept of a wave spectrum. Neumann (ref. 3–69) was the first to deal with the concept of a wave-frequency spectrum from which statistical properties could be obtained. Using Neumann's concepts, Pierson et al. (ref. 3–70) developed a model for the prediction of wind-driven sea and ocean swell spectra. The model has experienced considerable modification and improvement and still remains the most widely used model for forecasting ocean wave characteristics or statistics. The concept of an equilibrium spectrum was introduced by Phillips (ref. 3–71). This provided additional insight into the parameters that must be included in the gravity wave spectra and on the shape of the high-frequency part of the spectrum. A recent summary of wave spectra models for a complete range of wave numbers has been given by Pierson and Stacy (ref. 3–15).

Generally, wave spectra models have been quite successful. For example, a NOAA National Data Buoy Center report (ref. 3–72) provides analyses of ocean-wave spectra as determined by hindcasts. The development of these models has required the acquisition of a large amount of information about waves. Data concerning waves are routinely col-

lected by ships at sea. Wave heights, periods, and dominant direction of travel are recorded and radioed ashore in a special code by many ships at 00:00, 06:00, 12:00, and 18:00 G.m.t. These measurements are collected, stored at national data centers, and used to produce statistical summaries of the waves for the various areas of the oceans. The cost of collecting, storing, and analyzing data of this kind amounts to millions of dollars annually.

Also, a very small number of weather ships have wave recorders that measure the rise and fall of the sea surface as a function of time at a point. These spectra have been studied and used to develop wave-forecasting techniques and to aid in the design of ships. Wave records of this nature are obtained routinely at four or five locations in the North Atlantic and at one location in the North Pacific.

A consortium of oil companies has used wave recorders on their drilling rigs to collect a large amount of wave data during hurricanes in the Gulf of Mexico. The substantial effort to obtain wave data in these ways is a measure of its present value. However, this level of effort is inadequate for the future needs of the United States and the other nations of the world.

The reports from ships are estimates, not measurements, of the wave conditions. They are also concentrated along shipping lanes and do not adequately describe conditions on a uniformly spaced grid over the oceans. Moreover, they tend to be substantially in error, and the data obtained before a few years ago had built-in biases that tended to group reported wave heights near 5 and 10 m and to report high waves inadequately. In one study, in which these estimates of wave heights were compared with measured wave heights, the estimates frequently differed by a factor of 2 (either too high or too low) from the measured values. Approximately 1200 ships report wave conditions in this way every 6 hr, primarily in the Northern Hemisphere.

The shipborne wave recorder data are of high quality and have proved invaluable for many scientific investigations. However, the number of ships is too few and their locations too random to provide an adequate data base.

In addition, predictions of wave spectra are based on local conditions, primarily because this is all the information that is available. However, very-large-scale phenomena (storms, global currents, etc.) alter or determine the wave spectrum. For this reason, recourse must be continually made to observations of measured wave characteristics typical of those given by Hogben and Lumb (ref. 3–73). Moreover, in coastal regions, the open ocean waves must be considered in combination with local topography to develop realistic estimates of the wave spectra.

If global meteorological data were available, more accurate models for the prediction of wave spectra could possibly be developed. Such models would need to be verified by global wave statistics, however. Therefore, remote sensing appears to not only offer the opportunity to evaluate and improve wave spectra but to be the only way presently available to do so.

Requirements

The complete wave frequency or number spectrum need not be measured. Various parts of the spectrum must be measured, however, so that present models can be used to infer the complete spectra. In addition to the measurements of wave spectra or wave statistics, data on meteorological conditions are also required. These data are needed not only at the point of wave measurement but also globally, because of the large-scale phenomena that govern local wave spectra.

Technical Approach

The acquisition of sufficient data to develop a global picture of the local wave spectrum and its expected extreme is required. By using presently available models (e.g., Pierson et al. (ref. 3–70) and Pierson and Stacy (ref. 3–15)), a complete wave

spectrum can be developed from the significant wave height $H_{1/3}$ or the surface wind. Both together permit some checking of the models. The significant wave height can be obtained by the present satellite altimeter, although the accuracy may not be as great as desired. Surface wind can be obtained from microwave backscatter, but a higher accuracy may be needed.

Imaging radar can also be used to generate wave statistics. Imaging radar gives a picture of wave patterns that is at present a qualitative picture of the wave field. Therefore, the fact that waves can be seen makes the imaging radar a powerful tool for the oceanographer. The most exciting prospect is that of mapping wave patterns and wave buildup during large storms. This wave buildup occurs under cloud cover that only active microwave sensors can penetrate. It is in these large storms that the bigger, more damaging waves are generated.

In addition to mapping storm waves, the mapping of swell over continental shelves will permit the study of wave refraction in coastal regions. The continental shelves will be valuable real estate in the next few decades as a place to put man's machinery, such as offshore airports, powerplants, and oil rigs. The ability to predict wave climates in these areas and to verify these predictions by observations is another important contribution that imaging microwave sensors can make to oceanography. Again, the ability of active microwave sensors to penetrate clouds during storms is a most important attribute.

The capability for global monitoring of sea state and ocean waves, which will be provided by spaceborne imaging radar, is also a very important contribution. This is particularly true for oceans in the Southern Hemisphere, where wave measurements in the open ocean are so widely scattered that many areas of the ocean are essentially unknown. Little shipping and almost no land observation points are present in the Southern Hemisphere oceans between latitudes 20° and 40°, so that the interaction between wind and waves and the buildup of waves is practically unmonitored.

All of this information can be used to generate a global picture of the expected wave spectra or the wave statistics characteristic of these spectra. These data would establish a reference state for the ocean. This state could be considerably more accurate and detailed and with better resolution than the present tabulation by Hogben and Lumb (ref. 3–73) or those from the U.S. Department of Commerce (ref. 3-72).

With the acquisition of a reference condition, continued monitoring of the oceans can be used to reveal any changes that occur because of storms or other large-scale phenomena. These two goals, the development of more accurate global wave statistics and the monitoring of the magnitude of their changes, should be ample justification for the program.

The many advantages provide motivation to attempt to sense more completely the total wave spectrum. At present Krishen (ref. 3–63), Valenzuela et al. (ref. 3–65), and Daley (ref. 3–64) have used microwave backscatter to measure the high wave number (above 0.1 cm^{-1}) part of the wave spectrum. The use of the longer wavelength radar, or perhaps imaging radar, to sense the lower frequency portions of the spectrum should be considered. This is because the ultimate goal must be a tabulation of the complete wave-number spectrum and, in the future, possibly the directional wave-number spectrum, on a global basis. Active microwave systems are now the only sensing technique that can be used to measure wave spectra directly.

Applicability

The use of remote sensing to establish a reference picture of global wave statistics would provide data needed to plan shipping routes, design ships and/or offshore structures, and aid in the planning of future ports. This reference condition is especially needed in costal regions where the influence of the local topography on incoming open ocean

waves makes prediction of sea state quite difficult.

The monitoring of local variations from an established reference condition probably has its most immediate applicability in the routing of ships. The financial benefits obtained by routing ships around areas of heavy seas are quite large and can be easily accomplished with present remote-sensing technology. Other advantages would be in the monitoring of large-scale storms and their influence and the tracing of various surface pollutants, such as oil spills or the intrusion of saltwater into freshwater. Over longer periods, the compilation of wave statistics and their variation can reveal any unusual or significant changes in topography. In addition, there are a number of specific coastal problems that these data can help resolve.

When the depth of the water becomes less than half the wavelength of a spectral component in a wave spectrum, the speed of the component is affected by the depth. The shallower the water, the slower the wave travels. Complex offshore submarine topography turns the waves away from deeper regions and focuses them at shallower regions. Shallow areas off the coasts of parts of the continents, called continental shelves, are as much as several hundred kilometers wide. The depths in these shallow areas are often complex, and the waves are refracted in ways both difficult to describe and to compute.

All structures to be built in such shallow-water areas require design wave data so that the structures can withstand the forces on them produced by the high waves during a storm. Also, the continued action of the lower waves can erode the material around the structure base and cause it to collapse. With the many proposed offshore structures around the coasts, the problem of adequate designs for them will become increasingly more pressing during the next few decades.

One area studied in the past and under renewed theoretical analysis is the New York Bight, especially as affected by the Hudson Submarine Canyon. Offshore sites just 10 or 20 km apart in this area can, at times, be exposed to waves 10 times higher at one site than at another.

During selected conditions with appropriate offshore deepwater waves, data can be obtained that will provide verification for wave refraction studies in shoal water. Moreover, potential sites all over the world can be surveyed concerning wave refraction effects for preliminary, and perhaps even final, design considerations. The actual images will have to be recovered because the waves become shorter and change direction as the water becomes shallower, so that the concept of a spectrum representative of an entire area is not applicable.

A scientist familiar with the needs of the user community could rather easily select approximately 500 sites on a global basis for obtaining daily data, some over the deep ocean and others at coasts, so that in the course of each year a global data base of approximately 180 000 coastal refraction patterns and deep-water wave-number spectra could be obtained.

Finally, advantages will be gained by improved predictive models to forecast wave spectra. The present numerical spectral wave forecasting models are quite good. They incorporate many physical features of the generation and propagation of waves but not all the variously proposed theoretical features of waves. However, any numerical model of a physical phenomenon of the oceans can be improved because there are always increasing levels of complexity that need to be modeled. At present, the problem is lack of an adequate verification data base on which to build improved numerical spectral forecasting models. The measurements to be made by satellites would provide the kind of data needed to develop greatly improved numerical wave-forecasting models by providing a means to determine the errors in the present models. The need will always exist for forecasting wave conditions for as many days as possible into the future. The forecast problem involves wave spectra and

weather, but improvement in wave forecasts is a necessary requisite for improvement in weather forecasts.

POLAR ICE FIELDS

The polar regions are a fundamental part of the Earth heat engine, yet the way in which they interact with the other parts of the atmosphere/ocean/ice/land system is poorly known because they have existed behind what has been called an "observational barrier." Most polar geophysical studies are based on a paucity of data; relatively short-time series of measurements acquired at a few points spread over vast distances. The state and behavior of the Earth surface is one aspect of the interaction-exchange problem that can be said to be the most important in polar regions, where changes of phase of water into snow and ice occur over large areas at small times scales, and where large permanent floating and grounded ice masses are involved in a complex feedback process with atmospheric and oceanic circulation. This problem can be studied only by using satellite remote-sensing techniques.

In the vast array of remote-sensing techniques available for polar studies, microwave remote sensing, both passive and active, promises to be the most useful tool. The polar regions are in the dark for a large part of each year and when they are in their sunlit periods they are normally cloud covered. Therefore, sensors that can observe the polar surface at all times, such as microwave sensors, are needed to provide the sequential synoptic imagery needed for elucidation of the complex cause and effect processes of these vast regions.

Scope

Polar ice includes three distinct forms of ice that have widely divergent properties:

1. Sea ice, which covers large parts of polar oceans and some subpolar seas, contains brine, averages one to several meters in thickness, and ranges in age from hours to several years.
2. Icecaps and glaciers, which are composed of freshwater ice that averages several kilometers in thickness for Antarctica and Greenland and is tens of thousands of years old.
3. Lake ice and estuary ice, which is fresh and brackish water ice of a wide variety of thicknesses and ranges in age from hours to several months

In the following section, the three forms of ice are discussed in relation to active microwave remote sensing.

Sea Ice

Of all the forms of frozen water that exist on Earth, the one about which least is known is the sea ice that covers vast areas of the oceans; 10 percent in the Northern and 13 percent in the Southern Hemisphere. A good example of the paucity of knowledge is that, for the International Geophysical Year (IGY) period, essentially nothing is known about the extent and morphology of the winter sea ice surrounding Antarctica.

Individual ice floes have been observed to move 50 km in a day, and speeds of 10 to 20 km/day are common. Leads (cracks) and polynyas (large irregular openings) open and close at all times. The seasonal variations in areal extent of the ice canopies are large; approximately 15 percent for the Arctic and 80 percent for the Antarctic. In short, sea ice is the most rapidly varying solid on the Earth surface.

Although the feedback mechanism that exists within the air/ice/water system is not well defined, intuition and the few facts available suggest that the variation of the edge of the icepack must be of prime importance. On the time scale of months, air/sea interaction at the edge of the pack would cause an intensification of the atmospheric baroclinicity, which in turn would alter the surface ocean regime.

To monitor the seasonal patterns of surface heat exchange over polar oceans, one must systematically observe the location and extent of pack ice and the location and dura-

tion of large polynyas within the pack. Although meteorological satellites such as Tiros, Itos, and NOAA have given (and will continue to give) highly useful ice data, an alltime, all-weather capability of observing sea ice did not exist until the launching of Nimbus 5 in December 1972.

The electronically scanning microwave radiometer (ESMR) on Nimbus 5, operating at a frequency of 19 GHz (1.55 cm), is providing the first daily synoptic view of polar sea ice distribution. The NASA remote-sensing flights during the 1971 and 1972 Arctic Ice Dynamics Joint Experiment (AIDJEX) pilot experiments, which flew an ESMR identical with that aboard Nimbus 5, have provided data that allow the interpretation of ice types shown on the microwave brightness temperature maps obtained from space. The difference in brightness temperature between seawater and ice at 19 GHz is approximately 120 K; therefore, the ice edge on the maps shows up clearly and can be positioned geographically with an accuracy of 30 km, the nadir resolution of the 1.4° beamwidth of the ESMR.

The ice-edge positions shown in ESMR images differ considerably from the averages shown for winter months in the U.S.S.R. and U.S. Antarctic atlases. The actual ice edges are more irregular than the ones deduced from aircraft and ship reports shown in the atlases and are more extensive (farther north) in several areas, such as the Ross Sea. Of special note are the large polynyas revealed in the Ross and Bellingshausen Seas, which are not shown at all in the atlases.

Gloersen et al. (ref. 3–74) have used aircraft microwave images to show that it is possible to distinguish first-year sea ice (1.15 m thick) from multiyear sea ice (1 to 3 m thick) and to estimate amounts in mixtures of the two. Campbell et al. (ref. 3–75) have compared ESMR and aircraft microwave images of the Arctic ice canopy to delineate its gross morphology.

Although ESMR is a prime tool to study gross characteristics of sea ice morphology and dynamics, it does not provide the kind of high-resolution data needed for a wide variety of scientific and commercial purposes. To test the existing and developing numerical models for sea ice dynamics and thermodynamics, high-resolution sequential imagery of select areas is badly needed. The optimum sensors for this program would appear to be active microwave sensors.

American radar imaging of the polar sea ice dates back to the early 1960's (ref. 3–76). In a flight by a military aircraft from the North American Continent to the vicinity of the North Pole, a long strip of imagery was obtained with an X-band real aperture system. The ability of the radar to distinguish various classes and ages of ice was first shown in Anderson's analysis of these images. In 1967, the NASA Earth Resources Aircraft Program (ERAP) P–3A aircraft flew north of Point Barrow with the 13.3-GHz scatterometer. Although ground parties were on the ice to make thickness measurements, their lack of mobility prevented measurements from being more than of marginal utility, and the ice types had to be determined by analysis of aerial photographs made simultaneously with the scatterometer runs. Unfortunately, the more interesting ice morphologies occured some miles from the ice party's location. By comparing the photographs with ice atlas photographs and information gleaned from conversation with ice observers, Rouse (ref. 3–77) was able to make tentative identification of ice types and to show that the multiangle scatterometer observations could be well correlated with ice type.

In 1970, another NASA ERAP mission was conducted north of Point Barrow, with the ice party restricted to the uninteresting fast ice within a few miles of Point Barrow. In this mission, a series of scatterometer lines were flown with both 13.3- and 0.4-GHz instruments; the same area was imaged with the 16.5-GHz DPD–2 multipolarized imaging radar by flying the imager in a box around the area covered by the scatterometer. Parashar et al. (ref. 3–78) were able to make

excellent identification of ice types by detailed stereoscopic analysis of photographs of the area. The classification by ice type was then converted into effective ice thickness, using the average ice thickness appropriate to each kind of ice. The results were then interpreted in terms of ability to measure ice thickness with the various radars, but most of the work concentrated on what could be done with individual incident angles appropriate to an imaging radar that might be used operationally. Figure 3–40 shows the encouraging result at 13.3 GHz. Note that there is an ambiguity between the very thinnest ice category (new ice, less than 5 cm thick) and ice approximately 1 m thick. Fortunately, this ambiguity can be resolved by image interpretation, for the new ice has a characteristic texture quite different from that of the older first-year ice. It was found that the 0.4-GHz data could resolve this ambiguity if needed, but that the lower frequency by itself could not distinguish between the thicker multiyear ice and ice approximately 0.5 m thick. Indications from image analysis of the DPD–2 were that four categories (open water, ice less than 18 cm thick, ice 18 to 90 cm thick, and thicker ice) could be readily identified on the images, even though the images were somewhat saturated. The identification was an indication that the ambiguity in intensity between new ice and meter-thick ice did not exist on the cross-polarized image, but saturation on the film prevented assurance that this conclusion was correct. Parashar et al. (ref. 3–78) have also developed a theory that seems to explain the observations.

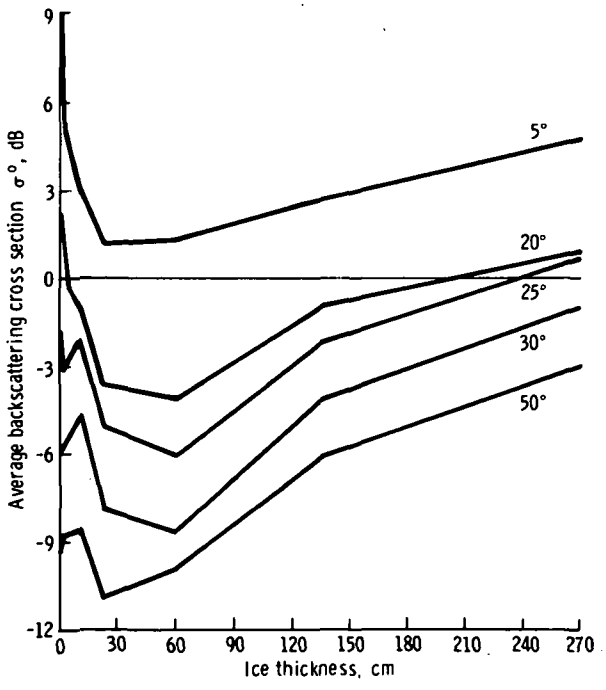

FIGURE 3–40.—Experimental σ° compared to ice thickness for different incident angles (frequency of 13.3 GHz, vertical transmit/vertical receive polarization).

The Arctic and Antarctic Institute of Leningrad has engaged in imaging of sea ice for at least 6 yr (ref. 3–79). The Soviets believe that they can clearly distinguish thin ice, thick first-year ice, and multiyear ice. In the late spring of 1973, an ice map of the entire shipping region across the north of the Eurasian Continent was prepared using the Toros 16-GHz real aperture radar imager. The system is presumably being used operationally in connection with directing shipping convoys along this route. In fact, the Soviet participants in the 1973 joint Bering Sea passive microwave experiment used the Toros images for "ground truth" to identify whether the passive microwave was able to distinguish water and ice and one ice type from the other. The Soviets have stated that the radar definitely distinguished more different ice types than did the passive microwave sensors.

The first American active microwave experiment on sea ice in which sequential images of ice were obtained took place north of Point Barrow during April and May 1973 when a joint U.S. Geological Survey (USGS)/Cold Regions Research and Engineering Laboratory (CRREL) team used an X-band side-looking airborne radar (SLAR) mounted in a Mohawk aircraft. In 2 weeks, nine flights were made over selected large areas of sea ice (200 by 50 km) to the east, north, and west of Point Barrow.

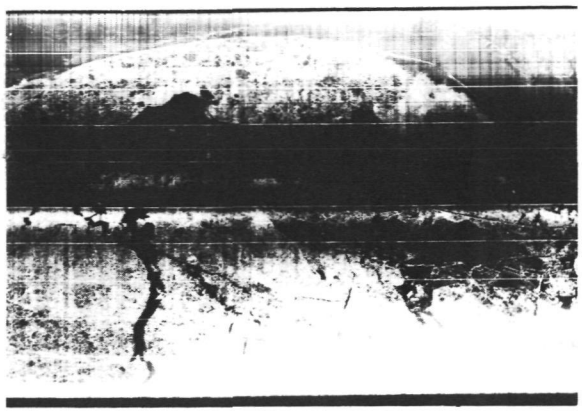

FIGURE 3–41.—An X-band SLAR image from the April 28, 1973, mission west of Point Barrow.

Figure 3–41 shows a portion of the April 28 mission data from west of Point Barrow. The coast can be seen with Wainwright at the upper left and Icy Cape at the upper right. The zone of shorefast ice shows clearly, as does the coastal lead. The pack ice is clearly seen to be composed of numerous fragmented floes and leads and has undergone strong recent deformation. The pack was made up of mostly first-year ice with some multiyear ice.

Figure 3–42 shows the same area 5 days later on May 3. The shorefast ice remained the same during this period, but the pack ice can be seen to have undergone strong deformation. Major lead changes occurred while the pack was translated only a few kilometers to the west.

A comparison of figures 3–41 and 3–42 with figure 3–43 reveals that SLAR shows the difference in ice types. Figure 3–43 shows a segment of the pack ice on May 2 approximately 190 km north of Harrison Bay (240 km northeast of Point Barrow). In this image, numerous undisturbed large ice floes can be seen, and the ridges appear as white linear features. The ice in this area was far less deformed than the ice west of Point Barrow.

Although much work remains to be done on these data, SLAR remote sensing of sea ice provides discernment of the following features.

1. Leads and polynyas can clearly be distinguished from ice.
2. Thin ice (pancake, frazil, gray) can

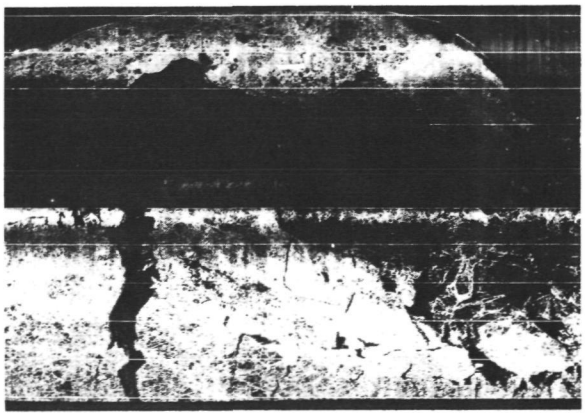

FIGURE 3–42.—An X-band SLAR image from the May 3, 1973, mission west of Point Barrow.

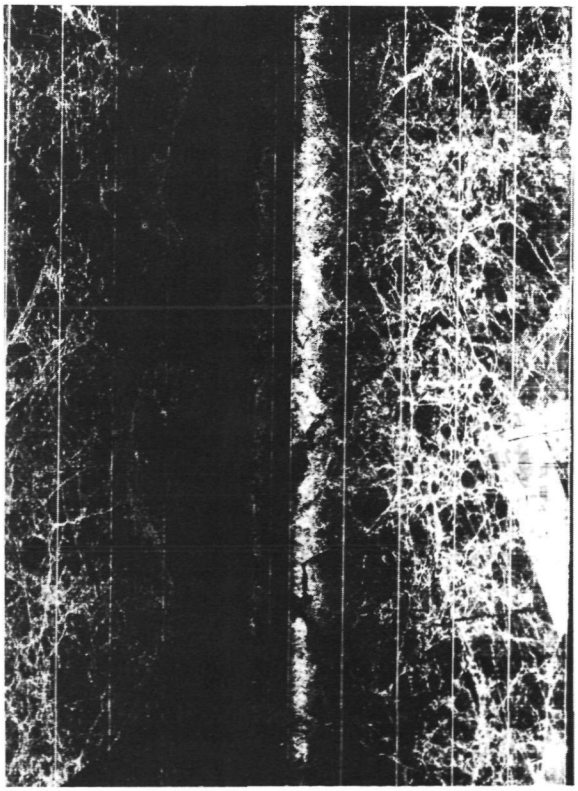

FIGURE 3–43.—An X-band SLAR image showing Arctic Ocean pack ice.

be distinguished from open water in leads and polynyas.

3. Ridges can generally be distinguished from leads, especially when the leads are large.

4. Ice floe shape and size can clearly be observed.

5. Land (permafrost) can clearly be distinguished from shorefast ice, water, and pack ice.

6. Ice-type distinction is good enough to permit distinctions between water, thin ice, thicker first-year ice, and the thicker multiyear ice.

Icecaps and Glaciers

Approximately 85 percent of the freshwater on Earth exists as ice in Antarctica and Greenland. Glaciological research in those areas has been aided greatly by the development of radio echo sounding techniques, which has made possible the delineation of bedrock topography and the measurement of ice thickness. Both these variables are needed to test recently developed numerical models. However, if the complex interaction between icecaps and glaciers and climate are to be understood, the ice/air interface events must be understood, especially the accumulation rate.

The ESMR images of the Arctic and Antarctic from Gloersen et al. (ref. 3–80) show very interesting signature variations on icecaps. For Greenland, brightness temperature differences of 323 K occur across the icecap, with the highest brightness emittance corresponding roughly to the highest elevation of the icecap. Although the cause of these variations is not fully understood, they are apparently not due to variation of the physical temperature of the ice, but to the emissivity variations probably induced by variations of the small-scale structure. Such crystal metamorphosis could be caused not only by temperature variations but also by pressure gradients within the ice.

In the ESMR images of the Antarctic icecap, no such correlation with elevation occurs; instead, the lowest brightness temperatures occur near the center of the continent, which would be expected if the variation in brightness temperatures was predominantly due to the variations in the physical temperature of the ice. Thawing and recrystallization of the surface ice does not occur on the Antarctic cap as it does in Greenland.

As interesting as these passive microwave measurements of icecaps are, they will be useful only for gross structure studies, whereas an urgent glaciological need exists for detailed measurements of the surface structure of icecaps and glaciers. It is precisely in this area that SLAR techniques could prove highly useful.

The Jet Propulsion Laboratory (JPL) has recently obtained L-band sounder profiles on Alaskan glaciers and on Greenland. The data show signal returns from structural features below the surface. The Greenland profiles show a tilted, layered structure that looks as if it had been formed by surface flow.

The only two-dimensional SLAR images of glaciers and icecaps are those obtained by V. V. Bogorodsky and V. S. Loshchilov of the Arctic and Antarctic Research Institute of Leningrad.[2] These Soviet scientists have obtained numerous SLAR (S-band) images of Siberian glaciers. All were obtained through a dry snow cover over nontemperate glaciers (those having temperatures below 273 K within the ice mass). In the great majority of images, the foliation planes formed by the annual accumulation processes were clearly visible. Most of the images were of glaciers with a snow cover thicker than several meters.

From the glaciological point of view, these data are exciting because one of the most difficult things to measure in glaciers is the rate and pattern of accumulation and ablation. As a glacier flows, the deposited layers of snow metamorphose into ice, which slowly flows downslope. Therefore, the pattern of foliation planes observed is due to two processes: accumulation/ablation and flow. Thus, to deduce the recent accumulation history of

[2] Personal communication, J. W. Campbell.

a glacier from the foliation planes, one must allow for the dynamics. This may not be too difficult for slow-moving nontemperate glaciers.

Bogorodsky and Loshchilov believe that SLAR measurements of glaciers can be used for accumulation studies. They have also obtained images of Arctic ice islands (pieces of icecaps that have calved off an ice shelf and drifted about within the matrix of sea ice floes). These images all showed the ice to have a parallel banded structure, with the bands having a spacing on the order of several hundred meters. They do not know what these bands are, but surmise that they were formed by the accumulation process existing on the icecap where the island was formed. The structural differences between ice island and sea were so great that distinguishing between the two was always possible.

Lake and Estuary Ice

Several of the world's major shipping routes are covered by lake or brackish ice for several months a year (i.e., Gulf of St. Lawrence and Baltic Sea), and great efforts are being made to extend the navigable season in these areas. To do this, two uses of sequential radar imagery are necessary: (1) as input into numerical models of ice dynamics and thermodynamics, and (2) as routing maps to direct ship traffic through the thinnest ice in an area.

A considerable part of the Asian and North American tundra is lake covered, and during the winter these lakes freeze both fully and partly (not to the bottom). Measurement of the ice cover on these lakes is important for many biological studies.

During the Skylab 4 overflights, SLAR imagery was obtained of the ice covers in Lake Ontario and the Gulf of St. Lawrence. These data show that radar remote sensing of lake and brackish ice can make it possible to distinguish the following features:

1. Leads and polynyas can clearly be distinguished from all forms of ice.
2. Rafted ice can be distinguished from undisturbed ice.
3. Shorefast ice can be distinguished from moving ice.
4. Ice floe size and shape can clearly be observed.
5. The approximate age of ice can be observed in terms of gray, gray-white, and white ice.
6. Ridges can generally be distinguished from small leads.

Bogorodsky and Loschilov, who have made SLAR X-band observations of lake ice in the Soviet Union, agree with these six tentative conclusions.

A very interesting phenomenon was observed on the tundra lakes east of Point Barrow during the USGS/CRREL experiment. In figure 3–44, a SLAR image of a series of thaw lakes to the east of Point Barrow is shown. Some of the lakes appear white (strong return), whereas others appear dark (weak return). After comparing this and other SLAR images with surface measurements, it was concluded that the lakes that appear white in the images are frozen all the way to the bottom (to the

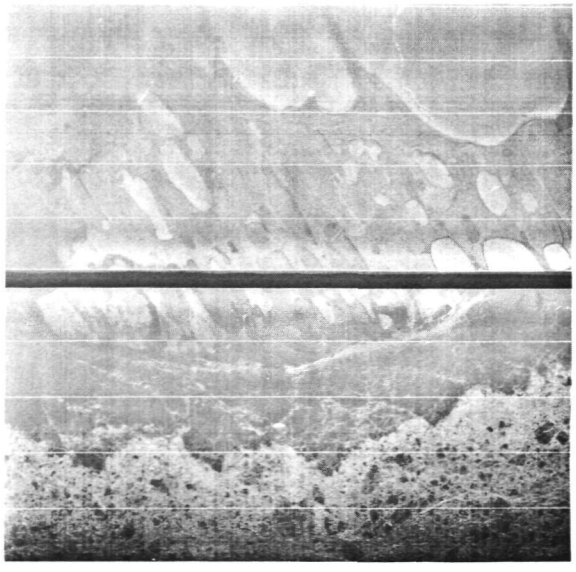

FIGURE 3–44.—An X-band SLAR image showing frozen thaw lakes east of Point Barrow.

permafrost table) and the lakes that appear dark have a water layer beneath the ice cover. This finding is important from several points of view. Such images could provide information to local communities concerning which lakes to tap for a winter water supply. The biological regime between completely and partly frozen lakes is different, the latter having far more fish.

Conclusions

Satellite-borne active microwave sensors offer the only means of obtaining high-resolution imagery of polar ice during all times, thus penetrating the "observational barrier" that has hampered much-needed research. Sequential synoptic active microwave imagery of sea ice is urgently needed to test and help develop numerical models of air/ice/ocean interaction. Such data will greatly enhance the usefulness of ESMR imagery of the gross characteristics of the sea ice canopies.

The only remote-sensing means capable of observing subsurface structures of ice-caps and glaciers is active microwave. The SLAR images of glaciers clearly delineate the accumulation foliation planes through several meters of snow cover. Those of ice-caps reveal a subsurface parallel banded structure. Such images promise to provide needed data on accumulation amounts, and patterns may help in determining surface flow patterns. Satellite radar is the best way to track and study the metamorphosis of ice island (bergs).

Active microwave imaging of lake and estuary ice will provide high-resolution, sequential, synoptic data needed to extend the navigable season in busy waterways such as the Gulf of St. Lawrence and the Baltic Sea.

The SLAR can be used to determine which tundra lakes are frozen to the bottom and which are not, an important logistical and ecological technique.

Although the potential of active microwave sensors that currently exist has been demonstrated as ice sensors, neither U.S. nor U.S.S.R. scientists yet know what frequency (or combination of frequencies) or what polarization (or combination of polarizations) is best for monitoring either sea ice or lake ice. Although earlier theories might be used to permit some extrapolation or interpolation, these too need improvement and further verification. Hence, in addition to further flights over the ice, both theoretical research and research with a microwave spectrometer that can be transported onto the ice seems to be needed if the optimum system parameters are to be established.

PART E

TECHNICAL APPROACHES

INSTRUMENTATION

Radar altimeters, scatterometers, and imaging radar are the major instruments needed to accomplish the applications discussed earlier in this chapter. This section describes the instrumentation in terms of its functions, future developments, constraints, and applications.

Altimetry

Introduction.—Satellite altimetry has demonstrated the capability for determining mean sea level. Although past efforts have not achieved the ultimate goal in spatial and height resolution, it is attainable in the next decade. On attaining this goal, satellite altimetry will enable improved knowledge of

the geoid, increasing the number of terms in the knowledge of the gravity field and the upward extension of the surface field. Also, the position and density of underwater topographic features can be determined from geoid undulations and satellite tracking. In addition, from waveform analysis of the radar altimeter return, global knowledge of sea slopes, currents and eddies, and estuarine characteristics is possible. From proper choice of orbit parameters and system concepts, an altimeter can provide a global synoptic description of the ocean surface. Figure 3–45 shows the differences between the "computed" and "measured" sea surface from one of the last Skylab experiments as a typical example of a first test (ref. 3–45).

Satellite altimetry.—Satellite radar altimetry has the potential to significantly improve knowledge of the geoid and sea state on a global basis. Although the data collection capabilities are limited to nadir, the short-pulse altimeter concept for the simultaneous measurement of surface-height variations and sea state has experimental verification warranting its deployment into space. Both the scientific value and the applications were emphasized in the Terrestrial Environment Solid Earth and Ocean Physics Study conducted during August 1969. Based on available data, the NASA EOPAP [3] (ref. 3–45) recognized the importance of satellite altimetry and has adopted a long-range physical ocean sensing program with objectives that rely heavily on this sensor.

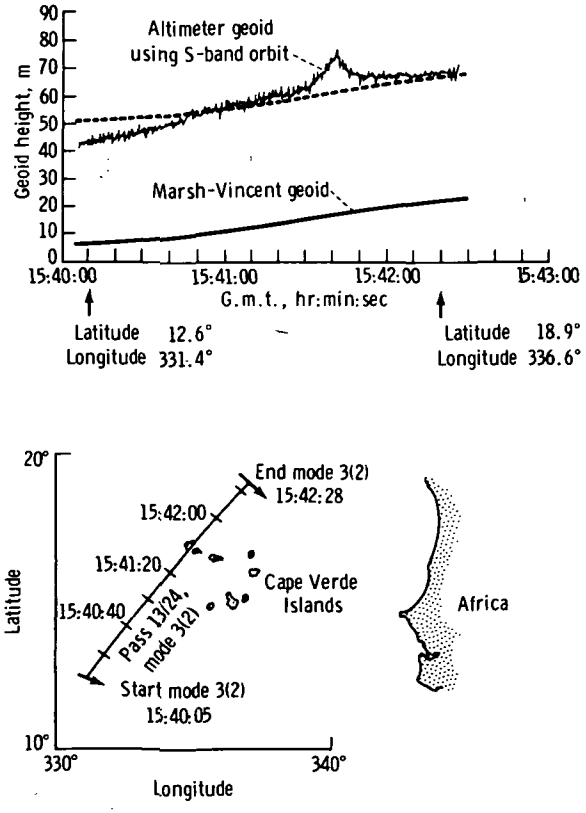

FIGURE 3–45.—Skylab altimeter pass over the Cape Verde Islands.

In all the activities to date, the role of altimetry has been visualized to include detection of dynamic ocean features (tides, waves, currents, etc.) or mapping of permanent mean ocean surface topography (geoid). The subsurface geological features have been known to affect the ocean geoid, and results obtained with the Skylab altimeter have correlated this relationship. These correlations could result in new applications of altimetry for bathymetric positioning of underwater topographic features (ref. 3–50).

The Skylab S193 experimental altimeter has demonstrated a system bias change of less than 20 cm in approximately 6 months of orbital operation. Altitude noise levels slightly less than 1 m have been maintained.

Altimeter tracking over the Great Salt Lake and the Great Lakes obtained altitudes above mean sea level for these features that correlate very nearly to those listed on maps. For mapping the ocean topography (ref. 3–81), a typical system error model has been produced (table 3–VI). Both the uncorrected magnitude and the residual of the best-known corrections that are applied to the data are shown.

Antenna beam pointing and antenna height bias are the two factors that are most critical to mapping surface topography. True

[3] NASA: Earth and Ocean Physics Applications Program. Vol. I—Executive Summary, Vol. II—Rationale and Program Plan, Sept. 1972 (NASA internal document, restricted distribution).

satellite heights are difficult to determine when short orbit arcs are used for analysis of the data. Also, the altitude of the satellite is continually changing, which affects the antenna pointing. Therefore, methods have been developed to extract pointing information from the altimeter waveforms and then to apply corrections to the altitude based on this information.

Figure 3–45 also shows data obtained from a pass over the Cape Verde Islands on September 3, 1973. For comparison, the Goddard (Marsh-Vincent) geoid (refs. 3–44 and 3–50) is shown on the graph. The absolute difference between the altimeter geoid and the Goddard geoid of approximately 45 m is well within the estimated orbit uncertainty. The dotted line on the graph is the geoid shifted for shape comparison. The overall comparison is good except for the 12-m undulation in the vicinity of the Cape Verde Islands. Detailed analyses of the altimeter footprint, noise characteristics, and ground-track indicate that the altimeter was not over land during any part of the pass. Because dynamic sea-surface effects could explain only a few meters of the undulation observed, the geoid undulation observed is surmised to be a real feature.

Figure 3–46 illustrates the altimeter-derived geoid for a pass of data taken on the Skylab 3 mission on September 13, 1973. These data were taken as the altimeter passed over the Mid-Atlantic Ridge in the North Atlantic. Excellent agreement with the general shape of the geoid is again seen and the offset is well within the expected orbit accuracy. A comparison of the altimeter geoid with the bottom topography in the area also shows excellent correlation.

The Skylab altimeter data analysis results are representative of numerous data that have been studied. The instrument performance was excellent, and the geoid shape information derived correlates well with the Goddard global geoid. Also, a strong correlation appears to exist between the derived geoid and underwater topographic features. The agreement between Sklab data and the predictions of system models has been extremely close (ref. 3–82). For example, figure 3–47 illustrates the agreement between

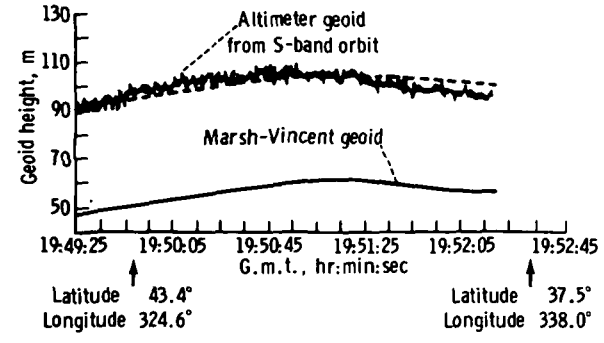

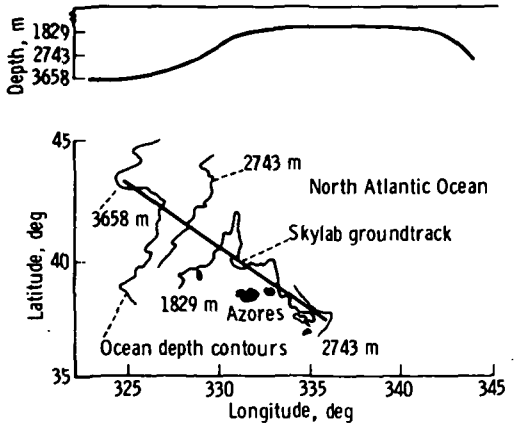

FIGURE 3–46.—Skylab altimeter pass over the Mid-Atlantic Ridge in the North Atlantic.

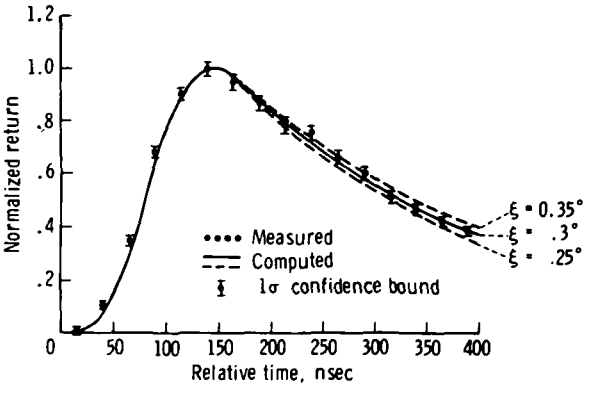

FIGURE 3–47.—A comparison between Skylab data and the predicted waveform (where ξ is pointing offset from nadir).

Skylab data and a predicted waveform for a 0.3° pointing error. The low one-sigma variation indicates the quality of that system for determining pointing.

Future developments.—The AAFE pulse compression altimeter development will increase the radar sensitivity and flexibility. This increase improves the radar performance over the NRL nanosecond pulse radar and establishes the feasibility for use in satellite altimetry. The GEOS–C altimeter experiment is primarily intended to demonstrate the operational utility of altimetry for geodesy and oceanography. Thus, the GEOS–C altimeter experiment follows the Skylab S193 altimeter experiment in a planned sequence of developments leading to an operational satellite system for oceanographic applications. The GEOS-C altimeter capability to measure mean-sea-level and ocean-wave heights will be greatly improved over the S193 altimeter. Experiments with GEOS-C (ref. 3–83) will be improved over the Skylab experiment because of improved orbital determination for GEOS-C. The orbital determination capability of the GEOS-C experiment will represent the best in the state of the art in this technology and will show from planned experiments what factors limit this technology for an operational oceanographic satellite. The next planned altimeter is for SEASAT–A and will have two modes of operation. In mode A, the altimeter will have a maximum range noise of 31 cm at a data output rate of 10 Hz, and in mode B, a 10-cm range noise at a data output rate of once per second. An internal calibration mode will provide a capability of an absolute range accuracy calibration to within ±25 cm. Ocean backscatter coefficients will be determined to ±1 dB, and the measurement of significant wave height $H_{1/3}$ of the ocean surface will be determined to ±25 percent of $H_{1/3}$ or 0.5 m, whichever is greater, in the $H_{1/3}$ range of 1- to 20-m wave height. The requirements for mode B are the same as for mode A except that $H_{1/3}$ will be accurate to ±10 percent or 0.5 m, whichever is larger, and that all the data outputs specified will be determined in real time onboard the satellite instead of by ground processing. The mode B goal will be achieved by the use of an onboard maximum-likelihood processor, which will adaptively change the tracking and sea-state algorithms as a function of signal-to-noise ratio and sea state.

Applications.—The immediate application of active microwave sensors is in the area of measuring sea state. The ability of mapping sea state globally and synoptically by active remote sensors would provide reference data needed to plan shipping routes, design ships, design offshore structures, and help plan future ports. The knowledge of sea state will also enable the testing of present meteorological and oceanographic models and aid in improving the understanding of the air/sea interactions so that better models can be derived for forecasting sea state and weather.

The intrinsic values of monitoring sea state are not limited to the consideration of wave forces or energy. The knowledge of sea state in the form of a wave spectrum can be used to measure ocean-surface currents (ref. 3–66). The information on global and synoptical ocean surface current systems will be very cost effective in efficiently deploying ships. Understanding mass transport, heat transport, and current systems has dominant effects on economies of marine communities and global weather predictions.

Scatterometers

Introduction.—Active microwave sensors have been used to measure range, reflection or scattering coefficient, and shape of the returned pulse from various objects or scenes. The ability with which a scene or object scatters incident microwave energy can be assessed by measuring the radar-scattering cross sections at various frequencies, polarizations, and incident angles. A microwave scatterometer is a special-purpose radar that is used to quantitatively measure the target reflectance or scattering cross section. Microwave scatterometers are usually simpler than conventional radars because range and velocity measurement capability and the high

spatial resolution (short pulse) requirements are eliminated. Long-pulse and continuous-wave scatterometers have been used to measure the scattering signatures of rough surfaces such as terrain or the ocean. The quantity of interest is the radar-backscatter coefficient, which is the backscattered power per unit area normalized for antenna gain, range loss, and the transmitted power.

The result of measurements taken to date reveals the following information about the dependence of the backscattering cross section from the ocean on windspeed:

1. A range of radar wavelengths exists for which backscatter is primarily dependent on surface windspeed, relatively insensitive to large-scale roughnes.
2. Backscatter at and near the vertical (0° incident angle) monotonically decreases with increasing windspeed.
3. Backscatter from incident angles greater than 20° from the vertical monotonically increases with increasing windspeed.

A representation of these three features of ocean backscatter as a function of windspeed and incident angle for 2- to 3-cm wavelength radar illumination is shown in figure 3–48. For windspeeds less than 1 m/sec, essentially no sensible backscatter is seen at any angle of incidence; the strong radar return at 0° incident angle is from specular mirror reflection (shown as a dotted line). As the windspeed increases toward 2 m/sec, patches of roughness begin to appear on the surface where turbulent gusts at the surface exceed the threshold for wind-to-water coupling. The small capillary waves generated by these gusts produce some backscatter at all angles of incidence with very rapid rates of change of backscatter as compared to windspeed.

At windspeeds above approximately 1.5 m/sec, the total surface is essentially covered with wind-driven capillary waves from which the large waves will grow. The approximate magnitude of backscatter cross section at 0° and 55° incident angles in figure 3–48 has been formed from good, but sparse, data taken between the extremes of approximately

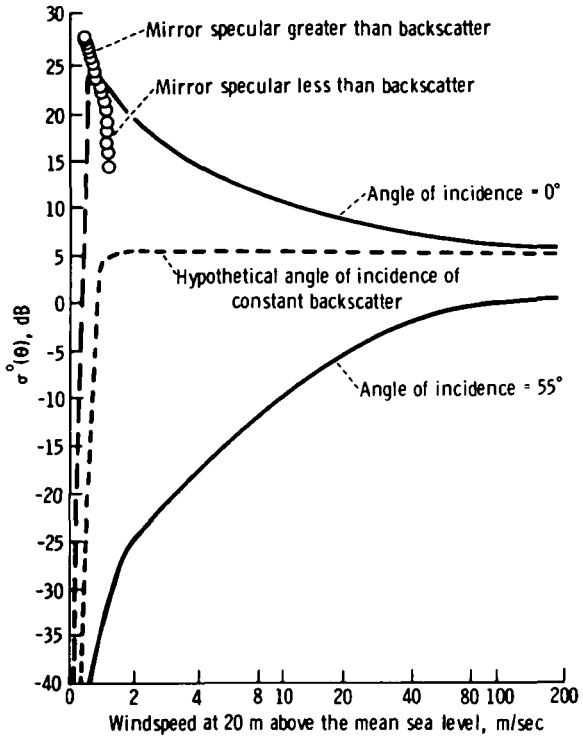

FIGURE 3–48.—Representation of approximate magnitude of backscatter cross section from the ocean at 2- to 3-cm radar wavelengths.

2- to 30-m/sec windspeeds. The continuation of the curves beyond 30 m/sec shows that the monotonic changes in backscatter cross section initiated at low windspeeds probably do not stop abruptly but become very slight at higher windspeeds. The local slope of the curves at high windspeeds shows that extremely accurate measurements of the backscatter must be made to sense small-percentage changes in windspeeds, but this accuracy is required over only a small range of backscatter values. Alternatively, the local slopes at low windspeeds show that less-accurate measurements are required to sense small-percentage windspeed changes.

The set of curves for backscatter is compared to windspeed at all angles of incidence between 0° and 55° lies between the curves shown in figure 3–48, being far apart at low windspeeds and close together at high windspeeds.

Because the change of backscatter compared to windspeed has a change in sign at some incident angle between 0° and 20°, a hoped-for discovery would be an incident angle for which the backscatter cross section is constant for all windspeeds. This constancy would provide a natural reference backscatter cross section and eliminate the requirement for absolute backscatter cross-section measurements for windspeed measurements. The dashed line in figure 3–48 shows that this hoped-for "hypothetical incident angle of constant backscatter" lies at approximately the average level of the backscatter as compared to windspeed for incident angles between 5° and 20°.

Other aspects of backscatter measurements present both an opportunity and a problem:

1. The upwind, downwind, and crosswind viewing directions give different values for backscatter cross sections.
2. The sensitivity of backscatter to upwind, downwind, and crosswind viewing directions is different at each incident angle.
3. The sensitivity of backscatter to upwind, downwind, and crosswind viewing angle at each incident angle is also windspeed dependent.

Figure 3–49 shows typical data of this kind. An interesting observation is that the upwind-downwind dependency was predicted and explained rather well 20 yr ago at NRL, assuming specular points as the backscatter mechanism and wave tank measurements of the probability distributions of surface facets as compared to windspeed. These statistics included not only the distributions of surface slope normals but also the distributions of the areas of these specular reflecting surfaces. Because NRL could not measure these same statistics in other directions, the crosswind dependency was not predicted. The problem created by this feature of ocean backscatter is obvious: with perfect instrumentation—that is, no error in the backscatter measurements but no knowledge of the viewing direction with respect to the wind direction—a radar cross-section data spread of many decibels will be obtained. For example, in figure 3–49, a 6-dB spread exists upwind to crosswind at a 13.9-m/sec windspeed, 40° incident angle, with an average backscatter coefficient over all wind heading angles of −10 dB, whereas at a 6.5-m/sec windspeed, the average is approximately −15.5 dB, with an upwind-to-crosswind spread of 4 dB.

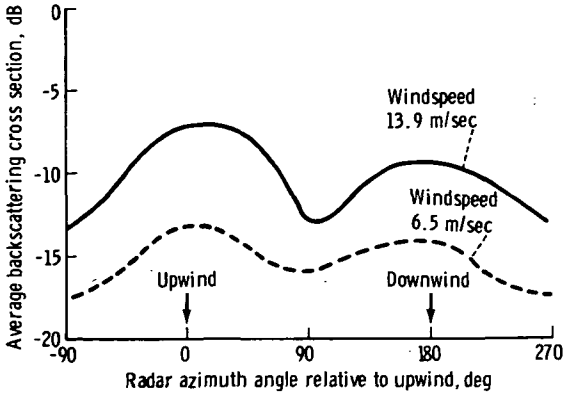

FIGURE 3–49.—Langley Research Center values of σ° compared to wind heading (vertical transmit/vertical receive polarization; incident angle of 40°).

This problem can only be solved either by knowing the viewing direction with respect to wind directions or by viewing the surface from enough different directions so that the upwind, downwind, and crosswind curves can be obtained as input data. However, this method represents an opportunity because, with this curve as input data, the wind direction in that resolution cell has also been measured. These resolution-cell data at many incident angles in a swath along the satellite path are required to properly map the windfields over the oceans and/or the pressure fields at the 100 000-N/m^2 level.

Scientists working with scatterometry data have recognized and accepted the facts illustrated by figures 3–48 and 3–49 and, finding that the data are repeatable, are starting to design their instruments, data-gathering procedures, and data-processing algorithms to solve the problems and take advantage of the directional data to the extent possible, given the satellite platform constraints.

With proper system design, satellite-borne

scatterometry will provide a majority of the input data required for mapping the windfields over the oceans with refresh times of less than 12 hr.

Typical scatterometer measurements.—Radar observations of the scattering cross sections from the ocean surfaces have been conducted for nearly 30 yr. In almost all cases, only the backscattering cross sections have been measured.

The NRL has conducted the most comprehensive measurements of the backscattering cross sections from ocean surfaces (refs. 3–84 to 3–89). These measurements have been conducted at several frequencies and polarization combinations. Both airborne and ground sensors have been used by NRL. A summary of the significant NRL measurements is given in table 3–VII.

The NASA has flown numerous missions with spaceborne and airborne sensors over ocean surfaces (refs. 3–63, 3–90, and 3–91). Scatterometer data have been collected at 0.4 and 13.3 GHz. Spaceborne radar data at 13.9 GHz (Skylab S193) have also been obtained. Backscattering cross-section data have also been collected by LaRC at 13.9 GHz. Table 3–VII also presents a summary of the NASA measurements. Other data, such as those recorded by Newton and Rouse (ref. 3–92), are available.

The interaction of the ocean surface winds and waves is a complex phenomenon. A mathematical model of ocean surface roughness as a function of surface wind velocity is not available. The large volume of the radar-backscattering cross-section data gathered over rough oceans has aided in the understanding of the interaction of waves and winds on the ocean surface. In this section, typical radar-backscattering cross-section data are presented. Problem areas and future efforts for their resolution are also outlined.

Experimental studies of the sea echo at 9.2-, 3.2-, and 1.25-cm wavelengths have been

TABLE 3–VII.—*Available Radar Backscattering Cross Sections Over Water/Ocean Surfaces*

Type of measurement and organization	Wavelength or frequency	Polarization combinations [a]	Approximate range of angles of incidence, deg	Range of winds or waves
Spaceborne experiments:				
JSC	13.9 GHz	VV, VH, HV, and HH	0 to 53	2.1 m/sec to more than 28.3 m/sec.
Airborne experiments:				
NRL	0.428, 1.228, 1.25, 4.425, and 8.91 GHz	VV, VH, HV, and HH	0 to 89	2.1 m/sec to 24.7 m/sec.
JSC	13.3 GHz	VV	0 to 60	3.1 m/sec to more than 28.3 m/sec.
	0.4 GHz	VV, VH, HV, and HH	0 to 60	
	13.9 GHz	VV, VH, HV, and HH	0 to 50	
LaRC	13.9 GHz	VV, VH, HV, and HH	0 to 50	3.1 m/sec to 20.6 m/sec.
From platform/bridges:				
NRL	8.6 mm, 1.25, and 3.2 cm	VV	0 to 80	0 to 12.9 m/sec.
Wave tank measurements:				
NRL	9.375 GHz	VV and HH	10 to 86	Millimeter waves of wavelengths from 1.6 to 6 cm.

[a] VV=vertical transmit/vertical receive; VH=vertical transmit/horizontal receive; HH=horizontal transmit/horizontal receive; and HV=horizontal transmit/vertical receive.

described by Kerr and Shain (ref. 3–93). These measurements were primarily aimed at studying the frequency dependence of the radar return at higher angles of incidence (grazing angles as much as 4°). The surface winds and waves have not been reported in these measurements.

Measurements of both the ocean-surface contour and the backscattering cross sections were conducted by MacDonald (ref. 3–84). These measurements were conducted at 1.25 GHz with an airborne radar, and the data corresponding to VV and HH polarization combinations were gathered. These data are shown in figure 3–50.

The details of ocean-surface wind, significant wave height, and mean-square slopes are also given by MacDonald (ref. 3–84). At higher angles of incidence (40° to 82°), the radar cross section decreases from −30 to −60 dB. Data given in figure 3–50 show a strong dependence of windspeed with horizontal polarization returns relative to vertical returns. The range of wind velocities for these measurements extended from 0 to 15 m/sec.

The widely quoted experiments by Grant and Yaplee (ref. 3–85) of NRL were performed at wavelengths of 8.6 mm and 1.25 and 3.2 cm; some results are shown in figure 3–51. These data were taken with a bridge-mounted radar system using VV polarizations. The surface wind velocities ranged from 0 to 12.9 m/sec. The height of the radar above the water surface was 50 m.

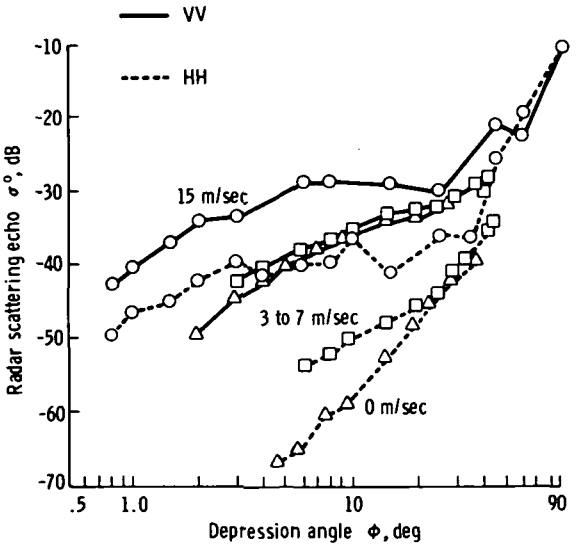

FIGURE 3–50.—Naval Research Laboratory data at 1.25 GHz (ref. 3–84).

These measurements show a rapid decrease in the backscattering cross section as a function of angle of incidence for surface windspeeds below 1 m/sec. At normal incidence for scattering, cross section decreases with an increase in surface wind velocity. For 1.25-cm and 8.6-mm wavelengths, the scattering cross section increases with wind velocity for incident angles higher than 20°.

These measurements do not include the effects of wind direction and winds in excess of 12.9 m/sec on the backscattering cross section. Furthermore, data corresponding to VH, HV, and HH polarizations were not acquired.

From 1964 to 1971, personnel of the NRL acquired numerous sea return data using a single four-frequency airborne radar. The four major measurement programs (refs. 3–64 and 3–86 to 3–89) conducted by NRL were Puerto Rico (1965), North Atlantic (1969), Joint Ocean Surface Study I (JOSS I) (1970), and JOSS II (1971). Surface truth measurements were established by ground-based observations.

A summary of NRL measurements and ground data measurements is given by Daley (ref. 3–64). The NRL measurements are given as the median normalized radar cross section (MNRCS). The scattering cross section per unit area has been defined as normalized radar cross section (NRCS).

To establish the average value of the backscattering cross section $\sigma°$, the probability distribution of the NRCS must be known. For a Rayleigh-distributed NRCS, $\sigma°$ can be computed by adding 1.6 dB to MNRCS. Both theory and experiment have shown that the sea return may have a probability density distribution other than that specified by Rayleigh. Hence, the average-to-median ratio

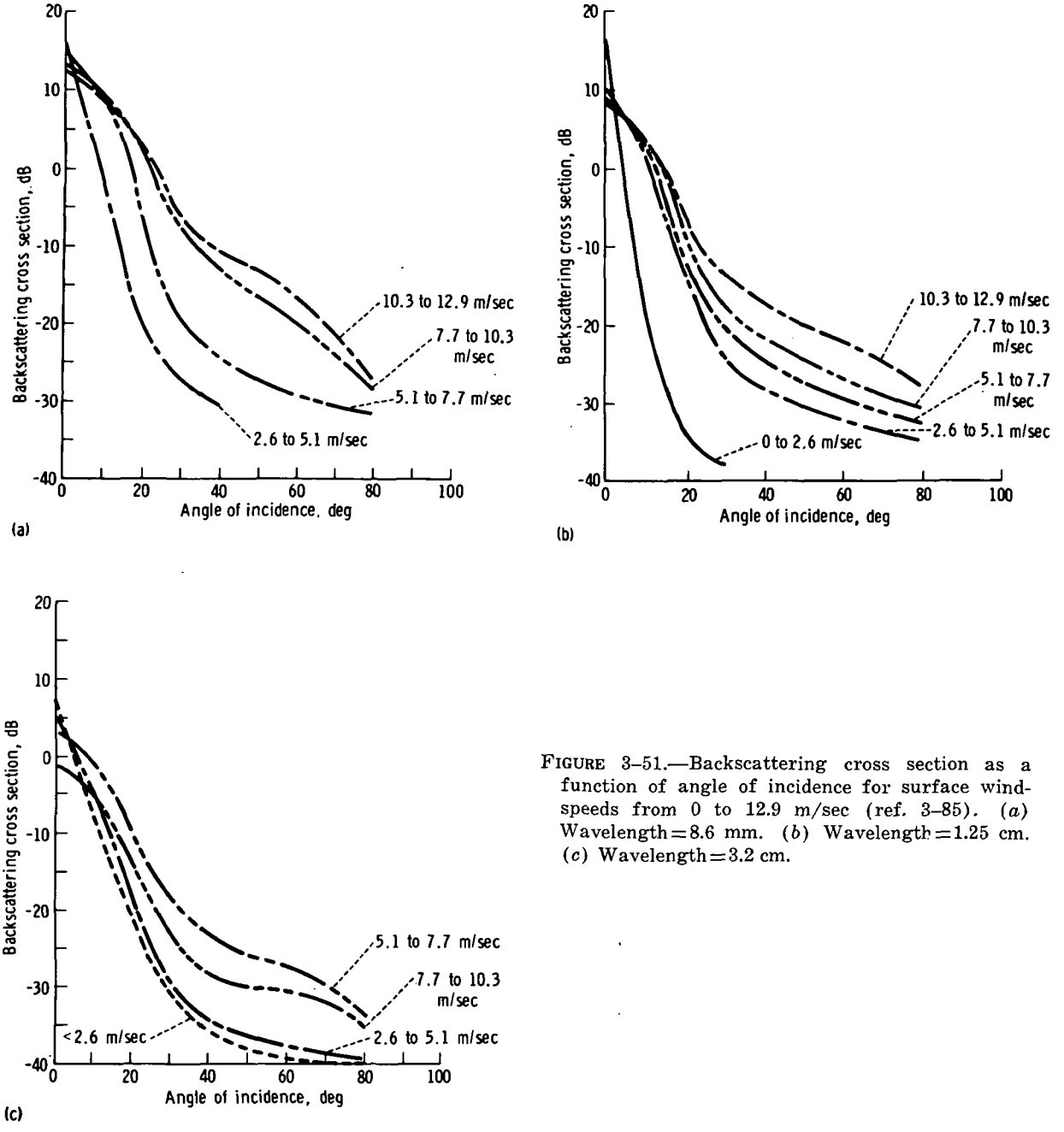

FIGURE 3–51.—Backscattering cross section as a function of angle of incidence for surface wind-speeds from 0 to 12.9 m/sec (ref. 3–85). (*a*) Wavelength=8.6 mm. (*b*) Wavelength=1.25 cm. (*c*) Wavelength=3.2 cm.

may differ from 1.6 dB and depend on the sea-surface roughness.

The previously published data, with the exception of JOSS II (ref. 3–89), do not define the illuminated area in terms of the two-way antenna pattern. Corrections to the NRL data are given by Daley (ref. 3–64). Typical NRL data acquired during the JOSS II mission are given in figure 3–52. The MNRCS decreases with increasing wind velocity at vertical incidence. The NRL measurements have been used to develop models for the frequency dependence of radar-backscattering cross section from the ocean surface. A more recent

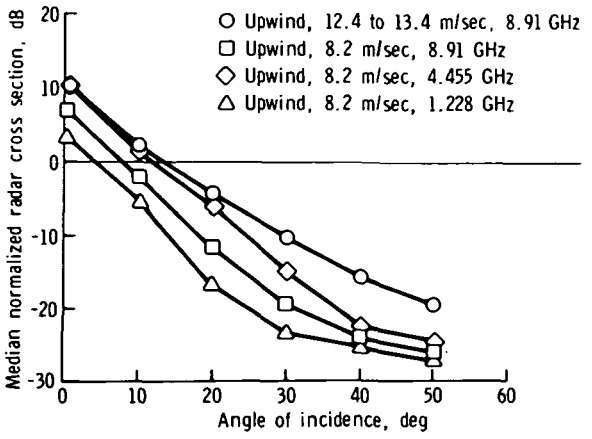

FIGURE 3–52.—Median normalized radar cross section as a function of incident angle for various frequencies and windspeeds (vertical transmit/vertical receive polarization).

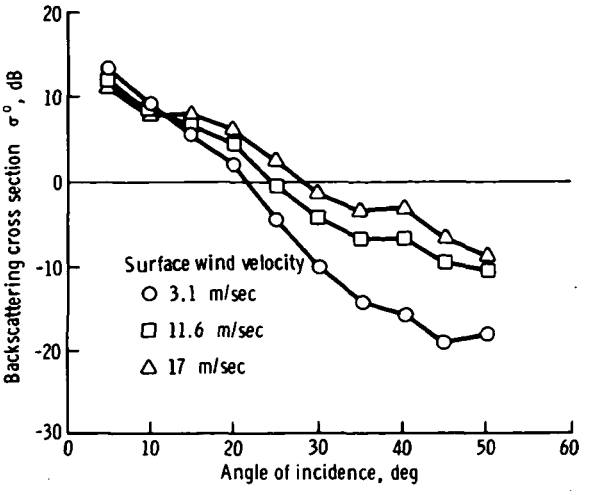

FIGURE 3–53.—Backscattering cross section as a function of angle of incidence for 13.3-GHz scatterometer for mission 119 (vertical transmit/vertical receive polarization).

analysis of NRL data shows correlations between surface wind velocity and the normalized radar cross section. Backscattering from capillary waves has also been investigated by NRL (ref. 3–94).

During a period of several years, many aircraft missions have been flown by NASA JSC to study the dependence of radar return on such parameters as local windspeed, wind direction, and the spectrum of the sea. Data have been collected using scatterometers at frequencies of 0.4, 13.3, and 13.9 GHz. Extensive surface truth has been compiled, including wind and wave measurements. Airborne laser profilometers were used to measure sea-surface spectra. Photographs of the ocean and clouds are also available for detailed correlation analysis. For the 0.4- and 13.3-GHz scatterometers, the data are collected simultaneously for incident angles between 60° and −60° (ref. 3–95) by using coherent Doppler wave techniques.

The digital-processing program yields the backscattering cross section as a function of the angle of incidence. The typical backscattering cross sections for 13.3 GHz are given in figure 3–53 (ref. 3–63). These data are for NASA JSC mission 119. For the 13.3-GHz scatterometer, a strong dependence of the backscattering cross section on surface-wind velocity has been shown (ref. 3–61).

The NASA 13.9-GHz RADSCAT (also known as AAFE RADSCAT) is a multiple-polarization system. Data corresponding to VV, HH, VH, and HV polarization combinations and radiometer vertical- and horizontal-polarization data (ref. 3–96) can be collected. The system antenna can be moved automatically, corresponding to 0°, 10°, 20°, 30°, 40°, and 50° pitch angles, or can be manually adjusted at each of these angles. Figure 3–54 is a typical example of the data gathered over ocean scenes using this system.

The most recent addition to active microwave measurements over ocean scenes has been the data acquired with Skylab S193 operated in several modes both in-track and crosstrack (ref. 3–97). Scatterometer data corresponding to VV, VH, HH, and HV polarization states were gathered. An altimeter was also used to collect backscattering cross-section data to approximately a 16° incident angle.

Ocean-surface measurements were made simultaneously for detailed data analysis, and data have been gathered over oceans having calm to hurricane conditions. Examples

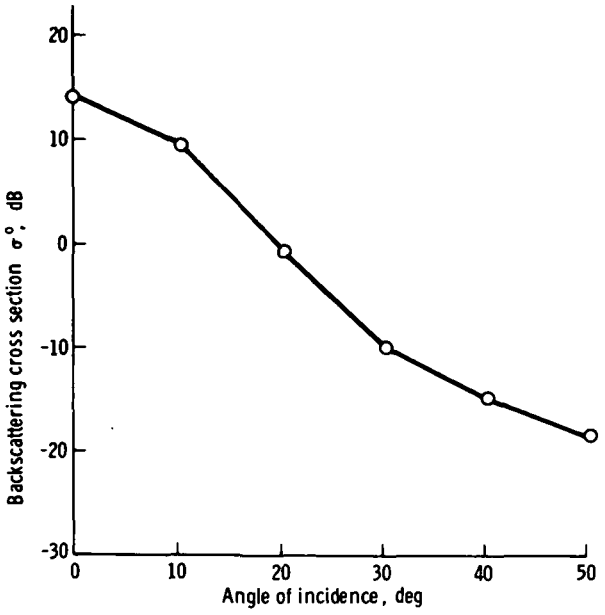

FIGURE 3–54.—Backscattering cross section as a function of incident angle for a 13.9-GHz aircraft RADSCAT (upwind: 6.7 m/sec; vertical transmit/vertical receive and horizontal transmit/horizontal receive polarizations).

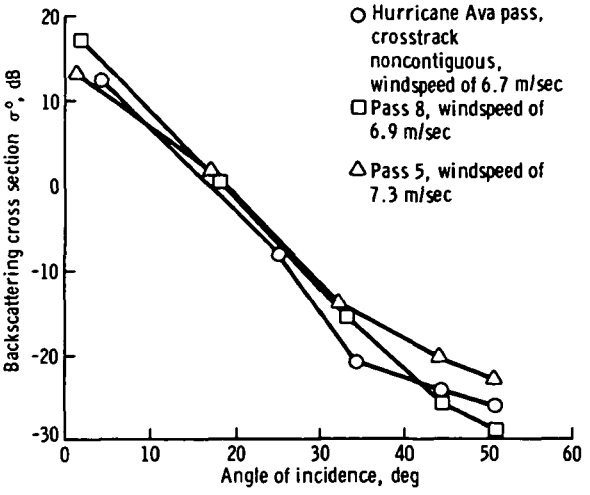

FIGURE 3–55.—Comparison of S193 scatterometer backscattering cross sections for EREP passes 5 and 8 and Hurricane Ava pass.

of S193 data are given in figures 3–55 and 3–56. In these figures, Earth Resources Experiment Package (EREP) (passes 5 and 8) and Hurricane Ava data are given. The S193 scatterometer data show a strong dependence on ocean-surface wind velocity.

Relationship between backscattering cross sections and ocean-surface wind velocity.— This section summarizes significant results in the investigation of the correlation between radar backscattering coefficient σ° and the ocean-surface windspeed W. This correclation has been investigated intensively during the past decade (refs. 3–63, 3–89, 3–91, 3–92, and 3–96) and much σ° data have been acquired by using airborne and spaceborne sensors. The major sources of active microwave data are NRL, JSC, and LaRC.

The relationship between σ° and W is currently being investigated. However, certain conclusions have been made based on aircraft- and spacecraft-acquired data analysis:

1. For angles of incidence beyond about 25°, the backscattering cross section increases with windspeed to 25 m/sec of wind for 13.3-, 24-, 1.25-, 13.9-, 4.455-, and 8.91-GHz frequencies.

2. Near and at vertical incidence, the scattering cross section decreases with surface windspeed. This fact has been observed at all frequencies thus far investigated.

The remote sensing of ocean-surface winds can be more effectively accomplished by measuring the ratio Q_0 defined by Krishen (ref. 3–63).

$$Q_0 = \frac{\sigma^\circ \text{ at or near vertical}}{\sigma^\circ \text{ at or near } 45^\circ \text{ incident angle}} \qquad (3\text{–}14)$$

The investigation of the winds over oceans can be divided into two parts for remote sensors: windspeed and wind direction. Detection of windspeeds using active microwave sensors has been done successfully, but little has been accomplished concerning the wind direction detection. The prediction of wind detection has been investigated by LaRC (ref. 3–96). This aspect of the problem still requires more research.

To study the effect of the wind on the backscattering cross section, the directional spectrum of the high-frequency gravity-capillary

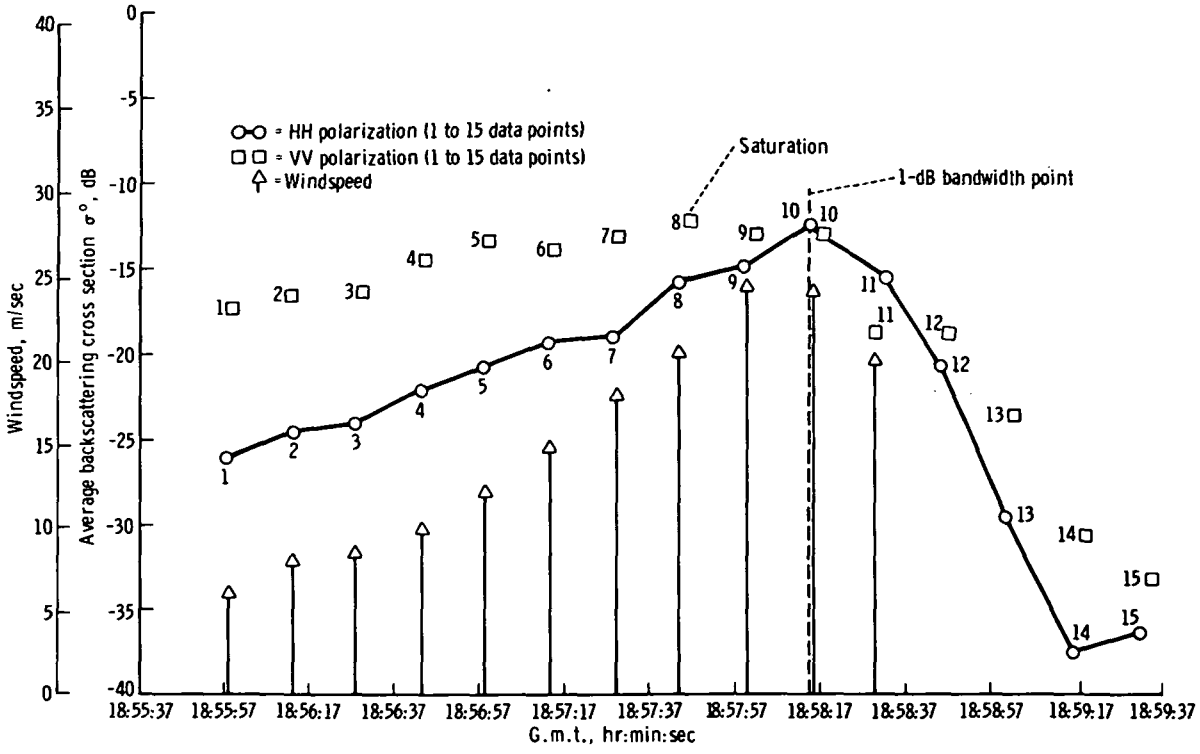

FIGURE 3–56.—Skylab S193 backscattering cross section as a function of time (roll angle of 46.6°; incident angle of 50.7°; Hurricane Ava pass). Data points 1 to 13 refer to locations in figure 3–59.

structure of the sea could be expressed as

$$W(Z) = kZ^{-k_3} \qquad (3\text{–}15)$$

where k and k_3 are constants, $Z = (p^2+q^2)^{1/2}$, and p and q are radian wave numbers on the ocean surface.

At higher angles of incidence, the backscattering cross section can be expressed, in part empirically and in part caused by scattering from a small gravity-capillary structure, as (ref. 3–63)

$$\sigma^\circ{}_{ij}(\theta) = k_1 W^{k_2} |\alpha_{ij}|^2 \cos^4\theta \ (\text{cosec}\,\theta)^{k_3} \qquad (3\text{–}16)$$

In equation (3–16) α_{ij} is defined as

$$\alpha_{HH} = \frac{\epsilon - 1}{(\cos\theta + \sqrt{\epsilon - \sin^2\theta})^2} \qquad (3\text{–}17a)$$

$$\alpha_{VV} = \frac{(\epsilon-1)\,[(\epsilon-1)\sin^2\theta + \epsilon]}{(\epsilon\cos\theta + \sqrt{\epsilon-\sin^2\theta})^2} \qquad (3\text{–}17b)$$

$$\alpha_{VH} = \alpha_{HV} = 0 \qquad (3\text{–}17c)$$

where ϵ is the complex dielectric constant of the surface and k_1 and k_2 are constants (k_1 is related to constant k).

The cosec θ form given in equation (3–16) can be simplified and expressed in cot θ form as (ref. 3–63)

$$\sigma^\circ{}_{ij}(\theta) = k_1 W^{k_2} |\alpha_{ij}|^2 (\cot\theta)^{k_3} \qquad (3\text{–}18)$$

In figure 3–57, the experimental and calculated data (using eq. (3–14)) for upwind mission 119 NASA JSC 13.3-GHz data are shown. The values of constants are $k_1 = 0.026$, $k_2 = 1.324$, and $k_3 = 5.47$.

Table 3–VIII is the 1.25-cm data reported by Grant and Yaplee (ref. 3–85). The values of k_1, k_2, and k_3, using cot θ form, are $k_1 = 0.00107$, $k_2 = 1.64$, and $k_3 = 5.03$.

These studies have also demonstrated that scatterometers can be used to determine the directional spectrum of small gravity and

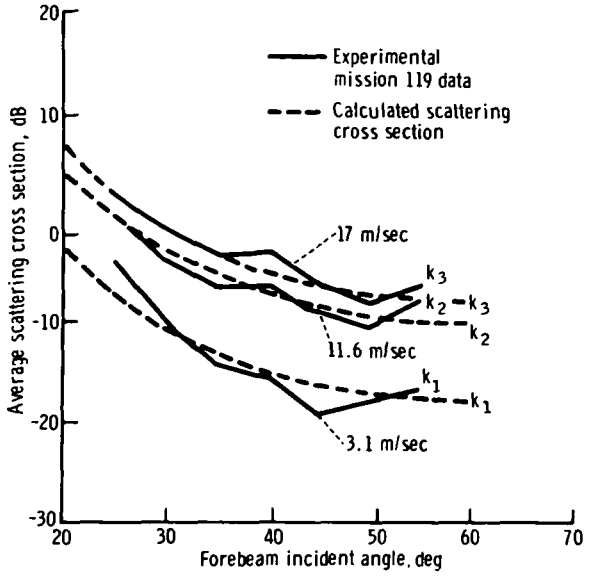

FIGURE 3–57.—Comparison of calculated and experimental scattering cross section for mission 119.

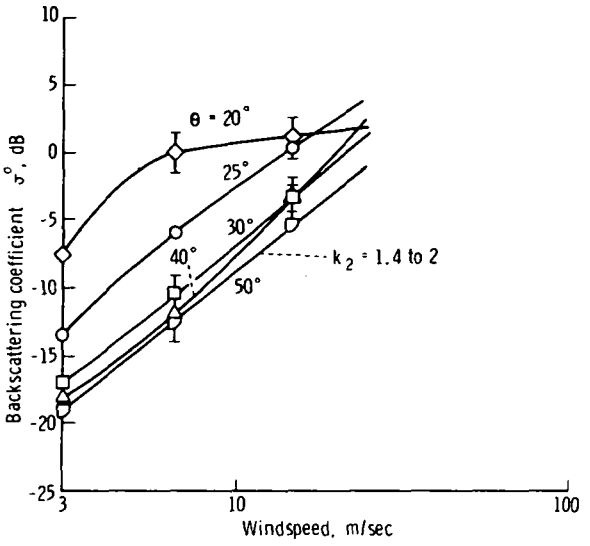

FIGURE 3–58.—Langley Research Center values of backscattering coefficient as a function of windspeed (frequency of 13.9 GHz; vertical transmit/vertical receive polarization; downwind).

capillary waves at various surface-wind velocities.

Measurements by NRL have also been analyzed to determine dependence of σ° on W. The values of k_2 are somewhat smaller (ranging from 0.2 to 1.9) compared to the values for NASA data. However, the operating frequency of NASA scatterometers (13.3 GHz) is higher than for NRL radar.

The LaRC has acquired 13.9-GHz data for various windspeeds. The values of k_2 for these data (ref. 3–96) range from 1.4 to 2.0 (fig. 3–58).

From the data shown in figure 3–58, the measured power factor k_2 apparently lies somewhere between 1.4 and 2.0 at those incident angles at which the radar return is dominated by the capillary wave structure. Initially, this may appear to be a trivial range of uncertainty. Nevertheless, many arguments have been generated among various groups because the value of k_2 and the instrument characteristics essentially define the accuracy and the upper limit on the measurement of windspeed.

TABLE 3–VIII.—*Backscatter as a Function of Mean Windspeed and Angle for the 1.25-cm VV Case*

Mean windspeed, m/sec	Backscatter, dB, for—			
	θ=20°	θ=30°	θ=40°	θ=50°
3.9	−14.0	−25.0	−28.75	−31.10
6.4	−12.4	−21.25	−25.00	−27.60
9.0	− 9.0	−17.8	−22.5	−24.4
11.5	− 7.5	−14.2	−17.5	−20.2

The Skylab EREP Hurricane Ava pass provides backscattering cross sections for a wide range of wind velocities. A quick-look evaluation (refs. 3–98 and 3–99) of the Hurricane Ava data shows a strong dependence of σ° on the wind velocity. The S193 RADSCAT gathered data in a crosstrack (right only) mode for nominal pitch angles of 0°, 15.6°, 29.4°, 40.1°, and 48°. The actual angles attained by the S193 antenna differed from these nominal angles.

The highest pitch angle data (average 46.6°) were taken from approximate areas shown in figure 3–59. The photograph was prepared by NOAA.

The scatterometer data corresponding to average roll angles of 31.35°, 40.61°, and

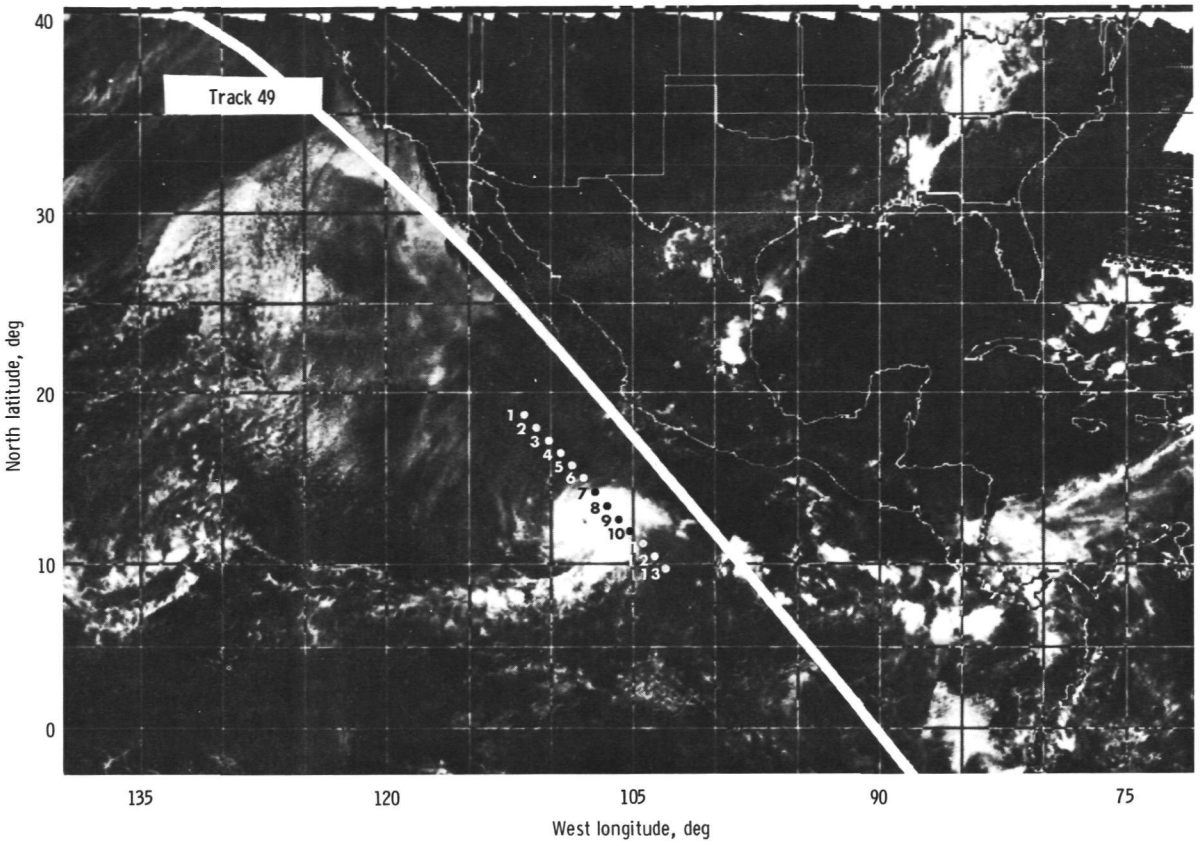

FIGURE 3–59.—Composite photograph showing approximate locations, from north to south, of 13 of the data points plotted in figure 3–56.

46.6° are given in figures 3–56 and 3–60 as a function of time. The wind velocities in these figures were taken from the report prepared by Hayes et al.[4]

During this pass, Skylab was in the solar inertial mode. The data drop after G.m.t. 18:58:17 is due to attenuation by the 0° Doppler filter. The dashed line marked 1-dB bandwidth point corresponds to a Doppler filter attenuation of 1 dB. No Doppler filter corrections have been done for the data given in these figures. In figure 3–59, locations of points 1 to 13 of figure 3–56 have been shown.

To study the wind dependence for data presented in figures 3–56 and 3–60, a function of the form

$$\sigma^\circ = k_1 W^{k_2} \qquad (3\text{–}19)$$

was used. A least-mean-square fit yields the following results (ref 3–98):

1. For the average roll angle 31.35°, $k_2 = 0.65$.
2. For the average roll angle 40.61°, $k_2 = 0.60$.
3. For the average roll angle 46.6°, $k_2 = 1.89$.

This wind dependence has been investigated for the data only to G.m.t. 18:48:17; the wind direction was very nearly downwind for these data points. No atmospheric corrections were made to the data.

Problem areas.—The comparison of backscattering cross sections from the various ex-

[4] Hayes et al.: A Preliminary Analysis of the Surface Truth Data To Be Correlated With the Skylab 2 Data Obtained for S193 Microwave Investigators. Informal report prepared for NASA JSC under contract NAS9–13642, Aug. 1973 (unpublished data).

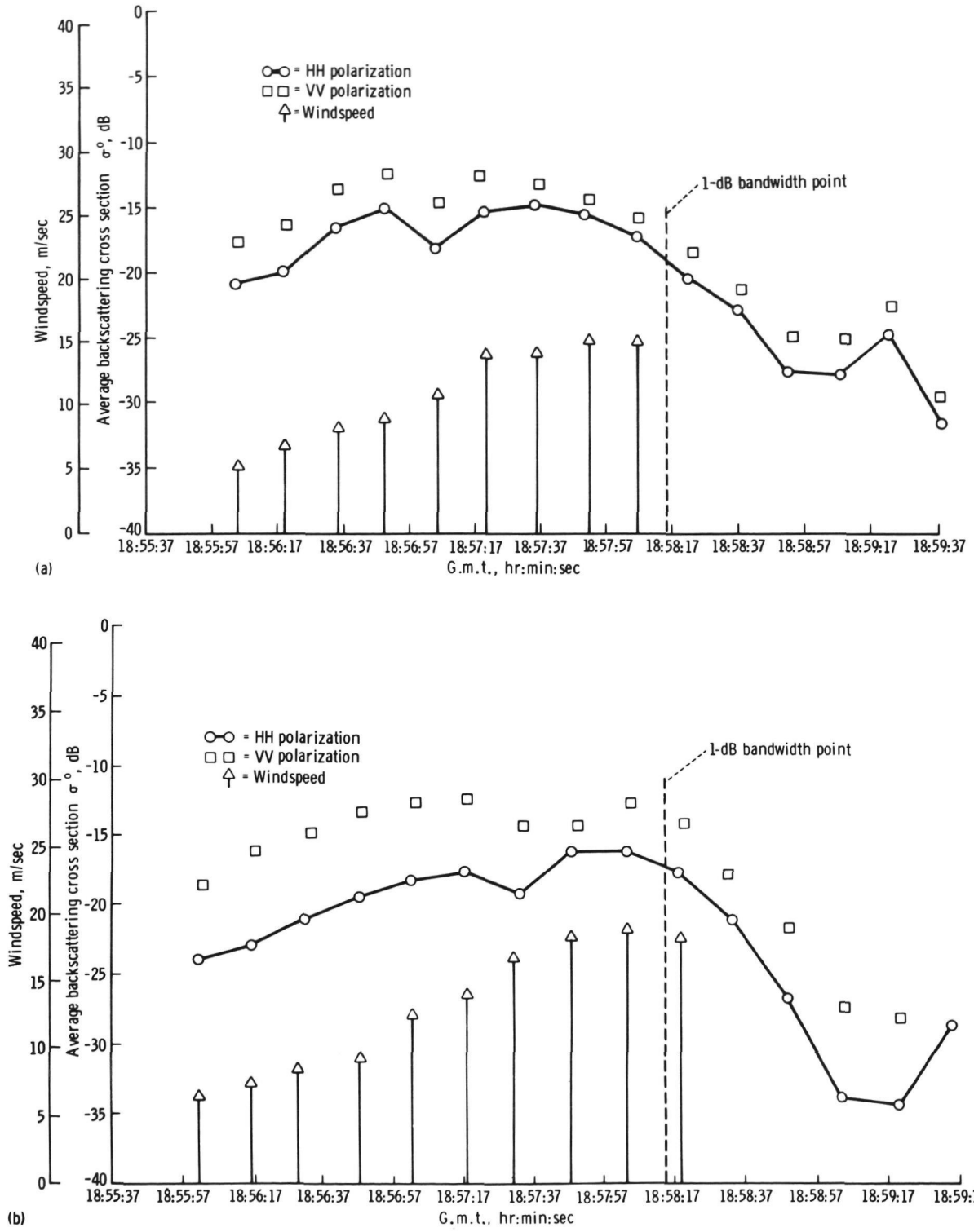

FIGURE 3–60.—Skylab S193 backscattering cross section as a function of time for Hurricane Ava pass. (*a*) Roll angle=31.35°; incident angle=33.92°. (*b*) Roll angle =40.61°; incident angle=43.8°.

periments reveals a wide spread of values under supposedly indentical ocean conditions. This disagreement has caused concern within the community of applications investigators. The sources of disagreement cannot easily be identified, and many of them still remain unknown. Common sources of disagreement fall within the following categories.

Description of the sea: The sea surface and its environment are a complex phenomenon. The identification of the ocean scene has not been given adequately in a majority of experiments. Ocean-surface data (sea spectra, surface-wind velocities, fetch, duration, effect of distant storms, surface contaminants, etc.) and intervening medium data (temperature, pressure, moisture, cloud cover, rainfall rate, spray, etc.) have not been fully specified. Even for the cases in which these data are partially given, the accuracies of the measurements and the methods of data processing differ greatly. For example, the height at which the surface winds are measured differ between experiments.

System and calibration problems: A thorough evaluation of the systems used for measuring ocean backscattering cross sections has not been reported in many investigations, and the precision and accuracy of the radar system has been neither measured nor documented. One-time determination of precision and accuracy is not sufficient because these measurements should be performed just before or after data have been collected with the system. The usual difficulties are encountered in accurate calibration for an absolute measurement of the radar cross section. The calibration methods for various radars differ significantly.

Platform perturbations: The changes in the attitude of the aircraft or spacecraft cause errors in the measurements. In many investigations, the effects of platform attitude variations are not properly compensated. Furthermore, the relative direction of flight should be properly maintained with respect to the known surface-wind vector for experimental aircraft missions. Otherwise, an unknown bias may be added to the data, as illustrated in figure 3–50.

Data collection and processing techniques: Subtle differences are observed in data collection techniques among various investigations. The extent of averaging of the data differs for various experiments. When several hours are required for collection of σ° as a function of angle-of-incidence data, the wind velocities may have changed direction significantly. When large areas are averaged, a nonuniform windfield could exist.

The algorithms used for processing the data differ in many cases. In several investigations, the value of backscattering cross section is referenced to an arbitrary number.

Future research and development.—The performance of NASA 13.3- and 13.9-GHz scatterometers has been fully demonstrated by aircraft and Skylab missions. However, these systems were basically experimental. These programs have indicated a need for improving both hardware and software capabilities. Also, procedures for collecting the data should be revised for an operational system.

The decade ahead requires systems that can be run reliably for extended periods of time. Also required are computational techniques that will automatically yield backscattering cross-section data without manual processing. To achieve this goal, the following recommendations for research and development are given:

1. Improved radar calibration techniques: After each data collection period, a calibration period should follow. The frequency of these calibrations will depend on the performance of the system. Some technique of external calibration should be adopted. Corner reflectors over smooth deterministic targets can be used for airborne and spaceborne scatterometers. Internal calibrations are undesirable because they do not involve all the paths through which the actual returned energy goes.

2. Improved systems design: Improvements are needed in the reliability of the antenna pointing, switching logic, and polariza-

tion isolation. System drifts, resolution, and noise-level fluctuations must be reduced in future airborne and spaceborne systems.

3. Data-processing techniques: For operational systems, highly efficient data-processing techniques are needed; no reliable data display techniques have yet been advanced. Onboard processing of the data should be explored, and the digitally processed data should be color coded to display ocean winds and waves for visual interpretation and use. These programs should be capable of processing large volumes of reflectivity data and displaying these data on a world map.

4. Calibration data measurements: For spaceborne and airborne instruments, the calibration data corresponding to each subsystem are usually measured in the laboratory. The amplifier, mixer, and filter gains are some examples. For instruments flown for extended periods, these internal gains change with time. To alleviate this problem, automatic calibration modes should be designed to check all calibration data needed to calculate backscattering cross sections from raw data.

Imaging Radars

An imaging radar has been selected as one of the active instruments for the SEASAT–A payload. An imaging radar was flown in space during the Apollo 17 mission, when the Apollo lunar sounder experiment used synthetic aperture techniques to map the lunar surface and to sound the near-lunar subsurface. Imaging radars have been flown on numerous aircraft and have detected several ocean surface and ice phenomena that are of interest to oceanographers.

Almost all ocean and ice mapping requirements can be fulfilled with radars using synthetic aperture techniques from satellites or with radars using synthetic or real aperture techniques from aircraft. The width of surface imaged from an aircraft platform is approximately 10 to 20 km. However, the width imaged from spacecraft can be 1 to 200 km, which is comparable to the width of an ERTS photograph. Aircraft platforms can be either dedicated aircraft or commercial aircraft. Dedicated aircraft have the advantage of being the most flexible for observation, parameter modification, and target selection. Radars carried aboard commercial aircraft could provide quasi-global coverage, particularly when there are no imaging radars in space. Spacecraft are the only way to obtain global coverage, which is vitally important to the monitoring of wave climatology and polar ice. The tradeoffs between aircraft and spacecraft are discussed further in this section.

The use of either spacecraft or aircraft imaging radars is suggested for the following research and application programs:

1. The mapping of ocean-wave buildup in storms.
2. The global monitoring of ocean-wave spectra.
3. The mapping and monitoring of oil slicks.

Imaging radar observables.—The use of imaging radars for oceanographic observations has been generally overlooked, although these radars have been flown in numerous configurations and over numerous portions of the Earth. However, the following phenomena have appeared in existing imagery.

1. Ocean waves with wavelengths of 50 m or more.
2. Ocean-wave diffraction patterns near shores and structures.
3. Oil-slick patterns caused by internal waves.
4. Slicks from oil and/or freshwater.
5. Ocean-wave differences at current boundaries.
6. Kelp beds.
7. Sea ice cover (floes, leads, polynyas, and ridges).
8. Ocean-wave attenuation in shallow areas.
9. Lake ice cover (floes, leads, polynyas, ridges, and estuary ice cover).

Thus, the imaging radar apparently senses two different aspects of the ocean surface: the longer gravity waves, which disturb the ocean surface with scales larger than the ra-

dar resolution; and the relative abundance of very small capillary waves, which disturb the ocean surface with scales near the radar wavelength.

Some instrumental constraints.—A primary requirement for imaging radars is that they be carried on aircraft or spacecraft platforms. These moving platforms provide the motion that carries the radar past the target so that its Doppler history can be mapped to a single point (synthetic aperture) or so that the target is backscattering for only a short period when it is in a narrow antenna beam (real aperture).

An aircraft platform is advantageous because radars can be varied and the observation area can be easily targeted. Radar parameters such as wavelength can be as short as approximately 1 cm and as long as a few meters, and resolutions and polarizations can be changed with moderately little difficulty.

Investigators at JPL have developed a multifrequency synthetic aperture radar that operates at wavelengths of 3.5 and 25 cm and 2 m, with a nominal resolution of 10 to 30 m. This JPL radar is configured to operate on the NASA CV–900 operated by the NASA Ames Research Center. Another aircraft dedicated to active radar experiments would be a valuable asset to ocean, ice, and other observations. The primary advantage of the dedicated aircraft would be the ability to target its observation area and to allow targets to be imaged at different angles of incidence. Jet aircraft fly at altitudes of slightly less than 15 km; thus, image swath widths could be 15 km either side of the aircraft.

Aircraft platforms for imaging radars can also be provided by large commercial jets, which routinely fly regular routes. Using spacecraft construction techniques, an imaging radar would have low weight, power, and volume. The NASA has developed other nonradar instruments to be carried aboard commercial aircraft. If this commercial aircraft were flown on ocean routes, oceanographers would be provided with ocean-wave spectra across an ocean basin. If this commercial aircraft were flown over the North Pole, daily images of sea ice could be obtained to help monitor ice motion. Imaging radars operating daily on a commercial aircraft could provide valuable quasi-global radar images during the next decade when global monitoring by spaceborne imaging radars is not possible. This period would occur before SEASAT–A is operating, several years after SEASAT–A is shut down, and before Space Shuttle follow-ons are launched and operating.

Satellites and the Space Shuttle will provide the only platforms for truly global coverage. In addition, spaceborne imaging radars can have swath widths of 1 to 200 km and will provide imaging capabilities similar to ERTS space photography. Spacecraft platforms for imaging radars in the 1970's and 1980's include the automatic unmanned SEASAT–A, presently scheduled for launch in 1978; the manned adaptable Space Shuttle Spacelab missions, scheduled for launch in the early 1980's; and Space Shuttle launched, automatic, and unmanned spacecraft, scheduled for launch in the late 1980's. Current plans for SEASAT–A operating parameters are given in table 3–IX.

In summary, both aircraft and spacecraft platforms are needed for radar imaging of ocean and ice phenomena. Aircraft have swaths as much as 15 km but can be easily targeted to areas of interest, if an aircraft is dedicated to active microwave remote sensing. Quasi-global coverages can be obtained with radar images carried aboard commercial aircraft, which will provide valuable data when no spacecraft are in orbit. Radar imagers on spacecraft have the advantage of providing global coverage with wide swaths of 200 km, which yield imagery like that obtained at optical wavelengths by the ERTS spacecraft.

Finally, a need exists for a real aperture radar imager that could be carried on a slow-moving or stationary lighter-than-air ship or that could be stationed on land. This type imager would be extremely valuable for mapping oil slicks that are fairly local and generally slow moving and that may not easily

be imaged by the fast-moving platforms needed for the other ocean and ice phenomena.

Research problems and applications.—The research problems addressable by imaging radar techniques are generally related to (1) ocean waves and their behavior in storms and near currents, shorelines, and structures; (2) behavior of oilspills under the influence of winds and currents; and (3) sea and lake ice dynamics and iceberg motion.

Ocean surface waves: The imaging radar is the only instrument presently existing that can provide maps of the behavior of ocean waves under heavy cloud cover in storm conditions. Tropical cyclones and high-latitude storms generate wavefields of great destructive capability at precisely those times when wave information is most difficult (if not impossible) to obtain. The radar is a promising instrument for providing these data. Present indications are that a spaceborne or airborne radar with 10-m resolution can image wavefields in all wavelengths from approximately 20 m in length to some unknown upper limit. Images of wave systems and amplitude measurements are required when the wave patterns change appreciably in space. This requirement is also needed near hurricanes and storms or in the vicinity of shorelines, jetties, harbor mouths, and offshore structures. Similarly, images are useful near current boundaries such as the Gulf Stream.

TABLE 3–IX.—*SEASAT-A Imaging Parameters*

Wavelength, cm	21.4
Frequency, GHz	1.3
Swath width, km	10 000 and 200
Image length, km	10 to 100
Nadir angle at beam center, deg	20
Angle of incidence at beam center, deg	22
Surface resolution:	
Swath of 10 or 100 km, m	25 by 25
Swath of 200 km, m	100 by 200
Signal-to-noise at beam center, dB	10 to 15
Orbital altitude, km	800
Orbital inclination, deg	108

In the open ocean, images by themselves may not be required; instead, a spectral description is adequate for the spatial homogeneity. The desired quantity is the distribution of wave energy among various wavelengths propagating at varying angles (i.e., the two-dimensional power spectral density). The current thinking is that imaging radar probably gives the slope spectrum rather than the amplitude. These two spectra are related by simple algebraic transformations.

Oilspills: Because of the damping effect of oils on capillary wave structure, oilspills (both natural and manmade) should be visible on imaging radar pictures. For example, it should be possible to assay the existing amount of surface oil cover in a region such as the eastern Gulf of Mexico, which will soon be opened for oil exploration and drilling, and, once in possession of these baseline data, determine if significant increases in that coverage have occurred because of the drilling operations. Furthermore, the drift of oilspills under the influence of currents and winds may be observed, especially in bad weather. This observation is probably best accomplished from aircraft optimized for coastal zone viewing.

Sea and lake ice dynamics and iceberg motion: The discussion related to polar, sea, and lake ice dynamics and the iceberg motion study using a SLAR is given in the section of this chapter entitled "Polar Ice Fields."

Recommendations: imaging radars.—In the first few years of the 1970's, the potential benefits of observing ocean and ice phenomena with a spacecraft imaging radar have been established by many programs, which have shown that ocean wave and ice patterns, forms, and structures appear in radar images. In the remainder of the 1970's and in the 1980's, imaging radars will be flown on SEASAT and the Space Shuttle. For the SEASAT and Space Shuttle missions, the first missions to carry imaging radars in Earth orbit, the radar parameters are being established by well-organized and well-operated programs of user/instrumenter interactions, such as the SEASAT user and instru-

ment working goups. No doubt exists that these early imaging radars will observe and measure interesting and important ocean and ice phenomena.

The scientific and application values of these radars can be further enhanced by careful surface-truth verifications. These surface-truth programs are presently underway and must be continued throughout the 1970's and 1980's. For imaging radars, it is very important to establish the physical surface mechanism of ocean waves that modulates the echo power and to establish the relationship that will convert a two-dimensional transform of a radar image into a two-dimensional wave spectrum. Also, the monitoring of wave buildup in large storms is very important. Ice observation programs must be continued so that the relationship between radar and echo and ice form can be established.

Measurement characteristics.— Experiments concerning nanosecond radar returns from the ocean surface have been conducted by NRL from a fixed tower in Chesapeake Bay, from ships, and from aircraft (ref. 3–100).

The ability of the radar to profile is shown in figure 3–61. The upper trace is a laser profile of sea surface taken along the aircraft groundtrack. The bottom trace was obtained simultaneously by an NRL nanosecond radar. In this comparison, the spot size of the laser was approximately 0.05 by 1 m, and the spot size of the radar was approximately 10 m.

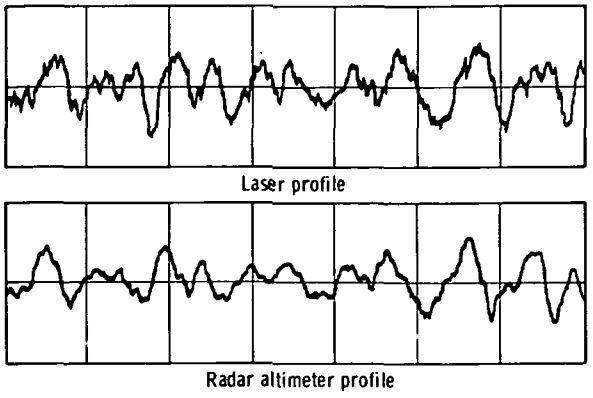

FIGURE 3–61.—Radar ocean profile return.

The poorer resolution of the radar does not affect its ability to return significant information on the vertical structure of the sea surface. The only information lost by the use of 10-m resolution is basically from the shorter water waves and capillary waves, which contain only a small percentage of the entire energy of the wave spectrum. In the surface contour radar, the average of a set number of returns would provide the range from the aircraft to the spot on the ocean illuminated by the radar. As the radar is scanned crosstrack, it will provide a crosstrack profile of the sea surface. As the aircraft advances downrange, successive crosstrack profiles are recorded, which produce a three-dimensional plot of the ocean surface.

Experimental apparatus.—A block diagram of the surface contour radar is shown in figure 3–62. The ranging circuitry would consist of a discriminator, a range-time to pulse-height converter, and a low-pass filter. The output of this circuitry would be a plot of range time, which is equivalent to vertical sea structure as compared to clock or experiment time. These data would then be digitized and stored on tape. All the components shown in figure 3–62 and the components of the ranging capability are readily available.

The elliptical wobble plate, which would be approximately 50 cm in diameter, would be mounted in the lower portion of an aircraft fuselage, although not so low as to be within the airstream. The 10° off-nadir scanning would not require significant modifications to the fuselage of the aircraft.

Physical parameters of the experiment.— Typical values of parameters for the proposed experiment are given in table 3–X. The proposed experiment could use commercially available components. A reasonable estimate for the total volume of the experiment would be 6 m^3, with approximately one-fourth of this volume located in the lower part of the fuselage. No particularly difficult power, data rate, or interface requirements are presented by this experiment, which should be easily accommodated in the NASA Wallops Flight

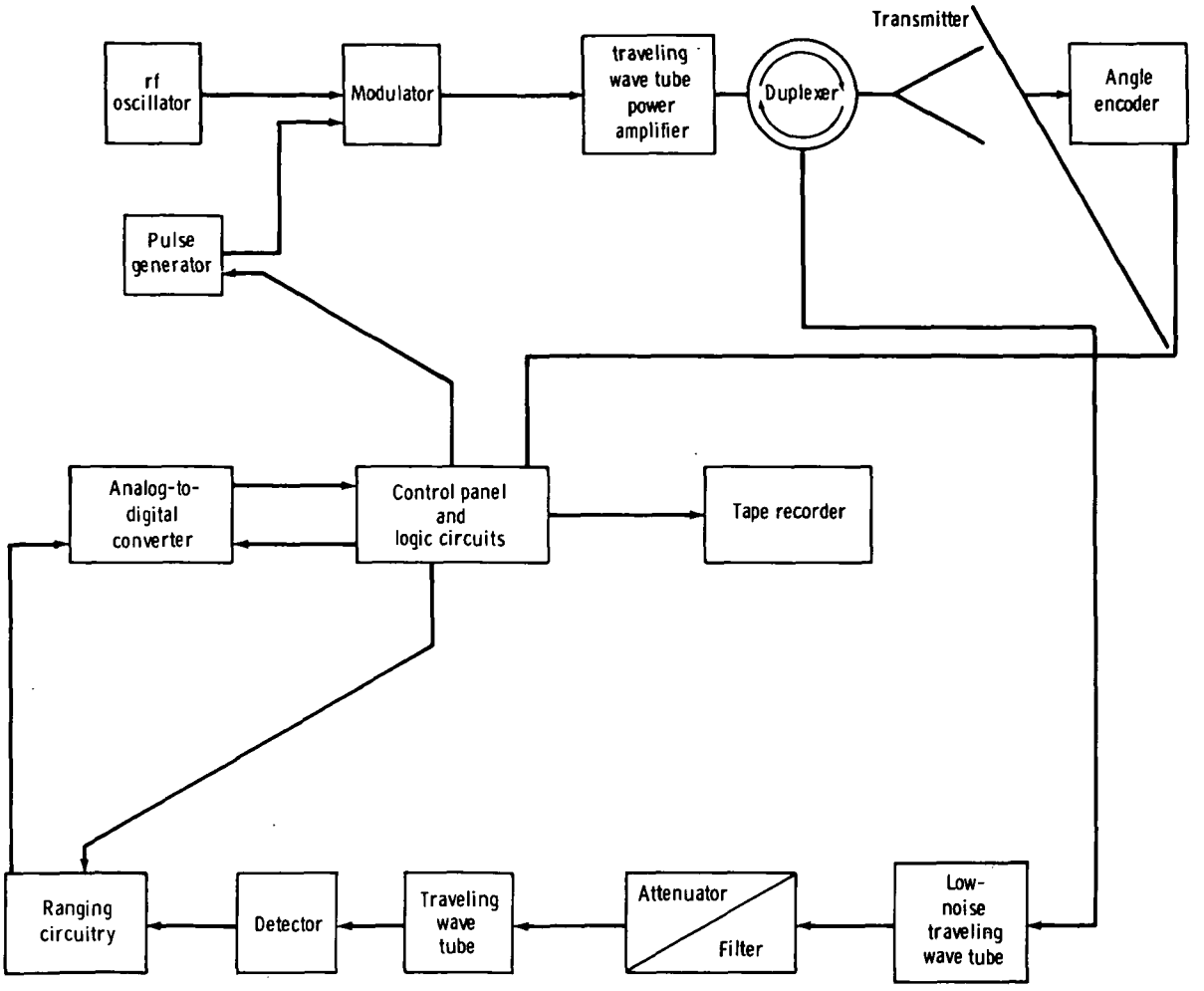

FIGURE 3–62.—Block diagram of surface contour radar.

Center experimental aircraft or another similar plane.

Surface analytic altimeter.—Altimetry technology has rapidly advanced beyond the capability of present satellite orbital determination and geodesy. Both orbital determination and geodetic improvements will be aided by the GEOS–C experiments. The ability of an altimeter to measure ocean-wave heights is useful to ocean meterology without the need for either orbital or geodetic improvements. This capability gives the altimeter a favorable enough cost/benefit position to recover the longer term investment of improved geodesy and orbital determination needed to realize ocean topography goals such as measuring tides, boundary currents, eddy currents, and surge currents. Therefore, the possibility should be investigated that this capability (or some equivalent or better capability) to measure the properties of ocean waves will justify either added investment in altimeter capability or investment in radar imaging instrumentation.

The microwave technology that gives a basis for expanding the measurement capability is represented in the Skylab S193 altimeter orbital performance analysis. More specifically, certain anomalous operating conditions of this instrument highlighted the need for future altimeter designs to include automatic alinement of the antenna in the

TABLE 3–X.—*Typical Parameter Values*

Aircraft altitude, m	300
Aircraft velocity, m/sec	70
Approximate antenna beamwidth, deg	1.2
Antenna diameter, m	0.5
Radar spot size, m	7
Radar wavelength, mm	8
Radar pulse width, nsec	1 to 2
Scan rate, Hz	10
Pulse rate, pps	500
Scan angle, deg	10
Ground swath, m	100

vertical direction. Furthermore, the analysis concluded that the average return waveform contains the information required to exercise the desired control primarily by wave-shaping effects caused by pointing error, but also by the Doppler content of the returns.

The effects of antenna pointing error on the return waveshape are given in reference 3–101, which also contains a discussion of how to use this information for nadir pointing control. The change of return signal Doppler content as a function of pointing error is as follows:

1. If the pointing error is forward along the subsatellite path, the power spectral density of the returns will be skewed toward positive Doppler.

2. If the pointing error is backward along the subsatellite path, the power spectral density of the returns will be skewed toward negative Doppler.

3. If the pointing error is orthogonal to the subsatellite path, the power spectral density of the returns will peak around zero Doppler.

These effects did appear in the Skylab S193 altimeter mode III data analysis for return signal space/time decorrelation in which crosstrack pointing errors showed up by increasing significantly the decorrelation times of the signals following the peak of the return. A second type of anomalous operating condition occurred during the Skylab S193 altimeter experiments.

1. Antenna pointing errors as large as 2° from the vertical did not cause the altimeter to "automatically abort" the experiment. Instead, the instrument exhibited a "pseudotrack lock" condition characterized by large standard deviations of altitude track jitter error accompanied by automatic gain control readings indicating anomalously low return signal power.

2. In some instances, the attitude error of approximately 2° rapidly decreased (during the proces of Skylab attitude control attempting to bring the spacecraft to the Earth pointing condition). In these cases, the "pseudotracked" altitude was rapidly decreasing, whereas the received signal strength was rapidly increasing, until the pointing error was approximately three-fourths of the antenna 3-dB beamwidth, at which point the altimeter operations switched to "true altitude track lock," characterized by approximately a 0.5-m tracking error jitter and a high received signal level. Unfortunately, this sequence of operation was initially considered to be proof that the S193 altimeter could not track high-altitude rates. However, analysis of both the orbit (in which the observed rapidly decreasing altitude could not have been real) and the Skylab attitude history (showing that the Earth pointing attitude was being initialized) disproved this contention. In fact, with the given conditions, the altimeter, by its nature, had to operate just as it was observed to operate.

The effect of the only satellite altimetry technology available reveals the following information:

1. Future altimeters will require better antenna pointing and better pointing error resolution.

2. The altimeter can provide this needed pointing control.

3. The antenna pointing should be done electronically by using a simple array to eliminate torquing of the satellite.

An altimeter design that has these capabilities is also given a "natural" added capability in the following respects:

1. It can be programed to have its antenna pointing at the vertical to receive the altitude return, and/or it can be pointed to receive the return from angles off vertical incidence.

2. Signal processing of the returns from angles off vertical incidence will yield the wave-directional spectra of the ocean surface and, possibly, the power spectral density of these waves.

Instrument requirements.—The proposed surface analytic altimeter instrumentation will require a phased array antenna. Beam forming and pointing will be controlled by the altimeter from the average wave shape and Doppler information contained in the returns from the vertical (altitude returns). On alternate pulses (or the second pulse of dual pulses), the antenna will be pointed to illuminate and receive returns from off-vertical incidence. The alternate on/off vertical illumination is to be sequenced around a circle at a radius $R(t)$ from the subsatellite path. For SEASAT geometrics, this circle would have a radius of approximately 25 km. The surface analytic function is performed on the returns from this off-vertical scanning shown in figure 3–63. The short pulse scanning the surface off vertical incidence produces down-chirp frequency-modulated returns with a different down chirp for each wavelength composing the surface. The area A_0 represents the altimeter footprint. Areas $A_1, A_2, A_3 \ldots A_i \ldots A_j$ show the location of the surface from which returns at time t are equal to 2700 nsec (where the time of altitude return is $t=0$). These areas sweep outward across the ocean waves at the rate

$$\frac{d}{dt}R(t) = \frac{d}{dt}\sqrt{cht} \doteq \frac{250 \text{ m/nsec}}{\sqrt{t}} \qquad (3\text{–}20)$$

where spacecraft altitude is 800 km. This produces a down-chirp frequency modulation of returns from each surface wavelength $\lambda_{0, 1, \ldots, i, j}$ of

$$f(t, \lambda_i) = \frac{250}{\sqrt{t}\,\lambda_i} \qquad (3\text{–}21)$$

where $f(t, \lambda_i)$ is in gigahertz. The physical mechanism and geometry involved is shown in figure 3–64. The surface length of short radar pulse δ_{pulse} equals $(c\tau)/[2 \cos (ct/h)]$, where c is the speed of light, τ is pulse duration, h is satellite altitude, and t is time after altitude return. The frequency of the change in signal strength (amplitude) of the returns changes as a function of time. The short length of the radar pulse illuminates only portions of the ocean wavelength, and strong returns will come preferentially from the side of the waves toward the radar creating these down chirps $f_i(t, \lambda_i)$, which are func-

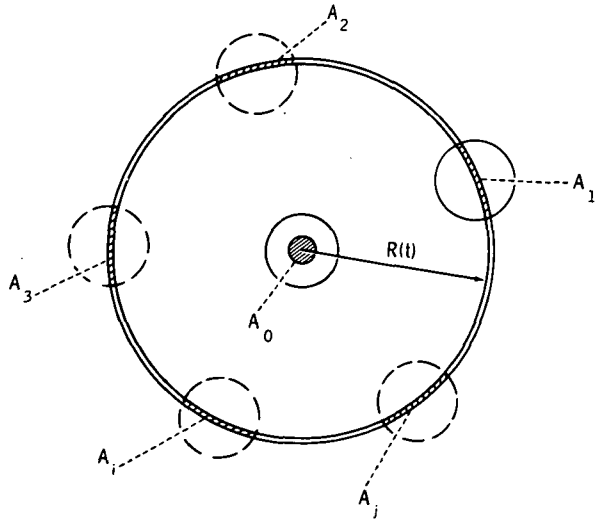

FIGURE 3–63.—Antenna illumination of ocean surface for surface analytic altimetry.

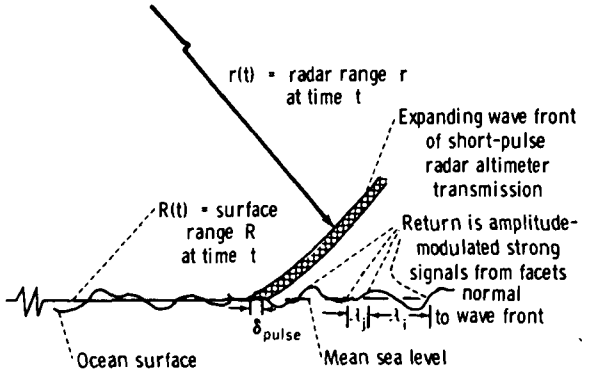

FIGURE 3–64.—Physical mechanisms involved in creation of down-chirp frequency modulation of returns from ocean surface with wavelengths λ_i, λ_j longer than δ_{pulse}.

tions of surface wavelength λ_i. Figure 3–65 shows the log-log plot of surface wave down-chirp modulation (frequency as a function of time) for ocean wavelength λ_s from 25 to 1000 m. One reason for selecting the off-vertical scan circle radius of 25 km is that pulse compression circuitry is at least as feasible as a signal process matched to the returns. Figure 3–66 shows the surface wave down-chirp modulation for λ_s from 25 to 500 m. Twenty-percent resolution of these wavelengths appears feasible. Simply stated, 1-μsec pulse compression circuits matched to these chirps could be selected so that no frequency overlap would occur between them over the bandwidth from 8 to 225 MHz. That set of pulse compression circuits comprises a matched receiver for the signal parameter of interest (i.e., the surface wavelengths in radial direction of each off-vertical step). The approximately 15 outputs obtained from each radial sweep at the 25-km radius should be converted from analog to digital and sent to ground processing. Probably, the only further processing required would be accumulating these numbers for approximately 2 sec

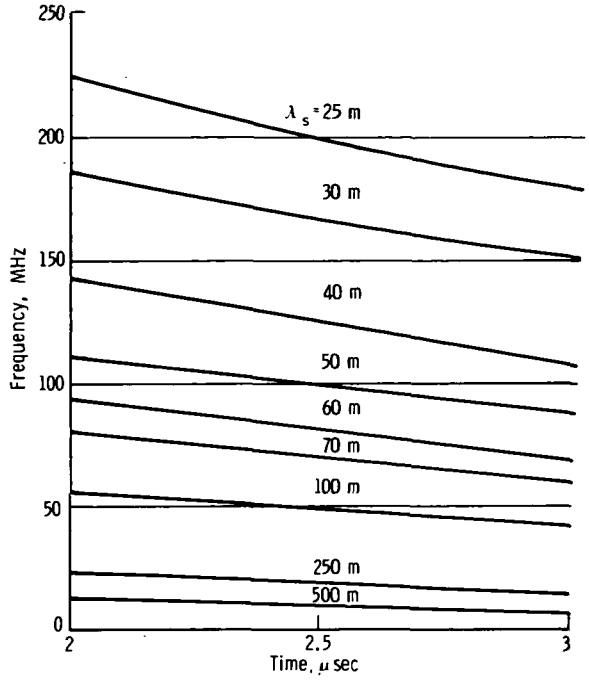

FIGURE 3–66.—Ocean surface wave down-chirp modulation in the 2- to 3-μsec window containing returns from the off nadir pointing surface analytic altimeter. From this plot it appears feasible to achieve 20-percent resolution of surface wavelengths using approximately 15 chirp pulse compression delay lines to cover the range from 25- to 500-m ocean wavelengths.

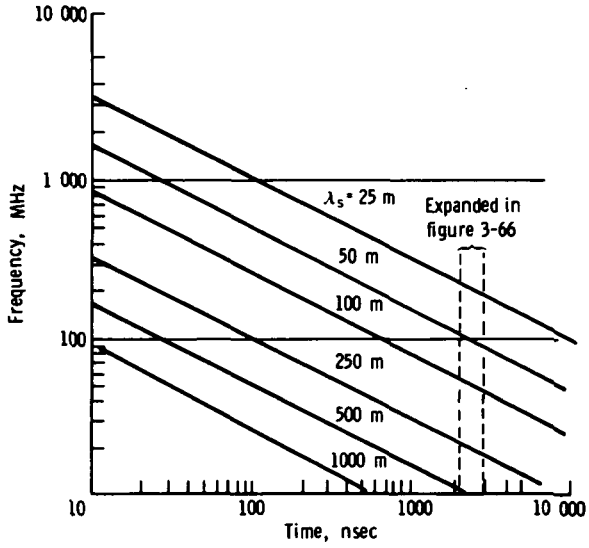

FIGURE 3–65.—Log-log plot of ocean surface wave down-chirp modulation as a function of time after altitude return. The surface analytic altimeter signal processor could be pulse compression delay lines tuned to these down chirps.

and plotting them as an amplitude contour obtained around the circle. Of course, this is a distortion of the wave directional spectra, but it should serve as a "first look" process. Spectra of particular interest can be extracted for the transformation processing required to map wave direction in latitude and longitude.

Undoubtedly, a different transformation will be required to use the same data in the wave forecasting algorithms, and a different transformation will be required for some other application.

These transformations should probably be done from the raw data (or, at most, edited raw data) so that less processing is required to get the data-editing quick-look function performed.

Technical approach.—Conceptual design

studies on future design and applications of satellite altimetry are required to determine a basic question. Should altimeter instrumentation become more complex by adding capability natural to its particular radar geometry, or should it be made less complex (restricted to altitude tracking only)? The answer to this question requires determining the possibilities, the payoffs, the needs for overlap and supportive data from different instruments, etc. The possibility exists that, in a fully instrumented oceanographic satellite, the need for accurate altitude measurements for 1 yr to solve ocean tide and circulation problems will be all that is required from the altimeter. This postulation assumes that the other instrumentation will obtain all the information for ocean meteorology. If this case were true, a much-simplified altimeter designed for 5- to 10-yr orbital operation may be the final configuration specified.

A laboratory research and development study should be undertaken to demonstrate the pulse compression performance obtainable for the ocean-surface-wave down-chirp-type signals. This class of chirp signal is different because it is not a linear frequency modulation with time. It is independent of transmitted carrier frequency or phase, and the down-chirp modulation ceases only at the horizon where it equals the speed of light divided by the surface wavelength.

Applications studies should be made to determine if the 25-km radius for obtaining wave directional spectra can be increased or should be decreased. Data processing required to apply these measurements should be studied.

Applicability.—The proposed surface analytic altimetry instrumentation simply extends the capability of an altimeter to measure the physical properties of sea state. The application of altimetry to ocean meteorology is improved. The application of altimetry to geodesy and static and dynamic oceanology will be that expected from altimetry with an accuracy of 10 cm.

Radar spectrometers and dual-frequency interferometers.—Several other instruments that have potential for determining ocean-wave spectral characteristics also advantageously use the "tilt modulation" effects described previously. One instrument is the "wave spectrometer." This instrument emits a short pulse for which the (effective) spatial width is less than one-half the length of the gravity waves to be observed (e.g., a pulse width of 10 nsec will provide a spatial resolution of approximately 5 m at a 15° incident angle, which is adequate to resolve gravity waves longer than 10 m). As this pulse travels out across the longer gravity wave, it illuminates specularly reflecting regions, the scattering characteristics of which vary with the slope (and position) over the longer wave. Hence, the received signal as compared to time (as would normally be displayed on an A-scope) will carry an amplitude modulation pattern corresponding to the period of the longer gravity wave. By Fourier transforming this amplitude function, a signal spectrum is produced, which is directly proportional to the ocean-wave slope spectrum along the radar line of sight. Both the first and second mechanisms described in the preceding section are responsible, to some degree, for the operation of the spectrometer. However, the third mechanism should not affect the spectrometer because the return on the A-scope is essentially instantaneous and will not be changed by the orbital velocity of the specular scatterers.

The dual-frequency interferometer is basically a frequency-domain implementation of the wave spectrometer described previously; it transmits two closely spaced frequencies, f_1 and f_2 ($\Delta f = f_2 - f_1$ ranging between 1 and 100 MHz). The correlation function of the power return at the two frequencies is then taken at the output of the receiver. Theoretical analyses have shown that this function, as compared to separation wave number $\Delta k = (2\pi\Delta f)/c$, is proportional to the slope spectrum of the longer wave components along the radar line of sight. This technique has not been demonstrated experimentally. From the theoretical models, unanswered questions

still exist about the magnitude of the desired portion of the correlation function containing the slope spectrum. Questions must also be answered concerning performance in the presence of noise and the average time required to observe a given level of sea echo correlation coefficient. However, the technique appears attractive at this point because of its simplicity and potentially low data-rate requirements compared to the wave spectrometer.

Dual-frequency wave-height sensor.—Work is underway at LaRC to use dual-frequency radar techniques to measure significant wave heights and probability density function of large ocean waves. The technique has been described by Weissman (ref. 3–102), and the basic results are summarized here.

If a vertical viewing radar transmits two microwave signals at frequencies f_1 and f_2 from an altitude H above mean sea level, if the antenna pattern is ignored, and if the radar illuminates a statistical ensemble of specularly reflecting wave heights, then the absolute value of the time average of the product of the returning signals is

$$|\bar{R}(\Delta k)| = \frac{|\langle E(f_1)\,E^*(f_2)\rangle|}{\sqrt{\langle|E(f_1)|^2\rangle\langle|E(f_2)|^2\rangle}} = |\langle e^{i2\Delta k h}\rangle| = \left|\int_{-\infty}^{\infty} P(h)\,e^{i2\Delta k h}\,dh\right| \tag{3–22}$$

where

$R(\Delta k)$ = the correlation coefficient

Δk = difference wave number $= [2(f_1 - f_2)]/c$

c = speed of light

h = height of a specularly reflecting wave

$P(h)$ = probability distribution function of heights

$E(f)$ = electric field of the scattered signal

$*$ = complex conjugate

$i = \sqrt{-1}$

$\langle\ \rangle$ = ensemble average

Thus, performing measurements by transmitting a sequence $<f_1, \Delta f_2, \ldots, \Delta f_n>$, the significant wave height $H_{1/3}$ and some features of the probability density function can be measured. The latter measurement may have some applicability to the detection of ocean currents. This is strictly a vertical viewing measurement and requires narrow-beam antennas.

This technique is a frequency analog of the impulse altimeter. If complex expression (magnitude and phase) for $R(\Delta f)$ is Fourier-transformed from the frequency domain Δf to the time domain, the solution to the impulse response of a rough surface is obtained.

Bistatic high-frequency local wave directional sensor.—A concept will be described that may provide the directional wave-height spectrum near a fixed point of interest on the ocean as a satellite passes overhead. This concept is illustrated in figure 3–67 where the point on the sea is shown as a buoy; actually this point could be a ship, island, tower, or coastal site as well. Also, although figure 3–67 indicates the satellite as the receiver and the surface point as the transmitter, the converse is actually a more desirable situation. In that configuration the satellite would transmit a low power signal (less than 10-W average), which would be stepped through the hf region (from 2 to 30 MHz). The spacecraft antenna could be an electrically small omnidirectional loop or dipole pair. The user below (e.g., a ship) would receive both the direct signal from the satellite and a sea-scattered signal at a given delay time (corresponding to a given range from the ship). Thus, collection and use of the sea-state data would be at the user's option and would require carrying onboard only a receiver, a simple digital processor, and a schedule of satellite passes (which need not be directly overhead).

The principle supporting the technique is Bragg scatter. In the bistatic configuration, a contour of constant time delay is an ellipse, in general, which becomes a circle when the satellite is directly overhead. The waves from which scatter is taking place are exactly one

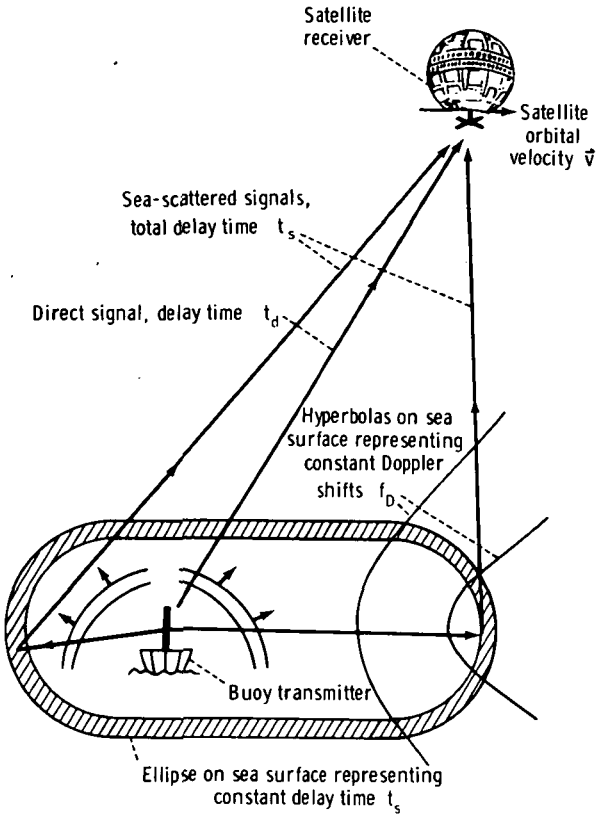

FIGURE 3–67.—Illustration showing concept of bistatic high-frequency local wave directional sensor.

radar wavelength long (when the satellite is overhead); thus, by sweeping from 2 to 30 MHz, one is measuring the heights of the ocean waves (as the strength of the received signal), the lengths of which range between 150 and 10 m.

Wave directionality is obtained by the Doppler imposed on the scatter by the satellite velocity. The greatest Doppler originates from that portion of the time-delay circle directly ahead of the satellite, with zero Doppler at the sides and the greatest negative Doppler from behind. For the satellite directly overhead, the scattered sea-echo Doppler is described by a simple cosine function of angle from the satellite track. An example of the Doppler spectrum produced at 5 MHz by an isotropic sea is shown in figure 3–68. Any departure from this shape represents the directional nature of the ocean waves and can

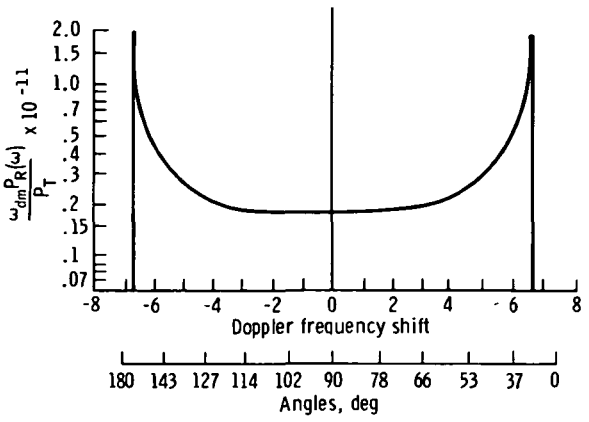

FIGURE 3–68.—Example of Doppler spectrum produced at 5 MHz by an isotropic sea (where ω_{dm} is maximum satellite-induced Doppler shift, $P_R(\omega)$ is average received power spectral density, and P_T is average transmitted power).

be obtained by straightforward digital processing of the signal spectrum. The angles designate the direction of the ocean waves with respect to the satellite track, which produces the Doppler at that point.

This technique, which is straightforward and easy to implement, has the advantage of requiring no data processing aboard the satellite. Furthermore, because the users receive the direct signal also, they have all the information they need to calibrate the system and remove unknown transmitter/receiver drifts and path losses. Because the ionosphere will pose the ultimate limitation on such a system, this self-calibrating feature is very desirable. A thorough system study and experimental evaluation of the concept is currently underway at Batelle-Columbus Laboratories under Wallops Flight Center support.

Microwave radiometry.— Observations (refs. 3–32 and 3–103) of the surface-roughness effect have indicated an apparent dependency on observational frequency, increasing with increasing frequency. In addition, surface-roughness effect is a function of the angle of observation and polarization of the radiation received. Increases of 1.1 K of the horizontally polarized brightness temperature at 19.34 GHz and 55° inci-

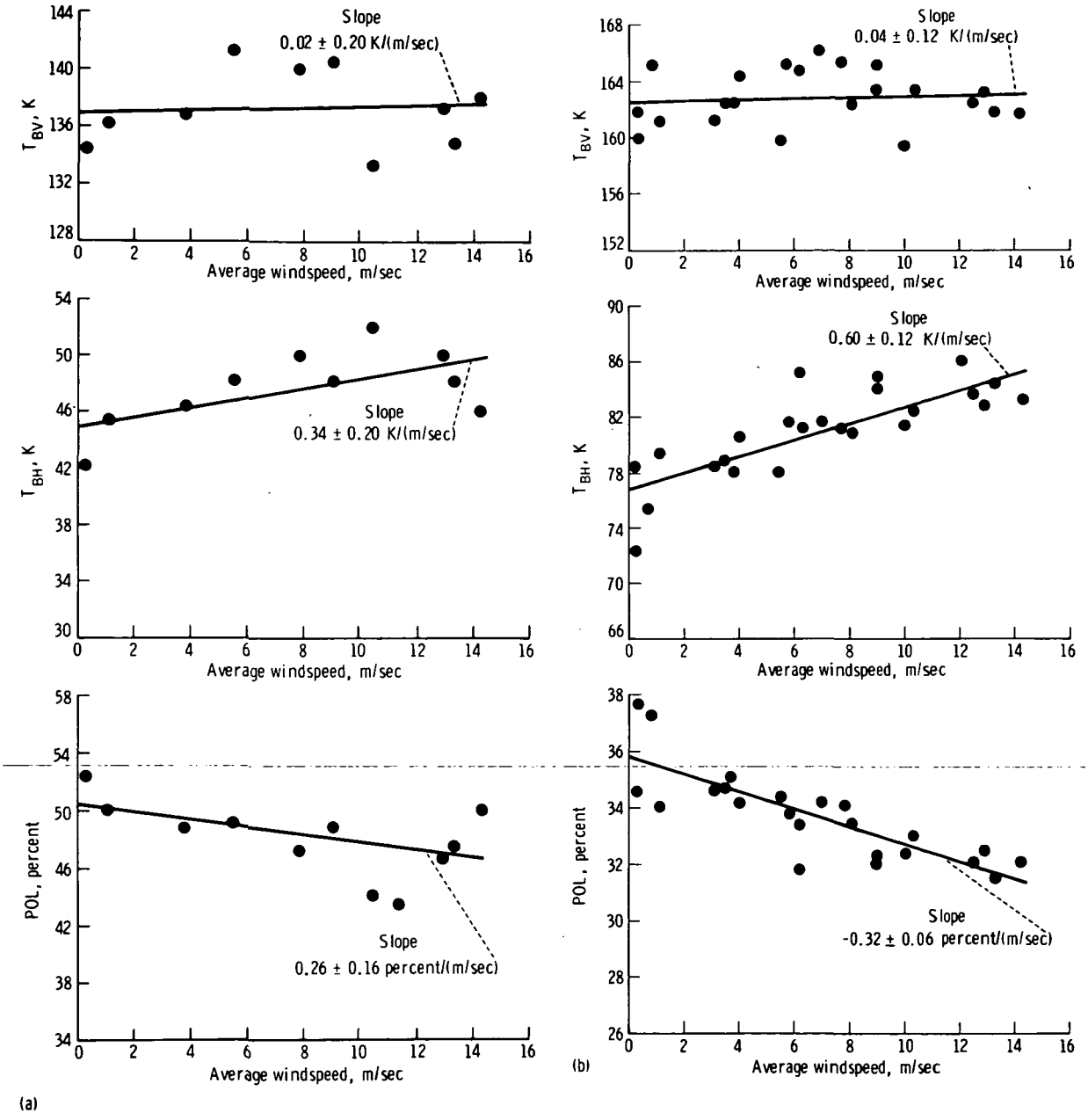

FIGURE 3–69.—Measurements of the surface roughness effect made from Argus Island Tower of Bermuda where T_B is brightness temperature, V is vertical polarization, H is horizontal polarization, and

$$POL=\frac{T_{BV}-T_{BH}}{T_{BV}+T_{BH}}\times 100.$$ (*a*) Frequency=1.41 GHz. (*b*) Frequency=8.36 GHz.

dent angle with 1-m/sec changes in windspeed have been measured. Measurements of the surface-roughness effect made from Argus Island Tower of Bermuda at 1.41, 8.36, and 19.34 GHz (ref. 3–32) are shown in figure 3–69. The surface-roughness effect is closely coupled to the local windfield, rapidly responding to changes in the local wind;

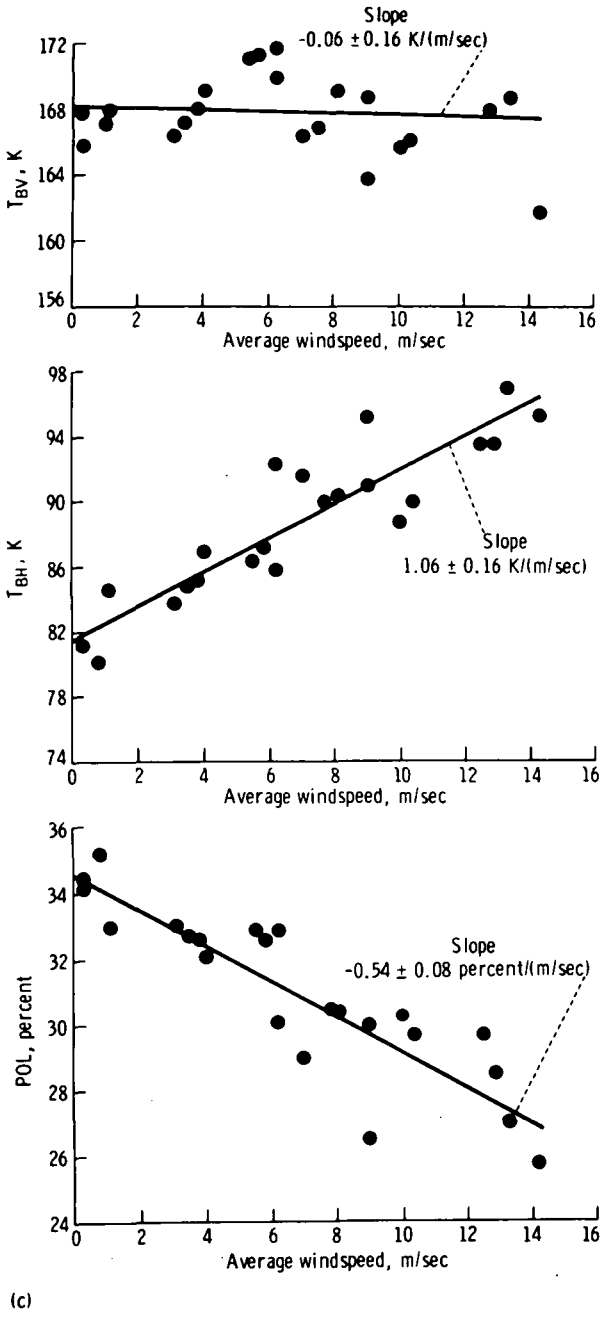

FIGURE 3–69 (concluded).—Measurements of the surface roughness effect made from Argus Island Tower of Bermuda where T_B is brightness temperature, V is vertical polarization, H is horizontal polarization, and $POL = \frac{T_{BV} - T_{BH}}{T_{BV} + T_{BH}} \times 100$. (c) Frequency = 19.34 GHz.

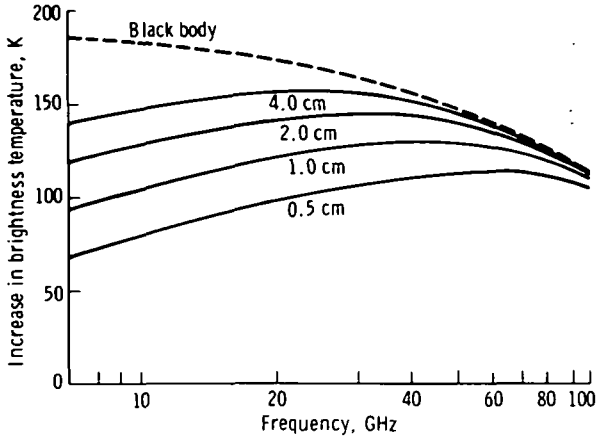

FIGURE 3–70.—Brightness temperature of foam as a function of microwave frequency.

hence, it is relatively insensitive to the energy content of low-frequency gravity waves. Evidence indicates that the surface roughness effect is primarily dependent on the mean-square surface slope.

Observations of the sea-foam effect (refs. 3–104 and 3–105) have shown it to have a very high brightness temperature (approaching the physical temperature of the sea) compared to the average sea surface. Recent laboratory and aircraft-borne measurements [5] are shown in figure 3–70. The evidence available indicates that the spectrum of the brightness temperature of foam is relatively flat at microwave frequencies, with a slight decrease with decreasing frequency. The high brightness temperature of foam is consistent with the foam serving as a matching layer to the sea rather than to inherent high loss in the foam. Unless the high brightness temperature of foam results primarily from very high loss of the foam, which seems unlikely, the brightness temperature will decrease with decreasing frequency when foam thickness of only a fraction of the observational wavelength is reached. The brightness temperature of foam is much less dependent on polarization and incident angle than is the compact sea surface.

[5] Unpublished data from James P. Hollinger, 1974.

Clearly, more detailed measurements as a function of the observational parameters of frequency, polarization, and incident angle over the range of foam characteristics, such as thickness, bubble-size distribution, water content, and degree of spatial uniformity, are required to fully understand the microwave properties of ocean foam. In addition to incomplete knowledge about the microwave characteristics of foam, the determination of the brightness temperature dependence on windspeed caused by sea foam is further complicated because the foam coverage of the sea surface does not depend only on the local wind. The foam coverage also depends on the air/sea temperature difference, the duration and fetch of the wind, and the history of the wave spectrum of the sea area being observed. An analytical model including these parameters and depending on the dissipation (by breaking waves) of energy transferred from the wind to the wave spectrum has been developed by Cardone (ref. 3–106) to predict whitecap coverage. This model is in reasonably good agreement with microwave measurements at high windspeeds (refs. 3–30 and 3–31). In addition to whitecaps, considerable wind streaking (thin lines of foam oriented in the direction of the wind) occurs at high windspeeds. Above approximately 12 m/sec, streaking contributes more to the total white water visible on a photograph than do whitecaps (ref. 3–107). The details of the microwave brightness temperature of streaks compared to that of whitecaps are not presently clear and result in difficulty in interpreting the detailed whitecap/streak/windspeed/brightness-temperature interrelationship. However, the general increase of microwave brightness temperature with windspeed caused by increasing coverage of the sea with foam is well established.

The increased noise temperature (ref. 3–103), which results from sunlight reflecting or scattering off the water, is shown in figure 3–71, where brightness temperature is plotted as a function of time. These data were obtained by pointing microwave radiometers at a fixed viewing angle over water (at the complementary Sun elevation angle) and allowing the image of the Sun to pass through the antenna beams. The closed points represent data obtained when the water surface was smooth, and the open points correspond to the data obtained when the surface was roughened by waves. The data show that, under calm conditions, the noise input to the receiver can significantly increase when solar radiation reflects specularly into the antenna, particularly at the lower microwave frequencies. When the water surface is very rough, the scattering generally becomes diffuse and causes a quasi-isotropic increase in brightness temperature, which may be tens of degrees at the lower microwave frequencies. In addition to showing the increased noise temperature in a radar receiver, these data imply that ocean roughness can be inferred by radiometrically measuring the microwave glitter pattern of the Sun.

Solar microwave interferometer.—The proposed instrument, the solar microwave interferometer imaging system (SMIIS), represents a novel application of the radio astronomers' very long baseline interferometry (VLBI) and forward scatter radar concepts and technology. The SMIIS can serve as a research tool for ocean studies but has limited operational potential. The history of both technologies are thus pertinent. Because the function of SMIIS (i.e., obtaining microwave imaging of the Earth environment) is also the function of any other proposed radar imaging systems being considered by the Active Microwave Workshop, the history and technology of radar imaging is also pertinent.

Present state of the art.—The applicable technology is contained in the previously stated historical connections to VLBI, forward scatter radar, imaging radar, short baseline interferometry, and phased arrays technologies. The present state of the art in satellite microwave antenna technology is specifically of interest because of the rela-

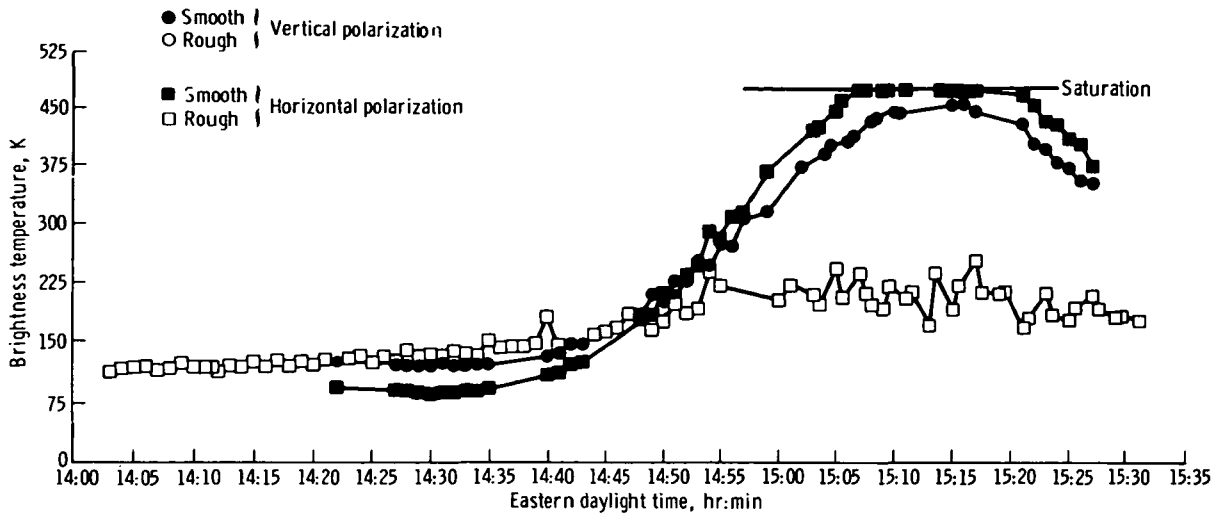

(a)

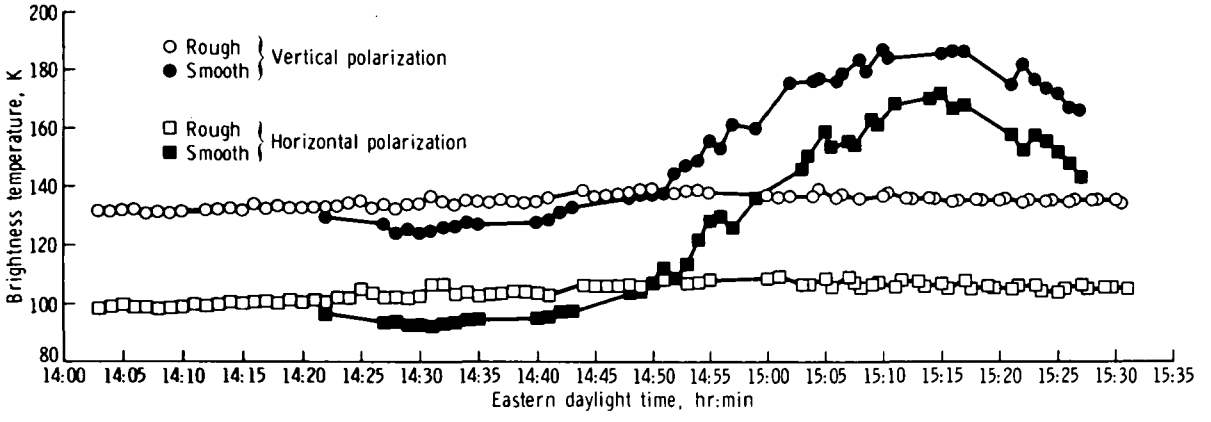

(b)

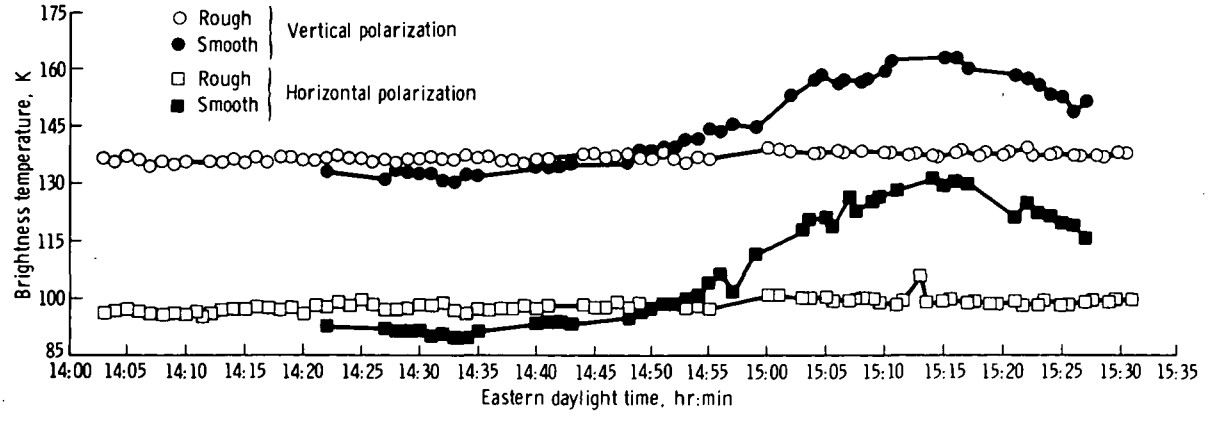

(c)

FIGURE 3–71.—Change in brightness temperature as a function of time. (*a*) Frequency =1.4 GHz. (*b*) Frequency=4.0 GHz. (*c*) Frequency=7.5 GHz.

tively large apertures and antenna pointing requirements for SMIIS.

The standard questions regarding onboard as compared to ground-site data processing associated with all satellite-borne imaging instruments must also be studied for the SMIIS. Thus, the communication/ground-site data processing and the inverse onboard data processing/communication state of the art is pertinent.

Qualitative concept description.—Figure 3–72 shows the proposed SMIIS instrumentation. The satellite (at 800-km altitude) has one antenna pointing directly at the Sun and another antenna pointing at the glistening surface of the Earth (i.e., the region surrounding the Sun-to-satellite specular reflection point).

The Sun-pointing antenna receives the solar noise by way of the direct ray path. This broadband noise radiofrequency signal is band-limited (to the level required for the desired imaging resolution of the system) and baseband detected by using a coherent local oscillator. The band-limited bipolar noise signal obtained and the time lags generated from the coherent local oscillator are recorded (or communicated to the ground) and stored as the reference phase and amplitude modulation for the VLBI-type correlation processing that follows. All surface elements contained within the glistening surface are also illuminated with the same solar microwave noise, except for propagation path noise differences and some signal decorrelation. The amount of signal decorrelation will be one of the problems requiring further investigation; however, for S-, C-, and X-band wavelengths, these illuminated points fall within the first (or first few) Fresnel zones of every point source of noise at the Sun generating the incident microwave noise.

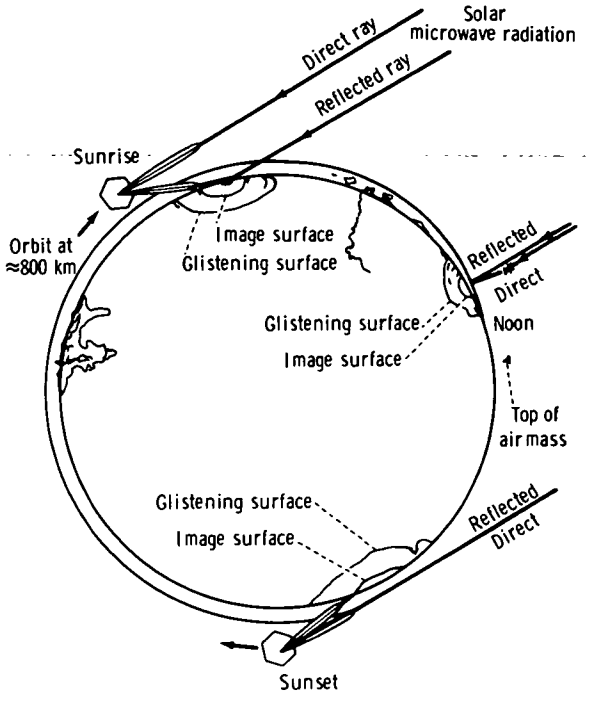

FIGURE 3–72.—Earth environment mapping using the SMIIS. Note the changes in the size and shape of the imaging and the glistening surfaces for satellite sunrise, noon, and sunset. Also note that the direct ray signal always precedes the forward scatter signal in time.

The forward scatter from the surfaces, facets, wavelets, etc., in the glistening surface provides the communication link between the VLBI remotely illuminated antenna and the satellite VLBI master antenna. These multiple-reflected signals from the glistening surface are received at the satellite and beat to baseband bipolar video by using the same receiver-coherent local oscillator that was used to obtain the direct ray reference signal. This composite baseband is time-tagged, recorded (or communicated to ground), and stored. The VLBI process is then applied to the record obtained from the reflectors in the glistening region. This process consists of applying the first-order Doppler correction (i.e., that computed for the ray reflection point in the glistening region), then running a cross-correlation of the forward scatter record with this first-order Doppler-corrected reference record. Strong correlation peaks will be generated in this time record; in fact, each peak will be a range pulse compression for a strong forward scatterer. The range pulse compression actually applied depends on the bandwidth of the reference record B_{REF} and the time length of that record R_{REF}. The width of the cor-

relation peak will be approximately $1/B_{REF}$, whereas the amplitude of the correlation peak will be proportional to the product of the reference record length T_{REF}, the forward scatter signal strength from each surface element A_i, and the match of the first-order Doppler correction to the Doppler frequency of that signal. The VLBI process completes the imaging process by successive correlations using differentially corrected Doppler reference records. This process is essentially a Doppler correction sweep across the glistening surface, in which each detected forward scatterer is positioned in azimuth by the Doppler correction that maximizes its correlation peak. The resultant range/azimuth map of correlation peaks comprises the polar microwave interferometer image.

Quantitative description of the SMIIS.— The following questions are among the first to be answered in designing the SMIIS:

1. Is enough solar microwave power available at the frequencies best suited to Earth environment planning?
2. If so, how large must the antenna apertures be to at least get the direct ray at adequate signal-to-receiver noise to enable interferometer processing?
3. What is the best antenna to use?
4. What bandwidth and reference signal duration will be required to provide adequate resolution?
5. What processing must be done at the receivers as opposed to what can or should be done at the ground sites?

The approximate answers to the first three questions can be obtained from the information presented in figure 3–73. The solid line shows the microwave power of the quiet Sun (in dBm/m²-Hz) in the range of frequencies from 30 MHz to 300 GHz. This microwave power is increasing at the rate of approximately 12 dB/decade, and, for frequencies above 4 GHz, the microwave noise power from an antenna with a 1-m² aperture will exceed the noise power from the best cooled parametric amplifier receivers available with present state of the art (shown by the dashed line). Figure 3–73 shows that

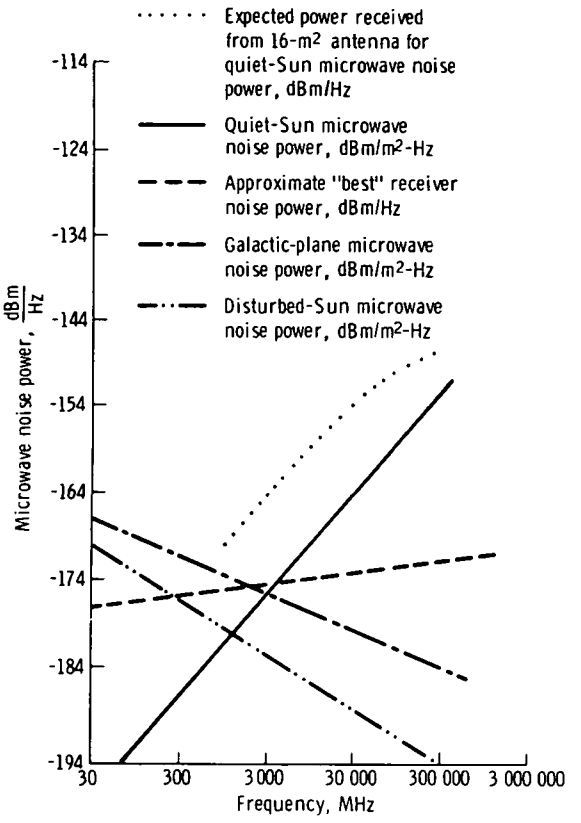

FIGURE 3–73.—Plot of solar and galactic-plane microwave noise power compared with frequency. Also shown is the approximate noise power of state-of-the-art, cooled, parametric amplifier receivers. Note that at 3000 MHz the SMIIS can use either solar or galactic-plane noise as the reference signal, thus giving day/night operation (ref. 3–108).

for almost all microwave frequencies suited to Earth environment mapping, enough microwave power is available from the quiet Sun to let the Sun be the transmitter in the SMIIS. Also shown is a dotted line, which illustrates the expected received power from a 16-m² antenna. This illustration indicates that for antenna apertures approximately as large as those required for radar mapping, the SMIIS could work at frequencies from 1 GHz and up. The microwave noise power available using the galactic plane as the transmitter for SMIIS with a 16-m² antenna aperture is sufficient for Earth environment mapping applications requiring frequencies below approximately 30 GHz. The 6-dB

signal to noise obtainable at 30 GHz is adequate for the SMIIS processes.

An initial assessment of the bandwidth required to provide adequate resolution for Earth environment mapping can be obtained from the requirement for wave directional spectra over the ocean. This data product is considered useful if ocean wavelengths from 50 m to 1 km are resolved in synoptic maps of the ocean suface. A 10-m/range resolution using SMIIS requires approximately a 30-MHz bandwidth bipolar video reference signal (because this is one-way propagation of electromagnetic waves; the resolution is at 3.3 nsec/m). Azimuth resolution of approximately 10 m requires approximately a 10-μsec duration of the bipolar video reference signals; that is, the differential Doppler from each reflecting center will cause detectable decreases in the cross-correlation peaks from records exceeding 10 μsec in duration. In the majority of cases, a much longer delay than 10 μsec will occur between the direct ray from the Sun and the reflected rays from the Earth environment; thus, much longer reference signals could be taken. However, the 300:1 pulse compression gain obtained from correlation processing the 10-μsec-duration 30-MHz-bandwidth signals should be adequate for SMIIS mapping.

The answer to question 5 is twofold.

1. The low-noise baseband receiver signal process should be performed onboard to preserve the best signal-to-noise ratio in the bipolar video signals.

2. The onboard as compared to ground data-processing tradeoffs, which must be made for radar mapping systems, apply to the SMIIS. However, the power, weight, and volume required for the radar systems transmitter can be applied to onboard data-processing electronics for the SMIIS; thus, all SMIIS data processing can be done onboard and still save power, weight, and volume over radar systems with similar mapping performance.

Impact of microwave technology.—The concepts embodied in the SMIIS bridge the present gap between the sophistication of the state of the art in radio astronomy (VLBI) and the state of the art in synthetic aperture radar. Because the microwave signals transmitted by the Sun (and/or the galactic plane) contain essentially all frequencies and polarizations possible, even the postulated performance of polypanchromatic radar (ref. 3–109) can be obtained with SMIIS. This attainment would represent a significant advance in the microwave mapping state of the art.

Requirements.—Generally, the same requirements are needed for the SMIIS instrumentation on a satellite as for any high-resolution microwave radar imaging instrument, except for one very significant difference. Radar images require a high-power transmitter, transmitted signal modulation electronics, and a matched receiver/demodulator for each microwave band used, whereas SMIIS does not require any transmitter or modulation electronics because it uses cosmic noise sources in the transmitter/transmitted signal modulator role. The fact that SMIIS has been described and initially designed as receiving its reflected signals from the region of forward scattering surfaces does not limit the system to operation in this viewing direction (i.e., this is not a requirement or limitation); it is simply the direction from which the strongest reflected signals are expected and, as such, represents the easiest direction for high-signal-to-noise, high-density mapping operation.

Electronically scanned multifrequency array antennas would be required to obtain SMIIS operation in many frequency bands with minimum use of satellite space. These antennas would not be a requirement of early experimental versions of SMIIS, but the technology of these array antennas should be nurtured for use with future operational versions of SMIIS.

Onboard data-processing requirements will be equivalent to those for radar imaging systems with the same need for growth, from the minimum amount possible to the maximum amount required, and for Earth en-

vironment monitoring and reporting missions that will evolve.

Technical approach.—Conceptual design studies should be done to determine the total capability of SMIIS instrumentation and to identify research and development requirements and feasibility demonstration experiments that can be done with existing instrumentation (for instance, the Massachusetts Institute of Technology Haystack radar performing SMIIS-type mapping of the lunar surface, possibly using radio stars instead of the Sun as transmitters).

Feasibility/applications studies should be done to determine design specifications for experimental SMIIS instruments aimed at specific applications missions.

A project to develop SMIIS instrumentation, data processing, and data use would be appropriate. One possibility would be to use one of the large antennas at Wallops Flight Center to get the direct ray reference bipolar video record while simultaneously obtaining the reflected ray record from an airborne platform. Both ocean and Earth could be viewed at all incident angles and at any distance from the reference station to obtain design data related to these parameters.

Continuing research and development is warranted in the area of real-time correlation technology (such as that presently underway at the General Electric Research and Development Center using charge-coupled devices that give a 32-bit correlator operating at 10 MHz on a single large-scale integration flatpack). Special developments for SMIIS applications may justify short-term funding in this technology.

Applicability.—The Earth environmental mapping capabilities of the proposed SMIIS extend from monitoring solar disturbances and mapping the ionosphere, using the low-frequency end of the spectrum, to mapping atmospheric phenomena using the high-frequency end of the spectrum. Only the development of receiver technology at millimeter and submillimeter wavelengths is required to close the gap between microwave imaging and long-infrared imaging instrumentation.

Other Active Microwave Sensors

Wave motion sensor.—A new technique being developed at the Applied Physics Laboratory of Johns Hopkins University (APL/JHU)[6, 7, 8] is potentially capable of mapping the significant height $H_{1/3}$ of ocean waves over a wide field of view beneath either an aircraft or a satellite. The technique directly measures the Doppler broadening of a radar signal caused by the orbital motion of the waves to determine significant wave height. This technique is significantly different from conventional Doppler techniques because there is no contamination of the sea motion broadening by the much larger Doppler broadening caused by platform motion and finite antenna beamwidth. The technique is capable of measuring the shape of the power spectrum of the Doppler-broadened echo. However, the displacement of the received center frequency from the transmitted frequency is not measured. Much of the following information is extracted from the Bush-Gotwols proposal.[9]

Present state of the art.—The most extensive series of Doppler-broadening measurements have been performed by the NRL (refs. 3–110 and 3–111). These measurements showed that the width of the Doppler-broadened spectrum is of the form $\omega_d = C(H_{1/3})^{1/2}$, where C is a constant for a given frequency and polarization. The full width at half maximum of the Doppler-broadened spectrum Δf, will always be converted to velocity units by the use of the (nonrelativistic) Doppler relation $\Delta f = 2\Delta v_d/\lambda$. This

[6] Bush, G. B.; Katz, I.; and Kropfli, R.: APL/JHU Memorandum BPP7IU–31, 1971 (unpublished data).

[7] APL/JHU: Phase-A Study for the SEASAT–A Mission. APL/JHU, vol. 1, sec. 2.6, July 1973 (unpublished data).

[8] Bush, G. B., and Gotwols, B. L.: The Wave Motion Sensor—A new Technique for Remotely Mapping the Significant Height of Ocean Waves. APL/JHU proposal submitted to NASA Wallops Flight Center, Apr. 1974 (unpublished data).

[9] *Ibid.*

facilitates the comparison of measurements taken at different frequencies. The measurements indicated that Δv_d was almost independent of the angle between the radar viewing direction and the predominant direction of the waves. Also, indirect evidence revealed that, because of the effect of "spray" at the air/sea interface, the Doppler broadening of horizontally polarized radiation was greater than that for the vertically polarized component. The simple relationship $\omega_d = C(H_{1/3})^{1/2}$ is used in the new technique. Katz (ref. 3–112) has previously proposed use of this relationship to measure ocean-surface roughness from a satellite by an entirely different method, which is limited to a narrow field of view.

The platform motion problem.—A better appreciation of the new technique will be obtained if the difficulties inherent in conventional radar Doppler-broadening measurements are first analyzed. Consider the highly simplified scheme shown in figure 3–74 in which a single high-gain antenna illuminates the surface of the ocean with a continuous wave (CW) transmission. Assume that the same antenna is simultaneously used to receive the reflected signal (ignore the associated technological difficulties). For the geometry shown in figure 3–74, the range of radial velocities between the half-power points of the antenna pattern is given approximately by

$$\Delta v_d = 2v_p\theta \qquad (3\text{–}23)$$

Assuming a highly directional antenna with a 1¼ beamwidth and a platform velocity of 7 km/sec (typical of a satellite), the full width at half maximum of the received spectrum will be approximately 244 m/sec. In contrast, the broadening caused by the orbital motion of the waves is approximately 1 m/sec for a significant wave height of 1 m. Any attempt to measure wave-motion-induced broadening is highly impractical, because the width of the composite spectrum consists of 1 part caused by orbital wave motion and 244 parts caused by platform motion. This pessimistic appraisal can be improved by considering various alternative schemes (coherent short-pulse radar, off-nadir pointing, etc.), but the improvement does not appear to be substantial enough to bring the broadening by the two mechanisms even close to equality.

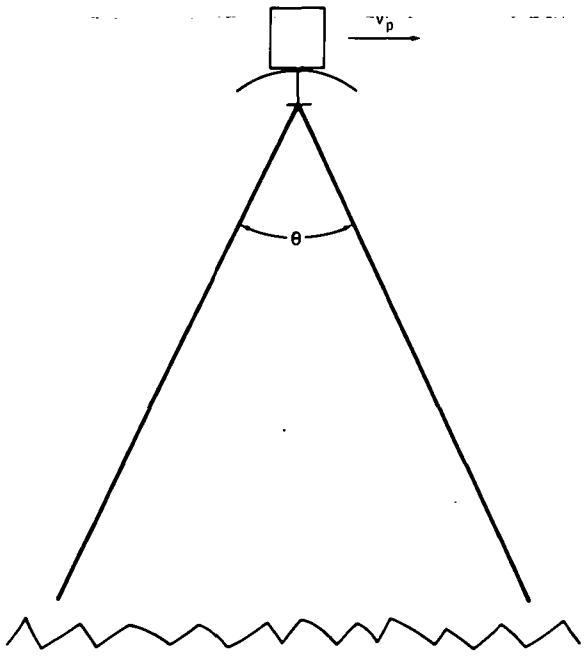

FIGURE 3–74.—Simplified diagram of a moving CW radar illuminating a rough ocean, where v_p is relative platform velocity.

The diffraction pattern in the plane of the transmitter.—Another way to consider the broadening caused by platform motion contains the key to the solution of this problem. Consider the diffraction pattern that is formed in the plane that contains the transmitting aperture (fig. 3–75). The correlation length of the intensity fluctuations in this plane can be estimated by using the Van Cittert-Zermike theorem (ref. 3–113). This theorem states that the correlation length l_a of the spatial fluctuations in the intensity caused by an extended source of diameter L and at distance h is given by

$$l_a = 1.22\, h\lambda/L \qquad (3\text{–}24)$$

If it is assumed that L is defined by the half-power points of the antenna pattern, then (approximately)

$$L = h\theta \approx h\lambda/D \qquad (3\text{–}25)$$

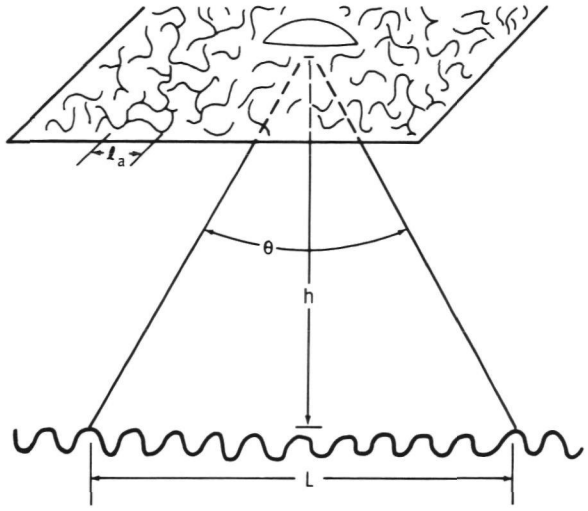

(a)

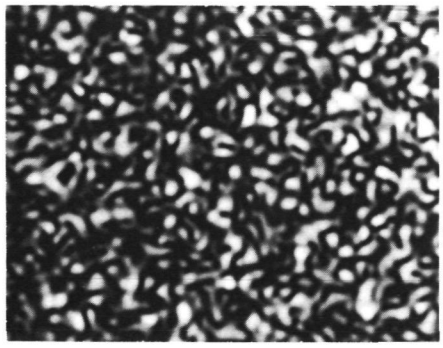

(b)

FIGURE 3–75.—Diffraction pattern. (*a*) Diagrammatic view of the diffraction pattern formed in the plane of the transmitter by radiation that is reflected from the surface of a rough ocean. (*b*) Photograph of an actual diffraction pattern created by reflecting the light from a laser off a rough surface.

where D is the diameter of the transmitting aperture and λ is the wavelength. Combining equations (3–24) and (3–25) yields the simple result

$$l_a = 1.22D \qquad (3\text{–}26)$$

By considering diffraction integral for this problem, if the transmitting aperture is moved l units to the right, the (intensity) diffraction pattern will translate as a rigid body l units to the left. Thus, the relative velocity between the transmitting-receiving aperture and the rest frame of the diffraction pattern of the rough ocean is $2v_p$. Therefore, the correlation length l_a corresponds to a correlation time $\tau \approx l_a/(2v_p) \approx D/(2v_p)$ and to a bandwidth $\Delta f \approx 1/\tau = (2v_p)/D$. This bandwidth is identical to that given by equation (3–23) from Doppler-broadening arguments (after conversion to consistent units). This equality of bandwidths supports the theory that platform motion broadening may be analyzed either by considering the range of radial velocities intercepted by the antenna beam or by considering the transmitting-receiving antenna as moving through the diffraction pattern of the rough ocean. Thus, if a way could be found to sit at a fixed point in the rest frame of the diffraction pattern, the temporal fluctuations in the received signal that are caused by the motion of the ocean waves could be measured without having to contend with the large fluctuations caused by platform motion.

The solution.—The solution to the platform motion problem is to arrange a series of

receiving antennas in a line that is parallel to the relative velocity vector of the moving platform. Because the diffraction pattern translates as a rigid body in a direction opposite to the platform velocity, N antennas can obtain N measurements (spaced in time) of the intensity I at a fixed point x_0 in the rest frame of the diffraction pattern. Imagine a coordinate system attached to the rest frame of the rigidly translating diffraction pattern, with the X-axis parallel to the velocity vector. Consider the short-term time-averaged power that an antenna centered at point x delivers to its load (i.e., $P(x, t)$) rather than the intensity $I(x, t)$. Then, for each point in the diffraction pattern (e.g., $x=x_0$), the following set of measurements can be made.

$$P(x_0, t), P(x_0, t+\tau_1), P(x_0, t+\tau_2), \ldots P(x_0, t+\tau_{N-1}) \quad (3\text{–}27)$$

Thus, the autocorrelation function for $N-1$ discrete lags is

$$\{P(x, t) \cdot P(x, t+\tau_i)\} \quad (3\text{–}28)$$

where braces indicate a spatial average along the X-axis. Assuming that the statistical properties of the rough ocean are stationary in time and homogeneous in space, it follows from the ergodic theorem that the space and time averages are equal. Thus,

$$R_p(\tau_i) = \langle P(x_0, t) P(x_0, t+\tau_i) \rangle = \{P(x, t) \cdot P(x, t+\tau_i)\} \quad (3\text{–}29)$$

where angular brackets indicate a time average, and, because of the assumption of homogeneity, the x_0 argument of R_p is suppressed. This result shows that the moving antenna system will obtain the same autocorrelation function as a hypothetical single stationary transmitter-receiver antenna that constructs an autocorrelation function by averaging over time.

After reasoning that the moving multi-antenna experiment is capable of measuring the same autocorrelation function as a single stationary receiving antenna, attention can be focused on the stationary antenna experiment. Because of the numerous scatterers that contribute to the reflected signal, a reasonable assumption is that the voltage induced across the output terminals of the stationary receiving antenna consists of band-limited noise with a Gaussian joint probability distribution function. The autocorrelation function of this noise voltage will be of the form

$$R_r(\tau) = v(t) v(t+\tau) = R_{vr}(\tau) \cos \omega_0 \tau \quad (3\text{–}30)$$

After linear amplification in a receiver, detection in a full-wave square-law detector, and filtering in a low-pass filter, the autocorrelation function of the short-term time-averaged power will be given by

$$R_p(\tau) = k^2 \delta^4 [1 + 2R_{vr}^2(\tau)] \quad (3\text{–}31)$$

where k is a constant that depends on the receiver gain and δ is the standard deviation of $v(t)$. Thus, $R_{vr}(\tau)$ can be calculated from equation (3–31), and, in turn, the shape of the Doppler-broadened power spectrum may be obtained by taking the Fourier transform of $R_{vr}(\tau)$.

The most important difference between the stationary and moving platform equipment with N antennas is restricted to obtaining $R_p(\tau_i)$ for $N-1$ discrete lags. Thus, the detail in which the power spectrum is desired will determine both the number of antennas and the separation between them. If only the width Δf of the power spectrum is desired, the use of only two antennas with an appropriately chosen spacing should be sufficient.

A practical wave-motion sensor that uses two antennas is shown in figure 3–76. Because this configuration is not restricted to vertical pointing antennas, a wide swath could be examined.

Further investigation of the relationship between the parameters measured by the wave-motion sensor and the statistical description of the ocean is needed. The problem of how well a practical device would operate in the presence of finite receiver noise should also be analyzed.

Surface contour radar.—Under the sponsorship of the AAFE Program, the NRL is developing an instrument for measuring the

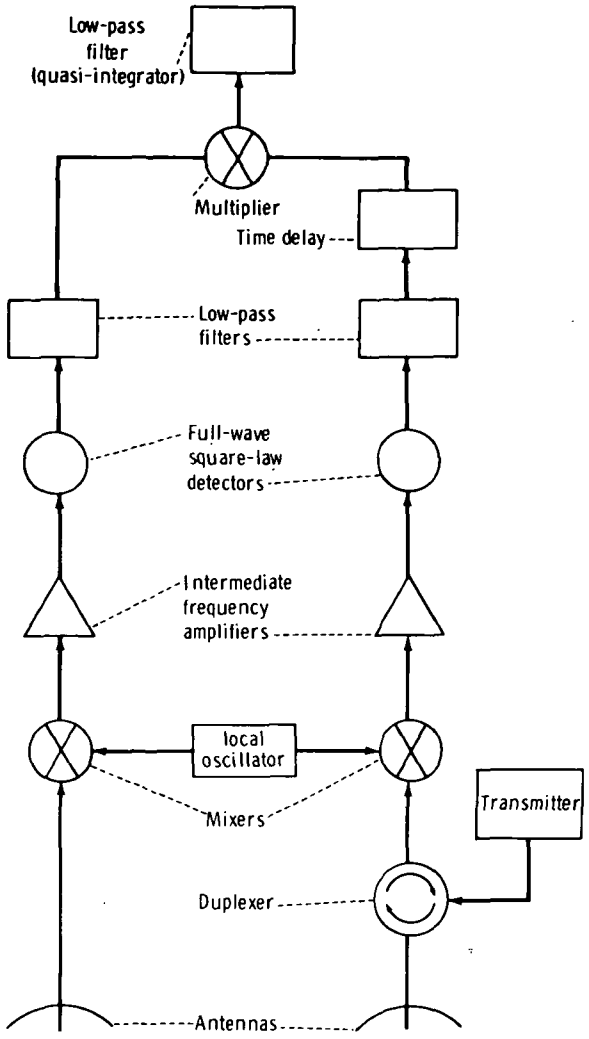

FIGURE 3–76.—A practical wave-motion sensor.

surface contours of the Earth in three dimensions. Surface contours, especially roughness of ocean surfaces, have been inferred from measurements made with other sensors; for example, scatterometers and radiometers, photography, etc. Profiling with radars or lasers provides two dimensions along the groundtrack. A sensor that profiles and scans crosstrack simultaneously will provide a three-dimensional surface contour of the sea.

Although surface contours can be measured over land and ocean areas, this discussion will be restricted primarily to coastal and ocean areas.

Scanning across the groundtrack measures the three-dimensional surface contours along the swath path from which wave heights could be determined directly. The use of data from each swath enables analysis of a slice of any angle across the Earth and determination of its spectra. Combining the analyses of slices at various angles across the swath could yield the directional wave spectra, which are fundamental to location and prediction of present and future sea-state conditions. Scanning in coastal areas will show how waves are affecting shorelines. Measuring the swells and breakers in shoaling water gives indications of the bottom topography.

Experimental technique.—The proposed experiment would consist of scanning a series of radar pulses crosstrack from the aircraft flightpath and recording the time and amplitude of the radar returns. The basic experimental scheme is shown in figure 3–77.

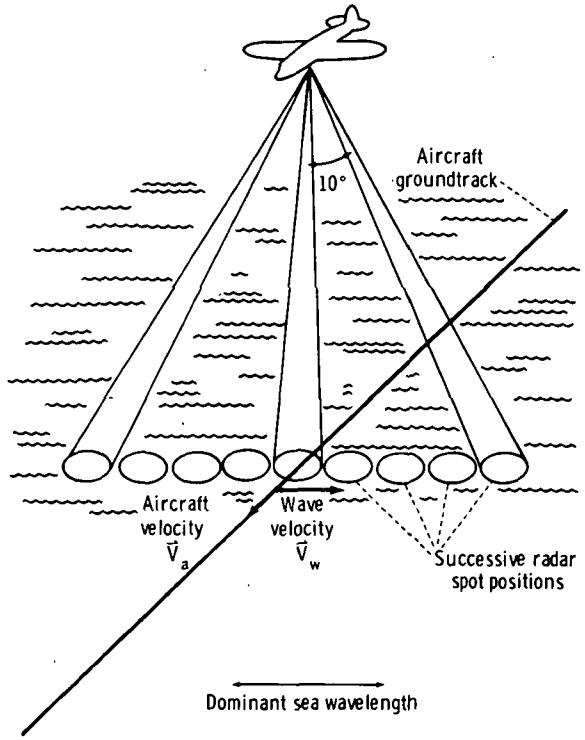

FIGURE 3–77.—Basic experimental scheme for a surface-contour radar system.

Figure 3–78 illustrates the pattern of scan on the ocean surface. The aircraft radar will operate in a beamwidth-limited mode. This choice of operation is made to avoid ambiguities that would occur in scanning a pulse-width-limited radar beam. However, the radar pulse width will still be very narrow, approximately 1 nsec, to enable resolution of the vertical structure of the sea surface.

Observed phenomena.—The laser has been the primary instrument for use in profiling the sea surface. However, the laser has constraints because it must operate at low altitudes and cannot penetrate clouds. The NRL (ref. 3–100) showed that a nanosecond pulse radar viewing in the vertical can profile the sea very accurately and measure the same profile and spectra that would be measured by a wave pole located in the same vicinity. The question arises as to what the radar would measure if it viewed away from the vertical. In figure 3–79, spectra measured by the radar were compared with those measured by the wave pole at angles of 0°, 10°, 20°, 30°, and 45° from the vertical, respectively. The high degree of correlation shows that only minor degradation is noted.

The understanding of ocean backscattering has just begun; thus, the factors causing disagreements between various data have to be explored. The potential offered by multiple frequencies and polarizations has not been investigated. Repeated measurements must be taken to understand the reliability of the prediction of ocean scenes from backscattering cross-section data.

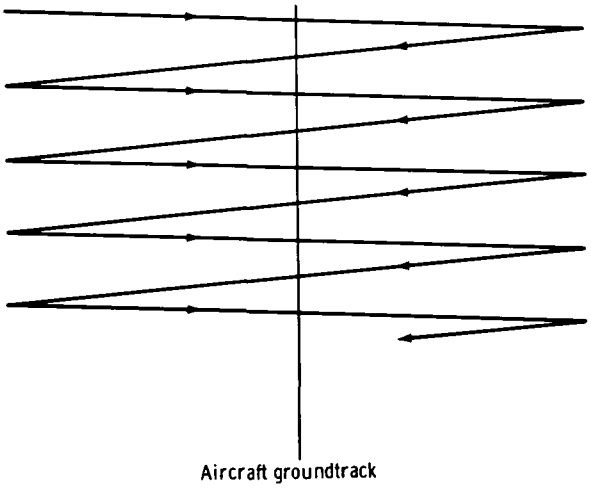

FIGURE 3–78.—Scan pattern on the ocean surface.

Applicability.—Scatterometer data gathered synoptically from the oceans of the world may allow production of accurate worldwide field maps and/or worldwide sea-level pressure maps.

The atmospheric sea-level pressure field specifies the conditions in the planetary boundary level or, for numerical weather prediction models, the properties of the 100 000-N/m^2 surface. This surface pressure field or the equivalent 100 000-N/m^2 surface then serves as the long-sought elusive reference surface for vertical temperature profile radiometer (VTPR) soundings; thus, the vertical structure of the entire atmosphere can be specified for numerical weather prediction models.

The height contour pattern of the planetary boundary layer 100 000-N/m^2 surface is complicated and consists of closed depressions and elevations corresponding to the highs and lows of conventional weather charts. If the pattern can be specified correctly, the bottom of the atmospheric soundings obtained over the oceans by the VTPR infrared sounding system, now operational on NOAA spacecraft, can be correctly related to this 100 000-N/m^2 reference surface, and an integration of the VTPR-computed sounding then yields the heights of all other constant pressure surfaces used in numerical weather prediction models. The most difficult part of the present use of these VTPR soundings is the determination of conditions near the sea surface, and scatterometer/altimeters can help solve this problem. Because the circulation patterns of the constant pressure surfaces become simpler with elevation and turn into the planetary wave patterns at the 100 000-N/m^2 surface, defining the complicated 100 000-N/m^2 surface correctly and integrating VTPR soundings up to the other reference surfaces will provide a more ac-

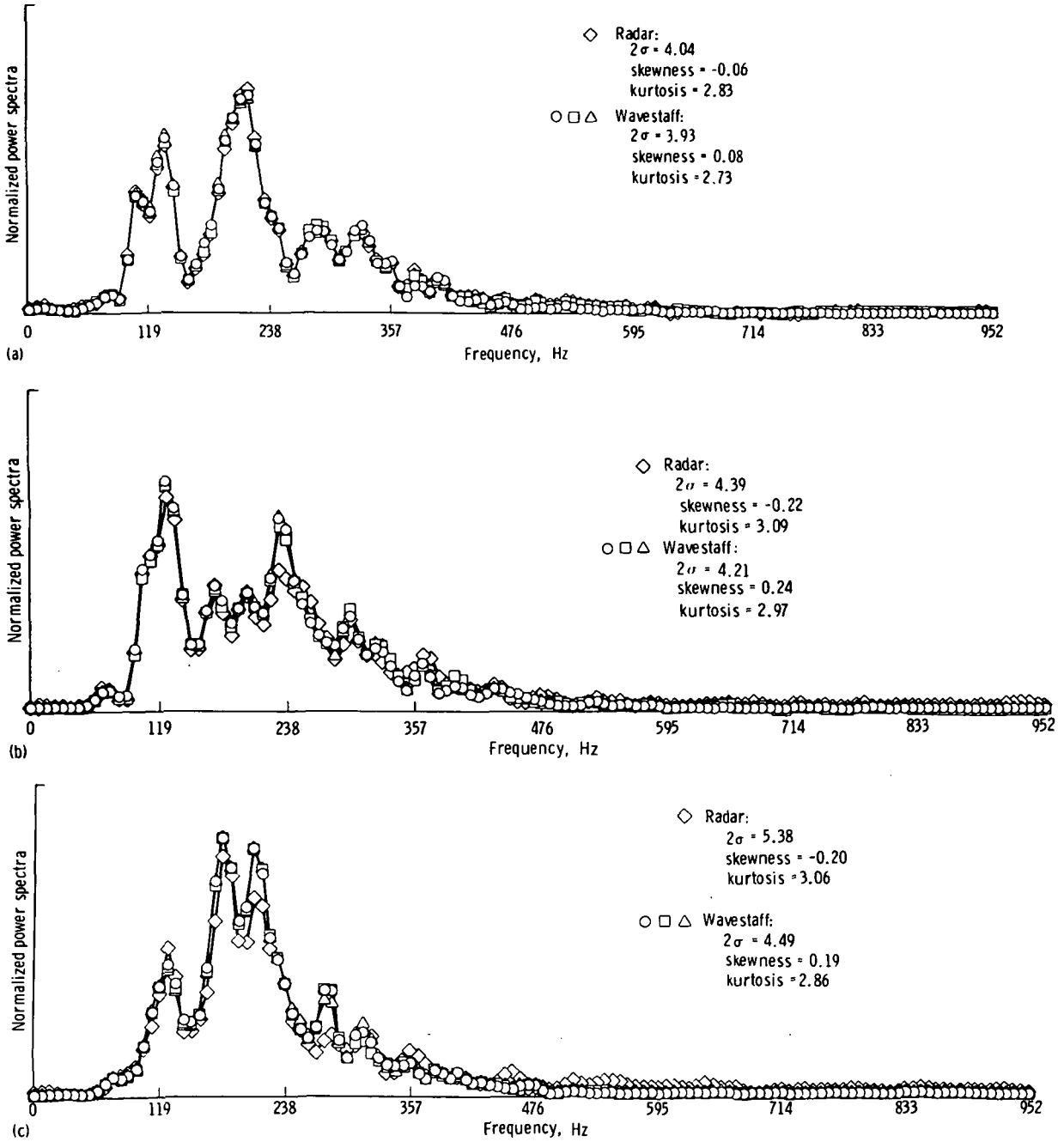

FIGURE 3–79.—Normalized power spectra for radar and wavestaffs for various look angles. (*a*) Look angle=0°. (*b*) Look angle=10°. (*c*) Look angle=20°.

curate initial value specification than, for instance, starting at a higher reference level and integrating both up and down.

Weather forecasts.—Improved weather forecasts on a global basis depend on (1) basic research on the physics of atmospheric, oceanic, continental, and solar interactions; (2) the development of numerical models of

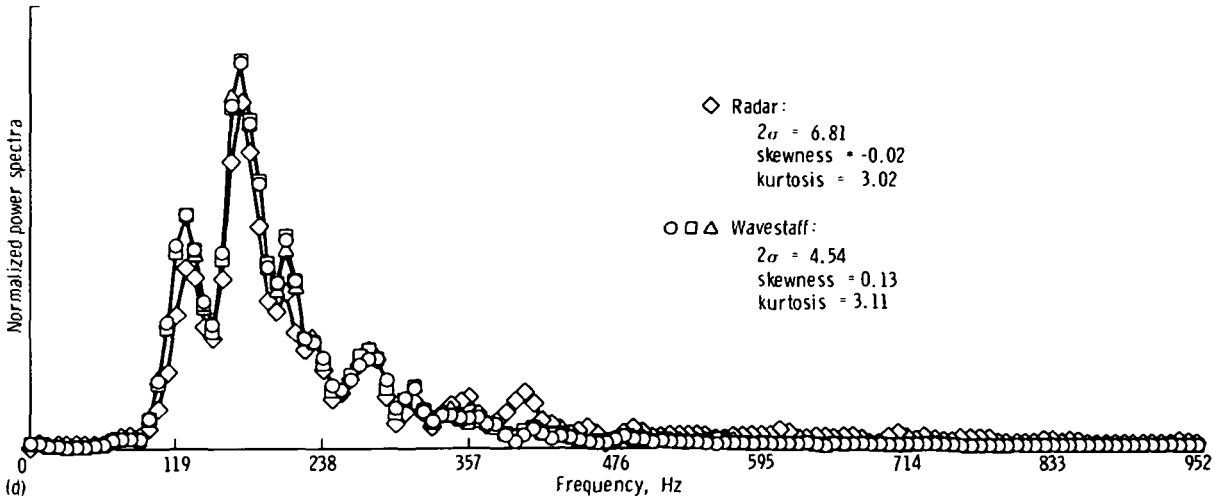

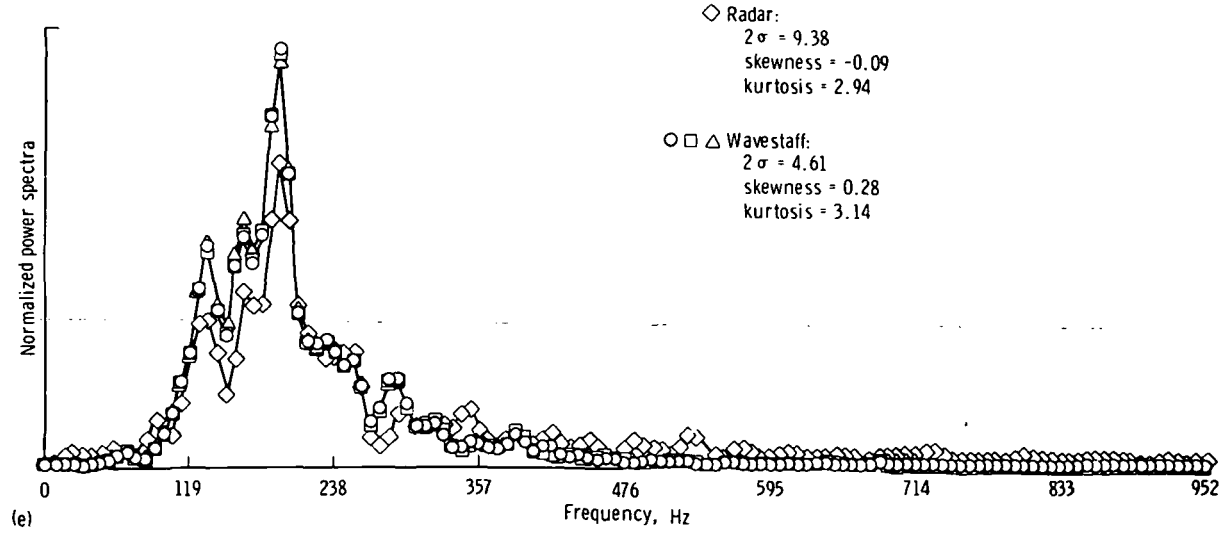

FIGURE 3–79 (concluded).—Normalized power spectra for radar and wavestaffs for various look angles. (*d*) Look angle=30°. (*e*) Look angle=45°.

the atmosphere and its interactions with the land, sea, and solar radiation; and (3) the collection of an adequate and correct data base for the initial value specification of the numerical weather forecasting model. Scatterometers will provide data for item 3 and produce an improvement in the accuracy and an increase in the range of validity of the forecasts produced by the numerical models described in item 2.

Numerical weather prediction models are continuously being refined, improved, and updated so that they can be run on computers of increasingly higher capacity and speed. Nevertheless, the models all depend on the accuracy with which the initial values are specified when the computation of the forecasted weather is started.

When random-error fields with errors of a size known to exist in the actual initial value data are introduced into a numerical model, the effects of these error fields double each day; thus, after 4 days they are 16 times as great, and the forecasted conditions no

longer agree with what actually happened. Reducing the error field in an initial value specification by a factor of 2, in effect, makes a 3-day forecast using better data as accurate as a 2-day forecast using the less-correct data.

Random-error fields are one way to study the effects of bad data; however, the situation is actually more complicated. Over the oceans, especially in the Southern Hemisphere, entire circulation patterns can be incorrectly specified as to the central pressure of a low and the horizontal extent and spacing of the isobars around the low. The proposed instruments for SEASAT–A can substantially reduce this source of error. Not only will weather forecasts over the oceans be improved by the data to be obtained, but also the forecasts over continental areas, such as the western half and the east coast of the United States, could be improved in the 2- to 3-day time frame.

Satellite-borne scatterometer systems should help improve forecasts substantially for 2 to 4 days for the Northern Hemisphere and should make possible, for the first time, 2- to 3-day forecasts for the Southern Hemisphere.

Global heat transports.—Another aspect of the proposed instrumentation for SEASAT–A, which includes a scatterometer, is that it provides a truly global oceanic data base, when combined with VTPR, for numerical weather prediction. The data base over the continents is reasonably adequate. Modeling interactions between the two hemispheres should be possible. Satellite heat budget studies show that the heat flux driving the Northern Hemisphere cyclones in the winter originates from as far as 30° south and has a magnitude at the Equator almost equal to the value at 40° north. The correct description on a day-to-day basis of this important global feature will be an essential step in fulfilling the stated goal of the National Weather Service of NOAA for providing reliable weather forecasts in the time range from 5 to 10 days.

Tropical cyclones.—An example of the value of this active microwave system is the potential contribution it can make in obtaining data on the winds and pressures on tropical cyclones wherever they occur. These tropical cyclones are called hurricanes in the North Atlantic Ocean, typhoons in the North Pacific Ocean, cyclones in the Indian Ocean, and willy-willies in the South Pacific Ocean near Australia and New Zealand. They are located by means of a characteristic cloud pattern by the NOAA Applications Technology Satellite spacecraft and tracked every 45 min or more as they move across the oceans. When their locations are known, ships avoid them almost completely. Thus, although their presence is known (recently there were four typhoons in the North Pacific Ocean at one time), their intensity and potential for damage when moving over land are not known from spacecraft data.

To determine the strength of a hurricane, the United States sends reconnaissance aircraft flights into hurricanes on a routine basis whenever they pose a threat to land. These aircraft measure the winds in the hurricane and determine the central pressure. Forecasting the movement of hurricanes is very difficult, partly because the atmosphere surrounding them is presently not well enough defined by measurements at a fine enough scale.

However, other nations do not have aircraft reconnaissance flights; although they know a hurricane is approaching, they have no information on its severity. Typhoon winds and rains caused much loss of life and damage in the Philippine Islands in 1973, and, in 1970, cyclone winds in the Bay of Bengal caused a storm surge combined with heavy rains that drowned 300 000 people in the Ganges Delta region of Bangladesh.

The problem is so acute for many nations that a special commission has been organized to attempt to find ways to obtain better data on the intensity of the surface winds in these storms as they approach populated areas. At the World Meteorological Organization meeting in Tokyo (Oct. 2 to 7, 1972), held for the study of the means of acquisition and communication of ocean data, a plea was made by the commissioner of this group for

better data on the severity of these storms. Synoptic coverage of the oceans by using satellite-borne scatterometry can solve this problem, as demonstrated by experiments performed during the Skylab Program.

The test version of this instrumentation (S193) on Skylab has scanned both a hurricane and a tropical storm in a way that may prove to have been the equivalent of having had 25 ships close enough to the storm to define the strength of the winds and the level of the central pressure.

The operational version on SEASAT–A could scan all the tropical cyclones present over the oceans twice a day and yield data on the winds and pressures. This one accomplishment would be an immediate aid to India, Burma, the Philippine Islands, many Pacific islands (such as Guam), Madagascar, New Zealand, Australia, and Mexico. Just as the adequate warning service of the National Weather Service has greatly reduced the number of lives lost and the property damage caused by hurricanes in the United States, similar benefits from this system should be possible for other nations. As more experience with the system is gained, it might be possible in a decade or more to dispense with aircraft reconnaissance of tropical cyclones.

Wave forecasting.—Of all oceanic phenomena, the waves, or storm seas, generated by high winds blowing over large areas of the ocean offer the most ever-present and rapidly varying patterns. The waves can grow in height from 5 m from crest to trough (as an average of the highest waves) to 17 m within 12 to 18 hr as the winds increase. Individual waves larger than 25 m from crest to trough have been measured, and waves larger than 30 m high have been estimated. Scatterometers and altimeters together can measure parameters needed for a wave forecasting model.

PLATFORMS

Satellites

Although the central theme of the Active Microwave Workshop is the application of active microwave systems to Earth observations, the question of integrating these systems with other sensors has to be considered. This section assesses three types of ocean-oriented spacecraft that use radar and several other types of sensors. The multisensor approach has the merit of yielding considerably more information from the simultaneous use of an array of instruments than could be obtained from their operation separately. This philosophy has been successfully used in SEASAT–A.

Three generalized types of useful oceanic observatories are: (1) a geodynamics/ocean topographic satellite, (2) an oceanic/marine atmospheric physics satellite, and (3) a marine water quality/biologic/fisheries satellite.

A geodynamics/ocean topographic satellite.—This system, which has evolved from the EOPAP project, would determine the marine geoid and superimposed local ocean topographic features, with the aim of understanding the space and time variations in the shapes of both surfaces caused by geodynamic and oceanographic effects and their interactions. Examples of geodynamic effects are tectonic plate motion, polar wandering, and solid Earth tides; examples of oceanographic effects are oceanic currents, deep sea tides, storm surge, and wind setup. The prime sensor would be a precision altimeter with an altitude error of approximately 2 to 5 cm, a precision that would require ionospheric, tropospheric, and ocean-wave-height corrections. The spacecraft would probably have a symmetrical drag-free configuration, laser reflectors, and satellite-to-satellite tracing capability. The orbit would be circular and inclined at 105° to 115° retrograde. By maintaining this satellite or similar ones in orbit for periods of approximately one decade, many highly significant Earth and ocean dynamics experiments could be performed, including measurements of continental drift and their relationship to earthquakes and a mapping of the major ocean currents and their time variations.

The oceanic/marine atmospheric physics satellite.—This spacecraft measures sea surface and maritime atmospheric parameters that help establish the near-ocean-surface

marine environment. These parameters are also of importance for weather forecasting over both land and water and for longer term climatological studies. The measurement functions of this satellite would include all-weather observations of surface and upper-level pressures, windspeeds, and directions; atmospheric profiles of water vapor, liquid water, and rainfall rates; air temperature profiles; sea-surface temperatures; wave heights, lengths, and directions; wave refractive patterns; and ice thickness, leads, polynyas, and general coverage.

The orbit would probably be circular, near-polar, and prograde, with an inclination of 75°. As such, the orbit would be non-Sun-synchronous and would process through a day/night cycle in a few weeks. The altitude would be chosen as a compromise between swath width, resolution element, power, and precision rate, but it would probably be near Earth at 1000- to 2000-km heights.

The sensor complement would include (1) an imaging radar for observing wave amplitude spectra and refractive patterns, shoreline dynamics, ice cover, and other similar features; (2) a combined scatterometer/multifrequency microwave radiometer for observing surface windspeeds and directions, atmospheric water vapor and liquid water content, and sea-surface temperature and salinity; (3) multifrequency/multiwavelength microwave and infrared sounders for determining temperature, pressure, and humidity profiles in the atmosphere; and (4) a multispectral thermal infrared imager capable of yielding quantitative land, sea surface, and cloudtop temperatures.

This combination of instruments is complex; however, the value of simultaneous observations of the relevant parameters for maritime environmental forecasts is great enough to warrant this complexity. If achievable, this second observatory would represent a highly significant advance in the data base required for a several-day global weather and maritime forecast.

Water quality, biological assay, and fisheries identification.—This system would rely heavily on spectral reflectivity analysis for determination of near-surface chlorophyll content, pollution, and sediment load. The required information could be derived from a multispectral imager optimized to the parameters of interest and, equally important, from data obtained by the two spacecraft mentioned previously. Of particular importance in the latter category are sea temperature, salinity, and current location.

The requirements for multispectral analyses imply a Sun-synchronous orbit and particular choices of look angle with respect to Sun angles so that illumination conditions on the ocean surface are uniformly maintained. Thus, this sensor complement may not be flown on the ocean/atmospheric physics platform, at least in a research mode, because the orbit for the research mode is deliberately designed to scan through a day/night cycle relatively quickly to observe diurnal effects. Operational spacecraft may not be so constrained, however.

Using these data, one may estimate primary biological productivity, water mass identification, sediment transport, and general condition of the ocean. Location of potential fisheries can probably be inferred from such information.

SEASAT–A.—This satellite is the first spacecraft dedicated to meeting in part the EOPAP objectives in ocean dynamics. The SEASAT–A is an outgrowth of a diversity of scientific and technological work conducted by NASA, the Department of Defense, the Department of Commerce, and several other institutions in both the measurement of required physical quantities and the implementation of appropriate sensors on the spacecraft and on the ground.

Description of the program.—SEASAT–A is a research-oriented program consisting of spacecraft precision groundtracking systems and data-processing and modeling capabilities that address both scientific and applications problems in ocean-surface dynamics. The satellite will carry an array of active radar and passive microwave and infrared instruments with the capability of observing

the ocean on a day/night near all-weather basis. This group of sensors will allow SEASAT–A to make quantitative measurements of oceanic, atmospheric, and geodetic parameters not only in clear weather but also under wind and wave conditions perhaps approaching hurricane force and over regions under persistent cloud cover.

The mission profile for SEASAT–A is tentatively as follows: lifetime, 1-yr minimum; orbit, approximately an 800-km altitude at an inclination of 108° (retrograde); eccentricity, less than 0.006 for a nearly circular orbit; and period, 100 min, resulting in 14.5 orbits/day. This orbit is nonsynchronous and will process through a day/night cycle in approximately 4.5 months. The orbit spans almost all the unfrozen oceans of the world from the Antarctic to the Alaskan North Slope and the Arctic Archipelago. The orbit is also optimum for fine-grained mapping of the geoid over the open ocean.

Instruments and sensors.—Each of the sensors proposed for SEASAT–A has predecessors that have been successfully flown on spacecraft and/or aircraft. Good-to-excellent assessments of the capabilities of these prototypes are available for wind and wave conditions approaching gale force, and enough is known of their theory of operation to make reasonable estimates of their performance under other, more severe environmental conditions. The selection of instruments was made to determine ocean-surface conditions in accordance with user data requirements set forth during NASA-sponsored meetings in early 1973. The sensors form a set of integrated, interactive, and mutually supporting devices, the simultaneous use of which brings about a genuinely synergistic effect wherein the total information derived from the sensor package is greater than the sum of the individual outputs. Meeting the user data requirements in their totality has not been possible because of limitations on system performance, but the five sensors described constitute a significant first step toward an optimum configuration.

Compressed pulse radar altimeter (CPRA): The CPRA has two distinct functions: the measurement of the altitude between the spacecraft and the ocean surface to an rms precision near ± 10 cm and the determination of significant wave heights along the subsatellite path. When combined with accurate orbital determinations, the altitude may be used to decipher the topography of the sea surface, including spatial variations in the geoid and time variations caused by ocean dynamics.

Coherent imaging radar (CIR): Wave information will be obtained by using a CIR to obtain images of the ocean on a sampled basis. Such a radar can function through clouds and moderate rain to yield wave patterns near shorelines and in storms and can see waves with a length greater than approximately 50 m. The CIR can also provide high-resolution pictures of ice, oilspills, current patterns, and similar features. Computations can be performed on the radar data to yield a quantity called the wave directional spectrum, which gives the relative distribution of wave energy among different wavelengths traveling in various directions, and this factor, together with the surface wind velocity, is the fundamental information needed in forecasting wave conditions on the ocean.

Microwave wind scatterometer (MWS): The third radar system, an MWS, is intended to measure surface windspeed and direction by sensing the small capillary waves induced by the wind over the ocean. Previous aircraft experience and recent Skylab data taken over the Pacific Hurricane Ava in June 1973 indicate that this sensor seems useful in winds approaching 25 m/sec, yielding speeds with an error of ± 2 m/sec and directions to $\pm 20°$.

In the SEASAT–A configuration, the output of the scatterometer will be measurements of lower windspeeds and directions taken over two 450-km-wide swaths equally displaced about the vertical by 300 km. In 12 hr, these swaths map out a quiltlike pattern of areas over the portion of the oceans between 72° north and 72° south latitude with enough density of observations so that an essentially complete chart of surface winds will be obtained.

An experimental variation of the MWS, termed the "wave spectrometer," is expected to be operated simultaneously with the MWS as an alternative, less complicated, and less complete method of obtaining wave directional spectra along a 300-km-wide swath about the vertical.

Scanning multifrequency microwave radiometer (SMMR): The SMMR is a passive microwave device that simultaneously senses the microwave energy emitted by and reflected from the ocean, ice, and atmosphere. To separate the various contributions to the signal from these sources, several microwave frequencies (6, 10, 18, 21, and 37 GHz) are used, each chosen for maximum sensitivity to one of those geophysical parameters. The scanning feature will enable low-resolution images of objects along its line of sight to be constructed from the signals received.

The SMMR serves several functions. First, the SMMR is a windspeed instrument that senses the increase in emitted microwave energy caused by roughness, foam, and streaks on the ocean when higher windspeeds create wave breaking and whitecaps. The estimated observable range of speeds is from approximately 10 m/sec to perhaps 50 m/sec. The upper limit has yet to be firmly established. Thus, the range of speeds measurable from SEASAT should be extended by the SMMR from the 25-m/sec limit of the scatterometer up toward hurricane-force winds. Second, the SMMR appears capable of measuring sea-surface temperature with an accuracy of 10 K even through light clouds where present infrared devices are useless. Third, the other frequencies are used for determining atmospheric liquid water and water vapor content, quantities that are needed for models of oceanic and atmospheric boundary-layer processes and for important corrections to the precision altimeter measurements. Icefields and ice cover will also be observed with low resolution from the SMMR.

Maps of higher ocean-surface winds, temperatures, and overlying atmospheric water content will be the output of the SMMR. These maps will be combined with the wind data from the MWS to yield a global quantitative chart of windspeed below hurricane force. The measurements will be equivalent to some 20 000 ship reports a day. When these measurements are combined with available ship and buoy surface information on wind and pressure, the atmospheric pressure field over the entire ocean, except perhaps near reserve storms, can be computed. This computation will also be possible in the data-sparse Southern Hemisphere. Such results should help improve the 24-hr weather forecasts substantially. This improved predictive capability for winds implies an approximately equal improvement in forecasting waves, especially when assisted by the data on the initial state of the sea obtained from the radar altimeter and imager.

Infrared radiometer (IRR): The purpose of this sensor is to provide images of thermal infrared emission from ocean, coastal, and atmospheric features that will help interpret the measurements from the other four microwave instruments. In addition, the IRR will have atmospheric correction channels that will enable temperatures to be deduced from the imagery with a precision of better than 1 K in clear air. The device will be similar to scanning radiometers flown on Nimbus and the NOAA Improved Tiros Operational Satellite.

The total system.—The informational output of the instrument complement will constitute three classes. The first class will be measurements of wave height, wave directional spectrum, and surface windspeed and direction over the global ocean with a repeat time of 12 to 36 hr on a somewhat uneven grid that is at least as fine as 250 km in most parts of the world. The second class will be sea-surface topography from which currents, setup tides, and other similar features may be deduced in selected regions over a time scale of days or weeks. The third class is high-resolution imagery, both radar and infrared, made over selected areas at specified times on selected time and space scales.

The interrelationships among these several

classes of data are presented in table 3–XI, which illustrates the complex nature of the contribution that each sensor makes to the geophysical parameters being measured. Table 3–XI indicates the importance of carrying the full sensor complement to achieve the measurement objectives.

SEASAT–A is thus an integrated observatory addressing the objectives discussed previously. Table 3–XII outlines the capabilities of the spacecraft system in meeting the requirements set forth by the users at the start of the program. Not all of the desiderata have been met; in particular, the operationally determined requirements demand more than one spacecraft. Thus, the request for continuous coverage of wind and waves with an update every 12 hr, the desire for 100-km surface resolution on the SMMR channels, and the requirement for all-weather temperature resolution of 0.25 K have been impossible to achieve. It does not appear feasible to reach a global overall ±10-cm accuracy in geoid, altimeter, and tracking needed to reduce the ultimate errors in current measurements to the level of 20 cm/sec. These considerations must await further work.

Nevertheless, these data will be valuable for both research purposes and for demonstration of near-operational uses in marine and weather forecasting. The program plan calls for assembling all the data in compatible format through a command and control center at the Goddard Space Flight Center, reducing and interpreting them as geophysical quantities, and disseminating them to research scientists in an orderly way. In addition, on a few occasions during the life of the satellite, a real-time quasi-operational exercise will be conducted in which the wind/wave/imagery information will be sent out on communications channels to users, such as the NOAA National Meteorological Center or the Department of Defense Fleet Nu-

TABLE 3–XI.—*Physical Parameter Measurement Methods*

Measurements and sensors	Physical parameters								
	Atmospheric water content	Surface winds, speed, and direction	Wave heights, length, and direction	Wave near shores and storms	Geoidal heights	Surface currents, speed, and direction	Tides, tsunamis, setups, storm surges	Sea surface temperatures	Ocean, ice, atmosphere, and land features
Radar backscatter (scatterometer)		X	X						X
Microwave emission (microwave radiometer)	X	X	X			X		X	X
Altitude and roughness (radar altimeter)		X	X	X	X	X	X		X
Radar images (imaging radar)		X	X	X		X			
Infrared images (IRR)	X					X		X	X
Ocean geoid (external data)					X	X	X		X
Satellite position (external data)	X	X	X	X	X	X	X	X	X
Other observations (external data)	X	X	X	X	X	X	X	X	X

TABLE 3–XII.—*Capability of SEASAT–A in Meeting User Requirements*

Physical parameter	Instruments	Range [a]	Precision	Resolution or IFOV [b]	Total FOV [c]	Comments
Wave height $H_{1/3}(x, y)$	Pulse altimeter and coherent altimeter	1.0 to 20 m	±0.5 m or ±10 percent	2- by 7-km spot	2-km swath	Along subsatellite track only
Directional sea wave spectrum $\psi(\lambda, \theta, x, y)$	Imaging radar (two-dimensional transform)	ψ: Unknown l_w: 50 to 1000 m θ_w: 0 to 360°	ψ: — l_w: ±10 percent θ_w: ±10°	50-m resolution	20- by 20-km squares	Global samples at 250-km intervals
	Two-frequency wave spectrometer	ψ: Unknown l_w: 6 to 500 m θ_w: 90° sector	ψ:— l_w: ±10 percent θ_w: ±90°	8- by 25-km spot	300-km swath about nadir	Global samples at 150-km intervals
Surface wind field $W(x, y)$	Scatterometer	W: 3 to 25 m/sec θ_w: 0 to 360	±2 m/sec, ±10 percent; ±20°	≤50-km spot	Two 450-km swaths	Global, 36 hr (low speeds)
	Microwave radiometer	W: 10 to 50 m/sec θ_w: Unknown	±2 m/sec, ±10 percent	≤100-km spot	900-km swath about nadir	Global, 36 hr (high speeds)
Surface temperature field $T(x, y)$	IRR	−2 to 35 K	±.25 to 1 K	1- to 17-km IFOV	1500-km swath about nadir	Global, 36 hr (clear air only)
	Microwave radiometer	0 to 35 K	±1.5 K	100-km spot	900-km swath about nadir	Global, 36 hr (clouds and light rain)
Geoidal heights $h(x, y)$ (above reference ellipsoid).	Pulse altimeter and coherent altimeter	7 cm to 200 m	±7 cm	2- by 7-km spot	18-km spacing along equator	Sampled throughout 1 yr
Sea surface topography $J(x, y)$ (departures from geoid).	Pulse altimeter and coherent altimeter	7 cm to 10 m	±7 cm	2- by 7-km spot	2-km swath	Along subsatellite track only
Oceanic, coastal, and atmospheric features (patterns of waves, temperature, currents, ice, oil, land clouds, and atmospheric water content).	Imaging radar	High resolution	All weather	25 or 100 m	100 or 200 km	Sample directly or stored images
	IRR	High resolution	Clear air	1 to 7 km	1500-km swath	Broadly sampled images
	Microwave radiometer	Low resolution	All weather	15 to 100 km	900-km swath	Global images

[a] The l_w is wavelength of waves, θ_w is directional angle of the waves, and W is windspeed.
[b] Instantaneous field of view.
[c] Field of view.

merical Weather Center, with less than a 3-hr delay. Another exercise visualized is one in which near real-time radar images of the icefields along the Northwest Passage are obtained and estimates are made of their usefulness to real or hypothetical ship passages.

An important element in interpreting the SEASAT–A data and extending its utility will be a combination of the information obtained from this spacecraft and the considerable data on oceans and atmosphere available from other sources. The environmental/meteorological satellites, ships, buoys, and transoceanic aircraft are obvious sources for marine and weather data. In the case of ocean-wave forecasts, a land-based high-frequency skywave radar that is intended for operational detailed monitoring of wave spectra near the continental United States is expected to be in service. Its fine-grained data complement the necessarily coarser-space open ocean-wave spectral data from SEASAT–A. Similarly, research data on currents, tides, the geoid, and the other parameters of interest will be amalgamated with the SEASAT–A data by individual researchers interested in specific problems.

Scientific problems.—In addition to being an applications satellite, SEASAT–A will be an important research tool in several areas of geophysics, as shown by the following list of scientific problems that it can address.

Oceanography: The mapping of major ocean currents and their time and space variations in selected regions will be achievable by a combination of infrared imagery to yield positions and precision altimetry for estimates of surface speeds.

Global deep-sea tides should be extractable from altimetry measurements with errors of perhaps a few tens of centimeters during a year of data taking; in contrast, only a few dozen measurements of open ocean tides presently exist.

Altimeter sensing of a tsunami in the Pacific Ocean may be possible if one or more of those earthquake-caused waves occurs during the lifetime of the satellite. The information obtained may assist in determining the energy content of the tsunami and help reduce the problem of overwarning that now exists. However, an operational warning system cannot be predicated on the basis of satellite altimetry.

Ice dynamics can be studied with repeated radar imagery taken in the polar regions. The size and extent of leads and cracks establish the heat exchange between air and water and, hence, determine much of the weather in those regions.

The generation, spatial distribution, and radiation of waves by storms and hurricanes may be investigated with radar imagery. Using detailed wave spectra, wave/wave interaction may be studied as a process that cascades energy from short to long waves, which result in high sea states. Little is known quantitatively about the surface-wave regime on continental shelves under severe storm conditions. Similarly, interactions of storm surf with shorelines and coastal structures can be observed during bad weather.

Oceanographers have never been able to gain the overview of their domain required to understand synoptic or planetary scale events in the sea. The SEASAT–A should provide a very important vantage point for that view.

Boundary-layer meteorology: The greatly increased knowledge of the surface temperature, wind, and pressure fields over the oceans will aid in understanding large-scale atmospheric circulation and air/sea heat exchange. The effects of the sea temperature on hurricane growth, jetstream deflection, and global climatology may be illuminated by these measurements. Poleward transport of heat by oceanic currents can be assessed more accurately, and the effect on the overall heat balance can be assayed.

Geodetic science: The prime geodetic output of SEASAT–A will be a precise fine-scale equipotential surface (geoid) over the ocean. *This measure of the Earth may be used to* determine gravimetric deflections of the accuracy of the new North American datum. Gravity anomalies caused by large underwater features such as sea mounts and

trenches may also be observed. The discrepancies between spirit leveling and sea-level measurements along the coasts may be resolved by the precise knowledge of sea-surface topography.

The improved gravity fields should result in more accurate satellite orbital determination. The influence of polar wandering and other nonrigid Earth motions may be measured more readily, and the origins of the motions can be sought using orbital analysis and accurate tracking.

Engineering science: A high-technology system such as a spacecraft always results in many important developments in technology and engineering science. Although it is difficult to specify exactly what the yield of SEASAT–A in this regard will be, a safe speculation would be that significant advances are expected in areas of short pulse and coherent radars, in tracking technology, and perhaps in data handling and dissemination. Other technologies presumably will be upgraded during the program.

Aircraft

Aircraft provide mobile, variable altitude platforms to fulfill four needs:

1. Providing a relatively inexpensive means to field test hardware.
2. Collecting data to verify theoretical models.
3. Collecting ground-truth data to verify the performance of satellite systems.
4. Conducting near-shore fine-scaled quick-response studies.

For many features, the temporal requirements for observation in the coastal region are considerably more frequent than for the open ocean. For specific coastal phenomena, such as circulation, the observation may well be tidally dependent and require multiple observations during the tidal cycle. Observations should be sensitive to seasonal variations and persistent wind conditions. However, continuous observations over extended periods and regions are not required and can be accomplished on a geographically selective basis. Hence, the aircraft platform complements satellite systems by increased temporal coverage for coastal requirements.

Aircraft in the aerospace program have been used for testing and establishing feasibility for space techniques and for providing several levels of monitoring in multistage sampling systems. These roles will continue for microwave development and for sea truth and instrument validation for experimental and operational satellite systems. Because of spatial resolution limitations of microwave systems and increased levels of temporal coverage needed for coastal operations, aircraft rather than geostationary platforms will be responsible primarily for active microwave selective coverage in the coastal region. Hence, imaging radar systems developed for aircraft can play an operational role in understanding coastal dynamics.

Lighter-Than-Air Airships

A unique opportunity exists with the station-keeping capability of relatively vibration-free airships. The plan position indicator radar (without clutter rejection circuits) can be combined with time-lapse photography techniques to monitor wave refraction effects in a continuous manner. In particular, wave energy focusing effects can be quantitatively evaluated over regions with approximately a 30- to 50-km radius, which is sufficient for many coastal activities.

The dirigible can monitor specific activities at sea on a very economical basis. Such activities include fishing operations and dumping of wastes into the ocean. For research, dirigibles offer the advantage of maintaining a specific area of ocean in the field of view of its instrument payload with varying observation angles, solar angles, etc.

Some benefits that ocean scientists could derive if they used the unique range, load, endurance, and flight characteristics potentially offered by airships are as follows:

1. Mounting of the largest microwave antennas ever flown.
2. Shortening of transit times (compared to ships) to remote ocean observation areas.

3. Unsurpassed staying power compared to airplanes or helicopters.
4. Stable and vibration-free flight.
5. Roominess onboard and good habitability characteristics.
6. Ability to carry a variety of oceanographic sensors, including very large listening arrays that can be towed without self-generated hull and propeller noise.
7. Capability to process observational data in flight and repeat the experiments on scene if required.
8. Opportunity to observe remotely from the air and simultaneously sample the ocean in situ for ground truth.

Being a function of volume, their performance could be tailored to the particular ocean work assignment involved. Nonrigid airships (the so-called blimp type) could be sized at approximately 0.1 million cubic meters for coastal work. Larger airships of the rigid or structural class, perhaps 0.55 million cubic meters, would be used for protracted mid-ocean missions. Ocean-related payloads might range from 5000 to 35 000 kg. Maximum speeds should exceed 60 m/sec. Refueling from surface ships or use of nuclear propulsion, for which lighter-than-air airships are peculiarly suited because of their low energy requirements, would insure impressive station-keeping capabilities.

Data Collection Platforms

The NASA Synchronous Meteorological Satellite A (SMS–A) was launched in June 1974. The SMS–B is to be launched in January 1975. The backup satellite, the NOAA GOES–A, is scheduled to be launched in August 1975. The GOES–A will be stored in orbit to replace either SMS–A or SMS–B should the need arise.

The subpoint locations for SMS–A and SMS–B are expected to be near 75° and 135° west longitude, respectively. The first satellite will be temporarily located near 100° west longitude. The second satellite will be positioned near 20° west longitude to support the GARP Atlantic Tropical Experiment (GATE). At the conclusion of GATE, the satellites will be moved to their designated operating positions.

From the Earth-synchronous orbit, 35 000 km above the Equator, the satellite will (1) provide near-continuous day/night imaging of the Earth surface and cloud cover over an area with a radius of at least 55° great circle around the satellite subpoint; (2) rebroadcast that imagery in a "slowed-down" mode for direct reception by suitably equipped regional user stations; (3) monitor the space environment in terms of solar energetic particles, X-rays, and the geomagnetic field; (4) broadcast environmental service products such as charts, analyses, and advisories to remote locations; and (5) collect and relay environmental data sensed by a variety of widely dispersed in situ platforms such as river and rain gages, seismometers, tide gages, buoys, ships, and automatic weather stations.

For the environmental data collection subsystem, the spacecraft is being designed with a capacity to collect and relay environmental observations from 10 000 or more individual observing platforms within each 6-hr period. Sensor data will be transmitted to the spacecraft either in an interrogated or self-timed mode of operation, using frequencies in the lower ultrahigh frequency (400 to 500 MHz) band. The preferred data format is the American Standard Code for Information Exchange, which is the U.S. Government standard, and is computer compatible. A platform equipped with a 10-dB gain antenna and a 5-W transmitter can operate effectively at an antenna elevation angle of 7.5°. The data received at the satellite will be transponded at S-band frequencies (nominal 1694 MHz). Data collected from these platforms will be relayed through the satellite and acquired by the National Environmental Satellite Service (NESS) Command and Data Acquisition Station at Wallops, Va., and relayed to a central location in Washington, D.C. As the program evolves to a fully operational status, these data will be disseminated routinely in a standard format over environmental data communications circuits.

The long-awaited plan for the operational GOES data-collection subsystem is nearing completion. The plan includes a questionnaire to be completed by those planning to establish data collection platforms. The responses to the questionnaire will be used by NESS to evaluate the need for the service, assign the channels to be used, and determine priorities for collection. Interface requirements for the self-timed and interrogated data-collection platform radio sets have been developed.

The system will be available for international participation by environmental services agencies/organizations in programs of mutual interest. Consistent with World Meteorological Organization practices, participating user agencies will bear the cost of the in situ platforms and environmental sensors, the radio equipment to establish the platform-satellite communications link, and the standard communications terminal equipment (teletypewriters) in their operating facilities. If the user has a unique need for dissemination from Washington, D.C., he may choose to provide, at his cost, for special communications between his facility and Washington, D.C.

The use of the data-collection system will be limited to the collection of environmental data in accordance with applicable International Telecommunication Union regulations concerning use of the allocated frequency bands. Environmental data are defined as observations and measurements of the physical, chemical, or biological properties of the oceans, rivers, lakes, solid Earth, and atmosphere (including space).

REFERENCES

3–1. APEL, J. R., AND SHERMAN, J. W. III: Monitoring the Seas From Space: NOAA's Requirements for Oceanographic Satellite Data. NOAA Rep. AOML–LORS (Miami, Fla.), June 1973.

3–2. U.S. COAST GUARD: An Analysis of the Potential Applications of Space Telecommunications Systems to U.S. Coast Guard Missions. Contractor Report by Westinghouse Defense and Electronics Systems Center, Baltimore, Md., 1975. (Available from the National Technical Information Service, Springfield, Va.)

3–3. CROMBIE, D. D.: Doppler Spectrum of Sea-Echo at 13.56 Mc/s. Nature, vol. 175, 1955, pp. 681–682.

3–4. KERR, D. E., ed.: Propagation of Short Radio Waves. MIT Radiation Laboratory Series, vol. 13, McGraw-Hill Book Co., 1951.

3–5. RUCK, GEORGE T.; BARRICK, DONALD E.; STUART, WILLIAM D.; AND KRICHBAUM, CLARENCE K.: Rough Surfaces. Radar Cross Section Handbook, vol. II, Ch. 9, Plenum Press, 1970.

3–6. SKOLNIK, MERRIL IVAN, ed.: Sea Echo. Radar Handbook. Ch. 25, McGraw-Hill Book Co., 1970.

3–7. WRIGHT, JOHN W.: A New Model for Sea Clutter. IEEE Trans. Antennas Propagat., vol. AP–16, no. 2, Mar. 1968, pp. 217–223.

3–8. BARRICK, D. E.: First-Order Theory and Analysis of MF/HF/VHF Scatter From the Sea. IEEE Trans. Antennas Propagat., vol. AP–20, no. 1, Jan. 1972, pp. 2–10.

3–9. CHAN, H. L., AND FUNG, A. K.: Backscattering From a Two-Scale Rough Surface With Application to Radar Sea Return. NASA CR–2327, 1973.

3–10. CHIA, R. C.: The Theory of Radar Scatter From the Ocean. CRES TR–112–1, Center for Research in Engineering Science, Univ. of Kansas, Oct. 1968.

3–11. KATZIN, MARTIN: On the Mechanisms of Radar Sea Clutter. Proc. IRE, vol. 45, no. 1, Jan. 1957, pp. 44–54.

3–12. SCHOOLEY, ALLEN H.: Upwind-Downwind Ratio of Radar Return Calculated From Facet Size Statistics of a Wind-Disturbed Water Surface. Proc. IRE, vol. 50, no. 4, Apr. 1962, pp. 456–461.

3–13. VALENZUELA, G. R.: Depolarization of EM Waves by Slightly Rough Surfaces. IEEE Trans. Antennas Propagat., vol. AP–15, no. 4, July 1967, pp. 552–557.

3–14. MOORE, R. K.; CLAASSEN, J. P.; FUNG, A. K.; WU, S. T.; AND CHAN, H. L.: Toward RADSCAT Measurements Over the Sea and Their Interpretation. CRES TR–186–6, Center for Research in Engineering Science, Univ. of Kansas, Aug. 1971.

3–15. PIERSON, W. J., JR., AND STACY, R. A.: The Elevation, Slope, and Curvature Spectra of a Wind Roughened Sea Surface—Final Report. NASA CR–2247, 1973.

3–16. WU, S. T., AND FUNG, A. K.: A Non-Coherent Model for Microwave Emission and Backscattering From the Sea Surface. J. Geophys. Res., vol. 77, no. 30, Oct. 1972, pp. 5917–5929.

3–17. VALENZUELA, G. R.: Scattering of Electromagnetic Waves From a Tilted Slightly Rough Surface. Radio Sci., vol. 3, no. 11, Nov. 1968, pp. 1057–1066.

3–18. GUINARD, N. W., AND DALEY, J. C.: An Experimental Study of a Sea Clutter Model. Proc. IEEE, vol. 58, no. 4, 1970, pp. 543–550.

3–19. BRADLEY, G. A.: Remote Sensing of Ocean Winds Using a Radar Scatterometer. Ph.D. Dissertation, Univ. of Kansas, 1972.

3–20. CLAASSEN, J. P.; FUNG, A. K.; MOORE, R. K.; AND PIERSON, W. J.: Radar Sea Return and the Radscat Satellite Anemometer. Proceedings of Engineering in the Ocean Environment (Newport, R.I.), Sept. 1972, pp. 180–185.

3–21. SUTHERLAND, A. J.: Spectral Measurements and Growth Rate of Wind Generated Water Waves. Tech. Rep. 84, Stanford Univ., Dept. of Civil Engineering, Aug. 1967.

3–22. STOGRYN, A.: The Apparent Temperature of the Sea at Microwave Frequencies. IEEE Trans. Antennas Propagat., vol. AP–15, no. 2, Mar. 1967, pp. 278–286.

3–23. COX, C., AND MUNK, W.: Measurements of the Roughness of the Sea Surface From Photographs of the Sun's Glitter. J. Opt. Soc. Amer., vol. 44, no. 11, Nov. 1954, pp. 838–850.

3–24. ULABY, F. T., AND FUNG, A. K.: Effects of Roughness on Emissivity of Natural Surfaces in the Microwave Region. IEEE Southwest Conf. Proc., Apr. 1970, pp. 436–440.

3–25. LYNCH, P. J., AND WAGNER, R. J.: Rough-Surface Scattering: Shadowing, Multiple Scatter and Energy Conservation. J. Math. Phys., vol. 11, no. 10, Oct. 1970, pp. 3032–3042.

3–26. WILLIAMS, G. F., JR.: Microwave Radiometry of the Ocean and the Possibility of Marine Wind Velocity Determination From Satellite Observations. J. Geophys. Res., vol. 74, Aug. 20, 1969, pp. 4591–4594.

3–27. DROPPLEMAN, J. D.: Apparent Microwave Emissivity of Sea Foam. J. Geophys. Res., vol. 75, Jan. 1970, pp. 696–698.

3–28. NORDBERG, W.; CONAWAY, J.; AND THADDEUS, P.: Microwave Observations of Sea State From Aircraft. Quart. J. Roy. Meteorol. Soc., vol. 95, Apr. 1969, pp. 408–413.

3–29. HOLLINGER, JAMES P.: Passive Microwave Measurements of the Sea Surface. J. Geophys. Res., vol. 75, no. 27, Sept. 1970, pp. 5209–5213.

3–30. ROSS, DUNCAN B.; CARDONE, VINCENT J.; AND CONAWAY, JACK W., JR.: Laser and Microwave Observations of Sea Surface Conditions for Fetch-Limited 17- to 25-M/S Winds. IEEE Trans. Geosci. Electronics, vol. GE–8, no. 4, Oct. 1970, pp. 326–336.

3–31. NORDBERG, W.; CONAWAY, J.; ROSS, D. B.; AND WILHEIT, T. T.: Measurements of Microwave Emission From a Foam Covered, Wind Driven Sea. J. Atmos. Sci., vol. 28, Apr. 1971, p. 429.

3–32. HOLLINGER, JAMES P.: Passive Microwave Measurements of Sea Surface Roughness. IEEE Trans. Geosci. Electronics, vol. GE–9, no. 3, July 1971, pp. 165–169.

3–33. STOGRYN, A.: Equations for Calculating the Dielectric Constant of Saline Water. IEEE Trans. Microwave Theory Tech., vol. MTT–19, no. 8, Aug. 1971, pp. 733–736.

3–34. BARRICK, D. E.: Wind Dependence of Quasi-Specular Microwave Sea Scatter. IEEE Trans. Antennas Propagat., vol. AP–22, 1974, pp. 135–136.

3–35. KRISHEN, K.: Detection of Oil Spills Using 13.3 GHz Radar Scatterometer. J. Geophys. Res., vol. 78, no. 12, Apr. 1973, pp. 1952–1963.

3–36. WRIGHT, JOHN W., AND KELLER, W. C.: Doppler Spectra in Microwave Scattering From Wind Waves. Phys. Fluids, vol. 14, no. 3, Mar. 1971, pp. 466–474.

3–37. SHEMDIN, O. H.; LAI, R. J.; REECE, A.; AND TOBER, G.: Laboratory Investigation of Whitecaps, Spray and Capillary Waves. Tech. Rep. 11, Coastal and Oceanographic Engineering Laboratory, Florida Univ., Dec. 1972.

3–38. WRIGHT, J. W.; KELLER, W. C.; AND DUNCAN, J. R.: Fetch and Windspeed Dependence of Doppler Spectra. Radio Sci., vol. 9, Oct. 1974, pp. 809–819.

3–39. STILWELL, DENZIL, JR.: Directional Energy Spectra of the Sea From Photographs. J. Geophys. Res., vol. 74, no. 8, Apr. 1969, pp. 1974–1986.

3–40. SVERDRUP, HENRY U., AND MUNK, W. H.: Wind, Sea and Swell: Theory of Relations for Forecasting. Pub. No. 601, U.S. Navy Hydrographic Office, 1947.

3–41. APEL, J. R.; PRONI, J. R.; AND CHARNELL, R. F.: Observations of Oceanic Internal and Surface Waves Using Remote Sensing Techniques. J. Geophys. Res., Feb. 1975. (To be published.)

3–42. DOLAN, R.: Coastal Land Forms: Crescentic and Rhythmic. Geol. Soc. Amer. Bull., vol. 82, Jan. 1971, pp. 177–180.

3–43. GREENWOOD, J. ARTHUR, ET AL.: Oceanographic Applications of Radar Altimetry From a Spacecraft. Remote Sensing Environ., vol. 1, no. 1, Mar. 1969, pp. 71–80.

3–44. VINCENT, S., AND MARSH, J. G.: Global De-

tailed Gravimetric Geoid. NASA TM X–70492, 1973.

3–45. VONBUN, F. O.: Spacecraft Missions and Experiments Important to Geodynamics. The XVII Plenary Meetings, COSPAR (São Paulo, Brazil), 1974.

3–46. KOLKER, M., AND WEISS, E.: Space Geodesy Altimetry Study. NASA CR–1298, 1969.

3–47. VON ARX, W. S.: Absolute Dynamic Topography. Limnol. Oceanogr. Suppl., vol. 10, 1965, pp. R265–R273.

3–48. VON ARX, W. S.: An Oceanographic Satellite. Proceedings of the Joint Oceanographic Assembly (Tokyo), 1971, p. 112.

3–49. ROME, H. J., AND CRUMP, E.: Near Real-Time Estimation of Vertical Deflections at Sea. IEEE International Conference on Engineering in the Ocean Environment, 1973, pp. 549–559.

3–50. MCGOOGAN, J. T.; LEITAO, C. D.; WELLS, W. T.; MILLER, L. S.; AND BROWN G. S.: Skylab Altimeter Applications and Scientific Results. AIAA Conference on Scientific Experiments of Skylab (Huntsville, Ala.), Oct. 30 to Nov. 1, 1974.

3–51. MILLER, L. S., AND BROWN, G. S.: Engineering Studies Related to the Skylab Program. NASA CR–137462, 1974.

3–52. CREPON, M.: Influence de la pression atmospherique sur le niveau moyen de la Mediterranée Occidentale et sur le flux à travers le détroit de Gibraltar. Ashiers Oceanographiques, 15, 1964.

3–53. KAULA, W. M., ed.: The Terrestrial Environment: Solid Earth and Ocean Physics. NASA CR–1579, 1970.

3–54. THIERET, D.: Geole—Système d'Aide à la Géodesie. Centre National d'Etudes Spatiales, PR/AM/DA 72–T–62, 1972.

3–55. HENDERSHOTT, M. C.: The Effects of Solid Earth Deformation on Global Ocean Tides. Geophys. J. Roy. Astron. Soc., vol. 29, 1972, pp. 389–402.

3–56. PEKERIS, C. L., AND ACCAD, Y.: Solution of Laplace's Equations for the M_2 Tide in World Oceans. Phil. Trans. Roy. Soc. London, Ser. A265, 1969, pp. 413–436.

3–57. MUNK, WALTER H., AND CARTWRIGHT, D. E.: Tidal Spectroscopy and Prediction. Phil. Trans. Roy. Soc. London, Ser. A259, 1966, pp. 533–581.

3–58. ZETLER, BERNARD D., AND MAUL, GEORGE A.: Precision Requirements for a Spacecraft Tide Program. J. Geophys. Res., vol. 76, no. 27, 1971, pp. 6601–6605.

3–59. CARTWRIGHT, D. E.: Tides and Waves in the Vicinity of St. Helena. Phil. Trans. Roy. Soc. London, Ser. A270, 1971, pp. 603–649.

3–60. MUNK, WALTER H., AND ZETLER, BERNARD D.: Deep-Sea Tides: A Program. Science, vol. 158, no. 3803, 1967, pp. 884–886.

3–61. FOMIN, LUCK M.: The Dynamic Method in Oceanography, Elsevier Pub. Co., 1964.

3–62. NEUMANN, GERHARD: Ocean Currents. Elsevier Pub. Co., 1968.

3–63. KRISHEN, K.: Correlation of Radar Backscattering Cross Sections With Ocean Wave Height and Wind Velocity. Geophys. Res., vol. 76, Sept. 1971, pp. 6528–6539. (See also Krishen, K.: Mathematical Model for the Relationship of Radar Backscattering Cross Sections With Ocean Scene and Wind Velocity. Proceedings of the Seventh International Symposium on Remote Sensing of Environment, vol. III, Univ. of Michigan, May 1971, pp. 1861–1877.)

3–64. DALEY, J. C.: Wind Dependence of Radar Sea Return—Composite Surface Model. J. Geophys. Res., vol. 78, no. 33, Nov. 1973, p. 7823.

3–65. VALENZUELA, G. R.; LAING, M. B.; AND DALEY, J. C.: Ocean Spectra for High Frequency Waves From Airborne Radar Measurements. J. Mar. Res., vol. 29, no. 2, 1971, p. 69.

3–66. HUANG, NORDEN E.; CHEN, DAVIDSON T.; TUNG, CHI CHAO; AND SMITH, JAMES R.: Interaction Between Steady Non-Uniform Currents and Gravity Waves, With Applications for Current Measurements. J. Phys. Oceanogr., vol. 2, Oct. 1972, pp. 420–431.

3–67. PIERSON, WILLARD J., JR., AND MOSKOWITZ, LIONEL: A Proposed Spectral Form for Fully Developed Wind Seas Based on the Similarity Theory of S. A. Kitaigorodskii. J. Geophys. Res., vol. 69, no. 24, Dec. 1964, p. 5181.

3–68. CORNISH, VAUGHN: Ocean Waves and Kindred Geophysical Phenomena. Cambridge Univ. Press, 1934.

3–69. NEUMANN, G.: On Ocean Wave Spectra and a New Method of Forecasting Wind Generated Seas. Tech. Memo. 43, U.S. Army Coastal Engineering Research Center (Fort Belvoir, Va.), 1953.

3–70. PIERSON, WILLARD J., JR.; NEWMANN, GERHARD; AND JAMES, RICHARD W.: Practical Methods for Observing and Forecasting Ocean Waves by Means of Wave Spectra and Statistics. Pub. No. 603, U.S. Navy Hydrographic Office, 1955.

3–71. PHILLIPS, OWEN M.: The Dynamics of the Upper Ocean. Cambridge Univ. Press, 1966.

3–72. Environmental Conditions Within Specified Geographical Regions, Final Report. U.S. Department of Commerce, The National Data Buoy Center, National Ocean Survey,

NOAA Mississippi Test Facility, Apr. 1973.

3–73. HOGBEN, NEIL, AND LUMB, F. E.: Ocean Wave Statistics. National Phys. Lab., London, H.M.S.O., 1967.

3–74. GLOERSEN, P.; NORDBERG, W.; SCHMUGGE, T. J.; AND WILHEIT, T. T.: Microwave Signatures of First-Year and Multi-Year Sea Ice. J. Geophys. Res., vol. 78, no. 18, June 1973, pp. 3564–3572.

3–75. CAMPBELL, W. J.; GLOERSEN, P.; NORDBERG, W.; AND WILHEIT, T. T.: Dynamics and Morphology of Beaufort Sea Ice Determined From Satellites, Aircraft and Drifting Stations. NASA TM X–66291, 1973.

3–76. ANDERSON, V. H.: High Altitude, Side-Looking Radar Images of Sea Ice in the Arctic. Proceedings of the Fourth Symposium on Remote Sensing of Environment, Univ. of Michigan, Apr. 1966, pp. 845–857.

3–77. ROUSE, JOHN W., JR.: Arctic Ice Type Identification by Radar. Proc. IEEE, vol. 57, no. 4, Apr. 1969, pp. 605–611.

3–78. PARASHAR, S. K.; BRIGGS, A. W.; FUNG, A. K.; AND MOORE, R. K.: Investigation of Radar Discrimination of Sea Ice. Proceedings of the Ninth International Symposium on Remote Sensing of Environment, vol. I, Univ. of Michigan, Apr. 1974, pp. 323–332.

3–79. GLUSHKOV, V. M., AND KOMAROV, V. B.: Side-Looking Radar System TOROS and Its Application to the Study of Ice Conditions and Geological Explorations. Proceedings of the Seventh International Symposium on Remote Sensing of Environment, vol. I, Univ. of Michigan, May 1971, p. 317.

3–80. GLOERSEN, P.; WILHEIT, T. T.; CHANG, T. C.; NORDBERG, W.; AND CAMPBELL, W. J.: Microwave Maps of the Polar Ice of the Earth—From Nimbus 5 Satellite. NASA TM X–70493, 1973.

3–81. MCGOOGAN, J. T.: Precision Satellite Altimetry. IEEE International Convention and Exposition, Mar. 1974, pp. 34–31 to 34–37.

3–82. MCGOOGAN, J. T.; MILLER, L. S.; BROWN, G. S.; AND HAYNE, G. S.: The S–193 Radar Altimeter Experiment—Onboard Skylab for Earth Surface Profile Measurement. Proc. IEEE, vol. 62, June 1974, pp. 793–803.

3–83. VONBUN, F. O.: Geodetic Satellite Mission and GEOS–C Spacecraft. Space Research XI, COSPAR, vol. 1, Akademie-Verlag (Berlin), May 1971, pp. 457–467.

3–84. MACDONALD, F. C.: The Correlation of Radar Sea Clutter on Vertical and Horizontal Polarization With Wave Height and Slope. IRE Nat. Conv. Rec., pt. 1, Mar. 1956, pp. 29–32.

3–85. GRANT, C. R., AND YAPLEE, B. S.: Backscattering From Water and Land at Centimeter and Millimeter Wavelengths. Proc. IRE, vol. 45, no. 7, July 1957, pp. 972–982.

3–86. DALEY, J. C.; BURKETT, J. A.; DUNCAN, J. R.; AND RANSONE, J. T., JR.: Sea Clutter Measurement on Four Frequencies. Rep. 6806, Naval Res. Lab., Washington, D.C., Nov. 29, 1968.

3–87. DALEY, J. C., ET AL.: Upwind-Downwind-Crosswind Sea Clutter Measurement. Rep. 6881, Naval Res. Lab., Washington, D.C., Apr. 1969.

3–88. DALEY, J. C.; RANSONE, J. T., JR.; AND BURKETT, J. A.: Radar Sea Return—Joss 1. Rep. 7268, Naval Res. Lab., Washington, D.C., May 1971.

3–89. DALEY, J. C., ET AL.: Radar Sea Return—Joss 2, Final Report. Rep. 7534, Naval Res. Lab., Washington, D.C., Feb. 1962.

3–90. MOORE, R. K.: Radar Scatterometry—An Active Remote Sensing Tool. Proceedings of the Fourth Symposium on Remote Sensing of Environment, Univ. of Michigan, Apr. 1966, pp. 339–373.

3–91. MOORE, RICHARD K., AND PIERSON, W. J., JR.: Worldwide Oceanic Wind and Wave Predictions Using a Satellite Radar-Radiometer. J. Hydron., vol. 5, no. 2, Apr. 1971, pp. 52–60.

3–92. NEWTON, RICHARD W., AND ROUSE, JOHN W., JR.: Experimental Measurements of 2.25-cm Backscatter From Sea Surfaces. IEEE Trans. Geosci. Electronics, vol. GE–10, no. 1, Jan. 1972, pp. 2–7.

3–93. KERR, F. J., AND SHAIN, C. A.: Moon Echoes and Transmission Through the Ionosphere. Proc. IRE, vol. 39, no. 3, Mar. 1951, pp. 230–242.

3–94. WRIGHT, JOHN W.: Backscattering From Capillary Waves With Application to Sea Clutter. IEEE Trans. Antennas Propagat., vol. AP–14, no. 6, Nov. 1966, pp. 749–754.

3–95. KRISHEN, K.; VLAHOS, N.; BRANDT, O.; AND GRAYBEAL, G.: Results of Scatterometer Systems Analysis for NASA/MSC Earth Observation Sensor Evaluation Program. Proceedings of the Seventh International Symposium on Remote Sensing of Environment, vol. II, Univ. of Michigan, May 1971, pp. 1451–1473.

3–96. SWIFT, C. T., AND JONES, W. L., JR.: Satellite Radar Scatterometry. IEEE International Convention and Exposition, Mar. 1974, pp. 34–41 to 34–46.

3–97. Historical Logbook, S–193 Microwave Radiometer/Scatterometer/Altimeter. No.

72SD234, rev. A, vols. 1 to 10, General Electric Corp., Oct. 1972.

3–98. KRISHEN, K.: Contribution to Ocean Panel Including Reports on Some Sea Return Experiments, Ocean Surface Windspeed Sensing and Scatterometers. Tech. Rep. LEC–3896, Lockheed Electronics Co., Inc., July 1974.

3–99. MOORE, R. K., ET AL.: Simultaneous Active and Passive Microwave Response of the Earth—the Skylab RADSCAT Experiment. Proceedings of the Ninth International Symposium on Remote Sensing of Environment, vol. I, Univ. of Michigan, Apr. 1974, pp. 189–217.

3–100. YAPLEE, B. S.; SHAPIRO, A.; HAMMOND, D. L.; AND ULIANA, E. A.: Ocean Wave Height Measurements With a Nanosecond Radar. Proceedings of the Seventh International Symposium on Remote Sensing of Environment, vol. III, Univ. of Michigan, May 1971, pp. 1879–1893.

3–101. APEL, J. R., ed.: Sea Surface Topography From Space. NASA CR–130293, 1973.

3–102. WEISSMAN, D. E.: Two Frequency Radar Interferometry Applied to the Measurement of Ocean Wave Height. IEEE Trans. Antennas Propagat., vol. AP–21, Sept. 1973, pp. 649–656.

3–103. SWIFT, C. T.: Microwave Radiometer Measurements of the Cape Cod Canal. Radio Sci., vol. 9, July 1974, pp. 641–653.

3–104. STOGRYN, A.: The Emissivity of Sea Foam at Microwave Frequencies. J. Geophys. Res., vol. 77, Mar. 1972, pp. 1658–1666.

3–105. HOLLINGER, JAMES P.: Remote Passive Microwave Sensing of the Ocean Surface. Proceedings of the Seventh International Symposium on Remote Sensing of Environment, vol. III, Univ. of Michigan, May 1971, pp. 1807–1817.

3–106. CARDONE, V. J.: Specification of the Wind Field Distribution in the Marine Boundary Layer for Wave Forecasting. Rep. TR 69–1, Geophys. Science Lab., New York Univ., Dec. 1969.

3–107. ROSS, DUNCAN B., AND CARDONE, VINCENT: Observations of Oceanic Whitecaps and Their Relation to Remote Measurements of Surface Wind Speed. J. Geophys. Res., vol. 79, no. 3, Jan. 20, 1974, pp. 444–452.

3–108. Reference Data for Radio Engineers. Fourth ed. International Telephone & Telegraph Corp., Stratford Press, Inc., 1961.

3–109. MOORE, RICHARD K.; WAITE, WILLIAM P.; AND ROUSE, JOHN W., JR.: Panchromatic and Polypanchromatic Radar. Proc. IEEE, vol. 57, no. 4, Apr. 1969, pp. 590–593.

3–110. VALENZUELA, G. R., AND LAING, M. B.: Study of Doppler Spectra of Radar Sea Echo. J. Geophys. Res., vol. 75, no. 3, Jan. 1970, p. 551.

3–111. LAING, M. B.: The Upwind/Downwind Dependence of the Doppler Spectra of Radar Sea Echo. IEEE Trans. Antennas Propagat., vol. AP–19, no. 5, Sept. 1971, pp. 712–714.

3–112. KATZ, I.: Utilization of a Radar Altimeter for Determination of Ocean Roughness. IEEE EASCON Conv. Rec., Oct. 1970, pp. 266–269.

3–113. BORN, MAX, AND WOLF, EMIL: Principles of Optics. Third ed. Pergamon Press, 1965.

APPENDIX 3A

ORBITAL ERRORS

Ever since orbits have been computed—of celestial bodies during the last several centuries or of artificial satellites during recent times—orbital errors in position and velocity have attracted the attention of analysts. Orbital errors were a major consideration when rockets and artificial satellites were first launched. As space missions increased and became more sophisticated, requirements for the reduction of orbital errors became increasingly important.

Presently, orbital accuracies in the meter, decimeter, and even centimeter region in position and in millimeters per second or less in velocity are needed for Earth and ocean dynamic satellite missions [1] (ref. 3A–1).

Such missions as Skylab, GEOS–C, and particularly SEASAT–A required orbital ac-

[1] NASA: Earth and Ocean Physics Applications Program. Vol. I—Executive Summary, Vol. II—Rationale and Program Plan, Sept. 1972 (NASA internal document, restricted distribution).

curacies commensurate with requirements to determine the gross features of the sea surface topography (ref. 3A–2).

Figures 3–45 and 3–46 depict the orbital height differences (quasi-errors) of the Skylab missions. Figure 3–45 shows a 25-m height variation and figure 3–46 shows a 40-m height variation, which can be seen from the difference of the "measured" sea surface and the "computed" sea surface, assuming that the bias error in the radar altimeter is small compared with these values mentioned. Experience indicates that crosstrack errors and along-track errors may be three to eight times as large, respectively (ref. 3A–3). The GEOS–C has an altimeter that can measure spacecraft height above the oceans within 0.5 to 1.0 m. Experience with Skylab certainly justifies the belief that these rather small values are attainable [2] (refs. 3A–4 and 3A–5). This knowledge, in turn, dictates that orbital height errors must be known to the same order of accuracy. Only the orbital radial component (height) is of importance for ocean altimetry.

PRESENT STATE OF THE ART

A realistic estimate of the errors must include all errors associated with the basic measurements (tracking systems), electromagnetic propagation (troposphere and ionosphere), tracking station location, timing, basic physical constraints, and, in particular, the gravity field of the Earth. In addition, the errors have to be separated into random errors, which are subject to statistics, and bias errors, which stay more or less constant during the measurement processes. The bias errors are more harmful because they do not decrease inversely as the square root of the number of samples. An increase in the number of measurements does not decrease the total error of the spacecraft position and velocity.

UNDERSTANDING THE PROBLEM

A brief outline will be given on the general subject of orbital uncertainty estimates, which will be interpreted as orbital errors. Both theoretical error analyses and orbital uncertainty estimates are discussed in some detail.

Orbital Uncertainty Estimates

Orbital uncertainty estimates (refs. 3A–3 and 3A–6) are based on practical orbital determination and include all errors (known and unknown) that appear when an orbit is calculated. The principle is rather simple and is depicted in figure 3A–1. Orbits, which are calculated for 2-day time intervals, overlap by 1 day. The maximum and minimum position differences in the overlap region are recorded as a measure of the uncertainty associated with the orbit. These arcs have different data sets, different tracking stations, and, as mentioned, describe reality.

Orbital Errors Using Error Theory

In many cases, particularly during project planning phases, error analyses have to be performed on a theoretical basis only, because the tracking system to be used is not yet built and/or the spacecraft is not designed. These techniques have been used for basic designs of range and range-rate systems, the Apollo Tracking Network, and plans for a new orbiting tracking system, which is presently under investigation (refs. 3A–7 to 3A–11).

Figures 3A–2, 3A–3, and 3A–4 show some examples of the orbital uncertainty estimates

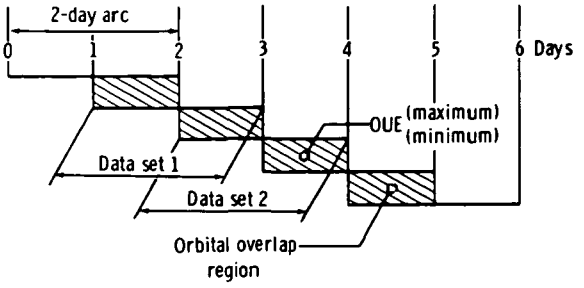

FIGURE 3A–1.—Schematic illustrating principle of orbital uncertainty estimates. Orbits are "connected" at that time within the overlap region where the position differences are at a minimum (case of 100-percent overlap).

[2] Personal communication, McGoogan, 1974.

that have been obtained for the Orbiting Geophysical Observatory IV (OGO–IV) and GEOS–I and GEOS–II. Thus, the OGO–IV spacecraft orbital uncertainty estimates during the 30-day period depicted in figure 3A–2 cover the band between 50 and 700 m; that is, the average position error should be approximately 300 m. Similarly, from figure 3A–3, if one determines a GEOS–1 orbit with the Goddard minitrack system only, the orbital uncertainty estimates cover a band from 30 to 210 m during the 15-day timespan. If good optical data are used, orbital uncertainty estimates vary between only 0 and 30 m. However, these values are still, to a certain extent, relative rather than absolute values.

An error analysis (refs. 3A–7 to 3A–11) for the 30-day OGO–IV orbit has been performed, and the result is superimposed on the orbital uncertainty estimates shown in figure 3A–2. The orbit uncertainties, based on the

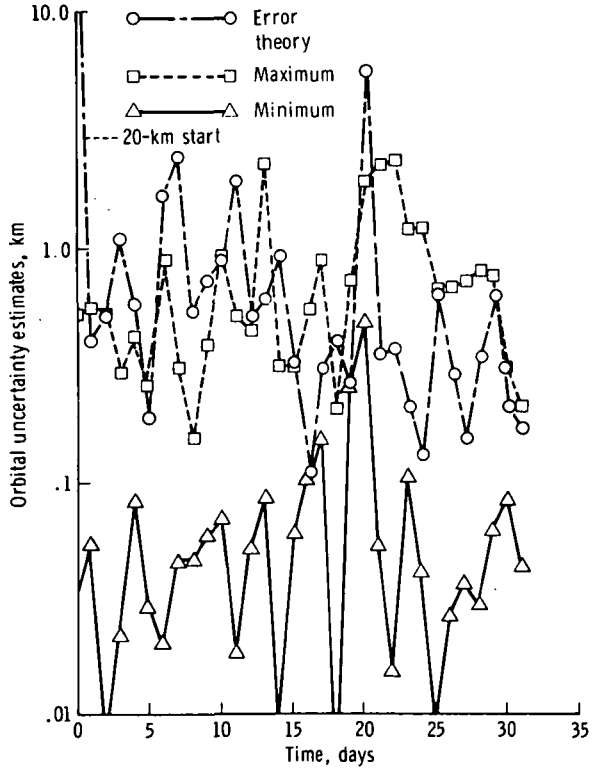

FIGURE 3A–2.—Orbital uncertainty estimates for OGO–IV.

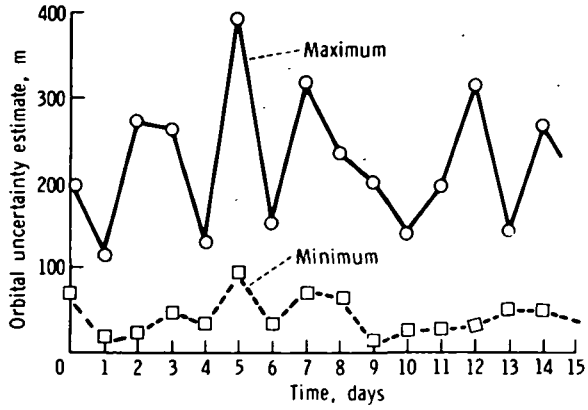

FIGURE 3A–3.—Orbital uncertainty estimates for GEOS–I.

error theory applied, fall within the upper regions of the error as determined by the overlap method. This agreement is considered good because a 50-percent "error-of-the-error" determination is an acceptable first theoretical estimate.

As previously mentioned, it is very difficult to make accurate theoretical predictions of expected orbital errors. Tracking system error parameters (refs. 3A–11 to 3A–15) have to be determined and chosen from previous orbital analyses. The information presented in figure 3A–2 shows that these theoretical errors are on the high side because rather large system bias error values are used in the error theory, and biases contribute most to the orbital errors. Noise contributions reduce statistically with an increase in the number of measurements used, whereas bias contributions, by their nature, stay constant (refs. 3A–7 to 3A–9) regardless of the number of measurements taken and actually used.

During the past few years, considerable progress has been made in reducing orbital errors because of improvements in determining (1) the Earth gravity field model (the major contributor to orbital errors); (2) the mathematical orbital systems models; and (3) the errors in the tracking system, although this has not been fully exploited at this time.

This paragraph gives some examples of orbital uncertainty estimates for GEOS–II us-

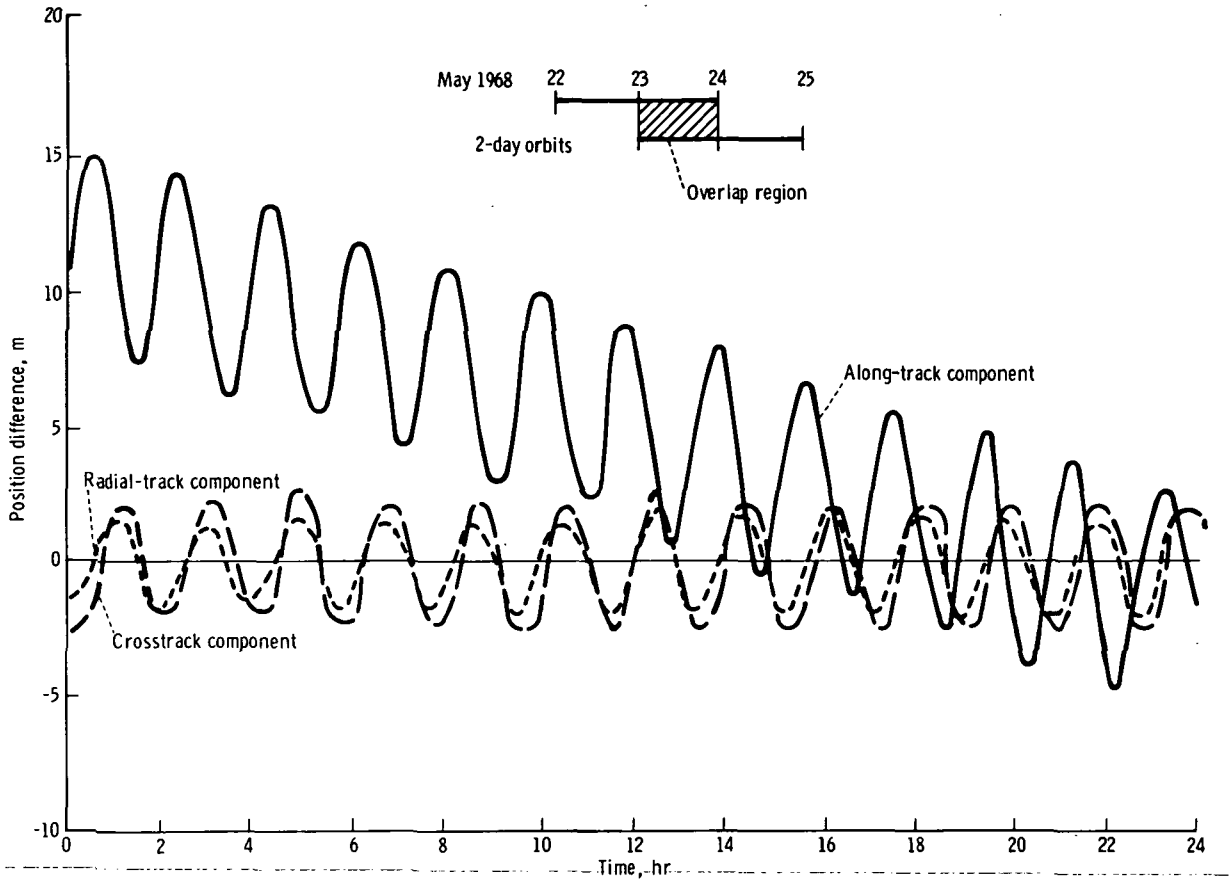

FIGURE 3A–4.—Satellite overlap position differences for GEOS–II (GEM–6 model, Naval Weapons Laboratory Doppler).

ing Naval Weapons Laboratory Doppler and optical data. The examples concern three different gravity fields: namely, the Goddard Earth models (GEM–1 and GEM–6) and the Smithsonian Astrophysical Institution (SAO). Figure 3A–4 shows the orbital uncertainty estimates for a 1-day overlap in the along-track, crosstrack, and radial-track components of the orbit. It is interesting to note that the GEM–6 errors in altitude are smaller than the GEM–1 errors (2-day computation shown in fig. 3A–5). However, if one intends to project the orbit 10 days into the future, the GEM–6 model performs this task very well (fig. 3A–5). Assuming that the GEM–6 model is better than the GEM–1 model, one should expect a good performance because, during the projection period, the satellite orbit depends solely on the gravity field. Finally, figure 3A–4 shows the behavior of the orbital uncertainty estimates over a 24-hr period of overlap. Only the along-track component has much deviation. Radial-track and crosstrack components linearly cancel out, as they should from orbital energy consideration. The sinusoidal-like variations do have orbital periodicity, as theoretically expected (ref. 3A–9).

IMPACT OF MICROWAVE TECHNOLOGY

The only metric measurements taken from orbit that are closely related and/or dependent on accurate orbital information are radar altimeter data. All other oceanographic measurements, such as wave height, wave direc-

Gravity field	June 1 to 3, 1968			June 10 to 13, 1968		
	Radial track, m	Cross-track, m	Along track, m	Radial track, m	Cross-track, m	Along track, m
GEM-1	13.0	26.6	289	6.6	30.6	922
GEM-6	8.6	25.3	91	11.8	33.2	555
SAO-2	9.3	51	366	26.2	78	948

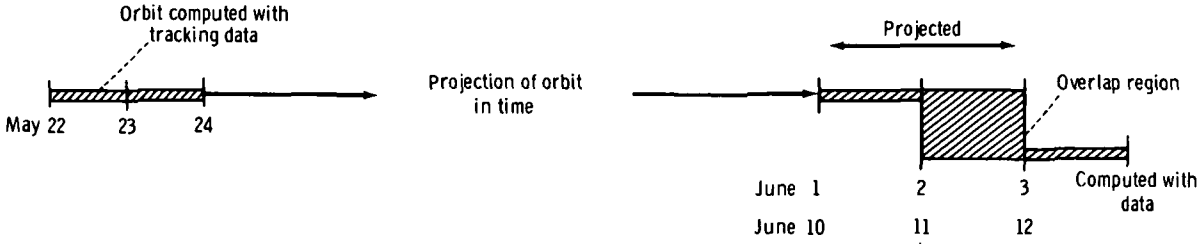

FIGURE 3A–5.—Satellite overlap projected position differences in meters for GEOS–II.

tion, and microwave images, are not so dependent on accurate position and thus on orbit determination. Spaceborne altimeter systems such as those flown (or to be flown) on Skylab, GEOS–C, and SEASAT have a substantial effect on the orbital error determination. Instead of having only a few minutes of tracking data, one can obtain such data almost continuously along the orbit (except over land areas).

The effect in this case is twofold. First, the orbital errors will be reduced (more tracking and an improved gravity field); second, the sea surface topography can actually be measured for the first time (ref. 3A–2). The Skylab results are tremendously encouraging in this respect. Much sea surface topography information[3] has already been extracted from Skylab data, and the analysis is just beginning. Relating this fact to the increased coverage that GEOS–C will have as compared to Skylab, gravity field and sea surface topography improvements will be substantial.

Thus, sea-surface topography errors that are, at present, approximately 2 to 15 m or more will be reduced. The estimates are that GEOS–C will reduce these geoidal error values on a global scale from 0.5 to 2 m in 2 to 3 yr, facilitating the way for the SEASAT–A mission with the ultimate goal of determining the sea surface topography to within 0.1 to 0.2 m (ref. 3A–1).[4]

REQUIREMENTS

Orbital height errors have to be reduced considerably if the EOPAP requirements for the sea-surface topography are to be satisfied. As shown in figures 3–45, 3–46, 3A–1, 3A–4,

[3] Personal communication, McGoogan, 1974.

[4] Also, see Earth and Oceans Physics Applications Program. Vol. I—Executive Summary, Vol. II—Rationale and Program Plan, Sept. 1972 (NASA internal document, restricted distribution).

and 3A–5, orbital errors are still in the meter range. However, when proper boundary conditions are imposed on the oceans,[5] the errors in determining the sea-surface topography may be smaller, by a factor of 3 to 5, than those of the orbital height under certain restraining conditions. For example, a nodal distance of 19° (half wavelength of error) and a 1-m orbital height error would contribute only 0.10 to 0.15 m to the geoid error. Any orbital altitude bias error would transform directly into an equivalent geoid error. For instance, a constant height error results from an error in the Earth gravitational parameter. Thus, another requirement for accurate altimetry is the better determination of this parameter.

REFERENCES

3A–1. The Terrestrial Environment: Solid-Earth and Ocean Physics. NASA CR–1579, 1970.

3A–2. VONBUN, F. O.: A Simulation of Synthetic Aperture Radar Imaging of Ocean Waves. Paper presented at 1974 Annual URSI Meeting (Boulder, Colo.), Oct. 1974.

3A–3. VONBUN, F. O.: Satellite Trajectory Determination and Their Expected Errors, OGO IV, GEOS–1. Dynamics of Satellites, Springer-Verlag (Berlin), 1970, pp. 89–97.

3A–4. VONBUN, F. O.: Sea Surface Determination From Space—The Goddard Geoid. USNC/URSI–IEEE Meeting (Boulder, Colo.), Oct. 1971.

3A–5. VONBUN, F. O.: Spacecraft Missions and Experiments Important to Geodynamics. The XVII Plenary Meetings, COSPAR (São Paulo, Brazil), 1974.

3A–6. SIRY, J. W., AND STEWART, D. J.: Goddard Orbit Information. NASA TM X–63892, 1969.

3A–7. VONBUN, F. O., AND KAHN, W. D.: Tracking Systems, Mathematical Models and Errors, Part I—Theory. NASA TN D–1471, 1962.

3A–8. KAHN, W. D., AND VONBUN, F. O.: Tracking Systems, Mathematical Models and Errors, Part II—Least Squares Treatment. NASA TN D–3776, 1966.

3A–9. BONAVITO, N. L.: An Analysis of Satellite Positional Uncertainty by Statistical Mechanics. NASA TN D–5259, 1969.

3A–10. VONBUN, F. O., AND MENGEL, J. T.: Tracking and Communications for Planetary Manned Missions. J. Spacecr. Rockets, vol. 5, no. 5, July 1968, pp. 863–865.

3A–11. COOLEY, J. L., AND MARLOW, A.: Orbital Error Studies—Tracking From a Synchronous Spacecraft. NASA TM X–551–69–7, 1969.

3A–12. SCHROEDER, CLARENCE A.: Electronic Interferometer Tracking. IEEE Transactions on the Fifth National Symposium on Space Electronics and Telemetry (Washington, D.C.), Sept. 19–21, 1960, pp. 1–9.

3A–13. KRUGER, B.: The Range Rate Error Due to the Averaging Techniques of Doppler Measurements. NASA TM X–55203, 1965.

3A–14. KRUGER, B.: Effects of Correlated Noise With Applications to Apollo Tracking Problems. NASA TN D–4121, 1968.

3A–15. MARSH, J. G., ET AL.: Intercomparison of the Minitrack and Optical Tracking Networks Using GEOS–I Long Arc Orbital Solutions, Part I. NASA TM X–63161, 1967.

[5] Personal communication, Mathews, 1974.

APPENDIX 3B

NATIONAL PRIORITY AREAS FOR COASTAL ZONES

The VIMS study is summarized in the following information. Remote sensing of temperature and salinity are two high-priority items, whereas sea state is a low-priority item.

The priorities for environmental data are as follows:

1. Water pollution and ecosystem balance
   a. Water pollution:
      (1) Toxic wastes, biocides, and heavy metals 9
      (2) Sewage, nutrients, and oxygen-demanding wastes .. 9
      (3) Radioactivity 9

(4) Oil 9
(5) Suspended sediment 8
(6) Thermal effluent 9
b. Estuarine and coastal ecosystems:
(1) Producers:
(a) Wetlands; etc. 9
(b) Phytoplankton 9
(c) Coastal vegetation 9
(2) Hydrography
(a) Dissolved oxygen 9
(b) Salinity 9
(c) Temperature 9
(d) Currents and circulation 9
(3) Chemical cycles 8
(4) Mathematical models 9
2. Natural resources:
a. Food
(1) Fish 8
(2) Shellfish 7
b. Water supply 5
c. Minerals 3
3. Extreme events: prediction, survey, and assessment of coastal storms, earthquakes, and tsunamis:
a. Sea state 4
b. Surge, tides, and sea level 4
c. Littoral response, shoals, and shorelines 4
4. Other aids to shipping and navigation:
a. Ice cover 2
b. Shoals, shorelines, seastate, and currents 2

The following list enumerates the remote measurables defined by VIMS. Nos. 13, 15, and 16 were not included in the matrix.

1. Ice
2. Sea level (altimetry)
3. Sea state
4. Tides
5. Salinity
6. Water color
7. Water-surface temperature
8. Oilslicks
9. Bathymetry
10. Shorelines
11. Shore topography
12. Coastland vegetation and land use
13. Benthic vegetation
14. Fish schools
15. Coastal mammals
16. Bioluminescence

The areas in which active microwave systems may be applicable are indicated in table 3B–I.

The following items are recommended by VIMS for a coastal zone oceanography program.

1. Remote sensing of salinity (top priority).
2. Development of common satellite for oceanography and meteorology.
3. Development of computer-simulation models of major estuaries.
4. Accurate mapping of coastal wetlands.
5. Development of remote sensing as the primary method for detecting suspended sediments.
6. Provision for data acquisition of selected areas by command.

The approach taken by ODU to establish priorities was to circulate a questionnaire to universities, industries, institutions, and State and local governments. The results again show that more disciplines require tem-

TABLE 3B–I.—*Order of Priority of Remote Measurables Defined by VIMS* [a]

Remote measurable	Percent score	Percent score with weighting factor removed
Water-surface temperature	19.0	17.7
Water color	15.0	13.6
Salinity	14.4	13.2
Coastland vegetation and land use [b]	12.7	11.8
Oil [b]	8.3	7.7
Bathymetry	7.1	7.7
Tides [b]	5.5	6.4
Shorelines [b]	4.8	5.0
Shore topography [b]	3.7	4.1
Sea state [b]	2.8	4.1
Sea level and altimetry [b]	2.6	3.2
Ice	2.3	3.6
Fish schools	1.9	1.8

[a] Current and circulation data can be derived by means of several of the remote measurables.
[b] Denotes active microwave sensing potential.

perature/salinity measurements than sea-state measurements. The following priorities in coastal zones have been established by ODU as a result of the questionnaires.

1. Biological oceanography:
   a. Pollution
   b. Fisheries
   c. Coastal geography and cartography
   d. Hazards to shipping and coastline
2. Marine geology
   a. Baseline studies: physical, chemical, biological, and geological environment
   b. Pollution
   c. Shoreline processes
   d. Oil and mineral resources not urgent
3. Chemical oceanography:
   a. Pollution
   b. Studies related to establishing fertility of coastal waters
4. Physical oceanography/meteorology:
   a. Water-mixing dynamics
   b. Baseline data for understanding physical regime
   c. More data on spatial and temporal distribution of parameters for mathematical models

The following information needs in coastal zones have been defined by ODU.

1. Pollution:
   a. Pathways of pollution in biological systems and tolerance
   b. Importance of estuaries in general ecology and influence of pollution
   c. Good hydrological information
   d. Adequate instrumentation
2. Fisheries:
   a. Physical oceanographic studies
   b. Systematic study of specimens
   c. Population dynamics
   d. Effects of environmental alteration
3. Geological processes:
   a. Suspended sediment circulation and transport in deep and shallow water
   b. Bathymetry data
   c. Wave energy
4. Chemistry:
   a. More emphasis on transport and long-term deposition of pollutants
   b. Analytical methods for specific organic pollutants in all waters
   c. Upgrade gathering, monitoring, treatment of basic data
   d. Physical and chemical properties of particles in water
   e. Mathematical description of natural water systems
5. Physical oceanography/meteorology:
   a. Physical data of water system
   b. Effluent characteristics
   c. Nutrient distribution
   d. Incoming radiation and effective back radiation
   e. Evaporation and precipitation
   f. Improved predictions with math models

The number of disciplines requiring remote measurables defined by ODU are listed in table 3B–II.

The following information is a description of ODU recommendations for the coastal zone oceanography program.

1. Data for improving knowledge of coastal water-mixing processes.

2. Need for large engineering data base of reliable data:
   a. Surface waves
   b. Wastes and pollution
   c. Sea/shore interactions
   d. Seabed conditions

TABLE 3B–II.—*Number of Disciplines Requiring Remote Measurables Defined by ODU*

Remote measurable	Number of disciplines
Water mixing	4
Surface temperature	4
Salinity	4
Suspended sediments	4
Sea level	3
Nutrients	3
Sea state	2
Bathymetry	2
Vegetation and soils	2
Oil	2
Shorelines (cartography)	2
Radiation	1
Evaporation	1

3. Coordination of oceanographic and meteorological observations with ERTS programs: World Weather Watch, GARP, and Integrated Global Ocean Station System.

4. Establishment of communications between NASA and director of IDOE to discuss cooperative efforts.

5. Establishment of a coastal zone management system needed for coordinating disciplinary interests.

Item 2 seems to be a probable area for active microwave techniques.

The problems considered by ODSI are presented in table 3B–III, and a priority listing that reflects the ODSI, VIMS, and ODU studies is given in table 3B–IV. The areas in which active microwave techniques may be appropriate are indicated in table 3B–IV. Note that wave measurements are at the bottom of the list.

The desired measurables as a function of resolution requirements are shown in table 3B–V. One of the most notable aspects of the chart is that spatial resolutions as small as 10 m are required. For this reason, perhaps the microwave studies of coastal regions would be restricted to those done from aircraft.

TABLE 3B–III.—*National Priority Area Issues and Most Relevant Data Types for Each Area in the Coastal Zone Defined by ODSI*

Priority area	Issue	Relevant data types
Pollution	Locate sources of discharge	Petroleum
	Determine types of discharge	Bioassays
	Determine extent of pollution effects	Water temperature
	Determine assimilative capacity	Currents
	Determine optimal siting for industry	Salinity
	Effect enforcement	Water density
	Assist rapid cleanup	Permeability
		pH
		Tides
		Metals
		Plankton
		Color
		Bathymetry
		Particulates
		Porosity (bottom)
		Bottom O_2 uptake
		Bacteria
		Sediment pH
Fisheries	Locate new fishing areas	Fish
	Improve scouting operations	Plankton
	Improve catching operations	Currents
	Forecast abundance	Bathymetry
	Improve management	Water temperature
		Nutrients
		Mammals
		Freshwater inflow
		Bioassays
		Salinity
		Dissolved gases
		Dissolved organics
		Color
Hazards to shipping and coastlines.	Identify hazards to navigation	Winds
	Provide climatology	Water temperature
	Monitor ocean phenomena	Currents
	Assist rescue operations	Ice

TABLE 3B–III.—*National Priority Area Issues and Most Relevant Data Types for Each Area in the Coastal Zone Defined by ODSI—Concluded*

Priority area	Issue	Relevant data types
		Waves Air temperature Precipitation Clouds Barometric pressure Breakers and surf Tides Bathymetry Humidity Solar radiation Topography
Coastal geography and cartography.	Assess mineral resources Improve coastal surveys Identify land use Monitor shoreline processes	Bathymetry Sediments Topography Land use Soils and geology Currents Tides Vegetation Water temperature Sediment settling rate Radioactive tracer concentration Particulates Color Metals Petroleum

TABLE 3B–IV.—*A Comparison of Coastal Zone Data Requirements Established by ODSI, VIMS, and ODU*

ODSI, remote measurable	ODSI, percent score	VIMS, weighting factor	ODU, number of disciplines
Currents[a]	7.5	9	4
Bathymetry	7.2	9	2
Water temperature	7.0	9	4
Tides[a]	5.0	4	3
Petroleum[a]	0.8	9	2
Sediments	4.6	8	4
Winds[a]	4.5	4	2
Color	4.5		
Plankton	4.3	9	1
Salinity	4.3	9	4
Precipitation	4.0		
Vegetation[a]	3.9	9	2
Air temperature	3.9		
Fish	3.7	8	
Bioassays	3.7		
Nutrients	3.7	9	3
Topography[a]	3.7	4	2
Water density	3.5		1
Freshwater inflow	3.5	5	1
Particulates	3.5	9	1
Metals	3.1	9	1
Land use	3.1		2
Waves[a]	3.0	4	2

[a] May be appropriate for active microwave techniques.

TABLE 3B–V.—*Remote-Sensing Requirements for Water Pollution Monitoring*

Remote measurable	Type[a]	Spatial resolution, m	Spectral resolution	Spectral range	Temporal resolution	Solar elevation, deg	Low angle from nadir, deg	Area coverage, km
Temperature	A	10	±1 K	10 to 12 μm	2 hr	NA[b]	NA	20 by 20
	B	100	±1 K	or	7 days			150 by 150
	C	1000	±1 K	3 to 5 μm	7 days			300 by 300
Currents	A	10	0.01 m/sec	0.4 to 0.8 μm	2 hr	NA	NA	20 by 20
	B	100	0.05 m/sec		7 days			150 by 150
	C	1000	0.05 m/sec		7 days			300 by 300
Salinity	A	NA	NA	NA	2 hr	NA	NA	NA
	B	100	±0.5‰	MW[c]	6 hr			150 by 150
	C	1000	±0.5‰	MW[c]	7 days			300 by 300
Surface winds	A	10	±0.1 m/sec	0.4 to 0.8 μm	NA	30 to 60	−5 to 30	NA
	B	100	±0.5 m/sec	or MW[c]	6 hr			150 by 150
	C	1000	±0.5 m/sec		7 days			300 by 300
Oil	A	10	0.1 μm	0.3 to 0.8 μm	2 hr	30 to 60	−5 to 30	20 by 20
	B	100	0.1 μm	or MW[c]	6 hr			150 by 150
	C	1000	0.1 μm		7 days			300 by 300
Plankton	A	10	0.05 μm	0.4 to 0.8 μm	1 day	30 to 60	−5 to 30	20 by 20
	B	100	0.05 μm		7 days			150 by 150
	C	1000	0.05 μm		7 days			300 by 300
Sediments	A	10	0.05 μm	0.4 to 0.8 μm	1 day	30 to 60	−5 to 30	20 by 20
	B	100	0.05 μm		7 days			150 by 150
	C	1000	0.05 μm		7 days			300 by 300
Bathymetry	A	10	10 percent	0.4 to 0.8 μm	30 days	30 to 60	−5 to 30	300 by 300
	B	100	of aver-					
	C	1000	age depth					
Tides	A	1000	±1 K or	10 to 12,	2 hr	30 to 60	−5 to 30	20 by 20
	B	1000	0.1 μm	3 to 5, or	6 hr			150 by 150
	C	1000		4 to 11 μm	7 days			300 by 300
Nutrients	A	10	0.015 μm	0.4 to 0.8 μm	1 day	30 to 60	−5 to 30	20 by 20
	B	100	0.015 μm		7 days			150 by 150
	C	1000	0.015 μm		7 days			300 by 300
Chemical and toxic wastes	A	10	0.015 μm	0.3 to 0.8 μm	5 hr	30 to 60	−5 to 30	20 by 20
	B	100	0.015 μm		7 days			150 by 150
	C	1000	0.015 μm		7 days			300 by 300

[a] A=locate source; B=determine effect; C=model inputs.
[b] NA=not applicable.
[c] MW=microwave.

CHAPTER 4

Active Microwave Sensing of the Atmosphere

Active Microwave Working Group

Atmosphere Panel:

WILLIAM R. BANDEEN, *Cochairman*
ISADORE KATZ, *Cochairman*

David Atlas
Gordon A. Beals
Charles W. Bostian
Thomas A. Croft
Richard J. Doviak
Roger M. Lhermitte
Hans J. Liebe
Gordon E. Peckham
Allan C. Schell
Paul L. Smith, Jr.
Robert A. Stokes
Richard R. Weiss
Raymond Wexler
Carl A. Wiley

The meteorological satellite program is now in its 15th year. Beginning with the launch of Tiros 1 on April 1, 1960, 18 experimental Tiros, Nimbus, and geostationary Applications Technology Satellite (ATS) satellites carrying meteorological instruments have been launched. Research with early television pictures led to many discoveries concerning the organization and movement of cloud patterns and their relationship to meteorological processes; limited operational use of television pictures in weather forecasting began soon after the launch of Tiros 1. Subsequent experimental satellites carried omnidirectional and multichannel scanning radiometers. The radiometer data were applied in many different ways, including studies of radiation balance, mapping of cloud cover, tracking of storms, determination of surface temperatures and cloud-top heights, inference of mean tropospheric water vapor content, and global mapping of mean stratospheric temperature.

The first geostationary satellite to carry a meteorological instrument (a spin scan cloud camera) was ATS–1, launched on December 7, 1966. Time-lapse "movies," made from images of the planetary disk taken approximately every 20 min from an altitude of 26 000 km, showed dramatically the short-term weather motions from space. New knowledge of wind, circulation, and wave features deduced from cloud motions; of interhemispheric mass transport; and of mesoscale systems (such as squall lines, tornadoes, and other severe weather) was acquired. The development of a technique to determine winds by tracking clouds was of major importance, and wind data determined from ATS–3, after more than 6 yr in orbit, are used operationally by the National Oceanic and Atmospheric Administration (NOAA).

Nimbus 3, launched in April 1969, departed markedly from its predecessors by carrying three new classes of experiments. The first experiment class, the monitor of

ultraviolet solar energy (MUSE), monitored wavelengths affected by the photochemical processes associated with the generation and destruction of ozone. A second experiment class, the interrogation, recording, and location system (IRLS), demonstrated the feasibility of locating moving platforms (such as balloons and buoys), collecting in situ measurements from them, and determining atmospheric winds and ocean currents from their movements. The third experiment class, the satellite infrared interferometer spectrometer (IRIS), which also provided global measurements of stratospheric ozone, was perhaps most dramatic in demonstrating the ability to remotely sense vertical profiles of temperature in the atmosphere. This ability was accomplished by suitably "inverting" spectral radiances measured over the 15-μm absorption band of CO_2. The success was so dramatic that vertical profiles from the satellite infrared spectrometer (SIRS) on Nimbus 3 and 4 were used operationally by NOAA from May 1969 to November 1972 when they were replaced by soundings from a new vertical temperature profile radiometer (VTPR) on the NOAA–2 operational satellite.

Many of the spacecraft and instrument technology and data applications techniques are used in the operational satellite system after they are tested and proved on experimental satellites. The previously mentioned evolution of vertical sounders from SIRS on Nimbus 3 and 4 to VTPR on NOAA–2 is a good example. The first Tiros operational satellite (TOS), Environmental Sciences Service Administration 1 (ESSA–1), was launched in February 1966. The first second-generation improved TOS (ITOS–1) was launched in January 1970. To date, 14 operational satellites (and prototypes) have been successfully launched.

Nimbus 5, which was launched on December 11, 1972, carried for the first time radiometers sensing emission in the microwave region of the spectrum. Data from a single-channel electrically scanning microwave radiometer (ESMR) have demonstrated the potential of the measurement for mapping sea ice through clouds and for delineating precipitating cloud systems over the oceans of the world. Data from the Nimbus 5 microwave sounder (NEMS) have shown the ability of the NEMS to sound atmospheric temperature through cloudiness. The addition of microwave channels to infrared sounders of the future will markedly improve their accuracy and utility.

Skylab, launched in May 1973, carried numerous experiments for Earth observations, including a multispectral camera, an infrared spectrometer, a multispectral scanner, and a composite active/passive microwave system. Although these experiments were designed primarily for Earth resources survey and oceanography, of particular interest to the atmosphere panel is the active/passive radiometer/scatterometer (RADSCAT)/altimeter system, designed to measure ocean-surface characteristics (such as roughness) from which surface winds may be inferred. This experiment is mentioned in chapter 3 and discussed further in chapter 5.

The first Synchronous Meteorological Satellite (SMS) carrying a two-channel visible and infrared spin scan radiometer (VISSR), which is the prototype of the Geostationary Operational Environmental Satellite (GOES) soon to be placed in service by NOAA, was launched on May 17, 1974. The SMS provides, for the first time, continuous viewing of weather features, both day and night; it also collects and relays environmental data from remote platforms such as buoys, ships, and automatic stations. Also, the ATS–6—NASA's first three-axis-stabilized geostationary satellite carrying an advanced two-channel (visible and 11-μm infrared) radiometer—was launched on May 30, 1974, and is operating successfully.

Nimbus 6 carries eight sensors, including advanced atmospheric sounders, radiometers, and a data collection and platform location system. Of particular interest are the two passive microwave instruments. One instrument, an advanced ESMR, has a single spectral band (37 GHz; wavelength λ of 0.81 cm) with dual polarization, a conical scan, and an

instantaneous field of view (IFOV) of 25 km. The other instrument, the scanning and microwave sounder (SCAMS), will map tropospheric temperature profiles, water vapor abundance, and cloud-water content. It will sense radiation in the 60-GHz (O_2) absorption region, the 22-GHz water vapor absorption region, and the 31-GHz window region of the spectrum.

The evolution of meteorological satellites is illustrated in figure 4–1, in which the satellite and the date of the first launch for each series (except Skylab) is shown. Nimbus-G, SEASAT–A, Space Shuttle, and Tiros-N are approved future missions. The Earth Observatory Satellite (EOS) and the Synchronous Earth Observatory Satellite (SEOS) are only concepts; they are shown merely to illustrate possible types of future missions.

Tiros-N will carry an advanced atmospheric sounder (including both infrared and passive microwave channels), an advanced radiometer imaging in the visible and infrared, and an advanced data collection and platform location system. Nimbus-G (to be launched in 1978) is scheduled to carry the following nine instruments: (1) scanning multichannel microwave radiometer (SMMR), (2) coastal zone color scanner (CZCS), (3) solar and backscattered ultraviolet and total ozone mapping system (SBUV/TOMS), (4) Earth radiation budget (ERB), (5) lower atmospheric composition and temperature experiment (LACATE), (6) stratospheric and mesospheric sounder (SAMS), (7) stratospheric aerosol measurement (SAM II), (8) measurement of air pollution from satellites (MAPS), and (9) temperature humidity infrared radiometer (THIR). Of particular interest to the atmosphere panel is the SMMR. The payload for SEASAT–A (to be launched in 1978) has not been officially determined, but a tentative payload, including several active microwave instruments, includes the following:

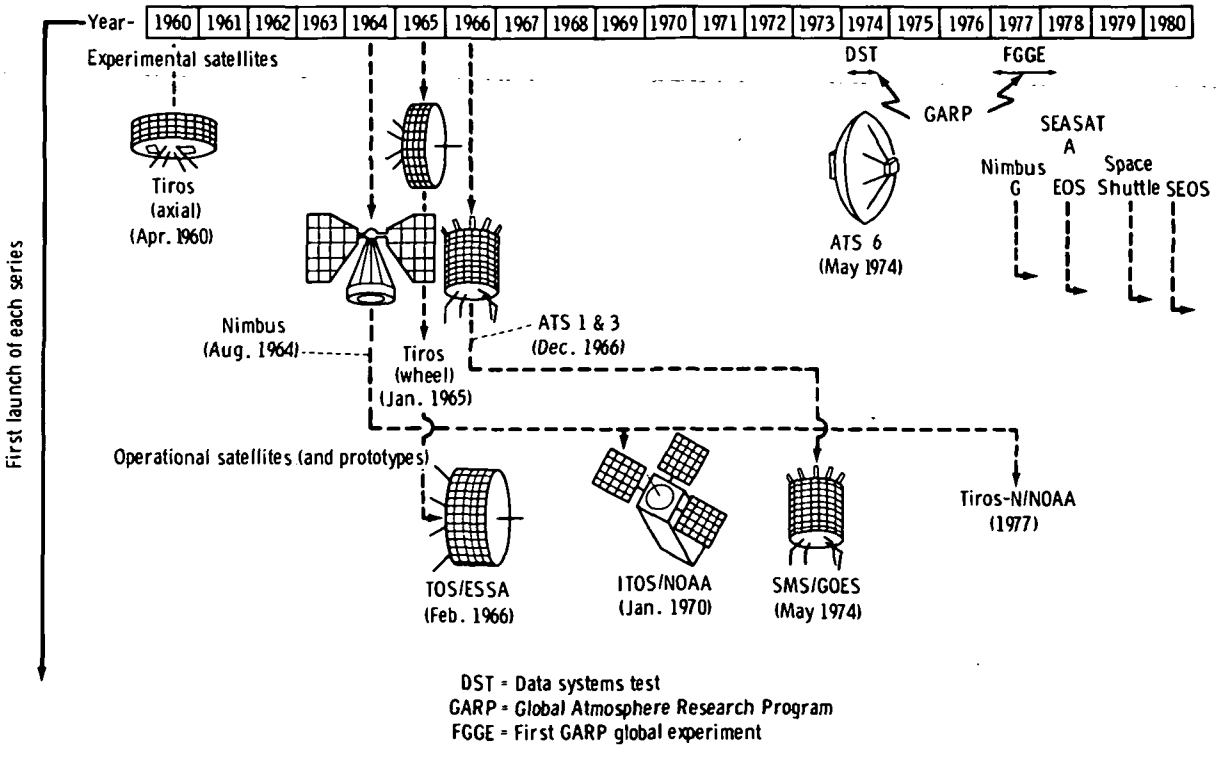

FIGURE 4–1.—Evolution of meteorological satellites (and other satellites with meteorological instruments).

(1) SMMR, (2) fan beam scatterometer (FBS), (3) radar altimeter (RA), (4) visible and infrared radiometer (VIR), and (5) synthetic aperture radar (SAR) or wave directional spectrometer (WDS).

DISCIPLINE OBJECTIVES IN THE ATMOSPHERIC SCIENCES

The decade of the 1960's saw the development of a comprehensive meteorological satellite program, with a concomitant increase in capabilities for useful application on a scale previously impossible. In the early 1970's, environmental problems came forcefully to public attention. Presently, a unique combination of opportunities and challenges exists—a new capacity for useful applications to the needs of society at a time when the influence of public opinion provides a driving force toward solutions for pressing problems. These circumstances are likely to have far-reaching influences on the development of atmospheric sciences in the coming years. A recent report prepared by the Committee on Atmospheric Sciences of the National Research Council, National Academy of Sciences (ref. 4–1), lists four meteorological objectives that can contribute most to the solution of pressing problems in the 1970's.

1. Weather prediction: To extend the capability for useful predictions of the weather and atmospheric processes

2. Atmospheric pollution: To contribute to the development of the capability to manage and control the concentrations of air pollutants

3. Climate and weather modification: To establish mechanisms for rational examination of deliberate and inadvertent means for modifying weather and climate

4. Weather danger and disaster warning: To reduce substantial human casualties, economic losses, and social dislocations caused by weather

The six NASA meteorology program objectives are as follows. (Objectives 2 to 5 correspond to the four meteorological objectives of the Committee on Atmospheric Sciences.)

1. Operational support: Support the development of the operational meteorological satellite system.

2. Weather prediction: Develop space technology for determining the vertical structure of the atmosphere globally, which, when supplemented by simulation techniques, models, and conventional observations, will provide required data with emphasis on large-scale long-term weather forecasts.

3. Atmospheric pollution: Develop a space-sensing capability to identify and quantitatively monitor the distribution of natural and manmade pollution in the lower and upper atmosphere on global and regional scales.

4. Climate and weather modification: Apply space-acquired data from remote sensors, data collection systems, and/or in-flight experiments requiring unique orbital conditions (such as a gravity-free environment) to the development of models and the establishment of mechanisms for the rational examination of deliberate and inadvertent means for modifying weather and climate.

5. Weather danger and disaster warning: Develop and establish a system for continuous observation of atmospheric features to permit early identification and quantitative measurement of atmospheric conditions conducive to the formation of severe atmospheric phenomena (e.g., thunderstorms, tornadoes, hurricanes, etc.) and to serve as a basis for timely warning to the public.

6. Processes and interactions: Investigate fundamental atmospheric processes and interactions on various temporal and spatial scales (within the atmosphere, in response to solar inputs, and at the air-surface interface) through the observation of the structure, composition, and energetics of the atmosphere for the purpose of effectively applying space capabilities in pursuance of the previously mentioned objectives.

The scientific and meteorological communities of the world, represented by the International Council of Scientific Unions (ICSU) and the World Meteorological Organization (WMO), have defined and undertaken an

ambitious and extensive international research program, the GARP. The Joint Organizing Committee (JOC) for GARP has been formed by these two organizations to provide leadership and direction to this program. At the first meeting in April 1968, the JOC provided the following definition and objectives for GARP:

> A program for studying those physical processes in the troposphere and stratosphere that are essential for an understanding of the transient behavior of the atmosphere as manifested in the large scale fluctuations which control changes of the weather; this would lead to increasing the accuracy of forecasting over periods from one day to several weeks, and the factors that determine the statistical properties of the general circulation of the atmosphere could lead to better understanding of the physical basis of climate.

Those objectives are closely analogous to objectives 2 (weather prediction) and 4 (climate and weather modification) of the NASA meteorological program.

The GARP has expanded rapidly, and it now involves a series of interrelated theoretical and observational subprograms. The GARP Atlantic tropical experiment (GATE) and the FGGE scheduled for 1977 to 1978 are particularly noteworthy. Also, a DST was conducted during 1974 to test elements of FGGE in preparation for the complete experiment (fig. 4–1).

The FGGE in intended to provide detailed measurements of the large-scale state and motions of the entire atmosphere over a period of a year or more (1977 to 1978). The main objectives of FGGE (ref. 4–2) are directed at developing more realistic numerical models of the atmosphere, assessing the ultimate limits of weather predictability, and designing appropriate weather observing systems for prediction of the large-scale features of the general circulation.

The basic data requirements for FGGE have been defined by JOC and are summarized in table 4–I. In addition to these parameters, an auxiliary list of desirable parameters has been defined. These additional requirements are soil moisture; reflected, scattered, and emitted radiation; albedo and radiation balance; snow and ice cover; cloud cover (and type); precipitation areas; ozone; and ocean temperature above the seasonal thermocline.

Because of the development time required, it is not practical to consider an orbiting radar to support FGGE in the period 1977 to 1978. The purpose of this discussion of GARP is to present briefly the scope of a major ongoing international effort that is in accord with several of the meteorological objectives of NASA and the National Academy of Sciences. In this framework, it is not

TABLE 4–I.—*The JOC Data Requirements for FGGE* [a]

Basic parameters	Horizontal resolution, km	Vertical resolution		Accuracy
		Troposphere	Stratosphere	
Mid and high altitudes				
Temperature	500	4 levels	3 levels	±1 K
Wind	500	4 levels	3 levels	±3 m/sec
Relative humidity	500	2 degrees of freedom	.....	±30 percent
Sea surface temperature	500	.....	.....	±1 K
Pressure (reference level)	500	.....	.....	±0.3 percent
Low altitudes				
Temperature	500	4 levels	3 levels	±1 K
Wind	500	4 levels	3 levels	±2 m/sec
Relative humidity	500	2 degrees of freedom	.....	±30 percent
Sea surface temperature	500	.....	.....	±1 K

[a] One measurement per day is required; 2 per day are desirable.

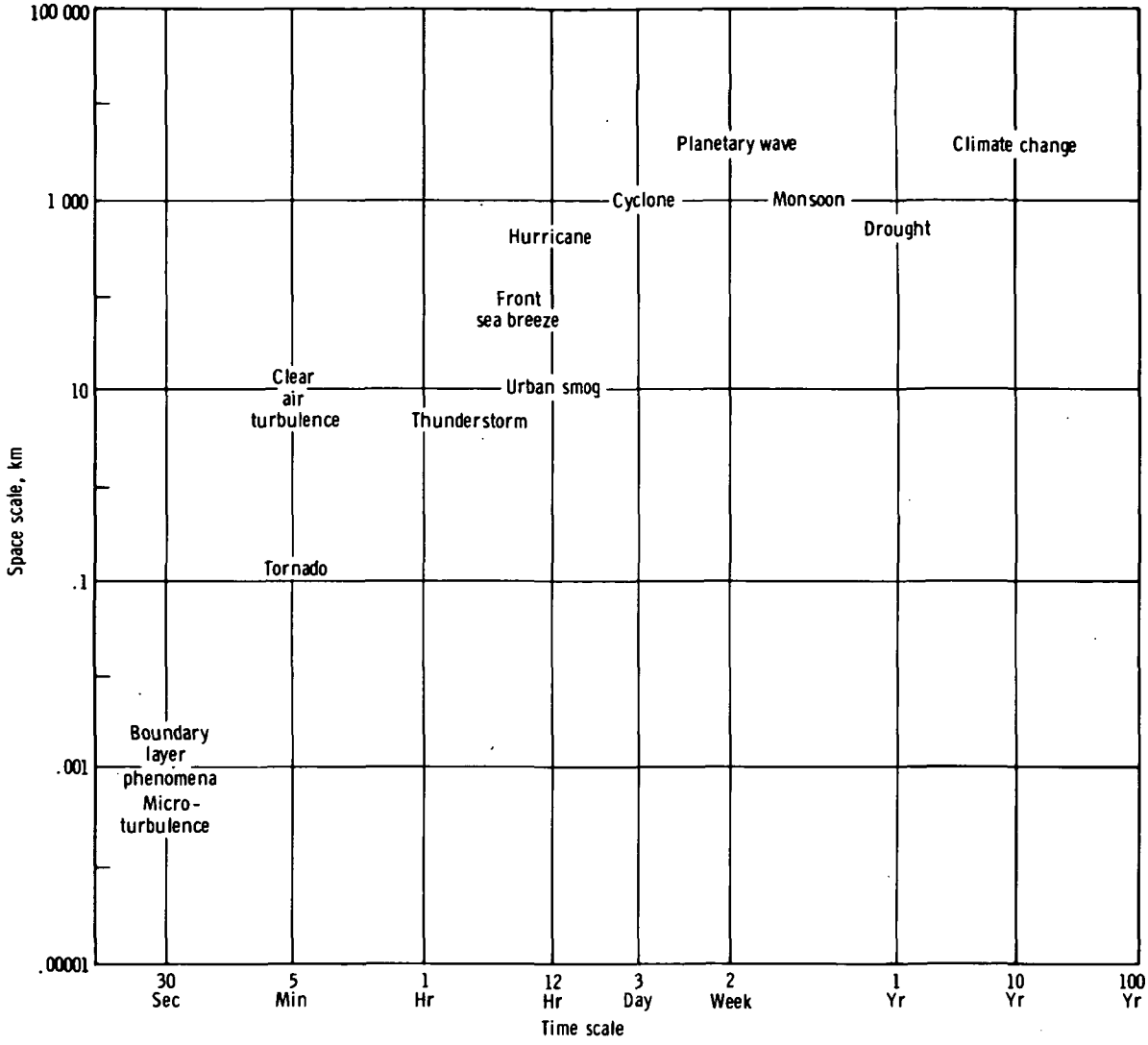

FIGURE 4–2.—Time and space scales of meteorological phenomena.

unreasonable to contemplate an active microwave system that could contribute to the success of a similar program in the future.

The FGGE is concerned primarily with atmospheric phenomena having time scales of approximately a week or longer. However, many important meteorological phenomena have shorter time scales, some of which are illustrated in figure 4–2. With reference to the NASA meteorology program objectives and figure 4–2, the geostationary satellite is peculiarly applicable to program objective 5 (weather danger and disaster warning), which involves phenomena having time scales less than 12 hr. The idea of orbiting an active microwave system at the geostationary altitude (36 000 km) has indeed seemed well beyond serious consideration in the past. However, with the approach of the Space Shuttle era and in terms of the tremendous technological advances of the past decade and of those advances that will surely come in the future, it seems appropriate to assess again the possible applications to the atmospheric sciences of active microwave systems in either near-Earth or geostationary orbits.

PART A

MEASUREMENT TECHNIQUES AND PRINCIPAL APPLICATION AREAS

APPLICATIONS OF CONVENTIONAL PULSE RADAR SYSTEMS TO METEOROLOGICAL OBSERVATIONS

Radars have been used for meteorological observations since shortly after the development of centimetric radar equipment in the early 1940's. The history of the meteorological uses of radar can be traced in references 4–3 to 4–13. In addition, the proceedings or preprint volumes from the series of radar meteorology conferences (formerly called weather radar conferences), published by the American Meteorological Society, provide an excellent history of the development and application of radar technology in meteorology.

The most important aspect of radar for meteorological observations is its ability to observe precipitation at distances up to several hundred kilometers, which makes it a true remote sensor for meteorological applications. Ground-based weather radars have been useful mainly for subsynoptic scale, or "mesoscale," observations. They readily provide observations with space continuity impossible to attain with the ordinary synoptic weather-reporting network. Such radar observations are of enormous value in a wide variety of applications, including short-term forecasting for local areas or terminal points and for many research investigations.

However, to extend the value of weather radar observations to the synoptic scale remains difficult. The area covered by a single ground-based weather radar set is too small to encompass most synoptic-scale features of interest, and techniques for meshing observations from numerous radar installations to provide coverage of larger areas are only now being developed. The so-called "Ligda montages" (ref. 4–14), which were synthesized from the observations of many radar systems located at different sites, were the first attempt to assemble data from several radars, thus providing examples of how synoptic-scale patterns can be discerned in radar observations. The development of automated techniques for meshing such observations is one objective of the NOAA digitized radar experiments (D/RADEX) program now in progress (ref. 4–15).

Weather radar observations are of value in forecasting for periods of up to 6 hr. A limiting factor is the variability of precipitation in space and time; the plan-position-indicator (PPI) scope of a weather radar set operating during a typical summer afternoon of convective activity reveals a process of continuous evolution. Cells and storm systems grow and decay. Old cells disappear from the scope and new ones form; sometimes cells merge, and less frequently they even split. It is even difficult to define a "cell" or "storm" or "echo" in an objective way, although there have been recent developments in this direction (ref. 4–16). These conditions greatly inhibit the use of radar observations of precipitation for forecast purposes, when extrapolation over appreciable intervals of space or time is required.

Hydrology is another important area in which weather radar is finding increasing application. Weather radar observations are ideally suited for such tasks as mapping accumulated precipitation amounts over specific watershed areas, particularly when short time intervals are involved (as in the case of flash-flood situations). This application places stringent demands on making accurate quantitative measurements of echo intensities with radar systems that are calibrated accurately. Even then, the problem of relating the radar measurements to precipitation rates and amounts has yet to be completely solved.

Characteristics of Ordinary Pulse Weather Radars

Weather radar observations provide a variety of information concerning the precipitation responsible for the echoes. This

information can be divided into two categories, according to whether it can be extracted from single "snapshot" observations (for example, single PPI scans) or whether repetitive observations over an interval of some minutes or hours are required. Such categorization may be helpful in evaluating the potential use of satellites as weather radar platforms because orbiting satellites provide primarily a "snapshot" capability. Obtaining repetitive radar observations in most instances requires operating from geosynchronous satellites or a system of multiple satellites.

The "snapshot" category of information includes the observation of the location, size, and shape of the precipitation regions from two- or three-dimensional imagery. Also, the precipitation structure can be determined from the pattern of the echoes and the "texture" of individual echo elements, and the intensity and intensity gradients can be determined from relative or absolute measurements of echo intensity. These characteristics are usually adequate to deduce the basic nature of the precipitation process; for example, stratiform compared to convective, airmass compared to squall line, etc. That information, together with synoptic information such as environmental wind data and the characteristics of the airmass, can be used to develop short-term forecasts of the future behavior of the precipitation in the area surveyed by the radar. However, the typical rapid evolution of the precipitation restricts the time period of validity of any such forecasts.

The situation can be improved somewhat by making repetitive observations over a period of time. They yield a second category of information, which is related to the movement (speed and direction) and time evolution or to persistence (duration) of the precipitation regions. The situation, with respect to repetitive observations, is seldom as clear-cut as it might at first appear. For example, even with echo patterns having fairly well defined cellular elements, it typically takes more than 15 min to establish reasonably good estimates of cell movements. However, the lifetimes of convective cells are often on the order of 30 min, and new cells have a tendency to develop alongside old ones, so that movement and evolution interact in a complicated way. Moreover, the direction of cell movement is usually different from that of the storm system as a whole.

The essential conclusion is that, although "snapshot" radar observations provide useful information about the space distribution of precipitation at a given time, repetitive observations are still necessary in most operational applications such as forecasting. Even so, the length of time over which the observations can be extrapolated to develop the forecasts is typically rather short. There remains the prospect that this time might be extended by developing numerical weather prediction models using current and past precipitation data as input, thus providing forecasts of the future course of development of the precipitation.

The observational capabilities of weather radar may possibly be extended by adding Doppler, multiple polarization, and/or multiple wavelength features to the radar system. The merits of adding these features are discussed in other sections of this chapter.

In the usual ground-based weather radar applications, the choice of radar wavelength is determined mainly by a compromise between the difficulties caused by attenuation (as the wavelength decreases below 10 cm) and the expense of obtaining the desired angular resolution (beamwidth) at long wavelengths. Research radars can operate at 10-cm wavelengths to virtually remove attenuation difficulties and can accept the increased expense required to obtain good beamwidth resolution. Operational radars tend to be designed for the 10-, 5-, or sometimes even the 3-cm wavelength regions. For a fixed beamwidth, the variations in available transmitter power and receiver sensitivity generally serve to keep the overall system sensitivity (in terms of minimum detectable radar reflectivity factor) over this range of wavelengths approximately inde-

pendent of the selected wavelength. Airborne weather radars generally operate at 5- or 3-cm (or even shorter) wavelengths to take advantage of the smaller sizes of the equipment.

The antenna beamwidths ordinarily used in weather radars range from approximately 1° to 3°, although there are exceptions beyond these limits in both directions. The narrower beamwidths are usually found in research weather radar systems. A lower bound near 1° is set even for these radar systems by some combination of tradeoff relative to (1) the huge antennas needed to reduce the beamwidths below 1°, (2) the increased scanning time required (because the number of angular elements to be scanned increases in proportion to the inverse of the product of the beamwidths), and (3) the increased amounts of data (from the greater number of angular elements) that have to be handled. For many purposes, good vertical resolution is more important than good horizontal resolution, so there can be advantages in using height-finder-type antennas.

Operational network weather radars typically have somewhat larger beamwidths. For example, the U.S. Air Force FPS–77 has a beamwidth of approximately 1.6°, whereas the National Weather Service WSR–57 has a beamwidth of approximately 2.2°. Beamwidths of 3° or larger are found only in airborne weather radars and in a few other radars in which the primary use involves relatively short-range observations.

The other characteristics of weather radars are generally governed by various practical considerations. Usually, values of peak power and pulse duration are comfortably within the state of the art, there seldom being any real requirement, when observing precipitation, to press for the relatively modest improvements in sensitivity that might be obtained by pushing those values toward the state-of-the-art limits. Upper limits on the pulse repetition frequency (PRF) are related to considerations of maximum unambiguous range and to the fact that precipitation echoes have pulse-to-pulse time correlations up to 5 to 20 msec (at $\lambda = 10$ cm); thus, little can be gained in the assessment of echo mean intensity by increasing the PRF beyond a certain value.

Weather Radar Observations From Orbiting Satellite Platforms

It is only natural to ask whether it is possible to combine the capabilities of radar observation of weather with the advantages offered by a satellite platform. Orbiting satellite platforms would provide the potential for a significant increase of the radar coverage to the synoptic scale, as well as extending observations to the remote oceans and other areas that are not presently covered by any weather radar system. Another advantage of the satellite platform is a possible use of shorter wavelengths because the radar signals do not have to traverse long paths through rain, thereby reducing the importance of attenuation.

The idea of installing a weather radar on a satellite was considered even before the first Tiros satellite went into orbit (refs. 4–17 to 4–21). Radars, however, require heavy transmitters and large amounts of prime power; therefore, they were not well suited to the early satellite technology. The amount of weight and power that can be carried in space has increased. It is therefore appropriate to reconsider the practicality of satellite-borne radars and the nature of the meteorological information that could be obtained with them.

Dennis (refs. 4–22 and 4–23) reviewed the early proposals and discussions of satellite weather radars and concluded that weather radar observations from an orbiting satellite would be of little meteorological value. He noted two basic problems in the use of satellite-borne radar systems:

1. The need for separating the contributions of the precipitation and of the ground or sea surface underneath to the echoes limits the radar observations to a narrow subsatellite swath. He suggested that the swath width might be smaller than 40 km. This limitation can be overcome by using tech-

niques that permit separating the ground and precipitation contributions to the echoes.

2. As previously noted, radar observations of precipitation cannot be extrapolated very far in either time or space. An orbiting satellite providing observations on a 12- or 24-hr return cycle would therefore be of little value to the usual operational applications of weather radar data, such as mesoscale analysis and forecasting. However, this problem only tends to restrict the effective application of satellite weather radar observations to the monitoring of precipitation in longer, persistent meteorological systems such as hurricanes.

Dennis' findings essentially halted serious consideration of satellite-borne weather radars. A 1969 report (ref. 4–24) included only a brief mention of the use of satellite radars for precipitation measurements. Although the material in this report outlines only possible solutions and there are few specific details, its tone is quite optimistic. It is mentioned that an average power of 20 W would still be adequate for a radar installed aboard a synchronous satellite. The radar would operate at a wavelength of 2 cm, use a 10-m-size antenna, have a range resolution of 75 km, and have an azimuth resolution of 150 km. Such a radar should be capable of detecting rain extending 1 km in height with a rainfall rate greater than 10 mm/hr.

A textbook of radar meteorology, authored by V. D. Stepanenko (ref. 4–12), devotes a chapter to the use of radar and microwave radiometry in satellites for obtaining meteorological and hydrological information. A translation of textbook section 9.6, "Features and Effectiveness of the Detection of Clouds and Rain With Pulse Radar From Satellites," is included as appendix 4A to this chapter. He considers radars with both a downward-looking scanning pencil beam and a fixed planar (fan) beam.

As an example of the scanning pencil-beam system, he considers an X-band (λ=3 cm) radar in a satellite at an altitude of 400 km. The scanning angle is 78°. The beamwidth in the along-track dimension is 3.5°; in the across-track dimension, it is 0.51°. The PRF is 1150 Hz; and, with a peak power of 300 kW and a pulse duration of 1 μsec, the satellite can detect a rainfall rate of 1.5 mm/hr. Four satellites are supposed to be required. The author implies that, with the scanning narrow-pencil-beam radiation pattern, the effect of Earth echo is not important.

Earth echo is noted by Stepanenko to be important when a fixed planar beam is used. This type of antenna is considered mainly because it is simpler to construct than a scanning pencil-beam antenna and because it also allows the necessary minimum number of pulses on target to be readily obtained. Coverage of the Earth surface is obtained with two fixed antennas oriented perpendicular to the orbit plane of the satellite. (Although not stated explicitly, it is presumed that the antennas point to opposite sides of the satellite.) When the altitude is 400 km, a common receiver/transmitter is switched between the two antennas at a rate of 16 Hz. The width of the radiation pattern is 30° in the direction perpendicular to the groundtrack and 0.23° in the direction along the groundtrack. The peak power is 300 kW, and the pulse duration is 5 μsec. Four satellites insure complete coverage of the Earth surface.

It is expected that, in the absence of clutter, this radar could detect a rainfall rate of 2 mm/hr. Over water, this minimum value increases to a rate of 3.1 mm/hr; over land, to a rate of 8.0 mm/hr.

To improve the sensitivity in clutter conditions, Stepanenko proposes a dual-band radar much like that proposed by Keigler and Krawitz (ref. 4–21). Advantage is taken of the different variation with frequency of the strength of the clutter and the precipitation echoes. The dual-frequency radar is assumed to operate at wavelengths of 3 and 0.8 cm; identical antenna patterns are assumed. The peak power at 3 cm is 300 kW; at 0.8 cm, it is 30 kW. With these specifications, the minimum detectable rainfall rate over the sea is 0.7 mm/hr.

Stepanenko also considers the possible

characteristics of a radar in synchronous orbit. With a beamwidth of 0.43°, a peak power of 300 kW, a minimum detectable signal of 10^{-15} W, and a pulse duration of 1 μsec, a rainfall rate greater than 4 mm/hr can be detected with the radar wavelength being either 0.8 or 2 cm, but not 0.3 cm. The beam resolution in the tangential dimension is 80 to 90 km; in the radial direction, it varies from 0.2 to 6.5 km with the scan angle increasing from 0.2° to 7°. Stepanenko also states that, in future years, it should be possible to measure the rainfall intensity in addition to simple detection.

In the period since Dennis' study, dramatic advances in radar technology and significant developments in the atmospheric sciences have occurred. Among the latter are the development and use of numerical models for weather prediction and the modeling of cloud and precipitation processes from cloud scale to synoptic scale. Thus, it seems reasonable to reexamine the situation to determine whether meaningful satellite weather radar experiments or applications can be defined in terms of these more recent developments.

The fundamental limitation noted by Dennis is that the "snapshot" views of the precipitation distributions provided by weather radar on an orbiting satellite cannot be extrapolated very far in either space or time because of the inherent time and space variability of precipitation. Thus, Dennis believed that the utility of such observations for weather analysis and forecast purposes would be virtually insignificant. The precipitation observations differ greatly in this respect from the once- or twice-a-day observations of pressure, temperature, humidity, and windfields that are vital in weather forecasting, whether done by manual methods or with the aid of numerical models. There is considerable validity to Dennis' arguments; and, before embarking on a satellite radar project, it may be well to consult the meteorological community concerning the potential usefulness of global precipitation observations in the "snapshot" format.

Dennis suggested that at least 10 observations would be needed during the lifetime of meteorological systems to derive much meaningful information. With observations available on a once- or twice-a-day basis, this suggests that one should concentrate his attention on storms with lifetimes on the order of a week or more. This implies that the primary targets of interest will be persistent cyclonic storms, including hurricanes and typhoons and also extratropical cyclonic storms, many of which have durations sufficient to permit the acquisition of 10 or more sets of observations. An alternative would be to use a constellation of weather radar satellites to increase the frequency of observation.

Tropical storms are perhaps the easiest meteorological targets to observe from a satellite. Their size makes them easy to find, and their persistence makes it possible to acquire repetitive observations from low-altitude satellites. The fact that these storms spend most of their lifetimes over water simplifies the technological problems of separating rain-echo signals from surface-echo clutter. Satellite-borne weather radar observations on a once- or twice-a-day return cycle would provide a history of the development and distribution of precipitation within the storms during their entire lifetimes. Such observations are not available from other sensors or other weather radar platforms.

Satellite-borne weather radar observations of tropical storms, especially over the remote oceans, would aid research into the genesis and behavior of such storms and aid in attempts to develop physical and numerical models describing them. The observing capability could be used to support large-scale research programs such as GATE, FGGE, or Project Stormfury (concerned with hurricane modification by silver iodide seeding, which is scheduled to be resumed in the Pacific Ocean in 1976). Data from meteorological radars aboard orbiting satellites could provide valuable observations for such research efforts. The horizontal distribution of precipitation over the oceans can be obtained from microwave radiometric observa-

tions; thus, any satellite-borne weather radar system should probably be complemented by a radiometer on the same spacecraft, with possible use of the same antenna and maybe the same receiver front end for the two systems.

Some significant characteristics of tropical storm systems are outlined in table 4–II. Table 4–III gives estimates of the minimum and the desired radar observational capabilities to provide useful information for hurricane studies. The minimum requirements are based primarily on the characteristics of present-day numerical hurricane models. In general, these models are concerned only with two-dimensional distributions of precipitation or with a vertical structure represented by a small number of levels. Microwave radiometer techniques appear to be capable of meeting the minimum requirements for two-dimensional mapping of precipitation over water.

The desired observing capabilities are based on anticipated future development of hurricane models and extrapolation from the capabilities of presently available ground-based weather radar systems. Here, much finer resolution is specified in the horizontal direction, with still somewhat finer resolution generally being desirable in the vertical dimension. The necessary vertical resolution can only be achieved by use of active microwave techniques. Whereas nonattenuating wavelengths would be required to obtain quantitative echo-intensity measurements, the acceptable range of wavelengths for satellite-borne radars extends to much shorter values than is the case for ground-based weather radars. (See the section entitled "Attenuation Considerations.")

TABLE 4–III.—*Capabilities Needed for Satellite Radar Observations of Tropical Storms*

Minimum capability:	
Determine the two-dimensional (horizontal) distribution of precipitation echoes with resolution as follows:	
Horizontal, km	20
Time, hr	12
Reflectivity factor	semiquantitative
Desired capability:	
Determine the three-dimensional distribution of precipitation echoes with resolution as follows:	
Horizontal, km	2
Vertical, km	1
Reflectivity factor, dB	3
Time, hr	12
Determine wind velocities with resolution as follows:	
Horizontal, km	[a] 2
Vertical, km	1
Wind velocity:	
Magnitude, m/sec	2.5
Direction, deg	20
Determine storm movement with resolution as follows:	
Magnitude, m/sec	1
Direction, deg	10

[a] For some purposes, the horizontal resolution requirements of the wind measurements can be relaxed to 10 to 20 km.

The observing capability required for any specific investigation has to be determined by reference to the detailed scientific objectives. Thus, the present estimates indicate design goals that may serve as a basis for deciding whether the needed capabilities can even be approached by satellite-borne weather radar systems.

TABLE 4–II.—*Some Characteristics of Tropical Storm Systems*

Typical overall dimensions of precipitation region:	
Diameter, km	560
Height, km	18
Lifetime, weeks	1 to 3
Reflectivity factor range of interest, dBZ[a]	20 to 70
Windspeed, m/sec	0 to 75

[a] $dBZ = 10 \log_{10} Z$ (where Z is radar reflectivity factor in mm^6/m^3).

Concerning the modeling of hurricanes, the present numerical models (refs. 4–25 to 4–31) attempt to describe the development of the hurricane, and some of them include precipitation fields as part of the output. The models do not use precipitation data as input (ref. 4–32), but precipitation observations from a satellite weather radar would be one source of data against which to verify the models. Such observations might also be used to help periodically update the models as they simulate the life cycles of the storms.

The latent heat released during the formation of precipitation affects the air temperature, which, in turn, influences the storm dynamics. The height at which the heat is released is therefore very important in the numerical hurricane models. If it is released at low levels, a much stronger vortex circulation develops. To the extent that the latent heat release can be localized on the basis of radar observations of precipitation, satellite weather radar observations could provide additional important information for the verification (or revision, if necessary) of the models and perhaps also for use in updating models operating in real-time applications. The difficulty is that most of the latent heat is released during the condensation of water vapor to form cloud droplets. It may or may not be possible to relate observed regions of precipitation to the regions of latent heat release.

The development of hurricane numerical models has been fairly recent, and it can be reasonably expected that significant advances in the models will occur during the next decade. Previous experience has shown that it takes approximately 5 yr to advance a numerical model that involves precipitation processes to the point at which it is suitable for meaningful comparisons with actual observations of the hurricane models.

Many extratropical cyclonic storms also persist long enough to allow significant repetitive observations from orbiting satellites. However, the development of numerical models for such storms incorporating the precipitation process lags behind the work on tropical storms. Consequently, requirements for observing precipitation distributions in extratropical cyclones would apparently have to be based mainly on proposed uses in forecasting applications.

Applications of Satellite Weather Radar Observations

It is proposed that the meteorological information obtainable from a satellite-borne conventional pulse radar would include global mapping of rainfall intensity, measurements of storm maximum echo heights, and measurements of the height of the melting layer, which is characterized by a significant increase of radar signal intensity (bright band) observed mainly in stratiform precipitation. Rainfall intensities are now being mapped over the oceans by the ESMR installed on Nimbus 5. Thus, the principal value of an active microwave system would be to provide height resolution and thus allow the three-dimensional mapping of precipitation (i.e., inside cyclonic storms, as discussed in the section entitled "Weather Radar Observations From Orbiting Satellite Platforms"). In the absence of a vertical resolution capability, however, the active system provides little advantage over passive radiometric techniques. Over the oceans, radar could probably distinguish rain echoes from sea clutter to a distance of approximately 200 km from the subsatellite point. This distance is reduced to less than 800 km for precipitation over land.

In the future, satellite weather radar observations may be valuable in providing precipitation distributions for use as input to the numerical weather prediction (NWP) models. The horizontal grid spacing of the present NWP models is basically incompatible with the spatial variations of precipitation as observed by radar, the former being much too large. Partly because of this, the NWP models do not presently use precipitation data as input. In fact, moist convection and precipitation processes are just being incorporated into such models as the

limited fine mesh (LFM) model of the National Weather Service.

However, the precipitation process contributes a significant amount of latent heat in the atmosphere. This heat can be insignificant over the short term of a few days, but it could become increasingly important for longer periods.

Latent heat is not now an input for numerical weather prediction. Many numerical modelers consider the effects of precipitation to be second order in the models; thus, bringing the effects into the models would probably not have a major impact on the prognoses; however, there are suggestions to the contrary (ref. 4–33). Tracton's work suggests that an ability to identify local areas of strong convection and their relationship to regions of cyclogenesis would be helpful in improving the numerical forecasts. If that is the case, the models will eventually advance to the stage at which they can accept precipitation data as input. In that event, the global coverage obtainable from an orbiting satellite would be a definite asset. Modification of the numerical models and testing with available global rainfall data would be required before global rainfall data on an operational basis could be properly utilized.

The maximum echo height is a good indicator of the intensity of a storm. Rain associated with middle-latitude cyclonic storms has maximum echo heights ranging from 5 to 8 km. Thunderstorms have maximum heights generally above 10 km; hailstorms, above 13 km. Severe storms with tornadoes may exceed 20 km. Comparisons of the distribution of maximum echo heights in both tropical and extratropical storms at 12-hr intervals may indicate storm development or dissipation during the period. The maximum echo height is also a good indicator of the rate of rain production in convective storms.

The height of the melting layer is detected by radar as a "bright band," which is characterized by a significant increase of radar reflectivity at this level due to the partial melting of frozen hydrometeors. The 273-K level is generally located approximately 300 m above the peak of the bright band. A downward-looking radar can be expected to measure the height of the 273-K level to an accuracy of 200 m (to approximately 50 km from nadir). The accuracy will decrease to approximately 1 km at 150 km and to 2 km at 300 km. Further analysis of accuracy at different distances for nadir is required.

The heights of the 273-K level in rain should be useful as an input in numerical weather prediction. Temperature soundings of the atmosphere are now being determined from infrared and passive microwave measurements in satellites. However, these soundings can only be made in clear or partly cloudy regions. The heights of the 273-K level in rain areas would provide useful supplementary information.

The height of the melting layer would also be useful as a measure of the intensity and state of development of tropical storms and some extratropical storms. Tropical storms are initially "cold core," and they develop into hurricanes as "warm core." The resulting horizontal temperature gradient is a measure of the intensity of the storm. Measurements of the height of the melting level in different parts of the storm can be used to determine the temperature gradient.

Another possible application of weather radar observations from an orbiting satellite is in developing a global climatology of precipitation echoes. This application uses the synoptic observing capability of the satellite-borne radar system and, by concentrating on climatology, circumvents its limitation to "snapshot" observations. Radar climatological information is useful in a variety of military, communication system design, and other applications. To develop the necessary climatology, the satellite radar observations would have to be made in conjunction with visible and infrared observations of the same weather systems, preferably from geostationary satellites. Moreover, for many regions of the world, weather radar observations providing a sufficient basis for developing the climatology may already exist.

Satellite Radar for Meteorological Observations

There are three possible methods for configuring a radar in a low- or medium-orbit satellite for meteorological observations:

1. A fixed side-looking fan-beam antenna that provides the greatest swath width and has the simplest antenna system. However, this system requires larger power than other systems because of the wide swath. The wide elevation beam means that it cannot obtain height information about the precipitation, nor can it obtain a measure of the precipitation intensity because the degree of beam filling is unknown. Two antennas looking out opposite sides of the spacecraft can increase the coverage. This system operates over water better than over land because the background clutter is less over water.

2. An antenna beam that rotates continuously and provides at least two looks at the target (once when the satellite is approaching and once when it is receding). Either a fan-beam antenna or several contiguous pencil beams can be used to achieve the desired coverage. Generally, the coverage of a rotating antenna is slightly less than that of a fixed side-looking antenna. A possible variation of this type of system is one that scans a sector forward or aft of the satellite.

3. A downward-looking scanning pencil-beam antenna that covers a swath usually less than that obtained with the previous two solutions and requires a more complicated antenna. This system has the advantage of allowing measurement of the precipitation height and, because the precipitation usually fills the resolution cell, measurement of the precipitation intensity.

Each approach to satellite meteorological radar design has its particular advantages and limitations. The downward-looking scanning pencil-beam system is selected here as offering the most appropriate solution for meteorological observations. This system has the advantage of being able to map the distribution of precipitation in three dimensions.

The characteristics of a downward-looking scanning pencil-beam radar are listed in table 4–IV. Rather than describe the logical development of the radar design, brief comments will be offered to explain why these parameters were chosen. The major design criteria that had to be observed are (1) there should be sufficient signal-to-noise ratio (SNR) available for detecting a reasonable amount of precipitation, (2) the radar resolution cell (beamwidth and pulse duration) must be sufficiently small to exclude ground echo, and (3) the radar must be able to provide vertical resolution of approximately 1.5 km.

The radar operations frequency of 35 GHz was chosen to take advantage of the smaller antenna and the larger radar reflectivities possible at the higher frequencies. Satisfactory operation can also be achieved at a lower frequency. The reflectivity of precipitation does not increase as rapidly with increasing frequency above 35 GHz, and suitable components are more difficult to achieve.

To obtain good height resolution, the beamwidth must be small. A 0.2° beamwidth was selected as being the smallest that is likely to be achieved in the near future with a spaceborne antenna at that wavelength. This corresponds to an antenna that is 300

TABLE 4–IV.—*Characteristics of a Satellite Meteorological Radar Using a Downward-Looking Scanning Pencil-Beam Antenna*

Frequency (0.86-cm wavelength), GHz	35
Antenna beamwidth (conical beam), deg	0.2
Antenna size (diameter), m	2.6
Transmitter power:	
Average, W	16
Peak, kW	3.5
Pulse duration, μsec	2
Pulse repetition frequency, Hz	2300
System noise temperature, K	3000
System losses, dB	6
Scanning angle (from nadir), deg	45
Minimum rain intensity (with 13-dB SNR), mm/hr	2 (or 28 dBZ)
Swath coverage (from nadir), km	400
Orbit height, km	400

wavelengths in diameter. The pulse duration has a lesser effect on altitude resolution than the beamwidth; a value of 2 μsec was selected. With this beamwidth and pulse duration, the altitude resolution at nadir (along the groundtrack) is 0.6 km and increases to 1.5 km at 400 km for the groundtrack at the edge of swath coverage.

The orbit height of 400 km was chosen somewhat arbitrarily and should be examined further to determine optimum orbit coverage. The 400-km orbit height and the need for 1.5-km height resolution results in a swath of 800 km (400 km on either side of the groundtrack). This is the approximate coverage needed with one satellite to insure one observation per 12 hr. To obtain a revisit time of 3 hr, four such satellites are required.

One of the most unusual aspects of this radar design is the high PRF. An ambiguous range is accepted in this design to obtain continuous ground coverage. If there is to be one pulse per beam position and if the satellite is to travel no more than one resolution cell in the scan time, the PRF must be 2300 Hz. This PRF corresponds to an unambiguous range of 65 km. Atmospheric precipitation will extend over a range interval smaller than 65 km; thus, there is no "foldover" of the rain echo and no ambiguity as to the determination of the true range. To achieve quantitative measurements of precipitation echo intensity with a single pulse-per-beam position, some form of coding will be needed on the transmitted waveform.

However, one important antenna design factor must be considered as a consequence of such a high PRF. When the radar echo returns to the satellite, the transmitting beam is looking at some other part of its coverage. Thus, there must be separate receiving and transmitting beams displaced in angle. With an orbiting satellite at an altitude of 400 km, the separation is approximately 3.3 beamwidths at the nadir and 4.7 beamwidths at the edge of the swath coverage. This factor complicates the antenna design, but it should be possible to achieve.

The minimum detectable rain intensity with this system is 2 mm/hr, corresponding to a reflectivity factor Z of 28 dBZ.[1] This could be traded with transmitter power. If the minimum detectable rain is increased to 4 mm/hr, then the average power can be reduced to approximately 5 W.

The most demanding component of the radar is the antenna. The type of antenna needed might be obtained with a frequency-scan linear array feeding a parabolic cylinder, an organ-pipe scan feeding a parabolic torus or a two-dimensional lens, or a mechanically rotating set of four switched paraboloid reflectors. The frequency-scan linear array feed is attractive because of its simplicity. The displacement of transmit and receive beams might be achieved by simply tuning the receiver to a different frequency than the transmitter. The possible limitations of the frequency-scan antenna are the wide bandwidth needed for the 2-μsec pulse and the possible high loss in the transmission line (snake feed).

This design of meteorological radar also has utility for Earth-sensing applications other than the atmosphere; that is, it can be used as a scatterometer or even as a precision altimeter with the inclusion of pulse compression.

Attenuation Considerations

Microwave attenuation is relatively small for a satellite-borne radar compared to that for ground-based radar. In the case of widespread precipitation, the reflectivity factor Z in rain is constant below the melting layer, and it is sufficient to measure Z in the upper portion of the rain to determine rain intensity. In the melting layer, attenuation may be increased perhaps by a factor of 3 over that of rain, but the depth of this layer is only approximately 400 m; thus, the total attenuation is relatively small. Above the 273-K level, the attenuation for snow is one-tenth or less that of rain and can generally be neglected.

In thunderstorms, supercooled water can exist at very low temperatures. However, the

[1] $\mathrm{dBZ} = 10 \log_{10} Z$.

probability of freezing increases with drop size and decreasing temperature. A 1-mm-diameter raindrop has a high probability of freezing at 263 K; a 0.5-mm-diameter raindrop, at 259 K. The greatest attenuation would be expected in a hailstorm in which wet hail can exist at temperatures as low as 258 K. However, the portion of a thunderstorm containing large raindrops or wet hail at temperatures below 263 K is limited to small horizontal regions ($\approx$5 km). In addition, the reflectivity factor, at an altitude of approximately 6 km (temperature approximately 258 K) in severe storms containing supercooled water or wet hail, exceeds 50 dBZ and is approximately the same as that in rain below the 273-K level. Therefore, a measurement of a Z value exceeding 50 dBZ at 6 km is indicative of a severe storm. The attenuation above the 6-km level generally will be relatively small.

In summary, attenuation will not normally be a problem in measuring precipitation reflectivity from a satellite above 6 km (in the case of convective storms) and below the 6-km level (in stratiform), even at wavelengths as low as 8 mm. In limited areas associated with severe storms, there may be moderate attenuation so that the value of the reflectivity at 6 km may be underestimated. More information on attenuation characteristics in the upper portions of severe storms is desirable.

Use of a Geostationary Satellite as a Weather Radar Platform

A satellite-borne weather radar system can be used to study, for the first time, the evolution and migration of precipitation in large-scale tropical storms. However, for truly effective monitoring of precipitation, it is necessary to scan a large area rapidly, perhaps once every 15 min when a storm is developing.

The requirements of large-area coverage and frequent observations dictate the use of a geostationary satellite for the radar system platform. Unfortunately, the orbit height (36 000 km) of such satellites places severe constraints on the performance parameters for a useful system.

A radar system designed for monitoring severe weather conditions should be capable of a horizontal resolution of approximately 10 to 20 km and a vertical resolution of 1.5 km. The total power consumption of the system should be low, and the size and weight of the antenna should be minimized. These considerations dictate the use of a short-wavelength (3 to 9 mm) radar system or even a CO_2 laser system such as the one discussed in the section entitled "Carbon Dioxide Pulsed Continuous-Wave Doppler Radar." However, optical radiation does not penetrate clouds.

Of course, even the millimeter wavelengths are strongly attenuated by atmospheric water vapor and oxygen (see the section entitled "Atmospheric Transmission and Ocean Reflectivity in the Neighborhood of the 5-mm Oxygen Band"), so the operating wavelengths should be carefully selected to be in an atmospheric window. At millimeter wavelengths, the state of the art of microwave device development is not as advanced as at the longer centimeter wavelengths; consequently, some components are not generally as reliable or readily available. However, received sensitivity is approximately the same at 3 mm as at 9 mm, and it is believed that there are no severe technological limitations in using short-wavelength radar.

In fact, existing systems have adequate performance characteristics to permit storm detectability from geosynchronous altitudes. For example, a 3-mm radar system using a 4-mm-diameter antenna could easily detect a tropical storm and measure maximum echo heights on a more or less continuous basis. Such a radar operating at an altitude of 36 000 km would be capable of 1-km vertical resolution at the nadir, which would be adequate for meteorological purposes. However, to achieve a reasonable horizontal resolution of 30 to 40 km requires a beamwidth of approximately 1 mrad, which is beyond the reach of technology in the near future.

The major obstacle in using a geostationary

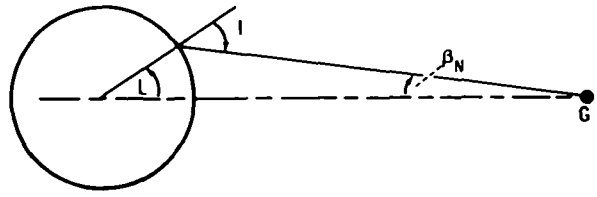

FIGURE 4–3.—Geometry of a geostationary platform, where I is inclination, β_N is nadir angle, and L is latitude.

platform is the problem faced by all side-looking ranging systems (namely, the loss of height resolution when scanning away from the nadir). The geometry of the situation is illustrated in figure 4–3; the relationship between latitude and the apparent inclination of the radar beam from the vertical is shown in table 4–V.

Even with a large 9-m parabolic antenna, which would possibly have an angular resolution of 0.5 mrad, the echo-height ambiguity is greater than +1.5 km for storms at a latitude of only 11°, simply because of geometric effects. Larger uncertainties would obviate the use of the system for measurements of maximum echo height.

It appears that angular resolutions of approximately 0.1 mrad, which could be achieved with the CO_2 lidar discussed in the section entitled "Carbon Dioxide Pulsed Continuous-Wave Doppler Radar," would be required to obtain useful meteorological information at a latitude of 45°. Until the deployment of large linear antenna arrays becomes a practical possibility, the angular resolution problem inherent with microwave systems may essentially limit the use of geostationary platforms to the study of equatorial weather.

TABLE 4–V.—*Variation of Inclination With Latitude*

Latitude, deg	Nadir angle, deg	Inclination from vertical, deg
5.6	1	6.6
11.4	2	13.4
17.3	3	20.3
23.6	4	27.6
30.4	5	35.4
38.0	6	44.0
47.0	7	54.0
59.5	8	67.5

MULTIWAVELENGTH AND DUAL POLARIZATION RADAR FOR WEATHER DETECTION FROM SATELLITES

This section concerns possible improvements of radar capabilities for the observation and measurement of precipitation by the use of two or more operating frequencies. The concept of multifrequency radar has been discussed in the literature (refs. 4–34 to 4–36) and is introduced in this section with the expectation that it will become feasible in a time frame of 5 to 10 yr and may contribute to a more accurate determination of precipitation and clouds.

At present, radars are used to detect precipitation and, in fact, to determine rainfall intensity. These determinations are made by assuming a relationship between rainfall rate and radar reflectivity, which is determined empirically. Unfortunately, there is no unique relationship between these two parameters because they vary with the raindrop distribution in different ways. Different droplet distributions can result in the same rainfall rate and still yield different radar reflectivities. It is therefore necessary to find additional parameters measured simultaneously that will resolve the uncertainty.

A parameter that is being proposed is radar-signal attenuation. It will be shown that, if reflectivity is estimated at both attenuating and nonattenuating wavelengths, rainfall rates can be determined with greater accuracy.

Another parameter is polarization. Larger raindrops are more oblate in shape than smaller raindrops, which are more nearly spherical. It is known that nonspherical raindrops cause depolarization of electromagnetic waves. Thus, although quantitative analysis has yet to be made, it is likely that polarization measurement will improve the knowledge of drop size.

Although all other techniques in this section apply to low-altitude satellites, it is also suggested that information on drop-size spectra can be obtained using a Doppler radar from a geostationary satellite.

Because cirrus clouds result in very small attenuation values but are detectable with ultrasensitive radars, their presence can also be determined by simultaneous measurements of reflectivity and attenuation at different frequencies.

Backscatter, Attenuation, Drop-Size Spectra, and Error Analysis

The weather radar equation can be expressed in the following form (ref. 4–11):

$$P_r=\frac{C_1}{R^2}\sum_i \sigma_i \tag{4–1}$$

where P_r is the power received from a volume of atmosphere containing precipitation, C_1 is a constant containing the fixed radar parameters, R is the radar range, and σ_i is the radar cross section of the ith droplet. The value of σ for an individual water drop of diameter D is given by the Rayleigh expression for cross section

$$\sigma=\frac{\pi^5}{\lambda^4}|k|^2D^6 \tag{4–2}$$

where $d\ll\lambda$, λ is the radar wavelength, and the atmospheric attention coefficient k is

$$k=\frac{m^2-1}{m^2+2} \tag{4–3}$$

where m is the complex index of refraction.

Equation (4–2) is valid for rain if λ is greater than approximately 5 cm. For smaller λ, the more complex Mie theory must be used to obtain the correct radar cross section, which is given by

$$\sigma=\frac{\pi D^2}{4\alpha^2}\left|\sum_{i=1}^{\infty}(-1)^i(2i+1)\,(a_i-b_i)\right|^2 \tag{4–4}$$

where the rain attenuation coefficient α is $\pi D/\lambda$, and a_i and b_i are coefficients that depend on the refractive index and α.

Equation (4–1) can also be written

$$P_r=\frac{C_2|k|^2}{R^2}Z \tag{4–5}$$

where

$$Z=\sum_i N_iD_i^6 \tag{4–6}$$

where Z is the reflectivity factor (conventionally expressed in mm^6/m^3, N_i is the drop-size distribution (m^{-3}), and D is the raindrop diameter (mm). For non-Rayleigh scattering, the effective radar reflectivity factor Z_e should be substituted for Z. The reflectivity η is the backscattering cross section per unit volume and is given by

$$\eta=\frac{\pi^5}{\lambda^4}|k|^2Z_e \tag{4–7}$$

The liquid-water content M_w is given by

$$M_w=\rho_w\frac{\pi}{6}\sum_i N_iD_i^3 \tag{4–8}$$

where ρ_w is water density.

If the radar wavelength is less than approximately 5 cm, the attenuation must be taken into account when clouds and rain exist over the transmission path. Gunn and East (ref. 4–37) give the following expressions for the attenuation due to Mie scattering cross section Q_s, absorption cross section Q_a, and total droplet cross section Q_t for rain and clouds.

$$Q_s=\frac{\lambda^2}{2\pi}\sum_{i=1}^{\infty}(2i+1)\,(|a_i|^2+|b_i|^2) \tag{4–9}$$

$$Q_t=\frac{\lambda^2}{2\pi}(-\mathcal{R}\varepsilon)\sum_{i=1}^{\infty}(2i+1)\,(a_i+b_i) \tag{4–10}$$

and

$$Q_a=Q_t-Q_s \tag{4–11}$$

Calculations of Q_t have been made by Haddock (ref. 4–38) and Medhurst (ref. 4–39), from which estimates of total attenuation can be made. The total attenuation will depend on the number density of raindrops and is represented by

$$\kappa=\int_0^{\infty}Q_t(mD)n(D)\,dD \tag{4–12}$$

where κ is attenuation in dB km^{-1}, Q_t is in units of dB km^{-1} cm^3, and $n(D)$ is the number

of drops per cubic centimeter in the size range dD.

Measurements of attenuation by different investigators show moderately good agreement at various wavelengths between 0.6 and 10 cm (ref. 4–40). In terms of available data, one may conclude that the theory is completely adequate. It is quite likely, however, that the spread in the experimental measurements is explained by the spatial variations in precipitation and drop-size distributions.

Drop-size distributions generally follow the Marshall-Palmer (ref. 4–41) distribution, which is expressed by

$$n(D) = n_0 \exp(-\Lambda D) \qquad (4\text{–}13)$$

where n_0 and Λ are constants. It should be clear from equations (4–6) and (4–12) that, if the exact drop-size distribution is known and the radar beam is filled, the values of radar reflectivity and attenuation are uniquely established. This suggests the possibility that if Z and the attenuation coefficient k are measured at two or more electromagnetic wavelengths, then the drop-size distributions can be determined. This concept is developed by Goldhirsh and Katz (ref. 4–36), in which two radars at different frequencies are used to measure Z and k simultaneously to obtain drop distributions in rain. The analysis of this concept is as follows.

Two simultaneous equations are derived, one representing reflectivity at a nonattenuating wavelength (i.e., S-band) and the other representing attenuation at a shorter (attenuating) wavelength (i.e., X- or K-band). Let P_{10} and P_3 be the powers received from the same precipitation at S-band (10 cm) and X-band (3 cm), respectively. One can then determine that

$$P_{10}(R) = \frac{C_{10} Z(R)}{R^2} \qquad (4\text{–}14)$$

and

$$P_3(R) = \left[\frac{C_3 \eta_3(R)}{R^2}\right] 10 \exp\left(-0.2 \int_0^R k_3 \, dR\right) \qquad (4\text{–}15)$$

where η is normalized reflectivity, the subscripts 10 and 3 refer to radar wavelengths in centimeters, and C is the radar constant for each radar.

Consider now a range interval ΔR equal to, or greater than, the pulse length. If the reflectivity is uniform over ΔR, one can determine the attenuation in terms of the backscattered power.

$$k_3 = \left(\frac{5}{\Delta R}\right) \log\left[\frac{R^2 P_3(R)}{(R+\Delta R)^2 P_3(R+\Delta R)}\right] \qquad (4\text{–}16)$$

One can also find k_3 by substituting equation (4–13) into equation (4–12):

$$k_3 = n_0 \int_0^\infty Q_{t_3}(D) \exp(-\Lambda D) \, dD \qquad (4\text{–}17)$$

in which the unknowns are n_0 and Λ, and $Q_{t_3}(D)$ is total attenuation at 3 cm.

Using the fact that, at S-band, Z depends on the sixth power of D, one can determine that

$$Z_{10} = n_0 \int_0^\infty D^6 \exp(-\Lambda D) \, dD = \frac{N_0 6!}{\Lambda^7} \qquad (4\text{–}18)$$

Note that equation (4–18) is also only a function of n_0 and Λ.

Dividing equation (4–17) by equation (4–18) gives

$$\frac{k_3}{Z_{10}} = \frac{\Lambda^7}{6!} \int_0^\infty Q_{t_3}(D) \exp(-\Lambda D) \, dD \qquad (4\text{–}19)$$

in which the left side is obtained by measurements at the two radar frequencies and the right side is a function only of Λ. Because $Q_{t_3}(D)$ is a known function of m (which depends on wavelength and temperature) and D, the right side is calculable. With Λ determined, n_0 is determined by using equation (4–17) or (4–18). These calculations show that the drop-size distributions can be determined; therefore, the precipitation characteristics in terms of rainfall intensity, radar reflectivity, and also liquid water can be effectively measured. It was only assumed that the radar beam is filled with precipita-

tion particles. The analysis leading to equation (4–19) can be repeated using any other attenuating wavelength.

The determination of Z at S-band requires a knowledge of the radar parameters (e.g., antenna and receiver gain, line losses, etc.) that comprise the radar constant C_{10} in equation (4–14). On the other hand, the determination of the attenuation coefficient k, as given by the form of equation (4–16), requires only a relative power measurement, and it therefore does not require a knowledge of these radar parameters. The measured ratio k/Z may contain errors primarily due to uncertainties in the S-band parameters. A method, which is described here, using two radars operating at attenuating wavelengths (K- and X-bands) as well as an S-band radar for surveillance can overcome this disadvantage. The general idea is to measure the attenuating coefficients over a common zone of uniform rain at both K- and X-bands. Through a comparison of these two independent measurements, the parameters n_0 and Λ may be ascertained as before.

Because the attenuating coefficients have the form of equation (4–17), the ratio k_1/k_3 is given by

$$\frac{k_1}{k_3}=\frac{\int_0^\infty Q_{t_1}(D)\exp(-\Lambda D)\,dD}{\int_0^\infty Q_{t_3}(D)\exp(-\Lambda D)\,dD} \tag{4–20}$$

in which the only unknown on the right side is Λ. The left side is obtained by a measurement of the powers of the two frequencies.

$$\frac{k_1}{k_3}=\frac{\log\left[\dfrac{R^2P_1(R)}{(R+\Delta R)^2P_1(R+\Delta R)}\right]}{\log\left[\dfrac{R^2P_3(R)}{(R+\Delta R)^2P_3(R+\Delta R)}\right]} \tag{4–21}$$

Again, after Λ is determined, n_0 is determined from equation (4–17).

In their initial treatment, Goldhirsh and Katz (ref. 4–36) performed an error analysis to determine the radar accuracy requirements. They estimated the error in Λ for ± 1-dB measurement errors and the rain-rate errors as given by the Marshall-Palmer distribution, assuming $n_0=0.08$. This procedure led to unacceptably large errors in rainfall rate. A more realistic analysis is described in which error bounds were obtained by allowing both Λ and n_0 to vary for selected radar measurement errors. From equations (4–17) and (4–18), one obtains one value for Λ and n_0 for a given set of values of Z and k_3. Taking Z to be in error by ± 2 dB and k_1 and/or k_3 to be in error by 25 percent or ± 1 dB (these are likely to be achievable in practice) allows the calculation of errors first in Λ and n_0, from which one can find rainfall-rate errors. These are shown in figure 4–4, where rainfall-rate error is plotted against actual rain rate for the various pairs of measurements (k_3 and Z, k_1 and Z, and k_1 and k_3). Notice that error bounds, using the k_1 and Z (at 10 cm) and the k_1 and k_3 combinations, are within reasonable limits. The k_3 and Z curves are clearly too large. The upper curve labeled "zero error in k_3" contains only the ± 2-dB error in Z. Clearly, as the radar accuracies are improved, so are the precipitation parameters. As stated later, the goals should be to achieve relative radar accuracies of approximately ± 0.2 dB, which

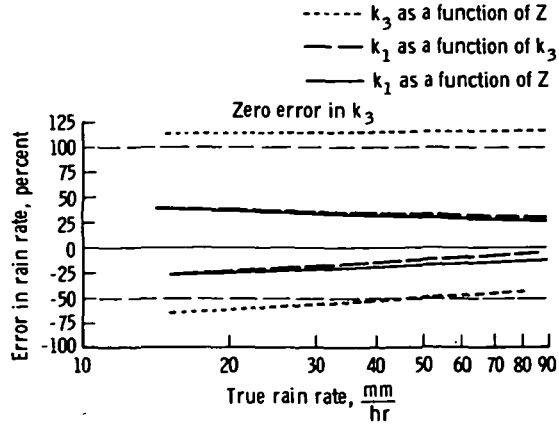

FIGURE 4–4.—Error in rain rate plotted against true rain rate for three pairs of measurements with a ± 2-dB error in Z and a ± 25-percent error in k (except the top curve, which contains only the ± 2-dB error in Z).

yield quite acceptable accuracies in drop sizes, liquid-water contents, and rain rates.

Determination of Optimum Wavelengths

The preceding discussion indicates that the attenuating wavelength should be as short as possible so that large attenuations per unit length (needed to obtain high accuracy from these multiple wavelength measurement methods) are obtained. It must be noted that, if the wavelength is too short, maximum penetration into the rain becomes a problem.

Two factors determine penetration. As the wavelength becomes shorter, the cross section of the rain increases as $1/\lambda^4$ in the Rayleigh region and somewhat slower in the Mie region. At the same time, the attenuation caused by the return from the rain at the maximum range of interest is increasing as $1/\lambda$. These two opposing factors cause the radar return to first rise with decreasing wavelength, go through a maximum, and then decrease. As the required penetration distance decreases, the wavelength at which maximum return is observed will shift toward shorter wavelengths. This is due to the decreasing influence of the attenuation factor as range decreases.

For a satellite-borne meteorological radar, the optimum wavelength will be much shorter than for a ground radar. Rain rarely extends above 10 km, except for large thunderheads and severe storm regions. Characteristic path lengths through rain will then be on the order of 10 km (or slightly more) to allow for normal incidence resulting from scanning.

In addition, the intensity of precipitation usually decreases with increasing altitude above the 273-K level. This relationship puts the least attenuating portion of the rain path closest to the radar and the most reflecting portion of the path farthest from the radar. This fact further enhances the ability to use short wavelengths.

In contrast to this situation, a ground radar should have a working range an order of magnitude greater than 10 km to measure rain over a satisfactory area. Furthermore, it is desirable to observe less dense rain beyond rain cores. As a result, radars at X-band, C-band, and even S-band are favored.

To determine optimum attenuating and nonattenuating wavelengths for the satellite case, the variation in the relative radar return from a resolvable element of rain seen through a uniform column of rain of length r is calculated by graphic means. The range of possible operating wavelengths is then determined by selecting the wavelength interval around the wavelength of maximum return that is not too far down from maximum to yield a good SNR.

The calculation can be done for a 10-km rain path length and for two rainfall rates (8 and 0.8 mm/hr). The range of operating wavelengths will be taken as those that are less than 16 dB down from the peak return at the greatest rainfall rate.

To calculate radar return against wavelength, observe that the return radar power P_r is given by

$$P_r = \frac{P_t G_t A_r V}{(4\pi R^2)^2}(\eta 10^{-2\alpha r})$$

$$= \frac{\frac{P_t 4\pi}{\Delta\phi^2} A_r (\Delta r R^2 \Delta\phi^2)}{(4\pi R^2)^2}(\eta 10^{-2\alpha r})$$

$$= \frac{P_t A_r \Delta r}{4\pi R^2}(\eta 10^{-2\alpha r}) \qquad (4\text{–}22)$$

where

P_t = transmitter power
G_t = radar antenna gain
Δr = range resolution
A_r = radar antenna cross section
R = radar range
r = range through rain
$\Delta\phi$ = antenna beamwidth
α = rain attenuation coefficient
V = volume of resolvable element of rain
η = rain reflectivity
λ = operating wavelength

The condition $A_r = 2\pi\lambda$ makes the beamwidth equal at all wavelengths. Then, the same resolvable element of rain will be observed at all wavelengths.

The input data are the values of η and α as a function of λ as given by Mitchell (ref. 4–42). These data, plotted with λ as a parameter and rainfall rate as the independent variable, were replotted with λ as the variable (for rainfall rates of 8 and 0.8 mm/hr). The resulting graphs of $\lambda^2\eta e^{-2\alpha r}$ for these two rainfall rates are given in figure 4–5 with $r=10$ km.

The optimum wavelength calculated by using the previously described method varies from approximately 1.8 cm (for 8 mm/hr) to 0.8 cm (for 0.8 mm/hr). If the attenuating wavelength return is allowed to fall no more than 10 dB below the peak return for 8-mm/hr rainfall, then the attenuating wavelength can be as short as 0.8 cm for the 8-mm/hr case. The wavelength shortens to approximately 0.5 cm for the 0.8-mm/hr case.

The nonattenuating wavelength for 8-mm/hr rainfall is approximately 5 to 6 cm (C-band) for which the response is less than 10 dB down from the peak response. However, for 0.8-mm/hr rainfall, the nonattenuating wavelength must be shorter. For $\lambda=3$ cm, the response is down 18 dB from the peak response of 40 dB for 8-mm/hr rainfall and $\lambda=1.8$ cm.

As noted before, the attenuating wavelengths are in the Mie region. This fact has an important consequence. If the nonattenuating and attenuating wavelengths were both in the Rayleigh region, measurement at two wavelengths would produce all the data obtainable. The Z value and attenuation at any other Rayleigh wavelength would be predictable from the measurements at the first two wavelengths.

However, if the attenuating wavelengths fall in the Mie region, it will become apparent from the following discussion that measurements done at other wavelengths permit the determination of additional parameters specifying drop-size distribution.

To determine whether the scatter is in the Mie region at 1-cm and 8-mm/hr rainfall, refer to the rain parameter diagram (ref. 4–43) in figure 4–6. Here, D_0 is the median

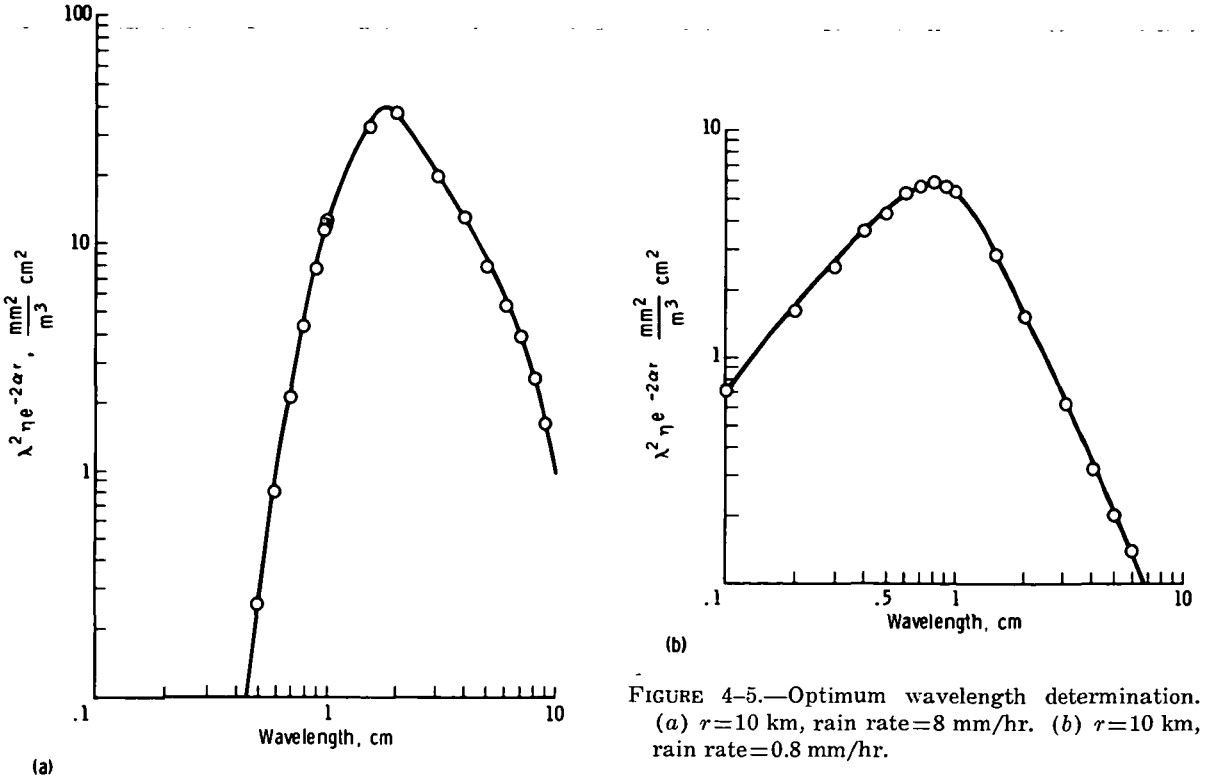

FIGURE 4–5.—Optimum wavelength determination. (*a*) $r=10$ km, rain rate=8 mm/hr. (*b*) $r=10$ km, rain rate=0.8 mm/hr.

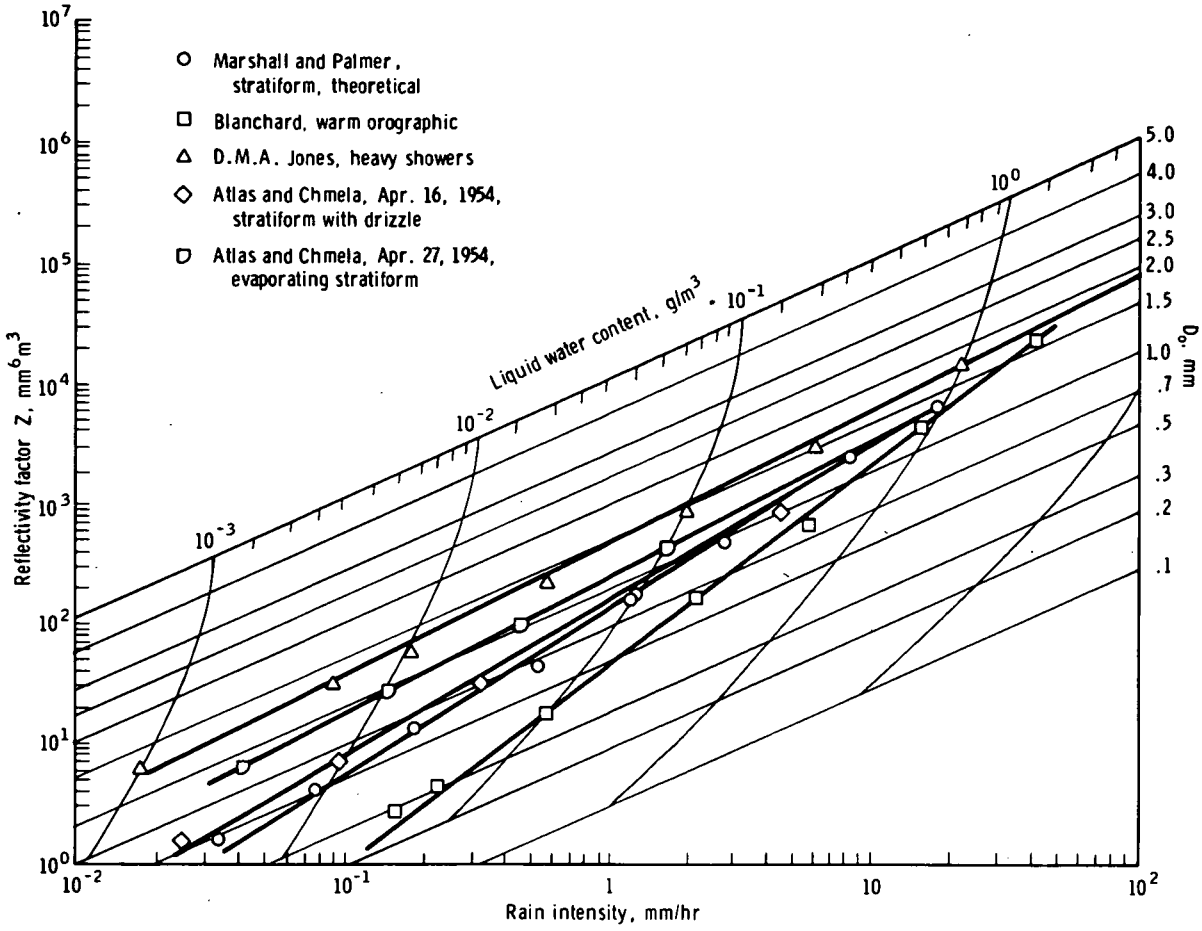

FIGURE 4–6.—Relationship of reflectivity factor Z, liquid water content, median diameter of the volume D_0 and rain intensity for a mean size spectrum (ref. 4–43).

diameter of the volume. For a rain intensity of 8 mm/hr, this diameter varies from 1.0 to 1.5 mm, depending on rain type.

Using an average value of $D_0=1.25$ mm, then $\alpha=\pi D/\lambda$ is 0.4 at $\lambda=1$ cm. Referring to a plot by Gunn and East (ref. 4–37) of the deviation of the attenuation and backscatter cross sections from Rayleigh (as a function of λ and α), it is seen that for $\alpha=0.4$ and $\lambda=1$ cm, the backscatter cross section is still very close to its Rayleigh value (fig. 4–7). However, the attenuation is about seven times greater than its Rayleigh value. This is a substantial deviation. Therefore, the scatter is in the Mie region for attenuation but not for target cross section. The attenuation constant is approximately 1.5 dB/km, giving a total attenuation increment of 3 dB for a 2-km path increment.

For 0.8-mm/hr rainfall, a shorter wavelength is required to get a substantial attenuation increment in 2 km. For this rate, the shortest practical attenuating wavelength is approximately 0.5 cm. Referring to the nomogram again, one sees that the median drop size is approximately 0.8 mm and α equals 0.58. Figure 4–7 shows that the attenuation differs from Rayleigh by a factor of 4.7. This is also a substantial deviation, as in the 8-mm/hr case.

If more operating wavelengths in the Mie region are available, simultaneous equations can be set up that take into account the deviation from Rayleigh of both cross section

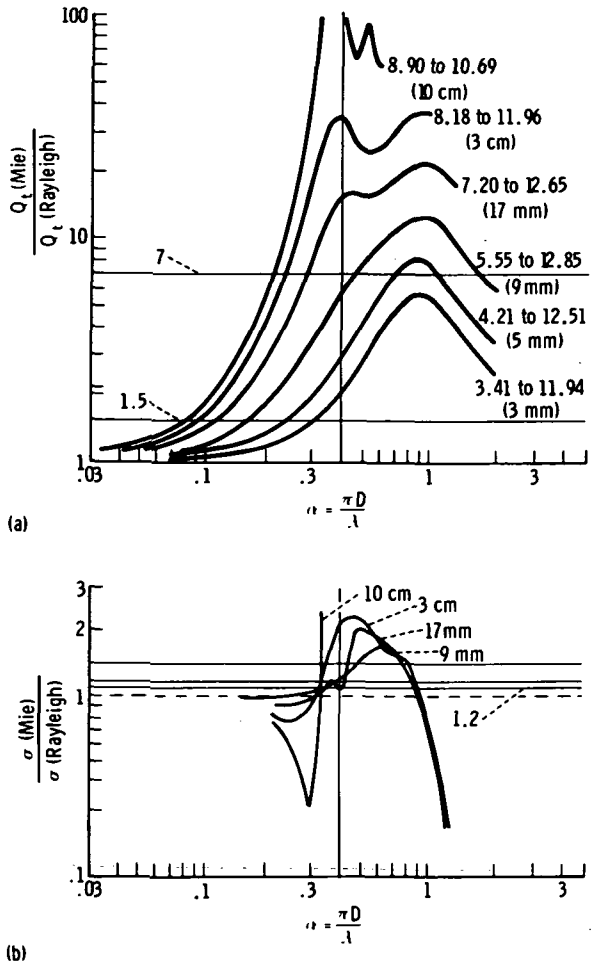

FIGURE 4–7.—Ratio of actual attenuation and actual backscattering to that given by the Rayleigh approximation for water at 291 K. (*a*) Ratio of actual attenuation to Rayleigh attenuation approximation. The complex refractive index and the wavelength (in parentheses) are shown for each curve. (*b*) Ratio of actual backscattering to Rayleigh backscattering approximation.

and attenuation. More parameters describing the deviation of the distribution from standard must be obtained to prevent overconstraint of the equation set. Indeed, the set of simultaneous equations is an approximation of an integral equation in which a finite number of data points are available. The standard distribution is then the preliminary estimate of the solution of the integral equation by recursion (successive approximations).

The number of radar frequencies used should obviously be at a minimum for a satellite application. However, the preceding discussion shows that wavelengths of approximately 0.5, 1, and 6 cm are needed to effectively measure rainfall intensities from 8 to 0.8 mm/hr. X-band and S-band may have to be added for very high rainfall rates (16-mm/hr and greater). Only a pair of these frequencies need to be operated simultaneously. The selection of a 0.5-cm wavelength must be avoided because it falls on the O_2 absorption band. However, a slightly different wavelength that still provides a satisfactory choice may be selected. Operation very close to an O_2 line in the absorption band may be advantageous. By selection of the correct wavelength, a situation may be obtained where the radiation is not greatly absorbed at high altitudes, but is heavily absorbed at low altitudes. This situation occurs because the O_2 line is narrow at high altitudes and therefore does not greatly attenuate the operating wavelength, which is offset from the line center as shown in figure 4–8.

At low altitudes, pressure broadening widens the O_2 band and attenuation becomes

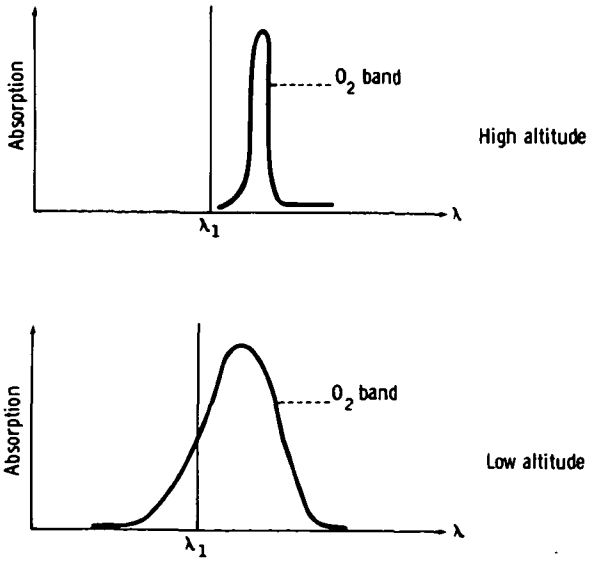

FIGURE 4–8.—Relationships of operating wavelength λ to the O_2 60-GHz absorption band.

very large. In the active microwave case, this may constitute a technique for eliminating ground clutter and thereby remove the swath-width limitation caused by the presence of ground clutter. In fact, by using a series of operating frequencies close to the center of an O_2 line, it may be possible to sound the atmosphere for precipitation without ranging, as in the passive case. This would be useful when large incident angles are used to obtain wide swath widths.

It should be mentioned that Atlas and Ulbrich (ref. 4–34) found that, in any case, the attenuating wavelength should be shorter than 1.5 cm so that the extinction coefficient will be independent of wavelength. This restriction may be a source of error when X-band must be used as the attenuating wavelength for extremely high rainfall rates.

Calibration

To increase the accuracy of the two-wavelength method for measurement of liquid-water content, it is desirable to calibrate the system. This calibration can be done by measuring the total attenuation through the rain path at selected calibration locations. Because the satellite radar has measured the total attenuation from maximum echo height to the Earth surface at the attenuating wavelengths, an independent measurement of the total attenuation will reveal any systematic errors in attenuation measurement that cause the two independent measurements to differ. The errors can then be removed or calibrated out, thereby improving the accuracy of the satellite system.

Primary calibration measurements would be made by measuring the intensity of the attenuating wavelength at ground stations. However, to get calibrations over a wider range of meteorological conditions, a second method is proposed that involves reflection of the satellite radar beam from the ocean surface.

The possibility of accurate determination of ocean-surface reflectivity depends on the unusual fact that the reflectivity of a smooth seawater surface is constant to a high degree of accuracy for angles of incidence up to approximately 40°. This condition occurs because circular polarization is composed of equal amounts of the linearly polarized components in the plane of incidence and normal to the plane of incidence. Brewster's angle for seawater occurs at an approximately 90° angle of incidence (i.e., 83° at 9 GHz and 283 K). The two linear polarizations deviate from their common reflectivity at vertical incidence, one increasing and the other decreasing. When Brewster's angle is near grazing, the rates of increase and decrease are approximately equal for a region around normal incidence. The average increase and decrease, observed by use of circular polarization, is almost constant in this region.

In figure 4–9, the emissivity E for smooth seawater is plotted for E_{par} (parallel), E_{per} (perpendicular), and E_{cir} (circular) polarization. The emissivity is almost constant to 40°. For a smooth surface, the reflectivity is 1 minus the emissivity; therefore, the plot indicates that the reflectivity for circular polarization is also almost constant to approximately 40°, which makes circular polarization applicable to radar measurements.

To apply this observation to the measurement of the molecular temperature of an

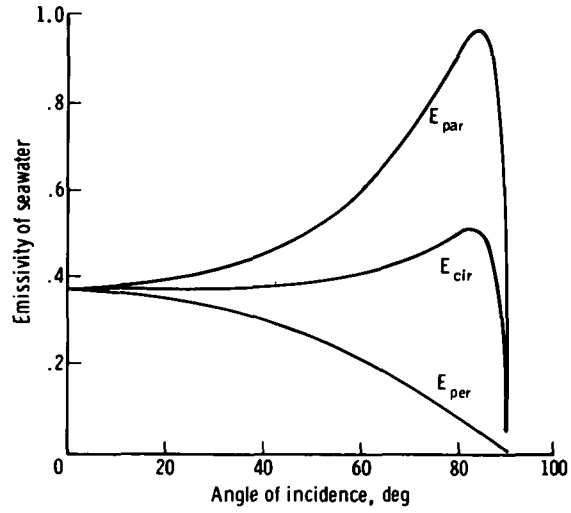

FIGURE 4–9.—Emissivity of smooth seawater plotted against angle of incidence for parallel, circular, and perpendicular polarizations.

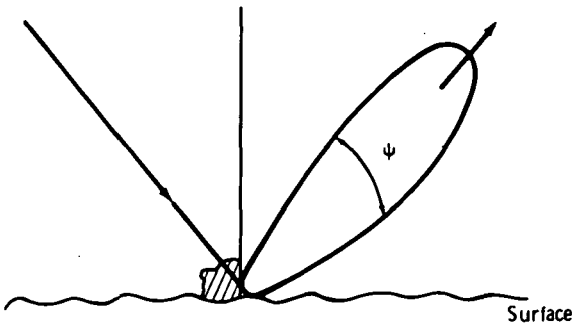

FIGURE 4–10.—Forward scattering by surface facets.

actual rough sea, the facet theory of reflection can be used. According to this theory, the incident beam will be scattered by the facets into a forward-scattered beam formed by specular reflection from the facets (Kirchhoff scattering) as shown in figure 4–10.

In addition, there is a pattern of diffracted radiation emanating in all other directions as shown by the crosshatching in figure 4–10. Obviously, the facet theory will be of little help in predicting the magnitude of the diffracted radiation. This diffuse radiation is scattered from irregularities having a size comparable to the radar wavelength (i.e., small ripples in the case of X-band).

In determining seawater temperature, it is assumed that all the power is in the forward-scattered lobe and that the power diffracted out of this lobe could be neglected. Because the sea-surface slopes do not exceed approximately 20°, all the reflected rays will be reduced by the same reflectivity factor. The reflectivity factor for all the power in the lobe should then be the same as that of a ray incident on a smooth seawater surface and normal to the surface.

A test of the soundness of this simple model of the scattering process was provided by measurements of the sea-surface temperature.[2] With 1- to 1.5-m waves, the radiant temperature of the sea computed using this simple model was higher than the measured radiant temperature by 0.7 K. The radiometer was a third-generation instrument with an accuracy of approximately 0.1 K (ref. 4–44).

The error is of the correct sign, if the model does not account for reflectivity outside the main lobe. The extra reflectivity not accounted for by the facet model (Kirchhoff approximation) will cause the model to predict a radiant temperature that is in error by $\Delta T = T_M \Delta P$, where T_M is the radiant temperature in the main lobe and ΔP is the fraction of the power scattered out of the main lobe. Then $\Delta P = 0.7/280 = 0.0025$. That is, 0.35 of the power is scattered into the main lobe (at 2.65 GHz), and 0.0025 of the power is scattered out of the main lobe. The total diffracted scattered power is then 21.5 dB below the main lobe power.

To clarify this rationale, note that maximum wave slopes lie between 10° and 20°, depending on sea state; therefore, the main lobe has a beamwidth of 20° to 40°. The ratio of the solid angle subtended by the main lobe (¼ rad) to the hemispherical solid angle subtended by the diffracted energy is 25 (or 14 dB). The average diffracted power density should then be down from the main-lobe power density by -21.5 dB $+(-14$ dB$) \approx -36$ dB.

Fortunately, Moore (ref. 4–45) gives the reflectivity of water near vertical incidence. The data are given for a lake rather than the sea, but they serve to estimate the magnitude of that reflectivity. Moore's data at 3.8 GHz show that the radar return is down approximately 35 dB at 30° from nadir. It then seems reasonable that the diffracted power density is approximately 36 dB down from the main-lobe power density in the case of the sea, thus showing that the radiometer results are consistent with the experimentally determined reflectivity patterns of the sea.

The preceding analysis also shows that energy diffracted out of the main lobe may be neglected in calculating the main-lobe pattern with little resulting error.

The measurement technique then consists of directing a radar beam straight down and

[2] Ho, W.; Hidy, G. M.; VanMelle, M. J.; and Love, A. W.: Radiometric Observations of Sea Temperature at 2.65 GHz. North American/Rockwell Space Center, Thousand Oaks, Calif., unpublished data.

moving it away from the nadir both along-track and crosstrack while measuring the magnitude of the radar return. To use these data for obtaining rainfall attenuation, an alternate expression for the radar return will be used that involves the directivity of the power reradiated from the surface and the illuminated surface area.

The two methods of received power calculations (radar cross-section analysis and target reflectivity pattern analysis) are compared in equations (4–23) and (4–24), where P_d is power density from radar antenna, P_{re} is power reradiated in radar direction, and P_{rec} is power received by radar. The radar cross-section analysis is

$$P_d = \frac{P_t G_t}{4\pi R^2} e^{-\alpha R} \qquad (4\text{–}23a)$$

$$P_{re} = \sigma \frac{P_t G_t}{4\pi R^2} e^{-\alpha R} \qquad (4\text{–}23b)$$

$$P_{rec} = \sigma \frac{P_t G_t A_r}{(4\pi R^2)^2} e^{-2\alpha R} \qquad (4\text{–}23c)$$

The target reflectivity pattern analysis is

$$P_d = \frac{P_t G_t}{4\pi R^2} e^{-\alpha R} \qquad (4\text{–}24a)$$

$$P_{re} = A_s G(2\phi) \frac{P_t G_t}{4\pi R^2} e^{-\alpha R} \qquad (4\text{–}24b)$$

$$P_{rec} = A_s G(2\phi) \frac{P_t G_t A_r}{(4\pi R^2)^2} e^{-2\alpha R} \qquad (4\text{–}24c)$$

where

P_t = radar transmitter power
G_t = radar antenna gain
R = radar range
α = attenuation coefficient
σ = radar cross section
A_s = illuminated surface area
A_r = radar antenna cross section

The reflectivity pattern of the surface is $G(\Psi)$, where $\Psi = 0$ on the main-lobe axis. When the radar beam is at depression angle ϕ, then Ψ along the line of direction to the radar is 2ϕ, as shown in figure 4–11.

It is assumed that the pattern rotates as ϕ changes, without changing shape. This holds true because, if the facet theory is accepted, the slope distribution of the sea will produce the same distribution of power around $\Psi = 0$, regardless of ϕ.

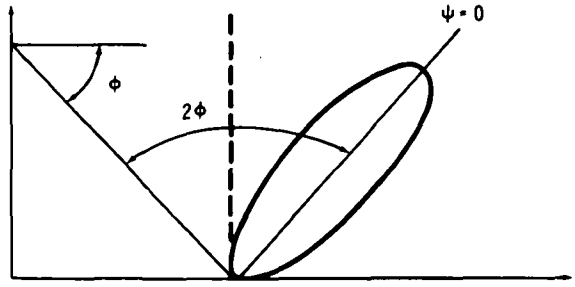

FIGURE 4–11.—Reflectivity pattern of the surface.

By definition, $\sigma = \sigma^\circ A_s$, where σ° is the target reflectivity. By setting equation (4–23b) equal to equation (4–24b) and canceling terms, one determines that $\sigma = G(2\phi)A_s$. Therefore, $\sigma^\circ = G(2\phi)$. In the special case of the radar looking at the nadir, $\Psi = 2\phi = 0$ and

$$\sigma^\circ = G(0) = \rho_{av} \frac{4\pi}{\Delta\psi^2} \qquad (4\text{–}25)$$

where ρ_{av} is the average reflectivity of the surface.

If the surface reflectivity ρ is unity and the surface is perfectly smooth, the beamwidth of the reflected power becomes the beamwidth of the illuminating antenna and

$$\sigma^\circ \rightarrow G_t = \frac{4\pi}{\Delta\phi^2} \qquad (4\text{–}26)$$

If for circular polarization, ρ is independent of Ψ over the range of incident angles and facet slopes under consideration, then the incident power density P_{inc} multiplied by the integral of $G(\Psi)$ over the hemisphere will be equal to simply ρP_{inc}; that is,

$$P_{inc} \int_0^{2\pi} G(\Psi)\, d\Omega = \rho P_{inc} \qquad (4\text{–}27)$$

where $d\Omega$ is the differential solid angle and

$$\int_0^{4\pi} G(\Psi)\, d\Omega \approx \int_{\Omega_a} G(\Psi)\, d\Omega = \rho \qquad (4\text{–}28)$$

where Ω_a represents the main lobe of the an-

tenna. This relationship is true even if $G(\Psi) \rightarrow G_t(\Psi)$ when the surface becomes smooth.

Then, the return power measured by the radar as it scans its beam around the nadir outside the main lobe can be written

$$P_r(\phi) = ka(\phi) G(2\phi) \exp (-2\alpha h \sec \phi) \quad (4\text{–}29)$$

where h is altitude and $a(\phi)$ is a resolvable element of area (depending on the radar antenna beamwidth $\Delta\phi$ and on range resolution Δr). Therefore

$$G(2\phi) = \frac{P_r(\phi) \exp (2\alpha h \sec \phi)}{ka(\phi)} \quad (4\text{–}30)$$

and

$$\int G(2\phi)\, d\Omega = \int \frac{P_r(\phi) \exp (2\alpha h \sec \phi)}{ka(\phi)} d\Omega = \rho \quad (4\text{–}31)$$

This is an integral equation which can be solved for α.

The preceding discussion presents only an outline of a possible measurement method. A thorough error analysis is needed to establish feasibility.

Once attenuation for the total path is known for a series of measurements (using fixed ground stations and the sea surface) for a large selection of rainfall rates and types, a calibration factor can be used to adjust the total attenuation measured by the radar. The calibration factor is adjusted so that the one-way and the radar attenuations agree statistically for that set of observational data.

Cross-Polarization for the Determination of Drop-Size Distribution and Melting Layer Height

Electromagnetic waves propagating through precipitation are depolarized by the nonspherical shape of the particles. At frequencies sufficiently high so there is an appreciable variation of the dipole moment as a function of orientation, the cross-polarization can be measured and used as an indicator of the type or size of precipitation particles. Typically, at frequencies of 9 GHz or higher, depolarization is sufficiently strong to be used for studying atmospheric precipitation effects.

Rain appears as an anisotropic medium to short-wavelength radio waves. Raindrops assume an oblate spherical shape as they fall, and their axes are oriented within a relatively small range of canting angles. Consequently, a differential phase shift and attenuation exists between horizontally and vertically polarized fields, and this differential refractivity causes a change in polarization along the path. A radar, viewing a rain cell at a wavelength such that the cell is penetrated, has returns that depolarize as a function of the intensity and type of precipitation.

The strong dependence of radar echo on drop diameter enables a multiwavelength radar to measure parameters of the drop-size distribution. Larger drops are more oblate than smaller drops. Therefore, the ratio of the cross-polarized return provides an additional measure of the drop-size distribution. In effect, the number of measurements is doubled, allowing some determination of the departure from an exponential distribution to be assessed.

For a medium containing particles with a number density n, the attenuation coefficient is

$$k = k_0 \left(1 + \frac{2\pi n}{k_0^2} \mathcal{R}eF_s\right) \quad (4\text{–}32)$$

where F_s is the parallel-polarized forward-scatter amplitude and $k_0 = 2\pi/\lambda$. Considering the particles as dielectric oblate spheroids having a vertical semiaxis c and a horizontal semiaxis a, the difference in index of refraction for vertically and horizontally polarized waves is

$$\Delta k = k_0 \left\{ n \frac{4\pi a^2 c}{3} \left[\frac{\epsilon - 1}{(\epsilon - 1) a^2 c I_c + 2} - \frac{\epsilon - 1}{(\epsilon - 1) a^2 c I_a + 2} \right] \right\} \quad (4\text{–}33)$$

where ϵ is permittivity and I_c and I_a are integrals for the oblate spheroid (ref. 4–46). Using a Laws and Parsons drop distribution and the drop ellipticity relation of Spilhaus (ref. 4–47), the differential phase change per unit length through 50-mm/hr rainfall at 3-cm wavelength is approximately 7×10^{-5} rad/m. For the two-way propagation through a 9-km rain cell, the calculated phase change between horizontal and vertical polarization components is approximately 70°.

The previous discussion indicates that the use of circular polarization is advantageous for meteorological measurements by satellite radar. The principal return is received by transmitting circular polarization and receiving the opposite sense. Measurement of the two senses of circular polarization could be made by an appropriate combination of two linear polarization returns. In any event, two receivers are needed.

The depolarization of the radar return from a cell within a region of precipitation is produced by two causes. The first cause is the propagation through the anisotropic medium, with its different attenuation and refractivity to horizontal and linear polarization. The second cause is the variation in radar cross section with polarization caused by particle ellipticity in the particular cell being observed. These causes can be quantified in a straightforward manner. The depolarization ratio is the ratio of received power having the same sense of circular polarization as the transmitted power to the power received with the orthogonal-sense circular polarization. The ratio is

$$\chi(z)=\left|\frac{1-C(z)\,\exp\left(-j2\int_0^z \Delta k\,dz\right)}{1+C(z)\,\exp\left(-j2\int_0^z \Delta k\,dz\right)}\right|^2 \qquad (4\text{–}34)$$

where z is the distance from the radar to the cell being observed, $C(z)$ is the polarization reflection ratio at the cell, and j is equal to $\sqrt{-1}$. For a spherical particle, C is unity.

Measurement of χ as a function of z (a relative power measurement) thus affords a determination of the complex index of refraction. From this information, and assuming a relationship of drop ellipticity with size, one can determine the parameters of the drop-size distribution.

The choice of frequencies of operation is consistent with the earlier discussion of drop-size distribution using a multiwavelength radar. The difference in dipole moment is appreciable where the path attenuation is significant. In fact, the depolarization measurement can be used in the same manner as the attenuation measurement in a two-wavelength determination of drop-size spectrum. This additional constraint permits the determination of the three parameters in a three-parameter drop-distribution model. This determination permits closer approximation of the actual drop-size distribution.

To show this effect, a depolarization parameter $p_d(\lambda)$ is defined such that

$$P_{2t}=[1-\exp\,(-\int p_d(\lambda)\,dl)\,]P_{1i} \qquad (4\text{–}35)$$

where P_{1i} is the incident power in polarization 1, P_{2t} is the transmitted power in polarization 2, and l is the path length. The parameter P_{2t} is related to the scattering matrix of the raindrop. The expression for l, analogous to equations (4–30) and (4–31), is

$$p_d(\lambda)=\sum_D Q_{12}(D,\lambda)N_D \qquad (4\text{–}36)$$

where attenuation Q_{12} is derivable from the scattering matrix. Note that $p_d(\lambda)$ goes to zero as λ approaches infinity.

If it is assumed that both senses of circular polarization are attenuated equally and reflected equally by the resolvable element of range at range R, the ratio of powers F_p in the two polarizations at range R (at the attenuating depolarizing wavelength) is

$$F_p(R)=1-\exp\left[-\int_0^R 2p_d(\lambda,R)\,dR\right] \qquad (4\text{–}37)$$

and at range $R+\Delta R$ is

$$F_p(R+\Delta R) = 1 - \exp\left[-\int_0^R 2p_d(\lambda, R)\, dR - 2p_d(\lambda, R)\, \Delta R\right] \quad (4\text{–}38)$$

Solving for $\exp[-2p_d(\lambda, R)\Delta R]$, one obtains

$$\frac{1-F_p(R+\Delta R)}{1-F_p(R)} = \exp[-2p_d(\lambda, R)\, \Delta R] \quad (4\text{–}39)$$

Thus, the value of the depolarization parameter at range R is derived in terms of the measured quantities $F_p(R)$ and $F_p(R+\Delta R)$. The three parameters in a three-parameter drop-size model must then be set to satisfy equation (4–36) as well as equations (4–30) and (4–31).

Measurements of cross-polarization can also be used to assess the melting layer. The strong depolarization produced in the melting layer is caused by the irregular shapes of particles as they melt and re-form. Indications are (ref. 4–48) that the polarization properties of the melting layer, when added to the principal-polarization echo-strength data, permit a good assessment of the layer depth. Experimental measurements have shown the strong polarization properties of the melting layer. Hendry and McCormick (ref. 4–49), using a dual-channel-polarization diversity radar operating at 1.8-cm wavelengths, observed the depolarization in rain, snow, and the melting layer.

By transmitting circular polarization and receiving both senses of circularly polarized returns, Hendry and McCormick observed a relative level of cross-polarization approximately 10 dB below the main returns. This level is approximately 20 dB greater than the cross-polarization of moderate snow and corresponds to the cross-polarization of rain at rates of approximately 50 mm/hr. Note that these levels are ratios of returns and not the absolute levels of the returns. The melting level can be distinguished from rainfall because the cross-polarization level remains approximately constant with depth, whereas in rainfall the cross-polarization increases with depth. Thus, a high depolarization that is constant with depth is an indicator of the melting layer, and an increasing depolarization is a characteristic of rainfall. The rate of increase of the cross-to-copolarization power is a function of the rainfall rate.

Implementation of polarization measurements does not impose new or unusual requirements on the satellite radar. The antenna must be designed to have good polarization separation, with two output channels having essentially identical radiation patterns. A typical requirement for the antenna-integrated cancellation ratio for each channel is 26 dB; this value is representative of good antenna design. The cross-polarization ratio of 5-mm/hr rainfall at 1.8 cm is under 20 dB; therefore, measurements at this rainfall rate should be possible with good antenna control. By using a dual-polarization feed and two receivers, the radar can be used to produce any polarization desired for an experiment.

The use of polarization measurements extends beyond the inference of meteorological phenomena. Circular polarization is widely used for weather clutter cancellation in the navigation and traffic control radars for marine and air services. There is a need for much more data, particularly data on a global scale, that show the statistics of depolarization. From a comprehensive measurement program, enough data could be extracted to develop reliable models for radar return depolarization so that radar designers and users could take appropriate account of weather effects on the subclutter visibility that can be expected from circular polarization.

Using Doppler Techniques to Measure Drop-Size Spectra From a Geostationary Satellite

A geostationary satellite has the capability of measuring the Doppler spectrum of precipitation resulting from differential fall rate. Because this satellite is almost stationary with respect to the Earth, the satellite or the Earth motion produces only a very small Doppler shift. If such a Doppler radar

observes precipitation, there is therefore practically no smearing of the fall-rate spectrum, as in the case of lower orbit satellites (such as discussed in the section entitled "Satellite-Borne Radar With Doppler Capability").

The drop-size distribution and liquid-water content cannot be directly inferred from the fall-rate spectrum because of the component of the wind vector projected on the line of sight. However, if the reflectivity of the rain is also measured, both the drop spectra and wind component can be obtained. This determination is accomplished by varying the assumed wind-velocity component and calculating the drop-size distribution that would be present for each assumed velocity. Only one assumed velocity will yield a size distribution for which the reflectivity is the observed reflectivity. Then, the wind component, size spectrum, and liquid-water content are known.

This procedure must start at maximum echo height. Then, as the size distribution of each increment in range is computed, the corresponding attenuation for the cell can be calculated. The total attenuation from maximum echo height to each successive cell can then be used to obtain the true reflectivity from the measured reflectivity. This technique is subject to the same restrictions on swath width as discussed elsewhere in this report.

Cirrus Cloud Detection

Clouds are generally not detected by ground-based microwave radars. Exceptions are very dense cumulus clouds and cirrus clouds. As an example, figure 4–12 shows a cirrus cloud detected on a high-sensitivity S-band radar. In this photograph, the cirrus cloud extends between 6 and 12 km in altitude and between 10 and 86 km in range. The inside of the cloud appears black because of the "slicing" circuitry that was used to obtain a measure of reflectivity of the clouds. The strongest return in the cloud was in the 76- to 79-dBm slice, which corresponds to approximately 20 dBZ ($dBZ = 10 \log_{10} Z$).

Definitive results from radar studies of cirrus clouds are not available, although tools for such research are presently in existence. The fact that cirrus clouds are visible on sensitive radar comes from the rather large size of the ice particles. Jones (ref. 4–50) gives the following expression for the density of water droplets in ice clouds:

$$n(D) = [-2.67 M_t^{-1/3}(D - 0.25)] \times 10^{4.1} \quad (4\text{–}40)$$

for droplet diameters ≥ 0.25 mm, where M_t is total ice content in grams per cubic meter. Note that these particles are in the millimeter region, compared to liquid cloud drops that have peaks in their distributions at less than 10 μm. Although further research is required in this area, satellite-borne ultrasensitive radar might well be used to study the occurrence, density, and thickness of cirrus clouds.

The multiwavelength radars discussed in this section have an obvious applicability in cirrus detection. Water clouds attenuate microwave frequencies much more than ice clouds. As an example, at approximately 263 K and for $\lambda = 0.9$ cm, the attenuation is 1.2×10^{-3} dB/km/g/m^3 compared to 3×10^{-3} dB/km/g/m^3 for water and ice, respectively, for one-way paths. With the difference in attenuation being two orders of magnitude, it may be possible to distinguish between water and ice clouds. Similarly, this technique might also be applied in distinguishing between rain and snow.

SATELLITE-BORNE RADAR WITH DOPPLER CAPABILITY

In the past few years, as previously mentioned, satellites have provided meteorologists with day-and-night monitoring of cloud systems on a global scale. Geostationary satellites are currently observing cloud formation over large regions on Earth, and the observations are frequently repeated so that the movement of cloud systems can be detected and measured. Orbiting satellites operate from a much lower altitude, are capable of better resolution, and can also carry a greater variety of experiments.

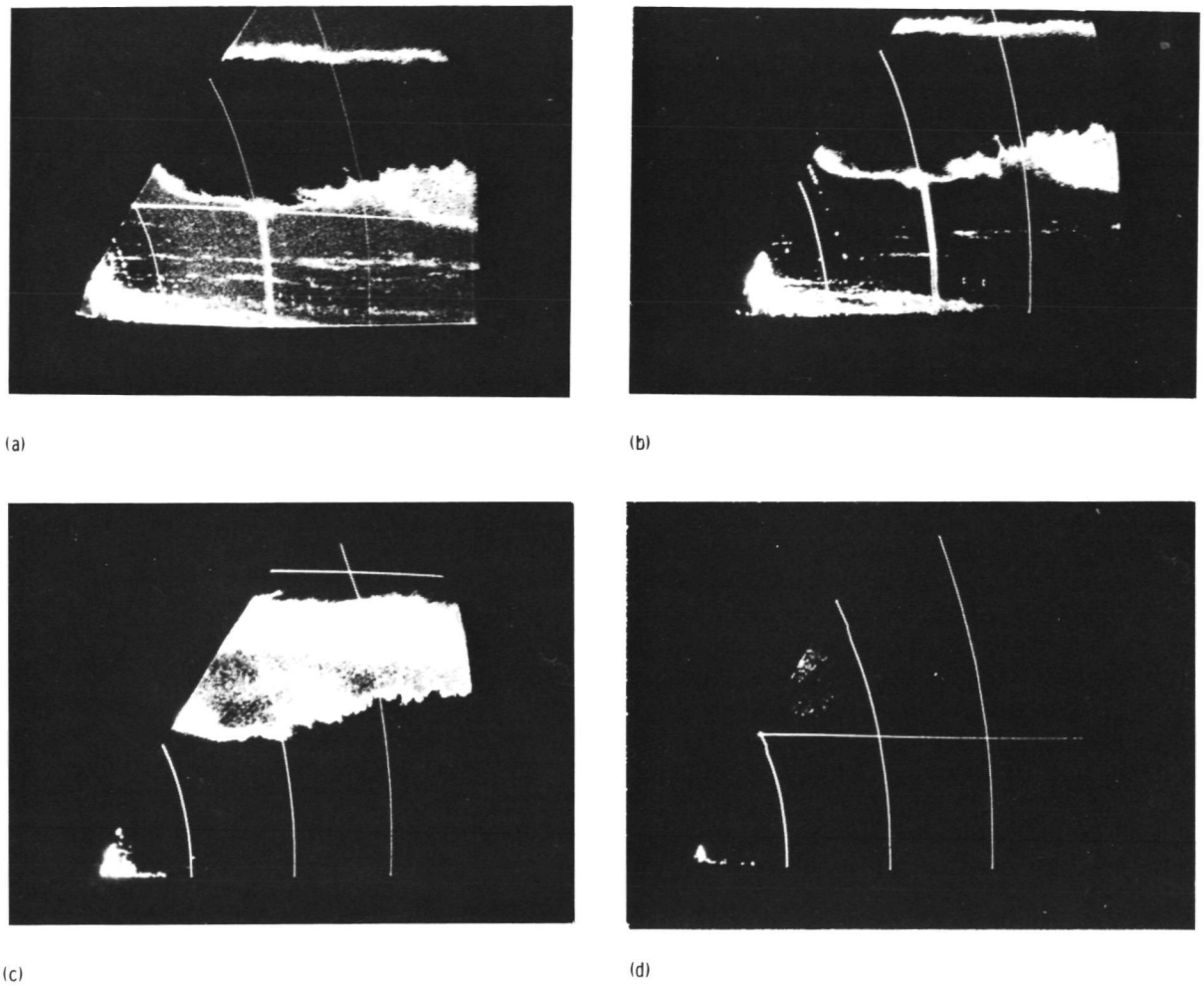

FIGURE 4–12.—Cloud and clear-air echoes with a slicer azimuth of 270°. (*a*) Window: 100 to 103 dB. (*b*) Window: 94 to 97 dB. (*c*) Window: 76 to 79 dB. (*d*) Window: 61 to 64 dB.

Indeed, meteorological satellites are now widely accepted as indispensable tools for the monitoring of cloud and cloud-top temperature with infrared sensors either from low-altitude orbits with substantial swath or from a geostationary orbit.

Passive microwave radiometers, which are now being flown on several Nimbus experiments, have also demonstrated excellent operational capabilities. However, such systems do not have the unique ranging capability of an active microwave system (radar).

None of the existing meteorological satellite capabilities include the monitoring of vertical and horizontal distribution of precipitation inside large meteorological systems (hurricanes; intertropical convergence zones; large, persistent squall lines; etc.), which could be achieved by use of a satellite-borne radar.

The constant day-to-day monitoring of the precipitation system associated with a hurricane over regions where there are no ground-based or shipborne radars is certainly one of the most significant examples of the use-

fulness and uniqueness of the satellite-borne meteorological radar.

Also, the observation of severe storm continental mesoscale systems could improve severe storm forecasts and warnings. These systems tend to lie along extended bands (squall lines) but are usually contained within a zone 200 to 400 km ahead of the cold front surface position (ref. 4–11). The squall-line zones can sometimes extend for more than 1400 km along the front and their duration can exceed 1 day, although the squall lines themselves have lifetimes of several hours and lengths of less than 300 km. It should be noted that even in the continental United States, where radar observations can easily be made, the monitoring of such precipitation systems over areas of a size comparable to that provided by satellite coverage would require the difficult compilation of data provided by a large number of ground-based radars.

A comprehensive study (ref. 4–22) on the feasibility of satellite-borne radars for meteorological observations was done by Stanford Research Institute under NASA sponsorship. This study concluded that such a facility had very little practical value for the mesoscale study of precipitation mainly because of the limited coverage and low sampling rate allowed by that system. However, the observation of large-scale, persistent meteorological features by satellite does not require the time and space resolution that is common to ground-based radars observing this type of weather over much smaller areas. This section will be mainly concerned with the possible use of Doppler radar techniques for the monitoring of windfields inside such precipitation systems, using precipitation particles as tracers for air motion.

In the case of a satellite placed in a low-altitude orbit, the use of Doppler radar techniques is made difficult by the very large groundspeed of the satellite. The major effect is a natural spread in the Doppler because of the different radial velocities of scatterers in various parts of the beam. It is evident that this effect is decreased for narrow beams and that it is a function of the beam scanning angle and direction. As an example, using parameters applicable to the proposed system, one finds that the maximum standard deviation of the Doppler spectrum due to this effect is 6 m/sec for a satellite groundspeed of 6.9 km/sec.

It must be noted that the satellite speed combined with the conical beam scan (which will be proposed in this section) also constitutes a useful capability, because the same target will be "seen" from different directions for which the target speed will result in different Doppler velocity components. Because this report will consider the possible application of Doppler radar methods for the measurements of atmospheric motion, it is appropriate to present the following brief review of the subject.

Doppler Radar Methods

Doppler radars provide a means for monitoring the radial velocity of targets (approaching or receding motion). If atmospheric targets are moving at the surrounding airspeed, such as in the case of precipitation particles, the method can easily be extended to the measurement of atmospheric air motion. Precipitation particles, or manmade targets ("chaff"), released in the atmosphere are considered as tracers for the air motion.

A single Doppler radar provides observations and mapping of the radial velocities of precipitation particles only. The information has the form of a spectrum of radial velocities that is produced by the distribution of particle velocities inside the scattering volume. In the case of turbulence, the spectrum is influenced by the space variability of the motion. In this case, the size of the scattering region controls the spread or variance of the Doppler spectrum; that is, the ability of the radar to effectively resolve these motion scales. This method has been used for observing the vertical velocities of precipitation particles with the radar beam pointed vertically so that particle size or air vertical velocity can be derived from the observed data. For example, cloud physics pa-

rameters, such as growth by deposition and riming, have been observed in winter storms. Horizontal wind can be probed by a method involving complete 360° scanning of a tilted radar beam, essentially providing different radial velocity components of the same wind, if the radar is inside a widespread precipitation system where the wind is horizontally homogeneous. These techniques are not applicable to the study of the structure and kinematics of localized convective storms, which basically require the simultaneous use of several Doppler radars installed at different locations and observing the same storm. In this method, the radar beams cooperatively scan the same region and thereby provide several radial components of the particle velocities, so that two- or three-dimensional velocity can be observed (ref. 4–51).

A dual-Doppler-radar system that provides two-dimensional velocity estimates is the first and most important step in this direction. In this method, two Doppler radar beams scan a common atmospheric region, a tilted plane intersecting the line joining the two radars. A set of such planes provides three-dimensional scanning of the region of interest.

At any point in a tilted plane, two different radial velocity components can be observed from the radial velocity samples acquired by the two radars. Two noncollinear radial velocity estimates can then be used to compute the two-dimensional velocity vector at that point on the plane.

Removing the contribution due to terminal velocity from the observed radial velocities, and assuming again that particles are moving at the airspeed, leads to the expression of the components u' and v' of the three-dimensional air velocity projected on the tilted plane. Inspection of the vector windfield can reveal patterns of convergence and vorticity of the observed motion field that are useful for descriptive modeling of storm kinematics.

If the convergence of the motion field in the tilted plane is computed, then the velocity component w' normal to the plane can be evaluated from the following equation of continuity for a noncompressible fluid:

$$\frac{\partial u'}{\partial x'} + \frac{\partial v'}{\partial y'} + \frac{\partial w'}{\partial z'} = 0 \qquad (4\text{–}41)$$

In this equation, x' and y', respectively, are rectangular coordinates parallel and perpendicular to the baseline. The use of the equation of continuity, which relies on steady-state kinematic conditions in convective storms, is very important because it virtually removes the need for a third radar, which would bring more complexity. The dual-Doppler-radar method has been presented and discussed in several papers (refs. 4–51 to 4–54), and an example of the motion fields observed by this method is shown in figure 4–13.

It must be noted that, although single-Doppler-radar measurements yield limited information on wind, fields of mean Doppler velocities may generate characteristic features (signatures) that can, under certain circumstances, be related to significant meteorological events, such as vortex motion (ref. 4–55).

An example of how a display of single-Doppler velocity fields can be used to infer mesocyclone characteristics is shown in figures 4–14 and 4–15, where a PPI sector

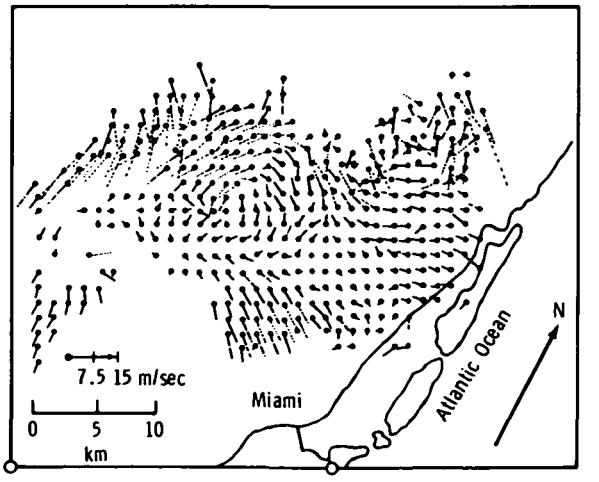

FIGURE 4–13.—Example of a motion field observed with a dual-Doppler-radar system inside a convective storm; plane tilt, 14°.

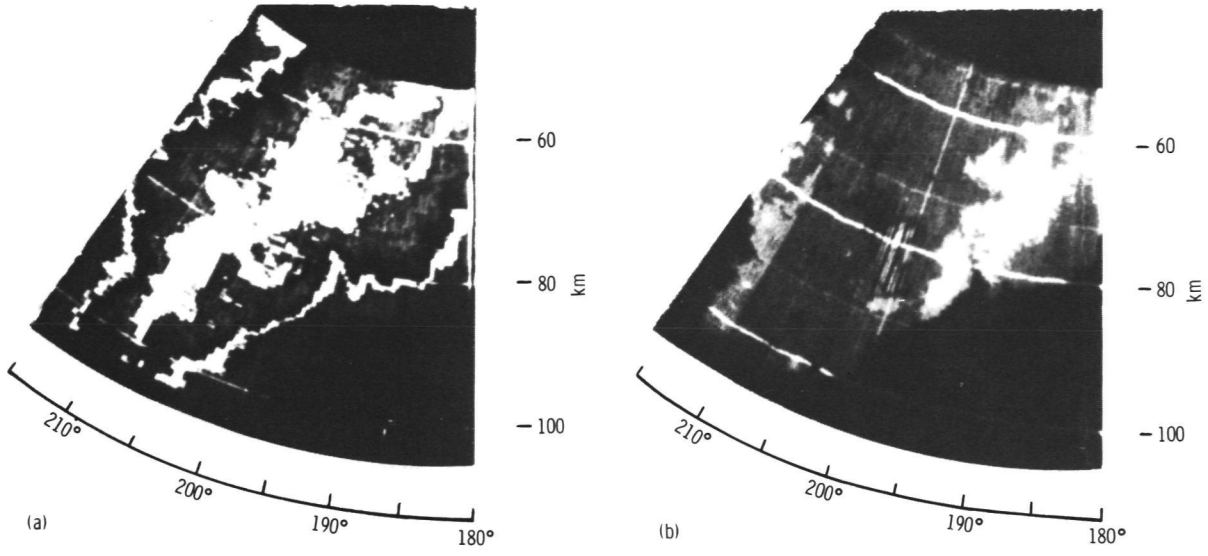

FIGURE 4–14.—Plan-position-indicator reflectivity and isodops. The elevation angle is 1.9°; range marks are at 60, 80, and 100 km. Reflectivity categories are dim (<21 dBZ), bright (21 to 31 dBZ), black (31 to 44 dBZ), dim (44 to 57 dBZ), and bright (>57 dBZ). Velocity categories are dim (<13 m/sec), bright (13 to 21 m/sec), and brightest (>21 m/sec). Positive radial velocities are angularly strobed. Mesocyclone-type signature between 193° to 203° and 75 to 90 km. (*a*) Plan-position-indicator reflectivity. (*b*) Plan-position-indicator isodops.

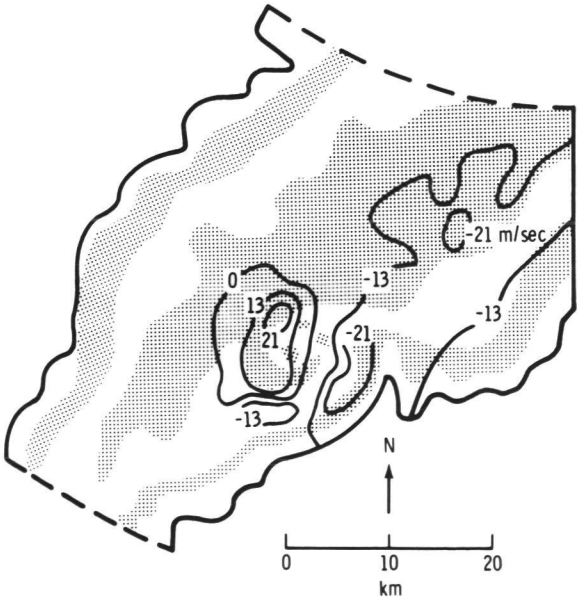

FIGURE 4–15.—Overlay of figure 4–14 reflectivity and radial velocity fields; tilt, 1.9°.

displays constant Doppler velocities (isodops) and constant echo power resolved with a 10-cm Doppler radar (0.8° beamwidth, 1-μsec pulse width). In figure 4–14(*b*), PPI trace brightness is used to indicate Doppler magnitude in the form of isodops. Figure 4–14 shows the echo pattern obtained simultaneously with the radial velocity field. Note the "hooklike" feature, which suggests mesocyclonic circulation. The isodop and reflectivity fields are overlayed in figure 4–15 to facilitate pattern comparison. It can be shown that circularly symmetric cyclonic motion forms a symmetric couplet of closed isodops with an equal number of lines encircling positive and negative velocity maximums. The nearly symmetric isodop pattern (fig. 4–15) indicates cyclonic rotation consistent with the reflectivity pattern. It can be shown that a signature pattern for circularly symmetric convergence is identical to a vortex pattern, but rotated by 90°. The apparent reflectivity spiral in the figures suggests convergence, a view supported by the clockwise angular displacement of isodop maximums about the vortex center.

In short, it is noted that single Doppler isodop displays may indicate storm structure, and it is expected that displays of satellite-derived radial velocity could likewise exhibit similar dynamic features.

Although pulse Doppler radars have been used extensively for research, there is no radar operated by the National Weather Service that is equipped for Doppler measurements. However, methods for using single Doppler radars are now being effectively developed so that the operational use of the Doppler radars may become effective in the next few years.

Doppler Radar Signal Processing

The velocity information contained in the Doppler radar signals can be expressed by a spectrum of speed related to the distribution of radial velocities of the precipitation particles in the pulse volume. The spectrum width is due to the actual statistics of precipitation particle velocities; however, in the case of a moving platform, substantial smearing of the spectrum can also originate from the change of radial velocities throughout the finite angular size of the radar beam. Such smearing is overwhelming in the case of a fast-moving radar, so that spectrum width may have little meteorological significance. However, the spectrum first moment or "mean Doppler" can contain meteorologically significant information. This estimate of the spectrum first moment can be obtained by simple processing systems, such as the signal covariance estimator, which is now used in ground-based Doppler radar applications (refs. 4–53 and 4–54). Also, quantitative mean Doppler estimates of slightly larger variance can be obtained by a simple device measuring the signal phase change (ref. 4–56).

The covariance estimator allows the tracking of the mean Doppler through any of the frequency ambiguity regions associated with the signal sampling rate (radar pulse repetition rate). Moreover, it is not biased by the occurrence of noise, which only increases the uncertainty or variance of the estimate. The only limitation of the covariance estimator for an accurate mean Doppler measurement occurs when spectrum width approaches the spacing (i.e., PRF) between frequency ambiguity lines.

Satellite-Borne Radars

An important limitation in the application of ground-based radar measurements to mesoscale and global-scale studies is the lack of mobility and the very limited coverage of the radars. The installation of radar systems aboard an airplane allows observations over much larger regions on Earth. If such methods for monitoring precipitation and possible atmospheric motion are implemented aboard an orbiting satellite, observations over the entire Earth will be provided.

The applicability of Doppler radar techniques to satellite instrumentation is made difficult by the high groundspeed of the satellite, which causes a Doppler frequency shift much larger than that due to the ground velocity of precipitation particles moving with the atmospheric wind.

In the case of a vertically pointing beam for which the axis is perpendicular to the satellite trajectory, the satellite motion does not produce a mean Doppler shift, but results in a smearing of the Doppler frequencies because of the finite size of the beam inherent in any antenna system. Note that it has been stated earlier that only the smearing of the spectrum limits the accurate recovery of mean Doppler because the velocity ambiguity region can be specified by beam position and satellite speed.

The limited coverage of a vertically pointing beam carried by an orbiting satellite will scarcely be acceptable as the means for probing large meteorological systems. It is indeed necessary that the satellite provide complete coverage on the Earth surface, at least in regions that are significant in terms of occurrence of precipitation systems. That coverage must be of the same nature as the cloud coverage provided by the infrared and visible sensors flown in orbiting satellites (such as NOAA–2 and NOAA–3) or geo-

stationary satellites (such as ATS–3 or GOES).

This report presents an example of two possible methods that would provide satisfactory solutions.

Doppler Radar Wavelength Selection

To determine the characteristics of a Doppler radar, it is necessary to specify certain meteorological objectives. First, assume a range resolution of 1 to 2 km and a 2-km "angular" resolution to provide meteorologically useful data on mesoscale systems and a vertical velocity resolution of 1 m/sec.

Range and velocity can be simultaneously resolved with a pulse Doppler radar. Velocity resolution ΔV is related to wavelength λ and dwell time $N_s T_s$ as

$$\Delta V = \frac{\lambda}{2N_s T_s} \qquad (4\text{–}42)$$

where N_s is the number of echo samples used to derive a mean Doppler estimate and T_s is effectively the sample spacing (i.e., pulse repetition time). The maximum velocity V_m that a pulsed Doppler radar can unambiguously resolve is given by

$$V_m = \pm \frac{\lambda}{4T_s} \qquad (4\text{–}43)$$

Velocities in excess of V_m will result in Doppler spectrum aliasing, so that the mean Doppler velocity estimates may pass discontinuously from $-V_m$ to $+V_m$ for two adjacent radar sample volumes. However, by assuming spatial continuity of velocity, these ambiguities can be resolved, provided that a mean velocity at an initial location is correctly identified. To remove range ambiguities, T_s must be sufficiently large so that all echoes associated with one transmitted pulse are received before the echoes associated with the following pulse. The value T_s is given by

$$T_s = \frac{2R_m}{c} \qquad (4\text{–}44)$$

where R_m is the range to the most distant target. Combining equations (4–43) and (4–44)

$$\lambda = \frac{8R_m V_m}{c} \qquad (4\text{–}45)$$

where c is the velocity of propagation. Satisfying simultaneous requirements of large V_m and R_m necessitates long wavelengths. However, because the wavelength must be kept small to maintain good angular resolution with reasonable antenna diameters, R_m and V_m must be limited to the smallest acceptable values. However, to achieve an accurate mean velocity estimate, $2V_m$ should be large compared to the Doppler spectrum width so that there is no significant folding bias. For low-orbiting side-looking radar moving at a groundspeed of 7 km/sec and having 0.3° beamwidth, the 6-dB velocity spectrum width will be approximately 34 m/sec. A value of $2V_m = 75$ m/sec will provide the requisite accuracy, assuming precipitation plus ground clutter targets would be received over a range interval of approximately 55 km (fig. 4–16). Therefore, substituting $R_m = 55$ km and $V_m = 37.5$ m/sec into equation (4–45) yields $\lambda = 5.5$ cm for the

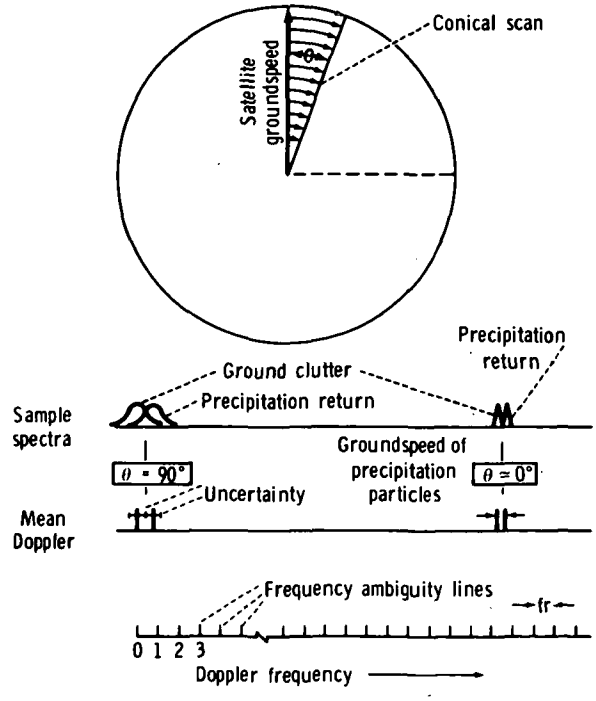

FIGURE 4–16.—Variation of the Doppler spectrum position and width with the scan angle θ.

minimum wavelength necessary to eliminate range ambiguity within the spatial limit of R_m. Thus, a minimum wavelength of 6 cm appears acceptable for satellite-pulsed Doppler operation.

In addition to Doppler considerations, the choice of the operating wavelength always may be conditioned by a compromise between the contradictory requirements of (1) narrow beams with practical-size antennas and (2) acceptable penetration of the radar signals in the precipitation systems. In this preliminary investigation, it appears that a decrease of the wavelength below X-band (3.2 cm) drastically increases the attenuation of the radar signals and therefore reduces the penetration of the signal and the significance of the quantitative data. On the other hand, a wavelength longer than 5 or 6 cm no longer improves the signal penetration performance significantly, and yet does result in an increased antenna size to meet the same angular resolution requirements.

The optimum wavelength lies somewhere between 3 and 5.6 cm. At a 3.2-cm wavelength, the beamwidth provided by a 12-m dish is 0.2°, and the two-way attenuation in a 15-km path in a 25-mm/hr rainfall is 13 dB. For the same conditions, but at a 5.6-cm wavelength, the beam size is 0.3°, and the attenuation becomes 2.6 dB, which is substantially less than in the 3-cm-wavelength case. It must be noted that, in the case of Rayleigh scattering, and neglecting attenuation, the sensitivity of a 3-cm-wavelength radar with respect to a 5.6-cm-wavelength radar is improved by 5 dB for the same angular resolution and overall radar characteristics.

A continuous-wave (CW) Doppler radar has no unambiguous velocity limit, and the maximum resolvable velocity is dictated by receiver bandwidth. Equation (4–42) applies equally well to a CW Doppler, except that there is continuous transmission during the dwell time $N_s T_s = T_{dw}$. For sufficiently small λ, T_{dw} can be made sufficiently small without changing ΔV so that the entire transmission can occur in a time that permits range resolution equivalent to that of a pulsed Doppler (i.e., 1 km). Solving equation (4–42) for λ, with $T_{dw} = 6.7$ μsec, yields $\lambda = 13$ μm.

Thus, a CW CO_2 Doppler radar (i.e., $\lambda \approx 10$ μm), transmitting for a duration of 6.7 μsec, should provide a velocity and range resolution of 1 m/sec and 1 km, respectively, and a Doppler radar at either of two wavelengths (6 cm and 10 μm) must be considered. It is interesting to note that wavelengths between these two limits would not meet the requirements of resolution without ambiguities.

Low-Altitude Orbit Satellite

The capability of a low-orbit satellite can be compared to NOAA–2 and NOAA–3 observational capabilities, which provide monitoring of large-scale time-persistent precipitation systems. With a Sun-synchronous polar orbit, the satellite acquires observational data for approximately noon or midnight at any point on Earth.

The low-altitude orbiting satellite method presented here is associated with difficult technological problems in extracting the Doppler velocity information from the backscatter signal, but it seems to be the only practical answer to a complete Earth coverage with acceptable resolution.

Low-altitude orbiting satellites are generally flown in an inclined (polar) orbit. This type of orbit provides excellent coverage in tropical regions where large, time-persistent meteorological systems occur. This section discusses a possible application based on the use of a circular quasi-polar orbit with a 58° inclination angle. The satellite altitude is 556 km with an orbit period of 1.6 hr. The angle of inclination of 58° [3] is chosen to maximize the latitude to which complete Earth surface coverage is obtained. In the example discussed here, the radar scans every surface region between ±68° latitude at least once in 12 hr (fig. 4–17).

The swath coverage across the orbital trajectory is obtained by rotating a tilted nar-

[3] A Sun-synchronous orbit could also be accepted.

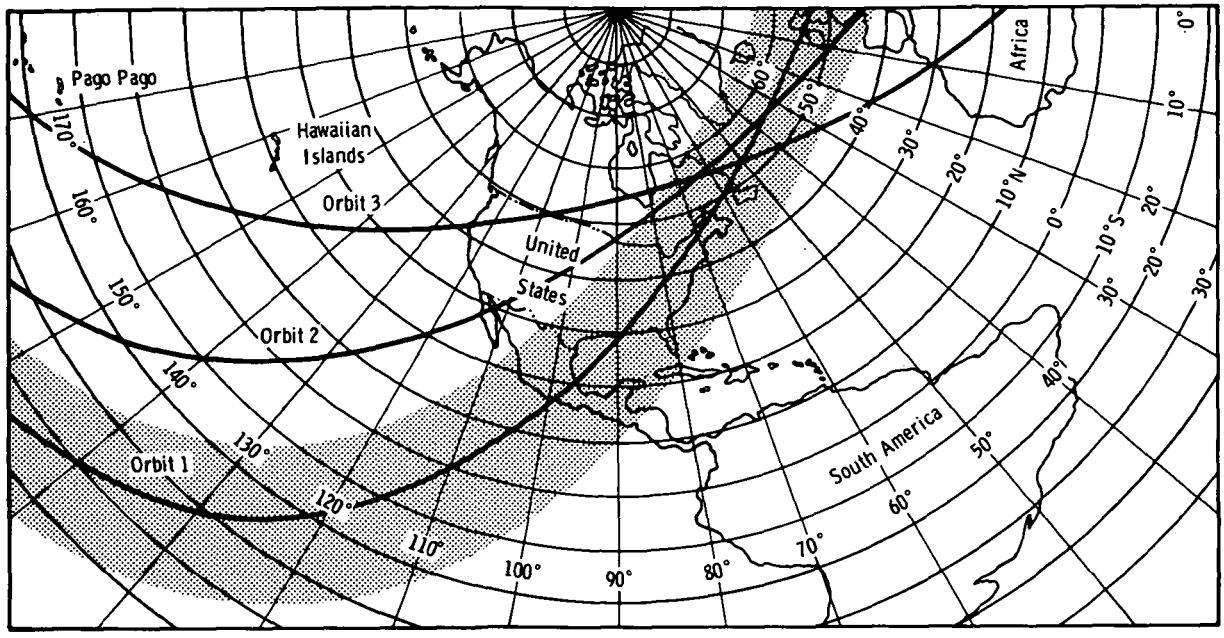

FIGURE 4–17.—Example of radar coverage available from an orbiting satellite at an altitude of 556 km. The orbit is quasi-polar with an inclination angle of 58°. The swath coverage is obtained by spinning a satellite carrying a tilted beam about a vertical axis.

row antenna beam around a vertical axis. The total swath width, which is approximately 2000 km, is obtained with a beam nadir angle of 60°. The configuration of the satellite in orbit and the swath geometry are shown in figure 4–18.

In the case of a pulse radar and an antenna radiation pattern free of any side lobes, the expected radar return is indicated in figure 4–19. There is a region contaminated by the ground or sea clutter that increases with the beam size. If the beam size is too large, the ground clutter occupies a substantial range interval; and the beam is no longer filled by the atmosphere in the "ground clutter free" part of the return. The maximum beam size that still allows substantial beam tilting for atmospheric observation can be determined as a function of the cross-swath range and the altitude h of the satellite, or the grazing angle γ.

For small beams, range gating of the radar signals in the range interval where only atmospheric targets occur will provide an effective means for probing the horizontal and vertical distribution of atmospheric targets (fig. 4–19). The process involved in range gating effectively selects scattering regions controlled by the radar pulse width. Small grazing angles, such as presented here (20°), favor horizontal resolution; the vertical resolution is controlled mainly by the beam size. With a 0.3° beam, a 20° grazing angle, and a 1000-km slant range, the vertical resolution is approximately 5 km; and, because of beam tilt, the horizontal resolution in the direction of the beam is approximately 2 km. The range gating will not affect the range resolution across the beam, which is still controlled only by the beam size.

However, the relationship between the mean altitude and horizontal position of the range gates depends on the beam tilt and limits complete atmospheric coverage. The simultaneous use of several contiguous, narrow beams (which is proposed later) can improve the coverage capability.

If there are no side lobes in the radiation

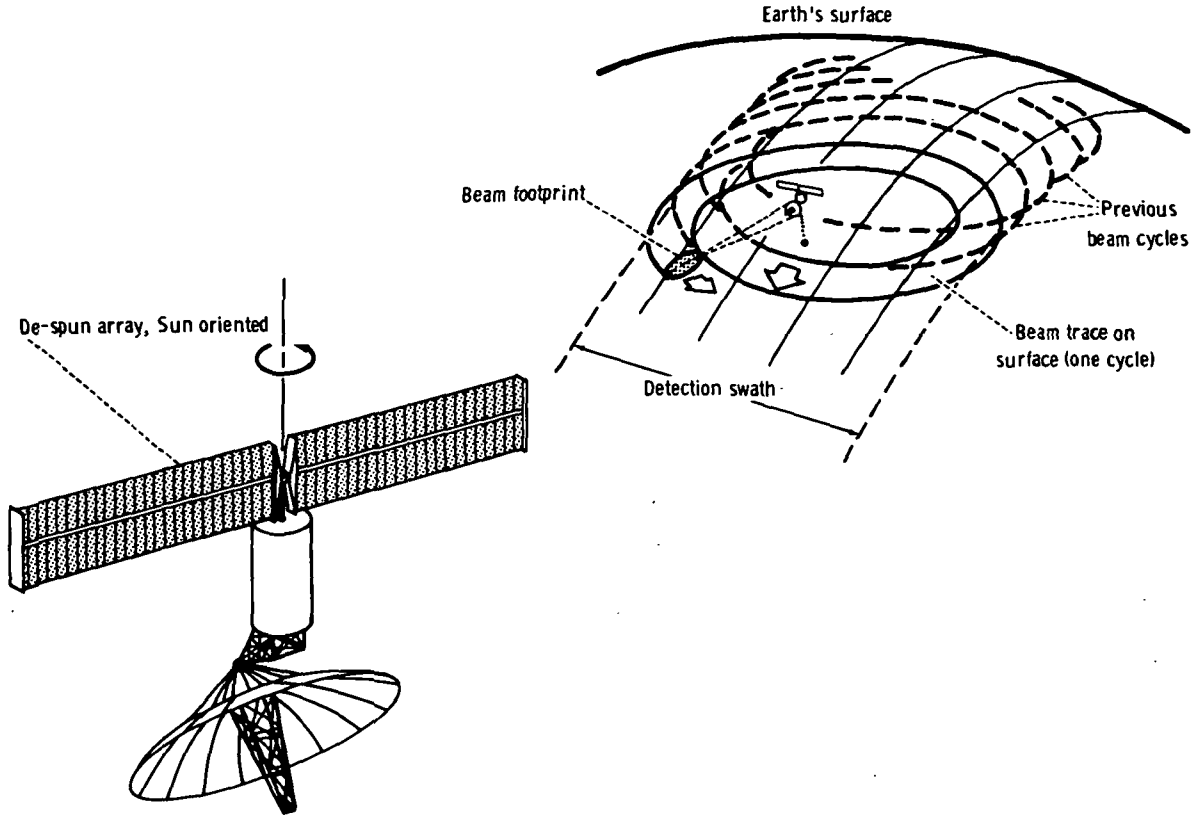

FIGURE 4–18.—Illustration showing the swath of an antenna producing beams that rotate about a vertical axis. The beam footprint is actually composed of a set of adjacent beams distributed radially.

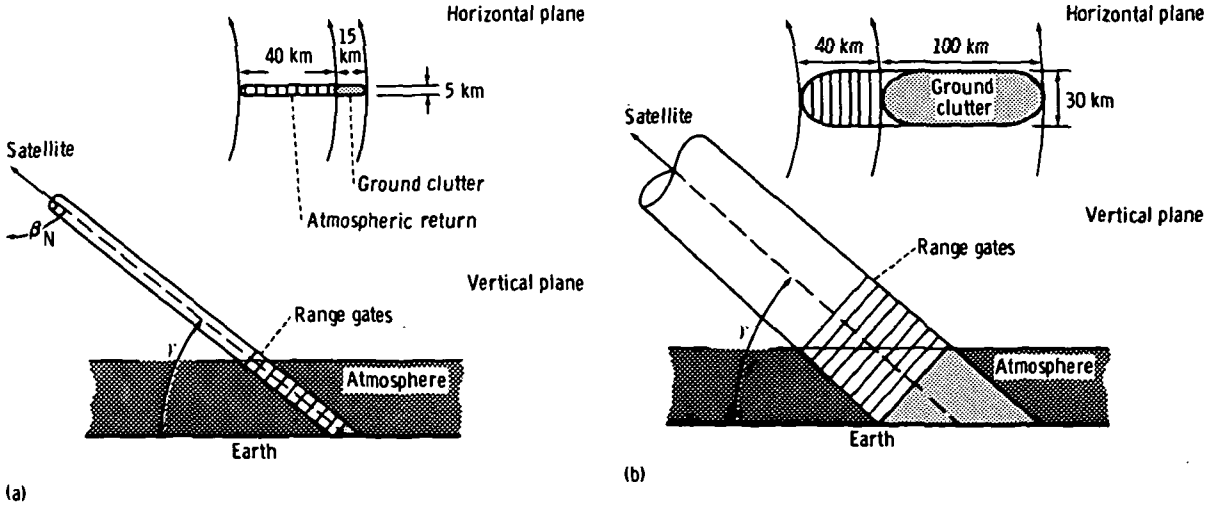

FIGURE 4–19.—Influence of the beam size on the importance of ground clutter and the filling of the beam by atmospheric returns. (*a*) Narrow beam (0.3°). (*b*) Wide beam (2°).

pattern, no backscattering is received between the transmitted pulse and the first echo coming through the main beam from the top of the precipitation system detected by the radar (β_n = nadir angle). To increase the sampling rate and thus facilitate the operation of the system as a Doppler radar, it is possible to send radar pulses separated only by the time (approximately 500 μsec) that is required by the radar depth of ground clutter plus the time that is required for atmospheric return, which is a distance of approximately 50 km with the grazing angle discussed here. However, the presence of side lobes may limit this possibility, because there will be additional ground returns occurring from directly below the satellite and beyond (fig. 4–20).

Indeed, at the range at which the atmospheric return is selected, there will also be a contribution from ground clutter "seen" through the side lobes at the same range. The significance of the effect varies with the sea or land backscattering coefficient and the side-lobe level. Preliminary investigations of the clutter problem indicate that the worst effect is due to the near-inside lobe. With a near-inside lobe level of -28 dB or less, 20 to 30 dB of signal-to-clutter ratio can be achieved with 3-mm/hr rain intensity observed over mountains or cities.

If the side-lobe effect can be neglected, a

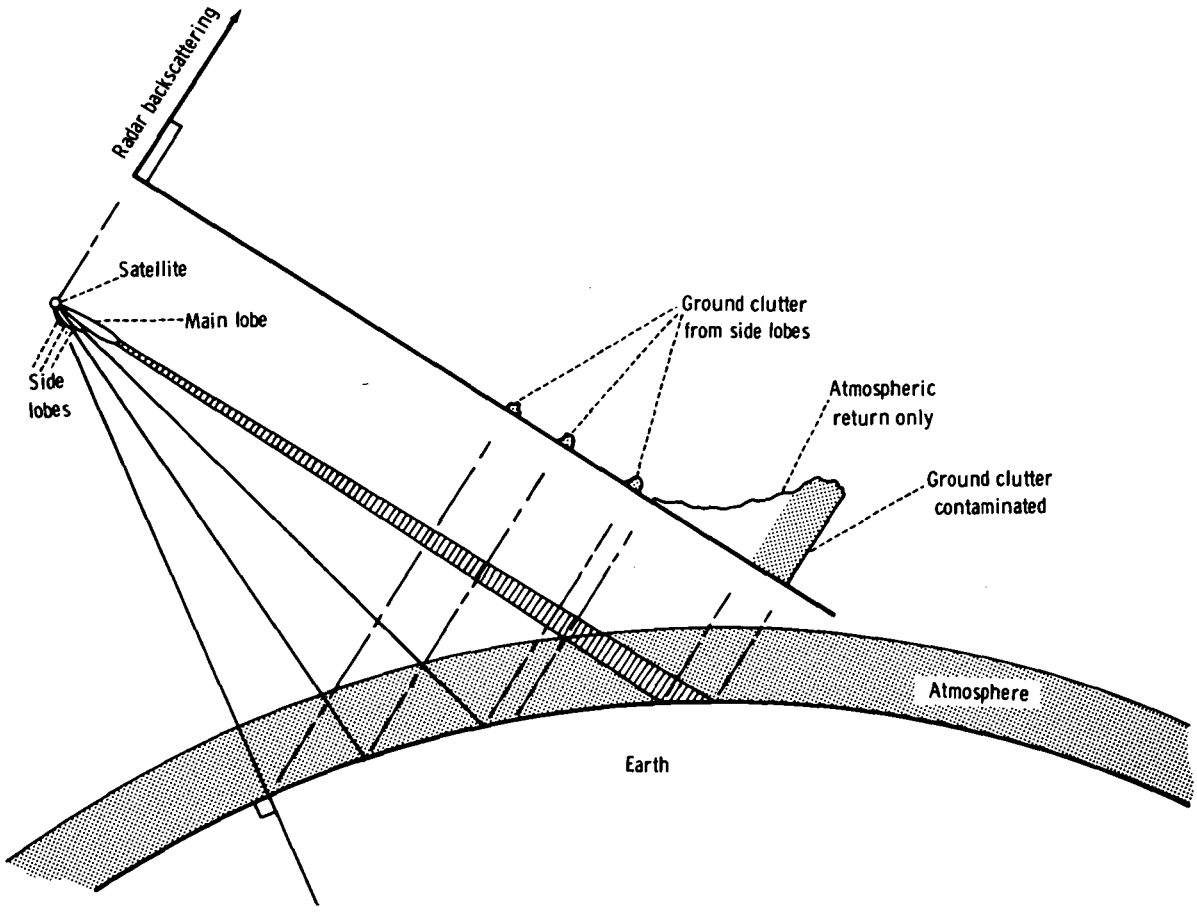

FIGURE 4–20.—Influence of the side lobes in the radiation pattern on the signal received by the satellite radar receiver.

high repetition rate of more than 2 kHz can be used without impairing the range gating of the signal. The critical issue is the selection of atmospheric echoes free of ground-clutter contamination, which implies a range side-lobe level at least greater than 50 dB. Although the discussion here implies a microwave pulse Doppler radar process, other coding methods such as pseudonoise coding can be investigated, as well as the use of a 10-μm radiation provided by a CO_2 laser.

As an example, preliminary investigations show that a 5.6-cm-wavelength pulse radar having the following characteristics

Pulse duration, μsec	10
Receiver bandwidth, MHz	0.2
Antenna effective aperture, cm^2	10^6
Overall noise figure, including losses, dB	10
Peak power, kW	5

provides a signal 15 dB above the receiver noise for precipitation filling the beam at a range of 1000 km and having a reflectivity factor $Z=10^3$.

In the case of the single pencil beam mentioned previously (fig. 4–19(*a*)) (0.3°) and a grazing angle of 20°, the radial size of the beam footprint is 40 km. Because the effective satellite groundspeed is 6.9 km/sec, the scan time per complete revolution as required for full coverage is 6 sec.

There are approximately 1000 different beam positions in each scan, so the time available to sample each position is only 6 msec, which is less than the round-trip time to the targets from the satellite. It is therefore imperative to reduce the scan rate. However, the necessity for full coverage of the swath will require the development of a multibeam capability. A 5- to 10-beam system and an overall scan rate of 40 sec can meet the scan requirements. The beams are contiguous and are used simultaneously with a single transmitter and a single shared receiver. The power required for this type of operation is within current practice.

Considering the echo-free region as mentioned before, the pulse repetition rate can be increased to 2 kHz and still resolve atmospheric and ground targets. Under these conditions, more than 40 samples of the Doppler signal can be available for processing for each beam and range rate.

Neglecting the Earth rotation speed, the Doppler frequency shift V_D due to the satellite velocity is expressed by

$$V_D = V_s \cos\theta \sin\beta_N \qquad (4\text{–}46)$$

where V_s is the satellite velocity, θ is the beam scan angle, and β_N is the beam nadir angle.

In the vertical plane, the spectrum smearing ΔV_D that is due to the satellite motion is mainly controlled by the elevation component of the beam $\Delta\beta_N$, where

$$\Delta V_D \approx V_s \cos\Delta\beta_N \cos\Delta\theta \qquad (4\text{–}47)$$

The Doppler spread in the direction of azimuth scan is expressed by

$$\Delta V_D \approx V_s \sin\Delta\theta \sin\Delta\beta_N \qquad (4\text{–}48)$$

In these expressions $\Delta\beta_N$ and $\Delta\theta$, respectively, are the elevation and azimuth beamwidths, and $\Delta\beta_N=\Delta\theta$ for pencil beam.

The total smearing due to the combined effects is given by

$$\Delta V_D = V_s[(\cos\beta_N \cos\Delta\theta \Delta\beta_N)^2 + (\sin\Delta\beta_N \sin\beta_N \Delta\theta)^2]^{\frac{1}{2}} \qquad (4\text{–}49)$$

With a 0.3° conical beam size, a satellite groundspeed of 7 km/sec, and a grazing angle of 20°, the spectrum smearing due to satellite motion will be approximately 34 m/sec (spectrum standard deviation of $\sigma_v=10$ m/sec) for $\Delta\theta=90°$ and 12 m/sec ($\sigma_v=3.5$ m/sec) in the forward direction.

At C-band and with a sampling rate (pulse repetition rate) of 2 kHz, the mean of spectra with a width smaller than 50 m/sec can still be processed by use of optimum estimators, such as the covariance estimator mentioned in the section entitled "Doppler Radar Signal Processing."

It can be shown that, with a signal dwell time of 0.05 sec (time during which the beam rotates by one beamwidth for a total conical scan time of 50 sec) and a spectrum standard deviation of 10 m/sec, the standard deviation

σ_v of the mean Doppler estimate is approximately 2 m/sec.

For a satellite groundspeed of $V_s = 7.0$ km/sec and $\beta_N = 60°$, $V_D \approx 6$ km/sec in the forward direction. At C-band, this is equivalent to a Doppler frequency shift of approximately 200 kHz. Assuming a sampling rate of 2 kHz will place the spectrum in the 100th frequency ambiguity region. However, the satellite groundspeed is extremely stable, and the sampling rate can also be easily made very stable and accurate. Various schemes are available to reduce the velocity ambiguity problems. It may be possible, for example, to use the ground Doppler shift as a reference. The range-gated ground return is expected to occupy a well-defined mean frequency position, which can be used as a reference, thereby allowing the unambiguous resolution of the groundspeed of atmospheric targets.

The continuous change of the scan angle during the beam rotation, combined with the satellite groundspeed, produces continuous variations of the mean Doppler frequency shift and spectrum smearing. If the radar is equipped with onboard processing systems capable of tracking spectrum mean frequency at four or five range gates in the atmospheric region and one in the ground clutter, this information can be continuously transmitted to Earth with low-bandwidth systems also telemetering scan angle and satellite position. The processing of this information by a ground-based computer can provide estimates of quasi-horizontal velocity in regions where atmospheric targets are "seen" from different angles during the satellite motion.

Table 4–VI outlines tentative specifications for such a satellite system. The critical part of these specifications is the maximum PRF that can be used. In the case of a radiation pattern free of side lobes and with the grazing angle of 20°, the minimum time between successive pulses is 400 to 500 μsec. This repetition rate of 2 kHz, which places the forward Doppler in the 100th ambiguity region, should still allow discrimination between atmospheric and ground-clutter speed with 35-m/sec-or-less Doppler smearing. Signal covariance estimators or equivalent are needed for accurate tracking of spectral mean.

TABLE 4–VI.—*Tentative Specifications for a Multibeam Doppler System*

Radar wavelength, cm	5.6
Peak power (per beam), kW	5
Average power, W	100
PRF (stability better than 10^{-4}), kHz	2.5
Pulse width, μsec	10
Antenna beamwidth, deg	0.3
Beam footprint on the ground, km	5 by 15
Beam nadir angle, deg	60
Grazing angle, deg	20
Conical scan, beam scan time, sec	40
Satellite displacement during complete scan, km	280
Angular displacement of the antenna beam during echo round trip, deg	0.13
Satellite orbit	polar inclined
Satellite altitude, km	≈500
Satellite orbit time, hr	1.6
Satellite groundspeed, km/sec	≈7
Forward-groundspeed Doppler shift, kHz	≈200
6-dB Doppler smearing (max), m/sec	35
Nonambiguous velocity interval, m/sec	70

This first example is an attempt to describe a possible specific solution for a low-orbit satellite-borne weather radar capable of a coverage comparable to that obtained with orbiting satellites now used in meteorology. The radar is primarily a conventional radar and could serve as a reference for further discussion and development. The choice of the wavelength implies the availability of large antennas, such as the one recently flown with ATS–F. The technology of large dish antennas to be used aboard satellites will certainly improve in the next few years, but for the present it appears that geostationary satellites are reserved for imagery done in the infrared or visible part of the spectrum, for which well-collimated beams are easy to obtain.

In summary, if the radar method is restricted to low-altitude orbiting satellites for

which the groundspeed is large, then the application of Doppler techniques will be very difficult, but not impossible. Also, low-altitude orbiting satellites require the use of beam scanning techniques that produce a swath of sufficient dimension so that complete coverage from orbit to orbit is obtained. A conical scanning method, which is easy to obtain simply from the spinning of the satellite, has been presented. This scanning method also allows the same point on Earth to be probed from a different direction during the satellite motion, therefore offering some possibilities of resolving quasi-horizontal velocity.

The design and implementation of such methods must be preceded by a thorough feasibility study. The purpose of the example presented earlier is to focus the discussion on a specific system for which such a feasibility study can be done.

In addition to the measurement of precipitation, the most significant contribution that active microwaves may make to atmospheric measurements is to observe the windfield inside precipitation systems. Ideally, the meteorologist would like to have synoptic maps of windfields at several altitudes and, under certain conditions, measured as frequently as several times an hour. Such global-scale maps would improve forecasting and would also allow accurate assessment of global atmospheric motion. When used in conjunction with the passive optical satellites, the maps would permit the identification of precipitating clouds and the assessment of their severity.

The Doppler wind-measurement method presented here is a unique capability available only to active microwave systems and only requires that the detectable tracers have no motion relative to the winds. Naturally, the active technique permits the measurements to be made on both the light and dark parts of the orbit.

The microwave Doppler weather measurements rely on basically the same backscattering phenomenon as the conventional radar. The unique aspect of the measurement is that the method is sensitive to the motion of each of the particular scatterers.

Preliminary study indicates that current state-of-the-art equipment can provide useful Doppler measurements. The system recommended in this section uses a conical scan obtained by rotating a tilted pencil-beam antenna. A low-altitude orbit (500 km) is used to reduce the required antenna dimension. The radar frequency would lie in the C- to X-band region. The coverage provided by a single satellite is sufficient to guarantee at least two passages a day over the global region between $\pm 70°$ latitude. The scanning pattern provides two observations for each pass over more than 70 percent of the swath, with sufficient angular diversity to obtain representative wind magnitude and direction. Accuracy of approximately 2 m/sec is available for each measurement. Altitude resolutions of 5 km (two-way 3-dB points) are available with current technology and may be improved in the future. The principal limitation is ground clutter, which requires a narrow-beam ($<0.3°$) antenna.

The scanning technique produces a swath with a width in excess of 2000 km. Availability of two-dimensional windfields would provide a snapshot of the entire windfield of a tropical-storm system such as a hurricane. If the storm were at a higher latitude (20°), two or more such snapshots spaced by 1.6 hr would be obtained.

The instrument needed in an advanced system would require an approximately parabolic 11-m antenna, a 1-kW peak-power transmitter operating at C-band, a low-compression coded waveform (1 MHz, time bandwidth <100), and an onboard system that processes reflectivity and mean Doppler speed.

Available technology indicates that the electrical equipment, exclusive of the solar cells but including the antenna and signal processor, might have a total weight of less than 500 kg. Data reduction on board the satellite would reduce the downlink average data rate to 4×10^5 (5-bit) samples/sec, even with no data editing. On the ground, cor-

rections for the satellite orbit and the attitude errors would be inserted. Even with communications delays, initial systems should be able to achieve 24-hr timeliness, with future systems achieving satellite sampling-time timeliness by the use of geosynchronous satellite communication systems.

The first priority is a thorough feasibility study to determine optimum parameters. Next, an experimental study should demonstrate the measurement principles and carry out the data reduction. Early experimental models should then be tested on existing platforms. The meteorological significance of these preliminary results should be reassessed; and, finally, a full-scale system should be planned and executed.

Geosynchronous Satellite

The geometry of a geosynchronous satellite is shown in figure 4–21. Assuming a convective precipitation cell at a great circle distance L from nadir, the expected radar echoes, if detectable, would probably have a time/distance dependence similar to that sketched in figure 4–21. The round-trip time delay τ_0 is approximately 0.25 sec, and the ground return is expected to be significantly higher than the return from precipitation. However, at shorter wavelengths (i.e., 10 μm), regions of precipitation could be masked by cloud cover. If $\tau_n < \tau_0$, where τ_n is the time delay for ground echoes detected at 0° nadir angle, no side lobes or main beam intersect the Earth; and the distance L to which precipitation targets alone are detected to height h (and delay τ_n) is given by the approximate expression

$$L = \frac{\sqrt{2hR_s}}{1+\frac{R_s}{R_E}} \qquad (4\text{–}50)$$

This expression indicates, for example, that if the measurement of vertical motion at a constant 10-km height is required, clutter-free observations can be made to distances L of approximately 330 km from nadir. Although a 700-km-diameter area may be sufficient to observe motion along a particular

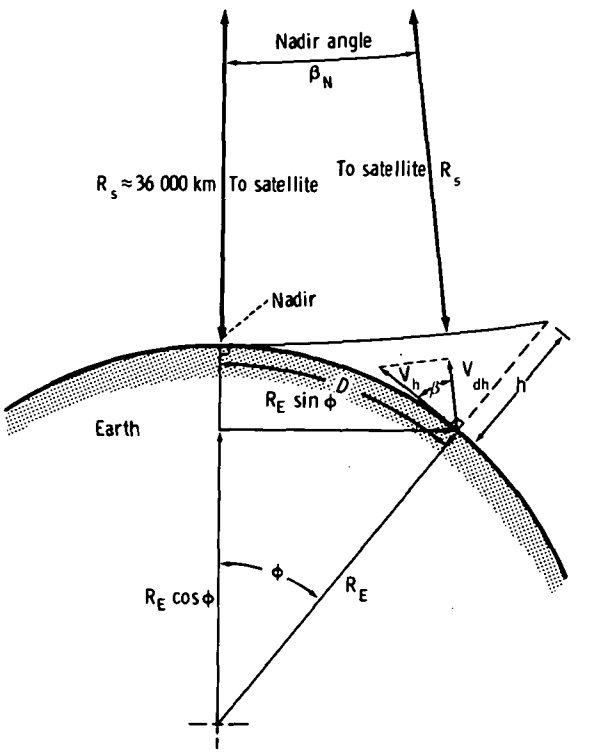

FIGURE 4–21.—Geometry of a satellite in a geosynchronous orbit.

entire squall line (for $h \geq 10$ km), it is too small to cover the vast area over which squall lines can form and would be restricted to equatorial regions. A ground-based radar can make observations over a diameter of 400 km; therefore, no great advantage in area surveyed would be derived from the use of a geostationary satellite radar for vertical velocity measurements.

It must be noted that the distance L from nadir, for which accurate vertical velocity measurements can be made, is also limited by the presence of the projection V_{dh} of velocity V_h on the radar radial direction. For small nadir angle β_N,

$$\frac{V_{dh}}{V_h} = \cos\beta \approx \left(\frac{1}{R_E}+\frac{1}{R_s}\right)L = \left(1.88\times10^{-4}\right)L \qquad (4\text{–}51)$$

where L is in kilometers. The contribution to radial velocity due to a 30-m/sec horizontal motion, for example, is 1.6 m/sec at

300 km from nadir. Therefore, to keep vertical velocity contamination below 2 m/sec, L must be less than 350 km, which limits the area of surveillance of vertical wind to a 700-km-diameter circular region.

The solution involving the use of a satellite in a high-altitude (36 000 km) geostationary orbit requires the availability of an extremely narrow beam. Because the radiating antenna size is limited, such a narrow beam can only be obtained with a very short wavelength. However, operation near vertical incidence involves less strict range ambiguity considerations, and wavelengths as small as 1 cm may be used. For example, if a 10-m dish, such as the one recently flown with ATS–F, could be used at 1-cm wavelengths, a beamwidth of approximately 0.06° with a beam footprint of approximately 45 km on the Earth surface would be obtained. This resolution is much poorer than the resolution (a few kilometers) provided by infrared and visible sensors installed aboard geostationary satellites such as ATS–3 and GOES, but it could still provide information on large-scale systems.

In addition, the use of such a short wavelength will be associated with prohibitive absorption of the radar signals (approximately 10 dB/km two ways, for a 25-mm/hr precipitation), so that penetration of the storm and quantitative observations would be questionable.

It can be concluded that, even if radar antennas (space qualified at 1-cm wavelength) can ultimately reach a 10- to 20-m size, the operation of 1-cm microwave radar aboard a geostationary satellite will still be highly questionable. The problem may be overcome only by substituting a CO_2 laser-type system operating at 10 μm, which might offer a more appropriate solution for geostationary satellite operation. At least, this system meets the resolution requirements, although coverage is still restricted to equatorial regions.

Carbon Dioxide Pulsed CW Doppler Radar

The purpose of this section is to determine whether mesoscale information can be derived from a 10-μm Doppler radar in synchronous orbit. In particular, an attempt is made to answer the question, "Can organized vertical motion of precipitating regions be resolved?"

The objective is to determine the parameters required for a 10.6-μm radar to detect and resolve the vertical velocity in a precipitation cell 2 km in diameter. A quantum-limited detector is assumed when the receiver noise power is (ref. 4–57)

$$P_N = B\left(\frac{h_1 c}{\eta\lambda} + kT_a\right) \qquad (4\text{–}52)$$

where

B = bandwidth $= 0.7/\tau_p$ (where τ_p is dwell time $= 2\Delta h/c$)
$T_a = 300$ K
k = Boltzmann constant, 1.38×10^{-23} J/K
η = quantum efficiency of detector = 80 percent
h_1 = Planck constant, 6.6×10^{-34} J-sec

Substituting these values into equation (4–52) yields

$$P_n = \frac{1.05\times10^{8}}{\Delta h}(2.48+0.414)\times10^{-20} = \frac{3\times10^{-12}}{\Delta h} \qquad (4\text{–}53)$$

where Δh is in meters. The precipitation backscatter cross section per unit volume σ_v as compared with reflectivity factor Z is plotted in figure 4–22 for $\lambda = 10.6$ μm. Transmitted peak power in excess of 1 MW would be required to detect a 30-dBZ precipitation cell of 2-km diameter with a 2-km vertical resolution, even if absorption is neglected. Although detection of precipitation is impractical, clouds have scatter cross sections that are orders of magnitude larger than precipitation; hence, cloud boundaries may be detected from geostationary altitudes. Further work along this direction may be required if significant meteorological information can be derived from cloud vertical velocities viewed over limited (several hundred kilometers) equatorial regions.

Reducing the satellite orbiting altitude to a lower value (e.g., 400 km) will result in considerable sensitivity gain (40 dB) if the

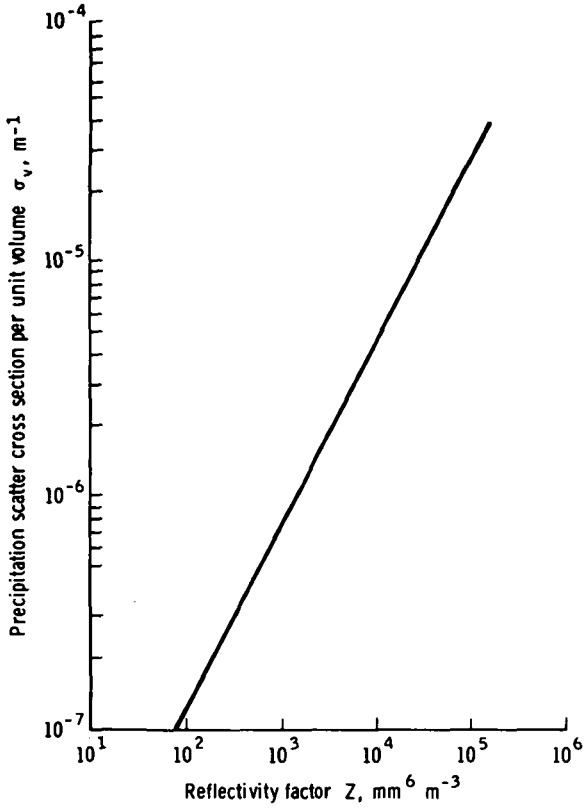

FIGURE 4–22.—Precipitation backscatter cross section per unit volume σ_v compared with reflectivity factor Z for $\lambda = 10.6$ μm.

other parameters are fixed. Therefore, thin clouds of lower water content can be used as tracers of air motion. Rensch and Long (ref. 4–58) made theoretical computations concerning fog scattering and attenuation. The authors show that, for $\lambda = 10.6$ μm and the droplet radius for maximum number density $a_m = 1$ μm, σ_v is approximately 3×10^{-7} m^{-1}/mg m^{-3}. Thus, for water clouds with water content of 10^3 mg m^{-3} which is appropriate for cumulus clouds, σ_v is 3×10^{-4} m^{-1}, which is an order of magnitude larger than the return from precipitation. This discussion does not provide a comprehensive treatment, but it does illustrate that the CO_2 Doppler laser has definite advantages in sensitivity and resolution for measurements of cloud motion, although it cannot penetrate thick cloud regions. Furthermore, returns from particulate matter for satellite-borne lasers ($\lambda =$ 0.7 μm) have been theoretically demonstrated to be possible (ref. 4–59). Investigations concerning CO_2 scatter cross section from in situ atmospheric aerosols and the spatial distribution and density of these aerosols should be vigorously pursued to determine the feasibility of clear-air detection of atmospheric motion from satellites. Although the CO_2 laser will not penetrate heavy cloud systems, the ability to detect and resolve speed and location of cloud particles may constitute an attractive alternative to a 6-cm microwave system.

Absorption of 10.6-μm radiation by water vapor for the entire atmosphere at normal incidence is less than 2 dB (ref. 4–60). Absorption of CO_2 laser radiation due to atmospheric airborne dioxide has also been computed. The total two-way absorption is less than 6 dB. Rain scatter and absorption losses have been computed by Rensch and Long (ref. 4–58), who have assumed a Gaussian distribution of drop size fitted to the tabulated size distribution of Laws and Parsons. By far, the largest attenuation is associated with propagation through cloud. Theoretical computations on fog attenuation, assuming a cloud droplet-size distribution of the form

$$N(a) = C\left(\frac{a}{a_m}\right)^6 e^{-6(a/a_m)} \qquad (4\text{–}54)$$

(where C is a constant and a_m is the droplet radius for maximum number density), show a 10.6-μm total attenuation normalized to liquid water density of approximately 1.5×10^{-1} dB/km/mg m^{-3} for mean drop radii between 20 and 10 μm. Larger droplet diameters produce decreasing attenuation for constant water content. Liquid-water concentration in cumulus clouds may be several g/m^3, and thus the attenuation rate due to cloud droplets may exceed 100 dB/km, overwhelming the absorption due to precipitation itself. The experiments of Chu and Hogg (ref. 4–61) of CO_2 attenuation verified that fog attenuates considerably more than raindrops.

Considering all the possible loss mechanisms, it appears that a CO_2 laser will, at

best, be able to measure only the motions of cloud boundaries.

Doppler radar measurements at a 10-μm wavelength may be attractive for several reasons. Calculation shows that detection of cloud particles is feasible from an orbiting satellite. Surveillance of larger areas of atmospheric motion than that achieved with microwave radar may improve because microwave radar is limited to detection of precipitation regions. A 10-μm-wavelength Doppler radar has range and velocity information contained in a single pulse of several microseconds' duration, resulting in mean velocity information being acquired at a rate much faster than that possible with a microwave system.

The measurement of cloud motion with a CO_2 Doppler radar may have an advantage over present techniques of mapping cloud positions photographed from geostationary satellites, because the radar can resolve cloud height. Although the radar measures only radial velocities, the measurement of air motion from two directions is possible so that vector wind direction can be achieved. The use of a CO_2 laser aboard a satellite may have an advantage over ground observations, because turbulence degradation of coherency should not be as severe when looking at clouds from above.

Vertical motion from geostationary satellites appears to be limited to observations of cloud tops. Vertical motion measurements will be constrained by the location of the geostationary satellite to regions near the equator.

APPLICATIONS OF BISTATIC MICROWAVE SYSTEMS TO ATMOSPHERIC RESEARCH

An active microwave system is one that incorporates both a transmitter and a receiver. In the situation most commonly considered, both the transmitter and receiver are in the same place; they are often in the same cabinet or in the same vehicle, or at least in sufficient proximity to permit the same operators to attend to both devices. This arrangement of equipment is called "monostatic." When the microwave transmitter and receiver are distant from one another, the system is termed "bistatic." The actual separation distance required to permit a choice between these two descriptive terms has not been agreed upon, but generally the bistatic name is applied to any system for which the analysis of the radar return requires consideration of the separation.

Bistatic radar systems have been used very effectively in applications as diverse as planetary astronomy observations and lunar surface soundings by orbiting spacecraft. It is therefore very likely that the bistatic techniques developed during the last decade will be used to considerable advantage in future active microwave applications.

The separation of transmitter from receiver often leads to inherent advantages, and one of these advantages usually accounts for the choice of a bistatic system in any given application.

In some circumstances, one wishes to measure the behavior of microwave propagation along a particular radio path. If the transmitter and receiver are at opposite ends of the path, the signal has to traverse the path in only one direction, and the loss is only one-way instead of two-way, as in the conventional monostatic radar case. Therefore, for path sounding, the bistatic approach may lead to a much lower requirement for signal strength and reception capability because of the decrease in the total loss of the system.

When the transmitter and receiver are close together, the receiver must be designed so that it can operate with the interference that inevitably results because of the presence of the nearby transmitter. By separating the transmitter and receiver, these problems are usually eliminated, or at least alleviated. The result is that comparatively simple modulations can be used; in fact, CW modulation becomes practical, and other quasi-continuous modulations may also be readily accommodated. This generally leads to a simplification of the hardware and, therefore, a decrease in cost, provided, of course, that

the objective of the system can be met with the bistatic configuration.

Many kinds of radio-wave scatterers do not produce a large backscatter return, although they may scatter a very large amount of energy through small angles. If a microwave transmitter is directed at such a body of scatterers and the receiver shares the same antenna, it will obtain a small return. A similar receiver located behind the scatterers and just off the transmitter-scatterer axis would receive a relatively strong return. It is sometimes possible to configure a bistatic radar system to take advantage of this effect, whereby small scattering angles lead to a large radar cross section.

In some circumstances, it is helpful to have a variable scattering angle to permit the measurement of radar cross-section variation with respect to the scattering angle. In the case of the lunar bistatic scattering experiment, the variation of the cross section with respect to angle permitted an inference of the Brewster angle, from which the dielectric constant of the lunar surface could be determined independently of the scattering model adopted by the observer. The measurement of the dielectric constant by direct return is comparatively inaccurate.

In some circumstances where the radio path from transmitter to receiver is almost straight and the signal is rather stable, the polarization of the signal can be controlled; therefore, its polarization changes can be observed with a high degree of accuracy. This may permit polarization analyses that would be impractical with a monostatic system.

Strictly speaking, one-way transmission experiments fall into the bistatic active microwave system category. Systems of this type operating in the millimeter-wavelength region are often the best suited for fundamental studies of the gaseous constituents of the atmosphere and the forward-scattering properties of hydrometeors. It is likely that, in the area of transmission experiments, bistatic techniques will be used for atmospheric problems in the next few years. For many meteorological and atmospheric physics studies, it is important to know the size, composition, shape, and orientation of hydrometeors. The best experimental approach to determining these parameters is to transmit a known polarization (linear or circular) from a satellite to a ground antenna that is instrumented to carry out a precise polarization analysis of the scattered signal. Such studies are of considerable importance to theoretical modeling of the scattering of microwaves by an assembly of nonspherical hydrometeors. In addition to the obvious importance to atmospheric physics, the results are of crucial importance to advanced satellite communications work.

The rationale for current satellite communication experiments is the lack of available channels in the frequency range below 10 GHz, where atmospheric effects are relatively unimportant. Above 10 GHz, microwave radiation interacts strongly with raindrops and ice particles, and measurements of attenuation and depolarization are planned or in progress to characterize these interactions. The goals of these experiments are primarily to gather statistical data and advanced communications technology, but meteorological information can and should be gathered as well.

After a series of investigations of 10- to 30-GHz attenuation and depolarization, theoretical models for propagation through rain were developed for terrestrial paths. These models involve the size and shape distributions of the raindrops and provide insight into the relationship between these distributions and observed attenuation and depolarization. The distributions generally accepted for ground rainfall are of questionable validity at high altitudes. In addition, Earth-satellite paths must penetrate the melting layer, and little is known about the ice-particle size and shape distribution in this layer. The planned propagation experiments will provide new information concerning both of these distributions.

An additional consideration is the possible depolarization by ice crystals in cirrus clouds. This effect may be important to meteorology. The available information is insufficient to

support a quantitative prediction; but qualitatively, if the ice crystals show some degree of alinement, it should be possible to calculate their size and number by measuring their depolarizing effects at two frequencies using linear polarization. If ice-crystal orientation is random, their effects in circular polarization may be a good indication of their number and composition.

The high degree of stability of the background signal can be used to allow accurate studies of gaseous atmospheric constituents. The scintillations in the signal, if detectable, would provide a clue to the observation of atmospheric turbulence. Heavy precipitation should be detectable by this means if the signal is stable and well calibrated in amplitude. The total water content could be determined by observing and measuring signal absorption. It might be possible to measure the vertical distribution of a constituent by taking advantage of the pressure broadening of its absorption lines, using a forward-propagated signal at multiple wavelengths. One might even sweep the transmitted signal frequency across an absorption band to provide a complete frequency sample of the shape of the band of some particular molecule of interest. By choosing different absorption bands that are characteristic of different constituents, one could measure the specific atmospheric constituents individually.

PART B

ADDITIONAL APPLICATIONS AND RELATED TOPICS

THE MEASUREMENT OF SURFACE PRESSURE FROM A SATELLITE BY ACTIVE MICROWAVE TECHNIQUES

Although it is now possible to map the temperature structure of the atmosphere from satellites, pressure measurements are still limited by the coverage of ground-based instruments. More data are required from wider areas as an input to long-period numerical forecasts. Satellite methods for pressure measurement should be investigated. The following data requirements for a set of global meteorological measurements sufficiently accurate to provide initial conditions for a numerical forecast up to 2 or 3 weeks ahead have been specified by GARP (ref. 4–62):

1. Wind components: ± 3 m/sec
2. Temperature: ± 1 K
3. Pressure of reference level: ± 0.3 percent
4. Water vapor pressure: ± 100 N/m^2
5. Time average interval: 2 hr
6. Horizontal space average: 100 km
7. Vertical space average: eight levels at 100 000, 90 000, 70 000, 50 000, 20 000, 10 000, 5000, and 1000 N/m^2, respectively.

Such a vast amount of data can possibly be collected in the necessary time and at a reasonable cost only by the use of remote-sounding instruments on satellites. Although a geostationary satellite provides the most convenient platform for such closely spaced observations, it has the disadvantage of being at a very large distance (36 000 km), so that the antenna size required to achieve an acceptable ground resolution or to intercept sufficient energy of a return echo may be prohibitive. Therefore, for the purpose of this discussion, it is assumed that the instrument is mounted on a satellite orbiting at approximately 1000 km.

An accuracy of ± 0.3 percent in a pressure measurement corresponds to a height change of only 20 m, so that the height at which the pressure is measured must be known to within this value. This requirement renders the measurement of the three-dimensional pressure field very difficult. In principle, the desired accuracy might be achieved by a radar or lidar technique, but any pressure-

dependent contributions to atmospheric backscatter are so weak that measurement is impossible with reasonable source powers and receiver apertures. This leaves only methods that measure surface pressure. Of course, the hydrostatic approximation, in conjunction with the measured temperature field, will allow reconstruction of the entire pressure field from the surface pressure, so that the restriction is not serious.

It has been proposed that atmospheric pressure could be deduced from measurements of the optical length of a path through the atmosphere. In practice, the dispersion between two different wavelengths must be measured. Unfortunately, this effect is very small. In the visible spectrum, dispersion can give a time difference of approximately 5×10^{-10} sec, and calculations by Liebe (ref. 4–63) give rather smaller times in the 5-mm O_2 band. To measure pressure to 0.3 percent, the time resolution must be approximately 1.5×10^{-12} sec. This is many orders of magnitude less than the equivalent length of a pulse reflected from the ocean surface (waves of 5 m in depth are equivalent to a time difference of approximately 3×10^{-8} sec). The only practical method for achieving such resolutions is to have separate transmitting and receiving stations on satellites, so spaced that the path between them includes some of the atmosphere. One would probably measure the phase of a continuous signal rather than timing the arrival of a pulse. Such a technique is not possible for reflection from the ocean surface, because the roughness of the surface renders the echo incoherent.

The most promising methods for surface-pressure measurement depend on measuring the intensity of energy reflected from the surface both in an atmospheric absorption band and at a nearby wavelength. The attenuation of the light in the atmosphere by Rayleigh scattering in clouds and the surface reflectivity are slowly varying functions of wavelength. Therefore, the ratio of the intensities at the two wavelengths is a measure of the atmospheric absorption due to the absorption band, from which the total amount of gas in the atmosphere and, hence, the surface pressure can be deduced.

The chosen absorption band must be due to a major constituent (e.g., O_2). Absorption bands of variable minor constituents such as water vapor or ozone must be avoided. Even CO_2 is probably not sufficiently evenly mixed for this purpose. Possible microwave O_2 bands occur at 0.76 μm and 5 mm.

Under favorable conditions, the absorption will need to be measured to 1 part in 80 to achieve the required accuracy of 300 N/m^2 in the surface pressure. (See the section entitled "Water Vapor.")

The Sun does not provide a suitable source at either wavelength. At 0.76 μm, under broken-cloud conditions, a substantial amount of sunlight is reflected back from the cloud top and does not traverse the entire atmosphere. (This fact has been used to determine cloud-top altitude.) An active, pulsed source allows discrimination against such cloud reflections. At 5 mm, the cloud reflectivity is negligible; but the Sun reflected in the rough ocean surface provides a signal weaker than thermal emission from the ocean and atmosphere, from which it cannot be distinguished. An active manmade source is then required. For the purpose of numerical estimates of minimum-required transmitter power, reflection at normal incidence from the ocean surface is considered. Rather higher powers would be required for operation over a land surface or over the oceans at nonnormal incidence.

At 0.76 μm, the most practical source is probably a dye laser pumped by either a flash lamp or a ruby laser. If a 1-J pulse (4×10^{18} photons) is assumed, the number of photons returned into an entrance aperture of 30 cm at a satellite height of 1000 km can be deduced from the ocean-surface reflectivity calculated by Krishen (ref. 4–64). The fraction returned is approximately 1.5×10^{-13} or 6×10^{5} photons. If the atmospheric transmission is 0.37 and if a photomultiplier with a quantum efficiency of 0.1 is used, the number of photoelectrons will be 2×10^{4} and the accuracy of intensity measurement will be $1/(2\times10^{4})^{1/2}$

$=1/140$. This assumes (1) that reflected sunlight can be reduced to a negligible amount by filtering and using a narrow field of view, and (2) that dark current in the photomultiplier is eliminated by cooling the tube, if necessary.

The overall efficiency of the laser system is unlikely to exceed 0.05 percent, so that 2000 J of electrical energy would have to be stored (400 μF at 3300 V). If a measurement is required every 10 sec, the power consumption would be 200 W. In addition to this high power consumption, the lifetime of the flash tube (approximately 10^5 flashes) may present a problem. However, the method seems feasible in principle, but it compares poorly with other methods discussed in this report.

This method has been previously investigated by Singer (ref. 4–65). Singer concludes that rather high power would be needed, but his calculations are based on a "gray" surface with albedo 0.1, which gives a value of 3×10^{-15} for the fraction of power returned compared with 1.5×10^{-13} from Krishen's calculation (ref. 4–64) for an ocean reflectivity.

At a frequency of 50 GHz, solid-state sources can provide powers approaching 1-W continuous wave (ref. 4–66), whereas vacuum devices can provide more if necessary.

The return signal from a 1-W transmitter is calculated to be approximately 5×10^{-3} W into a receiver aperture of 30-cm diameter. (The reflectivity is higher in the microwave region than in the visible region because of the larger dielectric constant of water.) If the receiver and blackbody source are at temperature T, if the intermediate-frequency bandwidth is Δf, and if the time constant after rectification is t, then noise-equivalent power is $4kT(\Delta f/t)^{1/2}F$, where k is the Boltzmann constant and F is the noise factor of the receiver (approximately 10 in practice). (The Rayleigh-Jeans' approximation for the blackbody radiation function is applicable to the microwave part of the spectrum.) Assuming an intermediate-frequency bandwidth of 30 MHz and assuming an integrating time constant of 1 sec, the SNR is 500:1, which should be adequate for the present purpose.

The O_2 5-mm band is the most promising for the proposed measurements; and, in the next section, atmospheric transmission in this region of the spectrum is considered in detail.

Atmospheric Transmission and Ocean Reflectivity in the Neighborhood of the 5-mm Oxygen Band

This section considers several factors that will affect the received signal strength. At normal incidence, the ocean reflection is predominantly specular if the surface structure is large compared with the radiation wavelength (ref. 4–64). Waves on the ocean surface cause an angular spread in the reflected radiation so that the proportion of the reflected energy intercepted by the receiver entrance aperture decreases as the wave amplitude increases. From Krishen's results (ref. 4–64), values for the radar-scattering coefficient σ° of 18 to 8 dB are obtained corresponding to sea states induced by wind of 5 to 25 m/sec. The fraction of incident power reflected into the receiver P_r is approximately related to σ° by

$$P_r \approx 0.28\left(\frac{d}{R}\right)\sigma^\circ \qquad (4\text{–}55)$$

where d is the aperture diameter and R is the radar range. The values quoted in the introduction of the section entitled "The Measurement of Surface Pressure From a Satellite by Active Microwave Techniques" correspond to an intermediate value for windspeeds of approximately 10 m/sec.

At normal incidence, there is only a slight variation in backscattering cross section with frequency due to dispersion in the dielectric constant. Away from normal incidence, the reflected power drops rapidly and varies with the roughness of the surface on a scale comparable with the wavelength, so that rather different behavior is expected. It is assumed that measurements are to be made at or near normal incidence.

There will be some fluctuation of the inten-

sity of the reflected power with time. To reduce the effects of those fluctuations, it is necessary to average a number of independent measurements at each frequency and to insure that the different frequencies are measured close together in time.

Although the 5-mm O_2 band has a complicated structure caused by rotational transitions between magnetic-line structure levels, in the wings of the band the absorption can be represented by a single Lorentz line. To obtain the most sensitive measure of surface pressure, it will be shown that the transmission on a double pass through the atmosphere should be e^{-1}. This occurs at a frequency of about 50 GHz (the band center is at 60 GHz), where the single-line approximation should apply. The pressure and temperature dependence are given in equation (4–56), where the exponents have been chosen to match Liebe's (ref. 4–63) results obtained by detailed, line-by-line calculations:

$$k=\frac{C\left(\frac{p}{p_0}\right)^{x(\nu)}\left(\frac{T}{T_0}\right)^{y(\nu)}}{1+\left(\frac{\nu_c-\nu}{\gamma_c}\right)^2} \qquad (4\text{–}56)$$

Here, k is the atmospheric absorption coefficient, C is a constant, p is the pressure, T is the temperature, ν is the frequency, ν_c is the band center frequency, γ_c is the width of the Lorentz line, and p_0 and T_0 are standard pressure and temperature.

The transmission for a double pass through the atmosphere is $\tau=\exp(-A)$, where the zenith absorption $A=2\int_0^\infty k\,dz$ and z is the vertical coordinate.

The atmosphere is quite accurately in hydrostatic equilibrium so that

$$p_a g\ d_z=-dp \qquad (4\text{–}57)$$

where p_a is the density and g is the acceleration of gravity. This may be written

$$\frac{dz}{z_0}=-\frac{T}{T_0}\frac{dp}{p} \qquad (4\text{–}58)$$

where $z_0=(RT_0)/(M_m g)$ (for the scale height at temperature T_0, and where R is the gas constant and M_m is the mean molecular weight for the atmosphere). Hence

$$A=2z_0\int_0^{p_G} k\,\frac{T}{T_0}\frac{dp}{p} \qquad (4\text{–}59)$$

where p_G is the ground pressure and k is the atmospheric attenuation coefficient.

Most of the absorption will occur in the lower part of the atmosphere where the temperature falls approximately linearly with height. The dry adiabatic lapse rate is obtained by considering the temperature T that would be attained by a block of air if expanded adiabatically from the ground pressure p_G and ground temperature T_G to the pressure p at a particular height.

$$T=T_G\left(\frac{p}{p_G}\right)^q \qquad (4\text{–}60)$$

where $q=(\gamma_r-1)/\gamma_r\approx 0.3$ and $\gamma_r=C_p/C_v$ is the ratio of specific heats for air.

If $p/p_G\approx e^{-z/z_0}$ is substituted into equation (4–60) and the exponent is expanded, then

$$T\approx T_G\left(1-\frac{qz}{z_0}\right) \qquad (4\text{–}61)$$

Lapse rates other than dry adiabatic may be described by changing the value of q. Equation (4–59) may be evaluated by making use of equations (4–56) and (4–60) for T, such that

$$A=\frac{\frac{2az_0}{x+q(y+1)}\left(\frac{p_G}{p_0}\right)\left(\frac{T_G}{T_0}\right)^{y+1}}{1+\frac{\nu_c-\nu^2}{\gamma_c}} \qquad (4\text{–}62)$$

If detector noise is the limiting factor, the frequency of operation should be chosen to give maximum transmission variation with changes in ground pressure. This maximum occurs when $A=1$ at a frequency of 51 GHz, where $x=2$ and $y=-2.6$ (figs. 4–23 and 4–24). If the received signal is s, the sensitivity to variations in p_G, T_G, and q is given by

$$\frac{\Delta s}{s}=-2\left(\frac{\Delta p_G}{p_0}\right)+1.6\left(\frac{\Delta T_G}{T_0}\right)-\frac{0.8\Delta q}{1-0.8\Delta q} \qquad (4\text{–}63)$$

If the surface pressure is required to an accuracy of 300 N/m^2, $(\Delta s)/s$ is equal to ± 0.6

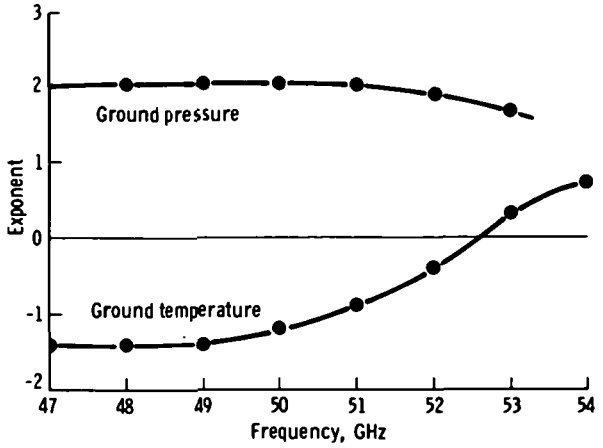

FIGURE 4–23.—Dependence of absorption coefficient on ground pressure and temperature.

percent and T_G must be known to ± 0.4 percent or 1 K and q to ± 0.006 (lapse rate of ± 0.25 deg/km).

This simple model is intended only to give an appreciation of the way the atmospheric transmission depends on ground pressure and atmospheric temperatures. In practice, corrections for possible temperature variations would have to be applied through a more precise model and through the pressure calibration obtained from passes over ground stations where surface pressure is accurately known.

It has been shown that in the wings of the 5-mm O_2 band, the absorption coefficient for the two-way pass through the atmosphere should vary as $p_G^2 T_G^{-1.6}$, so that quite accurate values for surface temperature are needed if surface pressure is to be deduced. The exponents of pressure and temperature as functions of frequency are plotted in figure 4–23. These detailed, line-by-line calculations were based on a standard atmosphere with a constant lapse rate, maintained in hydrostatic equilibrium as ground temperature is changed (fig. 4–25). Notice that at a frequency of 52.5 GHz, the atmospheric transmission becomes largely independent of temperature. This is further emphasized in figure 4–26, which shows the variations in ground temperature and in lapse rate that produce a change in atmospheric transmission equivalent to a 300-N/m² change in surface pressure. The transmission of the two-way pass through the atmosphere at 52.5 GHz is approximately 0.12; therefore, it is still quite feasible to operate an instrument

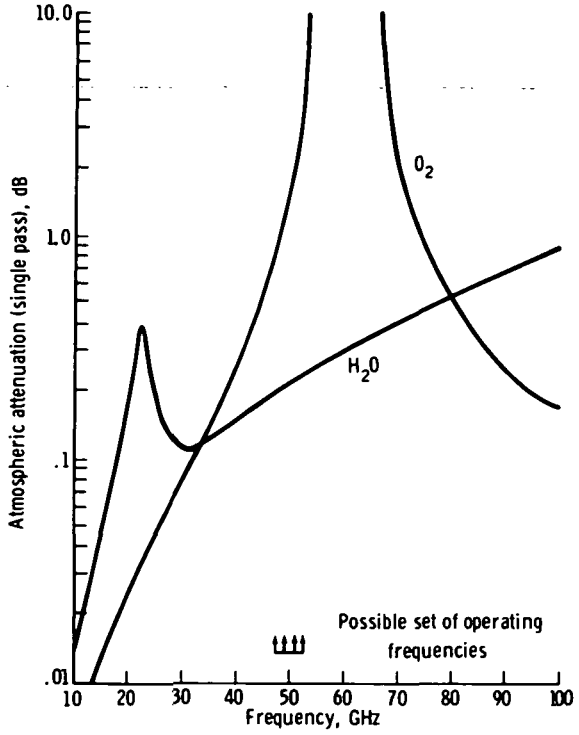

FIGURE 4–24.—Atmospheric O_2 and water vapor absorption.

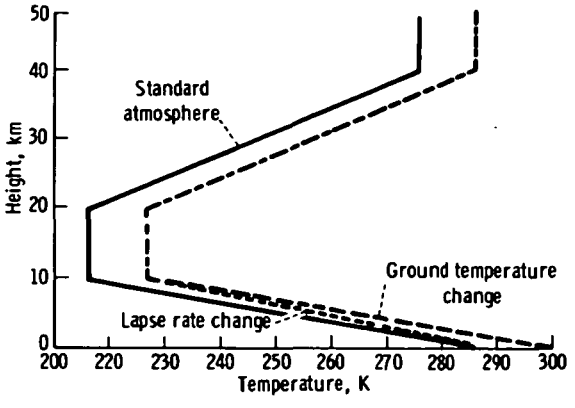

FIGURE 4–25.—Standard atmosphere and variation in T_G and lapse rate used in figure 4–23. (Variation exaggerated by a factor of 10.)

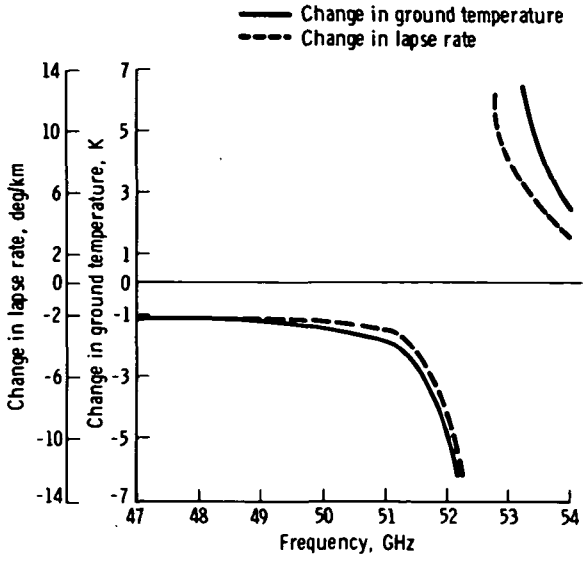

FIGURE 4–26.—Change in ground temperature and lapse rate to give atmospheric transmission change equal to 300-N/m² change in ground pressure.

at this frequency, even though this transmission is less than the optimum transmission for maximum sensitivity to surface pressure.

In fact, there are some advantages in moving farther into the absorption band. Although the absolute change in signal for a given pressure change is greater at an atmospheric transmission of e^{-1}, the fractional change increases with the absorption. At an overall transmission of 0.12, the signal needs only to be measured to a precision of 1 part in 80 for a 0.3-percent accuracy in pressure, compared with 1 part in 150 at transmission e^{-1}. The corrections for water-vapor absorption, cloud transmission, etc., then need be less accurate.

In table 4–VII, s is the received signal, s_0 is the signal that would be received in the absence of atmospheric absorption, and Δs is the change in s for a change Δp_G in surface pressure p_G.

Water-vapor absorption must be considered for the following reasons:

1. Water-vapor partial pressure makes a significant contribution to surface pressure (up to 500 to 800 N/m²).

2. Water-vapor absorption occurs at 50 GHz and must be allowed for, even if the interest is only evaluation of the O_2 absorption. Also, the presence of water vapor affects the middle of the O_2 lines and hence the O_2 absorption coefficient itself.

The first effect is quite small because of the total required accuracy of 300 N/m², and the water-vapor content could probably be estimated accurately enough without measurement.

The absorption caused by water vapor around 50 GHz is a slowly varying function of the absorption coefficient, being proportional to y^2, and could be included in the interpretation of cloud transmissivity and ocean reflectivity so that the amount of water vapor need not be known. The effect of changes in the width of the O_2 line caused by the presence of water vapor is small, but further calculations are necessary to determine whether a measurement of the water-vapor content would be required.

If such a measurement proved necessary, an instrument similar to the surface-pressure sounder could be built, operating over the 22-GHz water-vapor absorption band for example. Much lower precision would be needed for this measurement of the total water vapor.

Benoit (ref. 4–67) gives the following expression for the absorption coefficient of clouds in this region of the spectrum:

TABLE 4–VII.—*Attenuation at 2 Frequencies for a Double-Pass Atmospheric Transmission*

Frequency, GHz	Atmospheric transmission (double-pass)	Relative signal change $(\Delta s)/s$	Absolute signal change Δs
51.0.....	e^{-1}	$-2(\Delta p_G)/p_G$	$-0.74 s_0(\Delta p_G)/p_G$
52.5.....	0.12	$-3.7(\Delta p_G)/p_G$	$-.45 s_0(\Delta p_G)/p_G$

$$\alpha = \rho_c \nu^b e^a \qquad (4\text{–}64)$$

where ρ_c is the density of water in cloud in g/m^3, ν is the frequency, b is equal to 1.95 for a water cloud and 1.006 for ice, and the constant a depends on temperature. For water, $a = 6.866\ (1 + 0.6045T)$; for ice, $a = -8.261\ [1 - (1.767 \times 10^{-2}\ T) - (4.374 \times 10^{-4}\ T^2)]$, where T is in degrees Celsius. For the present purpose, it is sufficient to note that to remove the effects of cloud from the measurements, it will be necessary to allow for an absorption with components varying approximately as ν and as ν^2, in addition to the clear atmospheric absorption.

Although no detailed study has been made of attenuation caused by rain, it will be a smooth function of frequency, which can be allowed for by a polynomial similar to the cloud case over the range of frequencies of interest.

Proposed Instrument Concepts

The measurement of atmospheric transmission cannot be made absolutely, because the ocean-surface reflectivity and land transmissivity are unknown. In addition, such absolute measurements are technically extremely difficult because of variation in transmitter power and receiver sensitivity. The basic measurement will be the ratio of signal strengths at one or more pairs of frequencies sufficiently well separated so that the O_2 absorption differs substantially (i.e., the frequency separation must be approximately the width of the band, which is about 4.5 GHz). One pair of frequencies would suffice if cloud transmission and ocean-surface reflectivity were independent of frequency. Two pairs would be needed to allow a linear variation in these quantities with frequency.

The main difficulty in the design of the hardware is to devise a system architecture that provides equal transmitter power and receiver gain at both frequencies, because calibration to the required accuracy is probably beyond the state of the art. A possible approach is shown in figure 4–27. The transmitter chain consists of the output of an oscillator tuned at the mean frequency f_0 mixed with the output of a CW oscillator at half the difference frequency f_1, followed by a power amplifier. The sum and difference frequency outputs from the mixer are equal in amplitude, and the amplifier-antenna chain should have equal gain at the two frequencies. The receiver consists of a local oscillator at frequency $f_0 + \Delta f$, slightly offset from the mean frequency so that, at the output of the first mixer, the two frequencies $f_0 + f_1$ and $f_0 - f_1$ give rise to closely spaced components $f_1 \pm \Delta f$. These are reduced in frequency by a second mixer and passed through a common intermediate-frequency amplifier before being separated by filters, detected, and compared. Because the intermediate-frequency amplifier is common to both frequencies, gain drifts do not affect the final ratio.

Although the prime measurement will be relatively independent of temperature, it will be necessary to make some temperature corrections. The necessary temperature accuracy will be obtained as a result of more detailed calculations, but temperature will certainly not be required to an accuracy smaller than ± 1 K; probably much less accurate values will suffice. (See the section entitled "Atmospheric Transmission and Ocean Reflectivity in the Neighborhood of the 5-mm Oxygen Band.") Probably the most convenient source of such information would be a passive temperature sounder mounted on the same satellite. If such an instrument were available, it would be worth considering in some detail how the information from active and passive measurements might be combined to the benefit of both.

So far, the system has been described as a CW system making an overall transmission measurement. Some modulation will be necessary to distinguish the signal from thermal emission and to insure that the transmitter does not operate during reception of the echo. This transmission measurement could be affected by backscatter in the atmosphere from clouds and rain. Although the backscatter from clouds is probably negligible, backscatter from rain is possibly a significant factor.

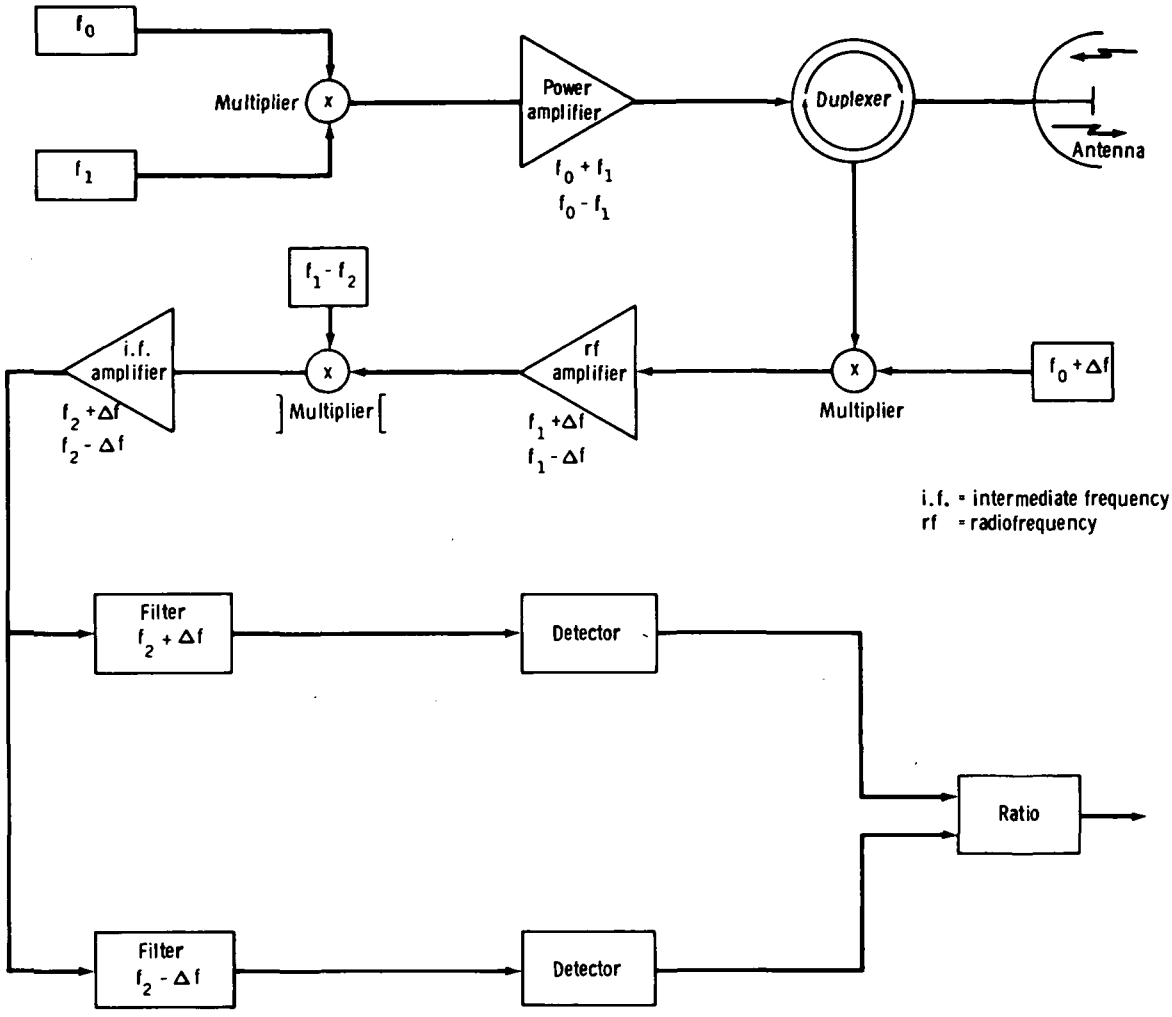

FIGURE 4–27.—Block diagram of possible transmitter and receiver configuration to obtain an accurate ratio of intensities at two frequencies.

Backscatter could be allowed for either source by estimating a correction or, instrumentally, by using a pulsed or coded source so that the surface echo may be distinguished by its time of travel.

Because the ocean reflectivity changes so rapidly as one scans away from normal incidence, unless a large increase in transmitter power or antenna size can be tolerated, the instrument will have to look vertically downward. This imposes a restriction on the ground coverage that can be achieved with a single satellite. A small scan of a few degrees might be accommodated; it would allow the pressure gradient and hence the geostrophic wind to be deduced. Larger transmitter powers and/or antenna sizes would also allow operation over land.

Summary

An active microwave sounder operating in the 5-mm O_2 absorption band and mounted on an Earth-orbiting satellite has been proposed as a means for the remote measurement of atmospheric surface pressure. At 52.5 GHz, the O_2 absorption has been shown to be largely independent of the temperature structure of the atmosphere, but depends strongly

on the surface pressure. A measure of the absolute transmissivity of the atmosphere at this frequency allows surface pressure to be deduced. Such a measurement can be made by reflecting a signal from a satellite transmitter off the ocean surface. Measurements at nearby frequencies allow the effects of varying ocean-surface reflectivity, clouds, and water vapor to be included.

The total water-vapor content of the atmosphere may also be measured by a similar instrument operating near the 22-GHz water-vapor absorption line.

METEOROLOGICAL APPLICATION OF SURFACE WINDS OVER OCEANS

The atmosphere panel noted with great interest the proposals for remote sensing of sea state with active microwave systems, especially the suggestions that wind direction, as well as windspeed at the surface, can be inferred. Surface wind information, if used in conjunction with a variational analysis scheme (such as that proposed by Y. Sasaki (ref. 4–68)), can greatly improve the initial analysis on which operational weather forecasts are based. Other applications include improved prediction of hurricanes and storm surges, and improved understanding of atmospheric processes.

This section is a review of (1) the capabilities that have already been demonstrated for inferring the surface wind from sea-state backscatter, (2) the unique advantages of determining surface winds in this way, and (3) the several NASA meteorological program objectives into which such wind determinations will fit. Finally, an estimate will be made of the meteorological benefits that would accrue from implementing a program to infer sea-surface winds from satellites.

Inference of Surface Wind From Backscatter

Earlier chapters of this report include reviews of previous experimental work relating radar backscatter to the windspeed and directions over the ocean. These are discussed specifically in chapter 3 in the section entitled "Large-Scale Phenomena." In summary, an empirical functional relationship between windspeed and radar cross section has been found. A smaller but significant dependence was also found between scattering cross section and the orientation of the wind. The results suggest that a four-beam array similar to an aircraft Doppler navigation system (but measuring backscattered power instead of Doppler shifts) could provide sufficient information to determine both windspeed and wind direction at the ocean surface. The signal disappears when the winds are nearly calm because of a lack of short-wavelength ocean waves. However, the absence of signal is a definite indication of light or calm winds. In very light winds, there is minimal interest in wind direction.

Meteorological Program Requirements for Winds Over Oceans From Satellite Microwave Systems

Over the oceans, surface windspeed alone can be inferred radiometrically, but determination of wind direction requires an active system. The determination of wind vector by Doppler techniques using the signal returned from precipitation particles (see the section entitled "Satellite-Borne Radar With Doppler Capability") is another possible means of determining winds with microwave systems. However, sufficiently large precipitation particles occupy only a small fraction of the atmosphere at any one time. Determining winds from sea-state condition is the only possible method, other than cloud motion, to obtain wind information from the nonprecipitating regions of the atmosphere.

Wind-velocity vectors inferred from the radar sea cross section can be considered as surface wind without ambiguity. In contrast, there can be considerable height uncertainty when winds are derived from cloud motions. For example, cloud elements are not truly conservative; and, therefore, pattern recognition schemes for tracking clouds are somewhat indefinite. Furthermore, it is not possible to be very accurate concerning the

infrared radiating temperature of cloud tops unless the cloud layer is a thick overcast. If tall cumulus towers are tracked, there is no unique way of knowing at what level the winds match the cloud motion.

There is a unique complementarity between winds determined from Doppler measurement of precipitation particles and winds inferred from sea state. This complementarity occurs because the same clutter that is essential for the operation of the Doppler technique would distort the backscatter signature from the sea surface. Thus, each technique works best when the other works least.

Three of the NASA meteorology program objectives would be served by having surface winds over ocean areas derived from wave backscatter. The first of these is weather prediction. A continuing objective in support of weather prediction is to develop the technology for determining the vertical structure of the atmosphere as an input into numerical prediction models. It has been shown recently (ref. 4–69) that knowing the vertical structure of the state variables (pressure, temperature, and composition) and the approximate time and space derivatives of these variables does not constitute sufficient information to update a numerical prediction model of the type used by most of the major weather centers. The measurement of the wind at one level within the atmosphere is also required. The determination of near-surface winds meets this requirement. Thus, a satellite with a payload similar to that planned for SEASAT–A could continuously provide the data set required to update numerical prediction models.

An additional application in support of numerical weather predictions would be an approximate extension to better coverage of the pressure-measuring scheme proposed in the section of this chapter entitled "The Measurement of Surface Pressure From a Satellite by Active Microwave Techniques." However, this measurement scheme would be considerably less sensitive at angles differing much from vertical incidence. Using the derived surface winds together with the geostrophic relationship would allow approximate reconstruction of the pressure gradient and thus the complete surface-pressure field. The application would require the observation of sea backscatter at several angles of incidence to obtain the wind measurement in the vicinity of the subpoint where the pressure measurements are made.

Operational numerical prediction models of the mid-1970's do not attempt to use wind data for the initial analysis. Instead, only pressures (or the height of constant pressure surfaces) are used to generate the assumed initial condition windspeeds. However, it is likely that, by the time an active microwave surface wind system is flown, the numerical prediction models may derive the initial condition windspeeds through a procedure such as Sasaki's (ref. 4–68) variational analysis scheme, which can use wind information as well as pressure information. A significant portion of the present error in weather predictions for more than 24 hr ahead can be attributed to an imperfect initial state of the numerical models. Any improvement of the fidelity of the initial conditions will certainly increase the accuracy of synoptic-scale weather forecasts in the realm of 2 to 6 days.

The second meteorology program objective served by the measurement of winds over the oceans is weather danger and disaster warning. Specifically, the winds surrounding hurricanes or typhoons can be measured. Empirical techniques are available for estimating maximum winds near the storm center from the character and diameter of the central, dense, cirrus overcast as viewed in visual wavelengths by satellite sensors. However, the primary consideration for public warning would be the distance that gale- or hurricane-force winds extend outward from the center; this distance is not uniquely determined by the maximum wind. The microwave system flown on Skylab 1 (experiment S193) successfully mapped a major section of the surface windfield of Hurricane Ava on June 5, 1973, in the eastern Pacific. Even if the windfield were measured only every 12 hr, such a measurement would supply a major

piece of warning information that is now missing (unless ships or aircraft are in the vicinity of the storm). In a prediction context, low-level wind data are most vital. For instance, measurement of winds in the lowest levels of a hurricane have had more value in modeling hurricane strength than winds measured higher in the storm (ref. 4–32).

Finally, the measurement of surface winds over the tropical oceans is necessary for a better understanding of tropical dynamic processes on scales between the single cumulus scale and the planetary scale. It is believed that a major factor in the development of cumulus clusters is the presence of large-scale divergence in the upper troposphere. It is normally assumed that there must be compensating convergence near the surface, but the low-level convergence has not been directly observed (because of a lack of suitably spaced wind measurements). The use of satellite-derived winds from wave backscatter offers the first opportunity to directly measure the low-level convergence.

Anticipated Results

Predicting the weather itself is more accurate than predicting improvements in forecasting models. However, a modest statement of anticipated results can be offered. Assuming the existence of an operational satellite family based on SEASAT–A technology, one could expect, by the early 1980's, to see an improvement resulting from the greater density of data over ocean areas. The improvement in forecasting will be most notable in the range of 3 to 6 days. It may then be possible to predict the general nature of the weather 4 or 5 days ahead with the same skill that meteorologists now have in forecasting 2 days ahead. A definite improvement in 1- to 2-day forecasts on the west coast should also be expected.

In the area of hurricane warning, it should be possible, a few years after SEASAT, to see definite improvements in the prediction of storm surges and the location of destructive winds once the storm is close enough for hurricane warnings. It is not possible to know at this time how much improvement might be expected in the form of reduced "watch" areas by better long-term prediction of a hurricane's path.

One can look forward to a considerably improved understanding of dynamic-scale interaction in the Tropics. This understanding (leading to better parametrization of the role of cumulus-scale clouds in the Tropics), when combined with the global capability to update numerical prediction models, will also lead to improved weather forecasts, especially in the range of 3 to 6 days ahead.

METEOROLOGICAL APPLICATIONS FOR SEA-ICE MAPPING IN POLAR REGIONS

The Earth-atmosphere system constitutes a large (and inefficient) heat engine. The Tropics can be considered the "fire box" of the engine, absorbing an excess of incident solar radiation compared to the long-wave radiation lost to space. The polar regions, however, lose more radiation to space than they receive from the Sun. The resultant meridional gradient of net (absorbed solar minus emitted long-wave) radiation ultimately results in the energy that drives the atmospheric and oceanic circulations.

Important factors governing the radiation lost to space in the polar regions (and, hence, the meridional gradient of the net radiation, which affects the energetics of the atmospheric circulation, in turn affecting weather and climate) are the interactions among air, ice, and water in the polar regions. For example, the flux of heat from the polar sea surface to the atmosphere can be as much as three orders of magnitude greater from open water than from ice cover.

The ESMR flown on Nimbus 5 in December 1972 has already provided much new knowledge concerning the gross characteristics of sea-ice morphology and dynamics. This instrument operates at a frequency of 19.35 GHz ($\lambda = 1.55$ cm) and has a spatial resolution of approximately 30 km. A similar instrument is scheduled to fly on Nimbus-F late in 1975.

Chapter 3 of this report discusses the additional requirement for high-resolution sequential imagery of selected areas to test existing and developing models for sea-ice dynamics and the energy exchange in the ice-water-atmosphere system. The type of instrument suggested by the ocean panel as being most suitable for these investigations is an SAR. The atmosphere panel endorses this recommendation by the ocean panel as one of interdisciplinary interest between the oceanic and atmospheric scientists.

MOLECULAR TRANSFER CHARACTERISTICS OF AIR BETWEEN 10 AND 150 GHz

Applications are dependent upon the ability to describe the somewhat complicated interaction between microwave energy and the molecules that comprise the atmosphere. The complete body of experimental evidence on a one-way attenuation through the total atmosphere, summarized in figure 4–28, is somewhat inconclusive. Its origin in molecular water vapor and O_2 absorption is well known; however, analytical schemes are needed to establish (by accurate correlations to meteorological variables) the utility of a particular remote-sensing method.

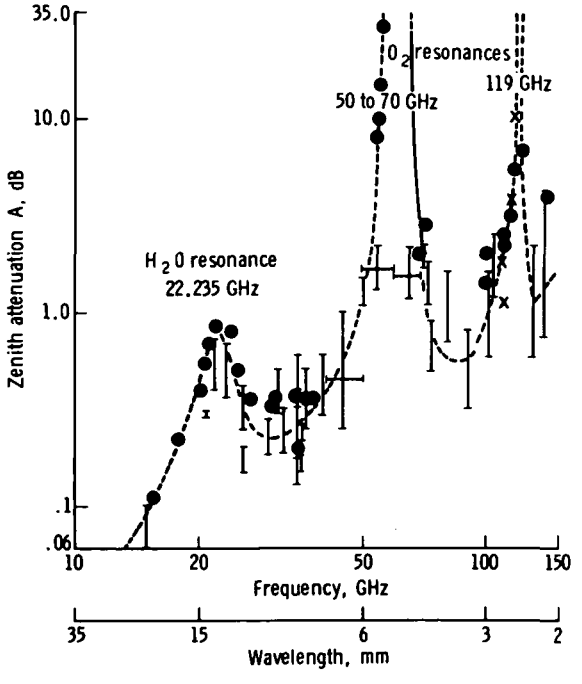

FIGURE 4–28.—Measured clear-sky zenith atmospheric attenuation in the range of 10 to 150 GHz (ref. 4–70).

The transfer properties of the total atmosphere are estimated from homogeneous gas conditions using numerical integration for modeled vertical pressure and temperature profiles. The H_2O and O_2 spectra for the homogeneous gas are discussed in the sections entitled "Water Vapor" and "Air" concerning their variability with frequency ν, dry air pressure p, water vapor pressure p_w, and temperature T as it occurs over the altitude range of $h=0$ to 90 km. Such a description of electromagnetic medium properties is, of course, fundamental to all active microwave remote-sensing schemes.

An emergent microwave signal is affected in amplitude, phase, and direction (refractive bending) by the intervening atmosphere; and the interaction can be a strong function of frequency. In addition, under special circumstances (O_2-microwave-spectrum (O_2-MS) Zeeman effect when $h>45$ km), a dependence on polarization and orientation can occur. Such behavior lends itself to active remote-sensing applications of atmospheric conditions, because the H_2O and O_2 resonance spectra are uniquely related to water vapor contents and to the dry airmass.

Gaseous transfer characteristics are expressed for homogeneous conditions in terms of attenuation coefficient k (in dB/km) and phase dispersion $\Delta\phi$ (in rad/km) by

$$k=0.1820\nu(N''_d+N''_w) \qquad (4\text{–}65)$$

and

$$\Delta\phi=0.02095\nu(\Delta N_d+\Delta N_w) \qquad (4\text{–}66)$$

where ν is the microwave frequency in GHz, and N''_d and N''_w are molecular extinction spectra of dry air (O_2 and ozone (O_3)) and of water vapor (H_2O and H_2OOH_2), and N_d and N_w are the corresponding dispersion spectra, all in units of ppm.

Cumulative transfer characteristics are evaluated by

$$\left.\begin{aligned} A &= \int_{h_i}^{h_f} k(l)\, dl \\ \Delta T &= \int_{h_i}^{h_f} \Delta\phi(l)\, dl \end{aligned}\right\} \qquad (4\text{–}67)$$

where A is zenith attenuation in decibels, ΔT is zenith dispersion in radians, dl is an increment of the ray path, h_i is the initial altitude, and h_f is the final altitude where $k(l)$ and $\Delta\phi(l)$ are essentially zero (h_f is approximately 90 km for O_2 and approximately 25 km for H_2O).

Water Vapor

Two rotational lines of the H_2O spectrum are centered at 22 and 183 GHz. The resonant part caused by these lines is evaluated by equations (4–65) and (4–66) using

$$\left.\begin{aligned} N''_w &= \sum_i (SF'')_i \\ \Delta N_{wc} &= \sum_i (SF')_i \end{aligned}\right\} \qquad (4\text{–}68)$$

where F is the pressure-broadened line, and the line strength S is given by

$$S = \frac{\nu}{\nu_0} S^\circ \left(\frac{300}{T}\right)^{3.5} p_{wc} \exp\left[w\left(1-\frac{300}{T}\right)\right] \qquad (4\text{–}69)$$

and for the intensity distribution of strongly air-broadened H_2O lines one assumes the shape

$$\left.\begin{aligned} F'_G &= \frac{2\nu_0(\nu_0^2-\nu^2)}{(\nu_0^2-\nu^2)^2+(2\nu\gamma_l)^2} \\ F''_G &= \frac{4\nu^2\gamma_l}{(\nu_0^2-\nu^2)^2+(2\nu\gamma_l)^2} \end{aligned}\right\} \qquad (4\text{–}70)$$

where the linewidth γ_l is given by

$$\gamma_l = \gamma^\circ\left[m_d\left(\frac{300}{T}\right)^{0.6} p + \left(\frac{300}{T}\right) p_{wc}\right] \qquad (4\text{–}71)$$

The line parameters given in table 4–VIII are at $T=300$ K (ref. 4–71).

The line spectrum of H_2O is not sufficient to account for water-vapor microwave attenuation away from the two line centers. A residual attenuation exists that can be postulated to consist of two parts: (1) the low-frequency wings of all H_2O rotational lines above 200 GHz, and (2) the microwave spectrum of a water vapor dimer H_2OOH_2.

The residual H_2O (monomer) attenuation can be estimated by

$$k_M \approx 4\times10^{-3}\, p_{wc}\left(\frac{\nu}{60}\right)^2\left(\frac{300}{T}\right)^{2.5} \qquad (4\text{–}72)$$

where k_M is in dB/km, p_{wc} is in torr, ν is in gigahertz, and T is in kelvin (e.g., when $p_{wc}=1$ torr, $T=280$ K, and $\nu=60$ GHz, then $k_M \approx 5\times10^{-3}$ dB/km).

The theory of a dimer attenuation k_D was treated in detail by Poon (ref. 4–72). The theoretical findings between 10 and 100 GHz can be roughly expressed by

$$k_D \approx 0.2\times10^{-3}\, p_{wc}^2\left(\frac{\nu}{60}\right)^{2.4}\left(\frac{300}{T}\right)^{17} \qquad (4\text{–}73)$$

(e.g., when $p_{wc}=10$ torr, $T=280$ K, and $\nu=60$ GHz, then $k_D \approx 65\times10^{-3}$ dB/km). Sketchy experimental evidence exists to somewhat support equations (4–72) and (4–73); however, much more experimental data need to be

TABLE 4–VIII.—*Line Spectrum Parameters at T=300 K for H_2O at 22 and 183 GHz*

Label	Individual lines of the H_2O microwave spectrum	
	1	2
Center frequency ν_0, GHz	22.23515	183.31012
Strength parameter S°, Hz/torr	[a] 13.9	[a] 322.0
Temperature exponent w, units	2.14	.653
Width (H_2O) γ°, MHz/torr	[a] 18.0	[a] 19
Broadening effect (air) m_d, units	.209	.21

[a] Unit of measurement fixed by the related equation.

gathered at different frequencies, temperatures, and close-to-saturation pressures.

The resonance dispersion ΔN_w offers a concept to measure the variability of atmospheric water vapor. The differential phase delay between two phase-coherent signals with frequencies on either side of the molecular resonance is a measure of the total amount of water vapor along the path. Such dual-frequency signals could be transmitted from a geostationary satellite and received by many ground stations. The technique has been investigated for line-of-sight ground-level paths (refs. 4–73 and 4–74). The integrated resonance dispersion for a vertical (zenith) path (fig. 4–29) provides some quantitative data. The calculation was based on equations (4–66), (4–67) (where $\Delta L = \Delta T c/2\pi\nu$), and (4–68) to 4–71). For the frequency pair 25.2 and 19.2 GHz, one obtains a phase change of 0.41° (0.015 mm/torr), which is sufficiently linear with each torr of ground-level water-vapor pressure.

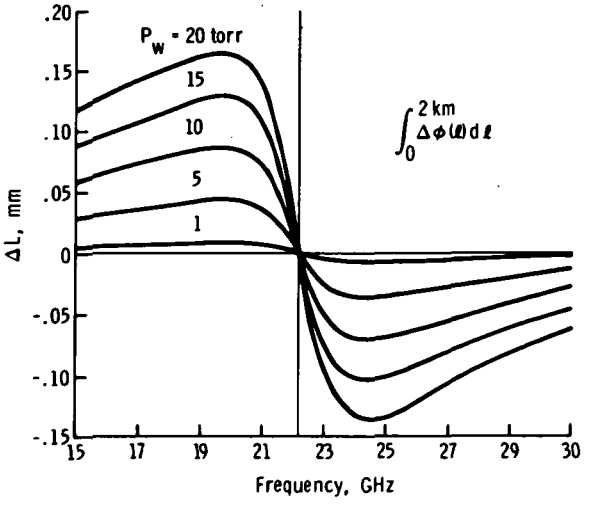

FIGURE 4–29.—Integrated resonance dispersion due to 22-GHz water-vapor line for vertical path through model atmosphere; p_w is water-vapor pressure at ground level (ref. 4–71). The model atmosphere was $p_0=760$ torr, $T_0=290$ K, and $p_w=1$ to 20 torr for ground-level conditions; exponential water-vapor distribution with 2.5-km scale height; $T=T_0-6.5h$ (km) and $p=p_0(T/T_0)^{5.53}$ for $h \leq 10$ km; $T=225$ K and $p=155\exp(-0.015)$ for $h > 10$ km.

The much stronger 183-GHz line, for a signal pair 187 and 179 GHz, yields a differential phase delay of approximately 50° per torr of ground-level water vapor; but it is associated with higher attenuation (approximately 15 dB).

Air

For all atmospheric transmission problems, it is sufficient to consider i less than or equal to 44 individual lines of the O_2-MS. Of these, 43 lines are centered around 60 GHz and 1 line at 119 GHz. Propagation parameters are evaluated using the following expressions for equations (4–65) and (4–66):

$$\left.\begin{aligned} N_d'' &= \sum_i (SF'')_i \\ \Delta N_d &= \sum_i (SF')_i \end{aligned}\right\} \qquad (4\text{–}74)$$

where N_d'' and ΔN_d are in ppm.

Each line strength is given in air by

$$S_i = 0.2090 \frac{\nu}{\nu_0^i} p\,[S^\circ \psi(T)]_i \qquad (4\text{–}75)$$

where S_i is in hertz and the temperature function (relative to $T_0=300$ K) is

$$\psi(T) = \left(\frac{300^3}{T}\right) \exp\left[-6.895\times10^{-3} N(N+1)\left(\frac{300}{T}-1\right)\right] \qquad (4\text{–}76)$$

where N is a quantum number.

Each pressure-broadened ($p \approx 1$ to 800 torr) line is described by the Lorentzian shape

$$\left.\begin{aligned} F' &= \frac{z}{\gamma_l(1+z^2)} \\ F'' &= \frac{1}{\gamma_l(1+z^2)} \end{aligned}\right\} \qquad (4\text{–}77)$$

where $z=(\nu_0^i-\nu)/\gamma_{l_i}$ is a dimensionless frequency.

The pressure-broadened linewidth (in megahertz) is

$$\gamma_{l_i}(p) = m_a(\gamma^\circ p - \xi p^2 + \cdots)\left(\frac{300}{T}\right)^{0.85} + \gamma^\circ m_w \frac{300}{T} p_w \quad (4\text{–}78)$$

where $m_a = 0.93$ and $m_w = 1.25$ are the broadening efficiencies in air and water vapor, respectively, and ξ (approximately equal to 0.0016 MHz/torr^2) is an empirical overlap coefficient (ref. 4–63). Table 4–IX

TABLE 4–IX.—*Spectroscopic Parameters of O_2 Microwave Line Spectrum*

O_2 line	Center frequency ν_0, GHz	Quantum number N		Strength S°, Hz/torr[a]	Width γ°, MHz/torr[a]	Remarks
		+	−			
1.....	48.942 4	.....	43^-	0.000 024	1.79	
	49.451 4	.....	41^-	.000 073	1.79	
	49.961 8	.....	39^-	.000 216	1.79	
	50.473 6	.....	37^-	.000 598	1.79	
5.....	50.987 3	.....	35^-	.001 564	1.79	
	51.503 02	.....	33^-	.003 860	1.79	
	52.021 17	.....	31^-	.008 985	1.79	
	52.542 23	.....	29^-	.019 707	1.79	
	53.066 80	.....	27^-	.040 717	1.79	
10.....	53.595 68	.....	25^-	.079 186	1.79	
	54.129 96	.....	23^-	.144 84	1.79	
	54.671 145 (20)	.....	21^-	.248 87	1.79	
	55.221 372 (20)	.....	19^-	.401 19	1.79	
	55.783 819 (20)	.....	17^-	.605 61	1.79	
15.....	56.264 778 (10)	1^+	.....	.348 69	2.26	Doublet
	56.363 393 (20)	.....	15^-	.853 87	1.79	98.62
	56.986 180 (20)	.....	13^-	1.120 4	1.79	
	57.612 49	.....	11^-	1.359 5	1.79	
	58.323 885 (10)	.....	9^-	1.515 0	1.79	Doublet
20.....	58.446 580 (10)	3^+	.....	.925 05	1.89	122.72
	59.164 215 (10)	.....	7^-	1.526 3	1.79	
	59.590 978 (10)	5^+	.....	1.341 0	1.81	
	60.306 044 (10)	.....	5^-	1.348 7	1.81	Doublet
	60.434 776 (10)	7^+	.....	1.562 6	1.79	128.74
25.....	61.150 565 (5)	9^+	.....	1.589 9	1.79	
	61.800 169 (10)	11^+	.....	1.458 8	1.79	
	62.411 223 (10)	13^+	.....	1.227 2	1.79	Doublet
	62.486 255 (10)	.....	3^-	.963 36	1.89	75.03
	62.998 00	15^+	.....	.954 01	1.79	
30.....	63.568 520 (10)	17^+	.....	.689 76	1.79	
	64.127 777 (20)	19^+	.....	.465 60	1.79	
	64.678 92	21^+	.....	.294 21	1.79	
	65.224 120 (20)	23^+	.....	.174 37	1.79	
	65.764 744 (20)	25^+	.....	.097 074	1.79	
35.....	66.302 06	27^+	.....	.050 820	1.79	
	66.836 77	29^+	.....	.025 041	1.79	
	67.369 51	31^+	.....	.011 621	1.79	
	67.900 73	33^+	.....	.005 083	1.79	
	68.430 8	35^+	.....	.002 096	1.79	
40.....	68.960 1	37^+	.....	.000 815	1.79	
	69.488 7	39^+	.....	.000 299	1.79	
	70.016 9	41^+	.....	.000 104	1.79	
	70.544 9	43^+	.....	.000 034	1.79	
44.....	118.759 343 (10)	.....	1^-	.597 25	2.10	Isolated line

[a] Relative to $T_0 = 300$ K.

lists the parameters for 44 lines labeled by line number or the quantum number $N^{\pm}$ (where ν_0 is center frequency, $S°$ is strength, and $\gamma°$ is width).

Transfer properties of homogeneous dry air.—The clean, dry atmosphere sustains a constant mixing ratio up to $h \leq 80$ km for all gases that might have a measurable influence on microwave transfer properties. An exception is ozone. The stronger lines of ozone in the microwave part of the spectrum are listed in table 4–X. A maximum zenith attenuation between 0.16 and 0.75 dB to ground level and a half-linewidth of approximately 30 MHz for an observation platform at $h=$ 12 km gives these lines some potential for the remote sensing of the atmospheric ozone content (refs. 4–75 and 4–76). However, the much stronger effects as a result of O_2 shall be emphasized here. Attenuation (eq. (4–65)) and dispersion (eq. (4–66)) related to the atmospheric O_2-MS are calculated using equations (4–74) to (4–78). The dependences on temperature and pressure follow from equations (4–75), (4–76), and (4–78). Results can be categorized as continuum, line, double-line (doublet), and line-Zeeman spectra in terms of altitude h increases.

1. Altitude $h<10$ km: All lines, except one at 119 GHz, are merged into a continuum spectrum under the influence of pressure broadening. Nonlinear (with respect to pressure) overlap effects are taken into account

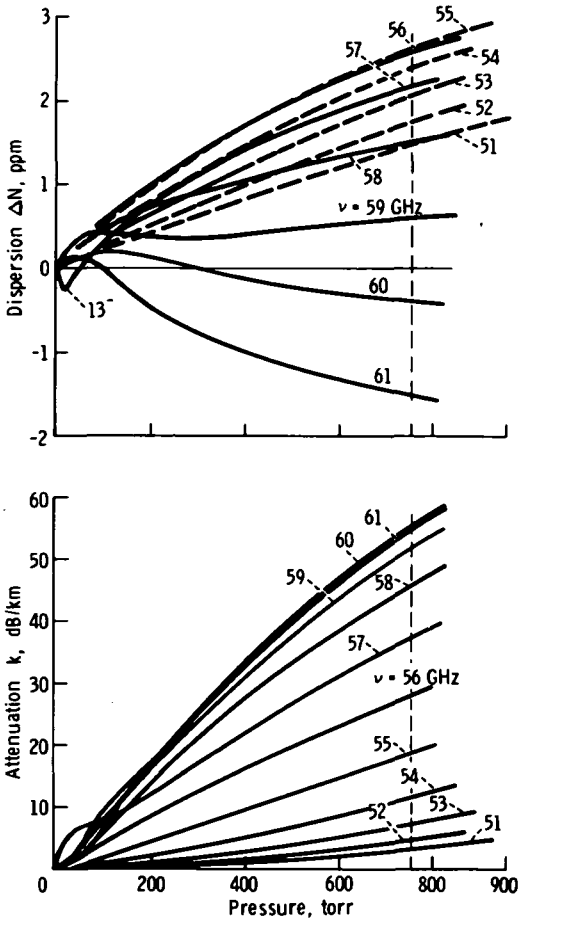

FIGURE 4–30.—Pressure profiles of the O_2 microwave continuum spectrum between 51 and 61 GHz at $T=300$ K. For dry air, multiply vertical scales (k and ΔN) by the factor 0.225. Simulated altitude range $h \approx 0$ to 20 km.

TABLE 4–X.—*Stronger Spectral Lines of Ozone in the 10- to 150-GHz Frequency Band* [a]

Center frequency, GHz	Maximum absorption of pure gas, dB/km [b]	Zenith absorption (maximum), dB [c]
96.2288	426	0.16
101.7368	803	.3
110.835	1230	.4
124.086	1750	.5
125.389	1030	
136.883	300	
142.172	2330	.75

[a] Data from refs. 4–75 and 4–76.

[b] Relative to $T_0=300$ K.

[c] Calculated for U.S. Standard Atmosphere (1962) (ref. 4–77) and daytime ozone distribution (maximum of 5×10^{13} molecules/cm^3 at $h=20$ km).

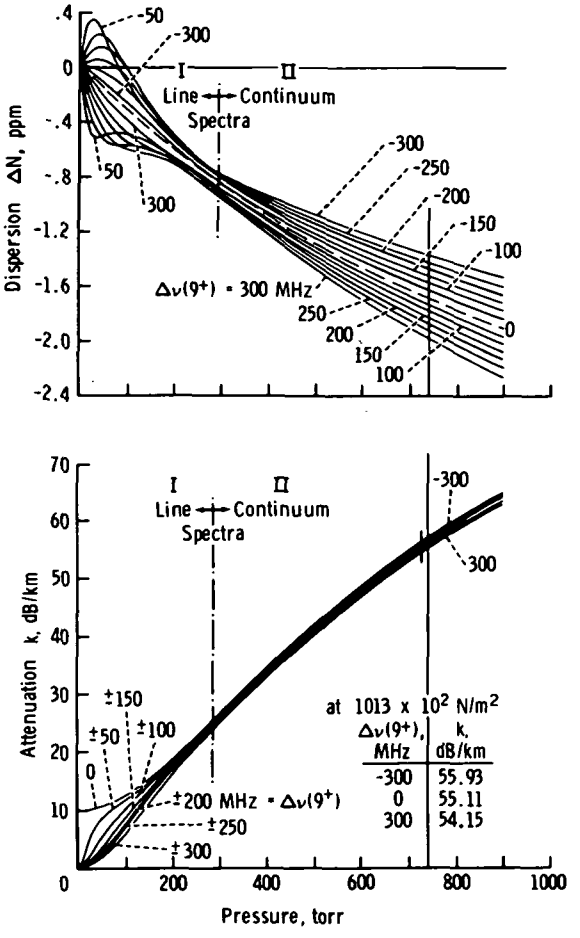

FIGURE 4–31.—Pressure profiles of the O_2 microwave spectrum in the vicinity ($\Delta\nu=\nu-\nu_0$) of the 9⁺ line ($\nu_0=61.1506$ GHz). For dry air, multiply vertical scales by 0.225. Simulated altitude range $h \approx 0$ to 20 km.

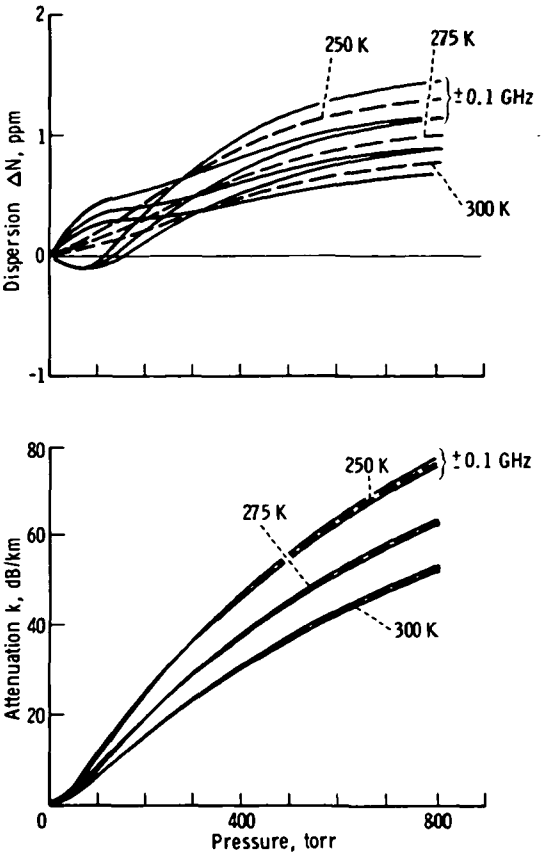

FIGURE 4–32.—Pressure profiles of the O_2 microwave continuum spectrum for $T=250$ to 300 K. The differential pressure sensitivity for $\nu\pm0.1$ GHz (58.8 ±0.1 GHz) is shown. For dry air, multiply vertical scales by 0.225. Simulated altitude range $h \approx 0$ to 20 km (ref. 4–78).

by the empirical parameter η. The results are given in figures 4–30, 4–31, and 4–32. The conversion factor from O_2 to air intensity (0.225) was experimentally verified. The attenuation can be approximated by a power-law form

$$k=\frac{Cp^{x(\nu)}T^{y(\nu)}}{1+\left(\frac{\nu_c-\nu}{\gamma_c}\right)^2} \qquad (4\text{–}79)$$

where C is a constant.

The pressure dependence on h is governed by the hydrostatic equation

$$p(h)=p_0e^{-h/H} \qquad (4\text{–}80)$$

where p_0 is the surface pressure, and $H=0.0293T(h)$ is the pressure scale height. An average atmospheric temperature $\bar{T}(h)=239$ K yields $H=7.0$ km (ref. 4–72). The vertical temperature profile, however, is not given by any simple physical model for $h<80$ km and must be taken from tables for model atmospheres.

2. Altitude $h>30$ km: An isolated line spectrum is displayed. The summation in equation (4–74) can be reduced to the response of a single line plus an unstructured background term. An example displays pressure profiles in the vicinity of the 9⁺ line (fig. 4–31). The response of the four O_2-MS doublets falls in the same category. The

normal line spacing is roughly 500 MHz, whereas the doublets are separated only by approximately 100 MHz. The example given in figure 4–33 shows the more complicated pressure dependence of k and ΔN. The doublet is suited to experimentally study the overlap effects (whereby the problem is reduced to two lines instead of $i=1$ to 43).

3. Altitude $h>45$ km: Zeeman-splitting of each O_2-MS line in the Earth magnetic field becomes noticeable and causes anisotropic, polarization-dependent transfer properties

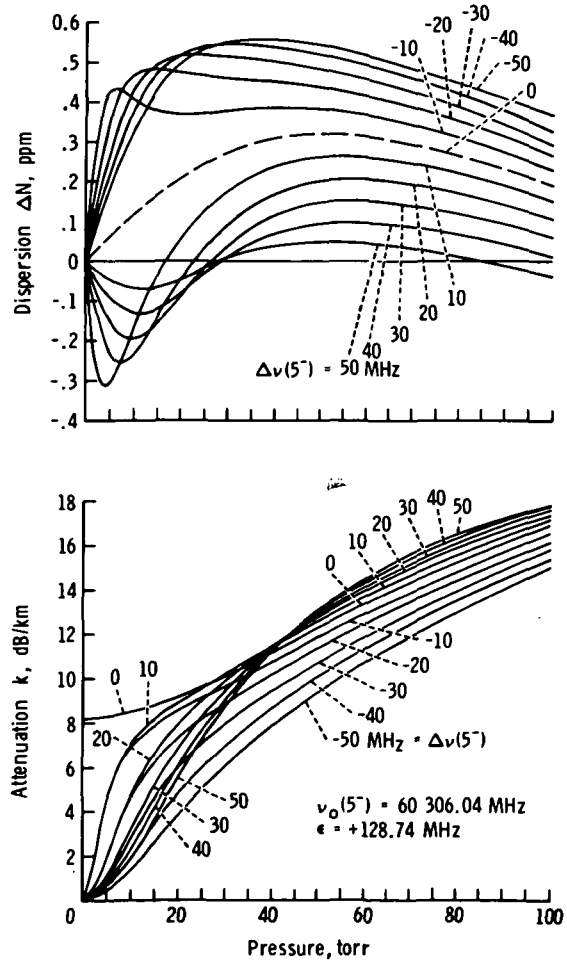

FIGURE 4–33.—Pressure profiles of the O_2 microwave line spectrum (300 K) in the vicinity ($\Delta\nu=\nu-\nu_0$) of the $5^-/7^+$ doublet (the separation to ν_0 (7^+) is given by ϵ). For dry air, multiply vertical scales by 0.225. Simulated altitude range $h\approx 15$ to 40 km.

(ref. 4–63). At these altitudes, the lines are only a few megahertz wide, although individual Zeeman components are not resolved. Each O_2-MS line assumes a constant width under the influence of a magnetic field and rapidly approaches zero intensity as the pressure drops below 1 torr. An example (fig. 4–34) treats the case of the 1^+ line, which splits into two σ-components when the magnetic-field vector of linearly polarized radiation is assumed to be perpendicular to the direction of the Earth magnetic-field strength in the plane perpendicular to the propagation direction.

For remote-sensing applications, it is important to know the frequency, pressure, and temperature sensitivities of O_2-MS transfer characteristics for a given condition. An example is given in figure 4–32.

Transfer properties of the total dry airmass.—The total atmospheric O_2-MS contains all the cases discussed in the previous section concerning transfer properties of homogeneous dry air (oxygen). The complexity of the problem is underlined by the various homogeneous gas conditions presented in figures 4–30 to 4–34. A solution of equation (4–67) was approximated by assuming a spherically stratified atmosphere with $i=151$ homogeneous slabs for $h=0$ to 90 km and a numerical integration based on Simpson's rule as follows:

$$\left.\begin{aligned} A &= 0.5\sum (k_i+k_{i+1})\,\Delta l_i(\theta) \\ \Delta T &= 0.5\sum (\Delta\phi_i+\Delta\phi_{i+1})\,\Delta l_i(\theta) \end{aligned}\right\} \qquad (4\text{–}81)$$

where A is in decibels and ΔT is in radians. The slant-path-length increments Δl_i are calculated along a straight-line path using an algorithm based on the starting angle against zenith θ (ref. 4–63). The results for three different initial altitudes ($h_i=h_l=0$, 10, and 20 km) are shown in figure 4–35.

Molecular emission produces an antenna noise temperature proportional to the integral over the attenuation rate and temperature distribution along the path at which the antenna is looking. This is the basis for the

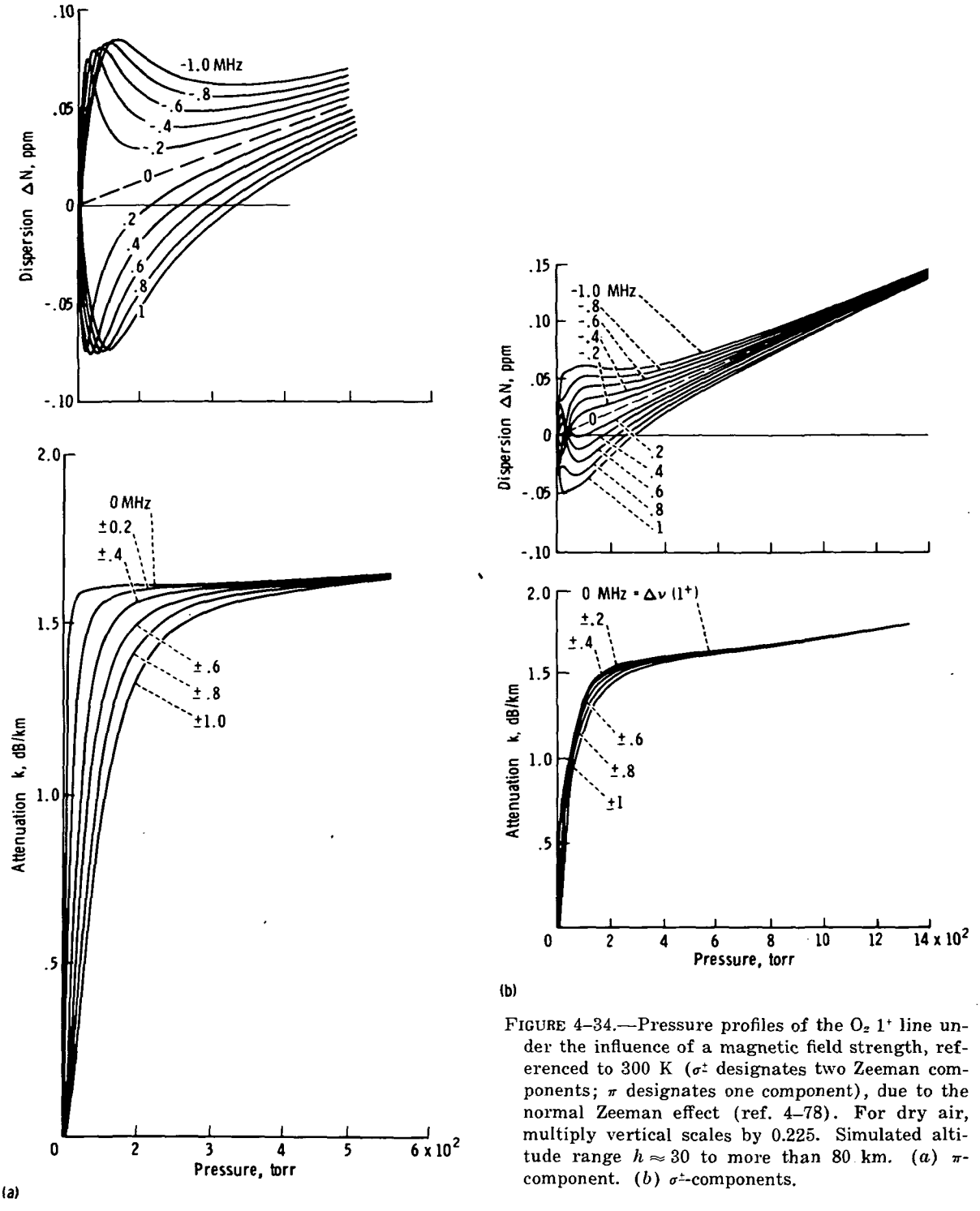

FIGURE 4–34.—Pressure profiles of the O_2 1^+ line under the influence of a magnetic field strength, referenced to 300 K ($\sigma^{\pm}$ designates two Zeeman components; π designates one component), due to the normal Zeeman effect (ref. 4–78). For dry air, multiply vertical scales by 0.225. Simulated altitude range $h \approx 30$ to more than 80 km. (*a*) π-component. (*b*) $\sigma^{\pm}$-components.

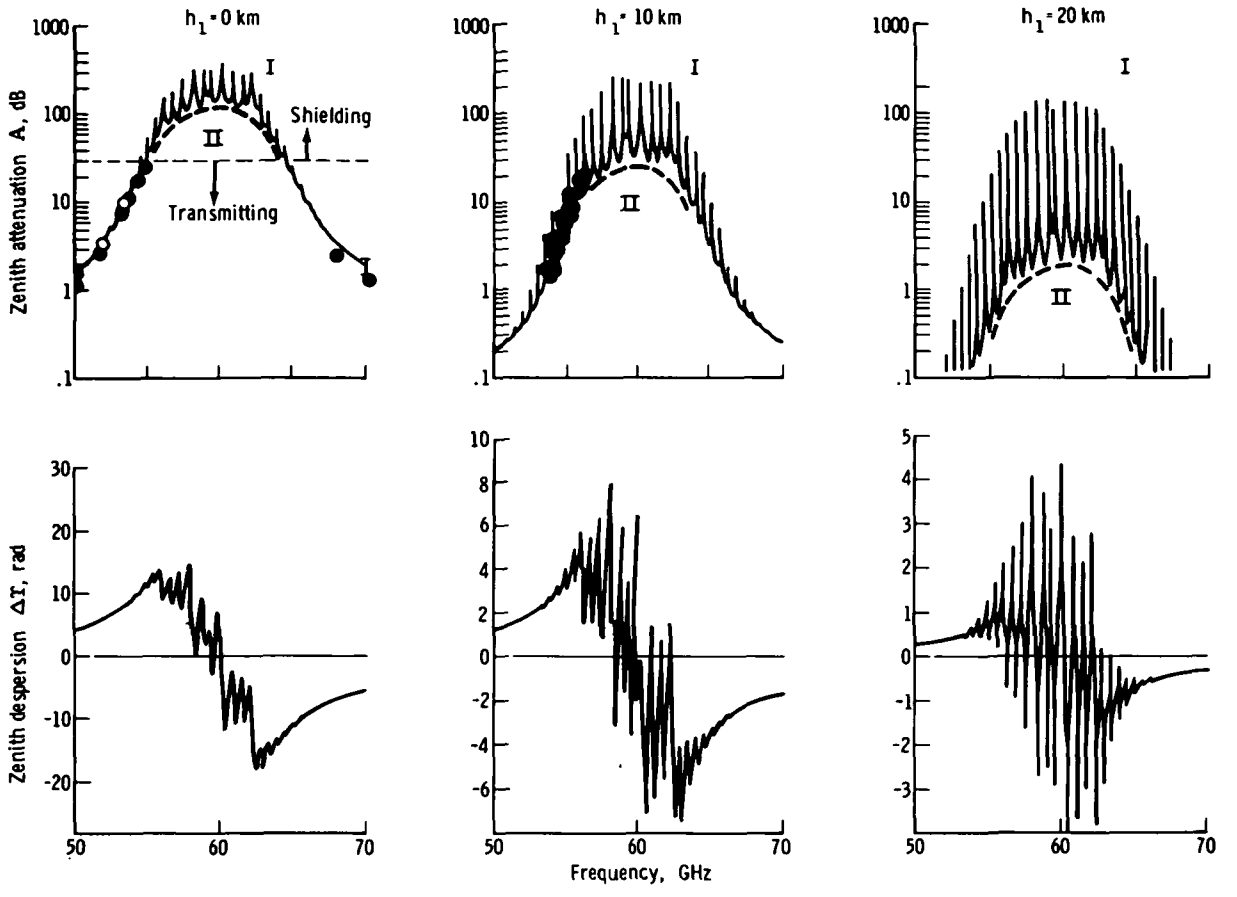

FIGURE 4–35.—One-way attenuation A and phase dispersion ΔT due to the O_2 microwave spectrum between 49 and 72 GHz for a zenith path through the U.S. Standard Atmosphere 1962 (ref. 4–77) from three different initial altitudes h_1 to outer space (I-line, II-continuum spectra). (For experimental points for $h_1=0$, see fig. 4–30.)

passive (radiometric) remote-sensing application to globally map vertical temperature structures from a satellite. In active systems, this atmospheric noise poses a problem because it sets an ultimate limit to the receiver sensitivity. Across the O_2-MS band, the noise temperature varies between 3 K ($A=0$ dB) and 300 K ($A>50$ dB), which is, however, still of no concern because mixer noise is considerably higher.

The resonance dispersion ΔN_d offers a concept to measure the variability of the dry airmass. The differential phase delay between two phase-coherent signals with frequencies on either side of the 60-GHz band is a measure of dry air conditions. The extreme values of O_2-MS zenith dispersion from $h=0$ to outer space (fig. 4–35) are shown in table 4–XI. The nondispersive delay $\Delta\tau$ caused by the vertical refractivity profile is approximately 7000 psec for a zenith path at 60 GHz. Moving the sensing frequency pair into the edges of the O_2-MS band increasingly favors the gas mass at the lower altitudes.

The same differential principle applies to attenuation in the semitransparent O_2-MS portions ($55<\nu<65$ GHz). By defining an equivalent altitude h_k for the zenith O_2-MS attenuation A (fig. 4–35) (where the homogeneous ground-level attenuation coefficient k (fig. 4–36) equals A), one obtains $h_k=$ 18 km (at a maximum of 60.4 GHz) and

TABLE 4–XI.—*Extreme Values of O_2-MS Zenith Dispersion*

Frequency ν, GHz	Zenith dispersion ΔT, rad	$\Delta L=(\Delta Tc)/(2\pi\nu)$, mm	$\Delta\tau=\Delta T/(2\pi\nu)$, psec
58.3	+15	+12	+40
	33	26	85
62.6	−18	−14	−45

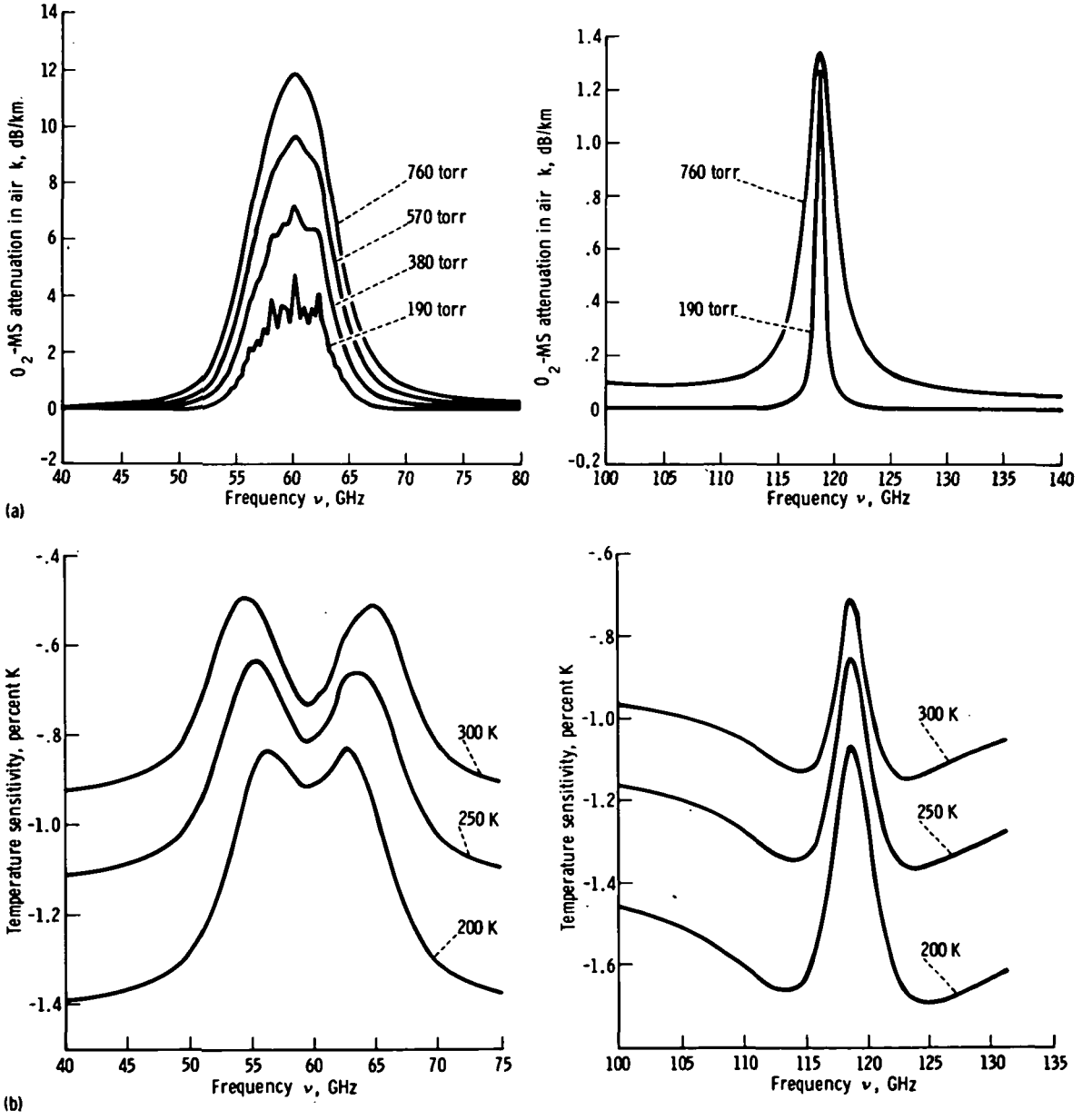

FIGURE 4–36.—The O_2 microwave spectrum attenuation and its pressure and temperature sensitivities to various atmospheric conditions over the 40- to 140-GHz band (ref. 4–78). (*a*) Attenuation in air k compared with frequency $\nu(T=300$ K). (*b*) Temperature sensitivity compared with frequency $\nu(p=760$ torr).

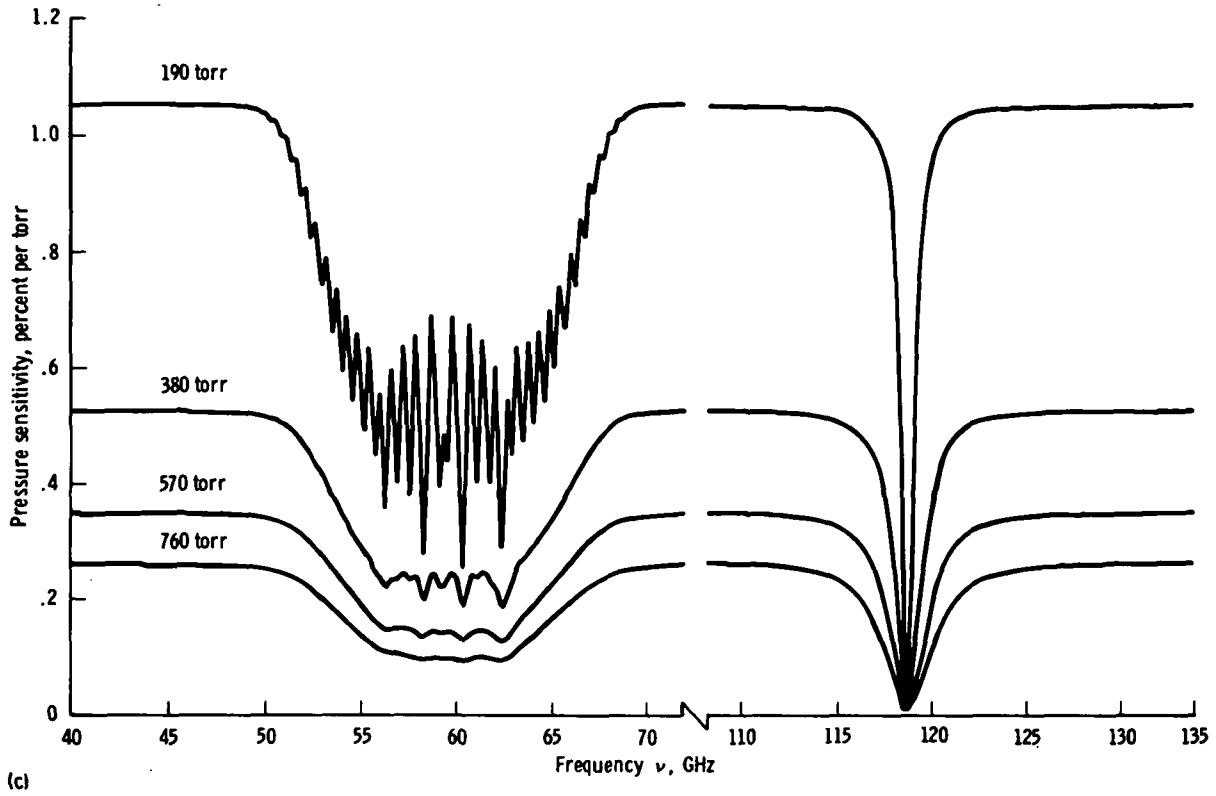

FIGURE 4–36 (concluded).—The O_2 microwave spectrum attenuation and its pressure and temperature sensitivities to various atmospheric conditions over the 40- to 140-GHz band (ref. 4–78). (*c*) Pressure sensitivity compared with frequency $\nu(T=300$ K).

$h_k=5$ km (for $50<\nu<55$ GHz and $66<\nu<72$ GHz).

A proposal has been made to measure surface pressure by a differential intensity measurement of two satellite-based radar signals reflected from the Earth surface (ocean), whereby one frequency lies in the semitransparent O_2-MS range and the other is remote from the O_2-MS in a transparent range. (See the section entitled "The Measurement of Surface Pressure From a Satellite by Active Microwave Techniques.") The calculations for the U.S. Standard Atmosphere, 1962 (ref. 4–77) yield the values of h_k given in the previous paragraph, which predict essentially constant opacity ($h_k=5$ km); hence, the attenuation response of the total airmass may be evaluated by equation (4–79). The values of x and y at a particular frequency (figs. 4–30 to 4–34) are the significant parameters for a radar sensing of surface pressure.

One can conceive possibilities for atmospheric research with a microwave system consisting of a transmitter on one spacecraft and a receiver on another. (See the section entitled "Applications of Bistatic Microwave Systems to Atmospheric Research.") Atmospheric occultation at frequencies in the two O_2-MS bands centered at 60 and 119 GHz can exploit the properties of individual O_2-MS lines when the closest approach to ground level is $h>15$ km. Two possible applications are:

1. The peak attenuation of the two $N=15^{\pm}$ lines (table 4–IX) is independent of temperature and thus a good indicator of stratospheric pressure (ref. 4–63).

2. The fact that the transfer characteristics in the vicinity of the $1^{\pm}$ lines (fig. 4–34) are dependent in the least complicated manner upon strength and orientation of the

Earth magnetic field suggests magnetometer applications.

Conclusions

Technically, there are several promising remote-sensing concepts that can benefit from or are affected by H_2O and O_2 spectroscopic transfer characteristics. The following research will provide a basis for the development of remote-sensing schemes operating in the 10- to 150-GHz frequency range:

1. The translation of molecular theory on millimeter wave properties of air into engineering terms.

2. The description of analytical schemes to predict propagation phenomena on the basis of meteorological variables, together with examples of unique atmospheric transfer properties.

Laboratory work is recommended to better define the spectroscopic parameters of atmospheric microwave transfer characteristics as a function of pressure, composition, temperature, and magnetic-field strength over the range of these variables encountered in the atmosphere.

REFERENCES

4–1. The Atmospheric Sciences and Man's Needs, Priorities for the Future. Printing and Publishing Office, National Academy of Sciences (Washington, D.C.), 1971.

4–2. Report of the Planning Conference on the First GARP Global Experiment. World Meteorological Organization and International Council of Scientific Unions (Geneva, Switzerland), Sept. 1972.

4–3. LIGDA, MYRON G. H.: Radar Storm Observation. Compendium Meteorology, Amer. Meteorol. Soc. (Boston, Mass.), 1951, pp. 1265–1282.

4–4. MARSHALL, J. S.; HITSCHFELD, WALTER; AND GUNN, K. L. S.: Advances in Radar Weather. Advances in Geophysics, vol. II, H. E. Landsberg, ed. Academic Press (New York), 1955, pp. 1–56.

4–5. VAN BLADEL, J.: Les Applications du Radar à L'Astronomie et à La Météorologie. Gauthier-Villars (Paris, France), 1955.

4–6. MARSHALL, J. S., AND GORDON, W. E.: Radiometeorology. Meteorol. Monogr., vol. 3, no. 14, July 1957, pp. 73–113.

4–7. BATTAN, LOUIS J.: Radar Meteorology. Univ. of Chicago Press, 1959.

4–8. ATLAS, DAVID: Advances in Radar Meteorology. Advances in Geophysics, vol. X, Academic Press (New York), 1964, pp. 317–478.

4–9. STEPANENKO, V. D.: Radar in Meteorology. Gidrometeoizdat (Leningrad), 1966. (Partial translation available from Joint Publications . Research Service, Washington, D.C.)

4–10. KOSTAREV, V. V.; CHERNIKOV, A. A.; AND SHUPYATSKII, A. B., eds.: Radar Meteorology. Translation of the 1968 Proceedings of the Third All-Union Conference. Israel Program for Sci. Transl., 1971. (Available as IPST 5809.)

4–11. BATTAN, LOUIS J.: Radar Observation of the Atmosphere. Univ. of Chicago Press, 1973.

4–12. STEPANENKO, V. D.: Radar in Meteorology. Second ed. Gidrometeoizdat (Leningrad), 1973.

4–13. SMITH, PAUL L., JR.; HARDY, KENNETH R.; AND GLOVER, KENNETH M.: Applications of Radar to Meteorological Operations and Research. Proc. IEEE, vol. 62, no. 6, June 1974, pp. 724–745.

4–14. LIGDA, M. G. H.: Middle Latitude Precipitation Patterns as Observed by Radar. Rep. 574 T, Dept. of Oceanography and Meteorology, Texas A. & M. Univ., Jan. 1957.

4–15. MCGREW, RUSSELL G.: Project D/RADEX (Digitized Radar Experiments). The 15th Radar Meteorology Conference, Amer. Meteorol. Soc. (Boston, Mass.), 1972, pp. 101–106.

4–16. OSTLUND, STELLAN SVEN: Computer Software for Rainfall Analyses and Echo Tracking of Digitized Radar Data. Tech. Memo. ERL WMPO–15, NOAA Environmental Research Labs. (Boulder, Colo.), 1974.

4–17. WEXLER, HARRY: Observing the Weather From a Satellite Vehicle. J. Brit. Interplanet. Soc., vol. 13, no. 5, Sept. 1954, pp. 269–276.

4–18. WIDGER, WILLIAM K., JR., AND TOUART, C. N.: Utilization of Satellite Observations in Weather Analysis and Forecasting. Amer. Meteorol. Soc. Bull., vol. 38, no. 9, Nov. 1957, pp. 521–533.

4–19. MOOK, CONRAD P., AND JOHNSON, DAVID S.: Proposed Weather Radar and Beacon System for Use With Meteorological Earth Satellites. IRE Third National Convention on Military Electronics (New York), 1959, pp. 206–209.

4–20. KATZENSTEIN, H., AND SULLIVAN, H.: A New

Principle for Satellite-Borne Meteorological Radar. Proceedings of the 8th Weather Radar Conference, Amer. Meteorol. Soc. (Boston, Mass.), 1960, pp. 505–515.

4–21. KEIGLER, J. E., AND KRAWITZ, L.: Weather Radar Observations From an Earth Satellite. J. Geophys. Res., vol. 65, no. 9, Sept. 1960, pp. 2793–2808.

4–22. DENNIS, ARNETT S.: Rainfall Determinations by Weather Radar on Meteorological Satellite Radar. NASA CR–50193, 1963.

4–23. DENNIS, ARNETT S.: Fundamental Limitations on Precipitation Observations From Satellites. NASA CR–52848, 1963.

4–24. Radar for Meteorology. Useful Applications of Earth-Oriented Satellites. Panel 4, App. G, NASA CR–101401, 1969, pp. 69–73.

4–25. KRISHNAMURTI, T. N.; KANAMITSU, M.; CESELSKI, B.; AND MATHUR, M. B.: Florida State University's Tropical Prediction Model. Tellus, vol. 25, no. 6, 1973, pp. 523–535.

4–26. KURIHARA, YOSHIO, AND TULEYA, ROBERT E.: Structure of a Tropical Cyclone Developed in a Three-Dimensional Numerical Simulation Model. J. Atmos. Sci., vol. 31, no. 4, May 1974, pp. 893–919.

4–27. MATHUR, MUKUT B.: Multiple-Grid Primitive Equation Model to Simulate the Development of an Asymmetric Hurricane. J. Atmos. Sci., vol. 31, no. 2, Mar. 1974, pp. 371–393.

4–28. MILLER, BANNER I.; CHASE, PETER P.; AND JARVINEN, BRIAN R.: Numerical Prediction of Tropical Weather Systems. Mon. Weather Rev., vol. 100, no. 12, Dec. 1972, pp. 825–835.

4–29. OOYAMA, KATSUYUKI: Numerical Simulation of the Life Cycle of Tropical Cyclones. J. Atmos. Sci., vol. 26, no. 1, Jan. 1969, pp. 3–40.

4–30. ROSENTHAL, STANLEY L.: Circularly Symmetric, Primitive Equation Model of Tropical Cyclone Development Containing an Explicit Water Vapor Cycle. Mon. Weather Rev., vol. 98, no. 9, Sept. 1970, pp. 643–663.

4–31. SUNDQVIST, HILDING: Numerical Simulation of the Development of Tropical Cyclones With a Ten-Level Model, pt. I. Tellus, vol. 22, no. 4, 1970, pp. 359–390.

4–32. ANTHES, RICHARD A.: Data Assimilation and Initialization of Hurricane Prediction Models. J. Atmos. Sci., vol. 31, no. 3, Apr. 1974, pp. 702–719.

4–33. TRACTON, M. S.: The Role of Cumulus Convection in the Development of Extra-Tropical Cyclones. Preprints, Eighth Conference Severe Local Storms, Amer. Meteorol. Soc. (Boston, Mass.), 1973, pp. 337–342.

4–34. ATLAS, D., AND ULBRICH, C. W.: The Use of Attenuation and Reflectivity for Improved Measurements of Water Content and Rainfall Rate. IUCRM—Colloquium on Fine Scale Structure of Precipitation and E.M. Propagation (Nice, France), Oct. 21, 1973.

4–35. ECCLES, P. J., AND ATLAS, D.: A New Method of Hail Detection by Dual-Wavelength Radar. The 14th Radar Meteorology Conference, Amer. Meteorol. Soc. (Boston, Mass.), 1970, pp. 1–6.

4–36. GOLDHIRSH, JULIUS, AND KATZ, ISADORE: Estimation of Raindrop Size Distribution Using Multiple Wavelength Radar Systems. Radio Sci., vol. 9, no. 4, Apr. 1974, pp. 439–446.

4–37. GUNN, K. L. S., AND EAST, T. W. R.: The Microwave Properties of Precipitation Particles. Quart. J. Roy. Meteorol. Soc., vol. 80, no. 346, Oct. 1954, pp. 522–545.

4–38. HADDOCK, F. T.: Scattering and Attenuation of Microwave Radiation Through Rain, Report of NRL Progress. Naval Research Laboratory (Washington, D.C.), June 1956, pp. 15–21.

4–39. MEDHURST, RICHARD G.: Rainfall Attenuation of Centimeter Waves: Comparison of Theory and Measurement. IEEE Trans. Antennas Propagat., vol. AP–13, no. 1, Jan. 1965, pp. 550–564.

4–40. WEXLER, RAYMOND, AND ATLAS, DAVID: Radar Reflectivity and Attenuation of Rain. J. Appl. Meteorol., vol. 2, no. 2, Apr. 1963, pp. 276–280.

4–41. MARSHALL, J. S., AND PALMER, W. MCK.: The Distribution of Raindrops With Size. J. Meteorol., vol. 5, no. 4, Aug. 1948, pp. 165–166.

4–42. MITCHELL, R. L.: Radar Meteorology at Millimeter Wavelengths. Rep. SSD TR–66–117, U.S. Air Force, Space Systems Division, 1966.

4–43. ATLAS, D., AND CHMELA, A. C.: Physical-Synoptic Variations of Drop-Size Parameters. Proceedings of the 6th Weather Radar Conference, Amer. Meteorol. Soc. (Boston, Mass.), 1957, pp. 21–29.

4–44. HARDY, WALTER N.; GRAY, KENNETH W.; AND LOVE, A. W.: An S-Band Radiometer Design With High Absolute Precision. IEEE Trans. Microwave Theory Tech., vol. MTT–22, no. 4, Apr. 1974, pp. 382–390.

4–45. MOORE, RICHARD K.: Ground Echo. Radar Handbook, ch. 25, Merrill I. Skolnik, ed., McGraw-Hill Book Co., 1970.

4–46. RUCK, GEORGE T.; BARRICK, DONALD E.; STUART, WILLIAM D.; AND KRICHBAUM, CLARENCE K.: Radar Cross Section Handbook, vol. I, George T. Ruck, ed., Plenum Press, 1970.

4–47. SPILHAUS, A. F.: Raindrop Size, Shape, and Falling Speed. J. Meteorol., vol. 5, no. 3, June 1948, pp. 108–110.

4–48. MCCORMICK, G. C., AND HENDRY, A.: The Study of Precipitation Backscatter at 1.8 cm With a Polarization Diversity Radar. The 14th Radar Meteorology Conference, Amer. Meteorol. Soc. (Boston, Mass.), 1970, pp. 225–230.

4–49. HENDRY, A., AND MCCORMICK, G. C.: Deterioration of Circular-Polarization Clutter Cancellation in Anisotropic Precipitation Media. Electron. Lett., vol. 10, no. 10, May 1974, pp. 165–166.

4–50. JONES, R. F.: Size-Distribution of Ice Crystals in Cumulonimbus Clouds. Quart. J. Roy. Meteorol. Soc., vol. 86, no. 368, Apr. 1960, pp. 187–194.

4–51. LHERMITTE, ROGER M.: Atmospheric Probing by Doppler Radar. Atmospheric Exploration by Remote Probes, vol. 2, National Academy of Sciences, 1968, pp. 253–285.

4–52. LHERMITTE, ROGER M.: Dual-Doppler Radar Observation of Convective Storm Circulation. The 14th Radar Meteorology Conference, Amer. Meteorol. Soc. (Boston, Mass.), 1970.

4–53. LHERMITTE, ROGER M.: Kinematics of Sea Breeze Storms. Geophys. Res. Newsletter, vol. 1, no. 3, July 1974, pp. 123–125.

4–54. LHERMITTE, ROGER M.: Real Time Monitoring of Convective Storm Processes by Dual Doppler Radar. Atmospheric Technology, no. 6, National Center for Atmospheric Research (Boulder, Colo.), 1975.

4–55. DONALDSON, RALPH J., JR.: Vortex Signature Recognition by a Doppler Radar. J. Appl. Meteorol., vol. 9, no. 4, Aug. 1970, pp. 661–670.

4–56. DOVIAK, R. F.; SIRMANS, D.; AND LEMMON, L.: Doppler Velocity and Reflectivity Structure Observed Within Tornadic Storms. Journal de Recherches Atmospheriques, May 1974.

4–57. JOSEPH, A. S.: Heterojunction PbSnTe Detectors Solve IR System Problems. Electro-Opt. Syst. Design, vol. 5, Oct. 1973, pp. 24–29.

4–58. RENSCH, D. B., AND LONG, R. K.: Comparative Studies of Extinction and Backscattering by Aerosols, Fog, and Rain at 10.6μ and 0.63μ. Appl. Opt., vol. 9, no. 7, July 1970, pp. 1563–1573.

4–59. ELTERMAN, LOUIS; TOOLIN, ROBERT B.; AND ESSEX, JOHN D.: Stratospheric Aerosol Measurements With Implications for Global Climate. Appl. Opt., vol. 12, no. 2, Feb. 1973, pp. 330–337.

4–60. MCCOY, JOHN H.; RENSCH, DAVID B.; AND LONG, RONALD K.: Water Vapor Continuum Absorption of Carbon Dioxide Laser Radiation Near 10μ. Appl. Opt., vol. 8, no. 7, Dec. 1968, pp. 1471–1478.

4–61. CHU, T. S., AND HOGG, D. C.: Effects of Precipitation on Propagation at 0.63, 3.5, and 10.6 Microns. Bell Syst. Tech. J., vol. 47, no. 5, May–June 1968, pp. 723–759.

4–62. The Planning of the First GARP Global Experiment. GARP Publ. no. 3, World Meteorological Organization (Geneva, Switzerland), 1969.

4–63. LIEBE, H. J., AND WELCH, W. M.: Molecular Attenuation and Phase Dispersion Between 40 and 140 GHz for Path Models From Different Altitudes. NASA CR–138495, 1973.

4–64. KRISHEN, K.: Mathematical Model for the Relationship of Radar Backscattering Cross Sections With Ocean Scene and Wind Velocity. Proceedings of the Seventh International Symposium on Remote Sensing of Environment, vol. III, Univ. of Michigan, May 1971, pp. 1861–1877.

4–65. SINGER, S. FRED: Measurement of Atmospheric Surface Pressure With a Satellite-Borne Laser. Appl. Opt., vol. 7, no. 6, June 1968, pp. 1125–1127.

4–66. WATTS, B. E.; HOWARD, A. M.; AND GIBBONS, G.: Double-Drift Millimetre-Wave Impatt Diodes Prepared by Epitaxial Growth. Electron. Lett., vol. 9, no. 8/9, May 1973, pp. 183–184.

4–67. BENOIT, ANDRE: Signal Attenuation Due to Neutral Oxygen and Water Vapor, Rain and Clouds. Microwave J., vol. 11, Nov. 1968, pp. 73–80.

4–68. SASAKI, Y.: An Objective Analysis Based on the Variational Method. J. Meteorol. Soc. Japan, ser. 2, vol. 36, no. 3, June 1958, pp. 77–88.

4–69. GHIL, M.: On Balance and Initiatization—Obtaining Data for Solving Initial-and-Boundary-Value Problems for Equations of Large Scale Dynamic Meteorology. Rep. IMM 400, Courant Inst. of Mathematical Sciences, New York Univ., Dec. 1973.

4–70. THOMPSON, W. I., III: Atmospheric Transmission Handbook. NASA CR–117173, 1971.

4–71. LIEBE, H. J.: Calculated Tropospheric Dispersion and Absorption Due to the 22-GHz Water Vapor Line. IEEE Trans. Antennas Propagat., vol. AP–17, no. 5, Sept. 1969, pp. 621–627.

4–72. POON, R. K.: Atmospheric Opacity Near Half Centimeter Wavelength. Ph.D. dissertation, Massachusetts Inst. of Technology, May 1974.

4–73. SULLIVAN, JOHN F., AND RICHARDSON, HAROLD

M.: Propagation of 15.6–31.2 GHz and 45–90 GHz Coherent Signal Pairs. AGARD Conf. Proc. No. 107 on Telecommunications Aspects on Frequencies Between 10 and 100 GHz, Sept. 1972, pp. 10/1–10/11.

4–74. THOMPSON, M. C.; WOOD, L. E.; AND JONES, H. B.: Phase and Fading Characteristics in the 10 to 40 GHz Band. Dept. of Commerce, Office of Telecommunications, Institute for Telecommunications Sciences Tech. Memo. prepared for NASA–LRC (Contract No. L–48, 854), Oct. 1972.

4–75. WATERS, J. W., AND PETRO, L. D.: Microwave Spectrum of Atmospheric Ozone. MIT–QPR No. 96, Research Laboratory of Electronics, Massachusetts Inst. of Technology, Jan. 1970, pp. 42–48.

4–76. WATERS, J.: Ground-Based Microwave Spectroscopic Probing of the Strato- and Mesosphere. Ph.D. dissertation, Massachusetts Inst. of Technology, Dec. 1970.

4–77. U.S. Standard Atmosphere, 1962. Superintendent of Documents, U.S. Government Printing Office (Washington, D.C.), 1962.

4–78. LIEBE, H. J.: Studies of Oxygen and Water Vapor Microwave Spectra Under Simulated Atmospheric Conditions. Dept. of Commerce, Office of Telecommunications, Institute for Telecommunications Sciences (Boulder, Colo.), 1974.

APPENDIX 4A

This appendix is based on a translation of section 9.6, entitled "Features and Effectiveness of the Detection of Clouds and Rain With Pulse Radar From Satellites," from Radar in Meteorology by V. D. Stepanenko (ref. 4–12).

UTILIZATION OF SCANNING BEAM RADAR

The capability of detecting a meteorological target with radar increases with the increase in transmitter power P_t and receiver sensitivity P_{min}. When interfering echo signals from the surface of the Earth are absent (as will often be the case for scanning-pencil beams produced by ground-based radar used for detection of the upper portion of clouds and rain), the required values of the radar parameters may be found from the basic radar equation.

When using radar in satellites, the widths of the radiation pattern $\theta_1\theta_2$ cannot be arbitrary; rather, they must be selected to insure a total angle of scan that will cover the Earth without any gaps. The radar-detection range depends on the orbit height and the given width of the region of coverage. The minimum height of the orbit is about 200 km; consequently, it is also the minimum detection range. This appears to be a disadvantage that is absent with ground-based radar; and, in the case of satellite-borne instruments, the limitations imposed by the present level of radar development prohibit the detection of weakly reflecting targets.

However, one of the advantages of using radar aboard satellites is the significantly large value of the beam-filling factor k_z at great distances in comparison with that for Earth-based radar (fig. 4A–1). In the latter case, the maximum range of showers and thunderstorms (the vertical dimensions of which are approximately 10 km) does not exceed 300 to 350 km. At greater ranges, they are located beneath the Earth-based antenna beam ($k_z=0$). At smaller ranges (200 to 250 km), the filling factor is only approximately several hundredths, even for narrow beamwidth ($\theta\approx1°$). In the same conditions, it is possible for satellite radar to have values of k_z of greater magnitude. This is readily shown from figure 4A–1. The magnitude of the beam filling factor at the Earth surface is

$$k_z' = \frac{h'}{\theta_2(H+h-h')\ \operatorname{cotan} A} \quad (4A\text{–}1)$$

After the pulse reaches the Earth surface

$$k_z'' = \frac{h}{(H\ \operatorname{cotan} A + B\epsilon' \cos^2 A)\,\theta_2} \quad (4A\text{–}2)$$

with

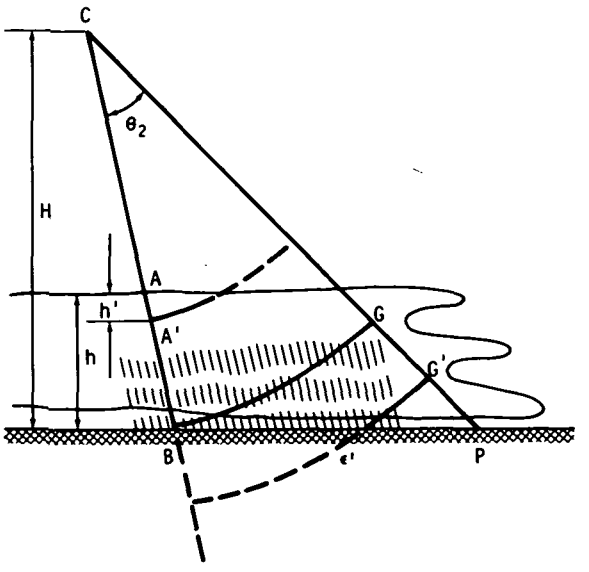

FIGURE 4A-1.—Geometry for computing the filling factor for satellite radar.

$$CG \geq \frac{H-h}{\sin(A-\theta_2)} \qquad (4A\text{–}3)$$

and

$$k_z'' = \frac{(BP - B\epsilon')\sin A}{\left(\frac{H}{\sin A} + \frac{B\epsilon'}{\cos A}\right)\theta_2} \qquad (4A\text{–}4)$$

Another advantage of using radar in a satellite is the possibility of detecting clouds and rain from overhead (i.e., with a large viewing angle). As a result of this path, microwaves in the attenuating layer (troposphere) of the atmosphere are attenuated less than for Earth-based radar. This circumstance modifies the optimum wavelength choice in the direction of much shorter waves (ref. 4A-1).

The classical radar equation and the radar equation for meteorological targets are necessary not only to determine the attainable values of the radar parameters but also to guarantee complete coverage of the Earth surface. To do so requires the utilization of a system of four radar-equipped satellites (ref. 4A-1).

A series of about 10 echo pulses must be received. The number of these pulses N_r is determined by the pulse repetition frequency f_p, the scanning speed of the beam V_γ, and the width of the antenna radiation pattern in the vertical plane θ_2.

$$N_r = 0.5\,\frac{f_p\theta_2}{V_\gamma} \qquad (4A\text{–}5)$$

The value of f_p is limited by the average transmitted power and the maximum operating range of the radar. Because of the first condition, the permissible value of f_p must be selected as $f_p \leq \bar{P}/(P_t t_p)$, where $\bar{P}$ is the average power and t_p is the radar pulse duration.

With present-day transmitters, $\bar{P} \approx 300$ W. Because the optimum wavelength for meteorological radars in satellites appears to be $\lambda = 2$ to 3 cm (ref. 4–9), $P_t \approx 3\times10^5$ W. The duration of the transmitted pulse T, to achieve the desired resolution, must be equal to 1 μsec. Then $f_p \leq 10^3$ Hz.

The second condition is concerned with the maximum radar range. In this case (with f_p in hertz)

$$\frac{1}{f_p} \gg \frac{2R_m}{c} \qquad (4A\text{–}6)$$

and

$$f_p \leq \frac{1.5\times10^5}{R_m} \qquad (4A\text{–}7)$$

For the satellite radar with pencil beams, meteorological targets will be detected within the range interval of 30 to 40 km, even with large scanning angles, because they are located in the troposphere. Consequently, to obtain readings of distance relative to the surface of the Earth, it may be assumed that $R_m = 30$ km. Then, $f_p \leq 5\times10^3$ Hz. However, the possibility of obtaining received echoes at the time the radar transmitter is turned on must be considered. It is easy to show that pulses, transmitted at a frequency of 600 Hz, will not be received from a range of 500 km each second pulse. With $f_p = 1200$ Hz, the echo will not be received on every fourth pulse, and so forth. To set the "blind" zone beyond the limit R_m, it is possible, for example, to take $f_p = 1000$ to 1150 Hz. Then, $\bar{P} = P_t f_p t_p = 3\times10^5\times1150\times10^{-6} = 345$ W.

Returning to equation (4A–5), in which

the scanning speed V_γ enters, one can show that

$$V_\gamma = \frac{2\gamma_s V_{pr}}{0.8\theta_1 H} \qquad (4A\text{–}8)$$

where γ_s is the scanning angle and θ_1 is the width of the radiation pattern in a plane perpendicular to the plane of the orbit. From equations (4A–5) and (4A–8)

$$\theta_1\theta_2 = \frac{4N_r\gamma V_{pr}}{0.8 f_p H} \qquad (4A\text{–}9)$$

The satellite velocity of motion projected on the Earth surface V_{pr} is related to its velocity of rotation around the Earth V_{kr} by

$$V_{pr} = \frac{V_{kr}R_E}{R_E+H} \qquad (4A\text{–}10)$$

with

$$V_{kr} = \frac{2\pi(R_E+H)}{T_s} \qquad (4A\text{–}11)$$

where T_s is orbital period in seconds.

Equation (4A–10) does not take into account the Earth rotation V_e. Generally, the receiving antenna beam along the Earth has a velocity

$$\mathbf{V} = \mathbf{V}_{pr} + \mathbf{V}_e \qquad (4A\text{–}12)$$

The magnitude of the vector velocity is

$$V = R_E\Omega_e \cos\phi \qquad (4A\text{–}13)$$

where Ω_e is the angular velocity of the Earth rotation, and ϕ is the terrestrial latitude of the subsatellite point.

For satellites with circular polar orbits

$$V_{pr} = [(V_{kr})^2 + (V_e)^2]^{\frac{1}{2}} \qquad (4A\text{–}14)$$

Analysis of equation (4A–9) shows that the necessary width of the radiation pattern also depends on the required angle of scan, the orbit height, and the number of pulses transmitted and received.

The scanning angle γ_s and the distance from the satellite to the Earth depend on the orbit height, the required longitudinal angular width of the coverage, and the number of satellites. The widths of the radiation pattern $\theta_1\theta_2$ are also determined by these parameters. This limits the use of narrow radiation patterns for the purpose of achieving large detection range and satisfactory resolution.

As an example, consider a single search of the Earth surface with four satellites with $N_r=10$ pulses, $\gamma=78°$, $H=400$ km, $f_p=1150$ Hz, and $V_{pr}=7.2$ km/sec. Substituting in equation (4A–9) yields $\theta_1\theta_2=1.78°$. This is achieved with $\theta_2=0.51°$ and $\theta_1=3.5°$.

With the indicated radar characteristics from the radar equation by Stepanenko (ref. 4–12), the ratio of the received power to the transmitter power for a detection probability of 0.9 can be readily obtained. Then

$$\frac{P_r}{P_t} = 5.2\times10^{-6}\frac{Z}{R^2}kk_z \qquad (4A\text{–}15)$$

where R is given in km, Z is in mm^6/m^3, and k is the attenuation factor.

According to experiments, the radar reflectivity Z is different for various atmospheric conditions and varies within the limits $10^{-3}\ mm^6/m^3 \leq Z \leq 10^6\ mm^6/m^3$.

Then, with $R=400$ km, the beam filling factor $k_z=0.3$, and the attenuation factor $k=0.5$, the ratio P_r/P_t will vary from 5×10^{-25} to 5×10^{-16}. For $R=1000$ km, $7.8\times10^{-26} < P_r/P_t < 7.8\times10^{-17}$.

If the radar receiver sensitivity is taken to be $P_{min}=10^{-14}$ W and the transmitter power $P_t=300$ kW, then $P_r/P_t=3.3\times10^{-20}$ (ref. 4A–2). Comparing this ratio with the required ratio of P_r/P_t for clouds and rain, one can determine those regions of rain that are detectable from satellites. Presently, clouds without rain cannot be detected with radar methods from satellites because the great distances result in a very small ratio of P_r/P_t. Increasing this ratio to insure the possibility of detecting nonrain clouds and measuring their upper height is possible with passive infrared radiometer methods.

Analysis of table 4A–I shows that, with a 400-km orbit, it is possible to detect moderate and heavy rain within the range of coverage.

UTILIZATION OF RADAR WITH FIXED, PLANAR RADIATION PATTERNS

This type of pulse radar is of interest because of the simpler antenna construction and the greater number of pulses on target.

TABLE 4A–I.—*Maximum Detection Ranges of Clouds With Pulse Radar of Selected Characteristics*

Characteristic	Maximum detection range, km			
	200	400	600	800
k_z	0.5	0.3	0.1	0.08
Z_{min}, mm^6/m^3	64	415	2880	5100
I_{min}, mm/hr [a]	.46	1.50	5.08	7.25

[a] I_{min}=minimum detectable intensity of rain.

Coverage of the Earth surface with such a satellite is obtained with two fixed, planar beams oriented perpendicular to the orbit plane of the satellite.

The radar has the following parameters: wavelength of 3 cm, radiated pulse power of 300 kW, receiver sensitivity of 10^{-14} W, pulse width equal to 4 to 5 μsec, angular width of the radiation pattern in the horizontal plane $\theta_1=0.23°$, and angular width of the radiation pattern in the vertical plane $\theta_2=30°$.

The radar has two antennas that are alternately switched to the receiver-transmitter. The frequency of switching is

$$F_{pod}=1.9\times10^{-6}\,\theta_1 h(H+R_E)\left(1+\frac{H}{R_E}\right)^{1/2}k_{per} \qquad (4A\text{–}16)$$

where k_{per} is the coefficient of overlap.

With $H=400$ km, the value of $F_{pod}\approx 16$ Hz. The width of the radiation pattern θ_1 is selected to obtain sufficient antenna gain, subject to the manufacturing restriction that $D_a/\lambda=300$, where D_a is antenna diameter. The width of the radiation pattern $\theta_2=30°$ insures complete coverage of the Earth surface with four satellites at an orbit height of 400 km.

One of the disadvantages of fixed planar beams is that unwanted clutter is almost always reflected from the sea or the Earth surface, together with the desired echoes from clouds and rain. These reflections create background that makes it difficult to extract the signals from the meteorological targets that are of interest.

In this case, the minimum detectable intensity of rain I_{min} (in mm/hr) can be expressed by the following relationship (ref. 4–12) :[1]

$$I_{min}=\left(\frac{8\pi\theta_1\theta_2^2\lambda^2R_m^3m_1P_r+m_2P_t\lambda^4h\tan\beta\,S(\beta)\,k}{\alpha 8\pi\times10^{-16}\,P_t h\theta_2R_m k k_z}\right)^{1/\gamma} \qquad (4A\text{–}17)$$

TABLE 4A–II.—*Calculation of* I_{min} in mm/hr *According to Equation (4A–17)*

Condition	Maximum detection range, km			
	300	400	500	600
Without clutter	1.5	2.0	2.8	3.4
Clutter from land	9.1	8.0	7.0	7.3
Clutter from water surface	2.0	3.1	2.8	3.7

Using the previously mentioned radar characteristics and with $m_1=m_2=1$, $k_z=5\times10^{-2}$, $k=0.4$, $\alpha=220$, and $\gamma=1.6$, one can determine with equation (4A–17) the value of the rain intensity with $\beta=40°$ and the scattering coefficient $S(\beta)=10^{-1.8}$, corresponding to a grass-covered ground; and $S(\beta)=10^{-3.4}$, corresponding to a water surface (table 4A–II).

Analysis of the table shows that the contribution of the clutter is substantial. However, the minimum detectable rain intensity is increased three to six times compared to the rain intensity in the absence of clutter. The characteristics are such that, in the presence of clutter, the minimum detectable rain becomes less, despite the increased range. This is explained by the fact that the echo signals from volumetric meteorological targets decrease as the square of the range, and the echoes from the area targets as the range cubed.

These calculations show that, with an increase in the angle of sighting β, the contribution of the clutter increases because of an increase of the multiplier $\tan\beta$ in the second term of the numerator of equation (4A–17).

In such a manner, the effectiveness of

[1] *Translator's note:* The quantity γ has a different meaning in eq. (4A–17) than it does in eq. (4A–9).

radar with planar beams for detecting meteorological targets from satellites is degraded by the harmful effect of the Earth surface.

To increase the effectiveness, it is necessary to attempt to reduce the effect of the ground reflection. To a large degree, this problem can be solved by using a multiwavelength radar.

In the microwave region, the scattering coefficient of the Earth surface $S(\beta)$ and, consequently, the effective scattering area are weakly dependent on the wavelength; but for rain, the scattering coefficient is proportional to λ^{-4}. This effect can be used to remove the significance of ground clutter.

The difference of the minimum received signals is

$$P_{\lambda_1 \min} - P_{\lambda_2 \min} = m_1 P_{\lambda_1 sh_1} + m'_1 P_{\lambda_1 e} - m_2 P_{\lambda_2 sh_2} - m'_2 P_{\lambda_2 e} \quad (4A\text{–}18)$$

Let the noise powers $P_{\lambda_1 sh_1}$ and $P_{\lambda_2 sh_2}$ and also the coefficients of the distinction be the same. Then, according to the theory of radar reception, the difference of the internal noise increases by $\sqrt{2}$.

To effectively use this method, it is necessary for the radiation patterns at both wavelengths to be the same. Accordingly, they will have the same angular resolution and filling factor k_z.

Substituting in equation (4A–18) the relationship in equation (4A–17) and calculating its relative rain intensity, the following expression is obtained:

$$I_{\min} = \left(\frac{1}{\alpha 64\pi^2 \times 10^{-19} \, h k_z \left(\frac{P_{t_1} k_1}{\lambda_1^2} - \frac{P_{t_2} k_2}{\lambda_2^2} \right)} \left\{ \sqrt{2}\, P_{\min} R_m^2 \theta_1 \theta_2 + \frac{h \tan \beta [S_1(\beta) \lambda_1^2 P_{t_1} k_1 - S_2(\beta) \lambda_2^2 P_{t_2} k_2]}{8\pi \theta_2 R_m} \right\} \right)^{1/\gamma} \quad (4A\text{–}19)$$

An analysis of this formula reveals that, with other conditions equal, the sensitivity of the dual-wavelength radar will increase with the difference in the denominator of the multiplying term and will decrease with the difference in the numerator of the second sum of the braces.

As one version of a dual-wavelength radar, an instrument was examined that operated at wavelengths of $\lambda = 0.8$ cm and $\lambda = 3$ cm. The main reason for selecting these bands was that, at these wavelengths, detailed scattering coefficient data $S(\beta)$ are available for various surfaces of the Earth with various viewing angles.

Solving the equation for $I_{\min}$ with $P_{t_1} = 300$ kW, $P_{t_2} = 30$ kW, $k_1 = 0.2$, and $k_2 = 0.4$ and assuming the other radar parameters are the same as before, the values in table 4A–III are obtained for the minimum detectable intensity of rain.

A comparison of the values of tables 4A–II and 4A–III reveals the advantage of two-band radar.

In addition to the detection of rain, an interesting problem is the possibility of measuring its intensity from satellites. Although the solution of this problem depends on overcoming a series of difficulties connected with the necessity to automatically process and measure the backscatter signal power under space conditions, the achievements of electronics and processing systems design offer hope for successful use of spaceborne two-band meteorological radar in the coming years for the detection of storms and for the measurement of rain. In this regard, it is tempting to present the possibility of installing such meteorological radars on geostationary satellites at orbit heights of 35 700 km.

Using equation (4A–15) (the radar equation) with a beamwidth $\theta = \lambda/D_a = \lambda/400 \approx 0.0025$ rad, $P_t = 3 \times 10^5$ W, $I_{\min} = 4$ mm/hr, $P_{\min} = 10^{-15}$ W, $t_p = 1$ μsec, attenuation coefficient $k = 0.5$ at $\lambda = 2$ cm, $k = 10^{-1}$ at $\lambda = 0.8$ cm, $k = 10^{-3}$ at $\lambda = 0.3$ cm, and with the value $k_z = 0.3$, the following required values for P_r/P_t are obtained.

For λ equal to 0.3, 0.8, and 2 cm, the cor-

TABLE 4A–III.—*Minimum Detectable Intensity of Rain (mm/hr) With Two-Band Radar*

Surface	Maximum detection range, km	Depression angle to near edge of coverage, deg			
		10	30	50	70
Land	300	0.5	1.8	3.6	4.0
Sea		.42	.42	.42	.42
Land	400	0.76	1.76	3.16	3.5
Sea		.7	.7	.7	.7
Land	500	0.95	1.73	2.9	3.1
Sea		.93	.93	.93	.93
Land	600	1.2	1.79	2.8	3.0
Sea		1.16	1.16	1.16	1.16

responding ratios of P_r/P_t are 5×10^{-21}, 7×10^{-20}, and 5.9×10^{-20}. At this time, the technically achievable values of these ratios appear to be $P_r/P_t=10^{-15}/(3\times10^5)\approx 3.3\times10^{-21}$. Thus, it appears that areas of rain will be detected from satellites at λ equal to 0.8 and 2 cm. With the selected values of θ and t_p, the geometrical resolution in the tangential dimension amounts to 80 to 90 km; and, in the radial direction, the measurements are from 6.5 to 0.2 km, with angle of scan γ_s increasing from 0.2° to 7°.

REFERENCES

4A–1. KMITO, A. A., ET AL.: Systems for Receiving and Transmitting Meteorological Information. Gidrometeoizdat (Leningrad), 1971.

4A–2. DOMBKOVSKAYA, E. P.: Determination of Sea Surface Temperature and Atmospheric Humidity From Satellite Measurements of the Thermal Radio Emission of the Earth-Atmosphere System. Satellite Meteorology, V. G. Boldyrev and N. F. Veltishchev, eds., Gidrometeoizdat (Leningrad), 1969.

C. 5

CHAPTER 5

Active Microwave Sensor Technology

Active Microwave Working Group

Technology Support Group:

WALTER E. BROWN, JR., *Cochairman*
M. I. SKOLNIK, *Cochairman*

Louis H. Bauer
Chi-Hau Chen
D. E. N. Davies
Richard G. Fenner
H. L. Groginsky
Preben E. Gudmandsen
Donald Howell
Rolando Jordan
Richard W. Larson
Leonard J. Porcello
Gerald G. Schaber
F. C. Williams

INTRODUCTION

Radar technology is concerned with ways and means to provide information about a reflecting area. During the past two decades, major advancements have been made in this technology, and sophisticated techniques have been developed for locating the direction and range to a reflecting area. Furthermore, other characteristics of the reflection, such as amplitude, phase, Doppler frequency, and polarization, have been used to identify additional properties of the target area. The radar provides its own illumination, and there is no question that the target information contained in the echo is unique. The wavelength, bandwidth, polarization, and modulation of the illuminating signal are selectable by the experimenter, thus providing a wide choice of operational parameters over a frequency spectrum of approximately three decades (150 MHz to 150 GHz).

The amount of information concerning a target area contained in the echo (reflection) is enormous. For example, a comparison between a photographic picture element (pixel) (visible spectrum), which has a high information content, and an element of a radar image is shown in table 5–I.

The radar echo per unit areal element contains as much or more information than the photograph. Each representation of the target area contains unique information because the wavelength range is different, and the surface reflection represents the response to the respective illumination wavelengths.

TABLE 5–I.—*A Comparison of Photographic and Active Microwave Data Content*

Photographic pixel	Radar image
X-angle	X-angle
Y-angle	Y-angle
Frequency (color)	Frequency
Albedo	Amplitude
Polarization	Polarization
No comparables	Phase (absolute)
	Doppler
	Phase jitter

For example, a wheatfield can be observed on both an areal photograph and a radar image. The two output sensor images do not necessarily contain the same information because the image areas may be covered by a wide-wavelength separation, from 3×10^{-5} to 25 cm. Because each image has a different information content, the wheatfield may be "visible" to one sensor or the other, or both. The objectives are to determine the relationship between the surface property and the echo characteristic and to enhance the effects to reduce the measurement uncertainty. This area is a major endeavor for radar technology.

One purpose of this chapter is to provide a link between the recommendations of the science or application studies and the implementation aspects of the radar. Thus, the technology support group (TSG) has contributed comments on feasibility, suggested baseline functional descriptions of the various types of active microwave sensors, and submitted some examples of existing radar techniques and examples of the results. This chapter also includes an example of how the data are used to obtain scientific results. Data handling, particularly for high-rate information systems (i.e., imaging radar), is a major problem area. Hence, a special section has been devoted to the data-management aspects. The last section is concerned with future development and reflects the concern of technologists for obtaining factual information about the measurement process.

Science and Application Guidelines

The various science and applications measurement recommendations were compiled and summarized to determine how many different types of systems may be required and to ascertain the major categories of essential microwave sensor parameters. These summaries are intended to serve only as guidelines for instrument development, not as specifications.

A summary of active microwave sensor parameters (resolution, swath width, and surface coverage) is given in table 5–II. These parameters were inferred from the science and application objectives to measure spatial and time-varying phenomena with various physical dimensions.

Most of the science and application objectives are related to imaging radar techniques in that they are concerned with the location of physical phenomena in two directions and sometimes in three dimensions, with resolutions that vary from 3 m to 40 km in areal (x, y) locations and 1 to 2 km in elevation (z). For subvehicle track profile measurements that require altimeter or sounder experiments, the accuracies and resolutions are 2 to 10 cm in range for surface profiles and 5 cm to 50 m for subsurface profiles. For

TABLE 5–II.—*Summary of Active Microwave Sensor Parameter Guidelines*

Application	Resolution, m	Swath width, km	Surface coverage
Imaging radar			
Earth/land	3 to 15	>20	Selected areas
	10 to 30	>40	Global
	30 to 100	≥100	Global
Atmosphere	1000 to 2000	.....	Hemisphere
	10 000	.....	Hemisphere
Earth/ocean	10 to 30	10 to 100	Global
Scatterometry			
.....	40 000	>100	Global
Altimetry			
.....	1 to 3 (elevation)	10 (diameter)	Global

upper surface profiles (i.e., cloud water), accuracies of approximately 1 km would be useful. One other sounder, the surface pressure sensor, would be measuring the slope of the oxygen absorption line to within a fraction of 1 percent. The following are the most stringent requirements:

1. Amplitude: Generally within 15 percent.
2. Dynamic range: 50 dB.
3. Polarization: Within 1°.
4. Range (time delay): 2 to 10 cm (10^{-10} sec) (correction for variations in index of refraction not expressed).
5. Frequency: Within 10 percent.
6. Phase: Within 5°.
7. Doppler frequency: Within 1 percent.

A large majority of the ocean and Earth/land science and application objectives could be realized with a single imaging radar system operating perhaps in various modes (in incident angle, swath width, or resolution). There are some special-purpose radar systems required for geoid measurements and surface-wind determination.

The atmospheric science and applications objectives have, in general, a different class of radar design criteria. The discussion of these criteria is contained in chapter 4.

The surface-sounding radar requirements are, in a sense, an extension of the altimeter radar design and may be restricted to aircraft programs for the next several years.

General System Considerations

The design of imaging radar systems for spacecraft leads to a set of system parameters that are interrelated. A change in one parameter implies changes in most of the others. This section will delineate some of the tradeoffs required for an acceptable system.

The antenna design is one of greatest importance because its proper selection is required to give an image with low ambiguous returns in either range or azimuth. The theoretical azimuthal resolution of a synthetic aperture radar (SAR) system is equal to one-half of the along-track length of the antenna. However, a small azimuthal beamwidth returns energy with a high Doppler bandwidth. To unambiguously sample the data, according to the Nyquist criteria, a high pulse repetition frequency (PRF) must be used. Thus, to avoid successive pulse mixing, the radiation of the antenna must be confined to a narrow set of angles in the crosstrack dimension, which results in a large antenna dimension in the crosstrack dimension (fig. 5–1).

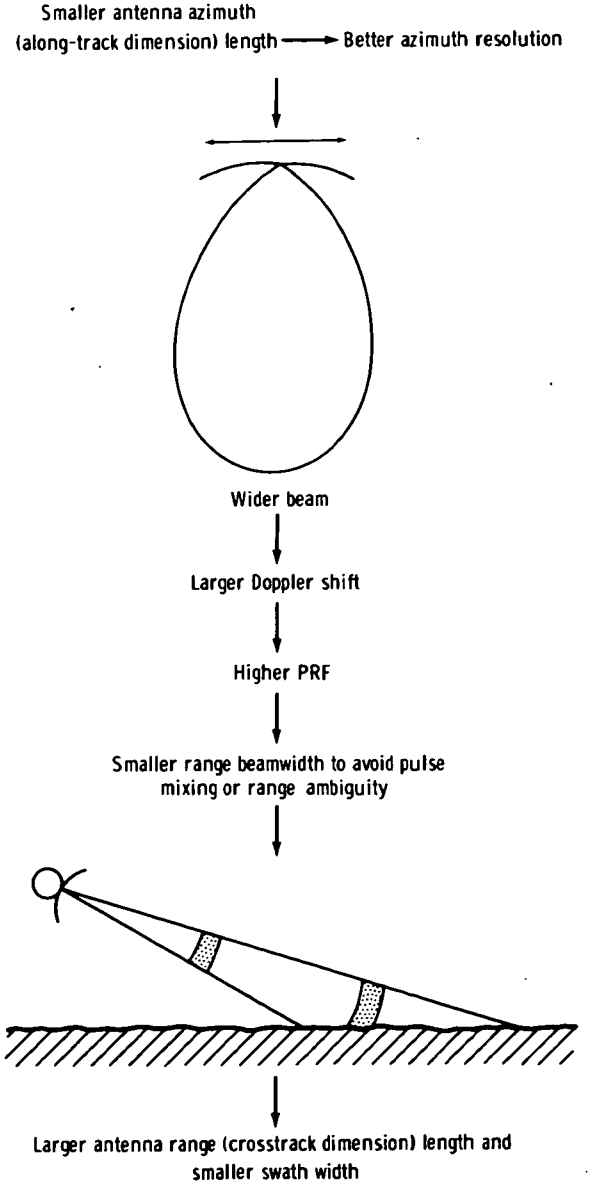

FIGURE 5–1.—Diagram showing that a decrease in one dimension of the antenna requires an increase in the other dimension to avoid ambiguities.

Given a required swath width or PRF, the antenna length in azimuth must be sufficiently large to limit radiation in the azimuth dimension to give low azimuthal ambiguities. These ambiguities are returns from areas other than the area being imaged, which, when sampled periodically and processed, map in identical locations as those of the desired surface returns. These ambiguities are reduced by sampling the data with several pulses (2 to 5) every time the spacecraft moves a distance equal to the antenna length. The illumination pattern of the antenna may be weighted to minimize the returns coming in through the antenna side lobes. In the range dimension, ambiguities can also result from successive pulse mixing, and these ambiguities are again reduced by limiting radiation by means of a large crosstrack antenna with illumination tapering. The implication of this antenna design, to keep ambiguities at a low level at orbital altitudes, results in a required minimum antenna area that follows a curve such as that shown in figure 5–2 for variations in spacecraft or aircraft altitudes. The antenna look angle also has a significant effect on the minimum area required for unambiguous illumination of the surface. As the antenna crosstrack length is increased from the nadir direction, the resultant echo shape is increased in duration. Thus, for a given PRF, to avoid consecutive pulse mixing, the radiation must be confined to look-angle widths, which, in turn, implies longer antenna crosstrack dimensions. The required antenna area then varies with the look angle as shown in figure 5–3. Another factor that will be affected by raising the look angle for a given system bandwidth is the radar system range resolution (fig. 5–3).

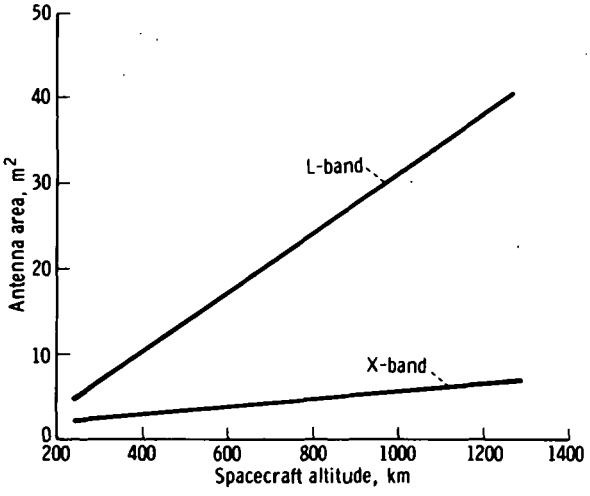

FIGURE 5–2.—Minimum antenna area required for X- and L-band radar systems with a 30° look angle from nadir.

The transmitter power required to yield an acceptable image is another parameter that needs careful consideration. The following information is required before these parameters may be determined:

1. The minimum detectable backscatter coefficient required of the radar.
2. The angle of incidence necessary for the measurement.
3. The necessary resolution.
4. The antenna characteristics.

The orbital characteristics presumably are known. For a given set of user conditions, the radiated power average required varies inversely with wavelength unless sophisticated multiple-feed antenna systems are used. Figure 5–4 shows a plot of the transmitter power required for a system with a 15° incident angle and is indicative of the dependence of power on wavelength. Thus, if wavelength is not a user requirement, a tradeoff between power and antenna area is involved in wavelength selection.

The accuracy (relative or absolute) of the measurement is one parameter having a great impact on the capability of an imaging radar system to measure a given phenomenon. The side-looking coherent imaging radar system provides the user a measure of the radar-backscatter coefficient of each resolution element on the surface being imaged. Because of numerous factors, this measurement will have an uncertainty in its absolute value. However, through careful design and implementation, this uncertainty can be reduced to arbitrarily low values at the expense of complexity, power, weight, etc.

A given resolution element, when illumi-

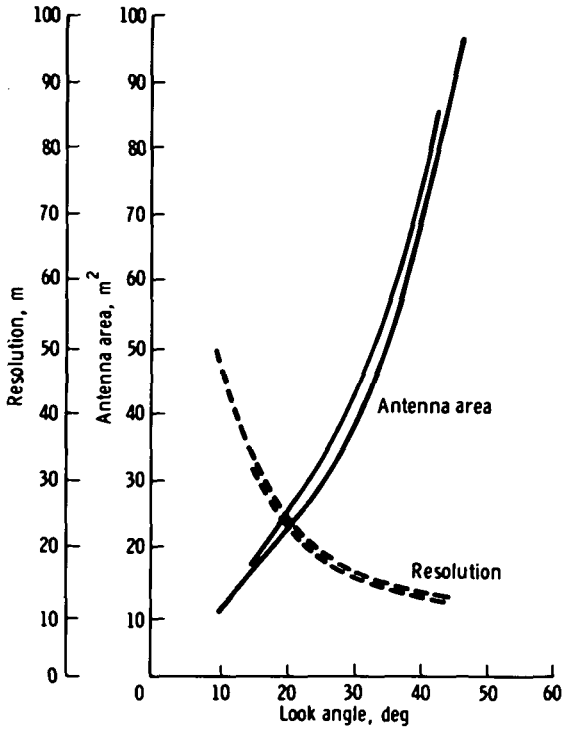

FIGURE 5–3.—Required antenna area and resolution as a function of incident angle.

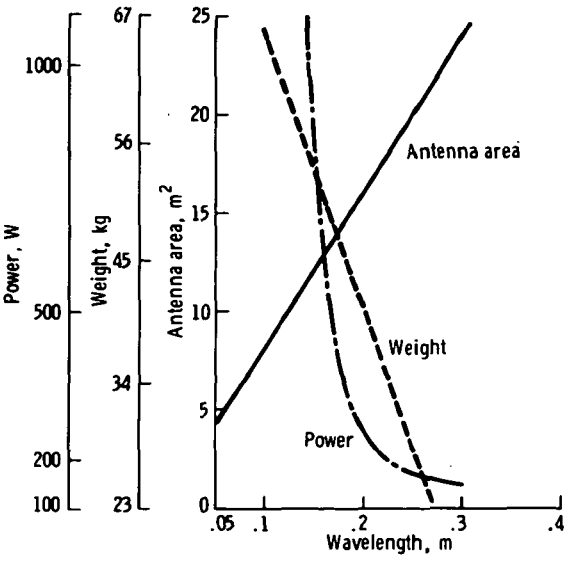

FIGURE 5–4.—Antenna area, radar power, and weight as a function of wavelength for a single feed antenna system at an altitude of 1000 km, with a 70-km swath width, 33- by 33-m resolution, and 15° look angle.

nated by a coherent source of electromagnetic energy, will exhibit a variation in its measured backscatter value as the antenna moves in location. This effect is known as target scintillation or "speckle." This variation is also observed when a large number of returns are added coherently to improve system resolution, which is done with a synthetic aperture system. To reduce the error in the estimated value of the backscatter coefficient of the resolution element being observed, the measurement process can be made repeatedly, and the measured values can be added noncoherently. Coherent addition implies that both quadrature elements of the measurement are added vectorially; whereas, in noncoherent addition, only the magnitude of the resultant vector is added. This concept of separate or independent measurements taken and summed is also known as multiple-look processing or noncoherent averaging in an SAR system. Thus, as a prime consideration early in the study of a potential imaging radar system, it is necessary to know the degree of precision to which a measurement at each resolution element must be made so that the user is able to accomplish his required task. The implementation implications of multiple-look processing are many. The major impact lies in the data-reduction process and, to some extent, in radiated power.

If the data-reduction process is accomplished on board a spacecraft, then each separate or independent look requires a separate digital processor. If the looks are accomplished in azimuth, then a large two-dimensional buffer is required to combine the separate looks that are gathered at slightly different delays. If the data-reduction process is accomplished on the ground, then a large data telemetry system or data storage device is required.

The data rate that the radar system will generate is similar to that of a photographic system and depends on the swath width, resolution, and vehicle velocity. If multiple-look processing is involved, this factor will also affect the data rate, if the data are

recorded or telemetered to Earth unprocessed. The data rate DR_r out of the radar system is given approximately as

$$DR_r = \frac{2N_{r1}N_L v S_r}{r_r r_a} \qquad (5\text{–}1)$$

where N_{r1} is number of bits per data sample, N_L is number of looks, v is vehicle velocity, S_r is swath width, r_r is range resolution, and r_a is azimuth resolution. The data rate DR_r out of the digital processor is given by the following equation:

$$DR_r = \frac{N_{r2} v S_r}{r_r r_a} \qquad (5\text{–}2)$$

where N_{r2} is the number of processor bits per data sample. These two equations differ by the ratio

$$\frac{2N_{r1}N_L}{N_{r2}} \qquad (5\text{–}3)$$

In general, N_{r1} will always be smaller than N_{r2}. However, the data rate out of the processor will be somewhat smaller than the radar system output, particularly if multiple looks are involved. The complexity of an onboard processor must be considered in any decision for its inclusion.

The following criteria must be satisfied to make a proposed application attractive in an overall sense:

1. The application or mission must have a degree of national importance or benefit that justifies the cost.
2. The technology either must be available or must be attainable with an acceptable level of risk.
3. The radar signature base and the proposed data-analysis techniques either must be available or must be attainable with high probability.

The judgment and applications pertaining to the first and second criteria are probably outside the scope of this workshop. However, the TSG believes that current technology and understanding of signature bases and analysis techniques are sufficiently advanced so that several of the proposed applications appear highly attractive in terms of the second and third criteria. These applications have relatively low technical risks and therefore will offer a high possibility of success from a purely technological viewpoint. If any of these same applications also happen to be cost-effective from a national viewpoint, then they lead to excellent candidate missions upon which to base a long-term program. Of course, none of the proposed applications are totally without problems, and each requires some level of further study and technique development, which will need to be planned and implemented.

Applications that appear to be low risk from a technological viewpoint include the following:

1. Use of an imaging radar for a variety of ice surveillance roles, including determination of the ice lead and polynya structure at high latitudes, iceberg detection in shipping lanes, monitoring drift and decay of icebergs off Antarctica, and lake-ice reconnaissance in the Great Lakes and St. Lawrence River shipping lanes.
2. Use of a radar profilometer for generating profiles of the ocean surface on a global scale, building upon the experience achieved in the Skylab S193 experiment and other experiments.
3. Use of a radar scatterometer for windspeed estimation for inputs to global weather models.
4. Use of an imaging radar for the observation of geologic structure and lithology.
5. Use of an imaging radar for a variety of applications that stem from the ability to observe land/water boundaries. (These applications include observations of lake levels and stream overflow, the analysis of watershed runoff, and the study of coastal and shoreline features.)
6. Use of an imaging radar for observations of ocean-surface patterns on a global basis.
7. Use of an imaging radar for gross land-use classification.
8. Use of a suitable multiband imaging radar with sophisticated analysis techniques

for estimation of crop acreage in agricultural contexts characterized by a small number of possible crops and moderate to large fields.

This list is not meant to be exhaustive. It reflects, in large part, the experience and comprehension of TSG members.

PART A

FUNCTIONAL DESCRIPTIONS OF SELECTED ACTIVE MICROWAVE SYSTEMS

In chapters 2, 3, and 4 of this document, the Earth/land panel, oceans panel, and atmosphere panel, respectively, have established requirements for several active microwave measurements. Although certain common features are present in these measurements, several basic types of measurements can be distinguished, and a class of sensors can be associated with each type.

MAJOR CLASSES OF CANDIDATE SYSTEMS

The following four classes of active microwave measuring systems appear to offer the greatest utility to the three user panels:

1. Scatterometers designed to measure electromagnetic scattering properties of surfaces (without emphasis on spatial resolution).
2. Altimeters designed to accurately measure the vertical distance between the sensor and the scattering surface directly beneath it or to profile the surface beneath it.
3. Sounders designed to penetrate the uppermost boundary of the medium beneath the sensor and to observe the vertical structure of this medium by means of a delicate balance between reflection due to vertical gradients and transmission through these gradients.
4. Imaging systems designed to measure the scattering properties of surfaces, usually with lateral spatial resolution finer than that required in any of the preceding classes.

Other useful radar-measuring configurations (e.g., a Doppler radar designed to observe the radial velocities of scatterers) can be treated in an analogous manner, but these configurations will be omitted in this report because they are less critical to the stated needs of the user panels.

For the purpose of this document, the term "functional description" will be a description of an active microwave system that answers the following fundamental questions:

1. What physical attribute of the scatterer does the system measure?
2. How does the system perform the measurement?
3. What are the principal parameters that characterize the output of the system?
4. In what form is the output provided to the user?
5. What are the principal sources of measuring system error, and how do they affect performance?

Questions 1 to 5 relate to figure 5–5. The answer to question 1 describes the input in terms meaningful to the sensor. Question 2 applies to the "transfer characteristic" of the measuring system, whereas question 3 describes the output in terms consistent with questions 1 and 2. Question 4, strictly a format question, may be critical to proper

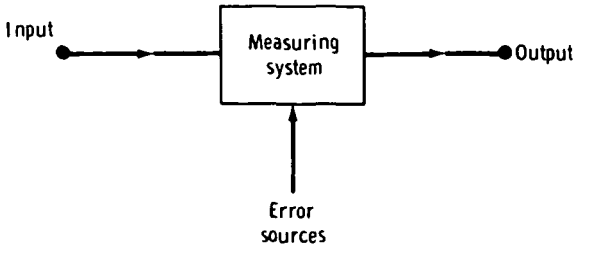

FIGURE 5–5.—Diagram of the basic measurement process.

data management. Question 5 is self-explanatory.

The topics of parameter interplays and system design tradeoffs sometimes are included in a functional description of a system. In general terms, a functional description provides a mathematical model on which to base a design exercise, whereas the parameter tradeoff question relates to the question of optimizing a design for a specific mission. However, a discussion of tradeoffs does provide useful insights and is included for some of the sensors.

Finally, two additional questions may arise in a functional description:

6. What level of performance does current technology permit, and how may this performance level be extrapolated into the future?

7. What are order-of-magnitude estimates of weight, power, volume, cost, expected lifetime, and other variables that are potentially important in experiment selection and planning?

The answers to these last two questions must come from design exercises that begin with a set of proposed mission objectives and design constraints and that are then optimized over all variables.

FUNCTIONAL DESCRIPTIONS BY CLASS

In this section, functional descriptions of the four principal classes of active microwave sensors are provided.

Radar Scatterometer

The radar scatterometer is a special-purpose instrument that measures the relative value of the radar-backscatter coefficient at a range of angles. Because no spatial resolution is required other than the area illuminated by the antenna, this system is less complex than other systems that require a high degree of spatial resolution. The data rate generated by a scatterometer is also much lower than imaging systems because the coarser resolution does not require close spatial sampling of the surface. Measurements of the relative radar-backscatter coefficient of the surface at various angles, polarizations, and wavelengths are used to infer characteristics regarding the surface (such as wind velocity and direction for the ocean and surface roughness for the land).

The scatterometer measures the microwave backscatter cross section of a surface for various angles of incidence. During flight over an area of interest, radar backscatter as a function of incident angle is generated from which some physical attributes of the surface can be inferred. These measurements may be taken at different polarizations or wavelengths to enhance interpretation of the surface characteristics. These measurements are taken by illuminating the surface with microwave energy and measuring the portion of this energy that is reflected back to the transmitting/receiving antenna. The output of the scatterometer system is a set of data points corresponding to radar-backscatter measurements as a function of angle and spacecraft position. These data are presented to the user as a plot of radar backscatter as a function of angle for each data cell on the surface.

System noise is the primary source of error in the measurement of radar backscatter. Radar scatterometers have been built that measure a minimum backscatter coefficient of -30 dB. However, this does not in any way mean that more sensitive microwave scatterometers cannot be built. Most observed phenomena have backscatter coefficients exceeding this value. Because of the simplicity of the radar scatterometer, its weight, excluding the antenna system, is usually in the tens of kilograms and power consumption is in tens of watts. Thus, the scatterometer is suitable for spacecraft use.

The scatterometer consists of (1) a microwave transmitter, (2) an antenna, (3) a microwave receiver, and (4) a detector and data integrator. Variation of these four basic components results in the two basic scatterometer types: the beamwidth-limited scatterometer and the pulse-width-limited scatterometer.

The beamwidth-limited scatterometer consists of a long-pulse-width transmitter, a pencil-beam antenna, a microwave receiver and down-converter, and a detector with an integrator. The transmitter pulse is sufficiently long to simultaneously illuminate the area of the antenna footprint. The return energy from the illuminated area is down-converted, amplified, narrow-bandpass-filtered, then square-law-detected and integrated as shown in figure 5–6. Because all the energy entering the antenna illuminates the surface, the sensitivity of backscatter coefficient varies as the square of the range to the surface. To obtain a backscatter function from which to infer surface characteristics, the pencil-beam antenna will be scanned in elevation while measurements are taken. In addition, the antenna may radiate and receive energy at different polarizations as an aid in inferring surface characteristics.

The pulse-width-limited scatterometer differs from the beamwidth-limited scatterometer in that a shorter pulse is transmitted to the surface by a fan-shaped antenna beam. The return echo is then time-gated to obtain elevation angle resolution. The received energy processing is the same as that for the beamwidth-limited scatterometer, except that a number of channels are required for the measurements. Each of these channels is time-gated for a slightly different delay from the transmitted pulse, and, consequently, each of these channels processes energy corresponding to a different range of elevation angles from the spacecraft. Scanning of the antenna angle in elevation is not needed to generate a backscatter function. As with the beamwidth-limited scatterometer, different polarizations can be used as an aid to data interpretation.

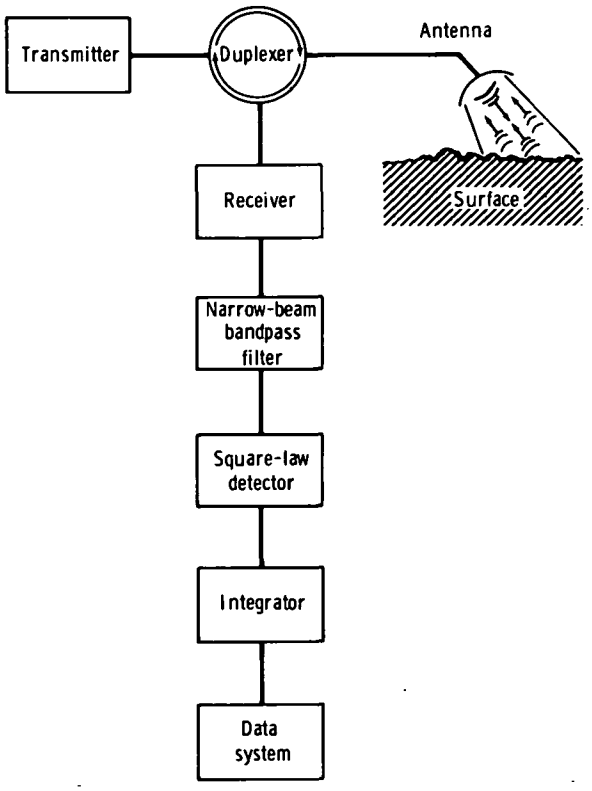

FIGURE 5–6.—Block diagram of scatterometer.

Radar Altimeter

The radar altimeter has played an important role in navigational and landing systems for aircraft and spacecraft. Remote-sensing applications of radar altimeters impose requirements for high measurement accuracy that depend not only on the altimeter but also on the control or monitoring of the motion of the platform on which the system is mounted.

To gain a proper perspective of the use of an altimeter as a remote-sensing instrument, the basic operating principles of a simple altimeter system will be considered. Figure 5–7 shows a block diagram of a radar altimeter that could represent several actual implementations.

On command from the timing system, the transmitter generates a modulated radio-frequency (rf) waveform that is directed by the duplexer to the antenna port. The antenna directs the radiated energy toward the target surface and subsequently collects that portion of the energy reflected or scattered back in the direction of the antenna. Once collected by the antenna, the returned signal is directed by the duplexer to the receiver input. The receiver processes the returned signal and provides an output from which

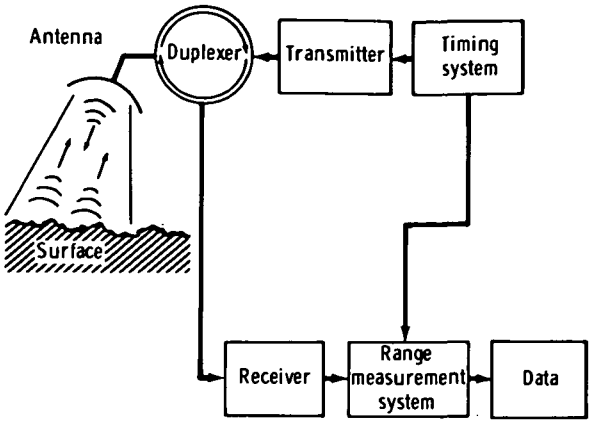

FIGURE 5–7.—Block diagram of simplified radar altimeter.

the two-way propagation delay can be determined. Because the velocity of propagation is known, the range to the target may be computed directly from the time-delay measurement.

To fully address the question of accuracy in terms of limiting factors, a particular implementation must be specified (e.g., frequency-modulated continuous wave, pulse, interrupted continuous wave (ICW), etc.), which, in many cases, is dictated by the given application. An in-depth discussion of the various radar altimeter implementations is beyond the scope of this report; instead, a comment on those aspects of system accuracy that relate primarily to a given application and that are common to all altimeter systems is provided.

For the applications that require the true range between the vehicle and the surface, some means of correcting for vehicle attitude and altitude changes must be provided. In addition, the timing system must have high long-term stability to insure that measurements made over a long period of time are repeatable.

If profiling is the desired measurement (i.e., measurement of the variation in surface height over a confined area), the long-term stability of the timing system needs to be good only for the desired measurement period, but measurement-to-measurement stability must be extremely high. Again, fluctuation in the system platform attitude and altitude can introduce serious errors unless steps are taken to correct for such variations.

Measurement of surface roughness may not require attitude or altitude correction, but measurement-to-measurement stability is still required.

In general, the achievable accuracy of a radar altimeter system depends on the measurement type and frequency and on the particular system implementation. Typical range measurements with present-day altimeter systems can be made with an accuracy of ± 30 m, whereas profiling measurements can be made with an accuracy of ± 60 cm.

Radio Subsurface Sounders

The radio subsurface sounder is a device to measure subsurface layers and boundaries. Radio subsurface sounders operate on the following principles:

1. That low frequencies can penetrate the surface of the Earth for some particular ground situations.
2. That the power reflected back to the sounder can be detected.
3. That adequate resolution in range can be realized.

This technique is only applicable to aircraft operations because of the large reflection from the air-surface boundary. Because the aircraft is at a given altitude above the surface, this strong reflection can be removed by range gating and can be minimized by viewing the surface at an incident angle other than normal. The special situations in which ground losses are small enough to enable the radio subsurface sounder to be useful include the polar ice and the inland ice in Greenland and Antarctica. An experiment application for a radio subsurface sounder is described in a subsequent section.

Image-Forming Radars

Of the various active microwave sensors, the imaging radar is most in demand. Radar

imagery is unique because it enables the scientific investigators to view the Earth at microwave frequencies in a manner exactly analogous to viewing the Earth with their eyes.

Several analogies can be drawn between a radar-imaging system and the more familiar photographic system, and they may be of value in understanding the basic principles of the imaging radar. A radar image is a record of the intensity of microwave energy reflected from each resolution cell within the radar field of view, just as a photograph is a record of the intensity of light reflected from each resolution cell within the camera field of view.

The radar system may be designed for a single-frequency or multiple-frequency operation with single- or multiple-polarization capability, which is analogous to monochromatic (black and white) or multispectral (color) photography with or without polarizing filters.

While the similarity between radar and photographic imagery is important, it is the inherent difference, both in measurement capability and information content, that makes the imaging radar an extremely valuable tool for Earth resources applications. In terms of measurement capability, imaging radar has the distinct advantage of providing its own illuminating source and is therefore not restricted to daytime operation. Within certain frequency bands, microwave signals are relatively unaffected by clouds, fog, and so forth, which results in an all-weather measurement capability.

Even more valuable than an all-weather day/night sensing capability is the ability to view the Earth in a band of frequencies outside the visible portion of the electromagnetic spectrum. The complex interaction between microwave energy and the Earth surface produces images that reveal striking contrast and subtleties in the structure and surface cover of the Earth, which are relatively unnoticed in even the most careful analysis of conventional photography.

Despite the similarity of output product, the image-forming process of an imaging radar is quite different from that of photography. The resolving power of a camera is determined by the lens and the granularity of the film. Angular resolution is accomplished by constructing a lens of a sufficient number of wavelengths in diameter to yield an image with the required quality of detail.

Whereas a camera lens is the functional equivalent of a microwave antenna, the longer wavelength of electromagnetic energy at microwave frequencies prohibits the construction of antennas large enough to have a resolving capability similar to that of a lens. To achieve acceptable resolution with antennas of limited size, it becomes necessary to use special signal-processing techniques. To achieve high resolution in the crosstrack dimension of the image, the radar return signal is processed so that it yields the magnitude of the reflected signal as a function of time. Because the time delay between transmission and reception of a signal is proportional to range (distance to the target), high resolution in the range measurement can be achieved by finely resolving the return signal in time. The bandwidth of the radar is therefore a limiting factor in achieving range or crosstrack resolution.

In the azimuth, or along-track dimension, high resolution can only be achieved by providing a large antenna aperture in that dimension. A real aperture radar (RAR) provides a large antenna aperture by means of the actual physical dimensions of the antenna. An SAR achieves a large antenna aperture by processing, storing, and adding vectorially (usually by optical means) the return from different positions within the beam. The positions within the beam are resolved by measuring the Doppler frequency shift of the return signal. The Doppler frequency shift and the scanning coverage in the along-track dimension are produced by the motion of the radar vehicle.

A typical real aperture system is shown in figure 5–8. Microwave pulses of the proper magnitude and duration are produced in the transmitter and radiated by the common

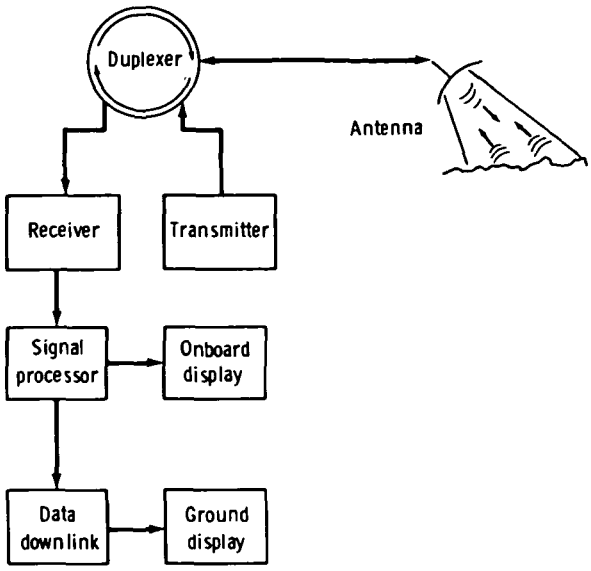

FIGURE 5–8.—Block diagram of a real aperture system.

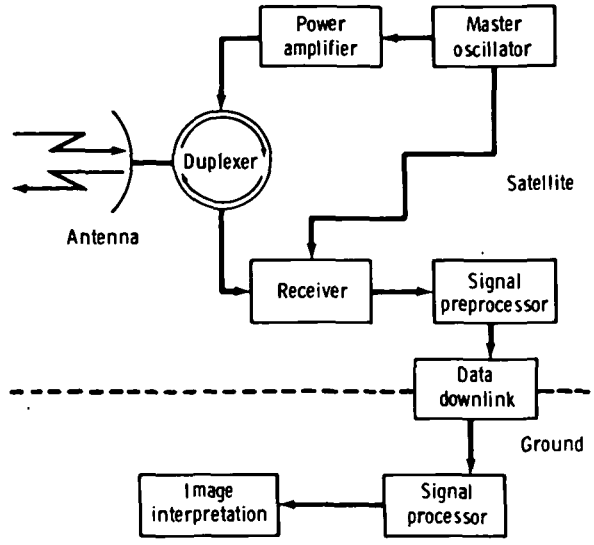

FIGURE 5–9.—Block diagram of an SAR system.

transmit/receive antenna. The duplexer switches the antenna from transmit to receive at the appropriate times. The return echoes are amplified and transmitted to an Earth station where output data are prepared in the desired format. Onboard signal processing and near-real-time display of the image may be provided if required.

A block diagram of an SAR suitable for satellite application is shown in figure 5–9. A coherent pulsed microwave signal is generated in the master oscillator, amplified, and transmitted through the antenna. Echoes intercepted by the antenna are directed to the receiver by the duplexer. The amplified echoes are preprocessed in the satellite to reduce their bandwidth, stored if necessary, and sent to a ground facility by means of the data downlink.

The combination of satellite preprocessor and ground processor analyzes the microwave echoes for time of arrival (corresponding to crosstrack position of a resolution cell), Doppler frequency (corresponding to alongtrack position of a resolution cell), and amplitude (corresponding to intensity of the reflection from a resolution cell). The signal-processing task is discussed in part B of this chapter.

A result of the differences between photography and imaging radars is that there are different performance parameter tradeoffs, but no differences in output product to the user. In both cases, the product consists of photographic negatives, photographic prints, or videotape in black and white or false color (exactly as in the present Earth Resources Technology Satellite (ERTS) outputs).

The major performance parameters that affect radar cost and realizability are range resolution, azimuth resolution, coverage (swath width), dynamic range, antenna side-lobe levels, number of different frequencies, number of different polarizations, and accuracy of backscatter measurement. A detailed discussion of the interactions between these parameters is given in part B of this chapter. In summary, the tradeoffs are as follows:

1. Improved range resolution requires increased transmitter average power. For SAR, there is a small increase in processing complexity.

2. Improved azimuth resolution in RAR requires a longer antenna, which increases the weight and complexity of the satellite. However, the longer antenna provides higher gain, thus lowering the required transmitter power. For SAR, improved azimuth resolu-

tion has no effect on the antenna or transmitter power but greatly complicates the signal processor.

3. Increased swath width requires increased transmitter power and, for SAR, requires an increase in the length of the antenna. Long antennas, in turn, decrease azimuth resolution capability and are more difficult and expensive to build and operate.

4. Improved resolution or increased coverage strongly impacts the data distribution problem and increases the data downlink bandwidth.

5. Improved dynamic range and lower side-lobe levels increase the data downlink bandwidth and, for SAR, increase the complexity of the ground-signal processor.

6. Multiple-frequency systems require duplication of the entire radar system: transmitter/receiver, antenna, data downlink bandwidth, and signal-processor capacity. However, if reduced coverage is acceptable, only the transmitter/receiver and antenna need to be duplicated.

7. Multiple polarizations require duplication of the entire radar system, except the transmitter.

8. For an RAR with fixed azimuth resolution requirements, the antenna size is inversely proportional to frequency. For this reason, designers use the highest operating frequency that also exhibits other acceptable characteristics such as low atmospheric attenuation.

9. Improved range resolution is normally provided by narrow transmitted pulse widths in a side-looking radar system. For SAR, chirp modulation is often used to improve range resolution and to lower peak power requirements.

10. Azimuth resolution of RAR is a function of the physical bandwidth. From the viewpoint of the radar system designer, very large antennas are preferred. Practical limitations on the maximum size depend on mechanical construction tolerance and the electrical accuracy required. For side-looking airborne radars, antenna dimensions of 150 to 300 wavelengths are common.

11. Accuracy of backscatter measurement depends on radar calibration. Calibration is a difficult process at best and becomes more so at broader bandwidths corresponding to better crosstrack resolution.

The ability of a camera to generate a true image of a scene depends on a lens that images the scene on film without geometric distortion and that images a point source into a small spot with minimum Airey rings. Furthermore, this ability depends on an emulsion and film process that provides a

TABLE 5–III.—*Present and Predicted Satellite Side-Looking Radar Performance*

Parameter	SAR		RAR	
	Present	5-year projection	Present	5-year projection
Resolution, m	10	3	1000 to 3000	500 to 1000
Range azimuth, m	<10	.....	.....	
Coverage:				
Along track, km	Continuous	Continuous	Continuous	Continuous
Across track, km	50 to 100	100 to 200	241	322 to 805
Dynamic range (point targets), dB	60	80	.....	
Dynamic range (distributed targets), dB	−20	−25	60	80
Peak side-lobe levels, dB	−30	−40	−25	−25
Different frequencies, number	1 to 3 (L- to X-band)	3+ (uhf to Ku-band)	4	4
		2	.....	
Different polarizations, number	0 to 2	2	2	2
Absolute calibration accuracy, dB	>4	≈3	>4	≈3
Relative calibration accuracy, dB	≈0.5	≈0.3	≈0.3	<0.2

predictable relationship between the intensity of reflected light at a point and the image gray level. With radar imagery, there are corresponding effects. Geometric distortion can occur because of inaccuracies in the relationship between time delay and ground range in the crosstrack direction or, for SAR, between Doppler shift and ground range in the along-track dimension. Both of these distortions tend to be negligible when vehicle trajectory is well known (e.g., as with a satellite). Camera spot size corresponds to SAR resolution in both crosstrack and along-track dimensions; camera Airey-ring amplitude corresponds to SAR side-lobe levels. The relationship between brightness and gray level in film corresponds to the dynamic range limitations in the radar receiver. The present and predicted performance parameters for RAR and SAR are summarized in table 5–III.

A typical SAR that would be suitable for the Space Shuttle and that has three frequencies, two polarizations, and other aforementioned parameters is described in a subsequent section. The satellite portion of such a radar will weigh approximately 500 kg and require 2 kW of prime power.

A general system description and tradeoff considerations for real aperture side-looking airborne radar (SLAR) are presented in part B.

PART B

EXAMPLES OF CURRENT RADAR TECHNOLOGY AND APPLICATIONS

USE OF SLAR FOR EARTH RESOURCES MAPPING

The design and manufacture of SLAR evolved primarily from requirements established by military users. In recent years, emphasis has been directed toward improved moving-target detection and higher resolution fixed-target capabilities. Improvements in both these parameters are important for tactical applications; however, the applicability of state-of-the-art military systems to the general remote-sensing problem is not well established.

The potential of SLAR for Earth and ocean remote-sensing applications has begun to emerge only in the past decade. Earth scientists and engineers have found that the radar map is an extremely useful tool. To the casual observer, a radar map may appear very similar to high-resolution photographs and may seem to warrant similar interpretations. However, full use of the data available in radar imagery requires a general understanding of the operating principles of SLAR and the microwave reflectivity characteristics of the terrain being mapped. The radar imagery will enhance certain features and suppress others.

This section briefly summarizes the basic principles and tradeoff considerations for SLAR. There are two fundamental types of SLAR sensors available to the remote-sensing user: real aperture and synthetic aperture. The primary difference between the two types is that a synthetic aperture system is capable of significant improvements in target resolution but requires equally significant added complexity and cost. The remote-sensing users must have a good understanding of the resolution required for each sensing mission.

The advantages of real aperture SLAR include long-range coverage, all-weather operation, in-flight processing and image viewing, and lower cost. The fundamental limitation of the real aperture approach is target resolution. However, the RAR is well suited for airborne missions that require real-time data with moderate resolution.

Synthetic aperture processing is the most practical approach for remote-sensing prob-

lems that require higher resolution (more than 30 to 40 m). However, various synthetic aperture design approaches are available, depending on the degree of resolution required. To obtain resolution improvement, sacrifices must often be made regarding range coverage, in-flight processing, and cost.

During the next 5 to 10 yr, the use of SLAR for remote sensing should expand dramatically. Based on known requirements, it appears that a mapping radar with a resolution of approximately 30 m will be in demand for airborne remote-sensing applications, particularly in the Earth-science fields.

A 30-m resolution requirement is not readily obtainable from an RAR. However, a cost-effective approach to this requirement is available that will retain the advantageous features of the RAR. This approach uses synthetic aperture processing and is known as a coherent-on-receive radar.

Resolution is not the only criterion used in selecting an airborne remote-sensing radar. Much work has been done in recent years on the detection and classification of terrain features by multifrequency and multipolarization measuring techniques. These techniques, which will not be discussed in this section, may be applicable to all SLAR systems, depending on the particular remote-sensing problem.

Basic Principles

Radar mapping systems depend on the principles (1) that all material reflects a portion of the electromagnetic energy radiated on it, and (2) that electromagnetic energy travels in straight lines and at constant velocities. Energy directed from an antenna in a beam is reflected from the ground, which can be considered as an extended array of scatterers. A radar map is obtained by scanning the ground and displaying the amplitude-modulated returns on a cathode-ray tube (CRT) or photographic film. The magnitude of ground reflections depends in a complex way on such factors as incident angle, target size and shape, material properties, and so forth. In general, a larger surface reflects more radar-transmitted energy than a small surface. Strongest reflections usually occur when the radar beam arrives at right angles to the reflecting surface. Certain materials are better reflectors than others. Of the commonly used structural materials, wood is the poorest reflector, whereas steel is the best reflector. Masonry without metal reinforcement is a fair reflector. Lakes, rivers, runways, or similar smooth, horizontal terrain features reflect radar signals as a flat mirror reflects a beam of light. Little of the radiated energy that strikes this type of terrain, at low grazing angles, is reflected back to the radar receiver.

The SLAR often produces photoradar maps of the terrain on one or both sides of the aircraft flightpath. The SLAR differs from other scanning radar systems in that the antenna is fixed to the aircraft, and its radiation pattern is perpendicular to the groundtrack. Scanning the area is accomplished only by the movement of the aircraft in flight.

The SLAR systems use an antenna beam pattern having a very narrow dimension in the horizontal direction and having wide angular coverage in the vertical direction, thus illuminating a long narrow strip of ground from beneath the aircraft to some maximum range. Therefore, the antenna beam illuminates the ground at many different ranges and incident angles. If not corrected, this condition would make correlating the strength of the radar returns with actual terrain features very difficult.

To compensate for the effects of range, the vertical gain pattern of the radar antenna is designed to be a function of the slant range or incident angle at which a given ground-patch is viewed. This type of antenna pattern is commonly called a cosecant-squared beam. At one altitude and assuming flat terrain of homogeneous properties, the radar returns from all ranges out to a maximum could theoretically be made equal. Practically, this condition can be attained only within some tolerance (usually ± 2 dB) over a limited range of vertical angles. Changes in

altitude can be compensated to some extent by tilting the vertical beam.

A typical real aperture SLAR system is shown in figure 5–10. The timing circuit synchronizes both the transmitting and recording systems. Radar power pulses of the proper magnitude and duration are produced in the modulator and then converted by the transmitter to rf pulses with the desired frequency characteristics. These pulses are then radiated by the antenna, which also picks up the returning target echoes. The duplexer switches the antenna from transmit to receive at the appropriate times. The return echoes are amplified, processed, and converted to intensity-modulated traces on a CRT. A mirror-lens optical system causes the light from the CRT to expose moving film in a recording system to build up a photoradar map of the areas to either side of the flightpath. The direction of film travel is perpendicular to the CRT trace. The film speed is proportional to the aircraft speed over the ground and provides the scanning motion to the film.

Figure 5–11 is a highly simplified representation of SLAR image recordings. Large elevated target masses, such as mountains, result in long shadows (or areas) from which there is no return (fig. 5–11(*a*)). Excessive shadowing can obscure important terrain features; however, a moderate amount of shadows is often desirable to highlight geographical features.

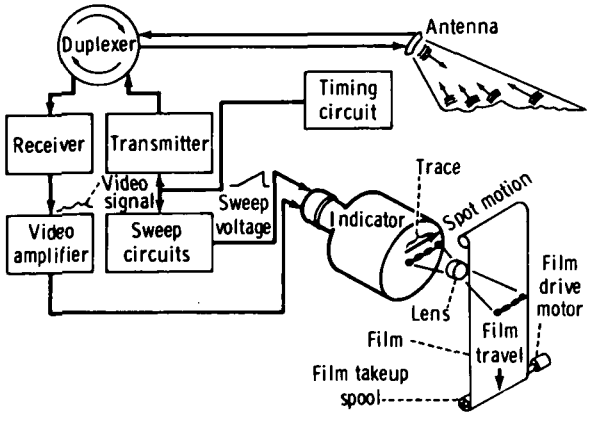

FIGURE 5–10.—Typical real aperture SLAR system.

Flying at higher altitudes will decrease the amount of shadowing in the radar image. Figure 5–11(*b*) shows the relative amplitude of echo signals that would be obtained from the targets illustrated. Figure 5–11(*c*) depicts the intensity of the CRT trace as it is modulated by the signal represented in figure 5–11(*b*). The larger signal amplitudes cause maximum intensity, whereas little or no light is produced by the shadow areas.

Radar echoes illustrated in figure 5–11 represent only one line segment of operation. In actual practice, a new line segment is produced for each 15 to 30 cm of aircraft travel over the ground. The length of the CRT trace on the film represents a fixed distance, which is the length of ground segment being viewed by the radar. Therefore, if the trace length on the film is 10 cm and represents a distance in range of 50 km, the film must move 10 cm when the aircraft travels 50 km over the ground to maintain a uniformly scaled photoradar map. Examples of actual radar imagery are presented in the section of this chapter entitled "Real Aperture SLAR Applications."

A synthetic aperture SLAR uses signal storage and processing techniques to simulate the performance of an antenna aperture that is much longer (in the direction of flight) than the actual physical antenna used. This technique results in improved azimuth resolution beyond that available from the beamwidth of the physical antenna. The physical antenna scans the terrain in the same way as the real aperture SLAR. At intervals along the flightpath, a signal is transmitted and the phase and amplitude of the returns are measured and stored. After the physical antenna has traversed a distance L, the stored signals can be combined to produce a return similar to that obtained from a real antenna having a physical length D.

With an SAR system, it is possible to focus at each range separately by the proper adjustment of the phases of received signals before summation; this capability is called a focused synthetic array. If the aperture is focused at infinity for returns from all

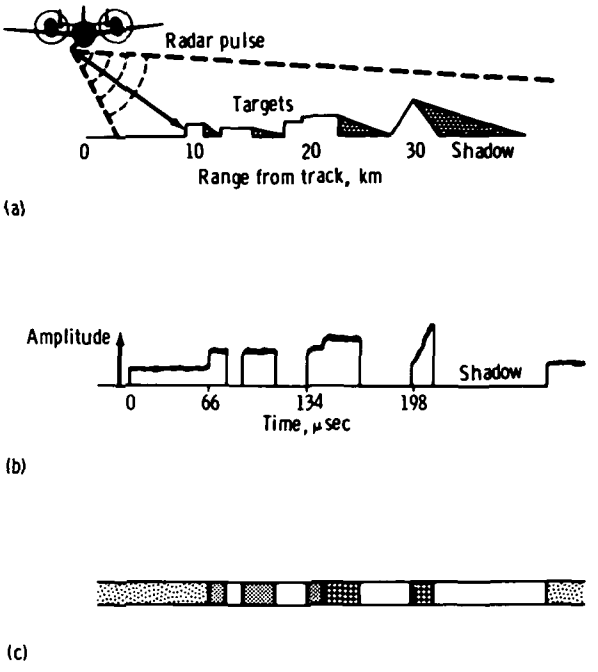

FIGURE 5–11.—Simplified representation of SLAR image recording. (*a*) Targets and shadow effect. (*b*) Radar return echoes. (*c*) Intensity of CRT trace.

ranges, the capability is called an unfocused SAR. Usually, this processing is accomplished on the ground after a flight by using an optical correlator. Recently, work has been performed on digital correlators that can operate on a real-time basis in the air. Optical correlators of the required quality are not suitable for aircraft installation, primarily because of their bulk.

The SAR systems usually incorporate chirp techniques to obtain high range resolution without requiring excessively high peak power transmitters. A coherent signal is required to generate chirp signals and to form a synthetic beam. Generally, such systems use a stable local oscillator (STALO) to generate the transmitted signal and to serve as a local oscillator in the receiver. A pulsed power amplifier is used to produce the high power transmitted signals.

Important System Considerations

The selection of an SLAR for remote sensing requires that certain key performance parameters be evaluated by the user. The user must understand the performance and cost tradeoffs so that a cost-effective selection can be made. Some of the more important characteristics that should be considered are presented in the following paragraphs.

Resolution.—A key parameter often used to judge the quality of mapping radar is resolution. With SLAR, resolution is defined as the minimum separation between two targets that will appear individually on the imagery. Whereas the ultimate system resolution is a function of several parameters, the most important criterion is the size of the radar pulse rectangle projected on the ground. At a given instant of time, the ground area (ΔR by ΔY) is simultaneously superimposed in the radar receiver (fig. 5–12). This area is called the pulse-rectangle or ground-resolvable area. Objects within the pulse rectangle are recorded as if they were all located at the center of the rectangle, and two objects that occupy the same pulse rectangle appear as a single return on the imagery. The integrated reflectance of all ground area and of all objects within the ground-resolvable area at any given instant are, in essence, presented as one value of reflectance to the sensor. When this composite reflectance value differs from those in adjacent pulse rectangles, the sensor can discriminate between targets. If a single "hard" target (such as a small truck) is in flat, open surroundings and is illuminated by the radar, it probably will be the dominant reflector in the pulse rectangle. The radar accordingly records, as a single target, the composite reflectance of the truck and the surrounding area within the pulse rectangle. To the radar, the truck is as large as the ground-resolvable area. If objects are separated by a distance greater than the corresponding dimension of the pulse rectangle, they will be imaged separately.

One should be careful to distinguish the difference between detection and resolution associated with a mapping radar. Resolution is commonly defined as the ability of the

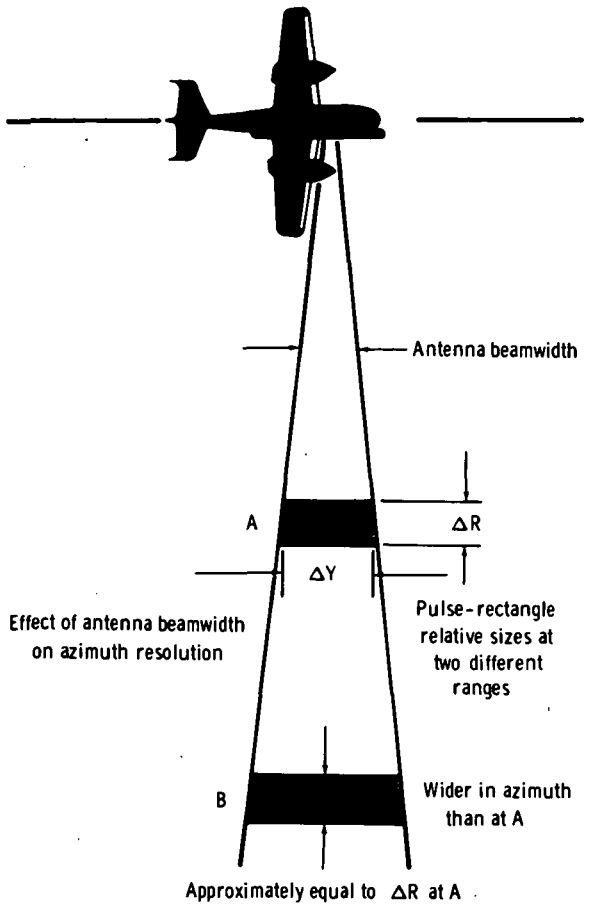

FIGURE 5–12.—Real aperture resolution.

radar to distinguish two targets of equal reflectivity separated by the resolution distance. However, this definition does not imply that the radar cannot detect a target smaller than the resolution cell. If a target has sufficient reflectivity, the radar will detect a target, such as a vehicle, a powerline pole, a corner reflector, and so forth, even though it may be physically much smaller than the resolution cell of the radar. Because of this difference in detection and resolution, users of RAR are often amazed by the detail in the imagery, because of the many small features that are detected when resolution is not required to distinguish them from surrounding objects.

For real aperture noncoherent SLAR, the pulse rectangle (ground-resolvable area) is primarily determined by the radar antenna beamwidth and transmitted pulse length. Range resolution, which is in the direction of radiated energy (perpendicular to the flightpath), is determined by the bandwidth of the transmitted signal. The inherent range resolution $c\tau/2$ is transformed into ground resolution by

$$\Delta R = \frac{c\tau}{2\cos\psi} \qquad (5\text{–}4)$$

where ΔR is ground range resolution, τ is transmitted pulse width (3 dB), ψ is beam depression angle, and c is speed of light. For an RAR and small horizontal antenna beams, the azimuth resolution is a function of half-power beamwidth $\theta_{-3\text{ dB}}$.

$$\theta_{-3\text{ dB}} = \frac{K\lambda}{D} \qquad (5\text{–}5)$$

where K is efficiency factor of antenna aperture, λ is transmitted wavelength, and D is antenna aperture length. The azimuth resolution ΔY is given by

$$\Delta Y = R\theta_{-3\text{ dB}} = \frac{RK\lambda}{D} \qquad (5\text{–}6)$$

where R is range.

Azimuth resolution can be improved by decreasing the wavelength λ (increasing frequency) or by increasing the physical dimension of the antenna. Either approach has a limit in a practical radar design. In decreasing the wavelength λ, the problems of atmospheric attenuation and the efficient generation of large amounts of power become more difficult. The problems of an excessively large antenna are quite obvious when considering airborne or spacecraft installations.

For the unfocused synthetic array for which no adjustments are made in the return-signal phases before integration, there is a limit to the effective synthetic antenna length that can be generated. The criterion often used is that the difference between the round-trip distance from the target to the center of the array and the round-trip distance from the target to the extremity of the array should not differ by more than $\lambda/4$ (fig. 5–13).

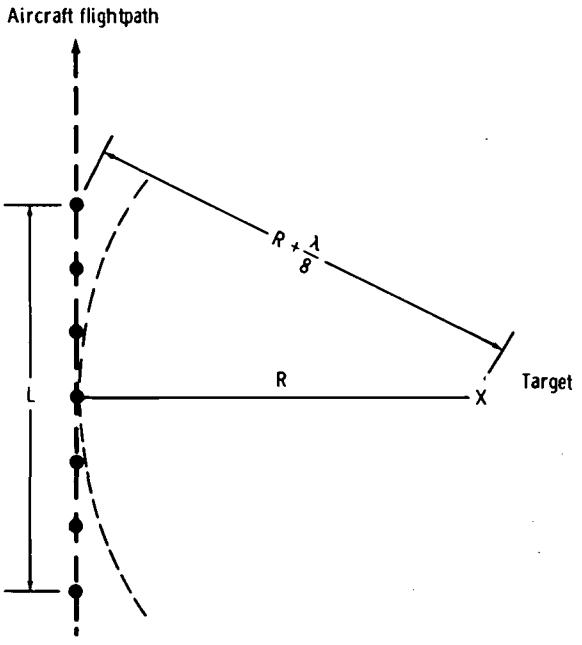

FIGURE 5–13.—Unfocused synthetic antenna.

When this rule is used, the best azimuth resolution obtainable from an unfocused radar is

$$\Delta Y_u = \tfrac{1}{2}\sqrt{\lambda R} \qquad (5\text{–}7)$$

Although range is still an important criterion, it is less important with the unfocused synthetic array than with the RAR. More importantly, the azimuth resolution at long ranges is not a function of the physical antenna length D.

If the radar processor makes adjustments in the signal phase received at each point of the synthetic antenna (focusing), the restrictions that limited the maximum synthetic antenna length of the unfocused antenna no longer apply. The best obtainable azimuth resolution from the focused SAR is

$$\Delta Y_f = \frac{D}{2} \qquad (5\text{–}8)$$

The smaller the physical aperture, the wider the physical beamwidth; and, consequently, the longer the portion of the flightpath during which the returns of a given target can be processed to form the synthetic aperture. This expression also forms the limit at short ranges for the azimuth resolution of the unfocused processor.

Distortion.—Image distortion is as important, in many respects, as system resolution. A distorted image makes it difficult to make the proper interpretation of actual terrain features. Although there are many sources, the types of distortion errors that should be given special consideration are azimuth resolution distortion, display distortion, and antenna motion distortion.

In the discussion of resolution, the pulse rectangle of the RAR was shown to grow in azimuth direction as the target range was increased (fig. 5–12). As a result, objects that are approximately equal in range and azimuth dimensions will be shown to be extended in azimuth, relative to range. This fact also obtains for targets mapped by an unfocused SAR, but to a lesser degree because azimuth dimensional relationships remain constant for focused SAR.

Display distortion can result from several factors, including nonlinear sweeps and improperly designed optics. However, most errors of this type can be minimized by proper hardware design. Skew distortion of the image will occur if no compensation is made for aircraft drift and antenna squint angle. If a slant-range presentation is used, a foreshortening of targets at close range will occur When ground range is displayed based on assumed level terrain, the image will be distorted if the terrain is sloping or irregular. If the antenna is rigidly fixed to the aircraft, buffeting and turbulence may smear and distort the radar image.

If the antenna pattern is not continually positioned perpendicular to the aircraft groundtrack, some form of correction must be provided to prevent square objects from being recorded as skewed parallelograms and circular objects from becoming elliptical. Generally, this skew distortion is corrected by yaw stabilization of the antenna and by providing drift information from the navigation system to the deflection yoke of the CRT. The true direction of the antenna beam is not

necessarily perpendicular to the face of the antenna array. The deviation of the beam from the orthogonal is called the squint angle. If the CRT traces are rotated an amount equal to the sum of drift and squint angle and expanded by the cosecant of the sum angle, the radar image will be free from skew distortion and range error.

Some radars display slant range from the aircraft to the target, which is reasonably accurate for small depression angles but causes close-in targets to appear farther away than the true distance from the aircraft groundtrack. The close-in distortion can be improved by a nonlinear sweep signal on the CRT, making the map dimensions proportional to true ground range. However, the aircraft altitude above some reference plane must be accurately known. This reference plane is normally measured with respect to the terrain directly below the aircraft flightpath. If the topography is highly irregular or sloping, range errors will still exist for all target areas not located on the reference plane.

For a radar system to generate high-quality photoradar maps, the aircraft should move over the ground at a constant velocity and maintain a stable attitude with respect to the ground. If the attitude of the aircraft varies, the movements may have adverse effects on the radar image. Roll, pitch, and yaw motions may be due to meteorological variables and autopilot discrepancies caused by improper operation or malfunction.

For RAR, the degree and precision of motion compensation or stabilization is relatively minor. Stabilization of the antenna about the yaw axis to within a beamwidth is generally all that is required for good-quality RAR imagery.

Stabilization of the antenna is a vitally important factor for high-resolution SAR. A greater degree of motion stabilization and correction is required as the resolution requirement becomes more extreme. Turbulent aircraft motion along the flightpath can "bend" or distort the synthetic antenna return. Generation of a high-resolution map is based on accurate determination of phases and Doppler frequencies of the return signal. If motion errors are not detected and appropriate corrections are not made, the map quality will be degraded to an unacceptable degree. Usually, the antenna is stabilized by a system of roll, pitch, and yaw gimbal drives that are controlled from signals generated in a motion compensation subsystem of the radar.

Range coverage and swath width.—For remote-sensing applications, range coverage and swath width are very important considerations that have a direct influence on the total cost effectiveness of any radar mapping mission. A radar with greater range coverage and swath width will undoubtedly result in lower operational cost, and will require less time, equipment, and manpower. This cost reduction is extremely important in commercial remote sensing.

For real aperture mapping radars that use the analog signal integration of the CRT and film, the maximum mapping range is limited primarily by transmitter power, antenna aperture size, and atmospheric attenuation. When digital processing is used, the overall complexity and cost of the processor may impose some practical restraints on swath width. The rapid development of LSI (large-scale integration) integrated circuits is making the use of real-time digital processing more attractive.

Real aperture X-band mapping radars that cover as much as a 200-km swath width are now in production. Usually, the SAR is limited to smaller swath widths (15 to 30 km) because of hardware complexity and transmitter power limitations.

All-weather capability.—In an RAR system with a fixed antenna size, the azimuth resolution is improved in proportion to the frequency of the transmitter. For this reason, designers use the highest transmitter frequency that also has other acceptable characteristics, such as low atmospheric attenuation. The X-band is a reasonable compromise between achieving high resolution and selecting a frequency with desirable propagation

characteristics. The X-band is the highest microwave frequency range that has acceptable low attenuation and backscattering properties through cloud cover and moderate rainfall. A real or unfocused SAR operating at Ka-band would provide better azimuth resolution for a given antenna length, but at the price of increased propagation losses and severely limited performance in weather conditions in which water droplets are formed.

Another important advantage of radar for geological survey applications is the ability of this type sensor to provide some penetration of foliage to reveal the rock formations below. In vegetated areas, the X-band radar imagery has revealed faultlines that were not detectable in photoimagery, even though relatively little foliage penetration is obtained at X-band. A lower transmitter frequency (e.g., 400 MHz) would provide much better foliage penetration, but the loss in azimuth resolution for an RAR makes this impractical. The SAR could provide good resolution and some foliage penetration by operating at these lower frequencies.

Availability of data.—The timeliness or turnaround time required for radar data is primarily a function of the mission objectives. When the terrain being mapped is static or slowly changing, such as mountain ranges or agricultural areas, it might appear that real-time data are not required. However, this is not the case. For example, when mapping an area to detect geological features (such as faults, fractures, and minor topographical features), the correct amount of shadowing must be produced on the map. The proper degree of shadowing will enhance the topography, whereas too much or too little shadowing will result in lost information. An airborne operator able to view imagery during flight can optimize the shadows by adjusting the flight altitude.

When the terrain is in a state of continual change, such as in ice-field mapping or oil pollution detection, a large time delay in transmitting the information to a ground station where it is processed, interpreted, and disseminated to the using agencies may be unacceptable.

When large areas are to be surveyed, it is practical to construct map mosaics from adjacent strips of radar imagery. Good-quality mosaics require that the overlap of each strip be properly controlled and that the amount and direction of the image shadows be the same for each strip. Real-time monitoring of the radar data by a qualified operator is vital to producing good-quality mosaics.

Real-time film developing for current SLAR systems is accomplished by onboard film-processing laboratories in the larger aircraft systems or by self-contained monobath-processing cameras. With the latter approach, exposed film passes under a metering roller at which time it comes into contact with chemical-processing fluid. Processing fluid is vacuum pumped from a sealed monobath tank into a processing tray and returned to the tank. After the film has been processed, it moves into view over a lighted viewing panel, which presents ground targets in the viewing area a few seconds after the area is illuminated by the radar.

Real Aperture SLAR Applications

This section briefly describes some environmental and geological applications of SLAR. Although these applications are not a complete listing, they give some indication of the versatility of SLAR as a remote sensor.

Oil and mineral exploration.—The usefulness of SLAR in locating gas and oil fields and mineral deposits lies in the ability of the radar to provide a large-area map, which enables surface lineaments to be detected. Analysis of the density and directional distribution of surface lineaments can isolate oil- and gas-bearing subsurface structures. This detailed radar lineament analysis is possible because the radar provides an image that enhances the geological features better than conventional aerial photography. The SLAR has the unique capability of operating with a wide selection of depression angles, which allows the operator to enhance the topographic features in areas of high or low relief.

An example of the imagery produced is shown in figures 5–14 and 5–15, which illustrate some of the features of the AN/APS–94D SLAR. The wide-area surveillance capability of a real aperture SLAR is demonstrated in figure 5–14. Swath width on this image is 100 km (50 km on each side of the aircraft flightpath). The enhancement of geographical features by SLAR is shown in figure 5–15.

Another advantage of SLAR for geological exploration is the ability to image simultaneously from both sides of the aircraft to facilitate making two radar mosaics of the terrain with opposite look directions. Thus, the imagery interpreter is better able to locate less-pronounced lines or fractures that might not be visible from a particular look direction.

The SLAR does not, of course, provide complete knowledge of geological features; however, it provides much information that permits surface exploration to be concentrated in areas with the highest probability of success.

Ice mapping and classification.—The SLAR imagery provides information on the amount and nature of ice cover for either saltwater or freshwater areas. The principles of operation are somewhat different from the mapping of ground areas because ice, under certain conditions, appears transparent to the microwave energy and does not reflect energy to indicate its presence. Thus, ice imagery requires careful interpretation. Different types and amounts of ice cover are illustrated in figure 5–16. The bright lines and areas in the image represent the points of greatest radar echo. The echoes result primarily from interface between ice and water or discontinuities or cracks in the ice that are nearly perpendicular to the line of sight. The pres-

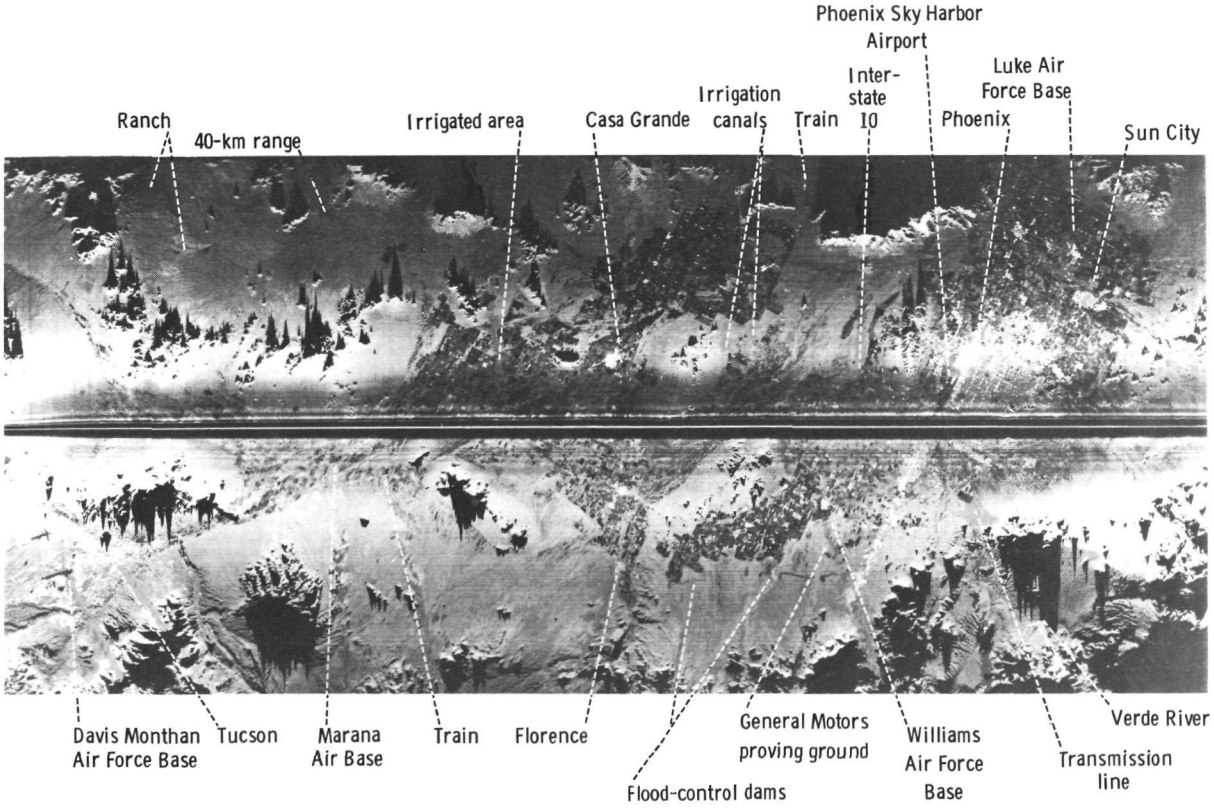

FIGURE 5–14.—Wide-area surveillance capability of a real aperture SLAR (AN/APS–94D fixed-target imagery of central Arizona).

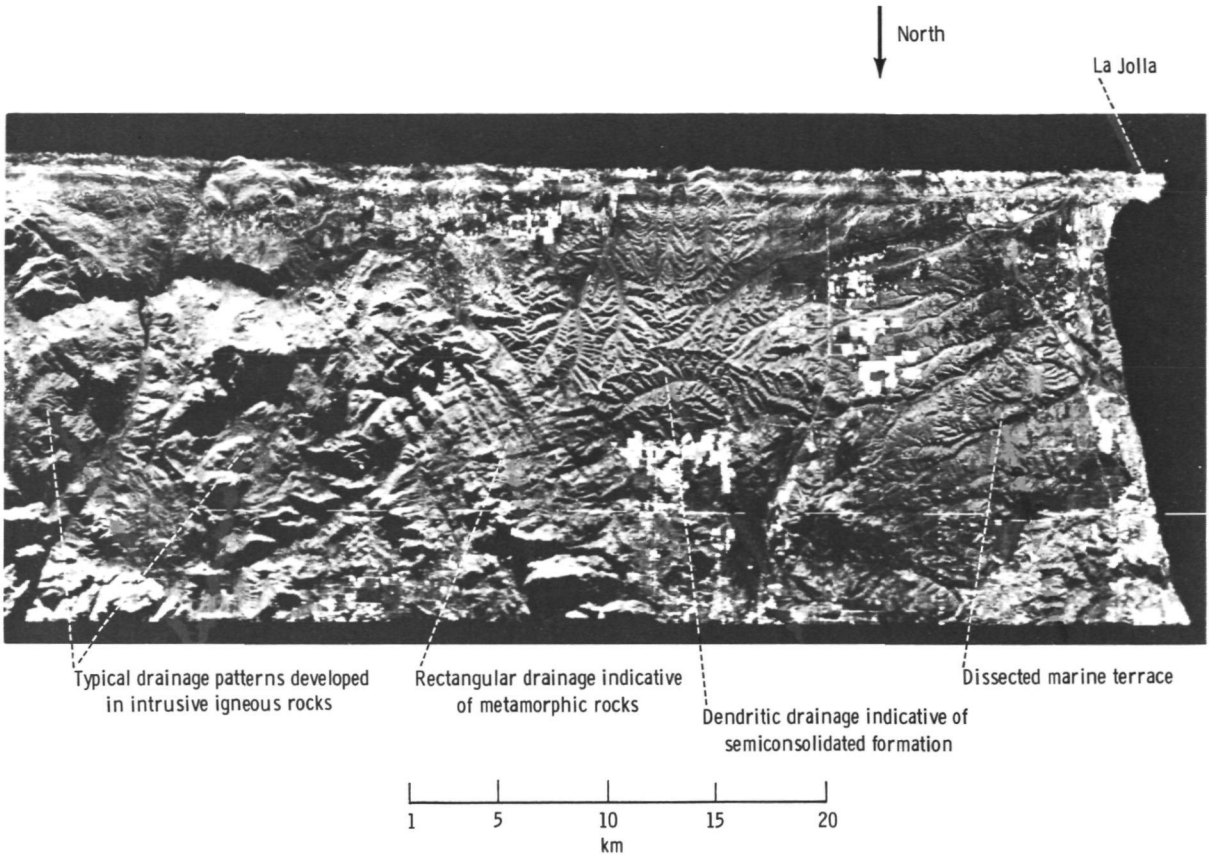

FIGURE 5–15.—Enhancement of geographical features by SLAR (AN/APS–94D fixed-target imagery of La Jolla, Calif., with a 25-km range and a single antenna).

ence of clear ice in the upper portion of figure 5–16 is primarily evidenced by the presence of pressure ridges and cracks. The clear area in the left portion of figure 5–16 shows the greatest amount of radar reflection and indicates the turbulent flow of ice in that area. The interpreter's ability to determine the nature of the ice cover is aided by knowledge of other meteorological conditions, such as the temperature, force, and direction of the surface wind.

The ability of SLAR to produce imagery through cloud cover and surface storms is particularly important because the information is of greatest value during these conditions. A radar operating at a wavelength of approximately 3 cm can penetrate cloud cover that would prevent visible and infrared (IR) sensors from producing ice imagery.

Icepack tracking.—The location of icepacks and icebergs is of prime importance to surface vessels in the area. The best information on the movement of these hazards is obtained by periodic mapping of the area with side-looking radar. The movement of ice on the water is governed by both winds and tides. Present experience indicates that the location can be determined accurately enough to permit safe passage of surface ships if an SLAR map can be obtained every few days. The required frequency of reconnaissance flights depends on the wind conditions and the particular areas involved. Attempts to predict the movement of ice by the speed and direction at the time of reconnaissance would not be useful because of the erratic nature of the movement and the inability to measure low velocities with a high degree of accuracy.

The ability of the SLAR to produce a

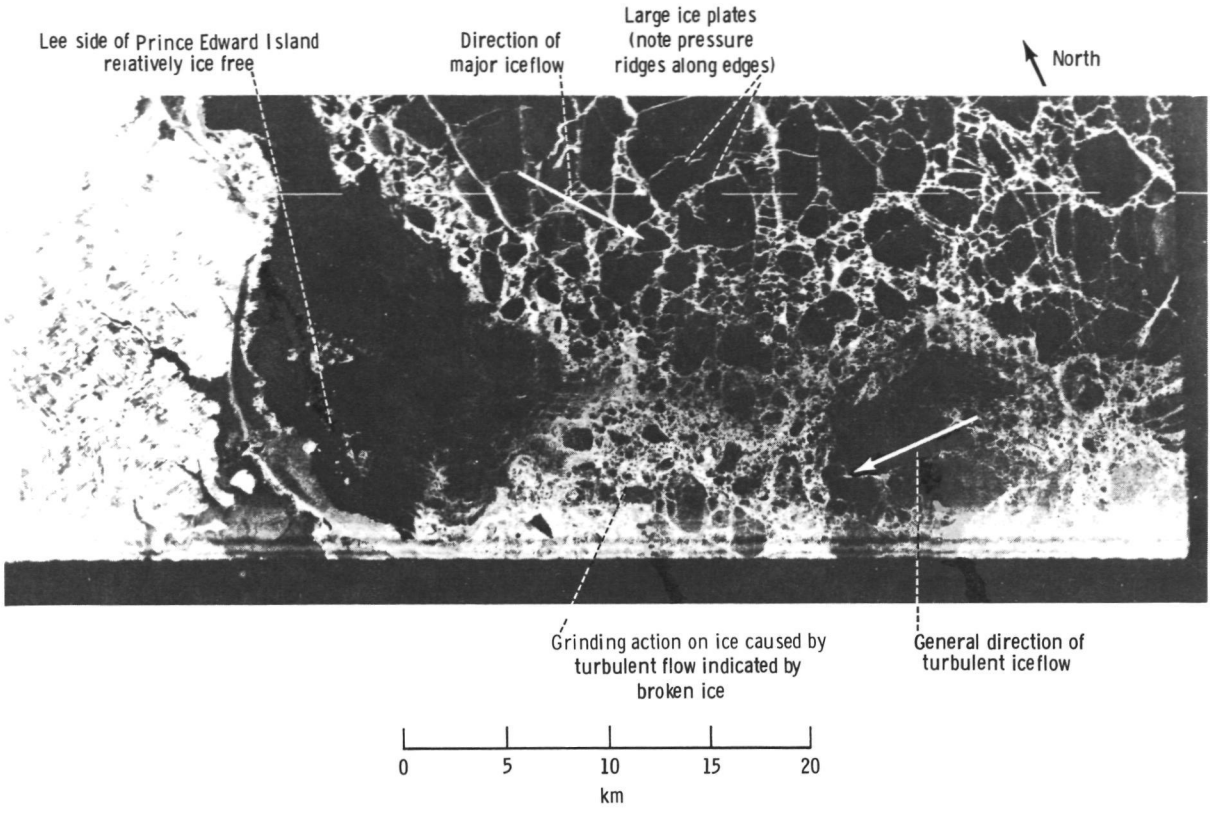

FIGURE 5–16.—The SLAR imagery of varying types and amounts of ice cover (AN/APS–94D fixed-target imagery of the northwest tip of Prince Edward Island).

200-km-wide radar map under adverse weather conditions is again a great advantage. Because icebergs produce large radar echoes, resolution is not of particular importance, and the radar can be operated on the largest scale factor and greatest range.

Oil pollution detection.—With the ever-increasing demand worldwide for crude oil and petroleum products, accidental spills from ships and offshore wells are becoming an increasing danger. To combat this potential hazard, the U.S. Coast Guard has developed an Airborne Oil Surveillance System (AOSS). The AOSS is a multisensor system consisting of an X-band side-looking radar, a Ka-band imaging microwave radiometer, a multichannel IR line scanner, and a multispectral low-light-level (LLL) television (TV) system. The AOSS is designed to detect and map oilspills anywhere within a 40-km range of the aircraft flightpath. The system was flight tested in early 1974. The following are functions of the AOSS:

1. To detect oilspills on the sea.
2. To indicate the magnitude of oilspills (both area and approximate thickness).
3. To assess cleanup operations and forecast dangers to coastal areas.
4. To identify the oil type (signature).

This set of complex requirements cannot be satisfied by a single sensor; thus, the AOSS combines microwave techniques and other methods using radiation from the ultraviolet to the IR region. The mission concept is depicted in figures 5–17 and 5–18.

The side-looking radar will provide long-range routine surveillance of an area as much as 40 km on each side of the aircraft. The microwave radiometer covers the area directly below the aircraft flightpath (not

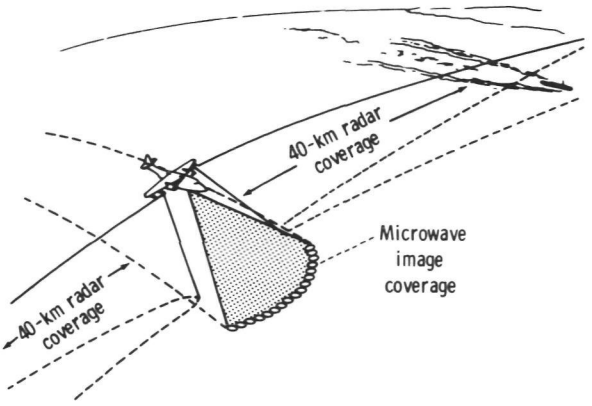

FIGURE 5–17.—Routine AOSS surveillance at a 1524-m altitude (ship detection and routine ocean slick mapping mode).

mapped by the radar). The radar imagery provides the location and approximate area of the oilspill, and once the oilspill has been identified, a short-range inspection is made by other sensors that classify and measure characteristics of the oilslick.

The active microwave sensor advantageously uses contrast in reflection properties between clean and polluted seas. Small-amplitude waves of short length are continually generated on both calm and high seas. These waves are efficient reflecting surfaces for microwave radiation. A thin film of oil damps these small gravity and capillary waves, forming a surface of lower radar reflectivity. Active microwave sensors can easily detect the change in microwave reflectivity caused by oil, except in the presence of very calm sea states (with prevailing winds less than approximately 1 m/sec). A summary of other requirements for the radar used on the AOSS is given in table 5–IV.

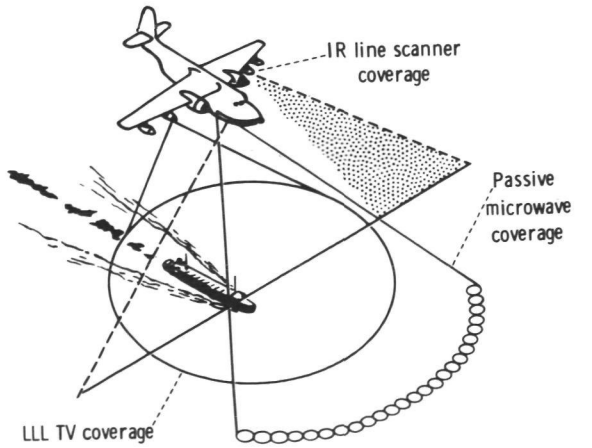

FIGURE 5–18.—Diagram of AOSS short-range pollution inspection and documentation (low-altitude ship and pollution inspection and documentation mode).

Tradeoff Considerations

The basic principles of an SLAR sensor have been examined, and some of the important considerations in the system design have been reviewed. In summary, the significant desirable features of an SLAR sensor are long-range coverage, broad swath width, adequate resolution and detection capability, all-weather operation, in-flight processing and imagery viewing, reliable design approach, moderate system acquisition costs, and low operational costs.

Although real-time film processing that uses wet chemical developing is available, a dry-film-processing camera would be a definite improvement in terms of operational costs and handling problems.

The most direct approach to improving azimuth resolution in RAR is to extend the physical length of the antenna. However, improved resolution is obtained at the expense of additional atmospheric and weather attenuation effects. When improved azimuth resolution is required, some type of synthetic processing technique can be used, but careful

TABLE 5–IV.—*Requirements for Radar Used on AOSS*

Range:	
Ship detection, km....	0 to 40
Oil spill detection, km.	15 to 25
Swath width, km.....	80
Detection requirements	
Ships, m	$\geq$25 by 80 (or larger)
Large spills (major dimension), km.....	$>$1.5
False alarm rate, max/hr..	1
Data	Hardcopy (film)

thought should be given to how much resolution is required to accomplish the task.

Resolution tradeoff considerations.—A tradeoff between SAR and RAR can only be made when the specific application of the radar is considered. For many environmental applications, such as geological fault surveys, geological exploration, ice reconnaissance, and water-level surveys, large-area moderate-detail imagery is required. The initial purchase cost, maintenance cost, and total mission operating cost of a high-resolution SAR is not justified solely for these applications. The greater swath-width coverage of the real aperture system more than offsets the lower resolution associated with this type of airborne radar. Usually, wide-range swath width and high resolution are incompatible because of practical limitations on the complexity of processing and recording equipment.

If fine topographical detail is required to obtain the desired target intelligence, the high-resolution SAR has an advantage. Some possible applications might include land use and urban studies. Again, the specific applications of the radar system may indicate whether the need to resolve the fine detail occurs frequently enough to justify a high-resolution radar.

An aircraft system used for environmental applications probably will contain multispectral sensors such as optical, IR, microwave, and magnetic sensors. In such instances, the most cost-effective system might include a side-looking radar for rapid large-area coverage. The SLAR provides gross detail and draws attention to probable areas in which closeup, highly detailed data are required.

Alternate approaches to synthetic aperture processing.—As an aid to selecting a cost-effective system, the azimuth resolution obtainable from various approaches will be reviewed.

For RAR, the best obtainable azimuth resolution is

$$\Delta Y_r = \frac{\lambda R_s}{D} \qquad (5\text{–}9)$$

For an unfocused SAR, the azimuth resolution is

$$\Delta Y_u = \tfrac{1}{2}\sqrt{\lambda R_s} \qquad (5\text{–}10)$$

Finally, the fully focused SAR azimuth resolution is

$$\Delta Y_f = \frac{D}{2} \qquad (5\text{–}11)$$

where λ is wavelength, D is effective antenna real aperture length, and R_s is slant range. The preceding expressions represent the resolution obtainable in an ideal system. In actual system designs, the overall resolution may be somewhat less than these predicted values. A graphic comparison of the theoretical resolution obtainable when λ is 3.2 cm and D is 3 m is shown in figure 5–19. Note that for a focused synthetic processor, resolution can be improved by decreasing the antenna length D (curve D in fig. 5–19). The unfocused example (curve C in fig. 5–19) assumes a uniformly weighted filter with

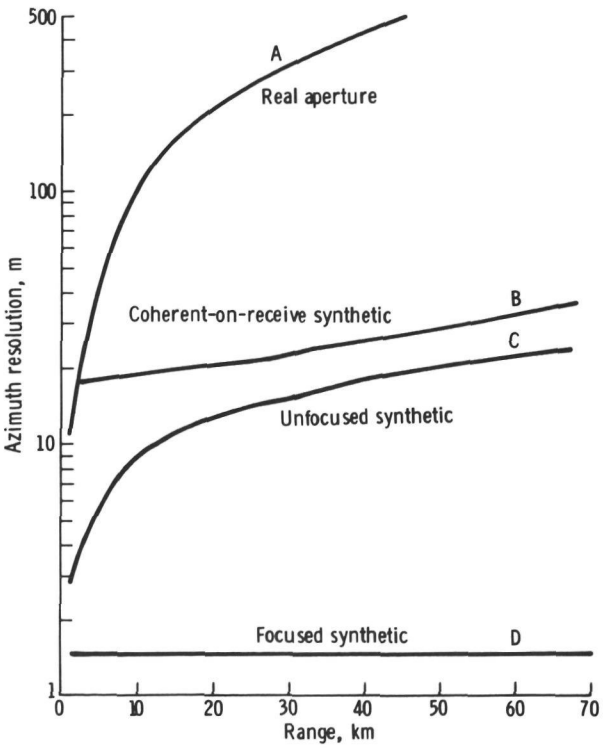

FIGURE 5–19.—Ideal azimuth resolution as a function of range, where λ equals 3.2 cm and D equals 3 m.

bandwidth varying as a function of the square root of range. A more practical design approach might use a Taylor weighting to minimize side lobes and a fixed bandwidth (curve *B* in fig. 5–19).

Cost tradeoff considerations.—Although precise cost comparisons are difficult to make, no system concept can be selected without some rough estimate of the overall cost, including both the airborne sensor and ground-processing equipment. It is fairly safe to state that system acquisition costs are heavily influenced by the resolution requirements. The RAR systems are the least expensive, and the focused synthetic radar is, of course, at the high end of the cost scale. The relative cost of X-band SLAR as a function of azimuth resolution is illustrated in figure 5–20.

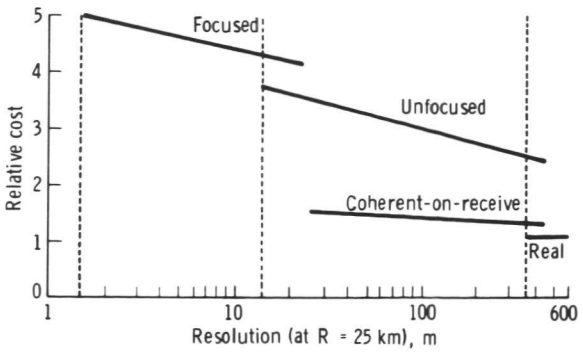

FIGURE 5–20.—Relative cost of X-band SLAR as a function of azimuth resolution.

Recommended future system developments.—Because of the wide diversity of requirements, no single SLAR design will meet all remote-sensing requirements in a cost-effective manner. In some applications, the RAR will be adequate; in others, state-of-the-art synthetic radars with multiple frequency and multiple polarization may be needed. However, for the vast majority of remote-sensing problems, a radar with moderate resolution (30 m) appears to be adequate. For these problems, an X-band unfocused synthetic aperture or Doppler-beam-sharpened design approach is recommended. There is nothing really new about the basic concept of Doppler beam sharpening; in fact, such radars are now in existence. However, the design approach briefly described in the following paragraphs represents a lower cost alternative to the fully coherent unfocused synthetic radar design. Some tradeoffs considered in selecting the coherent-on-receive approach are summarized in table 5–V.

A list of key performance characteristics of a mapping radar that should satisfy numerous remote-sensing applications during the next 5- to 10-yr period is given in table 5–VI. This radar is primarily intended for remote-sensing problems that require moderate resolution.

TABLE 5–V.—*Summary of Tradeoff Considerations*

Performance improvement	Recommended method	Alternate method	Reasons for not selecting alternate
Range resolution	Short transmitter pulse.	Pulse compression.	Klystron or traveling-wave tube must be used instead of a simple, inexpensive magnetron transmitter.
Azimuth resolution ..	Coherent-on-receive synthetic aperture.	Increase frequency of RAR.	Range decrease is caused by atmospheric losses, and more expensive microwave components are needed.
		Increase antenna length of RAR.	Antennas 5 m or less can be carried by business aircraft, whereas larger antennas would require transport-size aircraft.
		Fully coherent synthetic aperture.	Although the fully coherent design has highest ultimate resolution potential, the coherent-on-receive design provides an order-of-magnitude improvement over real aperture and retains magnetron transmitter.

TABLE 5–VI.—*Coherent-on-Receive Radar Parameters*

Transmitter:	
Tube type	Magnetron
Frequency	X-band
Peak power output, kW.	50
PRF, pulse/sec	750
Pulse width, μsec	0.2
Receiver:	
Minimum discernible signal, dBm	−95
Bandwidth, MHz	7
Antenna:	
Gain, dB	35
Elevation pattern shape.	$\csc^2 \theta$
Stabilization	Yaw plane
Antenna length, m	3
Polarization	Horizontal
Look direction	Both sides of aircraft
Processor type	Unfocused synthetic coherent-on-receive
Range resolution, m	30
Azimuth resolution (at 25 km), m	30
Range scale, km	25 or 50
Maximum swath width, km.	100
Data display	Real-time using dry silver film recorder

Coherent-on-Receive System

In a coherent radar system, the echo is processed to extract both amplitude and phase information, as opposed to a noncoherent radar system in which only amplitude information is processed. A coherent system will generally produce far better performance than a comparable noncoherent system. There are two basic approaches for achieving coherent operation. The most commonly used approach (i.e., the fully coherent system) uses a STALO and a power amplifier transmitter. Each transmitted rf phase is locked to the STALO, which is required to have very limited phase and frequency variations during the observation time of any representative target.

The coherent-on-receive technique is a method for generating a coherent signal from a magnetron transmitter. The phase of a magnetron transmitter will be approximately random from pulse to pulse. Coherence is obtained by measuring the phase of the echo from that pulse. Removal of the transmitted phase from the echo phase eliminates the random pulse-to-pulse phase variations so that the signal may be processed as a coherent signal. Thus, the signal is not coherent until it is received by the radar and the random phase error is removed.

The coherent-on-receive operation is generally not economical in systems requiring modulation, or chirp, of the transmitted phase. Such intrapulse modulation is generally required only when the desired range resolution of a mapping radar is high. The desired range resolution is available by transmitting a fairly short pulse (0.1 to 0.2 μsec), which is still long enough for practical peak-power considerations.

The key element of the coherent-on-receive radar is the measurement of the phase of each transmitted pulse and the subtraction of that phase from the subsequent echo train. The significant steps in accomplishing this operation are summarized as follows:

1. At the time of transmission, a sample of the transmitter is injected into the receiver (fig. 5–21).
2. The phase angle θ_t of the transmitted signal is measured in the receiver and stored.
3. The phase angle θ_t corresponding to the transmitter phase is subtracted from the echo signal phase history that resulted from the transmitted pulse.
4. This operation is repeated for each radar-transmitted pulse.
5. The echo signal pulse train can now be processed as a pulse-to-pulse coherent signal.

Any errors in the magnetron, the STALO, or the intermediate frequency will be converted into phase errors by the phase-measurement circuit. These sources of frequency errors must be minimized to keep the resulting phase error within acceptable limits.

Antenna.—Because the coherent-on-receive radar is a variation on the unfocused synthetic aperture technique, the physical aperture of the antenna does not affect the system azimuth resolution. The major considerations that determine the antenna size are (1) gain adequate to provide the desired

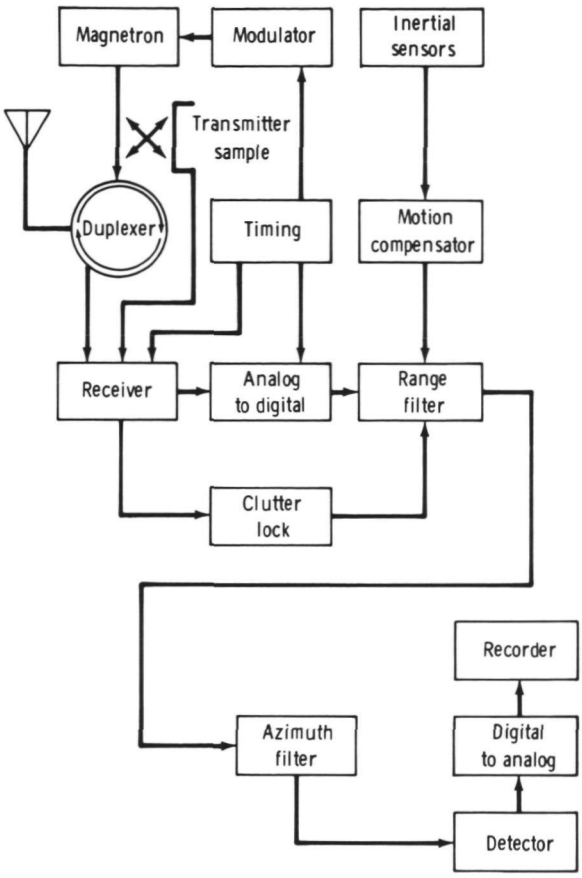

FIGURE 5–21.—Simplified block diagram of coherent-on-receive SLAR.

operating range, and (2) size small enough for convenient installation on a medium-sized aircraft.

A 3-m X-band phased-array antenna will have less than a 1° beamwidth (3 dB) in the azimuth plane. If the elevation pattern has a cosecant-squared shape, the peak antenna gain will be approximately 35 dB.

The optimum polarization depends on the intended remote-sensing application. For example, for oilslick detection, vertical polarization would be best, but horizontal polarization is optimum for geological survey work. An antenna with selectable polarization would solve both problems if the added cost can be justified. Horizontal is probably the best selection if only one linear polarization is to be used.

Receiver/transmitter.—The receiver/transmitter has all the elements of a standard noncoherent radar. The major differences include a local oscillator that has greatly improved frequency stability, and a sample of the transmitted pulse is summed into the receiver. These modifications make it possible to compare the relative phase of the transmitted signal and the received echo on a pulse-to-pulse basis. Typical characteristics of the receiver/transmitter are given in table 5–VII.

The stability requirements for the local oscillator for this system are more stringent than for noncoherent radar. The local oscillator consists of a highly stable crystal oscillator and a multiplier chain to obtain the X-band output. The basic frequency is chosen to obtain the best short-term frequency stability. The oscillator has a short-term stability of 1 part in 10^{10} when averaged over a 1-sec period.

Processor.—A simplified block diagram of a Doppler-beam-sharpened fixed-target processor is shown in figure 5–21. The video data are sampled by the analog-to-digital (A/D) converter and converted to digital numbers or words. Following the A/D conversion, a buffer stores data at the conversion rate of the A/D converter and writes out the data at a slower rate to fill the interpulse period completely.

The range filter removes the spectral offset frequency and divides the signal into in-pulse and quadrature channels, with each channel operating at half the input data rate. This result is achieved by first multiplying the signal by exp $(-j\omega_0 t)$, where ω_0 is the signal offset frequency. This multiplication shifts the spectrum to zero, but it also produces an

TABLE 5–VII.—*Typical Characteristics of the Receiver/Transmitter*

Peak power output, kW	50
PRF, pulse/sec	750
Pulse width, μsec	0.2
Minimum discernible signal, dBm	−95
Receiver bandwidth, MHz	7

undesirable spectrum centered about $2\omega_0$. A low-pass-filter operation eliminates the spectrum centered at $2\omega_0$. The azimuth filter is a nonrecursive convolution-type bandpass filter. The optimum filter bandwidth in terms of resolution and signal-to-noise ratio would be a function of the square root of range. A substantial hardware savings and only a minor loss of performance result from choosing the bandwidth to be independent of range. An aircraft-velocity-dependent bandwidth is not difficult to implement. Such an implementation causes the final display resolution to be independent of aircraft velocity.

Clutter lock.—During normal operating conditions, the antenna will not always be directed normal to the flightpath. High crosswinds will cause the aircraft heading and the flightpath to differ by several degrees. Because of such a drift angle, the azimuth clutter spectrum is no longer centered on zero Doppler (fig. 5–22). Also, the resulting offset frequency f_{offset} is not constant but depends on range. If the clutter spectrum is not centered on zero Doppler, the azimuth filters designed to filter near-zero Doppler may not function correctly. Two basic approaches to the frequency-offset problem are possible. One approach would use aircraft drift angle and altitude and calculate a correction frequency as a function of range. (The drift-angle input from the aircraft would have to be accurate to approximately 0.1°.) The azimuth filters may then be recentered on the main loads of the return spectrum. A second approach would measure the offset frequency from the clutter return and correct accordingly. The latter approach is generally recommended for these radars. Special effort is necessary to insure that very large point targets do not introduce false offset errors as they enter or leave the antenna pattern.

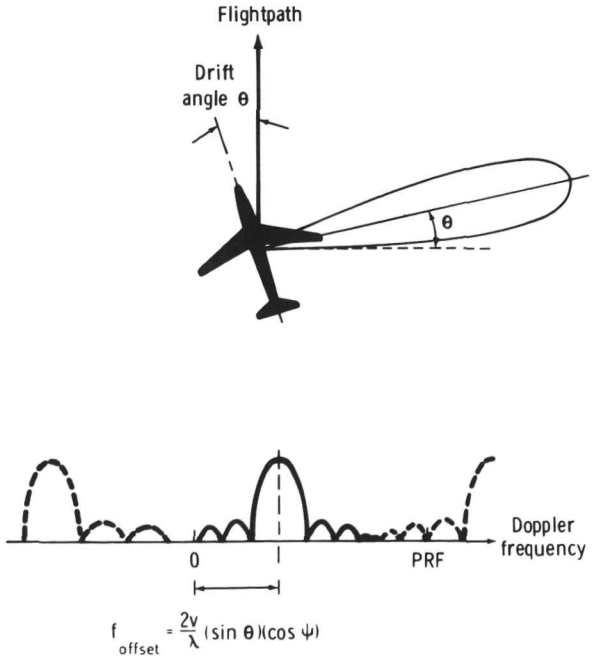

FIGURE 5–22.—Effect of drift angle on antenna direction and azimuth clutter spectrum, where v is aircraft velocity, λ is transmitted wavelength, and ψ is depression angle to target.

Motion compensation.—For coherent or synthetic aperture mapping radar systems, it is preferable that the aircraft fly in a perfectly straight line. The target azimuth phase histories would then be predictable and easily processed for improved resolution. Aircraft usually do not follow perfectly straight-line flightpaths. Deviations from the straight-line flightpath produce errors in the phase history of any target echo. These errors may be corrected by using crosstrack and vertical accelerometers on the antenna. The accelerometer outputs may be high-pass-filtered and integrated to measure crosstrack displacements, which, in turn, may be used to calculate range errors. Range errors are converted to phase errors, and the necessary corrections are generated as a function of range.

Recorder.—Real-time wet chemical film processors are now used on some mapping radars. Recent developments in dry-film processing and fiber optics make it feasible to consider the development of a real-time dry-film-processing camera for mapping radar data. This development would reduce operating costs and minimize storing and handling of corrosive monobath chemicals.

Dry silver film, now available commer-

cially, uses heat processing rather than the wet monobath developing. However, this dry film has a lower sensitivity than wet-processing film, which means that the radar image recorder must provide higher light levels to properly expose the film. New design concepts include the use of a CRT with high-intensity phosphors and fiber-optic faceplates. The dry silver film is exposed by moving it directly over the fiber optics. The fiber-optics technique provides an increase in the percentage of light gathered from the CRT phosphor and applied to the film. Previously used double-lens optical systems, using an $f/1.4$ lens, direct approximately 5 percent of the available light onto the film. A fiber-optics system could increase this technique to near-70-percent efficiency. Dry silver film is developed and fixed by passing it over a heated plate. The radar image could then be available for near-real-time viewing.

Special Applications of SLAR Image Data

A detailed geologic evaluation of 25-cm (L-band) SLAR images obtained over Death Valley, California, was recently completed (ref. 5–1). This study is a good example of the type necessary to properly quantitize and characterize the poorly understood interaction of active microwave signals with a terrain interface having diverse roughness scales. The following is a summary of the work represented in reference 5–1.

Summary of Death Valley Study

The salt flats and large gravel fans that characterize the floor of Death Valley, California, produce sensitive 25-cm radar-backscatter variations (image gray tone) that are correlated with systematic changes in surface-roughness parameters. The large range (0.01 to 2 times the wavelength of 25 cm) in "Lambert" and "Lommel-Seelinger" type surface roughness permitted a detailed investigation of the irregularity scale causing the change from diffuse to specular radar backscatter as theorized by the Rayleigh criterion. The agreement was good, and the transition point was found to be more clearly identified with a specific size range of surface irregularity than it was previously thought to be.

Backscatter variations within Death Valley very well describe the previously mapped geologic units, and it is suggested that long-wavelength radar systems are scientifically optimized for surface roughness investigation when antenna depression angles are restricted between 45° and 90°.

A major conclusion is that an airborne or spacecraft multifrequency radar system should provide image data of significant land use and economic resource potential, especially over the 680 million acres of extremely arid to semiarid lands in the United States.

Experiment Description

During the spring of 1969 and 1970, 25-cm-wavelength side-looking radar images covering a total of 13 300 km^2 were obtained over Death Valley. These flights, including both east- and west-look directions, were intended as system function tests of a prototype planetary imaging radar.

The radar system [1] was operated in a side-looking mode with a unique 0° to 45° look angle off vertical and with a slotted antenna array. Horizontally polarized radiation was transmitted, and horizontally polarized backscatter was recorded on 35-mm film, which was processed by optical correlation techniques. The radar equipment was flown aboard a NASA Convair 990 jet aircraft [2] operated by the Airborne Sciences Office of Ames Research Center in Mountain View, Calif.

The Death Valley area was chosen as the radar system calibration site because of the nearly total lack of leafy vegetation on the Death Valley floor and the extremely low

[1] Synthetic aperture optical recorder: 70-μsec sweep (transmitter 10-MHz sweep in 1.5 μsec); 6-kW peak power; 15-W average power; 18° antenna beamwidth in azimuth looking forward and 9° looking back; 1215-MHz frequency.

[2] The 1970 flight, south run: 7925-m altitude; 254-m/sec speed. The 1970 flight, north run: 3048-m altitude; 200-m/sec speed.

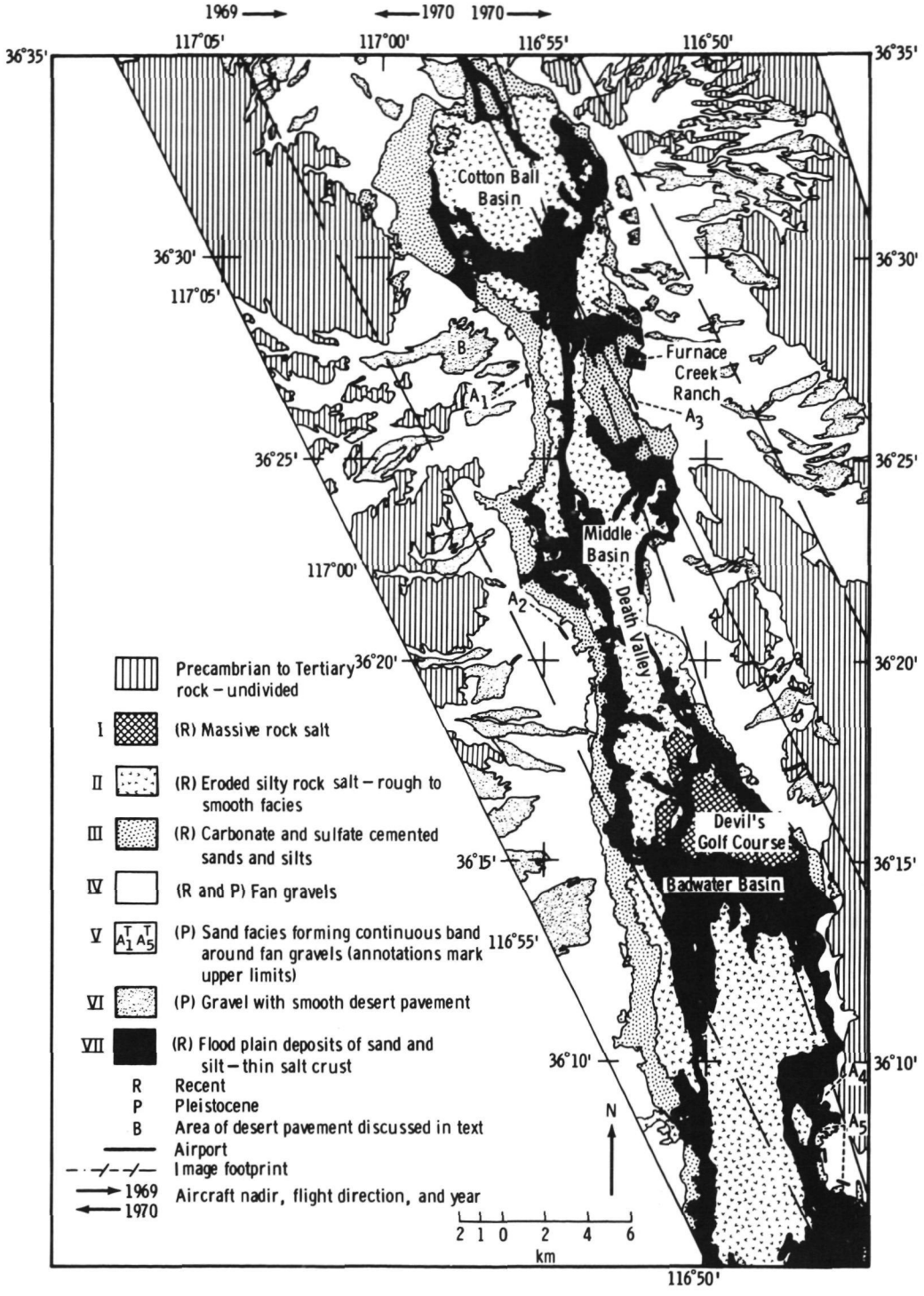

FIGURE 5–23.—Index map of Death Valley showing correlation of geology with 25-cm backscatter units (I, most diffuse; VII, most specular). See figure 5–24.

(4 cm/yr) precipitation rate. Death Valley has also been well described from geological (ref. 5–2), hydrological (ref. 5–3), and botanical (ref. 5–4) viewpoints.

The scale of the original 35-mm radar image film is approximately 1:600 000, although that portion of the crosstrack image nearest the flight line is considerably foreshortened because of inherent characteristics of the image acquisition and processing techniques. Ground resolution in range is approximately 60 to 100 m at the 45° incident angle, whereas azimuth resolution at any angle is approximately 20 m.

Schaber and Brown (ref. 5–5) discussed the geological potential of images obtained near Flagstaff, Ariz., with the same 25-cm-wavelength radar system, and a discussion of the effect of surface textures and complex dielectric constant on (10° to 70° look angle) K-band (0.86-cm wavelength) SLAR images of arid regions has been published by MacDonald and Waite (ref. 5–6).

The Death Valley investigation includes detailed roughness-calibrated radar response from many distinct sedimentary surfaces on the giant gravel fans and salt pans characterizing the extremely arid Death Valley floor.

Characterization of Geological Units on the Radar Images

Figure 5–23 is a generalized geological map of Death Valley (ref. 5–2) illustrating seven major geological surfaces clearly defined by backscatter variations on the 25-cm radar images shown in figure 5–24.

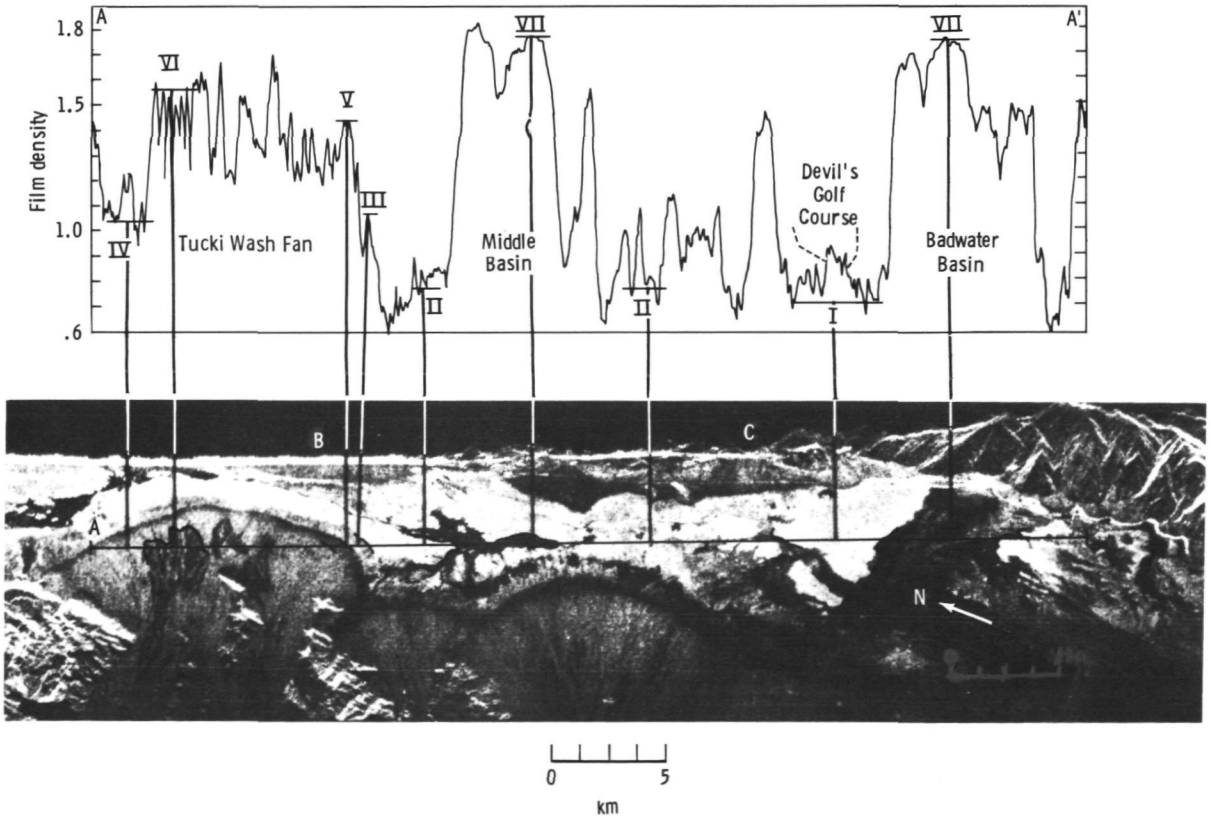

FIGURE 5–24.—West-looking radar image (25 cm) of Death Valley showing correlation of radar backscatter units I to VII with film photometric scan data taken at indicated profile *A* to *A'*. The profile is 32.7 km long.

Unit I is the highest backscattering flat-lying surface on the images and covers the least areal extent within Death Valley (20.7 km^2). This unit is represented by the Devil's Golf Course at Badwater and is composed of Quaternary massive rock salt with an extremely rough surface that elevated and protected against seasonal flooding. Vegetation of any kind is virtually absent (fig. 5–25(*a*), 5–25(*b*), and 5–25(*c*)).

Three additional decreasing rough facies of the Quaternary chloride zone are grouped together in figure 5–23 as unit II (fig. 5–26(*a*) and 5–26(*b*)). All facies listed in unit II are lacking in vegetation.

The third highest backscattering, unit III, delineated on the radar images is composed of two facies of Quaternary carbonate salt-impregnated Pleistocene lake deposits and five facies of miscellaneous Quaternary sulfate and carbonate salts (fig. 5–27(*a*) and 5–27(*b*)). Pickleweed and several species of phreatophytes having brine affinities comprise the sparse vegetation.

FIGURE 5–25.—Photographs of Devil's Golf Course (unit I) shown in geological map (fig. 5–23) and radar image (fig. 5–24). (*a*) Landscape photograph of massive rock salt of the Devil's Golf Course (unit I) that gave a highly diffuse (nearly isotropic) backscatter over incident angles ranging from 12° to 40°. Gnomon has wand length 31 cm above tripod base, gray-tone chart on gnomon leg is divided into 2.5-cm increments; black rule has small divisions of 1 cm and large divisions of 5 cm.

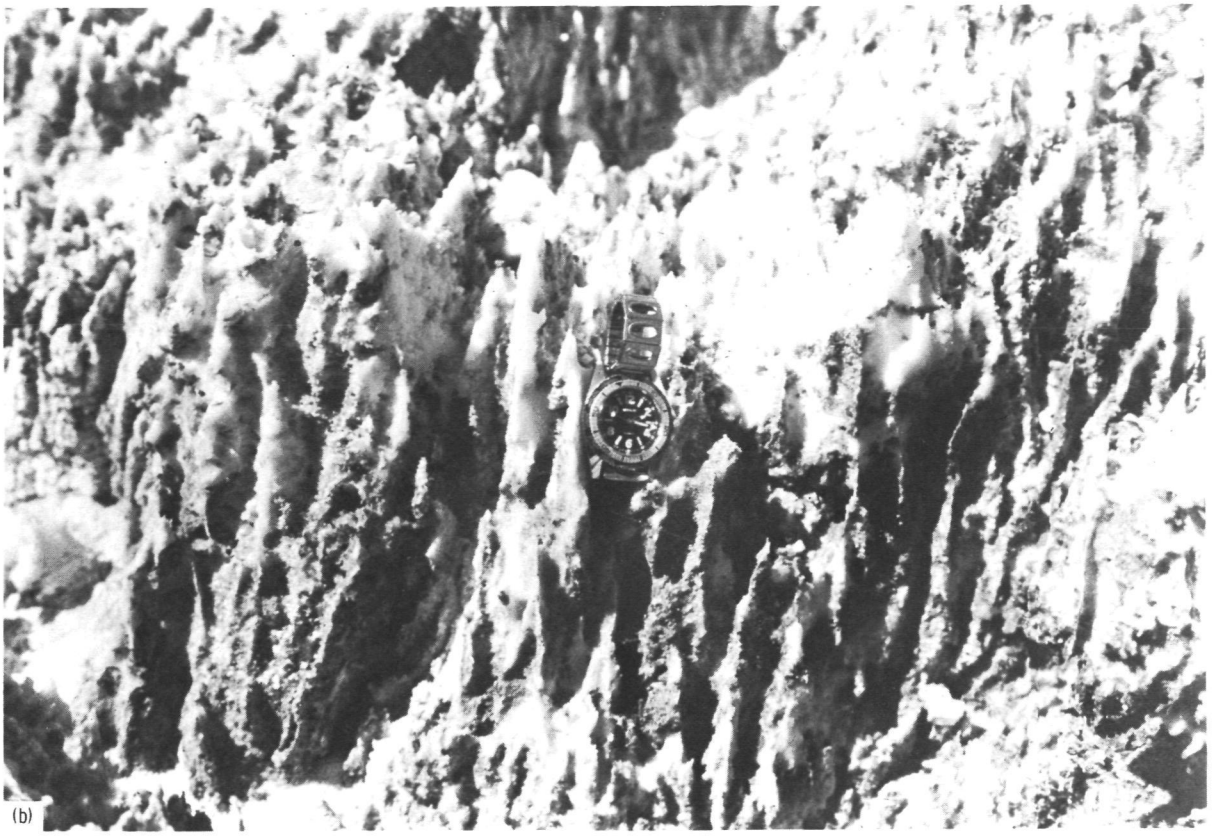

(b)

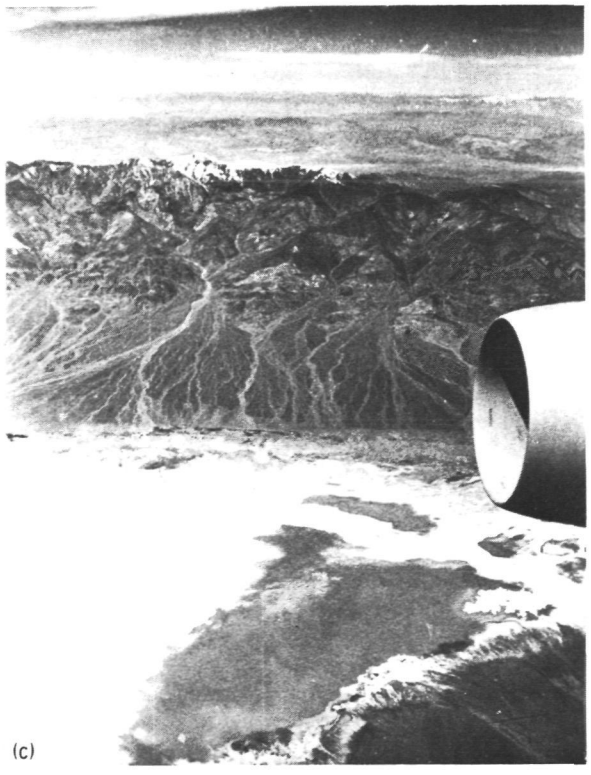

(c)

FIGURE 5–25 (concluded).—Photographs of Devil's Golf Course (unit I) shown in geological map (fig. 5–23) and radar image (fig. 5–24). (*b*) Closeup view of extreme 2- to 3-cm ($\lambda/10$) roughness. (*c*) Aerial view of Devil's Golf Course (dark heart-shaped unit) taken during radar overflight. Notice the reversal photographic and radar albedos for Devil's Golf Course (unit I) and flood plain (unit VII) (fig. 5–24).

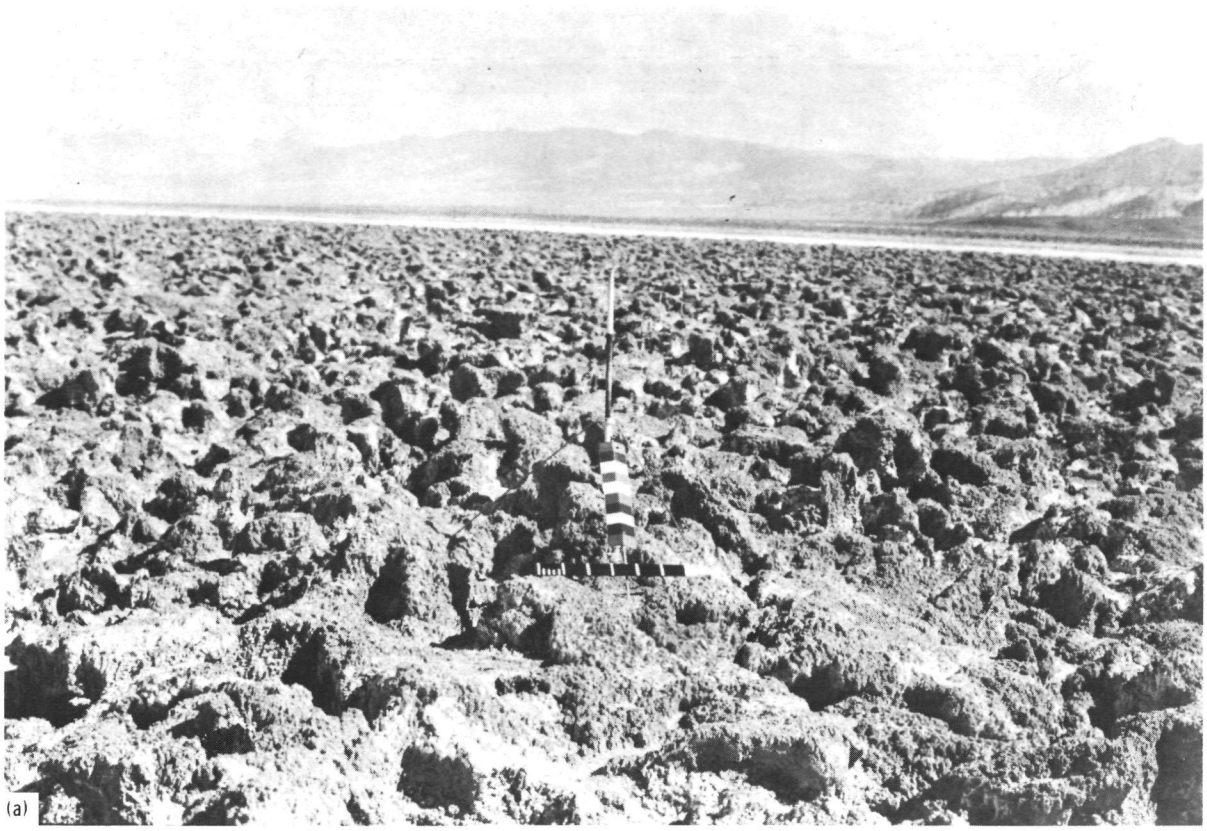

FIGURE 5–26.—Photographs of silty rock salt with rough facies (20 to 40 percent silt) that gave highest backscatter within unit II (fig. 5–24). Gnomon has wand length 31 cm above tripod base; gray-tone chart on gnomon leg is divided into 2.5-cm increments; black rule has small divisions of 1 cm and large divisions of 5 cm. (*a*) Landscape photograph.

Unit IV is limited to only the younger of the Upper Pleistocene and Recent gravels of the giant gravel fans. The Pleistocene materials are loose pebble-to-cobble-size varnished gravel with significant concentrations of boulders (fig. 5–28). Although not varnished, the Recent fan gravels are similar and exist in washes as much as 3 m below the level of the older Pleistocene materials.

Unit V represents the only distinct radar signature on the images that could not be related to a specifically mapped geological material. This unit is imaged as a narrow (100 to 200 m wide) dark band that is consistently found at the very base of the gravel fans in contact with the high backscattering unit III of the Death Valley salt pan (fig. 5–24). Another characteristic of the dark band on the images is that it is generally darkest (greater film density and weakest backscatter) at the very base of the gravel fans and becomes more diffuse (reduced film density and increased backscatter) within a few hundred meters toward the head of the fan. Field investigation revealed that the dark band was resulting from weak signal return from a boulder-free sandy zone distinguished by a lag of small rock fragments (fig. 5–29) that becomes systematically larger upslope on the fan. The relationship of gravel size to backscatter power within unit V will be discussed later in this section.

The relatively low backscattering (unit VI) was unexpectedly found to be well cor-

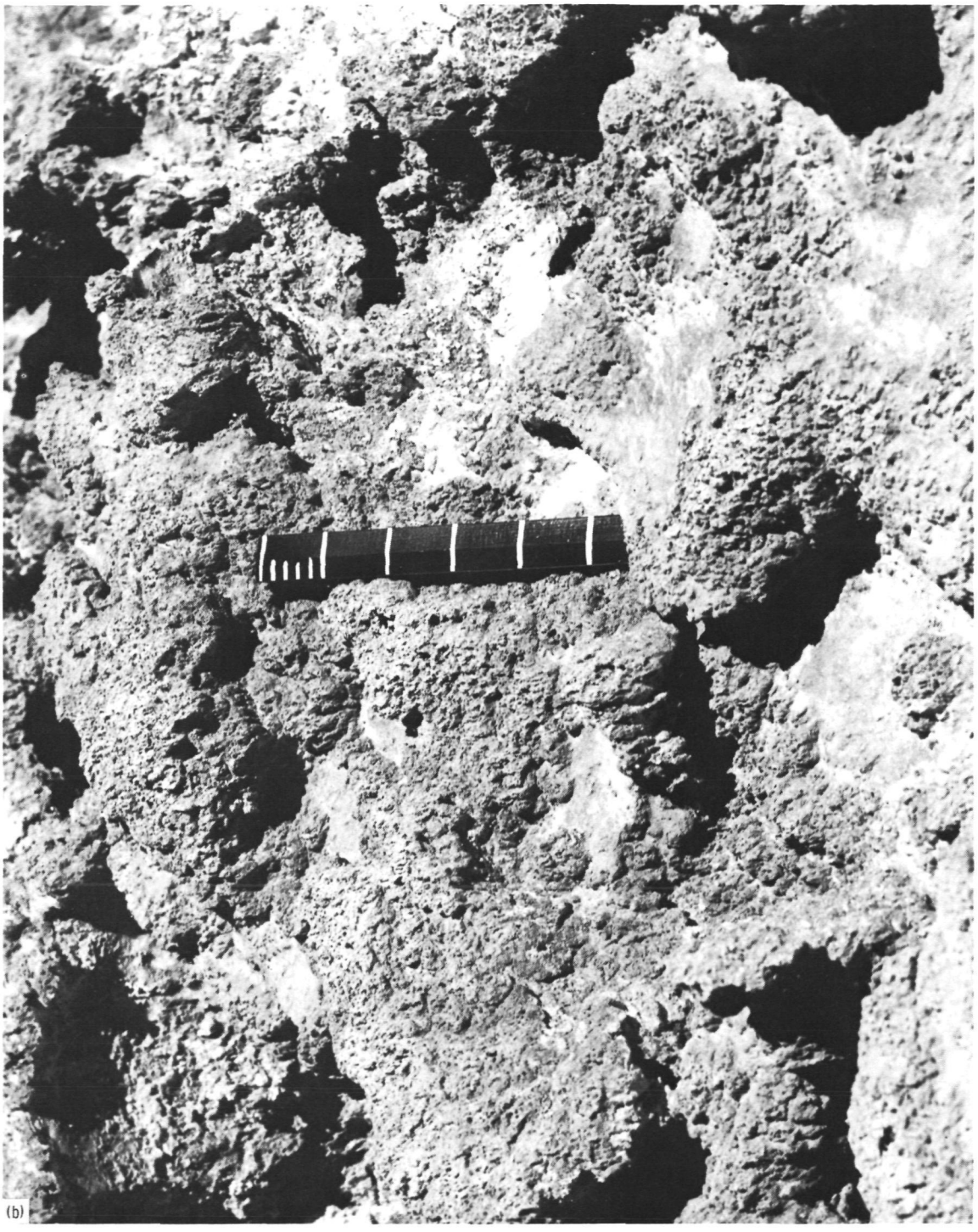

FIGURE 5–26 (concluded).—Photographs of silty rock salt with rough facies (20 to 40 percent silt) that gave highest backscatter within unit II (fig. 5–24). Gnomon has wand length 31 cm above tripod base; gray-tone chart on gnomon leg is divided into 2.5-cm increments; black rule has small divisions of 1 cm and large divisions of 5 cm. (*b*) Closeup view; small-scale roughness at 1 to 2 cm equal dimensional hummocks of silt.

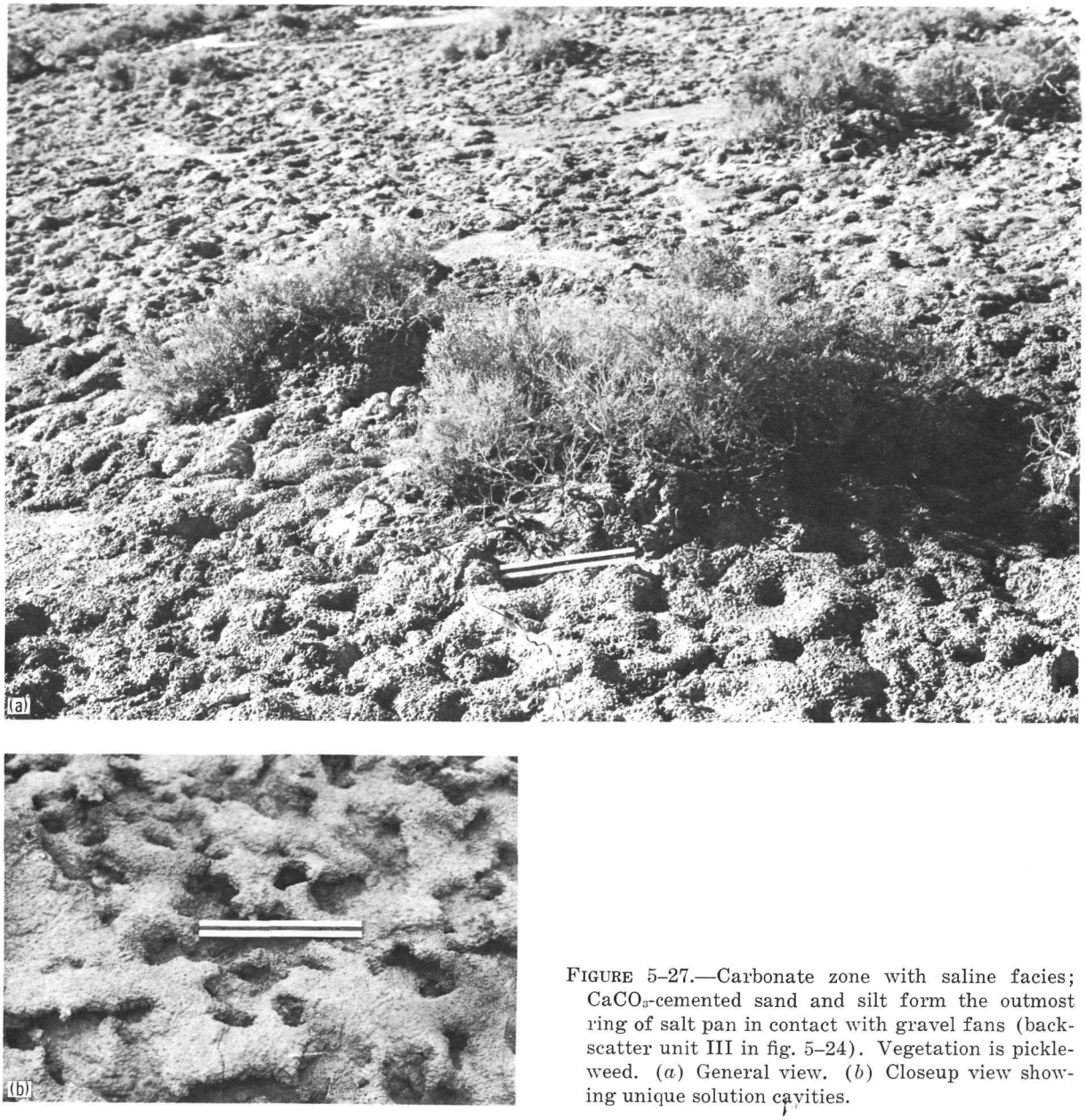

FIGURE 5–27.—Carbonate zone with saline facies; $CaCO_3$-cemented sand and silt form the outmost ring of salt pan in contact with gravel fans (backscatter unit III in fig. 5–24). Vegetation is pickleweed. (*a*) General view. (*b*) Closeup view showing unique solution cavities.

related with the oldest of the Upper Pleistocene fan gravels (figs. 5–23 and 5–24). The reason for such anomalous radar behavior lies in the fact that the unit VI surface is smooth "desert pavement," whereas the younger gravels have rough surfaces. The boulders and cobbles forming the original surface of these deposits have disintegrated to produce smaller, angular rock fragments. The "fitting together" of these weathering products forms the smoothest desert pavements in Death Valley (fig. 5–30). The desert-pavement surfaces are elevated above the present Recent washes near the head of the fans. Excellent representation of the desert pavement (unit VI) on radar images as compared to conventional photography is shown in figures 5–31 and 5–32(*a*), 5–32(*b*),

FIGURE 5–28.—Younger of the upper Pleistocene boulder gravels forming giant alluvial fans (radar unit IV). Notebook (21 cm long) is shown in foreground.

and 5–32(*c*). Vegetation is lacking except for xerophytes along the washes.

The lowest backscattering material in Death Valley is referred to as unit VII and is represented by the Recent flood-plain deposits that seasonally flood the lower parts of the Death Valley salt pan (figs. 5–23, 5–24, and 5–33). The floodplains are mostly flat and level expanses of occasionally damp or brine-soaked sandy silt and clay; part is encrusted with salt. The salt crust on the floodplain ranges from a thin delicate efflorescence to a firm crust several centimeters thick (ref. 5–2).

Surface Roughness Data and Correlation With Radar Backscatter

Theories pertaining to scattering of microwave signals from terrain have been the subject of much discussion for many years (refs. 5–6 to 5–10). The only two terrain parameters affecting the radar-scattering coefficient are surface roughness and the complex permittivity. Almost all workers agree that surface roughness is the dominant causative factor in amplitude variation of the returned signal (effecting image gray tone). Radiated energy is reflected in a specular (mirror-like) manner, according to Snell's Law, from a "smooth" surface and is reflected in a diffuse (energy scattered in all directions) manner from a "rough" surface. The question usually encountered in interpretation of SLAR images concerns the scale of roughness necessary to change from specular (*smooth*) to diffuse (*rough*) scattering. One of the major objectives of the Death Valley radar study was to approach this question from an empirical rather than a theoretical viewpoint.

FIGURE 5–29.—Closeup view of small-scale surface lag and underlying loose sand characteristic of the base of radar unit V. This surface was dominated by specular reflectivity.

The most quoted theoretical relationship with regard to radar "smoothness" is the so-called Rayleigh criterion that considers a surface "smooth" for

$$h < \frac{\lambda}{8 \sin \gamma} \qquad (5\text{–}12)$$

where h is height of surface irregularities, λ is wavelength of radar system, and γ is grazing angle of the incident radar wave.

In deriving this criterion, Rayleigh considered rays 1 and 2 (fig. 5–34) incident on a surface with irregularities of height h at a grazing angle γ. The path difference between the two rays is expressed as

$$\Delta r = 2h \sin \gamma \qquad (5\text{–}13)$$

and the phase difference is expressed as

$$\Delta\phi = \frac{2\pi}{\lambda} \Delta r = \frac{4\pi h \sin \gamma}{\lambda} \qquad (5\text{–}14)$$

Rayleigh thus argued that for $\Delta\phi = \pi$, the surface is "rough," whereas, for $\Delta\phi = 0$, it reflects specularly and is "smooth." In obtaining the Rayleigh criterion, an arbitrary choice halfway between the two examples (i.e., $\Delta\phi = \pi/2$) is made to represent the transition from diffuse to specular backscatter.

Peake and Oliver (ref. 5–7) used a truck-mounted radar-radiometer system to compare radar backscatter variation with change in a normalized roughness parameter ξ for three frequencies (X-, Ku-, and Ka-bands), where

$$\xi = \frac{d \cos \theta_i}{\lambda} \qquad (5\text{–}15)$$

and where d is particle diameter, θ_i is angle

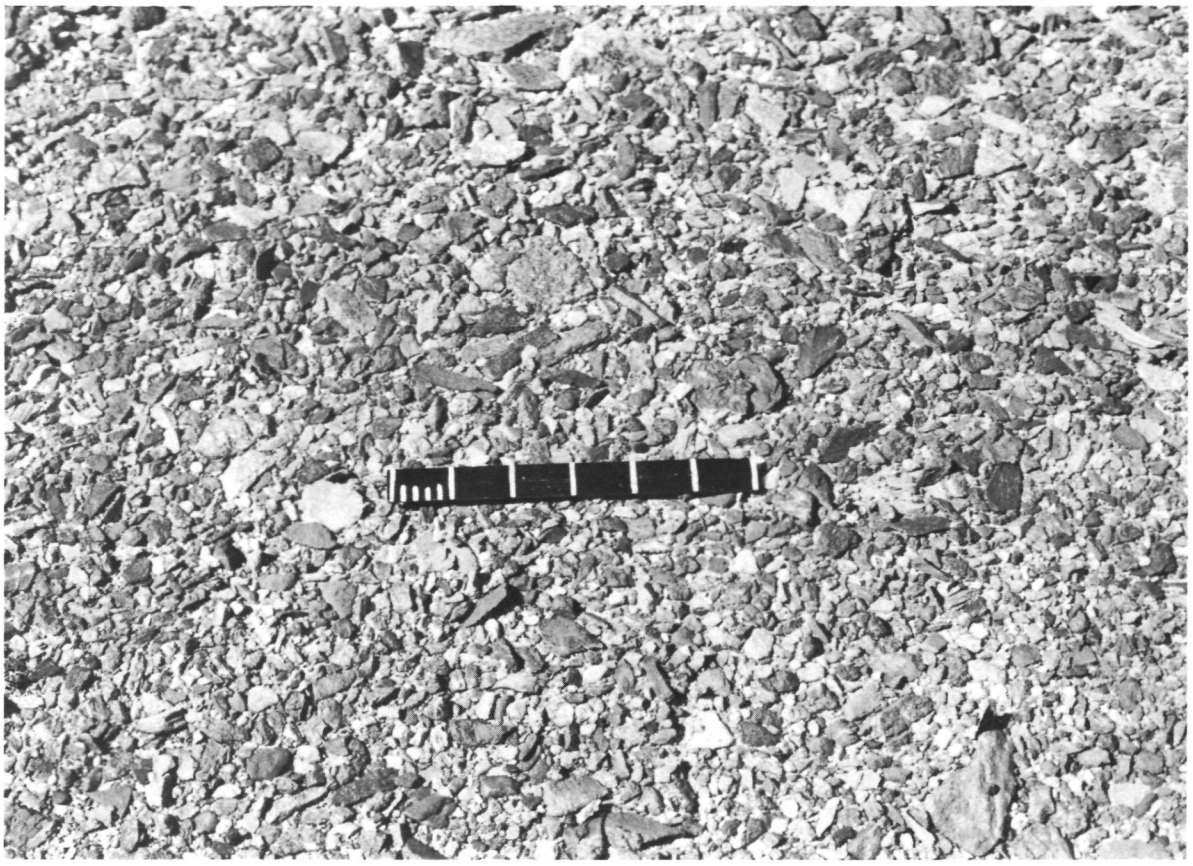

FIGURE 5–30.—Desert pavement ("varnished") formed on surface of oldest of upper Pleistocene fan gravels (radar unit VI). Surface of pavement rocks extremely polished.

of incidence, and λ is wavelength. These researchers found that the transition between specular and diffuse scattering occurs at approximately $\xi = 0.3$. This value appears to be slightly large for the 25-cm SLAR data of Death Valley.

Absolute calibration of the radar return power was not obtained during the Death Valley overflights. Therefore, relative exposure energies were obtained from the film (type 3414) $D \log_e$ sensitometry curve (fig. 5–35).

To quantitatively evaluate the relationship between relative return power and surface-roughness parameters, a total of 11 photometric scans were made across various regions of the radar images. Figure 5–24 illustrates the clear variations in film density observed for the seven major radar-backscatter units described previously. Table 5–VIII lists the physical roughness parameters for these seven radar terrain units and the relative power (dB) values representative of each. In figure 5–36, these data are plotted with relative radar power as a function of the sum of parameters A, B, and C (at $\lambda/10$ scale) for each of the seven radar terrain units. Average vertical roughness ranges from approximately 0.01 to 2 λ.

The significant aspects of figure 5–36 are the two distinct curve slopes with the inflection occurring at a vertical roughness representative of approximately 3 to 5 cm. It appears from this correlation that the change-over from primarily diffuse (rough) to pri-

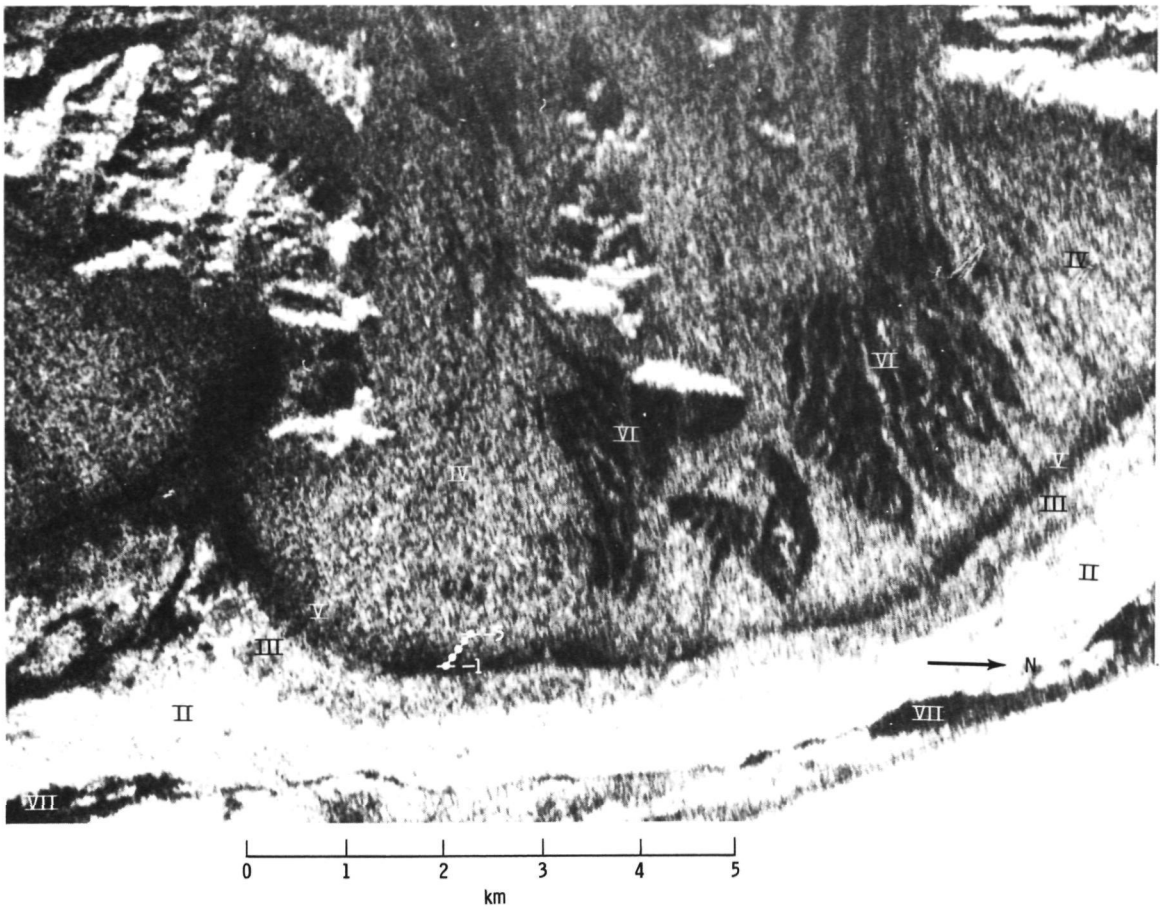

FIGURE 5–31.—Enlargement of west-looking 25-cm radar image of Tucki Wash gravel fan. Roman numerals represent radar backscatter units. Dots indicate sample locations 1 to 5.

TABLE 5–VIII.—*Roughness Parameters and Relative Backscatter Power*

Backscatter unit	Parameter A: macrovertical relief, cm [a]	Parameter B: average distance between macrorelief facets, cm [a]	Parameter C: percent area covered by microroughness [a b]	Roughness parameter α [c]	Film density	Relative power, dB
I	49.0	60.0	100.0	209.0	0.700	0.0
II	29.0	44.0	97.0	170.0	.749	—.4
III	6.0	15.0	20.0	42.0	1.163	—2.4
IV	12.0	10.0	40.0	62.0	1.266	—3.0
V	1.5	6.0	15.0	22.5	1.580	—4.4
VI	1.0	2.0	8.0	11.0	1.600	—4.5
VII	.2	2.0	.0	2.2	1.756	—5.3

[a] Roughness parameters A, B, and C represent averages of many field measurements.
[b] at $\lambda/10$ scale.
[c] Parameter α equals the sum of parameters A, B, and C.

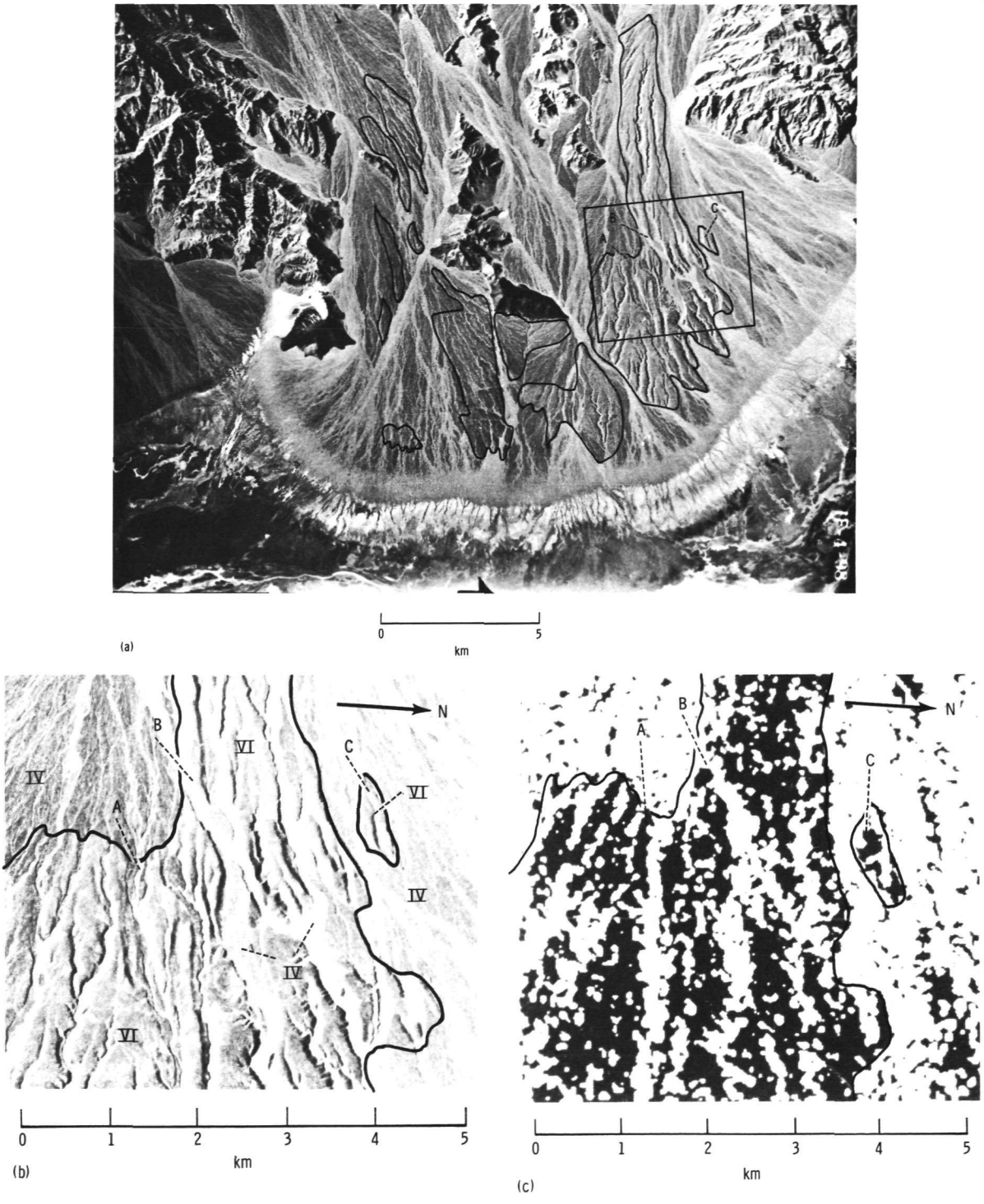

FIGURE 5–32.—Photographs of Tucki Wash gravel fan together with computer representation of digitized radar image for designated area. (*a*) Aerial photograph of Tucki Wash gravel fan with desert pavement regions delineated. Area in rectangle is for reference to figures 5–32(*b*) and 5–32(*c*). Points *A*, *B*, and *C* designate recent washes. (*b*) Enlargement of area indicated in figure 5–32(*a*). Recent washes are indicated at points *A* and *B* and outer part of desert pavement at point *C*. (*c*) Computer representation of digitized radar image of same area shown in figure 5–32(*b*) (processed to enhance pavement region). Note points *A*, *B*, and *C*. Computer enhancement performed at Jet Propulsion Laboratory Image Processing Laboratory.

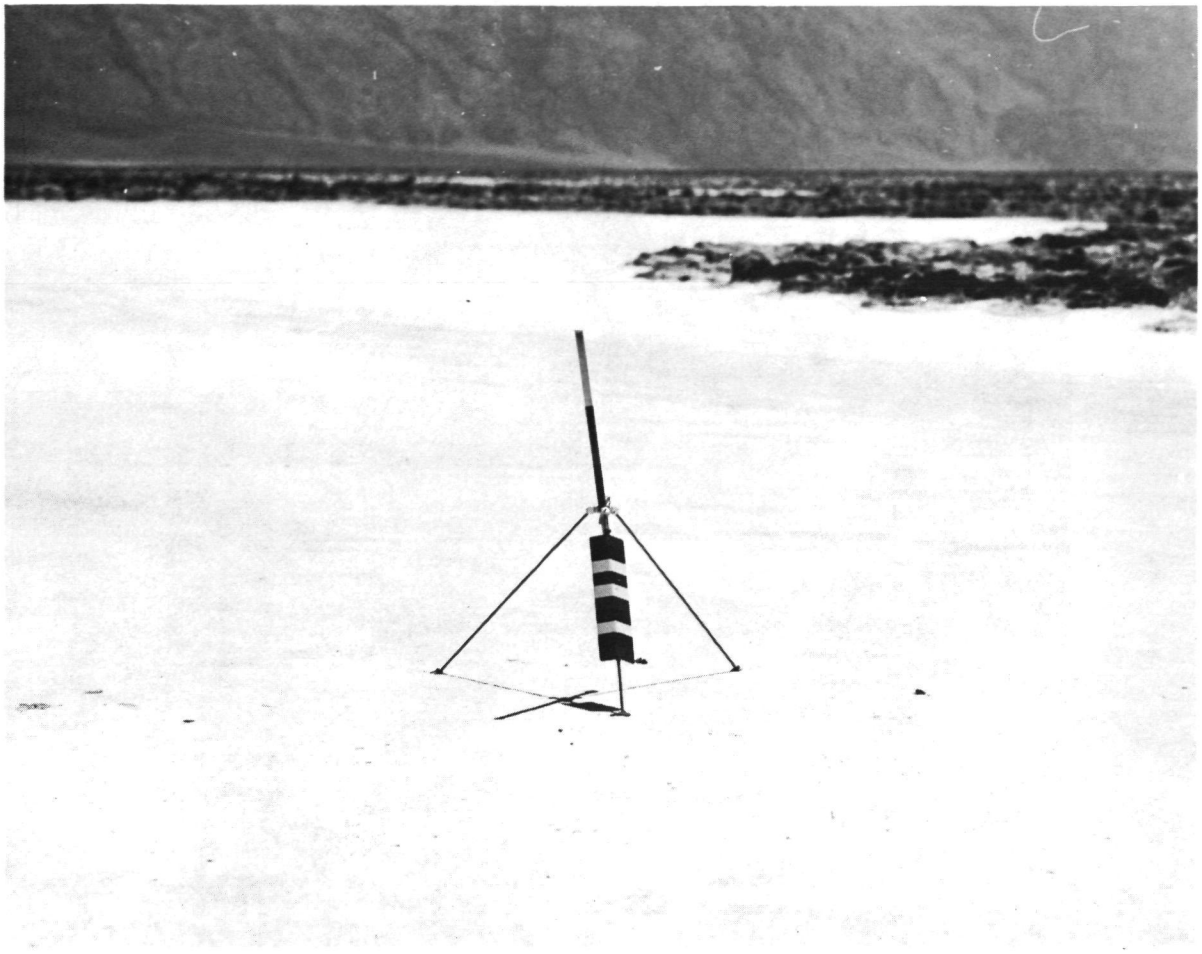

FIGURE 5–33.—Recent flood-plain surface (radar unit VII) giving essentially no radar return. Surface is coated with less than 1 cm of sodium chloride. Surface in background is eroded rock salt that is 15 cm higher than flood plain.

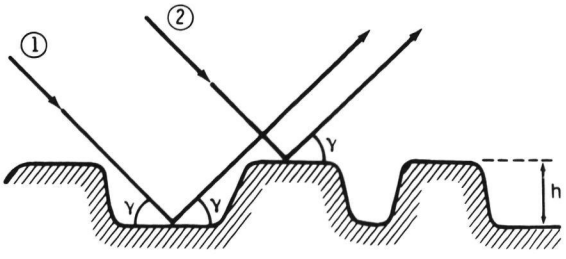

FIGURE 5–34.—Derivation of the Rayleigh criterion (after Beckmann and Spizzichino (ref. 5–10)). Numbers 1 and 2 represent incident rays.

marily specular (smooth) scattering may occur rather abruptly.

Two distinct types of surface roughnesses within Death Valley have made this region ideal for a detailed investigation of radar-scattering processes. The first is the chemical or solution roughness of the salt facies characterizing the salt pan of Death Valley floor (units I, II, and III) (figs. 5–25, 5–26, and 5–27). These surfaces have extremely rough reentrant cavities, with the concordant high points forming a flat and level plain on the scale of several meters. These salt-pan surfaces appear to be perfect examples of a "Lambert" roughness.

The second form of roughness encountered within Death Valley is that characteristic of

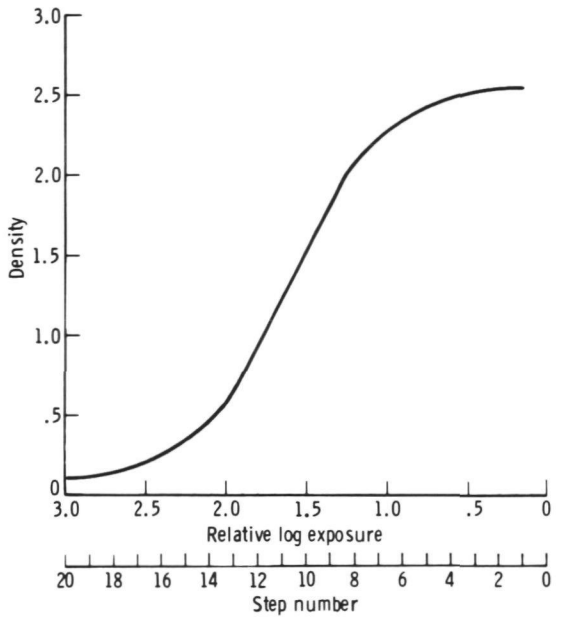

FIGURE 5–35.—Sensitometry curve D log$_e$ for the film type and processing used for Death Valley radar images. (Film type: Kodak High Definition Aerial 3414.) Steps equal 1.5-dB increments; 1.0 to 2.0 relative log exposure equals 10 dB.

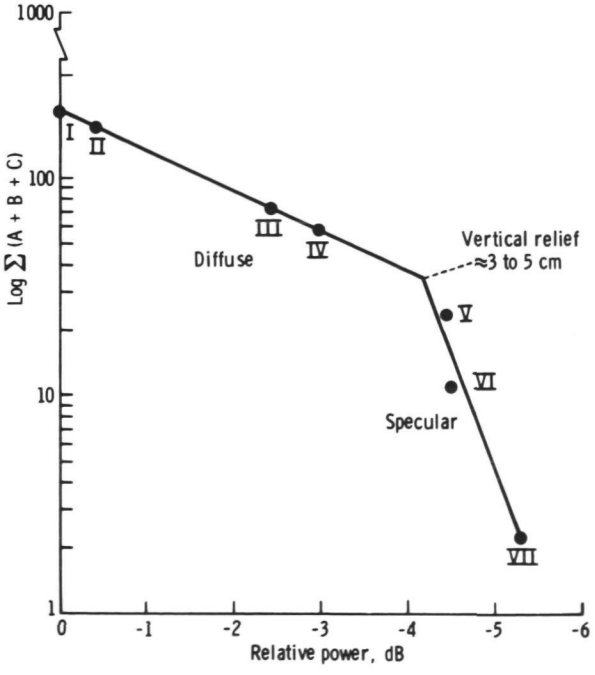

FIGURE 5–36.—Relative power as a function of surface roughness parameters log $\Sigma(A+B+C)$ for each of the seven radar terrain units.

the giant gravel fans. The gently sloping (2.5°) fans have a generally flat sand and gravel surface on top of which is resting many point scatterers in the form of perched or partly buried cobbles and boulders (fig. 5–28). This type of roughness with many independent point scatterers is called the "Lommel-Seelinger" type (ref. 5–7).

The gravel fans provided a suitable surface on which to quantitatively assess the relationship between frequency distribution of scatterers (rocks) and relative radar power. The gravels were found to be graded by size in a band several hundred meters wide at the base of the fans. The lower portion of this band has earlier been described as the weak radar-backscattering radar unit V (figs. 5–23, 5–24, and 5–31).

Five surface gravel samples (TWF–1 to TWF–5) were collected from 1-m^2 areas, starting at the very base of unit V on the Tucki Wash Fan and extending through this unit up the fan into the larger boulder unit IV for a total distance of 400 m (fig. 5–31). Samples were collected at 100-m intervals together with surface relief data. Figure 5–37 illustrates the presampling distribution of the gravels within each 1-m^2 sample station. Figure 5–38 shows the cumulative percent of total rocks as a function of mean rock diameters. The rock diameters increase consistently from sample TWF–1 to TWF–5.

The sample site locations annotated on the radar image of the Tucki Wash Fan (fig. 5–31) suggest that the area between samples TWF–2 and TWF–3 is the approximate visual contact between the dark band (unit V) and the lighter, coarser gravel deposits (unit IV). This contact should then represent the transition zone between specular and diffuse scattering. A photometric scan was made along the sampling line, and these data were converted to relative power by means of the film sensitometry curve (fig. 5–35). These data were correlated with both surface relief and rock-size percentages for the sample areas on the Tucki Wash Fan as shown in figures 5–39 and 5–40. Both diagrams indicate that the break in slope characterizing

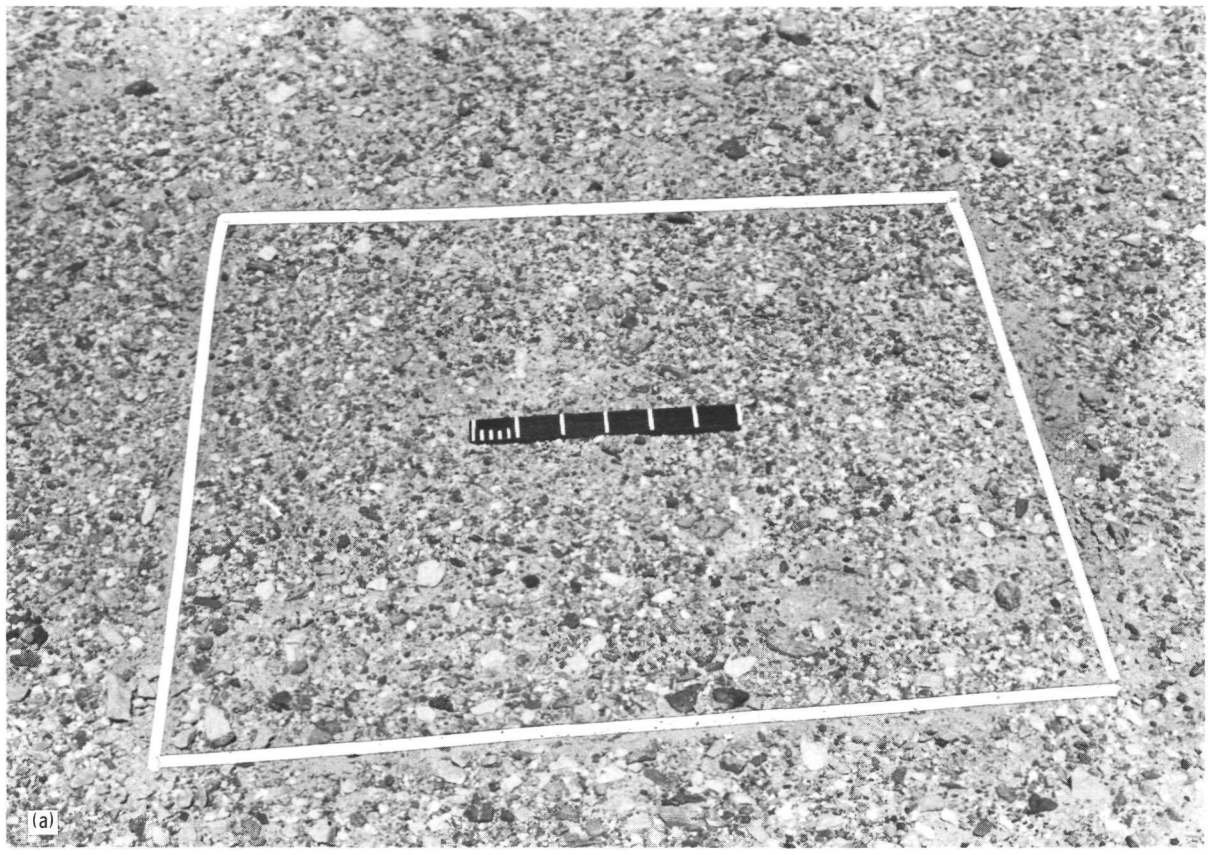

FIGURE 5–37.—Presampling photographs of five 1-m² sample sites (TWF–1 to TWF–5) at the base of Tucki Wash Fan (see fig. 5–31). Samples included all surface lag in 1-m² areas shown by white lines. (*a*) Sample site 1.

the specular-diffuse transition occurs as visually observed in the region between samples TWF–2 and TWF–3 at approximately the −1.0-dB (relative) power level.

The breaks in slope on figure 5–39 further indicate that 4.1 cm and 6.7 cm should be the minimum and maximum height to characterize the minimum and maximum surface roughness for the initiation of primarily diffuse scattering at 25 cm and at this particular radar grazing angle of 55.62°. The average relief value (4.1 cm) is the same as that shown by the curve inflection in figure 5–36 and is thought to be more significant regarding the radar behavior than the maximum relief data.

To compare this "smooth"/"rough" surface boundary with that of Rayleigh for the dividing line between "smooth" and "rough" surfaces, the value for the radar grazing angle (55.62°) and the wavelength (25 cm) need only be substituted as

$$h < \frac{25 \text{ cm}}{8 \sin 55.62} \qquad (5\text{–}16)$$

$$h < 3.8 \text{ cm} \qquad (5\text{–}17)$$

The value calculated from field measurements of average vertical relief (fig. 5–39) and the theoretical value agree well.

Figures 5–38 and 5–40 show that the cumulative percent of rocks characterizing the transition-zone gravels on Tucki Wash Fan should be as follows: 0.1 percent, $\lambda/2$ (12.5 cm) ; 5.5 percent, $\lambda/4$ (6.24 cm) ; 27 percent, $\lambda/8$ (3.125 cm) ; and 70 percent, $\lambda/16$ (1.562 cm). The mean (50 percent) gravel size

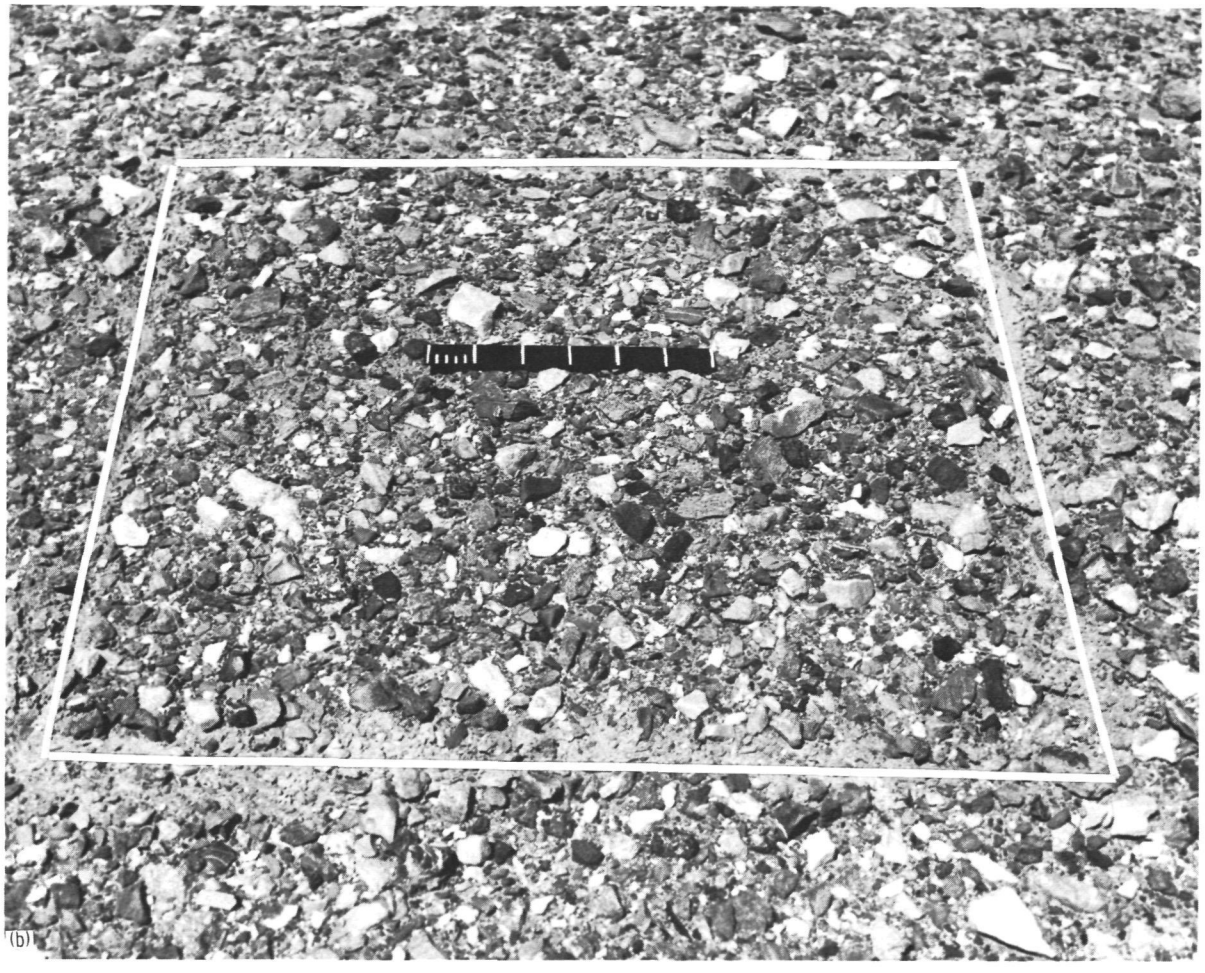

FIGURE 5–37 (continued).—Presampling photographs of five 1-m² sample sites (TWF–1 to TWF–5) at the base of Tucki Wash Fan (see fig. 5–31). Samples included all surface lag in 1-m² areas shown by white lines. (*b*) Sample site 2.

would be $\lambda/13$, or 1.92 cm. The gravel composing the average surface relief ($\approx$4 cm) of the transition zone is equivalent to the larger 25 percent of the bulk gravel sizes.

Peake and Oliver (ref. 5–7) give a normalized roughness parameter of $\xi=0.3$ (eq. (5–15)) for the transition point between specular and diffuse backscatter at the X, Ku, and Ka radar frequencies. The ξ value (fig. 5–39) associated with the average relief transition point is 0.13, or approximately 2.3 times less than that measured by Peake and Oliver. A value of $\xi=0.3$ would give an average surface relief of 9.1 cm by using the normalized roughness relationship of equation (5–15) (for an incident angle of 34.38° and a wavelength of 25 cm). A surface with this relief in the Death Valley study area is primarily a diffuse scatterer on the 25-cm image data.

Complex Dielectric Constants and Radar Penetration

The rather elevated dielectric constants ϵ of sodium and calcium salts found in the Death Valley salt pan are shown in table 5–IX. Unit III, composed of calcite ($CaCO_3$) cemented sands and silts, has a surface roughness distinctly less imposing than that

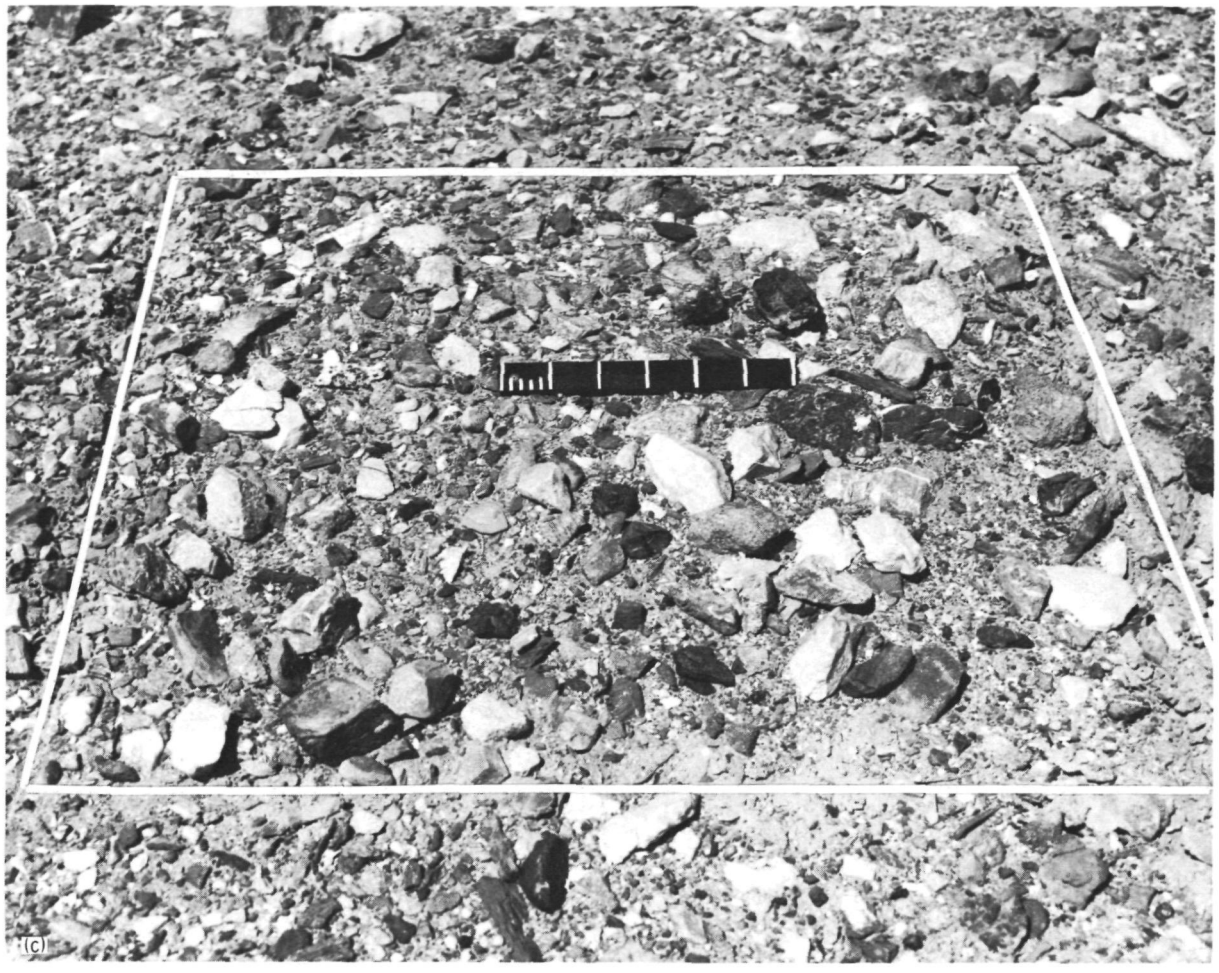

FIGURE 5–37 (continued).—Presampling photographs of five 1-m² sample sites (TWF–1 to TWF–5) at the base of Tucki Wash Fan (see fig. 5–31). Samples included all surface lag in 1-m² areas shown by white lines. (*c*) Sample site 3.

of the bouldery fan gravels of unit IV (figs. 5–27 and 5–28) ; however, the backscattering ability in the 25-cm images places the surface roughness slightly above that of the boulder gravel deposits (unit IV) (table 5–VIII). Although these studies have shown clearly that the surface roughness is the dominant cause of the diverse backscatter within Death Valley, there is some evidence to suspect that the elevated ϵ of $CaCO_3$ and the presence within this material of abundant solution cavities (which cause resonance effects) may be contributing to the abnormally high diffuse return (fig. 5–27(*b*)). The 25-cm radar may be penetrating a minimum of 0.5 to 1.0 λ (12.5 to 25 cm) into the surface of unit III.

Surface profile data.—The 25-cm radar images also contain high-resolution surface profiles as a result of the 0° to 45° off-nadir angle (fig. 5–24). The vertical range accuracy over flat regions is between 1 and 2 m, but it is somewhat degraded (10 to 20 m) over mountainous terrain because of complexities in the timing reference of signals returning from areas of high vertical relief.

The profiles from smooth, flat surfaces are characterized by "spiking" or fluctuations in the spectral power caused by multiple side lobes (fig. 5–24, point *B*) ; this spiking is not

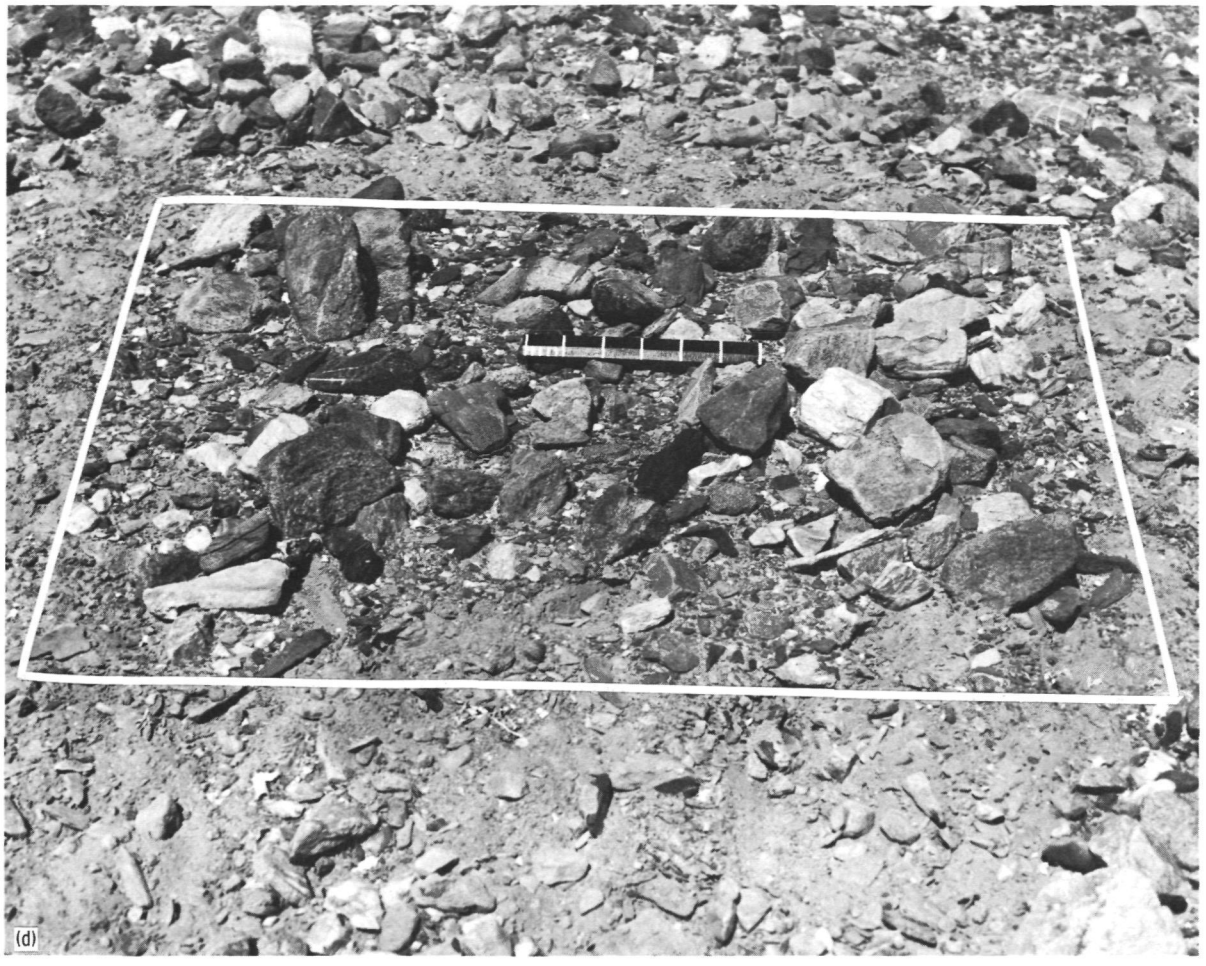

FIGURE 5–37 (continued).—Presampling photographs of five 1-m² sample sites (TWF–1 to TWF–5) at the base of Tucki Wash Fan (see fig. 5–31). Samples included all surface lag in 1-m² areas shown by white lines. (*d*) Sample site 4.

observed over the rougher mountainous terrains (fig. 5–24, point *A*). The scientific value of such profiles would be extremely high over regions of little or no photogrammetric control.

TABLE 5–IX.—*Materials Present in Death Valley Salt Pan*

Material	Composition	ϵ(1.0 MHz)
Calcite	$CaCO_3$	7.5
Halite	NaCl	5.9
Gypsum	$CaSO_4 \cdot 2H_2O$	5 to 11.5
Dry, sandy soil		2.5

Concluding Remarks

The Death Valley region is an excellent area for radar feasibility studies involving detailed geologic analysis of SLAR images. The region is characterized by a variety of materials with diverse dielectric properties and a large range in surface roughness. In addition, the extreme aridity in Death Valley minimizes the effects of vegetation and high soil moisture.

The major conclusions of the present investigation can be summarized as follows:

1. Many types of recent sedimentary surfaces and active sedimentation processes can

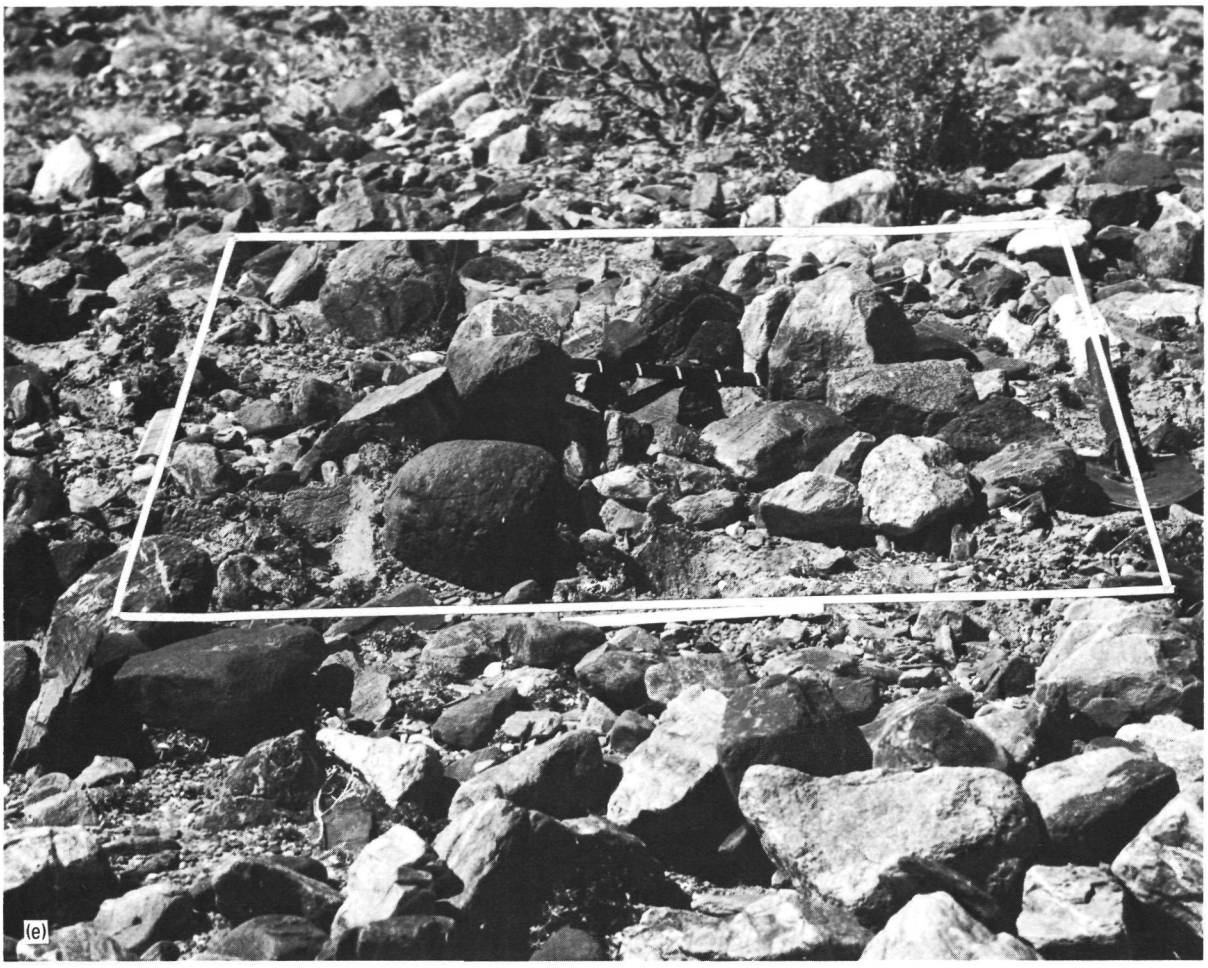

FIGURE 5–37 (concluded).—Presampling photographs of five 1-m² sample sites (TWF–1 to TWF–5) at the base of Tucki Wash Fan (see fig. 5–31). Samples included all surface lag in 1-m² areas shown by white lines. (*e*) Sample site 5.

be recognized by their surface roughness using only single-frequency SLAR image data. When SLAR is used in conjunction with more conventional sensors, the recognition potential becomes very good.

2. The height of surface irregularities responsible for the transition from specular to diffuse 25-cm radar scattering is restricted to a relatively smaller size range ($\lambda/5$ to $\lambda/8$) than previously thought and is well defined by the assumptions given in the Rayleigh criterion.

3. Antenna depression angles restricted between 45° and 90° appear to optimize the image data for surface backscatter information and appear to eliminate extensive radar shadowing effects that distract from geologic material characterization on more conventional SLAR data formats (10° to 70° off-nadir angles).

Future Applications

The radar images evaluated in this section are unique because they were obtained with a prototype of a planetary orbiting radar specifically designed to return high-resolution surface images from the cloud-covered planet Venus, possible in the early 1980's. The investigation of images from the 25-cm system

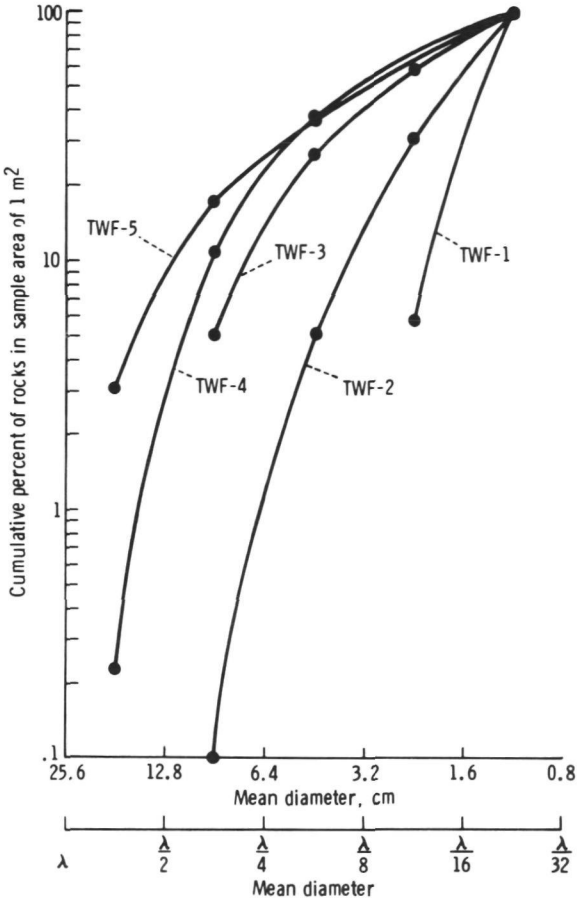

FIGURE 5–38.—Mean diameter of rocks from sample sites TWF–1 to TWF–5 with diameters given in centimeters and λ-ratios. Rocks measured totaled 3314.

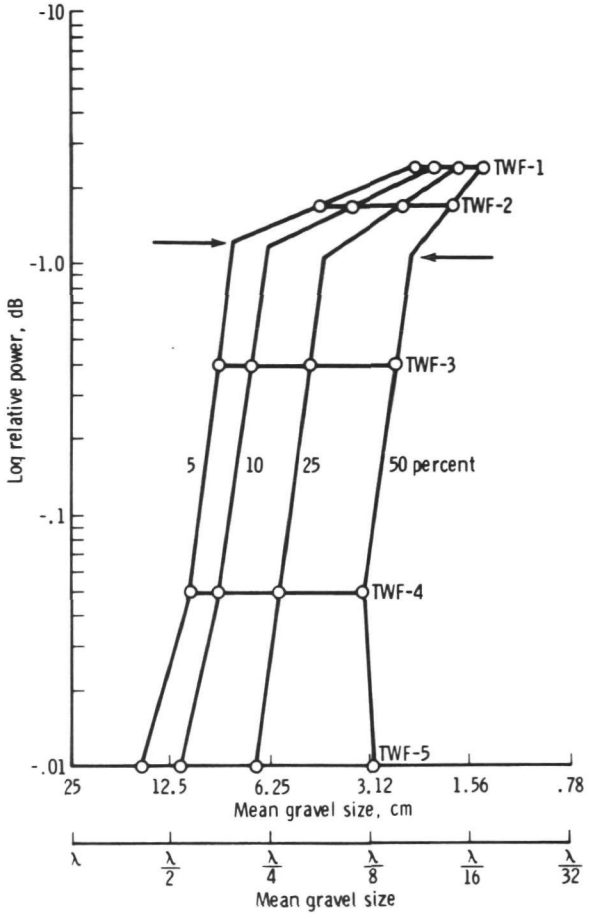

FIGURE 5–40.—Log relative power as a function of mean gravel size for TWF–1 to TWF–5 samples. Size distributions for 5, 10, 25, and 50 cumulative percent are shown.

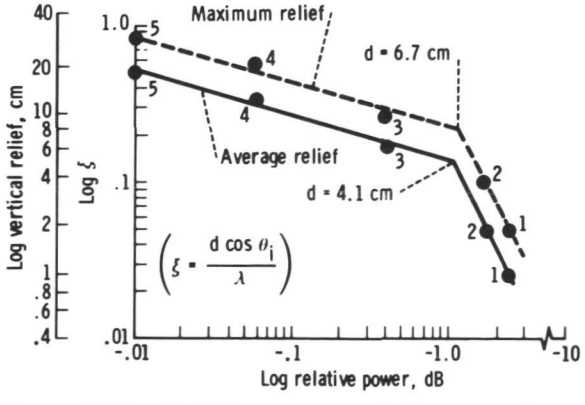

FIGURE 5–39.—Relative power variation as a function of average and maximum vertical reliefs for TWF–1 to TWF–5 sample sites (which are numbered 1 to 5).

are being conducted with that long-range goal in mind; however, the terrestrial benefits of such research studies are apparent.

The extremely good sensitivity of the radar system to variations in surface roughness appears to result from (1) the low frequency (1215 MHz); (2) the 45° to 90° antenna depression angle range, which emphasizes surface backscatter at the expense of conventional morphologic image portrayal; and (3) the high-resolution capability of the synthetic aperture system.

Surface moisture can substantially alter the complex dielectric constant and thus affect the backscatter power returned by sur-

face roughness alone. There are, however, an estimated 4×10^{10} m^2 of extremely arid land, 50×10^{10} m^2 of arid land, and 110×10^{10} m^2 of semiarid land within the limits of the contiguous 48 States (ref. 5–11). These relatively undeveloped regions could be the focal point of proposed airborne, Space Shuttle, and spacecraft radar-imaging applications such as the following:

1. Research on development of arid land recreational areas and other aspects of land use.
2. Detection of alluvial deposits for sand and gravel and for water potential.
3. Classification of active sedimentary processes (i.e., monitoring of aeolian activity and defining the extent of silt deposition after floodwaters recede).

Strategic Air Command, X-band (9500 MHz) SLAR images of Death Valley have been acquired recently. A full discussion and comparison of the X- and L-band images will be published in the near future; however, one enlargement of these high-resolution (15 m) X-band data is presented (fig. 5–41) for comparison with specific details on the L-band images.

The conspicuous dark band (unit V) around the base of the gravel fans on the L-band data (fig. 5–31) is present on the X-band image (fig. 5–41), but the area cannot be well delineated because of the less-distinctive tonal contrast between units V and III (the carbonate facies of the outer salt pan). Similarly, the contrast between units III and II on the X-band data is not as sharp as shown on the L-band images.

However, the desert pavement (unit VI) detail is somewhat better on the X-band image because this radar has a higher resolution and a more pronounced shadowing effect. The incident angle of the X-band data in the center of figure 5–41 is 72.3°, whereas the incident angle in the center of the L-band image (fig. 5–31) is 38.2°. The desert-pavement areas are very clearly defined on both radar frequencies as a result of the extremely smooth desert varnish surface (fig. 5–30). The pavement would probably be specular even on K-band images for this reason.

Within the salt pan, the X-band data appear to define geologic contacts between various chloride, sulfate, and carbonate facies differently than the L-band data. However, verification and discussion of the causal relationships must be delayed until further study of the X-band images is completed.

A SHUTTLE RADAR MICROWAVE SUBSYSTEM FOR EARTH RESOURCES APPLICATIONS

Introduction

The microwave subsystem considerations are discussed as a design example for a radar for Earth resources applications to be used in conjunction with the Shuttle Spacelab. This system with a multiplicity of frequencies and polarizations—L-band (25-cm wavelength), S-band (10-cm wavelength), and X-band (3.2-cm wavelength) at two orthogonal linear polarizations—has been tentatively selected. The Space Shuttle vehicle constrains the antenna to approximately 8 m in length and 3 m in width.

The frequencies and antenna size comprise the major constraints on the system described here and determine the sensor altitude, coverage, and major hardware parameters. The sensor performance is summarized as follows:

1. Frequencies:
   a. L-band (25 cm)
   b. S-band (10 cm)
   c. X-band (3.2 cm)
2. Polarization:
   a. Transmit: Vertical or horizontal
   b. Receive: Vertical or horizontal
3. Imagery: Synthetic array; four looks in azimuth; 10-m range and azimuth resolution on the ground.
4. Coverage: Offset of 75 to 275 km either side of the satellite groundtrack.
5. Swath width:
   a. At minimum offset: 40 km
   b. At maximum offset: 100 km

The major microwave subsystem parameters are outlined as follows:

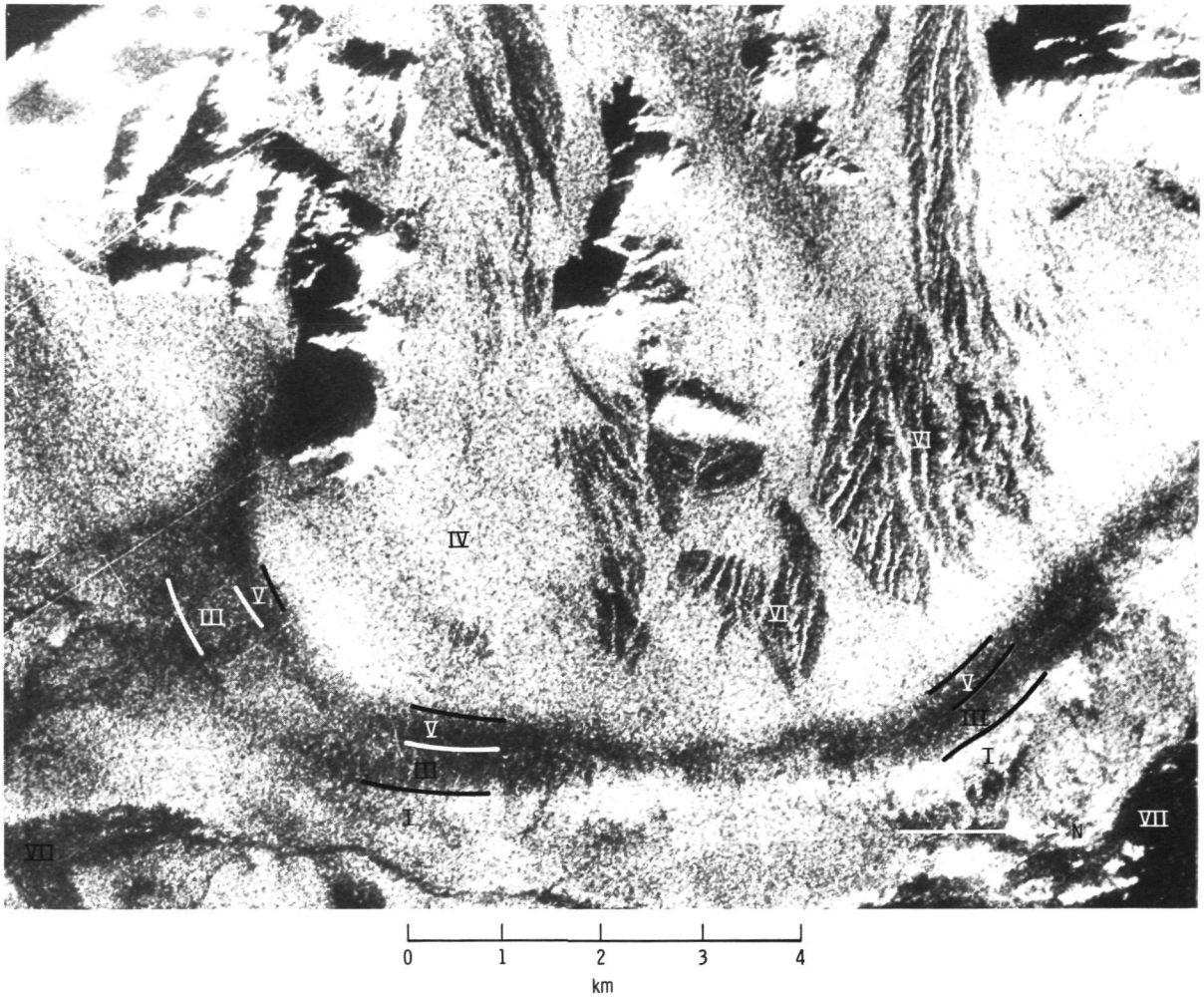

FIGURE 5–41.—Enlargement (10 times) of X-band SLAR image of Tucki Wash Fan. Radar look direction from lower right to upper left; flight altitude, 10 363 m. Compare annotations with figure 5–31. Incident angle (center of image) equals 72.3°, taking into consideration the 2.5° eastward slope of the fan. Dark streaks from upper left to lower right are artifacts of image acquisition. (Strategic Air Command photograph.)

1. Antenna: Dual linear polarization; planar array:
   - *a.* L-band: 2 m high; 8 m long
   - *b.* S-band: 0.75 m high; 8 m long
   - *c.* X-band: 0.25 m high; 8 m long
2. Transmitter: Switchable to either polarization; 2000 pulse/sec:
   - *a.* L-band: Solid state; 60-W average
   - *b.* S-band: Solid state or tube; 200-W average
   - *c.* X-band: Traveling-wave tube (TWT); 600-W average
3. Receiver: Dual channel for both polarizations; parametric amplifier input stage:
   - *a.* L-band: 1-dB noise figure
   - *b.* S-band: 1.5-dB noise figure
   - *c.* X-band: 2.5-dB noise figure
4. Pulse compression:
   - *a.* Chirp: As required to provide acceptable transmitter peak powers and 10-m ground resolution in range for varying offset distances
   - *b.* Off-nadir angle: 45°

To arrive at the design, two limitations must be considered: the antenna aperture constraints (8 by 3 m) on the imagery requirements and the antenna aperture constraints on the antenna design, such as off-track distance requirements, polypolarization, and multifrequency. The approaches to designing optimum transmitters must be considered for the three frequency bands, particularly the X-band transmitter, which requires an average power of approximately 600 W.

The major conclusion concerning the aperture constraint is that the 8- by 3-m aperture imposes a severe limitation on the available swath widths and on the extent of off-track range that is achievable. The maximum achievable offset for the system at an altitude of 200 km is 275 km, and the maximum swath width available at this offset is 100 km. These limitations are described in detail in this section.

Multiple-polarization use of the 8- by 3-m antenna aperture is an important consideration. In this preliminary analysis, the 8- by 3-m aperture was divided into three 8-m strips, each representing a slotted array at L-, S-, and X-bands, respectively, and all having an elevation beamwidth of 12° (fig. 5–42). Reasonable-sized offset ranges and swath widths are attained at all three frequencies.

Radar-power requirements are also fixed when the aperture is divided in the previously mentioned manner. For a signal-to-noise ratio of 15 dB, a 10-m ground resolution is required; and, for a geometric back-

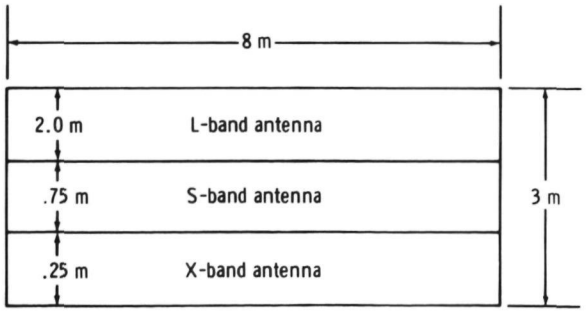

FIGURE 5–42.—Aperture sharing.

scattering coefficient of −14 dB, the radiated power requirements for a resolution cell 340 km away are as follows: X-band, 600 W; S-band, 200 W; and L-band, 60 W.

System Tradeoffs and Performance

The system tradeoffs considered here determine the radar parameters, PRF, antenna weighting, pulse compression ratio, pulse compression technique, transmitter peak power, and so forth, which draw a desired balance among swath width, available offset ranges, and image quality (given the antenna aperture constraints and transmitter constraints).

At the start of this balancing process, it is necessary to decide how the available aperture is to be shared by the three frequencies and to include dual polarization for each frequency. The 8- by 3-m antenna aperture will be partitioned into three 8-m-long antennas, one each for L-, S-, and X-bands (fig. 5–42). Antenna mechanization is discussed in a subsequent section.

Once aperture sharing is known, the radar PRF, based on the allowable signal-to-ambiguity ratio, can be selected. Also, if the PRF and the antenna elevation pattern are known, the available swath widths and maximum offset range can be determined within the limits of signal-to-ambiguity constraints.

This initial tradeoff process is discussed in the subsections on orbit geometry and on angle ambiguity control and PRF choice. The next section contains a view of image-quality optimization factors that relate to the microwave subsystem. Tropospheric and ionospheric propagation effects are detailed in a separate subsection, which concludes that, from a Space Shuttle altitude of 200 km and at 45° from the vertical, propagation problems are those usually associated with the troposphere (e.g., rain). However, above a 400-km altitude, Faraday rotation by the ionosphere may be an important factor.

Orbital geometry.—The basic geometry associated with a side-looking SAR in orbit around a spherical Earth is shown in figure 5–43. The equations used in determining ϕ,

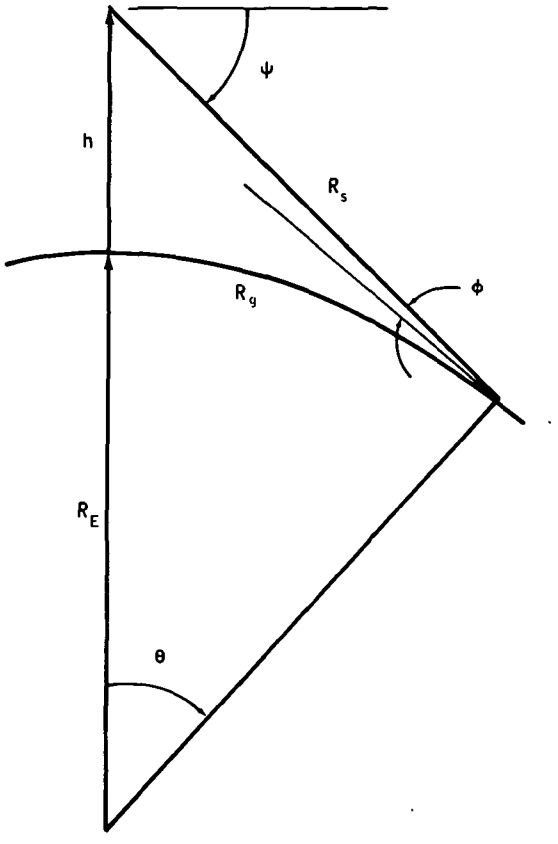

FIGURE 5–43.—Basic orbital geometry of side-looking SAR.

ψ, and R_s as functions of R_g are

$$\theta = \frac{R_g}{R_E} \qquad (5\text{–}18)$$

where ϕ is the elevation beamwidth, ψ is the depression angle, R_s is the slant range, R_g is the ground range, and R_E is the Earth radius.

$$\psi = \arctan\left[\frac{h + R_E(1-\cos\theta)}{R_E \sin\theta}\right] \qquad (5\text{–}19)$$

$$R_s = \frac{R_E \sin\theta}{\cos\psi} \qquad (5\text{–}20)$$

Figure 5–44 shows ϕ, ψ, and R_s as functions of R_g for $h=200$ km. The spherical Earth effects are particularly important at the smaller values of ϕ, where a small change in ψ can cause a large change in illuminated ground range R_g, which makes extremely

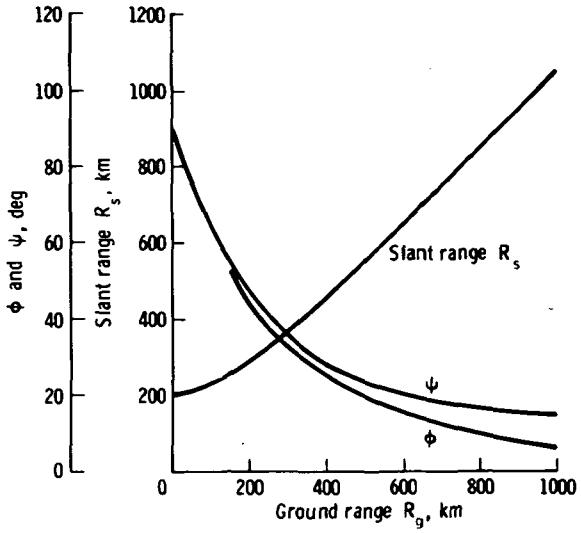

FIGURE 5–44.—Plot of ϕ, ψ, and R_s as functions of R_g ($h=200$ km).

small elevation beamwidths necessary to control range ambiguities.

Angle ambiguity control and PRF choice.—A pulsed radar return spectrum is shown in figure 5–45 for a real antenna with a uniform weighting function. The widths of the returns about each PRF line are independent of the carrier frequency; only the real antenna length l and the vehicle speed v affect the widths.

As the real antenna scans over a point scatterer, the Doppler shift varies and the antenna traverses the regions to be processed as illustrated in figure 5–46. The overlapping

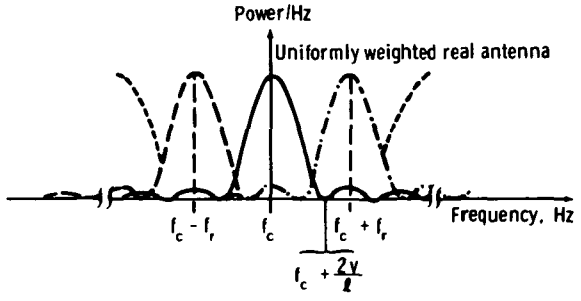

FIGURE 5–45.—Pulsed radar return spectrum for a real antenna with a uniform weighting function (where f_c is carrier frequency and f_r is return frequency).

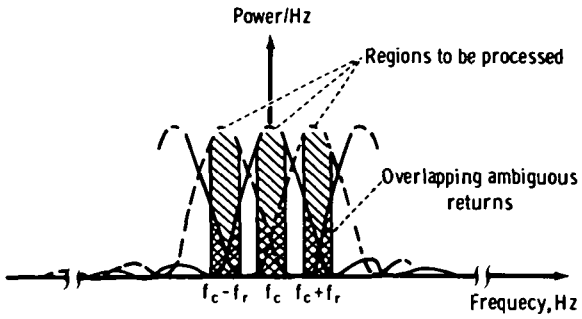

FIGURE 5–46.—Azimuth ambiguities.

returns from adjacent PRF lines are processed simultaneously with the desired returns. The result is an ambiguous synthetic array azimuth pattern. The synthetic aperture azimuth pattern required to hold the azimuth ambiguities to −18 dB is given in figure 5–47. It has been assumed that it is desired to hold the sum of all azimuth ambiguities to −15 dB.

A conservative specification on real antenna, mean, far-out azimuth side lobes $\bar{G}_{SL}$ can be derived as follows. The Doppler frequency extent of the side-lobe region is $\pm 2v/\lambda$. Therefore, the processed region near each PRF return line contains the contributions from $N=4v/f_r$ other PRF lines. At a nominal PRF of $2v/l$, $N=2l/\lambda$. Next, arbitrarily let it be required that the sum of all N contributions be −10 dB relative to the −27-dB peak of figure 5–47; then, the following equation results:

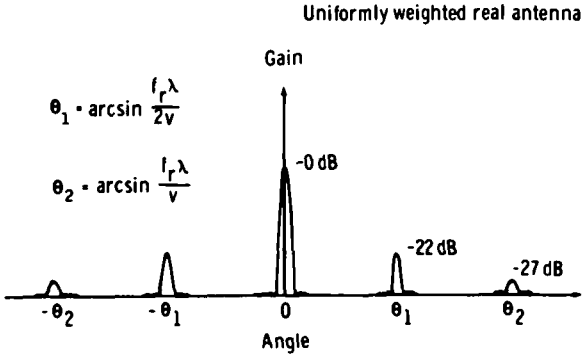

FIGURE 5–47. Synthetic aperture azimuth pattern required to hold azimuth ambiguities to −18 dB.

TABLE 5–X.—*Azimuth Far-Out Side-Lobe Level Requirements*

f_c	N, dB	$\bar{G}_{SL}$, dB
X-band	27	−32
S-band	22	−29.5
L-band	18	−27.5

$$20 \log_{10} G_{SL} + 10 \log_{10} N = -37 \text{ dB} \qquad (5\text{–}21)$$

The resulting requirements on average azimuth side-lobe levels for $l=8$ m are given in table 5–X.

The PRF can be adjusted so that, when it operates with four independent azimuth looks, the worst-case azimuth ambiguities (in the outer two processing regions of fig. 5–48) are −18 dB. For these particular ambiguities, the proper PRF choice is approximately $2v/l$. Similar considerations for three, two, and one azimuth looks yield the PRF as a function of the number-of-looks curve plotted in figure 5–49. The figure also shows $c/2f_r$ (the slant-range distance between transmitter pulses), which is an important measure of ground-range coverage, as shown in the following section.

Range ambiguity control and ground-range coverage.—From the previous section, it is noted that $c/2f_r < R_s$. Thus, many range am-

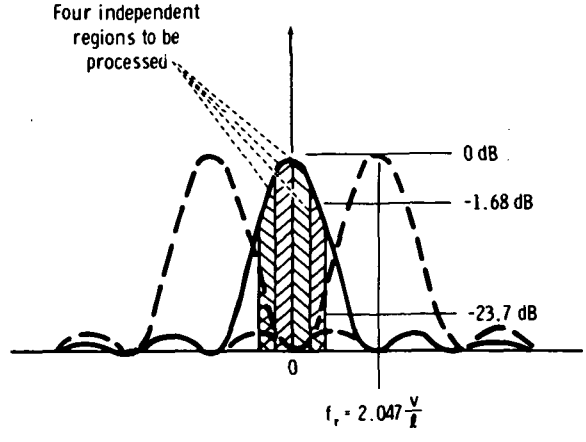

FIGURE 5–48.—Azimuth ambiguity adjustment for four independent azimuth looks.

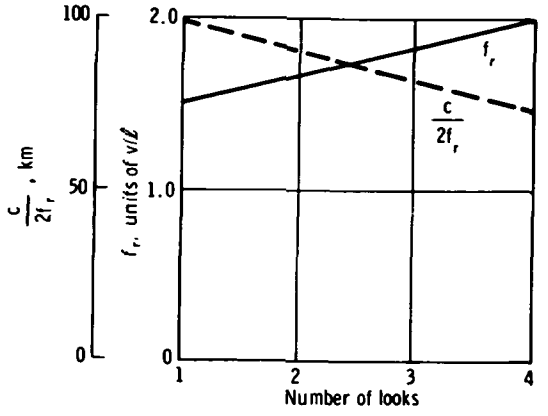

FIGURE 5–49.—The PRF and interpulse slant range compared with number of looks.

biguities will result unless the antenna elevation pattern is used to reject undesired returns (fig. 5–50). The ambiguous ranges are kept in the side lobes of the real antenna elevation pattern. Figure 5–51 illustrates the situation for smaller depression angles; a

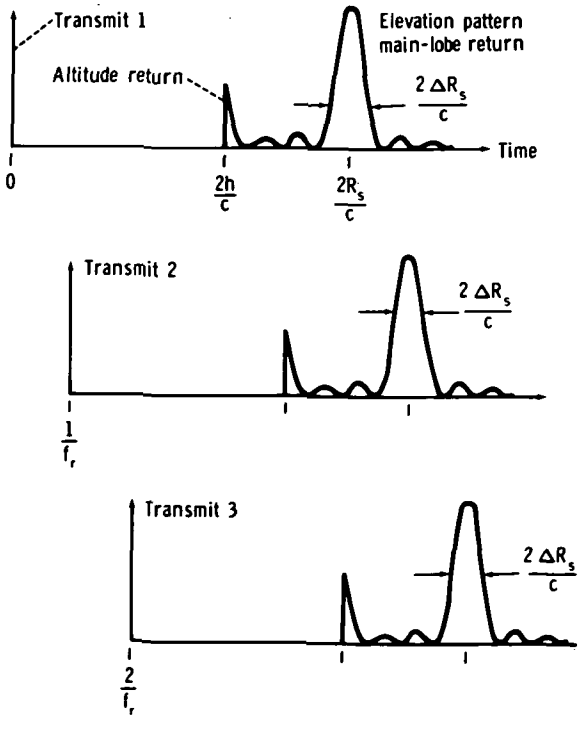

FIGURE 5–50.—Range ambiguity control (large depression angle).

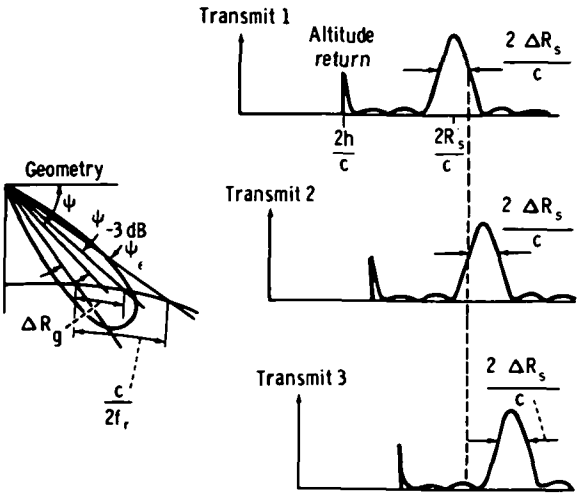

FIGURE 5–51.—Range ambiguity control (small depression angle).

given elevation beamwidth covers a greater slant range than before. Thus, to realize the maximum coverage from a given PRF choice, the real antenna elevation beamwidth must become a function of depression angle (or of ground range). The PRF should be adjusted as a function of altitude and antenna elevation pointing angle to cause the altitude returns to fall outside the desired range coverage. A small compromise in angle ambiguity level or in range coverage may be required at certain combinations of altitude and elevation pointing angle.

To estimate elevation beamwidth requirements and to estimate ground-range coverage, it was assumed that the elevation aperture of the real antenna is uniformly weighted and that the worst-case range ambiguities (at the edges of the range coverage) must be −18 dB relative to the desired returns at the edges of the range coverage. As before, the −18-dB figure was determined by interpreting the −15-dB specification to apply to the sum of all ambiguities.

Figure 5–52 shows the power return as a function of time for the following conditions: The worst-case range ambiguities (−18 dB) are present, the elevation aperture is uniformly weighted, and the ground-range coverage is that encompassed by the −3-dB one-

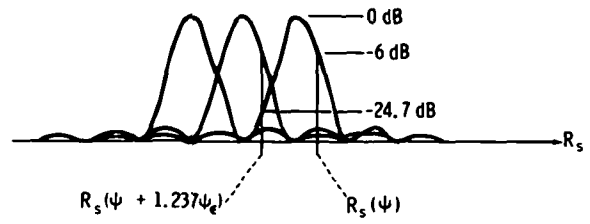

FIGURE 5–52.—Antenna elevation pattern adjusted for −18-dB range ambiguities.

way elevation pattern $\psi_{-3\ dB}=0.443\psi_\epsilon$. It can be shown that

$$\frac{c}{2f_r}=R_s(\psi+\psi_\epsilon)-R_s(\psi-\psi_\epsilon) \qquad (5\text{–}22)$$

$$\Delta R_g=R_s(\psi+0.443\psi_\epsilon)-R_s(\psi-0.443\psi_\epsilon) \qquad (5\text{–}23)$$

The results plotted in figure 5–53 can be derived from these two equations. This figure is for the case in which the real antenna elevation is continuously adjusted to optimize the ground-range coverage, limited only by the ambiguity levels previously discussed. Antenna design problems, radar power output, and elevation pointing accuracy problems have been ignored to show that the maximum theoretical limits are under only the ambiguity constraints.

Good coverage is still possible for a single elevation angle. Figure 5–54 shows three discrete coverage zones obtained at an altitude of 200 km from a real antenna elevation beamwidth of 12°.

As a trial design, the aperture constraints assumed were (1) that the 3-m vertical aperture available was shared among X-, S-, and L-bands without physically overlaying the antennas, and (2) that the elevation beamwidths of the three antennas were equal. These assumptions resulted in three antennas, each 8 m long, having vertical apertures of 0.25, 0.75, and 2.0 m at X-, S-, and L-bands, respectively. The elevation beamwidths of the three antennas are 6.4° minimum and are weighted to generate the 12° beam.

A conservative specification on real antenna far-out elevation side lobes can be derived as follows. The slant range extent of the side-lobe region is $R_{s_m}-h$, where R_{s_m} is the slant range to the horizon. The maximum number of range ambiguities is

$$M=\frac{R_{s_m}-h}{c/2f_r} \qquad (5\text{–}24)$$

At a nominal PRF of $2v/l$ and with $l=8$ m, $c/2f_r=76.9$ km; thus, $M=18.3$. Next, arbitrarily assume the requirement that the sum of all M contributions be −10 dB relative to the −24.7-dB level of figure 5–52. The following equation is the result:

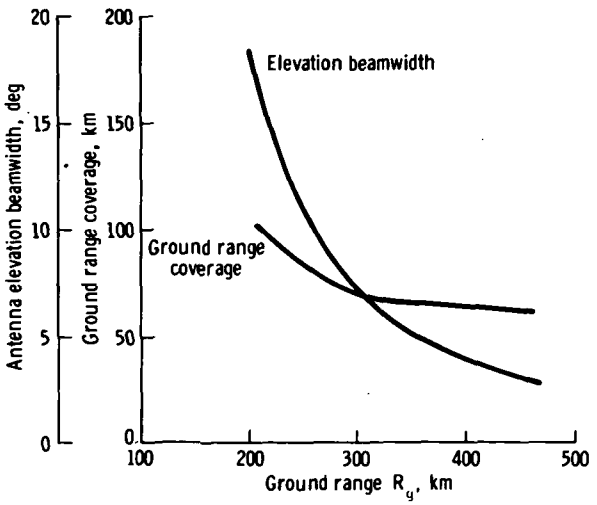

FIGURE 5–53.—Ground range coverage and antenna elevation beamwidth as a function of ground range (ambiguity constraints only); $h=200$ km, $l=8$ m, $f_r=2.047$ v/1, four azimuth looks.

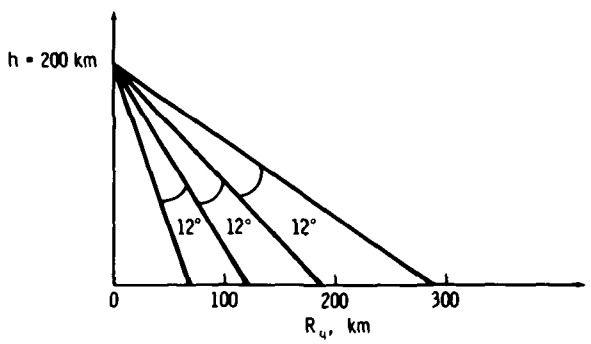

FIGURE 5–54.—Ground range coverage with one elevation beamwidth.

$$20 \log_{10} \bar{G}_{SL} + 10 \log_{10} M = -34.7 \text{ dB} \qquad (5\text{–}25)$$

The resulting requirement on average elevation side-lobe level is $\bar{G}_{SL} < -23.7$ dB.

Image-quality performance.—For the final radar design, a complete resolution and side-lobe budget to allocate all error sources must be developed to specify tolerances throughout the system so that overall performance requirements can be met. Some typical error sources for the transmitter/receiver section are described below.

The dominant contributors to integrated side lobes by the transmitter/receiver are (1) quadratic phase errors between the transmitted pulse and the pulse compression decoding signals, and (2) amplitude ripples across the transmitted pulse.

Figure 5–55 shows the effect of quadratic phase error for cosine-on-a-pedestal weighting functions defined by

$$h(x) = \frac{1 + 2F \cos x}{1 + 2F}, \qquad -\pi < \chi < \pi \qquad (5\text{–}26)$$

where x is the phase difference between transmitted pulse and the decoding signals and where the main beam broadening factor

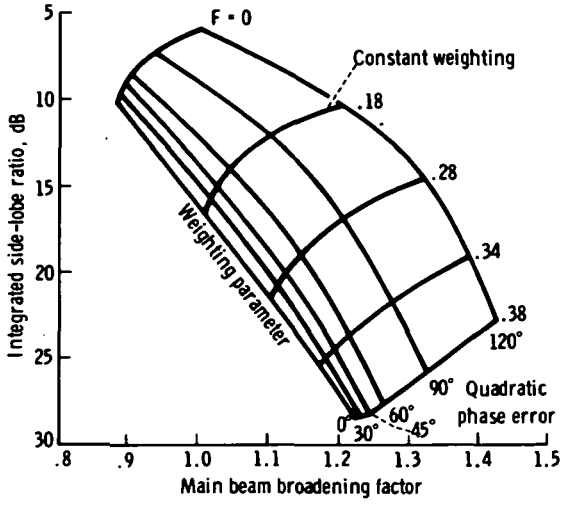

FIGURE 5–55.—Resolution effects of quadratic phase error on integrated side-lobe ratio and main beam broadening.

F is 0.886 for a uniformly weighted compression filter. For example, this figure shows that for a designated parameter (given an integrated side-lobe ratio (ISLR) of 27 dB and a broadening factor of 1.2 with no quadratic phase error), the effect of 30° of quadratic phase error is to degrade the ISLR by 0.5 dB and to degrade the resolution by approximately 1 percent.

Amplitude ripples are caused by ripples across the transmitter bandpass and by ripples on the modulating pulse. A ripple of ±1.5 percent produces two −42-dB side lobes.

For performance in the azimuth dimension, similar criteria apply, except that these criteria are now applied on a pulse-to-pulse basis. Thus, pulse-to-pulse coherence must produce short-term (over an array time) quadratic phase errors of less than approximately 30°. Random-phase errors result in an ISLR equal to the variance of the phase error (in radians). For example, a standard deviation of random-phase errors of 0.02 radian results in an ISLR of −34 dB.

Propagation effects.—In the formation of a synthetic array map from an orbital platform, the radar signal traverses both a portion of the lower ionosphere and the troposphere. The free electrons in the ionosphere cause the index of refraction to vary in time and space. In addition to being dispersive, the medium is doubly refracting, producing a Faraday rotation of a linearly polarized wave. The random fluctuation in index induces random-phase errors on the signal.

The index of refraction in the troposphere also varies in time and space, principally because of varying amounts of water vapor. However, the index is not frequency dependent; thus, the medium is not dispersive. In addition to inducing random-phase errors on the signal, the troposphere may contain precipitation that produces attenuation and backscatter, which are frequency dependent.

For a radar-platform altitude of 200 km, it is found that (for a rather severe ionospheric electron density profile) the Faraday rotation is less than 1° (two way) at 1 GHz, decreas-

ing as f^{-2} with increasing rf. Phase errors resulting from the ionosphere are estimated to be negligible (as is the dispersive effect) for frequencies above 1 GHz.

Tropospheric-induced phase errors are also found to be negligible at a 10-m resolution for any frequency below 10 GHz. The only serious propagation effect is found to be that caused by precipitation in the lower troposphere. Warm-front rain can produce backscatter so that barren ground ($\sigma^\circ \approx 10^{-2}$) will produce an echo less than 15 dB above the precipitation echo at frequencies above 6 GHz. Thunderstorms produce the same limitation at frequencies above 2 GHz, but they are much less common.

If the radar altitude is increased, the Faraday rotation is the only effect that changes materially. For the electron-density profile that produces less than a 1° round-trip rotation at 1 GHz and a 200-km altitude, the Faraday rotation increases to approximately 10° at a 400-km altitude, assuming the same off-nadir angle. This increase may begin to affect the dual-polarization signature information needed for surface classification (e.g., crop identification).

Probably, only precipitation will produce a significant tropospheric effect. It will occur at the upper end of the 1- to 10-GHz band.

Hardware Discussion

The hardware aspects of the microwave subsystem, antenna, transmitter, receiver, exciter, and pulse compressor are discussed in this section. The antenna and transmitter are the critical items in a satellite radar; the antenna is critical because of its large size, and the transmitter is critical because it is the major consumer of prime power and the unit in which the greatest voltage and current stresses occur. Therefore, these two units are covered in more detail than the receiver, exciter, and pulse compressor, which do not exhibit any major problems in the transition from airborne to satellite radars.

Antenna design considerations.—This antenna discussion is divided into three areas: antenna requirements, general design problems, and a candidate design. The various system requirements, frequencies, polarizations, and so forth, are examined with respect to their effect on antenna design and performance. Typical design considerations, which include multiple-frequency band operation, rf and signal bandwidth, manifolding, multipacting, and aperture phase tolerances, are discussed. A possible approach that has potential for satisfying the basic requirements is presented.

Antenna requirements: The necessary radiation pattern performance in both the azimuth and elevation directions is determined by the permissible level of interference contributed by ambiguities. With the elevation pattern, sufficiently steep sides and low side lobes at certain angles are required to avoid interference in the range interval of interest from multiple-time-around returns, near-in returns (particularly the altitude line), and the returns for the same range on the opposite side of the vehicle. The azimuth pattern must provide a sufficiently low side-lobe level to avoid undue contribution to interference from the integrated ambiguities. The required performance depends on the overall system design because some contributions to interference can be avoided by other means; for example, the altitude line can be moved with a small change in rf.

In general, the more complex the antenna becomes in terms of polarization flexibility or multiple-frequency operation within the same aperture, the more difficult it will be to provide precise control of the pattern shape and side lobes. With a single polarization and operation in a single-frequency band, rms side-lobe levels (beyond the first few) of approximately 45 dB below the main beam gain can be expected. However, if one antenna is interleaved or overlaid with another at a different frequency or polarization, 30 dB may be difficult to achieve. From preliminary system considerations (see section entitled "Angle Ambiguity Control and PRF Choice"), the requirements on the levels of side lobes beyond the first two do not appear severe in either principal plane. Azimuth

side lobes of 32 dB down and elevation side lobes of 24 dB down appear adequate.

An rf bandwidth of approximately 1 percent within a particular band to accommodate some flexibility in the location of the instantaneous bandwidth should not pose difficulty. An instantaneous bandwidth of perhaps 20 MHz, depending on resolution, requires careful attention because the requirement applies not only to the pattern and its variations with frequency, but equally to the phase and amplitude transfer characteristics from the electromagnetic field at points in the far field of the antenna to the current and voltage at the output terminals.

The provision of simultaneous reception on two orthogonal polarizations, while transmitting on one, imposes significant complexity. The degree of orthogonality required of the antenna would be a function of the required experiments (within the constraints imposed by Faraday rotation).

Obtaining polarization diversity concurrent with operations at widely separated frequency bands (greater than an octave) from a single aperture is not deemed feasible if delicate side-lobe and pattern control is needed. Use of separate antennas and radars appears to be the most practical approach; hence, the degree of commonality between designs and the ease of scaling are important considerations.

Design tradeoffs: The previously mentioned considerations pose many problems. Among the design considerations included are tolerance effects, pattern and polarization considerations, and multipacting effects.

Aperture phase tolerance: The problem of maintaining aperture phase tolerances is associated with antennas that are electrically long with respect to a wavelength. Failure to maintain phase tolerance results in increased side-lobe levels, filling in of the nulls, and, to a lesser extent, decreased gain. Errors in the excitation of the antenna can result from either electrical causes or mechanical distortions. The effects on the radiation pattern are indistinguishable. The error budget must be allocated between electrical and mechanical causes. Thermally induced distortions can be particularly severe when illumination of the antenna by the Sun is possible from many directions. However, numerous methods exist to deal with this problem. The antenna may be partially isolated from the heat source (the Sun) by a cover. The thermal coefficient of expansion may be minimized by use of materials such as graphite-fiber-reinforced plastics, which have been applied for communication spacecraft antennas. Another possible solution is the use of very high thermal conductivity materials that minimize temperature gradients. Still another partial solution is to use mesh structures that have high optical transparency.

In general, the errors in the antenna that cause degradation of the pattern can be divided into three classes, depending on their distribution over the radiating aperture:

1. Slowly varying systematic errors along the antenna caused by factors such as bending of the main support structure.

2. Errors associated with groups of elements caused by positional errors in mounting and phase and amplitude errors in the excitation of the feed manifold.

3. Small-scale random errors associated with the individual elementary areas of the antenna.

Elevation pattern: Assuming that mapping on either side of the Space Shuttle is desirable, two beam types can be considered: (1) a symmetrical beam (with respect to the Space Shuttle elevation plane) that requires the vehicle only to be rolled to map similar swaths on either side, and (2) a shaped or asymmetrical beam that requires the vehicle to yaw 180° to map an identical swath on the opposite side. This comparison is illustrated in figure 5–56.

Azimuth side lobes: Aperture distribution tapering may prove desirable in the azimuth plane to reduce side-lobe clutter contribution within a range ring. Standard Taylor distributions could then be used to optimize gain for the given side-lobe level. Only a moderate

increase in feed complexity will result from such tapering of the aperture distribution.

Polarization diversity: Polarization diversity creates a severe design problem that requires ingenuity for its solution; it complicates the design to the extent that very wide band performance is impractical.

The candidate design is configured to provide two orthogonal, linearly polarized antenna patterns with separate output ports for each polarization. Thus, received orthogonal signals can be processed individually in accordance with the particular experiment. Transmission can be accomplished on either polarization with appropriate switching in the transmitter. Furthermore, by dividing the transmitter output between the two linear antennas with the proper phase relationship, circular polarization can also be obtained. If done electronically, these switching schemes can be relatively complex. It may be worthwhile to consider in-flight adjustment or component substitution to simplify the design.

Multipactor effects: The operation of rf devices in the vacuum environment of space presents the microwave engineer and designer with electrical breakdown problems, which can be more serious than those caused by ionized discharge. The problem arises because the mean free path of electrons in the space environment may be larger than the dimensions of the rf components. Under such conditions, a secondary emission resonance (multipacting) may occur. Multipactor discharge is not necessarily a high electric field phenomenon; components operated at rf power levels as low as 1 W, when the frequency is greater than a few tens of megahertz, are susceptible. The problem is familiar to designers of microwave tubes; however, the need for designers of other active microwave devices to focus attention on the subject became evident only when suspected multipactor failures occurred in space probes.

Candidate antenna design: A strong candidate and one of the most straightforward designs for the type aperture contemplated

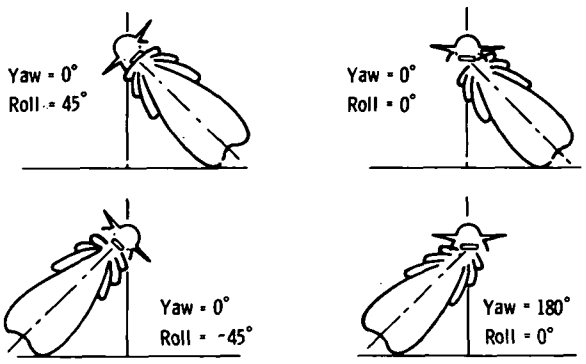

FIGURE 5–56.—Elevation pattern coverage.

is illustrated in figure 5–57. The design is the planar array of waveguide slots that produces linearly polarized radiation with the direction of polarization of the electric field parallel to the long dimension of the array. The slots used for this design are displaced shunt slots in the broadwalls of identical parallel guides. Each guide is the required length to form the proper beamwidth at the frequency of operation. The arrangement of slots along each waveguide can be designed to generate a phase and amplitude distribution that causes shaped beam or low side-lobe patterns, if either is desired.

An X-band planar array antenna designed for a space application is shown in figure 5–58. The array is 7.7 m long and 1.23 m high. The array has a structural backing that (1) supports the radiating panels that form the aperture, (2) provides support and attaching points for the waveguide corporate feed that

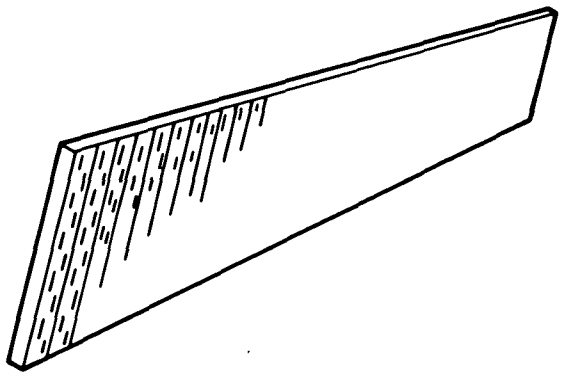

FIGURE 5–57.—Linearly polarized slotted array.

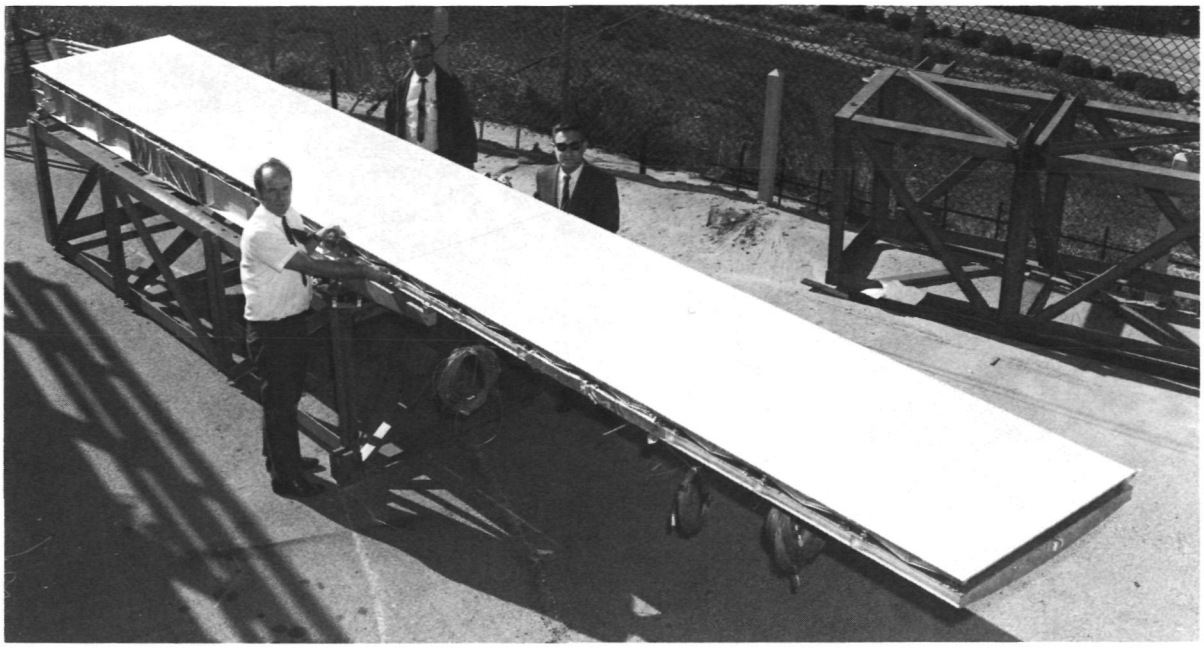

FIGURE 5–58.—An X-band planar array antenna.

distributes power to the array, and (3) protects the array and feed from uneven thermal radiation that would otherwise cause intolerable amounts of physical distortion. The array has been built and tested electrically. Environmental testing, including static tests, vibration tests, and thermal tests, was performed successfully.

Extension of the basic array design described previously yields a design that operates with two orthogonal orientations of linear polarization in which a second array is added. This addition can be accomplished in several ways; the most direct way is to add a second array in front of the first. The front array, if constructed with waveguides that use inclined shunt slots on the guide edges, can be overlaid on the rear array with spaces between the waveguides that allow the rear array to radiate unimpeded through the structure of the front array. This design is shown in figure 5–59.

Transmitter design considerations.—The transmitter designer must choose between solid-state and tube-type transmitters. For the average powers under consideration (X-band, 600 W; S-band, 200 W; and L-band, 60 W), the X-band transmitter will almost certainly be a tube type; the L-band transmitter will almost certainly be solid state; and the choice for the S-band transmitter will require additional study. Considerations affecting the choice of tube or solid-state transmitters for the satellite radar are discussed in this section.

Solid-state power amplification: As single sources of high rf power, vacuum tubes are presently secure in their transmitter role. At the lower frequencies, for which solid-state amplification is more efficient and opportunities exist for effectively combining the outputs of several devices, the solid-state approach may offer performance competitive with or superior to that of the tube. Therefore, an evaluation of high-power solid-state transmitter configurations implies consideration of both of the devices and the methods of power accumulation.

Solid-state devices: Three important classes of solid-state devices for the generation and/or amplification of microwave power are transistors, transferred electron devices (TED), and avalanche transit-time devices. The modes of operation, although

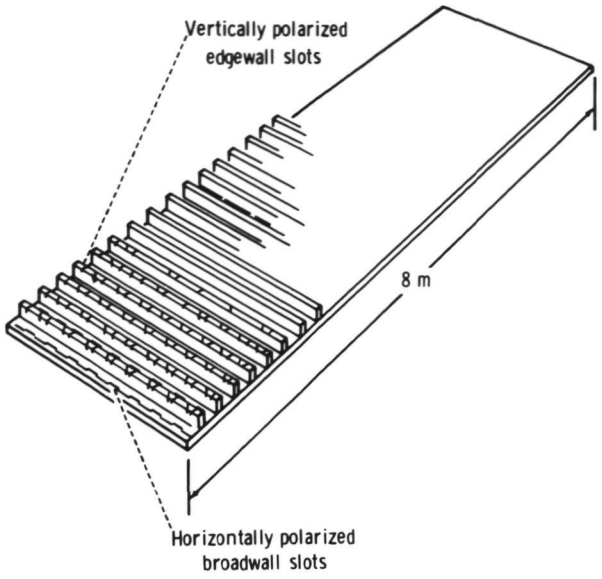

FIGURE 5–59.—Dual-polarized waveguide slot array concept.

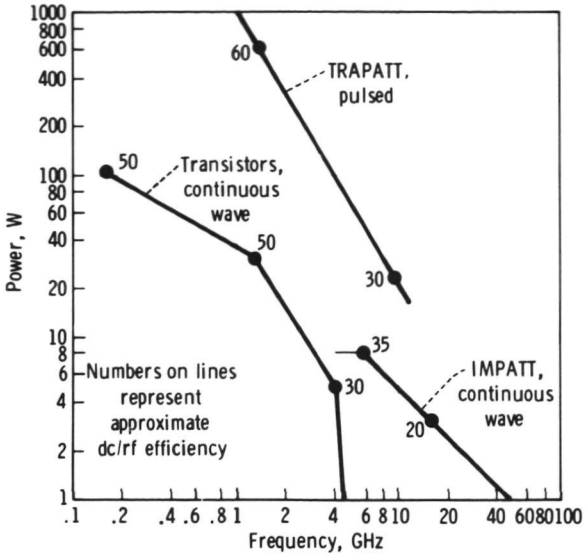

FIGURE 5–60.—Power capabilities of solid-state devices.

considerably different among these classes, have some common characteristics. A prime characteristic is the common requirement for relatively low operating voltages of less than 100 V, depending on the frequency and power desired. A second, less-desirable characteristic is the average power-output limitation caused by thermal effects in which a single device is limited roughly to the 10- to 100-W range, depending on thermal resistance of the design. The present power capability of single devices is shown in figure 5–60. Higher power can only then be obtained through a combination of these devices. The applicability of these devices is summarized in table 5–XI.

The rf power accumulation: When more microwave power is required than can be provided by a single solid-state device, accumulation techniques must be used. These techniques are divided into three areas following the natural interface breakdown of modern systems. Each area is considered independently in the following discussion.

First, there is the combination of devices or chips within a single package. Researchers have shown that both series and parallel techniques are feasible and result in substantial power improvements. Parallel thermal mounting results in increased heat dissipation, whereas interconnection flexibility allows control over impedance levels. This method has the most potential for power/cost improvement because of the applicability of multiple-chip processing on a common heat sink. Mounting circuit complexity may even

TABLE 5–XI.—*Summary of Solid-State Source Candidates*

Device	Appraisal
Transistors	Strong contender below 4 GHz.
TED	Not recommended because of low power and efficiency.
TRAPATT [a] devices.	High peak powers for moderate-to-low pulse widths (<10 μsec) and low-duty factors <1 percent; possible use depending on system final requirements.
IMPATT [b] devices (GaAs) [c].	Moderate efficiencies 20 to 30 percent; highest average power above 4 GHz.

[a] Trapped plasma avalanche triggered transit.
[b] Impact avalanche transit time.
[c] Gallium arsenide.

be reduced if impedance changes result in easier match requirements. Perhaps, 9 to 12 devices will be an optimum number connected in a series-parallel arrangement, mounted on a diamond heat sink.

After maximizing the power from a single package, the next step is to combine packages within a single component. This step is more difficult because distributed effects begin to have an important role. Linear techniques are usually limited to a low number of packages (three to four) due to interaction and power saturation in the downstream devices. Presently, radial configurations appear to have more potential (using symmetry for circuit stability and maintaining equal phase and power levels at all devices).

The third area of power accumulation is concerned with combining the outputs of various independent amplifiers or oscillators to sum the power, while maintaining stability and minimizing circuit losses. Spatial accumulation (or combining in space as is done with multielement radiators) acts independently, using spatial interference to produce the desired summation. This technique can only be used when it is necessary to have all the power available at one port or terminal. Otherwise, circuit accumulation must be used. Usually, hybrids or two-way Wilkinson circuits are used for this purpose. Although both circuits supply the necessary isolation between the power components, they are only two-way circuits requiring n stages of accumulation (2^n-1 combining circuits) for 2^n power components, which is cumbersome and impractical where $n \geq 4$.

Reliability: The chief advantage of solid-state devices in this application is in their improved reliability over vacuum-tube transmitters. Solid-state devices, in general, have demonstrated the capability of long life under normal operating temperature ranges, such as 473 K, at the junction. Elevated junction temperatures are common, however, for high-power devices, and result in reduced expected lifetime. A tradeoff is necessary to balance the mean time before failure (MTBF) with the power required for each device. An example of this relationship is shown in figure 5–61 for silicon IMPATT devices. As indicated, temperatures approaching 573 K are to be avoided because the lifetime is reduced sharply.

A related aspect of reliability is the failure mode of a system. If all the rf power is generated by a single device, its failure forces a system failure. However, when many devices are integrated to supply the necessary power, failure of some of the devices will only reduce the system capability. In fact, an increase in system MTBF may be obtained by a slight overdesign on the number of devices required. A 20-percent increase in devices will increase the system MTBF by a factor of 100 (fig. 5–62).

Tube transmitter: The major tradeoffs required for the definition of tube transmitters lead to—

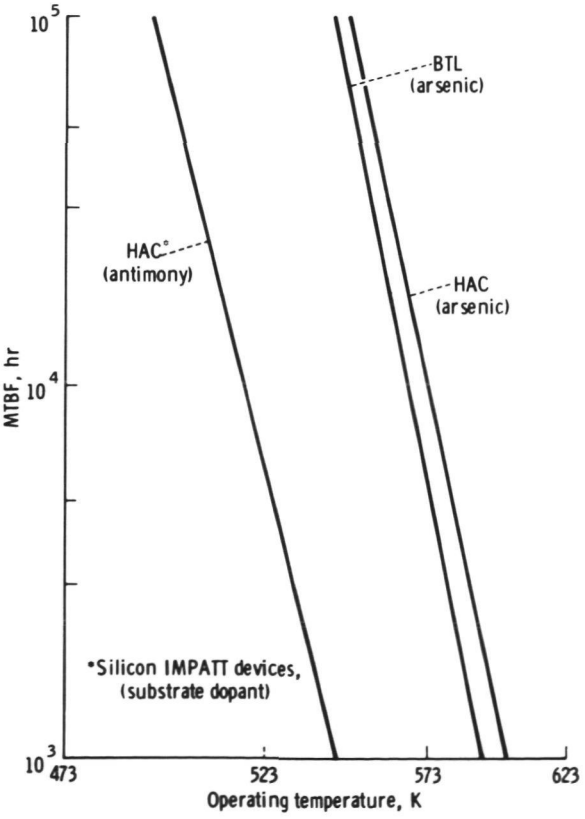

FIGURE 5–61.—Life expectation of silicon IMPATT devices related to junction temperature. Silicon IMPATTS. Hughes Aircraft Corp. (HAC), Bell Telephone Laboratories (BTL).

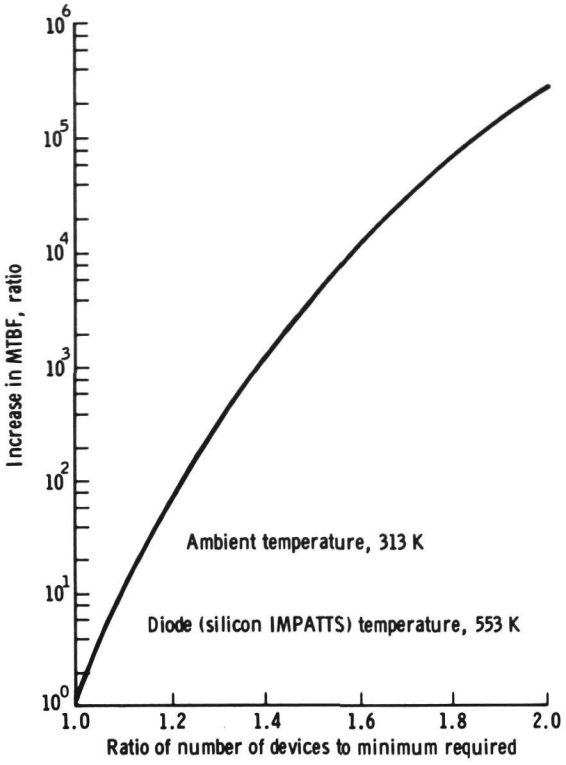

FIGURE 5–62.—Improvement of MTBF through redundancy of solid-state devices.

1. Choice of power amplifier tube.
2. Definition of high-voltage power and modulator circuits.
3. Selection of high-voltage medium and interconnection techniques.
4. Specification of high-power microwave components.
5. Mechanization of the control and monitor functions.

The average power levels range from approximately 60 W at L-band to 600 W at X-band. Using a PRF of 2000 Hz and a compressed pulse width of 0.05 μsec as nominal values and assuming that the duty cycle is not limited by swath width and corresponding listening-time requirements, the duty-cycle values corresponding to pulse-compression practical limits of 1 (no compression) and 2500 are 0.0001 and 0.25, respectively. Average power and corresponding peak-power limits for these and intermediate-duty cycles are shown in figure 5–63.

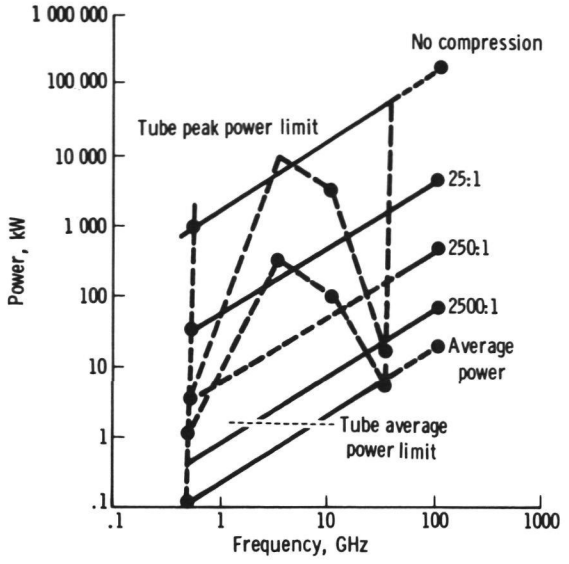

FIGURE 5–63.—Average and peak power transmitter requirements.

Also shown in this figure are average- and peak-power limits of existing high-reliability tube technology. A minimum bandwidth of 100 MHz is assumed to permit frequency agility. This bandwidth requirement excludes all tubes, except the TWT and crossfield amplifiers (CFA), below 5 GHz. Above 5 GHz, the broadband klystron (2 percent bandwidth) is a usable candidate. At the very lowest frequencies, the TWT is usually peak-power-limited by practical length and weight restrictions. At the higher frequencies, all linear beam tubes and the crossfield devices are both peak- and average-power-limited by focusing problems and the low thermal capacities of the small rf circuit structures that intercept the electron beam.

It is generally recognized that the sources of most failures in high-power transmitters are the high-voltage circuits and the critical tube interfaces. High-voltage power supplies at the 10-, 20-, and 30-kV levels, with peak powers as much as 100 kW and average powers to 1 kW, have been developed for space application. The tube-interface problem has also been addressed with the development of very simple pulse modulators, fail-safe bias supplies, and internal control-monitor circuits that limit the pulse width and duty

cycle and, in the event of a detected fault, automatically command the transmitter to a safe mode.

The rf breakdown at low-pressure levels by ionization of residual gases or by multipacting is a source of transmitter failure even in moderate rf power circuits. Both problems may be solved by use of pressurized rf lines or by a carefully designed and fabricated vacuum assembly.

The vented or vacuum approach requires control of the rf fields and element spacings to eliminate all low-order multipactor modes and choice of materials with low secondary-emission coefficients. In the vented approach, outgassing must be limited to prevent ionization breakdown, which implies choice of suitable materials and isolation of all surfaces from contamination during the extended test activities between manufacture and completion of launch.

The choice of high-voltage insulation, modulator circuits, rf duplexing and switching elements, and the detailed mechanization of the monitor and control unit will all depend on the power level of the transmitter. For the lowest power levels, a solid dielectric high-voltage insulation is advantageous. For higher power levels involving increased thermal losses, solid dielectrics are sometimes damaged by differential expansion, and the choice of a gas or an oil dielectric is preferred.

Similarly, a low-duty-cycle single-waveform transmitter using a TWT, klystron, or CFA may efficiently use a line-type cathode modulator, whereas a requirement for waveform flexibility would indicate the use of a tube modulation electrode, such as a mode anode, aperture grid, or shadow grid in combination with appropriate bias and modulation waveform coupling circuits.

Receiver design considerations.—The major element of receiver design for the Space Shuttle is low noise to minimize transmitter power requirements. A plot of noise figure as a function of frequency is shown in figure 5–64 for various solid-state-receiver front-end candidates, including balanced mixers,

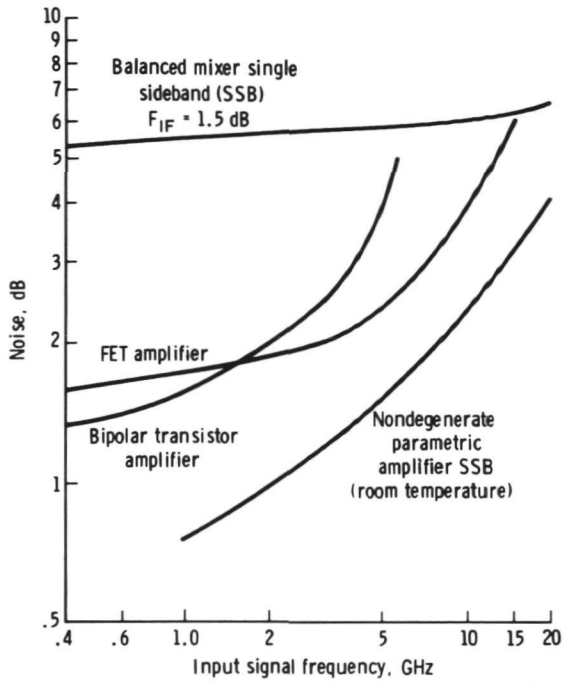

FIGURE 5–64.—Receiver front-end noise performance as a function of frequency.

transistor amplifiers, field-effect transistor (FET) amplifiers, and parametric amplifiers. Although noise figure is an important characteristic to the system designer, other characteristics, such as bandwidth, dynamic range, gain, reliability, and cost, must be considered.

The balanced mixer can be designed and fabricated in almost any form (stripline, waveguide, or microstrip) and can be designed in a single- or double-balanced configuration. Designs vary from 10 percent to multioctave bandwidth. These devices commonly employ Schottky barrier diodes for low noise and high reliability. The dynamic range of the mixer is a function of the diodes and the local oscillator (LO) power level. With local oscillator power in the 10-mW range, the two-dioxide mixer exhibits a 1-dB signal compression at an input level of approximately 3 dBm. It is possible to terminate the image port in the mixer and obtain a 1- to 2-dB noise figure improvement. The penalty is a reduction in bandwidth and a considerable increase in circuit complexity.

Low-noise bipolar transistor amplifiers are relatively simple and can be fabricated in stripline or microstrip. The design techniques are mature; and, with available devices, octave bandwidths are feasible. The gain per stage varies from 20 dB at 400 MHz to 7 dB at 6 GHz. For a 20-dB gain amplifier, 1 dB of gain compression typically occurs at a 5- to 10-dBm output.

Considerable effort is being expended on gallium arsenide (GaAs) FET amplifiers. The noise figures shown on figure 5–64 are presently available in the laboratory; however, commercial devices are available with a 5-dB noise figure and an 8-dB gain at 8 GHz. Amplifiers can be constructed in coaxial or microstrip and are capable of a 10-percent bandwidth. Typically, 1-dB gain compression occurs at a 10-dBm output. Device-reliability data are not presently available.

The parametric amplifier is the most complex of the practical spacecraft front-end candidates, but it offers the lowest noise figure. Amplifiers presently used in airborne radar systems use one or two varactor stages and have signal bandwidths from 3 to 10 percent and gains of 15 to 20 dB. The pump power and frequency requirements depend on operating frequency and required noise figure. Typical levels are 20 to 100 mW in the frequency range from 12 to 50 GHz. The Gunn diode oscillator can easily meet these requirements. The parametric amplifier is further complicated by the necessity for maintaining the temperature at or below room temperature. Typically, 1-dB gain compression occurs at a −35-dBm input power level. The high-level input signals normally are handled by switching the amplifier out of the receive line.

Although complicated, the parametric amplifier continues to be the best choice from a low-noise viewpoint. If an ultra-low-noise figure is not required, the bipolar amplifier is the prime candidate below 6 GHz. Between 1975 and 1979, the FET amplifier will be the prime candidate above approximately 6 GHz if its reliability can be demonstrated.

Exciter design considerations.—The primary function of the exciter is to provide a coherent low-noise drive for the transmitter oscillator (TO) and a receiver LO signal to heterodyne the received target returns to an intermediate frequency. The requirement for a stable centerline with low close-in noise dictates that any generation scheme begin with one or more very-high-frequency (vhf) crystal oscillators.

The exciter configuration also varies depending on the type of pulse compression waveform selected. The tradeoffs involve not only the compression ratio but also the method of generation; that is, analog or digital.

The exciter power-level requirements are determined mainly by the type of transmitter selected. Tube-type systems require approximately a 100-mW range for TO drive and a 20-mW range for LO drive. Power levels as much as 500 mW are required for all solid-state designs. Exciter configurations presently in production vary from the all-varactor multiplier-chain type to the high-frequency up-converter type.

The prime candidate for the proposed radar is the basic up-converter configuration shown in figure 5–65. The stable pump source is typically a Gunn or transistor voltage-controlled oscillator harmonically locked to a vhf crystal oscillator. The reference generator provides the signal to be up-converted, generally at a frequency of two to three times the required output bandwidth. This signal can be programed by a vhf synthesizer to provide frequency hopping. The generator can also be designed to provide active chirp or translate a passive pulse compression waveform. This signal can be gated easily to

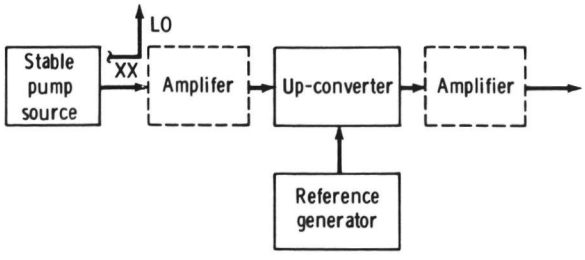

FIGURE 5–65.—Up-converter exciter configuration.

eliminate TO interference on receive. To obtain the required output drive, a Gunn or transistor amplifier must be used either in the pump port or in the output port.

Pulse-compression considerations.—Pulse compression is a means of reducing the peak power required of the transmitter while maintaining the necessary range resolution. Reduction of transmitted peak power has the attendant advantages of lower operating voltages, implying reduced size and weight and increased reliability; and the reduction eases rf breakdown problems throughout the high-power portion of the microwave circuitry. However, peak-power reduction has the disadvantage of having range side lobes that must remain low; otherwise, the background clutter that these side lobes cause will become objectionable.

Pulse-compression technology is highly developed and presents little technical risk in meeting the range of requirements anticipated for the Space Shuttle radar. The available waveforms may be divided into two major categories: (1) analog waveforms of which chirp (linear frequency modulation (FM)) is the most common, and (2) phase-coded waveforms.

The choice of compression ratio is a tradeoff between the desire for low peak transmitted power and the desire to minimize the pulse-compression system complexity.

Range side-lobe performance is another important factor in choosing the compression ratio. Good peak side-lobe performance is difficult to obtain at very low compression ratios ($<13:1$). At high compression ratios, the far-out side lobes cause concern because compressed pulses generally have a side-lobe "plateau," typically 30 to 35 dB below the main lobe, that extends to $\pm\tau$ from the main lobe, where τ is the transmitted pulse width. High-pulse-compression ratios thus lead to a wide plateau and reduced image quality. This phenomenon occurs for both analog chirp and phase-coded waveforms.

Range side-lobe performance: Good range side-lobe performance is required for mapping applications. Typical requirements are that close-in side lobes be 25 dB down from the main lobe and that far-out side lobes be 30 to 35 dB down.

Chirp systems provide good side-lobe performance if frequency weighting is used on receive. A small mismatch loss is incurred (approximately 1.2 dB for 35-dB first side lobes in the absence of errors). The mismatch loss can be eliminated by using nonlinear FM at the expense of increased difficulty in implementation.

Side lobes of phase-coded waveforms depend strongly on the particular code used. Simple-frequency weighting is generally ineffective, but some side-lobe reduction can be obtained by weighting the taps on a tapped-delay line compression filter. As in the case of linear chirp, there is a penalty in signal-to-noise ratio. A tradeoff occurs between implementation complexity and side-lobe performance. Figure 5–66 indicates that binary codes, which have the simplest implementation, have only moderately low side lobes. Polyphase codes have lower side lobes but require more complex implementation.

Reduction of range side lobes in a binary phase-coded system can be effected by transmitting complementary codes on alternate PRF's. In this system, the range side lobes for a zero-Doppler return pulse average to zero. The cancellation is imperfect for

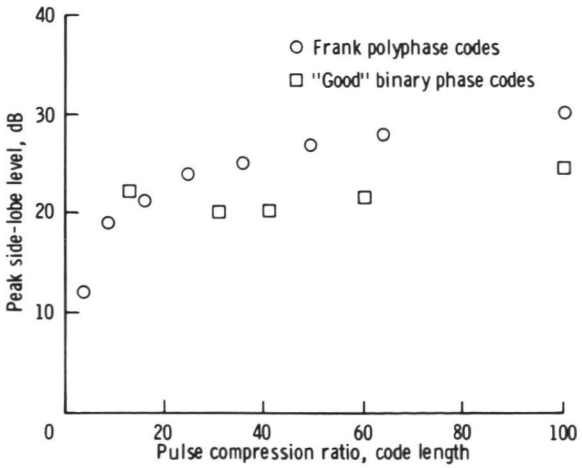

FIGURE 5–66.—Side-lobe levels for phase-coded pulse compression waveforms.

Doppler-shifted targets, but a significant overall improvement in side-lobe level is still obtained.

Generation of the transmitted waveform: The binary phase codes are easiest to generate, requiring only a biphase modulator in the drive signal path to the transmitter. Polyphase codes require a somewhat more complex coder, the complexity depending on the length of the code.

Chirp waveforms can be generated in an analog fashion or in an approximate fashion by using a stepped-phase approximation. In the latter instance, the coder is similar to that used for polyphase codes. Recent studies indicate that the side-lobe performance of the phase-coded approximation is very respectable.

Analog generation is usually somewhat more complex, particularly when frequency agility and coherency are required; polyphase codes are recommended for the Space Shuttle radar system.

COMBINED RAR AND SAR IMAGING

The conventional imaging radar system uses the side-looking geometry. There are other active microwave imaging systems, including the microwave hologram radar and active scanning systems, that can provide imagery from different aspects or look directions.

Down-looking radar systems have a geometry that is identical to that of an IR system or aerial camera. The microwave hologram radar system uses the synthetic aperture technique to realize along-track resolution (refs. 5–12 and 5–13), and crosstrack resolution is obtained by using a phased array antenna (i.e., a real antenna aperture) (refs. 5–14 and 5–15). Microwave hologram radars can be operated in a continuous-wave mode (as compared to pulse transmissions of conventional radars); hence, the range resolution of the conventional radar is replaced by the angular resolution of the phased array antenna. An example of a microwave hologram system is illustrated in figure 5–67 (ref. 5–16). A microwave hologram radar

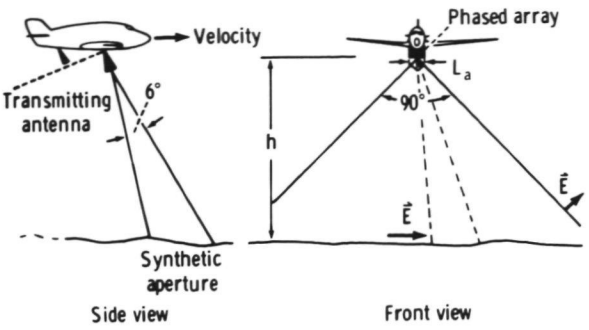

FIGURE 5–67.—Hologram radar geometry (L_a=azimuth length; **E** is the electromagnetic vector).

must be designed for operation at the shortest wavelength possible if fine crosstrack resolution is to be realized.

Basic requirements for the construction of a hologram are that the radiation is sufficiently coherent, that the scattered wavefront received from the image is adequately sampled in two dimensions, and that the sampled wavefront is recorded as wave-transmittance variations on a surface that is an image of the aperture.

Each antenna element has a 90° crosstrack beamwidth (45° each side of vertical when the aircraft is level) and a 6° along-track beamwidth (fig. 5–67). A single transmitting element located behind the receiving array illuminates the terrain. Variations in aircraft velocity are compensated for by varying the velocity of the recording film. This technique was the only motion compensation used in the existing experiment system built by the Environmental Research Institute of Michigan (ERIM).

Both the receiving array and the transmitting antenna are directed forward of the vertical to avoid persistent receiver saturation from very strong specular backscatter signals. The forward squint angle most commonly used has been 12° (a 30° angle was used for one ERIM flight). Backscatter energy from the field of view is compared with a reference frequency in each of the 100 receivers, and the phase-detected outputs are multiplexed into a CRT display which exposes a photographic film. In each dimension, the pattern thus recorded is a hologram

of the microwave frequency "view" from the aircraft. A model of the backscattered microwave signals can be reconstructed with optical waves, which then produces an image of the area viewed.

For nearly vertical viewing, the theoretically achievable resolution in the along-track synthetic aperture direction is given by

$$\rho_x = \frac{\lambda}{4 \sin (\theta/2)} \qquad (5\text{–}27)$$

where θ is the real antenna beamwidth in this direction. Theoretical resolution in the crosstrack phased array direction is given by

$$\rho_y = A \frac{\lambda}{L_a} h \sec^2 \theta_y \qquad (5\text{–}28)$$

where A is a constant of the order of unity that depends on the aperture weighting, L_a is defined in figure 5–67, θ_y is the angle measured from the vertical, and h is the altitude above ground level.

Because the image is three dimensional, direct visual viewing of the relief can theoretically be accomplished. However, because the scaling factors from microwave to light space could not be used in the present experimental system, severe distortions and minor aberrations occur in the reconstructed image. The experimental system does not provide positive indications of terrain relief through use of a mode that causes lines of constant slant range R_1 corresponding to transverse angle θ_1 to appear on the terrain image (fig. 5–68). In this mode, two microwave frequencies are transmitted and the signals from regularly spaced range intervals interfere. The range contour interval is given by

$$\Delta R_c = \frac{c}{2 \Delta f} \qquad (5\text{–}29)$$

where c is the velocity of light and Δf is the difference between the two transmitted frequencies. Slant-range contour lines are not the same as map contour lines. Optical processing for this ranging mode is accomplished in the same manner as for the imaging mode. Radar signal processing can be accomplished by optical or digital-processing techniques.

Similar radar geometry can be realized by

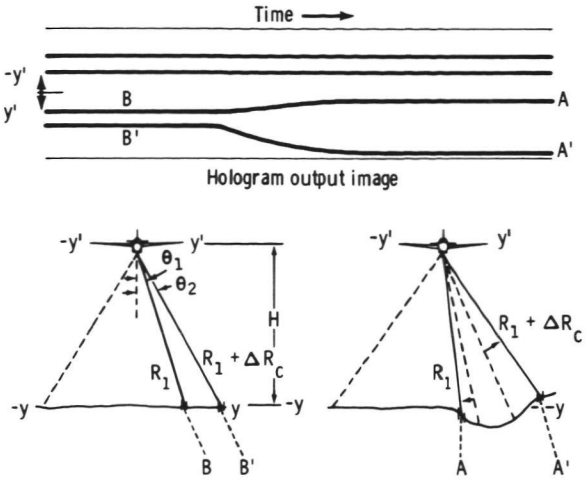

FIGURE 5–68.—Range-contouring geometry for a hologram radar.

using a scanning antenna, scanning in the crosstrack direction and transmitting a pulse-modulated signal to achieve range resolution. Again, the system must be operated at the shortest possible wavelength to realize finest resolution. System designs have been conducted for the application of microwave hologram radars to spacecraft (ref. 5–17).

Examples of imagery obtained from an experimental microwave hologram radar system are given in figures 5–69 and 5–70. The imagery shown in these figures was obtained by using the parameters shown in table 5–XII.

RADAR SCATTEROMETERS

The following two sections present different aspects of the art of radar scatterometry.

TABLE 5–XII.—*Parameters for Illustrated Imagery of a Hologram Radar System*

[See figs. 5–69 and 5–70]

Altitude, m	300
Swath width, m	[a] 600
Frequency, GHz	16.8
Along-track resolution, m	1.5
Crosstrack resolution, m	6
Contour intervals, m	30

[a] 300 m both sides of nadir.

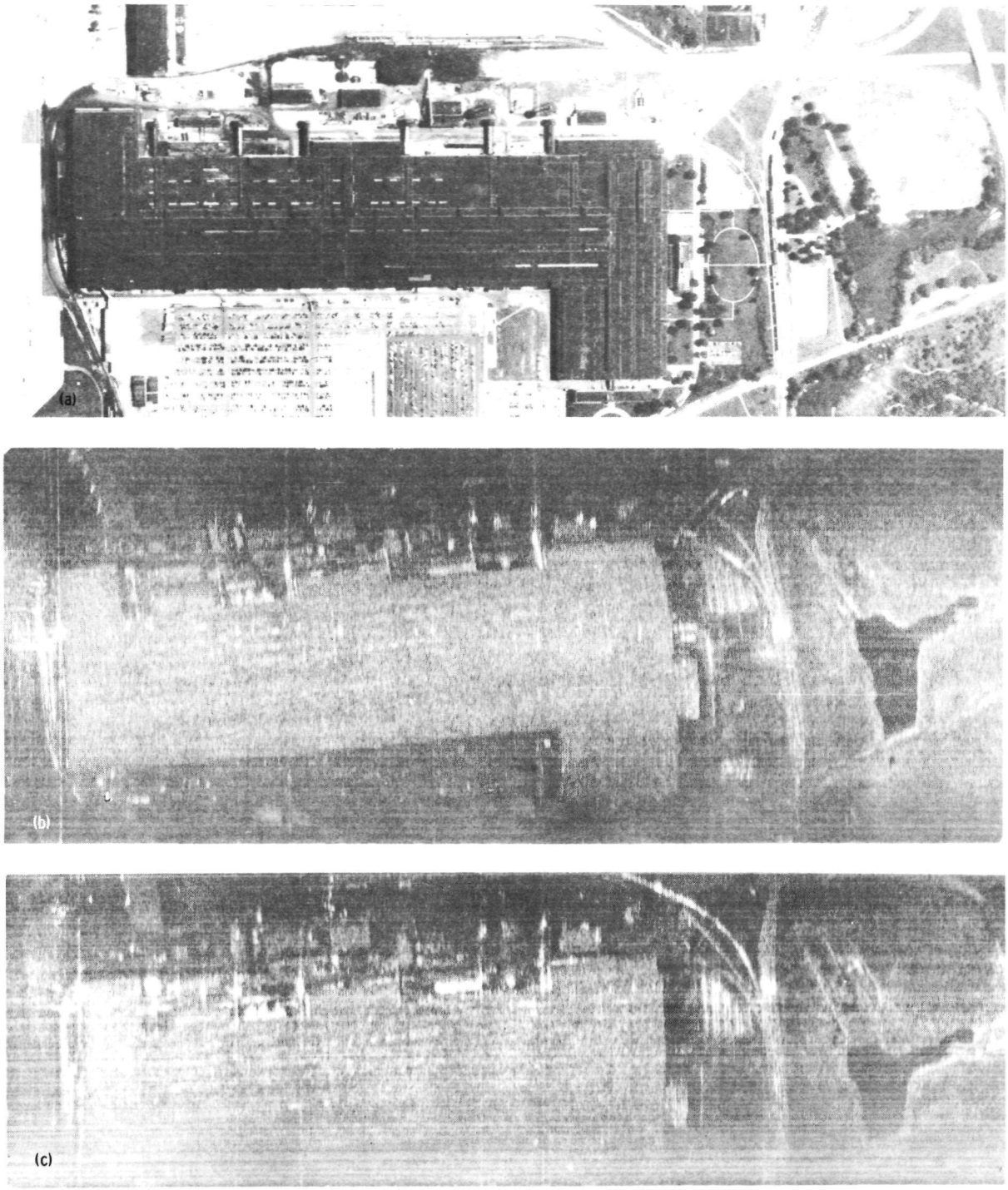

FIGURE 5–69.—Microwave hologram images and a photograph of Willow Run Airport at General Motors Plant. (*a*) Photograph of Willow Run Airport. (*b*) Microwave hologram image of Willow Run Airport; continuous wave operation, 4-mW average power. (*c*) Microwave hologram image of Willow Run Airport; continuous wave operation, 100-mW average power.

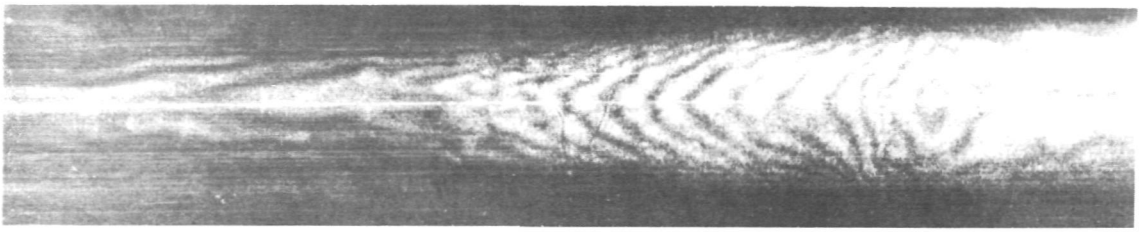

FIGURE 5–70.—Microwave hologram of hill west of Chattanooga, Tenn. (maximum altitude, 520 m; minimum altitude, 300 m).

The first section describes the two basic types of scatterometers, and the second section discusses the different modes of operation and previous experience with radar scatterometers as spacecraft and aircraft sensors.

Radar Scatterometry Design Considerations

Radar measurements have been useful in remote-sensing applications because of the capability to infer from them many characteristics of a target such as range, relative velocity, geometric form, and material composition. A microwave scatterometer is a special-purpose radar used to quantitatively measure only the target reflectance or scattering coefficient. In general, microwave scatterometers are simpler than conventional radars because range and velocity measurement capability and the high spatial resolution (short pulse) requirements are eliminated.

Long-pulse (beam limited) scatterometers have been used to measure the scattering signatures of rough surfaces such as the terrain or the ocean. The quantity of interest is the normalized radar cross section σ°, which is the backscattered power per unit area normalized for antenna gain, range loss, and the transmitted power. In the beam-limited mode, the return in a given range cell comes simultaneously from many scatterers over the entire antenna footprint; therefore, the radar return can be interpreted by using the methods of statistical analysis. To assure antenna-beam-filled conditions, the pulse length τ must satisfy the criterion

$$\tau > \frac{2H\beta}{c \cos \theta_i} \qquad (5\text{–}30)$$

where H is altitude, β is antenna half-power beamwidth (total angle), c is speed of light, and θ_i is surface angle of incidence.

Pencil antenna beam scatterometer.—A simplified block diagram of a microwave scatterometer that uses a narrow-beam antenna is given in figure 5–71. This type of instrument typically operates in a long-pulse or ICW mode (i.e., the receiver is cut off only during the pulse transmission period). The received pulses are shifted in center frequency by the Doppler effect of target and instrument platform motion and have a continuous power spectrum over a finite bandwidth because of the Doppler frequency spread across the antenna footprint. The received signals are down-converted, amplified, narrow-bandpass-filtered, square-law-detected, and integrated.

The normalized radar cross section of the surface can be found from the conventional radar range equation

$$\sigma^\circ = \frac{P_r (4\pi)^3 R_s^4}{P_t G^2 \lambda^2 A} \qquad (5\text{–}31)$$

where P_r is power in return pulse, P_t is

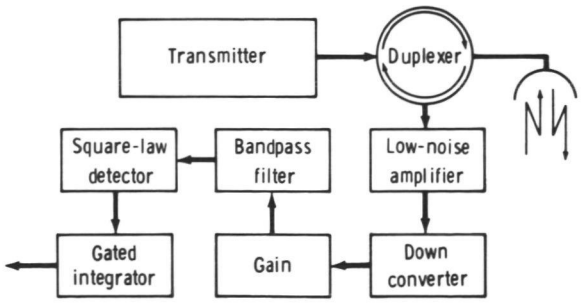

FIGURE 5–71.—Simplified block diagram of a microwave scatterometer that uses a narrow-beam antenna.

power in transmitted pulse, R_s is slant range to illuminated area, λ is free space wavelength, A is effective illuminated area (antenna footprint), and G is antenna gain. For the case of a beam-limited scatterometer at satellite altitudes (where curved Earth effects are important), the normalized radar cross section is

$$\sigma^\circ = \frac{P_r (4\pi)^2 H^2 L_{\text{atm}}^2 \cos\theta_i}{P_t G \lambda^2 (1-k)^2 \cos^2\phi\eta} \qquad (5\text{–}32)$$

where H is satellite altitude, L_{atm} is one-way atmospheric power loss factor, θ_i is Earth incident angle, k is $H(\tan^2\phi)/2R_E$, R_E is Earth radius, ϕ is nadir angle, and η is antenna efficiency $= (G\beta^2)/(4\pi)$. Because of the antenna-beam-filled conditions, the antenna gain appears as the first power, and the altitude (range) is squared; whereas, in the generalized radar range equation, the gain is squared, and range is to the fourth power.

Unfortunately, the output voltage from the square-law detector is corrupted by rectified received antenna noise. A gated ideal integrator is used to average the detector output for several return pulses, yielding a measurement of signal plus noise. This measurement is followed by an integration of noise alone (square-law detector output in the absence of return pulses). The subtraction of these measurements yields an estimate of the received power.

The form of the radar equation appropriate to the design of a scatterometer is

$$(S/N)_{\text{in}} = \frac{P_t G \lambda^2 \sigma^\circ \cos^2\phi\eta}{(4\pi)^2 H^2 \cos\theta_i L_{\text{atm}}^2 L_s^2 K T_s B_{\text{if}}} \qquad (5\text{–}33)$$

where $(S/N)_{\text{in}}$ is input signal-to-noise ratio, L_s is system power loss factor, k is Boltzmann constant, T_s is system noise temperature, and B_{if} is predetection intermediate frequency bandwidth. The precision of the scatterometer measurement is

$$\frac{\Delta\sigma^\circ}{\sigma^\circ} \approx \left[\frac{1}{B_{\text{if}}\tau_{s+n}}\left(1+\frac{1}{(S/N)_{\text{in}}}\right)^2 + \frac{1}{B_{\text{if}}\tau_n}\left(\frac{1}{(S/N)_{\text{in}}}\right)^2\right]^{1/2} \qquad (5\text{–}34)$$

where $\Delta\sigma^\circ/\sigma^\circ$ is normalized standard deviation in measuring σ°, τ_{s+n} is total integration time of noise-contaminated signal, and τ_n is total integration time for noise alone.

Figure 5–72 is a plot of $\Delta\sigma^\circ/\sigma^\circ$ as a function of $(S/N)_{\text{in}}$ for various integration times, where τ_{s+n} is assumed equal to τ_n. The intermediate frequency bandwidth B_{if} is 11 kHz and is assumed to be approximately the Doppler spread and equal for the "signal-plus-noise" and "noise-alone" measurements. A sufficient integration yields good measurement standard deviations for negative $(S/N)_{\text{in}}$.

A sample link calculation for a typical high-inclination-orbit satellite is given in the section entitled "A Shuttle Radar Microwave Subsystem for Earth Resources Applications." The total transmit/receive cycle is assumed to be 21 msec (PRF of approximately 47 pulses/sec) with an idealized 33.3-percent transmitter duty cycle. The integration time required for the σ° measurement was based on $\sigma^\circ_{\text{min}} = -30$ dB and on $\Delta\sigma^\circ/\sigma^\circ = 50$ percent. Because the signal-plus-noise integration period is 33.3 percent of the transmit/receive cycle, the required measurement time t_m is equal to 3τ. For applications in which large ground coverage is required, the maximum allowable measurement (integration) time is based on the antenna slew rate and the allowable smear (caused by platform motion) of the antenna footprint.

Fan-beam antenna scatterometer.—The operation of a fan-beam antenna microwave scatterometer is equivalent to several simultaneous pencil-beam systems. The effective multiple pencil-beam operation is achieved by filtering the Doppler-shifted radar return to subdivide the broad beam into an arbitrary number of resolution cells. A simplified block diagram is shown in figure 5–73. The system is beam limited in each Doppler cell, although it may not be beam limited simultaneously over the entire fan beam. Because of differences in slant range across the antenna footprint, separate range gates are required for each channel.

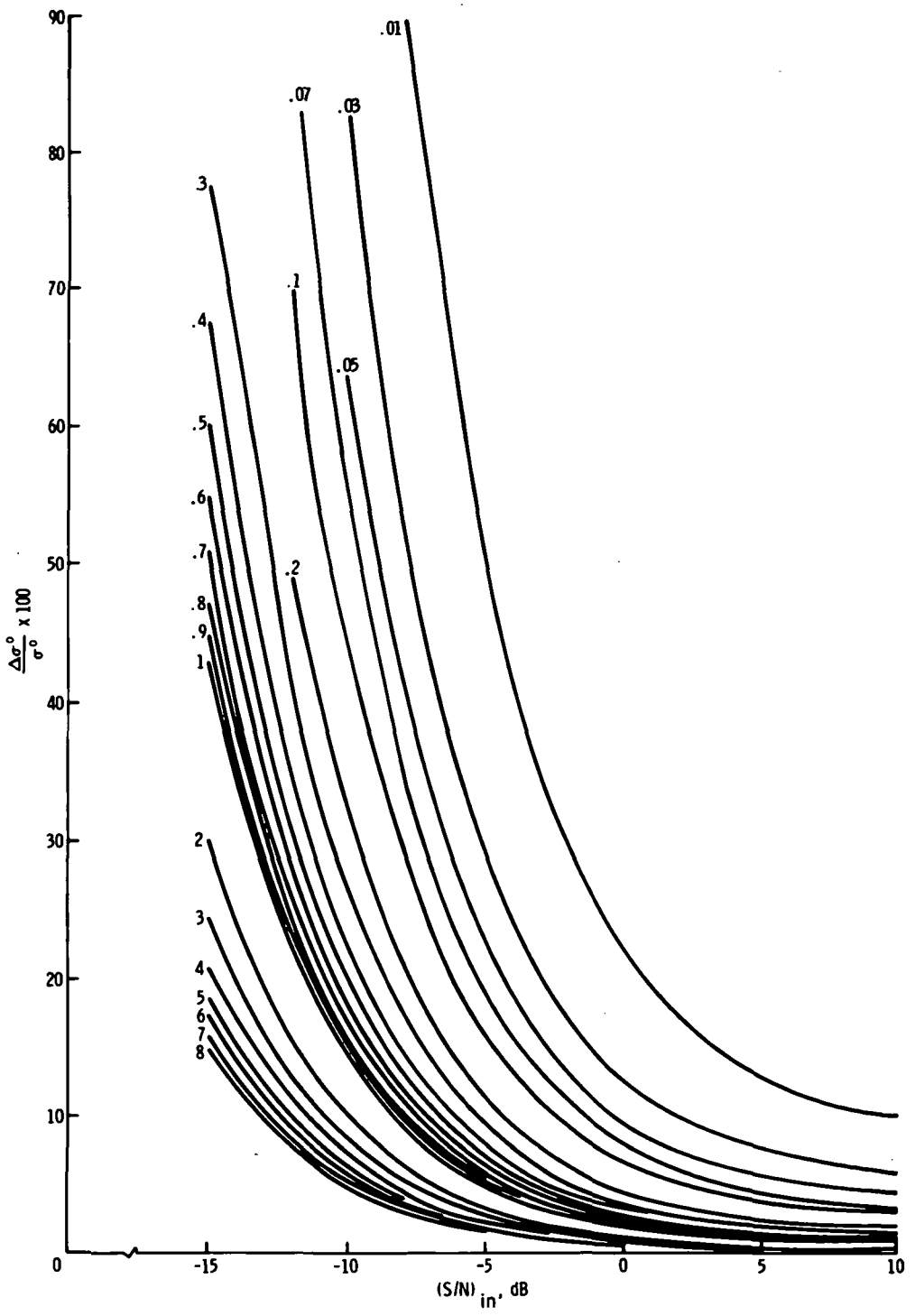

FIGURE 5-72.—Plot of $\Delta\sigma^\circ/\sigma^\circ$ as a function of $(S/N)_{in}$ for integration times indicated; τ_{est} is assumed equal to τ_n; the intermediate frequency bandwidth B_{if} equals 11 kHz and is assumed to be approximately the Doppler spread.

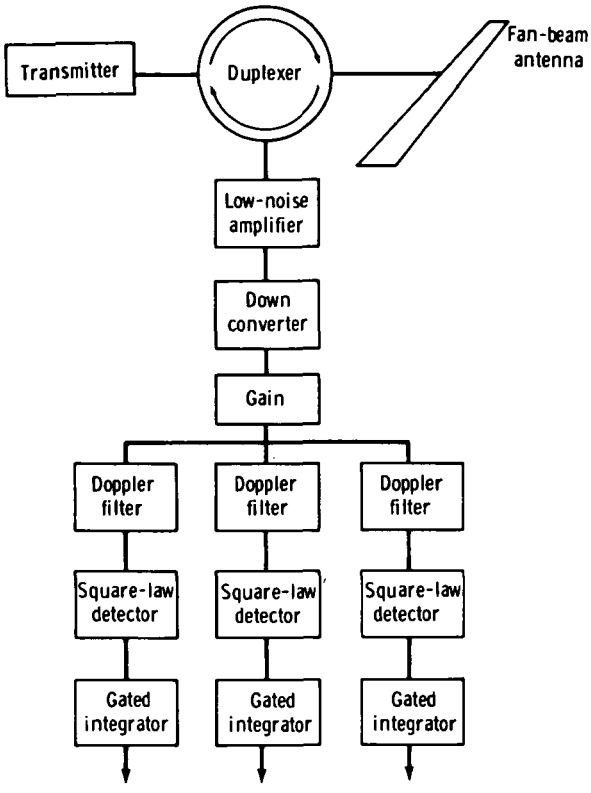

FIGURE 5–73.—Simplified block diagram of a fan-beam microwave scatterometer.

The equations used for this scatterometer are essentially identical to those used for the pencil-beam instrument. However, corrections must be made for differences in slant range, antenna gain, and effective beamwidth for each fan-beam receiver channel. Because of the multibeam aspects of the fan-beam instrument, the equivalent ground coverage (relative to a pencil-beam scatterometer) can be achieved with lower antenna slew rates, and, in some instances, without slewing the antenna at all. This characteristic results in longer available integration times and, thus, lower transmitter power requirements. However, the increase in transmitter power to compensate for the loss in the fan-beam antenna gain is greater than the savings. The system parameters for a satellite fan-beam scatterometer (to give the equivalent performance as the pencil-beam system described earlier) are P_t of 125 W, PRF of 74 pulse/sec, number of Doppler channels is 20, and antenna beamwidth is 0.5° by 20°.

Radar Scatterometry Applications

Radars capable of measuring backscattering cross sections from ocean or land have been generally referred to as scatterometers (ref. 5–18). Such systems may use continuous wave (CW) signals with or without Doppler processing or FM and pulse techniques.

A CW scatterometer depends on its antenna to distinguish among returns from various angles. The capability of radar to separate returns from different ranges can be used advantageously together with directive antenna beams to simplify the scattering measurements (ref. 5–19). A fan beam can be used to illuminate a narrow strip along the ground, and the range resolution permits separation of signals from different angles.

Another way to measure a scattering coefficient is to use Doppler bandwidths corresponding to a resolution cell on the ground. In such systems, a CW signal is transmitted. Contractors have built CW Doppler radars for various NASA programs (refs. 5–20 to 5–22).

The 0.4-GHz scatterometer and the 13.3-GHz scatterometer are similar. In both systems, a fan-shaped beam (fig. 5–74) il-

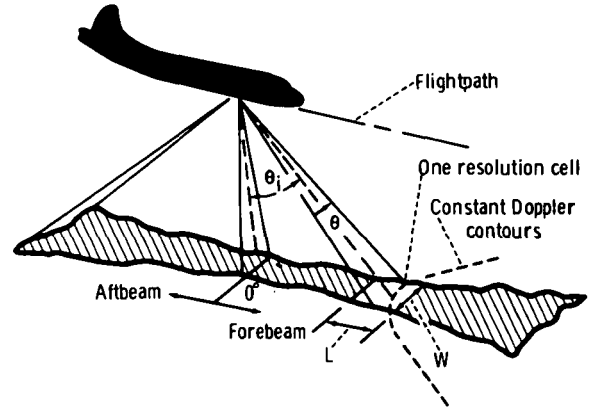

FIGURE 5–74.—The 13.3-GHz scatterometer resolution cell geometry; θ is radar beamwidth, θ_i is incidence angle, L is resolution cell length, and W is resolution cell width or $f(h, \theta_i, \theta)$.

luminates the ground. Doppler frequencies are used in digital processing to separate returns from various resolution cells. In the 0.4-GHz scatterometer, an intermediate frequency is used to record returns from $-60°$ to $60°$ on a positive frequency axis. However, in the 13.3-GHz scatterometer, a zero intermediate frequency is used, and returns corresponding to fore-and-aft beams are separated by using a sign-sensing technique. In this section, the details of the 13.3-GHz NASA aircraft scatterometer and the Skylab S193 13.9-GHz scatterometer are discussed. This discussion concludes with future hardware recommendations.

The NASA Lyndon B. Johnson Space Center 13.3-GHz scatterometer.—A circuit diagram of the 13.3-GHz system is shown in figure 5–75. The microwave energy is radiated by an antenna that has wide fore-and-aft beams and a narrow transverse beam. The returned energy may be separated using the Doppler equation as a function of incident angle:

$$f_d = \frac{2v}{\lambda} \sin \theta_i \qquad (5\text{–}35)$$

where f_d is Doppler frequency, v is aircraft ground velocity, λ is wavelength of the transmitted power, and θ_i is angle of incidence.

The returned energy is received simultaneously from all incident angles and is divided equally into two channels, one of which is 90° out of phase with the other. The data for each channel, detected by a direct-to-audio technique, are amplified and recorded on an FM tape recorder. The fore-and-aft-beam data are separated by use of a sign-sensing technique. To calibrate the system, a ferrite modulator is used to provide an absolute power reference level of the transmitted signal. The $\sigma°$ as a function of θ_i information is obtained by subtracting known system losses and aircraft altitude and velocity factors and by comparing the remainder with a reference signal level.

Skylab S193 radiometer/scatterometer.—The Skylab S193 radiometer/scatterometer (RADSCAT) sensor consists of a combina-

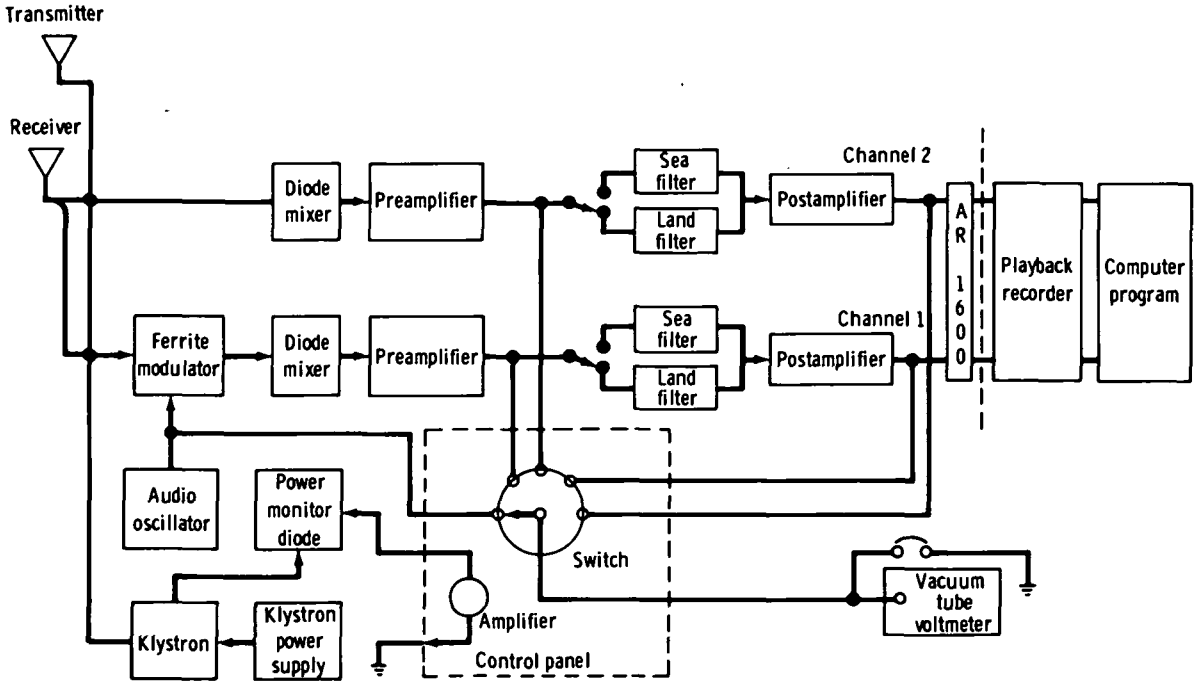

FIGURE 5–75.—Block diagram of 13.3-GHz scatterometer system.

tion of active and passive microwave sensors designed to perform scientific experiments to study the Earth from space.

The radiometer measures the radiometric brightness temperature from areas on the surface of the Earth as a function of incident angle in the interval of frequencies from 13.8 to 14.0 GHz. The mean value of the thermal noise signal of the Earth is compared to the measured mean noise signal of two known temperature sources to yield a precise measurement of the emission temperature of the resolution cell of the Earth. The brightness temperatures for both vertical and horizontal polarizations can be measured with the Skylab S193 radiometer.

The scatterometer measures the backscattering cross sections of an illuminated area on the Earth. The incident energy can be radiated with horizontal or vertical polarization. Corresponding to each incident polarization, both vertically and horizontally polarized backscattered energy can be measured. The angles of incidence range from 0° to 52°.

The radiometer and scatterometer can operate both jointly and separately in various scanning and polarization modes. A summary of these modes follows.

In-track noncontiguous mode: The in-track noncontiguous (ITNC) mode is used for a joint radiometer and scatterometer operation. In this mode, only the pitch angle is varied. A resolution cell on the ground (fig. 5–76) is seen by the radiometer and

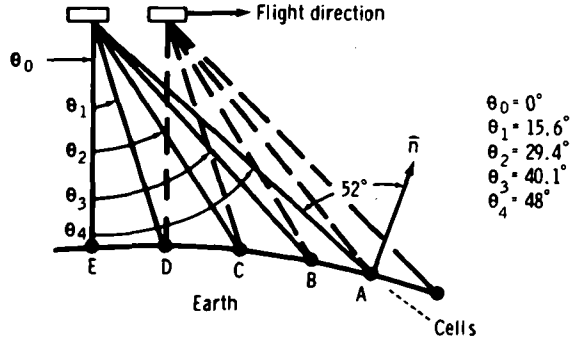

FIGURE 5–76.—The RADSCAT ITNC scanning mode with varied pitch angle θ; **n** is local vertical vector.

scatterometer at approximately the following pitch angles: 0°, 15.6°, 29.4°, 40.1°, and 48°.

During each dwell at a given pitch angle, the following measurements are taken:

1. Scatterometer data with vertical transmit/vertical receive (VV), horizontal transmit/horizontal receive (HH), vertical transmit/horizontal receive (VH), and horizontal transmit/vertical receive (HV) polarizations.
2. Radiometer and noise data with vertical and horizontal polarizations.
3. Radiometer reference voltages (R_1 for calibration and R_2 as baseline).

The measurement sequences are shown in figure 5–77. In this mode, the roll angle is always zero.

Crosstrack noncontiguous mode: In the crosstrack noncontiguous (CTNC) mode, the roll angle is varied identically to the ITNC mode, and the pitch angle remains zero. The motion of the field of view is shown in figure 5–78, in which individual cells are viewed from only one antenna position. Because of the motion of the antenna in the pitch direction, the cells lie on a curved arc. As shown in the figure, there are three forms of this mode: left scan, right scan, and left/right scan. The outermost cell is viewed at approximately 52° (corresponding to a 48° gimbal angle), and the innermost cell, at approximately 0° at all times.

The sequence of measurements is shown in figure 5–77. Only combined RADSCAT data can be gathered in the CTNC mode. In the sequence mode, data for all polarization combinations are gathered automatically for radiometer and scatterometer systems.

In-track contiguous mode: The pattern of the in-track contiguous (ITC) scanning mode (fig. 5–79) is similar to the ITNC mode, except that the antenna is scanned much faster and no dwell occurs at any antenna pitch angle. The entire in-flight path is eventually scanned at all incident angles with this process.

The scan cycle time is chosen so that at the vehicle velocity, the resolution cell at inci-

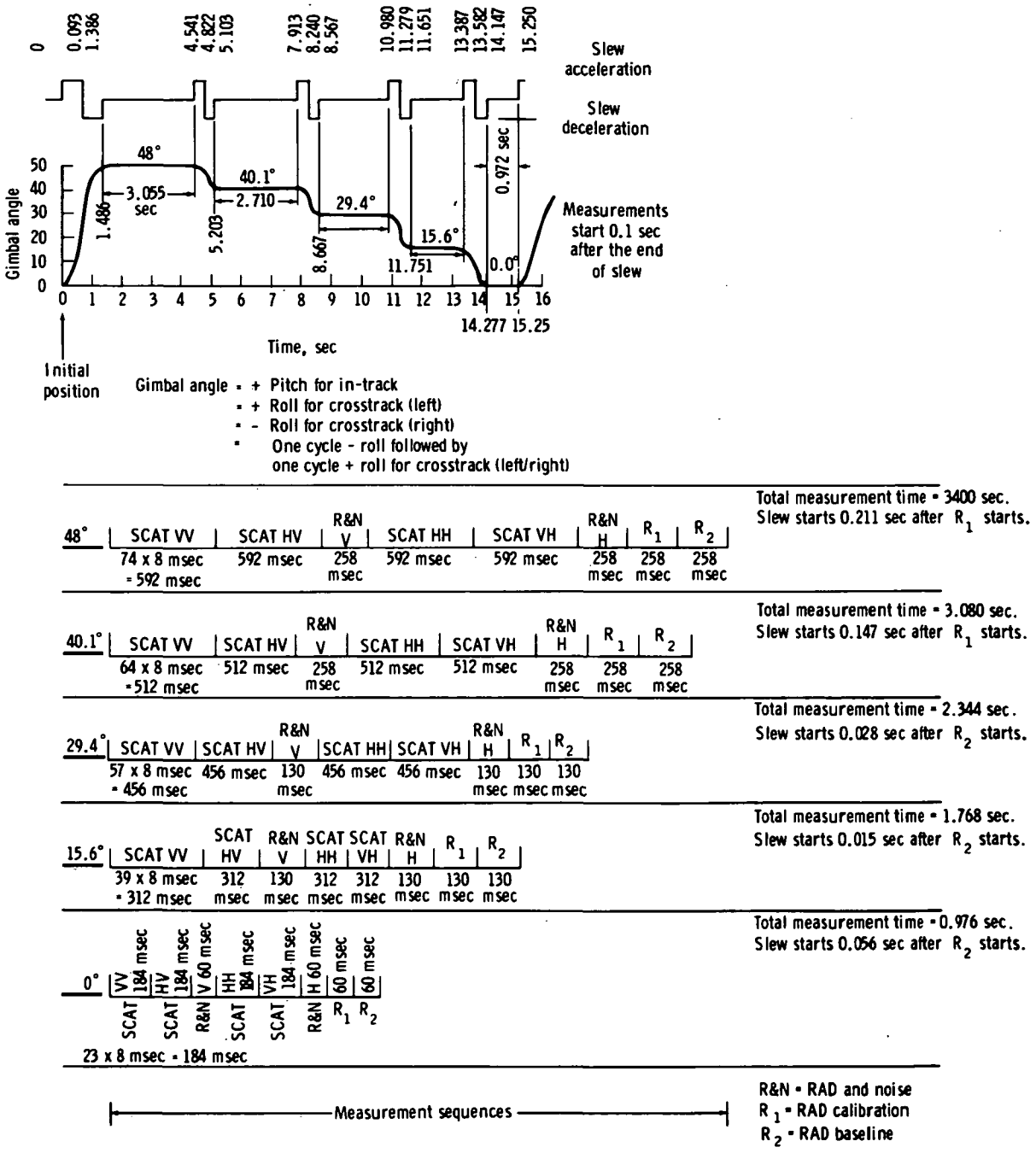

FIGURE 5–77.—Measurement sequence for ITNC and CTNC modes.

dent angle 48° overlaps the previous cell by approximately 25 percent; the 40.1° cell overlaps its predecessor by less than 20 percent, and so forth. At the 0° incident angle, gapping rather than overlap occurs. The measurement sequence is explained in figure 5–80.

The radiometer data are taken during skew periods between two pitch angles corresponding to scatterometer data angles. In

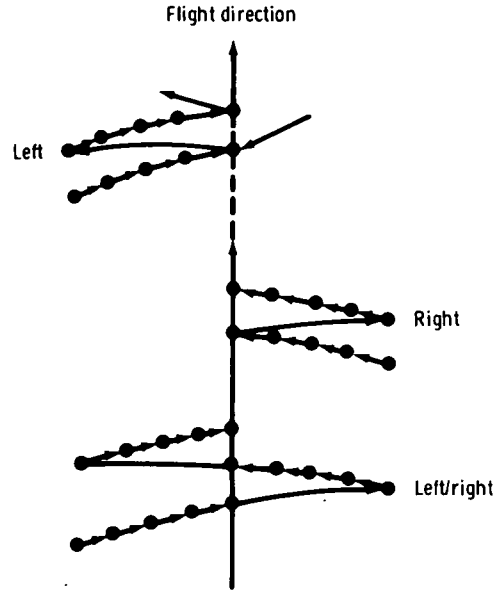

FIGURE 5–78.—Motion of the field of view, CTNC mode.

this mode during a given pass, only one transmitted polarization can be chosen. Data corresponding to the vertical or horizontal polarization are received. As the vehicle progresses on successive scans, the entire path is viewed at 48° and less, except for gapping at the low angles.

Crosstrack contiguous mode: The crosstrack contiguous (CTC) mode contains the following three submodes:

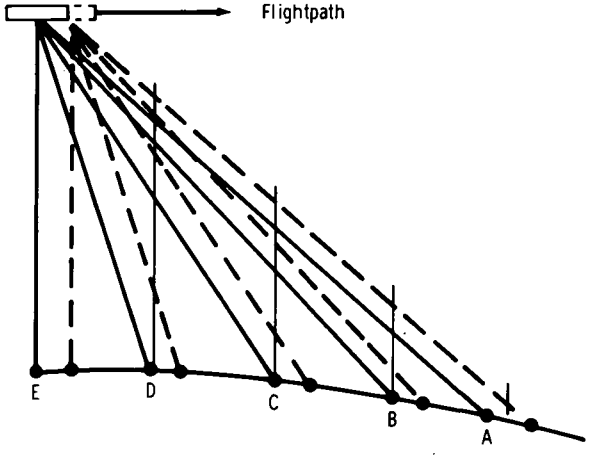

FIGURE 5–79.—The ITC mode.

1. The RADSCAT: In this submode, the astronaut can select one in-phase polarization pair, VV or HH.

2. Radiometer: In this submode, data corresponding to vertical and horizontal polarization are recorded.

3. Scatterometer: In this submode, data for. VV and HH polarization combinations are recorded.

The CTC mode provides a side-to-side linear scan covering ±11.375°. As indicated in figure 5–81, the CTC is a mapping mode. To compensate for the satellite forward velocity, which could cause skewing of the pattern perpendicular to the flightpath, the pitch gimbal is scanned slightly backward as the roll angle oscillates between its limits. Measurements are made for every 1.896° of beam center motion, ranging from −11.375° to 11.375° in roll. The measurement times and sequences are shown in figure 5–82. The pitch offset angles for this mode can be chosen as incident angles of 0°, 15.6°, 29.4°, or 40.1°.

Future research and development.—The performance of NASA 13.3- and 13.9-GHz RADSCAT scatterometers has been fully demonstrated by aircraft and Skylab missions. However, these systems were basically experimental in nature. These programs have indicated a need for improving both hardware and software capabilities. Procedures for collecting the data should be revised for an operational system. The following research and development are recommended:

Improved radar calibration techniques: A calibration period should follow each data-collection period. The frequency of these calibrations will depend on the performance of the system. Some technique of external calibration should be adopted. Corner reflectors over smooth deterministic targets can be used for airborne and spaceborne scatterometers. Internal calibrations are undesirable because they do not involve all paths that the actual returned energy traverses.

Improved systems design: Improvements

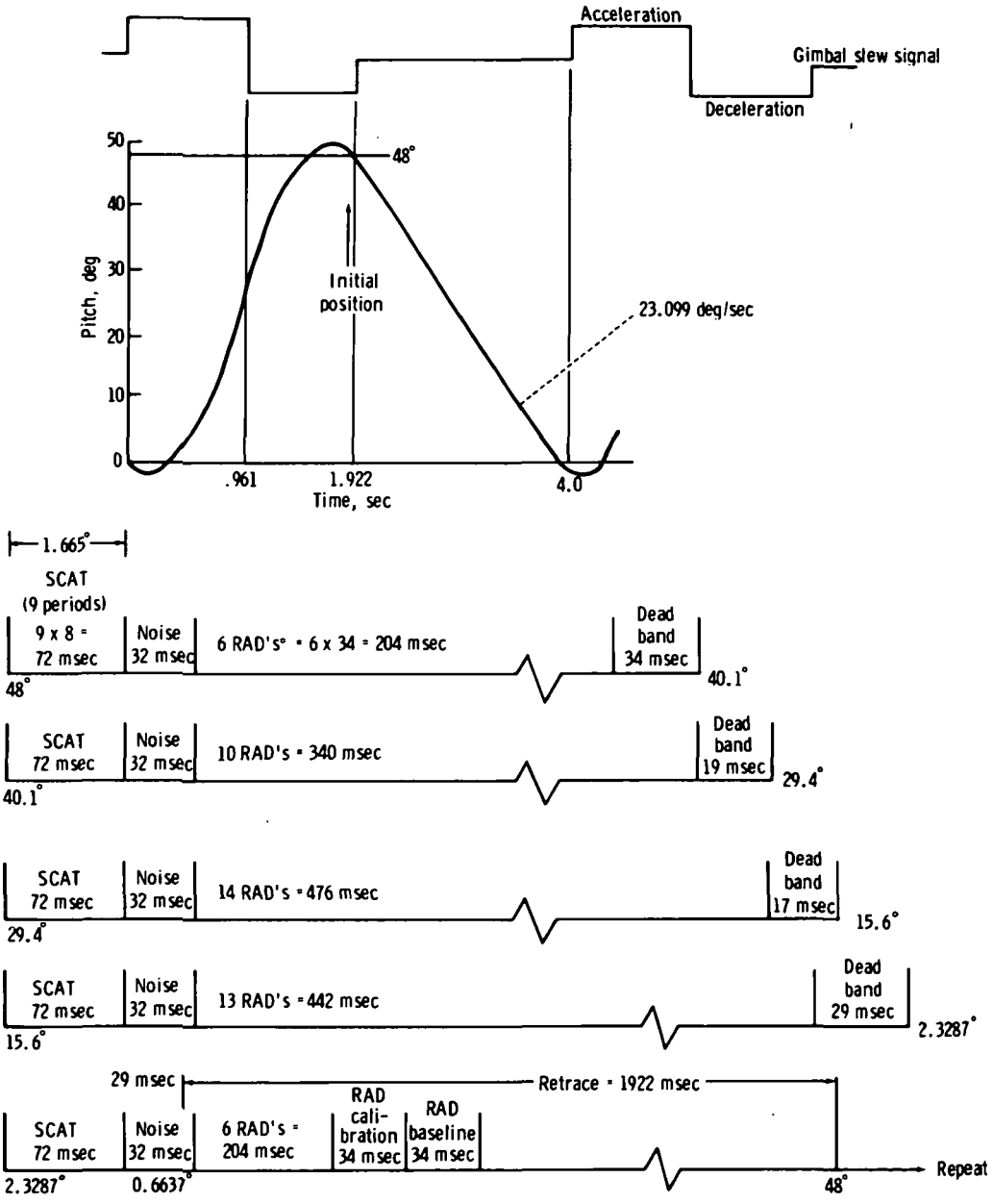

One selected polarization pair from VV, VH, HV, and HH (Example: HV means: SCAT transmit = H; SCAT receive and SCAT noise and RAD = V).
*Each radar measurement period is 32 msec plus 2 msec readout.

FIGURE 5–80.—Measurement sequence for the ITC mode.

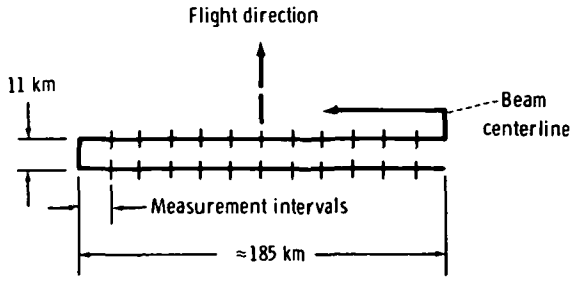

FIGURE 5–81.—The CTC mode.

are needed in the reliability of the antenna gimbaling, switching logic, and polarization isolation. System drifts, resolution, and noise-level fluctuations have to be reduced in future airborne and spaceborne systems.

Data-processing techniques: For operational systems, highly efficient data-processing techniques are needed; no reliable data-display techniques have been advanced to date. Onboard processing of data should be explored, and the digitally processed data should be color coded to display ocean winds and waves for visual interpretation and use. These programs should be capable of handling large volumes of reflectivity data and displaying these data on a world map.

Calibration data measurements: For spaceborne and airborne instruments, the calibration data corresponding to each subsystem are usually measured in the laboratory. The amplifier, mixer, and filter gains are some examples. For instruments flown for extended periods, these internal gains change. To alleviate this problem, automatic calibration modes should be designed to check all calibration data needed to calculate backscattering cross sections from raw data.

Applicability.—Multifrequency, multipolarization scatterometers can be used to measure winds and waves at the surface of the ocean and to detect development and progress of storms. These surface measurements can be used to predict weather and to forecast storm developments. Sea-state forecasting will aid in the navigation and routing of ships.

SUBSURFACE SOUNDERS

This section is concerned with airborne or spaceborne electromagnetic systems used to detect subsurface features.

The skin depth of a wave propagating into the ground, defined as the depth at which the electromagnetic field decays to e^{-1} of its value at the surface, is given by

$$\delta = \left(\frac{2\rho}{\mu_0 \omega}\right)^{1/2} \qquad (5\text{–}36)$$

where ρ is resistivity of the ground material (ohm-m), μ_0 is magnetic permeability of free space (H/m), ω is angular frequency $=2\pi f$, and f is frequency of the electromagnetic wave (Hz). Resistivities for normal ground rank between 10 ohm-m for clay soil to 3000 ohm-m for gravel and rock (ref. 5–23). To sound such ground to any appreciable depth, very low frequency (vlf) will have to be used. At 10 kHz, a skin depth of approximately 15 m will result for a ground with a 10-ohm-m resistivity, for example. With a resistivity of 1000 ohm-m, the corresponding skin depth is 150 m. At a frequency of 100 MHz, the skin depths are 0.15 and 1.5 m for the same resistivities.

The resistivities vary with the content of water and with the temperature. In permafrost regions, the ice contained in the ground may cause resistivities of approximately 100 000 ohm-m.

Radio-Wave Method

Soundings at a vlf with active devices are impractical because of interference from radio transmitters with signals that are propagated over very long distances along the surface of the Earth. However, one may take advantage of these vlf signals for investigation of subsurface features by using the so-called wave-tilt method. At a given position at the ground (fig. 5–83), the vertically polarized radio surface wave radiated from a vlf station may be resolved into the three components shown. The ratio between the longitudinal and the vertical electrical components is the wave tilt, which is dependent on the resistivity of the ground.

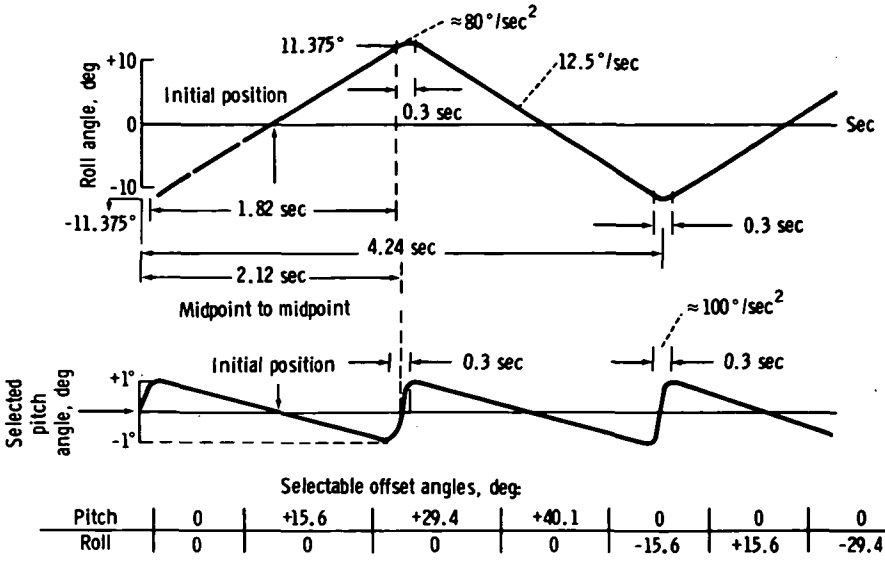

Selectable offset angles, deg:

Pitch	0	+15.6	+29.4	+40.1	0	0	0	0
Roll	0	0	0	0	-15.6	+15.6	-29.4	+29.4

Scan-measurement pattern:

Twelve measurement periods (M1 to M12) of 151.5 msec each. The same measurement sequence in each.
Beam center roll motion per measurement = 1.896°.

Measurement 151.5 msec		Total beam center angular measurement excursion = 22.75°											
		M1	M2	M3	M4	M5	M6	M7	M8	M9	M10	M11	M12
Beam center motion = K x 1.896°	From: K =	±6	±5	±4	±3	±2	±1	0	±1	±2	±3	±4	±5
	To: K =	±5	±4	±3	±2	±1	0	±1	±2	±3	±4	±5	±6

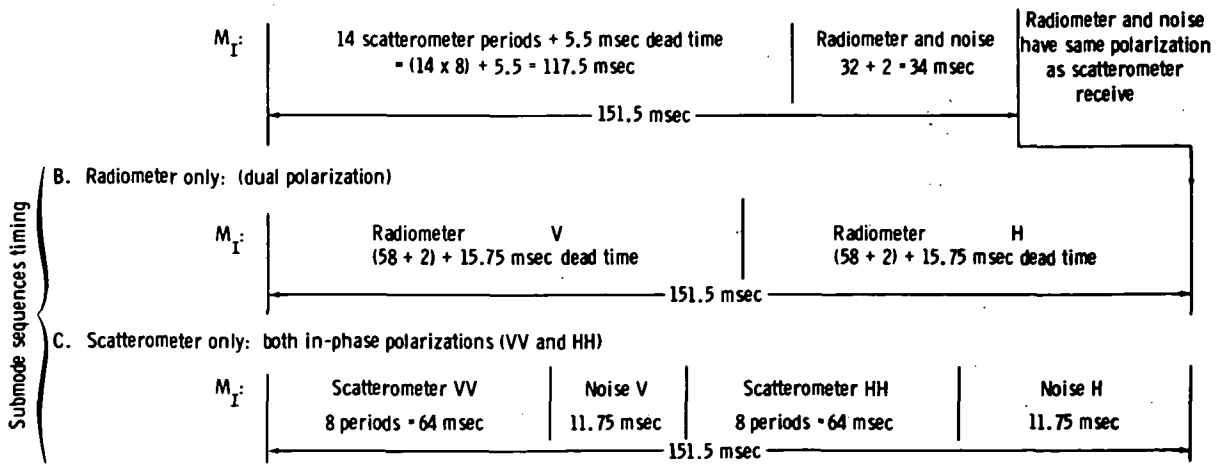

FIGURE 5-82.—Measurement sequences for the CTC mode.

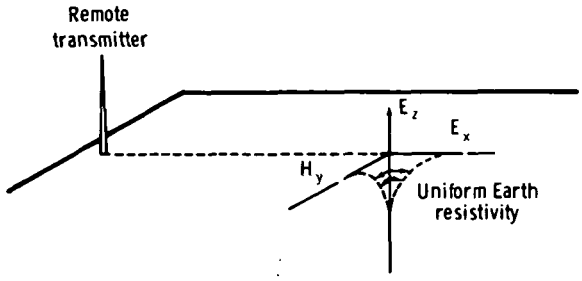

FIGURE 5–83.—Electromagnetic field components of a vertically polarized radio surface wave.

If the ground consists of layers of different resistivity, which will be penetrated by the radio wave, the layering will be reflected in the wave tilt. In simple cases in which the ground consists of two or three horizontal layers, the inverse problem may be solved eventually by using the signals from two radio stations.

Measurements may be carried out at ground level with a dipole that can be turned about a horizontal axis so that the actual wave tilt (approximately a few degrees from vertical) may be determined. Measurements may also be conducted from a low-flying aircraft using the so-called E-phase system. This system is based on the fact that the wave tilt $W=E_x/E_z$ has equal in-phase and quadrature-phase components. The E_x and E_z components are measured with two short dipole antennas, one horizontal and one vertical. Aircraft roll causes leakage of E_z into the horizontal antenna, but this signal is in phase. Therefore, by measuring the quadrature-phase component of W, errors caused by leakage are avoided.

The airborne measurements are conducted by flying approximately 60 m above the ground. The wave tilt is a local effect; that is, when passing a boundary between two regions with different resistivity, the wave tilt changes almost abruptly when measured at ground level. At heights over the ground, an "integration" effect occurs so that the change in wave tilt is smoothed out. To obtain a good resolution, the measuring height should be as low as possible. A resolution of approximately 25 m is obtained when measured at a height of approximately 60 m over the terrain.

In an existing system, the various signals of importance for computing the wave tilt, as well as an altimeter signal, are recorded on analog and magnetic tape recorders operated during the flight along lines in the terrain. A flightpath camera eases identification of the data relative to existing maps. Data reduction is conducted after completion of the flights.

The method of wave-tilt measurement based on the in-phase and the quadrature-phase components is valid only if conductive currents in the ground dominate over displacement currents; that is, low-resistivity ground. When conductive currents are not dominant, the true sensitivity can often be computed, although this computation requires some knowledge of the ground.

Two-Antenna Method

Another method of measuring the ground resistivity, which is the reciprocal of the conductivity, is to measure the change in coupling between two antennas caused by the influence of the ground.

The two antennas are small loops (magnetic dipoles) mounted 3 m apart in each end of a dielectric rod. The rod is held parallel to the ground with the loops at 45° to horizontal. One loop is used for transmitting and the other for reception at a low frequency. Far from the ground, the coupling signal between the two antennas is phased out. At low heights over the ground, the transmitted signal causes currents in the conductive ground, and these currents produce a signal at the receiver output. The conductance of the ground directly under the horizontal rod can be determined by computation.

In principle, the conductivity of two horizontal layers may be determined by measurements at more than one frequency. The measurements are conducted from a helicopter; to avoid the influence of the helicopter, the antenna rod is extended far under the vehicle. The height of the rod over the ground should be as low as feasible—60 m,

for example—because this technique also is relying on a local effect. The resolution is approximately 25 m and is of particular application for conducting ore detection.

Radio Echo Sounding

Because of the interference problem, sounding at a vlf, which permits penetration to appreciable depths, seems impractical. At vhf, that is, at frequencies above 30 MHz, the interference problem may be of minor importance in remote areas, but the absorption in the ground is very large; therefore, only moderate depths are reached. For example, at 100 MHz, silty clay soil with a water content of 15 percent (weight) gives an absorption of 2.5 dBm (ref. 5–24); thus, a system with a large system sensitivity (ratio between transmitted power and minimum detectable power) is required to reach appreciable depths. With an existing pulse radar system, a layer with a reflection coefficient of −10 dB should be observable at a depth of approximately 20 m. However, the reflection of the surface is, in this case, large (−3.5 dB); therefore, the received surface pulse becomes very large and tends to saturate the receiver so that near-surface reflecting interfaces may not be detectable.

The radio echo sounding method seems useful for detection of reflecting interfaces only in special cases over ground with small losses. Examples are polar ice (i.e., glaciers in polar regions and the inland ice in Greenland and Antarctica), areas of permafrost (although presence of unfrozen water may give high attenuation), some desert areas (except in cases where the content of salt is appreciable), and lunar soil and rock.

Simple radar systems have been designed for radio echo sounding of polar ice at several frequencies below 500 MHz. The systems rely on the facts that the absorption in the ice is very low (0.02 dBm at 253 K) and that the radio wave velocity V is independent of the ice temperature (until 273.25 K) and pressure ($V=169$ m/μsec, since $\epsilon=3.2$). The systems are used for airborne measurement of the thickness of icecaps and for detection of stratifications in the ice, which establish horizons in the ice and give information about the flow pattern of ice.

Typical airborne systems operate at 60 and 300 MHz and are flown simultaneously 300 to 1000 m over the surface of the ice (ref. 5–25). The principle of the measuring system is shown in figure 5–84, which illustrates a standard pulse radar system with a dipole antenna array mounted under the wing of the aircraft. The received echoes are displayed on an A-scope (real presentation of the video signal) and on a Z-scope (intensity modulated presentation). Both oscilloscopes are photographed, the A-scope intermittently and the Z-scope by a continuous moving film. The latter gives continuous profiles for each flight line. For position identification, the films are supplied with time marks that relate to marks on the recording of the inertial navigation data.

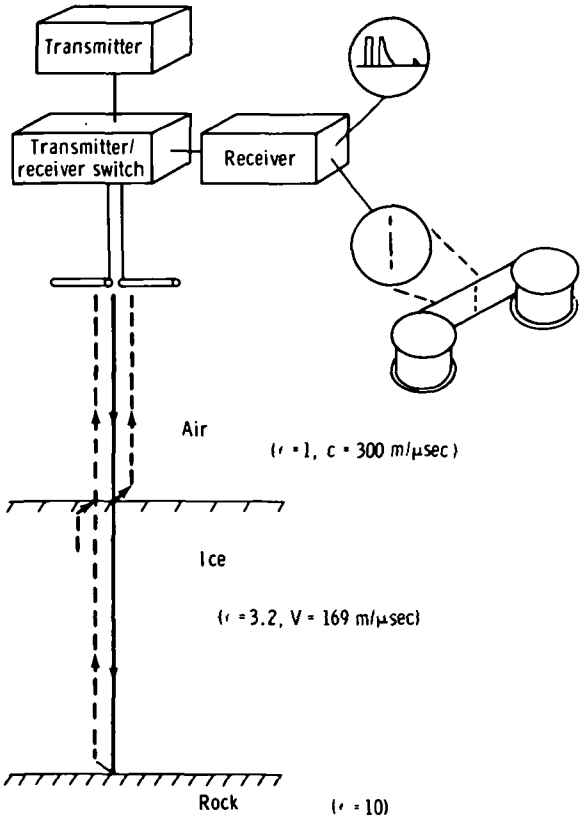

FIGURE 5–84.—Operational diagram of a radio echo sounder.

The system at 60 MHz is able to detect bedrock echoes in the greater part of the ice sheets in Greenland and Antarctica; that is, through more than 4500 m of ice. Stratification echoes have been detected down to approximately 3000 m below the surface, but this performance is dependent on the ice temperature (losses are temperature dependent). The vertical resolution relies on the pulse width. With the shortest pulse (60 μsec), a resolution of 6 m is obtained. In areas with thick ice in which the total absorption is large, a wide pulse (1 μsec) and corresponding narrow bandwidth (1 MHz) are used, giving a resolution of 100 m. In the other directions, the resolution is determined with the antenna radiation pattern. At 60 MHz, the antenna is a linear array of four dipoles mounted transverse to the flight direction. Therefore, good resolution is obtained transverse to the flight direction, whereas the longitudinal resolution is relatively poor, although refraction effects in the surface improve the situation. Because of the large radiation fore and aft, the bedrock features are generally represented by hyperbolas. A computer technique exists to correct for this effect. At 300 MHz, this effect virtually does not exist because a rectangular array of four dipole (backfire) antennas is used. However, this system is less sensitive and is designed for measurement over shallow ice only.

An improved version of ice-sounding radar is presently being tested. With an increase of the system sensitivity (increased transmitter power) and an introduction of a pulse compression technique, a vertical resolution of approximately 10 m should be obtained at all depths.

In several instances, the attempt has been made to sound temperate glaciers and ice sheets with the same technique. So far, these attempts have been unsuccessful because of scattering from a multitude of water inclusions in the glaciers. In polar ice, crevasses and ice lenses cause a similar effect.

The Apollo 17 lunar sounder system has been flown on both the Earth and Moon. This sounder system relies on direct reflection from surface and subsurface interfaces (as the previously mentioned system).

The system uses frequencies at 150, 15, and 5 MHz, which were chosen for various depths and resolutions of sounding of lunar rocks and soils in which electromagnetic waves are much less attenuated than in similar Earth materials. At all frequencies, the SAR technique is used, which gives a large dynamic range and low side lobes. A functional diagram is shown in figure 5–85 (ref. 5–26). The figure illustrates how along-track resolution ρ_x is obtained, despite the wide regular beamwidth of the antennas, by using a coherent radar (i.e., one in which both transmitter and receiver are phase referenced to a stable master oscillator) in conjunction with data storage and processing. A given terrain element of range R is observed by the radar while moving along a track subtended

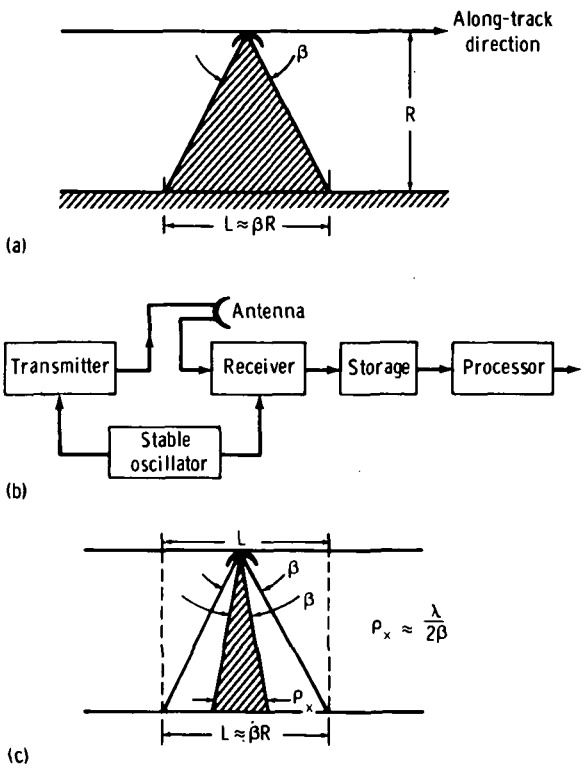

FIGURE 5–85.—Functional diagram of the Apollo 17 lunar sounder system SAR. (*a*) Physical beamwidth. (*b*) Simplified block diagram. (*c*) Improved along-track resolution ρ_x.

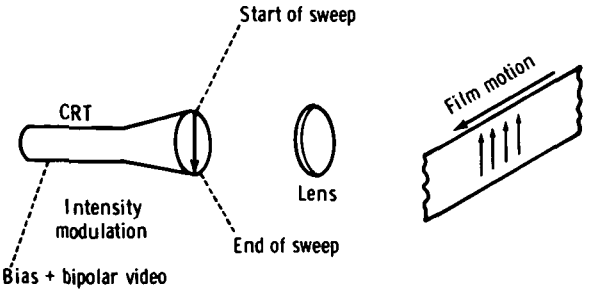

FIGURE 5–86.—Simplified diagram of the lunar sounder system SAR optical recorder.

by an angle β. Stored data collected during the observation time and processed to synthesize an antenna aperture of length L yield the improved along-track resolution ρ_x.

Systems parameters, such as system bandwidth and time-bandwidth product of the transmitted signal, are chosen so that the range/depth resolution is proportional to wavelength. At 5 MHz, a free-space resolution of 700 m is obtained. The resolution in the surface material will be finer given by ρ_x/n, where n is the refractive index. The along-track resolution in free space is obtained by the synthetic aperture technique to be 5λ, or 300 m at 5 MHz.

The video outputs of the radar systems are recorded (stored) on a CRT film-type optical recorder with all signals on the same 70-mm film, the 150-MHz system having a bandwidth of 16 MHz (fig. 5–86). This film is later processed on the ground in a coherent optical system (fig. 5–87) to perform the necessary along-track and/or range-processing operation. This processor is equipped

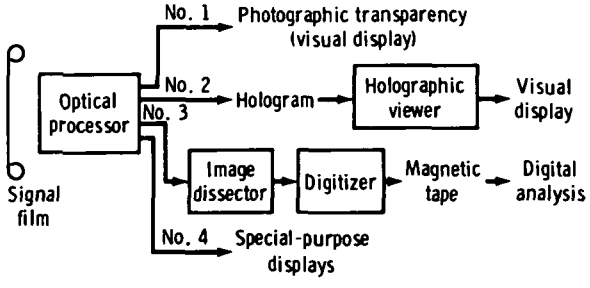

FIGURE 5–87.—The lunar sounder system SAR basic processor/display system.

with several alternate readouts, including a photographic hardcopy, a hologram, and a digital tape.

A prototype was flown at approximately 10 km above the Earth. Penetration in the Greenland ice cap was observed at 150 MHz, and a series of layers was recorded down to approximately 140 m, the limitation in depth being the result of the small power available (95-W peak). A combination of the features of the two sounders mentioned here may result in a system that may be used from low-orbit satellites to sound polar ice sheets and glaciers.

The 2-m mode of the lunar sounder can be used for an image of the ocean and solid-Earth surface from nadir to approximately 30 km. A distorted "cylinder perspective" image strip is obtained, with an average resolution of approximately 5λ. The prototype was used to obtain images of wave crests on the ocean, which showed the spacing and orientation of the crests.

The antenna patterns of the lunar sounder have very wide angular beamwidths (ref. 5–26); therefore, the system can be used as a scatterometer (ref. 5–27). The wide angular beamwidth gives the system the capability to receive reflected energy from small regions over wide angles in both the crosstrack and along-track directions. The measurement of reflection vis-a-vis angle is precisely the purpose of a scatterometer (ref. 5–18). Using an optical setup to focus (or position) the range in the same plane as the Doppler spectrum is obtained, the amount of reflection from any location within an angular beamwidth can be found (ref. 5–27). The resolution of the system used as a scatterometer is identical to that of focused SAR in the range direction (an inverse function of the bandwidth and approximately 5λ). In the Doppler direction, the half-power resolution is that of unfocused SAR ($[(\lambda R)/2]^{\frac{1}{2}}$, where R is range). From an altitude of 10 km, this resolution is approximately 150 m for the 2-m sounder mode. These resolutions compare favorably with those of a conventional scatterometer.

Experiment Application for a Subsurface Sounder

This section outlines an example of one experimental approach to detect the presence and determine the location of subsurface geological structures from an aircraft. The sensor used would be capable of performing large-area surveys of subsurface Earth resources, such as subsurface water tables, mineral deposits, oil location, and geological structure formation for mining purposes.

Prior development.—Electromagnetic subsurface sounding with active radio instrumentation has been used successfully in the geophysical exploration for groundwater and mineral deposits. Most sounding systems are CW that use at most a few frequencies. More recent developments use a pulse transient approach, which is still a variation on CW exploration (ref. 5–28). Both techniques have been operated on the ground or from low-flying aircraft, with the depth of exploration from 100 to 400 m. The techniques rely on a simple, anomaly/no-anomaly decision or on model fitting for interpretation. In the latter instance, the types of realistic geological models that can be computed are limited, and a large question of uniqueness exists in the interpretation. Two obvious areas of improvement in state of the art are greater depth of exploration and a more direct means of interpreting data. A time-delay approach, analogous to active seismic exploration for oil, is an attractive method for improving the means of interpretation. However, it has been thought that the frequency range needed for significant penetration, in typical geological materials, is in the kilohertz range. In this frequency band, dispersion is so great at bandwidths required for adequate resolution that a time-delay scheme is not practical (ref. 5–29). A notable exception to the previous discussion is Antarctic ice sounding (ref. 5–25), which operates successfully in the high-frequency (hf) region (35 MHz–8 m) because of the low loss tangent (and thus also low dispersion) of the ice. A second exception is lunar material (because of the complete absence of water) as was demonstrated by the Apollo 17 deep sounding lunar experiment.

This section describes a time-delay system that will operate in a wide range of geological materials and to depths greater than have been achieved from previous airborne instruments. This instrument operates in the hf range (100 kHz to 10 MHz) to avoid significant dispersion in materials with conductivities as high as 10^{-2} $(\text{ohm-m})^{-1}$ or loss tangents as high as 1.0.

Observed phenomena.—The previously mentioned experiment uses radar techniques to observe the discontinuities in dielectric constant on and within the surface layer of the Earth. From the phase information in the echo and the time-delay or equivalent frequency shift, the nature of the dielectric discontinuity and its location can be inferred. The analysis includes computer ray-tracking techniques and iterative techniques for establishing the depth of the subsurface feature. The detection of the presence of a subsurface discontinuity is unambiguous. The location determination depends on knowledge about the dielectric constant of the intervening material. Thus, the uncertainty in depth varies as the square root of the uncertainty in the dielectric constant. Most Earth subsurface materials in their natural state (the type with loss tangents less than 0.5) in the hf range (100 kHz to 10 MHz) have a dielectric constant between 9 and 16. Hence, the maximum likely uncertainty is 14 percent. The typical depth of penetration varies with the loss tangent of the intervening layers. A diagram that indicates typical performance is given in figure 5–88.

Experiment technique.—The experiment approach uses coherent radar techniques at long wavelengths and records the echoes on an optical recorder. (These measurements could be performed from an aircraft.) The basic technique uses the long-frequency sweep (used by FM altimeters) and the coherent format to increase the average effective power radiated to a level at which the successful observation of the subsurface features is highly probable. The combination

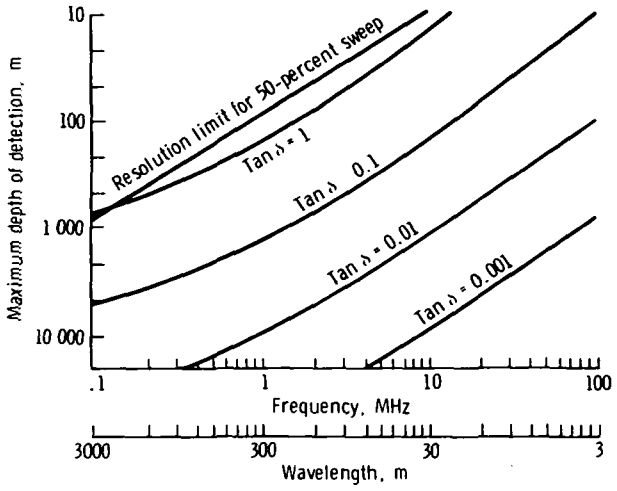

FIGURE 5–88.—Maximum depth of penetration and resolution as a function of frequency for various loss tangents, where tan δ is loss tangent.

of the coherent radar, the long linear FM sweep, and the optical recorder are the new aspects of this sounder.

The linear sweep and a typical response are characterized in figure 5–89. The apparatus consists of a linear sweep generator,

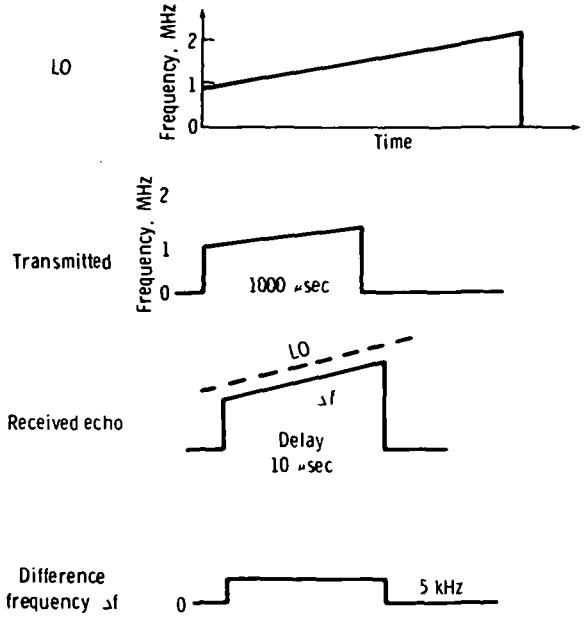

FIGURE 5–89.—Diagrams of typical frequency compared to time for the long-wavelength sounding radar.

transmitter, antenna, and receiver. The video output from the receiver is recorded on film by an optical recorder. The film is then processed by an optical correlator to produce an image film that is digitized, processed, and used to print out the subsurface feature locations.

The antenna consists of a deployable reel-type unit mounted in the tail of an aircraft. The maximum length is variable from 300 to 30 m. The matching of the transmitter to the antenna to minimize ringing or range side-lobe levels poses one of the most difficult problems associated with this experiment.

Once the instrument is installed on the aircraft, flights must be at relatively low altitudes over areas where conditions favor detection of known subsurface features. The preliminary data-acquisition flights may be used to verify the sounder performance and data reduction and interpretation techniques. One such area is the Chuckwalls Valley, which is northeast of Salton Sea in southern California.

The system operates over a 50-percent bandwidth; that is, 100 to 150 kHz or 2 to 3 MHz. The system is tunable in discrete steps over the range from 100 kHz to 10 MHz. The choice of frequency depends on the depth of penetration desired, the loss in the material, and the resolution required. The antenna is a deployable reel-type unit, and the antenna length may be adjusted as needed to operate at the highest possible efficiency.

System performance.—The system presented is an adaptation of FM altimeter radar techniques to low frequencies for use in a sounding mode. The transmitted frequency is a repetitive linear ramp of long duration. The transmitted frequency also serves as the reference frequency; sweep bandwidth must be kept high to attain adequate resolution. However, because the received frequency is mixed with a replica of the transmitted frequency and the sweep rate is slow, the system achieves significant bandwidth reduction to improve the signal-to-noise ratio with no appreciable loss in range

resolution. During data processing, a further bandwidth reduction may be attained to select returns from directions normal to the flightpath, such as pools of water beneath the aircraft. This technique is also known as Doppler filtering.

If the transmitted waveform has a frequency that sweeps over a total bandwidth B in an interval of T seconds, the frequency of a return delayed by Δt seconds will be $f_s = B\,\Delta t/T$.

The signal return has a duration of T seconds, and if it is passed through a filter of bandwidth $1/T$ at a center frequency f_s, then a return that has a delay of Δt with a total uncertainty of $1/B$ will pass through this filter. The noise bandwidth is also $1/T$; thus, a reduction of noise power by $1/TB$ may be achievable. This effect is equivalent to the time bandwidth product TB signal-to-noise ratio improvement that can be obtained with a conventional chirp pulse-compression system, but the system is not limited by dispersed pulse length compatible with round-trip delay time to the first surface.

The resolution is equivalent to

$$\Delta R = \frac{c}{2B\sqrt{\epsilon}} \qquad (5\text{–}37)$$

where c is velocity of light and ϵ is dielectric constant, which is essentially limited only by the total bandwidth sweep of the system.

The maximum depth of exploration for an ideal system without Doppler filtering has been computed on the following basis. The return power from a first surface of reflectivity γ_1 at a range R is given by

$$P_r = \frac{P_t G^2 \gamma_1 N \lambda_0^2}{(4\pi)^2 (2R)^2} \qquad (5\text{–}38)$$

where P_t is transmitted power, G is antenna pattern gain, N is antenna efficiency, and λ_0 is radio wavelength in free space. Equation (5–39) gives the return power from a subsurface layer located at a depth d in a medium for which the loss tangent is $\tan \delta$:

$$P_r = \frac{P_t G^2 N \lambda_0^2 (1-\gamma_1)^2 \gamma_2 L_1}{(4\pi)^2 (2R)^2} \qquad (5\text{–}39)$$

where γ_2 is the subsurface reflection coefficient and L_1 is the material loss. The loss in the material is given by

$$L_1 = 10^{-5.48 \tan \delta\, \epsilon_1^{1/2}\, d/\lambda_0} \qquad (5\text{–}40)$$

where ϵ_1 is dielectric constant. The expected noise comes primarily from sources outside the antenna. The noise power may be expressed by

$$P_n = kT_a BN \qquad (5\text{–}41)$$

where k is Boltzmann constant, T_a is ambient noise temperature, B is noise bandwidth of the system, and N is antenna efficiency. The expected ambient noise temperature T_a caused by manmade noise in rural environments follows the following relationship within 10 dB from quiet areas to noisy areas:

$$T_a = \frac{3 \times 10^7}{f^{2.5}} \qquad (5\text{–}42)$$

where the frequency f is in megahertz.

System parameters used to calculate the performance curves in figure 5–88 are as follows:

1. Peak power: 10 W
2. System bandwidth: 0.5 f (f=carrier frequency)
3. Noise bandwidth: 1000 Hz
4. Frequency sweep duration: 1 msec
5. Antenna efficiency: 0.01
6. First surface dielectric: 10 to 15 (ref. 5–30)
7. Second surface dielectric: 2 (oil)

Engineering development.—Airborne radar-sounding systems have demonstrated the ability to detect dielectric discontinuities beneath glaciers. The problem of designing a sounding radar instrument to detect discontinuities below moist Earth materials is more complex because the propagation loss of radio waves is greater in these materials than in ice. Increasing the peak radiated power can only alleviate this problem to a certain extent at the expense of a more cumbersome instrument. Operation at lower altitudes restricts the transmitted energy because the transmitted pulse length must not exceed the minimum round-trip elapsed time of the radio wave. The technique discussed would

circumvent this problem by using a technique that has been previously used at much shorter radio wavelengths in radio altimetry. With this technique, reception is simultaneous with transmission, and the waveform separation is accomplished by an instantaneous frequency separation of the transmitted frequency from the received frequency. This technique requires some unique characteristics of portions of the sounding radar for proper operation.

Description.—The sounding radar system shown in the functional diagram (fig. 5–90) consists of a sweeping LO, a low-noise power amplifier, an antenna, and a high-level mixer. The LO generates a linear frequency sweep that is amplified by a low-noise power amplifier, and this power is radiated by the antenna. The return signal is coupled from the transmitter-antenna line by a directional coupler into a high-level mixer. The return signal is then mixed with the transmit waveform. The output of the mixer is a waveform for which the frequency is directly proportional to the range of the reflecting surface. The output of this mixer is passed through a high-pass filter and amplified before recording in an optical recorder. The data stored in the optical recorder film are processed by taking a two-dimensional transform of the data film in an optical processor, filtering through a narrow-pass spatial filter in azimuth, and recording in an output data film. The result is an image for which the dimensions are along-track distance and cross-track distance (depth of discontinuity).

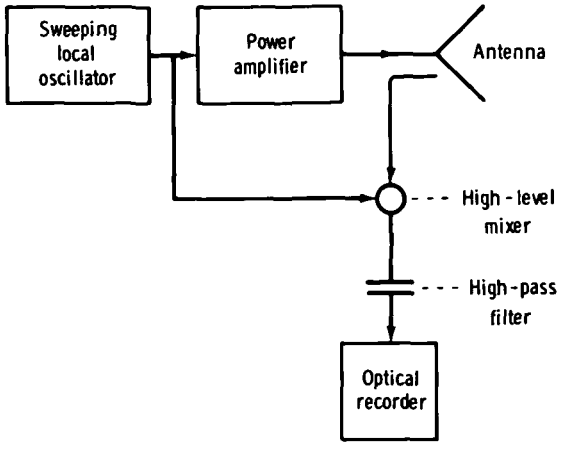

FIGURE 5–90.—Functional diagram of sounding radar system.

DOPPLER FILTERING AND MOVING TARGET INDICATOR

Some radar applications mentioned in earlier chapters have required some form of Doppler filtering or moving-target indicator (MTI) to determine the velocities or velocity spread of targets such as precipitation or ocean waves. Doppler radar provides information on the relative velocity between the targets and the radar; the information can be derived from many types of radar waveforms by using coherent processing.

The simplest form of Doppler radar involves pure CW transmissions. The returned signal spectrum is broadened by the Doppler spectrum of target movements, and the spectrum will be shifted in frequency when the radar is located on a moving platform. For CW transmissions, the desired spectrum will be contaminated by the Doppler spectrum of unwanted returns from land/sea. The width of this unwanted spectrum is set by the basic line width of the radar coherent reference convolved with the Doppler spread of groundspeed seen by the radar beam shape. For large dynamic range requirements, the Doppler spectrum seen by side lobes may also be significant and may set a limit on side-lobe levels. The Doppler resolution is therefore determined by this spectrum of unwanted clutter; and, for CW transmission, this can only be improved by reduction of antenna beamwidth and side-lobe levels.

For most applications, Doppler processing is combined with ranging, which enables range gating to be used to exclude (or reduce) unwanted responses outside the principal region of interest. As with SAR, coherent signal processing is necessary. This will entail either coherent transmissions or storage of phase information on each transmitted pulse referred to a stable LO (coherent-on-receive). The basic limit on Doppler resolution is set by the stability

(spectral line width) of the phase reference over the integration period of the radar. This limit will be further degraded by the Doppler spectrum from moving clutter such as returns from the surface of the Earth.

Discrimination and analysis of the Doppler return are performed by filtering the bipolar video waveform. The MTI techniques require the use of a high-pass filter response. Such a system rejects targets at or near the reference Doppler frequency, as conditioned by the filter response, but there is no classification of target velocities. The information relating to the relative speed between the radar and the ground can often be extracted from an appropriate range gate to provide a "clutter-locked" reference.

Doppler classification of targets within a range cell requires the use of multiple bandpass filtering (or digital fast-Fourier-transform (FFT) techniques) for each cell of interest. This technique is pulse Doppler or range-gate filtering and can lead to a very large number of filters (or associated digital storage) when targets may exist at any range. The storage is proportional to the product of the number of range cells and Doppler filters for a given dynamic range. The frequency response of the bandpass filtering is also repeated at multiples of the PRF.

The main limitation on measuring target velocity from a satellite or aircraft-borne radar wil be the residue of this unwanted spectrum from side lobes in range and azimuth. The problems of seeing slow-speed targets such as precipitation near the surface of the Earth can place severe constraints on the design of large narrow-beam antennas with low side lobes.

Traffic moving along a road in England seen from an aircraft-mounted, side-looking radar incorporating MTI processing is shown in figure 5–91. The corresponding radar map without MTI processing is shown for comparison.

In principle, the raw radar data from a coherent imaging radar could be subjected to different digital processing to obtain either optimum Doppler performance or maximum resolution as required by different users. Nevertheless, some compromise of certain radar parameters would be necessary to meet conflicting requirements of different applications.

The attainment of compatibility between Doppler processing and certain other features of radar systems can create system constraints, which are as follows:

Pulse compression: Doppler processing is fully compatible with pulse compression; but, with FM chirps, there are range errors proportional to Doppler; and, with other forms of code, there are increased range side-lobe levels caused by decorrelation effects from Doppler-shifted signals. Strong targets in range side lobes can contaminate the Doppler spectrum.

Multifrequency transmissions: Doppler processing may be applied simultaneously on multifrequency radars, but both the Doppler shifts and the blind speeds will be different at each frequency (for the same PRF).

Frequency agility: Doppler processing is not compatible with frequency agility unless steps are taken to transmit groups of pulses on each frequency, which also leads to a loss of signal pulses.

Synthetic aperture: The available coherent reference in this type radar may also be used for Doppler processing. There are errors in along-track range for moving targets because of the matched filter characteristics of the receiver.

Scanning beams: Doppler processing may be used with either mechanical or electronic beam scanning, but there is a broadening of the Doppler spectrum as a result of the movement (scanning) of the antenna beam. This broadening is generally significant only for very low Doppler speeds of high scan rates. The effect can be avoided with step scan, switched multiple beams, or Nyquist rate scanning.

Antenna null steering: Null steering in the directional pattern of the radar antenna may be used to reduce Doppler returns from

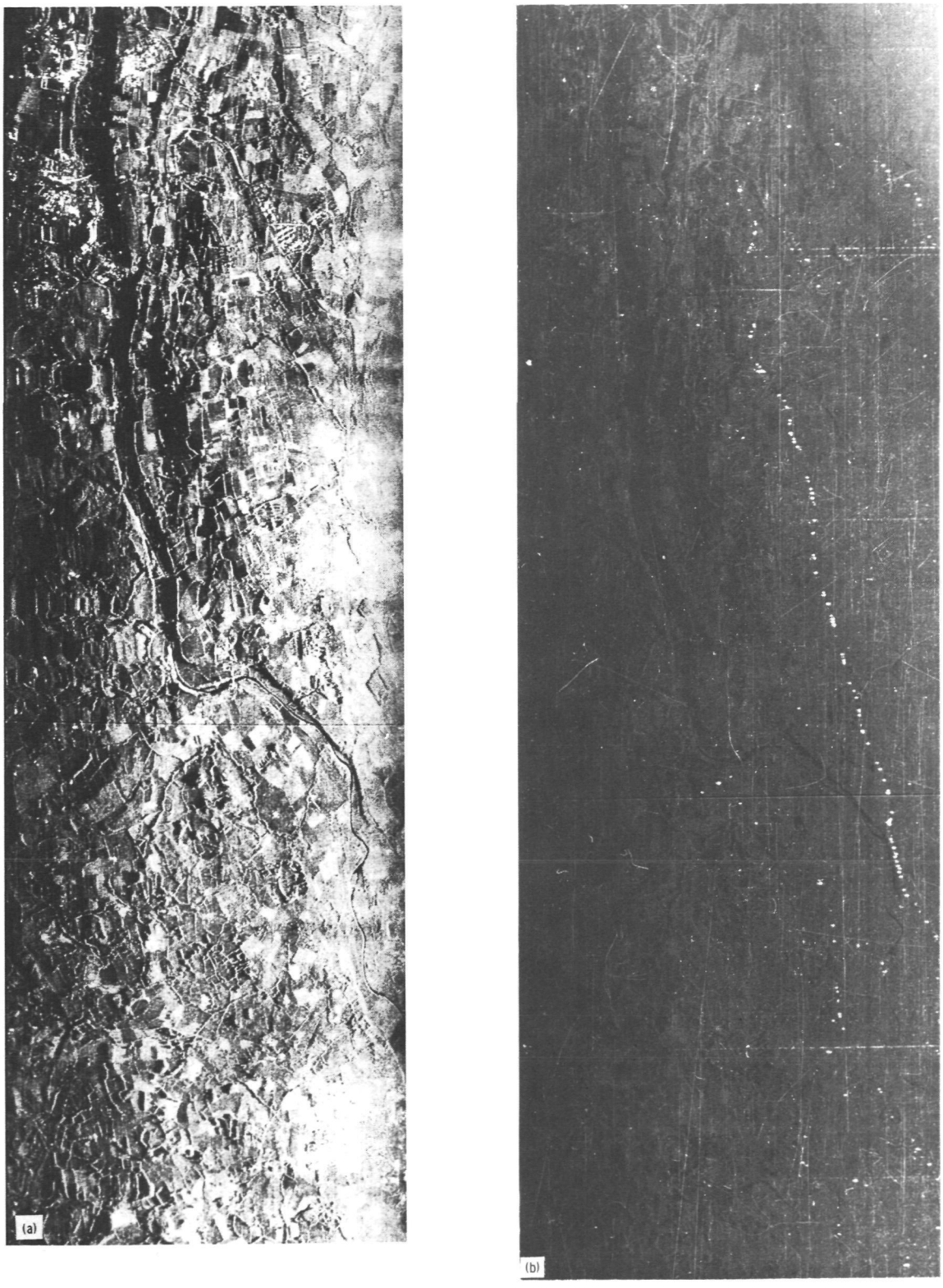

FIGURE 5–91.—Example of MTI. (*a*) Normal map. (*b*) Image with MTI processing.

c. 6

strong targets (such as the ground) where they mask wanted returns from precipitation. This technique is compatible with Doppler processing, but the null pattern should be constant over the integration time of the Doppler processing.

ANTENNAS AND ARRAYS

The current state of the art in antennas for spacecraft applications is discussed briefly in this section. A review of several of the more advanced antenna techniques is also included. These techniques are mostly used for ground radar installations and would require specialized development for spaceborne applications. The objective is to make users aware of the potential characteristics of such schemes because they are likely to be of increasing value for future systems.

Current State of the Art

Spacecraft have used parabolic reflection antennas 10 m in diameter in the Applications Technology Satellite (ATS) program. Using petals made of wire mesh hinged to a central hub, this antenna has a surface accuracy good to a 3-cm wavelength. This design is shown in figure 5–92. Antennas of these dimensions could also be produced for operation at millimeter wavelengths, which would probably require a continuous surface reflector or close mesh within a sandwich material.

Antennas with significant increases in diameter above 10 m would be more difficult to produce. One possible configuration is an inflatable balloon-type structure, but it is not clear whether this type antenna could maintain its tolerance with meteorite damage. Very large antennas could also encounter severe alinement problems, particularly related to heating from the Sun.

Antenna array systems.—During the past decade, new antenna techniques have been applied to radar systems. These techniques are based mainly on phased-array principles together with new developments in signal-processing technology and components. The antenna techniques include the following:

1. Electronic beam scanning.
2. The formation of multiple beams from a common aperture.
3. Placing and steering directional zeros in the antenna directional pattern.
4. Self-focusing and adaptive arrays.
5. Multiplicative processing arrays.
6. Arrays using separate patterns on transmit and receive to reduce the total number of elements.
7. Minimum-redundancy thin arrays.

Coherent synthetic aperture arrays should also be included in this list; however, they are discussed in more detail in other sections.

Electronic scanning and multiple beam forming.—Several relevant applications exist for electronic beam scanning for spaceborne radars where it is necessary to move the antenna beam at high rates or where it is convenient to use antenna array elements mounted over the surface of a given spacecraft (conformal arrays). Several phased arrays are now used on satellites.

The high cost of two-dimensional phased arrays for ground radars is caused by the need to handle very large power. In space applications, power levels are much less, and, for most instances, linear arrays incorporating one dimension of scan will be adequate. In some instances, the complication can be reduced by using array-thinning techniques, which are discussed later. Electronic scanning would not be relevant for very narrow beams from planar arrays because of the numerous elements.

An N-fold increase of data rate from a given radar-receiving aperture can be obtained by forming N separate independent beams from the aperture. This ability to make simultaneous measurements in multiple directions could have applications to scatterometers and narrow-beam sounders because it has the capability to increase resolution without loss of coverage or beam dwell time.

Multiple beams may be generated in a variety of ways, such as using multiple feeds

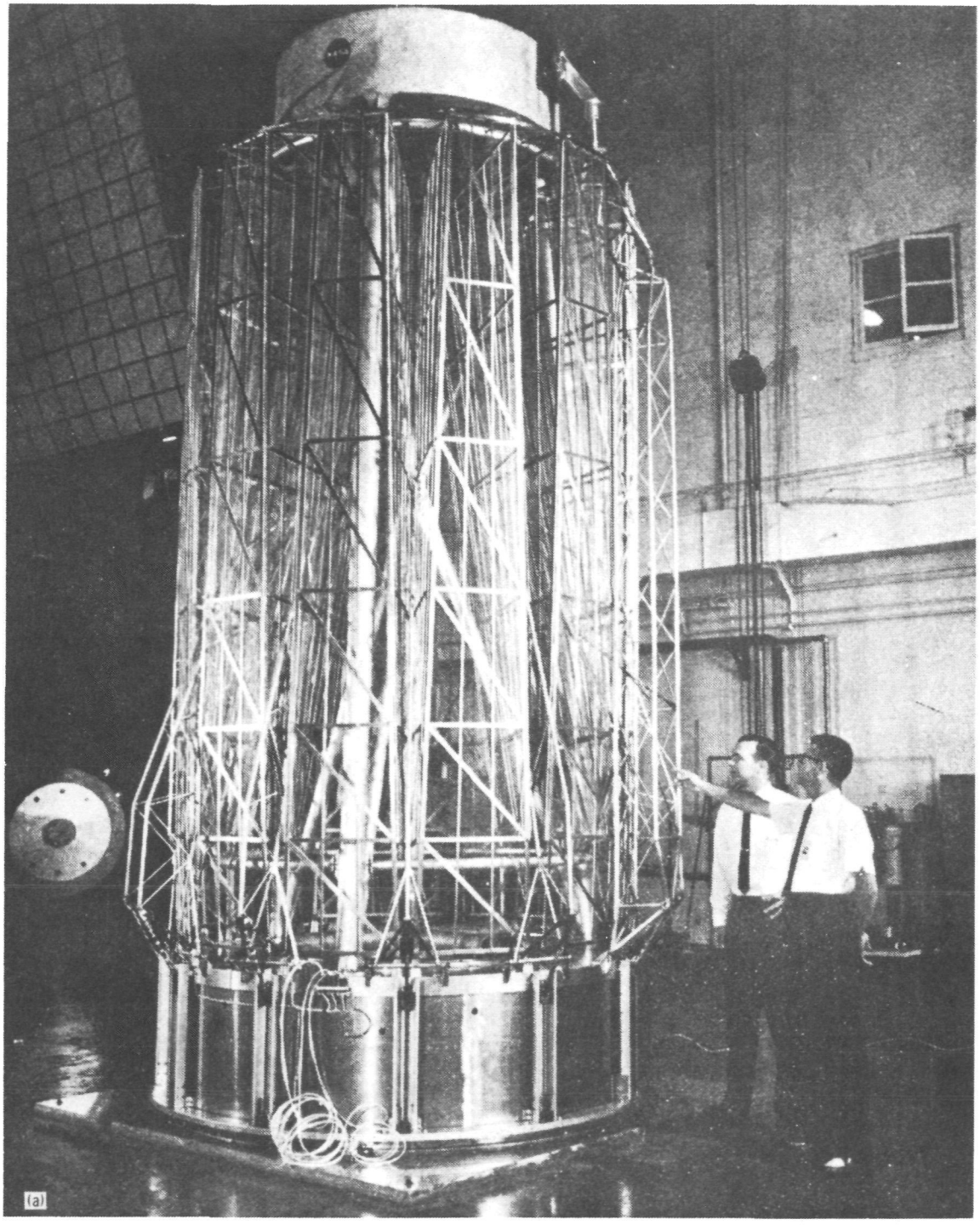

FIGURE 5–92.—Large space-erectable antenna reflector 9 m in diameter developed for the ATS program. The model has a paraboloidal structural design that can be collapsed for packaging into a launch-vehicle nosecone and then erected on command to its original shape. Each petal is permanently attached to its two adjacent petals before, during, and after erection. (*a*) Collapsed antenna.

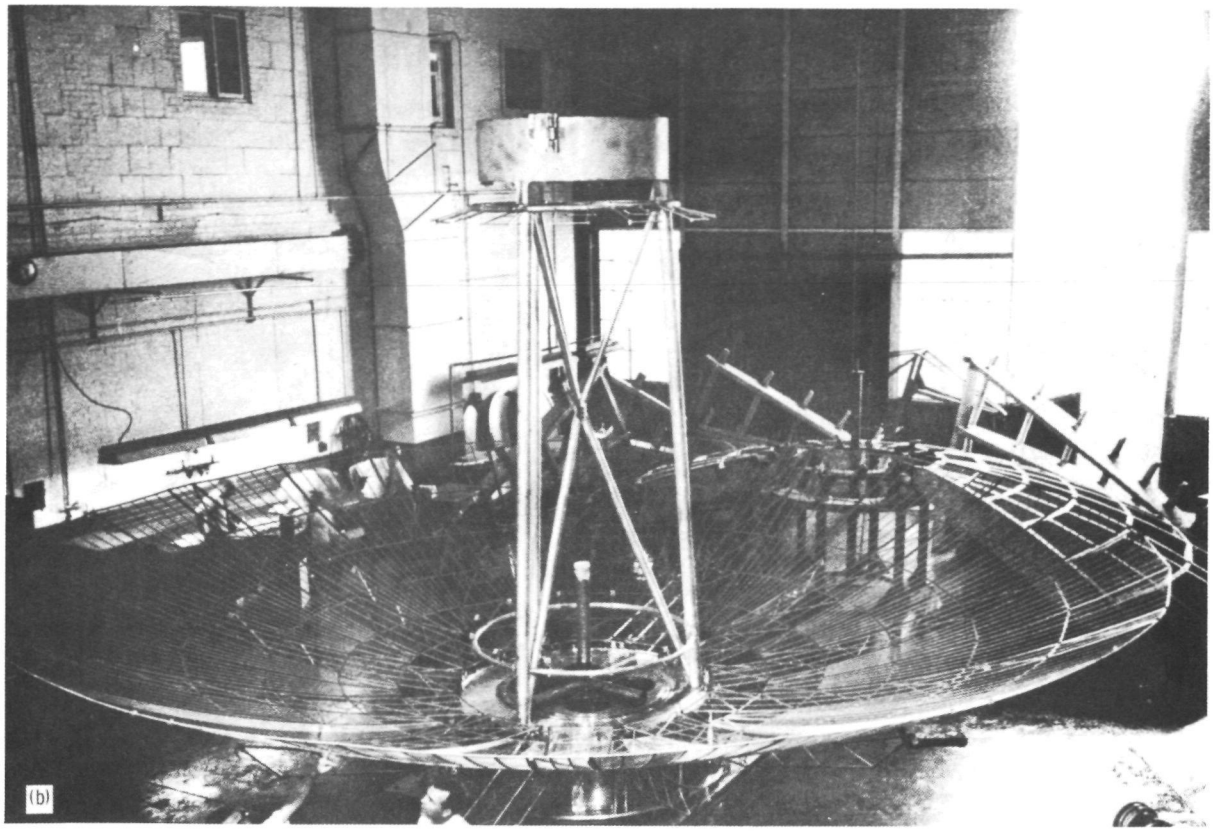

FIGURE 5–92 (concluded).—Large space-erectable antenna reflector 9 m in diameter developed for the ATS program. The model has a paraboloidal structural design that can be collapsed for packaging into a launch-vehicle nosecone and then erected on command to its original shape. Each petal is permanently attached to its two adjacent petals before, during, and after erection. (*b*) Erect antenna.

to parabolic or spherical reflections. Multiple-beam matrix networks, such as the Butler matrix network, can be used to generate independent beams from the output of antenna arrays. Monopulse tracking and zero steering can also be combined with multiple-beam matrix networks.

A group of high-data-rate radar systems is based on broad-beam (floodlight) transmission and either multiple-beam or Nyquist rate electronic beam scanning on reception. These systems offer very high angular data rates and derive their performance from more complex receiver processing, which benefits from the decreasing cost of digital velocity. An account of such radar systems using low-redundancy array techniques is discussed in the section entitled "Radar Systems Using Low-Redundancy Arrays."

Multiple beams may also be generated by digital FFT processing of the output of a receiving array, and synthetic aperture processing may be regarded as performing this technique in the Doppler domain.

Multiplication of directional patterns and thinned arrays.—Multiplicative arrays in which the output of array elements are demondulated by multiplying them in various combinations have been used for many years in radio-astronomy arrays. These arrays can provide incoherent antenna beams using the product of the signals from two crossed linear arrays (Mills cross). Work in this field has led to studies of large arrays

with low filling factors called minimum-redundancy arrays. The possible application of these arrays is discussed in more detail in the section entitled "Multiplicative Signal Processing."

Some radar applications described in earlier chapters need to use very large antennas in space. The requirement is often for very small beamwidths but without the need for high antenna gain. In such instances, it appears worthwhile to consider schemes that offer pencil beams generated from two crossed linear arrays, which might be technically easier to implement.

The Mills cross-type multiplicative beam applies only to reception. An alternative is to transmit using one linear array and to receive using the other array, thus forming a two-way pencil beam from the spatial product of the patterns. In this instance, there is a loss of transmitter power in the volume of the transmitter beam outside the common pencil-beam volume. If required, this loss of power may be removed by forming a set of multiple fan beams with the linear receiving array.

Adaptive arrays and zero steering.—Adaptive arrays control some aspect of the directional performance of the array to optimize some aspect of the received signal (using some automatic optimization process). The "self-phasing" performance is sometimes conducted by using separate pilot frequencies. Such arrays have had more application in communications than in radar.

Zero steering (null steering) arrays control the angular location of directional nulls in the antenna pattern to avoid illuminating and receiving signals from a specified direction, generally to avoid receiving some unwanted signals. This aspect of the system may be made adaptive. A possible application for such a system for spaceborne radar is the use of steered nulls to reduce Doppler clutter from ground returns. In such instances, it is possible to use a directional null to insert a corresponding null into the unwanted Doppler clutter spectrum. This effect can improve the capability of the radar to see returns from moving precipitation at the Doppler frequency of this null. The section entitled "The Extension of Meteorological Satellite Radar Coverage by Antenna Null Steering" gives a more detailed account of the use of null steering for improving Doppler performance.

The Application of Nonredundant Arrays to RAR and SAR Systems

Nonredundant arrays are linear (or planar) thinned arrays that are used in radio astronomy to synthesize the directional properties of filled receiving apertures. This section discusses how such techniques may be applied to radar systems to reduce substantially the number of antenna array elements. A particularly convenient radar-system configuration involves combining nonredundant arrays with within-pulse scanning of a receiving beam together with either frequency-agile transmissions or Doppler processing on reception to reduce effects of unwanted target cross products in the demodulation process. Schemes with square-law detection and multiplicative processing are discussed.

The application of such techniques to coherent SAR systems to reduce the amount of storage and processing of data needed for such systems is discussed.

Nonredundant arrays.—Nonredundant or partly filled arrays are used to a significant extent in radio astronomy but have found little application in radar systems. This section discusses several radar systems in which nonredundant and multiplicative arrays can provide significant reduction in the number of elements in the field of phased arrays for certain radar applications.

Aperture synthesis techniques have been used for coherent processing (i.e., for synthetic aperture side-looking radar) and for noncoherent receive-only applications (such as radio astronomy). For noncoherent applications, the synthesis procedure uses the fact that the cross-product signals from a pair of elements spaced a distance D apart in

a linear array is independent of the location of the elements in the array (provided the spacing D is maintained). The demodulated output of all receiving arrays consists of various weighted combinations of self-products and cross products of all element outputs; therefore, a substantial economy of elements (and associated processing) is possible if the duplication of any interelement spacing in the array can be avoided. Figure 5–93 shows a four-element array that contains all the interelement spacings from $D=1$ to $D=6$. This is a well-known example of a nonredundant array that contains all the spatial frequency components of a uniform seven-element array (ref. 5–31).

The conventional additive directional pattern of the array of figure 5–93 is most unattractive, having very high side-lobe levels, but the directional pattern of the output of the array after square-law detection is

$$D(p) = \frac{\sin(7p)}{\sin p} \qquad (5\text{–}43)$$

where $P = (\pi d)/\lambda \sin\theta$. This is the form of the normal pattern of a seven-element array. A conventional filled linear array involves a substantial duplication of element spacings. In most instances, it is difficult to produce arrays with each spacing occurring only once; thus, a compromise situation with a limited amount of duplication is acceptable. Low-redundancy arrays are the result of such a compromise.

Two reasons why such arrays have not found significant application in radar systems are as follows:

1. The radiated pattern from such arrays is unattractive because of very high side lobes. This can result in large amounts of the transmitted power residing outside the main beam.

2. The assumption that the cross product from a pair of elements (of fixed spacing) is independent of their location in the array is true only for incoherent signals (such as radio astronomy).

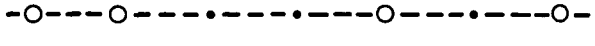

FIGURE 5–93.—Four-element array containing all the interelement spacings of a seven-element filled linear array.

Because there is no direct equivalent of nonlinear receiver signal processing for transmission, nonredundant arrays incorporating a low filling factor will exhibit high side lobes, which makes them unsuitable for transmission because of the significant loss of transmitter power. This problem can be overcome for radars incorporating floodlight transmissions together with either multiple beams or within-pulse scanning on reception. The widely spaced (low redundancy) arrays may then be used for the receiving array of such radars. A second area of potential application is coherent SAR, in which the minimum redundancy technique may offer a possible method for reducing the number of transmissions and associated storage required for the synthetic aperture process.

Radars incorporating floodlight transmitter coverage.—These forms of radar use phased-array techniques in conjunction with a floodlight transmitter. Figure 5–94 shows a sector illuminated by a floodlight transmitter, covered by a group of N fixed receiving beams. This type radar has the advantage of a very high data renewal rate. Figure

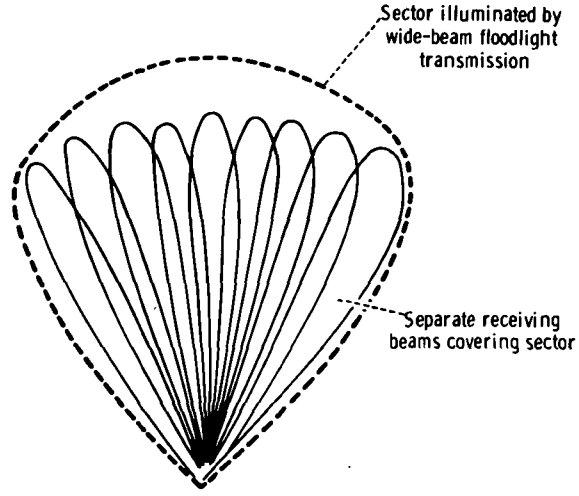

FIGURE 5–94.—Sector coverage by floodlight transmission and multiple-beam reception.

5–94 shows that both range and bearing are obtained on all targets within the coverage sector of the radar for each pulse repetition period.

The range performance of such a radar need not be significantly worsened by the use of floodlight transmissions. Although the radar range equation (as normally quoted) indicates that the maximum range is a function of the transmitting antenna gain, it is evident that the time average distribution of transmitting power is, for most conventional radars, uniform over the arcs of cover.

Comparing the radar configuration of figure 5–94 using a static floodlight coverage of a sector with the sequential illumination of each direction with a narrow antenna beam, it is clear that, in the former instance, data are obtained at a far higher renewal rate, but N times the number of pulses on each target are received, each containing $1/N$ of the energy (where N is the number of beam positions within the sector). The effect of such a system on maximum range performance is mainly dependent on the capability of the radar system to integrate these pulses, and this integration depends on target and noise statistics. In coherent integration, no loss of signal power would occur; but, for the more usual situation of incoherent integration, some reduction in maximum range would generally occur because of the less efficient integration. Therefore, such a radar will generally incorporate larger amounts of incoherent integration.

Various methods exist for generating such multiple beams, including multiple feeds to reflector or lens systems, special networks such as the Butler matrix, or sampling the outputs of the array followed by angular matched filters, such as digital FFT filtering. The third technique appears more suitable for the application of low-redundancy arrays by selecting the sampling points and processing to achieve the required array spacings. However, the application of low-redundancy arrays to radar can be conveniently described with reference to within-pulse scanning (ref. 5–32), which is another technique for receiving all the information on range and bearing from within an illuminated sector during a single pulse repetition interval.

Within-pulse scanning.—In this technique, a sector is illuminated with a floodlight transmission incorporating a pulse of duration τ, and a narrow receiving beam is scanned repetitively across this sector at a rate corresponding to $1/\tau$. Therefore, the scanning rate corresponds to the Shannon sampling rate or Nyquist rate, which means that pulses reflected from each target will be sampled by the scanning receiving beam, which effectively operates as a sampling switch for each direction. The technique is in operational use in the sonar field, but the radar application has been restricted to experimental devices (refs. 5–32 and 5–33).

Several alternative system configurations exist for providing Nyquist rate scanning of a receiving beam. The most well-known configuration is shown in figure 5–95. The output of each array element is subjected to single-sideband modulation at frequencies of ω_s, $2\omega_s$, $3\omega_s$, $4\omega_s$ . . . , where ω_s is the beam-scanning rate and equals $2\pi/\tau$. Such a scheme effectively adds a phase shift at uniform rates to each antenna element, thus producing a uniform movement of the array directional pattern along the sin θ scale. Each diffraction maximum of this pattern represents a beam that scans across the sector.

The noise factor of such a receiver is identical to that of a corresponding conventional receiving array provided that the

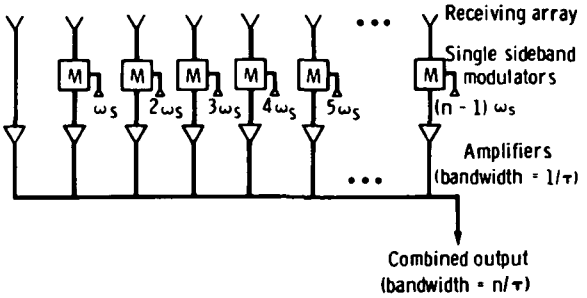

FIGURE 5–95.—Modulation scanning system to produce repetitive scanning of receiving beam at rate of ω_s ($\omega_s = 2\pi/\tau$).

bandwidth of the filters or amplifiers in each channel is restricted to $1/\tau$. However, although the bandwidth in each channel is $1/\tau$, the total bandwidth after summation of the channel outputs becomes n/τ (where n is number of channels), corresponding to the bandwidth of the sampled pulses (duration τ/n). Thus, the output represents the signals from N separate directions in space, which corresponds to the N-fold increase in bandwidth. The maximum range performance is not affected by the sampling process and corresponds to the previous examples of floodlight transmission.

The range resolution is determined by the transmitted pulse duration τ, and the side-lobe performance is set by one-way side lobes of the receiving array. A useful feature of the scanning receiver is that array amplitude tapers may be achieved by a single filter situated at the output of the combined array.

The MTI may also be applied to such a radar, and there is no reduction in performance due to scanning modulation, provided the pulse repetition interval is any integral multiple of the scan period.

Radar systems incorporating low-redundancy arrays.—Figure 5–96 shows the within-pulse scanning principle applied to the minimum-redundancy array of figure 5–90. The number of signal-processing channels is reduced in proportion to the number of elements in the array. Figure 5–95 also shows the frequency spectrum of such a scanning receiver when receiving a pure CW signal before and after detection. Before detection, there is a frequency component for each element of the thinned array. After square-law detection (at location X_2 in fig. 5–96), the "filled" spectrum corresponding to a seven-element array is produced.

The frequency spectrum of the output of a receiving array undergoing continuous scanning is a direct replica of the spatial frequency response of the array and associated signal processing. Figures 5–90 and 5–96 show how the square-law detection process produces a uniform filled spectrum giving the

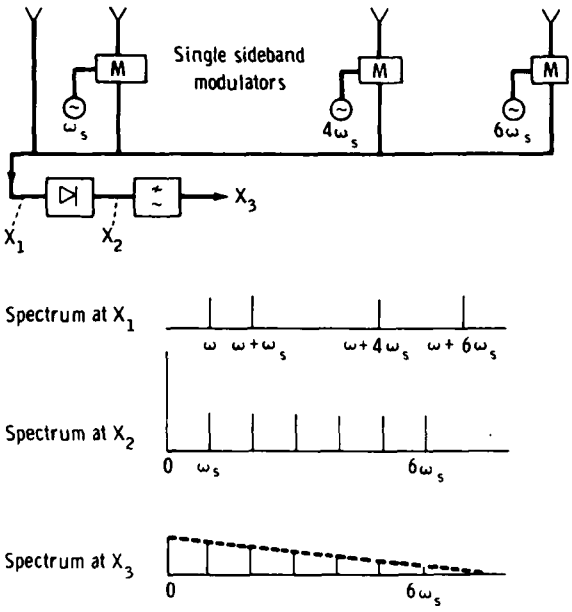

FIGURE 5–96.—Continuous electronic scanning of a nonredundant four-element array providing the directional pattern after demodulation of a filled seven-element array.

spatial frequency response of a filled array. However, because this spectrum corresponds to a $(\sin 7p)/(\sin p)$ power response, the side-lobe level would be too high for any radar application and would therefore require the application of amplitude tapers.

The adoption of the within-pulse scanning receiving system considerably simplifies such a tapering process. The capability for any side-lobe reduction technique appears to be determined by the range of possible amplitude tapers that could be applied to the thinned array. The well-known taper functions are not applicable to such nonuniformly spaced thin arrays. However, the output of the square-law detection enables separate access to each spatial frequency component of the processed pattern. Therefore, conventional taper theory can be applied at this point in the array processing. Apart from this additional degree of freedom in synthesizing the low side-lobe pattern, this technique has the additional advantages of enabling the taper to be applied after amplification and, hence, after the signal-to-noise

ratio has been defined. Another valuable feature is that, for many instances, the tapering function may be introduced by including a single filter at the output stage.

Figure 5–96 shows a simple low-pass filter included after detection to provide a triangular spectrum of spatial frequencies. This corresponds to a power response directional pattern of the following form:

$$D(p) = \left| \frac{\sin (7p)}{7 \sin p} \right|^2 \qquad (5\text{–}44)$$

This expression corresponds to the same side-lobe level as a uniform filled untapered array. Clearly, other filter responses corresponding to various low side-lobe patterns may be obtained by appropriate design of filters. The gain of such a thinned array is obviously reduced in proportion to the filling factor. The application of amplitude tapers causes the usual reduction of directivity (because of the slight increase of beamwidth).

The number of elements m in most low-redundancy array configurations is approximately given by $m=2\sqrt{n}$, where n is the number of element positions in a uniform filled array of the same dimensions. This fact means that the potential savings in elements and associated signal processing are most significant for large arrays and, particularly, for two-dimensional arrays used in radio astronomy. The significance of the reduction in gain greatly depends on the type of application for the radar.

Figure 5–96 illustrates the use of low-redundancy arrays for radar, but this particular example is of limited interest because it simulates a rather small array (seven elements) using four elements. Before considering designs for larger arrays and the use of other forms of demodulation, it is necessary to examine the multiple-target response of low-redundancy arrays and the effect of the coherence of the returns from targets.

Resolution and coherence.—If a directional receiver having a directional pattern $D(p)$ is illuminated by a source (or reflected signal from a target) of strength A_1 with frequency ω and direction θ_1, the receiver output will be

$$E_s = A_1 D(p_1) \cos (\omega t + \phi_1) \qquad (5\text{–}45)$$

where ϕ_1 is a general phase angle and $p_1 = (\pi d/\lambda) \sin \theta_1$. If this signal is square-law-detected and low-pass-filtered, the output will be proportional to

$$E_s = \frac{1}{2} A_1^2 D^2(p_1) \qquad (5\text{–}46)$$

A similar output would occur for separate excitation of the receiving array with a source A_2 at angle θ_2. However, for simultaneous excitation of the directional receiver, with both signals, the output after square-law detection and filtering becomes

$$E_s = \frac{1}{2} A_1^2 D^2(p_1) + \frac{1}{2} A_2^2 D^2(p_2) + A_1 A_2 D(p_1) D(p_2) \cos (\phi_1 - \phi_2) \qquad (5\text{–}47)$$

The first two terms are the outputs that would be predicted by superposition, and the third term is the cross product between two sources or targets.

Note that this cross-product term exists for all forms of directional receiver (whether using continuous apertures, filled arrays, or thinned arrays) and for all forms of demodulation. This cross-product term is an unwanted distortion, which reduces the ability to resolve multiple targets; thus, it needs to be reduced (ideally to side-lobe levels) relative to the wanted target self-products. Cross products between the signals from different element positions are the essential feature of a directional receiver; it is the cross product between different targets that must be removed (ref. 5–34).

For filled arrays with low side lobes, the target cross-product term is reduced because of the product $D(p_1) D(p_2)$. This fact shows that such cross products would be reduced to side-lobe levels if the angle between the two sources is greater than approximately one beamwidth.

Such target cross products fall off according to the autocorrelation of the predemodu-

lated directional pattern. Filled apertures use this property to reduce such effects. The amplitude of the target cross products is proportional to cos $(\phi_1-\phi_2)$, which represents the difference in phase of the returns from the targets A_1 and A_2. The phase difference will be random, which results in an average value of zero for the target cross product when averaged over all possible target positions.

For radio astronomy, the signals from two different radio sources are uncorrelated so that all such target cross-product terms average to zero, which explains the extensive use of thinned arrays in radio astronomy. However, for a radar system in which both targets may be illuminated from the same transmission, it may be necessary to introduce some deliberate variation of $(\phi_1-\phi_2)$ plus some averaging (integration) to integrate out the target cross products when a low-redundancy array is used.

The three principal methods for varying $(\phi_1-\phi_2)$ to achieve such results are as follows:

1. Movement of array: If the array moves relative to the target environment, the ranges (and hence the relative ranges) of the targets will change. To decorrelate returns from different targets by this method, it is necessary to obtain changes in $(\phi_1-\phi_2)$ in the region of one wavelength. Several such decorrelated responses must be averaged. Apart from the change of range, scintillation effects will occur because of complex targets, and changes of amplitude and phase returns will occur because of small changes of aspect angle. These effects will also help decorrelate the target cross-product returns.

2. Movement of targets: If the radar is used to obtain data on moving targets (using an MTI (or pulse Doppler) technique), Doppler filtering must be applied before detection. This technique necessarily removes most of the target cross products; it removes cross products between fixed targets and between moving and fixed targets, which leaves only cross products between moving targets. These cross products between moving targets will average to zero because of their relative movement. Thus, the unwanted cross products can be substantially reduced by the application of Doppler filtering followed by postdetector integration. The absence of scanning modulation effects for within-pulse scanning radars makes them particularly appropriate for MTI processing for certain applications, especially those involving very low speed targets.

3. Frequency agility: Changes in transmission frequency cause corresponding changes in the two-way phase delay to and from the targets and, hence, cause a change to $(\phi_1-\phi_2)$. Consequently, either multiple-frequency or frequency-agile transmissions for a radar incorporating low-redundancy arrays will enable the target cross-product returns to be decorrelated between successive pulses radiated at different frequencies. For distributed targets or clutter, it is generally necessary to change the transmission by an amount proportional to the transmitting bandwidth to decorrelate target returns from pulse to pulse. The technique of using frequency agility to reduce target cross-product effects has been demonstrated by Shearman et al. (ref. 5–35).

These three methods of reducing target cross products depend on noncoherent integration to average out the decorrelated returns. The extent of such integration will depend on the amount of decorrelation obtainable with the different methods and the degree of suppression of target cross products required. The level of cross products is proportional to the number of targets seen by the predemodulated directional pattern. The required integration is therefore substantially reduced for a thin target field (e.g., moving targets only). The only method not requiring integration is the filled aperture, which can be regarded as coherent integration of cross products within the array. The combination of low-redundancy arrays with within-pulse scanning is particularly convenient because the within-pulse scanning system requires the use of noncoherent in-

tegration for other purposes as previously discussed.

The unwanted effects of target cross products are not absent in filled arrays. Although there is considerable duplication of close element spacings, the relative weighting of element spacings in the spatial response of the array is triangular with no duplication of the largest spacing. This results in target cross products affecting the resolution of targets when closely spaced (within approximately two beamwidths of each other). For a nonredundant array, this effect can occur for all possible target directions.

Multiplicative signal processing.—The minimum-redundancy arrays discussed in the preceding section depend on the nonlinear performance of the demodulation process for their performance. In practice, all radar systems incorporate some form of nonlinear demodulation, but the effect on resolution performance is not very significant for filled arrays.

The use of multiplicative signal processing to demodulate the signals from directional arrays is an alternative form of nonlinear demodulations, which has been studied by many authors (refs. 5–34 and 5–35), and is used extensively in radio astronomy for noncoherent aperture synthesis and for synthesizing two-dimensional apertures from line arrays such as the Mills cross system (ref. 5–36).

Figure 5–97 shows how the directional pattern of a 36-element filled array can be obtained by multiplying the patterns of a 6-element wide-spaced array with a second 6-element closely spaced array. The array pattern multiplication theorem states that the overall directional pattern of an array is the product of the array factor and the directional pattern of each element. In figure 5–97, the short filled array is used as a single directional element, which is multiplied by the output of the wide-spaced array to synthesize a filled array of 36 elements.

No difference of principle exists between the adoption of square-law detection systems, such as those in figure 5–96, and the multiplication systems. Both techniques produce different combinations of self-products and cross products between signals from array elements. For example, a multiplier can be synthesized from three hybrids and two square-law detectors.

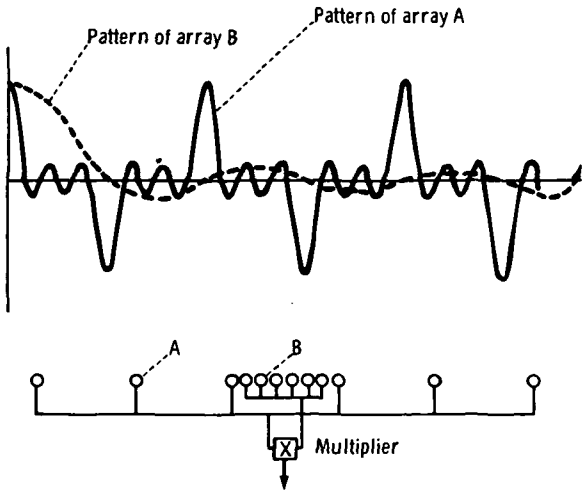

FIGURE 5–97.—Directional pattern of filled array produced by multiplying the output of the short filled array with the output of the wide-spaced array.

The scheme of figure 5–97 can be subjected to electronic scanning (for receive only) by appropriate phasing of the short and long arrays. There is a substantial economy of elements, phase shifters, and associated signal-processing equipment because the m_1 elements in the first array and the m_2 elements in the second array synthesize the directional pattern of an n-element linear array

$$D(p) = \frac{\sin np}{n \sin p} \qquad (5\text{–}48)$$

where $n = m_1 m_2$. This pattern is a power-law response; therefore, amplitude tapering would be necessary to achieve good side lobes.

The economy of elements increases with the size of the array; only 20 elements are needed for a 100-element-position array (20 percent filling) and only 68 elements for a 1000-element-position array (20 percent filling). Many configurations also exist for synthesizing planar arrays such as the Mills cross array (ref. 5–35), which produces an n-element planar array from two linear ar-

rays of m_1 and m_2 elements (again $n = m_1 m_2$).

Figure 5–98 shows a schematic diagram of a within-pulse scanning radar for such an array configuration. The long and short arrays are shown physically separated for convenience, but the arrangement of figure 5–97 would probably be chosen. The radar incorporates frequency agility and video integration to suppress cross products. The frequency agility is removed at each receiving channel of the radar before narrowband amplification and modulation to achieve the continuous electronic scanning process. Multiplication of the outputs of the two arrays is conducted in the intermediate-frequency section.

A further valuable feature of the multiplicative array configuration of figures 5–97 and 5–98 is that, because most element spacings are already repeated in the two basic arrays, a substantial reduction of cross products occurs before demodulation.

Applications.—The usual applications for either within-pulse scanning or multiple-beam systems incorporating floodlight transmissions involve high data rate coverage of a fixed sector. For applications to aircraft or spacecraft, this tends to suggest fore or aft surveillance for those situations in which conventional scanning might be inconvenient, when the data rate might be too low, or when the presence of scanning modulation might degrade the required Doppler performance. The within-pulse scanning-type system does not appear relevant to side-looking applications because the equivalence of bearing information is obtained by along-track movement of the craft.

Possible alternative applications of such systems include the provision of radar altimeter information over a wide arc of cover-

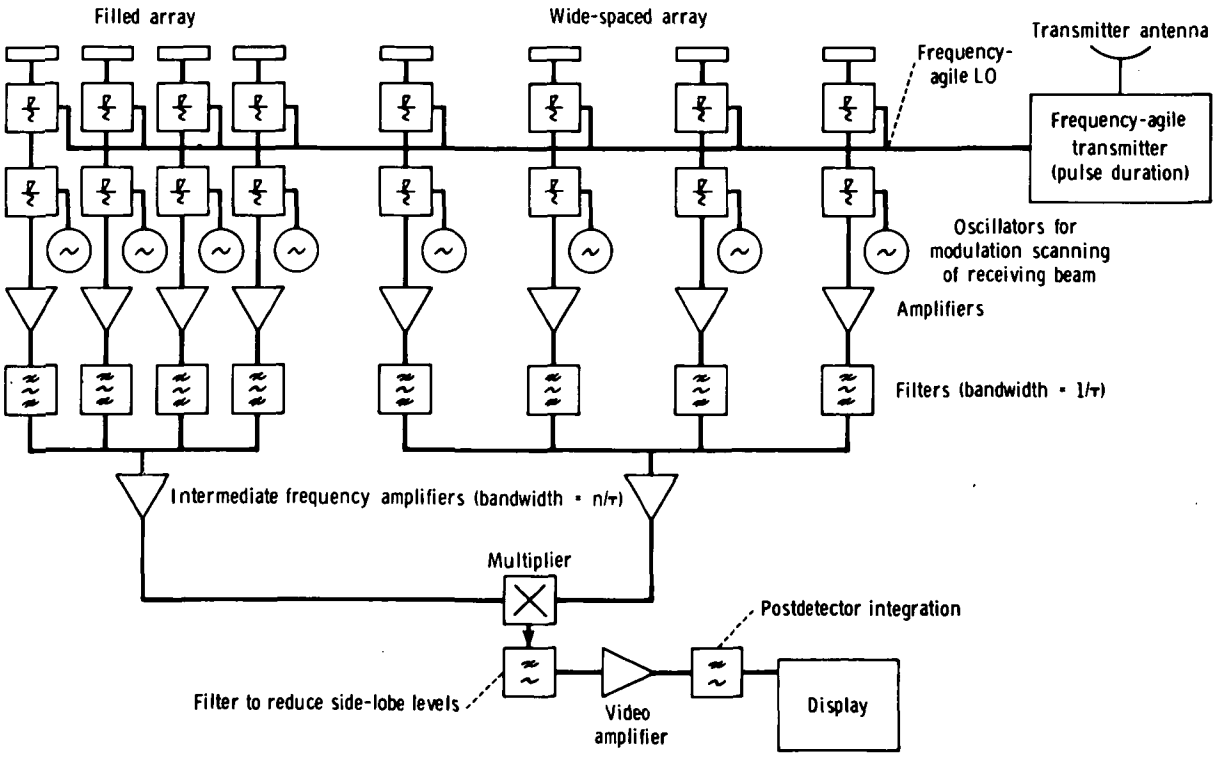

FIGURE 5–98.—Multiplicative array with within-pulse scanning on reception. Filled array containing m_1 elements multiplied by wide-spaced array containing m_2 elements to synthesize filled array with $n = m_1 m_2$ elements.

age below the craft; a further alternative might include scatterometer measurements over a similar wide arc. When the use of narrow fan beams or pencil beams is deemed advantageous, the previously discussed use of low-redundancy arrays offers substantial economies in numbers of elements required for the arrays and associated economies in processing circuitry.

Application of low-redundancy arrays to SAR.—The previous sections have been concerned with the application of low-redundancy arrays to the receiving aperture phased arrays for radar. This section concerns the possibility of extending the concept to synthetic aperture coherent radars with the objective of a significant reduction in the large amounts of data storage needed for such radars, particularly when using digital signal processing. The proposals are tentative and are meant to justify a more detailed study to establish the probable advantages for practical radar configurations.

The SAR uses phase-coherent transmissions (usually pulses). By storing and processing the received signals for many pulses, an equivalent two-way directional pattern of a long linear array can be synthesized. Details of such radars have been described in considerable detail in other sections.

The possible application of nonredundant arrays to the far-field patterns of the unfocused synthetic aperture is considered because this is a convenient direct extension of the far-field concepts of previous sections. However, the arguments also apply, with little modification, to focused arrays. The processed and filtered output of the radar is a signal that relates to a synthetic array in which each element position is the position of the physical array at the time of each transmission/reception. This processed output must be demodulated, and, as with the real arrays discussed previously, the detection process generates cross products between all possible pairs of element positions in the synthetic aperture. Again, there are substantial redundancies in such cross products, which suggest that it should be possible to reduce the number of transmission/reception positions in a given synthetic array length. This reduction would lead to some nonfilled pattern of transmission and reception positions within the synthetic array length, thus leading to a corresponding reduction of storage and processing.

Consider the original minimum redundancy array of figure 5–96. If an SAR moved along the line of this array transmitting and receiving only at the positions of the four elements, the output of the processor could be square-law-detected to provide the same postdemodulation directional pattern that would have resulted (before detection) from transmitting and receiving at all seven positions. This fact is certainly valid for the case of single-target directional patterns; the effect of coherence and unwanted multiple-target cross products will be discussed later.

The multiplicative scheme of figure 5–97 can also be translated into the synthetic aperture field. In this case, the radar would transmit and receive at the positions of the wide-spaced array and process this to produce the directional pattern of a synthetic array with wide element spacing. The resultant directional pattern would have angular diffraction lobes of the same form shown in figure 5–97. If the radar also transmitted and received at the locations of the shorter array, these outputs could be similarly processed to produce the synthetic pattern of a short filled array. The outputs of these two processed patterns can therefore be multiplied to produce a demodulated output having no diffraction lobes.

For such a scheme, the resolution of a synthetic aperture of n-element positions can be achieved by transmitting and receiving at m_1 and m_2 positions (where $n=m_1m_2$). This obviously represents a potentially valuable saving in storage and data processing. There is a loss of range performance as a result of the reduction of mean transmitted power by the same ratio. This loss can be recovered in principle by a corresponding

increase of peak transmitter power at those positions where the radar is activated.

A conventional SAR processes the output of the last n-pulse repetition intervals each time the physical aperture moves its own length. This is not possible with the previously mentioned two schemes, because the low-redundancy array configurations are not a continuous uniform series. For these cases, it is only possible to synthesize the required pattern at the end of the particular array pattern. To avoid gaps in the radar cover, it is also necessary to produce a processed output from the radar once for every position of the filled synthetic array. Figure 5–99 shows a different configuration of multiplicative array. The outputs of two thinned arrays having the same overall length but containing five and six elements, respectively, are multiplied. This figure shows that the resultant multiplicative pattern removes the diffraction lobes of the two constituent arrays. This resultant directional pattern is derived from 9-element positions and has a beamwidth and side-lobe level similar to the one-way pattern of a 21-element array (considering the power-law response).

The advantage of this configuration is that the output of the previous 9-element positions can be used to form such a pattern by synthetic aperture processing. However, this configuration does not solve the problem of deriving processed outputs from the radar for those positions of the real array at which there are no transmission and reception. This problem can be solved by tak-

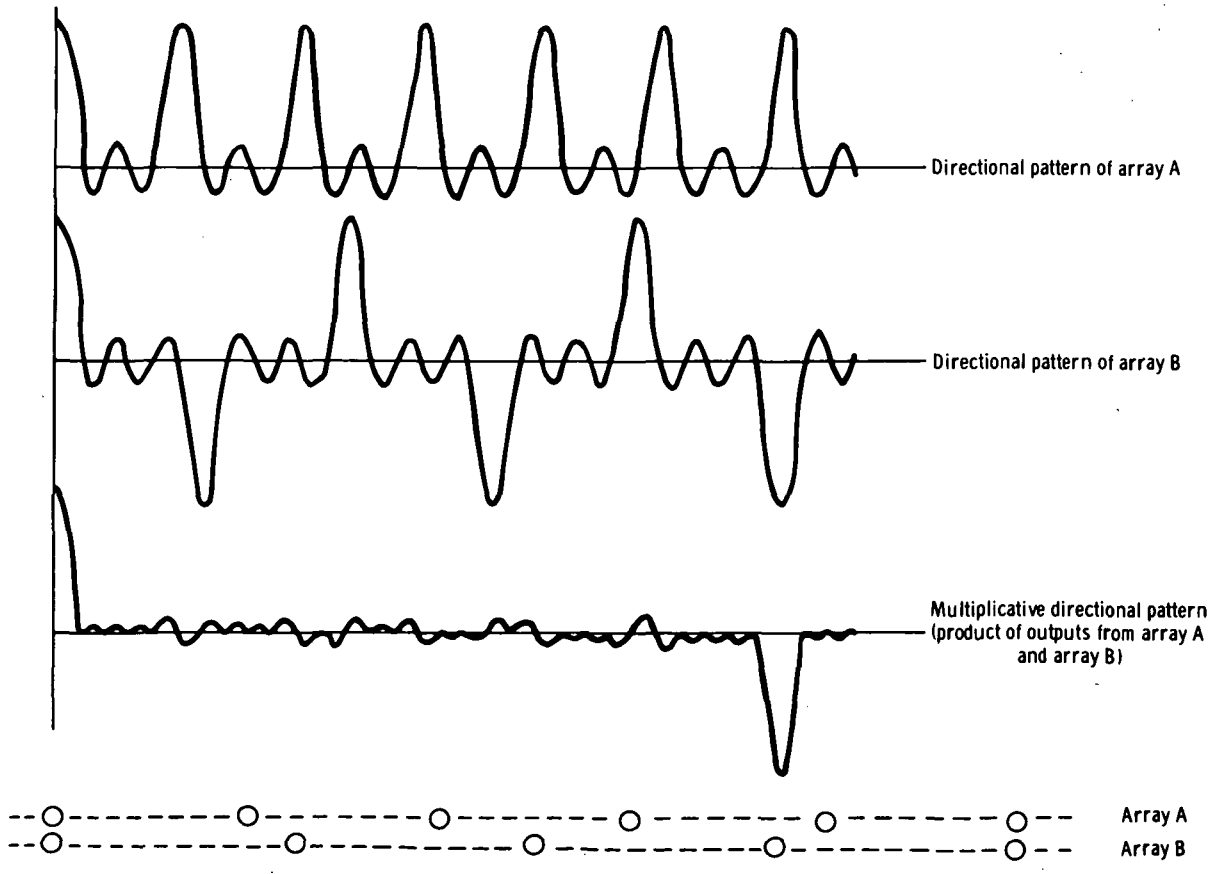

FIGURE 5–99.—Multiplicative product of outputs of two wide-spaced arrays that have the same total length but different numbers of elements.

ing the stored outputs from the active element positions and by processing these with different phase shifts to synthesize the beam outputs for the missing element positions.

It is also possible to apply this type technique to produce a continuous data output for the previous multiplicative configuration of figure 5–97. In this case, because the short filled array position is activated only infrequently, the resulting synthetic directional pattern changes slightly as the radar moves.

Because an SAR depends on some degree of coherence between the returns from each target over several transmissions throughout the length of the synthetic aperture, cross products between different targets will obviously arise. The methods of removing such target cross products, which were discussed earlier, will still apply in principle, but there are now rather different practical problems. For example, if frequency agility is used, it is still necessary to retain coherence over each synthetic aperture length so that the frequency-agile transmissions are interlaced with the other transmissions and the outputs added after demodulation. The obvious disadvantage of this approach is that it requires increased data storage in proportion to the number of different frequency transmissions per element position. Multifrequency transmissions with similar properties would be an alternative approach.

The most promising method of reducing cross-target products would probably be Doppler processing, but this restricts the applications to study of moving targets. In mapping areas of distributed targets (e.g., terrain), the level of cross products will be high.

For systems in which the low-redundancy array is used with SAR incorporating transmission to ground-based data processing, the telemetry bandwidth would be reduced. Nevertheless, it would be necessary to include some degree of buffering storage in the radar to smooth the flow of data.

Conclusions.—This section has shown how the nonredundant arrays used in radio astronomy may be used in radar applications for both RAR and SAR systems. Such schemes lead to an economy of elements in the array configuration in which typically $2\sqrt{n}$ elements are used to synthesize an n-element array; thus, the most significant savings are made for large arrays.

In the case of RAR, it is particularly convenient to combine low-redundancy arrays with within-pulse scanning. With such arrays, the demodulation process introduces target cross products that can be suppressed by using either frequency-agile transmission or Doppler filtering, followed by noncoherent integration. Such schemes offer attractive savings of array elements and associated processing for surveillance applications.

The application of low-redundancy arrays to SAR is more difficult to evaluate because it depends on the extent of target cross products for practical situations and their effect on the resultant radar maps. However, the potential storage savings should justify some further studies of these applications.

The Extension of Meteorological Satellite Radar Coverage by Antenna Null Steering

To use satellite-borne radar effectively for meteorological observations, ground clutter must not mask the returns from precipitation. A restriction is therefore imposed on the swath that can be covered by the satellite radar, because the range cell at extended crosstrack distances from the subsatellite point is inclined at an angle to the Earth, and returns from precipitation are masked by returns from the ground included in the cell (ref. 5–37). Narrowing the antenna beamwidth extends the crosstrack range. Also, MTI processing presents some promise for ground-clutter reduction, although this has been disputed. The backscatter from calm seas at low elevation angles may be sufficiently low to allow detection of moderate rainfall in the presence of sea clutter. However, over the land, clutter returns can be anticipated to be 5 to 25 dB stronger than returns from moderate rainfall.

The straightforward approach to avoid ground clutter by a meteorological satellite radar is to use an antenna beamwidth that is sufficiently narrow to minimize illumination of the Earth at the edge of the swath. Other considerations may restrict the antenna size below that needed for clutter reduction. This section outlines a method of ground-clutter reduction. The method consists of placing a null at the angle corresponding to the direction of the surface of the Earth at a given range. Techniques for accomplishing this task can vary from tilting a conventional antenna away from the Earth to controlling a null steering array. These techniques result in a gain reduction in the boresight direction.

The limitation on swath width.—A simple relationship exists between the satellite altitude, swath width, antenna beamwidth, and minimum detection height. A satellite is assumed to be at an altitude H above the Earth and to be detecting precipitation at a height h above the Earth at a crosstrack distance D from the subsatellite point (fig. 5–100). The radar pulse length is τ, which results in a range cell extent of $c\tau/2$. The boresight direction of the antenna is the direction of the precipitation target at height h, and the antenna pattern is assumed to have a null in the direction corresponding to the ground intercept point A. The angular width of the antenna pattern between the boresight and the first null is ϕ. For a conventional antenna, this is approximately equal to the half-power beamwidth. The relationships between the parameters shown in figure 5–100 are

$$h=r\cos\beta+\frac{c\tau}{2}\sin\beta \qquad (5\text{–}49)$$

$$(H+R_E)\sin\alpha=R_E\cos\beta \qquad (5\text{–}50)$$

$$r\sin\alpha=R_E\sin\theta \qquad (5\text{–}51)$$

$$D=R_E\theta \qquad (5\text{–}52)$$

leading to

$$h=r\phi\left(1+\frac{H}{R_E}\right)\sin\alpha+\frac{c\tau}{2}\sin\beta \qquad (5\text{–}53)$$

or

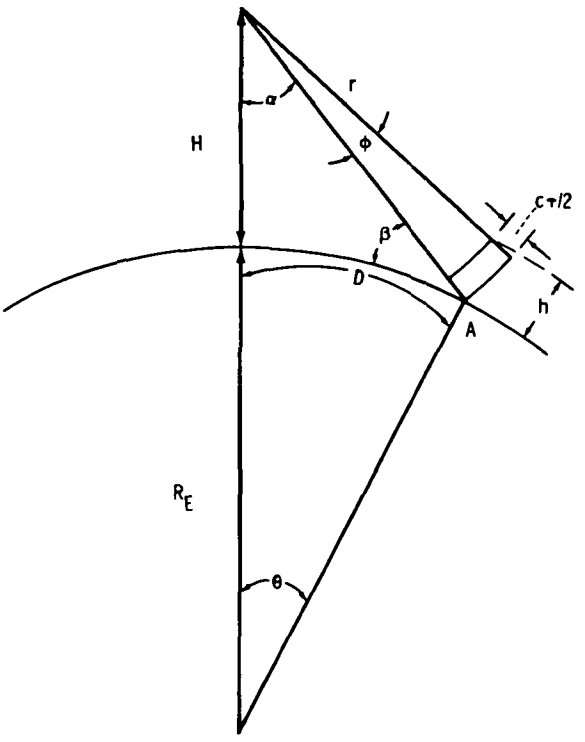

FIGURE 5–100.—Geometry describing the coverage of a satellite-borne radar.

$$h=D\phi\left(1+\frac{H}{R_E}\right)\left(\frac{\sin\theta}{\theta}\right)+\frac{c\tau}{2}\sin\beta \qquad (5\text{–}54)$$

If the radar pulse is short so that the range extent is small compared to h, the previous equation can be approximated by

$$h=D\phi\left(1+\frac{H}{R_E}\right) \qquad (5\text{–}55)$$

without incurring an error over 10 percent for the first 5000 km of crosstrack distance. The equation has been plotted for a range of parameters in figure 5–101. The crosstrack distance is greater for lower satellite altitudes.

The use of pattern nulls for clutter reduction.—Targets at heights below h will be masked by ground clutter because the antenna beam intercepts the Earth. However, if a pattern null were set at the direction of the ground intercept for a given range, the ground clutter would be substantially reduced.

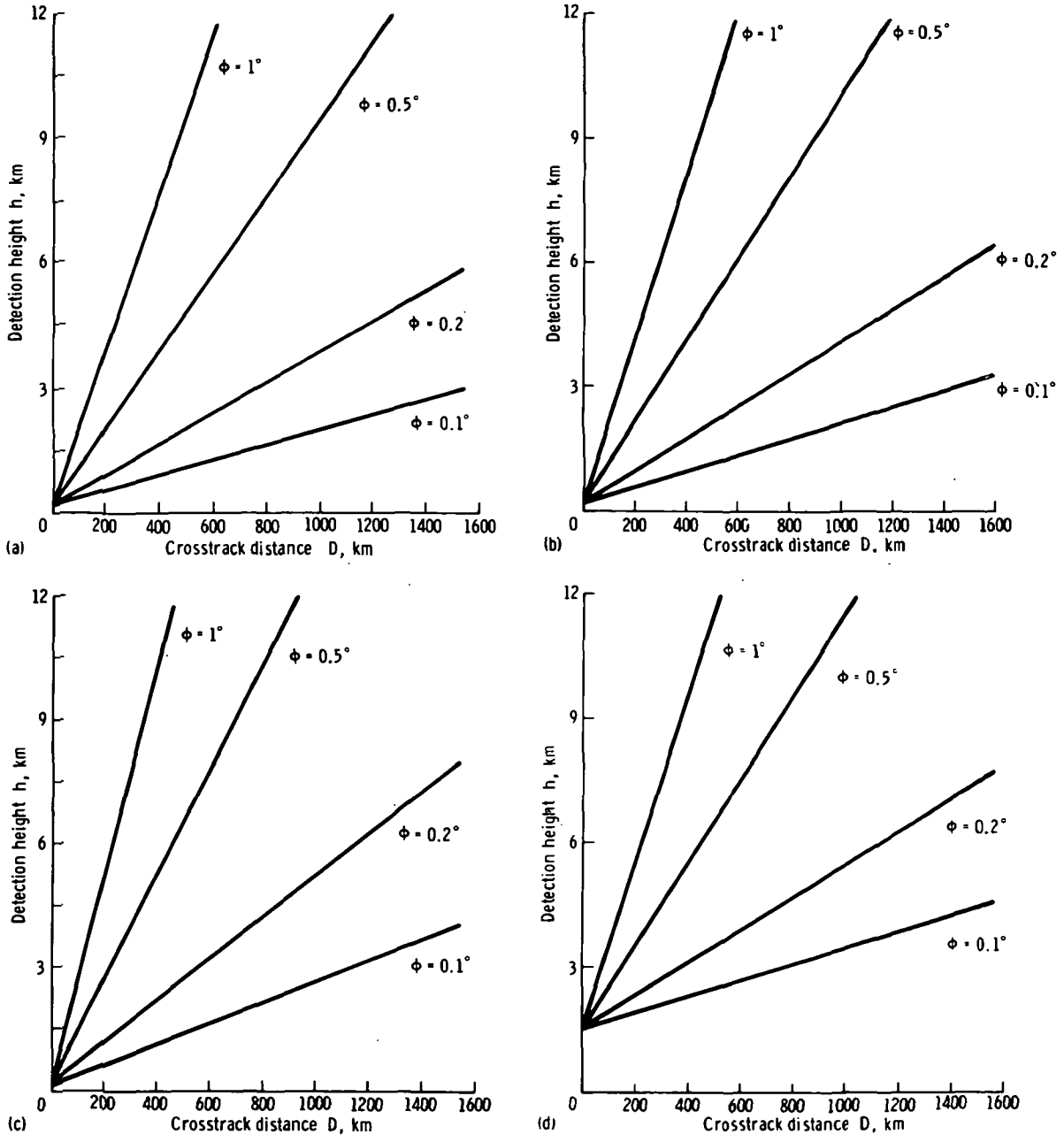

FIGURE 5–101.—Minimum detection height as a function of crosstrack distance for a range of parameters τ and H (ϕ=0.1°, 0.2°, 0.5°, and 1.0°). (*a*) H=322 km, τ=1 μsec. (*b*) H=965 km, τ=1 μsec. (*c*) H=2896 km, τ=1 μsec. (*d*) H=965 km, τ =10 μsec.

The nulls of the pattern of an array antenna can be positioned by the adjustment of the excitation coefficients of the array elements. The problem of maximizing the gain in a given direction while positioning a null at another direction has been studied by Drane and McIlvenna (ref. 5–38). The curve in figure 5–102 labeled "Null steering array"

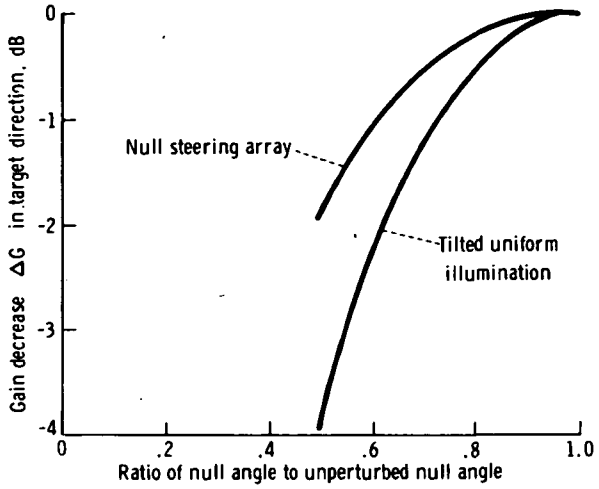

FIGURE 5–102.—Gain decrease in the target direction for null steered array and tilted uniform illumination.

shows the decrease in gain in the boresight direction as the null is steered into the main beam region. This figure illustrates that a null can be placed at an angle from boresight of one-half that of a conventional array, with an attendant reduction of 2 dB in one-way gain. This gain reduction would correspond to a lowering of radar sensitivity such that the minimum rainfall rate that could be detected would be increased by a factor of 1.78. Assuming that a 4-dB sensitivity margin could be built into the radar receiver, the ground swath width could be extended by a factor of 2 over that shown in figure 5–101.

Tilting the beam of a conventional antenna array away from the Earth will also achieve the desired result. However, the reduction in gain in the target direction is greater than that for a null steering array. The curve in figure 5–102 labeled "Tilted uniform illumination" shows the gain decrease as the antenna beam is pointed away and the null moves toward the ground intercept. For a tilt of one-half the peak-to-null angle, the gain in the target direction is lowered by approximately 4 dB, corresponding to an equivalent sensitivity to rainfall rates 3.4 times greater than that for the maximum gain direction.

The width of the null determines the number of range cells for which the ground clutter is effectively reduced. For the tilted antenna, the angular width of the null region for a clutter reduction of 26 dB, relative to the precipitation return direction, is 0.286 times the angle from the beam peak to the null. For the null steering array, the 26-dB clutter suppression zone is approximately 0.20 times the width of the unconstrained peak-to-null region. More than one null can be positioned near the ground-intercept direction to provide an extended region of clutter suppression.

Conclusions.—By steering the first null of the satellite antenna radiation pattern to coincide with the ground-intercept point, the crosstrack range of coverage of a meteorological satellite radar can be extended. Techniques exist for null steering by adjustment of the amplitude and phase of array excitation coefficients. As the null is steered into the main beam region, there is a directivity reduction. A simpler technique is to tilt the beam of a conventional antenna away from the Earth; however, this technique results in a larger gain decrease for a given null shift than for an optimized null steering array.

For example, consider a satellite at an altitude of 1000 km with an antenna beamwidth of 0.25°. At a wavelength of 0.8 cm, the crosstrack aperture size would be approximately 2 m. For a minimum detection altitude of 1.5 km, the maximum crosstrack distance from the subsatellite point would be 300 km. To cover ground ranges in excess of this distance, the null would be steered, extending the crosstrack distance to 650 km from the subpoint. The total swath width would be 1300 km, with an increase of 78 percent in the minimum detectable rainfall rate at the swath edges. The null steering must be linked to the range window so that the clutter-suppression zone corresponds to the desired set of range cells.

PART C

DATA MANAGEMENT

INTRODUCTION

The objective of data management is to provide a better data flow from the sensing of data to its application by the user. This effort is important because the data are increasing in complexity and volume, and the allowable time for reducing the data is limited in many instances. Data management should include, but is not limited to, the following: (1) onboard processing and transmission of the data to the ground, (2) ground handling and processing of the data, (3) machine interpretation of the data, and (4) distribution to the ultimate user.

As a major step in data reduction and in minimization of data-link bandwidth, as much onboard processing as possible should be performed within the practical constraints of the spacecraft or aircraft carrying the active microwave sensors.

A general block diagram of the data-management system is shown in figure 5–103 for a partial onboard processor. The figure traces the data flow from a sensor to the ultimate user.

Partial onboard processing will provide ephemeral data calibration, rough classification when appropriate, and as much bandwidth reduction as possible to reduce the telemetry load. Image restoration and registration will provide additional calibration when necessary, including geometric and atmospheric corrections, and will enter satellite ephemerides into the data. Image processing will provide enhancement, filtering, and, particularly in the case of SAR, the two-dimensional Fourier transform processing necessary to obtain the image. Pattern recognition and data compaction provide feature extraction, data classification, and, in many instances, conversion from image data to printed summaries. Data from the image-processing and pattern-recognition operation goes to either local or remote users.

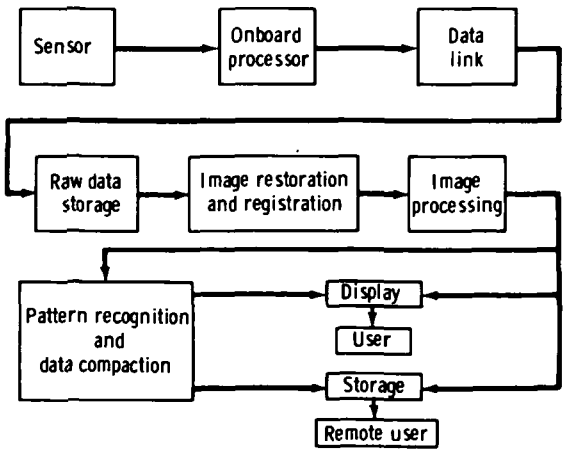

FIGURE 5–103.—Block diagram of the data management system for a partial onboard processor.

The approaches, equipment, and techniques are generally available for all functions shown in figure 5–103, except for the box labeled "Pattern recognition and data compaction." For research using satellite sensors, machine reduction is not necessary, and vast amounts of data are acceptable and even desirable. In this case, the effective data-management system on the ground must be an interactive system. Large computers alone cannot solve the data problem; thus, human interaction is needed to do the best research job.

The reverse is true in eventual operational usage. The managers, who must make decisions based on satellite data, will require inputs that are stripped of unnecessary information and are as compact as possible. For example, high-resolution radar maps of a region must be reduced to a table of hectares of wheat, rice, and so forth, together with an estimate of eventual yield for each. This function is the province of pattern recognition and data compaction. The techniques for accomplishing this task have not yet been developed for radar images and will require research effort.

The onboard processing and image processing required for SAR are discussed in the section entitled "Imaging Radar Data Reduction Considerations." The SEASAT–A ground data-processing system for radar images is a good example of an end-to-end data system and is discussed in detail in the section entitled "Imaging Radar End-to-End Data Systems." To illustrate how data may be processed for systems other than imaging radars, a brief discussion of the data handling and processing of the Skylab S193 altimeter, radiometer, and scatterometer is given in the same section.

Interpretation of the great mass of data that will be available from radar satellites requires at least partial automatic pattern recognition. Although much effort has been given to pattern recognition on other remotely sensed data, few results are available for active microwave systems. Hence, a specific recognition technique or data format cannot be suggested at this time. Appendix 5A to this chapter is devoted to a general discussion of pattern recognition with special reference to the active microwave data.

End-to-End Data System Overview

The term "end-to-end data system" is used to describe a system that converts analog radar signals into geographical quantities. The input "end" of the system is one or more analog signals from the radar, which, for most radars, would be a video-received output augmented with housekeeping information. The output "end" of the system is a measured geophysical quantity, which was estimated from some radar parameter. For example, the geophysical quantity could be significant wave height derived from the spread of surface echoes in an altimeter, windspeed derived from radar-scattering coefficient (which was derived from an echo power in a scatterometer), or ocean-wave spectra derived from a radar image. Between the input and output "ends" of this data system are other inputs such as ephemerides, instrument calibrations, housekeeping data, and propagation estimates. The propagation estimates may be provided by other space instruments.

The flow of radar data between the input and output is shown as the serial string of operations in figure 5–104. These functions are divided into two distinct groups. The first group includes functions performed on the spacecraft that transform the analog signal into a digital bit stream, a convenient form for storage in the spacecraft for eventual transmission to the ground.

The second group consists of the ground-based processing functions that begin with stored telemetry data and gradually convert the radar signals to geophysical quantities. Generally, the radar signals would be manipulated first and then converted to geophysical quantities using calibration curves. Once converted to geophysical quantities, the data would be distributed to users and archived for future data reductions.

The specific design of an end-to-end data system depends on the radar measurements flowing out of the instrument and the manipulations and algorithms required to convert these radar measurements to geophysical quantities. In some cases, like SEASAT–A, other instruments are flown and operated simultaneously, and several of the end-to-end data systems (like the one shown in fig. 5–104) must be tied together into an even larger system. However, in this section only single radar systems are considered.

The end-to-end data systems will depend

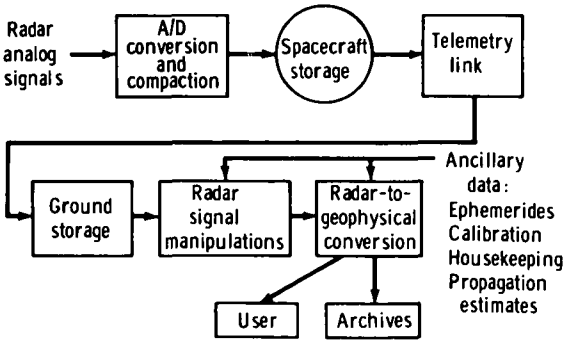

FIGURE 5–104.—Block diagram of an end-to-end data system.

on the number of spaceflights that a particular instrument has flown. For an instrument with no spaceflight experience, such as the imaging radar, many intermediate data products will be produced to ensure that individual processing steps are not breaking down. Also, the algorithms for converting radar measurements into geophysical quantities will be relatively crude. For other instruments such as radar altimeters and scatterometers, which have already flown in space, these algorithms will be more sophisticated and will be applied earlier in the data-processing chain, possibly onboard the spacecraft.

IMAGING RADAR DATA REDUCTION CONSIDERATIONS

Imaging radars have been proposed for SEASAT–A and Space Shuttle missions. Starting with a digitized version of video-amplifier output and ending with a digital-bit stream into an onboard storage, the data flow for an imaging radar requires that large volumes of data be reduced to maximize the output of radar instruments.

Synthetic Aperture Radar Data Acquisition

Synthetic aperture radar systems have generally gathered the data and recorded them for future processing on a ground-based correlator because the data-reduction process has not been amenable for real-time processing. With the advent of integrated circuits, especially large-scale integrated circuits, the possibility of digitally generating an image in real time with an onboard processor has become a reality.

A possible advantage of real-time processing of radar data onboard the spacecraft is that the total data content may be reduced if image data compression is used, thus eliminating one of the steps required to get the data to the user. However, a real-time processor still requires a complex piece of hardware that will require extra power and weight, and it may be more costly than an equivalent ground-based data digital correlator.

The synthetic aperture side-looking radar generates an image of the surface being observed by transmitting a coherent signal to the surface at a periodic rate and observing the return from all the resolution elements. During the data-reduction process, the two-dimensional data are passed through a two-dimensional matched filter corresponding to the ideal return from each cell. The following section describes the steps required to process these data digitally as an aid to determine at which point it would be best to stop the process onboard the spacecraft and to introduce the ground-based data-handling process.

Data-Reduction Processes

The data gathered by the coherent radar system may be thought of as being two dimensional. The first dimension, range, corresponds to the succeeding returns from a transmitted impulse and the echoes arriving from reflectors at increasing range. The second dimension, azimuth, corresponds to the returns at a constant range or time delay from succeeding pulses as the spacecraft travels in its trajectory. In a coherent system, the return from a single reflector is complex because it contains phase information and amplitude. The phase is relative to the constant stable LO and depends on relative delay in terms of fractional wavelength of the reflector. The amplitude is proportional to the transmitted waveform and the reflectivity of the target. The two-dimensional history of these returns uniquely determines the relative position and amplitude of this target relative to the radar system.

To obtain fine resolution in the range dimension, it is desirable to transmit a short rf pulse and receive through a wide-bandwidth receiver. Thus, one of the data reduction steps is pulse compression (i.e., range compression). A second process is azimuth compression, which corresponds to generating a focused synthetic array. Two other steps that may be performed are presumming and multiple-look processing. Presumming is an operation in the azimuth

dimension to reduce the azimuth bandwidth. Presumming simplifies the data processing and reduces memory storage requirements at the expense of azimuth resolution. Multiple-look processing involves generating separate images from independent data and superimposing these independent images to reduce the speckle caused by the statistical variation of the returns from each reflector. This section will examine the data contents at each step and estimate the complexity of each operation.

The basic radar data processor configuration is shown in figure 5–105. This processor need not be on the spacecraft and may be broken up at any of these basic blocks. Consequently, four options exist: (1) basic processing on the ground, (2) presumming onboard the spacecraft and range and azimuth compression on the ground, (3) only azimuth compression on the ground, and (4) all processing onboard the spacecraft. For a system with multiple looks, a fifth option exists: transmitting to the ground the composite image rather than the individual components. This technique will be discussed elsewhere in this chapter.

The data rate out of the radar N_A may be expressed as

$$N_A = \frac{2N_b(T+\tau)c(\mathrm{PRF})}{r_r} \qquad (5\text{–}56)$$

where N_b is number of bits per sample, T is

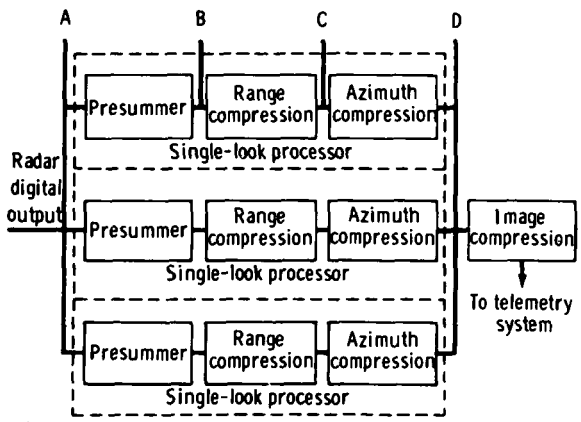

FIGURE 5–105.—Basic radar data processor configuration.

required sample interval in radar time, τ is dispersed transmitted pulse width, c is speed of light, and r_r is range resolution.

This equation may also be expressed as

$$N_A = 2N_b \frac{S_r S_a}{r_r r_a}\left(1+\frac{\tau}{T}\right) \qquad (5\text{–}57)$$

where S_r is radar space swath width, S_a is length images in 1 sec in azimuth, r_r is range resolution, and r_a is theoretical azimuth resolution. Because no processing has been done at this point, the theoretical azimuth resolution is

$$r_a = \frac{L_a}{2} \qquad (5\text{–}58)$$

where L_a is the antenna length along the velocity vector.

The presummer consists of several data storage arrays where a number of echoes are added on an ensemble basis, with or without time weighting. The presummer reduces the azimuth bandwidth at the expense of azimuth resolution. This azimuth bandwidth reduction also increases azimuth ambiguities. To reduce these ambiguities to acceptable levels, it is necessary to effectively oversample the azimuth data to a level higher than Nyquist's criteria by a factor K, varying from 1 to 2. Thus, after the presummer, the data rate N_B can be expressed by

$$N_B \quad \frac{2N_b T\left(1+\frac{\tau}{T}\right)vK}{r_r r_a'} \qquad (5\text{–}59)$$

where v is the spacecraft velocity, K is an oversampling factor, and r_a' is the desired azimuth resolution. Alternately, this expression may be written as

$$N_B = 2N_b \frac{S_r S_a}{r_r r_a'}\left(1+\frac{\tau}{T}\right) K \qquad (5\text{–}60)$$

The number of bits per sample N_b will be the same as before presumming, because no compression has taken place in either domain.

The range compression in the data system consists of a cross-correlation device. The effect is to compress the returns of the range-dispersed echoes. Because of the pulse-com-

pression effect, the data will now have an increased dynamic range (not signal-to-noise). The increase in dynamic range is given by

$$N_c = \log_2 (\tau B) \qquad (5\text{–}61)$$

However, the data stream per azimuth line is shortened by the dispersion length τ. The data rate at point C, shown in figure 5–105, of the range compression subsystem is

$$N_c = \frac{2(N_b+N_c)\,TcvK}{r_r r_a'}$$

$$= 2(N_b+N_c)\frac{S_r S_a}{r_r r_a'} K \qquad (5\text{–}62)$$

The azimuth compression subsystem is a cross-correlation device in which the signal is cross correlated on an ensemble basis with the azimuth-matched filter. Like the range compression subsystem, the dynamic range of the output will be greater than that of the input. The increase in dynamic range, in bits per sample N_d, is given by

$$N_d = \log_2 (TB_a) \qquad (5\text{–}63)$$

where T is the time the radar signal from a point reflector retains a Doppler frequency with a bandwidth B_a. In addition, the azimuth correlator will convert the data to baseband if a range offset occurs or if the data are in a complex mode (I and Q channels) computing the magnitude of the vector. In either instance, the output data content is

$$N_D = (N_b+N_c+N_d)\frac{S_r S_a}{r_r r_a'} \qquad (5\text{–}64)$$

At this point, the image may be formed directly where each pixel is characterized by $(N_b+N_c+N_d)$ bits per point.

The data storage DS required in the azimuth correlator is

$$DS = (N_b+N_c)\frac{S_r R_s \lambda}{r_r r_a'^2} \qquad (5\text{–}65)$$

where R_s is the range to the surface and λ is the radar system wavelength.

A radar image of a two-dimensional uniform target field processed with a two-dimensional matched filter will exhibit a variation of intensity in the output image from one resolution element to the next. This variation in apparent intensity is due to several factors such as (1) additive random noise caused by the radar system, (2) energy spillage from one resolution element to the next, and (3) variation of the apparent reflectivity of the resolution element with respect to angle of wave incidence. The latter term has been referred to as the reflection pattern of the target. The first factor is minimized by illuminating the target with sufficient power so that the signal-to-noise ratio is large. The second factor can be minimized by careful system design and by processing the data with suitable weighting functions to minimize both range and azimuth side lobes. Minimization of the third factor requires looking at the surface with either different wavelengths or different look angles; hence, the concept of multiple-look processing.

Multiple-look processing, to reduce image speckle, can be implemented using a variety of methods. These methods depend on either observing the terrain at several frequency bands or observing the terrain in different portions of the antenna beam. The first method is often referred to as obtaining multiple looks in range, whereas the second method is referred to as obtaining the multiple looks in azimuth. In either case, the image is generated by using these methods independently. The resultant signals are then noncoherently added. The result of this noncoherent addition is a more pleasing image because of the reduced speckle. This image is obtained by reducing the standard deviation of a uniform target field, which allows a more precise estimation of the surface backscatter coefficient. The improvement in image quality is not obtained without a price. If the different looks are obtained in range, the average transmitted power must be increased by the square root of the number of looks required, and the radar-receiver complexity is somewhat increased over the single-look case. If the looks are obtained in azimuth, the average

radiated power is reduced by the square root of the number of looks, but an image buffer must be added to the multiple processors. The total data storage in this image buffer N_{buf} is given by

$$N_{buf} = (N_L - 1)(N_b + N_c + N_a)\frac{S_r}{r_r}\frac{3R_s\lambda}{2(r_a')^2} \quad (5\text{–}66)$$

where N_L is number of looks.

Images have been successfully compressed to the extent that the total data transmittal is reduced by a factor of 30 to 50 from the uncompressed case. The impact of the image compression technique on the question of onboard radar data processing is very significant. A comparison of the basic (one look) processor data output and the radar system digitized data output (eqs. (5–64) and (5–58)) indicates that, for high-resolution processing, the data rate out of the processor may be no lower than if the data were telemetered back to the ground and processed. However, if an image compression technique were used, a significant reduction in data rate could be achieved by processing onboard the spacecraft. If the desired resolution of the imaging system is significantly worse than the theoretical resolution of the radar systems, the best point for data transmission to the ground may be at the output of the presummer (point B of fig. 5–105). At this point, for a given set of processing parameters, the data rate for the basic processor is at a minimum.

An examination of equation (5–65) gives an indication of the complexity of an onboard data processor for a spacecraft imaging radar system. As an example, the total data storage required for a radar (at an orbital altitude of 200 km, imaging a large swath width of 100 km, at a long wavelength of 0.2 m, and a resolution of 10 m) is approximately 32×10^6 bits. The current state of the art of shift registers suitable for a processor will store 4096 bits per chip. This processor would require 7800 integrated circuits. In the near future, charge-coupled-device digital shift registers are expected to have a significant effect on the digital processor implementation. Shift registers of 64×10^3 bits of storage and consuming two to three orders of magnitude less power are expected, making the digital processor a realizable device.

IMAGING RADAR END-TO-END DATA SYSTEMS

A purpose of the end-to-end data system is to transform data that are in engineering quantities into data that are in geophysical quantities. For an imaging radar, the starting data form is a two-dimensional array of power as a function of the orthogonal dimensions of range and azimuth. Azimuth is the along-track dimension and is a function of vehicle position as compared to time. The end data product will be some geophysical quality, such as wave spectra, as a function of position and/or time. Between these two end data products is a multiplicity of operations.

The End-to-End Data System for SEASAT–A

To better describe the end-to-end data system, the example of the SEASAT–A imaging radar will be used. The SEASAT–A, planned for launch in 1978, will have an imaging radar that will sample ocean surface phenomena in several modes. Sampled scenes with a wide swath of approximately 100 km (at a 25-m resolution) or 200 km (at a 100-m resolution) will be taken until the onboard storage of 10^9 bits is filled. Also, for global ocean-wave monitoring, patches 10 by 10 km (at a resolution of 25 m) will be taken at approximately a 100-km spacing until the onboard 10^9-bit storage is filled. In all these sampling modes, the radar data will be thinned by the presumming techniques described in the section entitled "Data Reduction Processes." The thinned data will be telemetered to the group and stored on telemetry tapes. These telemetry tapes will be processed to produce a radar image. This image is a convenient breakpoint and can be called the instrument output, and it is the

input to the end-to-end data system. Figure 5–106 shows the end-to-end system for SEASAT–A.

This radar image resembles space photographs obtained with Mariner, Pioneer, and ERTS spacecraft. Both digital and analog radar outputs are planned for SEASAT–A. The analog output is the familiar photographic radar image. The digital image is a collection of bits on magnetic tape, which are similar to the downlink products of the Mariner, Pioneer, and ERTS spacecraft.

These two radar image products, the analog photograph and digital tape, can be derived from two nearly independent processing paths. An analog path would proceed where telemetry tape was converted to a signal film, which would be compressed in an optical correlator to produce an image photograph that could be digitized to produce a digital image tape. The alternate digital path would directly correlate the telemetry tape data in a digital computer to produce the digital image tape, and a photographic playback would produce the photographic analog image.

These two products represent echo power as compared to range and azimuth. Obvious data transformation to more useful products would include conversion of range and azimuth to latitude and longitude and conversion of echo power to normalized surface cross section.

In addition to location tagging, time tags must be carried. Time tags will probably be carried from the initial telemetry tape. Also, during this image processing, obvious data dropouts and other radar flaws will be corrected.

Like the original images, the corrected

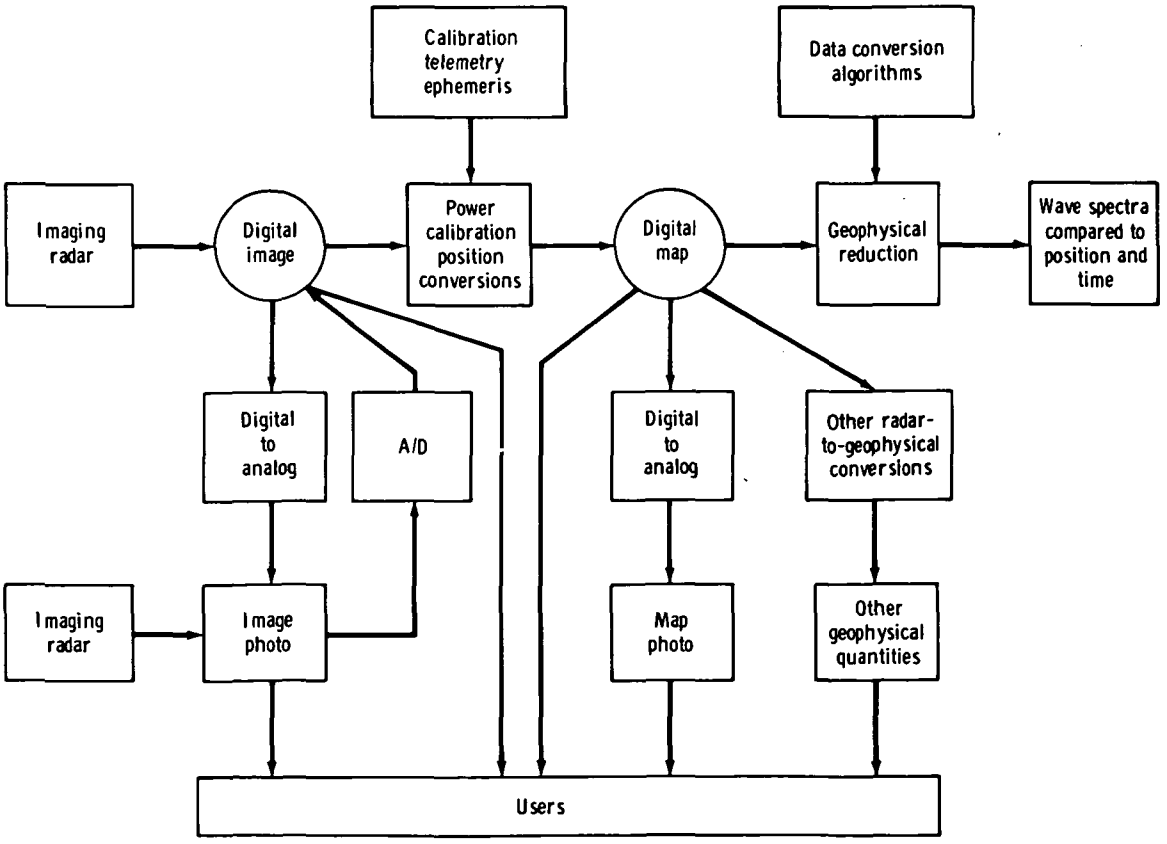

FIGURE 5–106.—End-to-end data system for SEASAT–A imaging radar.

and refined radar maps will be preserved as a digital image on magnetic tape. To separate the converted product from the original product, the term "map" is used for the corrected product, whereas the term "image" is used for the original product.

More processing will be needed to convert the mapped radar cross section to useful geophysical quantities. For example, a major objective of SEASAT–A is to convert these radar maps into wave spectra in a two-dimensional ocean wavelength space.

This example of SEASAT–A processing is illustrative of typical numbers for an imaging radar system. For example, the sampled swath with a 100-km width and 25-m resolution is 4000 pixels wide. Assuming images and maps of equal widths and lengths, there will be 4000 by 4000 radar pixels for a SEASAT–A frame as compared to 2400 by 3600 radar pixels for a single ERTS frame. Assuming eight bits per pixel, each picture has 1.28×10^8 bits (about the capacity of a standard computer tape). Photographic playback at a 15-μm spacing yields 60- by 60-mm negatives. For both ERTS and SEASAT–A radar imagery, the actual image length may be several times the image width, but these images can be reduced to square formats.

Several important points can be made by briefly reviewing this example of the SEASAT–A end-to-end data system.

1. The radar image data are similar to the photographic products from other spacecraft such as ERTS, Mariner, or Pioneer.
2. The user data products can occur at several points along the processing chain.
3. The radar parameters and/or operations can also enter at several points along the processing chain.
4. It is particularly important to have two types of products: the digital tape, which is the basic storage medium for the computer, and the photographic playback.
5. The ground-based processing must be flexible enough to accept new algorithms for computing geophysical quantities.

Other NASA radar imaging systems for the next decade will include aircraft test beds, possibly routine commercial aircraft, and the Space Shuttle. For the aircraft test beds, the data-processing steps outlined in figure 5–106 will be tested and proved, but a fixed and final system will probably not be built. However, if an imaging radar were built to operate routinely from a commercial aircraft, then an end-to-end data system similar to the one shown in figure 5–103 for SEASAT–A would be required. When imaging radar systems are carried onboard the Space Shuttle, an end-to-end data system will also be required. For the Space Shuttle flights, the end-to-end system must be flexible enough to keep up with changes in the Space Shuttle radar configurations, which will probably be improved with each Space Shuttle mission.

End-to-End Data Systems for Other Radar

Although not as complicated as a system for an imaging radar, end-to-end data systems for other radar types still require a degree of complexity. Figure 5–107 is a simplified flow diagram of the Skylab S193 altimeter, radiometer, and scatterometer.

This experiment was part of the Earth Resources Experiment Package (EREP), which combined several sensors. A combined data system was used to collect and record the data onboard the spacecraft. The basic flight-recording medium was a 28-track pulse-code-modulation tape recorder, and the tapes were returned by the crew after each mission. Once the tapes were recovered, a central data-processing system at JSC was used to reformat the tapes and correct any skew error that might have occurred. Fourteen-track tapes were then generated for each EREP sensor. These tapes contained essentially the raw experiment data. The data were used to assess experiment performance during the mission. The 14-track tapes were then subjected to further processing, which was unique to each experiment.

Altimeter data were time- and altitude-corrected with the Skylab data from the spacecraft. Altimeter calibrations and ephemeris correlations were input. Finally,

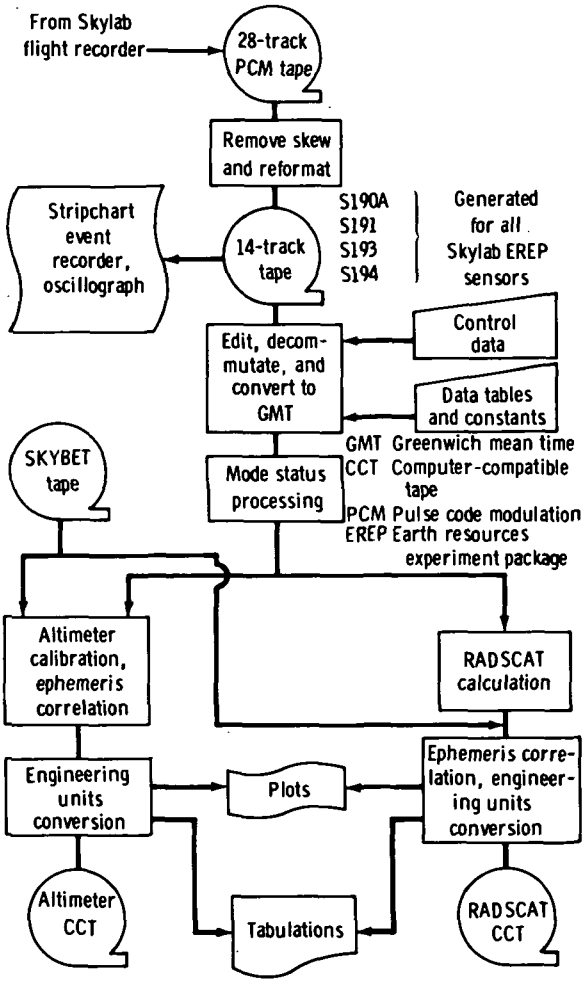

FIGURE 5–107.—Simplified diagram for data flow of the Skylab S193 altimeter, radiometer, and scatterometer.

engineering unit conversions were performed, and the information was recorded on a computer-compatible tape. In addition, plots and/or tabulations are generated as required.

The RADSCAT data received slightly different processing because certain calculations performed on the data were prerequisites to ephemeris correlation and conversion. The final output was a computer-compatible tape product. Plots and tabulations were also generated as required.

End-to-end data processing for altimeters, scatterometers, and radiometers may require several data reformats, attitude and time corrections, and calculations. The Skylab S193 experiment contained all three activities.

COMPUTER RECOGNITION CONSIDERATIONS

An important aspect of the conversion of radar measurements to geophysical quantities is the generation of fast and accurate algorithms. Interpretation of imaging radar data could require some form of pattern-recognition techniques in the image processing, and such techniques are useful to other radar data such as those from scatterometers, altimeters, and so forth. A discussion and techniques are presented in appendix 5A to this chapter, entitled "Pattern Recognition Considerations."

SUMMARY

The data management for a spacecraft radar has been defined in terms of an end-to-end data system, which performs the following three functions:

1. Sampling and compaction of data onboard the spacecraft.
2. Manipulation of radar data on the ground.
3. Conversion of radar measurements to geophysical quantities by means of pattern recognition and other machine techniques.

Division between these three functions is not always clear; and, as instruments are flown on more missions, the functions originally performed on the ground will eventually be moved closer to the data source and may in time be performed onboard the spacecraft.

The data processing for imaging radar onboard the spacecraft was examined in detail with the conclusion that several techniques can be used to compact the data before storage. The recent design study for the SEASAT–A imaging radar indicated that this data compaction was one of the outstanding research results in the design. It is recommended that compaction techniques

be studied further and that existing aircraft radars be modified to provide digital data so that these compaction techniques can be tested.

Data management for SEASAT–A imaging radar provided an example of a possible end-to-end data system for a future spacecraft imaging radar. This example indicated that—

1. A radar image is similar to the photographic products from other spacecraft such as ERTS, Mariner, and Pioneer.

2. The user products and the radar parameters enter the processing at several different points in the system (i.e., the ends of an end-to-end system are not singular points).

3. Two basic data products must be considered: computer digital tapes and analog photographs.

4. Ground processing must be flexible and adaptive.

5. A library for radar data is needed.

Automatic computer-processing and pattern-recognition techniques must be implemented near the user end of an end-to-end data system. The applications of these processes to imaging radar data will expand, based on previous work with multispectral data.

PART D

PROGRAM PLANNING

This section presents a discussion and recommendations for future activities necessary to support satellite microwave sensing. The need exists for a program that will provide information in the following areas:

1. Experimental test program to establish the interaction of electromagnetic waves and sensed parameters.
2. Component development.
3. Data processing.
4. Calibration.
5. Design and fabrication of a multifrequency system.

Each area will be discussed in greater detail in the following paragraphs.

Inputs to this section were obtained from joint discussions between the TSG and the three panels of the Active Microwave Workshop.

EXPERIMENTAL TEST PROGRAMS

A requirement exists to determine experimentally the characteristics of surface features when these features are sensed by electromagnetic waves in the microwave portion of the spectrum. The stated desires and requirements of the Earth/land panel for experimental data from controlled tests were adequate to keep several aircraft systems busy on a continuous basis.

Earth/Land

The Earth/land panel has suggested an aircraft research program the objective of which would be to provide the information that has been lacking or fragmentary in this important field of remote sensing. Two additional items are highlighted for future effort: small-scale surface-texture measurements and polarization signatures.

Small-scale surface texture.—The unique capability of active microwave systems to detect variations in surface texture of geologic materials is potentially one of the most useful applications of microwave remote sensing.

A recent example of the type of detailed feasibility study necessary for a thorough examination of SLAR surface texture analysis is included in the section entitled "Com-

bined RAR and SAR Imaging." This investigation, using radar images of Death Valley, clearly indicates the importance of multifrequency radar systems to delineate small-scale surface texture, and, thus, distinct lithologies.

Sufficient SLAR images are not yet available at diverse wavelengths, polarizations, and look directions over any particular study area for a comprehensive evaluation of optimum system design for surface-texture analysis.

As part of the NASA aircraft programs plan, it is proposed that an optimum SLAR system be designed for surface lithologic identification. The system would have the following characteristics:

1. A wide spread in wavelengths (i.e., 3 cm, 25 cm, 10 m).
2. Dual polarization (HH and cross) for at least the 3- and 25-cm wavelengths.
3. Incident-angle capability from 0° to 70° (0° to 45° nominal use).
4. Maximum attainable power.

The system would have surface-texture sensitivity ranging from 0.2 to 1.8 cm and should provide geoscience users with much greater success in mapping lithologic materials than previously encountered. The NASA Jet Propulsion Laboratory X-, L-, and P-band systems and the ERIM X- and L-band systems would have immediate application to this area of investigation.

Polarization signatures.—A unique polarization technique has been demonstrated by Martin (ref. 5–39) that appears almost unknown in the microwave-sensing community. The technique is the ability to change polarization at the PRF rate (e.g., 5000 times/sec). Thus, polarization changes can be obtained in small steps (e.g., 11.25° increments). This system can obtain polarization signatures (figs. 5–108 and 5–109) on a single pass over small areas.

Use of existing data and systems.—The initiation of several interim steps is proposed to reduce the time required to provide at least part of the needed experimental information.

The first approach recommended is to begin analysis of existing imagery. Considerable radar-image coverage of the United States exists at several locations. This imagery has had only limited analysis for resource applications. Several application areas could benefit from a well-planned pro-

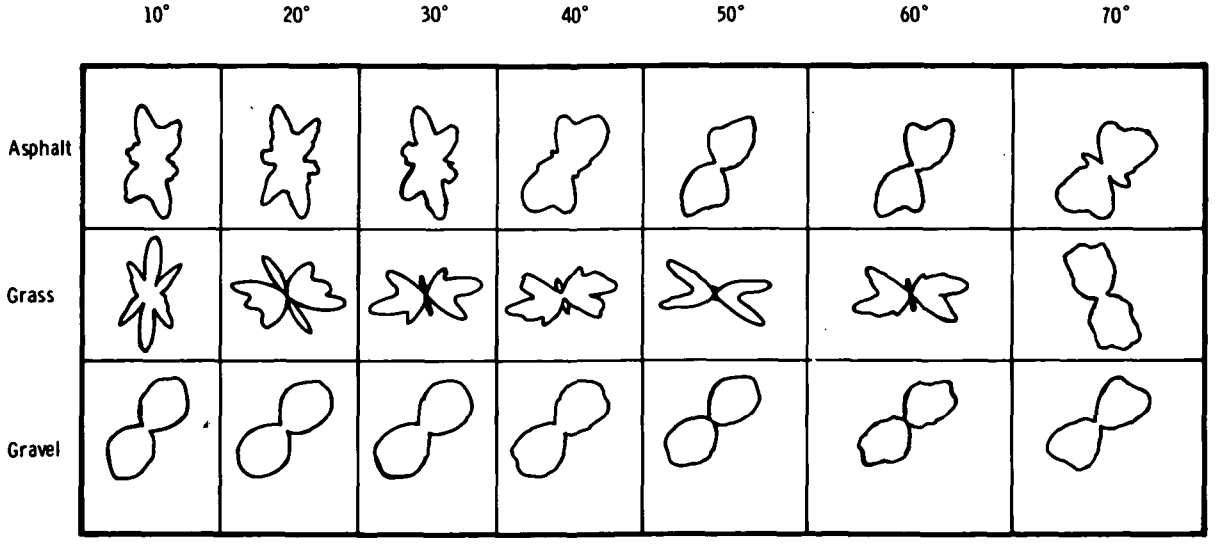

FIGURE 5–108.—Direct polarization profiles for asphalt, grass, and gravel at 8.505 GHz for various incident angles.

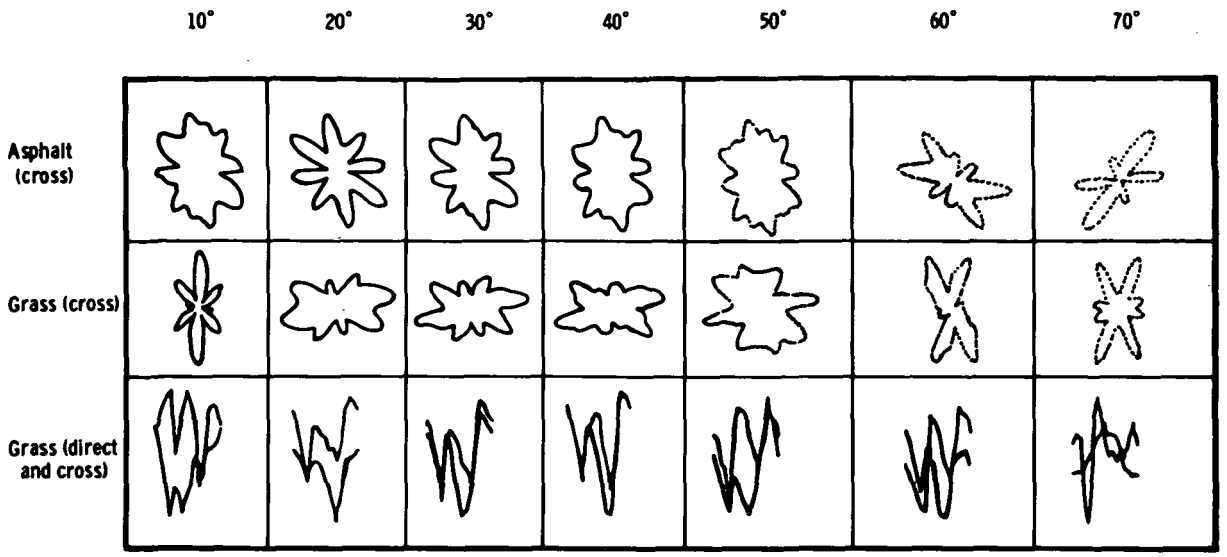

FIGURE 5–109.—Cross-polarization profiles for asphalt and grass at 8.505 GHz for various incident angles.

gram using these data. A fruitful area would be the comparison of ERTS multispectral scanner data with radar data in the area of geology and vegetation.

A second proposed approach is to use existing multiparameter systems in a coordinated measurement program. At least two existing systems have simultaneous frequencies on two or more wavelengths and two polarization channels. The use of these systems would provide much imaging information needed for both Earth/land and ocean applications.

Many of the reports and articles concerned with imaging radar classify the carrier wavelength or frequency into bands identified by letters, such as X-band. Presently, there are three recognized systems of band identification. To avoid confusion, in this section the carrier is specified by the wavelength expressed in millimeters, because wavelength is more meaningful to Earth scientists.

Oceans

In the area of ocean sensing, an effort is needed to determine which part or parts of the ocean wave reflect the radar energy, and further study is needed to develop methods to obtain two-dimensional wave spectra from imaging radar data. Most existing ice-measurement data provide information on physical parameters such as size and patterns. A need exists to use multiparameter radar systems to improve ice-type identification.

There is an established user requirement for the previously mentioned items. Consequently, high priority should be given to instituting programs that will supply the required information.

Atmosphere

The atmosphere panel has generated a requirement for radar observations of tropical storms. The requirements for such observations are presented as an item for a feasibility study. Tropical storms (including hurricanes and typhoons) appear to be promising targets for meteorological radar observations from orbiting satellites. Some characteristics of the storm systems are summarized in the following paragraphs, and minimum and desirable radar-observing capabilities are given.

Some significant characteristics of the storm systems are given in table 5–XIII.

TABLE 5–XIII.—*Significant Characteristics of Storm Systems*

Typical overall dimensions of the precipitation region:	
Diameter, km	560
Height, km	18
Lifetime, weeks	1 to 3
Reflectivity factor range of interest, dBZ	20 to 70
Windspeed range of interest, m/sec	0 to 75

Radar observations of the precipitation distribution in tropical storms throughout their life cycles are not now available. However, the Global Atmosphere Research Program Atlantic Tropical Experiment (GATE) radar program may provide a few sets of such observations.

Estimates of the minimum and the desired radar observational capabilities to provide useful information for hurricane studies are as follows:

1. Minimum capability: Determine the horizontal (i.e., two dimensional) distribution of precipitation echoes, with resolution as follows:
   a. Horizontal: 20 km
   b. Time: 24 hr
   c. Reflectivity factor: semiquantitative
2. Desired capability: Determine the three-dimensional distribution of precipitation echoes, with resolution as follows:
   a. Horizontal: 2 km
   b. Vertical: 1 km
   c. Reflectivity factor: 3 dB
   d. Time: 12 hr
3. Determine wind velocities, with resolution as follows:
   a. Horizontal: 2 km [3]
   b. Vertical: 1 km
   c. Wind velocity: 2.5 m/sec, 20°
4. Determine storm movement, with resolution of 1 m/sec, 10°.

The minimum requirements are based mainly on the characteristics of present-day numerical models. In general, those models deal with only two-dimensional distributions of precipitation or with a vertical structure represented by a few levels.

[3] For some purposes, the horizontal resolution requirements of the wind measurements can be relaxed to 10 to 20 km.

COMPONENT DEVELOPMENT

The equipment requirements of the applications panels are within the current state of the art, with the exception of possible deployment techniques for large space antennas. There is a need for deployable antennas for some imaging radar applications in the frequency range from 100 to approximately 40 000 MHz, having along-track dimensions of 5 to 20 m and crosstrack beamwidths of 6° to 15°. Side lobes in both dimensions must be kept below approximately −20 dB. A program should be initiated to develop a space-qualified antenna to meet these requirements.

DATA PROCESSING

Any plan designed to gather data from an aircraft for investigative purposes must include an adequate data-reduction facility to give the user/investigator the required data in a timely manner. If the same instrumentation is to serve a large number of user/investigators, at different wavelengths and polarizations, the data should take the form of a universally usable data-distribution method such as a computer-compatible tape. In the development of the instrumentation required, the merging of operational parameters (such as altitude, latitude, longitude, velocity, windspeed, wavelength, polarization, and swath width) with the data must be considered.

Future effort should be concerned with geometric fidelity of radar imagery and with the problem of producing images that are compatible with maps and other systems outputs such as ERTS. Consideration should be given to rectifying radar imagery and removing geometric distortion in the processing state of the data chain.

The recommendation concerning data processing and management is clear. Efforts must be initiated that will specify all phases of data processing and management from

the collection of the data to the data analysis and, where possible, the dissemination of the final product. More efficient data reduction algorithms are necessary for this effort.

The desired observing capabilities are based on anticipated future development of the hurricane models and extrapolation from the capabilities of presently available ground-based weather radar systems. Much finer resolution is needed in both the horizontal and vertical directions, and somewhat finer resolution is generally desirable in the vertical dimension. Moreover, nonattenuating wavelengths would be required to obtain quantitative echo intensity measurements.

The observing capability required for any specific investigation must be determined by reference to the detailed scientific objectives. Thus, the present estimate indicates design goals that may serve as a basis for deciding whether the needed capabilities can even be approached by satellite-borne weather radar systems.

CALIBRATION

Stated requirements for system calibration range from 2 to 5 dB, absolute, and from 0.1 to 3 dB, relative. The attainment of these requirements for some systems has not yet been demonstrated. Furthermore, the calibration must be maintained during extended periods of operation. A program is needed to establish the methods of calibration for each system, determine the level of calibration that can be achieved, and predict the degradation of calibration with time and environment during operation.

MULTIPARAMETER SYSTEM

The Active Microwave Workshop panels expressed the desire for multifrequency and multipolarization data. Of the three panels, the Earth/land panel specified imagery for two or more frequencies and at least two polarizations. This need, together with the shortage of existing data on simultaneous coverage with multiparameter systems, provides a strong justification to implement a program in the design and procurement of such a system and to institute an experimental measurements program.

SUMMARY OF RECOMMENDATIONS

The TSG has determined that a need exists for each of the following recommendations:

1. An experimental aircraft program for ocean wave and ice investigations.
2. An experimental aircraft program for Earth/land investigations.
3. A polarization signature study.
4. A coordinated program to analyze existing imagery.
5. A program to use existing multiparameter systems in the collection of needed data.
6. A feasibility study on the subject of equipment for the observation of tropical storms.
7. A program to develop large deployable space antennas.
8. A program to address the subject of data processing, data analysis, and data management.
9. A program to determine system calibration capabilities and methods of calibration.
10. The development of a multiparameter imaging system.

REFERENCES

5–1. SCHABER, GERALD G.; BROWN, WALTER E., JR.; AND BERLIN, GRAYDON L.: Surface Roughness Variations in Death Valley, California: Geologic Evaluation of 25 cm Radar Images. U.S. Coast Guard Interagency Rep. 65, Feb. 1975.

5–2. HUNT, C. B., AND MABEY, D. R.: Stratigraphy and Structure, Death Valley, California. U.S. Geol. Survey Prof. Paper 494–A, 1966.

5–3. HUNT, C. B.; ROBINSON, T. W.; BOWLES, W. A.; AND WASHBURN, A. L.: Hydrologic Basin, Death Valley, California. U.S. Geol. Survey Prof. Paper 494–B, 1966.

5–4. HUNT, C. B.: Plant Ecology of Death Valley, California. U.S. Geol. Survey Prof. Paper 509, 1966.

5–5. SCHABER, GERALD G., AND BROWN, WALTER E., JR.: Long-Wavelength Radar Images of

Northern Arizona—A Geological Evaluation. U.S. Geol. Survey Prof. Paper 800–B, 1972, pp. B175–B181.

5–6. MacDonald, H. C., and Waite, W. P.: Imaging Radars Provide Terrain Texture and Roughness Parameters in Semi-Arid Environments. Mod. Geol., vol. 4, no. 2, 1973, pp. 145–158.

5–7. Peake, W. H., and Oliver, T. L.: The Response of Terrestrial Surfaces at Microwave Frequencies. U.S. Air Force Avionics Lab. Rep., AFAL–TR–70–301, Ohio State Univ. Electroscience Lab., 1971.

5–8. Moore, R. K.: Radar Return From the Ground. Bull. of Engineering, no. 59, Univ. of Kansas Publications (Lawrence, Kans.), 1969.

5–9. Lundien, J. R.: Radar Responses to Laboratory Prepared Soil Samples: Terrain Analysis by Electromagnetic Means. Tech. Rep. 3–693, Rep. 2, U.S. Army Engineers Waterways Experiment Station (Vicksburg, Miss.), 1966.

5–10. Beckmann, Peter, and Spizzichino, Andre: The Scattering of Electromagnetic Waves From Rough Surfaces. Macmillan Press (New York), 1963.

5–11. AAAS Committee on Arid Lands: Off-Road Vehicle Use. Science, vol. 184, no. 4135, Apr. 1974, pp. 500–501.

5–12. Brown, William M.: Synthetic Aperture Radar. AGARD 12th Symposium of the Avionics Panel, Conf. Proceed. no. 20 (Paris, France), Apr. 1966.

5–13. Brown, William M.: Synthetic Aperture Radar. IEEE Trans. Aerosp. Electron. Syst., vol. AES–3, no. 2, Mar. 1967, pp. 217–229.

5–14. Ingalls, Arthur L.: Optical Simulation of Microwave Antennas. IEEE Trans., Antennas Propagat., vol. AP–14, no. 1, Jan. 1966, pp. 2–6.

5–15. Leith, Emmett N.: Optical Processing Techniques for Simultaneous Pulse Comparison and Beam Sharpening. IEEE Trans., Aerosp. Electron. Systems, vol. 4, no. 6, Nov. 1968, pp. 879–885.

5–16. Larson, R. W.; Zelenka, J. L.; and Johansen, E. L.: Results Obtained From the Univ. of Michigan Microwave Hologram Radar. Proceedings of the Seventh International Symposium on Remote Sensing of Environment, Univ. of Michigan, vol. II, May 1971, pp. 809–824.

5–17. Larson, R. W., et al.: Investigation of Microwave Hologram Techniques for Application to Earth Resources. Proceedings of the Ninth International Symposium on Remote Sensing of Environment, vol. III, Univ. of Michigan, Apr. 1974, pp. 1541–1569.

5–18. Moore, R. K.: Radar Scatterometry—An Active Remote Sensing Tool. Proceedings of the Fourth Symposium on Remote Sensing of Environment, Univ. of Michigan, Apr. 1966, pp. 339–373.

5–19. Skolnik, Merrill Ivan, ed.: Radar Handbook. McGraw-Hill Book Co. (New York), 1970.

5–20. The 400 MHz Scatterometer. NASA CR–101976, 1969.

5–21. Scatterometer Data Analysis Program. NASA CR–62072, 1967.

5–22. Historical Logbook, S–193 Microwave Radiometer/Scatterometer/Altimeter. General Electric Corp. Doc. no. 72SD4232, Rev. A, vol. 1–10, Oct. 1972.

5–23. Hoekstra, Pieter; Sellman, Paul V.; and Delaney, Allan J.: Airborne Resistivity Mapping of Permafrost Near Fairbanks, Alaska. U.S. Army Cold Regions Research and Engineering Laboratory (Hanover, N.H.), Mar. 1974.

5–24. Hoekstra, P., and Delaney, A.: Dielectric Properties of Soils at UHF and Microwave Frequencies. J. Geophys. Res., vol. 79, no. 11, 1974, Apr. 1974, pp. 1699–1708.

5–25. Gudmandsen, P.: Radio Echo Sounding of Polar Ice. Rep. D170, Laboratory of Electromagnetic Theory, Technical Univ. of Denmark, Lyngby, Dec. 1972.

5–26. Porcello, L. J., et al.: The Apollo Lunar Sounder Radar System. IEEE Proc., Special Issue on Modern Radar Technology and Applications, vol. 62, June 1974, pp. 769–783.

5–27. Jackson, Philip L.: Range Focused Doppler Spectra (RFD): A Transformation of SAR Signal Film for Radar Scattering Analysis. Proceedings of the Ninth International Symposium on Remote Sensing of Environment, vol. III, Univ. of Michigan, Apr. 1974, pp. 1571–1584.

5–28. Morrison, H. F.; Phillips, R. J.; and O'Brien, D. P.: Quantitative Interpretation of Transient Electromagnetic Fields Over a Layered Half-Space. Geophys. Prospect., vol. 17, no. 1, Mar. 1969, pp. 82–101.

5–29. Phillips, R. J.: Computer Study of the Feasibility of Electromagnetic Pulse Propagation in the Earth (abs.). Geophysics, vol. 31, no. 6, 1966, p. 1208.

5–30. Scott, James H.; Carroll, Roderick D.; and Cunningham, David R.: Dielectric Constant and Electrical Conductivity Measurements of Moist Rock: A New Laboratory Method. J. Geophys. Res., vol. 72, no. 20, Oct. 1967, pp. 5101–5115.

5–31. Moffett, Alan T.: Minimum-Redundancy

Linear Arrays. IEEE Trans., Antennas Propagat., vol. AP-16, no. 2, Mar. 1968, pp. 172–175.

5–32. DAVIES, D. E. N.: A Fast Electronically Scanned Radar Receiving System. J. Brit. IRE, vol. 21, no. 4, Apr. 1961, pp. 305–318.

5–33. EDGAR, A. K., AND JONES, I. L.: Flood-Lighting With Nyquist Rate Scanning. AGARD, Advanced Radar Systems, Nov. 1970.

5–34. SHAW, E., AND DAVIES, D. E. N.: Theoretical and Experimental Studies of the Resolution Performance of Multiplicative and Additive Aerial Arrays. Radio Electron. Eng., vol. 28, Oct. 1964, pp. 279–291.

5–35. SHEARMAN, E. D. R.; BICKERSTAFF, P.; AND FOFIADES, L.: Synthetic Aperture Skywave Radar: Techniques and First Results. Radar—Present and Future. Proceedings of the Int. Conf. IEEE, Oct. 1973, pp. 414–421.

5–36. MILLS, B. Y., AND LITTLE, A. G.: A High Resolution Aerial System of a New Type. Australian J. Phys., vol. 6, no. 3, May 1953, pp. 272–278.

5–37. DENNIS, ARNETT S.: Rainfall Determinations by Meteorological Satellite Radar. NASA CR–50193, 1963.

5–38. DRANE, C. J., JR., AND MCILVENNA, J. G., JR.: Gain Maximization and Controlled Null Placement Simultaneously Achieved in Aerial Array Patterns. Radio Electron. Eng., vol. 39, Jan. 1970, pp. 49–57.

5–39. MARTIN, D. P.: A Combined Radar-Radiometer With Variable Polarization. JPL Tech. Memo. 33–570, Oct. 1972.

APPENDIX 5A

PATTERN RECOGNITION CONSIDERATIONS

ESSENTIAL PROCESSING OF RADAR IMAGES

To extract the maximum useful information in data processing and pattern recognition, Nagy (ref. 5A–1) has identified the following necessary procedures.

1. Image enhancement by digital and/or analog means is needed as an aid for human interpretation of the data. Specific approaches in digital image enhancement include orthogonal transformations, linear transformation, two-dimensional filtering, and so forth. Difficulties may arise because the transformations required to reveal or emphasize one set of features may, in fact, degrade features desirable for another purpose. In this case, several transformations may be needed at the same time.

2. The need for exact (element by element) superimposition of two images of the same scene upon one another arises in preparing a composite image, chronological observations, and so forth. It is also desirable in many application areas to bring together radar images and multispectral sensor images of the same scene. In this instance, the geometric and radiometric correction techniques may be different, but the problems are identical. It is necessary to correct, although it may not be possible to completely eliminate, the differences that may occur between two images of the same scene.

3. Geometric distortions caused by changes in the attitude and altitude of the sensor can be corrected by digital techniques while preserving the resolution requirement.

4. Radiometric corrections are data corrections arising from a variety of sources, the most common of which are calibration corrections, empirical corrections for data recording and processing errors, and atmospheric corrections.

5. In the case of data dropouts, interpolation techniques must be used to compensate for data loss. In multifrequency and multipolarization operation, the amplitudes of the data from all channels must be scaled and calibrated to remove the variations among different channels.

6. The atmospheric effects of scattering and diffraction also degrade the images. It is necessary to assess and remove such effects, especially in the determination of surface reflectance. The removal of these effects

is also needed in the pattern recognition process in which ground-truth sites are used as training samples and the signatures are extended over other areas in the recognition process. If variations in the atmosphere are large enough to introduce significant variations in the signature, then the recognition performance will suffer. Atmospheric effects can be corrected by using the theoretical atmospheric model and the actual observations. The effects are highly dependent on the operating frequency and the turbidity and humidity of the atmosphere.

7. Once the images to be matched have been corrected for the previously mentioned sources of error, the relative location of the images must still be determined before an objective point-by-point comparison can be performed. Tracking and ephemeris data usually provide a first approximation to the position of the sensor at the time the data are acquired; but, for exact registration, more accurate localization is required.

AUTOMATIC PATTERN RECOGNITION CONSIDERATIONS

As with other sensors, the large amounts of data generated on an active microwave system make it desirable to use machine interpretation of the data whenever feasible. Machine interpretation requires the use of automatic pattern-recognition techniques. Although particular emphasis is placed on the automatic recognition of radar images, the techniques should be useful to other radar data, such as data from the scatterometer, altimeter, and so forth. Experience gained from the machine processing of other remotely sensed data, such as from ERTS–1, should be very useful for the automatic processing of the active microwave sensor data. The data acquisition and formatting may be different, but the basic recognition process entails the following three operations performed in sequence.

1. Preprocessing is performed to enhance the pattern characteristics that are important for recognition and to remove the irrelevant details. Preprocessing techniques are application dependent. Typical examples are Laplacian filtering for edge enhancement, regulation of input field size, and so forth. In most image-recognition experiments, the first step in the preprocessing phase entails reducing the radar image to digital form by means of a flying spot scanner and an A/D converter. The digitized image consists of an array of numbers, with each number representing the gray level at a particular point.

2. Feature extraction and selection is performed to obtain a pattern representation of lower dimensionality compared to the original input field. These features (properties) must also admit an effective decision function of a simple form. Features should be derived from spatial, tonal, and textual-contextual information of the images. The knowledge of which set of features to extract will guide the designing of the preprocessing operations, and the appropriate preprocessing of the image data will facilitate the extraction of significant features. These two closely related operations are the keys to the success of automatic recognition of radar images.

3. Classification, accomplished by applying a decision function to the feature set, is performed to assign the pattern to one of several preselected classes. The classes are defined according to a priori knowledge. The definition of pattern class may be modified at different levels of classification. For example, in radar discrimination of sea ice (ref. 5A–2), seven categories of sea ice can be identified with the scatterometer experiment. However, in an SLAR experiment, only four categories could be distinguished. Similar examples can be given in land-use classification. The training samples are usually required to obtain any reasonable recognition result. Typical classification or decision procedures are the maximum-likelihood decision rule, the nearest-neighbor decision rule, and the linear decision functions.

DATA FORMAT

Quantization introduces a nonrecoverable error in the specification of the amplitude of each image sample. The number of quantization levels required to maintain the quantization error below the subjective threshold of noticeability is strongly dependent on the characteristics of the image sensor and display. As many as 256 quantization levels may be required for flying a spot scanner display. For classification purposes, the data-format requirement is different. Suppose an image is divided into several subimages and each subimage is represented by a vector sample. If the number of samples (i.e., the sample size) is finite, which is typical in most remote-sensing problems, the mean recognition accuracy improves as the number of discrete values of the sample increases, until the number reaches a certain optimum number beyond which the recognition accuracy worsens. This result is due to the discrete nature of the feature measurement and the finiteness of sample size. The optimum number does not depend on the resolution and signal-to-noise ratio. Let the dimensionality of a vector sample be $n=q^N$ discrete levels, where N is the number of components of the vector. Thus, it has been shown that for two classes which are equally likely and have a finite number of samples, there exist optimum N and q, depending on the sample size, at which the mean recognition accuracy is the highest. For small sample size, the optimum q is 3 for $n \leq 5$. If the sample size is 40 and $N=2$, the optimum q is 6. If $q=2$ (i.e., binary measurements are used) and 500 samples are used, the optimum dimension is 23, which requires $N \leq 5$.

DATA ACQUISITION AND RECOGNITION ACCURACY

The recognition result depends strongly on how the data are gathered. Properly acquired radar images will greatly simplify the subsequent recognition operation. The recognition accuracy will definitely improve with multifrequency and multipolarization operations. The effect of taking measurements from several angles has been examined by Parashar et al. (ref. 5A–2). The percentage of correct recognitions of sea-ice types that they reported for the radar scatterometer is listed in table 5A–I.

The exact relationship between signal-to-noise ratio, spatial resolution, and recognition accuracy is not available. However, as the signal-to-noise ratio and the spatial resolution are improved to certain levels, the recognition accuracy reaches a saturation point at which further improvement is negligible.

PREPROCESSING AND FEATURE EXTRACTION TECHNIQUES

A general approach to preprocessing and feature extraction is the use of orthogonal transformation techniques. This approach emphasizes image enhancement. The Karhunen-Loeve transform may be applied to the digital imagery to provide a set of uncorrelated principal component images useful in automatic recognition, signal-to-noise ratio improvement, and data compression. Fast algorithms should be used to reduce the computational complexity in orthogonal transforms.

A more efficient computational approach is to sequentially select fewer (but good) features to achieve an acceptable recognition accuracy. The spatial and textural properties and the distance measures can be used to construct such features. Each feature can then be evaluated sequentially. The best features are used for classification. In most

TABLE 5A–I.—*Recognition Accuracies for Scatterometer Data*

Frequency	Number of classes	Number of angles	Percentage correct
13.3 GHz	7	12	66
13.3 GHz	7	6	64
13.3 GHz	4	12	87
13.3 GHz	4	6	85
400 MHz	4	12	75
400 MHz	4	6	62

instances, the underlying distribution of the features cannot be assumed, and nonparametric methods are needed. For preprocessing, one important problem is the boundary detection, which may be performed by a thresholding method using both local (gray-level association) and global (second-order gray-level distribution) information.

Another useful approach that significantly speeds up (by a factor of 2 or more) the classification and feature selection is to incorporate the Cholesky decomposition in the LARSYS program (a computer program developed by Purdue University).

NONSUPERVISED CLASSIFICATION AND CLUSTERING

"Nonsupervised learning" or "cluster seeking" are terms applied to methods of data analysis in which only the observed values are used explicitly to group samples according to some intrinsic measure of similarity. In remote-sensing experiments, this approach has been used (1) to alleviate the problem of multimodel probability distributions in supervised classification methods, (2) to circumvent the need for a priori selection of training samples, and (3) to condense the amount of information stored or transmitted.

This approach is suboptimal compared with the supervised classification. It is still necessary to collect the ground truth to reduce the errors that may arise in this approach. Clustering techniques can be used to effectively determine the homogeneity and inhomogeneity in Earth scenes as an initial step toward automatic scene identification.

ONBOARD CLASSIFICATION

Performing pattern recognition processing onboard the satellite (ref. 5A–3) may considerably reduce the amount of data to be sent back to the ground. For example, in terrain classification, it is envisioned that the data to be transmitted would be a set of coordinates delineating the boundaries separating large homogeneous areas (e.g., mountains and plains) together with a code for designating the pattern class on each side of the boundary. The original scene could then be reconstructed on the ground from idealized models of the pattern classes. The complexity of these models would be a function of the discrimination capability of the pattern recognition process. The main advantage of the onboard classification would be the reduction of the transmission bandwidth and the overall computational and storage requirements. A possible disadvantage would be the inadequate recognition accuracy available from the onboard processor.

In summary, the important points concerning radar image processing and recognition are as follows:

1. Both geometric and radiometric corrections for radar images can be performed in generally the same manner as for photographic products from other Earth resource programs.

2. Basically, the same image processing and pattern recognition techniques used for multispectral sensor data can be used for radar images.

3. More efficient preprocessing and feature extraction algorithms for radar images are needed.

REFERENCES

5A–1. NAGY, G.: Digital Image—Processing Activities in Remote Sensing for Earth Resources. Proc. IEEE, vol. 60, no. 10, Oct. 1972, pp. 1177–1200.

5A–2. PARASHAR, S. K., ET AL.: Investigation of Radar Discrimination of Sea Ice. Proceedings of the Ninth International Symposium on Remote Sensing of Environment, vol. I, Univ. of Michigan, 1974, pp. 323–332.

5A–3. DARLING, E. M., JR., AND JOSEPH, R. D.: Pattern Recognition From Satellite Altitudes. IEEE Trans., Syst. Sci. Cybernetics, vol. SSC–4, no. 1, 1968, pp. 38–47.

APPENDIX A

Abbreviations and Acronyms

AAFE	advanced application flight experiments
A/D	analog to digital
AGC	automatic gain control
AIDJEX	Arctic ice dynamics joint experiment
ALSE	Apollo lunar sounder experiment
AMW	Active Microwave Workshop
AOSS	Airborne Oil Surveillance System
ATS	Applications Technology Satellite
CAS	Cooperative Application Satellite
CCT	computer-compatible tape
CFA	crossfield amplifier
CIR	coherent imaging radar
CNES	Centre National d'Etudes Spatiales
CPRA	compressed pulse radar altimeter
CRREL	Cold Regions Research and Engineering Laboratory
CRT	cathode-ray tube
CTC	crosstrack contiguous
CTNC	crosstrack noncontiguous
CW	continuous wave
CZCS	coastal zone color scanner
DCS	data collection system
DME	distance measuring equipment
DOD	Department of Defense
D/RADEX	digitized radar experiments
DST	data systems test
EOPAP	Earth and Ocean Physics Application Program
EOS	Earth Observatory Satellite
ERAP	Earth Resources Aircraft Program
ERB	Earth radiation budget
EREP	Earth resources experiment package
ERIM	Environmental Research Institute of Michigan
ERTS	Earth Resources Technology Satellite
ESMR	electronically scanning microwave radiometer
ESRO	European Space Research Organization
ESSA	Environmental Science Services Administration
FBS	fan beam scatterometer
FET	field effect transistors
FFT	fast Fourier transform
FGGE	first GARP global experiment
FM	frequency modulation
GARP	Global Atmosphere Research Program
GATE	Global Atmosphere Research Program Atlantic Tropical Experiment
GEM	Goddard Earth Models
GEOS	Geostationary Earth Orbiting Satellite
GMT	Greenwich mean time
GOES	Geostationary Operational Environmental Satellite
GSFC	Goddard Space Flight Center
H	horizontal
hf	high frequency
HH	horizontal transmit/horizontal receive
HV	horizontal transmit/vertical receive
ICSU	International Council of Scientific Unions
ICW	interrupted continuous wave
IFOV	instantaneous field of view
IGY	International Geophysical Year
IMPATT	impact avalanche transit time
IR	infrared
IRIS	infrared interferometer spectrometer
IRLS	interrogation, recording, and location system
IRR	infrared radiometer
ISLR	integrated side-lobe ratio
ITC	in-track contiguous
ITNC	in-track noncontiguous
ITOS	Improved Tiros Operational Satellite
JOC	Joint Organizing Committee
JOSS	Joint Ocean Surface Study
JPL	Jet Propulsion Laboratory
JSC	NASA Lyndon B. Johnson Space Center
LACATE	lower atmosphere composition and temperature experiment
LaRC	Langley Research Center
LEST	large Earth survey telescope
LFM	limited fine mesh

LLL	low light level
LO	local oscillator
LSI	large-scale integration
MAPS	measurement of air pollution from satellites
mf	medium frequency
MNRCS	median normalized radar cross section
MS	microwave spectrum
MSS	multispectral scanner
MTBF	mean time before failure
MTI	moving target indicator
MUSE	monitor of ultraviolet solar energy
MWS	microwave wind spectrometer
NEMS	Nimbus-5 microwave sounder
NESS	National Environmental Satellite Service
NOAA	National Oceanic and Atmospheric Administration
NRCS	normalized radar cross section
NRL	Naval Research Laboratory
NWL	Naval Weapons Laboratory
NWP	numerical weather prediction
NWS	National Weather Service
ODSI	Ocean Data Systems, Inc.
ODU	Old Dominion University
OGO	Orbiting Geophysical Observatory
O_2-MS	oxygen microwave spectrum
OUE	orbital uncertainty estimates
PCM	pulse code modulation
pixel	picture element
PMIS	Passive Microwave Imaging System
PPI	plan position indicator
PRF	pulse repetition frequency
RA	radar altimeter
RADAM	radar of the Amazon
RADSCAT	radiometer/scatterometer
RAR	real aperture radar
rf	radiofrequency
rms	root mean square
SAM	stratospheric aerosol measurement
SAMS	stratospheric and mesospheric sounder
SAO	Smithsonian Astrophysical Observatory
SAR	synthetic aperture radar
SBUV/TOMS	solar and backscattered ultraviolet and total ozone mapping system
SCAMS	scanning and microwave sounder
SCR	surface-contour radar
SCS	Soil Conservation Service
SEOS	Synchronous Earth Observatory Satellite
SIRS	satellite infrared spectrometer
SLAR	side-looking airborne radar
SMIIS	solar microwave interferometer imaging system
SMMR	scanning multichannel microwave radiometer
SMS	Synchronous Meteorological Satellite
SNR	signal-to-noise ratio
STALO	stable local oscillator
TED	transferred electron devices
THIR	temperature humidity infrared radiometer
Tiros	Television and Infrared Observation Satellite
TO	transmitter oscillator
TOS	Tiros Operational Satellite
TRAPATT	trapped plasma avalanche triggered transit
TSG	Technology Support Group
TV	television
TWT	traveling wave tube
uhf	ultrahigh frequency
USCG	U.S. Coast Guard
USGS	U.S. Geological Survey
UTM	universal transverse Mercator
V	vertical
VH	vertical transmit/horizontal receive
vhf	very high frequency
VIMS	Virginia Institute of Marine Science
VIR	visible and infrared radiometer
VISSR	visible and infrared spin scan radiometer
VLBI	very long baseline interferometry
vlf	very low frequency
VTPR	vertical temperature profile radiometer
VV	vertical transmit/vertical receive
WDS	wave directional spectrometer
WMO	World Meteorological Organization

APPENDIX B

Units and Unit-Conversion Factors

In this appendix are the names, abbreviations, and definitions of International System (SI) units used in this report and the numerical factors for converting from SI units to more familiar units.

Names of International Units Used in This Report

Physical quantity	Name of unit	Abbreviation	Definition of abbreviation
Basic Units			
Mass	meter	m	
Time	kilogram	kg	
Temperature	second	sec	
Length	kelvin	K	
Derived Units			
Area	square meter	m^2	
Volume	cubic meter	m^3	
Frequency	hertz	Hz	sec^{-1}
Density	kilogram per cubic meter	kg/m^3	
Velocity	meter per second	m/sec	
Pressure	newton per square meter	N/m^2	
Work, energy, quantity of heat	joule	J	N·m
Power	watt	W	J/sec
Voltage, potential difference, electromotive force	volt	V	W/A
Electric resistance	ohm	Ω	V/A
Electric capacitance	farad	F	A·sec/V
Wave number	1 per meter	m^{-1}	
Specific heat capacity	joule per kilogram kelvin	J/kg·K	

Unit Prefixes

Prefix	Abbreviation	Factor by which unit is multiplied
pico	G	10^9
giga	M	10^6
mega	k	10^3
kilo	h	10^2
hecto	c	10^{-2}
centi	m	10^{-3}
milli	μ	10^{-6}
micro	n	10^{-9}
nano	p	10^{-12}

Unit-Conversion Factors

To convert from—	To—	Multiply by—
joule	British thermal unit (International Steam Table)	9.479×10^{-4}
joule	Calorie (International Steam Table)	2.388×10^{-1}
joule	electron volt	6.242×10^{18}
joule	erg	1.000×10^{7} [a]
joule	foot-pound force	7.376×10^{-1}
joule	kilowatt-hour	2.778×10^{-7}
joule	watt-hour	2.778×10^{-4}
kelvin	degrees Celsius (temperature)	$t_C = t_K - 273.15$
kelvin	degrees Fahrenheit (temperature)	$t_F = 9/5\ t_K - 459.67$
kilogram	gram	1.000×10^{3} [a]
kilogram	kilogram mass	1.000×10^{3} [a]
kilogram	pound mass (pound mass avoirdupois)	2.205×10^{0}
kilogram	slug	6.852×10^{-2}
kilogram	ton (short, 2000 pound)	1.102×10^{-3}
meter	angstrom	1.000×10^{10} [a]
meter	foot	3.281×10^{0}
meter	inch	3.937×10^{1}
meter	micron	1.000×10^{6} [a]
meter	mile (U.S. statute)	6.214×10^{-4}
meter	nautical mile (international)	5.400×10^{-4}
meter	nautical mile (U.S.)	5.400×10^{-4}
meter	yard	1.094×10^{0}
newton/meter^2	atmosphere	9.870×10^{-6}
newton/meter^2	centimeter of mercury (0° C)	7.501×10^{-4}
newton/meter^2	inch of mercury (32° F)	2.953×10^{-4}
newton/meter^2	inch of mercury (60° F)	2.961×10^{-4}
newton/meter^2	millimeter of mercury (0° C)	7.501×10^{-3}
newton/meter^2	torr (0° C)	7.501×10^{-3}
radian	degree (angle)	5.730×10^{1}
radian	minute (angle)	3.438×10^{3}
radian	second (angle)	2.063×10^{5}
watt	British thermal unit (thermochemical)/second	9.484×10^{-4}
watt	calorie (thermochemical)/second	2.390×10^{-1}
watt	foot-pound force/second	7.376×10^{-1}
watt	horsepower (550 foot-pound force/second)	1.341×10^{-3}

[a] An exact definition.

☆ U.S. GOVERNMENT PRINTING OFFICE: 1975 0—587-297

NATIONAL AERONAUTICS AND SPACE ADMINISTRATION
WASHINGTON, D.C. 20546

OFFICIAL BUSINESS
PENALTY FOR PRIVATE USE $300

SPECIAL FOURTH CLASS MAIL
Book

POSTAGE AND FEES PAID
NATIONAL AERONAUTICS AND
SPACE ADMINISTRATION
NASA-451

U.S.MAIL

POSTMASTER: If Undeliverable (Section 158 Postal Manual) Do Not Return

"The aeronautical and space activities of the United States shall be conducted so as to contribute . . . to the expansion of human knowledge of phenomena in the atmosphere and space. The Administration shall provide for the widest practicable and appropriate dissemination of information concerning its activities and the results thereof."

—NATIONAL AERONAUTICS AND SPACE ACT OF 1958

NASA SCIENTIFIC AND TECHNICAL PUBLICATIONS

TECHNICAL REPORTS: Scientific and technical information considered important, complete, and a lasting contribution to existing knowledge.

TECHNICAL NOTES: Information less broad in scope but nevertheless of importance as a contribution to existing knowledge.

TECHNICAL MEMORANDUMS: Information receiving limited distribution because of preliminary data, security classification, or other reasons. Also includes conference proceedings with either limited or unlimited distribution.

CONTRACTOR REPORTS: Scientific and technical information generated under a NASA contract or grant and considered an important contribution to existing knowledge.

TECHNICAL TRANSLATIONS: Information published in a foreign language considered to merit NASA distribution in English.

SPECIAL PUBLICATIONS: Information derived from or of value to NASA activities. Publications include final reports of major projects, monographs, data compilations, handbooks, sourcebooks, and special bibliographies.

TECHNOLOGY UTILIZATION PUBLICATIONS: Information on technology used by NASA that may be of particular interest in commercial and other non-aerospace applications. Publications include Tech Briefs, Technology Utilization Reports and Technology Surveys.

Details on the availability of these publications may be obtained from:

SCIENTIFIC AND TECHNICAL INFORMATION OFFICE

NATIONAL AERONAUTICS AND SPACE ADMINISTRATION

Washington, D.C. 20546